EXTRACTIVE METALLURGY OF RARE EARTHS

SECOND EDITION

EXTRACTIVE METALLURGY OF RARE EARTHS

SECOND EDITION

Nagaiyar Krishnamurthy
Chiranjib Kumar Gupta


CRC Press
Taylor & Francis Group
Boca Raton London New York

CRC Press is an imprint of the
Taylor & Francis Group, an **informa** business

CRC Press
Taylor & Francis Group
6000 Broken Sound Parkway NW, Suite 300
Boca Raton, FL 33487-2742

© 2016 by Taylor & Francis Group, LLC
CRC Press is an imprint of Taylor & Francis Group, an Informa business

No claim to original U.S. Government works
Version Date: 20151008

International Standard Book Number-13: 978-1-4665-7638-4 (eBook - PDF)

This book contains information obtained from authentic and highly regarded sources. Reasonable efforts have been made to publish reliable data and information, but the author and publisher cannot assume responsibility for the validity of all materials or the consequences of their use. The authors and publishers have attempted to trace the copyright holders of all material reproduced in this publication and apologize to copyright holders if permission to publish in this form has not been obtained. If any copyright material has not been acknowledged please write and let us know so we may rectify in any future reprint.

Except as permitted under U.S. Copyright Law, no part of this book may be reprinted, reproduced, transmitted, or utilized in any form by any electronic, mechanical, or other means, now known or hereafter invented, including photocopying, microfilming, and recording, or in any information storage or retrieval system, without written permission from the publishers.

For permission to photocopy or use material electronically from this work, please access www.copyright.com (http://www.copyright.com/) or contact the Copyright Clearance Center, Inc. (CCC), 222 Rosewood Drive, Danvers, MA 01923, 978-750-8400. CCC is a not-for-profit organization that provides licenses and registration for a variety of users. For organizations that have been granted a photocopy license by the CCC, a separate system of payment has been arranged.

Trademark Notice: Product or corporate names may be trademarks or registered trademarks, and are used only for identification and explanation without intent to infringe.

Visit the Taylor & Francis Web site at
http://www.taylorandfrancis.com

and the CRC Press Web site at
http://www.crcpress.com

Sri Krishnarpanam

Contents

Preface to the Second Edition xxi
Preface to the First Edition xxv
Authors xxix

Chapter 1 The Rare Earths 1

1.1 Introduction 1
1.2 Discovery 1
1.3 Special Characteristics 8
1.3.1 Electronic Configuration 8
1.3.2 Lanthanide Contraction 19
1.3.3 Basicity 20
1.4 Properties 21
1.4.1 Melting Point 21
1.4.2 Boiling Point 22
1.4.3 Allotropes 23
1.4.4 Resistivity 23
1.4.5 Magnetic Properties 24
1.4.6 Spectral Properties 24
1.4.7 Mechanical Properties 25
1.5 Reactivity 25
1.5.1 Air/Oxygen 25
1.5.2 Refractories 26
1.5.3 Nitrogen 26
1.5.4 Hydrogen 28
1.5.5 Carbon 28
1.5.6 Silicon 28
1.5.7 Sulfur, Selenium, Phosphorus 28
1.5.8 Refractory Metals 29
1.5.9 Acids and Bases 29
1.5.10 Water 30
1.6 Aqueous Systems 30
1.6.1 Trivalent State 30
1.6.2 Complexes 31
1.6.3 Tetravalent State 31
1.6.4 Divalent State 32
1.7 Applications 33
1.7.1 Metallurgy 34
1.7.1.1 Ductile Iron 34
1.7.1.2 Steels 36
1.7.1.3 Superalloys 40
1.7.1.4 Magnesium Alloys 41

1.7.1.5 Aluminum Alloys 41
1.7.1.6 Titanium Alloys 42
1.7.1.7 Copper Alloys 42
1.7.1.8 Zinc Alloys 42
1.7.1.9 Oxide Dispersion–Strengthened Alloys 43
1.7.1.10 Long-Range-Ordered Alloys 43
1.7.2 Magnets 43
1.7.3 Terfenol 51
1.7.4 Magnetic Refrigeration 53
1.7.5 Ceramics 53
1.7.6 Electronics 56
1.7.7 Chemical 57
1.7.8 Optical 59
1.7.9 Phosphors 61
1.7.9.1 Technology Transition in High-Efficiency Lighting 64
1.7.10 Nuclear 66
1.7.11 Hydrogen Storage 67
1.7.12 Superconductor 70
1.7.13 Miscellaneous 70
1.8 Global Rare-Earth Demand 73
1.9 Summary 81

Chapter 2 Resources 85

2.1 Introduction 85
2.2 Crustal Abundance 86
2.3 Minerals 87
2.3.1 Bastnasite 88
2.3.2 Monazite 93
2.3.3 Xenotime 94
2.3.4 Allanite 94
2.3.5 Apatite 97
2.3.6 Brannerite 99
2.3.7 Eudialyte 99
2.3.8 Euxenite, Fergusonite, Florencite, Gadolinite, and Loparite 99
2.3.9 Perovskite 100
2.3.10 Pyrochlore 100
2.3.11 Zircon 100
2.3.12 Others 101
2.3.13 Scandium Minerals 102
2.3.14 Promethium 102
2.4 Rare-Earth Deposits 102
2.4.1 Basic Geology of REEs 102
2.4.2 Distribution 105

2.5 Resources and Reserves 107
2.6 Occurrence 163
2.6.1 Argentina 163
2.6.2 Australia 163
2.6.2.1 Brown's Range 163
2.6.2.2 Dubbo Zirconia Project (DZP), Toongi 164
2.6.2.3 Eneabba 164
2.6.2.4 Cooljarloo/Jurien Bay 164
2.6.2.5 Cummins Range 165
2.6.2.6 Gilgai Intrusion 165
2.6.2.7 Jangardup 165
2.6.2.8 WIM-150 165
2.6.2.9 Murray Basin 165
2.6.2.10 Nolans Bore 165
2.6.2.11 Norraburra RE Deposit 166
2.6.2.12 Olympic Dam 166
2.6.2.13 Brockman (Hastings) Deposit 166
2.6.2.14 Mary Kathleen 166
2.6.2.15 Mount Weld 167
2.6.2.16 John Galt 168
2.6.2.17 Radium Hill 168
2.6.2.18 Syerston 168
2.6.2.19 Thuddungra 168
2.6.2.20 Yangibana 168
2.6.3 Bangladesh 168
2.6.4 Brazil 169
2.6.5 Canada 170
2.6.5.1 Denison Mine 170
2.6.5.2 Nechalacho/Thor Lake Mine Site, Northwest Territories 170
2.6.5.3 Yukon 171
2.6.5.4 Hoidas Lake 171
2.6.5.5 Kipawa 171
2.6.6 China 172
2.6.6.1 Bayan Obo 172
2.6.6.2 Ion-Adsorption Ore 175
2.6.6.3 Placers 176
2.6.6.4 Other Deposits 176
2.6.7 Egypt 177
2.6.8 Germany 177
2.6.9 Greenland 177
2.6.9.1 Kvanefjeld 177
2.6.10 India 178
2.6.10.1 Hard Rock Deposits 178
2.6.10.2 Placers 179
2.6.11 Indonesia 179

2.6.12 Japan 180
2.6.13 Kenya 180
2.6.14 Madagascar 180
2.6.15 Malaysia 180
2.6.16 Malawi 181
2.6.16.1 Kangankunde 181
2.6.16.2 Nanthace Hill 181
2.6.16.3 Songwe 182
2.6.16.4 Chilwa Island 182
2.6.17 Mozambique 182
2.6.18 Myanmar 182
2.6.19 New Zealand 182
2.6.20 Peru 182
2.6.21 South Africa 182
2.6.21.1 Buffalo Fluorspar 183
2.6.21.2 Phalaborwa Complex 183
2.6.21.3 Steenkampskrall 183
2.6.21.4 Zandkopsdrift 183
2.6.22 Sri Lanka 184
2.6.23 Sweden 184
2.6.24 Taiwan 184
2.6.25 Thailand 185
2.6.26 Turkey 185
2.6.27 United States 185
2.6.27.1 Elk Creek Carbonatite, Nebraska 186
2.6.27.2 Music Valley, California 186
2.6.27.3 Wet Mountains Area, Colorado 186
2.6.27.4 Diamond Creek Area, Idaho 187
2.6.27.5 Hall Mountain, Idaho 187
2.6.27.6 Lemhi Pass District, Idaho 187
2.6.27.7 Pea Ridge Iron Deposit and Mine, Missouri 188
2.6.27.8 Hicks Dome, Illinois 188
2.6.27.9 Mineville Iron District, New York 188
2.6.27.10 Bear Lodge Mountains, Wyoming 189
2.6.27.11 Mountain Pass, California 189
2.6.27.12 Bokan Mountain, Alaska 190
2.6.27.13 Iron Hill, Colorado 190
2.6.27.14 Gallinas Mountains, New Mexico 190
2.6.27.15 Pajarito, New Mexico 190
2.6.27.16 Placers 190
2.6.28 Former Soviet Union 192
2.6.28.1 Tomtor 193
2.6.28.2 Chuktukon 193
2.6.28.3 Kyrgyzstan 194

2.6.29 Venezuela 194
2.6.30 Vietnam 194
2.6.30.1 Nam Xe 194
2.6.30.2 Dong Pao 195
2.6.31 Zaire 195
2.7 By-Products and Coproducts 195
2.8 World Rare-Earth Production 197
2.8.1 Brazil 202
2.8.2 India 203
2.8.3 United States 203
2.8.4 Australia 205
2.8.5 China 207
2.8.6 Former Soviet Union 210
2.8.7 South Africa 211
2.8.8 Canada 211
2.8.9 Malaysia 212
2.8.10 Thailand 212
2.8.11 Sri Lanka 212
2.8.12 Zaire and Madagascar 213
2.9 Scenario for the Immediate Future 213
2.10 Summary 229

Chapter 3 Resource Processing 235

3.1 Introduction 235
3.2 Mining 236
3.2.1 Hard-Rock Deposits 236
3.2.2 Placer Deposits 236
3.3 Physical Beneficiation 236
3.3.1 Monazite 239
3.3.1.1 Froth Flotation 244
3.3.1.2 Bastnasite Flotation 244
3.3.1.3 Monazite Flotation 246
3.3.2 Bastnasite 247
3.3.3 Bayan Obo Ore 249
3.4 Beneficiation of Other Rare-Earth Minerals 251
3.5 Chemical Treatment 254
3.5.1 Monazite 254
3.5.1.1 Acid Treatment 254
3.5.1.2 Alkali Treatment 255
3.5.1.3 Indian Rare Earths Ltd. Practice 255
3.5.1.4 Monazite Breakdown Practices 258
3.5.1.5 High-Temperature Process 260
3.5.1.6 Chlorination 260

3.5.2 Bastnasite 261
3.5.2.1 Processing Bear Lodge Ore 266
3.5.2.2 Goldschmidt Process 266
3.5.3 Xenotime 269
3.5.4 Ion-Adsorption Ore 270
3.5.5 Elliot Lake Uranium Ore 273
3.5.6 Gadolinite 273
3.5.7 Euxenite, Fergusonite, and Samarskite 274
3.5.8 Loparite and Pyrochlore 276
3.5.9 Apatite 277
3.6 Separation Processes 279
3.6.1 Selective Oxidation 279
3.6.2 Selective Reduction 281
3.6.3 Fractional Crystallization 282
3.6.4 Fractional Precipitation 283
3.6.5 Ion Exchange 285
3.6.5.1 Method 285
3.6.5.2 Application 287
3.6.6 Solvent Extraction 290
3.6.6.1 Method 290
3.6.6.2 Organophosphorus Acids 293
3.6.6.3 Carboxylic Acids 300
3.6.6.4 Solvating Extractants 301
3.6.6.5 Amines 303
3.6.6.6 Synergistic Effects 306
3.6.6.7 Industrial Processes 307
3.6.6.8 Molycorp 308
3.6.6.9 Denison Mines 309
3.6.6.10 Indian Rare Earths 310
3.6.6.11 Mintek 318
3.6.6.12 Megon 319
3.6.6.13 Rhône-Poulenc 321
3.6.6.14 Thorium Ltd. 322
3.6.6.15 Yao Lung Chemical Plant 322
3.6.6.16 Spin-Off Processes 327
3.6.6.17 Dry Processes 328
3.7 Scandium 329
3.8 Summary 330

Chapter 4 Reduction 333

4.1 Introduction 333
4.2 Fundamentals 333
4.3 Metallothermy 337
4.4 Preparation of Rare-Earth Chlorides 339

4.4.1 Preparation of Hydrated Rare-Earth Chlorides 339
4.4.2 Dehydration of Hydrated Rare-Earth Chlorides 339
4.4.3 Dry Methods 345
4.4.4 Purification of Rare-Earth Chlorides 346
4.5 Reduction of Rare-Earth Chlorides 348
4.5.1 Early Attempts 348
4.5.2 Reduction in a Refractory Bomb 350
4.5.3 Reduction in a Tantalum Crucible 352
4.5.4 Intermediate Alloy Processes 353
4.5.5 Kroll-Type Processes 353
4.5.5.1 Lithium/Sodium Reduction of Yttrium Chloride 353
4.5.5.2 Lithium Reduction of Yttrium Chloride ... 355
4.5.5.3 Lithium Reduction of Rare-Earth Chlorides 357
4.5.5.4 Lithium Reduction of Dysprosium, Holmium, and Erbium Chlorides 358
4.6 Preparation of Rare-Earth Fluorides 363
4.6.1 Wet Method 363
4.6.2 Dry Methods 364
4.6.2.1 Reaction of Rare-Earth Oxides with Anhydrous HF 364
4.6.2.2 Reaction of Rare-Earth Oxides with Ammonium Bifluoride 366
4.6.3 Purification of Rare-Earth Fluorides 367
4.7 Reduction of Rare-Earth Fluorides 368
4.7.1 Lithium Reduction 369
4.7.2 Calcium Reduction (Ames Process) 371
4.7.2.1 Semicontinuous Reduction 372
4.7.2.2 Goldschmidt Process 374
4.7.3 Intermediate Alloy Process 376
4.7.4 Preparation of Scandium 379
4.7.5 Reduction of Samarium, Europium, and Ytterbium Halides 379
4.7.5.1 Reduction of $SmCl_3$ by Mechanical Milling 380
4.8 Oxide Reduction Processes 380
4.8.1 Reduction–Distillation: Lanthanothermy 382
4.8.1.1 Preparation of Samarium and Ytterbium ... 383
4.8.1.2 Preparation of Europium 383
4.8.1.3 Preparation of Samarium, Europium, Ytterbium, and Terbium 384
4.8.2 Reduction–Distillation: Other Reductants 386
4.9 New Reduction Procedures 397
4.9.1 Metallothermic Reduction in Molten Salt 398

4.10 Carbothermic Reduction 401
4.11 Electrolytic Production of Rare-Earth Metals 402
4.11.1 Chloride Electrolysis 403
4.11.2 Electrowinning at Room Temperature 408
4.11.3 Electrowinning Solid Metal Deposits 409
4.11.4 *In Situ* Preparation of Electrolyte 409
4.11.5 Commercial Electrowinning from Rare-Earth Chlorides 410
4.11.6 Oxide–Fluoride Electrolysis 411
4.11.6.1 Gray's Cell 412
4.11.6.2 Reno Cell Type 6 413
4.11.6.3 Reno Cell Type 12 415
4.11.6.4 Reno Continuous Cell Type 12 418
4.11.6.5 Cells for Electrowinning Lanthanum 419
4.11.6.6 Cell for Electrowinning Neodymium, Praseodymium, and Didymium 426
4.11.6.7 High-Temperature Electrowinning Cell 428
4.12 Recovery of Rare-Earth Metals as Alloys 431
4.12.1 Electrolysis of Chlorides 432
4.12.2 Electrolysis of Oxide–Fluoride Melts 435
4.12.2.1 Electrodeposition of Europium from Molten Fluoride 441
4.12.2.2 Electrochemical Reduction of Cerium Oxide to Metal 441
4.13 Current Efficiency 442
4.14 Summary 442

Chapter 5 Refining 447

5.1 Introduction 447
5.2 Origin of Impurities 448
5.2.1 Starting Materials 449
5.2.2 Crucible 451
5.2.3 Environment 452
5.3 Methods for Impurity Removal 453
5.4 Pyrovacuum Treatments 453
5.4.1 Distillation 454
5.4.2 Removal of Halogens/Halides 455
5.4.3 Degassing 457
5.4.3.1 Dehydrogenation 457
5.4.3.2 Denitrogenation 457
5.4.3.3 Deoxidation 458
5.4.3.4 Sacrificial Deoxidation 458
5.4.3.5 Carbon Deoxidation 460
5.4.3.6 Silicon Deoxidation 461
5.5 Pyrovacuum Techniques 462

5.5.1 Lanthanum, Cerium, Praseodymium, and Neodymium 463
5.5.2 Yttrium, Gadolinium, Terbium, and Lutetium 463
5.5.3 Scandium, Dysprosium, Holmium, Erbium, and Lutetium 473
5.5.4 Samarium, Europium, Thulium, and Ytterbium 475
5.5.4.1 Purification of Europium by Distillation 475
5.6 Electrorefining 478
5.6.1 Yttrium 478
5.6.2 Gadolinium 482
5.6.3 Cerium 489
5.7 Ultrapurification Methods 490
5.8 Zone Refining 490
5.8.1 Preliminary Studies 491
5.8.2 Lanthanum, Gadolinium, and Terbium 493
5.8.3 Lanthanum, Cerium, and Gadolinium 493
5.8.3.1 Redistribution of Interstitial Impurities 496
5.8.3.2 Redistribution of Metallic Impurities 497
5.9 Solid-State Electrotransport 500
5.9.1 SSE System 503
5.9.2 Residual Resistivity Ratio 505
5.9.3 Lanthanum 505
5.9.4 Praseodymium 505
5.9.5 Neodymium 506
5.9.6 Gadolinium 506
5.9.7 Terbium 506
5.9.8 Yttrium 507
5.9.9 Dysprosium and Holmium 507
5.9.10 Erbium 508
5.9.11 Lutetium 509
5.9.12 Samarium 510
5.10 Zone Refining and Electrotransport 510
5.10.1 Neodymium 510
5.10.2 Gadolinium 512
5.11 Iodide Refining 515
5.12 Miscellaneous Processes 515
5.12.1 Deoxidation by Oxyhalide Formation 516
5.12.2 Electrochemical Deoxidation of Rare-Earth Metals 517
5.13 Summary 520

Chapter 6 Rare-Earth Materials 523

6.1 Introduction 523
6.2 Misch Metal 523
6.2.1 Preparation of Mixed Rare-Earth Chlorides 524
6.2.2 Electrolysis of Chlorides 526

6.2.3 Electrolysis of Oxide–Fluoride Melts 528
6.2.4 Ames Process 532
6.2.5 Thermal Reduction Process 534
6.3 Rare Earth–Silicon–Iron Alloys 538
6.3.1 Reno (USBM) Process 538
6.3.2 BARC Process 541
6.3.3 Baotou Process 541
6.4 Rare Earth–Magnesium–Silicon Alloys 541
6.5 Rare Earth–Aluminum–Zinc Alloys 543
6.6 Yttrium–Aluminum Alloys 544
6.7 RE–TM–Mg Alloys 545
6.8 FCC Catalysts 545
6.9 Permanent Magnet Materials 546
6.10 Rare Earth–Co Permanent Magnets 546
6.10.1 Preparation of Magnet Material 549
6.10.1.1 Direct Melting 550
6.10.1.2 Reduction–Diffusion 550
6.10.1.3 Coreduction 555
6.10.1.4 Electrolysis 556
6.10.2 Preparation of Magnets 561
6.10.2.1 Sintered Magnets 562
6.10.2.2 Precipitation-Hardened Magnets 564
6.10.2.3 Bonded Magnets 565
6.11 Neodymium–Iron–Boron Magnets 567
6.11.1 Production of Nd–Fe–B Alloys 568
6.11.1.1 Direct Melting 568
6.11.1.2 Coreduction 568
6.11.1.3 Production of Consolidated Alloys 569
6.11.2 Production of Nd–Fe–B Magnets 575
6.11.2.1 Melt Spinning 576
6.11.2.2 Strip Casting 577
6.11.2.3 Hydrogenation–Disproportionation–Desorption–Recombination 577
6.11.2.4 Consolidation 580
6.11.2.5 Sintered Magnets 586
6.11.3 Preservation and Enhancement of Magnetic Properties 589
6.11.3.1 Super High-Energy Magnets 592
6.11.3.2 Two-Alloy Process 594
6.11.4 Corrosion Control by Coatings on Magnets 595
6.12 Sm–Fe–N Magnets 598
6.13 Lanthanum Substitution in Ferrites 599
6.14 Magnetostrictive Material (Terfenol-D) 601
6.15 Magnetic Refrigerants (Magnetocaloric Materials) 602
6.15.1 Magnetic Refrigeration 603
6.16 Thin Film Deposition Processes 605

6.16.1 Bubble Domain Memory Materials 606
6.16.2 Magneto-Optic Storage Media 606
6.17 NiMH Battery and Hydrogen Storage Materials 607
6.17.1 $LaNi_5$–Hydrogen System 607
6.17.2 Preparation of the Alloys 607
6.17.3 Alloys for Hydride Compressor 609
6.17.4 Preparation of Multicomponent RE–Ni–Mg Intermetallics 609
6.18 Special Rare-Earth Ceramics 610
6.18.1 Yttrium Aluminum Garnet, Nd:YAG Ceramics 610
6.18.2 Gadolinium Gallium Garnet 611
6.18.3 Scandia Ceramics 611
6.18.4 Rare-Earth Sulfides 612
6.19 Preparation of Rare-Earth Phosphors 612
6.19.1 Homogeneous Precipitation 612
6.19.2 Solid-State Reaction 614
6.19.3 Sol-Gel Synthesis 615
6.19.4 Melt Synthesis 616
6.19.4.1 Molten Salt Synthesis 616
6.19.4.2 Flux Method 617
6.20 Superconductors 617
6.21 Summary 621

Chapter 7 Recycling 627

7.1 Introduction 627
7.2 Materials for Recycling 636
7.3 Potential for Recycling 637
7.4 Processes for Recycling 640
7.5 Pyrometallurgical Processes 640
7.5.1 Smelting 640
7.5.2 Melt Spinning 643
7.5.3 Chlorination 645
7.5.4 Chemical Vapor Transport 646
7.5.5 Liquid Metal Extraction 646
7.5.5.1 Ames Process 647
7.5.6 Flux-Based Processes 649
7.5.6.1 Electroslag Refining 649
7.5.6.2 Molten Flux Process 650
7.5.6.3 Glass-Slag Method 650
7.5.7 Oxidation–Reduction and Other Options 651
7.6 Hydrometallurgy 652
7.6.1 Leaching and Precipitation 653
7.6.1.1 Rhône Poulenc Process 656
7.6.1.2 Hydrothermal Process 658
7.6.2 Leaching, Precipitation, Solvent Extraction 658

7.7 Separation of Individual Rare Earths 664
7.8 Magnets 668
7.8.1 In-Plant or Preconsumer Scrap 669
7.8.2 End-of-Life Scrap 669
7.8.2.1 Collection 669
7.8.2.2 Dismantling 670
7.8.2.3 Samarium–Cobalt 671
7.8.2.4 NdFeB 671
7.8.2.5 Mixed Sm–Co and Nd–Fe–B Scrap 671
7.9 Nickel–Metal Hydride Batteries 672
7.10 Phosphors 672
7.10.1 Composition of Recycled Lamp Phosphor 673
7.10.2 Physical Separation 675
7.10.3 Separation of Individual Phosphors 676
7.11 Glass-Polishing Powder 682
7.12 Catalysts 683
7.12.1 Fluid Cracking Catalysts 683
7.12.2 Automotive Exhaust Catalysts 684
7.13 Optical Glass 684
7.14 Miscellaneous Materials 685
7.15 Summary 685

Chapter 8 Analysis 687

8.1 Introduction 687
8.2 Chemical Methods 687
8.2.1 Gravimetry 687
8.2.2 Volumetry 688
8.2.2.1 Determination of Cerium 688
8.2.2.2 Determination of Europium 689
8.3 Analytical Separation of Rare Earths 689
8.4 Instrumental Methods 689
8.5 Spectroscopy 690
8.5.1 Spectrophotometry 690
8.5.2 Emission and Absorption Spectroscopy 693
8.5.3 Induction-Coupled Plasma Excitation 698
8.5.4 ICP-AES 698
8.6 ICP-MS 700
8.7 XRF 703
8.8 NAA 705
8.9 Other Instrumental Techniques 710
8.9.1 Cathode Ray–Excited Emission Spectroscopy 710
8.9.2 X-Ray–Excited Optical Luminescence Spectroscopy 710
8.9.3 Spark Source Mass Spectrometry 711
8.9.4 Secondary Ion Mass Spectrometry 711

8.10 Determination of Interstitials 711
8.11 Summary 713

Chapter 9 Environmental Aspects 717

9.1 Introduction 717
9.2 Contaminant Elements in Rare-Earth Ores 718
9.2.1 Radioactive Contaminants 718
9.2.2 Contaminants from Hard-Rock Mining 719
9.2.3 Rare-Earth Elements 720
9.3 Main Process Steps in Mining and Processing 720
9.4 Contaminant Release Points 721
9.4.1 Mine Pit 723
9.4.2 Tailing Impoundment 723
9.4.3 Waste Rock Stockpiles 724
9.4.4 Mill 724
9.4.5 Air Emissions 724
9.4.6 Mine Site 724
9.4.7 Head-End Processing 725
9.5 Environmental Aspects of Mining and Processing in China 725
9.5.1 Overview 725
9.5.2 Bayan Obo Facilities 726
9.5.3 Sichuan Mine 726
9.5.4 Ion-Adsorption Deposits 727
9.5.5 Processing 727
9.5.6 Wastewater from REE Separation and Refining 727
9.6 Entry Criteria for Rare-Earth Industry (China) 730
9.7 Research and Development on Cleaner Production in China 731
9.7.1 Technology Solutions to Environmental Problems 731
9.7.1.1 Fluorine Emission and Mitigation 731
9.7.1.2 Eco-Friendly RE/Th Separation 732
9.7.1.3 Wastewater Treatment 732
9.8 Environment-Friendly Processing outside China 734
9.8.1 General Outlook 734
9.8.1.1 Monazite and Xenotime 734
9.8.2 Recovery Rates 734
9.8.3 Mine Planning and Management 735
9.9 Mountain Pass 735
9.10 Bear Lodge 738
9.10.1 Water Contamination 738
9.10.2 Air Contamination 739
9.11 Mount Weld 739
9.12 Dubbo Zirconia Project 740

9.13 Kvanefjeld 741
9.14 Steenkampskrall Mine 742
9.15 Nechalacho Project 742
9.16 Summary 743

References 745

Index 809

Preface to the Second Edition

At the time of writing the Preface to the first edition, we realized and also wrote that the future of rare earths would be glorious and full of excitement, be it in science, technology, or commercial utilization. Subsequent events more than confirmed these expectations, and the rare earths have also become widely popular in the sense that a person on the street anywhere in the world knows that rare earths are useful and they are important. Thanks to the Internet, we could also evaluate who used the book and how the book we wrote was used. The readership profile that emerged helped in casting the second edition.

In the 10 years that have passed since the publication of the first edition of *Extractive Metallurgy of Rare Earths*, we realized that developments in the field pertained more to rare-earth materials processing (converting a rare-earth metal, alloy, or compound to a device-ready material) than to materials preparation (converting an ore or a concentrate to a sufficiently pure rare-earth metal, alloy, or compound). In fact, the basic knowledge structure on materials preparation was built and reached maturity in the period we covered in the first edition. Efforts continued and some interesting breakthroughs were achieved in the past 10 years, too, in the challenging area of rare-earth separation. On the whole, the requirement in the area of materials preparation (the essence of extractive metallurgy) at the present time is to translate the technically feasible processes into commercially viable processes. This needs to be done not only for the well-known and well-studied resource minerals monazite, bastnasite, and xenotime but also for numerous other minerals that pose challenges by the nature of their dissemination (especially extremely fine-grained occurrences) and complexity of their compositions in addition to low rare-earth concentrations.

Commercial viability has a new dimension now—community acceptability. For some time in the past and possibly forever in the future, the implementation of any extractive metallurgy process in a plant is possible only in a regime of strict regulations with liberal safety margins. This translates to minimization of energy consumption (direct and indirect), chemicals, and water, and minimization or elimination of liquid or gaseous effluents and solid waste. The regulations as regards radioactive materials (uranium, thorium, and their natural decay products) are stricter. Even the very processing of monazite is not allowed in Australia and China. These requirements are attempted to be implemented by various process and plant design innovations and suitable plant practices. As regards extractive metallurgy and rare earths, the focus of recent research efforts has been in trying out new reagents and processes, particularly for rare-earth separations. Regulatory changes have been outlined even in the metal and alloy production processes, which, in the case of rare earths, are not known to be particularly *polluting.* For the electrolytic production of misch metal, chloride electrolytes are not allowed in certain countries. Current and future rare-earth extractive processes need to be in tune with these parameters. The process metallurgy *per se* presented in this edition keeps this background in view.

The rare-earth industry has been through a strange transformation. Time and again it has been noted that rare earths are abundant, and deposits of rare earths

are widely distributed throughout the world. Major consumers (Japan, EU) never had large deposits in their own geographical boundaries but nevertheless had access to large deposits with fairly high reliability. The United States, Australia, China, and India needed the rare earths and also had deposits in their own boundaries. By the mid- and late 1980s, it was also clear that rare earths are vital and largely without substitute for all important technology devices including those for *green* electric power generation, lighting, and surface transportation, apart from military hardware. Yet, instead of a natural proliferation of mining and production facilities all over the world, the technology activities moved to China, and a decade and a half later, all stakeholders realized that this was not a sustainable arrangement. Then followed a flurry of activities to identify and develop new mines and production facilities. This has been the liveliest area of rare-earth extractive metallurgy. It has been extensively covered in this edition.

Limited natural availability of certain key rare-earth elements like Dy and Eu, general uncertainty in the continued availability of these and other elements from primary sources at a reasonable cost, and regulatory pressures on industrial procedures for primary rare-earth production have steadily contributed to the emergence of recycling as an important process option for the rare earths. Recycling as a materials supply route comes with a host of advantages that concerns economy, environment, reliability, energy, and ethics. There are also challenges to overcome, both relating to logistics to ensure accessibility of recyclable material, and process to ensure maximum retention of the value addition that occurred in primary processing. A new chapter on recycling addresses various issues in the recycling of rare earths—the advantages and limitations, and the methods used worldwide to manage them.

Precise quantification of the rare earths in various materials, be they ores, concentrates, and such starting materials, interprocess intermediates, as well as products such as metals, alloys, and compounds, is essential for the development of extractive processes for the rare earths. Depending on the matrix, co-occurring elements, and the relative concentration of various components, a number of analysis techniques have been developed and fine-tuned for the rare earths. Classical chemical methods, instrumental techniques based on absorption and emission of radiation, charge-to-mass ratio of the constituent nuclides, as well as propensity to radioactivation and the nature of radioactivity formed have all been used in the analysis of rare earths at various concentration levels—from a tenth of a ppm to tens of percent. Rare earths as a group as well as individual rare earth elements have been determined in rare-earth and non-rare-earth matrices. Non-rare-earth impurities have been determined in rare-earth matrices. All techniques relevant to extractive metallurgy of rare earths have been covered in the new chapter on analysis.

Apart from the scientific merit and engineering elegance of a flow sheet for rare-earth extraction and processing, including mining and beneficiation, that the scheme will become plant practice or would remain as one depends strongly on its environmental impact. The land, water, and energy use and plant emissions into the atmosphere, and types and quantities of liquid effluents and solid wastes, their storage, and disaster potential are all factors that determine the siting and continued existence of a rare-earth facility. It is becoming increasingly important that if the rare

earths are for green energy, their mining, extraction, and processing must also meet green standards. The new chapter on environmental aspects deals with such issues.

All features of the first edition that the authors perceived to be useful to readers have been retained in this edition as well, and new materials, as outlined above, have been added. We have made liberal (hundreds of them) use of tables and figures and accommodated varied approaches to solving current and potential issues in rare-earth technology. We wanted to reveal research gaps and areas that would benefit from further work. We expect the book to be useful to a broad spectrum of people spanning academic, research, and industrial backgrounds related in any way to rare-earth technology.

The idea of a second edition was mooted by Allison Shatkin, senior editor, Books, Materials Science & Chemical Engineering, Taylor & Francis, and has become a reality entirely because of her strong support. Amber Donley was tremendously helpful and supportive during the long process of manuscript preparation and publication, and so were Iris Fahrer and Adel Rosario in transforming the manuscript to the final book. Kizza Florence, Arlene Kopeloff, and Jennifer Ahringer of CRC Press helped with the development of the book at various stages. We are deeply grateful to them.

Steve Constantinides and Doris Schuler graciously permitted liberal use of material from their publications and presentations. Elsevier kindly accorded permission to use a remarkable number of tables and figures. The institutional support from Bhabha Atomic Research Centre, the publications of the US Geological Survey and Technology Metals Research have been invaluable resources for this book. In a way, we stood on the shoulders of such giants to create this work.

Yatin Thakur at BARC has been a trusted teammate in our authorship endeavor. He skillfully prepared the line drawings for the first edition and also the additional figures for the second edition.

We warmly acknowledge the support of our family members. I (NK) thank my wife Kusuma (a banker) and daughter Kavita (a civil engineer) for their time, support, and constant encouragement during the preparation of the manuscript, especially when the going got tougher and hours spent endless.

Nagaiyar Krishnamurthy
Chiranjib Kumar Gupta

Preface to the First Edition

A chronological account of the chemistry and metallurgy of the rare earths is arranged into three eras or ages. The basis of this division is the availability and purity of the rare-earth metals and materials and the scientific and engineering information about them. The period prior to 1950 may be called the *Dark Age*. The next two decades were the *Age of Enlightenment*. The period after the early 1970s may be considered the *Golden Age*. In the first three decades of this golden era, a number of remarkable advances and discoveries were made in the field of rare earths, and these have left an indelible mark on the global materials scenario. It is widely perceived that the future of the rare earths will be glorious and full of excitement, be it in science, technology, or commercial utilization.

The rare earths are a community of 17 metallic elements, all but one occurring naturally (14 lanthanides and 2 associated elements). They are found in combination in mineral deposits widespread throughout the world. Notably large reserves exist in China, the United States, and Australia. The word *rare* in *rare earths* arises more from the historical difficulty in separating and obtaining them as individual pure elements than from their inherent nonavailability. There have been major developments in the technologies for the production of separated high-purity rare earths. Highly efficient separation technologies have been key to the exploitation of the rare earths in a wide range of now commonplace applications that have slowly become an inseparable part of modern living.

At the Bhabha Atomic Research Centre in Mumbai, India we had a long, direct, and active association with rare-earth research and production practices. That has been the motivation to write, in 1992 an extensive review on the extractive metallurgy of the rare earths. This was published in the *International Materials Reviews*. With the publication of the review in 1992, its enthusiastic reception, and our progressively increasing involvement with the rare earths, we attempted to preserve the available information on the extractive metallurgy of the rare earths in the form of a book. This thinking gathered further momentum because we found that although a voluminous literature in the form of numerous conference proceedings, a highly rated series of volumes on the physics and chemistry of the rare-earth elements (edited by Gschneidner and Eyring), and important trade publications and newsletters is available, all of these publications have objectives different from that of our book. We are not aware of any other text that covers the subject in the manner we have attempted here. We have worked to bring together all relevant matters concerning the extractive metallurgy of the rare earths and related information that, at present, remains scattered in a variety of forms of published literature.

This book has been organized into seven chapters. Chapter 1, The Rare Earths, provides the background information on the properties and applications of the rare earths and highlights the links of these aspects to the totality of rare-earth extraction and processing techniques. The interesting sequence of the discovery of the rare earths is first presented, followed by a listing and discussion of the currently accepted

values and information pertaining to the various properties of the rare earths. A comprehensive account of all major applications of the rare earths is then provided.

Chapter 2, Resources, presents in detail all currently available information on the world's rare earth resources, their location, quality, and quantity. The resource utilization trends and patterns from the times when the rare earths were first produced as a commodity up to the present are presented. Factors leading to the unequal availability of the rare earths are highlighted, and the world's rare earth resources position is dealt with in the context of current and projected demands.

Chapter 3, Resource Processing, incorporates a detailed account of the techniques for the processing of the various rare earth resources and the separation of individual rare earth elements. While placing a strong emphasis on the modern methods of solvent extraction and ion exchange, the salient features of the classical methods of rare earth separation are covered in detail. Various options for the treatment of the as-mined rare earth resources by physical and chemical beneficiation methods prior to separation are discussed.

Chapter 4, Reduction, deals with the techniques for converting the pure rare earth oxide intermediates to the metals. The numerous scientifically interesting and technologically challenging procedures for rare earth metal reduction are described in considerable detail. Chemical as well as electrochemical reduction methods have been used and the variety in the actual processes has come about because of the different physical properties of the individual rare earth elements. Particularly, the melting and boiling points of the elements dictate the type of process best suited for reduction. These aspects are discussed.

Chapter 5, Refining, is devoted to the purification of the rare earth metals. Elucidation of the unique properties of the rare earth elements has been possible only with the availability of these elements in very pure forms; therefore, major efforts have gone into the development of suitable techniques such as pyrovacuum treatment, zone melting, and electrotrans- port to prepare metals of high purity levels. The chapter covers these refining techniques as applied to different rare earth metals.

Chapter 6, Rare-Earth Materials, is concerned with the techniques for the preparation of the numerous rare earth alloys and compounds and rare earth bearing materials. Among the materials described are the traditional products like misch metal and rare earth-iron-silicon alloys, as well as new materials like lanthanum-nickel alloys, permanent magnet materials based on samarium and neodymium, magnetostrictive and magnetocaloric materials. The procedures followed by various manufacturers of rare earth materials are outlined. The presentation also covers methods under investigation for newer materials.

Chapter 7 is an overview—a sojourn for the reader in the world of the rare earths. While going through this chapter one can develop a brief but significant acquaintance with the rare earths in their entirety.

In all the chapters, the text is liberally supported by tables and figures. Key property values and results have been listed in the tables, and the figures comprise line drawings of equipment and flow sheets of processes. References to original papers are extensively made in the text and all the references are grouped in one place at the

end of the book. The reference list will serve as a very useful guide for those who want to refer to the original sources for more information on specifics.

We hope this book will be useful to professionals involved with the extraction, separation, concentration, and production of the rare earth metals, alloys, and chemicals. They include process, production, and regulatory staff engineers; management as well as research and development professionals; graduate students; and libraries attached to universities and R&D establishments.

We would like particularly mention the contributions of certain people who have been especially involved, with the preparation of this book. The work pertaining to the production of the typed version of the manuscript in its finished form was very efficiently handled by PoonamKhattar. All figures for the book were drawn by Yatin Thakur. We are grateful to the editorial department of G+B, particularly to Catherine Bewick in the initial stages and to Sally Cheney, Lloyd W. Black, and Matt Uhler in the latter stages for supporting and encouraging us in the project.

Finally, we wish to dedicate this book to our wives, Chandrima Gupta and Kusuma Krishnamurthy, in gratitude for their unique contributions toward the completion of this work.

Chiranjib Kumar Gupta
Nagaiyar Krishnamurthy
Bhabha Atomic Research Centre, Mumbai, India

Authors

Dr. Nagaiyar Krishnamurthy was affiliated with the Materials Group, Bhabha Atomic Research Centre (BARC), Mumbai, India for nearly four decades, conducting and later formulating and guiding research in the extraction and processing of rare earths, reactive and refractory metals, and special less common materials.

He earned his BSc degree at the University of Madras in 1974, his MSc in 1980, and his PhD in 1992, both at the University of Bombay. His PhD dissertation was on the pyrometallurgy of group V refractory metals and their alloys with group IV metals.

He is a professor at the Homi Bhabha National Institute and has guided many students to complete their PhD. He has been a member of Indian Rare Earths Technology Development Council. In addition to the more than 100 original research papers published in peer-reviewed international journals, Dr. Krishnamurthy coauthored the first edition of *Extractive Metallurgy of Rare Earths* published by CRC in 2004. Earlier he coauthored the book *Extractive Metallurgy of Vanadium* published by Elsevier in 1991 and a monograph on the Binary Phase Diagrams of Tantalum published in 1996 by the Indian Institute of Metals.

Dr. Chiranjib Kumar Gupta retired as the director of the Materials Group, Bhabha Atomic Research Centre (BARC), Mumbai, India in January 2000 after decades of association with BARC. He was instrumental in formulating and directing the programs of the Materials Group in the areas of extraction and processing of refractory metals and materials. He pioneered the open aluminothermic reduction as a process of metal- and alloy-making and contributed extensively to the use of fused salt electrolysis for the preparation and refining of group V and VI refractory metals. He is an alumnus of Banaras Hindu University and guided numerous students to PhD in Mumbai University. Dr. Gupta has authored nearly 200 publications including half a dozen books on nuclear energy and refractory metals. He has been a recipient of numerous awards and honors.

1 The Rare Earths

1.1 INTRODUCTION

The term *rare earths* denotes the group of 17 chemically similar metallic elements that includes scandium, yttrium, and the lanthanides (Spedding 1978; Connelly et al. 2005). The lanthanides are the series of elements with atomic numbers 57 to 71, all of which, except promethium, occur in nature. The rare-earth elements, being chemically similar to one another, invariably occur together in minerals and behave as a single chemical entity. Thus, the discovery of the rare earths themselves occurred over a period of nearly 160 years, from 1787 to 1941 (Szabadvary 1988; Weeks 1956). The problem of separating them from one another for scientific study or industrial use then followed. This has been one of the most challenging tasks of rare-earth technology. While the attempts to separate the rare earths began with the work of Mosander during 1839–1841, much of the effort directed to the separation of various rare earths occurred from 1891 to 1940. During this period, from the available mixed and separated compound intermediates, many rare-earth alloys and metals were prepared, and commercial applications were developed for mixed or roughly separated rare earths. The following two decades, 1940–1960, were the most productive in terms of effective process development. Most important were the development of modern separation methods, which resulted in the availability of sufficient quantities of pure individual rare-earth compounds (Powell and Spedding 1959b) for the investigation of reduction processes to prepare pure metals and alloys (Beaudry and Gschneidner 1978) and evaluation of their properties. Beginning in the 1960s, much progress was made in the large-scale production of purer rare earths, in the identification of newer properties, and in their use in a variety of important commercial applications. The usable forms of rare earths encompass naturally occurring oxide mixtures and products synthesized from them, high-purity individual metals, alloys, and compounds. The current annual demand for rare earths is in the range of 125,000 t calculated as rare-earth oxides. The world rare-earth reserves are large and sufficient to support the present level of consumption for many centuries to come.

This chapter is a survey of the history, properties, and applications of the rare earths and highlights the background to their current status as materials of interest in the laboratory and products of use in technology and industry.

1.2 DISCOVERY

The discovery of rare-earth elements began in 1787 and went on for about 160 years to conclude in the 1940s (Szabadvary 1988; Weeks 1956). All the naturally occurring rare earths and all but one of all the rare-earth elements had been discovered by the first decade of the twentieth century, and the discovery of the remaining one rare earth had to wait until the discovery of nuclear reactions.

The rare-earth elements and their discoverers are listed in Table 1.1 and charted in Figure 1.1. The activity started at Ytterby, a village near Stockholm in Sweden. Ytterby was the site of a quarry that had been the source of many unusual minerals containing rare earths.

In 1787, Carl Axel Arrhenius, a lieutenant in the Swedish Royal Army and also an amateur mineralogist, found a black mineral, until then not mentioned by anyone, in Ytterby. The mineral was analyzed by the Finnish chemist Johan Gadolin in 1794. Gadolin found iron and silicate as constituents of the mineral and also a "new earth," which accounted for 30% of the mineral. The discovery of the new earth by Gadolin was confirmed by the Swedish chemist Anders Gustaf Ekeberg the following year. Ekeberg found that the mineral also contained beryllium, a metal that had been recently discovered by the French chemist Nicolas Louis Vanquelin. The mineral found by Arrhenius turned out to be an iron–beryllium–silicate. Ekeberg gave the name *yttria* to the new earth discovered by Gadolin and also named the mineral *gadolinite*.

Until the first decade of the nineteenth century, "earths" were universally considered to be elements. The fact that earths were not elements but compounds was first stated by the Hungarian chemist Antal Ruprecht but conclusively proved by Sir Humphrey Davy, who electrolyzed melts of earths and obtained metals from them. In the first decade of the nineteenth century, Davy separated numerous metals such as calcium, strontium, and barium from alkaline earths, and from then on, the metals were distinguished from earths. For example, chemists began to use the name *yttrium* for the metal instead of *yttria* even though the metal itself had not been produced in the pure state.

TABLE 1.1
Discovery of the Rare-Earth Elements

Year	Mineral/ Element	Discovered by	Named by	Confirmed by	Origin of Name
1787	Gadolinite	C.A. Arrhenius	A.G. Ekeberg		Person: J. Gadolin
1794	Yttria	J. Gadolin	A.G. Ekeberg	M. Delafontaine	Place: Ytterby
1751	Cerite	A.F. Cronstedt	J.J. Berzelius, W. Hisinger		Asteroid: Ceres
1804	Cerium	J.J. Berzelius, W. Hisinger	J.J. Berszelius, W. Hisinger		Asteroid: Ceres
1839	Samarskite	M.H. Klaproth, G. Rose			Person: Col. Samarsky
1839	Lanthanum	C.G. Mosander	J.J. Berzelius		Chemical behavior: to escape notice
1842	Didymium	C.G. Mosander	C.G. Mosander		Chemical behavior: twins

(*Continued*)

TABLE 1.1 (CONTINUED)
Discovery of the Rare-Earth Elements

Year	Mineral/ Element	Discovered by	Named by	Confirmed by	Origin of Name
1843	Erbium (known as terbium after 1864)	C.G. Mosander	C.G. Mosander	M. Delafontaine, J.L. Soret, H.E. Roscoe, A.J. Schuster, J.G. Marignac, J.L. Smith	Place: Ytterby
1843	Terbium (known as erbium after 1864)	C.G. Mosander	C.G. Mosander	M. Delafontaine, J.L. Smith	Place: Ytterby
1878	Ytterbium	J.C. Marignac	J.C. Marignac	M. Delafontaine, L.F. Nilson	Chemical behavior: between erbium and yttrium
1879	Samarium	P.E.L. de Boisbaudran	P.E.L. de Boisbaudran	P.T. Cleve	Mineral: samarskite
1879	Scandium	L.F. Nilson	L.F. Nilson		Place: Scandinavia
1879	Thulium	P.T. Cleve	P.T. Cleve		Place: Scandinavia (*Thule* is her ancient name)
1879	Holmium	P.T. Cleve	P.T. Cleve	J.L. Soret, P.E.L. de Boisbaudran	Place: Stockholm (medieval name)
1886	Dysprosium	P.E.L. de Boisbaudran	P.E.L. de Boisbaudran		Chemical behavior: difficult to access
1886	Gadolinium	J.C. Marignac	J.C. Marignac	M. Delafontaine, J.L. Soret	Person: J. Gadolin
1886	Praseodymium	C.A. von Welsbach	C.A. von Welsbach	A. Bettendorf	Chemical behavior: green twin
1886	Neodymium	C.A. von Welsbach	C.A. von Welsbach	A. Bettendorf	Chemical behavior: new twin
1901	Europium	E. Demarcay	E. Demarcay	G. Urbain	Place: Europe
1907	Lutetium	G. Urbain, C.A. von Welsbach	G. Urbain		Place: Paris (Roman name of Paris)
1947	Promethium	J.A. Marinsky, L.E. Glendenin, C.D. Coryell	J.A. Marinsky, L.E. Glendenin, C.D. Coryell		Legend: Prometheus

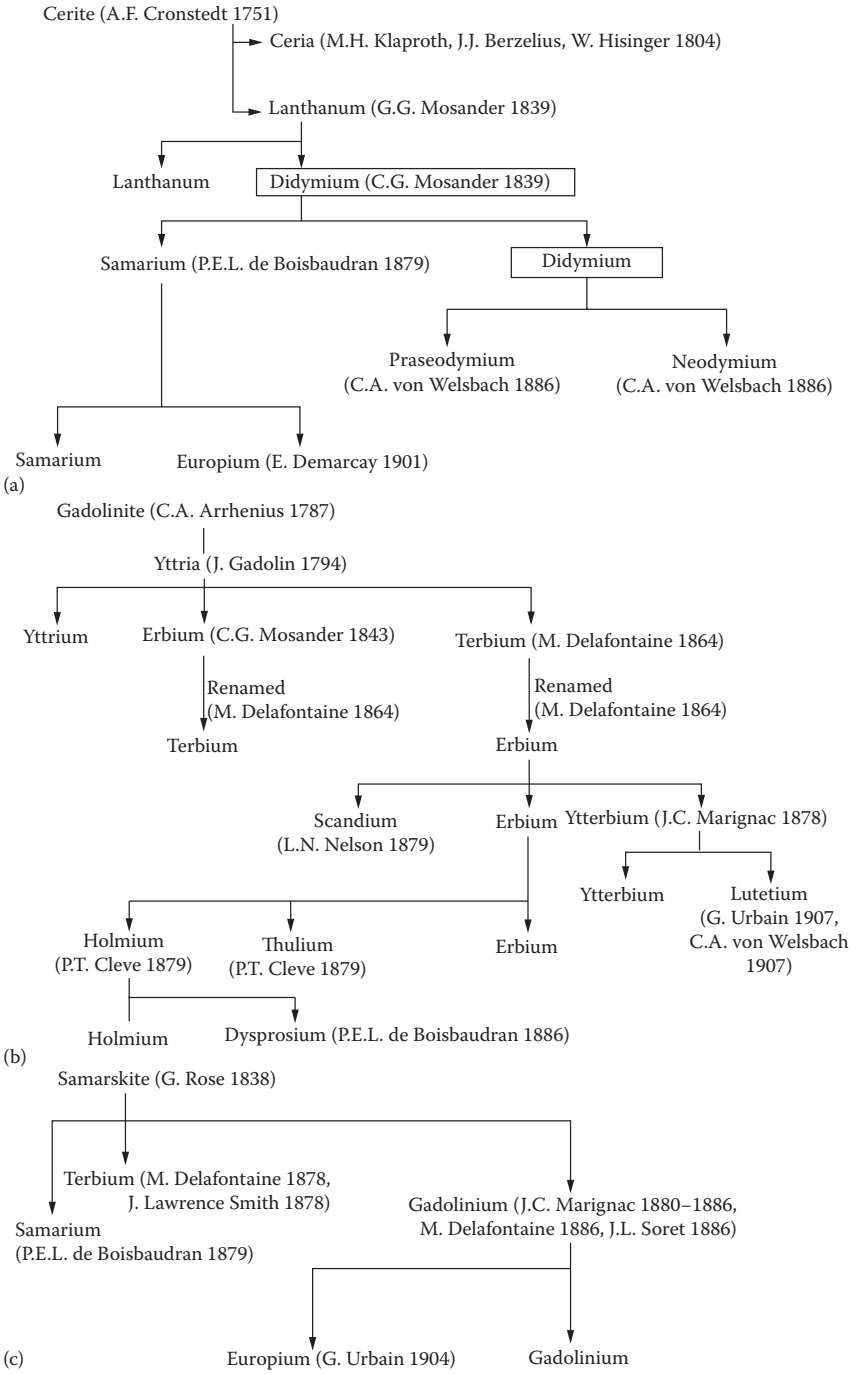


FIGURE 1.1 Discovery of rare-earth elements: (a) cerite sequence, (b) gadolinite sequence, and (c) samarskite sequence.

Interestingly, another new mineral, which was later shown to contain an unknown earth, had been discovered by A.F. Cronstedt in the Bastnäsgrube mine close to Rydderhyatten in Sweden in 1751, before gadolinite was discovered in Ytterby. This mineral was investigated by Jöns Jakob Berzelius and Wilhelm Hisinger in Sweden and independently by Martin Heinrich Klaproth in Germany. They reported simultaneously, in 1804, the discovery of a new element in the mineral. Klaproth was still considering earths as elements and named the new earth *ochroite earth*, while Berzelius and Hisinger stated that the earth was the oxide of a new element. They named the element *cerium* after the asteroid Ceres that had been discovered only 3 years earlier, in 1801. The mineral that contained cerium was named *cerite*.

Carl Gustaf Mosander, an associate of Berzelius, through his patient and painstaking investigations, established that both yttria and ceria were complex in nature and contained new elements. In 1839, Mosander separated a new element from ceria. Berzelius suggested to Mosander the name *lanthanum* for the new element (in Greek, *lanthano* means "to escape notice"). Mosander believed that the lanthanum he separated was not a pure element but might contain yet another new element. Continuing his experiments, he succeeded in 1842 in detecting that new element. He named the new element *didymium*. The element didymium, which was present in cerite, tracked lanthanum in some experiments, while it tracked cerium in some other experiments. It therefore got its name from the Greek word *didymos*, meaning twins, to denote that it accompanied cerium and lanthanum as a twin in the cerium mineral.

The possibility of gadolinite containing new elements in addition to yttrium was already indicated by the works of Heinrich Rose and Berzelius before Mosander turned his attention to this mineral. Reporting his results in 1843, Mosander mentioned not one but two more new elements in gadolinite. He named them *erbium* and *terbium*.

Beginning in the 1850s, a new analytical aid, spectroscopy, was used to identify and confirm the existence of new elements. In 1864, Marc Delafontaine, a Swiss-American chemist, used spectroscopic identification to unequivocally confirm the existence of yttrium, terbium, and erbium. He interchanged, probably unintentionally, the names given by Mosander for terbium and erbium, and the interchanged names have persisted ever since. What was called erbium by Mosander became known as terbium, and what was named terbium by Mosander came to be known as erbium.

There was considerable confusion surrounding terbium and erbium in the 1860s. Delafontaine himself became doubtful, while O. Popp, Johan Fridrik Bahr, and Robert Wilhelm Bunsen denied the existence of terbium while accepting that erbium existed. Charles Augustus Young, an American scientist, demonstrated in 1872 the existence of erbium in the solar spectrum, and the existence of erbium was doubted no more. The matter of terbium was finally resolved by Delafontaine and the Swiss chemist Jean Charles Marignac by 1877–1878. Delafontaine separated the terbium oxide from the mineral *samarskite*, which had been discovered in 1838 by the German mineralogist Gustav Rose. In 1878, J. Lawrence Smith, an American chemist and mineralogist, also reported the existence of terbium in samarskite. In

the same year, Marignac confirmed the presence of terbium in gadolinite, the mineral in which Mosander had originally found the element. Further confirmations of the existence of terbium were provided by the spectral analysis reports of J.L. Soret in 1880 as well as by Sir Henry Enfield Roscoe and A.J. Schuster in 1882.

Delafontaine reported in 1878 that the absorption spectrum of didymium separated from samarskite was not fully identical with the absorption spectrum of didymium separated from cerite. He suspected that didymium was not a single element. Interestingly, in 1879, the French chemist Paul Emile Lecoq de Boisbaudran disproved Delafontaine's report on the spectra but did find a new element in samarskite. He named the element *samarium* after the mineral samarskite in which it was detected.

Investigating gadolinite, Marignac not only had confirmed the existence of terbium in it but also was looking for more new elements in the mineral. He worked on the erbium fraction obtained from the mineral and separated an oxide and salts that were different from erbium in both chemical and spectral characteristics. In 1878, Marignac named the new element *ytterbium* because it stood between yttrium and erbium in its properties. In the same year, Marignac's ytterbium was also identified by Delafontaine in an yttrium niobate mineral called *sipylite*, which had been discovered in Virginia (USA) by John William Mallet in 1877.

The experiments on erbium described by Marignac were repeated in Sweden by Lars Frederick Nilson, and he also confirmed the existence of ytterbium and the statements of Marignac regarding it. Proceeding further, through an exceedingly intricate fractionation procedure, Nilson finally obtained a basic nitrate from gadolinite. He dissolved the salt in nitric acid, and the solution yielded a weak absorption line in the red and in the green spectrum. It also precipitated as an oxalate. Nilson considered this a new element and, in 1879, named it *scandium*, after Scandinavia.

In Sweden, Per Theodor Cleve investigated the erbium fraction remaining after the separation of ytterbium. Based on a spectrum taken by the Swedish physicist Tobias Robert Thalén, Cleve suspected that the erbium fraction could contain more elements. Proceeding with chemical separation and spectral analysis, he identified the existence of two new elements and named them *thulium*, after the legendary old name of Scandinavia, and *holmium*, after the Medieval Latin name of Stockholm. Before Cleve reported his discovery of the new elements in 1879, the Swiss chemist Soret had indicated, on the basis of absorption spectrometry results, the possibility that an unknown element was present in the erbium sample given to him by Marignac. Soret later stated that the unknown element mentioned by him corresponded to Cleve's holmium. The statements and discoveries of Soret and Cleve were confirmed in 1879 by Lecoq de Boisbaudran.

In 1886, Boisbaudran, following an elaborate, intricate, and wearisome method for the chemical separation and spectroscopic and fluorescence studies of rare-earth elements in gadolinite, concluded that the holmium discovered by Cleve contained another new element. He named it *dysprosium*.

Earlier, in 1880, Marignac investigated samarskite by chemical separations. He obtained the nitrate of a substance that differed in many respects from the other elements then known. He tentatively named it Yα and, after more investigations by him as well as by Delafontaine and Soret, in 1886, proposed the name gadolinium for Yα.

In 1885, Carl Auer von Welsbach, an Austrian chemist, began investigations on didymium. By then, it was already widely suspected that didymium might not be a single element, but chemical separation efforts to substantiate the presence of the new element were unsuccessful. Auer used fractional crystallization instead of the hitherto applied fractional precipitation to separate didymium. In 1886, he succeeded in obtaining two fractions of didymium ammonium nitrate. He further investigated them by absorption and spark spectrometry and concluded that the fractions belonged to different elements. He named the elements *praseodidymium* and *neodidymium*. In course of time, *di* disappeared from these names, and they came to be known as *praseodymium* and *neodymium*. Mosander's naming of the "element" didymium, meaning twins, was indeed prophetic.

Auer's discovery of praseodymium and neodymium was questioned by Henry Becquerel in 1887, but in 1890 Auer's experiments were repeated by A. Bettendorf, and the existence of praseodymium and neodymium was confirmed. The unseparated mixture of praseodymium and neodymium, however, continued to be referred to by the name didymium.

Samarium, discovered in 1879 in the original didymium by Boisbaudran, was also confirmed as a new element by Cleve. In 1886, the French chemist Eugene Demarcay announced that he separated a new element from samarium. He substantiated his claim only 15 years later in 1901 when he succeeded in preparing it as a pure substance in the form of a double nitrate with magnesium. He named the element *europium*. In 1904, europium was also separated from gadolinium by the French chemist Georges Urbain.

In 1905, Auer mentioned that Marignac's ytterbium probably contained new elements. Two years later, he published experimental results supporting his doubt and stated that ytterbium consisted of two elements. He named them *aldebaranium* and *cassiopeium*. Almost simultaneously, Urbain also reported that ytterbium consisted of two elements, which he named *neoytterbium* and *lutetium*. In the course of time, the names ytterbium (for neoytterbium) and lutetium survived. The name lutetium was derived from the ancient Roman name of Paris.

With the discovery of lutetium, incidentally the last member of the lanthanide series of elements, the story of the discovery of the naturally occurring rare-earth elements, which lasted for well over a century, ended.

Even though all the naturally occurring rare-earth elements had been discovered, the discoverers themselves did not realize that fact. For example, both Auer and Urbain continued to work on reporting new elements. But that was not to be. The theoretical explanation of the great similarity of the properties of the rare-earth elements and also the maximum limit for their number came in later years with the development of the atomic theory. Atomic numbers were introduced by van den Broek in 1912, and Henry Gwyn Jeffreys Moseley discovered, in 1913, a mathematically expressible relationship between the frequency of x-rays emitted by the element serving as an anticathode in the x-ray tube and its atomic number. Urbain subjected all the rare-earth elements discovered in later times to the "Moseley check," to determine their atomic numbers and thus confirm that they were true elements. The range of rare-earth elements, from lanthanum, with atomic number 57, to lutetium, with

atomic number 71, was established. Among these, the element with atomic number 61 was as yet unknown.

In 1941, researchers at the Ohio State University irradiated praseodymium, neodymium, and samarium with neutrons, deuterons, and alpha particles and produced several new radioactivities, which were most probably those of element 61. The formation of element 61 was also claimed in 1942 by Wu and Segre (1942). Chemical proof of the formation of element 61 was provided in 1945 at the Clinton Laboratory (now the Oak Ridge National Laboratory) by Marinsky et al. (1947), who used ion-exchange chromatography to obtain the element from the products of fission of uranium and of neutron bombardment of neodymium. They named the element *promethium* after Prometheus, who stole fire from the Gods for man (Szabadvary 1988). Promethium does not occur in nature.

1.3 SPECIAL CHARACTERISTICS

The close chemical similarity of all the rare-earth elements is, first of all, displayed in their occurring together in nature and further by the fact that it took nearly 160 years of effort by many great names in science to isolate and identify them. It has been borne out by experimental evidence that striking similarities among the chemical properties of the elements and their compounds are the consequence of strikingly similar electronic configurations.

1.3.1 Electronic Configuration

The electronic configurations of the rare-earth elements are listed in Table 1.2. Scandium, yttrium, and lanthanum are the elements that begin three successive series of transition elements. Their valence electron configurations are $ns^2(n-1)d^1$, with $n = 4$, 5, and 6, respectively. They have no *f* electron. The 14 elements following lanthanum, namely, cerium to lutetium, are the lanthanides (lanthanum-like) and have valence electron configurations represented by $6s^25d^14f^{n-1}$ or $6s^24f^n$. The $5d$ and $4f$ electrons have similar energies in the neutral rare-earth atoms, and this is the reason for two typical electronic configurations. The 14 elements from cerium to lutetium form the series known as the *inner transition* elements or *f* elements. It must, however, be stated that the electronic configurations given are not known with complete certainty, because of the great complexity of the electronic spectra of these atoms and the consequent difficulty in analysis.

The ionization potentials of rare-earth elements are comparatively low. The elements are therefore highly electropositive and form compounds that are essentially ionic in nature. While all the rare earths form M^{3+}, some of them also occur in +2 and +4 states. These states are always less stable than the +3 state. The occurrence of +2 and +4 states in certain rare earths, which is of considerable importance in rare-earth extractive metallurgy, is related to their electronic structures and ionization potentials. Special stability is apparently associated with empty, half-filled, and filled *f* shell configurations.

The rare earths scandium, yttrium, and lanthanum form only the M^{3+} ions because this results in the inert gas configuration. Lutetium and gadolinium form only the

TABLE 1.2
Properties of Rare-Earth Elements

Properties	Scandium	Yttrium	Lanthanum	Cerium	Praseodymium	Neodymium	Promethium	Samarium	Europium
				Atomic Properties					
Atomic number	21	39	57	58	59	60	61	62	63
Atomic weight	44.95591	88.90585	138.9055	140.115	140.90765	144.24	(145)	150.36	151.965
Crystal structure	cph < 1337; bcc > 1337	cph < 1478; bcc < 1478	dcph < 1478; fcc > 310 and < 865; bcc > 865	fee < −148; dcph > 148 and < 139; fcc > 139 and < 726; bcc > 726	dcph < 795; bcc > 795	dcph < 863; bcc > 863	dcph < 890; bcc > 890	rhomb < 734; cph > 734 and < 922; bcc > 922	bcc
Atomic volume, cm^3/mol at 24°C	15.059	19.893	22.602	17.2	20.803	20.583	20.24	20.000	28.979
Density, g/cm^3 at 24°C	2.989	4.469	6.146	8.16	6.773	7.008	7.264	7.520	5.244
Conduction electrons	3	3	3	3, 3.1	3	3	3	3	2
Valence in aqueous solution	3	3	3	3, 4	3	3	3	3, 2	3, 2
Color in aqueous solution, RE^{3+}	Colorless	Colorless	Colorless	Colorless	Yellow-green	Rose	Pink	Yellow; Sm^{2+} is deep red	Colorless; Eu^{2+} is pale yellow
Main absorption bands of RE^{3+} ion in aqueous solution in the range 200–1000 nm	–	–	–	210.5, 222.0, 238.0, 252.0	444.5, 469.0, 482.2, 588.5	354.0, 521.8, 574.5, 739.5, 742.0, 797.5, 803.0, 868.0	548.5, 568.0, 702.5, 735.5	362.5, 374.5, 402.0	375.5, 394.1

(*Continued*)

TABLE 1.2 (CONTINUED)
Properties of Rare-Earth Elements

Properties	Scandium	Yttrium	Lanthanum	Cerium	Praseodymium	Neodymium	Promethium	Samarium	Europium
Color of oxide, RE_2O_3		White	White	Off white (CeO_2)	Yellow-green; black (Pr_6O_n); pale blue (Pr_2O_3)	Pale blue	Pink	Cream	White
Number of isotopes: natural (artificial)		1 (14)	2 (19)	4 (15)	1 (14)	7 (7)	(15–18)	7 (11)	2 (16)
Thermal neutron absorption cross section: for naturally occurring mixture of isotopes, single isotopes (mass number of isotope), barns/atom		1.31	8.9	0.73	11.6	50	–	5600; 66,000 (149)	4300; 9000 (151); 5000 (152); 420 (153); 1500 (154); 13,000 (155)
Ionization potential, eV/g·atom		6.6	5.61	5.65	5.76	6.31	–	5.6	5.67
Electronegativity		1.177	1.117	(+3) 1.123; (+4) 1.43	1.130	1.134	1.139	1.145	(+2) 0.98; (+3) 1.152

(*Continued*)

TABLE 1.2 (CONTINUED)
Properties of Rare-Earth Elements

Properties	Scandium	Yttrium	Lanthanum	Cerium	Praseodymium	Neodymium	Promethium	Samarium	Europium
Thermal, Electrical, and Magnetic Properties									
Melting point, °C	1541	1522	918	798	931	1021	1042	1074	822
Boiling point, °C	2831	3338	3457	3426	3512	3068	–	1791	1597
Heat of fusion, kJ/mol	14.1	11.4	6.20	5.46	6.89	7.14	(7.7)	8.62	9.21
Heat of sublimation at 25°C, kJ/mol	377.8	424.7	431.0	422.6	355.6	327.6	(348)	206.7	175.3
Allotropic transformation temperature, °C	cph to bcc, 1337	cph to bcc, 1478	dcph to fcc, 310; fcc to bcc, 865	fcc to dcph, −148; dcph to fcc, 139; fcc to bcc, 726	dcph to bcc, 795	dcph to bcc, 863	dcph-bcc, 890	rhomb to cph, 734; cph to bcc, 922	–
Heat of transformation, kJ/mol	cph to bcc, 4.00	cph to bcc, 4.99	dcph to fcc, 0.36; fcc to bcc, 3.12	fcc to dcph and dcph to fcc, 0.05; fcc to bcc, 2.99	dcph to bcc, 3.17	dcph to bcc, 3.03	dcph to bcc, (3.0)	rhomb to cph, 0.2; cph to bcc, 3.11	–
Heat capacity at 298 K, C_p, J/mol·K	25.5	26.5	27.1	26.9	27.4	27.4	(27.3)	29.5	27.7
Standard entropy, $S°_{298}$, J/mol·K	34.6	44.4	56.9	72.0	73.9	71.1	(71.6)	69.5	77.8
Coefficient of thermal expansion, per °C	10.2×10^{-6}	10.6×10^{-6}	12.1×10^{-6}	6.3×10^{-6}	6.7×10^{-6}	9.6×10^{-6}	(11×10^{-6})	12.7×10^{-6}	35.0×10^{-6}
Thermal conductivity, W/(cm·K)	0.158	0.172	0.134	0.113	0.125	0.165	(0.15)	0.133	(0.139)

(*Continued*)

TABLE 1.2 (CONTINUED)
Properties of Rare-Earth Elements

Properties	Scandium	Yttrium	Lanthanum	Cerium	Praseodymium	Neodymium	Promethium	Samarium	Europium
Magnetic moment (theoretical for 3+ ion), Bohr magnetons		0	0	2.5	3.6	3.6	–	1.5	3.5
Magnetic susceptibility, emu/g·atom		191×10^{-6}	101×10^{-6}	2430×10^{-6}	5320×10^{-6}	5650×10^{-6}	–	1275×10^{-6}	$33{,}100 \times 10^{-6}$
Curie temperature, °C		None	None	None	None	None	–	None	None
Neel temperature, °C		None	None	−260.6	None	−253	–	−258	−165
Superconducting transition temperature, K	0.050 (at 18.6 GPa)	1.3 (at 11 GPa)	5.10	0.022 (at 2.2 GPa)					
Electrical resistivity, μΩ·cm	56.2	59.6	61.5	74.4	70.0	64.3	(75)	94.0	90.0
Hall coefficient, V·cm/A·Oe	-0.13×10^{-12}	–	-0.35×10^{-12}	$+1.81 \times 10^{-12}$	+0.709	$+0.971 \times 10^{-12}$	–	-0.21×10^{-12}	$+24.4 \times 10^{-12}$
Work function, eV	3.5	3.23	3.3	2.84	2.7	3.3	3.07	3.3	2.54
Density of liquid rare-earth metal, g/cm^3	2.80	4.24	5.96	6.68	6.59	6.72	(6.9)	7.16	4.87
Heat capacity of liquid rare-earth metal, C_p, J/mol·K	(44.2)	43.1	34.3	37.7	43.0	48.8	(50)	(50.2)	38.1

(*Continued*)

TABLE 1.2 (CONTINUED)
Properties of Rare-Earth Elements

Properties	Scandium	Yttrium	Lanthanum	Cerium	Praseodymium	Neodymium	Promethium	Samarium	Europium
				Mechanical Properties					
Yield strength, 0.2% offset, MPa	173	42	126	28	73	71	–	68	–
Ultimate tensile strength, MPa	255	129	130	117	147	164	–	156	–
Uniform elongation, %	5.0	34.0	7.9	22	15.4	25.0	–	17.0	–
Reduction in area, %	8.0	–	–	30	67.0	72.0	–	29.5	–
Young's modulus, GPa	74.4	63.5	36.6	33.6	37.3	41.4	(46)	49.7	18.2
Shear modulus, GPa	29.1	25.6	14.3	13.5	14.8	16.3	(18)	19.5	7.9
Bulk modulus, GPa	56.6	41.2	27.9	21.5	28.8	31.8	33	37.8	8.3
Poisson's ratio	0.279	0.243	0.280	0.24	0.281	0.281	(0.28)	0.274	0.152
Recrystallization temperature, °C	550	550	300	325	400	400	(400)	440	300
Vicker's hardness, 10 kg load, kg/mm^2	85	38	37	24	37	35	–	45	17
Compressibility at 25°C, cm^2/kg	2.26×10^{-6}	2.68×10^{-6}	4.04×10^{-6}	4.10×10^{-6}	3.21×10^{-6}	3.00×10^{-6}	2.8×10^{-6}	3.34×10^{-6}	8.29×10^{-6}

Properties	Gadolinium	Terbium	Dysprosium	Holmium	Erbium	Thulium	Ytterbium	Lutetium
			Atomic Properties					
Atomic number	64	65	66	67	68	69	70	71
Atomic weight	157.25	158.92534	162.50	164.93032	167.26	168.93421	173.04	174.967

(*Continued*)

TABLE 1.2 (CONTINUED)
Properties of Rare-Earth Elements

Properties	Gadolinium	Terbium	Dysprosium	Holmium	Erbium	Thulium	Ytterbium	Lutetium
Crystal structure	cph < 1235 bcc > 1235	cph < 1289 bcc > 1289	cph < 1381 bcc > 1381	cph	cph	cph	cph < 795 bcc > 795	cph
Atomic volume, cm^3/mol at 24°C	19.903	19.310	19.004	18.752	18.449	18.124	24.841	17.779
Density, g/cm^3 at 24°C	7.901	8.230	8.551	8.795	9.066	9.321	6.966	9.841
Conduction electrons	3	3	3	3	3	3	2	3
Valence in aqueous solution	3	3	3	3	3	3, 2	3, 2	3
Color in aqueous solution, RE^{3+}	Colorless	Very pale pink	Pale yellow-green	Yellow	Pink	Greenish tint	Colorless; Yb^{2+} is yellow	Colorless
Main absorption bands of RE^{3+} ion in aqueous solution in the range 200–1000 nm	272.9, 273.3, 275.4, 275.6	284.4, 350.3, 367.7, 487.2	350.4, 365.0, 910.0	287.0, 361.1, 416.1, 450.8, 537.0, 641.0	364.2, 379.2, 487.0, 522.8, 652.5	360.0, 682.5, 780.0	975.0	None
Color of oxide, RE_2O_3	White	Brown (Tb_4O_7)	Yellowish white	Yellowish white	Pink	White, greenish tint	White	White
Number of isotopes: natural (artificial)	7 (11)	1 (17)	7 (12)	1 (18)	6 (12)	1 (17)	7 (10)	2 (14)
Thermal neutron absorption cross section: for naturally occurring mixture of isotopes, single isotopes (mass number of isotope), barns/atom	46,000; 70,000 (155); 180,000 (157)	46	950; 130 (161); 680 (161); 240 (162); 220 (163); 2780 (164)	64	160	125	37	80

(*Continued*)

TABLE 1.2 (CONTINUED)
Properties of Rare-Earth Elements

Properties	Gadolinium	Terbium	Dysprosium	Holmium	Erbium	Thulium	Ytterbium	Lutetium
Ionization potential, eV/g·atom	6.16	6.74	6.82				6.25	5.0
Electronegativity	1.160	1.168	1.176	1.184	1.192	1.200	(+2) 1.02; (+3) 1.208	1.216
Thermal, Electrical, and Magnetic Properties								
Melting point, °C	1313	1356	1412	1474	1529	1545	819	1663
Boiling point, °C	3266	3223	2562	2695	2863	1947	1194	3395
Heat of fusion, kJ/mol	10.0	10.79	11.06	(17.0)	19.9	16.8	7.66	(22)
Heat of sublimation at 25°C, kJ/mol	397.5	388.7	290.4	300.8	317.1	232.2	152.1	427.6
Allotropic transformation temperature, °C	cph to bcc, 1235	cph to bcc, 1289	cph to bcc, 1381				fcc to bcc, 795	
Heat of transformation, kJ/mol	cph to bcc, 3.91	cph to bcc, 5.02	cph to bcc, 4.16				fcc to bcc, 1.75	
Heat capacity at 298 K, C_p, J/mol·K	37.1	28.9	27.7	27.2	28.1	27.0	26.7	26.8
Standard entropy, S°298, J/mol·K	67.9	73.3	75.6	75.0	73.2	74.0	59.8	51.0
Coefficient of thermal expansion, per °C	9.4×10^{-6} (at 100°C)	10.3×10^{-6}	9.9×10^{-6}	11.2×10^{-6}	12.2×10^{-6}	13.3×10^{-6}	26.3×10^{-6}	9.9×10^{-6}
Thermal conductivity, W/(cm·K)	0.105	0.111	0.107	0.162	0.145	0.169	0.385	0.164
Magnetic moment (theoretical for 3+ ion), Bohr magnetons	7.95	9.7	10.6	10.6	9.6	7.6	4.5	0

(*Continued*)

TABLE 1.2 (CONTINUED)
Properties of Rare-Earth Elements

Properties	Gadolinium	Terbium	Dysprosium	Holmium	Erbium	Thulium	Ytterbium	Lutetium
Magnetic susceptibility, emu/g·atom	356,000 × 10^{-6}	193,000 × 10^{-6}	99,800 × 10^{-6}	70,200 × 10^{-6}	44,100 × 10^{-6}	26,100 × 10^{-6}	71 × 10^{-6}	17.9 × 10^{-6}
Curie temperature, °C	17	−53	−185	−254	−253	(−241)	None	None
Neel temperature, °C	none	−43	−97	−143	−188	−216	None	None
Superconducting transition temperature, K	–	–	–	–	–	–	–	0.022 (at 4.5 GPa)
Electrical resistivity, μΩ·cm	131.0	115.0	92.6	81.4	86.0	67.6	25.0	58.2
Hall coefficient, V·cm/A·Oe	−4.48 × 10^{-12} (at 77 K)	–	–	–	–	−1.8 × 10^{-12}	3.77 × 10^{-12}	−0.535 × 10^{-12}
Work function, eV	(3.07)	(3.09)	(3.09)	(3.09)	(3.12)	(3.12)	(2.59)	(3.14)
Density of liquid rare-earth metal, g/cm^3	7.4	7.65	8.2	8.34	8.6	(9.0)	6.21	9.3
Heat capacity of liquid rare-earth metal, C_p, J/mol·K	37.2	46.5	49.9	43.9	38.7	41.4	36.8	(47.9)
Mechanical Properties								
Yield strength, 0.2% offset, MPa	15	–	43	–	60	–	7	–
Ultimate tensile strength, MPa	118	–	139	–	136	–	58	–
Reduction in area, %	56.0	–	30.0	–	11.9	–	92.0	–
Young's modulus, GPa	54.8	55.7	61.4	64.8	69.9	74.0	23.9	68.6
Shear modulus, GPa	21.8	22.1	24.7	26.3	28.3	30.5	9.9	27.2
Bulk modulus, GPa	37.9	38.7	40.5	40.2	4.4	44.5	30.5	47.6
Poisson's ratio	0.259	0.261	0.247	0.231	0.237	0.213	0.207	0.261

(*Continued*)

TABLE 1.2 (CONTINUED)
Properties of Rare-Earth Elements

Properties	Gadolinium	Terbium	Dysprosium	Holmium	Erbium	Thulium	Ytterbium	Lutetium
Recrystallization temperature, °C	500	500	550	520	520	600	300	600
Vicker's hardness, 10 kg load, kg/mm^2	57	46	42	42	44	48	21	77
Compressibility at 25°C (cm^2/kg)	2.56×10^{-6}	2.45×10^{-6}	2.55×10^{-6}	2.47×10^{-6}	2.39×10^{-6}	2.47×10^{-6}	7.39×10^{-6}	2.38×10^{-6}

Properties	La	Ce	Pr	Nd	Pm	Sm	Eu	Gd
Electronic Configuration								
Atom	$5d6s^2$	$4f^15d^16s^2$	$4f^36s^2$	$4f^46s^2$	$4f^56s^2$	$4f^66s^2$	$4f^76s^2$	$5f^75d6s^2$
M^{2+}	$5d$	$4f^2$	$4f^3$	$4f^4$	–	$4f^6$	$4f^7$	$4f^75d$
M^{3+}	[Xe]	$4f$	$4f^2$	$4f^3$	$4f^4$	$4f^5$	$4f^6$	$4f^7$
M^{4+}		[Xe]	$4f$	$4f^2$	–	–	–	
Radii, M^{3+}	1.061	1.034	1.013	0.995	0.979	0.964	0.95	0.938
Equilibrium Vapor Pressure								
Vapor pressure at m.p., Pa	34.7×10^{-9}	0.113×10^{-9}	14.67×10^{-6}	4.53×10^{-3}		0.773×10^{3}	0.121×10^{3}	18.67×10^{-3}
Temperature (°C) for vapor pressure 10^{-8} atm (0.001 Pa)	1301	1290	1083	955		508	399	1167
10^{-6} atm (0.101 Pa)	1566	1554	1333	1175		642	515	1408
10^{-4} atm (10.1 Pa)	1938	1926	1701	1500		835	685	1760
10^{-2} atm (1013 Pa)	2506	2487	2305	2029		1150	964	2306
1 atm (101,300 Pa)	3464	3443	3520	3074		1794	1529	3273

(*Continued*)

TABLE 1.2 (CONTINUED)
Properties of Rare-Earth Elements

Properties	Tb	Dy	Ho	Er	Tm	Yb	Lu	Sc	Y
				Electronic Configuration					
Atom	$4f^9 6s^2$	$4f^{10} 6s^2$	$4f^{11} 6s^2$	$4f^{12} 6s^2$	$4f^{13} 6s^2$	$4f^{14} 6s^2$	$4f^{14} 5d 6s^2$	$[Ar] 3d 4s^2$	$[Kr] 5d^1 6s^2$
M^{2+}	$4f^9$	$4f^{10}$	$4f^{11}$	$4f^{12}$	$4f^{13}$	$4f^{14}$			
M^{3+}	$4f^8$	$4f^9$	$4f^{10}$	$4f^{11}$	$4f^{12}$	$4f^{13}$	$4f^{14}$	[Ar]	[Kr]
M^{4+}	$4f^7$	$4f^8$							
Radii, M^{3+}	0.923	0.908	0.894	0.881	0.869	0.858	0.848	0.68	0.88
				Equilibrium Vapor Pressure					
Vapor pressure at m.p., Pa	0.115	94.66	71.99	49.33	0.246×10^6	2.53×10^3	1.293	10.27	0.28
				Temperature (°C) for Vapor Pressure					
10^{-8} atm (0.001 Pa)	1124	804	845	908	599	301	1241	1036	1222
10^{-6} atm (0.101 Pa)	1354	988	1036	1113	748	400	1483	1243	1460
10^{-4} atm (10.1 Pa)	1698	1252	1313	1405	964	541	1832	1533	1812
10^{-2} atm (1013 Pa)	2237	1685	1771	1896	1300	776	2387	1999	2360
1 atm (101,300 Pa)	3230	2567	2700	2868	1950	1196	3402	2836	3345

Note: bcc, body centered cubic; cph, close packed hexagonal or hexagonal close packed (hcp); dhcp, double hexagonal close packed; fcc, face centered cubic; m.p., melting point; ortho, orthorhombic; rhomb, rhombohedral.

M^{3+} ions because they then attain the stable $4f^{14}$ and $4f^{7}$ configurations, respectively. The most stable M^{2+} and M^{4+} ions are formed by those rare earths that can thereby attain f^0, f^7, or f^{14} configuration. Thus, Ce^{4+} and Tb^{4+} attain the f^0 and f^7 configurations, respectively, and Eu^{2+} and Yb^{2+} attain the f^7 and f^{14} configurations, respectively. In other words, the special stability of the f^0, f^7, and f^{14} configurations is an important factor in determining the existence of oxidation states other than +3 in the rare earths. However, there could be other thermodynamic and kinetic factors that are of equal or greater importance in determining the stability of the oxidation states.

1.3.2 Lanthanide Contraction

The term *lanthanide contraction* is used to denote the significant and steady decrease in the size of atoms and ions with the increase in atomic number as the lanthanide series is traversed from lanthanum to lutetium. Thus, as given in Table 1.2 and Figure 1.2, lanthanum has the largest and lutetium the smallest radius. The cause of the contraction is stated to be the imperfect shielding of one electron by another in the same subshell. As one proceeds from lanthanum to lutetium, both the nuclear charge and the number of 4*f* electrons increase by one with each succeeding element. Owing to the shape of the *f* orbitals, the shielding of one 4*f* electron by another is very imperfect. The atomic nucleus is poorly shielded by the highly directional 4*f* electrons, and as a result, at each increase of the atomic number, the effective nuclear charge experienced by the 4*f* electron increases, resulting in a reduction in the size or contraction of the entire 4*f* shell. With the successive increase in atomic number, such

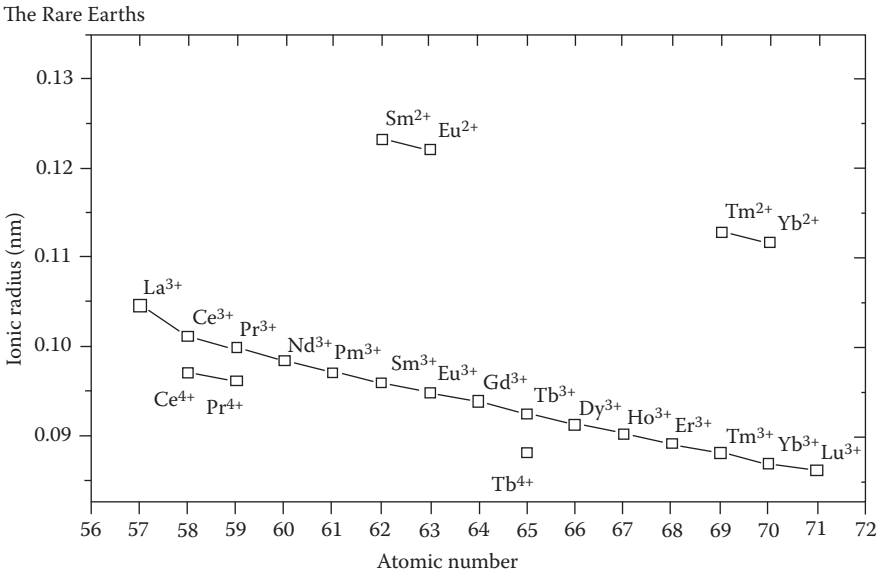


FIGURE 1.2 Lanthanide contraction.

contractions accumulate and result in the steady decrease in size. This is the famous lanthanide contraction.

Lanthanide contraction is the root cause of many of the features of the rare earths' chemistry. The chemistry of lanthanides is predominantly ionic and is determined primarily by the size of the M^{3+} ion. Even though the lanthanum atom and its tripositive ion are considerably larger in size than the corresponding yttrium species, the magnitude of lanthanide contraction is so much that the radii of the lanthanide species decrease to those of the yttrium species in the general holmium–erbium region. The similarity in the outermost electronic arrangement and the similarity in size due to lanthanide contraction explain the occurrence of yttrium in association with the heavier lanthanides. For essentially the same reason, it will be seen later that (1) yttrium compounds always concentrate with those of the heavier lanthanide elements in almost all fractionation procedures for the rare earths' separation, (2) considerable difficulty is experienced in separating yttrium from the heavier lanthanides, and (3) yttrium exhibits general similarities in solubility, crystal structure, and overall chemical properties with the heavier lanthanide metals. These factors, combined with the greater natural abundance of yttrium compared to the heavier rare earths, led to these rare earths being popularly called the *yttrium earths*. The chemistry of heavier rare earths is essentially the chemistry of yttrium.

The lanthanide contraction was sufficient for decreasing the atomic and ionic sizes of the heavier rare earths to those of yttrium but not to those of scandium. The atomic and trivalent ionic radii of scandium are far too small. Thus, scandium does not occur in rare-earth minerals, and its chemistry is significantly different from that of the other rare-earth elements.

1.3.3 Basicity

One of the important properties of rare-earth elements, related to their ionic size, which is in turn related to lanthanide contraction, is basicity. Basicity determines, in one way or another, certain important chemical features of rare earths relevant to their extractive metallurgy. Basicity determines the extent to which cations hydrolyze in aqueous solution, the relative solubilities of salts of all types, the ease with which salts containing oxyanions decompose when heated, and the stabilities of complex ions (Moeller 1961). A base tends to lose anions or electrons. Thus, those cations with the least attraction for anions or electrons are considered to be the most basic, and those with the strongest attraction, to be the least basic. Considering size relationships alone, the rare-earth ions are arranged as follows in order of decreasing basicity:

$$La^{3+} > Ce^{3+} > Pr^{3+} > Nd^{3+} > Pm^{3+} > Sm^{3+} > Eu^{3+} > Gd^{3+} > Tb^{3+} > Dy^{3+} > Ho^{3+} > Y^{3+}\ Er^{3+} > Tm^{3+} > Yb^{3+} > Lu^{3+} > Sc^{3+}.$$

Cerium(IV) is less basic than any of the tripositive species, and all of the dipositive species are more basic than the tripositive species (Moeller and Kremers 1945).

The variation in basicity is the basis of most of the fractionation procedures for separating the rare-earth elements from one another (Moeller 1961). In the so-called

classical separation procedures, exploiting the differences in basicity, a large variety of fractional crystallization and fractional precipitation methods had been used. Later, the techniques of ion exchange and solvent extraction, which again ultimately operate by exploiting basicity differences, have been used. The separations involving selective oxidation and reduction are also related to basicity because final removal from the contaminating tripositive species is usually effected by exploiting basicity differences between the different oxidation states of the element. Moeller (1961) emphasized that were it not for size-induced alterations in basicity, the separation of the rare-earth-metal species would be a nearly unsolvable problem.

A note of caution appears to be in order here. To readily achieve what has been implied in the previous paragraph, basicity differences should be large, the larger the better. Even though the size differences between the end members of the series or between two states of oxidation are substantial, the differences between adjacent members of the series in a given state of oxidation are, at best, very small. Therefore, generally, separations of adjacent members of rare earths remain most difficult. However, there are exceptions, like La^{3+}–Ce^{3+}.

1.4 PROPERTIES

In the elemental form, the rare earths are lustrous, iron gray to silvery metals. They are typically soft, malleable, and ductile and usually reactive. Their reactivity is especially pronounced at elevated temperature or when finely divided.

The physical properties of the rare-earth elements are listed in Table 1.2 (Cannon 1974; Gschneidner and Daane 1988; Gschneidner 1990; Gschneidner et al. 1995; McGill 1997).

1.4.1 Melting Point

The melting point increases in a regular manner across the series from lanthanum to lutetium with the exception of cerium, europium, and ytterbium. The melting point of lutetium is almost twice that of lanthanum. While considering the increase in the melting point by as much as 750°C, as the rare-earth series is traversed from lanthanum to lutetium, as unusual for a group of nearly identical elements, Gschneidner and Daane (1988) attribute the change in the melting point to the extent of hybridization of the 4*f* and 5*d*6*s* orbitals. The hybridization is the largest for cerium (the lowest-melting rare-earth metal) and decreases along the series from light lanthanides to heavy lanthanides. A lower melting point is associated with a greater amount of hybridization.

Various values have been reported for the melting points of the rare-earth metals, and this variety is traceable to the purity of the metal and the method used for the determination of the melting point. The temperature at which the rare-earth metal melts depends on its purity. If appreciable quantities of oxygen, carbon, and nitrogen are present in the sample, the measured melting points are likely to be high (Spedding et al. 1968). In small quantities, these impurities can lead to lower readings of the melting point (Gschneidner and Daane 1988). For example, early reports on the melting point of lanthanum put it at 806°C, but the currently accepted

value is 918°C. The determination of the La–C phase diagram by Spedding et al. (1959) revealed that the La–C eutectic melts at 806°C. Earlier, samples of lanthanum metal were prepared by fused-salt electrolysis using graphite electrodes, and melting point determinations using these samples, usually contaminated with carbon, led to the eutectic being reported as the pure metal's melting point. The availability of relatively large amounts of metallothermically prepared pure rare-earth metals in the 1950s led to more accurate determination of their melting points. Melting point determined by thermal analysis using a refractory metal crucible also needs to be checked for the possibility of the eutectic being reported as the melting point. In tantalum, however, the eutectic point and the actual melting point are very close to each other, differing by less than 1°C, in low-melting rare earths, but the difference may be appreciable in high-melting rare earths (Garg et al. 1996). The difference between the eutectic temperature and the actual melting point is much smaller in the corresponding rare earth–tungsten systems (Krishnamurthy et al. 2000).

The melting point of the rare-earth metal is an important parameter in the choice of the reduction process for metal production, both by metallothermic and electrolytic routes. Relatively inexpensive chloride reduction processes can be used for producing certain low-melting rare-earth metals (La, Ce, misch metal), whereas more expensive fluoride reduction methods are needed for the high-melting rare-earth metals (Gd, Y).

1.4.2 Boiling Point

The vapor pressures of all the rare-earth metals were systematically determined at Ames Laboratory in the 1950s using the Knudsen effusion technique for all the rare-earth metals except promethium. Their data along with the values for promethium are included in Table 1.2.

The boiling points of rare-earth metals do not exhibit a trend, even to the extent, the melting points displayed, across the series. Lanthanum metal, which is among the four lowest-melting-point rare earths, has the highest boiling point. In other words, it has the lowest vapor pressure at its melting point for any rare-earth metal. The most volatile rare-earth metal is ytterbium. At 1000°C, for example, the vapor pressure of lanthanum is one-billionth of the vapor pressure of ytterbium (Gschneidner and Daane 1988). The heat-of-vaporization data for the rare earths are also listed in Table 1.2. Habermann and Daane (1961) noted certain correlations among the vapor pressure (boiling point), heat of vaporization, and electronic structure of the rare-earth metals. For example, the divalent europium and ytterbium in the metallic state have no *d* electrons, resulting in weaker bonding. Consequently, the vapor pressure is higher, and the heat of vaporization is lower. Later, Gschneidner and Daane (1988) considered the electronic states of both the condensed phase and the final gaseous atom in correlating the electronic structure to boiling point and heat of vaporization.

Like the melting point, the boiling point of a rare-earth metal also strongly influences the method used for its preparation and purification. For example, the most volatile metals—europium, samarium, and ytterbium—are prepared by the reduction–distillation process, which is very similar to the Pidgeon process used for

magnesium (Pidgeon and King 1948). In these and other metals, the high vapor pressures are also exploited for the purification of metal by sublimation or distillation (Beaudry and Gschneidner 1978). On the other hand, the relatively high volatility of many of the rare-earth metals has been a major limitation in the application of ultrapurification techniques like solid-state electrotransport.

1.4.3 Allotropes

The crystal structures and lattice parameters of all the rare-earth metals, except samarium, promethium, and holmium, were determined quite early by Klemm and Bommer (1937). Their work confirmed the existence of the lanthanide contraction; discovered the multivalency in cerium, europium, and ytterbium; and confirmed that the rare earths crystallize in at least three different structures: fcc, bcc, and hcp. Final and finer details of room-temperature crystal structures of rare-earth metals were established at Ames Laboratory by various researchers between 1958 and 1971. The details of crystal structures, lattice parameters, and allotropic transformation temperatures of rare earths are summarized in Table 1.2.

Most of the rare-earth metals crystallize in the close-packed hexagonal structure. However, the stacking sequence along the *c*-axis is not identical for all. Lanthanum, cerium, praseodymium, and neodymium crystallize with one stacking sequence; gadolinium to lutetium crystallize in another; and samarium has yet another arrangement. Most of the rare-earth metals undergo allotropic transformation, and the high-temperature phase just below the melting point is invariably bcc. Europium, which is bcc even at room temperature, undergoes no transformation. Holmium, erbium, thulium, and lutetium also are monomorphic (cph) and do not undergo an allotropic transformation to the bcc phase before melting at atmospheric pressure. However, by application of pressure (~1 GPa), the bcc phase can be transformed in holmium and erbium. As regards the allotropic transformation temperatures, there is apparently no systematic trend across the lanthanide series (Gschneidner and Daane 1988).

The allotropic transformation is important in rare-earth-metal ultrapurification. The electrotransport mobilities of interstitial impurities in rare-earth metals depend on the crystal structure of the metal. Mobility is higher in the bcc phase. Thus, when no other complication crops up, electrotransport purification is best carried out in the bcc phase.

The light rare earths form solid solutions with each other, and so do the heavy rare earths. The solid solution is not perfect, and the liquidus and solidus lines are curved. When a light rare earth is alloyed with a heavy rare earth, two phases are likely to form.

1.4.4 Resistivity

The rare-earth metals are poor electrical conductors. Among the rare earths, room temperature resistivities are highest in the middle of the series. They also show anisotropy. Resistivity measured along the *c*-axis of a rare-earth-metal single crystal differs from that measured along the *a*- or *b*-axis in the basal plane. Rare earths are self-resistance heated during their purification by solid-state electrotransport.

The resistivity of the metal at 4 K is sensitive to the presence of impurities, particularly oxygen, nitrogen, and hydrogen, to the extent that it can be used for denoting the metal purity. A well-known method for estimating the total purity of a metal is to measure the ratio of its resistivities at 298 K and at 4 K, or even at 1 K. The impurities will be very low if the resistivity ratio obtained is very high. For certain rare earths, however, in spite of good purity, the resistivity ratio obtained may not be very high.

Among the rare earths, only lanthanum is superconducting at atmospheric pressure (Gschneidner and Daane 1988), and elemental lanthanum (fcc phase) is one of the better elemental superconductors [T_c = 6.1 K, $H_c(0)$ = 1600 Oe], like lead (T_c = 7.2 K) and niobium (T_c = 9.2 K). At a high pressure of 20 GPa, lanthanum has the highest known elemental superconducting transition temperatures (13 K). Certain lanthanum-based ceramic compositions are important superconducting materials.

1.4.5 Magnetic Properties

The 4*f* electrons determine the magnetic behavior of the rare-earth metals. In the completed 4*f* subshell, the magnetic effects of different electrons cancel each other out, but in the incomplete 4*f* subshell, they do not. All rare-earth metals, except scandium, yttrium, lanthanum, ytterbium, and lutetium, are strongly paramagnetic. On cooling, many of them become antiferromagnetic, and on cooling further, a number of these elements become ferromagnetic. If a magnetic field of sufficient strength is applied, all paramagnetic rare earths become ferromagnetic at low temperatures. The rare-earth metals display strong magnetic anisotropy; their magnetic behavior depends on the crystal axis.

The existence of ferromagnetism at room temperature in gadolinium was reported and confirmed by Klemm and Bommer (1937). Many of the detailed studies on the magnetic behavior of the rare-earth elements were carried out by the Ames group in the 1950s. Elucidation of the magnetic behavior of the rare-earth metals, as has been the case with their many other properties, was greatly dependent on the availability of the rare-earth metals at high levels of purity and in special forms such as large single crystals (Gschneidner and Daane 1988).

1.4.6 Spectral Properties

The trivalent rare-earth ions, except Ce^{3+} and Yb^{3+}, exhibit very sharp absorption bands in the visible and ultraviolet (UV) regions. These bands are caused by *f–f* transitions, and the sharpness comes because the electrons in the 4*f* inner shell of the rare earths are shielded from the chemical environment by the $5s^2p^6$ octet. Most of the rare-earth salts display colors that are characteristic of the tripositive ions. The striking colors persist in aqueous and nonaqueous solutions and are unaffected by alterations of anions present or the addition of complexing agents (Moeller 1971). The absorption bands and colors are listed in Table 1.2.

In the rare earths with electronic configurations of $4f^1$ and $4f^{13}$, no *f–f* transition is possible. Thus, Ce^{3+} and Yb^{3+} do not absorb in the visible region. They do, however,

absorb in the UV region due to transitions of the type $4f^n–4f^{n-1}5d$. The divalent ions of europium, samarium, and ytterbium display colors in aqueous solutions: Eu^{2+} is pale yellow, Sm^{2+} is deep red, and Yb^{2+} is yellow.

1.4.7 Mechanical Properties

Values for the elastic and mechanical properties of rare-earth metals reported in the literature vary widely. This is because of the variation in the impurity levels of the metals. Generally, the elastic property values increase with an increase in purity (Gschneidner and Daane 1988). The chosen values are listed in Table 1.2 (Gschneidner 1990). In the series, there is an increase in the elastic moduli with an increase in atomic number until a maximum is reached at thulium. Cerium, europium, and ytterbium have anomalously low values. The elastic constants of rare earths are similar in value to those of aluminum, zinc, cadmium, and lead.

The hardness and strength values of the rare earths (Gschneidner and Daane 1988; Gschneidner 1990) follow the same periodic trend displayed by the elastic constants. Cerium, europium, and ytterbium have anomalously low values. Mechanical properties improve from the light rare earths to the heavy rare earths. In the lower range, the strengths of rare-earth metals are similar to that of aluminum, and in the higher range, the values correspond to levels between aluminum and titanium.

1.5 REACTIVITY

1.5.1 Air/Oxygen

At room temperature, all the rare-earth metals are not affected by air the same way. Some corrode very rapidly, while some remain bright and shiny for years. A solid block of europium tarnishes immediately on exposure to air at room temperature, particularly when the air is moist. If left in that condition, it will be converted to an oxide of europium in a few days or weeks. Massive blocks of lanthanum, under similar conditions, will undergo surface corrosion in a few days and will develop a thick crust of oxide in a few months. Neodymium behaves in the same way as lanthanum; however, most of the heavy rare-earth metals will remain bright for a long time.

An increase in temperature and humidity accelerates oxidation of rare-earth metals (Gschneidner and Daane 1988). The rate at which lanthanum oxidizes increases by more than a factor of 10 when the relative humidity is increased from 1% to 75%. The oxidation of lanthanum at 1% humidity, which is 0.8 mg/cm^2 day at 35°C, increases to 5.1 mg/cm^2 day at 95°C, rising further to 32 mg/cm^2 day at 400°C and to 130 mg/cm^2 day at 600°C (Love and Kleber 1960). The value at 75% relative humidity is 210 mg/cm^2 day at 95°C. Under the latter conditions, praseodymium oxidizes at the rate of 55 mg/cm^2 day, neodymium at 20 mg/cm^2 day, and samarium at 1 mg/cm^2 day. The corresponding values for gadolinium through lutetium, scandium, and yttrium are 0–0.35 mg/cm^2 day. The oxide products formed by the oxidation of the light rare earths, lanthanum through neodymium, are the hexagonal (A)-form RE_2O_3 phase. Samarium through gadolinium form the monoclinic (β)-form RE_2O_3, and the remaining rare earths form the cubic (C)-form RE_2O_3 phase. The A-form oxides

react readily with water vapor in the air to form an oxyhydroxide, and this spalls, exposing the fresh metal surface, which undergoes oxidation. The C-type-structure oxides form a tight coherent stoichiometric gray-black coating, preventing further oxidation. It will be seen later that neodymium being prone to oxidation is a major technological issue in the production and use of NdFeB magnets.

The rate of oxidation is increased considerably if the metal contains one or more impurities such as fluorine, calcium, magnesium, carbon, iron, and any of the many *p*-group elements such as zinc, gallium, and germanium, and their congeners. Pure metals are attacked by oxygen and moisture slowly at first; however, once oxidation starts, the oxide apparently catalyzes the reaction, and oxidation is fast.

1.5.2 Refractories

The reactivity of rare-earth metals toward oxygen is due to the large negative free energy of formation of the oxide, and the free energy of formation of rare-earth oxide is among the most negative of all the elements in the periodic table. In other words, the rare-earth oxides are among the most stable of the oxides of all elements in the periodic table. At room temperature, only calcia is more stable than the rare-earth oxides. As a consequence, the rare-earth metals will attack and reduce most of the refractory crucibles, including zirconia, alumina, and magnesia and such refractory linings (Kremers 1961). The attack on refractories is particularly relevant when containment of the liquid rare-earth metal is considered. Rare-earth metals form solid solutions with oxygen. These solutions have greater stability (Alcock 1976), and this leads to the rare-earth metal picking up and dissolving oxygen from oxides of comparable (e.g., MgO) or greater (e.g., CaO) stability.

The Ellingham diagram showing the stabilities of certain well-known oxide refractories, rare-earth oxides, and rare-earth metal–oxygen solid solutions is given in Figure 1.3 (Okabe et al. 1998) and Figure 1.4 (Hirota et al. 1999). That the metal–oxygen solid solutions are far more stable than the lowest oxides of metal concerned at all temperatures is clearly revealed. Besides, the more dilute the solid solution is, the greater is its stability. The equivalent partial pressure of oxygen corresponding to various regions of the Ellingham diagram is also shown. Thermodynamically, all known oxide refractories will be attacked by the rare-earth metals, when heated together. It is also shown that the solution of oxygen in yttrium metal is the most stable metal–oxygen system among all the oxides and oxygen solutions.

1.5.3 Nitrogen

Rare-earth metals show a strong affinity for nitrogen. The mononitrides of rare earths are comparable in stability to those formed by metals such as titanium or zirconium (Pankratz et al. 1984). They have high melting points and very low decomposition pressures. The metals also form solid solutions with nitrogen. For example, cerium dissolves up to 0.3 wt.% nitrogen at 750°C. The equilibrium nitrogen pressures over these solutions will be still lower. Thus, the rare earths are very good getters of nitrogen from the environment and do not easily degas with respect to nitrogen.

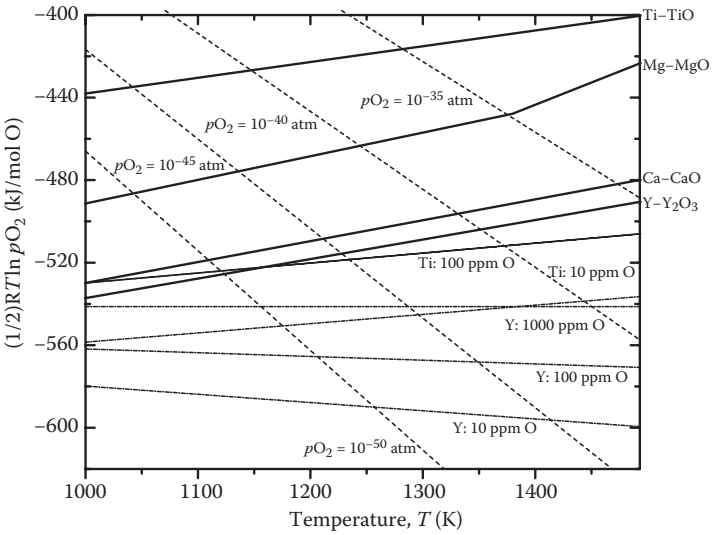


FIGURE 1.3 Ellingham diagram showing the stabilities of certain well-known oxide refractories, yttria, and titanium, yttrium-oxygen solid solutions. (From Okabe, T.H. et al. *J. Alloys. Compounds*, 237: 150–154, 1996.)

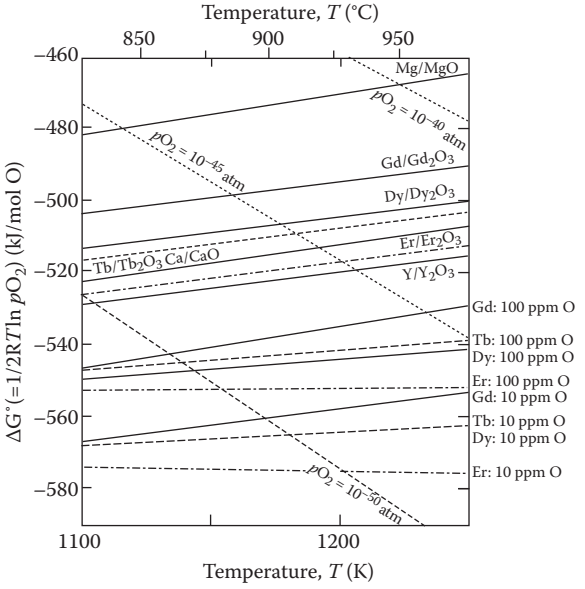


FIGURE 1.4 Ellingham diagram showing the stabilities of selected oxides and the oxygen chemical potential of RE-O (RE = Gd,Tb, Dy, Er) solid solutions containing 10 and 100 mass ppm of oxygen. (From Hirota K. et al., *J. Alloys. Comp.*, 282(1–2): 101–108, 1999.)

The reaction between rare-earth metals and nitrogen is, however, slow. High temperatures are needed to observe any appreciable reaction. Besides, the formation of a nitride layer on the surface greatly retards further nitridation.

1.5.4 Hydrogen

Rare-earth metals react with hydrogen and easily form hydrides at temperatures of 400–600°C. If hydriding is allowed to continue, when the metal is hydrided up to and beyond REH_2, the solid material fragments. When the hydrogen content is below REH_2, the material behaves like a metal and, at certain concentrations of hydrogen, conducts electricity better than even the pure metal. It is possible to load more hydrogen per unit volume in yttrium metal than in liquid hydrogen or water. The decomposition pressure of YH_2 is low even at fairly high temperatures and becomes 1 atm only at 1260°C (Spedding et al. 1968).

Unlike the yttrium hydride, several rare-earth-metal hydrides decompose and degas evolving hydrogen at relatively low temperatures. The brittleness and crumbling tendency of the hydride, combined with the possibility of easy hydrogen removal by degassing, has made hydriding–comminution–dehydriding a method to produce rare-earth-metal powder. It is, however, likely that the effort to drive off the last traces of hydrogen from the powdered hydride, by the use of high temperatures, will result in a partially sintered mass of powder (Gschneidner and Daane 1988).

1.5.5 Carbon

All rare earths are known to form dicarbides REC_2, and most of them (La–Sm, Gd–Ho, Y) form sesquicarbides, RE_2C_3. Monocarbides (e.g., ScC, LaC) and subcarbides (e.g., RE_3C_4, Sm, Gd–Lu) are also known (Goldschmidt 1967). The rare-earth carbides are high melting and form extensive solid solutions with oxygen and nitrogen. The solid solubility of carbon in rare-earth metals is also considerable (Massalski et al. 1990). For example, yttrium dissolves up to 1.3 wt.% C at 1520°C, and lanthanum takes up to 0.3 wt.% C at 775°C. The high stability of the lower carbides of rare earths and also of the carbon–RE solutions makes the attack of molten rare-earth metals on graphite crucibles an important factor leading to the contamination of rare-earth metals with carbon. Besides, these characteristics have rendered carbothermic reduction a useless method for rare-earth-metal preparation.

1.5.6 Silicon

Silicon, like carbon, forms rare-earth silicides and solid solutions. Rare-earth silicides are generally all disilicides represented by the formula $RESi_2$, but silicides of other stoichiometries have also been reported (Goldschmidt 1967).

1.5.7 Sulfur, Selenium, Phosphorus

The rare earths react exothermically with sulfur, selenium, and phosphorus. On heating a mixture of rare-earth metal with these elements, the reaction sets off and,

if precautions are not taken, could seriously damage the crucible, furnace, vacuum enclosures, etc. The strong exothermicity may afford preparation of sufides, selenides, and phosphides of rare earths by self-propagating high-temperature synthesis (SHS). On the other hand, at low temperatures, some of the rare earths, particularly heavy rare earths, hardly react with, for example, sulfur.

1.5.8 Refractory Metals

Among the refractory metals, niobium, molybdenum, tantalum, and tungsten are resistant to attack by liquid rare-earth metals. The metals listed above are in order of decreasing solubility in the liquid rare-earth metals at high temperatures, tungsten being the least soluble (Dennison et al. 1966a,b). Approximately 1.5 at.% tantalum dissolves in lutetium at the eutectic temperature, and the corresponding solubility of tantalum in scandium is about 3 at.%. When tungsten is used in place of tantalum, the solubility of tungsten in liquid rare-earth metals is about one-third of the solubility of tantalum. This makes tungsten the most inert container for holding liquid rare-earth metals. However, tungsten embrittles and has poor mechanical properties compared to tantalum. Thus, tantalum is a more useful crucible material for liquid rare earths in spite of its solubility in rare earths. The solubility of tantalum is a function of temperature, and for many rare-earth metals, it decreases from a high value at high temperatures to a very low value at temperatures just above the rare-earth metal's melting point.

Commenting on the interaction of tantalum with liquid rare-earth metals, Gschneidner and Daane (1988) have stated that the use of ceramic crucibles for metal preparation and purification puts an upper limit of 95–98 at.% purity of the rare-earth metals. The use of tantalum has allowed the purity level to rise to 99 at.% and higher.

1.5.9 Acids and Bases

All rare-earth metals readily dissolve in dilute mineral acids, and hydrogen is evolved. In a certain range, the rate of dissolution is proportional to the acid concentration (Gschneidner and Daane 1988). The attack on the metal by concentrated sulfuric acid is somewhat less (Kremers 1953). Rare-earth metals resist attack by hydrofluoric acid because REF_3 forms and coats the metal. This coating prevents further attack by the acid. A mixture of equal parts of concentrated nitric acid and 48% hydrofluoric acid attacks most rare earths only superficially and may be used to clean/pickle the rare-earth metals. This acid mixture may be used to separate tantalum from the rare earths because only tantalum dissolves in the mixtures, whereas the rare earths remain more or less intact (Gschneidner and Daane 1988). Rare-earth metals react with common organic acids but at slower rates than with mineral acids of the same concentration.

Rare-earth metals react, but slowly, with strong bases like sodium hydroxide. With a weak base like ammonium hydroxide, no reaction occurs. The lack of reactivity may be due to the formation of an insoluble rare-earth hydroxide coating on the metal surface.

1.5.10 Water

The reaction of rare earths with water varies depending on the metal. Generally, light rare-earth metals react with water slowly at room temperature and vigorously at higher temperatures. The heavy rare earths react very slowly. However, even with cold water, europium reacts to form $Eu(OH)_2 \cdot H_2O$, liberating hydrogen (Spedding et al. 1968).

1.6 AQUEOUS SYSTEMS

The standard oxidation potential data listed in Table 1.2 indicate that each of the rare-earth elements is a powerful reducing agent in aqueous acidic solution and forms the tripositive ion readily. The special stability of empty, half-filled, and completely filled 4*f* shells is reflected (Moeller 1967) in that the $4f^0$ cerium(IV) is much less readily reduced to the tripositive state than the $4f^1$ praseodymium(IV). For similar reasons, $4f^7$ europium(II) and $4f^{14}$ ytterbium(II) are weaker reducing agents than samarium(II).

1.6.1 Trivalent State

The rare earths are characteristically trivalent. In an aqueous solution, the tripositive rare-earth cations have a strong ionic character and form salts with a large variety of anions. The solubilities of such salts vary widely.

Rare-earth hydroxides are obtained as gelatinous precipitates from aqueous solutions by the addition of ammonia or dilute alkalies. Rare-earth hydroxides are definite compounds and are not just hydrous oxides. As mentioned earlier, $La(OH)_3$ is the most basic of the rare-earth hydroxides, and the basicity decreases across the series with an increase in the atomic number.

Rare-earth salts containing thermally unstable anions such as OH^-, CO_3^{2-}, and $C_2O_4^{2-}$, when heated, yield first the basic derivatives and finally the oxides. The hydrated salts, regardless of the nature of the anion, undergo thermal hydrolysis at high temperatures. Anhydrous compounds of rare earths containing thermally stable anions such as O^{2-}, F^-, Cl^-, and Br^- melt without decomposition at relatively high temperatures. These solids are also highly ionic.

The chlorides, bromides, nitrates, bromates, and perchlorate salts of rare earths are all soluble in water. When their aqueous solutions are evaporated, they precipitate as hydrated crystalline salts. For example, the rare-earth chlorides crystallize as hexahydrates. The light rare earths (La to Nd) can form heptahydrates. On heating, the hydrated chlorides lose HCl more readily than H_2O. The product is oxychloride. The bromides and iodides are quite similar to the chlorides. The iodides as well as the iodates and acetates are somewhat less soluble in water. The sulfates are sparingly soluble, and their solubility decreases with an increase in temperature. The rare-earth oxides, sulfides, fluorides, carbonates, oxalates, and phosphates are insoluble in water. Among the halides, only the fluorides are insoluble. The addition of hydrofluoric acid or fluoride ions to RE^{3+} solutions even in 3M nitric acid results in the precipitation of REF_3. This is a characteristic test for rare-earth ions. Rare

earths can also be precipitated as oxalates, another insoluble rare-earth compound, from a dilute nitric acid solution. The precipitation is not only quantitative but also specific to rare earths and is used for the determination of rare earths gravimetrically. Oxalate precipitation is also a useful procedure for rare-earth purification. The oxalate is calcined to the oxide.

Double salts of rare earths are common and extensively used. The most important are the double nitrates $2RE(NO_3)_3{\cdot}3MgNO_3{\cdot}24H_2O$ and $RE(NO_3)_3{\cdot}2NH_4NO_3{\cdot}4H_2O$, and the double sulfates $RE_2(SO_4)_3{\cdot}3Na_2SO_4{\cdot}12H_2O$ and $RE_2(SO_4)_3{\cdot}24H_2O$. The cerium-group double sulfates are only sparingly soluble in sodium sulfate, whereas those of the yttrium group are appreciably soluble. This characteristic makes it possible to achieve a fairly rapid separation of the entire group of rare earths into two subgroups.

1.6.2 Complexes

The formation of complex species is an important feature of tripositive rare-earth ions. It is improbable, however, that any hybrid *f* orbitals from the ions would take part in covalent bonding, and the large size of the RE^{3+} ions makes it possible for only certain types of complexes to be formed (Moeller 1961). Thus, (1) the number of rare-earth complexes is limited; (2) only species that can attract the RE cations as a result of their own small size, large charge, and chelating abilities will yield complexes; (3) stabilities of such complexes with respect to dissociation will be less than those of the tripositive transition metal ions; and (4) bonding in all complex species will be predominantly ionic. The coordination number is usually 7, 8, 9, or 10, and only in isolated cases, it is 6. Properties that depend directly on the 4*f* electrons are not affected by complexation. The complexes formed by tripositive rare-earth ions include complexes with citric acid, ethylene diamine tetraacetic acid (EDTA), and hydroxy ethylene diamine triacetic acid (HEDTA). The most important of the chelates are the species derived from the various polyamine polycarboxylic acids. Many of these have been isolated and characterized. These complexes are water soluble. However, the stabilities of the species in solution are of great importance because differences in the stabilities of the complexes have been used in conjunction with ion-exchange techniques to effect the separation of rare earths from one another (Powell 1961, 1979). The complex formation is pH dependent, and the stabilities of chelates are related to the ionic radii of the rare-earth ion. The stabilities of complex species invariably increase from La^{3+} to Eu^{3+} or Gd^{3+}, but for cations heavier than gadolinium, the stability may continue to increase, remain nearly constant, or pass through a maximum (Moeller 1967).

1.6.3 Tetravalent State

Cerium(IV) is the only tetrapositive rare-earth species that is stable in aqueous solution as well as in solid compounds (Moeller 1961). The III and IV valency states of cerium are often designated as cerous and ceric, respectively. Ceric oxide, CeO_2, hydrous ceric oxide, $CeO_2 \cdot nH_2O$, and ceric fluoride, CeF_4, are the only binary solid compounds of Ce(IV). Ceric oxide is obtained by heating cerium metal, $Ce(OH)_3$,

or any of the several Ce(III) oxosalts, such as the oxalate, nitrate, or carbonate in air or oxygen. CeO_2, white when pure, is quite inert and not attacked by even strong acids or alkalies. It can, however, be dissolved by acids in the presence of reducing agents to form Ce(III) solutions. Hydrous $CeO_2 \cdot nH_2O$ can be obtained as a yellow gelatinous precipitate, from Ce(IV) solutions on treatment with bases. The hydroxide is precipitated at a pH of 1. Ceric fluoride, CeF_4, is prepared by reacting anhydrous $CeCl_3$ or CeF_3 with fluorine at room temperature. Ceric fluoride is inert to cold water and is reduced to CeF_3 by hydrogen at 200–300°C.

Ce(IV) is obtained in solution by treatment of Ce(III) solution with strong oxidizing agents like ozone, peroxodisulfate, or bismuthate in nitric acid. Under alkaline conditions, oxidation of cerium to a +4 state is readily effected by $OC1^-$, H_2O_2, and O_2. In solutions, Ce(IV) can also be obtained by electrolytic oxidation. Cerium(IV) forms phosphates insoluble in $4NHNO_3$ and iodates insoluble in $6NHNO_3$ as well as insoluble oxalate. Precipitation as phosphate or iodate can be used to separate Ce(IV) from trivalent rare earths. Ce(IV) is extracted more readily than the RE(III) ions into organic solvents like tributyl phosphate. Ce(IV) can be used as an oxidizing agent.

Ceric oxide dissolves, undergoing reduction, in acids such as hydrochloric acid. In an acidic medium, reduction of cerium(IV) is effected by many reductants such as Fe^{2+}, Sn^{2+}, I^-, and H_2O_2. It dissolves in oxidizing acids such as nitric acid or sulfuric acid without undergoing reduction. The double ammonium nitrite of Ce(IV), the orange-red water-soluble salt $Ce(NO_3)_4 \cdot 2NH_4NO_3$, crystallizes readily from a concentrated nitric acid solution. It is both an excellent source of Ce(IV) and a useful analytical oxidizing agent.

Pr(IV) is a powerful oxidizing agent and oxidizes water itself. Therefore, it does not exist in aqueous solution. When Pr(III) salt or oxide is heated in air, Pr_6O_{11} forms. Both Pr(III) and Pr(IV) are present in the oxide.

The chemistry of Tb(IV) is similar to that of Pr(IV). The oxide Tb_4O_7 is obtained on igniting Tb(III) oxosalts in air. Tb_4O_7 contains both Tb(III) and Tb(IV). TbO_2 is obtained by oxidation of Tb_2O_3 with atomic oxygen at 450°C. The colorless compound TbF_4 is obtained by treating TbF_3 with gaseous fluorine at 300–400°C.

1.6.4 Divalent State

The divalent state of Sm, Eu, and Yb is well established both in solution and in solid compounds. These species are obtained (Moeller 1967) by (1) thermal reduction of anhydrous halides or chalcogenides with metals or hydrogen [e.g., solid oxide, chalcogenides, halides, carbonate, or phosphate of europium(II) may be obtained by reduction of the corresponding Eu(III) compound or from $EuCl_2$ by metathesis]; (2) electrolytic reduction in aqueous solution or in halide melts [e.g., Eu(II) and Yb(II)]; (3) chemical reduction in solution [Eu(II) using Zn in aqueous solution, Sm(II) using Mg in ethanol]; (4) thermal decomposition of anhydrous triiodides; and (5) controlled oxidation of free metals or their amalgams.

The divalent rare-earth cations are strong reducing agents in acidic aqueous solutions, and their reducing ability decreases in the order $Sm^{2+} \gg Yb^{2+} \gg Eu^{2+}$. Both Sm^{2+} and Yb^{2+} undergo instant oxidation to the tripositive species by the hydronium

ion and also by air. The oxidation of Eu^{2+} is, however, slower, and solutions containing Eu^{2+} can be readily handled. In an acidic solution, all three ions are rapidly oxidized by elemental oxygen. The RE^{2+} ions resemble group II ions, particularly Ba^{2+}. Thus, the hydroxides are soluble, and sulfates are insoluble. Eu^{3+} can be readily separated from the other rare earths by reduction with zinc to the dipositive state followed by the precipitation of the remaining tripositive rare earths as hydroxides by carbonate-free ammonia. The water-insoluble compounds, sulfates, carbonates, or fluorides of the divalent ions are relatively more resistant to oxidation. These ions have little tendency, compared to Ba^{2+} or Sr^{2+}, to form complex compounds.

1.7 APPLICATIONS

The rare earths have an ever-growing variety of applications in the modern technology. The first application of the rare earths and the beginning of the rare-earth industry date back to 1891 and were related to the inventions of the Austrian entrepreneur and scientist Carl Auer von Welsbach. He used the rare earths to solve what was, at that time, a major technical problem—the production of bright light. It was already known that a solid of suitable composition and large surface area, when brought into the hot zone of a gas flame, would glow, giving off the required bright light. The hitch was finding a suitable solid that would be the incandescent mantle. Auer solved the problem. First, he announced in 1866 the discovery of a gas mantle composed of zirconia doped with lanthana. That mantle was too brittle and produced cold blue light. Later, after persistent experimentation, in 1891 Auer came up with a gas mantle composed of 99% thoria and 1% ceria. The light from this mantle was not only white and bright and superior to electric light but it was also cheaper. This situation remained for several decades until about 1935, and an estimated 5 billion gas mantles had been produced and consumed in the world (Greinacher 1981). The Auer mantle was produced by a simple process. A cotton sock was saturated with a salt solution, which, upon ignition, resulted in a mixture of thorium–cerium oxides with a large surface area. Even today, light production from gas mantles remains in use in remote areas where electricity is unavailable or erratic and in some railroad signal devices.

The next important application of the rare earths also came from Auer's inventions. The search for a simple ignition system for his gas mantle lamps led him to discover (in 1903) and develop a pyrophoric alloy called flintstone. Beginning in 1903, the production of flintstone was the first major large-scale use for rare-earth metals. The flintstone, which is composed of 70% misch metal and 30% iron, was used in the lighters for the gas mantle. The name *misch metal* was coined by Auer for the alloy that contained lanthanum, cerium, and didymium in the same proportion in which they occurred in monazite. To produce misch metal, Auer founded a company in Carinthia, Austria in 1907. The company came to be known as Treibacher Chemische Werke and was the first company involved in the commercial production of rare earths. Auer used the fused-salt electrolysis method for the production of misch metal, and in 1908, over 800 kg of misch metal–iron flints entered the market. Following Auer's discovery, production of lighter flints was started by Ronson Metals in the United States in about 1915.

Greinacher (1981) noted that in the 22 years between 1908 and 1930, about 1100–1400 t of flints were produced from approximately 1300–1800 t of rare-earth oxides in the form of rare-earth chlorides. During the same time, about 7500 t of thorium nitrate were used for Auer incandescent mantles. The lighter flints are still very common and account for the consumption of a substantial fraction of the misch metal produced. Pyrophoric alloys, which give tracer shells their distinctive fiery trail, also contain misch metal as a constituent.

The production of intense light by electric arc was developed by Beck in Germany in 1910. These electric arc lamps have been used for a wide range of lighting purposes, including searchlights and cinema projectors. Historically, the third major use of rare earths was the addition of rare-earth fluoride as a wick in arc-light carbons (Greinacher 1981). Even though the electric arc struck and maintained between carbon electrodes emits light, it is low in intensity. The brightness is greatly increased if a cored carbon, consisting of an outer shell of carbon and an inner core made from carbon flour mixed with rare-earth oxides and fluorides, is used. The enhanced brightness and color come about because of the characteristic emission spectra of the core material (Bagchi 1988).

From these beginnings, and over many years, applications of rare earths have developed essentially in industrial and technology areas broadly classified as magnets, catalysts, electronics, glass, ceramics, metal alloys, phosphors, and others. The division of the total world rare-earth consumption among these application areas is summarized in Table 1.3 (Gschneidner 2011a,b). The proportion of rare earths (by volume) that is consumed in each of these categories is also listed for the year 2010. An element-wise listing of the major uses of rare earths is given in Table 1.4.

1.7.1 Metallurgy

Rare earths have major applications as metallurgical alloys. The oldest of these alloys is misch metal, which is, as mentioned earlier, an alloy consisting only of rare-earth metals, with the individual rare-earth elements present in the same proportion in which they naturally occur in bastnasite or monazite. Misch metal is the form in which the rare earths were introduced as constituents in numerous alloys for a variety of applications. A selection of alloys that benefit from rare-earth additions are described below.

1.7.1.1 Ductile Iron

The rare earths played a leading part in the discovery and commercialization of nodular iron (Linebarger and McCluhan 1981). Nodular iron has properties similar to mild steel and is essentially a ductile cast iron. Nodular iron results when the graphite flakes in cast iron are converted to nodules. In the 1940s, it was discovered that spheroidal graphite could be routinely produced in the laboratory in irons containing 0.02% Ce. The rare-earth elements cleanse the metal of elements that prohibit spherical graphite growth, and the compounds they then form provide heterogeneous substrates for graphite nucleation. Nodular iron has good mechanical and foundry properties and is an attractive engineering material, particularly in the automotive industry.

TABLE 1.3
Rare-Earth Application Areas

Application Areas	Subareas, Components, and Devices	Proportion of Total Rare-Earth Consumption in 2010, %
Magnets	Motors	20.8
	Disk drives and disk drive motors	
	Power generation	
	Actuators	
	Microphones and speakers	
	Magnetic resonance imaging (MRI)	
	Anti–lock breaking system	
	Automotive parts	
	Communication systems	
	Electric drive and propulsion	
	Frictionless bearings	
	Magnetic storage disk	
	Microwave power tubes	
	Magnetic refrigeration	
	Maagnetostictive alloys	
Catalysts	Petroleum refining	19.6
	Chemical processing	
	Catalytic converter	
	Diesel additive	
	Industrial pollution scrubber	
Electronics	Display phosphors (CRT, Plasma	7
	Display Panel [PDP], LCD)	
	Medical imaging phosphors	
	Lasers	
	Fiber optics	
	Optical temperature sensors	
Glass	Polishing compounds	24
	Optical glass	
	Ultraviolet (UV)-resistant glass	
	Thermal control mirrors	
	Colorizers/decolorizers	
Ceramics	Capacitors	6
	Sensors	
	Colorants	
	Scintillators	
Metal alloys	Hydrogen storage (NiMH batteries, fuel cells)	18
	Steel	
	Lighter flints	
	Aluminum/magnesium	
	Cast iron	
	Superalloys	

(*Continued*)

TABLE 1.3 (CONTINUED)
Rare-Earth Application Areas

Application Areas	Subareas, Components, and Devices	Proportion of Total Rare-Earth Consumption in 2010, %
Others	Water treatment Fluorescent lighting Pigments Fertilizer Medical tracers Coatings	6

Source: Gschneidner, Jr. K.A., *Material Matters*, 6(2), 2011b.

In the manufacture of nodular iron, rare earths are added as misch metal or mixed rare-earth silicides and not as pure rare-earth metals, mainly due to cost considerations (Davies 1981). Magnesium has emerged as competition for rare earths for graphite nodularization in cast iron, threatening the continued use of misch metal for this purpose (Falconnet 1988).

1.7.1.2 Steels

The deleterious effect of sulfur on the mechanical properties of freshly cast steel is well known. Iron sulfides form and concentrate at the boundaries between the grains of steel formed on solidification. Such steels are very brittle and fracture on working. Addition of rare earths to steel causes the sulfur content to be captured in the form of very stable compounds such as RE_2S_3 or RE_2S_2O. These compounds tend to form globular or spherical inclusions that do not concentrate at the grain boundaries, thus greatly enhancing ductility (Luyckx 1981). The sulfides and oxysulfides are very stable at steel-making temperatures, and unlike other sulfides such as those of manganese, they neither deform nor elongate under processing conditions. As the rare-earth concentration is increased, MnS inclusions are displaced by rare-earth oxysulfides or sulfides. The stability of granular rare-earth sulfides alleviates the detrimental effects of elongated MnS inclusions on toughness. Besides the improvements in the toughness characteristics of high-strength low-alloy (HSLA) steels, rare-earth additions also improve fatigue, creep, and several other mechanical properties (Collins et al. 1961; Linebarger and McCluhan 1981) of steels. The rare earths react quite efficiently with hydrogen in steel and also lower the hydrogen diffusion coefficient.

Rare earths are added to steel as misch metal, rare-earth silicides (RE content, 30%), and alloys such as Fe–Si–10RE, Mg–FeSi–0.1 to 0.2 RE. The effect of rare-earth metals in steels, in whichever form they are introduced, is the same, and the amount of misch metal usually added to ferrous alloys is about 0.1–0.2%. Such small additions do lead to considerable beneficial effects in both nodular iron and steels. Starting in the late 1960s, rare-earth additions to steel in the forms mentioned above became widely prevalent. The practice of adding rare earths to steel was reviewed by Wauby (1978). A few kilograms of misch metal were added to each metric ton

TABLE 1.4
Applications of Rare Earths

Rare Earth	Applications (of the Metal and Its Alloys and Compounds)
Rare earths	Raw material for myriad rare-earth chemicals and functional materials.
Lanthanum	Nickel–metal hydride (NiMH) batteries, phosphors for lighting, fluid-cracking catalysts for petroleum refining, $LaNi_5$ for hydrogen gas storage and management, metallurgical alloy additive to cast iron, steel and magnesium alloys, lighter flint, additive to optical glass (for cameras), lanthanum hexaboride ceramic (thermionic emitter) and other specialized ceramic compositions, Department of Defense (DOD) communication devices.
Cerium	Dominant rare earth with maximum number of uses. Polishing agent (for precision optical polishing) of glass, faceplates, mirrors, optical glass, silicon microprocessors, and disk drives; additive to glass; additive to (1) decolorize glass by keeping iron in its ferrous state, (2) block out ultraviolet light (medical glassware and aerospace windows), and (3) suppress discoloration of television glass; prevent polymers from darkening in sunlight; in phosphors, a sensitizer, in a variety of ceramics, including dental compositions and as a phase stabilizer in zirconia-based products; in catalytic converters, a stabilizer for the high-surface-area alumina; a promoter of the water–gas shift reaction; an oxygen storage component; and an enhancer of the NOX reduction capability of rhodium. Cerium is added to the catalyst for the production of styrene from methylbenzene to improve styrene formation; in fluid catalytic cracking (FCC) catalysts containing zeolites to provide both catalytic reactivity in the reactor and thermal stability in the regenerator; in steel manufacturing to remove free oxygen and sulfur by forming stable oxysulfides and by tying up undesirable tramp elements, like lead and antimony, in self-cleaning ovens, carbon-arc lighting, and misch metal.
Praseodymium	Highly valued as a bright yellow pigment for glass and ceramics, used in the scintillator for medical computerized axial tomography (CAT) scans; can partially substitute for neodymium in neodymium–iron–boron magnets for improved magnet corrosion resistance; used in electric vehicle motors and wind turbine generators; additive for high-strength metals; DOD guidance and control systems.
Neodymium	Most famous of the primary applications include neodymium–iron–boron ($Nd_2Fe_{14}B$) permanent magnets, indispensable and extensively used in every area of modern technology (both civilian and defense) that relies on superior performance, reliability, and miniaturization. Neodymium has a strong absorption band centered at 580 nm, which is very close to the human eye's maximum level of sensitivity, making it useful in protective lenses for welding goggles. It was also used in CRT displays to enhance contrast between reds and greens. It is highly valued in glass manufacturing for its attractive purple coloring to glass. Neodymium is included in many formulations of barium titanate, used as dielectric coatings and in multilayer capacitors essential to electronic equipment. Yttrium–aluminum–garnet (YAG) solid-state lasers utilize neodymium because it has optimal absorption and emitting wavelengths. Nd-based YAG lasers are used in various medical applications, drilling, welding, and material processing. Used by DOD in guidance and control systems, electric motors, and communication devices.
Promethium	Beta radiation source; fluid-cracking catalysts.

(*Continued*)

TABLE 1.4 (CONTINUED)
Applications of Rare Earths

Rare Earth	Applications (of the Metal and Its Alloys and Compounds)
Samarium	Primarily utilized in the production of permanent magnets ($SmCo_5$, Sm_2Co_{17}, Sm–Fe–N), still valued for their ability to function at high temperatures, beyond the operating limits of Nd magnets. Sm–Co magnets are used in precision-guided weapons due to their ability to operate at high temperatures. Used by DOD in guidance and control systems and electric motors.
Europium	Primary use relies on its unique luminescent characteristics. Excitation of the europium atom by absorption of ultraviolet radiation can result in specific energy-level transitions within the atom, creating an emission of visible radiation. In energy-efficient fluorescent lighting, europium provides not only the necessary red but also the blue. Several commercial red phosphors are based on europium for color TV, computer screens, and fluorescent lamps. Its luminescence is also valuable in medical, surgical, and biochemical applications. Combining Eu phosphor compounds with terbium phosphor compounds produces the white light of compact fluorescent lightbulbs, and they are a primary component in the production of T8 and T5 fluorescent tubes. No proven substitute for Eu in fluorescent lamps has been identified. No known substitutes for Eu as a red phosphor in television or liquid crystal display (LCD) screens. Also used as LED phosphor. Eu is also used to dope glasses and plastics for laser production, to investigate biomolecular reactions during drug screening trials, and as a counterfeiting indicator on banknotes. Used by DOD in targeting and weapon systems and communication devices.
Gadolinium	Gadolinium is usable for its high magnetic moment. Mixed with EDTA, it is used as an injectable contrast agent for patients undergoing magnetic resonance imaging. With its high magnetic moment, gadolinium can reduce relaxation times and thereby enhance signal intensity. The particularly stable half-full 4*f* electron shell with no low-lying energy levels creates applications as an inert phosphor host, for x-ray cassettes, and in scintillated materials for computer tomography. It has a potential application as the functional (magnetocaloric) material in magnetic refrigeration.
Terbium	Terbium is a high-intensity green emitter, primarily used in phosphors, fluorescent lamps, and projection televisions, as YAG (Tb:YAG). Terbium responds efficiently to x-ray excitation and is also as an x-ray phosphor. Terbium alloys were also used in magneto-optic recording films, such as TbFeCo. It is a superior but expensive substitute for dysprosium in neodymium–iron–boron (NdFeB) permanent magnets. Used by DOD in guidance and control systems, targeting and weapon systems, and electric motors.
Dysprosium	Dysprosium is an essential additive in NdFeB for electric vehicle and wind energy applications. Addition of either Dy or terbium (up to 6% of the magnet's weight) to NdFeB increases the value of intrinsic coercivity or resistance to demagnetization; resistance to demagnetization at higher temperatures also improved. Dy is used in special ceramic compositions based on BaTiO formulations, lasers, chalcogenide sources of infrared radiation, ceramics, nuclear fuel, phosphors, lighting, and catalysts. Used by DOD in guidance and control systems and electric motors.

(*Continued*)

TABLE 1.4 (CONTINUED)
Applications of Rare Earths

Rare Earth	Applications (of the Metal and Its Alloys and Compounds)
Holmium	Holmium has the highest magnetic moment of any naturally occurring element. Because of this, it has been used to create the highest known magnetic fields by placing it within high-strength magnets as a pole piece or magnetic flux concentrator. This magnetic property also has value in yttrium–iron–garnet (YIG) lasers for microwave equipment. Holmium lasers at a human-eye-safe 2.08 μm allow its use in a variety of medical and dental applications in both YAG and yttrium–lanthanum–fluoride (YLF) solid state lasers. Has applications as red and yellow pigments in glass and zirconia, and in calibration of γ-ray spectrometers.
Erbium	Erbium has application in glass and ceramic coloring (pink), as an amplifier in fiber optics, and in Er:YAG lasers for medical and dental use. It can neutralize discoloring impurities such as ferric ions and produce a neutral gray shade. It is used in a variety of glass products for this purpose. Lasers based on Er are ideally suited for surgical applications because of its ability to deliver energy without thermal buildup in tissue.
Thulium	Thulium products are mainly used in making crystals and lasers. An important application of thulium in the medical field, and relatively independent of its high cost, is the production of portable x-ray sources. These sources are available for about 1 year, as tools in medical and dental diagnosis as well as to detect defects in inaccessible mechanical and electronic components. This type of sources does not need excessive shielding. Usually, a small cap of lead is enough. Thulium can also be used in magnetic and ceramic materials (ferrite).
Ytterbium	Ytterbium is used in fiber-optic technology and lasers. It has a single dominant absorption band at 985 in the infrared, making it useful in silicon photocells to directly convert radiant energy to electricity. Ytterbium metal increases its electrical resistance when subjected to very high stresses. This property is used in stress gauges for monitoring ground deformations from earthquakes and nuclear explosions. It is also used as in thermal barrier system coatings on nickel, iron, and other transition metal alloy substrates. It is also usable as radiation source for portable x-ray units.
Lutetium	Specialist x-ray phosphors; single-crystal scintillators (baggage scanners, oil exploration).
Yttrium	In ceramics (yttria) for molten metal containment; yttria dispersion for strong alloys [oxide dispersion–strengthened (ODS) alloys, etc.]; yttria-stabilized zirconia in thermal plasma sprays to protect aerospace component surfaces at high temperatures; in fluorescent lighting phosphors, computer displays, and automotive fuel consumption sensors; oxygen and sulfur sensors in molten metals and process gas mixtures; YIG in microwave communication equipment for satellites; YAG with neodymium in lasers; yttrium–barium–copper oxide high-temperature superconductors. Used by DOD in targeting and weapon systems and communication devices.
Scandium	Scandium is mainly used in ceramics, lasers, phosphors, and certain high-performance alloys for the aerospace industry.

of special steel used in the manufacture of an Alaska oil pipeline because misch metal improves the physical properties of steel under arctic conditions. Because of its use in the Alaska pipeline steel, a major increase in demand occurred for misch metal in the period 1971–1978. In spite of the fact that the major consumption of rare earths is in the iron and steel industry, the annual tonnage of steel that is treated with lanthanides had indeed been very small (Haskin and Paster 1979). The use of rare earths in the form of rare-earth silicides or misch metal in steels grew explosively in the 1970s and peaked around 1975. Since then, the market for rare-earth products dropped off, following the availability of cleaner steel and the use of calcium for desulfurization (Falconnet 1988).

1.7.1.3 Superalloys

In the early 1960s, researchers at General Electric discovered that stainless steel containing both aluminum and yttrium possessed exceptional high-temperature corrosion resistance. Beginning then and continuing until about 1975, these alloys were produced for limited application in the nuclear industry (Davies 1981). This alloy, known as *fecralloy* to denote the presence of Fe, Cr, Al, and Y, has since been widely used for the fabrication of furnace-heating elements and has been considered as a replacement for ceramic substrates in emission-control catalysts for the automobile industry. Lanthanum is also used in high-temperature iron-based alloys (Davies 1981). An alloy with 200 ppm lanthanum combines oxidation resistance to 1100°C with good ductility and ease of fabrication.

Superalloys are essentially a class of heat-resistant alloys used in gas turbines, electric generators, jet engine exhaust nozzles, and reaction vessels, and, in general, as materials for use in intense oxidizing environments at high temperatures. Certain rare-earth elements are added to superalloys to enhance their oxidation resistance. Yttrium is the active component in the M–Cr–Al–Y (Fe–Cr–Al–Y stated earlier, Ni–Cr–Al–Y, Co–Cr–Al–Y) family of superalloys. The stability of the alumina–chromia skin that forms on oxidation is enhanced by traces of yttrium. These alloys, even when formed by vapor deposition, form an oxide coating that exhibits remarkable adhesion because yttrium acts to prevent the formation of voids at the oxide/substrate interface. Lanthanum and cerium also play a similar role in certain nickel and cobalt superalloy compositions. Cerium is used in amounts ranging from 100 to 300 ppm in certain high-strength nickel alloys to control sulfur and oxygen. Typically, 200–400 ppm of lanthanum is added in nickel-base and cobalt-base high-temperature alloys for gas turbine service. For example, lanthanum raises the operating temperature of nickel-base Hastelloy-K from 950°C to about 1100°C. Without lanthanum, these alloys exhibit less resistance to cyclic oxidation, and lanthanum probably results in a firmly bound oxide layer. Misch metal in small concentrations (0.03–0.05%) added to electrical-resistance alloys such as Ni–20Cr causes the formation of dense and more adherent surface oxides, leading to a tenfold increase in service life, from 1000 to about 10,000 h. The addition of cerium to the Cu78 high-temperature aerospace alloy (Al–8Fe–4Ce) of Alcoa for enhancing its oxidation resistance was noted as the first major industrial use of cerium metal. Usually, less than 1 wt.% of rare earths added in the form of individual metal leads to dramatic improvements in the performance of these superalloys.

1.7.1.4 Magnesium Alloys

The beneficial effects of the addition of rare earths to magnesium alloys were discovered in the late 1930s by Haughton and Prytherch (1937). Sauerwald (1947) discovered the exceptional grain-refining action of zirconium in magnesium. Murphy and Payne (1947) showed that the rare-earth additives are compatible with zirconium, and enhanced properties could be obtained by incorporating both rare earths and zirconium. Subsequently, zinc (Emley 1966) or silver was also included a desirable additive to these alloys.

At high temperatures, as compared to conventional magnesium alloys, magnesium alloys containing about 3% misch metal and 1% Zr show enhanced creep strength (Kremers 1961). Significantly higher strength at all temperatures was obtained by using Di (Nd + Pr) in place of misch metal as the alloying constituent. The new-generation magnesium alloys contain individual rare earths. One of the two magnesium alloys for use in high-performance engines for aircraft, space rockets, and satellites, possibly as castings, contains 4% zinc and 1% misch metal and can be used in applications seeing temperatures as high as 160°C. The other, which contains 5.5% yttrium, 3.5% other rare earths, and 0.5% zirconium, is stable at temperatures up to 280°C (Jackson and Christiansen 1993). A Mg–Al–Zn–Nd alloy has good corrosion resistance in a saline solution, and a Mg–Y–Nd–Zr alloy was shown to have good corrosion resistance, good castability, and stability up to 300°C. Rare earths refine the grain and improve strength, ductility, toughness, weldability, machinability, and corrosion resistance in the host alloys.

Improving upon the commercially available Mg–Y–Nd–Zr alloy, a lower-weight high-creep-resistance quaternary alloy Mg–Gd-Sc–Mn has been developed by researchers at TU Clausthal, in Germany (Hedrick 2001).

It has also been found that a melt-spun amorphous magnesium alloy containing 10 at.% cerium and 10 at.% nickel has good ductility and, in addition, a tensile fracture strength more than twice as large as conventional optimum age-hardened alloy.

1.7.1.5 Aluminum Alloys

A small amount of yttrium (100 ppm) in combination with zirconium was found to increase (by 50%) the electrical conductivity of aluminum transmission lines (Davies 1981). The addition of misch metal to aluminum-base alloys used for high-tension transmission lines has led to improved tensile strength, heat resistance, vibration resistance, corrosion resistance, and extrudability. An yttrium–magnesium–aluminum alloy has been developed in China for transmission cabling (McGill 1997).

The aluminum alloys 22Si–1MM and 2.5Cu–1.5Ni–0.8Mg–1.2Fe–1.2Si–0.15MM possess good high-temperature properties and fatigue strength and are used in the automobile industry, aircraft, small engine, and other fields. A new aluminum alloy composed of aluminum, iron, and cerium is also under development as a replacement for titanium components in specific applications in the range of 90–315°C. Cerium imparts the required corrosion resistance at elevated temperatures (Jackson and Christiansen 1993). Significant improvements in high-strength Al–Mg and Al–Li alloys have been obtained by the addition of scandium (McGill 1997).

The addition of scandium to aluminum increases the yield strength as it reduces the grain size. The scandium–aluminum alloy has been used in a premier line of

baseball and softball bats. The high-strength alloy allows the bats to have thinner walls, less weight, and greater rebound (Hedrick 1997).

A low-density glassy alloy containing about 90 at.% Al, up to 9 at.% transition metals, and about 5 at.% rare earths has been under development (Kilbourn 1988). The transition metals considered were iron, cobalt, and nickel, and the rare earths were cerium, neodymium, and yttrium. These materials, produced by melt spinning, have extremely high tensile strengths, about twice that of the best crystalline commercial alloy, and good ductility, in addition to low density. These characteristics are attractive for aerospace applications.

An Al–8 wt.% Fe–4 wt.% Ce alloy was made by the rapid solidification (RS) technique of melt spinning and processed further by powder metallurgy techniques. These alloys rely on the rapid gettering of oxygen by the rare earth. The stability of dispersed oxide particles thus formed improves the high-temperature performance of the alloys (Kilbourn 1988), particularly creep resistance, elevated-temperature tensile strength, thermal stability, and corrosion resistance. Compared to the heat-treatable ingot metallurgy products whose elevated-temperature properties are limited to 175°C, the RS Al–Fe–Ce alloys retain good strength even up to 340°C.

About 1–3% misch metal in an aluminum–carbon composite improves the wetting by carbon and, hence, the incorporation of graphite dispersoid in the metal matrix, resulting in a material with improved tensile strength.

1.7.1.6 Titanium Alloys

Yttrium, in concentrations of approximately 200 ppm, was found to improve ductility and ease of fabrication of vacuum arc–melted titanium alloys (Davies 1981). Microalloying of various commercial titanium alloys with rare earths has also resulted in improved strength, stress rupture, and oxidation resistance.

Rapidly solidified titanium alloys (the rare-earth addition, particularly Y, Nd, Er, or Ce, ranged from 1% to 2%) showed improvements by orders of magnitude in high-temperature yield strength, stress rupture life, and creep resistance. The most important of the rare-earth additives have been those with erbium or yttrium (Mahajan and Rama Rao 1988).

1.7.1.7 Copper Alloys

The addition of misch metal or yttrium to oxygen-free high-conductivity (OFHC) copper enhances oxidation resistance without affecting electrical conductivity. For example, the oxidation resistance at 600°C nearly doubled when 0.1 wt.% Y was added to copper.

Misch metal additions have been used to improve the hot workability and deep-drawing characteristics of bronzes containing less than 1 wt.% lead and also the wear resistance of highly leaded bronzes. Adding misch metal in leaded bearing bronze reduced the coefficient of friction by a factor of 4.

1.7.1.8 Zinc Alloys

Misch metal is a constituent in the alloy Galfan (Zn–5% Al–0.05% MM), used in galvanizing baths. This alloy, developed by the International Lead–Zinc Research Organization, is superior with respect to corrosion resistance and permeability to

standard galvanized steel sheets and wire of equal coating thickness and has comparable paintability and weldability properties (Radtke and Herrschaft 1983).

1.7.1.9 Oxide Dispersion–Strengthened Alloys

In oxide dispersion–strengthened (ODS) alloys, the high thermal stability of the rare-earth oxides such as Y_2O_3 and CeO_2 impart desirable properties, like high-temperature strength, creep resistance, and resistance to cyclic corrosive oxidation (Kilbourn 1988). Yttria (0.25–1.3%) is introduced into the nickel–chromium and iron–chromium alloys by mechanical alloying. The mechanical alloying is a high-energy ball-milling process that permits solid-state processing and results in the biggest improvement in properties. After mechanical alloying, the alloy powder is processed by powder metallurgy techniques. The products are high-temperature high-strength ODS alloys, which have found use in gas turbine blades, combustors, and other such applications.

1.7.1.10 Long-Range-Ordered Alloys

Long-range-ordered alloys such as $(Fe,Co)_3V$, $(Fe,Ni)_3V$, and $(Fe,Co,Ni)_3V$ are materials with potential for high-temperature applications. The addition of a small amount of Ce (<0.1%) together with titanium has been found to double the rupture ductility, substantially lower the creep rate, and considerably improve the rupture life of some of these alloys (Mahajan and Rama Rao 1988). In another application, mixtures containing Zr, Ce, and Y oxides of controlled particle morphology are plasma sprayed onto the metal surfaces to create barrier coatings for the protection of the metal substrates against high-temperature degradation.

1.7.2 Magnets

Magnets are fascinating materials, and the rare earths share a wonderful relationship with magnets and magnetism.

There are only two naturally occurring magnets. One is the mineral pyrrhotite, and the other is a type of the mineral magnetite. While ordinary magnetite is attracted to a magnetic field like iron and steel are, it does not become a magnet itself. Only a certain variety of magnetite with a particular crystalline structure (a mixture of magnetite and maghemite) has sufficient coercivity to remain magnetized and thus be a permanent magnet (PM). This mineral has been known as a *lodestone* or *loadstone*. It is mostly found at the surface of the earth; not buried at great depth. According to one theory, lodestones were magnetized by the strong magnetic fields surrounding lightning bolts. The ancient Greeks are credited with discovering lodestone, and the first reference to this material dates back to the sixth century BCE. The name *magnet* might have come from lodestones found in the ancient Greek city Magnesia.

King (2012), in a recent article, traced the 270 years of progress in magnet technology by presenting a visual of three magnets that were state-of-the-art materials in the years 1735 (lodestone), 1952 (ferrite), and 1985 (Nd–Fe–B). The picture is reproduced in Figure 1.5. Each magnet shown here produces half a joule of magnetic energy, yet the size has decreased a thousandfold. Another oft-repeated figure of Constantinides (2012a,b), also reproduced in Figure 1.5, demonstrates the dramatic decrease in magnet sizes over a 50-year period that have made possible many of the consumer devices as we know them today.

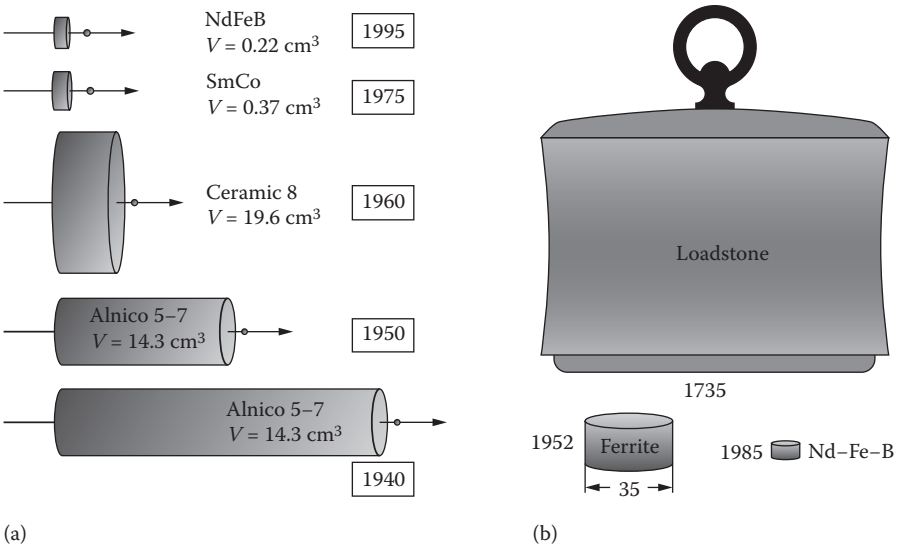


FIGURE 1.5 270 years of progress in magnet technology. (a) Each magnet here produces half a joule of magnetic energy, yet the size has decreased a thousandfold. • Lodestone • ferrite • Nd–Fe–B (b) Relative magnet size to generate 1000 gauss field at 5 mm from the pole face of the magnet. (From King, A., *Rare earth magnet R&D*, The Ames Laboratory, USDOE Iowa State University of Science and Technology, 2012; Constantinides, S., Material matters, 2012a; Constantinides, S., The demand for rare earth materials in permanent magnets. In *51st Annual Conference of Metallurgists*, 2012a,b.)

A complete listing of all PMs ever developed is given in Table 1.5. Before the 1930s, certain steels were the only PM materials known. Beginning in the 1930s, new PM materials were discovered with great regularity, in an effort to achieve higher remanence (B_r) and energy product (BH_{max}) and greater resistance to demagnetization. The first major breakthrough was the discovery of alnico in Japan in 1931. Alnico underwent improvisation over the next four decades. The hard ferrite magnet was developed in the 1950s and was being widely used by 1960. In the late 1960s, samarium alloyed with cobalt was first used in magnets, and in the 1980s, the cheaper and more powerful neodymium–iron–boron magnets also became available (Wernick 1995). The rare-earth magnets have since become and are set to remain as a major input to clean technologies and high-efficiency consumer and industrial devices (Constantinides 2012b). A consolidated picture of the PMs highlighting the characteristics of the rare-earth magnets that have earned them such adulation in technology is presented in Table 1.6 (Constantinides 2011a). A majority of all the PMs that were ever developed are in production till this date. The status of worldwide production and consumption of the four major PM types—alnico, ferrite, Sm–Co, and NdFeB, over the past 40 years is given in Figure 1.6 (Constantinides 2012a,b). Each PM material apparently has a technocommercial space all for itself. This is depicted in Figure 1.7 (Dent 2012), wherein the magnetic properties provided by the magnets and the temperature limits of their normal operation are given.

TABLE 1.5
Permanent Magnet Development Timeline

Material	First Reported	Reference	BHmax (MGOe)	Hci (Oe)
Carbon steel	c. 1600	Gilbert	0.2	50
Chrome steels	c. 1870	Hadfield	0.3	65
Cobalt steel	1916	Honda et al.	0.9	230
Remalloy	1931	Seljesater	1.1	230
Alnico	1931	Mishima	1.4	490
New KS	1934	Honda et al.	2.0	790
PtCo	1936	Jellinghaus	7.5	4300
Cunife	1937	Neumann et al.	1.8	590
Cunico	1938	Dannöhl and Neumann	1.0	450
Alnico, field treated	1938	Oliver and Shedden	5.5	640
Vicalloy	1940	Nesbitt and Kelsall	3.0	450
Alnico, DG	1948	McCaig, Bemius, Ebeling	6.5	680
Ferrite, isotropic	1952	Went et al.	1.0	1800
Ferrite, anisotropic	1954	Stuijts et al.	3.6	2200
Lodex	1955	Luborsky et al.	3.5	940
Alnico 8	1956	Koch et al.	4.5	1450
Alnico 9	1956	Koch et al.	9.2	1500
$RECo_5$	1966	Strnat et al.	16.0	7000
$RECo_5$	1970	Benz and Martin	19.0	8000
$RE_2(Co,Fe,Cu,Zr)_{17}$	1972	Strnat et al.	32.0	25,000
$RE_2TM_{14}B$	1984	Koon, Croat, Sagawa	26.0	25,000
		(Range of properties)	35.0	11,000
$RE_2TM_{14}B$	2010	(Numerous)	30.0	35,000
		(Range of properties)	52.0	11,000

Source: Constantinides, S. The demand for rare earth materials in permanent magnets. In *51st Annual Conference of Metallurgists*, Niagara Falls, Sept. 30–Oct. 3, Met. Soc. of CIM, 2012b.

Sintered magnets of the $SmCo_5$ type, the first of the rare-earth magnets to be available commercially, possess specific magnetic properties much superior to the well-known and hitherto well-established ferrite and alnico magnets. This is shown by the values in Table 1.6. The intermetallic $SmCo_5$, because of its hexagonal structure, exhibits a high degree of uniaxial anisotropy, resulting in extremely high coercivity, which, in turn, results in considerably greater energy product. The magnetic strength of Sm–Co compounds is predominantly from the cobalt atoms. Samarium apparently helps define an anisotropic structure *locking* the cobalt moments in place and rendering demagnetization difficult (Molycorp 1993).

The superior properties of rare-earth magnets not only permitted extensive miniaturization in a wide variety of consumer and industrial products but also resulted in performance characteristics hitherto unattainable. Both samarium and cobalt are

TABLE 1.6
Magnet Characteristics—Comparative Values for Major Types

Characteristic	Units	Alnico 5–7	Alnico 9	Ferrite 8	Ferrite 9	SmCo 1:5	SmCo 2:17	NdFeB 33EH	NdFeB 48M	Indicator
Flux density (Br)	Tesla	1.35	1.12	0.39	0.45	0.9	1.1	1.15	1.39	> is better
Energy product (BHmax)	kJ/m^3	60	84	28	37	175	230	230	370	> is better
Resistance to demagnetization (Hcj)	kA/m	59	115	245	370	2400	1600	2400	1115	> is better
Usable temperature range	°C	4 K to 520°C	4 K to 520°C	−40 to 150°C	−40 to 150°C	4 K to 520°C	4 K to 520°C	150 K to 200°C	150 K to 100°C	Minimum −40°C to 200°C
Induction change with temperature (RTC of Br)	%/°C	−0.02	−0.01	−0.2	−0.18	−0.045	−0.035	−0.11	−0.12	< is better
Second quadrant normal curve	Shape	Curved	Curved	Straight	Straight	Straight	Straight	Straight	Straight	Straight
Recoil permeability	B/H	2	1.3	1.04	1.04	1.03	1.05	1.04	1.05	~1
Corrosion resistance		Excellent	Excellent	Outstanding	Outstanding	Good	Good	Fair	Fair	Outstanding
Physical strength	MPa	55	55	65	70	120	120	285	285	>50 also “tough”
Electrical resistivity	μΩ·cm	47	50	10^6	10^6	55	90	180	180	> is better
Magnetizing field requirement	kA/m	120	240	480	800	2000	4000	2700	2700	<4000
Coefficient of thermal expansion	%/°C $\times 10^{-6}$	11.5	11	10 to 15	10 to 15	7 to 14	11 to 13	7.5 to −0.1	7.5 to −0.1	<15
Approximate current price (relative to NdFeB 33EH)		0.2	0.225	0.04	0.075	0.6	0.5	1	0.75	< is better

Source: Constantinides, S., Rare earth science community help needed for clean energy initiatives, Presentation at the 26th Rare Earth Research Conference (RERC 2011), Santa Fe, New Mexico, June 19–23, 2011a.

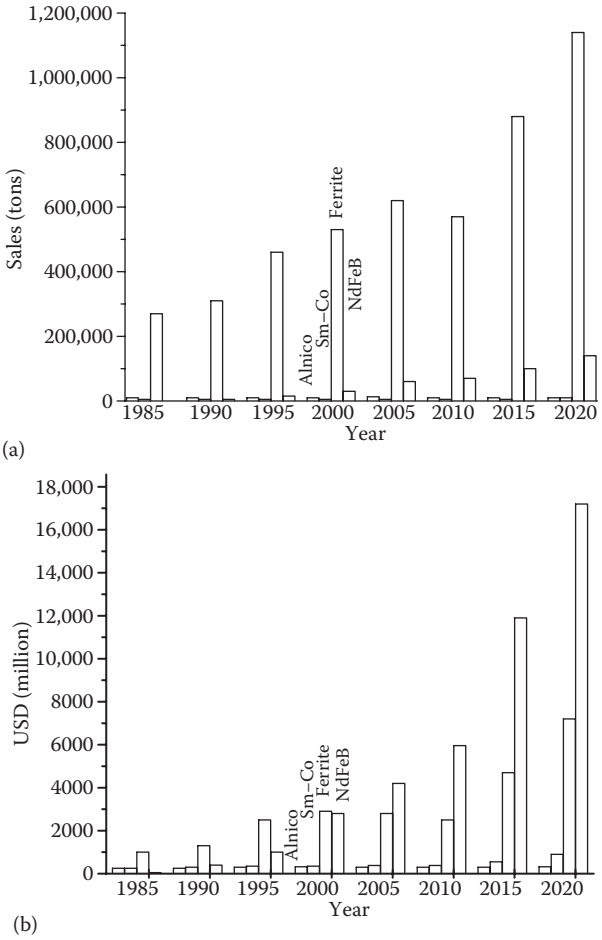


FIGURE 1.6 Permanent magnet sales (a) by volume and (b) by value for the four largest commercially available materials. (From Constantinides, S., The demand for rare earth materials in permanent magnets. In *51st Annual Conference of Metallurgists*, 2012b.)

expensive and limited in supply, and this made the $SmCo_5$ magnets expensive. The disadvantage of the high cost of samarium was sought to be offset by using misch metal in its place. The use of misch metal offers significant cost reduction, particularly for large-volume applications, such as in electric machinery. The theoretical energy product of $PrCo_5$ is 30% higher than that of $SmCo_5$, but $PrCo_5$ has substantially weaker anisotropy compared with $SmCo_5$ (Wallace et al. 1988). Praseodymium, which is more abundant than samarium, was considered to replace Sm in $SmCo_5$ materials (Kilbourn 1988). While praseodymium addition to samarium raises the strength of the magnet, it also increases corrodibility. Gadolinium is substituted for part of the samarium in temperature-stabilized grades of $SmCo_5$, which provide no change in flux output in the range of −40°C to 150°C (Constantinides 2012a,b).

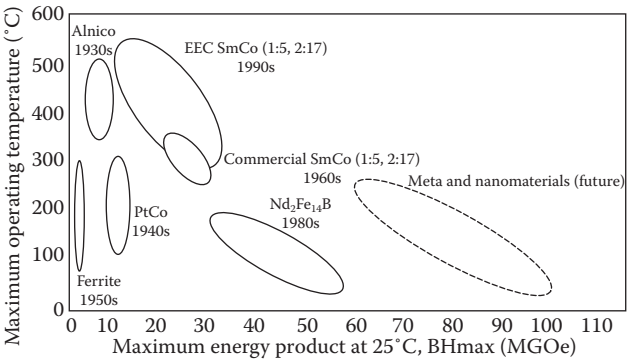


FIGURE 1.7 Operating temperature range for various magnets and their energy products. (From Dent, P.C., *J. Appl. Phys*., 111: 07A721, 2012.)

A new generation of samarium–cobalt magnets that not only permitted savings in raw material costs but also provided enhanced magnetic properties was based on the 2:17 alloy, Sm_2Co_{17}. This material was developed between 1969 and 1974. Electron Energy Corporation (EEC) (Dent 2012). In temperature-stabilized grades, gadolinium is substituted for part of samarium. The most widely used of the 2:17 alloys are of the type $Sm(Co, Cu, Fe, M)_x$, where M = Zr, Hf, or Ti, and x is in the range of 7.0 to 7.85. Higher-temperature grades, for use at over 500°C, have a higher cobalt and reduced-iron content in the magnet composition.

The continuing search for new PM materials has led to the emergence of certain rare earth–iron intermetallic compounds modified by interstitials such as nitrogen and carbon, for example, $Sm_2Fe_{17}N_3$ (Coey et al. 1991b). Interstitial modification has been found to bring advantages, like an increase in Curie temperature and development of a strong uniaxial anisotropy (Collocott et al. 1999). Sm–Fe–N magnets have excellent temperature stability. The material is produced as a powder by mechanical alloying. It is almost always converted to bonded magnets because any attempt to sinter by heating beyond about 450°C will result in the decomposition of the material with the release of nitrogen. For bonded magnets, Sm–Fe–N can have a higher-energy product than anisotropic neo powder. Sm–Fe–N magnets are relatively expensive because of the materials and processes involved (Constantinides 2012a,b Coey and Sun 1990; Wallace and Huang 1992).

The discovery of $Nd_2Fe_{14}B$ (Neo) magnets in 1984 ushered in a new era for the rare-earth transition metal-based PMs. The Nd–Fe–B magnets are high-strength magnets with a magnetic energy of up to 50 MGOe, which is a factor 2.5 times greater than that of $SmCo_5$ magnets, with high remanence and coercive force. There is a large potential for these magnets because iron, which is cheap and available in abundance (unlike the scarce and costly cobalt), is present as the main constituent (82.4 at.%). Neodymium is also in ample supply, being the third most abundant rare earth and constituting 13% of bastnasite and 18.5% of monazite ores.

Immediately after introduction in the market, the demand for and, hence, production of Nd–Fe–B magnets expanded rapidly, driven primarily by the growth of the personal

computer market. By 1990, 75% of all the Neo magnets were used in hard disk drives of PCs. Hard disk, CD, and DVD drives use small and reliable motors to spin the disks and for positioning the read/write head. The spindle drive motors comprise compression-bonded ring magnets made from melt-spun Magnequench powder. The quantity of magnet material per drive is small (~6 g), but the number of drives made is very large (660 million in 2011). Another important large-scale application in the initial years was the substitution of ferrite magnets with Nd–Fe–B magnets in small electric motors of automobiles, an application pioneered by General Motors. One more major use of Nd magnets was in magnetic resonance imaging equipment. The worldwide production of neodymium magnets was driven initially by the electronic industry (especially the manufacture of computers and portable devices like cell phones) as well as by automotive and industrial applications. The future growth of the Nd magnets will be determined by their use in two major green energy technologies, the use of Nd magnets in windmills and the use of Nd magnets in electric vehicles of all formats.

The main limitation of the Nd–Fe–B magnets is their lower Curie temperature (about 300°C). This leaves the field open for Sm–Co magnets (Curie temperature, 700–900°C) for uses where this property is of major importance. The coercivity of Nd–Fe–B high-strength PMs is enhanced by using Dy as an additive. Dysporium probably substitutes into the magnetic phase, creating $Nd_{2-x}Dy_xFe_{14}B$ with higher anisotropy (hence higher coercivity) than the unsubstituted material (Molycorp 1993). Even below the Curie temperature, the high-temperature performance of Nd magnets has been an issue of concern. The situation is depicted in Figure 1.8. Substitution of Dy results in improvement, but above 150°C, the samarium magnets have a superior energy product.

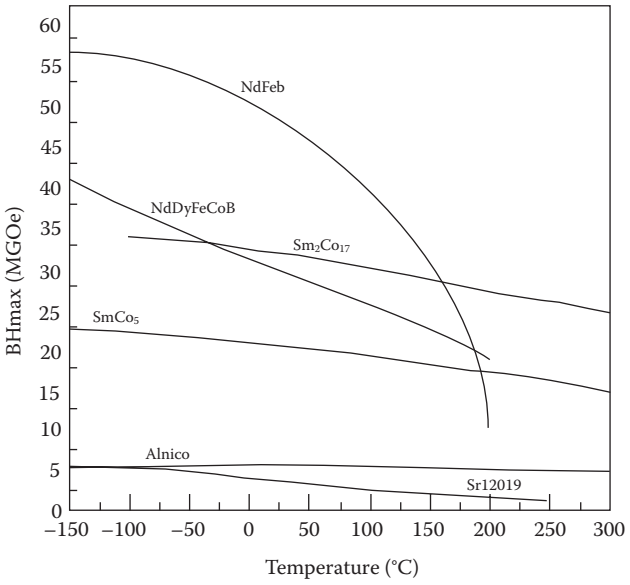


FIGURE 1.8 The temperature performance of the maximum energy product as a function of temperature for many common commercial magnets and some promising alternatives. (From Kramer, M.J. et al., *JOM*, 64(7): 752–763, 2012.)

Rare earth–Transition Metal™ permanent magnets are considered essential to many military weapon systems. Sm–Co magnets retain their magnetic strength at elevated temperatures and are preferred for military technologies such as precision-guided missiles, smart bombs, and aircraft. The superior strength at lower temperatures and, hence, smaller and lighter NdFeB magnets are also preferred in defense weapon systems.

The characteristics possible in rare-earth magnets have revolutionized magnet design in recent years, most notably in the production of high-performance electric motors, which convert electricity into mechanical motion, and electric generators, which, operating in reverse, convert mechanical motion into electricity.

As a pollution-free, energy-efficient alternative, electric drive systems are or could be part of a range of transport vehicles starting from the smallest, motor assisted bicycles; through cars, SUVs, and trucks; to even large mining and earth-moving equipment. Presently, the main commercial products using electric drives, exclusively or with an internal combustion engine, are electric bicycles, hybrid electric vehicles (HEVs), plug-in hybrid electric vehicles (PHEVs), and all electric vehicles (AEVs). The motor size in a typical electric bicycle is less than 1 kW, compared to a 55 kW traction motor in a Toyota Prius (HEV). The per-unit usage of magnet material ranges from 60 g for bicycles to 350 g for high-power scooters and 2400 g for the passenger car. PM motors (PMMs) and generators (PMGs) are used in, for example, Prius-class HEVs, to power the vehicle as well as to recapture energy associated with braking, respectively. Each Prius HEV requires an estimated 1 kg of Nd + Pr and perhaps 100–200 g of Dy in the various magnets required for operation. The Neo magnet material for use in these thus contains 4–10% Dy, primarily due to the high temperature of the application coupled with localized high demagnetization fields. Almost all mass-produced HEVs and electric vehicles (EVs), which include PHEVs and all-electric vehicles, use rare-earth PMs in the motors that propel them during electric drive operation. In PHEVs and HEVs, a gasoline engine (or generator) and an electric motor are constrained in size and weight to fit within a tight engine compartment, limiting the choice of motor size and operating characteristics. AEVs have no gasoline engine, which allows more flexibility and alleviates space constraints, making it easier to cool the motor.

Electric energy generation via wind power has been an industry holding out many possibilities as a renewable, nonpolluting alternative for nearly three decades. Wind turbine generators convert wind energy into electricity, and neodymium–iron–boron rare-earth PMs are used in wind turbines. Wind power as a viable technology alternative for electricity generation has been increasingly implemented all over the world in the past decade, and during this time, there has been a gradual progression toward larger, more powerful wind turbines. Permanent Magnet Generators (PMGs) used in megawatt-scale, next-generation wind turbines eliminate massive mechanical gearboxes and other components that are subject to reliability issues. The magnets in these large turbines contain an estimated 150–200 kg of Nd + Pr and perhaps 20–35 kg of Dy, per megawatt of generating capacity. Thus, larger turbines are more likely to use rare-earth PMs, to dramatically reduce the size and weight of the generator compared to non-PM designs such as induction or synchronous generators. Another trend is toward turbines equipped with electricity

generators that run at slower speeds, allowing better coupling with the turbine rotor. For a given power rating, slow-speed turbines require larger PMs. Constantinides (2011a) estimated that presently, direct-drive turbines require 600 kg of PM material per megawatt, which translates to several hundred kilograms (~310 kg REO) of rare-earth content per megawatt. The estimates for the future, given by him, reduced the quantity of PM material required per megawatt to 400 kg, possibly anticipating the development of a superior Nd magnet and/or a superior design for the windmill generator.

The rare-earth PM designs still make up only a small percentage of the market for wind turbines, as of now, and the situation will be changing, in all likelihood, in favor of greater use of the rare earths in the world wind power sector. Wind power requirements for rare earths depend on the total installed wind power (megawatts) and the fraction of this total that use PM generators. The numbers listed in Table 1.7 are very informative in this context. The table concludes with an estimate for not only the neodymium but also the critically important dysprosium additive.

In any case, possible uncertainties in the future supply of critically important rare-earth materials Nd and, particularly, Dy have also accelerated the development of alternatives like the superconducting generator turbines, which do not use PMs and which show promise for turbines in the 10 MW+ range. American Superconductor has been developing a 10 MW Sea Titan turbine prototype that uses a direct-drive high-temperature superconducting generator (Constantinides 2012a,b).

1.7.3 Terfenol

Magnetostriction is a property exhibited by certain materials, and these materials are known as magnetostrictive materials. A magnetic field applied to a magnetostrictive material makes it expand or contract, and conversely, when stress is applied to the magnetostrictive material, a magnetic pulse is generated. The property of magnetostriction was discovered in 1971, but it took another 15 years before commercial application of the phenomenon became possible with the development of suitable materials (Jiles 1994). Iron alloys of rare earths such as Tb, Sm, and Dy exhibit properties of very large magnetostriction. The Laves-phase alloy $Tb_{0.3}Dy_{0.7}Fe_{1.9}$ (terfenol-D), in particular, shows outstanding magnetostrictive properties. Terfenol-D was initially developed in the 1970s by the Naval Ordnance Laboratory (NOL) and named after terbium (TER), iron (Fe), and NOL; *D* comes from *dysprosium*. The technology for manufacturing the material was developed in the 1980s at Ames Laboratory under a US Navy-funded program (Clark 1979). The magnetostriction in an applied field exhibited by terfenol is approximately 100 times larger than that of nickel, the well-known metal exhibiting magnetostriction. Terfenol changes dimension in a magnetic field instantaneously, and this effect is essentially at the heart of advanced transducers and micropositioners. Its initial application was in naval sonar systems. Terfenol is also used in areas of high-power actuators, acoustic devices, broadband sonar devices, micropositioners, fluid control valves, and micropumps (Gschneidner and Daane 1988; McGill 1997). Terfenol-D was also slated for use as the smart material to control fluid flow in natural-gas fuel injection in light-duty diesel engines (Hedrick 2000).

TABLE 1.7
The Windmill Story

Country	Cumulative Installed Capacity as of End of 2010, MW	Installed during 2010			Forecast for Installation during 2020		
		Installed MW	% PM Generators	Neo Magnets Required, Metric Tons (Average, 600 kg/MW)	Installed MW	% PM Generators	Neo Magnets Required, Metric Tons (Average, 400 kg/MW)
China	44,733	18,928	95%	10,789	10,000	90%	3600
USA	40,180	5115	10%	307	15,000	75%	4500
India	13,065	2139	5%	64	5000	75%	1500
Spain	20,676	1516	5%	45	3000	75%	900
Germany	27,214	1493	5%	45	1500	75%	450
France	5660	1086	5%	33	1500	75%	450
UK	5204	962	5%	29	1000	75%	300
Italy	5797	948	5%	28	800	75%	240
Canada	4009	690	5%	21	800	75%	240
Sweden		604	10%	36	500	75%	150
Rest of world	30,501	4785	5%	144	15,000	75%	4500
Total	197,039	38,265		11,540	54,100		16,830
Dy requirement at 4.1 wt.%				473			690
Nd requirement at 27.5 wt.%				3174			4628

Source: Constantinides, S., Rare Earth Materials, In *SMMA Management Conference*, Spring, May 10–12, San Diego, CA, 2011.

Dysporium–terbium–iron magnetostrictive alloys are also being developed for use as actuators to allow precision positioning of the next-generation space telescope (NGST) (Hedrick 1998). Incidentally, NGST would have 6 to 12 times the surface area of the Hubble space telescope.

1.7.4 Magnetic Refrigeration

Gadolinium metal and alloys have been considered as the working substance in magnetic refrigeration cycles (Hashimoto et al. 1981). The underlying principle of magnetic refrigeration is that a gadolinium-based solid heats up in a strong magnetic field and cools when removed from the field. This system works even at room temperature but has the greatest prospects in cryogenic applications. Initially, GdPd was used, and later, the gadolinium–aluminum garnet (GAG) single crystal and intermetallics $(Dy_{0.5}Er_{0.5})Al_2$ and $TbNiO_2$ were used as magnetic refrigerants for cooling to as low as 4 K. The refrigerator using the magnetic refrigerant is called the active magnetic regenerative magnetic refrigerator (AMR-MR) (Gschneidner and Pecharsky 2006). The main advantages of the magnetic refrigerator are the compactness and large refrigeration power per unit volume. It is also reliable, vibration free, and more efficient than most cryogenic cooling systems, particularly below liquid nitrogen temperature (77 K).

Gschneidner et al. (1999) have reported two major breakthroughs in magnetic refrigeration. They successfully demonstrated that sub-room-temperature magnetic refrigeration is a viable and competitive technology vis-à-vis conventional gas-cycle compression/expansion refrigeration. In a laboratory prototype refrigerator using 3 kg of Gd spheres as magnetic refrigerant in a magnetic field of 5 T, they achieved a cooling power of 600 W, operating at a maximum temperature span of 30 K, while running the apparatus for more than 1200 h over a 10-month period. They also reported the discovery of the giant magnetocalorific effect (MCE) materials $Gd_5(Si_xGe_{1-x})_4$, which have MCEs ranging from 25% to 200% better than the known prototype magnetic refrigerants such as gadolinium. As an added attraction, their Curie temperatures are tunable from 40 to 290 K by changing the Si–Ge ratio in this material. These new materials can make magnetic refrigeration more efficient. Refrigeration systems based on the new material can have applications in home and automobile air-conditioning and in household appliances like refrigerators, freezers, and ice makers (Hedrick 1997).

Magnetic refrigeration has great potential for improving the energy efficiency of the refrigeration process using rare-earth PMs. Before this technology can capture a significant share of the refrigeration market, issues like the timeline for commercialization, projected demand, and material intensity of the commercial products need to be sorted out.

1.7.5 Ceramics

Rare-earth oxides, particularly ceria and yttria, are used as sintering aids in powder metallurgical fabrication due to their ability to eliminate weakening voids (Jackson and Christiansen 1993). For instance, during the sintering of silicon nitride, the Si–Y–O–N liquid phase is formed. On cooling, the nitride grains regroup, the yttrium

oxynitride cools into a microcrystalline intergranular bond between the grains, and this resists crack development. The silicon nitride thus obtained is used in hot-zone engine parts and high-speed cutting tools.

Yttria has a major use in the stabilization of the high-temperature cubic phase of zirconia. Yttria-stabilized zirconia (YSZ) is one of the best high-temperature, high-strength, and thermal shock-resistant refractory compositions that remain chemically stable at elevated temperatures. It has high thermal insulation properties and is used as a barrier coating to protect hot parts in jet engines. Due to the presence of oxygen defects, YSZ has an electrical resistivity that permits its use as an oxygen sensor in automobile exhaust systems. YSZ has also been adopted for use as an SO_2 sensor (Hedrick 2000). The concentration range of SO_2 can be sensed from 1 to 1000 ppm.

An integral part of the emission-control system in automobiles is the exhaust oxygen sensor, which feeds back information for control of the air–fuel ratio. This is necessary to ensure that the exhaust gas composition is very near the stoichiometric point so that the catalytic converter system, which not only oxidizes the hydrocarbons and carbon monoxide in the exhaust gases but also reduces the nitrous oxide, operates efficiently (Kennard 1981). Stabilized zirconia is a key material in this sensor. The stabilizer used is calcia, magnesia, or yttria. While calcia or magnesia stabilization has cost advantages, yttria stabilization results in better ionic conductivity. Ytterbia is still better but more expensive. Oxygen sensors based on YSZ also have use in industrial furnaces and in the measurement of oxygen content in molten glass, molten steel, and other metals. They are also used in research in solid electrolyte galvanic cells. In medicine, YSZ is used for hip replacement parts, and in dentistry, it is used for tooth filling. YSZ has also been used as an electrode in the high-temperature electrolysis of water. YSZ cells have been tested in certain advanced space programs for the production of O_2 from CO_2 (McCallum 1998).

The formation of a solid solution of ceria with, for example, trivalent cations such as Y or La results in oxygen ion vacancies that are mobile. Oxygen diffusion is fast, whereas the cation diffusion is slow. The defect fluorite structure thus formed has good oxygen conductivity and is considered a novel electrolyte for temperatures above 600°C.

A long-life (>5000 h) ceramic heating element for use in air up to 1900°C is based on $La_{0.84}Sr_{0.16}CrO_3$. This material combines electrical conductivity and structural rigidity in an oxidizing environment and has significantly extended the operating temperature range of compact furnaces in air.

Many application possibilities have been indicated (McGill 1997) for rare earths in ceramics. These include the use of La_2O_3, Y_2O_3, and CeO_2 with Ni, Co, Cr, or Zn as electrodes in fuel cells with a zirconia–yttria solid electrolyte and the use of $LaCrO_3$ and $LaCoO_3$ electrodes in magnetohydrodynamic generators. Rare earths containing perovskites have been considered for certain catalytic applications (Gunasekaran 1988). In fact, rare-earth perovskites, represented generally by $REMO_3$, where M is a transition metal, are of continuing interest in many developing technologies. These are electrocatalysis, high-temperature electrodes and electrolytes, and membranes for gas separation and sensors (Molycorp 1993). The wide range of application also results from a possibility for fine-tuning of the structure in these compounds.

The electrical conductivity of $CaCrO_3$ is fairly constant at around 0.1 $(\Omega\text{-cm})^{-1}$ in the range of 500–1900°C. The conductivity can be greatly increased by adding calcium and strontium at levels up to 20 mol.% to give $(La,M)CrO_3$. Further, the conductivity of $Ca_{0.84}Sr_{0.16}CrO_3$, already >2 $(\Omega\text{-cm})^{-1}$ at room temperature, rises to >10 $(\Omega\text{-cm})^{-1}$ above 300°C and remains close to this value up to 2000°C. There are two important uses for $(La,M)CrO_3$. One is as furnace-heating elements. The most important use is as the crucial intercell conducting material in solid oxide fuel cells (SOFC) (Minh 1993).

Ceramic fuel cells, also called SOFCs, generate electricity directly from the reaction of a fuel with an oxidant. Power is produced electrochemically by passing a hydrogen-rich fuel over the anode and air over the cathode and separating the two using an electrolyte. In producing electricity, the only byproducts of SOFC are heat, water, and CO_2. Prototypes like 1 MW microturbine power plant fuel cells operate at temperatures around 1000°C, where rare-earth ceramics such as $LaMnO_3$ (p-type conductor) and Sr-doped $LaMnO_3$ (cathode), which have a high electronic conductivity in oxidizing atmospheres, are considered attractive. Another perovskite, $(La,M)CoO_3$, has properties to be considered for possible use as catalytically active electrodes stable in high-temperature, aggressive environments for fuel cells and sensors (Molycorp 1993).

Fuel cells are a promising clean energy technology for vehicle propulsion, auxiliary power, and distributed power generation. Rare-earth elements are used in several different fuel cell chemistries. In particular, SOFCs for distributed power generation commonly use yttrium in their electrolyte and may also use lanthanum, cerium, nickel, and cobalt in other components. The National Energy Technology Laboratory (NETL) estimated that commonly used SOFC designs may require 21 g of yttrium oxide per kilowatt of fuel cell capacity (i.e., less than 0.5% of current yttrium production at 4 GW/year of new capacity). However, some commercially established stationary distributed power fuel cells as well as polymer electrolyte membrane fuel cells used in fuel cell vehicles do not rely on rare earth materials.

Pure cerium oxide has been used as an opacifier in ceramic glazes (Greinacher 1981). In the 1960s, praseodymium (Pr_6O_{11}, 90%) was used with zirconium oxide, in the ratio of 62–64% ZrO_2, 32–33% SiO_2, and 3–6% Pr_6O_{11} (Kudo 1988), as a beautiful yellow pigment in ceramics. Praseodymium is built into the zirconium silicate lattice and thereby results in the full optical splendor. The praseodymium pigment is stable at high temperatures.

Cerium sulfide, CeS, and yttria are also used as materials for making crucibles apart from their use as high-temperature materials (McGill 1993). CeS has one of the most negative free energies of formation for sulfides and has been proposed as a containment material for very reactive molten metals such as uranium and titanium (Krikorian and Curtis 1988). CeS has electrical conductivity like metal, high thermal conductivity, a high melting point (2442°C), and good thermal shock resistance, and is also machinable like a metal (Molycorp 1993). Samarium, europium, gadolinium, and dysprosium oxides are used in the nuclear industry in radiation-shielding ceramic compositions. Rare-earth (Eu, Sm, Ce) oxides have also been used to improve light fastness of lead chromate and titanium dioxide pigments and also to impart natural fluorescence to artificial teeth.

In 1971, Heartling and Land (1971) first reported achieving optical transparency in a ferroelectric ceramic material, lanthanum-modified lead zirconate titanate (PLZT) solid solution. The PLZT ceramics [$Pb_{1-x}La_x(Zr_{1-y}Ti_y)O_3$] have interesting applications in military and industrial devices. These applications include use in thermal/flash protection goggles, data display recorders, stereoviewing systems, eye safety devices such as electronic welding helmets, and image storage devices (Heartling 1981). The basic operation of these devices relies on the change in the optical properties of the ceramic with the strength and direction of the electric field applied to it, and the changes are brought about rapidly. The use of PLZT as an electromechanical transducer and its piezoelectrical properties have also been studied (McGill 1993). The rare earth used in these applications is lanthanum, and the PLZT is made by conventional ceramic fabrication methods of hot pressing and polishing. Remarkable effects on optical transparency are achieved when the amount of lanthanum exceeds 7 at.% in the ceramic.

The attractive thermionic properties of LaB_6 were identified by Laferty (1951) at General Electric Company, USA. This compound, with a melting point above 2500°C, also has low vapor pressure, low work function, and excellent thermionic emission current. It is superior to tungsten but is more expensive. It is used in the electron gun of electron microscopes, where high electron intensities are very desirable.

More than any other material LaB_6 shows resistance to attack by aggressive fluorine at very high temperatures. This property leads to many strategic applications involving fluorine gas. The resistance is conferred by the formation of an adherent fluoride film on the boride (Molycorp 1993; Holocombe and Kovach 1982).

Researchers in China have noted that when rare earths are incorporated in a cemented carbide, a 50–100% improvement in carbide tool life was observed. The improvement is, however, dependent on both the rare earth used and how it is incorporated in the mixture (Hedrick 2001).

Gas turbines for stationary power generation use yttria for thermal barrier coatings of turbine blades. In lesser amounts, yttria is also used in bond coatings, high-temperature overlay coatings, substrates, and structural supports. These coatings are applied during initial manufacture and, later on, as a maintenance requirement reapplied periodically over the decades of turbine life. The initial and recurring requirements for yttria in this application, when considered in the context of a large global power generation capacity, could qualify it as a significant global demand for yttrium in the future years.

1.7.6 Electronics

The hexaborides of rare earths are unique electrical resistor materials in that they have near zero temperature coefficient of resistance, a feature not seen in metals. The formation of glass frits and LaB_6 can be screen printed and fired to provide resistor components required in modern integrated circuitry (Molycorp 1993).

Rare-earth materials find use in electronic devices that convert one form of energy to another (Jackson and Christiansen 1993). Both input and output are electricity in some cases, but the output variance is determined by thermal or radiation energy. In these materials, the rare earths are added to synthetic garnet crystals such

as yttrium–iron, yttrium–aluminum, and gadolinium–gallium. Yttrium–iron garnets (YIGs; $Y_3Fe_5O_{12}$) have important uses communication devices. Yttrium and gadolinium are also used in garnets for microwave applications. Besides use as microwave filters, yttrium–aluminum garnet (YAG; $Y_3Al_5O_{12}$) crystals, when doped with small quantities of neodymium or erbium, can be used for lasers. The YAG single crystal has many desirable properties for use in high-power solid-state lasers. It is hard and optically isotropic and has sites suitable for trivalent rare-earth ion substitution without charge compensation. The most common solid-state laser is based on neodymium (Weber 1979). It is usually in a glass or YAG host. Neodymium is present at around 1–5 wt.% in the host. When exposed to intense broad-spectrum light, Nd atoms absorb the light and are pumped to an excited energy state. Then the lasing transition to a lower energy level occurs with light emission at or very close to 160 nm. The exact wavelength depends on the host. Neodymium-doped YAG (Nd:YAG) emits at 1064 nm, which is in the infrared (IR) region. This laser is quite popular in cutting, welding, and metal heat-treating applications. The Ho–YAG and Er–YAG lasers emitting at 2000 and 2900 nm, respectively, have been developed for use in microsurgery, in place of CO_2 lasers. Ho^{3+} ion lases at ≈2.08 μm, an eye-safe wavelength. Er–YAG lasers lasing at ≈2.9 μm have also been found useful in dental work (McCallum 1998). This wavelength is sharply absorbed by water. It is thus possible to deliver energy without thermal buildup in tissue. Single-crystal gadolinium–aluminum–scandium garnet (GASG) doped with nickel and chromium is likely to be used in tunable and high-power laser applications. Neodymium-doped $Gd_3Ga_5O_{12}$ (GGG) crystals are used in high-power pulsed lasers. A frequency-doubled 532 nm Nd:YAG laser with a green beam is suitable for medical use. Rare earths such as Pr, Nd, Ho, Er, and Tm in hosts such as $CaWO_4$, YAG, and $LiFY_4$ are materials for optically pumped or activated solid-state lasers with a wide variety of wavelengths.

Multilayer capacitors essential to electronic equipment require dielectrics with a high electric constant and a capacitance invariable over a wide temperature range, –50°C to 120°C. The so-called NPo dielectric material used in such capacitors contains neodymium–barium titanate formulations. The components are probably $BaO:Nd_2O_3:nTiO_2$ ($n \approx 3$–5) (Molycorp 1993). Rare earths have also been useful in the miniaturization of capacitors (La_2O_3, Gd_2O_3, Dy_2O_3) and in the production of thermistors (Haskin and Paster 1979). Gadolinium oxide has been used in making optical fibers. Significant quantities, several hundred tons, of cerium are used annually, in the form of cerium ammonium nitrate solution for etching on substrates in the electronic manufacturing industry (Kudo 1988).

1.7.7 Chemical

The single largest application of rare earths, in which the naturally occurring rare-earth mixture is useful, is the manufacture of rare earth-containing zeolite cracking catalysts required in petroleum refining (Wallace 1981; Venuto and Habib 1979). In a refinery, crude oil is distilled into different streams—the lighter-molecular-weight streams (comprising gasoline, kerosene, and diesel) and the heavier-molecular-weight streams. The heavies are processed further, to be broken down into lighter products. The fluid catalytic cracking (FCC) process breaks apart or cracks heavy input

streams into primarily gasoline and diesel fuel, but also light hydrocarbon gases, heavy oil, and coke. As revealed by the name, FCC catalysts are used for the cracking, and the main use of rare earths in petroleum refining is in the FCC unit.

In the early 1960s, it was discovered that incorporation of small amounts of zeolite in a silica–alumina matrix resulted in considerable enhancement in the performance of the catalyst in gas–oil cracking. From then on, zeolite cracking catalysts have largely replaced the amorphous silica–alumina catalysts used previously. Zeolites are made catalytically more active and thermally more stable at the operating temperatures by replacing the sodium in them with rare-earth ions. Rare earth-exchanged zeolites are prepared by many methods, and the rare-earth content of the catalyst may vary from 0.5% to 5%. The rare-earth starting material used for the manufacture of these catalysts is usually a mixture of (light) rare-earth (mainly lanthanum and cerium) chlorides or nitrates. Rare-earth usage in commercial petroleum cracking catalysts started in 1964.

FCC catalysts are manufactured to have composition and shape to increase the speed of the cracking process and to yield the right mix of products—in this case, light olefins (propylene and butylenes), gasoline, and diesel. Lanthanum and Cerium are added to the catalytic compounds, to take advantage of their ability to interact with the hydrogen (H) atoms found in the long-chain hydrocarbon molecules in the starting raw material. This interaction aids in the transformation of the heavy oil into useful petroleum products. The amount of REOs in FCC catalysts increased from an average of 1.2% in 1994 to about 2.9% in 2010. Higher REO content results in higher gasoline yield, but it also lowers octane content in the FCC gasoline. Presently, octane loss is not considered critical, because with increased blending of high-octane ethanol into gasoline, the need for higher-octane FCC gasoline has fallen. Cerium is used in some FCC additives (4% and 15% cerium oxide by weight) to reduce sulfur oxide (SOx) emissions, when sulfur in the crude is an issue.

In the chemical process industry, rare-earth elements have been used or considered for use as catalysts for ammonia synthesis, alkylation, isomerization, hydrogenation, dehydrogenation, dehydration, polymerization, refining of hydrocarbons, and oxidation (Molycorp 1964–1970, 1971–1976; Rosynek 1977; Peters and Kim 1981). Methanation catalysts contain rare earths; the ability of rare earths to form hydrides is useful here (Coon et al. 1978).

Catalytic converters have been used in automobiles since the 1970s to convert hydrocarbons, carbon monoxide, and nitrogen oxides in the engine exhaust to water, carbon dioxide, and nitrogen. The catalysts comprise γ-alumina and small amounts of precious metals, and are activated by ceria, which is about 5% by weight. CeO_2 is the primary rare-earth compound used here, usually in conjunction with platinum-group metals. Some La_2O_3 and Nd_2O_3 are also added to ceria. Ceria provides oxidation resistance at high exhaust temperatures, stabilizes rhodium and palladium dispersions, minimizes the interaction of rhodium with alumina, and enhances the oxidizing ability of the system. Efforts have also been made to substitute lanthanum-enriched palladium for the more expensive rhodium.

The role of ceria in automotive exhaust catalysts is complex. In addition to enhancing the catalytic activity of precious metals deposited on it, its function is described as “an oxygen storage component” that enhances performance when the

exhaust gases are fuel rich/air poor. Anyway, ceria is a crucial ingredient in the catalysts used to control vehicle exhaust emissions, and an average catalytic convertor contains approximately 50–75 g of CeO_2 (Molycorp 1993).

While the amount of cerium required per vehicle is not much, catalytic converters are used in practically every passenger vehicle. The demand for cerium in catalytic converters will continue to grow with increasing global automobile deployment and the continuing need for replacement vehicles. Cerium is the most abundant rare earth and can support the increased demand anticipated in both the short and medium terms.

The division of the total rare earths used in various streams of catalyst applications is as follows. The numbers pertain to the year 2008 (Goonan 2011). The total of 27,400 t REO used as catalysts was essentially accounted for by two bulk uses. FCC usage consumed 72% of the total, and automobile catalytic converters used the remaining 28%. In that year, 98% of the total of 18,200 t of lanthanum oxide consumed for catalysts went to fluid cracking and only 2% to automobile catalysts. Out of 8820 t of cerium oxide used for catalysts, only 22% went to fluid cracking, and 78% went to automobile catalysts. Apparently, rare-earth catalyst consumption for other chemical processes did not amount to a significant quantity.

1.7.8 Optical

The optics industry encompasses a vast range, from glasses through lasers and fiber optics to phosphors and fluorescent lights. Through the use of rare earths in these products, vast improvements in communication and vision have been achieved. The 4*f* electrons in the rare-earth elements possess narrow and sharp absorption–emission lines in the visible range, and this plays a central role in the use of rare earths in the optics and phosphor industries.

Rare earths are added to glass to perform certain specific functions—absorbing UV light, altering the refractive index, colorizing, and decolorizing. An early and continuing use of the rare earths is in the manufacture of glass. In 1896, Dressback patented and manufactured a mixture containing cerium and other rare-earth oxides for decolorizing glass (Riker 1981). This, incidentally, was the first commercial use of cerium. Iron oxide is always present as an impurity in glass and causes a yellow-green color. If decolorizing is necessary due to iron contained in the glass, cerium is added to oxidize the iron. While a chemical decolorization of iron is achieved by oxidation to the trivalent state, physical decolorization is achieved by selective absorption by didymium through optical compensation. A combination of chemical and optical decolorization may be used.

While small amounts of CeO_2 decolorize glass, ~1% CeO_2 makes glass yellow, and larger amounts of CeO_2 make glass brown. Neodymium colors glass bright red, praseodymium colors glass green, and their mixture colors glass blue. Holmium also colors glass blue. Erbium oxide gives a pale pink color to glass, and this color cannot be obtained by any other means (Riker 1981). Because of the stability of trivalent erbium, glass formulations with Er are colored pink. It is the only pink truly stable in glass melts. Pink coloration by erbium is used in ophthalmic materials like sunglasses as well as in decorative crystal glassware. Coloration in glass due to

impurities such as ferric ions can be neutralized or complemented by erbium absorption, resulting in the formation of a neutral gray, colorless shade. Incidentally, this is the dominant use for erbium, and erbium oxide of ~96% purity can be used for this purpose (Molycorp 1993). Further coloring effects are obtainable by combining rare earths with other elements, for example, titanium + cerium for yellow, selenium + neodymium for violet, and nickel + neodymium for red. Cerium is used only in conjunction with other coloring oxides.

In 1912, Crookes of England found cerium to be excellent for UV absorption without imparting color to the glass, a feature useful in protective eyeglasses. Crookes absorptive sunglasses contain the natural ratio of Nd to Pr together with a high amount of Ce to give a good UV cutoff. Glasses with 2–4% Ce_2O_3 (or Pr, Nd oxides) absorb UV and IR radiation and are used in the production of glassblowing and welding goggles. Didymium oxide has long been used in welders' goggles because of a high concentration of Nd and Pr, which effectively absorb yellow sodium light.

A neodymium-doped glass lightbulb has been introduced by GE for use in typical incandescent applications around the home. The powder-blue-colored bulb uses neodymium to absorb the yellow spectrum, which is more prevalent in the emission from a tungsten filament than from natural sunlight and provides a more sunlight-like light with richer colors and improved surface definition of the home environment (Hedrick 2001).

Neodymium oxide together with vanadium trioxide is used for making optical glass for photometers and Nicol prisms. Most cathode ray tube (CRT) faceplates use Ce-stabilized glass. Cerium prevents browning/fogging of glass under nuclear radiation (γ-rays and cathode rays). Large quantities of radiation-shielding windows, which provide very high transmission without darkening due to formation of color centers, were needed in the nuclear industry. As the result of much development work in the 1950s and 1960s, cerium is used in radiation-shielding windows. Cerium in container glass prevents colorization caused by UV radiation and protects the product.

Lanthanum was first used in the optical glass industry in 1935 by Morey (1938). Low-silica glass containing lanthanum oxide possesses a high index of refraction and low dispersion and is extensively used in the manufacture of camera and other lenses (Greinacher 1981). Optical glass for camera lenses is made from a "lanthanum–flint" composition containing La_2O_3 and B_2O_3 (Molycorp 1993). Lanthanum oxide does not impart color to the glass. Optical glasses containing up to 40% lanthanum oxide are made, and these are also corrosion resistant. Gadolinium is also added to optical glasses meant for use in magneto-optical and electro-optical systems. It is very important that the rare-earth materials introduced into the optical glasses be 99.9–99.995% rare-earth oxide (Riker 1981) and that no radiation-absorbing impurity oxides are present. In Japan, the world's largest manufacturer of optical glasses, consumption of La_2O_3 has been considerable because of large-volume production of autofocus single-lens reflex (SLR) cameras and video cameras. Praseodymium is used for vacuum-deposited antireflection coating on lenses and as a constituent in tinted glass filters for selective light absorption.

The rare-earth elements act as activators in laser glasses. Neodymium is the most popular rare earth for this purpose (Greinacher 1981), and this use has already been described. Neodymium can be incorporated in very large glass rods, and intense

pulses (up to 10^{15} W) can be generated from neodymium lasers (Singh 1988). A rare-earth laser crystal, neodymium (Nd^{3+})-doped lithium niobate ($LiNbO_3$), emits a continuous three-color beam: red, green, and blue. The red and green emissions are obtained by frequency doubling, and the blue emission is created by self-sum frequency doubling (Hedrick 2001). Glasses doped with rare earths such as Nd, Yb, Er, and Ho could possibly find future technological applications in the areas of luminescent solar concentrators and as light sources for fiber optics in addition to use as laser materials. Luminescent solar concentrators have been prepared using a combination of Nd^{3+} and Yb^{3+} with UO_2^{2+} or Cr^{3+}. Fluoride glasses for fiber waveguide sources contain Er^{3+}. Glass fibers containing rare earths can transmit data over exceptionally long distances without booster stations. The glass for these fibers, which may be composed of fluorides of lanthanum, zirconium, barium, aluminum, sodium, and hafnium, is formed by chemical vapor deposition, rather than through a melt, to minimize impurities (Jackson and Christiansen 1993). Erbium-doped fiber amplifiers (EDFAs) are used for optical communications in terrestrial long trunk and undersea cable applications (Auzel and Goldner 1999). This is the current major high-technology application of erbium. Optical telecommunications rely on signals transmitted down silica fibers. The signals use a wavelength of 1.55 μm, which is a low-loss wavelength window in the fiber. Incidentally, erbium lases efficiently at this wavelength in the fiber and can be pumped by light of other wavelengths, such as visible or near IR, thus enabling a very efficient optical method of amplification.

An EDFA contains lengths of fiber, doped with part-per-million levels of erbium spliced into the optical fiber at regular intervals. Along with the signal energy, the pumping energy is also transmitted down the fiber. The Er in the EDFA lases, amplifying the longer wavelength light signals that also propagate down the complete fiber.

The first application of cerium oxide or cerium-rich rare-earth oxide mixture in glass polishing began in the European glass industry by about 1933 and spread to the Canadian optical industry by about 1940 and to the United States in the following years (Duncan 1970; Horrigan 1981). Special REO compositions containing 50–90% cerium oxide, the remainder being other light rare-earth elements, are used to polish glass surfaces without abrading. Polishing agents such as rouge, silica, and zirconia are slow and dirty and leave minute scratches. REO compounds are much faster and cleaner and provide a superior finish. Polishing with REO is mostly a chemical reaction, and water plays an active role. In the use of ceria-based REO compositions for glass polishing, typically, the polishing powder is sprayed on spinning glass, where chemical dissolution and mechanical abrasion occur together to provide a superior polished glass surface (Goonan 2011). This is according to the chemical–mechanical hypothesis (Horrigan 1981). In the polishing process, the formation of a CeO–Si activated complex permits the rupture of O–Si–O bonds by hydrolysis. Subsequently, the complex CeO–Si breaks apart, the hydrated silica is swept away along with the alkalis released from the glass surface, and the process repeats.

1.7.9 Phosphors

Phosphors are used in devices that require color in the light exhibited. Not every phosphor contains rare-earth elements, but many of the present-generation phosphors

do (Goonan 2011). The radiant energy incident on the phosphor is reemitted as light of a certain color depending upon on the properties of the elements included in the phosphor. A certain amount of fine-tuning is possible here. Since a larger fraction of the electrical energy is converted into light than with conventional light sources, phosphor materials are significantly more energy efficient than older technologies, requiring a lot less electricity to produce the same output.

The first application of a rare-earth element in a sophisticated technology was in 1965, when a rare earth-containing alternative was introduced to the erstwhile red phosphor in color television picture tubes. The work of Levine and Palilla (1965) established that a material consisting of Eu doped in an yttrium-containing host, YVO_4:Eu^{3+}, was superior as red phosphor to the Ag-activated CdS red phosphor. The strong and sharp emission lines of europium at 610 nm without a yellow component, perceived by the eye as a wonderfully saturated red color tone, provided an evenly colored TV picture. Subsequently, YVO_4 was replaced by either Y_2O_3 or Y_2O_2S. Both these phosphors are better than the vanadate because their energy conversion efficiency is greater and their emission is a bit more orange. Color for television and computer screens is obtained through the use of three phosphors: a europium–yttrium compound for red, a terbium fluoride–zinc sulfide for green, and a cerium–strontium sulfide for blue. When activated by photons, these phosphors emit the luminescence that makes the screen attractively colorful. Each color TV screen requires approximately 5–10 g yttrium oxide and 0.5–1 g europium oxide (Jackson and Christiansen 1993). Since 1964, the TV industry has been using highly purified Y and Eu oxides in ton quantities. The purities required exceed 99.9%, and many individual impurities in excess of 100 ppm may be deleterious. The TV faceplate contains neodymium oxide, which blocks ambient light from ruining the picture.

A new rare-earth phosphor, lithium-doped Gd_2O_3:Eu^{3+}, was developed in South Korea for flat-panel field emission displays. This phosphor is said to have higher cathode luminescence than the widely used commercial phosphors, europium-doped yttrium oxide and europium-doped yttrium oxysulfide (Hedrick 2000).

Another phosphor with potential use for field emission arrays to produce compact lightweight displays that consume less electricity than CRTs is the green rare-earth phosphor $SrGa_2S_4$:Eu^{2+}. This could potentially substitute for the use of the standard green CRT phosphor ZnS:Cu, Al (Hedrick 1998). Several CRT phosphors contain Tb, for example, Tb:YAG and Tb:Y_2SiD_5, a phosphor for high-intensity green emission needed for projection TVs (Welker 1991; Ronda et al. 1993).

Rare earth-based phosphors are composed of rare-earth activators and host lattice. The optical spectral inertness of hosts such as lanthanum, gadolinium, yttrium, and lutetium ensure that they do not interfere with the activator emission spectra. There is an added advantage of close chemical similarity, which makes substitutional incorporation of rare-earth activators in these hosts possible. Besides, rare-earth hosts such as oxides, oxysulfides, phosphates, vanadates, and silicates are rugged materials compatible with high-temperature operations involved in tube processing and in their reclamation (McColl and Palilla 1981). Some more examples of CRT phosphors are Ce_2O_2S:Tb^{3+}, CaS:Ce^{3+}, and $SrGa_2S_4$:Eu^{2+} for green and $SrCl_5(PO_4)$:Eu^{2+} and ZnS:Tm^{3+} for blue (McGill 1993).

An organolanthanide phosphor (OLP) for potential commercial use in flat-panel displays was developed by researchers at the University of Oxford, UK. The polymer material is an organoterbium emitter. A high-efficiency organic electroluminescent device that produced a green light with a peak luminescence of 2000 cd/m^2 was also fabricated (Hedrick 2001).

Ce(III) has no absorption bands in the visible spectrum but does absorb strongly just outside it, in the UV region. Solids with Ce(III) often show strong optical absorption and luminescence in the UV or near UV. Cerium is used in several CRT phosphors. In fluorescent lighting, Ce is also used as a sensitizer for other lanthanide emitters.

A number of rare-earth phosphors have been developed for conversion of x-radiation into visible light, which then strikes photographic film (Rabatin 1981). Phosphors that consist of Tb^{3+}–Gd_2O_2S or Yb^{3+}–La_2O_2S, Eu–BaFCl, Tm–LaOBr, and La_2O_3–Tb have allowed significant reduction in the x-ray dosage required for medical radiographic data. For example, Tb-activated gadolinium oxysulfide, currently the most popular x-ray phosphor, enables up to 80% lower x-ray dosage to patients. In addition to reduced exposure of patients as well as staff, the advantages of rare-earth phosphors over the originally used calcium tungstate phosphor include need for less silver in the film and a sharper picture because of reduced patient movement within a shorter time interval (Jackson and Christiansen 1993). Eu-based phospholuminable phosphors are in use for the automation of x-ray detection systems. The phosphor used is Eu-doped BaFBr or its variants. The phosphor used absorbs the x-ray radiation. In a separate processing step, later, upon stimulation by a small spot laser beam, the phosphor emits visible radiation proportional to the absorbed dose (Crawford and Brixner 1991). Gadolinium compounds act as hosts in scintillator materials such as Eu:$(Y, Gd)_2O_3$, Pr, or Ce:Gd_2O_2S for computed tomography (Greskovich and Duclos 1997). The RE_2O_2S materials account for a significant fraction of the world's use of rare-earth elements. Important among these are Y_2O_2S for TV phosphors and other oxysulfides for x-ray screens. The luminescence of Tm under x-ray excitation is in the near UV (=375 nm) and blue (=465 nm). This closely matches the sensitivity of normal photographic film. Tm:LaOBr is a sensitive x-ray phosphor helpful in the reduction of x-ray exposure of patients (Molycorp 1993).

Scintillation is a flash of light produced in a phosphor by absorption of an ionizing particle or photon, and a scintillation counter is a device for detecting and counting scintillations produced by ionizing radiation. Scintillation detectors are used to detect x-rays and γ-rays. A lanthanum chloride compound doped with 10% trivalent cerium emits at 330 and 350 nm. This compound may be used as a scintillation detector. The cerium-doped lanthanum chloride compound has better energy resolution and improved response times compared with the thalium-doped sodium iodide—the most commonly used scintillation detector material (Hedrick 2000).

Rare earths are also useful as lamp phosphors. The three spectral lines most important to human vision are blue-violet near 450 nm, green near 535 nm, and orange-red near 615 nm. Lamp phosphors activated by Eu^{2+} supply the blue-violet color. Commercial phosphors based on the broad emission of Eu^{2+} at just the right spectral position for the blue are Eu:$Sr_5(PO_4)3Cl$, Eu:$BaMg_2Al_{16}O_{27}$, and Eu:$Sr_4Al_4O_{25}$. Trivalent terbium, holmium, and erbium are candidates for pure green

emission but had problems compared to the old trustworthy zinc silicate:Mn^{2+}. Thus, the addition of rare earths to the phosphors in fluorescent lamps makes the light appear more natural. Some of the phosphors using terbium's green emission are Tb:(La,Ca)PO_4, Tb:$CaMgAl_{11}O_{19}$, and Tb:(Ca,Cd)MgB_5O_{10}. Europium and terbium are used as activators, with yttrium, lanthanum, or gadolinium as hosts. The resultant light is stronger and leads to approximately 25% savings in capital and operating costs (Jackson and Christiansen 1993). Energy-efficient illumination, ranking high in visual efficiency, is given by rare-earth phosphors based on scandium also.

In another application, CaF_2:Eu is placed in front of a solar cell to convert UV sunlight into the visible region, where the solar cell can efficiently convert it into electricity (McCallum 1998).

Scandium, in small amounts, has been widely used by the lighting industry in the manufacture of metal halide lamps. Because of the hygroscopicity of the scandium iodide, it is incorporated by a special process that forms the iodide *in situ* in the lamp by reacting a small piece of scandium with elemental iodine. Scandium metal is used by lamp manufacturers in the form of uniform small disks (Davies 1981). Dysprosium is also used in metal halogen lamps to improve brightness (Kudo 1988).

At high temperatures, the atomic emission spectrum of dysprosium contains many lines in the visible region. Dysprosium is added to the lamp phosphor as an anhydrous halide, e.g., DyI_3. The salt dissociates in the lamp's hot center, absorbs energy there, and emits radiation efficiently to produce high-intensity illumination. The ions later recombine at the lamp's cooler wall surfaces (Molycorp 1993). The cycle repeats.

On rare earths in lamp phosphors, Thornton (1981) stated that the emission from rare-earth phosphor is not only useful but also made to order for the requirements of the human visual system for optimal seeing.

Rare-earth silicates are useful phosphor hosts. Yttrium orthosilicates are commercially used phosphor material and also have potential for projection TVs. The high efficiency and very fast decay time of Ce:$Y_2Si_2O_7$ make it suitable for CRT use. Ce:Gd_2SiO_5 is a potential scintillator for positron emission imaging and γ-ray detection (Molycorp 1993). A new class of luminescent materials represented by the blue-white phosphor Sr_2CeO_4, which has an unusual type of one-dimensional chain structure, has uses in flat-panel displays and fluorescent lighting. It was also useful in television and computer CRT monitors, and in temperature-sensing devices (Hedrick 1998). The samarium compound SrB_4O_7:Sm^{2+} is usable at above 100 GPa and to a temperature of 800 K. This is the material in a new optical pressure gauge developed for diamond anvil cells. Pressure measurement is based on a shift in the fluorescence line of the material. Traditionally, a shift in the fluorescence line of ruby was used for pressure measurement, and a samarium compound emits in the same range as ruby but with a higher intensity.

1.7.9.1 Technology Transition in High-Efficiency Lighting

Approximately 18% of electricity use, for instance, in US buildings goes into lighting—second only to space heating (DOE 2009). Modern technologies provide opportunities to significantly reduce energy demand from lighting. The traditional incandescent lightbulbs in widespread use today need considerably more energy

than twenty-first century alternatives, including fluorescent lighting, light-emitting diodes (LEDs), organic light-emitting diodes (OLEDs), and halogen incandescents.

New and improved incandescent halogen bulbs use 25–30% less energy on average and last up to three times longer than conventional incandescent lightbulbs. Normally, only a small portion of the energy used by an incandescent bulb is converted into light, while the rest is emitted as heat. Special reflective coatings are applied to gas-filled capsules that surround the bulb's filament in the halogen incandescents. The coatings act as a sort of heat mirror that bounces heat back to the filament, where it is transformed to light. The light given off by incandescent halogens resembles the familiar warm glow of old-fashioned bulbs. They are dimmable and are the most similar in shape and size to standard lightbulbs, but also reduce energy use. While these halogen incandescents may provide a smoother transition for consumers, they are less efficient and have shorter life expectancies than compact fluorescent lamps (CFLs) and LEDs. However, the halogen incandescents have been generally more acceptable to consumers.

The transition to new lighting technologies is underway around the world. Many countries now limit or prohibit the use of traditional incandescent lightbulbs. The first substitutes will likely be fluorescent lightbulbs (both compact and linear). Within a few years, the demand for LEDs and halogen incandescent lamps will grow, in many cases replacing the demand for fluorescent lighting. Fluorescent lightbulbs depend on phosphors made from terbium, europium, and yttrium. LEDs use much less rare-earth content than fluorescent lightbulbs, while OLEDs and halogen incandescents use no rare earths. The total rare-earth content in LEDs is estimated at one to two orders of magnitude lower than fluorescent lights of equivalent light output (GE 2010).

The efficacy of solid-state lighting (SSL) based upon InGaN LEDs has improved by >10× over the past decade: the efficacy of cool white LEDs surpasses linear fluorescent lamp (LFLs) efficacies (>100 lm/W), and that of warm white 1 W LEDs surpasses CFL efficacies (>60–70 lm/W). A 2015 efficacy target of 138 lm/W for warm white packages has been set by the US Department of Energy (DOE) (Setlur 2009).

In LED-based SSL, violet, blue, and green LEDs are based upon InGaN semiconductors, while the red and amber LEDs are based upon AlInGaP semiconductors. Both of these semiconductor systems have lower efficiencies in the green, yellow, and amber spectral regions. The limitations in InGaN (termed pc-LEDs) and AlInGaP efficiency make it necessary to use phosphor down-conversion to generate green and yellow light for high-efficacy LED packages, lamps, and fixtures. The maximum efficiency of blue and violet InGaN LEDs appears to be higher than the maximum efficiency for red (lmax = 600–630 nm) AlInGaP LEDs. The potential efficacy for a system that uses phosphor down-conversion of InGaN LEDs for the entire white spectrum could be greater than for systems using AlInGaP LEDs to generate red light. There has been extensive research and development on phosphors in LFLs/CFLs, CRTs, and x-ray films, but most of these traditional phosphors are not suitable for pc-LEDs (InGaN LEDs). This is usually because these phosphors do not strongly absorb violet or blue LED radiation, and there are issues of decay times and phosphor quenching. New phosphors needed to be specifically developed for pc-LEDs. Using Ce^{3+} and Eu^{2+} phosphors resolves some of the issues as regards decay

times. The challenges and additional requirements for LED phosphors are, however, balanced by larger potential composition spaces for LED phosphors vis-à-vis that for LFL/CFL phosphors.

Phosphor is used in conjunction with blue-emitting LEDs to create white light or other desired color points. While there are some instances where the use of a single phosphor will achieve the desired result [i.e., cool white, mid-color-rendering index (mid-CRI) to low-CRI LEDs], in many cases, it is necessary to use more than one phosphor to achieve a desired result. For example, high efficacy, warm white, high CRI, and tight color binning when using a broad distribution of blue pumps must be achieved through blending of phosphors (Setlur 2009).

Current phosphor usage (backlights for portable displays and indicators) in pc-LEDs is heavily skewed toward YAG:Ce. The properties of YAG:Ce also represent a benchmark for other LED phosphors. The absorption and emission transitions are parity and spin allowed, giving strong absorption of blue LEDs and a fast decay time that prevents saturation quenching. The quantum efficiency (QE) of YAG:Ce under blue LED excitation is >85%, even at 200°C, and there are no indications that YAG:Ce degrades under blue LED excitation or moisture. Besides, the synthesis of YAG:Ce is relatively straightforward and uses high-purity precursors (Y_2O_3, Al_2O_3, CeO_2) that have been qualified for use in traditional CFL/LFL/CRT phosphors. The rare-earth dopants in the variety of LED phosphor compositions mentioned are largely restricted to Eu^{2+} or Ce^{3+} broadband emitters (full width at half maximum [FWHM] > 70 nm) (Setlur 2009).

Over the past 10 years, many of the requirements for new LED phosphors have been met by the development of new phosphors, and the compositions have moved from the single family of phosphor compositions—the Ce3^{+}-doped aluminate garnets, $Y3Al_5O_{12}:Ce^{3+}$ (YAG:Ce)—to a variety of silicate, aluminate, nitride, oxynitride, sulfide, and fluoride compositions.

1.7.10 Nuclear

Rare earths have many applications in nuclear energy. One of the largest uses of Gd oxide was in General Electric Company's boiling water reactors (BWRs) as a burnable poison. Gadolinium oxide (about 5%) was mixed directly with uranium oxide in the fuel, which helps in achieving a uniform neutron flux during the lifetime of the fuel element. Gadolinium has not only a high neutron absorption cross section but also a burnup rate similar to that of ^{235}U; physical and chemical properties of gadolinia are similar to UO_2. Gadolinium is used as an oxide intimately mixed with UO_2 before pelletizing the fuel. About 2 t of Gd oxide was estimated to be in use in 26 operational BWRs in the United States. It is also usable, for a similar function, in pressurized heavy-water reactors (PHWRs). Besides gadolinium, the elements Eu, Sm, and Dy also have a large capture cross section for thermal neutrons. Europium is unique because, like hafnium, it has an uninterrupted series of five isotopes, ^{151}Eu, ^{152}Eu, ^{153}Eu, ^{154}Eu, and ^{155}Eu, each one forming on capture of a neutron by the isotope with one mass number less. All of these have large capture cross sections for neutrons. This property is valuable in the use of europium for control rods in compact nuclear reactors (Greinacher 1981), as, for example, in nuclear submarines. Europium hexaboride, EuB_6, has been considered as the neutron absorber material in fast breeder

reactors. This boride has both europium and boron (enriched in the isotope B-10) as neutron absorbers, and the novel neutron-absorbing properties of europium are combined with the hexaboride stability (Molycorp 1993; Pasto and Tennery 1977).

The neutron-absorbing isotope ^{167}Er has properties that can provide an extremely long lifetime for nuclear fuels for specialized reactors. It has been used in a U–Zr–H fuel in research submersibles. Erbia, Er_2O_3, is also used homogeneously mixed with UO_2 fuel for pressurized water reactors (Jonsson et al. 1992; Barchevtsev et al. 2002).

Yttrium has a low capture cross section for thermal neutrons and was considered as a material for tubing in molten salt nuclear reactors. Because of high hydrogen atom density and high-temperature stability, cerium and yttrium hydrides could be useful as neutron moderators (Greinacher 1981). The (n,β) reaction characteristic of Gd and Dy and the availability of these metals as thin foils have been very useful in neutron radiography.

In neutron radiography, like in x-ray radiography, an imaging beam is passed through the specimen, and the attenuated beam is recorded to produce an image of the internal details of the specimen. The recording medium in neutron radiography is also a standard x-ray film. This film, however, is insensitive to neutrons and so needs an aid to produce the image. The aid is a 0.025-mm-thick gadolinium foil placed in direct contact with the x-ray film. When exposed to the thermal neutron beam, the gadolinium absorbs neutrons and promptly emits β-radiation (electrons), and the x-ray file is sensitive to the β-radiation. Dysprosium is used for the same purpose but differently. In neutron radiography, dysprosium foil generally 0.1 mm thick is exposed to the attenuated neutron beam but in the absence of the x-ray film. The exposed dysprosium foil is then removed from the beam, and its β-decay (nuclear transformation by emission of β-rays) is used to produce an autoradiograph in contact with the x-ray film. This technique, using dysprosium, has been particularly suitable for radiography of highly radioactive materials (Davies 1981).

Dysprosium-doped crystals, particularly $CaSO_4$ or CaF_2, have been used in dosimeters for monitoring exposure to ionizing radiation, such as γ-rays or neutrons (Molycorp 1993). Such a crystal, on exposure to energetic radiation, creates *in situ* and quantitatively excited Dy atoms. When the crystal is heated, these atoms luminesce, producing a glow peak. The magnitude of the glow peak is related to the radiation dose (Molycorp 1993).

The exceptional thermal stability of monazite and xenotime structures, the absence of any phase transition up to their melting points, and their limited chemical reactivity have led to the rare-earth phosphates being considered as hosts for the long-term storage of radioactive wastes (Molycorp 1993).

1.7.11 Hydrogen Storage

An application for the rare earths that was identified in 1969–1970 concerns the hydrogen energy system. In 1969, Zijlstra and Westendorp (1969) of the Philips Research Laboratories, Eindhoven, identified the ability of the intermetallics REM_5 (where RE is the rare earth and M is iron, cobalt, or nickel) to absorb a large amount of hydrogen at room temperature. The following year, Van Vucht et al. (1970), also from Philips (the same laboratory), revealed the remarkable hydrogen absorption

properties of $LaNi_5$. This intermetallic absorbs hydrogen readily at room temperature to form the compound $LaNi_5H_6$, which has, per cubic centimeter, more hydrogen than even liquid hydrogen. More importantly, it also gives off hydrogen at a higher temperature, and the whole absorption and desorption cycle is essentially reversible with only a small hysteresis loop. It was recognized that lanthanum nickel intermetallic can be used commercially as a hydrogen storage medium and for related technological applications. Solid-state storage of hydrogen offers advantages in volume, weight, pressure, energy savings, and safety over cryogenic and compressed gas.

While $LaNi_5$ is most efficient in terms of both capacity and kinetics, it also remains more expensive than the majority of its rivals. Lanthanum in $LaNi_5$ can be partially replaced by cerium, praseodymium, neodymium, misch metal, or thorium, and nickel by Al, Co, Cr, Cu, Fe, or Pt. It is thus possible to vary the hydrogen absorption–desorption properties for various commercial applications or for basic research studies (McGill 1997; Gschneidner and Daane 1988; Buschow 1984).

There were some interesting technological firsts in the twentieth century as regards rare earths and hydrogen. The world's largest hydrogen storage vessel was made by Kawasaki Heavy Metal Industry (Omachi 1988). The vessel has a capacity of 175 Nm^3, carried a total of 1000 kg charge of La-rich misch metal–nickel alloy for hydrogen storage, and is operated at 700 kPa (at 30°C) stage pressure. Compared to high-pressure hydrogen storage of the same capacity, the vessel is 30% lighter and occupies only ~14% of the volume. In addition, in one cycle of absorption–desorption, hydrogen gas is upgraded in purity from 99.99% to 99.99999%. The Japanese also have been developing hydrogen-fueled cars and even have successfully road tested a Toyota wagon (2000 cc, four cycles) driving a 200 km stretch at 100 km/h. In this, a La–MM–Ni–Al alloy was selected for hydrogen storage (Omachi 1988).

The hydriding reaction between hydrogen and lanthanum nickel alloy is specific and is usable as a method for separation of hydrogen and also for purification of hydrogen, as mentioned in the previous paragraph. The metal hydride process for separation or recovery of hydrogen from industrial off-gas streams consists of two steps: hydrogen absorption and hydrogen desorption. The off-gas feed stream is passed through a packed bed containing the hydriding alloy while maintaining the hydrogen partial pressure in the stream at more than the equilibrium decomposition pressure (of the hydriding alloy) to enable absorption of hydrogen by the bed. In the second step, the absorbed hydrogen is recovered by desorbing the hydrogen from the bed either by increasing the bed temperature or by lowering the system pressure. This scheme has advantages, such as reaction specificity (only hydrogen reacts), high hydrogen recovery, product purity (>99.9%) and energy efficiency (Huston and Sheridan 1981). The metal hydride process has been investigated for hydrogen recovery from an ammonia purge gas stream generated during ammonia manufacture. When the objective is hydrogen purification, after absorption, residual gaseous impurities are expelled by simply desorbing a portion of the hydride.

The possibility of reversible hydrogen absorption–desorption over a range of temperatures has been used in hydride chemical compressors. Hydrogen is absorbed at low temperatures and pressures and desorbed at a higher temperature and pressure. At Brookhaven National Laboratory, USA, a $LaNi_{4.5}Al_{0.5}$ alloy was used, and

hydrogen pressures up to 7600 kPa were generated in capsules. The unit also delivered 1.2 m^3 of hydrogen at 4250 kPa in a continuous operation (Huston and Sheridan 1981).

Hydride heat pumps have been devised on the basis of the reversibility of the metal–hydrogen reaction and the heat of the chemical reaction. In these devices, which are closed units comprising two or more hydride beds, hydrogen functions as the energy carrier. With no moving parts in the system, heat can be pumped over large temperature differentials by a suitable choice of hydriding alloys, heat sources, and heat sinks. These hydride pumps can operate with low-grade heat. A demonstration unit made by Ergenics used $LaNi_5$ and $LaNi_{4.7}Al_{0.3}$. This unit generated hot water at 95–100°C from wastewater at 60°C and 20°C cooling water. In Japan, hydrogen heat pumps have been used as air-conditioning systems (Omachi 1988). The pump used 800 kg of MM–Ni–Ca–Al alloy and had a capacity of 630 MJ/h. This air conditioner, installed in an 18-room leisure house in a spa in Hokkaido, operated efficiently with energy input from the spa's hot water for cooling in the summer and warming in the winter. A larger chemical heat pump using 3500 kg of MM–Ni–Co–Al alloy, having a capacity of 1300 MJ/h, was also mentioned by Omachi (1988). A hydride refrigerator that could cool to as low as –240°C (33 K) without using electricity has been described by Jackson and Christiansen (1993). Overall, the operation was described as follows. In a chamber, lanthanum nickel hydride was heated to 104°C. Stored hydrogen gas was released, and this gas was passed through a heat exchanger and was then allowed to expand. The expansion cooled the gas considerably, and some liquid hydrogen was also formed. The gas was conducted to another chamber, where it was absorbed by the alloy to form the hydride. The cycle was then repeated using the new hydride until the cooling chamber attained the target temperature.

Many types of hydrogen-based rechargeable batteries containing rare-earth elements have been investigated (Jackson and Christiansen 1993; Züttel et al. 1999). They offer good cycling life, high energy and power density, effective protection from overcharging and undercharging, and superior low-temperature behavior. For nickel–metal hydride (NiMH) batteries, two families of metal hydrides are widely used. They are the AB_5 and AB_2 intermetallic compounds, where, in general, A is a late transition or a rare-earth element and B is one or more early transition elements. A popular AB_5 alloy is $Lm(Ni_{3.6}Mn_{0.4}Al_{0.3}Co_{0.7})$, where Lm stands for lanthanum-rich misch metal (≈50 wt.% La) (Kopera 2004).

NiMH batteries, using AB_5-type alloys as a cathode, which form hydrides up to AB_5H_6, have effectively replaced the previously popular nickel–cadmium batteries because they (NiMH) are environment friendly and have high energy density. NiMH batteries are ahead of nickel–cadmium in performance and lithium-ion types in cost. NiMH batteries found extensive use in portable electronic devices (Hedrick 2001). These batteries were also recommended as midterm technology for electrical vehicles by the United States Automotive Battery Consortium (Vogt 1998). They are used in both HEVs and pure electric vehicles (AEVs). By 2000, HEVs were commercially available in the United States. The HEV Honda Insight used a NiMH battery with 144 V output, and in the Toyota Prius, the battery produces 274 V. The driving ranges of the AEVs are from 55 to 240 km (Hedrick 2000). Beyond their traditional role in automobiles, batteries perform larger functions and are a key component in

new-generation vehicles—HEVs, PHEVs, and AEVs all require batteries to store energy for vehicle propulsion. Current-generation HEVs primarily use NiMH batteries, while lithium-ion (Li-ion) batteries are preferred for PHEVs and AEVs to meet requirements of greater storage capacity and higher power ratings (National Research Council 2010). HEVs rely on an internal combustion engine as the primary power source but use a battery to help collect energy captured during vehicle braking and deceleration. PHEVs generally incorporate a higher-capacity battery than HEVs, which can be recharged externally and used as the primary power source for longer durations and at higher speeds than is required for an HEV. AEVs use the battery as the sole power source. It is estimated that each current-generation hybrid-vehicle battery contains several kilograms of rare-earth element (REE) material. Most of the hybrid and electric vehicles sold in the United States were powered by NiMH batteries as of year-end 2010. Future demand for the rare-earth elements used in NiMH vehicle batteries will depend on public acceptance of electric vehicles as substitutes for internal combustion-powered vehicles, general economic growth worldwide, and acceptance of Li-ion batteries (which contain no rare earths) as substitutes for NiMH. The push for NiMH batteries for heavy-duty automotive applications apparently subdued sometime back because of the perceived superiority of Li-ion batteries. Safety concerns on the use of Li batteries in vehicles are presently shifting the focus to NiMH, which is set to see better days.

1.7.12 Superconductor

A topic that has generated considerable worldwide interest in the last quarter of the twentieth century is the high-critical-temperature (T_c) superconductivity. All the known high-T_c materials contained either yttrium or one of the lanthanides (Kilbourn 1988). A ceramic compound of Y, Ba, Cu, and O exhibits zero resistance at 90–100 K, making it possible to replace expensive liquid helium with the cheaper liquid nitrogen as a refrigerant for the superconductor. These new superconductors have already been fabricated in thin films, the form used in electronic circuits, on a laboratory scale in the United States. Large-scale commercial use of these superconductors will depend on whether these materials can sustain the high currents necessary in applications such as electricity pylons, power generators, electric storage units, and electric motors. Another potential application area is in devices where power losses are usually significant but currents are small. The major developments in the field have been extensively reviewed (Wu et al. 1978; Hatfield and Miller 1988). As far as the rare earths are concerned, the practical realization of commercial high-T_c superconductors, if and when it happens, would mean an unprecedented demand for several of the rare earths.

1.7.13 Miscellaneous

Substantial quantities of rare earths are used in a number of civilian and military applications that do not clearly belong to one category or another mentioned so far. It was estimated in 2012 that the U.S. Department of Defense (DoD) used an equivalent of less than 5% of the domestic consumption of rare earths (Grasso 2013). A profile of rare-earth use in a variety of defense-related applications is given in Table 1.8.

TABLE 1.8
Military Applications of Rare Earths

Area	Rare-Earth Element Used	Technology	Function/ Application	Selected Examples
Guidance and control systems	Nd, Pr, Sm, Dy, Tb	Compact and powerful magnets	Guidance and control of electric motors and actuators	Tomahawk cruise missile, smart bombs, Joint Direct Attack Munitions, joint air-to-ground fin actuator, predator unmanned aircraft
Defense electronic warfare	Numerous	Energy storage, density amplification, capacitance	Electronic warfare, directed-energy weapons	Jamming devices, electromagnetic rail gun, area denial system, long-range acoustic device
Targeting and weapon systems	Y, Eu, Tb	Amplification of energy and resolution	Targeting and weapons	Laser targeting, air-based lasers, Laser Avenger (counter-improvised explosive device [IED]), SaberShot photonic disruptor, FCS vehicle with laser weapon
Electric motors	Nd, Pr, Sm, Dy, Tb	Compact and powerful permanent magnets	Electric drive motors	CHPS future combat, integrated starter–generator, HUB mounted electric traction drive, Zumwalt DDG-1000, Joint Strike Fighter and more electric aircraft
Communication	Nd, Y, La, Eu	Amplification and enhanced resolution of signals	Radar, sonar, radiation and chemical detection	Sonar transducers, radar, enhanced λ-ray radiation detection, Multipurpose Integrated Chemical Agent Alarm (MICAD)

Source: Grasso, V.B., Rare earth elements in national defence: Background, oversight issues, options for congress, Congressional Research Service (CRS) Report R41744 (http://www.crs.gov), 2013.

Rare-earth metals have been useful as getter materials for removing residual oxygen in a small confined volume. The great affinity of the rare earths for oxygen is the basis of this application.

A remarkable application of cerium, developed in the 1980s, is in starch polyacrylonitrile copolymers, which absorb 500 to 1000 times their weight of water. These copolymers have been investigated in Japan for making baby diapers (Kudo 1988). For this application, cerium is used in the form of oxide or hydroxide, in quantities

of several hundred metric tons per annum. Cerium is also used as a high-pressure antiwear lubricant. Cerium fluoride is added to greases, pastes, and suspensions used as lubricants (Molycorp 1993).

An interesting application of rare earths, popular in the People's Republic of China, is to use the rare-earth elements as trace nutrients in agriculture. The positive effects of rare earths on plant growth have also been claimed by Buckingham et al. (1999) in Australia, while Diatloff et al. (1999), from the same country, have not found a positive effect on plant growth.

Rare earths have also been used in radiopharmaceutical therapy (Turner 1998). For this application, β-emitting radiolanthanides such as holmium-166 (half-life, 26.8 h), samarium-153 (half-life, 46.3 h), and lutetium-177 (half-life, 6.7 days) have been suggested as suitable. These radionuclides also emit γ photons of suitable energies for quantitative imaging on conventional γ cameras. Their half-lives correspond to the required irradiation time for the tumor cells and thus minimize radiotoxicity to normal tissues. All these qualify them as tools for radiopharmaceutical treatment of cancer patients for whom conventional therapy has failed.

Rare earths are also used in the paint and pigment industry (Desai 1988). Cerium compounds with or without the hydrous oxides of aluminum or silicon are extensively used in lead chrome paints to improve their light fastness. Titanium dioxide pigment is treated with cerous acetate to improve resistance to sunlight and outdoor durability, particularly for the pigment's applications in synthetic fibers, molding compositions of high polymers, paints, powder coatings, and wire coatings. A water-based yttrium coating to provide corrosion resistance and a lead-free primer for paints have been developed (Hedrick 2001). An yttrium hydroxide coating is applied by electrodeposition from an yttrium salt and converted to yttrium oxide during heat curing.

Rare-earth compounds also find use in the paint industry as dryers, in the textiles industry as oxidizing agents for self-cleaning ovens, and also in wastewater purification (McGill 1997). Lanthanide carboxylates are used as paint dryers. Cerium carboxylates promote drying of the resin coating by accelerating the cross-linking reactions within the polymer skin. Cerium salts are used as combustion additions. These salts, soluble in hydrocarbon, promote the complete oxidation of diesel fuels (Molycorp 1993). Cerium stearate controls the labile hydrogen in polyvinyl chloride (PVC), limits the high-temperature dehydrochlorination reactions, and hence confers high-temperature stability to PVC.

Cerium and titanium dioxide have been used to make an improved electrorheological (ER) fluid. The viscosity, stiffness, and heat transference of the fluid can be varied using an electric field. Under the field, the particles in the ER fluid are polarized and organize into structures, thus increasing the viscosity. Cerium-doped titanium dioxide in dimethylsilicone oil has five to six times higher shear stress than pure titanium dioxide. Potential applications are in viscous clutches, variable cushion shock absorbers, and other variable-coupling devices (Hedrick 2001). A process that allows cerium dioxide to be used as a sunscreen has been developed. Cerium dioxide particles were coated with a 10 nm layer of boron nitride, which eliminated agglomeration, provided cerium catalytic activity, and produced a slippery feel when incorporated into an organic thin film. The coated cerium particles had

higher transparency and greater UV-blocking ability than the common sunscreen ingredients such as titanium dioxide or zinc oxide. The improved sunscreen reduces sunburn, skin aging, and potential causes of skin cancer (Hedrick 2000). Rare-earth chelates with diketones were considered for use as antiknock compounds (McGill 1993), in place of the well-known lead compounds.

1.8 GLOBAL RARE-EARTH DEMAND

Approximately 20 years ago, Wayne D. Jackson and Grey Christiansen (1993) commented on world consumption of rare earths in just two sentences. They summarized: in 1988, world consumption of rare earths and their products was 40 million lb. (18,000 t), and the major consumer by weight was the chemicals industry, whereas the major user by value was the optical industry. Falconnet (1993) of Rhône-Poulenc considered rare-earth applications in two major categories: uses that demand separated (pure) rare earths and uses that do with naturally occurring pure rare-earth mixtures. As of 1990, only about 27% (8000 t) of total rare-earth consumption was in the form of separated rare earths. The actual quantity was 8000 t. Out of this, approximately 2000 t was used for magnet manufacture. Another major application for pure separated rare earth was phosphors. Falconnet (1993) foresaw a 16% annual growth for the magnet sector and about 6% annual growth for the phosphors. The total contribution from the three main applications of nonseparated rare earths, viz., catalysts, metallurgy, and glass ceramics, was expected to decrease as a whole from being nearly three-quarters of total rare-earth consumption by volume in 1990. Over the years, analyzing world rare-earth demand on an annual basis has shown that it has remained more or less the same. The focus has shifted more on accurately predicting the future requirements and possibilities of ensuring that the required rare-earth supply would indeed be available/accessible. It no longer remains the job of professional scientists involved full time in rare-earth processing, but of highly resourceful specialists who can track mineral industry nuances across the seven continents on a real-time basis.

Hatch (2011) looked at the end uses of rare earths from a different perspective. He divided them into broad categories: uses that enable the processing of engineered or other materials and uses within components, which are themselves used as building blocks within engineered products. As process enablers, rare earths participate in the life cycle of other materials and components, where the REEs do not stay with the processed material. Basically, the properties of simple REE compounds are utilized. Significant examples include fluid cracking catalysts, automotive catalytic convertors, and polishing media. The second group of end uses for rare earths begins with incorporating various REEs into sometimes-complex alloys and compounds and proceeds through their use in engineered components, sub-assemblies, and finally, a complex product or device. Usually, small amounts of REEs are used in the overall product, but their presence is critical for the functionality of the intended end application. Significant examples include permanent magnets, energy storage units, phosphors, and glass additives.

Rare earths, at least some of them, are indispensable to support every nation's mission as regards the green energy program—to provide electric power in a renewable,

environmentally benign, and ethically sustainable manner. Besides, the rare earths, or some of them, are indispensable for national security, for the creation and deployment of effective weapons and associated control and communication systems. It is simply not conceivable to continue living as most of us are used to, without an adequate and assured supply of rare earths to the domestic industries, for a long time to come.

Rare earths need to be used in relatively small amounts yet enable magnetic, electrical, and chemical processes to occur at significantly lower energy levels, allowing for increased energy efficiency apart from smaller-size products. As detailed above, rare earths have a broad range of uses, the most well known being in catalysts, magnets, and phosphors, with important and extensive uses also in electronics, glass, ceramics, and metal alloys, among others. The total world rare-earth consumption is rather unequally divided in these categories. Such a type of division is true only for the volume of rare-earth material used globally but even when the dollar value of material is considered. The data for the year 2010 are given in Figure 1.9. Approximately 60% of the total worldwide usage of rare earths is in mature markets, which include catalysts, glass making, lighting, and metallurgy. The newer high-growth markets (PMs, battery alloys, and ceramics) account for the remaining 40% of usage. The bulk of the rare earths (80%) used in the mature markets are lanthanum and cerium, which, incidentally, are the most abundant rare earths in the ores. In the new market segment, Nd, Dy, and Pr account for about 85% of rare-earth elements used (Goonan 2011). A current and future scenario is that these rare earths are required in quantities much more than what could be readily available from known or globally accessible resources.

Over a period of time, some of the applications become more popular and grow more rapidly than others. Some high-growth applications become subdued. As a result, with time, the relative proportion of rare earths used in each of the application categories changes. This is shown by the data in Table 1.9 and Figure 1.10. The components of world rare-earth consumption in the years 2000 and 2010 and projected consumption for the year 2020 are listed. Catalysts have historically been the largest end use for rare earths (seldom less than 20% of the total rare-earth consumption by volume), but the growth of mobile electronics and green technologies has spurred the development of compact and high-efficiency motors, utilizing rare-earth magnets, which now consume the largest amount of rare earths (>20% in 2010 and >33% in 2020, by volume). Over this decade, the expectation is that the demand for rare earths will grow at 7–9% per annum, increasing from ~125,000 t in 2010 to ~263,550 t in 2020, driven largely by a persistent shift to energy-efficient green products and an increased use of mobile electronics and electric vehicles (Anon 2010).

As noted earlier, the rare earths are not only essential material inputs to a range of industries, but also they relate directly to the consumers/final users. Presently 10 out of the 16 naturally occurring rare earths have well-defined applications. The rare earths that each application area relies on and the contribution of each of the individual elements expressed as a volume fraction of the total rare-earth requirement for the given application are given in Table 1.10. Translated into the quantity of each of these metals consumed, the year 2010 demand in terms of the tonnage of each of the rare-earth metals required is listed in Table 1.11. Taking into account the anticipated growth rate arrived at for each of the metals, the element-wise demand for the

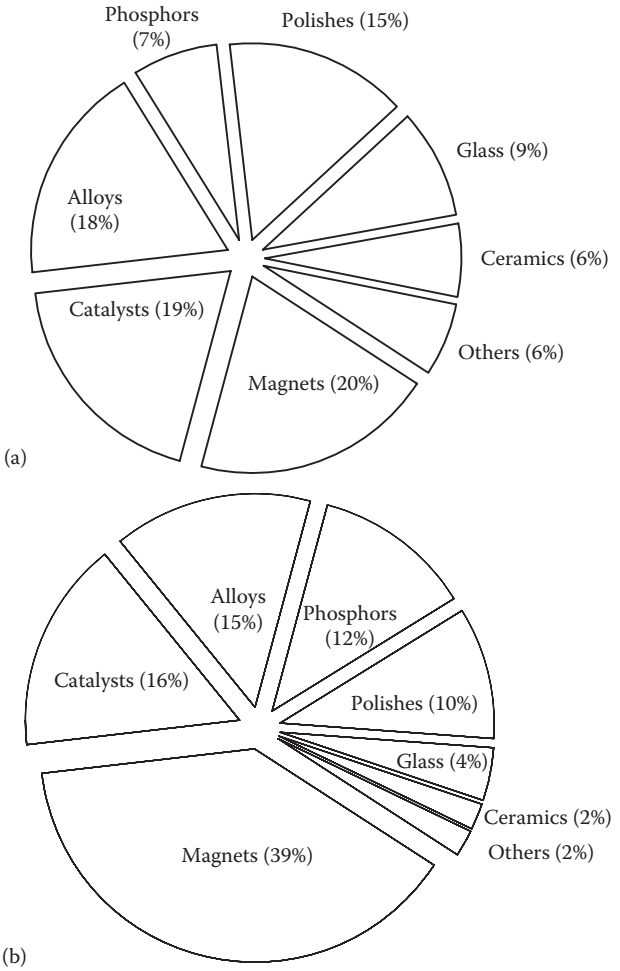


FIGURE 1.9 Global rare-earth consumption by end use (a) by volume and (b) by value in the year 2010. (From Anonymous, Rare earth elements. Enablers of high tech applications and green energy technologies, 2010.)

year 2020 has been worked out. Growth rates are nonuniform because of the reasons outlined below, and, as a consequence, the contribution from each of the rare earths to the total rare-earth usage changes.

Rare-earth demand in metal alloys has grown at an average of 5.8% per annum over the last decade. In non-battery alloy applications, the absence of any major developments either for or against the continued use of metallurgical alloys of rare earths points to continued growth in line with the global economy. The bulk of this application is supported by rare earths that are relatively more abundant and noncritical. For battery applications, growth will continue, possibly at a reduced rate. Lithium batteries have performance advantages over NiMH batteries and have already been preferred in PHEVs and AEVs. Rare earths are used in NiMH batteries, and their use is likely to continue in applications

TABLE 1.9
Components of Growth in World Rare-Earth Consumption (2000–2020)

	Consumption/Demand							
	2000		2010		2020		Average Growth Rate, %	
Application Area	Metric Tons	% of Total	Metric Tons	% of Total	Metric Tons	% of Total	2000–2010	2010–2020
Alloys (metallurgical)	4900	6.2	8600	6.9	14,050	5.3	5.8	5
Alloys (battery)	7600	9.6	13,400	10.7	18,050	6.9		3
Catalysts (FCC)	5600	7.1	7800	6.2	18,500	7.0	3.4	9
Catalysts (automotive and others)	11,950	15.1	16,700	13.4	33,000	12.5		7
Ceramics	3000	3.8	7000	5.6	13,800	5.2	8.8	7
Glass	14,000	17.7	11,000	8.8	14,850	5.6	–2.4	3
Magnets	10,500	13.3	26,000	20.8	88,600	33.6	9.5	13
Phosphors	6000	7.6	8500	6.8	20,200	7.7	3.5	9
Polishes	11,500	14.5	19,000	15.2	31,050	11.8	5.1	5
Others	4000	5.1	7000	5.6	11,450	4.4	5.8	5
Total	79,050	100	125,000	100	263,550	100	4.7	8

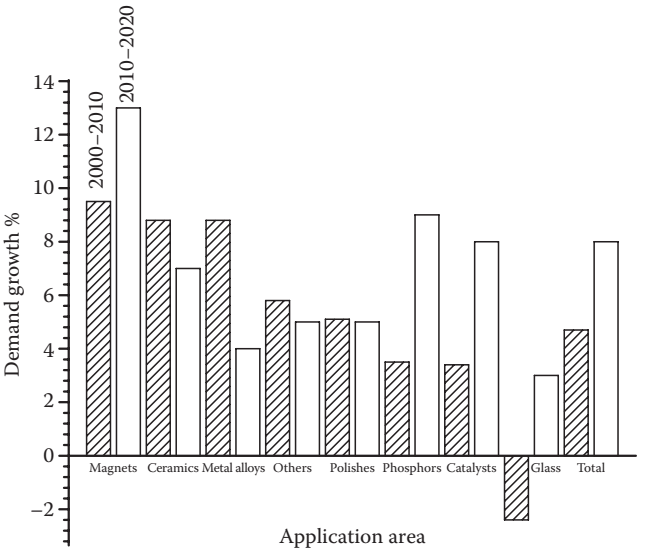


FIGURE 1.10 Growth of REE consumption by end use 2000–2010 and 2010–2020. (From Anonymous, Rare earth elements. Enablers of high tech applications and green energy technologies, 2010.)

that favor cost savings over energy and power performance. Besides, NiMH batteries are safer (e.g., less prone to fire hazards) than the Li-ion batteries, and this may work in favor of their continued use in heavy-duty applications. For example, La–Ni–H is still a very cost-effective and reliable method of storing electricity, for applications including Prius-class HEV battery packs (which use an estimated 2.3 kg of La per vehicle for this application) and others.

The rate of growth for rare earths in catalyst applications is estimated to be more now (2010–2020) than in the last decade (2000–2010). The demand for catalysts growing at above-average rates follows from a shift to heavy-oil sources for the production of oil. As the world shifts to higher-tier engine emission standards, above-average growth in catalysts used in automobiles to reduce environmentally harmful emissions follows. The demand for catalytic converters is likely to outpace the underlying demand for vehicles and generators.

As regards the phosphors, there are all reasons for an accelerated growth decade. There is a continuing worldwide shift to energy-efficient lighting in all formats, be it domestic, industrial, community, or highway lighting. It is easy to anticipate the demand for phosphors and, hence, the demand for the rare earths in phosphors to grow at accelerated rates. The shift away from incandescent lighting to CFL, LFL, and LED sources will translate to increased demand for rare-earth metals. The growth in LCD, LED, and plasma screen displays as well as mobile electronics with large and full-color displays will sustain an increasing demand for phosphors and, hence, the rare-earth metals.

Rare earth-based polishing has been used in the manufacture of CRT, LCD, and LED monitors, as well as high-quality mirrors, decorative glass products, and the

TABLE 1.10
End-Use Breakup among the Rare-Earth Elements in 2010

	Percentage of Application's Total Requirement Fulfilled by the Individual Rare-Earth Element										
Use	**La**	**Ce**	**Pr**	**Nd**	**Sm**	**Eu**	**Gd**	**Tb**	**Dy**	**Y**	**Other**
Magnets			23	69	0.8		2	0.2	5		
Catalysts—petroleum refining	90	10									
Catalysts—automotive	5	90	2	3							
Alloys—batteries	50	33.4	3.3	10	3.3						
Alloys—excluding batteries	26	52	5.5	16.5							
Phosphors	8.5	11				4.9	1.8	4.6		69.2	
Polishes	31.5	65	3.5								
Glass	25	67	1	3						3	1
Ceramics	17	12	6	12						53	
Others	19	39	4	15	2		1			19	1

Source: Long, K.R. et al., The principal rare earth elements deposits of the United States—A summary of domestic deposits and a global perspective, U.S. Geological Survey Scientific Investigations Report 2010–5220, available at http://pubs.usgs.gov/sir/2010/5220, 2010.

TABLE 1.11
Rare-Earth Metal Demand Forecast

Rare-Earth Element	2010 Demand, Metric Tons	% of Total REE Tonnage Consumed	Forecast Demand Growth Rate, %	2020 Demand Forecast, Metric Tons	% of Total REE Tonnage Consumed
Lanthanum	28,770	23.0	5–7	45,930–55,490	19.2
Cerium	48,980	39.2	4–6	75,460–91,260	31.6
Praseodymium	8700	7.0	10–12	22,700–27,150	9.5
Neodymium	23,420	18.7	11–13	63,840–76,300	26.6
Samarium	790	0.6	6–8	1390–1670	0.6
Europium	420	0.3	8–10	900–1080	0.4
Gadolinium	740	0.6	11–13	2050–2450	0.9
Terbium	440	0.4	9–11	1010–1200	0.4
Dysprosium	1300	1.0	12–14	4040–4820	1.7
Yttrium	11,250	9.0	7–9	21,740–26,090	9.1
Other	180	0.1	3–5	240–290	0.1
Total	125,000	100	7–9	239,000–288,000	100

Source: Anonymous, Rare earth elements. Enablers of high tech applications and green energy technologies, 2010.

wafers used to produce silicon chips. The secondary and fast-growing use of rare earth-based polishes in electronic components maintained an 8–12% per annum growth rate over the last decade. Collectively, the demand for rare earth-based polishes should continue growing faster than the global economy.

An important exception to across-the-board growth in the rare-earth sector is the application in glass. CRT monitors are commonly made using cerium oxide-stabilized glass. The rapid transition to LCD, LED, and plasma displays has led to a significant drop in the demand of CRT monitors and to a similar extent for rare earths in glass. This decline is partially offset by the growth in lanthanum consumption for use in glass to reduce the passage of UV rays and also for camera lenses. The number of items incorporating lanthanum, which, incidentally, is rapidly expanding in numbers even though per-unit consumption of rare earths is small.

In ceramics, rare earths have important applications. They have not been of significant use as structural ceramics but are extremely valuable as functional ceramics, both in the oxide and nonoxide categories. Rare earths are used in ceramics for a range of applications, from coloring additives to imparting enhancements in refractory, electrical, and hardness properties. The chemical inertness and stability at high temperatures of some of the rare-earth ceramics are remarkable, as are the special characteristics connected with superconductivity. Anticipated growth rates would be slightly above world economy growth rates due to an increasing demand for high-technology products and continued development of new applications. As far as development of new applications for rare-earth ceramics is

concerned, all that has been explored might turn out to be just the proverbial tip of the iceberg.

As referred to above in the context of the stability and rise of rare-earth demand growth rates, the complete application potential of rare earths may not have been fully comprehended by the potential users. Many of the least common rare-earth elements have never been thoroughly investigated for potential applications simply because the metals were unavailable. As new mines enter production and global production of erbium, holmium, thulium, and ytterbium increases, it is likely that new applications will be found for their unique physical, chemical, thermal, and electrical properties. This state of affairs is reflected by the information provided in Table 1.12. All the current and known potential applications of rare earths are divided among only 10 of the 17 rare-earth elements. A review 10 years from now will hopefully include more rare-earth elements in the applications matrix and demand projections.

The future global demand projections of rare earths will need to factor in the populous nations in Asia and Latin America becoming consumers of rare earth-enhanced devices growing to a level that is current in the industrialized countries, and their governments implementing green energy initiatives in the area of electricity generation and transportation. This will, in all likelihood, trigger unprecedented demand for rare earths, mostly post 2020.

Although the rare earths occur abundantly in nature, they were never cheap materials. This has resulted in current rare-earth users searching for a cheaper

TABLE 1.12
Energy-Critical Elements

	Photovoltaic Films	Wind Turbines	Vehicles		Lighting
Material	**Coatings**	**Magnets**	**Magnets**	**Batteries**	**Phosphors**
Lanthanum				*	*
Cerium				*	*
Praseodymium		*	*	*	
Neodymium		*	*	*	
Europium					*
Terbium					*
Dysprosium		*	*		
Yttrium					*
Indium	*				
Gallium	*				
Tellurium	*				
Cobalt				*	
Lithium				*	
Manganese				*	
Nickel				*	

Source: USDOE, Critical materials strategy, December 2011, US Department of Energy, http://energy.gov/sites/prod/files/edg/news/documents/criticalmaterialsstrategy.pdf, 2011.

solution even for established applications of rare earths. An urgent and ominous reason for looking for rare-earth substitutes has emerged post 2010. It has to do less with the cost but more with the current and future reliability of raw material supply for the rare earths, especially for the energy-critical rare earths. In the European Union as well as in the United States, the grouping of certain chemical elements as energy-critical elements has gained ground in industrial and governmental discourses. The concept of energy-critical elements evolved out of an important and urgent need to buffer green energy initiatives from the vagaries of raw material supply. Considering and qualifying certain essential key elements as energy-critical elements would help plans for developing and sustaining the supply of these materials either from domestic resources or from overseas resources that rank high on long-term reliability. The US DOE as well as institutions and stakeholders in the European Union and Japan have identified many of the rare earths as energy-critical elements. It is imperative that functional substitutions are concurrently developed for these materials. The substitution of rare earths has been pursued in many ways. One is through the use of new processes, another is through the use of new substances (Greinacher 1981; Falconnet 1988), and yet another is through the use of new devices. The efforts so far seem to suggest that while substitution of rare earths might be possible to some extent where metallurgical and magnetic properties are involved, in those applications based on optical, chemical, and certain special magnetic properties, substitution appears less likely. Thus, applications of rare earths in certain polishing applications, catalysts, phosphors, magnets, optical glass components, coloring and decoloring of glass, pigments, and intensifiers of x-rays will be long lasting. Coming back to the rare earths as energy-critical elements, the largest concentration of efforts has been directed toward "alternative rare earth-free magnets." Elegant summaries on this can be found in the work of Campbell (2012), Constantinides (2012a,b) and Kramer et al. (2012). The development of the 10 MW Sea Titan turbine prototype that uses a direct-drive high-temperature superconducting generator (Constantinides 2012a), development of OLEDs for lighting, and Li-ion batteries as an alternative to NiMH are some of the success stories that would, though seemingly ironic, insulate green technology development from rare earths and provide a glimpse of the way things will shape up if and when the rare-earth supply becomes too constrained.

1.9 SUMMARY

What are rare earths? How were they all discovered, and why did their discovery occur over an unusually long period of scientific endeavor? What are their properties? What types of interactions do they undergo? Apart from scientific curiosity, what had made researchers attempt to unravel the mystery surrounding the enigma called rare earths? These questions are briefly answered in this chapter. Notwithstanding the great scientific merit of studying the rare earths for their own unique characteristics, it is very clear that the rare earths are remarkably useful materials in an extensive range of technological fields. Most importantly, some of the rare earths provide the technology answer to the most important issue of our times: to maintain and enhance the standard of living of a growing number

of people, while consuming less energy and with no or minimal degradation of the environment. In many of these roles, they are simply unsubstitutable. The rare earths are extremely useful materials, and they are abundantly available in nature. Closer examination, however, reveals that crustal abundance and a gross statement on the rare earths being plenty in natural resources hide the highly unequal distribution of mineable rare-earth reserves among the nations of the world. Mining and processing of rare-earth deposits come with inevitable penalties of environmental degradation. This aspect will be visited again in later chapters. Provided that accessible and mineable rare-earth reserves are there, the logical effort then will be to produce the rare earths cheaply in sufficient quantities at the required quality. This is not possible without a good understanding of the physics and chemistry of the rare earths. To study the physics and chemistry of the rare earths, in turn, the rare earths are needed in pure form. This catch-22 situation, which persisted in the rare-earth industry during the first four decades of the twentieth century, was alleviated by the remarkable and highly rated research work conducted at Ames Laboratory under the leadership of Professor Frank H. Spedding, starting from the late 1940s. Largely through these efforts, the technology became available that brought the rare earths within the reach of any scientist who wished to study them. The success story of Ames and Rare Earths had a subplot involving Herbert Newby McCoy and Frank Spedding. Many research groups all over the world have investigated the rare earths and highlighted their scientific behavior and application possibilities.

This first chapter provides the backdrop needed to appreciate the remainder of the book. Specifically, this chapter provides the background necessary to understand the separation processes to isolate the rare earths from one another. Physical properties given are invariably related to their application potential in reduction and refining steps. Many of the applications listed also justify the necessity to take pains and obtain the required quantity of rare-earth material.

Among the numerous applications of the rare earths, one of the most spectacular has been their use in the new-generation PMs; rare-earth magnets are much more powerful than any PM hitherto developed and enabled the manufacture of smaller, lighter, and more energy-efficient motors and every other magnet-based device. A 31:68:1 ratio of neodymium, iron, and boron is used in the materials to produce rare-earth magnets with small amounts of dysprosium and terbium added to increase the magnets' strength at high temperature and praseodymium to augment magnetic field strength. The availability of compact and high-efficiency motors led to increased capabilities in mobile electronics, electric vehicles, and wind turbines apart from every household appliance including washers, dryers, and air conditioners. Gschneidner (2011a) did allude briefly to a life without rare earths. The development of electric cars relies on both powerful batteries and energy-efficient motors to provide both driving range and power comparable to the conventional internal-combustion-engine vehicles. Lanthanum and cerium, the most abundantly occurring of the rare earths, are used in the petroleum industry to convert heavy crude oil into gasoline and other refined products. Cerium and, to a certain extent, lanthanum and neodymium are used in catalytic converters, in combination with platinum-group metals, to reduce the emission of polluting gases from an internal combustion engine. Phosphors are materials that emit light when excited with an

energy input. LCD, LED, and plasma displays make use of compounds containing cerium, europium, yttrium, and terbium for their specific color properties and high energy-to-light conversion efficiency. The perennially improving capabilities of each generation of mobile phones are a lasting testimony of the ability of rare earths to improve energy efficiency and reduce size while providing pleasing visual splendor. Beyond the three major uses for rare earths noted above, other end uses include such items as glass, fiber optics, ceramics, plastics, polishes, lasers, and numerous concepts that await their turn to transit from the laboratory tables to the competitive market place.

The issue of some of the rare earths being classified as energy-critical elements and the consequences thereof were also briefly covered. The more a material becomes indispensable for a highly desirable technology application, the more serious will be the consequences should there be a problem on the availability or accessibility of the material. It has happened at least twice in the matter of RE magnets. The euphoria of Sm–Co magnets received a jolt as cobalt prices jumped 300% in the late 1970s in response to geopolitical pressures. A similar situation was recreated in 2010 when the vulnerability of neodymium magnets to raw material supply control was exposed. There was a fairly quick recovery from the event of 1980, but the lessons of 2010 are probably having a lasting effect. The ways in which technology and nations respond to such developments are also indicated in this chapter.

2 Resources

2.1 INTRODUCTION

The rare earths are moderately abundant elements in the earth's crust that occur in a large number of minerals, typically as carbonates, oxides, phosphates, and silicates. Rare-earth minerals are found in hard rock and placer deposits located throughout the world, with unusually large deposits occurring in a few countries. In most of the deposits, the disposition of the rare earths in the minerals is such that they can be recovered only as a coproduct or a by-product of certain other minerals. In a few deposits, however, the rare earths can be recovered as the primary or main product. Even though the number of rare-earth minerals is large, much of the actual world rare-earth supply comes from only a few of them. About a dozen more rare-earth minerals also occur in deposits that can be processed easily to supplement the existing rare-earth supply sources. The total rare earths contained in the world rare-earth reserves is considered sufficient to meet the foreseeable demand for these elements, far beyond the twenty-first century.

While the total rare-earth content in world rare-earth resources is large, the availability of individual rare-earth elements (REEs) has always remained highly unequal. This situation is the culmination of many factors, both inherent and transient. The inherent factor is that while each of the rare-earth minerals generally contains all the rare-earth elements, the concentrations of individual rare earths in the mineral are, as a rule, highly unequal. In each mineral, some REEs are present in high concentrations while some others are in very low concentrations, and this, in turn, varies from mineral to mineral. Besides, there is a wide variation in the contents of different minerals in the rare-earth deposits. The predominant mineral in world rare-earth deposits is enriched with respect to rare earths of lower atomic numbers and highly depleted with respect to rare earths of higher atomic numbers. The next most important mineral is also similarly disposed but to a lesser extent. As a result, the rare earths of lower atomic numbers are available more than the rare earths of higher atomic numbers. The transient factor relates to the by-product status of the rare-earth minerals and the occurrence of the element thorium in some of them. These factors affect the current production of the minerals and hence the availability of individual REEs present in them.

This chapter details the occurrence of the REEs in several different minerals, the occurrence of the minerals in various deposits, and the location of the deposits in different countries of the world. The composition of the mineral and the distribution of individual rare earths in the mineral and the quantity of rare earths contained in the deposit are presented. The status of the rare-earth deposits as a present or potential resource for rare earths is highlighted. An overall picture of the availability of rare earths, vis-à-vis their consumption, is given. The unequal availability of individual

REEs is mentioned, and estimates on the amounts of individual REEs theoretically recoverable from world rare-earth resources are provided.

2.2 CRUSTAL ABUNDANCE

The abundance or scarcity of an element is conveyed in a general way by its crustal abundance, which is its average concentration in the earth's crust. Many estimates of the crustal abundance of the rare earths have been made, and values that differ considerably from one another have been reported. This is apparent from the listing in Table 2.1. The values given by Lide (1997) have been adopted presently. In terms of inherent abundance in the earth's crust, the rare earths are not rare because the total rare-earth abundance (~240 ppm) is more than that of even carbon (200 ppm), and many of the individual REEs are more abundant than many better known metals. This is illustrated in Figure 2.1. Among the rare earths, the relative abundance varies widely—0.52 ppm for thulium to 66 ppm for cerium. Rare earths with even atomic numbers are more abundant than their odd-numbered neighbors (Kilbourn 1988). The rare earths with lower atomic numbers (lighter rare earths), as will be described later, have larger ionic radii and hence are more incompatible and therefore more strongly concentrated in the continental crust than the rare earths with larger atomic numbers (heavier rare earths). Thus lanthanum, cerium, praseodymium, and

TABLE 2.1
Abundance of REEs in the Earth's Crust

Element	Mason and Moore (1982)	Jackson and Christiansen (1993)	Sabot and Maestro (1995)	Wedepohl (1995)	McGill (1997)	Lide (1997)
Sc	22		10	16	5–10	22
Y	33	29	28	24	28–70	33
La	30	29	18	30	5–18	39
Ce	60	70	46	60	20–46	66.5
Pr	8.2	9	5.5	6.7	3.5–5.5	9.2
Nd	2.8	37	24	27	12–24	41.5
Sm	6	8	6.5	5.3	4.5–7	7.05
Eu	1.2	1.3	0.5	1.3	0.14–1.1	2.0
Gd	5.4	8.0	6.4	4	4.5–6.4	6.2
Tb	0.9	2.5	0.9	0.65	0.7–1	1.2
Dy	3	5.0	5.0	3.8	4.5–7.5	5.2
Ho	1.2	1.7	1.2	0.8	0.7–1.2	1.3
Er	2.8	3.3	4.0	2.1	2.5–6.5	3.5
Tm	0.5	0.27	0.4	0.3	0.2–1	0.52
Yb	3.4	0.33	2.7	2	2.7–8	3.2
Lu	0.5	0.8	0.8	0.35	0.8–1.7	0.8
Total	206.1	205.2	159.9	184.3	94.74–214.9	242.17

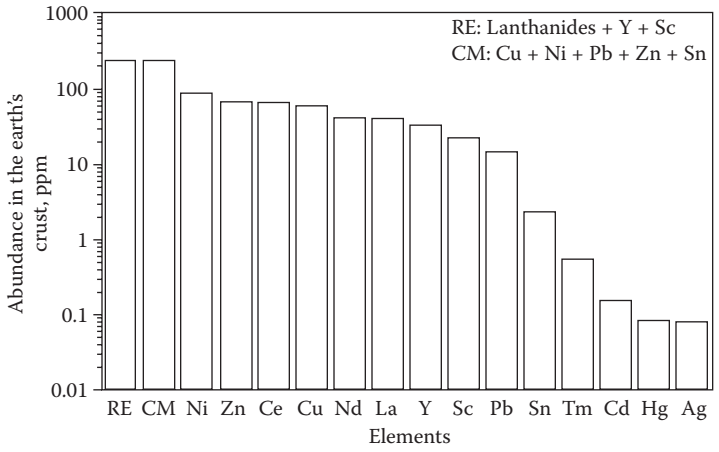


FIGURE 2.1 Abundance of rare earths and certain common elements in the earth's crust.

neodymium are the most abundant rare earths. The most abundant rare earth is cerium and the least abundant is thulium. Incidentally, cerium is more plentiful than copper; neodymium, yttrium, and lanthanum are each more plentiful than cobalt or lead; praseodymium, samarium, gadolinium, dysprosium, and erbium are each more plentiful than tin; and ytterbium and thulium, the least abundant of the rare earths, are each more plentiful than mercury or silver.

The extent to which a metal is used in technology and is available commercially is determined not only by its crustal abundance but also by many other factors (Hampel 1961). These include (1) the degree of metal concentration by natural processes into ore deposits, (2) the relative ease of obtaining the ore from the environment, and (3) the feasibility of extracting the metal from the ore. Unlike the common metals like copper and lead, which form fairly concentrated natural deposits, the rare earths occur widely distributed in low concentrations. Added to this, the nature of their mineralization and the complexity of the processes needed for their extraction seem to justify the adage "rare"—even though considering crustal abundance per se, they are not rare.

2.3 MINERALS

In nature the rare earths do not occur in the elemental state nor do they occur as individual rare-earth compounds. The rare earths, scattered dilutely in the earth's crust, occur as mixtures in many rock formations such as basalts, granites, gneisses, shales, and silicate rocks and are present in amounts ranging from 10 to 300 ppm (Sabot and Maestro 1995). Their strong affinity for oxygen has resulted in their being found mostly as oxidic compounds (oxides, carbonates, phosphates, and silicates) even though other combinations are possible. In rock-forming minerals, rare earths typically occur in compounds as trivalent cations in carbonates, oxides, phosphates, and silicates (Hedrick 2003). Rare earths occur in over 160 discrete minerals. Most

of these minerals are rare, but the rare-earth content in them, expressed as oxide, can be as high as 60% rare-earth oxide (REO). Many other minerals, in which the rare earths occur by atomic substitution, are also known (Aplan 1988). In total, nearly 200 minerals containing >0.01% rare earths are presently known (O'Driscoll 1991). As a rule, any rare-earth mineral usually contains all the rare-earth elements with some of them enriched and some others in very low concentrations.

United States Geological Survey brought out in 2002 a compilation of Rare Earth Element Mines, Deposits, and Occurrences in the world (Orris and Grauch 2002). The total number of rare-earth minerals listed as occurring in these deposits is 85. All these minerals are mentioned in Table 2.2, and the more important rare-earth minerals from the point of rare-earth extraction (Aplan 1988; Ferron et al. 1991; Jackson and Christiansen 1993) are listed in more detail in Table 2.3. Even though the rare-earth minerals are so many in number, about 95% of all the world rare-earth resources occur in just three of them, bastnasite, monazite, and xenotime apart from a special type of ore (ion-adsorption clay) with unique occurrence in China. These four therefore are the principal ore minerals for rare-earth extraction. Among these, again, bastnasite occurs most frequently, monazite is second, and the distant third position is shared by xenotime and the ionic clay. Other rare-earth minerals that have been or are now used as resources of rare earth include apatite, brannerite, euxenite, gadolinite, loparite, and uraninite. The minerals allanite, apatite, and other phosphorite sources, eudialyte, fergusonite, floreneite, parisite, perovskite, pyrochlore, zircon, and a few other naturally occurring rare earth-bearing materials are also considered potential rare-earth resources.

The first eight rare earths, lanthanum to gadolinium, are often referred to as the cerium subgroup of the REEs or light REEs (LREEs), and the remaining eight elements, terbium to lutetium, together with yttrium, are said to belong to the yttrium subgroup or heavy REEs (HREEs; Jackson and Christiansen 1993). Sometimes, the rare earths are divided into three subgroups. From lanthanum to neodymium are called "light rare earths," from samarium to dysprosium are known as "medium rare earths," and from holmium to lutetium, including yttrium, are called "heavy rare earths" (Sabot and Maestro 1995). In another classification (Kremers 1961), the light rare earths, from lanthanum to samarium, are called the "cerium group"; the middle rare earths, europium to dysprosium, are called the "terbium group"; and the heavies, holmium to lutetium and yttrium, are called the "yttrium group."

2.3.1 Bastnasite

Bastnasite, $(REE,Ce)(CO_3)F$, is a magma-derived fluorocarbonate mineral containing 65–75 wt.% REOs and hardly any thorium. Bastnasite (bastnäsite or bastnaesite) $[(Ce,La,Y)CO_3F]$, hydroxyl-bastnasite $[(Ce,La)CO_3(OH,F)]$, and parisite $[Ca(Ce,La)_2(CO_3)_3F_2]$ are all closely related. Bastnasite can be pale white, tan, gray, brown, yellow, or pink, with a pearly, vitreous, or greasy to dull luster. It usually forms small rounded hexagonal or short prismatic crystals. Both massive and granular varieties are known. As regards the geological environment, bastnasite is found in vein deposits, contact metamorphic zones, and pegmatites. Bastnasite occurs as

TABLE 2.2
Rare-Earth Minerals in World Rare-Earth Deposits

Mineral	Formula	Content (wt.%)		
		REO	ThO_2	UO_2
Aeschynite	$(Y,Ca,Fe,Th)(Ti,Nb)_2(O,OH)_6$	16–24	11–17	–
Allanite	$Ca(Ce,La,Y,Ca)Al_2(Fe^{2+},Fe^{3+})(SiO_4)(Si_2O_7)O(OH)$	–	–	–
Allanite (Ce)	$(Ce,Ca,Y)_2(Al,Fe^{2+},Fe^{3+})_3(SiO_4)_3(OH)$	3–51	0–3	–
Allanite (Y)	$(Y,Ce,Ca)_2(Al,Fe^{3+})_3(SiO_4)_3(OH)$	3–51	0–3	–
Anatase	$(Ti,REE)O_2$	–	–	–
Ancylite	$Sr(Ce,La)(CO_3)_2(OH)\cdot(H_2O)$	–	–	–
Ancylite (Ce)	$SrCe(CO_3)_2OH\cdot H_2O$	46–53	0–0.4	0.1
Apatite	$Ca_5(PO_4)_3(F,Cl,OH)$	–	–	–
Astrophyllite	$(K,Na)_3(Fe^{++},Mn)_7Ti_2Si_8O_{24}(O,OH)_7$	–	–	–
Baddeleyite	ZrO_2	–	–	–
Bariopyrochlore	$(Ba,Sr)_2(Nb,Ti)_2(O,OH)_7$	–	–	–
Bastnasite (Ce)	$(Ce,La)(CO_3)F$	70–74	0–0.3	0.09
Brannerite	$(U,Ca,Y,Ce)(Ti,Fe)_2O_6$	–	–	–
Britholite	$(Na,Ce,Ca)_5(OH)[(P,Si)O_4]_3$	–	–	–
Britholite (Ce)	$(Ce,Ca)_5(SiO_4,PO_4)_3(OH,F)$	56	1.5	–
Brockite	$(Ca,Th,Ce)(PO_4)\cdot H_2O$	–	–	–
Burbankite	$(Na,Ca)_3(Sr,Ba,Ce)_3(CO_3)_5$	–	–	–
Calcio-Ancylite (Ce)	$(Ca,Sr)Ce_3(CO_3)_4(OH)_3\cdot H_2O$	60	–	–
Carbocernaite	$(Ca,Na)(Sr,Ce,Ba)(CO_3)_2$	–	–	–
Caysichite	$Y_2(Ca,Gd)_2Si_4O_{10}(CO_3)_3(H_2O,O,OH)\cdot 3H_2O$	–	–	–
Cellophane	A hydroxylapatite-containing carbonate	–	–	–
Cerianite (Ce)	$(Ce^{4+},Th)O_2$	–	–	–
Ceriopyrochlore	$(Ce,Ca,Y)_2(Nb,Ta)_2O_6(OH,F)$	–	–	–
Cerite	$(Ce,La,Ca)_9(Mg,Fe^{3+})(SiO_4)_6(SiO_3OH)(OH)_3$	–	–	–
Cerite (Ce)	$Ce_9Fe^{3+}(SiO_2)_6[(SiO_3)(OH)](OH)_3$	–	–	–
Cheralite	$(Ca,Ce,Th)(P,Si)O_4$	–	≤30	–
Chevkinite	$(Ca,Ce,Th)_4(Fe^{2+},Mg)_2(Ti,Fe^{3+})_3Si_4O_{22}$	–	–	–
Churchite (Y)	$YPO_4\cdot H_2O$	–	–	–
Columbite	$(Fe,Mn)Nb_2O_6$, $(Y,U,Fe)(Nb,Ta)O_4$	–	–	–
Cordylite	$Ba(Ce,La)_2(CO_3)_3F_2$	–	–	–
Crandallite	$CaAl_3(PO_4)_2(OH)_5\cdot H_2O$	–	–	–
Daqingshanite	$Sr_{1.2}Ca_{0.6}Ba_{0.2}Ce_{0.75}La_{0.25}(PO_4)(CO_3)_{2.5}(OH)_{0.4}F_{0.1}$	–	–	–
Doverite	$YCaF(CO_3)_2$	–	–	–
Eudialyte	$Na_4(Ca,Ce)_2(Fe^{2+},Mn^{2+},Y)ZrSi_8O_{22}(OH,Cl)_2$	1–10	–	–
Euxenite	$(Y,Er,Ce,U,Pb,Ca)(Nb,Ta,Ti)_2(O,OH)_6$	34–58	1–5	0.4–12
Fapa Fluorapatite	$Ca_5(PO_4)_3F$	–	–	–
Fcer Fluocerite	$(Ce,La)F_3$	–	–	–
Ferg Fergusonite		–	–	–

(*Continued*)

TABLE 2.2 (CONTINUED)
Rare-Earth Minerals in World Rare-Earth Deposits

Mineral	Formula	Content (wt.%) REO	ThO_2	UO_2
Fergusonite	$(Y,Sr,Ce,U)(Nb,Ta,Ti)O_4$	32–62	1–3	1–6
Fersmite	$(Ca,Ce)(Cb,Ti)_2(O,F)_6$	–	–	–
Florencite	$(La,Ce)Al_3(PO_4)_2(OH)_6$	–	–	–
Florencite (Ce)	$CeAl_3(PO_4)_2(OH)_6$	–	1.4	–
Florencite (La)	$(La,Ce)Al_3(PO_4)_2(OH)_6$	1.4	–	–
Fluocerite (Ce)	$(Ce,La)F_3$	–	–	–
Fluocerite (La)	$(La,Ce)F_3$	–	–	–
Fluorapatite	$(Ca,Ce)_5(PO_4)_3F$	0–21	0–0.01	
Fluorite	$(Ca,REE)F$	–	–	–
Formanite	$(U,Zr,Th,Ca)(TaNb)O_4$	–	–	–
Gadolinite	$(Y,Ce)_2FeBe_2Si_2O_{10}$	36–40	0.3–0.4	–
Gagarinite (Y)	$NaCaY(F,Cl)_6$	–	–	–
Gerenite (Y)	$(Ca,Na)_2(Y,REE)_3Si_6O_{18}\cdot 2H_2O$	–	–	–
Gittinsite	$CaZrSi_2O_7$	–	–	–
Gorceixite	$(Ba,REE)Al_3[(PO_4)_2(OH)_5]\cdot H_2O$	–	–	–
Goyazite	$SrAl_3(PO_4)_2(OH)_5\cdot H_2O$	–	1.4	–
Hellandite	$(Ca,Na)_{2-3}Al_3(Al,Si)_2Si_{13}O_{36}\cdot 12H_2O$	–	–	–
Hingganite (Y)	$(Y,Yb,Er)_2Be_2Si_2O_8(OH)_2$	–	–	–
Huanghoite	$BaCe(CO_3)_2F$	–	–	–
Hydroxylapatite	$Ca_5(PO_4)_3(OH)$	–	–	–
Iimoriite (Y)	$Y_2(SiO_4)(CO_3)$	–	–	–
Joaquinite	$NaFe^{2+}Ba_2Ce_2TiNb(Si_4O_{12})_2(OH)_{0.5}F_{0.5}\cdot(H_2O)$	–	–	–
Kainosite	$Ca_2(Ce,Y)_2(SiO_4)_3CO_3\cdot H_2O$	–	–	–
Kamphaugite	$Ca(Y,REE)(CO_3)_2(OH)_2\cdot 3(H_2O)$	–	–	–
Karnasurtite	$(Ce,La,Th)(Ti,Nb)(Al,Fe^{3+})(Si,P)_2O_7(OH)_4\cdot 3(H_2O)$	–	–	–
Keiviite	$(Y,Yb)_2Si_2O_7$	–	–	–
Kuliokite	$(Y,REE)_4Al(SiO_4)_2(OH)_2F_5$	–	–	–
Lavenite	$(Na,Ca)_2(Mn^{2+},Fe^{2+})(Zr,Ti)Si_2O_7(O,OH,F)_2$	–	–	–
Lessingite	$Ca_2Ce_4Si_3O_{13}(OH)_2$	–	–	–
Leucophanite	$(Na,Ca)_2BeSi_2(O,OH,F)_7$	–	–	–
Loparite	$(Na,Ca,Ce,Sr)_2(Ti,Ta,Nb)_2O_6$	32–34	–	–
Lovchorrite	$Ce_2(TiO_3)_3\cdot 10CaSiO_3\cdot 2CeF_3$	–	–	–
Lueshite	$NaNbO_3$	–	–	–
Miserite	$KCa_6Si_8O_{22}(OH)$	–	–	–
Monazite (Ce)	$(Ce,La,Nd,Th)PO_4$	35–71	0–20	0–16
Mosandrite	$Na(Na,Ca)_2(Ca,Ce,Y)_4(Ti,Nb,Zr)(Si_2O_7)_2(O,F)_2F_3$	–	–	–
Orthite	$(Ca,Ce)_2(Al,Fe)_3Si_3O_{12}[O,OH]$	0–21	–	–
Parisite (Ce)	$Ca(Ce,La)_2(CO_3)_3F_2$	59	0–0.5	0–0.3
Perovskite	$(Ca,REE)TiO_3$	≤37	0–2	0–0.05

(*Continued*)

TABLE 2.2 (CONTINUED)
Rare-Earth Minerals in World Rare-Earth Deposits

Mineral	Formula	Content (wt.%) REO	ThO_2	UO_2
Perovskite	$(Ca,REE)TiO_3$	≤37	0–2	0–0.05
Plumbopyroclore	$(Pb,U,Ca)_{2-x}Nb_2O_6(OH)$	–	–	–
Polycrase	$(Y,Ca,Ce,U,Th)(Ti,Nb,Ta)_2O_6$	–	–	–
Polylithionite	$KLi_2AlSi_4O_{10}(F,OH)_2$	–	–	–
Priorite	$(Y,Er,Ca,Th)(Ti,Nb)_2O_6$	25–33	0.6–8	0.5–3
Pyrochlore	$(Ca,Na,REE)_2Nb_2O_6(OH,F)$	–	–	–
Rhabdophane (Ce)	$(Ce,La)PO_4{\cdot}H_2O$	–	–	–
Rhabdophane (La)	$(La,Ce)PO_4{\cdot}H_2O$	–	–	–
Rinkite (Rinkolite)	$(Ca,Ce)_4Na(Na,Ca)_2Ti(Si_2O_7)_2F_2(O,F)_2$	–	–	–
Rosenbuschite	$(Ca,Na)_3(Zr,Ti)Si_2O_8F$	–	–	–
Sahamalite	$(Mg,Fe^{2+})Ce_2(CO_3)_4$	–	–	–
Samarskite	$(REE,Fe^{2+},Fe^{3+},U,Th,Ca)(Nb,Ta,Ti)O_4$	–	–	–
Samarskite	$(Y,Er,Fe,Mn,Ca,U,Th,Zr)(Nb,Ta)_2(O,OH)_6$	10–36	0–4	4–16
Sphene (Titanite)	$(Ca,REE)TiSiO_5$	≤3	–	–
Steenstrupine (Ce)	$Na_{14}Ce_6Mn_2Fe_2(Zr,Th)(Si_6O_{18})_2(PO_4)_7{\cdot}3H_2O$	–	–	–
Stillwellite	$(Ce,La,Ca)BSiO_5$	–	–	–
Synchisite	$Ca(Ce,Nd,Y,La)(CO_3)_2F$	–	–	–
Synchysite (Ce)	$Ca(Ce,La)(CO_3)_2F$	49–52	1.6	–
Synchysite (Y) (Doverite)	$Ca(Y,Ce)(CO_3)_2F$	–	–	–
Tengerite	$Y_2(CO_3)_3{\cdot}n(H_2O)$	–	–	–
Thalenite (Y)	$Y_3Si_3O_{10}(F,OH)$	–	–	–
Thorite	$(Th,U)SiO_4$	≤3	–	10–16
Titanite (Sphene)	$CaTiSiO_5$	–	–	–
Uraninite	$(U,Th,Ce)O_2$	–	–	–
Vesuvianite	$Ca_{10}(Mg,Fe)_2Al_4(SiO_4)_5(Si_2O_7)_2(OH,F)_4$	–	–	–
Vitusite (Ce)	$Na_3(Ce,La,Nd)(PO_4)_2$	–	–	–
Wöhlerite	$Ca_2Na(Zr,Nb)(F,OH,O)_2Si_2O_7$	–	–	–
Xenotime	YPO_4	52–67	0–5	0–5
Yttrotantalite	$(Y,U,Fe^{++})(Ta,Nb)O_4$	–	–	–
Yttrialite	$(Y,Th)_2Si_2O_7$	–	–	–
Yttrocerite	$(Ca,Y,Ce,Er)F_2{\cdot}3H_2O$	22–50	–	–
Yttrofluorite	$(Ca,Y)F_2$	–	–	–
Zircon	$(Zr,REE)SiO_4$	–	0.1–0.8	–
Zirkelite	$(Ca,Th,Ce)Zr(Ti,Nb)_2O_7$	–	–	–

Source: Orris, G.J., and Grauch, R.I., Rare earth element mines, deposits, and occurrences: U.S. Geological Survey Open-File Report 2002–0189, 2002; Long, K.R. et al., The principal rare earth elements deposits of the United States—A summary of domestic deposits and a global perspective: U.S. Geological Survey Scientific Investigations Report 2010–5220. Available at http://pubs.usgs.gov/sir/2010/5220, 2010.

TABLE 2.3
Important Rare-Earth Minerals

Mineral	Formula	Rare-Earth Content (%)	Other Constituents (%)
Aeschynite	$(Ce,Ca,Th)(Ti,Nb)_2O_6$	Ce_2O_3 15.5–19.5; $(Y,Er)_2O_3$ 0.9–4.5	TiO_2 21.2–24; Nb_2O_5 23.8–32.5; Ta_2O_5 0–7; ThO_2 11.2–17.5; CaO 2.3–2.7; FeO 2.2–4.3; also Sn, Mn, Mg
Bastnasite	$(Ce,La,Pr)(CO_3)F$	Ce_2O_3 36.9–40.5; $(La,Pr,..)_2O_3$ 36.3–36.6	CO_2 19.8–20.2; F 6.2–8.5
Euxenite	$(Y,Ce,Ca,U,Th)(Ti,Nb,Ta)_2O_6$	$(Y,Er)_2O_3$ 18.2–27.7; $(Ce,La,\ldots)_2O_3$ 16–30	TiO_2 16–30; Nb_2O_5 4.3–47.4; Ta_2O_5 1.3–23; ThO_2 1–5; UO_2 0.4–12
Fergusonite	$(Y,Sr,Ce,U)(Nb,Ta,Ti)O_4$	Y_2O_3 31–42; $(Ce,La,..)_2O_3$ 0.9–6; Er_2O_3 0–14	$(Nb,Ta)_2O_5$ 46–57.5; ThO_2 1–3.4; UO_2 1.2–6; TiO_2 0–6; also ZrO_2, SnO_2, WO_3
Gadolinite	$(Y,Ce)_2FeBe_2Si_2O_{10}$	Y_2O_3 30.7–46.5; $(Ce,La,\ldots)_2O_3$ 5.23	FeO 10–13.7; SiO_2 23–24.5; ThO_2 0.3–0.4; BeO 9–10.2; also Ca, Mg
Loparite	$(Na,Ca,Ce,Sr)_2(Ti,Ta,Nb)_2O_6$	$(Ce,La,\ldots)_2O_3$ 32–34	TiO_2 39.2–40; $(Nb,Ta)_2O_5$ 8–11; CaO 4.2–5.2; Na_2O 7.8–9; also Sr, K, Si, Th
Monazite	$(Ce,La\ldots)PO_4$	$(Ce,La,\ldots)_2O_3$ 50–68	P_2O_5 22–31.5; ThO_2 4–12; U 0.1–0.3; ZrO_2 0–7; SiO_2 0–6
Orthite	$(Ca,Ce)_2(Al,Fe)_3Si_3O_{12}$ [O,OH]	Ce_2O_3 0–6; La_2O_3 0–7; Y_2O_3 0–8	BeO 3.8; also ThO_2
Parisite	$Ca(Ce,La\ldots)_2(CO_3)F_2$	Ce_2O_3 26–31; $(La,Nd,..)_2O_3$ 27.3–30.4; Y 8	CaO 10.4–11.4; CO_2 23–24.5; F 6–7
Priorite	$(Y,Er,Ca,Th)(Ti,Nb)_2O_6$	$(Y,Er)_2O_3$ 21.1–28.7; Ce_2O_3 3.7–4.3	TiO_2 21.8–34; Nb_2O_5 15–36.7; Ta_2O_5 0–1.3; CaO 1–4.1; ThO_2 0.6–7.9; UO_2 0.5–3; FeO 1.4–5.6; SnO_2 0–0.3; PbO 0.08; MnO 0–2
Samarskite	$(Y,Er,U,Ce,Th)_4(Nb,Ta)_6O_2$	Y_2O_3 6.4–14.5; Er_2O_3 2.7–13.4; Ce_2O_3 0.25–3.2; La_2O_3 0.37–1; $(Pr,Nd)_2O_3$ 0.74–4.2	Nb_2O_5 2.7–46.8; Ta_2O_5 1.8–27; ThO_2 0–4.2; UO_2 4–16; also Ti, Zr, Sn
Thorite	$ThSiO_4$		U_3O_8 10–16
Xenotime	YPO_4	Y_2O_3 52–62	ThO_2, UO_2 up to 5; ZrO_2 3; SnO_2, SiO_2 9
Yttrocerite	$(Ca,Y,Ce,Er)F_2{\cdot}3H_2O$	Ce 8.5–11.5; Y 14.3–37.7	Ca 19.7–32.7; F 37.7–41.6

Source: Aplan, F.F., The processing of rare earth minerals. In Bautista, R.G. and Wong, M.M. (eds.), *Rare Earths*, The Minerals, Metals and Materials Society, Warrendale, PA, 1988.

TABLE 2.4
REE Distribution in Bastnasite (w.r.t. 100% REO)

Rare Earth	Bastnasite, Mountain Pass	Bastnasite, Bayan Obo
La	33.2	23.0
Ce	49.1	50.0
Pr	4.34	6.20
Nd	12.0	18.5
Sm	0.789	0.800
Eu	0.118	0.200
Gd	0.166	0.700
Tb	0.0159	0.100
Dy	0.0312	0.100
Ho	0.0051	Trace
Er	0.0035	Trace
Tm	0.0009	Trace
Yb	0.0006	Trace
Lu	0.0001	Trace
Y	0.0913	0.500

veins or dissemination in a complex of carbonate–silicate rocks, occurring with and related to alkaline intrusives, for example, in California. Bastnasite occurs in quartz veins that cut micaceous schists and quartzite in Burundi. It is in fluorite-bearing veins and breccia filings in Permian sandstone, for example, in New Mexico (Jackson and Christiansen 1993).

The rare-earth content of bastnasite is approximately 70% REO, mostly of the lighter elements. Bastnasite is the primary source of light REO in the enormous deposit in Bayan Obo in China (800 million metric tons [Mt]; 6% REO) and at Mountain Pass, California, in the United States (3.3 Mt; 7.7% REO). The rare-earth content in bastnasite from these locations is given in Table 2.4 (Hedrick 1991). In addition, bastnasite is also the main REO mineral in Bear Lodge (Wyoming), Brockman in Australia, Pocos de Caldas in Brazil, Thor Lake in Canada, and Karonge in Burundi. Bastnasite is chemically susceptible to weathering, and this causes REO to dissolve and combine with available phosphates.

2.3.2 Monazite

The mineral monazite is a phosphate, mainly of the cerium group rare earths and thorium [$(Ce,La,Y,Th)PO_4$]. Monazite's resistance to chemical weathering and its high specific gravity are reasons for its association with other chemically resistant heavy minerals such as ilmenite, magnetite, rutile, and zircon in placer deposits. Because monazite is radioactive (alpha activity), its grains can be metamict, which means they have lost their crystalline structure owing to internal damage due to alpha particles arising out of radioactive decay. Crystals of monazite are yellow to brown or orange-brown with a vitreous and resinous or adamantine luster. Monazite

grains are usually equant to prismatic with wedge-shaped terminations. Both granular and massive forms exist (Long et al. 2010).

Monazite is found in many geological environments. It occurs as an accessory mineral in acidic igneous rocks, in metamorphic rocks, and in certain vein deposits. The primary monazite deposits have been exploited as rare-earth resources in a few instances. Notable among them are occurrences in Van Rhynsdorp and Naboomspruit (South Africa), in Colorado (United States), and in Bayan Obo (China). The most important monazite resources have been the beach placers. Alluvial, stream, and aeolian deposits have been less significant. Beach sand deposits contain, in addition to monazite, other heavy minerals like ilmenite, rutile, and zircon. Sometimes monazite co-occurs with placer gold or tin deposits (Aplan 1988). Monazite-bearing heavy mineral sand deposits are found in large quantities principally in Australia, Brazil, China, India, Malaysia, South Africa, and the United States. The rare-earth content and individual REE distribution in monazite are variable, as also its thorium content, depending on the location (Hedrick 1985b, 1992). This is shown in Table 2.5. Usually monazite contains about 70% REO, and the rare-earth fraction is constituted by 20–30% Ce_2O_3; 10–40% La_2O_3; significant amounts of neodymium, praseodymium, and samarium; and lesser amounts of dysprosium, erbium, and holmium. Yttrium content may vary from a trace to ~5% Y_2O_3, and thorium content of 4–12% is common. Some amount of uranium is also present in monazite.

2.3.3 Xenotime

Xenotime is a Y-bearing phosphate mineral (YPO_4) containing about 67% REO, mostly of the heavier elements. It is yellowish brown to reddish brown with a vitreous to resinous luster, occasionally gray, salmon pink, and even green. It is usually an accessory mineral in acidic and alkaline rocks, though it has been observed in mica schists and quartz-rich gneisses. Xenotime can easily be mistaken for zircon because of similarities in crystal habit and overall appearance. However, it is not as hard as zircon and demonstrates perfect {100} cleavage. Having undergone a weathering, transportation, and concentration process similar to that of monazite, xenotime co-occurs with it in placer deposits, but such deposits are relatively few. Usually the content of xenotime may range from 0.5% to about 5% of the monazite present. A rare occurrence where the proportion of xenotime is as high as 50% was identified in California (Sabot and Maestro 1995). Xenotime occurs in the placer cassiterite deposits in Malaysia and in certain Australian heavy mineral sands. Xenotime occurs also in the placer cassiterite deposits of Indonesia and Thailand and in the heavy mineral sands of China, as well as in the alluvial tin mines of Brazil (Highley et al. 1988). The rare-earth distribution in xenotime is given in Table 2.6.

In addition to the three major minerals, there are several other rare-earth minerals that are or could become important for the commercial recovery of rare earths.

2.3.4 Allanite

Allanite [$Ca(Ce,La,Y,Ca)Al_2(Fe^{2+},Fe^{3+})(SiO_4)(Si_2O_7)O(OH)$] is a rare earth-bearing member of the epidote mineral group. It is one of the more common REE-bearing

TABLE 2.5
Rare-Earth Distribution in Monazite from Different Locations (% of TREO)

Rare Earth	North Staradbroke Island, Queensland	Capel, Western Australia	East Coast, Brazil	Nangang, Guangdong China	India	Green Cove Springs, Florida	Bear Valley, Idaho	Mount Weld, Australia
La	21.50	23.90	24.00	23.35	23.00	17.50	26.23	26.00
Ce	45.8	46.02	47.00	42.70	46.00	43.70	46.14	51.00
Pr	5.3	5.04	4.50	4.10	5.50	5.00	6.02	4.00
Nd	18.6	17.38	18.50	17.00	20.00	17.50	16.98	15.00
Sm	3.1	2.53	3.00	3.00	4.0	4.90	2.01	1.8
Eu	0.8	0.05	0.0550	0.10		0.16	1.54	0.4
Gd	1.8	1.49	1.00	2.03		6.60	0.77	1.0
Tb	0.29	0.04	0.1	0.70		0.26		0.1
Dy	0.64	0.69	0.35	0.80		0.90	Tb,Dy: 0.31	0.2
Ho	0.12	0.05	0.035	0.12		0.11		0.1
Er	0.18	0.21	0.07	0.30		0.04		0.2
Tm	0.03	0.01	0.005	Trace		0.03		Trace
Yb	0.11	0.12	0.02	2.40		0.21		0.1
Lu	0.01	0.04		0.14		0.03	Ho–Lu: 0.15	Trace
Y	2.50	2.41	1.4	2.40	Eu–Y: 1.50	3.20	1.39	Trace
Major Constituents		**Taiwan Black Monazite**		**Taiwan Yellow Monazite**		**Australian Monazite**		**Indian Monazite**
REO		48.62		63.22		58.50		58.60
P_2O_5		20.14		30.27		27.50		30.1
SiO_2		18.66		1.62		2.83		1.7
ThO_2		0.41		3.21		6.40		8.8

Note: Australian monazite from Eneabba Co., Australia. Indian monazite from Indian Rare Earths Ltd., India.

TABLE 2.6
Rare-Earth Distribution in Important Rare-Earth Minerals (% of TREO)

	Ion-Adsorption Ore			Xenotime								
Rare Earth	Longnan	Xunwu	Uranium Residues, Canada	Malaysia	Guangdong, China	Gadolinite	Allanite	Apatite	Eudialyte, Revda, Russia	Loparite, Kola	Nechalacho Ore	Synchysite-(Y), Kutessaisk, Kazakhstan
La	1.82	43.4	0.80	0.50	1.20	1	20	25.78	15.2	27.8	17.28	14
Ce	0.40	2.40	3.70	5.00	8.00	2	40	46.22	29.7	57.1	39.55	26
Pr	0.70	9.00	1.00	0.70	0.60	2	10	4.00	2.9	3.7	4.89	2.7
Nd	3.00	31.70	4.10	2.20	3.50	5	20	14.4	12.7	8.7	19.10	9.8
Sm	2.80	3.90	4.50	1.90	2.20	5	2	1.6	3.4	0.91	3.77	3.5
Eu	0.10	0.50	0.20	0.20	0.20	Trace	0.03	0.5	1.3	0.13	0.44	0.08
Gd	6.90	3.00	8.50	4.00	5.00	5	1	1.5	3.0	0.21	3.06	3.5
Tb	1.30	Trace	1.20	1.00	1.20	0.5	0.1	0.1	2.8	0.07	0.40	0.7
Dy	6.70	Trace	11.20	8.70	9.10	6	0.3	1.02	4.3	0.09	1.84	4.3
Ho	1.60	Trace	2.60	2.10	2.60	1	0.1	0.10	2.9	0.03	0.31	0.8
Er	4.90	Trace	5.50	5.40	5.60	4	0.3	0.15	2.1	0.07	0.60	3.8
Tm	0.70	Trace	0.90	0.90	1.30	0.6	0.1	0.02	Na	0.07	0.11	0.3
Yb	2.50	0.30	4.00	6.20	6.00	4	0.3	0.08	1.6	0.29	1.20	1.2
Lu	0.40	0.10	0.40	0.40	1.80	0.6	<0.1		0.3	0.05	0.11	0.25
Y	65.00	8.00	51.40	60.80	59.30	60	3	4.40	21.4	0.14	7.80	29

minerals in igneous rocks such as granites, syenites, diorites, and associated pegmatites, but not in sufficient concentrations to be considered an ore of REE. Allanite grains are tabular and usually black, sometimes dark brown to brownish violet. It has a conchoidal fracture and is commonly metamict because of the alpha radioactivity due to thorium.

Allanite occurs in igneous, hydrothermal, and metamorphic environments. It may be found as small or disseminated crystals throughout the pegmatitic body or as veins varying in width from a fraction of an inch to several feet. The rare-earth content of allanite is normally limited to about 5% REO, but it may vary from 3% to 51%, depending on the source. The thorium content of allanite may vary from a trace up to 3%. The relatively low REO, usually scattered presence in the rock and the thorium content have prevented allanite from being processed on a large scale. However, allanite had been considered as a useful future resource (Nininger 1956) because it is available in very large quantities and might be produced at a lower cost per ton than monazite. At present, three deposits are considered to have potential for allanite mining (Jackson and Christiansen 1993). They are the Mary Kathleen uranium tailings in Queensland, Australia, the Alice Springs prospect in the Northern Territory, Australia (1 Mt, 4% allanite, 20% REO), and the deposits in Hall Mountain Group in Idaho, USA. The rare-earth distribution in allanite is given in Table 2.6.

2.3.5 Apatite

Apatite is a calcium fluorophosphate. It is found in carbonatites, alkaline igneous rocks, and some sediments. Apatite is not a rare-earth mineral but a rare-earth concentrating mineral (Aplan 1988). Rare-earth ions are similar in size to calcium ions and proxy calcium ions in the apatite lattice. The rare-earth content of apatite is highly variable and ranges from a trace to over 10% (as REO). The amount and distribution of rare earths are dependent on the nature of the host rock. The rare-earth distribution in Kola apatite is given in Table 2.6.

Apatite may constitute a substantial resource for rare earths. Unlike most of the rare-earth minerals, which are found only in small quantities in a potential ore body, apatite occurs in large quantities like bastnasite and monazite.

Large quantities of rare earth–bearing apatites occur at Kola Peninsula (~1% REO), Kovdor, and in the Vishnevye Mountains (>1% REO) in the former Soviet Union (Hedrick 1985b), in Phalaborwa in South Africa, and in the Mineville iron ore in New York State in the United States (Aplan 1988). Rare earth-bearing apatites have also been located in California placers (Hedrick 1986) and in Florida (Altschuler et al. 1967). Phosphorite deposits in Jordan and Morocco also contain rare earths. REEs in the apatite containing tailings of the Chadormalu iron ore concentrator in Iran have also been recently identified as a significant source of rare earths (Jorjani and Bagherieh 2007).

Phosphorite is a phosphate-rich sedimentary rock that contains between 18% and 40% P_2O_5. The apatite in phosphorite is present as cryptocrystalline masses referred to as *collophane*. Phosphorites in the large phosphoria formation of Montana, Utah, and Wyoming contain rare earths (0.16%) (Aplan 1988). The

TABLE 2.7
Content of REEs in Various Phosphate Rocks

Deposit	Florida	Morocco	Algeria	Russia	South Africa	Russia				
Origin	Pebble	Khoribga	Djebel Onk	Kola	Palfos	Kovdor	Jordan		Israel	
Lanthanides%	0.29	0.14–0.16	0.13–0.18	0.84–0.88	0.4	0.14	0.01		0.01	
Content of REEs in Various Phosphorite Phosphate Rocks (ppm)										
Deposit	**Y_2O_3**	**La_2O_3**	**CeO_2**	**Pr_6O_{11}**	**Nd_2O_3**	**Sm_2O_3**	**Eu_2O_3**	**Gd_2O_3**	**Tb_4O_7**	**Dy_2O_3**
Zhijin	434.2	273.2	162.7	45.8	198.2	35.2	8.5	42.9	5.9	35.5
Fanshan	248.9	1034	2170	285.0	1201	229.6	56.9	166.6	16.9	62.8
Deposit	**Ho_2O_3**	**Er_2O_3**	**Tm_2O_3**	**Yb_2O_3**	**Lu_2O_3**	**Sc_2O_3**	**ΣREO**	**LREO**	**HREO**	**LREO/ HREO**
Zhijin	7.4	20.4	2.3	12.0	1.4	6.8	1295.0	723.7	571.3	1.27
Fanshan	9.1	19.8	1.9	9.7	1.22–5513.2	4976.1	537.1	9.26		
Ore Composition (Phosphorite Ore—Fanshan Phosphorite)										
P_2O_5	**CaO**		**REO**		**MgO**		**FeO**		**Al_2O_3**	
33.8%	51.0%		0.55%		0.8%		1.5%		0.5%	

Source: Krea, M. and Khalaf, H., *Hydrometallurgy*, 58(3): 215–225, 2000; Koopman, C. and Witkamp, G.J., *Hydrometallurgy*, 58(1): 51–60, 2000; Wang, H. et al., *Hydrometallurgy*, 101(1–2): 41–47, 2010.

quantity of rare earths contained in phosphate sources has been estimated to be over 8 Mt REO (Cross and Miller 1988). The total reserve in the world is about 100 billion tons (Becker 1983; Ilyin 1998), which on average contains 0.5% REO. Table 2.7 shows the rare-earth content in various phosphorite reserves. In particular, Russia has abundant reserves of high-grade phosphorite ore at Kola, which contains up to 1% rare earths and is considered as the primary rare-earth resource in the country. Therefore, it is important to study the recovery of the rare earths from phosphorite, which is a phosphate mineral suitable for the manufacture of phosphoric acid (Wang et al. 2010). Rock phosphate, which is used for the production of fertilizer-grade phosphoric acid, contains minor quantities of REEs. It is often considered as a secondary source for REEs. Phosphate rocks generally contain about 50–300 mg of uranium and ≤100 mg of rare earths for every kg of rock, depending on the source (Cioroianu et al. 2001).

2.3.6 Brannerite

The uranium ore brannerite contains rare earths and occurs in pegmatites and conglomerates. Economically important quantities of brannerite occur in the Precambrian quartz pebble conglomerate at Elliot Lake, Ontario, Canada (Adams and Staatz 1973). The distribution of rare earths in the deposit is given in Table 2.6. Brannerite also occurs in association with gold in the Witwatersrand deposit in South Africa (Highley et al. 1988) and at Radium Hill, Australia (Adams 1971).

2.3.7 Eudialyte

Eudialyte is a somewhat rare, nine-member ring cyclosilicate mineral, which forms in alkaline igneous rocks, such as nepheline syenites. It is a zirconium mineral that can contain rare earths (1–3% REO) and could be rich in yttrium (0.2–1%) too (Ferron et al. 1991). Eudialyte was first described in 1819 for an occurrence in nepheline syenite of the Ilimaussaq intrusive complex of southwest Greenland. This silicate mineral also occurs in peralkaline granite, for example, at Pajarito in New Mexico, USA (Jackson and Christiansen 1993). The rare-earth contents of these deposits are 0.9% and 0.18% REO, respectively. Eudialyte deposits also occur in the former USSR and Canada. An advantage is that eudialyte tends to form as coarse-grained euhedral crystals that are easily dissolved in acids. In fact, its name alludes to its ready solubility in acid.

2.3.8 Euxenite, Fergusonite, Florencite, Gadolinite, and Loparite

The minerals euxenite and fergusonite are complex tantaloniobates of titanium, rare earths, thorium, and uranium. Euxenite $[(Y,Er,Ce,U,Pb,Ca)(Nb,Ta,Ti)_2(O,OH)_6]$ is an oxide mineral that forms a series with the mineral polycrase $[(Y,Ca,Ce,U,Th)(Ti,Nb,Ta)_2O_6]$. Other REO minerals, such as fergusonite, aeschynite, and samarskite, have similar properties. The co-occurring metal values and the heavy rare-earth content make euxenite processing attractive (Dayton 1958). Euxenite is black with a tabular to prismatic habit, indistinguishable from rutile, when found

in massive form. Unlike rutile, euxenite does not have any cleavage planes, and it undergoes conchoidal fracture. Euxenite is ordinarily found in granite pegmatites, commonly associated with quartz, feldspars, columbite (now called ferrocolumbite), tantalite (now called ferrotantalite or manganocolumbite), and monazite (Long et al. 2010). It occurs in the placer deposits of Idaho.

The mineral florencite is an aluminum phosphate. It occurs in the weathered zone of carbonatites. This mineral by itself can be relatively high in REO, but it is not known to occur in large quantities (Jackson and Christiansen 1993).

Gadolinite is a beryllium iron silicate mineral found in granites, granitic pegmatites, and placers. Gadolinite is a widespread but not abundant component of pegmatites and has been found in veins, lenses, and pockets in many locations, particularly in the United States (Kleber and Love 1963). Gadolinite deposits have also been found in Quebec and Yellowknife, Northwest Territories (Canada) (Hedrick 1985b). Gadolinite usually contains about 40% REO. The rare-earth distribution (Foos and Wilhelm 1954; Spedding and Powell 1954) is given in Table 2.6.

Loparite is basically a niobium ore that contains titanium and the rare earths. A large deposit of loparite occurs in the Kola Peninsula of the former Soviet Union. It occurs in association with the minerals aegirine, apatite, eudialyte, feldspar, nepheline, ramasayite, and titanite. The primary ore grades 2–3% loparite. The rare-earth content is 30–36% REO (Hedrick et al. 1997; Jackson and Christiensen 1993) from the cerium group. The rare-earth distribution in loparite is given in Table 2.6. Loparite occurrence has also been reported in the Parana Basin carbonatite near Sarambi, Paraguay (Hedrick et al. 1997).

2.3.9 Perovskite

Perovskite, which is a calcium titanate, is a rare-earth concentrating mineral where the rare earths substitute calcium. Rare earth–containing varieties, enriched essentially in the light rare earths, are mainly associated with alkalic igneous rock suites. A major prospect containing perovskite is at Powderhorn, Colorado, USA. Here the rock contains 0.36% REO (Jackson and Christiensen 1993). Large quantities of rare earths are reportedly contained in various perovskite ore bodies (Haskin and Paster 1979).

2.3.10 Pyrochlore

Pyrochlore is another rare-earth concentrating mineral (Aplan 1988; Highley et al. 1988). In this mineral, rare earths substitute in the alkali position. Large deposits of pyrochlore occur at St. Honoré and Oka in Quebec (Noblitt 1965) and Araxa, Brazil (Adams 1971), and at various places along the Rift Valley in East Africa.

2.3.11 Zircon

Zircon is also known to accept a spectrum of REEs in the mineral and can be considered as a probable source of yttrium and heavy lanthanides (Haskin and Paster 1979).

2.3.12 Others

It has been recently established that granite-like subalkaline rare metal metasomatites located near faults may serve as an important source of yttrium and other rare earths.

An unusual type of rare-earth ore known as ion adsorption-type ore is found at various locations in South China. The ion-adsorption ore is a weathered crust elution-deposited rare-earth ore. It is a unique rare earth-rich mineralized clay. Mild, humid, rainy climatic conditions and tectonically stable environment are suitable for such weathering processes to occur. At present, however, only two districts (both in southern China), where such conditions prevail, have the ion adsorption deposits. It only exists in China in Jiangxi, Fujian, Hunan, Guangdong, Yunnan, and Guangxi provinces and was discovered in 1969. The grade of these rare-earth deposits is low in the conventional sense, but not only the composition of the rare earths contained therein is very attractive, being particularly rich in the medium and heavy REEs (Chi and Tian 2008), but also the deposit is very easy to process.

The metallogenetic mechanism of this kind of ore could possibly be the weathering of granodiorite and volcanic rocks in humid and warm climate, being transformed into clay minerals such as kaolinite, halloysite, and montmorillonite (Tian et al. 2010). During the same progressive geological weathering, the rare-earth minerals could have also weathered in the original rocks, releasing the rare-earth ions that moved with migrating flow of natural water and adsorbed onto the clay minerals (Wan and Liu 2005). Thus, the rare earth in the weathered crust elution deposited rare-earth ore mainly exists with the ion-exchangeable phase adsorbed on clay minerals (Chi et al. 2005). Apparently, this kind of adsorption module has stable chemical properties and does not hydrolyze and revolute in neutral water. The weathering process also modifies the proportion of the various lanthanides originally found in the source rock, as they ultimately end up as the ion-adsorption ores. The composition of ion-adsorption ores depends on location. Laterite clays from Longnan (LN) in the Jiangxi Province yield heavy REE- and Y-rich material, whereas ore from Xunwu is light REE-rich (O'Driscoll 2003), but overall, they are relatively rich in Y and the mid-rare earths such as Eu, Sm, and Gd. As shown in Table 2.8 (Jun et al. 2010), LN rare-earth ore contains mainly heavy rare earth, and the yttrium element accounts for 68.94% and hardly any light REEs.

TABLE 2.8
Composition of Longnan Rare-Earth Ore

Element	**La_2O_3**	**CeO_2**	**Pr_6O_{11}**	**Nd_2O_3**	**Sm_2O_3**	**Eu_2O_3**	**Gd_2O_3**	**Tb_4O_7**
Content (wt%)	1.56	0.085	0.65	3.20	2.42	0.50	4.48	0.95
Element	**Dy_2O_3**	**Ho_2O_3**	**Er_2O_3**	**Tm_2O_3**	**Yb_2O_3**	**Lu_2O_3**	**Y_2O_3**	
Content (wt%)	6.90	1.56	4.33	0.55	3.48	0.50	68.94	

Source: Jun, T. et al., *Hydrometallurgy*, 101: 166–170, 2010.

2.3.13 Scandium Minerals

The abundance of scandium in the earth's crust is greater than the metals lead, tin, mercury, and silver. Yet, scandium rarely occurs in concentrated quantities. The reason is that scandium does not combine with ore-forming anions.

The rare-earth-element scandium does not usually occur in the rare-earth minerals. An important exception is the iron–niobium–rare earth deposit in Bayan Obo, China. This deposit contains scandium in concentrations ranging from 0.006% to 0.016% Sc_2O_3 in various ores and dispersed over the niobium and rare-earth minerals (CREI 1998).

The major source of scandium is uranium ores, which contain about 0.1% scandium. Some scandium is also recovered from wolframite. Scandium content in wolframite is of the order 500–800 ppm, and this was considered an important potential resource in the United States (Kleber and Love 1963). The only mineral that contains a large percentage (33–45%) of scandium is thortveitite. It is a scandium silicate in which variable amounts of yttrium and lanthanides, aluminum, iron, thorium, zirconium, and alkaline earths substitute for scandium. This mineral is very rare—only two sources are known. It was found in the granite pegmatites in northern Norway, and a variety called befanamite was found in Madagascar. Thortveitite is not considered an important source of scandium. Slags from blast furnaces used in the production of cast iron and tin smelting are also sources of scandium.

2.3.14 Promethium

Several rare earths are among the elements formed in the nuclear fission of uranium and plutonium. The spent fuel from nuclear reactors is the only source of the REE promethium (Wheelwright 1973).

2.4 RARE-EARTH DEPOSITS

2.4.1 Basic Geology of REEs

The REEs are usually not concentrated into mineable ore deposits. The principal occurrences of REEs are associated with the uncommon varieties of igneous rocks—alkaline rocks and carbonatites. REE-bearing minerals are also found in placer deposits, residual deposits formed from deep weathering of igneous rocks, pegmatites, iron-oxide copper–gold deposits, and marine phosphates.

Alkaline igneous rocks result from cooling of magmas derived by small degrees of partial melting of rocks in the earth's mantle. The complex sequence of formation of alkaline rocks can be surmised as a geologic process that extracts and concentrates those elements that do not fit into the structure of the common rock-forming minerals. The resulting alkaline magmas are unusually enriched in elements such as zirconium, niobium, strontium, barium, lithium, and the REEs. When these deep-seated magmas, rich in carbon dioxide and low in silica, ascend into the earth's crust, their chemical composition changes due to variations in pressure, temperature, and

composition of surrounding rocks. The result is diverse rock types that are variably enriched in the above-mentioned elements, including the REEs. The mineral deposits associated with these rocks are rich in variety and awkward to classify (Long et al. 2010). The distinctive features of these deposits and their rarity can result in classes that have only one or a few known examples. Magmas forming closer to the surface usually lose their carbon dioxide and other volatile matter and do not bear rare earths. The rare earths in carbonatites are almost exclusively the light REEs contained in minerals such as bastnasite, allanite, and apatite. Monazite, when present, contains the maximum amount of rare earths and a minimum amount of calcium and thorium.

Table 2.9 presents a relatively simple classification of mineral deposits that are rare earth-bearing. Some of the alkaline rocks that host, or are related to, REE ores are carbonatites and phoscorites—igneous rocks composed principally of carbonate and phosphate minerals, respectively. Economic concentrations of REE-bearing minerals occur in some of these alkaline rocks, skarns, and carbonate-replacement deposits associated with alkaline intrusions, veins, and dikes cutting alkaline igneous complexes and surrounding rocks, and soils and other weathering products of alkaline rocks (Long et al. 2010).

Deep chemical weathering of carbonatites causes the dissolution of calcite, dolomite, and apatite. The rare earths released as a result of this activity have an affinity for the phosphate radical and form superzene monazite. Pyrochlore is converted to florencite, and perovskite is converted to anatase by extreme lateritic weathering. Generally, the light rare-earth minerals are converted to heavy rare-earth minerals (Jackson and Christiansen 1993).

The weathering of all types of rocks yields sediments that are transported and eventually deposited in a wide variety of environments, such as streams and rivers, shorelines, alluvial fans, and deltas. The process of erosion concentrates denser minerals into deposits known as placers. Depending on the source of the erosion products, certain REE-bearing minerals, such as monazite and xenotime, can be concentrated along with other heavy minerals. Interestingly, the source need not be an alkaline igneous rock or a related rare-earth deposit. Many common igneous, metamorphic, and even older sedimentary rocks contain enough monazite to produce a monazite-bearing placer (Long et al. 2010). As a result, monazite is almost always found in any placer deposit. However, the types of placers with the greatest concentrations of monazite are typically ilmenite–heavy mineral placers, and cassiterite placers. Large amounts of rare-earth minerals such as monazite and xenotime are contained in placers. The high specific gravity placer minerals are also characterized by general chemical inertness. They remain stable during the erosion and transportation cycles of weathering. The major locations for placers are rivers, deltas, and coastlines. Heavy minerals are concentrated along the coast by a combination of tidal action, long shore currents, waves, winds, and natural traps such as a cape. Important placers for mining are recently formed beaches and dunes along the coastlines, as well as some older deposits that have become stranded due to land elevation or ocean withdrawal.

In certain tropical environments, rocks are deeply weathered to form a unique soil profile consisting of laterite, an iron- and aluminum-rich soil, as much as many

TABLE 2.9
Classification of REE-Bearing Mineral Deposits

Association	Type	Example
Peralkaline igneous rocks	Magmatic (alkali-ultrabasic)	Lovozero, Russia
	Pegmatite dikes (alkali-ultrabasic)	Khibina Massif, Russia
	Pegmatite dikes (peralkaline)	Motzfeldt, Greenland
	Hydrothermal veins and stockworks	Lemhi Pass, Idaho
	Volcanic	Brockman, Western Australia
	Metasomatic–albitite	Miask, Russia
Carbonatites	Magmatic	Mountain Pass, California
	Dikes and dilatational veins	Kangakunde Hill, Malawi
	Hydrothermal veins and stockworks	Gallinas Mtns., New Mexico
	Skarn	Saima, China
	Carbonate rock replacement	Bayan Obo, China
	Metasomatic–fenite	Magnet Cove, Arkansas
Iron oxide copper–gold	Magnetite–apatite replacement	Eagle Mountain, California
	Hematite–magnetite breccia	Olympic Dam, South Australia
Pegmatites	Abyssal (HREEs)	Aldan, Russia
	Abyssal (LREEs)	Five Mile, Ontario
	Muscovite (REEs)	Spruce Pine, North Carolina
	REEs–allanite–monazite	South Platte, Colorado
	REEs–euxenite	Topsham, Maine
	REEs–gadolinite	Ytterby, Sweden
	Miarolitic–REEs–topaz–beryl	Mount Antero, Colorado
	Miarolitic–REEs–gadolinite–fergusonite	Wasau complex, Wisconsin
Porphyry molybdenum	Climax-type	Climax, Colorado
Metamorphic	Migmatized gneiss	Music Valley, California
	Uranium–REEs skarn	Mary Kathleen, Queensland
Stratiform phosphate residual	Platform phosphorite	Southeast Idaho
	Carbonatite-associated	Mount Weld, Western Australia
	Granite-associated laterite	South China
	Baddeleyite bauxite	Poços de Caldas, Brazil
	Karst bauxite	Montenegro
Paleoplacer	Uraniferous pyritic quartz pebble conglomerate	Elliot Lake, Ontario
	Auriferous pyritic quartz pebble conglomerate	Witwatersrand, South Africa
Placer	Shoreline Ti–heavy mineral placer	Western Australia, India, Brazil
	Tin stream placer	Malaysia

Source: Orris, G.J., and Grauch, R.I., Rare earth element mines, deposits, and occurrences: U.S. Geological Survey Open-File Report 2002–0189, 2002.

tens of meters thick. The processes of soil formation commonly concentrate heavy minerals as residual deposits, resulting in an enriched metal layer over the underlying, unweathered bedrock. When a rare-earth deposit undergoes such weathering, it may be enriched in REEs in concentrations of economic interest (Long et al. 2010).

A particular type of REE deposit, the ion absorption type, is formed by leaching REEs from seemingly common igneous rocks and fixing the elements onto clays in soil. These deposits are only known in southern China and Kazakhstan, and their formation is poorly understood. This peculiar type of rare-earth deposit may be formed as a result of *in situ* lateritic weathering of igneous rocks. *In situ* weathering of REO-rich host rocks occurring under conditions of prolonged weathering with limited erosion can result in ion adsorption–type deposits wherein a high Si, Al clay crust adsorbs rare-earth ions from weathered minerals of a host rock (Clark and Zheng 1991a).

Pegmatites, a group of very coarse grained intrusive igneous rocks, begin as granitic magmas formed by remelting of crustal material (Jackson and Christiansen 1993). As the magma cools, crystals incorporating heavy REEs form first. This is followed by crystallization of the residual liquid, which is relatively rich in lighter REEs. Thus, monazite and allanite in pegmatites tend to be richer in the heavy rare earths than when they are found in other rocks. The overall rare-earth content of monazite is, however, decreased because it is likely to have more calcium and thorium. Among the pegmatites, the niobium–yttrium–fluorine family comprises a large number of subtypes formed in different geologic environments. These subtypes are granitic in composition and are usually found peripheral to large granitic intrusions. The REE-bearing pegmatites are generally small and are of limited economic interest.

Since the discovery of the giant Olympic Dam deposit in South Australia in the 1980s, the iron-oxide copper–gold type of deposit has been recognized as a distinct deposit type. The Olympic Dam deposit contains large amounts of REEs and uranium. Many other deposits of this type have been identified around the world, but information on their REE content is unknown (Long et al. 2010). Trace amounts of REEs have also been identified in magnetite–apatite replacement deposits.

Karst bauxites, aluminum-rich soils that accumulate in cavernous limestone (underlying karst topography) in Montenegro and elsewhere, are enriched in REEs but not in economically significant concentrations (Maksimović and Pantó 1996). Marine phosphate deposits also can contain as much as 0.1% REE oxides (Altschuler et al. 1966), and the recovery of rare-earth elements as a by-product of phosphate fertilizer manufacture has been considered.

REEs can be carried by hydrothermal solutions that are developed through the interaction of hot underground water with crustal material (Jackson and Christiansen 1993). The light REEs are less soluble than the heavier elements, and they therefore tend to settle out first, leaving the liquid more concentrated in heavy elements. As a result, hydrothermal deposits contain minerals such as xenotime, which are enriched in the heavy rare earths.

2.4.2 Distribution

Jackson and Christiansen (1993) listed 123 important rare-earth deposits located in 20 countries. A decade later, Orris and Grauch (2002) expanded the list of world

rare-earth deposits and tabulated 774 of them. Chen (2011) stated that there are about 34 countries with rare-earth deposits. Kanazawa and Kamitani (2006) noted that carbonatite/alkaline rocks constitute the majority of the world RE resources, and more than 550 carbonatite/alkaline complexes are distributed in the world. The information available on each of the obviously vast number of world rare-earth deposits is different both with respect to completeness and reliability. This limitation has been addressed by looking at the resource details through certain classification systems and standards. The details appear in Section 2.5. While agreeing that there are insufficient details on rare-earth deposits from every country due to either inadequate raw data or the parameters of permitted reporting, a broad working view on the status of rare-earth resources can be gleaned from the information compiled by the USGS geologists (Jackson and Christiansen 1993; Orris and Grauch 2002). Based on their reports, the types of deposits and the number in each type are given in Table 2.10. On the whole, there are approximately 400 hard rocks and 370 placers. Even though the USGS geologists did not elaborate on the criteria for the selection of their entries, it appears that occurrence of rare earth–containing minerals in enhanced concentration, possibly mineable in the best-case scenario, did guide the selection for listing. Out of all the rare-earth deposits covered by Orris and Grauch (2002), they provided

TABLE 2.10
Types of World Rare-Earth Deposits and Frequency of Their Occurrence

Type of Deposits	Number of Deposits
Carbonatite	97
Carbonatite with residual enrichment	42
Alkalic igneous	122
Hydrothermal Fe-oxide	4
Other igneous affiliated (including pegmatites and veins)	38
Ion adsorption	12
Metamorphic	16
Placer, shoreline	264
Placer, alluvial	78
Placer, uncertain origin	14
Placer, paleoplacer	13
Phosphorite	21
Other bauxite or laterite hosted	2
Other F deposits	7
Other Pb deposits	2
Other uranium deposits	8
Other uncertain	34
Total numbers of deposits	774

Source: Orris, G.J., and Grauch, R.I., Rare earth element mines, deposits, and occurrences: U.S. Geological Survey Open-File Report 2002–0189, 2002.

Note: Hard rock: 405, Placer: 369.

information on the quantity of rare earth contained therein for approximately one-fourth of them. These deposits have been chosen and listed in Table 2.11, where the information contained in the earlier report of Jackson and Christiansen (1993) and the later publication of Orris and Grauch (2002) combined. The location of the rare-earth deposits is also shown indicatively in Figure 2.2.

The rare-earth deposits are distributed all over the world. The occurrences are relatively less in Europe, southwest Asia, South America other than Brazil, and also northeast Africa. The discovery of many rare-earth occurrences happened when highly resourced searches were conducted for uranium deposits, in the heydays of nuclear energy (1950–1980). Radiometric surveys for uranium minerals conducted over huge geographical sectors led to thorium minerals revealing not only themselves but also the associated rare-earth occurrences. This was quite common in North America and Australia. A major reason for rare-earth deposits not being located in a geographical region could be that it has not been looked for seriously enough. Long et al. (2010) emphasized that long-term prospects for the discovery of new reserves and resources depend on sufficient exploration. US Geological Survey knew about 150 projects worldwide that are prospecting and exploring for REEs (US Geological Survey 2010). Most of this activity began by about 2008 and could yield information any time now.

Numerically, most of the deposits are located in the United States, followed by Australia, Brazil, China, Canada, India, Russia, and South Africa. These deposits belong to both the placers and hard-rock types.

The world rare-earth deposits are divided more or less equally between the placers and the hard rocks if only the numbers are considered. The placers are mostly found in recent or ancient shorelines and less frequently along present or former riverbanks. Monazite is the predominant rare-earth mineral in the placers. The countries having major placer deposits are Australia, Brazil, the United States, India, China, Taiwan, Malaysia, and also Vietnam. Placer deposits are also found in Argentina, Egypt, Mozambique, New Zealand, South Africa, Sri Lanka, and Uruguay.

As regards the hard-rock deposits, the maximum number is found in the United States, followed by Australia, Canada, Brazil, Burundi, South Africa, and China. Monazite is the major mineral found in most of the hard-rock deposits; bastnasite is predominant at a lesser number of sites. In the remaining deposits, the leading minerals are allanite, brannerite, apatite, and eudialyte, with anatase, davidite, florenite, gadolinite, perovskite, and xenotime limited to individual properties. The ion adsorption–type ore deposits of China are a class by themselves and, because of their highly selective occurrence, do not figure prominently in the general surveys. It has been noted by Long et al. (2010) that reliable data on REE reserves and resources in China, North Korea, and Russia are not available.

2.5 RESOURCES AND RESERVES

The term *resources* has been generally used to denote the deposits of a commodity, in this context, the rare earths, in or on the earth's crust in such forms and concentrations that economic extraction of the commodity is presently or potentially feasible. The term *reserve*, on the other hand, has been used to represent, in the present context, the specific bodies of rare earth-bearing material of known location, quality,

TABLE 2.11
Summary of World Rare-Earth Deposits

Location	Deposit Type, Host Rock, Principal Minerals	RE Minerals	Average Grade Resources, kt [Year]	Year of Discovery (Year of First Production) Annual Production, kt [Year] Status
			Argentina	
Rio Tercero Cordoba	Placer, fluvial	Monazite	0.0173% monazite containing 60% REO and 3.8% ThO_2 Ore: 31,700; monazite: 5.48	1957 (Not producing) No current production plans
			Australia	
Agnes Waters (Rocky Point) Queensland	Placer Marine Ilmenite, rutile, zircon, monazite, quartz	Monazite	1.36% ilmenite, 0.18% rutile Ore: 217,800	1956 Not producing –
Alice Springs Northern Territory	Magmatic Pegmatite	Allanite	1 Mt at 4% allanite Allanite contains 20% REO and 1.5% Th Ore: 1000 Allanite: 40	1987 (Not producing) Remote location may preclude development
Allied Eneabba Western Australia	Placer Shoreline	Monazite	Total reserves—150 Mt at 4% HM, 0.043 Mt monazite	– – Past by-product producer

(*Continued*)

TABLE 2.11 (CONTINUED)
Summary of World Rare-Earth Deposits

Location	Deposit Type, Host Rock, Principal Minerals	RE Minerals	Average Grade Resources, kt [Year]	Year of Discovery (Year of First Production) Annual Production, kt [Year] Status
Australind Western Australia	Placer Marine Ilmenite, rutile, zircon, leucoxene, monazite, quartz, garnet	Monazite	6 Mt at 0.03% monazite (15% HM) Ore: 6000 HM: 901 Ilmenite: 662; rutile: 3.6 Zircon: 61; leucoxene: 50	– Not producing –
Birthday Gift (Murray Basin) New South Wales	Beach sand		61 Mt at 3.6% HM	– – HM prospect; coarse-grained beach placer; resource estimate is indicated + inferred
Brockman Western Australia	Magmatic Rhyolite tuff, peralkaline granite Columbite, pyrochlore, bastnasite, xenotime, cassiterite, sphalerite	Bastnasite, xenotime	9.0 Mt at 0.15% Y_2O_3, 0.12% HREE, 1.3% Zr; 4.29 Mt at 0.123% Y_2O_3, 0.0355% REO, 0.440% Nb_2O_5, 1.040% ZrO_2 9.3 Mt at 0.215% REO [0.09% REO, 0.124% Y_2O_3 REO: 20 Ore: 9290]	1973 (Not producing) Undergoing feasibility study
Byfield (Bayfield) Queensland	Placer Marine Ilmenite, rutile, zircon, monazite, quartz	Monazite	1.14% heavy minerals, 0.05% monazite Ore: 2,400,000 HM: 27,360; monazite: 14	1956 (Not producing) Steep wind-blown sand dunes; awaiting feasibility study

(*Continued*)

TABLE 2.11 (CONTINUED)
Summary of World Rare-Earth Deposits

Location	Deposit Type, Host Rock, Principal Minerals	RE Minerals	Average Grade Resources, kt [Year]	Year of Discovery (Year of First Production) Annual Production, kt [Year] Status
Capel South Western Australia	Placer Marine Ilmenite, rutile, zircon, leucoxene, monazite, quartz	Monazite, xenotime	40% HM; 25.3 Mt at 0.06% monazite [1989]	1954 (1956) – Past by-product producer
Cataby Western Australia	Placer Marine Ilmenite, rutile, zircon, monazite, quartz	Monazite	7.7% heavy minerals, 0.1% monazite Ore: 8974 HM: 700; ilmenite: 490 Rutile: 49 Zircon: 84; monazite: 10.5	1976 (Not producing) Mining would be by open pit Past by-product producer
Cooljarloo/Jurien Bay Western Australia	Placer Marine Ilmenite, rutile, zircon, leucoxene, monazite, quartz	Monazite	Proven—431.3 Mt at 3.4% HM + probable—138 Mt at 3.0% HM; 177 Mt at 3.7% HM (0.2% monazite); 0.59 Mt at 0.009% monazite	1971 (1975) Cooljarloo is operating; Jurien Bay is on standby Past producer ore: 12,000 monazite concentrate: 2.5 [1988] Munbinea Shoreline—a group of former beaches; deposit is as much as 30 m below water table and is mined by dredging; HM fraction contains 0.2% monazite

(*Continued*)

TABLE 2.11 (CONTINUED)
Summary of World Rare-Earth Deposits

Location	Deposit Type, Host Rock, Principal Minerals	RE Minerals	Average Grade Resources, kt [Year]	Year of Discovery (Year of First Production) Annual Production, kt [Year] Status
Coolooa Queensland	Placer Marine Ilmenite, rutile, zircon, monazite, quartz	Monazite	0.00846% monazite Ore: 23,760; ilmenite: 170 Rutile: 42 Zircon: 32 Monazite: 0.7 [in 1975]	1948 (1956) Mining ceased in 1975; area is now a national park
Dongara Western Australia		Monazite	20 Mt at 6.6% HM	Prospect
Eneabba Western Australia	Placer Marine Ilmenite, rutile, zircon, kyanite, monazite, quartz	Monazite	0.05% monazite Proprietary	1968 (1974) Past producer monazite concentrate: 8.9 in 1987, 35.4 during 1984–1987; dredge, open pit
Eneabba West Western Australia		Monazite	150 Mt at 4% HM; 230 Mt at 3.1% HM; 43 Mt monazite	– Past producer, dredge operation

(*Continued*)

TABLE 2.11 (CONTINUED)
Summary of World Rare-Earth Deposits

Location	Deposit Type, Host Rock, Principal Minerals	RE Minerals	Average Grade Resources, kt [Year]	Year of Discovery (Year of First Production) Annual Production, kt [Year] Status
Jangardup Western Australia	Placer Marine Ilmenite, rutile, zircon, leucoxene, kyanite, staurolite, monazite, xenotime, quartz, garnet	Monazite, xenotime	6.8% heavy minerals, 0.0476% monazite, 0.0204% xenotime Ore: 30,000 HM: 2040 Ilmenite: 1679; rutile: 51 Zircon: 171; leucoxene: 61 Monazite: 14 [as of 1990]	1986 (None) Potential reserve Past producer HM concentrate: 270 [in 1990] Current HM producer; REE by-product potential
Jurien Bay Western Australia	Placer Shoreline	Monazite	2 Mt at 3% HM; 18.3 Mt monazite ore at 1% monazite	– Past producer
Kulwin (Koolwin) Victoria			24 Mt at11.5% HM	– HM prospect
Lake Innes New South Wales	Laterite hosted		12.4 Mt at 0.004%Sc	– – Ni–Co–Sc laterite deposit formed from weathering of a serpentine; Sc is enriched in the upper part of the lateritic profile

(*Continued*)

TABLE 2.11 (CONTINUED)
Summary of World Rare-Earth Deposits

Location	Deposit Type, Host Rock, Principal Minerals	RE Minerals	Average Grade Resources, kt [Year]	Year of Discovery (Year of First Production) Annual Production, kt [Year] Status
Mary Kathleen Queensland	Magmatic Skarn, calc-silicate metasediments, granite allanite, stillwellite uraninite, uph, garnet, fluorapatite, pyrite, ceriopyrochlore, pyrrhotite	Allanite, stillwellite	Ore ran 35% allanite, 40% garnet, 10% apatite 6.8 Mt tailings at 4% REO (1990) Ore: 6800 REO: 272 [1990]	– – Former uranium mine; underground uranium mine closed in 1963; production of uranium ceased in 1982; rare earths could be recovered from tails
Mount Weld Western Australia	Magmatic Carbonatite Apatite, pyrochlore, magnetite, ilmenite, monazite, quartz	Monazite, churchite, xenotime, florencite, goyazite, cerianite	Indicated 15.4 Mt at 11.2% REO + Y_2O_3 (5% cutoff) + 4.0 Mt at 0.36% Y_2O_3; 6.3 Mt at 16.2% REO; 15.2 Mt at 11.2% REO (including Y); 6.3 Mt at 17.2% REO	1948 (None) Not producing Pilot plant at site in 1993; could commence at 20,000–50,000 t/year of ore; REE–P resource; monazite has <0.3% ThO_2
Munmorah New South Wales	Placer Marine Ilmenite, rutile, zircon, monazite, quartz	Monazite	71.2 Mt at 0.81% HM, 0.006% monazite	1950 (1969) Past by-product producer; closed by government in 1977
Newrybar New South Wales	Placer Marine Ilmenite, rutile, zircon, monazite, tourmaline, quartz, garnet	Monazite	22 Mt at 1.1% HM, 0.0418% monazite	1935 (1990) Past producer; ore: 3500; rutile: 12; zircon: 10 [1990] dune and beach sand; dredge

(*Continued*)

TABLE 2.11 (CONTINUED)
Summary of World Rare-Earth Deposits

Location	Deposit Type, Host Rock, Principal Minerals	RE Minerals	Average Grade Resources, kt [Year]	Year of Discovery (Year of First Production) Annual Production, kt [Year] Status
Nobiac, Southeast New South Wales	Placer Marine Ilmenite, rutile, zircon, leucoxene, monazite, quartz, garnet	Monazite	2 Mt at 0.005% monazite	Past producer by-product monazite
Nolan's Bore Northern Territory	Carbonatite	Apatite, allanite	In places, REE grades exceed 10%	Advanced rare-earth project
North Stradbroke—Yarraman Queensland	Placer Marine Ilmenite, rutile, zircon, monazite, quartz	Monazite	311 Mt; 0.0015% monazite (1.5 % HM)	1947 (1949) Past producer by-product monazite Beach and dune deposits; first prod was planned for 1999; deposit is low grade with areas that contain up to 10% fines
Olympic Dam South Australia	Magmatic Olympic Dam Breccia Complex-granite breccia Chalcocite, bornite, chalcopyrite, uraninite, brannerite, hematite, bastnasite, fluocerite	Monazite, bastnasite, fluocerite, florencite	0.5% REE on average; 2000 Mt at 0.24%–0.45% La + Ce; 0.3285% REO Ore: 1500; Cu: 45; U_30_8: 1.5 [1988]	1975 (1988) REO in uranium is not recovered; underground REO associated with U_3O_8 in a major Cu/Au/Ag/U mine; potential REO by-product

(*Continued*)

TABLE 2.11 (CONTINUED)
Summary of World Rare-Earth Deposits

Location	Deposit Type, Host Rock, Principal Minerals	RE Minerals	Average Grade Resources, kt [Year]	Year of Discovery (Year of First Production) Annual Production, kt [Year] Status
Toongi (Dubbo) New South Wales	Alkalic igneous Altered trachytic intrusive		Indicated—10 Mt at 0.12% Y_2O_3, 0.75% REO, 2% ZrO_2, 0.04% HfO_2, 0.5% Nb_2O_5, 0.3% Ta_2O_5; inferred—40 Mt	– 50 pegmatites Prospect Advanced rare-earth project
Waroona North and South Western Australia	Placer Marine Ilmenite, leucoxene, zircon, monazite, quartz	Monazite	5 Mt at 14.2% HM Heavy minerals are 0.35% monazite Ore: 590 Monazite: 0.235 [1988]	1970 (1984) Past producer Open pit Dune and beach sand
WIM 150 (Drung South, CRA, Horsham) Victoria	Placer Fluvial Ilmenite, leucoxene, zircon, anatase, monazite, xenotime, quartz	Monazite, xenotime	0.75 Mt monazite + xenotime; 750 Mt at 4% HM; 2475 Mt at 0.138% monazite (1990); resource—4900 Mt at >2.8% HM (monazite is 1.4% of HM; xenotime is 0.4% of HM); proven—>1000 Mt at >3% HM; proven—0.58 Mt monazite, 0.17 Mt xenotime 1990; 2000; deposit contains 100,000 t Y_2O_3	1987 (None) In Murray Basin; fine-grained off-shore deposit; fine-grained nature of the sands (<50 μm) has prevented development Potential resource

(*Continued*)

TABLE 2.11 (CONTINUED)
Summary of World Rare-Earth Deposits

Location	Deposit Type, Host Rock, Principal Minerals	RE Minerals	Average Grade Resources, kt [Year]	Year of Discovery (Year of First Production) Annual Production, kt [Year] Status
Yangibana Western Australia	Magmatic Mica schist and gneisses intruded by alkaline granite and syenite. Gossan ore referred to as *ironstones*	Monazite	3.1 at 1.7% REO (1989); as much as 11% REO; 3.5 Mt at 3.09% monazite (1.7% REO)	Potential resource
Yoganup Extended Western Australia	Placer Marine Ilmenite, rutile, zircon, leucoxene, monazite, quartz	Monazite	>40 Mt ore; 13% HM; 0.056% monazite 1988 (ore)	1954 (1972) Past producer monazite: 1.7 [1986]; 1.75 [1987]; 1.8 [1988]
		Bangladesh		
Badarmokam		Monazite	1.765 Mt at 0.28% monazite	
Cox's Bazaar	Beach sand	Monazite	5.119 Mt at 0.04% monazite	
Shilkhali		Monazite	2.757 Mt at 0.14% monazite (1983)	
Subrang		Monazite	0.348 Mt at 0.59% monazite (1983)	
Teknaf		Monazite	1.94 Mt at 0.16% monazite (1983)	

(*Continued*)

TABLE 2.11 (CONTINUED)
Summary of World Rare-Earth Deposits

Location	Deposit Type, Host Rock, Principal Minerals	RE Minerals	Average Grade Resources, kt [Year]	Year of Discovery (Year of First Production) Annual Production, kt [Year] Status
			Brazil	
Acobaca Southern Bahia	Placer Marine Ilmenite, rutile, zircon, monazite, quartz	Monazite	0.47% monazite Monazite: 3.44 [1987]	1970s (None) Not producing
Anchieta (Parati, Imbiri, Pipa de Viho, Mãebá) Espírito Santo	Placer Marine Ilmenite, rutile, zircon, monazite, quartz	Monazite	Measured reserves—698 t monazite grading 60.02% REO (1986); 0.057 Mt at 0.71% monazite (1987); monazite contains about 5.2% ThO_2	1900s (Unknown) Probably mined out already Small modern beach placers, elevated bars
Aracruz Espírito Santo	Placer Marine Ilmenite, rutile, zircon, monazite, quartz	Monazite	Measured reserves—2964 t monazite grading 59.98% REO (1986); 0.282 Mt at 1.05% monazite	1970 (None) No production planned yet
Araxa (Barreiro) Minas Gerais	Weathered carbonatite with three separate deposits Beforsite, glimmerite, sovite, some pyroxenite	Monazite, gorceixite, goyazite, apatite, bariopyrochlore, calcite, ancylite, ceriopyrochlore	>450 Mt Nb ore at 2.5% Nb_2O_5, 4.4% REO + 0.8 Mt laterite ore at 13.5% REO, 2% Nb_2O_5, 0.05% U_3O_8 (1984); 0.546 Mt at 10%–11% REO (1982); 462 Mt at 0.033% REO	Nb–P producer; REE–Ba occurrence Barreiro Complex is circular and about 4.5 km in diameter; world's largest Nb reserve

(*Continued*)

TABLE 2.11 (CONTINUED)
Summary of World Rare-Earth Deposits

Location	Deposit Type, Host Rock, Principal Minerals	RE Minerals	Average Grade Resources, kt [Year]	Year of Discovery (Year of First Production) Annual Production, kt [Year] Status
BrejoGrande—Pacatuba Sergipe	Placer Shoreline	Monazite	0.062 Mt monazite	Sediments
Buena (Rio de Janeiro)	Placer Marine Ilmenite, rutile, zircon, monazite, quartz	Monazite	0.83% monazite Monazite: 0.3	1960s (Unknown) Past producer monazite: 3.8 [1987] Probably mined out already; open pit
Camaratuba Rio Grande do Norte	Placer Marine Ilmenite, rutile, zircon, tourmaline, monazite, xenotime, quartz, garnet	Monazite, xenotime	44.7 Mt at 0.55% monazite	1970s (Unknown) Past producer ore: 3160 [1981] Elevated dunes at the base of an ancient sea cliff; open pit
Careacu Minas Gerais	Placer	Monazite	2500 t monazite (1987)	Occurrence
Catalão I Goias Brazil	Carbonatite with residual enrichment Carbonatite, pyroxenite, serpentinized peridotite, glimmerite	Ce–Ba–pyrochlore, gorceixite, apatite, monazite, florencite, ancylite, goyazite, anatase, rhabdophane	2 Mt laterite at 12% REO; 5 Mt at 12% REO; 21 Mt at 1.02% REO; 4.6 Mt at 4% REE	– – Plug—6 km in diameter Nb–P producer; REE minor by-product (Ce) Ti resource

(*Continued*)

TABLE 2.11 (CONTINUED)
Summary of World Rare-Earth Deposits

Location	Deposit Type, Host Rock, Principal Minerals	RE Minerals	Average Grade Resources, kt [Year]	Year of Discovery (Year of First Production) Annual Production, kt [Year] Status
Cordislandia Minas Gerais	Placer	Monazite	8200 t monazite (1987)	– Not producing
Guarapari (Praia do Vaz, Vila Velha, Rastinga, Canto do Riacho, Praia de Diogo) Espírito	Placer Shoreline Ilmenite, rutile, zircon, monazite, magnetite, quartz	Monazite	Measured reserves—818 t monazite at 60.04% REO (1986); 950 t monazite (1987)	– Current(?); producer by-product monazite
Morro Dos Seis Lagos (Sao Gabriel da Cachoeira) Amazonas	Weathered carbonatite	Florencite, RE oxides and hydroxides	0.13 Mt REE; 1.50% REO in laterite cover	– 3 carbonatitic alkaline pipes that form laterite-covered hills; laterites average 230 m in depth Potential Nb–REE resource
Northeast dunes	Placer Marine Ilmenite, rutile, zircon, monazite, quartz	Monazite	145 Mt at 0.033% monazite	– Prospects
Pocos de Caldas (Morro do Ferro) Minas Gerais, Sao Paolo	Magmatic Highly weathered lujavrite and khibinite, nepheline syenite, phonolite; bauxite	Allanite, bastnasite, eudialyte, cerianite	>1.0 Mt at 4% REO, 1% ThO_2; 1.5 Mt bastnasite or 0.050 t REO (1990); 6 Mt at 3% REO	– Eudialyte contents range from 0% to 11% in the relatively small host bodies; was once one of the world's biggest baddeleyite deposits, but now nearly depleted; weathered magnetite stockwork in alkaline rocks; past producer U, Zr, bauxite

(*Continued*)

TABLE 2.11 (CONTINUED)
Summary of World Rare-Earth Deposits

Location	Deposit Type, Host Rock, Principal Minerals	RE Minerals	Average Grade Resources, kt [Year]	Year of Discovery (Year of First Production) Annual Production, kt [Year] Status
Prado Bahia	Placer Marine	Monazite, xenotime allanite	Measured reserves—4564 t monazite grading 19.98% REO	– Past by-product producer, current?
Sao Gonçalo do Sapucai area Minas Gerais Brazil	Placer Fluvial Ilmenite, zircon, gold, monazite, garnet	Monazite	28 M m^3 with 0.05 t monazite; 0.066% monazite Ore: 75,600; ilmenite: 630; zircon: 115; garnet: 33; gold: 1.4; monazite: 50 [1990]	
Sao Joao de Barra (Barra Sao Joao) Rio de Janeiro	Placer Shoreline Ilmenite, zircon, monazite	Monazite	Measured reserves—8177 t monazite grading 59.99% REO	– Producer by-product monazite? Grupo Barreiras and younger sediments—beach sand
Serra (Jacareipe) Espírito Santo	Placer Marine Ilmenite, rutile, zircon, monazite, quartz	Monazite	0.0436 Mt at 0.80% monazite	– Not producing Potential open pit 1960 (none) Ilmenite, rutile, zircon, monazite dune and beach sand, placers associated with veins, stockwork in gneiss

(*Continued*)

TABLE 2.11 (CONTINUED)
Summary of World Rare-Earth Deposits

Location	Deposit Type, Host Rock, Principal Minerals	RE Minerals	Average Grade Resources, kt [Year]	Year of Discovery (Year of First Production) Annual Production, kt [Year] Status
Serra Negra Minas Gerais	Carbonatite with residual enrichment Weathered carbonatite, peridotite, dunite, shonkinite, jacupirangite ana, Th, U, pyro	Apatite, anatase	200 Mt at 27.7% TiO_2—Ti concentrates contain >3% REE	– Hi LREE/HREE ratio Ti resource with potential by-product REE
Tapira (Minas Gerais)	Magmatic Weathered pyroxenite, syenite, sovite, silexite, jacupirangite	Anatase, hydroxylapatite, pyrochlore, apatite perovskite, limonite, magnetite, garnet	150 Mt at 0.03% REO; 166 at 0.03% REO	– 0.03% REO in anatase overburden at an operating phosphate mine Ti–P producer; potential for Nb, REE, vrm 1966 (1983)
		Burundi		
Karonge (Gakara)	Magmatic Metasedimentary rocks, gneiss, granite Fluocerite, cassiterite, monazite, barite, goethite, quartz	Bastnasite, monazite, rhabdophane, cerianite, fluocerite	Mineable ore—0.06 Mt at 3.0% bastnasite (1.59% REO)	REE deposit in quartz–barite–bas–monazite stockworks of uncertain affiliation, but assumed in references to have carbonatite source; weathering has produced rhabdophane and cerianite 1940s (1948) past producer (ore: 141; bastnasite concentrate: 2.8) [1967–1987] REE production ceased, due to irregular distribution of grade, in 1978

(*Continued*)

TABLE 2.11 (CONTINUED)
Summary of World Rare-Earth Deposits

Location	Deposit Type, Host Rock, Principal Minerals	RE Minerals	Average Grade Resources, kt [Year]	Year of Discovery (Year of First Production) Annual Production, kt [Year] Status
Kasagwe	Magmatic	Bastnasite	0.067 Mt at 3% bastnasite or 1.5% REO	– Unknown
		Canada		
Eldor (Ashra) Carbonatite Complex, Quebec	Syenite, calcite carbonatite, dolomite carbonatite, ankerite carbonatite, glimmerite, feldspathic breccia Apatite, pyrochlore, fersmite, zircon, rutile, baddeleyite, magnetite	Monazite	1.74% REO	Advanced rare-earth project
Kipawa Lake (Zeus), Ontario	Peralkaline quartz syenite, amphibole schist Fluorite, zircon, chondrodite, vlasovite, wöhlerite, gittinsite, hiortdahlite	Eudialyte, mosandrite, britholite, gittinsite, miserite, apatite	0.23% REO	Advanced rare-earth project Mineralization probably resulted from high-grade metamorphism without obvious igneous relics; geochemistry of some eudialyte-rich rocks strongly suggests metasomatic origin
Atlin-Ruffner Ontario	Other igneous-affiliated (including pegmatites and veins)	Allanite	0.0366 Mt at 2.29% CeO_2	– Pegmatite zone is 61 m long, 1.8 m wide, 49 m deep and contains allanite crystals of to 15 cm in size

(*Continued*)

TABLE 2.11 (CONTINUED)
Summary of World Rare-Earth Deposits

Location	Deposit Type, Host Rock, Principal Minerals	RE Minerals	Average Grade Resources, kt [Year]	Year of Discovery (Year of First Production) Annual Production, kt [Year] Status
Elliot Lake (Blind River) (Denison) (Ontario)	Magmatic Quartz–pebble conglomerate Uraninite, brannerite, monazite, zircon, pyrite, quartz	U-monazite, brannerite	106 Mt at 0.01% REO (1989)	1953 (1957) Past U producer with by-product REE, underground Grauch classifies as U deposit; Mariano as a Proterozoic quartz–pebble conglomerate
Elliot Lake (Blind River) (Rio Algom, Stanleigh) (Ontario)	Magmatic Quartz–pebble conglomerate Uraninite, brannerite, monazite, zircon, pyrite, quartz	U-monazite, brannerite	49.9 Mt at 0.0086% REO	– Past U producer with by-product REE; uranium producer potential for 152 t/year REO Underground
Elliot Lake (Blind River)–Quirke–Panel Ontario	Magmatic Quartz–pebble conglomerate Uraninite, brannerite, monazite, zircon, pyrite, quartz	Uraninite, brannerite, monazite	68.2 Mt at 0.0073% REO (1989)	1953 (1956) Past U producer with by-product REE; closed in 1990 Grauch classifies as U deposit; Mariano as a Proterozoic quartz–pebble
Lackner Lake (Nemegos) Ontario	– Nepheline syenite, ijolite, malignite, syenite	Pyrochlore, apatite	Zone 6—4.8 Mt (other ore zones with no REE not included); 69.9% mag, 21.9% apatite, 2.72% REO [grade of REO is for nonmetallic fraction (which is over 90 volume% apatite)]	– Nb–P potential

(*Continued*)

TABLE 2.11 (CONTINUED)
Summary of World Rare-Earth Deposits

Location	Deposit Type, Host Rock, Principal Minerals	RE Minerals	Average Grade Resources, kt [Year]	Year of Discovery (Year of First Production) Annual Production, kt [Year] Status
Oka Quebec	– Carbonatite, okaite, melteigite, urtite, alnoite Pyrochlore, britholite, apatite, ceriopyrochlore	Pyrochlore, britholite, apatite, ceriopyrochlore	221 Mt at 0.1% REO; 4.0 Mt at 0.31% Nb_2O_5, 0.39% REO, 3.8% P_2O_5	1956 Past Nb producer; potential REE resource
St. Honoré Quebec	– Carbonatite, syenite, nepheline syenite, ijolite	Bastnasite, pyrochlore, parisite, monazite	16 Mt at 0.0088% REO; as much as 4.5% LREE; REE range from 0.1% to 1.7%	– Nb producer; potential REE resource complex is 8 × 6.5 km; carbonatite core is surrounded by syenite and other alkaline rocks
Strange Lake (Lac Brisson) Quebec, Labrador	Magmatic Pegmatite in peralkaline granite Zircon, gadolinite, bastnasite, kainosite, pyrochlore, monazite, allanite, apatite, astrophyllite, fluorite	Gadolinite, bastnasite, kainosite, pyrochlore, monazite, allanite, apatite, astrophyllite	52 Mt at 0.54% REE, 0.31% Y_2O_3, 2.9% ZrO_2 (1983); 55 Mt at 0.38% Y, 2.99% ZrO, 0.29% Nb_2O_5, 0.076% BeO, unspecified REO; 1.3% REO and 0.66% Y	1979 Potential resource; could be started as a beryllium project Advanced rare-earth project 250 km NE of Schefferville; Be deposit; complex only partially exposed; peralkaline granite complex about 6 km in diameter; mineralization in roof zone of magma chamber 1.3% REE and 0.66% Y_2O_3 in a primary beryllium property

(*Continued*)

TABLE 2.11 (CONTINUED)
Summary of World Rare-Earth Deposits

Location	Deposit Type, Host Rock, Principal Minerals	RE Minerals	Average Grade Resources, kt [Year]	Year of Discovery (Year of First Production) Annual Production, kt [Year] Status
Thor Lake (Blachford Lake) Northwest Territories	Magmatic Peralkaline syenite, gabbro, granite Xenotime, gadolinite, Y-fluorite, bastnasite, parisite, synchysite, monazite, columbite, zircon	Xenotime, gadolinite, allanite, columbite, amphibole, fluorite	65 Mt at 0.3% Ta, 0.4% Nb, 1.7% REE, 3.5% Zr; proven—0.507 Mt at 0.17% Y oxide, 1.11% Be oxide; 0.51 Mt at 0.45% REO	1979 (None) Essentially a Nb_2O_5–Ta_2O_5 project; potential; by-product of Be mining; REE and yttrium occur in a primary beryllium property Advanced rare-earth project Small, remote deposit; the T Zone deposit has significant REE, Y, and Be mineralization; deposits are part of the Blachford Lake alkaline complex
Williams Lake-Maw zone Saskatchewan	Placer Paleoplacer Athabasca Group sandstone tour, qtz		Estimate—0.336 Mt at 0.25% Y_2O_3	– Y + HREE Occurrence
		China		
Bayan Obo (Baotou) (Inner Mongolia)	Magmatic Dolomite, trachyte, fenite Hematite, magnetite, monazite, rutile, bastnasite, martite	Bastnasite, monazite, aeschynite, allanite, apatite, parisite, huanghoite, fergusonite, fersmite, xenotime, daqingshanite, cordylite, carbocernaite, chevkinite, britholite	750 Mt at 4.1% REO; 48 Mt at 6% REO; 15,000 Mt at 35% Fe; 800 Mt at 6% REO (1990); 36 Mt REO	1951 (1957) Current producer The largest known RE deposit Open pit 6% REO in a major hematite mine

(*Continued*)

TABLE 2.11 (CONTINUED)
Summary of World Rare-Earth Deposits

Location	Deposit Type, Host Rock, Principal Minerals	RE Minerals	Average Grade Resources, kt [Year]	Year of Discovery (Year of First Production) Annual Production, kt [Year] Status
Beihei (Beihai, Peibhai?) District Guangxi	Placer Fluvial Ilmenite, rutile, zircon, monazite, quartz	Monazite	1%–2% HM; 530 Mt ore	– (1966) Producer by-product monazite Open pit; HM recovered from sands manually Mixed river and marine placers along coastline; as much as 60% of mined material may be from river sands; mined by farmers collectives
Guangdong (Guangdong)	Placer Fluvial Ilmenite, rutile, zircon, monazite, quartz	Monazite	2.3% heavy minerals; ore: 385,320 [1989]	1950s (1960s) Past producer Covers five separate mines and plants Open pit
Maoniuping Sichuan	– Quartz syenite, nordmarkite bastnasite; lesser monazite, allanite, britholite, xenotime, aeschynite, chevkinite	Bastnasite–barite–carbonate veins associated with nordmarkite	0.4 Mt proven resvs at 1%–8% REO (ave. 2%); 1%–8% REO	– Active REE producer
Nanyang (Nangang) Guangdong/ Hainan Island		Monazite, xenotime	Measured—8.2 Mm^3 at 0.79 kg monazite/m^3 (6500 t monazite), 41.9 kg ilm/m^3 [1982]	– Producer by-product monazite

(*Continued*)

TABLE 2.11 (CONTINUED)
Summary of World Rare-Earth Deposits

Location	Deposit Type, Host Rock, Principal Minerals	RE Minerals	Average Grade Resources, kt [Year]	Year of Discovery (Year of First Production) Annual Production, kt [Year] Status
Sai-Lao (Quoinghi) Guangdong/ Hainan Island	Placer Marine	Monazite	170 (ind. res); measured—2539 t monazite; 0.74 Mt ilm; 0.067 Mt zir (1982)	– Producer by-product monazite
Wuzhaung (Baoding) Guangdong/ Hainan Island	Placer Marine	Monazite	Measured—9 Mm^3 at 1.03 kg monazite/m^3 (9253 t monazite), 15.36 kg ilm/m^3, 3.0 kg zir/m^3 Monazite contains 5%–6% ThO_2 and 51% REO	– Producer by-product monazite
Xiuwen Guizhou	– Bauxites occur at the bottom of lower Carboniferous strata overlying Cambrian dolomites	Bauxite (RE)	0.1%–0.2% REO, 55%–80% Al_2O_3, and others [1996]	– Occurrence
Xun Jiang (Guangxi)	Placer Fluvial Ilmenite, rutile, zircon, monazite, quartz	Monazite	66.7 Mt at 6% HM (1982)	1975 (None) Not producing River plain deposit average of 5 m thick
Zhanjiang district Guangdong	Placer Mixed beach and river coastal plain	Monazite, xenotime	Measured—3.0 Mt; indicated—7.0 Mt	– Producer by-product monazite

(*Continued*)

TABLE 2.11 (CONTINUED)
Summary of World Rare-Earth Deposits

Location	Deposit Type, Host Rock, Principal Minerals	RE Minerals	Average Grade Resources, kt [Year]	Year of Discovery (Year of First Production) Annual Production, kt [Year] Status
			Egypt	
Nile Delta—Rosetta	Placer Marine Ilmenite, rutile, zircon, monazite, magnetite, garnet	Monazite	Reserves—4.6 Mt, resource—40 Mt, estimate—contains 0.18 Mt monazite; 44.4 Mt at 0.5% monazite (1989)	– (1929) Small past producer?
			Gabon	
Mabounié	Magmatic A carbonatite with florencite	Fluocerite	2.52% REO in the ore	– Mabounié polymetallic deposit in Gabon contains reserves of niobium, tantalum, rare earths, and uranium
			Greenland	
Ilimaussaq Gardar	Magmatic Agpaitic nepheline syenite; arfvedsonite lujavrite, pulaskite, foyaite	Pyrochlore, eudialyte; minor rinkite, steenstrupine, monazite, apatite, britholite	>6.6 Mt at 6% ZrO_2, 3% REO, 0.2% Y_2O_3 (1994); 30 Mt at 0.9% Y_2O_3	– One of the 10 alkaline intrusions of the Gardar Complex; apatite containing >16.0 wt% REO has been identified; U–Be–Zr–Nb mineralization; Jackson and Christiansen classify as carbonatite Zr, REE resource Advanced rare-earth project

(*Continued*)

TABLE 2.11 (CONTINUED)
Summary of World Rare-Earth Deposits

Location	Deposit Type, Host Rock, Principal Minerals	RE Minerals	Average Grade Resources, kt [Year]	Year of Discovery (Year of First Production) Annual Production, kt [Year] Status
			India	
Chatrapur Orissa Sands Complex/ OSCOMOrissa	Placer Marine Ilmenite, rutile, zircon, leucoxene, sillimanite, monazite, quartz, garnet	Monazite	Proven—240 Mt at 0.625% monazite, 9.6% ilm, 0.5% rut, 0.42% zir, 3.29% sill + inferred—350 Mt (1982); 224 Mt at 0.632% monazite or 0.3476% REO [1989]	1958 (1983) Sand dunes open pit By-product of Ti mining; belt of sand dunes is 1500 m wide and 19 km long; relatively low U + Th (50–60 ppm) in ilmenite concentrate Producer by-product monazite
Chavara (IREL) (Kerala)	Placer Marine Ilmenite, rutile, zircon, leucoxene, sillimanite, monazite, quartz, garnet	Monazite	Total for deposit 0.12 Mt monazite; 0.5%–1.0% monazite (1973); 118 Mt at 0.16% monazite or 0.0856% REO 18% heavy minerals, 0.135% monazite	1920s (1932) Producer by-product monazite By-product of Ti mining; monazite distribution is patchy; ore is 18% HM; open pit sands mined manually
Chavara (Quilon)—KMML Kollam Kerala	Placer Marine Ilmenite, rutile, zircon, leucoxene, sillimanite, monazite, quartz, garnet	Monazite	114.8 Mt at 0.16% monazite or 0.088% REO (1989)	1920s By-product producer; by-product of Ti mining; occurrence is patchy

(*Continued*)

TABLE 2.11 (CONTINUED)
Summary of World Rare-Earth Deposits

Location	Deposit Type, Host Rock, Principal Minerals	RE Minerals	Average Grade Resources, kt [Year]	Year of Discovery (Year of First Production) Annual Production, kt [Year] Status
Manavalakurichi Tamil Nadu	Placer Marine Ilmenite, rutile, zircon, leucoxene, sillimanite, monazite, quartz, garnet	Monazite	103.7 Mt at 2.5% monazite or 1.37% REO (1989)	1909 (1911) Producer by-product monazite By-product of Ti mining; open pit sands mined manually
Ranchi and Purulia Bihar	Placer Fluvial Ilmenite, rutile, zircon, monazite, apatite, columbite, magnetite, quartz	Monazite	86.5 Mt at 1.64% HM, 0.31% monazite, 0.03% apatite (1989)	1956 (None) Not producing Inland alluvium By-product REE from Ti mining
		Kenya		
Ruri Complex	Carbonatite, carbonatite agglomerate, nepheline syenite, phonolite plugs	Monazite, bastnasite, eudialyte	0.375 Mt at 6.4% monazite or 3.5% REO (1989)	1940s (None) Potential resource Complex of twin, deeply eroded, carbonatitic volcanoes; open pit
Mrima Hill	Supergene Sovite, lamprophyre, agglomerate, fenite	Monazite, gorceixite, goyazite, pyrochlore	6 Mt at about 5% REO (1966); 50.8 Mt at 0.59% REO	– Past Nb producer Potential REE—resource

(*Continued*)

TABLE 2.11 (CONTINUED)
Summary of World Rare-Earth Deposits

Location	Deposit Type, Host Rock, Principal Minerals	RE Minerals	Average Grade Resources, kt [Year]	Year of Discovery (Year of First Production) Annual Production, kt [Year] Status
		Malawi		
Kangankunde	Magmatic Dolomitic carbonatite, fenite	Monazite, staurolite, bastnasite, florencite–goyazite, daqingshanite	11 Mt at 1.97% REO; 11 Mt at 5% monazite (1983); 11 Mt at 0.62% REO Monazite almost thorium-free	– Advanced Rare Earth Project Carbonatite contains average of 7% euhedral green monazite crystals; high iron content; locally, REE of hydrothermal origin REE–Sr resource
		Madagascar		
Fort Dauphine	Placer Marine	Monazite	60 Mt at 1.49% monazite	– Past producer
Tolagnaro	Placer Marine	Monazite	75 Mt at 3.84% zircon, 0.96% monazite, 5.12% rutile	– A coastal lagoon
		Mauritania		
Bou Naga	Hydrothermal carbonatite	Monazite, bastnasite	3.66% REO; 0.1 Mt at 8% monazite or 4.4% REO [1970]	– (1968–1970) Past small producer? LREE dominant

(*Continued*)

TABLE 2.11 (CONTINUED)
Summary of World Rare-Earth Deposits

Location	Deposit Type, Host Rock, Principal Minerals	RE Minerals	Average Grade Resources, kt [Year]	Year of Discovery (Year of First Production) Annual Production, kt [Year] Status
		Mongolia		
Khaldzan-Buregtey Western Mongolia	– Peralkaline granite, gabbro, basalt, pantellerite dikes, syenite	Fergusonite, allanite, bastnasite, synchysite, britholite, monazite, chevkinitev	>1.2 Mt REE at 0.3% REE, >0.4 Mt Nb at 0.1% Nb, >8 Mt Zr at 2.0% Zr	1984 Host rocks have been metasomatized
Lugin Gol East Govi	– Nepheline syenite, ijolite, carbonatite dikes	Bastnasite, synchysite, parisite barite	0.023 Mt REO at 3.2% REO	1999 In Gobi desert; 20 carbonatite dike zones with 400 separate mineralized pods
Mushgai Khudag (Mushgia Khudag, Mushugai Khuduk, Mushugai-Hudag) South Govi	Magnetite–apatite rock, potassic alkaline volcanic rocks, carbonatite, melanephelinite, melaleucitite	Apatite, bastnasite	200 Mt at 1.5% RE; 6.1 Mt at 1.37% REO	Apatite has high REE
		Mozambique		
Angoche		Monazite	Estimated reserves—124 Mt at 4% HM	1988

(*Continued*)

TABLE 2.11 (CONTINUED)
Summary of World Rare-Earth Deposits

Location	Deposit Type, Host Rock, Principal Minerals	RE Minerals	Average Grade Resources, kt [Year]	Year of Discovery (Year of First Production) Annual Production, kt [Year] Status
Congolone	Placer Marine dune and beach sand	Ilmenite, rutile, zircon, monazite, quartz	166.8 Mt at 2.94% ilmenite, 0.2% zircon, 0.05% rutile, 0.0066% monazite [1990]	1992 Beach sands, dunes; four mineralized areas—Moma (Namalope-Tupuito), Congolone, Quinga, and Marrua
Moebase (Moebane) Zambezia	Placers Marine + aeolian	Monazite	1300 Mt at 3.8% HM 2 Mt of black sands reported to grade 78% ilm, 2% rute, 13% zir, 5% monazite	–
Quelemane Zambezia Mozambique		Monazite; minor loparite, sahamalite rutile	520 Mt at 4.5% heavy minerals	
		Namibia		
Eureka	Carbonate rocks Monazite, zircon, magnetite, graphite	Monazite	Proven: 0.03 Mt at 6.3% REE [1989]	– Carbonatite dikes on Eureka 99 farm, 38 km W of Usakos; resource estimate is to depth of 20 m; potential resource
Kalkfeld (Etaneno)	Magmatic Carbonatite, syenite, foyaite, iron ore	Eudialyte, monazite	20 Mt REO (1989)	– Th–REE occurrence Fe ore and carbonatites are enriched in La, Ce, neodymium, and thorite

(*Continued*)

TABLE 2.11 (CONTINUED)
Summary of World Rare-Earth Deposits

Location	Deposit Type, Host Rock, Principal Minerals	RE Minerals	Average Grade Resources, kt [Year]	Year of Discovery (Year of First Production) Annual Production, kt [Year] Status
		New Zealand		
Barrytown South Island/Westland	Placer Marine Ilmenite, rutile, zircon, magnetite, cassiterite, gold, monazite, scheelite	Monazite	10.8 Mt at 0.1–0.3% monazite [1970's]; 73.3 Mt at 0.001% monazite or 0.00055% REO [1989]	1960s Marine placer beach and dune sands extending over a distance of 16 km along the coast. Deposit averages 10 m thick Under development
Westport (South Island)	Placer Marine Ilmenite, rutile, zircon, magnetite, cassiterite, gold, monazite, scheelite	Monazite	Ore: 850,200 R2E [1989]	– Undergoing feasibility study
		Russia and Countries of Former Soviet Union		
Khibina(Khibiny) Kola Peninsula	– Foyaite, nepheline syenite, ijolite, rischorrite, urtite, pegmatites, carbonatite?	Apatite, eudialyte, burbankite, ancylite, synchysite, parisite, carbocernaite, cordylite, apatite, astrophyllite, loparite, mosandrite, lovchorrite, rinkite	9 Mt REO	P, NEPH producer; largest igneous apatite deposit in the world, in urtite–ijolite; REE minerals largely in alkaline rocks not carbonatite (Kogarko et al. 1995); small bodies of carbonatites contain as much as 9% REE, 6.5% Sr, 3% Ba

(*Continued*)

TABLE 2.11 (CONTINUED)
Summary of World Rare-Earth Deposits

Location	Deposit Type, Host Rock, Principal Minerals	RE Minerals	Average Grade Resources, kt [Year]	Year of Discovery (Year of First Production) Annual Production, kt [Year] Status
Kutessai-II Kyrgyzstan	– Granophyre, dikes	Monazite, xenotime, Y-synchysite, Y-parisite	0.088 Mt REE at 0.39% REE	– Active mine (1998) Advanced rare-earth project
Lovozero	– Lujavrite, foyaite, urtite, syenite, nepheline syenite; min also in alkaline pegmatites and hydrothermal veins	Loparite, eudialyte, rinkite, ancylite, mosandrite, monazite, burbankite, bastnasite, huanghoite, rhabdophane, synchysite, carbonate-fluorapatite	>1000 Mt at 0.8–1.5% REO	– Loparite min. is in urtite–foyaite–lujavrite rocks; eudialyte lujavrite complex is being assessed for Zr and Y Nb producer with by-product REE from loparite
Seligdar Siberia	Apatite rock, syenite porphyry	Apatite, monazite, allanite	300 Mt at 6%–8% P_2O_5	– P resource; potassic alkaline igneous complex; unclear if deposit high-temperature apatite-bearing carbonatite or phosphate mobilized from surrounding country rocks

(*Continued*)

TABLE 2.11 (CONTINUED)
Summary of World Rare-Earth Deposits

Location	Deposit Type, Host Rock, Principal Minerals	RE Minerals	Average Grade Resources, kt [Year]	Year of Discovery (Year of First Production) Annual Production, kt [Year] Status
Tomtor	Weathered carbonatite dolomite and calcite carbonatite, nepheline syenite	Pyrochlore, florencite, monazite, gorceixite, goyazite, rhabdophane, xenotime, bastnasite	Large resource with 8–31% REO, 3–8% Nb_2O_5	– REE–Nb resource 300 km^2 massif; contains as much as 37% RE oxides
		Saudi Arabia		
Ghurayyah	Microgranite	Aeschynite (Y), xenotime, monazite, sahamalite, pyrochlore	440 Mt at 0.15% REE + Y	– Enriched in HREE relatively to LREE
Jabal Hamra'	Silexite plug	Monazite, bastnasite	18 Mt at 0.21% Nb_2O_5, 0.18% Y_2O_3, 1.78% ZrO_2, 0.8% REO	–
Jabal Sa'id (Jabal Sayid)	Alkaline rocks, aplite–pegmatite	Brockite; allanite, pyrochlore	23 Mt (to 100 m below surface) at 0.6% REE + Y	–
Jabal Tawlah	Leucocratic microgranite, microsyenite, albitite sill	Pyrochlore, monazite	6.4 Mt at 0.42% Nb_2O_5, 0.62% Y_2O_3, 5.0% ZrO_2	– High HREE/LREE
Umm al Birak	Microgranite stock	Monazite, bastnasite, pyrochlore	6.6 Mt at 0.14% REE + Y	–

(*Continued*)

TABLE 2.11 (CONTINUED)
Summary of World Rare-Earth Deposits

Location	Deposit Type, Host Rock, Principal Minerals	RE Minerals	Average Grade Resources, kt [Year]	Year of Discovery (Year of First Production) Annual Production, kt [Year] Status
		South Africa		
Buffalo Fluorspar Transvaal	Magmatic Granite	Monazite, allanite, bastnasite	50 Mt at 1% monazite Open pit monazite is not reclaimed Ore: 50,000 CaF_2: 6500 Monazite: 500 [1989]	1943 (1948) Veins in leptite pendants of the Bushveld granite
Palabora (Phalaborwa) South Africa	Magmatic Weathered pyroxenite, carbonatite, phoskorite Bornite, chalcopyrite, apatite, pyroxene, hornblende, plagioclase	Apatite, synchysite, monazite	123.8 Mt at 0.105% REO [1989]; 652 Mt at 0.15% REO Ore: 123,840; apatite: 1858; REO: 130 [1989]; REO is not reclaimed	1912 (1932) Open pit; major copper producer Possible by-product REE recovery; apatite concentrates contain 0.4%–0.9% REO Potential by-product REE recovery
Pilansberg Complex (Pilanesberg, Pilaan's berg) Transvaal	Alkali igneous, foyaite, syenite, tinguaite	Britholite, eudialyte, pyrochlore, allanite, mosandrite	13.5 Mt at 0.7% REO + ThO_2, 1.2 Mt at 6.54% REO + ThO_2, and 0.024 Mt at 10% REO + ThO_2	– Britholite-bearing veins and small areas of eudialyte syenite
Richards Bay (Natal)	Placer Marine Ilmenite, rutile, zircon, magnetite, leucoxene, monazite, quartz, garnet	Monazite	6.5% heavy minerals, 0.023% monazite 4980 Mt at 0.023% monazite or 0.013% REO	1967 (1977) Dune and beach sand by-product producer Mines having three dredges and wet plants

(*Continued*)

TABLE 2.11 (CONTINUED)
Summary of World Rare-Earth Deposits

Location	Deposit Type, Host Rock, Principal Minerals	RE Minerals	Average Grade Resources, kt [Year]	Year of Discovery (Year of First Production) Annual Production, kt [Year] Status
Sandkopsdrif (Zandkops Drift)	Carbonatite, glimmerite, carbonatized intrusions Churchite, goyazite, apatite, pyrochlore vermiculite, ilmenite, titanite	Churchite, goyazite	57 Mt at 1% REO	Complex about 1 km in diameter Advanced rare-earth project
Steenkampskraal Cape Province	Metamorphic Gneiss Titanifereous magnetite	Monazite	Reserves— >0.2 Mt at 12.5% REO; approximately 20,000 t of monazite remained in 1986	– Monazite–apatite veins in gneiss; in 1996, restartup was planned for 1998; mine life was estimated at 10 years Active producer? Advanced rare-earth project
		South Korea		
Janghowon	Placer	Monazite	0.017 Mt monazite at a grade of 0.07% monazite [1968]	– 60 km north of Chongju; deposit is inland and believed to be composed of river sands; deposit type classification is uncertain
Kusipo	Placer Marine and fluvial	Monazite	Measured—0.0025 Mt monazite at a grade of 0.12% monazite	– 50 km north of Mokpo; deposit is along a coast and believed to be a marine placer or a mix of marine and alluvial sands

(*Continued*)

TABLE 2.11 (CONTINUED)
Summary of World Rare-Earth Deposits

Location	Deposit Type, Host Rock, Principal Minerals	RE Minerals	Average Grade Resources, kt [Year]	Year of Discovery (Year of First Production) Annual Production, kt [Year] Status
Kwangsangun	Placer	Monazite	0.048 Mt monazite at a grade of 0.05% monazite (1968)	– 10 km N of Kwangju; deposit is inland and believed to be composed of river sands; deposit-type classification uncertain
Namdaecheon River (Muju area)	Placer Fluvial	Monazite	0.028 Mt monazite at a grade of 0.14% monazite (1982)	– Deposits are associated with the Namdaechon river
Soun-Miyang	Placer Fluvial	Monazite	0.025 Mt monazite at a grade of 0.07% monazite (1968)	– 40 km NW of Chongju; deposit is inland and believed to be a river placer
Yongsanpo	Placer Fluvial	Monazite	0.02 Mt monazite at a grade of 0.07% monazite (1968)	– Deposit is inland and believed to be a river placer
		Sri Lanka		
Pulmoddai	Placer Marine Ilmenite, rutile, zircon, sillimanite, monazite, garnet, quartz	Monazite	6 Mt at 0.3% monazite; proven—4.0 Mt at 0.24% monazite, 56% ilm, 6.4–8% zir, 6.4% rut; 1.593 Mt at 70% heavy minerals, 0.15% monazite or 0.082% REO (1989)	1920s (1961) By-product of Ti mining; old beach deposit (1.2 m above sea level) and modern beach; deposit replenished by annual monsoon; by-product producer

(*Continued*)

TABLE 2.11 (CONTINUED)
Summary of World Rare-Earth Deposits

Location	Deposit Type, Host Rock, Principal Minerals	RE Minerals	Average Grade Resources, kt [Year]	Year of Discovery (Year of First Production) Annual Production, kt [Year] Status
			Sweden	
Norra Kärr	Alkali igneous Peralkaline syenite	Eud, zr	0.54% REO	– Eudialyte contains 1.3% Y Advanced rare-earth project
			Taiwan	
Chingshankangchow	Placer	Monazite	0.765 Mm^3 at 13.0% monazite, 20.4% ilm, 18.4% zir, 2.1% rut	– Offshore sand bar
Foulun		Monazite	0.23 Mm^3 at 11.5% monazite, 24.9% zir, 22.1% ilm, 3.2% rut	–
Peitungshanchow		Monazite	5 Mm^3 at 12.6% monazite, 25.9% zir, 22.7% ilm, 2.3% rut (1968)	– Offshore sand bar
Putaichow		Monazite	0.2 Mm^3 at 13.5% monazite, 25.0% zir, 22.0% ilm, 2.5% rut	– Offshore sand bar
Tingtouechow		Monazite	0.018 Mm^3 at 9.6% monazite, 20.9% zir, 19.5% ilm, 5.2% rut (1968)	–

(*Continued*)

TABLE 2.11 (CONTINUED)
Summary of World Rare-Earth Deposits

Location	Deposit Type, Host Rock, Principal Minerals	RE Minerals	Average Grade Resources, kt [Year]	Year of Discovery (Year of First Production) Annual Production, kt [Year] Status
Tungshanchow		Monazite	8.85 Mm^3 at 11.8% monazite, 18.0% zir, 16.5% ilm, 2.3% rut (1968)	– Offshore sand bar
Waisantingchow		Monazite	3.04 Mm^3 at 11.2% monazite, 18.9% ilm, 16.7% zir, 1.8% rut (1968)	– Offshore sand bar
Wangtzeliaochow		Monazite	0.55 Mm^3 at 10.9% monazite, 22.8% zir, 21.4% ilm, 3.1% rut (1968)	– Offshore sand bar
Wangyehchow		Monazite	0.96 Mm^3 at 12.1% monazite, 24.4% zir, 23.1% ilm, 5.0% rut (1968)	– Offshore sand bar
		Tanzania		
Wigu Hill	Weathered dolomitic carbonatite	Bastnasite, monazite, Ce–goyazite, synchysite, parisite	As much as 20% REO	– Carbonatite dikes; deposit shows extensive replacement by hydrothermal solutions rich in REE, Sr, F, BA, and silica
		Turkey		
Kizilçaören Eskisehir Turkey	Phonolite, trachyte, and alkaline pyroclastic rocks	Bastnasite	4.7 Mt at 2.78% REE (1990)	Bastnasite–fluorite–barite rock lenses associated with carbonatite dikes

(*Continued*)

TABLE 2.11 (CONTINUED)
Summary of World Rare-Earth Deposits

Location	Deposit Type, Host Rock, Principal Minerals	RE Minerals	Average Grade Resources, kt [Year]	Year of Discovery (Year of First Production) Annual Production, kt [Year] Status
		United States		
Bald Mountain Wyoming/Albany County	Magmatic Conglomerate Ilmenite, zircon, monazite, magnetite, hematite, quartz	Monazite	18.1 Mt at 0.13% monazite or 0.077% REO (1983); 0.011% ThO_2	1951 (None) Fossil fluvial placer Little Big Horn River area; two sites contain at least 1.0 kg monazite/t of rock; resource is poorly defined; potential open pit
Bear Lodge Mountains (southern) Wyoming	Magmatic Trachyte, phonolite, minor syenite and nepheline syenite, carbonatite monazite, xenotime, ancylite, bastnasite	Monazite, xenotime, thorite	726 Mt at 1.306% REO [1978]; 0.034% ThO_2	– Large low-grade resource of RE and Th Veins and disseminated deposits; samples ranged from 112 to 30,000 ppm with REE more abundant than Th; area incompletely explored; potential open pit; high thorium Advanced rare-earth project
Bear Valley Idaho/ Valley County	Placer Fluvial sands, gravel Ilmenite, magnetite, monazite, garnet, quartz	Monazite; minor loparite, xenotime, fergusonite	109.9 Mt at 0.0155% monazite or 0.010% REO [1982]; total production of 10,000 t REO	1950 (1955) Mining ceased in 1959 Includes porter placer; small past producer
Big Creek Idaho/ Valley County	Placer Fluvial Ilmenite, magnetite, zircon, monazite, garnet	Monazite, Y-lop, Y-euxenite	10,000 mt REO; 116.1 Mt at 0.04% monazite [1982]	1940s (1950) Past producer Date of shutdown unknown

(*Continued*)

TABLE 2.11 (CONTINUED)
Summary of World Rare-Earth Deposits

Location	Deposit Type, Host Rock, Principal Minerals	RE Minerals	Average Grade Resources, kt [Year]	Year of Discovery (Year of First Production) Annual Production, kt [Year] Status
Blackfoot Bridge Idaho, USA	Magmatic Mudstone Collophane, vanadinite, uraninite, REEs, pyrite, clay	Collophane, monazite	5.9 Mt at 0.16% monazite [1984]	– Monazite ~0.1% REE in P ore Mining to start in 2023 at close of Caldwell Canyon
Bokan Mountain (Ross–Adams) Alaska	Peralkaline, riebeckite, and aegirine granites, syenite, granite porphyry	Kainosite, allanite, thalenite, bastnasite, parisite, synchysite, monazite, britholite, tengerite, xenotime, iimoriite, fergusonite, sahamalite	6.2 Mt (indicated resource) at 0.09–0.46% REO + 0.09–0.4% Y_2O_3	– Potential resource REE, past prod. U REE-bearing pegmatites, dikes, and shear zones/ fractures in the central part of the complex and in veins in the outer parts and nearby country rocks; produced 98,000 mt of approx. 1% U_3O_8; because dikes generally <1 m thick and mineralogically complex, economic potential low Advanced rare-earth project
Brunswick—Altamaha (Georgia)	Placer Marine Ilmenite, magnetite, zircon, monazite, quartz	Monazite	65.85 Mt at 0.0288% monazite [1982]	1959 (None) Mining would be by dredge
Caldwell Canyon Idaho	Magmatic Mudstone Collophane, vanadinite, uraninite, REEs, pyrite, clay	Monazite	11 Mt at 0.155% monazite	– ~0.1% REE in P ore; mining to start in 2035 at close of Trail Creek

(*Continued*)

TABLE 2.11 (CONTINUED)
Summary of World Rare-Earth Deposits

Location	Deposit Type, Host Rock, Principal Minerals	RE Minerals	Average Grade Resources, kt [Year]	Year of Discovery (Year of First Production) Annual Production, kt [Year] Status
Cumberland Island Georgia	Placer Marine Ilmenite, rutile, zircon, leucoxene, monazite, quartz	Monazite	241 Mt at 0.0178% monazite or 0.011% REO [1982]	1940s (None) Sand Barrier island in National Park so development unlikely
Diamond Creek Idaho/Caribou	Magmatic Quartzite Monazite, xenotime, fluorite, hematite, feldspar, quartz	Monazite, xenotime	0.235 Mt at 1.96% monazite or 1.23% REO (1978); 0.21% ThO_2	– Would be an underground mine
Dora Bay, Alaska	Peralkaline, agpaitic nepheline syenite complex		2.8 Mt eudialyte	Prospect
Gallinas Mountains New Mexico	Magmatic Sandstone Fluorite, REEs, pyrite, quartz, clay	Bastnasite	0.046 Mt at 2.95% REO (1983)	About 1885 (1943) Fluorite mine closed in 1956 About 65 t of bas concentrate produced in the 1950s from Cu–F veins and breccia fillings probably associated with alkalic trachyte; open pit, underground; very small past producer
Gay and South Forty (Idaho)	Magmatic – Collophane, vanadinite, uraninite, REEs, pyrite, clay	Collophane, monazite	0.1% rare earths at phosphate property Ore: 18,000; P_20_5: 4590 Monazite: 18 [1989]	Unknown (1946); open pit

(*Continued*)

TABLE 2.11 (CONTINUED)
Summary of World Rare-Earth Deposits

Location	Deposit Type, Host Rock, Principal Minerals	RE Minerals	Average Grade Resources, kt [Year]	Year of Discovery (Year of First Production) Annual Production, kt [Year] Status
Gold Fork-Little Valley, Idaho/ Valley County, USA	Placer Fluvial Ilmenite, magnetite, zircon, gold, monazite, quartz	Monazite	296 Mt at 0.016% monazite or 0.0098% REO (1981)	1880s (1880s) Originally a gold placer producer
Green Cove Springs Florida	Placer Marine Ilmenite, magnetite, zircon, staurolite, monazite	Monazite	110.1 Mt at 0.0073% monazite or 0.0045% REO (1989)	1950s (1972) Active mine (1999); past by-product monazite producer; the only placer REO producer in the United States (1993); stopped producing monazite in 1994
Hall Mountain Group Idaho	Magmatic – Gold, zircon, apatite, monazite, hematite, quartz	Thorite, magnetite, gold, zircon, apatite, allanite, monazite	0.071 Mt at 0.026% Y_2O_3, 0.668% ThO_2	1930s (1930s); open pit, underground Mining ceased in 1940s
Henry, Idaho	Magmatic Mudstone Collophane, vanadinite, uraninite, REEs, pyrite, clay	Collophane, monazite	0.847 Mt at 0.189% monazite (1989)	– Mining halted in 1990 ~0.12% REE in P ore Open pit Past by-product producer?

(*Continued*)

TABLE 2.11 (CONTINUED)
Summary of World Rare-Earth Deposits

Location	Deposit Type, Host Rock, Principal Minerals	RE Minerals	Average Grade Resources, kt [Year]	Year of Discovery (Year of First Production) Annual Production, kt [Year] Status
Hicks Dome, Illinois	Magmatic Peridotite, intrusive breccia Thorite, xenotime, REEs, fluorite, barite, apatite, sulfides, hematite	Xenotime, bastnasite, churchite	14.7 Mt at 0.42% REO (1978); 0.15% ThO_2	– Potential resource; no production plans
Hilton Head Island South Carolina	Placer Marine Ilmenite, rutile, zircon, staurolite, magnetite, monazite, quartz, clay, garnet	Monazite	759.3 Mt at 0.008% monazite (1983)	1954 (None) Potential resource Dune and beach sand mining unlikely, active resort area
Horse Creek (Aiken County) South Carolina	Placer Fluvial Ilmenite, rutile, zircon, monazite, quartz, clay	Monazite, xenotime	19 Mt at 0.041% monazite or 0.026% REO (1983)	1950s (1955) Past producer of monazite; closed in 1958 Tuscaloosa Fmt sediments; flood plain; reconcentration of heavy minerals from Tuscaloosa Fmt; includes Hollow (Holley) Creek and other drainages
Husky Idaho	Magmatic Mudstone Collophane, vanadinite, uraninite, REEs, pyrite, clay	Collophane, monazite	23 Mt at 0.16% monazite (1989)	Unknown (1993) ~0.1% REE in P ore Open pit Start was planned in 1993 at 1,358,000 t/year

(*Continued*)

TABLE 2.11 (CONTINUED)
Summary of World Rare-Earth Deposits

Location	Deposit Type, Host Rock, Principal Minerals	RE Minerals	Average Grade Resources, kt [Year]	Year of Discovery (Year of First Production) Annual Production, kt [Year] Status
Iron Hill (Powderhorn, Cebolla Creek) Colorado	Magmatic Carbonatite, ijolite, nepheline syenite, pyroxenite, melasyenite, fenite Ilmenite, rutile, zircon, pyrochlore, apatite, monazite, fluorite, pyrite	Bastnasite, perovskite, synchysite, parisite, apatite, pyrochlore, monazite	36.3 Mt at 0.01% REO; 655.6 Mt at 0.397% REO (1989)	1880s (None) Not producing Ti resource/prospect Mining goal would be Nb_2O_5
Iron Hill (Powderhorn, Cebolla Creek) Colorado	Magmatic Carbonatite, ijolite, nepheline syenite, pyroxenite, melasyenite, fenite	Bastnasite, perovskite, synchysite, parisite, apatite, pyrochlore, monazite	36.3 Mt at 0.01% REO; 655.6 Mt at 0.397% REO (1989)	1980s (None); potential open pit; not producing Ti resource/prospect
Lemhi Pass Idaho	Magmatic Quartzite, phyllite, gneiss, schist Monazite, thorite, rutile, quartz, hematite, pyrite	Monazite, xenotime, bastnasite, allanite, ancylite, loparite, churchite	39 Mt at 0.81% monazite or 0.51% REO	1949 (None) Veins; thorium is dominant mineralization Would be mined underground for ThO_2
Maybe Canyon (Maybie) Idaho	Magmatic Mudstone Collophane, vanadinite, uraninite, REEs, pyrite, clay	Collophane, monazite	6.35 Mt at 0.16% monazite	Unknown (1966) ~0.1% REE in P ore; open pit

(*Continued*)

TABLE 2.11 (CONTINUED)
Summary of World Rare-Earth Deposits

Location	Deposit Type, Host Rock, Principal Minerals	RE Minerals	Average Grade Resources, kt [Year]	Year of Discovery (Year of First Production) Annual Production, kt [Year] Status
Mineville dumps New York	Magmatic Magnetite–hematite vein in gneiss Magnetite, martite, apatite, quartz, feldspar	Xenotime-bearing apatite	15.7 Mt at 1.04% REO, 0.0136% ThO_2 in dumps from former iron ore mine	1700s (1824) Past Fe producer; REE resource Open pit Apatite in mill tailings averages from 4% to more than 11% REO; magnetite–hematite ore body in metamorphic rocks
Monumental Summit Idaho	Quartzite, schist, calcareous rock	Rhabdophane	0.086 Mt at 3.6 kg REE/t	–
Mountain Fuel Idaho	Magmatic Mudstone Collophane, vanadinite, uraninite, REEs, pyrite, clay	Collophane, monazite	5.4 Mt at 0.166% monazite	Unknown (1986) Open pit ~0.1% REE in P ore
Mountain Pass California	Magmatic Carbonatite Allanite, monazite, barite, quartz	Bastnasite, parisite, monazite, sahamalite, allanite, cerite	Proven + probable—29 Mt at 8.9% REO (5% cutoff); >40 Mt at 7.68% REO; 28 Mt at 8.86% REO; 28.1 Mt at 12% bastnasite or 8.9% REO [1989]; 90 Mt at 5% REO	1949 (1965) Current producer Open pit The major REO producer in the United States

(*Continued*)

TABLE 2.11 (CONTINUED)
Summary of World Rare-Earth Deposits

Location	Deposit Type, Host Rock, Principal Minerals	RE Minerals	Average Grade Resources, kt [Year]	Year of Discovery (Year of First Production) Annual Production, kt [Year] Status
Music Valley California	Magmatic Gneiss Xenotime, monazite, gold, biotite, quartz	Xenotime, monazite	As much as 16% REO (1964); 0.05 Mt at 8.6% REO	1949 (None) Ore is highly radioactive RE value ranges from 3% to 14%
North and South Carolina Placers North and South Carolina	Placer Fluvial Ilmenite, rutile, zircon, sillimanite, staurolite, monazite, garnet, kyanite	Monazite	Monazite: 90; REO: 57 [1978]	1880s (1887) Series of separate placers No plans for production
North Henry Idaho	Magmatic Mudstone Collophane, vanadinite, uraninite, REEs, pyrite, clay	Collophane, monazite	3.2 Mt at 0.119% REO (1985)	Unknown (1991) Open pit to operate through 1994 ~0.1% REE in P ore
Oak Grove Tennessee	Placer Fluvial Ilmenite, rutile, zircon, leu– coxene, staurolite, monazite, garnet, kyanite, tourmaline	Monazite	174.6 Mt at 0.155% monazite or 0.09% REO (1982)	1960s (None) Sand of the McNairy Fm; alluvial terrace No plans for production

(*Continued*)

TABLE 2.11 (CONTINUED)
Summary of World Rare-Earth Deposits

Location	Deposit Type, Host Rock, Principal Minerals	RE Minerals	Average Grade Resources, kt [Year]	Year of Discovery (Year of First Production) Annual Production, kt [Year] Status
Old Hickory (Stony Creek) Virginia	Placer Shoreline Ilmenite, rutile	Monazite?	210 Mt at 6.5% HM; reserves—73 Mt at 8.1% HM, proven—27 Mt at 10.2% HM??	Active mine (1999) No REE prod
Pajarito Mountain New Mexico	Magmatic Alkalic igneous Syenite, melasyenite, quartz syenite Eudialyte, zircon	Eudialyte, monazite, apatite, kainosite	24 Mt at 0.18% Y_2O_3, 1.2% ZrO_2; 2.4 Mt at 0.167% REO	1984 (None) 0.18% Y_2O_3 in major potential source of yttrium in the United States Quartz-bearing syenite contains as much as 20% eudialyte and 5% fluorite; apatite containing as much as 19.2% REO has been found in the peralkaline granites
Pea Ridge Missouri	Hydrothermal Fe-oxide, breccia pipes assoc. with granite and syenite	Monazite, xenotime, allanite	0.6 Mt at 12% REO	– Potential resource
Pearsol Creek Idaho	Placer Fluvial Ilmenite, magnetite zircon, monazite, garnet, quartz	Monazite	172.5 Mt at 0.0186% monazite (1982)	1940s (1950) Unknown shutdown date
Ramey Meadows Idaho	Placer Alluvial	Allanite	1.7 Myd^3 at 13.5 lbs HM/yd^3	Occurrence

(*Continued*)

TABLE 2.11 (CONTINUED)
Summary of World Rare-Earth Deposits

Location	Deposit Type, Host Rock, Principal Minerals	RE Minerals	Average Grade Resources, kt [Year]	Year of Discovery (Year of First Production) Annual Production, kt [Year] Status
Silica Mine Tennessee	Placer Fluvial Ilmenite, rutile, zircon, leucoxene, monazite, quartz	Monazite	26.7 Mt at 0.013% monazite or 0.0079% REO [1989]	1930s [1942] HM stockpiled from past production of silica sand; producer but does not recover REO
Smoky Canyon Idaho	Magmatic Mudstone Collophane, vanadinite, uraninite, REEs, pyrite, clay	Collophane, monazite	35.5 Mt at 0.158% monazite	Unknown (1984) Phosphate mine Open pit; production was to continue through 2005 By-product producer?
Trail Creek Idaho	Magmatic Mudstone Collophane, vanadinite, uraninite, REEs, pyrite, clay	Collophane, monazite	27 Mt at 0.159% monazite [1984]	– Production was to start in 2005 0.1% rare earths at phosphate property
Wet Mountains Colorado	Magmatic Alkaline rocks, carbonatite dikes Thorite, xenotime, barite, hematite, quartz	Apatite, bastnasite, synchysite, xenotime, monazite	13.96 Mt at 1.0% REO [1989]; 2.5% REO	1960s (None) No plans for production REE, Nb, and Th occur in veins and carbonatite dikes; province includes Gem Park, McClure Mtn-Iron Mtn, Democrat Creek, and other occurrences ThO_2:REO ratio 2.2:1.0
Wooley Valley Idaho	Magmatic Collophane, vanadinite, uraninite, REEs, pyrite, clay	Collophane, monazite	11.5 Mt ore mined between 1955 and 1987	Unknown (1955) Mining ceased in 1987 0.11% rare earths at phosphate property; open pit

(*Continued*)

TABLE 2.11 (CONTINUED)
Summary of World Rare-Earth Deposits

Location	Deposit Type, Host Rock, Principal Minerals	RE Minerals	Average Grade Resources, kt [Year]	Year of Discovery (Year of First Production) Annual Production, kt [Year] Status
		Vietnam		
Cat Khanh Binh Dinh or Nghia Binh	Placer Coastal	Monazite, xenotime	8.97 Mt at 0.117% monazite (7.7% HM)	– 3 ore horizons in placer; current producer
Dong Pao Lai Chau	Syenite, quartz syenite	Bastnasite, parisite	Possible reserves: 7 Mt REO and proven + possible ore body 3: 0.645 Mt REO	– Metasomatic + weathered ore in Phong Tho district, 40 km from Nam Xe deposits; 60 ore bodies of various sizes have been identified in the Dong Pao area; they form irregular pods, lenses, and veins in shear zones
Mi Tho Binh Dinh	Placer Coastal	Monazite, xenotime	Possible—6574 t monazite + xenotime	– In Cat Khanh area; active producer?
Muong Hum	–	Allanite	0.4 Mt REO	–
Nam Xe North (Mau Xe North) Lai Chau	Limestone, marble, schist	Bastnasite, parisite	Possible reserves—7 Mt REO; proven + probable—7.8 Mt REO; proven—1.745 Mt REO	– Metasomatic + weathered ore; on N side of Nam Xe River in Phong Tho district; lenses, veins, disseminated ore in crushed zones of 1st affected by metasomatism; weathered ore contains 4–5% REO to depth of 20 m; primary ore contains an average of 1.4% REO

(*Continued*)

TABLE 2.11 (CONTINUED)
Summary of World Rare-Earth Deposits

Location	Deposit Type, Host Rock, Principal Minerals	RE Minerals	Average Grade Resources, kt [Year]	Year of Discovery (Year of First Production) Annual Production, kt [Year] Status
Nam Xe South (Mau Xe North) Lai Chau	Basic volcanics	Bastnasite, parisite	Proven + probable reserves—940 t REO; possible reserves—3.0 Mt REO; average of 10.6% REO	– Metasomatic + weathered ore; on S side of Nam Xe River in Phong Tho district; REE reserves include 3225 t of Y_2O_3
Quang Ngan Thua Thien-Hu	Placer Coastal	Monazite	3261 t of monazite + xenotime	Part of Thuan An group of deposits; aeolian dunes and beach sand
Vinh Mi (Vinh My) Vietnam Thua Thien-Hu	Placer Coastal	Monazite, xenotime	Possible reserves—2057 t of monazite	Coastal placer; part of Thuan An group of deposits; average deposit thickness 1.6 m
		Uruguay		
Atlantida	Placer Fluvial	Monazite	3.2% monazite	Meager data

Source: Jackson, W.D. and Christiansen, G., International Strategic Minerals Inventory Summary Report—Rare Earth Oxides, U.S. Geological Survey Circular 930-N, U.S. Geological Survey, Map Distribution, Denver, Colorado, 1993; Orris, G.J., and Grauch, R.I., Rare earth element mines, deposits, and occurrences: U.S. Geological Survey Open-File Report 2002–0189, 2002.

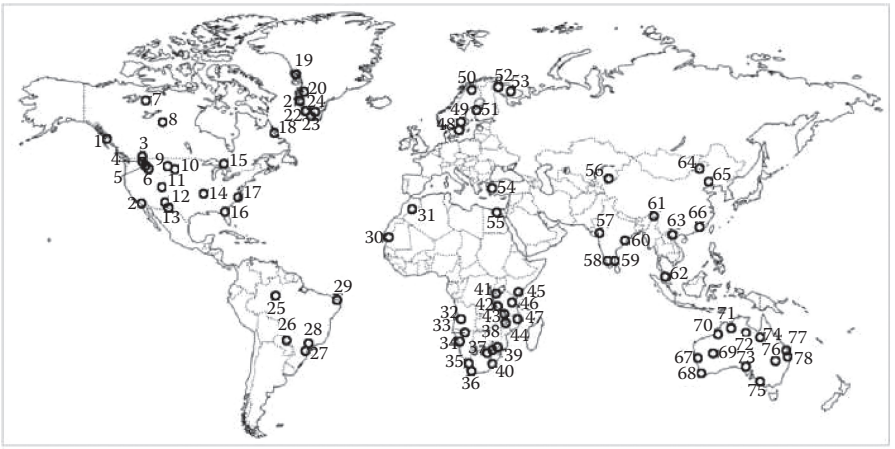


FIGURE 2.2 Locations of the rare-earth deposits in the world. Numbers explained in the adjoining Table 2.12.

and quantity, from which the rare earth can be extracted presently. Resources of rare earths, therefore, include reserves (Bureau of Mines Staff 1975).

A complete listing of definitions of reserves, resources, and related terms used presently is given in Table 2.13 and illustrated in Figure 2.3 (USGS 1980).

Chen (2011), quoting the USGS report of Long et al. (2010), noted that the term *deposit* is just the rare-earth resource, and the term *reserve* is defined as rare-earth resource for industrial production. REE resources are distributed between many mineral deposits, but only a proportion will be economic to develop and mine. By convention, that portion of resources that is economic to mine is classified as a *reserve*. That a rare-earth deposit contains reserves does not mean that it will be developed and mined—it means only that it is economic to do so.

There are more systems and national standards for classifying reserves and resources. They are the Canadian National Instrument 43-101, JORC, and SAMREC codes (JORC, The Australasian Code for Reporting of Exploration Results, Mineral Resources and Ore Reserves [Jorccode 2004]; SAMREC, South African Mineral Resource Committee [Samcode 2009]). The definition of these terms according to the JORC code (JORC 2012) is also given in Table 2.13, and the schematic of the relationship of the various terms is illustrated in Figure 2.4.

United Nations Group of Experts on Definitions and Terminology for Mineral Resources (Jackson and Christiansen 1993) had also put forward an international classification system for mineral resources. The United Nations resource classification is summarized in Figure 2.5. The whole of the *in situ* resources is divided into known deposits, extensions of known deposits, and newly discovered deposits and undiscovered deposits. The known deposits that are of greatest current interest are again divided into economically exploitable deposits (R1E), marginally economic

TABLE 2.12
Location of World Rare-Earth Deposits (Corresponding to Numbers in Figure 2.2)

Number	Place	Type of Deposit
1	Bokan Mountain	Alkali igneous rock-associated
2	Mountain Pass	Carbonatite-associated
3	Rock Canyon Creek, Canada	Hydrothermal other than alkaline settings
4	Snowbird, USA	Hydrothermal other than alkaline settings
5	Lemhi Pass, USA	Hydrothermal other than alkaline settings
6	Deep Sands	Alluvial placers
7	Nechalacho (Thor Lake)	Alkaline igneous rock-associated
8	Hoidas Lake, Canada	Hydrothermal exclusive of alkaline settings
9	Bald Mountain, USA	Paleoplacers
10	Bear Lodge, USA	Carbonatite-associated
11	Iron Hill, USA	Carbonatite-associated
12	Gallinas Mountains, USA	Alkaline igneous rock-associated
13	Pajarito Mountain, USA	Alkaline igneous rock-associated
14	Pea Ridge, USA	Iron–REE deposits
15	Elliot Lake, Canada	Paleoplacers
16	Green Cove Springs, USA	Marine placers
17	Carolina placers, USA	Hydrothermal deposits exclusive for alkaline settings
18	Strange Lake, Canada	Alkaline igneous rock-associated
19	Karrat, Greenland	Alkaline igneous rock-associated
20	Sarfartok, Greenland	Carbonatite-associated
21	Qeqertaasaq, Greenland	Carbonatite-associated
22	Tikiusaaq, Greenland	Carbonatite-associated
23	Kvanefjeld, Greenland	Alkaline igneous rock-associated
24	Motzfjeldt, Greenland	Carbonatite-associated
25	Pitinga, Brazil	Lateritic deposits
26	Chiriguelo, Brazil	Carbonatite-associated
27	Barro do Itapirapua, Brazil	Carbonatite-associated
28	Araxa, Brazil	Lateritic deposits
29	Camaratuba, Brazil	Marine placers
30	Bou Naga, Mauritania	Alkaline igneous rock-associated
31	Tamazeght Complex, Morocco	Alkali igneous rock-associated
32	Longonjo	Carbonatite-associated
33	Etaneno, Namibia	Carbonatite-associated
34	Lofdal	Carbonatite-associated
35	Steenkampskraal, South Africa	Hydrothermal other than alkaline settings
36	Zandkopsdrift, South Africa	Carbonatite-associated
37	Plinesberg Complex, South Africa	Alkali igneous rock-associated
38	Naboomspruit, South Africa	Carbonatite-associated

(*Continued*)

TABLE 2.12 (CONTINUED)
Location of World Rare-Earth Deposits (Corresponding to Numbers in Figure 2.2)

Number	Place	Type of Deposit
39	Palabora, South Africa	Carbonatite-associated
40	Richards Bay, South Africa	Marine placers
41	Karonge, Burundi	Hydrothermal other than alkaline settings
42	Nikombwa Hill	Carbonatite-associated
43	Kangankunde, Malawi	Carbonatite-associated
44	Songwe	Carbonatite-associated
45	Mrima Hill	Carbonatite-associated
46	Wigu Hill	Carbonatite-associated
47	Congolone, Mozambique	Marine placers
48	Norra Karr	Alkaline igneous rock-associated
49	Bastnas	Iron–REE deposits
50	Kiruna	Iron–REE deposits
51	Korsnas	Hydrothermal other than alkaline settings
52	Khibiny Complex	Alkaline igneous rock-associated
53	Lovozero Complex	Alkaline igneous rock-associated
54	Conakli	Alkaline igneous rock-associated
55	Nile Delta and Rosetta	Marine placers
56	Kutessay II	Alkaline igneous rock-associated
57	Amba Dongar	Carbonatite-associated
58	Chavara	Marine placers
59	Manavalakurichi	Marine placers
60	OSCOM, Gopalpur	Marine placers
61	Maoniuping/Dalucao, China	Carbonatite-associated
62	Perak, Malaysia	Alluvial placers
63	Dong Pao, Vietnam	Carbonatite-associated
64	Bayan Obo, China	Carbonatite-associated
65	Weishan, China	Alkaline igneous rock-associated
66	Xunwu/Longnan, China	Ion-adsorption clays
67	Eneabba, Australia	Marine placers
68	Jangardup, Australia	Marine placers
69	Mount Weld, Australia	Lateritic deposits
70	Cummins Range	Carbonatite-associated
71	Brockman, Australia	Alkaline igneous rock-associated
72	Nolans Bore, Australia	Hydrothermal other than alkaline settings
73	Olympic Dam, Australia	Iron–REE deposits
74	Mary Kathleen, Australia	Hydrothermal other than alkaline settings
75	WIM 150, Australia	Marine placers
76	Dubbo Zirconia, Australia	Alkaline igneous rock-associated
77	Fraser Island, Australia	Marine placers
78	North Stradbroke Island, Australia	Marine placers

TABLE 2.13
Classification of Reserves and Resources

Class	Definition
Resource	A concentration of naturally occurring solid, liquid, or gaseous material in or on the earth's crust in such form and amount that economic extraction of a commodity from the concentration is currently or potentially feasible.
Identified resources	Resources whose location, grade, quality, and quantity are known or estimated from specific geologic evidence. *Identified resources* include economic, marginally economic, and subeconomic components. To reflect varying degrees of geologic certainty, these economic divisions can be subdivided into *measured*, *indicated*, and *inferred.*
Demonstrated	A term for the sum of *measured* plus *indicated.*
Measured	Quantity is computed from dimensions revealed in outcrops, trenches, workings, or drill holes; grade and (or) quality are computed from the results of detailed sampling. The sites for inspection, sampling, and measurement are spaced so closely, and the geologic character is so well defined that size, shape, depth, and mineral content of the resource are well established.
Indicated	Quantity and grade and (or) quality are computed from information similar to that used for measured resources, but the sites for inspection, sampling, and measurement are farther apart or are otherwise less adequately spaced. The degree of assurance, although lower than that for measured resources, is high enough to assume continuity between points of observation.
Inferred	Estimates are based on an assumed continuity beyond measured and (or) indicated resources, for which there is geologic evidence. *Inferred resources* may or may not be supported by samples or measurements.
Reserve base	That part of an identified resource that meets specified minimum physical and chemical criteria related to current mining and production practices, including those for grade, quality, thickness, and depth. The *reserve base* is the in-place demonstrated (measured plus indicated) resource from which reserves are estimated. It may encompass those parts of the resources that have a reasonable potential for becoming economically available within planning horizons beyond those that assume proven technology and current economics. The *reserve base* includes those resources that are currently economic (*reserves*), resources that are marginally economic (*marginal reserves*), and some of those that are currently subeconomic (*subeconomic resources*). The term *geologic reserve* has been applied by others generally to the *reserve-base* category, but it also may include the *inferred reserve-base* category; it is not a part of this classification system.
Inferred reserve base	The in-place part of an identified resource from which inferred reserves are estimated. Quantitative estimates are based largely on knowledge of the geologic character of a deposit and for which there may be no samples or measurements. The estimates are based on an assumed continuity beyond the reserve base, for which there is geologic evidence.

(*Continued*)

TABLE 2.13 (CONTINUED)
Classification of Reserves and Resources

Class	Definition
Reserves	That part of the reserve base that could be economically extracted or produced at the time of determination. The term *reserves* need not signify that extraction facilities are in place and operative. *Reserves* include only recoverable materials; thus, terms such as *extractable reserves* and *recoverable reserves* are redundant and are not a part of this classification system.
Marginal reserves	That part of the reserve base that, at the time of determination, borders on being economically producible. Its essential characteristic is economic uncertainty. Included are resources that would be producible, given postulated changes in economic or technologic factors.
Economic	This term implies that profitable extraction or production under defined investment assumptions has been established, analytically demonstrated, or assumed with reasonable certainty.
Subeconomic resources	The part of identified resources that does not meet the economic criteria of reserves and marginal reserves.
Undiscovered resources	Resources, the existence of which are only postulated, comprising deposits that are separate from identified resources. *Undiscovered resources* may be postulated in deposits of such grade and physical location as to render them economic, marginally economic, or subeconomic. To reflect varying degrees of geologic certainty, undiscovered resources may be divided into two parts: hypothetical resources and speculative resources.
Hypothetical resources	Undiscovered resources that are similar to known mineral bodies and that may be reasonably expected to exist in the same producing district or region under analogous geologic conditions. If exploration confirms their existence and reveals enough information about their quality, grade, and quantity, they will be reclassified as identified resources.

Source: USGS, Principles of a resource/reserve classification for minerals, Geological Survey Circular 831, U.S. Geological Survey, Arlington, VA, 1980.

(R1M), and subeconomic (R1S). The R1E deposits generally refer to the deposits known usually as reserves.

The total quantity of rare earths contained in world rare-earth reserves was estimated in 1977 by United States Bureau of Mines (USBM) to be 7.7 million tons REO. Thereafter for a long time, through the 1980s, 47.6 Mt REO was the quoted figure (Clark and Zheng 1991a,b; Hedrick 1988; Sabot and Maestro 1995). In 1990, the figure was revised to 84 million tons. By the time the first edition of this book was ready, in 2003, the figure available was 88.0 Mt REO in reserves and 150 Mt REO if the reserve base is considered (USGS 2003). This value (150 Mt) remained the same till the last reserve base estimate from USGS in 2008. The reserve base estimates of the USGS were discontinued in 2009. The reserve estimates by USGS over the years 2004–2014 are listed in Table 2.14.

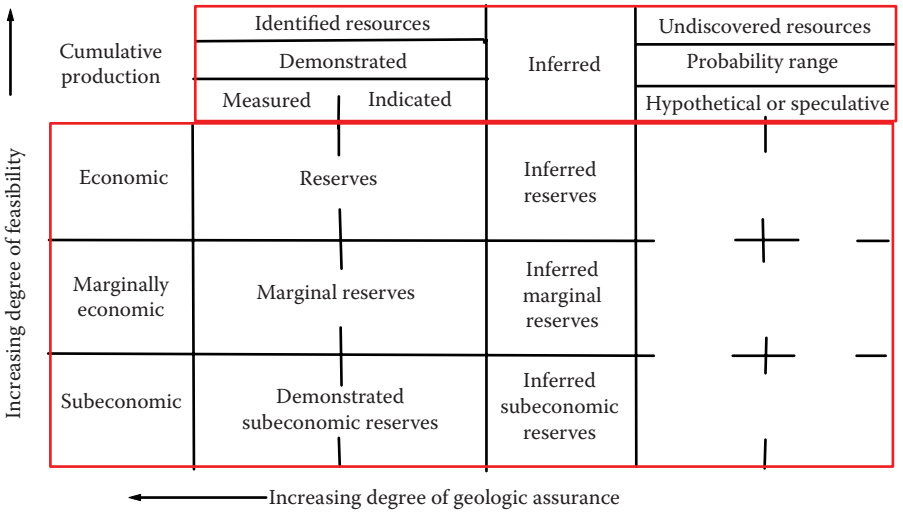


FIGURE 2.3 USGS classification of mineral resources. (From USGS, Principles of a resource/reserve classification for minerals, Geological Survey Circular 831, U.S. Geological Survey, Arlington, VA, 1980.)

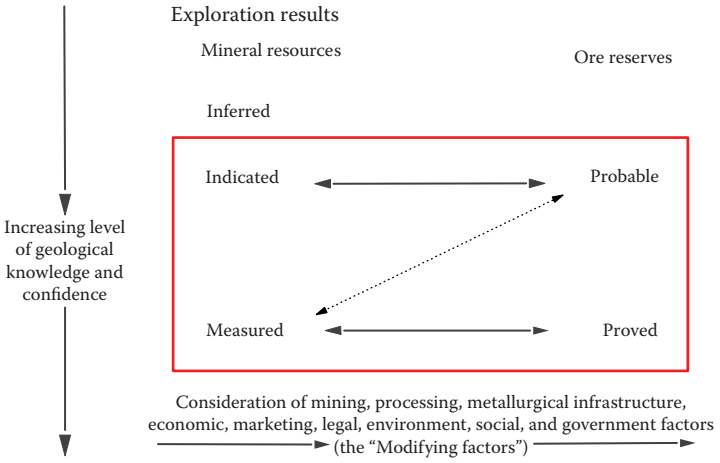


FIGURE 2.4 General relationship between exploration results, mineral resources, and ore reserves. (From JORC, *Australasian Code for Reporting of Exploration Results, Mineral Resources and Ore Reserves*, The JORC Code 2012 edition, AusIMM.)

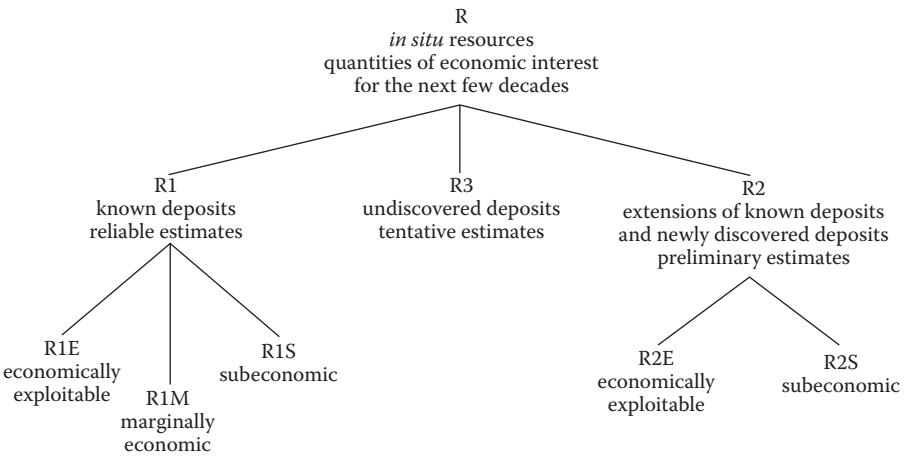


FIGURE 2.5 United Nations resource categories.

Chen (2011) provided estimates of world rare-earth reserves in his review. He emphasized major upward revision in the reserve estimates of Brazil and inclusion of significant estimates for Canada, Greenland, and Vietnam. The information given by Chen (2011) in diagrams is listed in Table 2.14. Significantly, the resource position emphasized by Chen was reflected in the USGS tabulation, three years later, in 2014. It may be noted in Table 2.15 that the values for the reserves of Australia are revised downwards, and Chen (2011) has chosen a significantly lower value for China's reserves but a higher value for Australia as compared to the values of USGS. It was mentioned by USGS that the reserves for Australia and Brazil were based on information from government reports. China supplies much of the rare earth to meet the global rare-earth demand. This supply apparently comes from a reserve base that is only 23% of the known global reserves (Chen 2011). The 23% figure for China's proportion of the world REE reserve base is markedly lower than the reported 50.0% of world REE reserves that China has according to the widely cited USGS Mineral Commodity Surveys (Cordier 2011, 2012; Hedrick 2009, 2010). The real value is likely to be more than that admitted by the Chinese but less than that estimated by USGS. The USGS data do not include a large number of Canadian and Australian deposits that have been delineated as REE resources. The NI 43-101 and JORC reporting requirements are stringent in Canada and Australia, and many of these resources may be classifiable as reserves in other jurisdictions. Under these circumstances, these resources would add to the worldwide total REE reserve base and therefore decrease the Chinese proportion of world reserves (Jordens et al. 2013; Simandl 2012).

Presently available rare-earth reserves data imply sufficient rare-earth availability in a geographically distributed manner. Large deposits that would support sustained production for decades are located in Australia, Vietnam, China, India, Russia (CIS), Greenland, Canada, United States, Brazil, and South Africa. However, the journey of the rare earths from reserves to marketable materials and devices is

TABLE 2.14
Global RE Reserve Estimates (2009–2010)

	Reserves				Deposits (Resources)	
	2009		2010		2010	
Country	Metric Tons REO	% of World Total	Metric Tons REO	% of World Total	Metric Tons REO	% of World Total
USA	13,000,000	13.19	15,504,000	1.06	11,771,600	7.23
Australia	5,400,000	5.48	3,330,600	2.34	13,420,500	8.25
Brazil	48,000	0.05	52,597,000	37.01	52,597,000	32.32
Canada			4,122,500	2.90	4,389,500	2.70
China	36,000,000	36.52	36,000,000	25.33	36,000,000	22.12
CIS	19,000,000	19.27	19,000,000	13.37	19,000,000	11.68
India	3,100,000	3.14	3,100,000	2.18	3,100,000	1.91
Malaysia	30,000	0.03				
Other countries	22,000,000	22.32				
Sri Lanka						
South Africa			1,254,000	0.88	1,254,000	0.77
Greenland			4,890,000	3.44	4,890,000	3.01
Malawi			107,000	0.08	107,000	0.07
Brundi			1000		1000	
Kenya			972,000	0.68	972,000	0.60
Kyrgyzstan			291,000	0.20	291,000	0.18
Turkey			130,500	0.09	130,500	0.08
Vietnam			14,800,000	10.42	14,800,000	9.10
World total	98,578,000	100	153,099,600	99.98	162,724,100	100.02

Source: Chen, Z., *Journal of Rare Earths*, 29(1): 1–6, 2011.

TABLE 2.15
Global RE Reserve Estimates (1996–2014; in Mt REO; USGS Data)

Year	China	Others[a]	CIS	USA	Australia	India	Canada	RSA	Brazil	Malaysia	World Total
1996	43.0	21.0	19.0	13.0	5.2	1.1	–	0.39	0.28	0.03	100.0
1997	43.0	21.0	19.0	13.0	5.2	1.1	0.94	0.39	0.28	0.03	100.0
1998	43.0	21.0	19.0	13.0	5.2	1.1	0.94	0.39	0.28	0.03	100.0
1999	43.0	21.0	19.0	13.0	5.2	1.1	0.94	0.39	0.28	0.03	100.0
2000	43.0	21.0	19.0	13.0	5.2	1.1	0.94	0.39	0.28	0.03	100.0
2001	43.0	21.0	19.0	13.0	5.2	1.1	0.94	0.39	0.28	0.03	100.0
2002	43.0	21.0	19.0	13.0	5.2	1.1	0.94	0.39	0.082	0.03	100.0
2003	27.0	21.0	19.0	13.0	5.2	1.1	0.94	0.39	0.11	0.03	88.0
2004	27.0	21.0	19.0	13.0	5.2	1.1	0.94	–	0.11	0.03	88.0
2005	27.0	22.0	19.0	13.0	5.2	1.1	–	–	–	0.03	88.0
2006	27.0	22.0	19.0	13.0	5.2	1.1	–	–	–	0.03	88.0
2007	27.0	22.0	19.0	13.0	5.2	1.1	–	–	–	0.03	88.0
2008	27.0	22.0	19.0	13.0	5.2	1.1	–	–	0.048	0.03	88.0
2009	27.0	22.0	19.0	13.0	5.2	3.1	–	–	0.048	0.03	88.0
2010	36.0	22.0	19.0	13.0	5.4	3.1	–	–	0.048	0.03	99.0
2011	55.0	22.0	19.0	13.0	1.6	3.1	–	–	0.048	0.03	110.0
2012	55.0	22.0	19.0	13.0	1.6	3.1	–	–	0.048	0.03	110.0
2013	55.0	41.0	–	13.0	1.6	3.1	–	–	0.036	0.03	110.0
2014	55.0	41.0	–	13.0	2.1	3.1	–	–	22.0	0.03	140.0

[a] Others means one or more of the countries: Burundi, Canada, CIS (countries of former Soviet Union), Egypt, Greenland, Indonesia, Kenya, Malawi, Namibia, South Africa, Sri Lanka, Taiwan, Thailand, Turkey, Vietnam, or Zaire unless they are separately listed.

long and particularly protracted in the present regulatory environment. This aspect will be revisited later in Section 2.9. If the main concern was a geographically distributed occurrence of the rare earths, the occurrence is indeed so.

2.6 OCCURRENCE

Rare-earth deposits are found at various locations in the world. The locations are marked on a world map in Figure 2.2. Current information on major deposits, selected from the lists of US Geological Survey (Jackson and Christiansen 1993; Orris and Grauch 2002), is summarized in Table 2.11. Generally those with a certain estimate on the quantity of rare earths available in the resource have been selected. Details and additional information on these and other deposits that became available at a later date are given in the following for various countries.

2.6.1 Argentina

A rare earth–uranium–thorium deposit is in San Luis Province, Argentina. The project, known as "Rodeo de los Molles," is located about 300 km southwest of Cordoba and 200 km northeast of San Luis. Minerals of economic significance include bastnasite, britholite, and allanite with 2.0–2.5% rare-earth content (RIC 1995).

2.6.2 Australia

Australia remains home to some of the world's major potential sources of REEs contained in its alkaline intrusive deposits, heavy mineral sand deposits, and rare-earth lateritic deposits.

Heavy mineral sand placer deposits comprising ilmenite, rutile, zircon, monazite, and, in a few cases, xenotime occur extensively along the Australian coast. There are approximately 15 placer deposits in western Australia, 7 in Queensland, and 5 in New South Wales. The west coast deposits are mainly paleobeach placers, and the principal deposits are located inland and 10–100 m above sea level. The deposits on the east coast have been formed by waves and wind and their combination.

2.6.2.1 Brown's Range

The Brown's range project is located 150 km southeast of Halls Creek in Western Australia. There are four deposits here—Wolverine, Gambit, Gambit west, and Area 5. The first three were discovered only in 2009 and 2010. All these deposits are breccia-hosted hydrothermal systems with xenotime mineralization (Hoatson et al. 2011). The total resource at the Brown's range project has been estimated at 6.48 Mt at 0.74% REO. The contained REO is therefore 48,000 t. The cutoff grade was taken as 0.15% REO. The largest share of this total is accounted by the Wolverine deposit (4.46 Mt of resource with an average REO content of 0.86%). The contained REO in this deposit is 38,270 t REO using a cutoff of 0.15% REO. Brown's range deposit can be mined by the open pit methods. Mining can progress to underground operations (at around 200 m below surface) for two of these deposits. At Wolverine and

Gambit deposits, the heavy rare-earth proportion to total rare earths is between 85% and 90%.

2.6.2.2 Dubbo Zirconia Project (DZP), Toongi

A rare-earth deposit is located at Toongi, which is 20 km south of the large regional town Dubbo in central New South Wales approximately 410 km northwest of Sydney. The multimineral deposit is located on the Toongi alkaline intrusive that contains hafnium, lanthanides, niobium, tantalum, yttrium, and zirconium in the igneous rock trachyte. The Toongi body comprises a very fine-grained mineral assemblage that contains eudialyte, armstrongite, natroniobite, bastnasite, and parasite, and very small amounts of ancylite–(Ce) (Hedrick 2007).

The estimated reserves at the DZP are 92.1 Mt, split between the measured resource of 54.9 Mt, which extends from the surface to 55 m of depth, and the inferred resource of 37.5 Mt, which extends from 55 to 100 m of depth (Gambogi and Cordier 2010). The measured and inferred grades in the trachyte were similar and contained 1.96% zirconium oxide, 0.04% hafnium oxide, 0.14% yttrium oxide, 0.46% niobium oxide, 0.03% tantalum oxide, 0.014% uranium oxide, and 0.75% REO. According to Gambogi (2011), proven and probable reserves of REO, including yttrium oxide, were estimated to contain 316,000 t of REO, based on a 1.5% cutoff grade (combined ZrO_2, Nb_2O_5, and REO).

The Dubbo open pit operation at 200,000 t/year of ore would produce 3000 t/year of zirconia equivalent, 600 t/year of columbium (niobium)–tantalum concentrate, and 1300 t/year of REO (yttria and lanthanide oxides) during a 400 year mine life. Alkane expected about 50% of the DZP's revenue to come from the range of zirconium products, 40–45% from the niobium–tantalum concentrate, and 5% to 10% from the yttrium–rare-earth concentrate (Hedrick 2004, 2006). Another definitive plan is based on a 20 year operation (~650,000 t/year ore) with a potential production of 4170 t/year of REOs. However, production was not expected to begin until 2014.

2.6.2.3 Eneabba

The Eneabba mineral sand deposit on the west coast north of Perth has been the major source of monazite in Australia. Additional mineral sand reserves occur in the adjacent Eneabba West deposit. The mineral sands of Eneabba also contain useful quantities of xenotime (Taylor 1991).

2.6.2.4 Cooljarloo/Jurien Bay

Mineral sand deposits occur at Jurien Bay and Cooljarloo in western Australia just south of Eneabba. Cooljarloo's deposits were estimated as 16 Mt of proven and 42 Mt of probable ore grading 3–5% heavy minerals, including monazite (Hedrick 1985a). Reserves at Jurien Bay were estimated at 25 Mt of proven and 1 Mt of probable ore grading 6–7% heavy minerals, including monazite. At Cooljarloo, the mined sand is composed of about 0.2% monazite, and at Jurien Bay, the sand contains 0.7% monazite. Total reserves were equivalent to 64,000 t REO at Cooljarloo and 100,000 t REO at Jurien Bay (Hedrick 1985a).

2.6.2.5 Cummins Range

Located near the junction of Halls Creek and King Leopald Orogens, the Cummins Range carbonatite is a subvertical zoned stock comprising central core of carbonatite enclosed by carbonated mica-rich pyroxenite passing outwards into a large zone of unaltered pyroxenite. It is deeply weathered and covered with a thin layer of aeolian soil. Explorations with widely spaced shallow drilling have confirmed deposits consisting primarily of apatite and monazite. The deposit is considered similar to Mount Weld, and economically important abundances of Nb, Ta, Zr, and Ti have also been found. Inferred resources are 4.17 Mt at 1.72% REO, 11.0% P_2O_5, 180 ppm U_3O_8, and 41 ppm Th at a cutoff grade of 1% REO.

2.6.2.6 Gilgai Intrusion

The Gilgai Intrusion, one of several *Alaskan*-type mafic–ultramafic bodies, is located 20 km west-southwest of Nyngan in Central New South Wales. Alluvial material of Cenozoic era covers the intrusion for up to 50 m. Explorations carried out in 1999–2001 revealed significant enrichment of scandium in the laterite above the Gilgai Intrusion. The laterite zone is layered, comprising hematitic clay at the surface, followed downwards by limonitic clay, saprolitic clay, weathered bedrock, and then fresh mafic–ultramafic rocks. Scandium is concentrated, with levels reaching 350 ppm, in the hematitic, limonitic, and saprolitic zones. Resources have been estimated to be 12.012 Mt at 261 ppm Sc (Hoatson et al. 2011). The deposit was considered minable via the open pit method, with the capacity of producing 30 t/year of 99.9% scandium oxide (Cordier 2009).

2.6.2.7 Jangardup

Jangardup mineral sand deposit, located 60 km south of Nannup in southwestern Australia, has moderate quantities of xenotime.

2.6.2.8 WIM-150

This deposit was named after Wimmera Industrial Minerals and is a major deposit of heavy mineral sands near Horsham in western Victoria (Taylor 1991). The WIM-150 deposit contains an estimated 32 Mt of heavy minerals in an area of about 40 km^2. This includes 580,000 t of monazite and 170,000 t of xenotime.

2.6.2.9 Murray Basin

About six times the amount of rare earths contained in the WIM-150 deposit occur in the four other deposits of Murray Basin, western Victoria (RIC 1993). The deposit is a commercial source of zircon and titanium minerals in addition to monazite.

2.6.2.10 Nolans Bore

Discovered in 1995, the Nolans Bore REE-U-Th deposit is located in the Reynolds Range of the Arunta Region, 135 km north-northwest of Alice Springs in the Northern Territory. Rare earth-bearing massive fluorapatite (averages 7% TREE) occurs as veins and forms 53–93% of the rock. The apatite crops out sporadically over an area 800 × 1700 m (Hoatson et al. 2011). Measured resources are 5.1 Mt

grading 3.2% REO, 13.5% phosphate, and 0.57% uranium oxide. Indicated resources are 12.3 Mt grading 2.8% REO, 13.4% phosphate, and 0.43% uranium oxide (Cordier and Hedrick 2008).

Annual production would generate four products during a 20 year mine life—20,000 t of REO, 150,000 t of phosphoric acid, 400,000 t of calcium chloride, and 150 t of uranium oxide. Production at the Nolans project was scheduled to be operating at 50% of capacity by 2011, scaling up to 100% of capacity by 2013 (Hedrick 2007).

2.6.2.11 Norraburra RE Deposit

This multimetal resource for Zr, Hf, Nb, Th, and the REE occurs in a 1500 × 800 m zone of weathered granite intrusive, near Temora in Central New South Wales. An estimate made in January 2011 infers the resource at 55 Mt at 1500 g/t Y, Nb, Th, Li, and REO. The REO and zirconia contents in this deposit are 16,000 and 55,000 t, respectively (Hoatson et al. 2011).

2.6.2.12 Olympic Dam

The Olympic Dam deposit is a huge multimetal (copper, uranium, gold, and rare earths) resource (Taylor 1991). The hard-rock ore body contains rare-earth minerals at a typical concentration of 5000 ppm. The minerals found are bastnasite, monazite, and florencite with a very minor amount of xenotime. Significantly, the most abundant of the rare-earth minerals in the deposit, bastnasite, is abnormally enriched in heavy rare earths and the usual europium depletion is absent.

2.6.2.13 Brockman (Hastings) Deposit

The Brockman multielement prospect is located 18 km southeast of Halls Creek in the Halls Creek Orogen of Western Australia. It is potentially a major source of yttrium and heavy rare earths that could be recovered along with other minerals. The area was first explored by radiometric surveys in 1954, and periodical explorations went on till December 2010. It was then reported that Brockman prospect was a JORC compliant resource with over 22 Mt containing 0.10% Y_2O_3, 0.79% ZrO_2, 0.31% Nb_2O_5, and 0.23% Ta_2O_5. Rare earths other than yttrium were not included in the report. Earlier, Taylor (1991) reported 8.97 Mt of resource up to 100 m of depth, grading, in percentage, 1.027 ZrO_2, 0.116 Y_2O_3, 0.437 Nb_2O_5, 0.026 Ta_2O_5, 0.038 HfO_2, 0.01 Ga, 12.1 Al_2O_3, and 0.105 REO. Additional 13.6 Mt resource of similar grades up to a depth of 250 m was also inferred. A factor responsible for the apparent delay in the exploitation of this resource is the fine-grained (<20 μm) hydrous nature of the ore minerals that would need specialized processing operations for value recovery (Hoatson et al. 2011).

2.6.2.14 Mary Kathleen

In Queensland, Mary Kathleen is the site of a major hard-rock deposit of uranium and rare earths. The ore body consists of steeply dipping uraniferous lenses in garnet skarns. The rare earths are hosted by the main uranium bearing components of the ore body—allanite (orthite) and stillwellite (lanthanum borosilicate). Allanite comprises about 35% of the ore as outcrop. The REEs are broadly distributed with the uranium mineralization. Approximately 85% of the REO is accounted by cerium

and lanthanum oxides. Nearly 9.5 Mt of the ore with 4.5% REO content has been mined from this deposit, processed, and retained in the tailings dam.

2.6.2.15 Mount Weld

The Mount Weld deposit is located 35 km south-southeast of Laverton in the Yilgam Craton of Western Australia. Exploration drilling of the Mount Weld resource began in the late 1960s, and presence of carbonatite was confirmed in 1967. The Mount Weld rare-earth deposit is one of the richest major rare-earth resources in the world (Taylor 1991). The Mount Weld complex comprises world-class REO and niobium/tantalum deposits developed within the Mount Weld carbonatite—an intrusive pipe approximately 3 km in diameter. The carbonatite is essentially coarse-grained dolomite and ankerite, with biotite and apatite also present. The main deposits (Nb, Ta, and REE) are hosted within the well-developed soil/regolith horizon that blankets the entire carbonatite and form shallow lenses and sheets within 20–100 m of the surface. The most important REO deposit, the Central Lanthanide Deposit (CLD), is located at the center of the carbonatite with the Nb/Ta and other deposits generally located towards the outer fringes. Discovered in 1988, the CLD represents a spectacular enrichment zone of REEs. The regolith above the central part of the carbonatite contains the most important REE concentrations ranging from 4% to 13.8%. At depths of 45–90 m below the surface, a 6- to 30-m-thick residual layer of apatite occurs near the base of the regolith with magnetite and vermiculite. Niobium- and tantalum-bearing minerals are concentrated in the apatite–magnetite residual zone.

The deposit is believed to be the largest and highest grade of its type in the world. Measured reserves at Mount Weld are 6.2 Mt grading 12.4% REO for a total content of 769,000 t of REO. Inferred resources are an additional 1.5 Mt grading 9.9% REO. The total resource at Mount Weld was 7.7 Mt grading 11.9% REO, equivalent to 917,000 t REO (Hedrick 2006).

The principal rare-earth mineral in the deposit is supergene monazite, and in some zones, the mineralization is predominantly churchite—hydrated yttrium phosphate mineral. The europium content of monazite is unusually high. Most importantly, the Mount Weld deposit is low in the radioactive element thorium (0.05%) (Hedrick 2002). Besides, the ore zones have low levels in other deleterious elements such as fluorine and calcium, which is a positive for both metallurgical and environmental reasons.

A separate group of polymetallic ore bodies in the north and northeast region of the Mount Weld carbonatite, designated the Crown Polymetallic Project, contains additional mineral resources, including rare earths. These include resources of 37.7 Mt of ore grading 0.024% tantalum oxide, 1.07% niobium oxide, 1.16% lanthanide oxides, 0.30% zirconium oxide, 42.8% iron oxide, 8.0% phosphate, 0.09% yttrium oxide, 11.3% aluminum oxide, and 4.0% titanium oxide (Hedrick 2007; Lynas 2008). In other words, the Crown deposit contains resources of 1.5 Mt of titanium oxide, 470,000 t of REO, 400,000 t of niobium oxide, 110,000 t of zirconium oxide, and 9070 t of tantalum oxide. The Mount Weld Crown Polymetallic Project is the second-ranked niobium deposit in the world behind the niobium deposit at Araxa, Brazil, and has an average grade of 1.07% niobium oxide (Hedrick 2006; Lynas 2008).

2.6.2.16 John Galt

This is a hard-rock deposit containing high-grade veins of xenotime in lithic quartz sandstone and is located about 120 km northeast of Halls Creek in the East Kimberley, Western Australia. The rare-earth distribution in the ore is generally similar to xenotime, but the yttrium content as a proportion of total rare earths is higher than normal (Taylor 1991).

2.6.2.17 Radium Hill

Rare earths occur associated with uranium minerals in the uraniferous titanium-rich minerals at Radium Hill. Lodes in high-grade metamorphic rocks at Radium Hill contain davidite. Incidentally, davidite–(La) (La,Ce,Ca) (Y,U)$(Ti,Fe^{3+})_{20}O_{38}$ was discovered at Radium Hill mine, South Australia in 1906. Davidite concentrates from the uranium tailings of the Radium Hill uranium mine contain significant quantities of scandium and other rare earths (Hoatson et al. 2011).

2.6.2.18 Syerston

The Syerston nickel–cobalt laterite near Fifield contains scandium in concentrations ranging from 20 to 370 g/t. Resources here are estimated to contain 76.8 Mt at 0.73% Ni and 0.13% Co with significant platinum group element credits.

2.6.2.19 Thuddungra

Mineralized laterites enriched in Ni, Co, and scandium formed from the weathering of underlying serpentinite occur at Thuddungra located 25 km northwest of Young, New South Wales. Resource estimates of this deposit indicate 168 Mt at 0.72% Ni, 0.07% Co, and ~40 g/t scandium (Hoatson et al. 2011).

2.6.2.20 Yangibana

The deposit is located 280 km northeast of Carnarvon in the Gascoyne Complex, Western Australia. In this hard-rock deposit, the REEs, in coarse-grained monazite, occur in a tightly folded iron stone dyke sequence that crop out over an area of 500 km^2. The rare-earth mineralization occurs over a distance of approximately 7 km with a width of several hundred meters. The estimated size of the resource is 3.5 Mt with an average grade of 1.7% REO (Taylor 1991). The monazite contains up to 20% Nd_2O_3 and 1600 ppm Eu_2O_3 (Hoatson et al. 2011).

2.6.3 Bangladesh

Heavy minerals including monazite occur in the Cox's Bazaar coastal area of Bangladesh. The beach sand deposits, located 100 km southeast of Chittagong along the coast and nearby islands, contain resources estimated at 5 Mt of heavy minerals (Hedrick 1985a). The monazite content of this deposit is low, only 0.04%. This is true of the majority of the total 16 mineral sand deposits in Bangladesh listed by Orris and Grauch (2002). A total of 17.6 Mt of heavy minerals in these 16 locations contains 19,000 t of monazite. Apart from the five deposits listed in Table 2.11, smaller deposits of heavy minerals occur in 11 other locations in the country. Total heavy mineral and monazite contents in the listed deposits are 11.9 Mt and 16,000 t,

respectively. The remaining 11 deposits account for only 5.7 Mt heavy minerals and 3000 t monazite. No rare-earth production has been reported from Bangladesh.

2.6.4 Brazil

The rare-earth reserves of Brazil are contained in various types of deposits—marine placers, fluvial or stream placers, alkaline intrusives, carbonatites, and lateritic ores (Hedrick 2004). The total rare earths contained in these deposits have been variously estimated from time to time (from 36,000 to 110,000 t REO). A major upward revision in the rare-earth resources of Brazil came about in the last few years. USGS (Gambogi 2013) revised figures for Brazilian rare-earth reserves to 22,000,000 t REO, based on data provided by the Departamento Nacional de Produção Mineral.

There are numerous beach sand deposits extending from the northern border of the state of Rio de Janeiro over the state of Espirito Santo to the state of Bahia, on the Atlantic coast. Monazite deposits also occur in the state of Parana. Jackson and Christiansen (1993) listed 14 monazite deposits, one bastnasite deposit, and one deposit of other rare-earth minerals in Brazil. The crude mineral sand of Brazil contains around 10% of heavy minerals of which between 10% and 15% is monazite. The monazite contains about 64% of the REOs, 5.5–6% of thorium oxide, and 0.15–0.2% of uranium oxide. The relative concentration of rare earths in monazite is given in Table 2.5. The rare-earth deposits at Sao Goncalo de Sapucai and Tapira are of particular interest (Jackson and Christiansen 1993). The Sao Goncalo de Sapucai deposit is the first inland placer to be dredged in Brazil. It is located on the Sapucai River in Minas Gerais.

At Tapira, which is an existing phosphate mine based on apatite, an anatase-bearing overburden currently stockpiled contains recoverable titanium and rare earths. A hard-rock deposit at Pocos de Caldas in Minas Gerais is a resource containing 1.5 Mt of bastnasite. The average rare-earth content of bastnasite in the deposit is 3.3% REO.

Hedrick (2004) indicated, Brazil's rare-earth reserves as 109,000 t contained in various types of deposits, including both placer and hard-rock types. Reserves of monazite contained in marine alluvial deposits were 42,000 t and, in stream placers, 40,000 t (Hedrick 2000). The hard-rock reserves were only 27,000 t REO. The reserves of marine origin were distributed in deposits primarily in the states of Rio de Janeiro (26,730 t), Bahia (10,186 t), and Espírito Santo (4136 t). The main placer reserves were in the states of Minas Gerais (24,396 t), Espírito Santo (11,372 t), and Bahia (3481 t). There was a downward revision of resource figures of Brazil to 44,000 t in the USGS Minerals Year Book 2005, and the figures given for deposits in the individual states were as follows: Minas Gerais (11,730 t), Bahia (5949 t), Espírito Santo (2527 t), and Rio de Janeiro (2454 t) (Hedrick 2005).

Henry Lazenby, in a dispatch to *Mining Weekly*, 20th June 2012 issue, mentioned reports of discovery of abundant rare-earth resources in Brazil. MBAC Fertilizer, a Brazil- and Latin America-focused phosphate and fertilizer producer, announced that it had established a combined measured and indicated mineral resource of 6.34 million tons, grading 5.01% TREOs for the Araxá project in Brazil. Using a cutoff grade of 2%, the National Instrument 43-101-compliant combined resource

comprises 8.4% phosphorus pentoxide (P_2O_5) and 1.02% niobium pentoxide (Nb_2O_5). The inferred mineral resource was estimated at 21.94 million tons at 3.99% TREOs, 7.86% P_2O_5, and 0.64% Nb_2O_5. The company noted that the Araxá deposit is a significant resource base of rare-earth oxides, with a high grade when compared with other deposits globally.

The Brazilian mining company World Mineral Resources reported the discovery of a large reserve of neodymium in the western state of Bahia, Brazil. The deposit holds about 28 million tons of neodymium, second only to China's Baotu. The ore grade (concentration) is 12.75% (DeGuire 2012).

2.6.5 Canada

In terms of rare-earth resources, Canada is one of the majors in the world. Canada is unique in that its rich rare-earth reserves are not constituted by placer monazite or a large hard-rock deposit with bastnasite as the principal mineral. The *other minerals* constitute the large rare-earth deposits of Canada.

Jackson and Christiansen (1993) mentioned five rare-earth deposits in Canada, all of which are hard-rock deposits. Three of these deposits contain uraninite, brannerite, and monazite, while the remaining two deposits contain gadolinite, zircon, monazite, allanite, fluorite, and pyrochlore or columbite and xenotime. Rare earths occur with uranium in the uranium deposit at Elliot Lake, Ontario (Drew et al. 1991). An yttrium–beryllium–zirconium deposit at Strange Lake, northeast of Schefferville on the Quebec–Labrador border, contains huge quantities of rare earths in addition to beryllium, pyrochlore, and fluorite (Argall 1980). An estimate of the reserve at Strange Lake was 25 Mt with 0.38% yttrium. Quest Rare Minerals Ltd. updated its resource estimate on its Strange Lake B-zone deposit. According to its NI 43-101 report, at a cutoff grade of 0.579% REO, the indicated resource estimate was 140.3 Mt grading 0.93% REO (Gambogi 2011).

Large deposits of rare earth-bearing pyrochlore occur at St. Honoré and at Oka in Quebec (Noblitt 1965). The rare-earth content of Oka pyrochlore averages almost 10% REO and ranges from 2.5% to 11.8% REO. Cerium, lanthanum, neodymium, and yttrium predominate in this pyrochlore, which also has 0.02–1.51% ThO_2 and 0.03–0.72% U_3O_8.

2.6.5.1 Denison Mine

The paleoplacer uranium-bearing quartz pebble conglomerate ore at the Denison mine, Elliot Lake district of Ontario, Canada, is composed of quartz pebbles cemented by a matrix comprising fine-grained quartz, feldspar, and sericite, amounts of pyrite (5–25%), and a wide variety of other heavy minerals (Derry 1960). Uranium, thorium, yttrium, and REE-bearing minerals occur as both primary (detrital) phases and secondary alteration phases within the cement matrix, with grain sizes in the range of 1–600 μm (Robertson and Steenland 1960; Burton and Fralick 2003).

2.6.5.2 Nechalacho/Thor Lake Mine Site, Northwest Territories

The Thor Lake REE–zirconium–niobium–tantalum–beryllium deposit is located on the north shore of Great Slave Lake and about 100 km southeast of Yellowknife in

the Northwest Territories. The deposit was discovered in the early 1970s and is the third largest REE resource in North America. The multielement mineral deposit occurs in a rare-metal peralkaline igneous intrusion at Thor Lake. The genesis of the deposit has been described to reflect both magmatic segregation and hydrothermal metasomatic overprinting. LREE mineralization is principally in allanite, monazite, bastnasite, and synchysite. HREE and tantalum are primarily found in fergusonite and zircon (Cox et al. 2010, quoted in Krahulec 2011).

The composition of the Nechalacho deposit can be seen in Table 2.6. This deposit has 88.5 Mt of inferred resources at a grade of 1.53% TREO (Cox et al. 2011). The most important RE mineral in this deposit is zircon as it has been reported to host over 65% of all REEs in the deposit. The major gangue minerals are quartz, K-feldspar, plagioclase, biotite, and iron oxides. Avalon had completed a NI 43-101 resource update on the Nechalacho deposit and announced the indicated resource as 359,000 t of REO (Gambogi and Cordier 2010).

2.6.5.3 Yukon

A major new source of rare earths has been discovered in the southern Yukon Territory, Canada. Over 1,500,000 t of ore is contained in a wide fluorite-bearing vein, which has a mineral assemblage of monazite and xenotime. The following composition has been reported for a representative rock outcrop of the deposit: 0.15% yttrium oxide, 0.62% niobium oxide, 1.10% zircon, 0.02% hafnium oxide, and 1.37% lanthanides consisting mostly cerium, lanthanum, and neodymium oxides.

2.6.5.4 Hoidas Lake

The most recently discovered REE deposit in North America is the Hoidas Lake vein deposit (Hedrick 2006) in northern Saskatchewan, a small but incompletely evaluated resource. Hoidas Lake is a remote northern Canadian lake, which lies approximately 50 km north of Uranium City, Saskatchewan. It is the site of Canada's most advanced REE mining project. This iron oxide–copper–gold type deposit contains rare earths primarily in apatite and allanite, and lesser amounts in bastnasite and chevkinite. Hoidas Lake deposits contain significant amounts of heavy REEs, including dysprosium. The mineralization is presumably hydrothermal, from an alkali or carbonatitic source at depth. Great Western Minerals Group reported a NI 43-101-compliant resource estimate for Hoidas Lake: 2.56 Mt reserves with 963,800 t in the measured category and 1.60 Mt in the indicated category at an average grade of 2.4% REO. Ongoing work at Hoidas Lake has delineated an extensive vein system that extends for at least 1 km along strike, but the limits of the system have not been established along strike or along dip. The zone's total extension remains unknown. The resource zone averages 75 m in width, comprising individual veins ranging from 1 to 11 m in thickness, averaging about 3 m each. Veins are continuous to 30 m depth and follow an anastomosing geometry (Halpin 2010).

2.6.5.5 Kipawa

A heavy rare earth–yttrium–zirconium deposit located in the Kipawa Alkaline Complex in Temiscamingue, Quebec was explored in 2009 by Matamec Explorations Inc. The deposit occurs across most of the Kipawa Alkaline complex, hosted in a

peralkaline syenite and granite about 200 m thick. The mineralogy is similar to certain other major deposits such as the Lovozero and Khibiny loparite massifs of Russia, the Ilimaussaq intrusion located in east Greenland, and the Parajito Mountain deposit of New Mexico. The deposit contains three main minerals (in decreasing order of rare-earth abundance): eudialyte, britholite, and zircon. In 1991, Unocal estimated the resources to be 1.26 Mt at grades of 0.15% yttrium oxide in the west zone, and 1.01 Mt at a grade of 0.14% Y_2O_3 in the east zone.

2.6.6 China

China is home to the largest rare-earth deposit in the world. The sum total of the rare earths contained in the country's deposits is unparalleled in quality and quantity. The actual quantity of REO contained in China's deposits remains a matter of continuous revision towards either side of the 48 Mt REO mark. Jackson and Christiansen (1993) noted that China probably has more rare-earth deposits than what has been reported. The data from China's Society of Rare Earths presented by Ministry of Environmental Protection indicate that China has 52 Mt of proven industrial reserves (Schuler et al. 2011). The details are in Table 2.16. It is not clear if the term *industrial reserves* in China's reporting is the same as *reserves* of USGS. In a later publication, Chen (2011) used the term *reserve* to denote rare-earth resources for industrial production. Besides, post-2010, USGS reported China's rare-earth reserves as 55 Mt. However, Shuler et al. (2011) did consider *reserves* of USGS and *industrial reserves* of China to be different. In 2010, an additional large rare-earth deposit in Central China's Hubei Province at the foot of Mountain Laoyin in Shiyan City was announced by China's Ministry of Commerce (Schuler et al. 2011). The grade and quantity of rare earths contained in this deposit have not been made public.

There are four main belts of rare-earth mineralization in China (Clark and Zheng 1991): (1) Inner Mongolia belt; (2) Fuji, Jiangxi–Guangdong, Guangxi–Hunan belt; (3) Hubei–Sichuan belt; and (4) Southeast China beach placer belt. Each of these belts has a unique type of rare-earth mineral occurrence. The Inner Mongolia belt contains the Bayan Obo rare earth–iron mine, which, with over 350 Mt of reserves, is the world's largest rare-earth mine. The principal minerals are bastnasite and monazite in a dolomitic iron formation. The Fuji, Jiangxi–Guangdong, Guangxi–Hunan belt occurs along the borders of the provinces mentioned and contains the relatively recently discovered and currently exploited ion-adsorption deposits. The deposits are lateritic zones containing bastnasite, synchysite, and allanite. The ore occurs in numerous small deposits. The Hubei–Sichuan belt occurs along the borders of these two provinces and consists of bastnasite and parisite occurring in barite and calcite veins associated with alkaline and carbonatite rocks. In the southeast China beach placer belt, beach placer deposits containing monazite and xenotime occur along the coastal areas of west Guangdong Province and Haian Island.

2.6.6.1 Bayan Obo

The Bayan Obo iron–rare earth–niobium ore bodies, discovered in 1927, are located 135 km northwest of Baotou in the Nei Monggol autonomous region of northern China. The Bayan Obo mine is China's largest iron mine with iron ore reserves of

TABLE 2.16
Distribution of REE Reserves in Tons REO

Provinces and Regions	Mineral	REE	Grades in % REO	Industrial Reserves	Measured Reserves	Inferred Reserves
Bayan Obo, Inner Mongolia	Bastnasite and monazite	Light REE in iron–Nb–LREE deposit	6	43.5 million	106 million	>135 million
Shandong	Bastnasite	La, Ce, Pr, Nd with high grade	7–10	4 million	12.7 million	>13 million
Sichuan	Bastnasite	Light REE with high grade	6–8	1.5 million	2.4 million	>5 million
Seven Southern Provinces (Jiangxi, Guangdong, Fujiang, Guangxi, Hunan, Yunnan, and Zhejiang)	Ion-adsorption deposit	Middle and heavy REE	0.1–0.3	1.5 million	8.4 million	>50 million
Others	–	–	–	1.5 million	2.2 million	>3.7 million
Total				52 million	131.7 million	>206 million

Source: Schuler, D. et al., *Study on Rare Earths and Their Recycling*, Oeko-Institut e.V., Darmstadt, Germany, 2011.

more than 1.5 billion t at 35% Fe. The rare-earth reserves of Bayan Obo exceed 48 Mt REO (800 Mt of ore at 6% REO). Niobium reserves have been estimated at 1 Mt of niobium. Kanazawa and Kamitoni (2006) have also mentioned of recent statistics that place the REO holding at 85 Mt. The ore has an extremely high LREE/HREE ratio (Chao et al. 1997; Smith and Henderson 2000). However, Chen (2011) arrived at a figure of 36 Mt (as of 2010) for the rare-earth reserve at Bayan Obo taking into account the original reserve value of 43 Mt and the quantity already mined so far during the past 30 years of production.

The genesis of the Bayan Obo deposit has been explained in many ways (Kanazawa and Miyawaki 1991), as a marine sedimentary–diagenetic deposit, as a sedimentary–metamorphic–hydrothermal deposit, as a marine facies volcanosedimentary deposit, and as marine facies volcanosedimentary carbonatite. It has also been interpreted (Drew et al. 1991) that the Bayan Obo iron–rare earth–niobium ore bodies were formed by hydrothermal replacement of Middle Proterozoic dolomite in an intercontinental rift setting. The original iron ore (hematite) bodies were formed syngenetically before REE–Nb mineralization. The hydrothermal fluid with an alkaline–carbonatite chemistry was derived from the upper mantle and printed the REE–Nb mineralization over the original iron bodies.

Clark and Zheng (1991a,b) have described the Bayan Obo deposit as occurring in a severely folded and faulted sequence of Middle Proterozoic slates, quartzites, dolomites, and limestones intruded by Hercynian granites and weakly metamorphosed. The main mineralization zones lie south of the Kuang Gow fault and occur primarily in what is known as the H8 dolomite.

The H8 dolomite occurs within a zone that extends 18 km in the east–west direction and is 2 km in width. The majority of the commercial deposits occur here. The H8 dolomite occurs throughout the zone and is more than 1000 m thick. Within the H8 dolomite, there are three main ore zones: the main ore body, the east ore body, and the west ore body. The main ore body and the east ore body have reserves of 20 and 15 Mt of REO, respectively. There are 16 medium ore bodies in the west mine.

The main ore body consists of tubular and/or lenticular bodies of REO bearing magnetite and hematite iron ores. A high but variable amount of fluorite is associated with both the ore and the surrounding dolomitic host rock throughout the Bayan Obo deposits.

At Bayan Obo, the REO-bearing iron ore as well as the host H8 dolomitic rocks are the sources of rare earths. The main ore body has an average REO content of 6.19%, the east ore body 5.17%, and the west ore body approximately 1% (Argall 1980). Dolomitic-type ores in the main and east ore bodies also contain a considerable amount of rare earths (2–4% REO). The primary rare earth-bearing minerals in the Bayan Obo ore bodies are bastnasite and monazite. These two together constitute approximately 80% of the REO occurring in the deposit. A total of 29 individual rare-earth minerals have been reported to be intergrown in the Bayan Obo deposit. Among these, 13 are stated to be new minerals (Clark and Zheng 1991a).

The rare earths in the ore at Bayan Obo occur as individual minerals, and less than 10% is dispersed isomorphically in other minerals. In the ore bodies (Clark and

Zheng 1991a), bastnasite and monazite are closely associated. Usually the quantity of bastnasite is 20–100% more than the quantity of monazite in the ore.

Monazite in the ores of Bayan Obo contains an average of only 0.26% of ThO_2. The REO and P_2O_5 together account for 98% of the monazite composition. The low thoria content and the high REO content make this a highly desirable mineral for rare-earth production. The thoria content of bastnasite varies in the range 0.02–0.28%, making this also a favorable mineral for rare-earth production. Fluorine occurrence is widespread in the mine, but more than 98% of the fluorine in the deposits occurs primarily as fluorite and as a minor component in bastnasite.

2.6.6.2 Ion-Adsorption Ore

The ion-adsorption ore deposits were first discovered in 1970 in Ganzhou in southern Jiangxi Province, which to date remains the principal region for ion adsorption–type deposits. Additional ion-adsorption deposits have been discovered in the provinces of Guangdong, Fujian, Zhejiang, Hunan, Guangxi, and Yunnan. The proportion of the total ion-adsorption deposits of China that occur in each of these provinces is given in Table 2.17.

The ion-adsorption deposits form as a result of *in situ* weathering of REO-rich host rocks, most commonly granitic or volcanic rocks. For their formation, therefore, there must be sufficient quantity of rare earth-bearing host rock occurring within the zone of weathering, and the weathering or lateritic process must be balanced so that prolonged weathering is possible but with limited erosion. The rare-earth cations from the host rocks are mobilized onto the aqueous phase and migrate downwards. Simultaneously with the weathering, various aluminosilicate minerals, such as kaolinite clays, form, and these in turn adsorb the RE^{3+} cations. The minerals are therefore called weathering crust elution deposited rare earths (Yang et al. 2013). Such weathering requires a mild, rainy, humid, and tectonically stable environment over a long period of time. All these conditions are met in southern China, and hence, a large number of ion adsorption–type REO deposits occur there.

The deposits are generally found in small mountains with a humus topsoil layer of 0.3–1 m, a full regolith layer of 5–30 m (the main ore body containing 0.03–0.15%

TABLE 2.17
Distribution of Ion-Adsorption Deposits in South China

Province	Jiangxi	Guangdong	Fujian	Guangxi	Hunan	Yunnan and Zhejiang	Total
% of ion-adsorption deposits occurring therein	36	33	15	10	4	2	100

Source: Schuler, D. et al., *Study on Rare Earths and Their Recycling*, Oeko-Institut e.V., Darmstadt, Germany, 2011.

REE), a semi-regolith layer of 2–3 m, and a bedrock layer. Unlike other rare-earth minerals that are in a solid-state mineral phase and tend to be associated with thorium and uranium, ion-adsorption rare-earth minerals occur in a trivalent cationic state, which is simply adsorbed onto clays. The ion-adsorption minerals are associated with very little, if at all, of radioactive elements. The ion adsorption-type rare-earth deposits account for only about 3% of China's total rare-earth reserves.

Even though the reserve estimate of rare earths in ion adsorption-type deposits in China is placed at 1 Mt REO, Clark and Zheng (1991a,b) state that it is likely to be several million metric tons REO. Over 100 individual mineralized occurrences have been identified in Jiangxi Province alone, and geologic studies have shown granitic outcrops, which are potential sources of ion-adsorption deposits, occupy very extensive areas in southern Jiangxi, western Fujian, and Guangdong provinces. The rare-earth contents of ion adsorption-type ores in several major deposits of southern Jiangxi and western Fujian provinces are given in Table 2.5. These deposits are special in that they are characterized by low cerium and high neodymium, samarium, europium, gadolinium, and terbium or high yttrium contents. So, depending on the REE required, the deposits may be selectively mined. The grades of ion adsorption-type deposits are the lowest (0.05–0.2% REO) among the various rare-earth deposits in China. This, however, is offset by the easier mining and beneficiation of these deposits apart from absence of any radioactivity baggage. The large environmental cost of mining ion-adsorption ore and relatively rapid depletion of this unique resource (the ratio of Chinese ion-absorbed clay reserves to the amount of this material extracted each year has reportedly fallen from 50:1 to 15:1 in the last 20 years) has been a major factor that forced Chinese authorities to author a quota system to limit rare-earth exports (Jordens et al. 2013).

2.6.6.3 Placers

Placer deposits containing monazite and xenotime occur at many locations in China (Clark and Zheng 1991a). The principal placer deposits are located along the coastal areas of west Guangdong and Hainan Island. The Nanshanhai deposit of Guangdong extends from the east to the west for about 9 km. It is 1.4 km wide and has an average thickness of 3.24 m. In addition to monazite (44,000 t) and xenotime (8200 t), zircon and ilmenite occur in the deposit. Reserves of monazite, equal in extent to that mentioned above, occur in fluvial and lacustrine placer deposits found widespread in Hunan, Hubei, Sichuan, and Jiangxi provinces. The average grade of placer deposits in China is 0.5–1.0% REO.

2.6.6.4 Other Deposits

Rare earth-bearing carbonatite deposits associated with alkaline rocks have been found in Taohualashan, Northern Nei Monggol, Zhushan, northwestern Hubei, Weishan, southern Shandong, and Xichang, Sichuan (Clark and Zheng 1991a). The main producing mine among these is the Weishan mine in Shandong Province. The principal ore mineral in this mine is bastnasite.

A massive alkaline igneous-type rare-earth deposit occurs in Mianning county, southwestern Sichuan. The ore body consists of mainly bastnasite with small amounts

of parisite, chernovite, and xenotime. The metals lead, molybdenum, and bismuth occur in association with the rare-earth minerals. This deposit is considered attractive because it is easy to beneficiate and is low in thorium content.

Apatites enriched in rare earths occur over the western part of China. The levels of REO are, however, too low (<0.1% REO) for commercial recovery. Phosphorite is also relatively abundant in China where the Zhijin phosphorite deposit in Guizhou province has reserves of more than 1.6 billion tons containing more than 1.4 million tons REO. Another deposit is in Fanshan (Wang et al. 2010).

2.6.7 Egypt

Fluorapatite is the principal phosphate mineral in the New Valley ore (65–80%) at Abu Tartur, situated in the Western Desert 50 km to the west of El-kharga town and 275 km from Assuite, Egypt. The reserve is estimated at 987.6 million tons with an average P_2O_5 of 25–30% and contains several minor constituents including rare earths (0.20% REO). Other constituents are dolomite 7.5–9.3%, montmorillonite 6.1–7.6%, pyrite 3.1–6.2%, gypsum 2.3–4.4%, and quartz 1.2–3.4%. Phosphate rocks have long been considered as potential source of uranium and lanthanides. Typically, the quantity of phosphates processed overshadows the fact that their uranium or rare-earth concentrations are usually very small. Studies have been conducted for a possible rare-earth recovery route for the Abu Tatur phosphates (Kandil et al. 2010).

2.6.8 Germany

Schuler et al. (2011) summarized the limited information available on European rare-earth deposits. According to The British Geological Survey (Walters et al. 2010), there has been no systematic, comprehensive evaluation of REE resources in Britain. Small rare-earth occurrences are known but have not demonstrated economic potential. The German Federal Institute for Geosciences and Natural Resources reports on a German deposit in Saxony with probable resources of about 40,000 t REO with an average grade of 0.5%. Heavy mineral sand deposits, similar to those in the east coast of Australia, occur at Cuxhaven in the North Sea Coast, Germany. Reserves have been estimated at 10 Mt of heavy minerals, including ilmenite, rutile, zircon, and possibly monazite (Hedrick 1985a). A potential rare-earth output of a maximum of 1400 t/year as a by-product of iron mining in the north of Sweden has also been indicated. The compilation of Orris and Grauch (2002) mentions reserves in Norway and Turkey. The largest and most important rare-earth resource in EU is the newly developed Kvanefjeld deposit in Greenland.

2.6.9 Greenland

2.6.9.1 Kvanefjeld

A major rare-earth deposit occurs at Kvanefjeld in Greenland. First discovered in the 1950s and studied extensively in the later years, the vast multielement resource

containing uranium, zinc, and the rare earths occurs in the Ilimaussaq intrusive complex on the southwest coast of Greenland (Greenland minerals 2011). The complex covers an area of 8 × 17 km. Kvanefjeld is located at the northwest corner. In the complex, a rock layer called lujavrite underlies the broad plateau. Lujavrite hosts the multielement ore. Rare earths, uranium, and zinc are strongly enriched in the uppermost sections of lujavrite, which is considered to be continuous at depth between outcrops at Kvanefjeld and at zone 2 (6 km from Kvanefjeld). Mineralized lujavrite sections are mostly preserved in the northern half of the Ilimaussaq complex, and apart from Kvanefjeld and zone 2, the ore deposits in locations known as zone 3 and Sorensen are also considered important resources.

Kvanefjeld is considered to be one of the largest multielement deposits of its kind in the world. It is also the world's second largest deposit of rare earths and the sixth largest uranium deposit. According to a pre-feasibility study estimate, the Kvanefjeld mine can produce 43,700 t of REO and 3900 t of uranium every year during a 23 year life span. The deposit is conducive to open cut mining methods.

According to the resource estimate made in 2011, Kvanefjeld resources amount to 619 Mt of ore containing an average of 10,585 ppm REO. The metal inventory comprises 6.6 million tons of REO (including 0.25 Mt heavy REO, 0.5 Mt yttria), 160,000 t. U_3O_8, and 1.6 Mt Zn. A large variety of rare-earth deposits occur in India of both the hard-rock and placer types. It is, therefore, a multicommodity project that would coproduce uranium, zinc, and the rare earths.

2.6.10 India

A large variety of rare-earth deposits occur in India of both the hard-rock and placer types.

2.6.10.1 Hard Rock Deposits

Rare-earth minerals in large concentrations occur in pegmatites in the states of Bihar, Rajasthan, and Andhra Pradesh, and in hydrothermally altered formations, particularly those associated with carbonatites, in the states of Rajasthan, Tamilnadu, and Gujarat. Vast occurrences of allanite within the granitic rocks are known in the districts of Madurai and Tirunelveli in Tamilnadu and in parts of Mayurbhanj and Koraput districts of Orissa. Allanite, even though it contains much less total REO (10–30%) than many other minerals, may best be reckoned in India as a potential source of rare earths in view of their extensive occurrence. Many of the allanites from parts of Bihar and Tamilnadu have been found to contain small amounts of europium and samarium. The Kanyaluka deposit in the Singhbhum district of Bihar contains pegmatites rich in xenotime. The deposits of uranium ore from Jaduguda contain appreciable amounts of dysprosium and gadolinium. Gadolinite occurs in the Mayurbhanj district of Orissa and in the Madurai and Salem districts of Tamilnadu. Chevkinite occurs in parts of Orissa and Karnataka; uranothorite occurs in parts of Karnataka, Tamilnadu, and Uttar Pradesh; and rare earth–bearing pyrochlore and zircon occur in the north Arcot district of Tamilnadu and in the sandstones of Madhya Pradesh, respectively. Yttrium occurs in association with lanthanides and like them is characteristic of

granite pegmatites. These deposits occur in the (1) Rajasthan and Bihar pegmatite belt; (2) Kanyaluka and Singhbhum district of Bihar; (3) Syenite pegmatites and alkali rocks like the carbonatites of Rajasthan, Gujarat, and Tamilnadu; and, possibly, (4) certain locations in Andhra Pradesh.

2.6.10.2 Placers

The most important rare-earth deposits of India are the beach sand deposits that contain monazite in addition to ilmenite, rutile, zircon, sillimanite, and garnet. In terms of reserves of beach sand deposits, India ranks second only to Australia. There are five major rare-earth placer deposits, four of which are in coastal areas. The fifth placer, yet unworked, is inland. The rare earths in the Indian placer deposits have been estimated at 2.7 Mt REO, placing India among the countries that can be considered rare-earth majors in terms of reserves.

The rare-earth placer deposits in India are found in the southwestern coast of the peninsula at Manavalakurichi in Tamilnadu, Chavara in Kerala, and the eastern coast in Gopalpur in Orissa. The Chavara beach deposits extend over a stretch of 22 km from Kayamkulam in the north to Neendakara in the south. The Manavalakurichi beach deposits extend to about 2 km in length from the mouth of the river Valliar touching Kadiapatnam village to the village Chinnavilai. Apart from the rich seasonal washings on the beach, the dunes containing relatively higher percentage of silica form an important source. Extensive dune sand deposits occur along the south Orissa coast over a stretch of about 150 km. Of the several deposits located, the one close to Chatrapur is an extensive single deposit with the highest grade of heavy minerals. It runs over a coast length of nearly 18 km, covering a total area of over 26 km^2 between Gopalpur in the south and the Rushikulya river in the north. In addition to the main deposits described above, extensive heavy mineral deposits also occur on the coasts of Andhra Pradesh and Maharashtra. It is reported (Jackson and Christiansen 1993) that resources on the coastal placers of India may be underestimated because the beach sands are apparently replenished by annual monsoons. Rare earths also occur in the inland placer deposits at Ranchi in the Jharkhand state and at Purulia in the West Bengal state.

There is a recent revision in the placer monazite resource figures in India. As of March 2014, the statewise resources of *in situ* monazite established by the Atomic Minerals Division of the Department of Atomic Energy are as follows: Odhisa 2.41 Mt, Andhra Pradesh 3.72 Mt, Tamil Nadu 2.46 Mt, Kerala 1.90 Mt, West Bengal 1.22 Mt, and Jharkhand 0.22 Mt. India has 11.93 Mt of monazite, which contains 1.07 Mt of thorium.

2.6.11 Indonesia

In Indonesia, the important rare-earth resource is xenotime, occurring in the cassiterite-rich placers in the Tin Islands, Belitung, Bangka, Tujuh Archipelago, Singkap, Kundur, and Karimun, which form part of the southern extension of the Tin belt of Southeast Asia. The deposits of the Belitung island are the most important. The total reserves of monazite and xenotime in cassiterite placers of the Tin islands have been estimated at approximately 5000 t. No actual mining or processing for rare-earth recovery appears to have been carried out.

2.6.12 Japan

In Japan, the titanium mineral sphene, containing rare earths, has been found (Ito 1991) in the syenitic rocks around the periphery of the Kamioka lead–zinc mine. The deposit is a holocrystalline syenitic rock that is composed essentially of diopside, feldspar, quartz with accessory sphene, apatite, epidote, calcite, amphibole, sphalerite, and others. The sphene content of the deposit is approximately 4–7%, and the total rare-earth content of the sphene is ~1.1% REO. Sphene is not commercially processed at present anywhere. It is a refractory and chemically stable silicate mineral.

Researchers at the University of Tokyo reported that they have discovered seafloor sediments in Japanese waters that contain an estimated 6.8 Mt of REEs (Kato et al. 2011) and catalogued some hotspots of rare-earth accumulation on the bed of the Pacific. Seafloor hydrothermal vents pump out REEs dissolved in their hot fluids. And these elements and others accumulate in potato-sized lumps, known as manganese nodules, on the sea floor. The elements also build up in sea-floor mud; but only a few spot measures of this source of REEs have previously been made. Kato et al. (2011) examined 2000 samples of sediments taken from 78 sites around the Pacific and found rare-earth concentrations as high as 0.2% of the mud in the eastern South Pacific and 0.1% near Hawaii. Some of the deposits are more than 70 m thick. The authors estimate that an area of 1 km^2 around a hotspot near Hawaii could hold 25,000 t of rare earths. Overall, the ocean floor might hold more than the 110 Mt of rare earths estimated to be buried on land.

2.6.13 Kenya

The Kwale Project is located 10 km inland from the Kenyan coast and 50 km south of Mombasa. Resources at Kwale are 200 Mt of heavy mineral sands containing 3.8 Mt of ilmenite, 1.1 Mt of rutile, 0.6 Mt of zircon, and lesser amounts of monazite (Hedrick 2002). Monazite occurs in the Kwale deposit in low quantities and will be recovered, blended with the tailings, and returned to the mining area (Hedrick 2003). Tiomin Resources Inc. had a mining lease from the Kenyan Mining and Prospecting Licensing Committee for its Kwale heavy mineral sands project.

2.6.14 Madagascar

The Farafangana heavy mineral prospect region on the southeastern coast is known to contain monazite and has previously reported reserves in the Tolagnaro deposits in the south and southeast of Madagascar of 50,000 and 260,000 t, respectively (Hedrick 2003).

2.6.15 Malaysia

Alluvial tin deposits in Malaysia contain cassiterite as the main economic mineral and, in addition, several other minerals such as ilmenite, monazite, xenotime, and zircon. Cassiterite and the associated minerals usually occur as free grains liberated from one another due to the natural breakdown process from the primary ore body. Monazite, xenotime, ilmenite, and zircon contents are highly variable and

depend on the location of the deposit. Data are available usually for the composition of tin tailings generated in mineral benefication for cassiterite, known locally as *amang*.

Alluvial tin deposits occur in various states in Malaysia, and the deposits in the Kinta valley of the Perak state are considered important. Analysis of an amang sample from this valley is given (Hussin et al. 1991) in Table 2.6.

The highest percentage of xenotime is found in the deposits at Jelepang (5%) and at Batu Gajah (3%) in the Kinta valley. The monazite content in the amang from Batu Gajah is 10%, whereas no monazite is present in the amang from Jelepang. Similarly the deposit in the state of Terengganu contains about 2% monazite but no xenotime. Even in some areas of Perak, as well as in the state of Selangor, xenotime presence does not exceed trace levels. By and large, monazite occurrence is more prevalent in amang, but useful quantities of xenotime are present. On average, Malaysian monazite (Sulaiman 1991) contains 25% Ce_2O_3, 2% Sm_2O_3, 2% Y_2O_3, 27% phosphate, 6% ThO_2, and 0.2% U_3O_8. A typical analysis of Malaysian xenotime is 35% Y_2O_3, 4% Dy_2O_3, 4% Yb_2O_3, 29% phosphate, 0.7% ThO_2, and 1.6% U_3O_8. Total rare-earth reserves in Malaysia have been estimated (Kanazawa and Miyawaki 1991) at a modest 30,000 t REO.

2.6.16 Malawi

Many rare-earth minerals, including the common monazite and bastnasite and the less common synchysite and florencite, are found in Malawi. They occur in carbonatites in the Chilwa province of southern Malawi (Malunga et al. 1991).

2.6.16.1 Kangankunde

The Kangankunde Hill rare-earth deposit is an intrusive carbonatite located 90 km north of Blantyre. Rising 200 m above the plains, the deposit has monazite in carbonatite dikes and veins and has an average thoria content of only 0.08%. Monazite is found as a pale green to colorless mineral disseminated throughout the carbonatite, in carbonatized fledspathic rocks, and in the surrounding eluvial soils. The rare-earth content in the carbonatite ranges from 1.6% to 16.2% REO with an average of 10% REO. The mean percentage concentrations of Sm_2O_3 (1.43), Eu_2O_3 (0.17), and Y_2O_3 (0.10) compare favorably with Mountain Pass bastnasite. The Kangankunde contains 11 Mt of ore with proven resources of 6 Mt. The deposit has an inferred resource of 107,000 t grading 4.24% REO with, as mentioned above, a very low thorium content.

2.6.16.2 Nanthace Hill

The minerals synchysite and bastnasite occur in Nanthace Hill as disseminated needles, 0.2–1 mm long, in sideritic carbonatite. The grade is 1–3.6% REO. Three mineralized zones, more than 10 m thick, within the apatite and carbonatite contain 600,000 t of ore with 1.7% REO up to a depth of 50 m. The apatite carbonatite of Nanthace Hill bears higher concentrations of yttrium and europium. The total REO content of apatite crystals ranges from 0.5% to 1.25%.

2.6.16.3 Songwe

The main mineral in the Songwe carbonatite is synchysite or bastnasite. Mineralized zones with thicknesses of more than 10 m show an REO content of more than 1%. Within 50 m depth, 1.4 Mt with 1.7% REO has been proved.

2.6.16.4 Chilwa Island

The minerals synchysite and florencite occur as disseminated fibrous aggregates in the Chilwa Island carbonatite. In the central core of the sideritic carbonatite, the rare-earth content is 5% REO. The mean Sm_2O_3, Eu_2O_3, and Y_2O_3 contents are 2.20%, 0.47%, and 1.64%, respectively. The sideritic carbonatite of the Chilwa Island contains apatite and pyrochlore. This apatite contains lanthanum (7.12%) and cerium (13.7%), whereas pyrochlore contains cerium (1.3–2.76%).

2.6.17 Mozambique

Placer deposits of heavy minerals including monazite occur in Mozambique at Congolone, which is on the coast, 15 km north of Angoche. The deposit consists of dredgeable reserves of 167 Mt grading 3.25% heavy minerals. The 5.42 Mt of heavy minerals in the reserve include 11,000 t REO (RICI 1990).

2.6.18 Myanmar

In Myanmar, monazite and xenotime occur in association with placer cassiterite and wolframite deposits. Columbite and tantalite also occur in these deposits, which are found in the Dawei and Myeik areas of southern Myanmar (Jackson and Christiansen 1993).

2.6.19 New Zealand

There are two placer deposits on the west coast of south island at Westport and Barrytown. These deposits contain ilmenite, rutile, zircon, and monazite like many other marine placers. Additionally, they contain magnetite, cassiterite, gold, and scheelite (Jackson and Christiansen 1993). The monazite reserves are considered only modest.

2.6.20 Peru

An alluvial mineral sand ore body that contains cerium, lanthanum, neodymium, and other rare earths occurs near Tacna in Peru. This ore body contains titanomagnetite and associated minerals (RIC 1997).

2.6.21 South Africa

With more than 1 Mt REO contained in her rare-earth deposits, South Africa is potentially a rare-earth major. There are five deposits; four of them are hard rock type and one is a placer. All five deposits are very large. At Buffalo fluorspar monazite occurs in association with fluorite and apatite; at the Phalaborwa complex, apatite is rare earth bearing; the Zandkopsdrift deposit comprises a carbonate-rich, magmatic

rock deposit with monazite and crandallite as the main rare earth-bearing minerals; at Steenkampskrall, the hard-rock deposit bears monazite vein; and Richards Bay placer deposit contains monazite.

2.6.21.1 Buffalo Fluorspar

The open pit mine is about 9 km northwest of Naboomspruit (Mookgophong) situated on the farm Buffelsfontein in the Waterberg District, Bushveld Complex, Limpopo Province, South Africa. The 14–16% grade (CaF_2) deposits consist of a network of fluorspar veinlets in sill-like bodies of fine-grained, pink granite in coarse, red Bushveld granite. This mine was the biggest single producer of acidic (hydrofluoric acid) grade fluorspar in the world, with an output of 240,000 tons/year around 1982/1983. During the 1990s, the price of fluorspar worldwide dropped to a point where this mine became uneconomical. Operations ceased in 2002 apparently due to legal problems. There was a feasibility study into the economic viability of rare-earth exploitation at Buffalo about 41,000 t/year of REO could be obtained from the Buffalo fluorspar mine.

2.6.21.2 Phalaborwa Complex

The largest open pit mine in South Africa is located at Phalaborwa, Limpopo Province, South Africa. The Phalaborwa mine contains magnetite, vermiculite, apatite, zirconium, titanium, and uranium, as well as copper. The deposit is hosted in an alkaline igneous complex comprising mainly pyroxenite with occurrences of pegmatites, foskorite, and carbonatite. In the carbonatite complex, the fluorapatite, $3Ca_3(PO_4)_2{\cdot}CaF_2$, deposits contain a significant amount of rare earths, typically 0.5–1.0% REO. The proportions of europium, samarium, and neodymium are considerably higher in Phalaborwa apatite (Eu 1.1%, Sm 5.0%, and Nd 13%). An advantage of apatite as a source of rare-earth products is the absence of thorium. The safe disposal of the radioactive element thorium is a vexation to monazite-based processes (Preston et al. 1996).

2.6.21.3 Steenkampskrall

The hard-rock monazite vein deposit at Steenkampskrall (71 km north of Vanrhynsdorp, Western Cape, South Africa) has been notable among the world's primary monazite deposits. The main vein is made up predominantly of monazite, which accounts for more than 91% of total REEs, with much lesser amounts of REE-bearing allanite, thorite, and xenotime. According to Great Western, the new NI 43-101-compliant resource estimate, at a cutoff grade of 1%, now includes 16,600 t of TREOs in the measured category and 67,000 t of TREO in the *in situ* indicated category. Overall, the latest resource in the *in situ* and tailings measured and indicated categories stands at 86,900 t.

2.6.21.4 Zandkopsdrift

The Zandkopsdrift deposit comprises a carbonate-rich, magmatic rock deposit containing significant REE-bearing mineralization within near-surface, deeply weathered phases that crop out. The carbonatite is exposed as a well-defined, outcropping hill, about 40 m above a surrounding plain. Zandkopsdrift has been the subject of a number of geological, mineralogical, and metallurgical investigations from the 1950s onwards. Most of the work was carried out by Anglo American in two phases over a 6-year period, including during the 1980s, when the rare-earth potential was investigated.

The main rare earth-bearing minerals of monazite and crandallite and the mineralization are similar to Mount Weld deposit in Australia (Elliott 2012). Europium, terbium, and dysprosium are contained at elevated levels at Zandkopsdrift. The concentration of radioactive elements averages 178 ppm for thorium and 47 ppm for uranium.

The Zandkopsdrift project contains 950,000 t TREO. Some 22.92 Mt at an average grade of 2.32% in the indicated resource category (532,000 t of TREO) and an additional 20.81 Mt containing 415,000 t of TREO in the inferred resource category applying a 1% TREO cutoff.

There are a series of higher-grade zones of sufficient size within the overall resource that could be exploited as discrete units within the deposit. The 2.5% cutoff zone is a discrete area referred to as the Zandkopsdrift B-zone, which contains some 450,000 t of REO. A high-grade zone of mineralization within the overall Zandkopsdrift resource, referred to as the Central Zone, consists of the mineralization above a grade of 2.0% TREO, with an average grade of the indicated mineral resources of 3.1% TREO and an average grade of the inferred mineral resources of 2.9% TREO. The production is due to start in the second half of 2015 and will reach full production within 1 year. The carbonatite to be mined is highly weathered; excavation will consist of a mix of free digging, ripping, and conventional drill and blasting methods.

2.6.22 Sri Lanka

Substantial deposits of heavy mineral sands occur concentrated along the beach on the northeast coastline centered at Pulmoddai, 56 km north of the Trinconamalee port (Panditharatna 1991). The deposits occur over a stretch 9 km long and 360 m wide. The mineral reserves of Pulmoddai have been estimated to be approximately 3.7 Mt. The Sri Lankan mineral sands have the distinction of being the richest in heavy mineral content. The heavy mineral content is in the range 60–75%, and the constituent minerals are ilmenite 70–80%, rutile 8–10%, zircon 8–10%, and monazite 0.2%. Interestingly, Pulmoddai's offshore deposits have been estimated to be between 0.95 and 1.34 Mt. It has also been estimated that about 14–16% of the quantity of heavy minerals mined is added to the deposits by accretion due to wave action during the monsoon season every year.

2.6.23 Sweden

A carbonatite-related REE deposit, the massive magnetite–apatite ore bodies with 0.7% TREO in the Kiruna iron ore district of northern Sweden, is considered as a resource similar to Bayan Obo.

2.6.24 Taiwan

Heavy mineral sand deposits occur along the southwest coast of Taiwan. About 550,000 t of mineral sands, containing about 10% black monazite, was reported in this deposit (Miao and Horng 1988). The black monazite is primarily composed of rare-earth phosphate and silica and also contains zirconium, titanium, uranium,

and thorium as minor constituents. The Taiwan black monazite is particularly low in thorium, containing only 0.41% ThO_2. The composition of this monazite vis-à-vis the minerals from Australia and India is shown in Table 2.5. The main difference between the black and yellow monazite is the silica and thorium contents.

2.6.25 Thailand

Rare-earth mineral deposits occur in Thailand in a wide range of geological environments. Monazite is the most common mineral in Thailand, and the occurrences of xenotime and microlite are also important. Significant quantities of monazite and small amounts of xenotime are invariably associated with tin and tungsten deposits. Both hard-rock and placer deposits are found in Thailand. The hard-rock deposits include *disseminated* rare earth-bearing lithophile granitoids and stockworks, rare earth-bearing tin pegmatites, rare earth-bearing quartz veins, and rare earth-bearing skarns and skarnoids. The placer deposits include alluvial placer deposits, recent and old beach sand deposits, and near- and offshore deposits. There are also some weathering crust deposits in the country. The grades of rare-earth ores in these deposits have been estimated to vary from low (<0.001% RE minerals) for most primary deposits, intermediate (0.01–0.001%) for pegmatite and alluvial placer deposits, to high (>0.01%) for weathering crust and placer deposits. The ore tonnages are considered to be small for the quartz vein, skarn type, and weathering crust deposits, intermediate for alluvial placer deposits, and large for disseminated granitic–pegmatitic and near offshore deposits.

Much of the cassiterite deposits of the Thai Peninsula are located in the western granitic belt (Pungrassami and Sanguansai 1991). The primary sources of tin, tungsten, and associated heavy minerals are pneumatolytic granite, pegmatite, apatite, and hydrothermal quartz veins. Beach sand deposits occur in Changwat Prachuap, Khiri Khan, and Changwat Chumphon. The monazite–cassiterite ratio in these deposits is in the range 0.0011–0.5203, and the xenotime–cassiterite ratio is in the range 0.00–0.0194. The reserves of cassiterite, monazite, and xenotime from the mines in the granitic belts and from offshore are only modest.

2.6.26 Turkey

A bastnasite deposit was found in midwest Turkey at Beylikahir, near Eskisehir. The resource was estimated to be 1 million tons with an average grade of 3.14% REO. The other constituents of the ore are fluorite, barite, calcite, and minor amounts of thorium-, iron- and manganese-containing minerals. The bastnasite mineral occurs as very fine yellowish particles as a cement material between fluorite and barite particles, or was intimately associated with these minerals (Kul et al. 2008).

2.6.27 United States

Before the discovery of the huge rare-earth deposit at Bayan Obo, China, the United States was ranked first as the country with the greatest amount of REO in its resources. With the identification of massive quantities of rare earths in deposits located in Australia, Brazil, Canada, Greenland, and, according to an earlier report,

Namibia, some of which will have to be unequivocally substantiated in the future, it can only be stated that the United States ranks among the major countries in terms of REO contained in their resources.

Jackson and Christiansen (1993) noted 32 monazite and 3 bastnasite deposits in addition to 5 deposits containing other rare-earth minerals in the United States. Rare-earth deposits occur distributively across the United States from inland California to the lower East Coast.

Deposits of monazite occur in the United States in Florida, South Carolina, Idaho, Georgia, Alabama, Virginia, Wyoming, California, and Alaska. Out of the 40 rare-earth deposits in the United States, only 13 are placer deposits of which 8 are fluvial placers and 5 are marine placers. Monazite occurs with ilmenite, zircon, magnetite, and other minerals in these deposits. Monazite from stream placers in Idaho is relatively low in thorium. The composition of a commercial monazite concentrate from Idaho was given in Table 2.5. Monazite from Florida contains about 4% ThO_2, which is much less than the thorium contents of monazite from Brazil (6% ThO_2) and India (8% ThO_2). Most of the monazite deposits in the United States are, however, hard-rock deposits. The mineral euxenite occurs in a placer deposit at Bear Valley, Idaho (Kremers 1961; Jackson and Christiansen 1993).

2.6.27.1 Elk Creek Carbonatite, Nebraska

A REE and niobium-rich carbonatite mass, referred to as the Elk Creek carbonatite, lies in the subsurface about 1.6 km southwest of the small town Elk Creek in southeastern Nebraska. The REEs occur principally in the minerals bastnasite, parisite, and synchisite and smaller amounts in monazite. Niobium occurs in pyrochlore. The Elk Creek carbonatite contains 39.4 million tons of ore containing 0.82% Nb_2O_5, making it possibly the largest niobium resource in the United States. The rare-earth resource has not been estimated (Gambogi and Cordier 2010).

2.6.27.2 Music Valley, California

Throughout Music Valley in Riverside County, California, distributed in an area of 9.7 × 4.8 km, mineralized zones containing monazite and xenotime occur. The estimated combined REO equivalent tonnage is 2.5 Mt for every 30 m of mining, and the structure is reportedly 120 m deep to the base of the synclinal trough. Xenotime occurrence in the Music Valley area was revealed during radiometric prospecting by the USGS for United States Atomic Energy Commission (USAEC) during 1949 and 1952. All the xenotime in this area occurs in pinto gneiss of probably Precambrian age (Evans 1964).

2.6.27.3 Wet Mountains Area, Colorado

A thorium and REEs deposit occurs in the Wet Mountains area of south-central Colorado. Thorium and REEs occur in veins, syenite dikes, fracture zones, and carbonatite dikes associated with three Cambrian alkaline complexes that intruded the surrounding Precambrian terrain (Long et al. 2010). The average concentration and reserves of thorium and rare earths in these deposits are 0.46% ThO_2 and 64,200 tons; 0.21% REO (light) and 73,270 tons; and 0.14% REO (heavy) and 48,850 tons, respectively (Armbrustmacher 1988). The Wet Mountains Area deposit is considered comparable to the Lemhi Pass REE–Th resource.

2.6.27.4 Diamond Creek Area, Idaho

Thorium and rare earth-bearing veins hosted by Proterozoic quartzite and siltite and by Mesoproterozoic granite occur in the eastern slope of the Salmon River Mountains. These veins are mineral fillings (hydrous iron oxide and disseminated thorium and REE) in fractured and sheared bedrock and are found over an area 4 × 0.8 km. Monazite is the primary rare-earth mineral in the region with smaller amounts of bastnasite and xenotime. Gold was also reported. Historical and recent investigations noted the potential for a larger, buried iron (Fe)–REE–thorium–apatite (FRETA) deposit, similar to the FRETA deposits in Mineville, New York, and Pea Ridge, Missouri. The resources have been estimated at 75,500 tons REO using an average grade of 1.22% REO. The USGS reported gold contents of 0.017, 0.07, and 0.348 oz. per short ton in three samples, while the highest gold content reported by the AEC was 3 oz. per short ton from one vein. The average thorium content was 0.12%. Hedrick (2010) listed an estimate of the amounts of REE in this deposit: 22,400 t of Ce, 17,125 t of Nd, 8220 t of La, 5480 t of Sm, 4795 t of Y, 3425 t of Pr, 3425 t of Gd, 1370 t of Dy, 1370 t of Eu, and a total 685 t of remaining heavy REE.

2.6.27.5 Hall Mountain, Idaho

Thorium-rich veins containing rare earths crop out in an area 1830 × 305 m at Hall Mountain in northeastern Idaho. The veins cut Precambrian quartzite and quartz diorite. Thorite is the primary thorium- and REE-bearing mineral in the veins in which a total of 30 minerals were identified by Staatz (1972). The vein averages 4.0% thoria, and thorium reserves here stand at 115,000 tons. The average REO concentration in the veins is only 0.05%. This resource is unlikely to be considered for rare earths.

2.6.27.6 Lemhi Pass District, Idaho

Numerous vein deposits enriched in thorium and rare earths occur within a 140 km^2 zone of a larger 400 km^2 area in the Central Beaverhead Mountains. Most of these are quartz–hematite–thorite veins that fill fractures, shears, and brecciated zones in Mesoproterozoic quartzite and silicate host rocks. The deposit is considered to be the largest concentration of thorium resource in the United States (van Gosen et al. 2009), and the REE resources here are approximately equal to the thorium resource. Investigation of the Lemhi Pass District of Idaho and Montana by the USGS delineated a combined indicated and inferred resource of 368,000 t REO and 277,000 t ThO_2 (Staatz et al. 1976). Aueralitic thorite–xenotime, monazite, and brockite are the main thorium and rare-earth minerals in the Lemhi Pass District. The veins are relatively enriched in the middle REE such as neodymium, samarium, europium, and gadolinium, as well as the heavy REE such as terbium to ytterbium and yttrium (Reed 2007). Hedrick (2010) reported the quantities that could be available from the Lemhi Pass District (in tons): Y 77,345; La 25,780; Ce 69,980; Pr 11,050; Nd 66,296; Sm 40,515; Eu 14,735; Gd 40,515; Tb 1840; Dy 14,730; Ho 1840; Yb 1840; Er ≤ 929; Tm ≤ 929; and Lu ≤ 929. Appreciable concentrations of copper, lead, zinc, and anomalous silver and gold enrichment are found in some of the thorium and rare-earth veins in the Lemhi Pass District. These elements could be having considerable by-product value (Reed and Gillerman 2008). Recent and ongoing work implied a potential for a larger mineralized system at depth.

2.6.27.7 Pea Ridge Iron Deposit and Mine, Missouri

Seven major iron ore deposits are known in the southeastern Missouri iron metallogenic province. The deposit at Pea Ridge has rare-earth mineralization in four igneous breccia pipes and in apatite associated with magnetite. REE-bearing breccia pipes cut through the Pea Ridge massive magnetite iron ore body (Long et al. 2010) located in Washington County, Missouri. The iron deposit as a whole contains concentrations of REE that may be economically recoverable as a primary product or as a by-product. Within the main iron ore deposit, rare earths occur as inclusions in apatite and as interstitial grains exsolved from apatite (Seeger 2008). REE-bearing minerals in the breccia include monazite, xenotime, and minor amounts of bastnasite and britholite. Other REE minerals at Pea Ridge are allanite, bastnasite, britholite, tengerite–(Y), and synchysite–(Y) (Hedrick 2007). The breccia pipes contain about 660,000 t REE reserves with an average grade of 12% REO (Whitten and Yancy 1990), amounting to a total of 72,000 t REO. Additional lanthanide resources—primarily in fine-grained monazite and xenotime that form inclusions in apatite—are contained in surface tailings. Apatite also contains minor amounts of REE in its structure.

2.6.27.8 Hicks Dome, Illinois

The 14.5-km-diameter dome-shaped structure (Hicks Dome, Hardin County, Southernmost Illinois) overlies a potentially wide area of REE and thorium mineralization at depth. A hole drilled near the apex of the dome intersected mineralized breccia at a depth of 490 m, which continued to the bottom of the hole at 897 m (Brown et al. 1954). Mineralization of the breccia contain Th and REE possibly residing in monazite. Resources have not been estimated.

2.6.27.9 Mineville Iron District, New York

REEs and thorium occur within apatite iron ores once mined in the Mineville Iron District, Essex County, New York. The iron deposits were mainly magnetite, martite, and apatite. The rare earth-containing apatite at Mineville occurs in association with magnetite ore in metamorphosed sedimentary and igneous rocks. The rare-earth content of the apatite averages 11.1% REO (range 3–35%). It also contains thorium (average 0.15%, range 0.01–0.33%) and uranium (average 0.032%, range 0.015–0.2%) (McKeown and Klamic 1956). The rare earths in the apatite include all elements except Pm and Tb. The contents of Ce, La, Nd, and Y are especially higher.

Iron deposits of Mineville–Port Henry area that are high in apatite are also enriched in phosphorus, thorium, and rare earths because these elements are concentrated in the apatite grains. Besides, the ore mineral magnetite is intergrown with rice-shaped grains of apatite. Iron ore was mined from this district intermittently from 1804 until the last operation in 1971. Large tailing piles and unmined part of magnetite ore bodies in the Mineville district contain rare earths. According to Staatz et al. (1980), two-thirds of the tailings piles were derived from apatite-rich ores. This represents 10 million tons of tailings. The apatite content of the tailings is about 8%. Thus, approximately 790,000 tons of apatite would be present in the tailing dump in the district. The average rare-earth content of the apatite is approximately 11.4% (McKeown and Klemic 1956). Thus, the tailing dump pile could contain approximately 88,400 tons REO.

2.6.27.10 Bear Lodge Mountains, Wyoming

Southern Bear Lodge Mountains, Crook County, Wyoming, is a large alkaline–igneous complex of disseminated vein REE–Th deposits. These deposits are hosted by middle tertiary alkaline intrusions consisting of primarily phenolite and trachyte. They intruded Paleozoic and Mesozoic sedimentary rocks, forming a dome 13 × 10 km in size. REE-bearing carbonatite dikes ranging in size from veinlets to 15 m in width intruded near the dome center (Bull Hill diatreme). The REE and thorium are incorporated into the minerals monazite, thorite, brockite, ancylite, and bastnasite.

Near the dome center (Bull Mountain) and adjacent areas, numerous carbonatite dikes are exposed. The oxide zone (the near surface part of the Bull Hill deposit) hosts a reserve of 4.5 million tons at 4.3% REO. A NI 43-101-compliant mineral resource (inferred) estimate for the Bull Hill Southwest deposit was 9.8 Mt averaging 4.1% TREO (Cordier 2009). According to the latest estimates, measured and inferred resources total to 11.88 Mt averaging 3.36% REO. The total contained REO is 394,420 t (Noble 2013). The Bear Lodge intrusive complex also hosts some Cu and Au sulfide mineralization and is locally enriched in Th, U, F, Ba, Sr, and Nb (Castor 2008b). The Bear Lodge disseminated deposits contain one of the largest concentrations of both REE and Th in the United States. Even though the grade of both commodities is lower in this deposit than in some other deposits, their size and potentially inexpensive mining (open pit) make them important potential resource of REE in the United States.

2.6.27.11 Mountain Pass, California

Bastnasite was not a well-known rare-earth mineral until the discovery in 1949 of a large bastnasite deposit in Mountain Pass, California (Evans 1966; Olson et al. 1954). Mountain Pass is part of a 130-km-long, north-northwest-trending belt of anorogenic ultrapotassic intrusions in southeastern California (Krahulec 2011). The Mountain Pass ore body is located near the west center of a block of pre-Cambrian metamorphic rocks composed of granite–biotite–garnet–hornblende–gneisses and schists that are cut by pegmatites and other dikes. Large areas of potash-rich igneous rocks, syneite, and shonkinite intrude into this complex, and next to these is the intrusion of rare earth-bearing carbonatite, which is also of pre-Cambrian age. Three principal rock types, namely, calcite–pink barite, dolomite, and silicified carbonate, form the carbonatite ore body. The minerals contained are, approximately, calcite/dolomite/ankerite, 50%; barite/celesite/ strontianite, 3%; bastnasite, 12%; and silica, 8%. The bastnasite ore body at Mountain Pass extends 750 m along a NW–SE strike and dips 40 m SW with an average thickness of 60 m. The deposit contains over 30 Mt proven and probable ore based on a 5% cutoff. The average rare-earth content is 8.9% REO (Wilson 1991). Mountain Pass has strong LREE enrichment and a high LREE/HREE ratio like Bayan Obo; however, unlike Bayan Obo, Mountain Pass is low in Fe (Castor and Nason 2004).

Long et al. (2010) mentioned that Molycorp estimates the remaining deposit at Mountain Pass (on the verge of the second phase of mine production beginning in 2012 after continuous production between 1952 and 2002 and a decade-long break between 2002 and 2012) to be 20–47 Mt of ore with an estimated average grade of 8.9% REO. The Mountain Pass deposit still has the third largest known REE resource in the world (Castor and Nason 2004).

2.6.27.12 Bokan Mountain, Alaska

The Bokan Mountain peralkaline granite complex covers about 7.7 km^2 area in the Prince of Wales Island in southeast Alaska. REEs along with niobium, uranium, and thorium occur in the numerous pegmatite, andesite, dacite, and apatite veins and dikes that cut the complex. An estimate by USBM (Warner and Barker 1989) suggested a total resource of 6.8 million tons of ore that averages 0.264% REEs, about one-third of which is yttrium. While HREEs are dominant in the central mineralized zone of the complex, the LREEs occur more peripherally. REE potential is estimated at about 4.26 Mt (equivalent to 16,630 t REO) if the cutoff is 0.39% REE.

2.6.27.13 Iron Hill, Colorado

Located near Gunnison in central Colorado, the Iron Hill intrusive complex is a carbonatite-related REE deposit. The REEs occur essentially in bastnasite, synchysite, and rhabdophane, and in lesser amounts in fluorapatite, pyrochlore, and monazite. The complex has the largest known exposed mass of carbonatite (2.5 km^2) in the United States. Resources at Iron Hill deposit contain an estimated 655 Mt of 0.397% REO, 0.0043% ThO_2, and 0.057% Nb_2O_5 (Van Gosen et al. 2009). The deposit is enriched in LREE.

2.6.27.14 Gallinas Mountains, New Mexico

Bastnasite is found within fluorite–copper sulfide deposits of the Gallinas Mountains, Lincoln County, central New Mexico. The minerals occur in two settings within the sandstones and siltstones of the Yeso Formation. They occur as veins that till the fissures in highly fractured zones and as mineral-rich masses that fill open spaces and veinlets in breccia zones. According to Soule (1946), bastnasite forms about 5% of the breccia deposits (Long et al. 2010).

2.6.27.15 Pajarito, New Mexico

The Pajarito yttrium–zirconium deposit in New Mexico is associated with a gabbro, syenite, quartz syenite, and alkali granite complex. Eudialyte, a zirconium silicate that contains Y, is the ore mineral that is disseminated in the syenite, quartz syenite, and alkali granite. The Pajarito deposit has a recoverable resource of 2.7 million tons grading 0.18% Y_2O_3 and 1.2% ZrO_2 (McLemore 2011; Sherer 1990).

2.6.27.16 Placers

In the United States, alluvial deposits of monazite are known to occur in the Carolina Piedmont of North and South Carolina, and the intermontane valleys of Idaho. Beach placers occur in northeastern Florida through southeastern Georgia. These three monazite placer districts (North and South Carolina stream placers, Florida–Georgia beaches, and Idaho stream deposits) are the largest volume placer REE–Th deposits known in the United States.

2.6.27.16.1 Idaho Placer Deposits

There are at least 11 monazite-bearing placer districts in the valleys of a region extending north of Boise, Idaho, along the western flank of the Idaho batholith. The primary source of the Th–REE minerals in these places is thought to be the quartz,

monazite, and pegmatite phases of the batholith. The common heavy minerals in the alluvial deposits (in generally decreasing amounts) are ilmenite, magnetite, sphene, garnet, monazite, euxenite, zircon, and uranothorite (uranium-rich thorite).

In the Idaho placers, the thorium oxide content of monazite is in the range from 2.2% to 6.24%. Total thorium reserves in the five important monazite districts here have been estimated to be 10,060 tons thoria. The reserves of REE would presumably be ten times the thorium reserves (typically monazite contains about 63% TREO and 2.2–6.24% ThO_2).

2.6.27.16.2 North and South Carolina Placers

Monazite-bearing alluvial stream placers occur in the valleys of the Piedmont of North Carolina and South Carolina, between the Catawba River in the northeast and the Savannah River in the southwest. The alluvium is deposited in flat valleys forming well-bedded, poorly graded layers of unconsolidated sediment (gravel, sand, clay, and clayey silt) at an average thickness of 4.5 m (Staatz et al. 1979). Monazite is found in all units but most abundant in the basal gravel layers and least in the clay layers. Various rivers carried monazite and other heavy minerals eastward from the Piedmont region resulting in all the regions in the coastal plain receiving various amounts of heavy minerals. The famous placer is the Horse Creek, which is southwest of Aiken, South Carolina, and is the site of first large-scale mining of stream placers for monazite and other heavy minerals in the Carolinas. Staatz et al. (1979) estimated a total reserve of about 5300 tons of thorium oxide, and potential thorium reserves seven times as high, for the 13 largest placer deposits of the Piedmont region of North and South Carolina. Using mean concentrations of REO (60–63%) and ThO_2 (5.67%) found in monazite from these placer deposits, an REE resource of roughly 58,400 tons is possible.

2.6.27.16.3 Florida–Georgia Beach Placers

The modern and raised Pleistocene and Pliocene beach deposits of Florida and southeastern Georgia host low-grade but persistent concentration of monazite. Heavy minerals constitute a small part of modern beach sands, and monazite forms a small part of the heavy minerals. However, because of the larger tonnage of suitable beach sand deposits and the ease of mining and processing of the material, these deposits represent a potential REE and thorium resource. According to Staatz et al. (1980), the beach placer deposits of this region contain total reserves of about 198,000 t of REO, 14,700 t of ThO_2, and 1490 t of uranium oxide, all of which are hosted in 330,000 t of monazite.

Generally, monazite-bearing sands in the raised Pleistocene and Pliocene beach deposits lie as much as 80 km inland, making them deposits of former shoreline. These relict shorelines lie 3–33 m above sea level. The monazite and associated heavy minerals in these deposits in southeastern United States were eroded from crystalline rocks of the Piedmont province (Mertie 1953), carried toward the Atlantic Ocean by streams and rivers, and eventually redeposited by coastal processes.

Marine phosphorite deposits can be enriched in REE, and minor amounts of REE minerals occur in phosphatic shale deposits. The Permian Phosphoria Formation is known to host low-grade (<0.1% REO) REE deposits in Idaho and Montana; however, no REO mineral is currently recovered in the phosphate operations (Castor 2008b). The sedimentary phosphate rocks of Florida contain about 0.024% Y_2O_3 and in total

0.05% total rare earths (Weterings and Janssen 1985). These rocks also contain uranium and vanadium. Phosphorite samples from the large Phosphoria Formation of Idaho, Montana, Utah, and Wyoming average 0.16% rare earths (~0.06% La, Nd etc., and 0.1% Y) (Aplan 1988). In the United States, a deposit occurs near Mescalero, New Mexico, that contains not only yttrium but also zirconium in a silicate mineral called eudialyte (Kilbourn 1990). The lanthanide elements are contained in complex mineralizations, such as in the eudialyte, in many of the hard-rock resources identified in the United States and elsewhere in the world.

2.6.28 Former Soviet Union

In Russia, large deposits of the mineral loparite occur in association with the minerals aegirine, apatite, eudialyte, feldspar, nepheline, ramsayite, and titanite in the Lovozero Alkali Massif, Kola Peninsula adjacent to Finland. The primary ore contains 2–3% loparite. The loparite ores are rich in light rare earths, and the rare-earth content is 32–34% REO. In addition, loparite contains 39–40% TiO_2, 8–10% $(Nb, Ta)_2O_5$, 4–5% CaO, and 8–9% Nb_2O_3. Thorium oxide content in the ore is 0.67%. The bulk of the CIS demand for the rare earths (Kosynkin et al. 1993) is supplied by loparite. Outside the former Soviet Union, loparite also occurs in the Parana Basin carbonatite near Sarambi in Paraguay (Hedrick et al. 1997).

Phosphate rocks of magmatic origin occurring at the Kola Peninsula of the former Soviet Union hold a considerable amount of yttrium and other rare earths. The yttrium content of Kola apatite averages 0.04% Y_2O_3 in the total rare-earth content averaging 1% REO. Rare earth-bearing apatite deposits also occur at Vishnevye Mountains, and the rare-earth content is more than 1% REO. Uraniferous phosphates containing rare earths occur at Schevchenko in Kazakhstan. The reserves, however, are limited. A fluorocarbonate rich in yttric rare earths, yttrosynchisite, occurs in Kutessaisk deposit, but reserves are limited. Deposits of rare earths are also found in Dnieprodzerzhinsk in the Ukraine, but the nature of this deposit is not known.

Kuzmin et al. (2012) listed three REE deposits in Siberia as most promising. They are given in Table 2.18. All these are situated in the Central and East Siberia regions. The Kii deposit is located in the Krasnoyarsk region (the central part of Siberia). Rare-earth metals are present in the three main ore mineral species—bastnasite, parisite, and monazite. The average content of the rare-earth metals is about 2%. The ore is poorly enriched but readily broken down for subsequent leaching. The high radioactivity of the ore is the main drawback of the deposit. Over 80% of the resources of REE and niobium-rich ores in Russia are concentrated in the two other deposits—Tomtor and Chuktukon. It is likely that only these deposits may seriously compete with the world-class deposits in Brazil and China for niobium and REE, respectively. The weathered carbonatite crusts are the basis of the REE ores of the Tomtor and Chuktukon deposits. Such types of ores are very similar and characterized by the high dissemination and intergrowth of the mineral species, which makes ore dressing very difficult and therefore inefficient (Kuzmin et al. 2012).

With regard to composition, the Tomtor ore is distinguished by quite a high aluminum and phosphorus content, and iron and manganese oxides are prevalent in the Chuktukon ore.

TABLE 2.18
Concentrations of Rare Metals in Ores of Largest Deposits (wt.%)

	Rare Metals	Rare-Earth Metals			
Deposit	**Nb Oxide**	**REE Oxides**	**Ce Group**	**Y Group**	**Including Y**
Tomtor, Burannyi site	7.0	10.0	9.0	1.00	0.420
Lovozero group (Kornasurt, Umbozero)	0.24	1.2	1.17	0.026	0.008
Chuktukon (REE ores)	0.5	7.0	6.58	0.42	0.130
Chuktukon (Nb ores)	1.2	3.0	2.76	0.24	0.084
Katuga	0.3–1.0	0.37	0.2	0.17	0.08
Bayan Obo, Inner Mongolia, China	0.1	6.0	5.86	0.14	0.030
Ionic ores, southern provinces of China	Mo, U, V, Co, Re	0.15	0.03	0.05	0.07

Source: Dobretsov, N.L. and Pokhilenko, N.P., *Russian Geology and Geophysics* 51: 98–111, 2010.

2.6.28.1 Tomtor

Crandallite, monazite, pyrochlore, titanium and iron oxides, kaolinite, and siderite are the main minerals of the Tomtor deposit. The REEs are mainly concentrated in monazite, and the niobium with a small amount of tantalum is found in the pyrochlore. All in all, the ore can be considered as a rich natural mixture of two concentrates—monazite and pyrochlore. The investigations carried out by different authors showed that physical liberation and separation of these constituents of the ore are practically impossible due to the high dissemination of the ore and intergrowth of the mineral species.

A rich rare-metal deposit occurs in Tomtor field located in the Sakha Republic (Yakutia) about 300 km away from the Arctic Ocean (Dobretsov and Pokhilenko 2010. The Tomtor ore contains niobium and the rare earths including scandium (0.1–0.3% Sc_2O_3). This is the largest deposit of scandium in Russia. The richest among the Tomtor deposits are at Burannyi site, and the resources here are described as redeposited weathering residuum of more depleted alkaline rocks and carbonatites. Composition of the Tomtor deposit is compared with other similar deposits in Table 2.18. The ores at Burannyi are richest in the world in Nb_2O_5 content—ten times or more than in other Russian deposits and three times of that in the Araxa deposit (Brazil).

2.6.28.2 Chuktukon

The ores of the Chuktukon deposit, unlike the Tomtor ores, are characterized by a high content of iron and manganese oxides. The average REE content is also high, but the niobium concentration is one tenth of that in the Tomtor ores. The ore body of the Chuktukon deposit is located on the surface in the form of a cupola. The area of the ore zone is relatively small and characterized by its large thickness, which increases to the dome part of the deposit up to 300 m. The ore is complex and principally consists of iron–manganese oxides (composition: 40–70% Fe_2O_3 and 1–20% MnO). The

ore contains about 1–2% phosphorus in the form of REE phosphates and apatite. The REE in the Chuktukon ore are mainly present as florensite, monazite, and cerianite. Phosphorus is relatively evenly distributed in different fractions throughout the ore. The granulometric composition of the ore is characterized by the presence of finely dispersed particles with a grain size of 0.074 mm, which constitute more than 50% of the material. The ore consists of agglomerates composed of particles of less than 1 μm in size. The particular dissemination of the minerals and intergrowth of the mineral species cause problems for the enrichment of these ores (Kuzmin et al. 2006).

2.6.28.3 Kyrgyzstan

The Kutessai II rare-earth deposit contains a complex ore. The rare-earth content of the Kutessai ore is enriched in the heavy rare earths with LREEs constituting 54.5%, HREEs constituting 43.7%, and 1.8% constituting losses during analysis (moisture, volatiles). Reserves at Kutessai II are 20.2 Mt ore with an average grade of 0.25% rare earths. Total rare earths in the deposit are 51,500 t (Hedrick 2002).

2.6.29 Venezuela

Deposits of rare earths and niobium occur at Cerro Impacto (Hedrick 1985a), 190 km southwest of Cindad Bolivar, Bolivar state. Intense weathering, as a result of the country's tropical climate, has leached the original carbonatite source rock to result in thick lateritic beds enriched in rare earths and other elements. Rare-earth contents range from 0.1% to 11%.

2.6.30 Vietnam

In addition to monazite and zircon in the mineral sands, Vietnam has large deposits of rare earths in carbonatites. These deposits were discovered in the late 1950s and occur in the Fan Si Pan Mountains in the north of the country.

2.6.30.1 Nam Xe

The most important rare-earth deposit occurs at Mau Xe (Nam Xe) situated at the northwestern part of the country (Kusnir 2000; Tirnh 1991). The Nam Xe rare-earth deposit belongs to the hydrothermal–metasomatic type. The deposit occurs as a series of barite–baritocelestite rare-earth carbonate veins. These veins vary in thickness from a few centimeters up to about 4 m. They are 200–1000 m long. The rare-earth content varies from 1.2% to 36.2% with an average of 9–13% (Tirnh 1991). The ore bodies are hosted in permo-carboniferous limestone. In addition to rare earths, the deposit contains significant amounts of minerals such as baritocelestite and barite. There are more than 35 minerals in the Nam Xe deposit. The main minerals are bastnasite, parisite, synchisite, baritocelestite, and barite, and the secondary minerals are calcite, ankerite, monazite, ortite, siderite, pyrite, galena, apatite, fluorite, phlogopite, limonite, magnetite, chlorite, and montmorillonite. The mineralization is complex, and all the minerals are closely intergrown. Primary ore has an average rare-earth content of 1.4% REO, mainly Ce, La, Nd, Pr, and Y. Gadolinium and europium are also present to the extent of 4% of the REO content. The weathered

zone to a depth of 20 m contains 4–5% REO. The reserves are huge—7.8 Mt REO out of which 1.7 Mt is proved at Nam Xe north alone. The ore is reported to be easy to process for recovery of rare earth, strontium, and barium. Additional reserves, smaller in quantity but richer in grade, occur on the south side of the river Nam Xe. About 3 Mt REO total reserves could be located here, and the average grade is 10.6% REO (Orris and Grauch 2002).

2.6.30.2 Dong Pao

The Dong Pao deposit is situated in the Tam Duong district of the northern province of Lai Chau, 40 km south of Nam Xe. The deposit is hosted in a paliogene syenitic intrusion. Approximately 60 ore bodies of various sizes, occurring as irregular pods, lenses, and veins, have been identified in the Dong Pao area. Resources here are also large. The deposit has reserves amounting to 7 Mt REO grading 5% RE and similar in quality to the Nam Xe resource (Kusnir 2000).

2.6.31 Zaire

Monazite is found in several tin and gold deposits in the Kivu region, Zaire (Hedrick 1985a). Reserves of monazite occur in two separate deposits in the Obaye mining sector. The Kabengelwa deposit and the Mashabuto deposit. The quantity is not substantial.

2.7 BY-PRODUCTS AND COPRODUCTS

In spite of the large identified world resources for the rare earths, their production and supply have been strongly influenced by the nature of rare-earth mineralization. Commercial mine production of rare earths is feasible in most of the cases only as a coproduct or by-product of some other mineral value. This is due to the fact that the concentration of rare earths in the reserves is usually not large enough for the extraction of rare earths alone to be economically viable. The prevailing market value of the rare earths would not, by itself, support entirely the mining and production costs involved in such an operation. As of 2009, the world mine production of rare earths seen in this context (Long et al. 2010) is given in Table 2.19.

When rare earth is extracted as a coproduct, the market value of the main product supports the cost of extraction of the rare earth, and the recovery of rare earths, in turn, makes the recovery of the main product economically more attractive. There is a sharing of mining and production costs between a coproduct and a main product, the latter carrying a major share of the overall input cost burden. When rare earths are recovered as a by-product, the situation is the same as that of its recovery as a coproduct except that the recovery and sale of by-product rare earths are not a necessary condition for making the recovery and the sale of the main product economically viable.

The recovery of rare earths as the primary product had been carried out from the Mountain Pass, California, bastnasite deposit. In fact, the Mountain Pass mine was the only active mine in the western world operated exclusively for the recovery of rare earths as no coproduct or by-product was commercially recovered (Wilson 1991). In China, bastnasite is mined as the main product in Sichuan 1 mine, and the ion adsorption-type ores in China are also processed, recovering the rare earths as the primary product.

TABLE 2.19
Production of REEs Mines in 2009

Country	Mine	2009 Output (Metric Tons REO)	Primary Product	By-Product
Brazil	Buena Norte	650	Ilmenite concentrate	Monazite concentrate
China	Bayan Obo	55,000	Iron ore	Bastnasite concentrate
China	Sichuan	10,000	Bastnasite concentrate	
China	South China	45,000	REEs	
India	Heavy-mineral sands	2700	Ilmenite concentrate	Monazite concentrate
Malaysia	Ipoh sand plant	380	Cassiterite concentrate	Xenotime concentrate
Russia	Lovozero	2500	Loparite concentrate	REE chloride

Source: Long, K.R. et al., The principal rare earth elements deposits of the United States—A summary of domestic deposits and a global perspective: U.S. Geological Survey Scientific Investigations Report 2010–5220. Available at http://pubs.usgs.gov/sir/2010/5220, 2010.

There has been a possibility of recovering rare earth as the main product in at least three deposits in Australia: Mt. Weld, Yangibana, and John Galt (Taylor 1991).

Historically, the only country where monazite recovery has been the purpose of mining beach sand deposits was Brazil. The principal attraction was the thorium content of monazite. In fact, all over the world, monazite was formerly mined solely for its thorium content (3–9%). Since 1920, however, the rare earths in the ore have been more important. From placer deposits of heavy mineral sands, rare earth has been invariably recovered as a by-product of ilmenite production in most of the cases, as a by-product of cassiterite mining in Southeast Asia, and in some cases as a by-product of placer gold (Aplan 1988).

Rare earths were recovered as a by-product of uranium extraction at Denison Mines, Elliot Lake in Canada. Much of the world's rare-earth production comes from its recovery as a by-product of iron ore mining at Bayan Obo, China. In the former Soviet Union, the supply of rare earth-bearing mineral loparite is associated with the large titanium recovery operations in the Kola Peninsula. A large potential exists for the recovery of rare earths from apatite as a by-product of phosphoric acid production from various locations in the world. Rare earths can be by-products if perovskites are ever processed for titanium recovery. True to its status as a by-product, the recovery of rare earths has not been a constant feature of the main product recovery in most of the cases, resulting in rare earth-rich tailings being accumulated for possible future recovery. These tailings may, in the future, be processed for rare-earth recovery, which would then assume the status of a pseudo main product.

The extraction of rare earths from anatase concentrates in Brazil has been cited as an example of possible new by-product sources of rare earths. Another example was

the possibility of by-product rare-earth production from the Olympic Dam copper–uranium–gold mine in South Australia.

The recovery of rare earths as a coproduct could be carried out in the processing of two of the Australian resources. The ore minerals of the Brockman deposit are very fine grained and not amenable to physical beneficiation to obtain concentration of any of the valuable minerals. Processing would therefore involve fine milling and chemical dissolution and separation by solvent extraction. There is the possibility therefore of recovery of values like ceramic-grade alumina and zirconia with the production of yttrium and rare earths as coproducts. The Toongi deposit in New South Wales is another suitable project for recovery of rare earths as a coproduct along with zirconia, tantalum, and niobium.

2.8 WORLD RARE-EARTH PRODUCTION

Rare earths were first produced commercially in the 1880s in Sweden and Norway from monazite. Production in Scandinavia was triggered by the invention in 1884 of the incandescent lamp mantle by Welsbach in Austria. Initially lanthanum, yttrium, and zirconium oxides were used for the mantle. Later, for improved light quality, only the oxides of thorium and cerium were used. Small amounts of neodymium and praseodymium oxides were also used for marking an indelible brand-name label on the mantle (Hedrick 2000). In the United States, production of rare earths started in 1893 in North Carolina. However, a small tonnage of monazite was known to be mined as early as in 1887. South Carolina started production of monazite in 1903. Production of monazite began in Brazil in 1887, and in India in 1911 (Hedrick 2004).

The published data on total world rare-earth production over the past 112 years (DiFrancesco et al. 2014) are shown as a graph in Figure 2.6. The century-old saga of

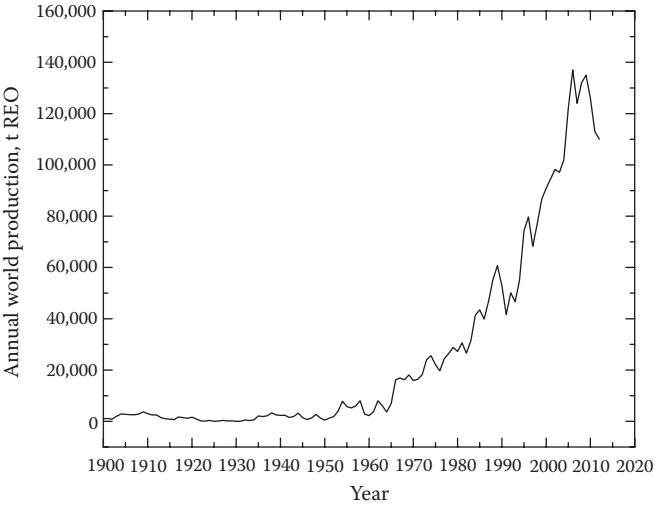


FIGURE 2.6 Total world rare-earth production over the past 112 years. (From DiFrancesco, C.A. et al., *Rare Earth Statistics*, U.S. Geological Survey, Reston, VA, 2014.)

world rare-earth production has certain interesting segments (Haxel et al. 2002), especially in the latter half. The picture during the 30 years (1983–2013) when world rare-earth production was derived from many countries is depicted in Figure 2.7. The rise and reign of China as the global provider of rare earths, the cessation of primary mine production of rare earths first in Australia and then in the United States, and, after a long gap, the reemergence of both these countries as rare earth producers happened during the years 1983–2013. The 30-year mine production detail compiled from data published in USGS Minerals Yearbook issued during the period are also given in Table 2.20.

Regular commercial mining of rare-earth reserves began approximately 100 years ago (Parker and Baroch 1971). India and Brazil were the principal sources of world rare-earth supply, with the United States occasionally contributing, until the late 1940s, when Australia and Malaysia also started regular production. Much of the world rare-earth supply between 1950 and 1985 came from the United States, which was the leading producer, and from Australia, which was the second. By 1985, however, China rose to second place, and by 1988, it overtook the United States to become the world's leading producer. China, United States, former Soviet Union, Australia, India, Brazil, and Malaysia have all been major or consistent rare earth-producing countries, with South Africa, Canada, Thailand, Sri Lanka, Madagascar, and Zaire contributing occasional or smaller amounts to world rare-earth production (Hedrick 1995, 1997; Jackson and Christiansen 1993).

Monazite was the major rare-earth resource mineral from the beginning of the industry until 1965. Thereafter, bastnasite production equaled or exceeded monazite production. Until 1988, bastnasite and monazite along with minor amounts of xenotime were the minerals that accounted for all the world rare-earth production. Loparite and other mineral resources might have been mined for supply in the then Soviet Union, but information on the quantity is unavailable. At present, bastnasite is the world's major source of rare earths. It constituted 62% of world output of rare-earth

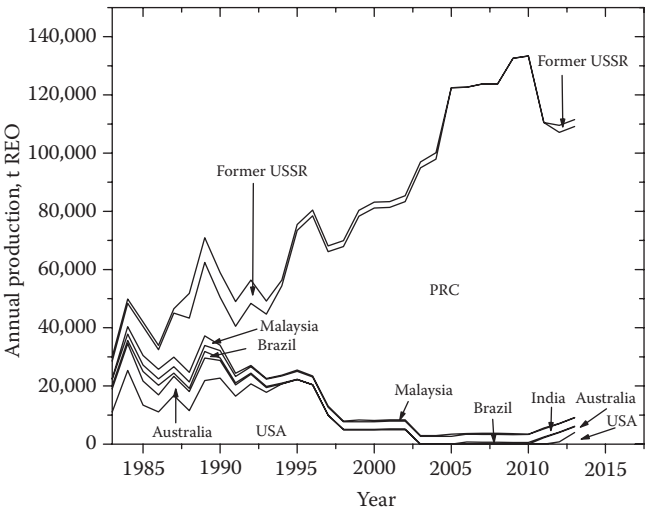


FIGURE 2.7 Breakdown of world rare-earth production 1983–2013.

TABLE 2.20
World Mine Production of Rare Earths (Metric Tons REO Equivalent)

Year	USA	Australia	Brazil	India	Malaysia	China	Former USSR	Other Countries	World Total[a]
1983	11083	7975	1100	2200	187	6000	1500	–	30,000
1984	25,311	9189	1100	2200	2563	8000	1500	–	49,900
1985	13,428	8250	3300	2200	3300	10,000	1500	–	42,000
1986	11,094	5820	3300	2200	3300	6750	1500	–	34,000
1987	16,710	6600	1100	2200	3300	15,100	1500	–	46,500
1988	11,533	6530	1100	2200	3300	18,660	8500	–	51,800
1989	21,875	7700	2280	2060	3300	25,220	8500	–	70,900
1990	22,700	6050	911	2500	1830	16,500	8500	–	59,000
1991	16,500	3850	719	2200	1090	16,150	8500	–	49,000
1992	20,700	3300	396	2200	427	21,340	8000	–	56,400
1993	17,800	1650	400	2500	224	22,100	4500	–	49,200
1994	20,700	–	256	2500	234	30,700	2000	–	56,400
1995	22,200	–	103	2700	448	48,000	2000	–	75,500
1996	20,400	–	–	2700	340	55,000	2000	–	80,400
1997	10,000	–	–	2700	418	53,000	2000	–	68,100
1998	5000	–	–	2700	202	60,000	2000	–	69,900
1999	5000	–	–	2700	625	70,000	2000	–	80,300
2000	5000	–	–	2700	446	73,000	2000	–	83,100

(*Continued*)

TABLE 2.20 (CONTINUED)
World Mine Production of Rare Earths (Metric Tons REO Equivalent)

Year	USA	Australia	Brazil	India	Malaysia	China	Former USSR	Other Countries	World Total[a]
2001	5000	–	200	2700	450	73,000	2000	–	83,400
2002	5000	–	200	2700	450	75,000	2000	–	85,400
2003	–	–	–	2700	250	92,000	2000	2200	99,100
2004	–	–	–	2700	250	95,000	2200	–	102,000
2005	–	–	–	2700	750	119,000	–	400	123,000
2006	–	–	730	2700	200	119,000	–	–	123,000
2007	–	–	650	2700	380	120,000	–	–	124,000
2008	–	–	650	2700	380	120,000	–	–	124,000
2009	–	–	550	2700	350	129,000	–	–	133,000
2010	–	–	550	2800	30	103,000	–	–	130,000
2011	–	2200	250	2800	280	105,000	–		110000
2012	800	3200	140	2900	100	100,000	2400	220	110000
2013	4000	2000	140	2900	100	100,000	2400	220	110000

[a] Includes Vietnam and Thailand, among others.

minerals in 1989, and the proportion rose to very high levels starting in 1994–1995 (Hedrick 1995, 1997). Incidentally, no bastnasite was produced before the 1950s.

Beginning in 1988, a new type of rare-earth ore, the ion-adsorption ore—occurring only in China—was mined. The production in 1988 was approximately 9000 tons REO, which was roughly half of total rare-earth production in China, that year. The production of ion-adsorption ore continued, constituting ≥25% of China's rare-earth production ever since. Monazite continued to be the second most produced rare-earth mineral until about 1994 when Australia stopped monazite production. With the decline in the supply of monazite, ion-adsorption ore became the second most important ore resource after bastnasite from 1995.

Monazite contains typically 50% REO as phosphate, and the light lanthanide fraction (La, Ce, Pr, Nd) constitutes more than 90% of the total rare-earth content while the other REEs make up 5–10%. The rare-earth content of bastnasite concentrate is constituted by as much as 99% of light rare earths (La–Nd), almost no heavy rare earths, and very little yttrium. Up to 60% of the rare-earth content of xenotime is yttria, and it also has a higher proportion of other heavy rare earths than monazite. Even though bastnasite and, particularly, monazite contain predominantly cerium, lanthanum, and neodymium (and only trace amounts of yttrium, 0.1% and 2.1%, respectively), because these minerals have been processed in much larger quantities as compared to the heavy lanthanide sources, such as xenotime, they were the principal sources of heavy lanthanides as well. With the steady increase in bastnasite production at the expense of monazite, the supply of heavy rare earths was increasingly constrained because monazite was significantly richer in heavy earths compared to bastnasite. With ion-adsorption ore being strongly enriched in the heavy rare earths, their mining in increasing quantities augmented the heavy rare-earth supply and ensured the continued decline of monazite production.

Monazite is a constituent in essentially all heavy mineral sand deposits. It is normally recovered and separated during processing but, in most cases, is either returned to tailings because of a lack of demand or stored for future sale. For instance, monazite was recovered in Australia at various localities as a by-product of beach sand mining for ilmenite, rutile, and zircon. In 1983, the proportion of by-product monazite production in Australia was 17,000 t/Mt of ilmenite. In 1988, only 7400 t of monazite was produced per million tonnes of ilmenite. Incidentally, over the same period, the annual monazite production in Australia decreased from 15,000 to 12,000 t (Taylor 1991).

The advantage of rare earths contained in monazite as a resource is owing to its widespread availability as a very low-cost by-product of heavy mineral sand processing. However, the demand shifted to thorium free rare earth mineral concentrates as industrial consumers became concerned with the potential liabilities of radioactive thorium, the costs of complying with environmental monitoring and regulations, and costs at approved waste disposal sites.

Taylor (1991) estimated the world rare-earth production in 1989 at 50,000 t of REO with 50% of this total constituted by bastnasite, 40% by monazite, and the balance mainly from the ion-adsorbing clay ores found in China. By 2000, the quantity of REO produced from monazite source was less than 5% of the t REO produced from all sources. Ion-adsorption ore provided 23% of world t REO requirement with

bastnasite essentially contributing the remaining 72%. By the end of the decade (2009–2010), when world (137,300 t REO) and China's production (129,400 t REO) were at their peaks, world rare-earth supply came from bastnasite (62.5%), ion-adsorption ore (33%), monazite (2.7%), and other ores (1.8%; Chen 2011; Yang et al. 2013).

In the 1990s, as mentioned earlier, monazite was a declining source of rare earths with production practically coming to a halt in Australia—the principal monazite producer in the world (Hedrick 1997). The declining importance of monazite as a raw material has been due to growing supplies of bastnasite and ion adsorption ores from China and also due to spotlighting of issues associated with the disposal of the radioactive element thorium contained in monazite. There was similarly a decline in the production of xenotime, as well, from the main producer Malaysia. The decreased supply of traditional minerals enhanced the importance of the *other ores* and their contribution to world production of mid and heavy rare earths.

2.8.1 Brazil

In Brazil, there are about a dozen and a half deposits of rare earths, most of them commercially exploitable. Out of these, only four have been known to be operating and two of these were making monazite concentrates. The status of the other projects is not known (Jackson and Christiansen 1993), including the huge niobium–rare earth–phosphorus resource at Araxa, which is now known as a major rare-earth resource outside China (Chen 2011; Gambogi 2011).

Many types of rare-earth deposits occur in Brazil. However, only placers have been mined commercially. A unique situation in Brazil was that the heavy mineral sand mining was conducted primarily for the thorium content of monazite rather than for ilmenite, rutile, or zircon. This is in contrast to the objectives of placer mining in other countries where monazite is considered only as a by-product with ilmenite the primary product.

Monazite was first produced in 1885 in Brazil from beach sand deposits. These deposits occurring over a stretch of 200 km on the southeast coast of Brazil were at places so rich in monazite that their exploitation was possible and actually easily performed using primitive technical resources. Such rich deposits were only a small fraction of total rare-earth occurrence in Brazil, and these were exhausted even before 1950. In 1950, systematic exploitation of sands, which are relatively poorer in monazite and more complex in composition, started. Monazite production continued in the states of Espirito Santo, Parana, and Rio de Janeiro (Hedrick 1985b). Production was also started in the heavy mineral sand deposit at Cumuru-xatiba in Bahia state, where monazite along with ilmenite, rutile, and zircon was recovered. The new projects underway in Brazil included the dredging operation on the Sapucai River, which would be producing 1600 t/year of monazite, equivalent to 900 t/year of REO, and the phosphate mine at Tapira where the rare-earth recovery plant would be producing 253 t/year of REO.

During the nearly 100 years of more or less continuous commercial production, Brazil's annual output seldom exceeded 3300 t REO and remained for the large part at the 1000–2000 t REO level. The rare-earth production in Brazil started

declining significantly in the 1990s. Annual production decreased to below 1000 t in 1990 and became 100 t in 1996. No significant production was reported from 1996 onwards till 2005. Production restarted in 2005, but the output remained in hundreds of metric tons only. Chen (2011) mentions INB (Industries Nucleares do Brazil S/A at Buena Norte) with a capacity of 1500 t/year REO as the important producer.

Technology Metals Research (2014), in its compilation of Advanced Rare Earth Projects on a global level, included the deposits at Araxa and Serra Verde. Chen (2011) included Ptinga deposit as an "under preparation" producer. It is generally believed that in Brazil also, the rare-earth output could be easily raised by a factor of 5, whereas in India, the output could go up by nearly 100%.

2.8.2 India

Mining of Indian beach sand deposits for recovering monazite values started in 1911. Prior to World War II, much of the world rare-earth supply was derived from Indian deposits in addition to Brazilian sources. From the beginning until 1953, world rare earth production did not exceed 5000 t REO per annum. Monazite was the only rare earth mineral mined in any quantity. Monazite mining has been continuing in India for over a hundred years, and annual production levels have remained essentially stable at a few thousand tonnes REO.

Out of the five major rare-earth mineral-bearing placer deposits in India, four are in production and all of these are in coastal areas. The fifth placer, yet unworked, is inland and removed from the necessary infrastructure. Three of the operating projects, Chavara in Kerala, Manavalakurichi in Tamil Nadu, and Chatrapur in Odhisa, are owned by the Government of India, and another project at Chavara is owned by the Government of Kerala. Almost all of the minerals in the beach sands, ilmenite, rutile, zircon, garnet, sillimanite, leucoxene, magnetite, and monazite, are recovered. Currently, the annual REO production in India is about 3000 t (Hedrick 1997). The output could go up by nearly 100%. In fact, Indian Rare Earths Limited has set up a monazite processing plant at Odhisa Sands Complex (OSCOM) to process 10,000 t of monazite (5800 t REO) per annum. Thorium is a by-product along with rare-earth chloride and trisodium phosphate as main products from the plant.

2.8.3 United States

Production of rare earths started in the United States in 1887, 2 years after the beginning of world rare-earth production in Brazil, from placer deposits in Burke County, North Carolina (Overstead et al. 1959) and continued until 1910. Since that time, the only domestic production of monazite has been from placer deposits in Idaho and Florida. The production was not very significant from 1910 until the time of World War II because, during that period, the United States imported almost all the monazites it processed principally from India and Brazil. Due to the war, both India and Brazil had restricted export of monazite, possibly for preserving the nuclear fuel material thorium for their own future energy requirements and also for building

domestic rare earth–processing industries (Kleber and Love 1963). This cutoff of major supplies led to exploration in the United States and to identification and development of several large deposits. The United States emerged as a major producer of rare earths with the discovery and development of the Mountain Pass bastnasite deposit in 1949. Monazite production also restarted in 1948 with the recovery of monazite as a by-product of mining Florida beach sands for titanium minerals and zircon. Since the early 1950s, monazite production was a part of very large-scale operations for the separation of gold and ilmenite. Mining for rutile, garnet, zircon, and other minerals was conducted in the states of California, Colorado, Georgia, Florida, Idaho, and the Carolinas. Later, these operations have been mainly confined to Florida and South Carolina. Up to the end of 1994, monazite was produced in Florida at Green Cove Springs by RGC (US) Minerals Inc., a subsidiary of the Australian company Renison Goldfields Consolidated Ltd. (RGC) as a by-product of ilmenite production from beach sands. The recovery of monazite ceased at the end of 1994 as world demand for radioactive thorium-bearing rare-earth ores decreased primarily due to increased thorium disposal cost.

The United States emerged as the major producer of rare earths with the discovery of the Mountain Pass bastnasite deposit in 1949 and its subsequent development. Mountain Pass began production in 1954. Since then, the Mountain Pass mine has been the most important provider of rare earths in the United States and, until the mid-1980s, the only source of commercial bastnasite in the world. Molycorp, the owner of Mountain Pass Mine, was the world's largest producer of REE from the mid-1960s to the mid-1990s. Molycorp mined bastnasite by open pit methods at Mountain Pass. Mine production at Mountain Pass was ≤10,000 t REO per annum from the start in 1962 till about 1975. Output was over 10,000 t REO between 1975 and 1996, after which it tapered to 5000 t from 1998 onwards till it stopped totally by 2002. In the best of times during 1975–1996, mine output from Mountain Pass exceeded 20,000 t REO, peaking to 25,000 t in 1984 and 22,000 t in 1995. As mentioned earlier, China's output caught up with Mountain Pass in 1992, and things were never the same again.

A few years before mining was stopped at Mountain Pass, the mine had operated below capacity and only intermittently. This has been caused to a certain extent by local environmental and regulatory problems but to a large extent by global rare-earth market factors, which posed a threat to the long-term viability of Mountain Pass as a supplier of REE for high-technology applications. By 1999 and 2000, nearly all (>90%) of separated REE used in the United States was from China's rare-earth resources.

Rare earths were not mined in the United States beginning 2003. The mine and plant at Mountain Pass, California, was kept on care-and-maintenance status. In the second phase of Mountain Pass operations, the shipment of stockpiled concentrates from the property resumed in 2004. In December 2010, Molycorp Inc. resumed mining at its Mountain Pass operation for the first time since 2002 and was preparing to resume milling operations (Gambogi 2011). A two-phase expansion plan was underway that would increase capacity to 19,100 t/year of REOs by year-end 2012 and 40,000 t/year by year-end 2013. After the restart in 2012, production was 800 t REO in 2012 and 4000 t in 2013.

The first US source known to have produced commercial quantities of xenotime is the Marion, North Carolina gold mine (RIC Insight 1990). The mixed heavy mineral sand concentrate produced in the mine contains monazite as its major constituent with lesser amounts of zircon and xenotime. Production started in 1989; however, no continuous production is indicated (Hedrick 1997). Towards the end of the last century, a possible increase in rare-earth production by new sources is linked to the development of the eudialyte deposit at Pajarito, New Mexico, and production of monazite from the placer deposit at Maxville in Florida. Apatite-rich tailings of the iron ore at Mineville, New York, can be developed into a large source of yttrium and other rare earths. In the United States, about 7000 t/year of REO could be recovered from the operating open pit phosphate mines if the producers considered it worthwhile. The United States has the potential to produce about 32,800 t REO per year, which is more than 50% over the average annual production in the best of times.

While some of these sources remain relevant to date for possible augmentation of rare-earth production in the United States, there are many from among the numerous rare-earth reserves in the United States that have been listed as Advanced Rare Earth Projects by analysts (Technology Metals Research 2014) of the rare-earth industry. More of this is given in Section 2.9.

2.8.4 Australia

Australia has been the primary producer of monazite in the world. Regular monazite production started in the country in the late 1940s. Since 1967, Australian beach sand deposits were the major source of supply, and until the late 1980s, Australia continued to dominate, contributing nearly 37% of world monazite output. Australia has been the fourth largest producer of rare earths in the world after China, the United States, and the former Soviet Union (Hedrick 1997). A large quantity of monazite was contained in heavy mineral sand mined in Western Australia, New South Wales, and Queensland. Much of this has been derived from North Stadbroke Island and the beaches from Southport South to New South Wales Border. The heavy mineral fraction of the Queensland and New South Wales deposits contained up to 2% monazite. A total of 265,000 t of monazite has been exported from Australia in the period 1952–1995. Production of monazite from the placer deposits ceased in 1995 (Hoatson et al. 2011).

A major reason for the decrease in monazite production leading to near-zero production from 1995 onwards was the decreasing world acceptance for thorium-bearing rare-earth concentrate, especially when access to thorium-free concentrates from China at competitive rates became possible.

Notwithstanding the status of no rare-earth production till recently, Australia remains one of the world's major sources of REEs from its heavy mineral sands and rare-earth laterite deposits. Worldwide there are many new projects that could start rare-earth production within a few years. The highest number of such projects is in Australia. Many placer and hard-rock projects are pending in Australia (Taylor 1991). One of them is the WIM-150, an inland dredging property. The WIM deposit is potentially a major source of rare-earth minerals; however, these minerals can be recovered only as by-products from the production of titanium minerals and

zircon from this deposit. The development of the WIM-150 deposit poses a number of technical challenges relating to the separation of fine-grained minerals. The projected mining rate of 20 Mt/year of this deposit could result in the production of 12,000 t/year of monazite and potentially up to 3000 t/year of xenotime. The size of this resource is sufficient to support an operation on this scale for more than 30 years (Taylor 1991). Eneabba mineral sand deposit was the principal source of monazite in Australia. In 1991, it was described as a declining source by Taylor (1991), who, however, stated that the development of additional mineral sand reserves in the adjacent Eneabba west deposit could sustain the Eneabba production level in the immediate future. At Eneabba, potential exists for the recovery of substantial quantities of xenotime from existing mineral sand operations. Actual production, however, has been very little because of limited industrial requirements of unprocessed xenotime. New mineral sand projects in Victoria and Western Australia can support increased future production of monazite and xenotime. In addition, there are a number of other potential sources of rare earths, some of them large and/or with attractively high europium and yttrium contents.

Monazite is invariably a constituent of all of placer deposits of heavy mineral sands. The principal potential rare-earth producers are those placer operations where the objective so far has been to recover titanium minerals and discard the other minerals. Recovery of REOs was not carried out in hard-rock operations either. The Olympic Dam multi-metal deposit in South Australia for the production of copper, uranium, and gold is a major resource with a potential operating life of more than 100 years. At the best average scale of operation, the quantity of rare earths mined in the ore may be of the order of 10,000 t/year of REO content. The advantage of this situation is that the rare earths are already being mined, and the major economic minerals will support a long-term operation. Besides, the environmental problems of processing rare-earth ores are circumvented in this operation because it already involves disposal of radioactive wastes. The key factor, however, is the development of technology to economically extract the rare earths from the existing process streams. At the Olympic Dam underground mine, while the potential to produce about 5000 t/year REO as a by-product of uranium recovery exists, there appear to be technocommercial and regulatory issues to resolve.

Mining and processing of the Brockman deposit would lead to coproduction of high-purity alumina, zirconia, yttria/rare-earth concentrate, niobium, and tantalum pentoxide. Although xenotime mineral has not been found, the distribution of yttrium and the REOs in the deposit is similar to the distribution found in xenotime. The minerals in this deposit are very fine grained, and it is not possible to produce a physical concentrate of any of the valuable minerals. All the minerals have to be first obtained in solution and then processed for separation. The feasibility of obtaining the ore in the solution has been demonstrated in a pilot plant. A mining rate of 300,000 t/year has been considered for the deposit. At this rate, the production of REO concentrate would be 450 t/year, which includes 275 t/year of yttrium oxide. The resource is sufficient to support this level of production for over 100 years. The Brockman deposit is a large potential source of yttrium and the other REOs. Current development of the source is hindered by remote location and high processing costs.

Other candidates for development were the Mount Weld rare-earth deposit in Western Australia, with a grade of 26% REO and yttrium, the deposit at Yangibana with a grade of 1.7%, the allanite deposit at Alice Springs at 0.8% REO, and the placer deposit at Cataby, which has a potential for 4000 t/year of monazite (Jackson and Christiansen 1993). In addition, there are a few dedicated resources in Australia that could be developed. These include tailings from the processing of Radium Hill uranium ore at Port Pirie, South Australia, tailings from old uranium extraction operations at Mary Kathleen, Queensland, and a carbonatite deposit at Cummins Range in Western Australia.

Mount Weld is considered one of the richest REE deposits in the world and a major commercially viable rare-earth operation outside China. Mount Weld was originally expected to come online in late 2011, initially producing at 11,000 t/year TREO and ramping up to 22,000 t/year (Hoatson et al. 2011).

Lynas commenced mining in Mount Weld by July 2008 (Lynas Corporation Ltd. 2008, p. 10). The plan was to recover 121,000 t/year of ore, grading 14.8% REO, by open pit methods followed by flotation processing at the Mound Weld site to produce 31,500 t/year of a 40% REO concentrate (Hedrick 2005). The concentrate was to be trucked to the port of Esperance, Western Australia, en route to Shandong Province, China, for processing. The destination was eventually changed to Malaysia.

2.8.5 China

China exceeded the US output to dominate the world supply of REE, starting from 1992. China's rare-earth production crossed the 50% level of world total in 1994, coinciding with the stoppage of monazite production in Australia. China's output kept steadily increasing while the US production remained steady up to 1996 and started tapering off thereafter. It was in 2003 when mine output of rare-earth minerals from the United States stopped completely that China breached the 90% share mark of total world rare-earth production. The contribution from China continued to rise and exceeded 95% in 2005 and has remained in that zone ever since. Mine production was primarily from bastnasite and other rare-earth minerals in Nei Mongol Autonomous Region, Sichuan Province (Mianning), and Weishan in Shangdong Province, and from ion-adsorption ores in Fujian, Guangdong, and Jiangxi Provinces in southeastern China (Gambogi 2011). According to an earlier information (Hedrick 2000), the rare-earth content of the iron ore mined at Baiyun Obo, Inner Mongolia, ranges from 400,000 to 500,000 t/year REO. However, only a portion of this material is processed annually to recover rare earths. There are also reports of China creating a buffer stock of 200,000 t REO from its annual mine output.

Mining has been going on in several rare-earth deposits in China. Apart from the locations mentioned already, placer monazite and xenotime deposits at Guangdong and Hunan provinces were also probably operational. Among all the production centers, the Bayan Obo deposit contributes to the major chunk of Chinese rare-earth production and also supports the frequent large increases in the country's rare-earth production levels.

Mining of the Bayan Obo deposit began in 1957, even though no rare-earth production was reported from China prior to 1980. In the 1980s, China emerged as the

major producer of rare earths. Chinese mine production capacity was about 6000 t REO in 1982 and rose phenomenally to over 20,000 t REO in 1985. Actual rare-earth production itself increased fourfold between 1983 and 1989, from 6000 to 25,220 t REO. Significant new production from 1987 onward was realized from the ion adsorption-type REO deposits of southern China.

Rare-earth production in China remained relatively low during 1990–1992 but started increasing beginning in 1994. In 1994, production was 30,650 t REO, which was 39% more than the 1993 level of 22,100 t REO. The production was mainly from the Bayan Obo mine. There was another sharp increase in rare-earth production between 1994 and 1995. In 1995, China was the leading producer of rare earths, producing a record 48,000 t REO, an increase of about 57% from the previous level. In 1995, production of rare earths at Baotou was 26,905 t REO, while Sichuan Province and Shangdong Province produced 8500 and 963 t REO, respectively. The production of rare earths from ion adsorption-type clays in southern China's provinces of Jiangxi, Guangalong, Hunan, and Fujian was 9770 t REO (Hedrick 1997). The contributions of various mines to the overall Chinese production of rare earths is shown in Figure 2.8.

The significant annual increase in levels continued through 1996–2002, with only a slight decrease from the previous year's level in 1997. Production picked up in 1998 crossing 60,000 t REO, and the production of rare-earth concentrates in China was 70,000 t REO in 1999. By 2000, rare-earth produced from the iron ore mined at Bayan Obo ranged from 40,000 to 50,000 t/year REO, and it usually accounts for the bulk of the frequent increase in the production level as well. Annual levels in 2000 and 2001 were 73,000 t REO, and the figure for 2002 is 75,000 t REO. Regional production in 1997 was as follows: Baotou, Inner Mongolia Autonomous Region 35,000 t REO; Shangdong Province 1200 t REO; Sichuan Province 11,000 t REO; Monazite concentrate production, all regions, 50 t REO; and ion-adsorption clays, all regions, 6000 t (Hedrick 1997).

The Baotou Iron and Steel Company (BISC) is by far the largest and most important rare-earth producer in China. The ore dressing plant of BISC splits the ore from Bayan Obo into two usable fractions—one for rare-earth extraction and the other for iron smelting. Canadian-based Advanced Material Resources Ltd. (AMR), in a joint venture, produces rare earths from bastnasite-bearing carbonatite at Mianning, Sichuan Province. AMR is also involved in rare-earth processing plants at Jiangyin, Jiangsu Province, and Zibo, Shangdong Province. In southern China, the major rare-earth producer is the Zhujiang smelter. The raw materials for this plant are xenotime and monazite from Guangdong placer deposits. Monazite is also available from the Xun Wa and Long Nan mines near Nanchung in Kiangsi. Monazite, which is easily available in southern China, was used as the principal raw material in the Yao Lung chemical plant (Zhang et al. 1982). Alluvial placer deposits of monazite in the Hunan Province were processed by the Taojiang smelter. Ion adsorption-type deposits are processed by the Jiangxi Rare Earth Company, Nanchang Rare Earth, and the Ganjia Rare Earth Company. Ion-adsorption ore of the Xunwu mine is processed by the Jiangnan Rare Earth material.

There are many other placer and ion-adsorption clay deposits in China that could be mined. The Bayan Obo mine accounts for 95% of REO reserves in China with the ion-adsorption ores and other types representing 3% and 2%, respectively. While

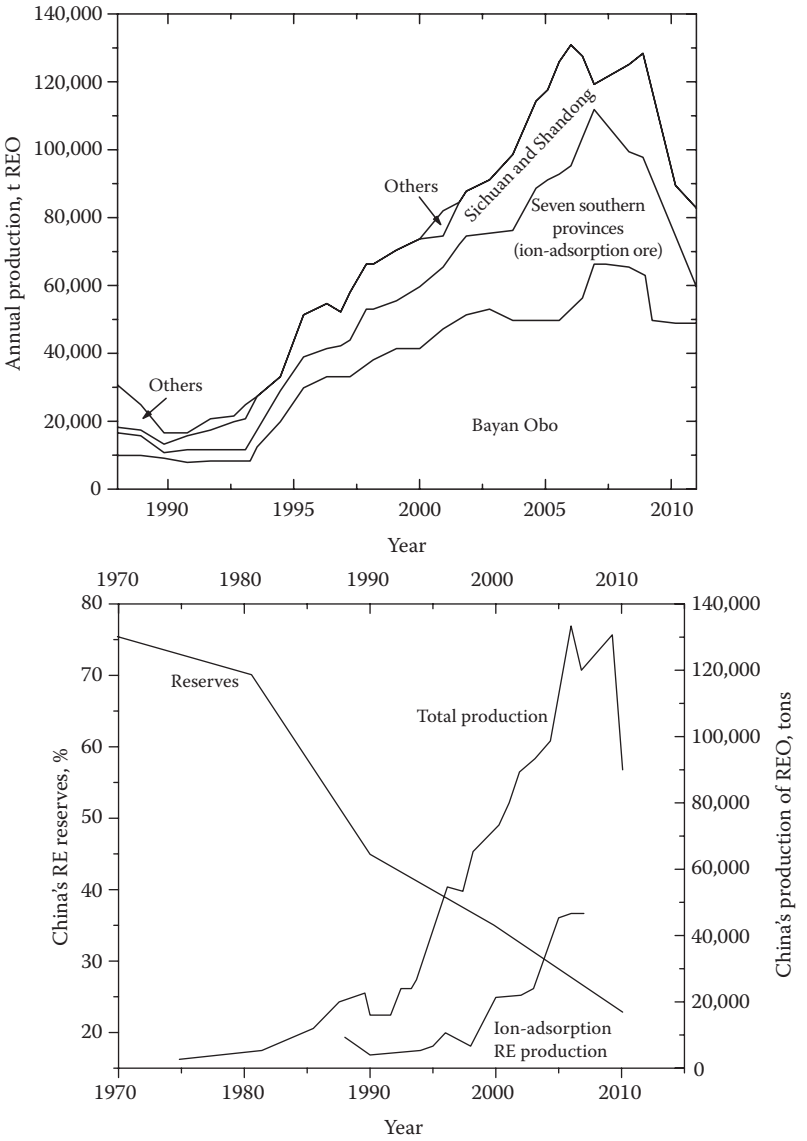


FIGURE 2.8 China's rare-earth reserves and components of production. (From Wubbeke, J., *Resources Policy*, 38: 384–394, 2013; Yang, X. J. et al., *Environmental Development*, 8(October): 131–136, 2013.)

the Bayan Obo mine is essentially a producer of light rare earths, the ion-adsorption ores are basically producers of both light and heavy rare earths. This factor can have a bearing on the production starting on these new projects. China could undoubtedly produce more REO than is reported, for example, by successfully treating Bayan Obo steel slag (Figure 2.8).

2.8.6 Former Soviet Union

The former Soviet Union is a major producer of rare earths and ranked fourth in the world in terms of annual rare-earth output, after China, the United States, and India. Annual production that used to be in the range of over 8000 t REO until the early 1990s decreased to the 2000 t REO/year level by 1994 and has remained so ever since.

The important sources of rare earths in the former Soviet Union are titanoniobates (loparite ore), phosphorites (apatites, monazite, and bone relics), and fluocarbonates (yttrosynchisite). Mine production of rare earths in Russia is essentially from loparite, which is recovered from the central Kola Peninsula's Lovozero Alkali Massif. Up to 6500 t equivalent REO has been mined annually from this source (Hedrick et al. 2007). Rare earths were first derived from loparite in 1934, and commercial mining of loparite started in 1951 at the Karnasurtsk mine of the Lovosersk Enrichment Works, Murmansk Province (Oblast). Later, production was at the Lovosersk Mining and Benefication Complex near Revda, Murmansk (Hedrick et al. 1997). Loparite mined from the Kola Peninsula was treated at the Irtysh Chemical Metallurgical Plant in east Kazakhstan, the largest rare-earth plant in the former Soviet Union, and the Sillamae Chemical Metallurgical United Works in Estonia. The Sillamae plant started to process loparite ore producing tantalum and niobium in 1970. Later it also started to extract rare-earth-metal oxides. The loparite deposit (at Lovozero, Murmanssk) was operated by AO Sevredmet's Lovozero Mining Combine until March 2000 and thereafter by the new public company Lovozero Mining Company (LMC). LMC operated the Umbrozero mining facility to produce loparite concentrate. The projected output from the concentrator was 5150 t/year of rare-earth carbonates (96% of Russian demand). LMC ships loparite concentrate for further processing to Solikamsk and then on for further refining and separation to Estonia, Kazakhstan, and Kyrgyzstan (Hedrick 2001). Solikamsk Magnesium Works (SMZ) has been producing rare-earth chlorides and carbonates from loparite concentrate, equivalent to 3000–4000 t of REO (Hedrick 2002, 2003). Presently, SMZ is the only consumer of loparite concentrate (Hedrick 2002).

Uraniferous phosphates are mined at Schevchenko in Kazakhstan. They are rich not only in the yttrium earths (14.2% Y_2O_3) but also in the middle elements (0.6% Eu_2O_3). The concentration of rare earths in the ore is, however, limited (0.7%). Rare earths are recovered concomitantly with phosphorus (25% P_2O_5 is the content in the ore) and uranium (0.16%). In the CIS, uraniferous phosphates have been providing over 50% of the yttrium oxide and 80% europium oxide. The production of rare earths is strongly tied to the demand and hence production of uranium from these resources (Kosynkhin et al. 1993).

The yttrosynchisite ore was mined from the Kutessaisk deposit. The deposit does not contain any valuable components other than the rare earths. The ore was treated at the Kirgiz works. The REO in the concentrate reaches 40–50%, and the yttrium content in the rare earths reaches 30–35%. However, the europium content was no more than 0.1%. The deposit was worked mainly for yttrium and is probably exhausted (Kosynkin et al. 1993).

The other rare-earth sources in the country are apatite and monazite. In the former Soviet Union, a considerable quantity of monazite occurs, possibly at Samotkanskii, and is probably produced, but no production data are available. Monazite from the Novotroitsk deposit has been processed in CIS for a long time (Kosynkhin et al. 1993). The REOs comprise 56% thorium oxide 8%, and phosphorus oxide 25.2%. Annual production figures have not been available.

The status of apatite is similar. The recovery of rare earths from apatite of the Kola Peninsula is likely to gain importance as these ores are a potential source of yttrium and europium. Commercial quantities of rare-earth products have been recovered in Russian Federation mainly from apatite.

Apart from the six major rare earth–producing countries mentioned above, world rare-earth production is contributed by South Africa, Canada, Malaysia, Thailand, Sri Lanka, Zaire, and Madagascar (Hedrick 1997; Jackson and Christiansen 1993).

2.8.7 South Africa

A hard-rock vein deposit, discovered in 1950 at Van Rhynsdorp (Steenkampskrall) in the Republic of South Africa, remained a major source of monazite for the decade 1953–1963, operated by Anglo American plc mine. Great Western Minerals Group Ltd. (GWMG) had plans to recommission the abandoned mine in the Western Cape (Gambogi and Cordier 2010). A certain amount of rare earths was also recovered from the Witwatersrand uranium deposit in South Africa (Highley et al. 1988). At Buffalo, fluorspar monazite occurs in association with fluorite and apatite; at the Phalaborwa complex, apatite is rare earth bearing; and Richards Bay placer deposit contains monazite. Although all three mines were operating, monazite was not recovered either at Buffalo fluorspar or at Phalaborwa. Only Richards Bay was recovering a monazite by-product. Richards Bay is a major beach dredging operation producing zircon and the second leading producer of heavy mineral sands in the world in 2003 from its Richards Bay Mine (RBM). RBM did not produce monazite in 2003 (Hedrick 2003).

In fact, South Africa has the greatest potential for REO production. As compared to an actual annual production of about 400 t REO, South Africa could produce about 41,300 t/year. This would be an increase of approximately 100 times its present production.

2.8.8 Canada

In Canada, rare earths have been produced as a by-product of uranium mining at Elliot Lake. A rare-earth recovery plant was in operation intermittently between 1967 and 1978 and, after modernization, has been in operation since 1986 at the Denison Mines, Elliot Lake, Ontario, for the recovery of yttrium and heavy rare earths from uranium leach solutions (Hedrick 1985b). In 1988, nearly 100 t of contained Y_2O_3 was produced from the source (Robjohns 1989). No significant production was reported in the 1990s (Hedrick 1995). Similarly, Canadian underground uranium mines have the potential for producing 610 t/year of REO but actually produce only about 150 t/year.

A possibility exists for rare-earth production in Canada by development of the Strange Lake deposit. This deposit, developed for its beryllium content, would yield about 4700 t/year of REO as a by-product (Jackson and Christiansen 1993).

2.8.9 Malaysia

Malaysia has been a rare-earth producer since the late 1940s. Monazite and more particularly xenotime have been obtained as by-products of placer cassiterite mining. Placer cassiterite deposits at Perak have been worked by Beh minerals/Mitsubishi Chemical Industries Ltd. for monazite and xenotime production. Deposits at Perak and at Selangor, west Malaysia, have been mined to produce monazite and xenotime. The annual mine production of monazite and xenotime during the best of times in Malaysia is given in Table 2.20. Annual production of rare earths in Malaysia, which was only 187 t REO in 1983, increased to 2563 t REO in 1984 and to 3300 t REO in 1985. Production remained steady until 1989, decreased to 1830 t REO in 1990, 1090 t REO in 1991, 427 t REO in 1992, and down to 224 t REO in 1993. The declining production was to culminate in the closure of the Asian Rare Earth Sdn. Btd. Plant in Ipoh, Perak State, in the face of overwhelming competition from China (*Mining Journal* 1994).

Australian company Lynas Corporation Ltd. shifted the location of its rare-earth separation plant from its original site in China to a new location in Malaysia. The site is located on the east coast of Malaysia at Kemaman, Terengganu. The separation plant would process rare-earth concentrate produced from Lynas's rare-earth deposit at Mount Weld. Lynas neared completion of its processing plant near Kuantan with an initial capacity of 11,000 t/year of REO. The REO capacity at Kuantan was being expanded to 22,000 t/year (Gambogi 2011).

2.8.10 Thailand

In Thailand, monazite and xenotime were recovered as by-products from alluvial tin mining and offshore tin dredging. Approximately 80–90% of the country's production of tin concentrates is from the Thai Peninsula (Pungrassami and Sanguansai 1991). From 1971 to 1989, the total production of monazite and xenotime in Thailand was 6400 and 655 t, respectively. Almost 99% of this production was from the Thai Peninsula. Monazite is produced mainly from deposits of Changwat Phuket, Phangnga, Ranong, Surat Thani, Chumphon, and Prachuap Khirikhan. Xenotime is produced mainly from deposits at Changwat Phuket, Phangnga, Ranong Trang, and Prachuap Khirikhan.

Annual production was less than 100 t REO in 1983 but was about 150 t REO during 1984–1986, and it increased to a steady 800 t REO between 1987 and 1989. Production decreased to about 230 t REO beginning in 1990 (Hedrick 1997).

2.8.11 Sri Lanka

In Sri Lanka, there is one placer deposit of heavy minerals in Pulmoddai, and this is an operating monazite property that produces monazite concentrate. Monazite is

recovered as a by-product during the processing and recovery of ilmenite, rutile, and zircon from this deposit. Production has been going on for many years at a modest level of about 110 t of REO per annum. Production was approximately three times this quantity in 1989. Production could be stepped up to 500 t REO per year (Jackson and Christiansen 1993).

2.8.12 Zaire and Madagascar

Zaire and Madagascar are the two countries reporting rare-earth production in small quantities. Monazite is produced in Zaire, and both monazite and bastnasite are produced in Madagascar (Jackson and Christiansen 1993).

In addition to the countries mentioned above, rare-earth minerals are probably produced in Indonesia, North Korea, Mozambique, and Vietnam, even though the regularity and extents are unknown. The Congolone beach placer in Mozambique was considered a monazite deposit that could begin production immediately (Jackson and Christiansen 1993).

2.9 SCENARIO FOR THE IMMEDIATE FUTURE

As it has developed, the technology-supported lifestyle of people in industrialized and prosperous countries is critically dependent on the rare earths, and so is the technology-enhanced life of the rapidly growing number of people in large developing economies. A remarkably elegant and overtly plain summary (Lifton and Hatch 2012) of the underlying reasons for such a status of rare earths was provided by Jack Lifton as follows, "The key factor to keep in mind when considering the importance of the rare earths is that their electronic properties have made possible the miniaturization of devices, which are able to convert motion into electricity; electricity into motion; electricity into light of all visible wavelengths; electricity into sound; and electricity into devices that absorb heat from their surroundings." It should be added here that for the performance of these functions, the rare earths are largely unsubstitutable by any other material or group of materials, and any attempt to substitute attracts performance and/or cost penalty.

Lifton (2013) also remarked that the supply of rare earths will shape the demand for them. Arguments can be advanced supporting this point of view, and instances can be listed where this assertion does not seem to be operating. The disposition of rare earths in the natural resources and the manner in which the individual rare earths are distributed in the ore deposits may force this situation in a way. Rare earths that are less abundant and more difficult to prepare are also the least used and the most abundant and readily produced rare earth, e.g., cerium is also the most used. According to a forecast, cerium demand would exceed its availability (Bruno 2013). Later, Kingsnorth observed, in apparent agreement with Lifton (on supply shaping the demand), that while cerium would continue to be in oversupply, the surplus of cerium would be diminishing in the later years because increased availability of reasonably priced cerium will drive new applications. Lanthanum is the second most available rare earth after cerium. It has similar production-demand situation like cerium. As regards lanthanum, two developments can push its future demand

to match production (default) or even past it. One is the status of NiMH batteries for automotive applications (including traction) vis-à-vis the Li-ion batteries. After all, the Li batteries may not obliterate the chances of NiMH in large device applications, at least not so fast as it was forecast some time back, mainly because of safety-related issues. Another development that could translate to increased and sustained demand for lanthanum is the La use in FCC to match the growth of heavy crude oil refining and in heavy shale oil production. An increase in the rare-earth content of ultrastable Y-zeolite (by rare-earth ion exchange) has been proposed as a means to increase the activity of Y-zeolite with high silica content (Groenenboom and Wieringa 1989). By weight, the REO content of REHY zeolite could increase to about 6–16% and of REY zeolite to about 8–20%. Primary processing of any rare-earth resources seeking neodymium, europium, or dysprosium ensures a concomitant supply of cerium and also lanthanum. The status as regards samarium and europium is different. Here, except for a brief period of sustained demand for samarium particularly as a material for the newly discovered high-performance magnets ($SmCo_5$ and Sm_2Co_{17}) in the 1970s and early 1980s, demand has not been tracking supply. For europium, a less abundant rare earth, demand has generally exceeded supply. It does seem that due to the interplay of a variety of technocommercial factors, in general, supply shaping demand would be more operational in the future than in the past for most of the rare earths.

Dysprosium is widely regarded as the foremost among the critical rare earths that will enable and sustain worldwide green technology initiatives. While mentioning several apparently unsolvable constraints in the continued and enhanced supply of dysprosium from primary sources, Gareth Hatch of TMR (Bruno 2013) foresees dependency on dysprosium to be kept in control through technology solutions in addition to improving the Dy recovery technologies at the head-end operations of the overall processing scheme. He has listed the following possibilities. Design changes (i) in the microstructure of the material: Nd–Fe–B magnet grades that require less Dy to do the same job as conventional grades, because of the way that the Dy is put into the magnet material, via grain-boundary diffusion processes; (ii) the use of polymer-bonded magnet material grades (most notably produced by Molycorp Magnequench and Aichi Steel) that require no Dy at all, and yet that can still operate at reasonably significant temperatures, because of the advanced microstructure that develops in such materials; and (iii) in the devices: figuring out ways to reduce the temperatures and/or magnitude of demagnetizing fields that magnets experience and hence the use of grades that contain less Dy. As a likely outcome in such a scenario based on improved economics in Nd–Fe–B magnets, there would be a broader usage of the magnets and potential increases in demand from the market as a whole for Nd + Pr.

The key components of the projected increase in RE demand up to the year 2016 are neodymium, dysprosium, europium, and cerium, all of which are essential for automation technology as well as polishing powders, FCC catalysts, wind turbines, and hybrid vehicles. Incidentally, the familiar picture of higher demand than supply for neodymium, terbium, dysprosium, europium, and yttrium is enlarged to include the elements cerium and lanthanum for which supply usually exceeded consumption in the past. With such selection of individual rare-earth elements for drivers of

global rare-earth demand in the immediate future, all known rare-earth mineral reserves remain in contention with focus shifting to reliability and continuity of supply, and alternatives to resources that are important as of now but may not last very long.

Commenting on the demand–supply and prices of rare earths, Dudley Kingsnorth, in a presentation at the AusIMM 2013 Critical Minerals Conference in Perth, Australia (Bruno 2013), suggested that global demand could increase to 160,000 tons in 2016 rising further to 200,000–240,000 tons in 2020 vis-à-vis 110,000 tons in 2012 and the historical high of 133,000 tons two years earlier, in 2010. This view is probably shared by other forecasters and analysts. As regards the supply, Kingsnorth (Bruno 2013) summarized it as follows. In 2009, China produced about 120,000 tons (another 35,000 tons, unregulated), accounting for 95% of the global market. The forecast demand for 2016 of 160,000 t REO (60–65% China) would be matched by a supply of 180,000–210,000 t REO (60–65% China). Rare-earth production could well be 240,000–280,000 t by 2020. The real supply of critically needed rare earths will only be slightly more than half of this tonnage and the rest would be cerium.

The ROW supply would remain very limited. The demand in 2020 will be 200,000–240,000 t REO (60–65% China) and supply 240,000–280,000 t REO. As regards the ROW supply from new deposits coming on line, Kingsnorth (Bruno 2013) reminded that after project commitment, both Lynas and Molycorp, with a background of over 50 years technology experience in rare earths, required at least three years for completing construction and start-up. Hence, another major light rare-earth project in production may not happen earlier than in 2017/2018. Latent capacity and robust technology backup will ensure that Mountain Pass and Mt. Weld will be the major ROW producers for the foreseeable future. Given the ongoing requirement for supply diversity, Kingsnorth summed up that there is unlikely to be more than one new ROW producer for light rare earth in production in 2020.

In the matter of heavy rare earths, China does not have any hard-rock deposits with economically recoverable heavy rare earths but relies on the only resource available in the world today, for terbium, dysprosium, and yttrium—the extremely inefficient and costly-to-process ion-adsorbed clays. As regards, europium, Lifton (2013) anticipates that it is not in short supply and will get less likely to be, even if its new production is limited to just China. As regards the ROW situation on heavy rare earths, it is apparent that resource ownership and technology background are usually not with the same company. Viability of the early (2016/2017) production start-up is thus dependent upon a small project with proven reserves teaming up with the appropriate technology partner. It is entirely possible and seems likely to happen that, by applying realistic techno-economic filters, there will be, in the latter part of this decade, no more than seven or eight ROW major rare-earth producers—i.e., the fruition rate of the large number of *potential* new projects listed by TMR will be in the range of 1–2%.

A variety of forecasts with different types of detailing have been made by analysts, rare-earth industry watchers, as well as by staff analysts of major institutions. An extensive listing of future relevant projects was compiled by TMR and updated periodically (Technology Metals Research 2014, http://www.techmetalsresearch.com/metrics-indices/tmr-advanced-rare-earth-projects-index/). The TMR listed

projects relate, on a global level, to resources that have been formally defined as a mineral resource or reserve under the parameters of codes such as NI 43-101, the JORC, or the SAMREC. The TMR Advanced Rare-Earth Projects Index, as updated on October 2014, consists of 57 rare-earth mineral resources, associated with 51 advanced rare-earth projects and 49 companies, and located in 34 regions within 16 countries. Information from the index is summarized in Table 2.21.

The development route of a rare-earth project, wherein a mineral deposit metamorphoses to a profitably operating mine, happens to be a long winding road with many milestones to pass and many decision points to tackle. The process, sufficiently complicated as it is, has become still more challenging in the present regulatory environment, which is becoming less forgiving as we move into the future. Long et al. (2010) remind us that the last REE deposit discovered and developed into a mine in the United States was the Mountain Pass mine in California. It was discovered in 1949 and put into production in 1953. Such remarkable speed was possible more than 50 years ago. It is not indicative of the time required to discover and develop REE deposits in today's regulatory climate. Besides, some of the major deposits scheduled to commence production by 2015 such as the Nechalacho deposit in the Northwest Territories (Canada) and Kvanefjeld (Greenland) will involve minerals and ore compositions that have never been successfully processed, and a great deal of industrial and academic research will be required to quickly bridge this knowledge gap.

Presently, there is actually no usable REE exploration and development record to draw upon for assessing the future pace of discovery and development, because, in the past 50 years, outside of China, there has been little REE exploration and almost no mine development. Long et al. (2010) have proceeded to describe the issues and processes involved in the development of a REE mine. This point is also addressed by analysts and forecasters in the rare-earth industry. The development phase of major REE deposits (from a JORC-compliant resource to commencement of production) is graphically depicted in Figure 2.9.

Chen (2011) counted that about six countries can provide the world with rare-earth products, citing data based on the 2009 USGS report and a report from the Ministry of Industry and Information Technology of China. With about 94% of the world supplies provided by China, 6% was contributed by Russia and Estonia, United States, India, Malaysia, and Brazil. It is important to note that this is the time period when China's export quota restrictions had not been announced, and the countries mentioned most probably did not have a premonition that such restrictions were coming so soon. In other words, these are the countries that would be producing rare earths irrespective of the stance of China. They should be counted as stable and *permanent* rare-earth producers. Incidentally, all of them are home to some of the largest rare-earth deposits.

Chen (2011) mentioned that out of a total of about 200 projects on rare-earth exploration, under preparation and exploitation, about 25 projects are promising to be the competitors of future multisupply. The status of these 25 projects is summarized in Table 2.22. Eight of them are former producers, seven companies are under preparation, and 10 projects are in the stage of exploration. The most promising among the non-China producers, which could get into production at the earliest, are Molycorp, Lynas, Simelt of Estonia, Great Western Group, and three Japanese joint

TABLE 2.21
Advanced Rare Earth Projects

Project, Owner, MR (Mt)	Grade of *In Situ* Rare-Earth Oxides (wt.%), Quantity of REO Available in the Deposit (kt)															
	La_2O_3	CeO_2	Pr_6O_{11}	Nd_2O_3	Sm_2O_3	Eu_2O_3	Gd_2O_3	Tb_4O_7	Dy_2O_3	Ho_2O_3	Er_2O_3	Tm_2O_3	Yb_2O_3	Lu_2O_3	Y_2O_3	TREO
Australia																
Browns Range, Northern Minerals Limited, 6.5	0.018	0.044	0.006	0.028	0.016	0.003	0.042	0.009	0.062	0.014	0.039	0.006	0.032	0.004	0.416	0.742
	1.17	2.86	0.39	1.82	1.04	0.20	2.73	0.59	4.03	0.91	2.54	0.39	2.08	0.26	2.70	48.23
Charley Creek (JV), Crossland Strategic Metals Ltd., 805.3	0.005	0.011	0.001	0.004	0.001	0.000	0.001	0.000	0.001	0.000	0.000	0.000	0.000	0.000	0.004	0.029
	40.26	88.58	8.05	32.21	8.05	0	8.05	0	8.05	0	0	0	0	0	32.21	233.54
Clay-Howells, Pancontinental Uranium Corporation, 805.3	0.005	0.011	0.001	0.004	0.001	0.000	0.001	0.000	0.001	0.000	0.000	0.000	0.000	0.000	0.004	0.029
	40.27	88.58	8.05	32.21	8.05	0	8.05	0	8.05	0	0	0	0	0	32.21	233.54
Cummins Range, Navigator Resources Limited, 4.9	0.468	0.814	0.084	0.273	0.033	0.006	0.020	0.000	0.009	0.000	0.001	0.000	0.000	0.000	0.034	1.740
	22.93	39.89	4.12	13.38	1.62	0.29	0.98	0	0.44	0	0.05	0	0	0	1.67	85.26
Dubbo Zirconia Project, Alkane Resources Ltd., 73.2	0.174	0.328	0.036	0.126	0.019	0.001	0.019	0.003	0.018	0.003	0.010	0.001	0.009	0.001	0.141	0.890
	127.37	240.10	26.35	92.23	13.91	0.73	13.91	2.20	13.18	2.20	7.32	0.73	6.59	0.73	103.21	651.48
Hastings, Hastings Rare Metals Limited, 36.2	0.003	0.013	0.002	0.007	0.005	0.000	0.007	0.002	0.019	0.004	0.017	0.002	0.014	0.002	0.112	0.210
	1.09	4.71	0.73	2.53	1.81	0	2.53	0.72	6.88	1.45	6.15	0.72	5.07	0.72	40.54	76.02
Milo, GBM Resources Ltd., 187.0	0.015	0.026	0.002	0.008	0.001	0.000	0.001	0.000	0.001	0.000	0.001	0.000	0.001	0.000	0.005	0.062
	28.05	48.62	3.74	14.96	1.87	0	1.87	0	1.87	0	1.87	0	1.87	0	9.35	115.94
Mount Weld CLD, Lynas Corporation Ltd., 14.9	2.323	4.625	0.502	1.764	0.237	0.052	0.106	0.009	0.024	0.003	0.006	0.001	0.003	0.000	0.074	9.729
	346.13	689.13	74.80	262.84	35.31	7.75	15.80	1.34	3.58	0.45	0.89	0.15	0.45	0	11.03	1449.62
Mount Weld Duncan, Lynas Corporation Ltd., 9.0	1.202	1.904	0.230	0.865	0.137	0.037	0.096	0.013	0.061	0.009	0.020	0.002	0.009	0.001	0.250	4.837
	108.18	171.36	20.70	77.85	12.33	3.33	8.64	1.17	5.49	0.81	1.80	0.18	0.81	0.09	22.50	435,330
Nolans, Arafura Resources Ltd., 47.2	0.501	1.277	0.155	0.539	0.060	0.010	0.026	0.002	0.008	0.001	0.002	0.000	0.001	0.000	0.035	2.620
	236.47	602.74	73.16	254.41	28.32	4.72	12.27	0.94	3.78	0.47	0.94	0	0.47	0	16.52	1236.64

(*Continued*)

TABLE 2.21 (CONTINUED)
Advanced Rare Earth Projects

Project, Owner, MR (Mt)	Grade of *In Situ* Rare-Earth Oxides (wt.%), Quantity of REO Available in the Deposit (kt)															
	La_2O_3	CeO_2	Pr_6O_{11}	Nd_2O_3	Sm_2O_3	Eu_2O_3	Gd_2O_3	Tb_4O_7	Dy_2O_3	Ho_2O_3	Er_2O_3	Tm_2O_3	Yb_2O_3	Lu_2O_3	Y_2O_3	TREO
Brazil																
Araxá, MBAC Fertilizer Corp, 28.3	1.180	2.079	0.191	0.583	0.063	0.014	0.029	0.003	0.012	0.002	0.003	0.000	0.002	0.000	0.047	4.208
	333.94	588.36	54.05	164.99	17.83	3.96	8.21	0.85	3.40	0.57	0.85	0	0.57	0	13.30	1190.86
Serra Verde, Mining Ventures Brasil Ltda., 412.0	0.035	0.055	0.007	0.021	0.004	0.000	0.003	0.001	0.003	0.001	0.002	0.000	0.002	0.000	0.025	0.159
	144.20	226.60	28.84	86.52	16.48	0	12.36	4.12	12.36	4.12	8.24	0	8.24	0	103.00	655.08
Canada																
Ashram Main, Commerce Resources Corp., 239.7	0.495	0.884	0.091	0.314	0.039	0.009	0.021	0.002	0.008	0.001	0.002	0.000	0.001	0.000	0.030	1.898
	1186.52	2118.95	218.13	752.66	93.48	21.58	50.34	4.79	19.18	2.40	4.79	0	2.40	0	71.91	4549.51
Ashram MHREO, Commerce Resources Corp., 9.4	0.351	0.702	0.080	0.300	0.047	0.012	0.031	0.004	0.015	0.002	0.004	0.001	0.003	0.000	0.062	1.614
	32.99	65.99	7.52	28.20	4.42	1.13	2.91	0.38	1.41	0.19	0.38	0.09	0.28	0	5.83	151.72
Buckton, DNI Metals Inc., 3433.5	0.005	0.008	0.001	0.004	0.001	0.000	0.001	0.000	0.001	0.000	0.000	0.000	0.000	0.000	0.004	0.026
	171.68	274.68	34.34	137.34	34.34	0	34.34	0	34.34	0	0	0	0	0	137.34	892.71
Buckton South, DNI Metals Inc., 496.7	0.005	0.009	0.001	0.004	0.001	0.000	0.001	0.000	0.001	0.000	0.000	0.000	0.000	0.000	0.004	0.026
	24.84	44.70	4.97	19.87	4.97	0	4.97	0	4.97	0	0	0	0	0	19.87	129.14
Clay-Howells, Canada Rare Earth Corp., 8.5	0.183	0.318	0.032	0.110	0.017	0.004	0.011	0.004	0.007	0.001	0.003	0.000	0.003	0.000	0.036	0.729
	1473.70	2560.85	257.70	885.83	136.90	32.21	88.58	32.21	56.37	8.05	24.16	0	24.16	0	289.91	5870.64
Eco Ridge, Pele Mountain Resources Inc., 59.3	0.037	0.071	0.007	0.023	0.004	0.000	0.003	0.000	0.002	0.000	0.001	0.000	0.001	0.000	0.008	0.157
	21.94	42.10	4.15	13.64	2.37	0	1.78	0	1.19	0	0.59	0	0.59	0	4.74	93.10
Elliot Lake Teasdale, Appia Energy Corp., 51.6	0.048	0.088	0.009	0.028	0.005	0.000	0.003	0.000	0.002	0.000	0.001	0.000	0.001	0.000	0.007	0.190
	24.77	45.41	4.64	14.45	2.58	0	1.55	0	1.03	0	0.52	0	0.52	0	3.61	98.04

(*Continued*)

TABLE 2.21 (CONTINUED)
Advanced Rare Earth Projects

Project, Owner, MR (Mt)	Grade of *In Situ* Rare-Earth Oxides (wt.%), Quantity of REO Available in the Deposit (kt)															
	La_2O_3	CeO_2	Pr_6O_{11}	Nd_2O_3	Sm_2O_3	Eu_2O_3	Gd_2O_3	Tb_4O_7	Dy_2O_3	Ho_2O_3	Er_2O_3	Tm_2O_3	Yb_2O_3	Lu_2O_3	Y_2O_3	TREO
Canada																
Foxtrot, Search Minerals Inc., 14.4	0.183	0.390	0.044	0.160	0.029	0.001	0.023	0.004	0.021	0.004	0.012	0.002	0.010	0.002	0.129	1.014
	26.35	56.16	6.34	23.04	4.18	0.14	3.31	0.58	3.02	0.58	1.73	0.29	1.44	0.29	18.58	146.02
Grande-Vallée, Orbite Aluminae Inc., 1209.6	0.009	0.019	0.002	0.009	0.002	0.000	0.001	0.000	0.001	0.000	0.001	0.000	0.001	0.000	0.006	0.050
	108.87	229.82	24.19	108.87	24.19	0	12.10	0	12.10	0	12.10	0	12.10	0	72.58	604.80
Hoidas Lake (JV), Great Western Minerals Group Ltd., 2.8	0.491	1.120	0.143	0.494	0.065	0.013	0.030	0.003	0.008	0.000	0.006	0.000	0.001	0.000	0.028	2.402
	13.75	31.36	4.00	13.83	1.82	0.36	0.84	0.08	0.22	0	0.17	0	0.03	0	0.78	67.26
Hoidas Lake (JV), Star Minerals Group Ltd., 2.8	0.491	1.120	0.143	0.494	0.065	0.013	0.030	0.003	0.008	0.000	0.006	0.000	0.001	0.000	0.028	2.402
	13.75	31.36	4.00	13.83	1.82	0.36	0.84	0.08	0.22	0	0.17	0	0.03	0	0.78	67.26
Kipawa (JV), Matamec Explorations Inc., 27.1	0.057	0.116	0.014	0.053	0.012	0.001	0.012	0.002	0.014	0.003	0.010	0.001	0.010	0.001	0.089	0.395
	15.45	31.44	3.80	14.36	3.25	0.27	3.25	0.54	3.79	0.81	2.71	0.27	2.71	0.27	24.12	107.05
Kipawa (JV), Toyota Tsusho Corp, 27.1	0.057	0.116	0.014	0.053	0.012	0.001	0.012	0.002	0.014	0.003	0.010	0.001	0.010	0.001	0.089	0.395
	15.45	31.44	3.80	14.36	3.25	0.27	3.25	0.54	3.79	0.81	2.71	0.27	2.71	0.27	24.12	107.05
Lavergne-Springer, Canada Rare Earth Corp., 16.9	0.311	0.536	0.055	0.185	0.022	0.005	0.012	0.001	0.005	0.001	0.002	0.000	0.001	0.000	0.026	1.163
	52.56	90.58	9.30	31.27	3.72	0.85	2.03	0.17	0.85	0.17	0.34	0	0.17	0	4.40	196.55
Montviel, Geomega Resources Inc., 250.6	0.372	0.716	0.075	0.242	0.025	0.005	0.008	0.001	0.002	0.000	0.001	0.000	0.000	0.000	0.007	1.455
	932.23	1794.30	187.95	606.45	62.65	12.53	20.05	2.51	5.01	0	2.51	0	0	0	17.54	3646.23
Nechalacho Basal, Avalon Rare Metals Inc.,_125.7	0.232	0.520	0.066	0.259	0.055	0.007	0.049	0.007	0.037	0.007	0.016	0.002	0.013	0.002	0.159	1.431
	291.62	653.64	82.96	325.56	69.14	8.80	61.59	8.80	46.51	8.80	20.11	2.51	16.34	2.51	199.86	1798.77

(*Continued*)

TABLE 2.21 (CONTINUED)
Advanced Rare Earth Projects

Project, Owner, MR (Mt)	Grade of *In Situ* Rare-Earth Oxides (wt.%), Quantity of REO Available in the Deposit (kt)															
	La_2O_3	CeO_2	Pr_6O_{11}	Nd_2O_3	Sm_2O_3	Eu_2O_3	Gd_2O_3	Tb_4O_7	Dy_2O_3	Ho_2O_3	Er_2O_3	Tm_2O_3	Yb_2O_3	Lu_2O_3	Y_2O_3	TREO
Canada																
Nechalacho Upper, Avalon Rare Metals Inc., 177.7	0.243	0.566	0.068	0.266	0.049	0.005	0.036	0.004	0.015	0.002	0.005	0.001	0.004	0.001	0.060	1.324
	431.81	1005.78	120.84	472.68	87.07	8.89	63.97	7.11	26.66	3.55	8.89	1.78	7.11	1.78	106.62	2352.75
Niobec, IAMGOLD Corporation, 1058.6	0.425	0.830	0.092	0.321	0.036	0.007	0.017	0.001	0.005	0.000	0.000	0.000	0.000	0.000	0.000	1.735
	4499.05	8786.38	973.91	3398.11	381.10	74.10	179.96	10.59	52.93	0	0	0	0	0	0	18,366.70
Strange Lake Enriched, Quest Rare Minerals Ltd., 20.0	0.150	0.360	0.039	0.140	0.036	0.002	0.039	0.009	0.066	0.015	0.049	0.008	0.051	0.007	0.470	1.441
	30.00	72.00	7.80	28.00	7.20	0.40	7.80	1.80	13.20	3.00	9.80	1.60	10.20	1.40	94.00	288.20
Strange Lake Granite, Quest Rare Minerals Ltd., 472.5	0.120	0.270	0.030	0.110	0.024	0.001	0.023	0.005	0.030	0.007	0.021	0.003	0.021	0.003	0.206	0.872
	567.00	1275.75	141.75	519.75	113.40	4.73	108.68	23.63	141.75	33.08	99.23	14.18	99.23	14.18	973.36	4120.20
Two Tom, Canada Rare Earth Corp., 40.6	0.288	0.544	0.056	0.188	0.032	0.003	0.019	0.002	0.008	0.001	0.002	0.000	0.001	0.000	0.038	1.182
	116.93	220.86	22.74	76.33	12.99	1.22	7.71	0.81	3.25	0.41	0.81	0	0.41	0	15.43	479.89
Germany																
Storkwitz, Seltenerden Storkwitz AG, 4.5	0.124	0.220	0.023	0.064	0.006	0.001	0.005	0.001	0.001	0.000	0.001	0.000	0.001	0.000	0.006	0.452
	5.58	9.90	1.04	2.88	0.27	0.05	0.23	0.05	0.05	0	0.05	0	0.05	0	0.27	20.34
Greenland																
Kvanefjeld, Greenland Minerals and Energy Ltd., 619.0	0.291	0.444	0.044	0.136	0.017	0.001	0.012	0.002	0.012	0.002	0.006	0.001	0.005	0.002	0.081	1.058
	1801.29	2748.36	272.36	841.84	105.23	6.19	74.28	12.38	74.28	12.38	37.14	6.19	30.95	12.38	501.39	6549.02
Sarfartoq, Hudson Resources Inc., 8.3	0.371	0.857	0.099	0.323	0.032	0.007	0.017	0.001	0.003	0.000	0.000	0.000	0.000	0.000	0.007	1.718
	30.79	71.13	8.22	26.81	2.66	0.58	1.41	0.08	0.25	0	0	0	0	0	0.58	142.59

(*Continued*)

TABLE 2.21 (CONTINUED)
Advanced Rare Earth Projects

Project, Owner, MR (Mt)	Grade of *In Situ* Rare-Earth Oxides (wt.%), Quantity of REO Available in the Deposit (kt)															
	La_2O_3	CeO_2	Pr_6O_{11}	Nd_2O_3	Sm_2O_3	Eu_2O_3	Gd_2O_3	Tb_4O_7	Dy_2O_3	Ho_2O_3	Er_2O_3	Tm_2O_3	Yb_2O_3	Lu_2O_3	Y_2O_3	TREO
Greenland																
Sørensen, Greenland Minerals and Energy Ltd., 242.0	0.306	0.477	0.044	0.129	0.016	0.001	0.012	0.002	0.011	0.002	0.006	0.001	0.005	0.001	0.090	1.102
	740.52	1154.34	106.48	312.18	38.72	2.42	29.04	4.84	26.62	4.84	14.52	2.42	12.10	2.42	217.80	2666.84
TANBREEZ, Rimbal Pty Ltd, 4300.0	0.116	0.217	0.021	0.080	0.015	0.002	0.017	0.003	0.019	0.004	0.016	0.002	0.013	0.002	0.127	0.653
	4988.00	9331.00	903.00	3440.00	645.00	86.00	731.00	129.00	817.00	172.00	688.00	86.00	559.00	86.00	5461.00	28,079.00
Zone 3, Greenland Minerals and Energy Ltd., 95.3	0.329	0.498	0.047	0.131	0.016	0.001	0.011	0.002	0.011	0.002	0.006	0.001	0.006	0.001	0.099	1.161
	313.54	474.59	44.79	124.84	15.25	0.95	10.48	1.91	10.48	1.91	5.72	0.95	5.72	0.95	94.35	1106.43
Kenya																
Mrima Hill High Grade, Pacific Wildcat Resources Corp., 26.9	2.123	3.051	0.315	1.009	0.128	0.034	0.083	0.010	0.045	0.007	0.017	0.002	0.011	0.002	0.209	7.045
	571.09	820.72	84.74	271.42	34.43	9.15	22.33	2.69	12.11	1.88	4.57	0.54	2.96	0.54	56.22	1895.11
Mrima Hill Main, Pacific Wildcat Resources Corp., 132.5	0.791	1.373	0.144	0.493	0.071	0.020	0.053	0.007	0.033	0.006	0.015	0.002	0.010	0.001	0.189	3.208
	1048.08	1819.23	190.80	653.23	94.08	26.50	70.23	9.28	43.73	7.95	19.88	2.65	13.25	1.33	250.43	4250.60
Kazakhstan																
Kutessay II, Stans Energy Corp., 18.0	0.044	0.052	0.010	0.022	0.011	0.001	0.009	0.004	0.016	0.001	0.009	0.001	0.009	0.001	0.070	0.259
	7.92	9.36	1.80	3.96	1.98	0.18	1.62	0.72	2.88	0.18	1.62	0.18	1.62	0.18	12.60	46.62
Mozambique																
Xiluvo, Promac Lda., 1.1	0.440	0.940	0.100	0.350	0.050	0.010	0.030	0.000	0.020	0.000	0.010	0.000	0.000	0.000	0.080	2.030
	4.84	10.34	1.10	3.85	0.55	0.11	0.33	0	0.22	0	0.11	0	0	0	0.88	22.33

(*Continued*)

TABLE 2.21 (CONTINUED)
Advanced Rare Earth Projects

Project, Owner, MR (Mt)	Grade of *In Situ* Rare-Earth Oxides (wt.%), Quantity of REO Available in the Deposit (kt)															
	La_2O_3	CeO_2	Pr_6O_{11}	Nd_2O_3	Sm_2O_3	Eu_2O_3	Gd_2O_3	Tb_4O_7	Dy_2O_3	Ho_2O_3	Er_2O_3	Tm_2O_3	Yb_2O_3	Lu_2O_3	Y_2O_3	TREO
Madagascar																
Tantalus, Tantalus Rare Earths AG, 435.0	0.017	0.031	0.004	0.013	0.002	0.000	0.002	0.000	0.002	0.000	0.001	0.000	0.001	0.000	0.010	0.082
	73.95	134.85	17.40	56.55	8.70	0	8.70	0	8.70	0	4.35	0	4.35	0	43.50	356.70
Malawi																
Kangankunde, Lynas Corporation Ltd., 2.5	1.262	2.109	0.199	0.594	0.045	0.008	0.015	0.003	0.003	0.000	0.001	0.000	0.000	0.000	0.000	4.240
	31.55	52.73	4.98	14.85	1.13	0.20	0.38	0.08	0.08	0	0.03	0	0	0	0	106.00
Songwe, Mkango Resources Ltd., 31.8	0.364	0.659	0.071	0.242	0.035	0.008	0.020	0.002	0.012	0.002	0.004	0.001	0.003	0.000	0.054	1.478
	115.75	209.56	22.58	76.96	11.13	2.54	6.36	0.64	3.82	0.64	1.27	0.32	0.95	0	17.17	470.00
Namibia																
Lofdal, Namibia Rare Earths Inc., 1.7	0.021	0.039	0.004	0.016	0.007	0.006	0.026	0.007	0.048	0.011	0.031	0.005	0.029	0.004	0.341	0.591
	0.36	0.66	0.07	0.27	0.12	0.10	0.44	0.12	0.82	0.19	0.53	0.09	0.49	0.07	5.80	10.05
Sweden																
Norra Kärr, Tasman Metals Ltd., 58.1	0.059	0.133	0.017	0.067	0.018	0.002	0.019	0.004	0.025	0.005	0.017	0.003	0.016	0.002	0.204	0.590
	34.28	77.27	9.88	38.93	10.46	1.16	11.04	2.32	14.53	2.91	9.88	1.74	9.30	1.16	118.52	342.79
Olserum, Tasman Metals Ltd., 7.8	0.083	0.189	0.023	0.090	0.021	0.001	0.021	0.004	0.021	0.004	0.012	0.002	0.011	0.002	0.130	0.617
	6.47	14.74	1.79	7.02	1.64	0.08	1.64	0.31	1.64	0.31	0.94	0.16	0.86	0.16	10.14	48.13
Turkey																
Aksu Diamas, AMR Mineral Metal Inc., 494.0	0.018	0.031	0.003	0.010	0.001	0.000	0.001	0.000	0.001	0.000	0.000	0.000	0.000	0.000	0.004	0.070
	88.92	153.14	14.82	49.40	4.94	0	4.94	0	4.94	0	0	0	0	0	19.76	345.80

(*Continued*)

TABLE 2.21 (CONTINUED)
Advanced Rare Earth Projects

Project, Owner, MR (Mt)	Grade of *In Situ* Rare-Earth Oxides (wt.%), Quantity of REO Available in the Deposit (kt)															
	La_2O_3	CeO_2	Pr_6O_{11}	Nd_2O_3	Sm_2O_3	Eu_2O_3	Gd_2O_3	Tb_4O_7	Dy_2O_3	Ho_2O_3	Er_2O_3	Tm_2O_3	Yb_2O_3	Lu_2O_3	Y_2O_3	TREO
Tanzania																
Ngualla, Peak Resources Ltd., 41.7	1.136	2.021	0.202	0.683	0.070	0.015	0.032	0.003	0.007	0.001	0.003	0.000	0.001	0.000	0.020	4.193
	473.71	842.76	84.23	284.81	29.19	6.26	13.34	1.25	2.92	0.42	1.25	0	0.42	0	8.34	1748.48
Wigu Hill Twiga, Montero Mining and Exploration Ltd., 0.5	2.020	2.560	0.190	0.450	0.026	0.006	0.008	0.001	0.002	0.000	0.000	0.000	0.000	0.000	0.007	5.269
	10.10	12.80	0.95	2.25	0.13	0.03	0.04	0.01	0.01	0	0	0	0	0	0.04	26.35
USA																
Bear Lodge, Rare Element Resources Ltd., 52.1	0.715	1.184	0.133	0.484	0.078	0.017	0.041	0.003	0.011	0.001	0.002	0.000	0.001	0.000	0.035	2.706
	372.52	616.86	69.29	252.16	40.64	8.86	21.36	1.56	5.73	0.52	1.04	0	0.52	0	18.24	1409.83
Bokan, Ucore Rare Metals Inc., 4.9	0.070	0.170	0.020	0.084	0.022	0.002	0.023	0.004	0.026	0.006	0.014	0.002	0.010	0.001	0.158	0.611
	3.43	8.33	0.98	4.12	1.08	0.10	1.13	0.20	1.27	0.30	0.69	0.10	0.49	0.05	7.74	29.94
La Paz, AusAmerican Mining Corp. Ltd., 128.2	0.008	0.017	0.002	0.007	0.001	0.000	0.001	0.000	0.001	0.000	0.000	0.000	0.000	0.000	0.005	0.044
	10.26	21.79	2.56	8.97	1.28	0	1.28	0	1.28	0	0	0	0	0	6.41	56.41
Mountain Pass, Molycorp Inc., 31.6	2.180	3.224	0.282	0.788	0.053	0.007	0.013	0.004	0.003	0.001	0.001	0.001	0.001	0.001	0.007	6.567
	688.88	1018.78	89.11	249.01	16.75	2.21	4.11	1.26	0.95	0.32	0.32	0.32	0.32	0.32	2.21	2075.17
Round Top, Texas Rare Earth Resources Corp., 905.9	0.002	0.009	0.001	0.003	0.001	0.000	0.001	0.000	0.004	0.001	0.004	0.001	0.006	0.001	0.028	0.063
	18.12	81.53	9.06	27.18	9.06	0	9.06	0	36.24	9.06	36.24	9.06	54.35	9.06	253.65	570.72

(*Continued*)

TABLE 2.21 (CONTINUED)
Advanced Rare Earth Projects

Project, Owner, MR (Mt)	Grade of *In Situ* Rare-Earth Oxides (wt.%), Quantity of REO Available in the Deposit (kt)															
	La_2O_3	CeO_2	Pr_6O_{11}	Nd_2O_3	Sm_2O_3	Eu_2O_3	Gd_2O_3	Tb_4O_7	Dy_2O_3	Ho_2O_3	Er_2O_3	Tm_2O_3	Yb_2O_3	Lu_2O_3	Y_2O_3	TREO
Republic of South Africa																
Glenover (JV), Galileo Resources PLC, 10.4	0.359	0.956	0.122	0.473	0.075	0.019	0.043	0.004	0.016	0.002	0.004	0.000	0.002	0.000	0.054	2.132
	37.34	99.42	12.69	49.19	7.80	1.98	4.47	0.42	1.66	0.21	0.42	0	0.21	0	5.62	221.73
Glenover (JV), Fer-Min-Ore (Pty) Ltd., 10.4	0.359	0.956	0.122	0.473	0.075	0.019	0.043	0.004	0.016	0.002	0.004	0.000	0.002	0.000	0.054	2.132
	37.34	99.42	12.69	49.19	7.80	1.98	4.47	0.42	1.66	0.21	0.42	0	0.21	0	5.62	221.73
Steenkampskraal, Great Western Minerals Group Ltd., 0.7	2.907	6.340	0.717	2.517	0.402	0.009	0.274	0.030	0.140	0.020	0.041	0.004	0.018	0.002	0.579	14.001
	20.35	44.38	5.02	17.62	2.82	0.06	1.92	0.21	0.98	0.14	0.29	0.03	0.13	0.01	4.05	98.01
Zandkopsdrift (JV), Frontier Rare Earths Ltd., 42.5	0.566	0.983	0.103	0.354	0.051	0.013	0.032	0.004	0.017	0.003	0.007	0.001	0.005	0.001	0.092	2.233
	240.55	417.78	43.78	150.45	21.68	5.53	13.60	1.70	7.23	1.28	2.98	0.43	2.13	0.43	39.10	949.03
Zandkopsdrift (JV), Korea Resources Corp., 42.5	0.566	0.983	0.103	0.354	0.051	0.013	0.032	0.004	0.017	0.003	0.007	0.001	0.005	0.001	0.092	2.233
	240.55	417.78	43.78	150.45	21.68	5.53	13.60	1.70	7.23	1.28	2.98	0.43	2.13	0.43	39.10	949.03
REO:	La_2O_3	CeO_2	Pr_6O_{11}	Nd_2O_3	Sm_2O_3	Eu_2O_3	Gd_2O_3	Tb_4O_7	Dy_2O_3	Ho_2O_3	Er_2O_3	Tm_2O_3	Yb_2O_3	Lu_2O_3	Y_2O_3	TREO
Total REO in ARPs:	23,150.00	42,360.10	4415.44	15,444.70	2295.02	349.41	1787.85	276.93	1571.20	289.41	1051.27	134.05	903.96	137.28	9596.64	103,781.00

Source: Technology Metals Research 2014, Available at www.techmetalsresearch.com/metrics-indices/tmr-advanced-rare-earth-projects-index/, accessed November 24, 2014.

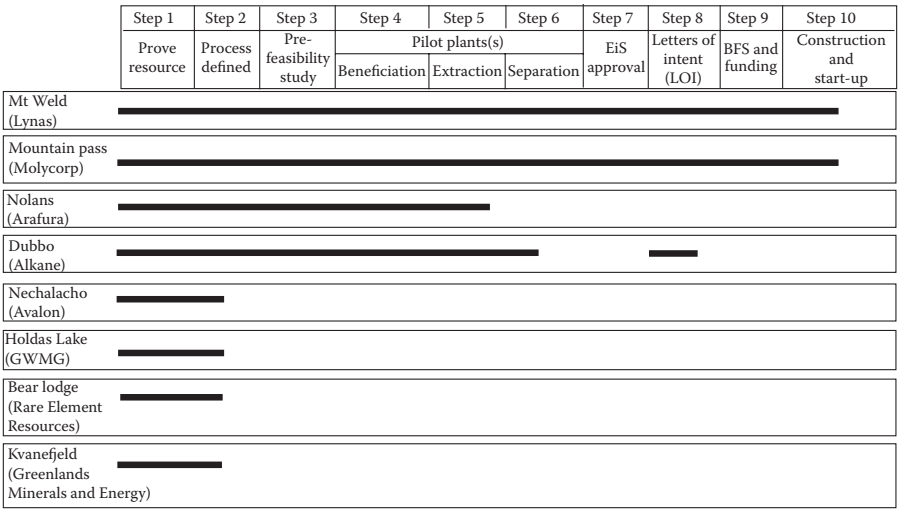


FIGURE 2.9 Development of REE deposits (from a JORC-compliant resource to commencement of production). (From Kingsnorth, D. J., Rare earths: Facing new challenges in the new decade, SME Annual Meeting, Figure 2.30, February 28–March 3, 2010, Phoenix, AZ.)

ventures in Vietnam, India, and Kazakhstan. The total production capacity out of China after 2015 should be more than 170,000 tons. When setting the target date, most companies planned for 2015. In reality, the projects needed much larger time for fruition.

Kingsnorth (2010) estimated for 2015, the global supply of rare earths to be in the order of 195,000–210,000 tons. Notwithstanding the many new projects that are expected to come online, the major producers in 2016—outside of China—will be Mountain Pass (Molycorp), Mt. Weld (Lynas Corp), Indian Rare Earths (IRE and Toyota Tsusho), and Kazakhstan (SARECO and Sumitomo). Kingsnorth sees recycling as also contributing to supply, while Great Western's Steenkapskraal mine in South Africa and Alkane's Dubbo zirconia project in Australia should enter production stage by that time as well.

It is likely that China may not possess the world's largest resources and reserves of the rare earths, but in the immediate future, the course of China remains the course of the rare-earth market. To reiterate, China produces 95% of the world's rare-earth supply and also consumes more than 75% of the world's rare-earth supply, creating rare earth–containing components and final assemblies that the rest of the world also uses (vacuum cleaners, automobile components, or wind turbine generators, for example). That title of the world's largest rare-earth resource holder may well belong to Greenland or Canada, christened the North Atlantic Mineral Resource Zone (NAMRZ) by Lifton (2013). However, China possesses the world's largest (by volume production capacity) rare-earth total supply chain, and its very large reserves of rare earths could provide for the world's demand for centuries. The

TABLE 2.22
Current Producers Out of China

Company	Location	Country	Current Capacity (t/year REO)	Target Capacity after 2015 (t/year REO)
		Current Producers		
Molycorp Minerals	Mountain Pass, California	USA	3000	40,000
Lovozersky Mining Company	Kamasurt Mine Kola Peninsula	Russia	3000–4400	15,000
Solikamsk Magnesium Works	Solikamsk Processing Plant, Urals	Russia		
Indian Rare Earths	Orissa, Tamil Nadu and Kerala	India	100	10,000
Toyota/Sojitz/Govt. of Vietnam		Vietnam	1800–2000	>2000
Neo		Thailand		
Lynas/Malaysia	Gebeng, Malaysia	Malaysia		
Indústrias Nucleares do Brasil S/A (INB)	Buena Norte	Brazil	1500	>1500
Total			9500–11,000	>68,500
		Under Preparation Producers		
Lynas Corp Mount Weld	Western Australia and a processing plant in Gebeng, Malaysia	Australia	10,500	21,000
Rareco/Great Western Minerals Group	Steenkramskaal, South Africa	South Africa/ Canada	3000	5000
Sumitomo/ Kazatomprom/ SARECO JV	Kazakhstan	Kazakhstan/ Japan	3000	15,000
Toyota/Sojitz/Govt. of Vietnam	Dong Pao, Vietnam	Vietnam/ Japan	300	5000
Toyota/Indian Rare Earths jv	Orissa	India India/ Japan	5000	10,000
Mitsubishi/Neo Material Technologies Pitinga	Brazil	Japan/USA/ Canada/Brazil	500	1000
Alkane resources	Dubbo, NSW, Australia	Australia	2600	6000
Total			24,900	63,000

(*Continued*)

TABLE 2.22 (CONTINUED)
Current Producers Out of China

Company	Location	Country	Current Capacity (t/year REO)	Target Capacity after 2015 (t/year REO)
		Exploration-Candidate Supplier		
Avalon Rare Metals Inc.	Nechalacho deposit rich in HREEs in NWT, Canada	Canada	0	5000
Quest Rare Metals	Strange Lake and others in Quebec/ Labrador, Canada	Canada	0	0
Ucore	Bokan–Dotson Ridge project Alaska	USA	0	0
Matamec	Kipawa deposit in Quebec, Canada	Canada	0	0
Arafura	Nolan's project, Australia	Australia	10,000	20,000
Great Western Minerals Group	Hoidas Lake, Canada	Canada	3000	5000
Rare Element Resources	Bear Lodge, Wyoming, USA	USA	0	0
Stans Energy Corp	Kutessay ll Mine	Orlovka Kyrgyz Republic	Kyrgyz Republic	0
Greenland Minerals and Energy	Kvanefjeld-Greenland	Greenland	0	10,000
Japan–Mongolia JV	Mongolia	Mongolia	0	0
Total			13,000	40,000
Grand Total			47,400–48,900	171,500

Source: Chen, Z., Global rare earth resources and scenarios of future rare earth industry, *Journal of Rare Earths*, 29(1): 1–6, 2011.

rare earths in the NAMRZ would need to be developed in every sense of the word to create a total rare-earth supply chain of the magnitude of the one in China. NAMRZ would need to put in place as much value addition as possible so as to capitalize on its vast resources of *all* of the rare earths.

As regards the rare-earth market in the latter half of the decade, the key factor is that China would continue to modernize, and her domestic total supply chain for rare earths will become more competitive. China's production capacity for rare earths will at all times exceed the prevailing world demand. For example, if in 2020, world

rare-earth demand will be 200,000–240,000 t, China's capacity for their production at the mine site will be 240,000–280,000 t (Bruno 2013). In this scenario, a check on continued Chinese dominance of the rare-earth total supply chain would most likely be the creation and rise of efficient non-Chinese total supply chains, with cost structures less than those in China. A possibly exists for the rise of India or Brazil, as a lower cost actor in the total supply chain space, but they will be saddled by the limitations of less centrally managed economies than China. As India gets into the production of rare earths, it is more likely to expand into the total supply chain and become a competitor, not a partner, of both Japan and then of China. The same would happen also with Brazil too (Lifton 2013).

In the complex total rare-earth supply chain, there is value addition at every stage, but the lowest value addition in the sequence occurs in the development of the mineral ore body into a producing mine. The supply chain is characteristically end-user directed, and maximum value addition, hence economic viability, happens in the last stages of the chain. Hence, a venture dealing with the early stages of the chain becomes more viable commercially to the extent it partners with one in the end stages of the sequence. The more one is in or partners with one who is placed in towards the end stages of the chain, the more are the chances of profitability. Lifton (2013) therefore anticipates increased viability when a group of junior miners (a *junior* miner is by definition an exploration and/or mine development company) partners with large end users with the skill sets in place from existing qualified technology vendors. He alludes that the Japanese lack and hence need to develop and consolidate the initial steps in the rare-earth total supply chain beyond Vietnam and also India. Apart from vertical integration as a prerequisite for long-term survival in the world rare-earth industry there may be room for only for one or two large entities in the light rare-earth space, Lifton (2013) predicted also that several non-Chinese medium/heavy rare-earth producers will remain viable by moving far down the supply chain to reach a reproducible profitability at the lowest cost.

If the projects outside China, following the path suggested by Lifton (2013) or any other path of smart evolution, could develop profitably and run smoothly, a reasonable multisupply system would form. Chen (2011) anticipated that after consolidation and with effective total production control, China would reduce its supply proportion to 64% and leave the remaining 36% to those producers out of China. The demand balance out of China could grow to 80,000–100,000 t by the end of the decade. There will be a great space to begin with for new producers.

World reserves are sufficient to meet forecast world demand well into the twenty-first century. Several very large rare-earth deposits in Australia, NAMRZ, Brazil, and China have yet to be fully developed. In the 2001 edition of Minerals Yearbook (Hedrick 2001), the tone was that the world demand was currently (2001) being satisfied by existing production and that the world resources should be adequate to fulfill demand for the foreseeable future. The perception was different in the 2006 edition. It went on to note that the world reserves were sufficient to meet forecast world consumption well into the next decade, existing production was currently not sufficient to meet increases in world consumption, and shortages exist for neodymium and dysprosium for magnet alloys and europium and terbium for phosphors (Hedrick 2006). This was even before China's restrictions came into force a few years later, to

be taken as the situation facing the whole of the world including China. As regards the US situation, Hedrick (2005) stated that the Mountain Pass deposit in the United States contains sufficient resources to meet the domestic demand if the foreign supply is compromised, and Hedrick (2006) modified it as follows: "Although the Mountain Pass deposit in the United States contains sufficient resources to meet domestic consumption for the light-group rare-earth elements for the next two decades, the deposit does not contain enough quantities of heavy-group rare-earth elements to meet existing or expected future consumption over this period."

In course of time, it is inevitable that placer monazite will reemerge as a source of rare earths. From the mid-1990s, companies have shifted away from using naturally occurring radioactive rare-earth ores. This trend has had a negative impact on monazite-containing mineral sand operations worldwide causing mine closures and reduced revenues. In the future, demand for monazite as an ore of rare earths is expected to increase because it will be more cost effective to recover owing to its abundance and availability as a low-cost by-product during processing for zircon and titanium minerals. Thorium, as a non-proliferative nuclear fuel is considered a likely substitute for uranium in the future, especially in a world concerned with the threat of nuclear terrorism. If consumption of thorium increases, monazite could resume its role as a major source of rare earths. Worldwide, space and regulatory requirements to dispose of radioactive waste products are expensive, severely limiting the use of low-cost monazite and other thorium-bearing rare-earth ores (Hedrick 2001, 2002, 2006).

2.10 SUMMARY

All rare earths except promethium occur in nature. Rare earths are a relatively abundant group of metallic elements in the earth's crust, occurring in over 200 minerals. As a rule, any rare-earth mineral usually contains all the rare earths, some of them enriched and some in very low concentrations. Although the minerals are numerous, about 95% of all world rare-earth resources occur in just three minerals: bastnasite, monazite, and xenotime. A dozen other minerals also have been or could be used as rare-earth resources.

Rare-earth deposits contain one or more rare-earth minerals. They are broadly divided into hard-rock deposits and placer sands. Bastnasite is found only in hard-rock deposits, whereas monazite and xenotime occur in both hard-rock and placer deposits. Deposits that have been traditionally considered as reserves correspond approximately to the *R1E resources* in the United Nations Resource Classification System. There are more systems and national standards for classifying reserves and resources. They are the Canadian National Instrument 43-101, JORC (The Australasian Code for Reporting of Exploration Results, Mineral Resources and Ore Reserves), and SAMREC (South African Mineral Resource Committee) codes. However, certain incongruity persists in the definition of reserves across the nations and this gets reflected in the numbers they use in representing their and others rare earth holding in ores and minerals.

World reserves (R1E resources) of rare earths have been estimated at 93.4 Mt REO in place, of which 93% occur in hard-rock (primary) deposits and 7% occur in

placer (secondary) deposits. These resources occur as follows: 20% in monazite and 80% in bastnasite and other minerals. Geographically, 52% of world REO resources are located in China, 22% in Namibia, 15% in the United States, 5% in Australia, 3% in India, and the remainder in several other countries. According to latest estimates, world rare-earth reserves are 88 million tons.

There are as many as 40 rare-earth deposits in the United States. The most important is the Mountain Pass bastnasite deposit, which has over 3 Mt of REO and the distinction of being the only rare-earth deposit in the world worked exclusively for the recovery of rare earths. Numerous other deposits of present and future relevance are in the United States. These include placer monazite deposits in the states of Florida, South Carolina, and Alaska, and deposits of other rare-earth minerals such as euxenite, eudialyte, apatite, and other phosphorites, and perovskites.

There are 35 rare-earth deposits in Australia: 28 are placers and 7 hard rock. Heavy mineral sand placer deposits containing monazite are widely distributed along the east and west Australian coasts. Major deposits at and near Eneabba have been the most important. The most promising and large reserves of monazite and xenotime are the WIM-150 deposit and four other deposits in Murray Basin. Other major deposits include the Olympic Dam multimetal deposit, the Brockman deposit, the Toongi deposit, and, for recovery of rare earths as a main product, the deposits at Mt. Weld, Yangibana, and John Galt.

Brazil has many placer deposits along the Atlantic coast and the only inland placer at Sao Goncalo de Sapucai on the Sapucai River. Monazite is the mineral in all these deposits. One of the two hard-rock deposits occur at Tapira, an existing apatite mine where rare earths occur in anatase overburden, and the other hard-rock bastnasite deposit occurs at Pocos de Caldas.

Many rare-earth deposits, hard rock and placers, occur in India. The hard-rock deposits, however, have been completely overshadowed by the extensive placer deposits of monazite-containing heavy minerals in the southwestern and eastern coasts.

In Canada, there are large rare-earth deposits that together contain more than 1 Mt REO. They include rare earth occurring in uranium ores at Elliot Lake, Ontario, a gadolinite deposit at Strange Lake, Quebec, and a columbite–gadolinite deposit at Thor Lake, Northwest Territories.

China has numerous rare-earth deposits, some of them unusual and some of them among the world's largest. The world's largest known rare-earth deposit, containing 48 Mt REO, occurs at Bayan Obo. It is an iron–rare earth–niobium resource. Bastnasite and monazite account for about 70% and 30%, respectively, in the rare-earth fraction. Monazite and xenotime placers occur at Guangdong, Guangxi, Hunan, Hubei, and Hainan Provinces in south China. The unusual ion adsorption-type ore occurs at Jiangxi, Guangdong, Fujian, Hunan, Guangxi, and southern Anhui Provinces. Bastnasite also occurs in Sichuan and Shangdong. The rare-earth deposits of China are great in quantity and, taken together, are relatively better balanced as regards light, middle, and heavy rare-earth content.

South Africa has more than 1 Mt of REO in its deposits, which include placer monazite at Richards Bay, rare earth-bearing apatite at Phalaborwa complex, and monazite co-occurring with apatite and fluorite at Buffalo fluorspar.

In the former Soviet Union, large deposits of the rare-earth mineral loparite and rare earth-bearing phosphate rocks of magmatic origin occur in the Kola Peninsula.

Heavy mineral sands containing monazite and, most importantly, xenotime occur in the placer cassiterite deposits in the Southeast Asia tin belt in Malaysia, Thailand, and Indonesia.

An enormous hard-rock carbonatite deposit containing bastnasite occurs at Etaneno in Namibia. This deposit, containing an estimated 20 Mt REO, is second in size only to the Bayan Obo deposit in China. Besides this and the deposits at South Africa, rare-earth resources are found in Africa at Malawi (hard-rock monazite, Kangankunde), Mozambique (placer monazite, Congolone), Burundi (hard-rock bastnasite, Karonge and Kasagwe), Kenya (hard-rock monazite, Rangwa/Ruri/Homa), Egypt (placer monazite, Nile Delta-Rosetta), Mauritania (hard-rock monazite, Bou Naga), and Gaban (hard-rock florencite, Mabounie).

Rare-earth deposits also occur in Argentina (placer monazite, Rio Tercero [Colorado]), Greenland (hard-rock pyrochlore and eudialyte, Ilimaussaq), New Zealand (placer monazite, Barrytown and Westport in South Island), Sri Lanka (placer monazite, Pulmoddai), Uruguay (placer monazite, Atlantida), Bangladesh (placer monazite, Cox Bazzar coastal area), Germany (placer monazite, Cuxhaven), Indonesia (placer monazite, Tin Islands), Japan (hard-rock sphene, Kamioka lead–zinc mine), Myanmar (placer monazite, Dawei and Myeik), Taiwan (placer monazite, Southwest coast), Turkey (hard-rock bastnasite, Eskisehir), Venezuela (lateritic beds, Cerro Impacto), Vietnam (hard-rock bastnasite, Nam Nam Xe), and Zaire (placer monazite, Kivu region).

In spite of the large identified world resources for rare earths, their production and supply have been affected because, except at Mountain Pass, the rare-earth minerals can be produced only as a by-product or coproduct of some other mineral value.

Monazite was the principal rare-earth source from the beginning of the rare-earth industry 100 years ago until 1965. Thereafter, production of bastnasite exceeded monazite production. In the 1990s, the status of monazite as a rare-earth resource diminished, and the production of bastnasite and, to a certain extent, that of other resources such as ion-adsorption ores have been increasing.

India and Brazil were the principal sources of world rare-earth supply until the late 1940s, when Australia and Malaysia also started regular production. Much of the world rare-earth supply during 1950–1985 came principally from the United States and secondly from Australia. By 1985, China rose to second place, and by 1988, it overtook the United States to become the world's leading producer. Rare-earth production in both China and the United States is primarily from bastnasite.

In 2002, world rare-earth production was 98,300 t REO. The leading producer was China (88,000 t REO), followed by the United States (5000 t REO), India (2700 t REO), and former USSR (2000 t REO). In 2003, while the world mine production reached 95,000 t REO, no production was reported from the US Mountain Pass deposit (Hedrick 2004). China produced 90,000 t REO, with India and Commonwealth of Independent States contributing 2700 and 2000 tons, respectively. In 1995, monazite started losing its importance due to problems associated with thorium disposal (probably only temporarily). While the total world REO production remained

practically at the same level, the contributions from two major countries—Australia and Malaysia—declined substantially. This has been made up by enhanced Chinese production.

Actual world rare-earth production is much less than the world production potential. If the presently operating mines had all produced REO instead of discarding or stockpiling it, the total world production could be more than double the actual world production. The status as regards individual countries is vastly variable. Further enhancement in rare-earth production is possible by exploiting new reserves. Worldwide there are many new projects that could begin rare-earth production within a few years.

Forecasts for rare-earth production expect a growing demand and a continuously rising market for rare earths. The world rare-earth consumption in the year 2000 was 80,000 t REO and is set to exceed 100,000 t REO by the year 2004. There could be no difficulty in ensuring the supply of rare earths to meet such demand. Besides, undiscovered resources are thought to be very large relative to expected demand (Hedrick 2004). In relation to the world cumulative production in the year 2003 (1,816,000 t REO), world rare-earth reserves (93,000,000 t REO) were very substantial. While the TREO content is an impressive figure of 93 Mt, the amount of individual rare earths theoretically recoverable from this vast reserve varies greatly because only 20% of the total reserves are in monazite and almost 80% are in bastnasite, with minor quantities in other rare-earth minerals. Bastnasite is poorer in heavy rare-earth content when compared to monazite. The individual rare-earth availability is strongly tilted toward the light rare earths (Figures 2.10 and 2.11).

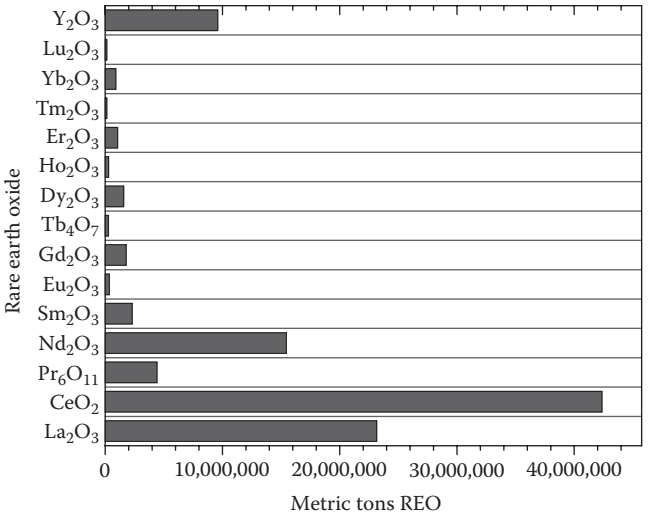


FIGURE 2.10 Quantities of rare earths available in APR resources.

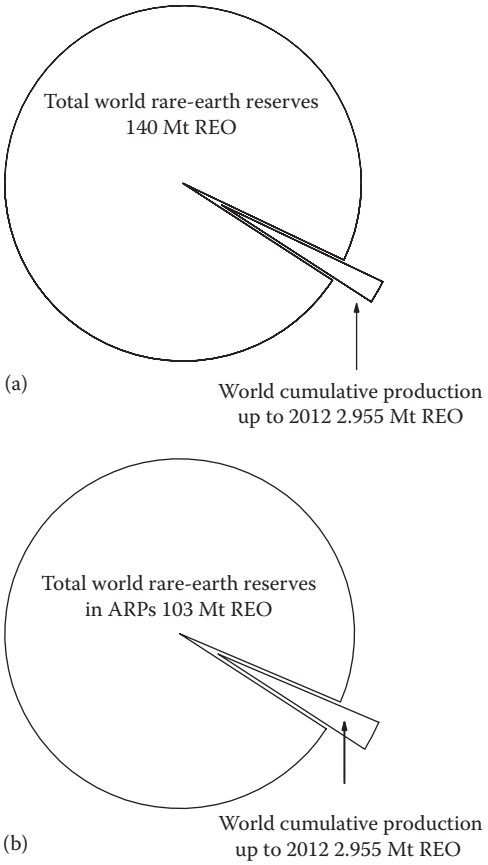


FIGURE 2.11 Estimated long-term availability of rare earths. (a) Total world rare-earth reserves and cumulative production up to 2012. (b) Total world rare-earth reserves in ARPs and cumulative production up to 2012.

3 Resource Processing

3.1 INTRODUCTION

In the overall rare-earth extraction flow sheet, the term *resource processing* refers to the group of unit operations, comprising both physical and chemical processing, used to obtain from the as-mined ore a compound that is either an end product in itself or an interprocess intermediate for the subsequent processing to the metal or alloy or other compound. Usually, these processes accomplish sequential removal of impurity compounds from the material being processed. In the case of rare earths, the resource processing involves not only the operations that result in such impurity removal but also special operations that achieve the difficult task of separating the considerable number of naturally co-occurring rare-earth elements (REEs) from one another.

Rare-earth minerals are numerous, and even the number of them that are found in ore deposits considered for extraction processing is more than a dozen. However, much of the actual extraction of rare earths is principally from the minerals bastnasite, monazite, and the special resource, China's ion adsorption ore. As described in the preceding chapter, all the rare earths generally occur together in all the minerals with large variations in relative proportions. Such an occurrence is the culmination of their similar chemical behavior, and it is this chemical similarity that has, in the past, made separation of rare earths from one another a daunting task.

The nature of the occurrence and distribution of the rare-earth minerals has generally ensured that they could be recovered only as a by-product or a coproduct. Therefore, except in one important case, Mountain Pass bastnasite, the process of physical beneficiation of the rare-earth mineral is the same as that used for the main product of the resource. The Mountain Pass bastnasite has a unique process of physical beneficiation.

Chemical beneficiation or chemical processing of the concentrate obtained after physical beneficiation usually involves hydrometallurgical and sometimes pyrometallurgical operations. Chemical beneficiation by hydrometallurgy techniques is preferred because, eventually, the concentrates would need to be processed by hydrometallurgical separation processes for isolating rare earths from one another. The chemical properties of rare earths make them amenable to ready dissolution and easy precipitation. Subtle and systematic differences in the basicity of the REEs have been used in developing possibilities for their separation. The sheer number of REEs that occur together ensured that the separation procedures, if feasible, would be laborious. However, the exhibition of stable multivalence in the most abundant and also in one of the least abundant rare earths has simplified, to some extent, the separation procedures. With the development of techniques like ion exchange and solvent extraction, it became possible to effectively work upon the inherent differences in rare earths' chemical behavior, however small they are, to effect their separation from one another.

This chapter deals with the various aspects of rare-earth resource processing. First, a brief description of the mining methods is presented. Then the procedures used for physical beneficiation to obtain the rare-earth mineral concentrate and the procedures used to chemically treat the concentrates to a mixed rare-earth oxide product are given. Next, the key feature of rare-earth extractive metallurgy, separation of the rare earths from one another, is covered. All important processes and those that have been rated as suitable for industrial operation are included. Even though, the industrial implementation of monazite processing has shrunk considerably, it is not because of lack of monazite resources but more due to regulatory load on commercial operations, and its ramifications. As pointed out in the concluding paragraphs of Section 2.9, this forced hibernation is unlikely to last too long. Besides, much of rare earth extractive metallurgy developed while processing of monazite.

3.2 MINING

3.2.1 Hard-Rock Deposits

Hard-rock rare-earth deposits are mined by open-pit and underground methods (Jackson and Christiansen 1993). At two of the world's largest rare-earth mines, Bayan Obo in China and Mountain Pass in the United States, the open-pit operations are the standard drill, blast, load, and haul-to-the-mill procedures. At Mount Weld, subsequent to the removal of overburden to a depth of 20–30 m, the rare-earth deposit would be mined using conventional open-cut methods (EPA 1992). At the Canadian uranium properties where rare earths could be recovered as by-products, underground room and pillar mining have been conducted.

3.2.2 Placer Deposits

Mining of placer sands that are under water or affected by a high water table is conducted by dredges. Shallower sands are mined using bucket-wheel units, while bucket-line and suction dredges are used for deeper material. Where water is not available, variations of open-pit excavation methods, such as scrapers, front-end loaders, shovels, and draglines, are used. Usually, drilling and blasting are not required but are useful when the sand is cemented by ferruginous or calcareous precipitates. In the past, in countries where inexpensive manual labor is available, the labor has been used to fill head-carried baskets or to work hand-operated sluices.

The as-mined ore is subjected to a physical beneficiation process after crushing and milling in the case of hard-rock ore, and in the as-mined condition in the case of placer sand.

3.3 PHYSICAL BENEFICIATION

The physical beneficiation of rare-earth minerals has been comprehensively reviewed in the recent publications of Zhang and Edwards (2012) and Jordens et al. (2013). Apart from the three most common RE minerals, bastnasite, monazite, and xenotime, new rare-earth deposits that are poised for development contain many new minerals, most

of them with unknown beneficiation characteristics. Generally, the RE mineral deposits are beneficiated through a combination of gravity concentration, magnetic separation, electrostatic separation, and froth flotation. RE minerals have relatively high specific gravities (between 4 and 7), and gravity separation can be used to concentrate by eliminating low-specific-gravity gangue minerals such as quartz (Ferron et al. 1991).

Separation of very fine particles can still be achieved for minerals with very large differences in specific gravity, such as gold from silicate gangue, by employing centrifugal gravity separators such as the Knelson, Falcon, and Mozley Multi-Gravity Separators (Falconer 2003; Gee et al. 2005). These fine particle separators are designed for semicontinuous operation where the valuable dense material is present in low concentrations (<0.1 wt.%).

A popular gravity separator used for fine particle sizes is a centrifugal gravity concentrator (Falconer 2003). The mineral slurry is introduced into a rapidly rotating bowl to generate centrifugal forces on the particles that are several times the force of gravity. The centrifugal forces on the particles trap high-specific-gravity material against the sides of the bowl to become the gravity concentrate, while lower-specific-gravity material flows along with the fluid to collect as gravity tailings (Falconer 2003). The contoured bowl design and water flow arrangements in one of the most common centrifugal separators, the Knelson concentrator, makes it very effective for applications where the desired high-specific-gravity mineral is present in very low concentrations (typically <1%). Various designs and procedures have evolved in the construction and working of such concentrators to handle a variety of feeds, different in size ranges and characteristics (Fullam and Grewal 2001). The development of centrifugal separators capable of continuous operation e.g., Knelson continuous variable-discharge (CVD) and the ability to process feed materials with up to 50% heavy mineral (HM) content make them valuable for REE mineral separation too (Fullam and Grewal 2001).

Gravity separations have been successfully experimented on in rare-earth deposits with very fine-grained mineralization in Turkey and Australia (Guy et al. 2000; Ozbayoglu and Umit Atalay 2000). In both these cases, the rare-earth minerals concentrated into the very fine (<5 μm) particle size range. To circumvent this, either the grinding steps needed modification to control excessive fine generation or a multigravity separator, designed to recover ultrafine particles via gravity separation, needed to be used. The modified grinding procedure was an attrition scrubbing step prior to further grinding to yield a product that was 100% −300 μm (suitable size limit for flotation), while decreasing −5 μm size fraction (slime losses) by approximately 8%. To adequately liberate the rare-earth minerals without excessive fine production, screening and secondary grinding steps are used after gravity and magnetic separations at a mine in Maoniuping (Jordens et al. 2013a), China, to produce a bastnasite flotation concentrate with a grade of 62% REO and a recovery of 80–85%.

The roasting of ore prior to gravity separation was suggested in a 1956 patent by Kasey (1956). A rare-earth carbonate ore was roasted at temperatures in excess of 1000°C to convert the carbonates into oxides, thereby increasing the mineral density and amenability to gravity separation. The roasted ore was quenched from the high temperature to render it friable and hence lead to a significant decrease in the

energy required for crushing and grinding operations (Fitzgibbon and Veasey 1990). However, this process does not appear to have been successfully applied on an industrial or pilot scale (Jordens et al. 2013).

The problem of rare-earth values in the minerals getting lost in the fine-size fractions produced in the comminution of finely grained rare-earth ores has been addressed in an unconventional way. Chistov et al. (1995) reported that subjecting the ore to a 2.45 GHZ, 5 kW microwave treatment that heated the ore (a complex niobium/rare-metal ore from Tomtor, Russia) to 540°C (approximate 600 s exposure time) prior to grinding reduced the formation of slimes (<5 μm) from 43% to 19%. This process, on scaling up to an industrial operation, would lead to considerable improvements in rare-earth recovery simply due to the decreased losses in desliming operations (Jordens et al. 2013).

The most common application of gravity separation is in monazite beneficiation from HM sands. Initially, the beach sand material is concentrated typically using a cone concentrator to produce an HM preconcentrate (20–30% HMs) before a more selective gravity separation, using a spiral concentrator to achieve concentrations of 80–90% HMs. At this point, a series of magnetic, electrostatic, and further gravity separation operations may be applied, according to each individual deposit's mineralogy (Ferron et al. 1991). Low-intensity magnetic separation can be used to remove ferromagnetic gangue minerals such as iron oxides, and high-intensity magnetic separation, to separate monazite and xenotime from other HMs.

Electrostatic separation techniques are used only when nothing else works. The comminution steps in mineral processing flow sheets are generally wet processes, and the electrostatic separation works with a dry powder. Energy requirements to drive off all moisture prior to electrostatic separation (drum type, belt type, plate type) can be significant (Kelly and Spottiswood 1989a). This is an issue with all ores that need some form of comminution prior to beneficiation treatment. HM sands and ion-adsorption ores do not need such grinding with slurried feed material.

Electrostatic separation exploits the differences in electrical conductivity between different minerals to effect separation (Higashiyama and Asano 2007; Kelly and Spottiswood 1989a,b,c). In rare-earth mineral processing, electrostatic separation is typically used in the separation of monazite and xenotime from gangue minerals with similar specific gravity and magnetic properties (Ferron et al. 1991; Zhang and Edwards 2012). Xenotime is more paramagnetic than monazite and concentrates with ilmenite during magnetic separation of HM sands. To separate xenotime from ilmenite, electrostatic separation is useful, as ilmenite is conductive, but xenotime is not. Electrostatic separation is a technique to separate ultrafine (<37 μm) coal particles and may be the solution to treat the fines produced in many currently operating mineral processing circuits that account for significant rare-earth losses (Higashiyama and Asano 2007; Jordens et al. 2013).

Magnetic separation of minerals is based on the difference in the behavior of mineral particles when in a magnetic field. The extent of beneficiation in a magnetic separator depends on the applied magnetic field strength, the magnetic field gradient, and the magnetic susceptibility of the mineral particles and accompanying fluid medium. The size range in which magnetic separation is effective depends on the dominant force on the particle (gravitational, magnetic, and fluid drag) under the

conditions of separation (Oberteuffer 1974) but is usually in the zone of 5 μm to 1 mm. The recovery of increasingly fine magnetic material (down to even nanoscale particles) is an area of active research (Jordens et al. 2013).

Magnetic separation is used in rare-earth mineral beneficiation to eliminate highly magnetic gangue or to concentrate the paramagnetic REE minerals monazite or xenotime. From the magnetic susceptibilities of individual REEs, Ito et al. (1991) predicted rare-earth minerals' magnetic susceptibilities based on their chemical compositions (for M^{3+} lanthanide ions). The results indicated that the elements from gadolinium to erbium had the highest magnetic susceptibilities of all the lanthanides, and the higher concentrations of Gd, Dy, and Er ions present in xenotime explain their threefold increase in magnetic susceptibility compared to monazite (Ito et al. 1991).

Gravity separation and magnetic separation are critical to monazite beneficiation from HMs in beach sands. They are used to eliminate strongly magnetic minerals such as magnetite prior to more selective separation steps and are also used to separate paramagnetic monazite from nonmagnetic HM gangue material such as zircon and rutile (Ferron et al. 1991; Tran 1991; Zhang and Edwards 2012). Xenotime, a paramagnetic mineral that is more susceptible to magnetic separation than monazite, may be isolated using these techniques; however, for fine grain sizes (<100 lm), flotation is the preferred means of separation (Rosenblum and Brownfield 1999; Zhang and Edwards 2012).

Magnetic separation is used in the beneficiation of Bayan Obo bastnasite to eliminate Fe-bearing gangue minerals prior to rare earth-specific separation steps and as a cleaning step for flotation feeds and concentrates (Chi et al. 2001; Zhang and Edwards 2012). In the case of China's second biggest rare-earth deposit, the Sichuan Maoniuping rare-earth ore, magnetic separation has been combined with gravity separation to achieve a bastnasite recovery greater than 55% without the need for flotation (Chi et al. 2001).

3.3.1 Monazite

In placer deposits, monazite occurs as a minor constituent along with sillimanite, garnet, and magnetite, while the major minerals are ilmenite, rutile, zircon, and quartz. Cassiterite occurs as the major mineral in the placer deposits of the Southeast Asia tin belt. Occasionally, trace quantities of other minerals, such as chromite, picotite, baddeleyite, and cinnabar, and native metals such as gold and platinum are also present. The beach sand deposits exhibit a considerable variation in mineralogy and chemical composition depending on the location (Hedrick 1985b). The flow sheets for their beneficiation are therefore variable in detail. However, as the task is essentially to separate the already finely divided minerals with quite similar physical properties, the flow sheets have several features in common. An outline of the major steps in processing by physical beneficiation is given in Figure 3.1.

The highest concentrations of HMs in beach sand are found in the Manavalakurichi (70–80% HMs and 4–7% monazite) and Chavara deposits (70–80% HMs and 0.7–1% monazite) of India. Preconcentration by wet gravity methods is generally not required for these deposits. The same is true of the Pulmoddai deposit (Panditharatna

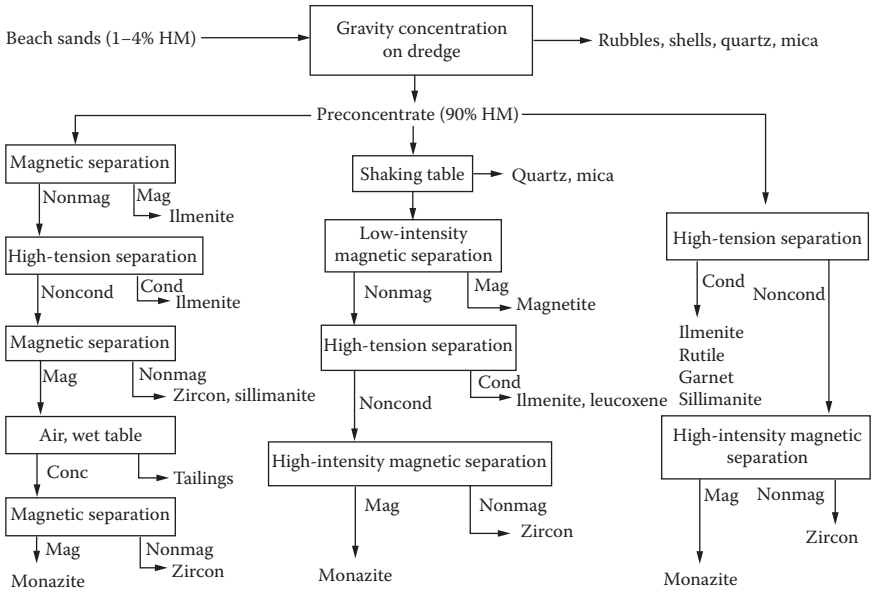


FIGURE 3.1 Physical beneficiation of beach sand minerals.

1991), which has 60–75% HMs, 70–80% ilmenite, 8–10% rutile, 8–10% zircon, and 0.02% monazite. With the Orissa deposit of India (20% HMs and 0.4% monazite), and for most other deposits throughout the world, bulk concentration of HMs is needed before actual separation of individual minerals is carried out (Bashir 1988). For example, a lean deposit containing 2–5% HMs is first concentrated to 20–30% HMs on cone concentrators. This product is then fed into spirals, which give a concentrate of more than 80% HMs.

The separation of HMs is then achieved by exploiting small gravimetric differences or the slight differences in magnetizability and surface ionization potential among the various co-occurring minerals (Anderson 1986; Aplan 1988; Bashir 1988; Parker and Baroch 1971). Among the beach sand minerals, the specific gravity of monazite is the highest. Ilmenite, garnet, xenotime, and monazite, in decreasing order of magnetizability, behave as magnetic minerals. In electrostatic separation, ilmenite and rutile behave as conducting minerals and at other times behave as nonconducting ones. Xenotime is more strongly magnetic than monazite and, in magnetic separation, concentrates with ilmenite. A poor electrical conductor, xenotime is electrostatically separated from ilmenite. Leucoxene, when present, can cause problems in the separation of monazite from ilmenite. A reduction roast at 600°C converts free hematite in leucoxene into magnetite and enables easy separation.

One of the simplest flow sheets for the production of a monazite concentrate from a placer deposit is shown in Figure 3.2. This figure outlines the process used to recover gold and monazite from a placer deposit in Idaho (Hill 1951; Jackson and Christiansen 1993). Gravity is the only method needed to produce an REO concentrate. Gold was removed earlier by amalgamation.

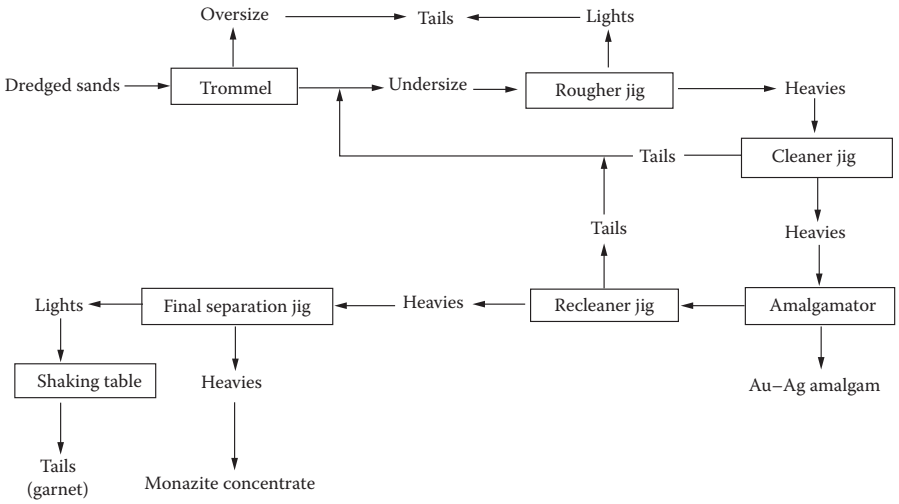


FIGURE 3.2 Concentration of placer minerals on board a dredge. (From Aplan, F.F., The processing of rare earth minerals. In Bautista, R.G. and Wong, M.M. (eds.), Rare Earths, pp. 15–34, The Minerals, Metals and Materials Society, Warrendale, PA, 1988; Ferron, C.J. et al., Beneficiation of rare earth oxide minerals. In Siribumrungsukha, B., Arrykul, S., Sanguan Sai, P., Pungrassami, T., Sikong, L., and Kooptarnon, K. (eds.), *Proc. Int. Conf. Rare Earth Minerals and Minerals for Electronic Uses*, Jan. 1991, Hat Yai, Thailand, pp. 251–269, Prince of Songkla University, Thailand, 1991.)

The dredging operations formerly conducted in the gold placers in Idaho and tin placers of Southeast Asia are similar. Before separation of the HM concentrate, just as the gold was removed by amalgamation in Idaho, cassiterite was recovered using a series of jigs in placer tin beneficiation, as shown in Figure 3.3 (Fujita and Leepawpanth 1991; Meechumna 1991). Further separation of HM dredge concentrate is achieved using a combination of high-intensity magnetic separation, high-tension separation, and dry and wet tabling to obtain the clean concentrate of REO minerals and other minerals (Sulaiman 1991). As mentioned earlier, the beach sands of Manavalakurichi in India and Pulmoddai in Sri Lanka need not be preconcentrated. It is directly put in for separation into its constituents using electrostatic and magnetic methods. Some of the mineral beneficiation practices for obtaining monazite concentrate are outlined in Figures 3.4 to 3.7.

A flow sheet to treat Egyptian beach sands containing approximately 30 wt.% HMs is given in Figure 3.8 (Moustafa and Abdelfattah 2010). Wet gravity concentration (Wilfley shaking table) is used to separate low-specific-gravity gangue, and then a low-intensity magnetic separation is used to discard any ferromagnetic minerals without removing paramagnetic monazite. The nonmagnetic stream that remains contains most of the monazite, zircon, and rutile as well as some of the gangue minerals. Gravity, magnetic, and electrostatic separations are then applied to effect further separations. Rutile collects in the conductor fraction after electrostatic separation (monazite and zircon are nonconductive), and diamagnetic zircon is removed from the paramagnetic monazite by magnetic separation.

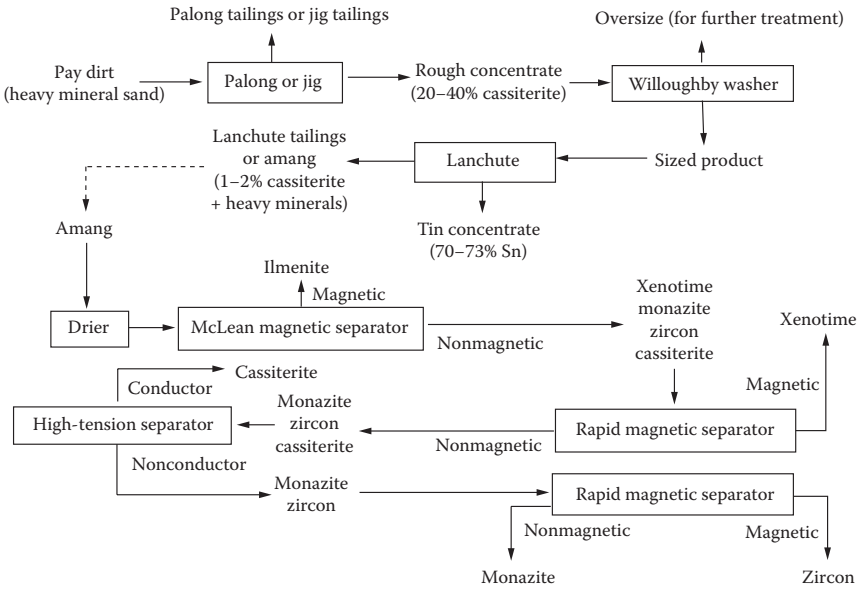


FIGURE 3.3 Physical beneficiation of cassiterite-bearing mineral sands of Southeast Asia.

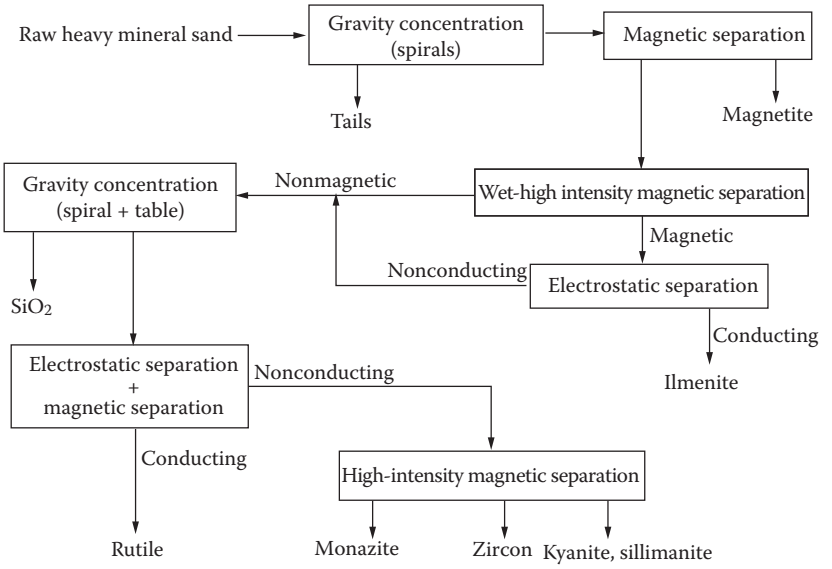


FIGURE 3.4 Beneficiation of coarse heavy mineral sand from Congolone, Mozambique. (From Ferron, C.J. et al., Beneficiation of rare earth oxide minerals. In Siribumrungsukha, B., Arrykul, S., Sanguan Sai, P., Pungrassami, T., Sikong, L., and Kooptarnon, K. (eds.), *Proc. Int. Conf. Rare Earth Minerals and Minerals for Electronic Uses,* Jan. 1991, Hat Yai, Thailand, pp. 251–269, Prince of Songkla University, Thailand, 1991.)

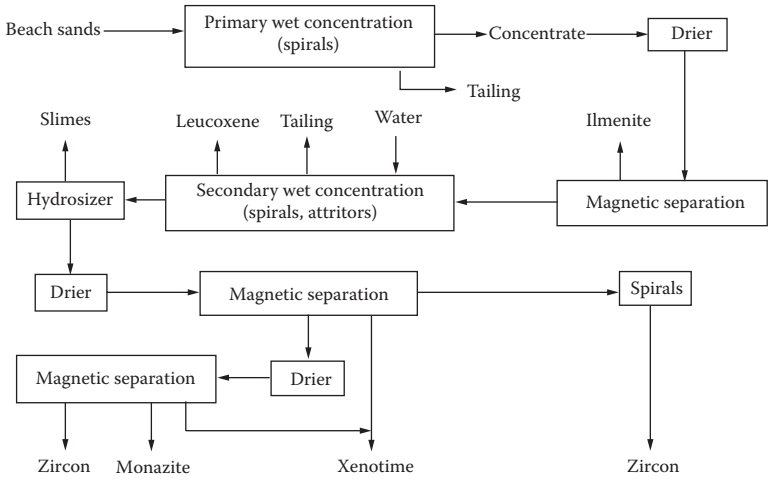


FIGURE 3.5 Beneficiation flow sheet at Cable Sands Pty Ltd. plants, Australia. (From Houot, R. et al., Recovery of rare earth minerals with emphasis on flotation process. In Siribumrungsukha, B., Arrykul, S., Sanguan Sai, P., Pungrassami, T., Sikong, L., and Kooptarnon, K. (eds.), *Proc. Int. Conf. Rare Earth Minerals and Minerals for Electronic Uses,* Jan. 1991, Hat Yai, Thailand, Prince of Songkla University, Thailand, pp. 301–324, 1991.)

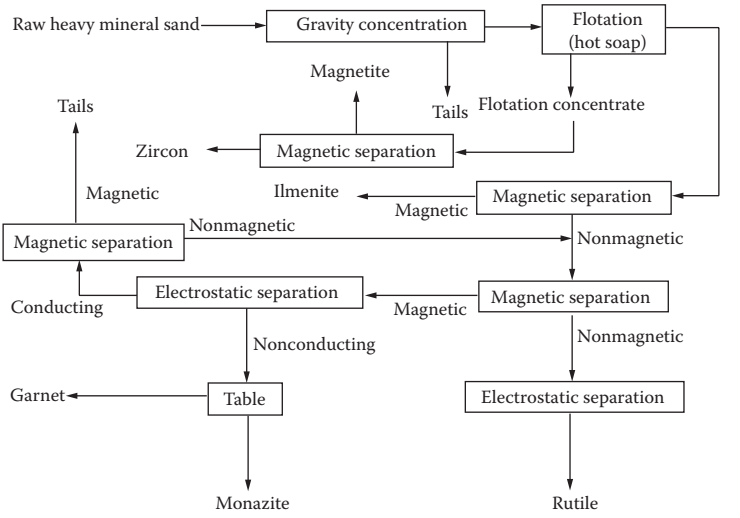


FIGURE 3.6 Beneficiation flow sheet at Zircon Rutile Ltd., Australia. (From Ferron, C.J. et al., Beneficiation of rare earth oxide minerals. In Siribumrungsukha, B., Arrykul, S., Sanguan Sai, P., Pungrassami, T., Sikong, L., and Kooptarnon, K. (eds.), *Proc. Int. Conf. Rare Earth Minerals and Minerals for Electronic Uses*, Jan. 1991, Hat Yai, Thailand, pp. 251–269, Prince of Songkla University, Thailand, 1991.)

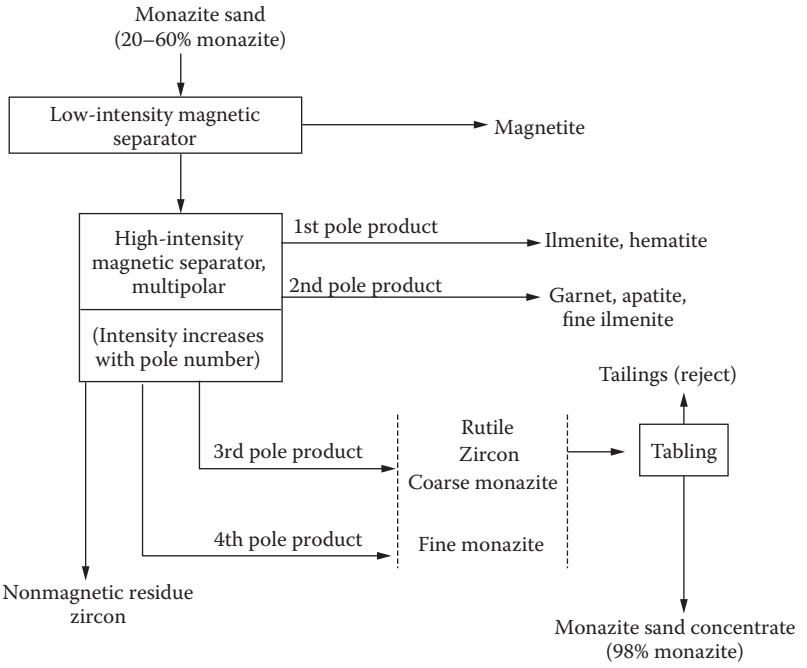


FIGURE 3.7 Flow sheet of the beneficiation of beach sand minerals in India.

3.3.1.1 Froth Flotation

Froth flotation is a popular and versatile ore beneficiation technique because it processes a wide range of fine particles and the technique can be tailored to the unique mineralogy of most deposits. Thus, froth flotation of rare-earth minerals has seen a large amount of research compared to other beneficiation techniques. The technique has been particularly effective for the beneficiation of bastnasite both at Mountain Pass and at Bayan Obo.

3.3.1.2 Bastnasite Flotation

Flotation is used to beneficiate bastnasite in many locations, including the two largest rare-earth deposits: Mountain Pass and Bayan Obo (Zhang and Edwards 2012). The collectors commonly used for bastnasite flotation are variants of hydroxamates, fatty acids, dicarboxylic acids, and organic phosphoric acids (Ferron et al. 1991; Jun et al. 2003). Typical depressants include sodium silicate, sodium hexafluorosilicate, lignin sulfonate, and sodium carbonate (Houot et al. 1991).

Fatty acids have been widely used as a collector in *mineral flotation*. To achieve a reasonable separation in bastnasite flotation (Bulatovic 2007, 2010; Cheng et al. 2007; Pradip 1981), elevated temperatures and the addition of large volumes of depressant are needed. At higher temperatures, there is a significant increase in the rate of collector adsorption onto bastnasite relative to gangue such as calcite and barite. Compared to fatty acids, hydroxamic acid (alkyl hydroxamate) has better selectivity. The improved flotation response is possibly due to collector molecules forming

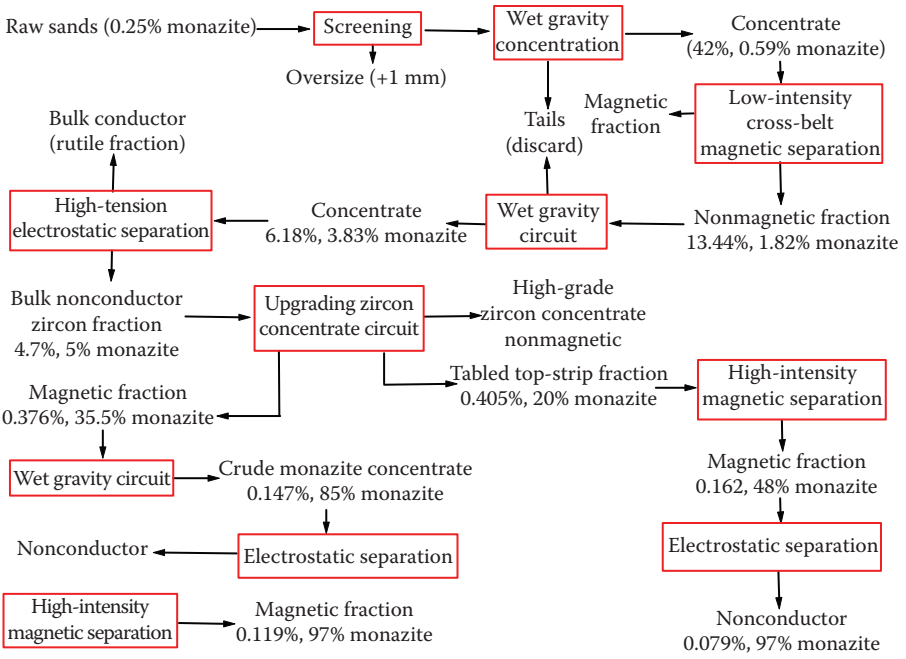


FIGURE 3.8 A flow sheet to treat Egyptian beach sands containing approximately 30 wt.% heavy minerals. (From Moustafa, M.I. and Abdelfattah, N.A., *Resour. Geol.* 60(3), 288–299, 2010.)

stabler chelates with rare-earth cations present on the mineral surface (Houot et al. 1991; Pavez et al. 1996). The effectiveness of hydroxamic acids is decreased by water hardness and decreasing pH because Ca^{2+} and Mg^{2+} ions consume large amounts of the collector, and excess hydrogen ions prevent the formation of the chelated compounds (Li et al. 1988).

The key process step in the beneficiation of the Mountain Pass ore is the heated flotation of bastnasite from calcite and barite using a fatty acid collector system (Fuerstenau and Pradip 1991). For the Bayan Obo rare-earth deposit, a very large iron ore deposit with a relatively small quantity of rare-earth minerals present among the iron mineralization, the common elements of its numerous proposed beneficiation flow sheets are a nonselective flotation, using a fatty acid, of rare earths and similar gangue minerals from the iron-bearing minerals followed by a more selective flotation step using a collector such as hydroxamic acid to beneficiate the REO concentrate (Chi et al. 2001; Luo and Chen 1984). The Bayan Obo deposit, with its complex mineralogy and a grain size of 10–74 μm, would have been impossible to process were it not for flotation (Zhang and Edwards 2012).

The selection of depressants depends on the composition of the ore deposit and the major gangue minerals in the flotation feed. At Mountain Pass, lignin sulfonate is added as a depressant to suppress the calcite and barite, but bastnasite is also affected to a certain extent (Houot et al. 1991; Morrice and Wong 1982). Sodium carbonate

is used extensively in bastnasite flotation to control the supply of carbonate anions. Sodium fluoride and sodium hexafluorosilicate have also been used as generic depressants for barite and calcite in the Mountain Pass process. At Bayan Obo, sodium silicate is used to depress iron-bearing and silicate minerals. Hydroxamic acid and sodium silicate are the two most important reagents for successful flotation of the Bayan Obo ores (Jordens et al. 2013).

While flotation is a very useful technique for the beneficiation of bastnasite, Li and Zeng (Jordens et al. 2013) recommend a process combining sizing, gravity, magnetic, and flotation separation steps for superior results, for example, at Mountain Pass (flotation at elevated temperatures), Weishan (flotation using hydroxamic acid), and Dalucao (magnetic and gravity separation). Dalucao is the second largest REE deposit in the Mianning-Dechang REE belt, Sichuan Province. It has mineralogy similar to that of the Maoniuping deposit. At the Maoniuping plant, such a combination yielded grades (62–70% REO) similar to the best-performing plants (Weishan produces a concentrate with a grade of 69.55% REO) while achieving recoveries that were significantly higher than the best performer among the other plants (85–92% REO recovery at Maoniuping versus 78.11% at Dalucao) (Jordens et al. 2013).

3.3.1.3 Monazite Flotation

Monazite flotation has been intensely investigated (Abeidu 1972; Luo and Chen 1984; Houot et al. 1991; Pavez and Peres 1993; Pavez et al. 1996). Monazite flotation is similar to that of bastnasite in terms of collectors used (fatty acids and hydroxamates) as the monazite surface will contain many of the same rare-earth cations present on the bastnasite and the increase in selectivity of these collectors with increasing temperature also applies to monazite flotation. Two of the typical monazite gangue minerals, zircon and rutile, require a depressant, sodium silicate (which is also used in bastnasite flotation), sodium sulfide, and sodium oxalate to enhance selectivity of flotation (Pavez and Peres 1993). In small quantities (10 mg/L), Zakharov et al. (1967) showed that sodium sulfide activated zircon, pyrochlore, and monazite minerals. As the dosage increased (up to 37.5 mg/L) pyrochlore and zircon were depressed, with the monazite flotation unchanged.

Sodium oxalate has been considered as both a depressant and an activator of monazite flotation. Sodium oxalate activates monazite when combined with a sulfonate collector (Bulatovic 2010; Houot et al. 1991). Another depressant of monazite, the starches, have been used with a variety of collectors, including sulfonates, cationic amines (Cuthbertson 1952), and phosphoric acid esters (Ferron et al. 1991). In a novel rare-earth flotation process, using phosphoric acid at an acidic pH and an organic depressant, monazite and an unspecified yttrium-bearing mineral were completely depressed to achieve separation through reverse flotation. The gangue—albite, chlorites, and aegirine—naturally hydrophobic, floated without the need for collector addition.

Apart from Bayan Obo and Mountain Pass, published literature on flotation as a means of REE concentration is limited. In the 1960s, a process for flotation of monazite and steenstrupine was investigated for the Kvanefjeld rare-earth deposit in Greenland. Sodium oleate was used as a collector and sodium silicate as a depressant (Sorensen and Lundgaard 1966).

Apatite is a potential source of REE. Examples of REE-rich apatite deposits include Kola and Kovdor in Russia, Palfos in South Africa, as well as sedimentary deposits in Jordan and Morocco. REEs in the apatite containing tailings of the Chadormalu iron ore concentrator in Iran could also be a source (Jorjani et al. 2007). Being an important class of minerals for the phosphate industry, apatites' flotation is well established. Fatty acid collector systems are common (Lu et al. 1998). Due to the similar chemical nature of common gangue minerals such as calcite and fluorite, fatty acids such as sodium oleate preferentially adsorb onto these gangue minerals instead of apatite. Apatite from the Kola Peninsula in Russia has been successfully recovered via flotation using a tall oil collector and sodium silicate as a gangue depressant. After six flotation stages (one rougher, two scavenger, and three cleaner stages), the resultant concentrate grade was 95% apatite with a 94% phosphate recovery (Houot 1982).

The rare-earth deposit in Mount Weld in Australia has a complex mineralogy. The rare-earth minerals in the ore body include monazite, cheralite, cerianite, florencite, and small quantities of rhabdophane. The gangue minerals are goethite, apatite, crandallite, dolomite, cryptomelane, and jacobsite. Two flotation schemes have been proposed for this resource. One uses a blended collector emulsion of fatty acid with an emulsifier (secondary amino–modified sulfonated fatty acid) and an oil as a froth stabilizer, with sodium sulfide, sodium silicate, and a starch as depressants (Chan 1992). In another scheme (Guy et al. 2000), a fatty acid collector had sodium sulfide, starch, and sodium silicate as the depressants. Apparently, new flotation processes rely on the use of new collectors with the same depressants (Jordens et al. 2014). An amine as a collector has the advantage of easy removal from mineral surfaces after flotation, if a suitable depressant can be developed.

When the constituents of HM deposits (beach sand deposits) are in a finer size range (between 15 and 100 μm), standard gravity methods are not very efficient, and there would be heavy losses of the mineral values. Flotation would be useful. In the former Soviet Union, for the production of bulk HM concentrate from fine-grained beach sand deposits, flotation was performed using fatty acid collectors (Zadorozhnyi 1965, 1967). Ferron et al. (1991) noted that bulk heavy mineral flotation can be performed efficiently using fatty acids or phosphoric acid esters as collectors. For separation of individual HMs, collector selection is dependent upon the ease of desorption prior to separation.

The dressing of South African monazite deposits occurring in association with copper minerals (Hill 1951) was done by flotation to recover both monazite and copper concentrates. Beneficiation by flotation had also been developed for Indian monazite (Viswanathan 1957) and for the recovery of monazite from molybdenum flotation tailings at the Climax Co. mine of Amax (Aplan 1988; Cuthbertson 1952). The flow sheet of the Climax Molybdenum Company's by-product plant, Colorado, is shown in Figure 3.9.

3.3.2 Bastnasite

The bastnasite ore of Mountain Pass has a distinctive beneficiation process. The process, in a simplified form, is shown in Figure 3.10. The blasted bastnasite rock is

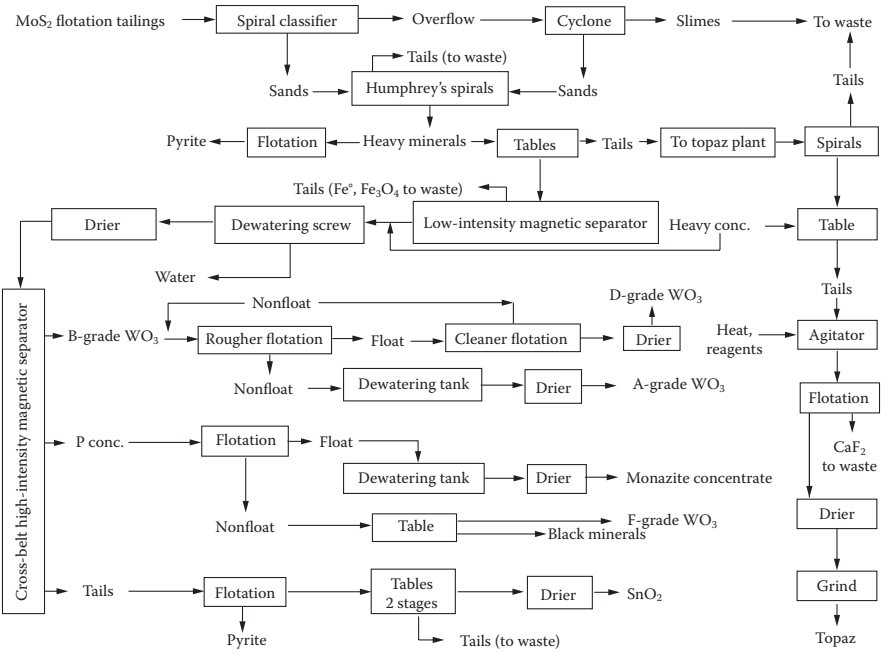


FIGURE 3.9 Flow sheet of Climax Molybdenum Company's by-product plant, Colorado. (From Aplan, F.F., The processing of rare earth minerals. In Bautista, R.G. and Wong, M.M. (eds.), *Rare Earths*, pp. 15–34, The Minerals, Metals and Materials Society, Warrendale, PA, 1988.)

crushed, and the crushed ore is built in layers to average 7% REO in blending piles, to be reclaimed and fed to the mill fine ore bin. The ore is withdrawn from the bin and conveyed to a ball mill, where the particle size is reduced to 100% passing 150 mesh. The ground ore is beneficiated by hot froth flotation.

The flotation characteristics of bastnasite are fairly well established (Fuerstenau and Pradip 1986; Aplan 1988). Various collectors such as fatty acids (oleic) (Morrice and Wong 1982), hydroxamates, and dicarboxylic acids (Xu 1985) have been proposed and/or used. Some of the gangue minerals associated with bastnasite, such as calcite, barite, and celestite, have flotation properties similar to bastnasite, and their separation by conventional fatty acid flotation is difficult.

Mountain Pass ore contains the gangue minerals barite, calcite, strontianite, and quartz. Prior to rougher flotation, the ore undergoes as many as six different conditioning treatments. Conditioning is carried out in large tanks (1800 mm × 2700 mm) with steam being bubbled through the pulp. The reagents are added stepwise in the pulp heated to 70–90°C, and the six-stage conditioning lasts for about 2 h. In the first stage, the ore slurry is mixed with soda ash, sodium fluosilicate, and steam. The next step is steam conditioning. In the third stage, ammonium lignin sulfonate is added in the presence of steam. In the fourth stage, the pulp is conditioned with steam, in the fifth stage with steam-distilled tall oil C-30, and in the sixth stage again with steam. The conditioned slurry, which contains 30–35% solids, is pumped

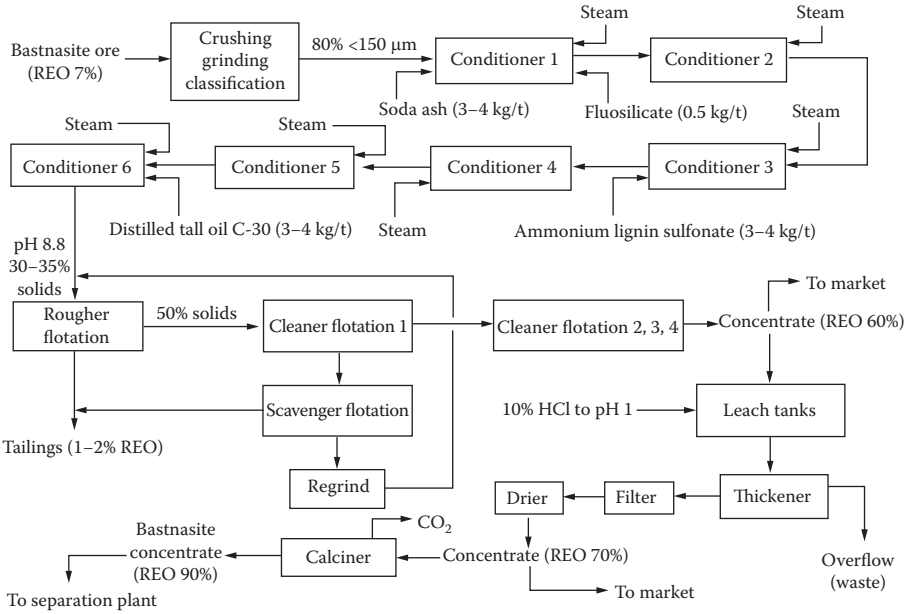


FIGURE 3.10 Simplified flow sheet for the recovery of bastnasite at the Molycorp plant. (From Aplan, F.F., The processing of rare earth minerals. In Bautista, R.G. and Wong, M.M. (eds.), *Rare Earths*, pp. 15–34, The Minerals, Metals and Materials Society, Warrendale, PA, 1988.)

to a rougher flotation circuit. Rougher flotation is carried out in flotation cells, each with a capacity of 1700 L. The tailings from rougher flotation average 1–2% REO. The rougher concentrate, which assays approximately 30% REO, is transported to cleaner cells for four-stage cleaning. These cells operate at 50% solids. Within the cleaning circuit, the tailings are recirculated. Only the tailings from the first cleaner are put through a scavenger flotation circuit. The tailings from the scavenger circuit are combined with rougher tailings and constitute the flotation plant tailings, which average 2% REO. The concentrate from the scavenger is reground and reverted to the rougher cells.

After four-stage cleaning, the final concentrate from the flotation circuit is thickened, filtered, and dried. The final dried concentrate of Mountain Pass contains 60% REO, and the overall recovery is 65–70% (Pradip and Fuerstenau 1988).

A higher recovery of 88% was obtained in a scheme (Ferron et al. 1991) shown in Figure 3.11. The complex bastnasite ore was beneficiated using a double-reverse gangue flotation followed by bastnasite flotation. A specially developed collector was used.

3.3.3 Bayan Obo Ore

Numerous minerals occur intimately intergrown in the rare earth–bearing Bayan Obo iron ore (Aplan 1988; Li et al. 1988). In physical beneficiation, in addition to

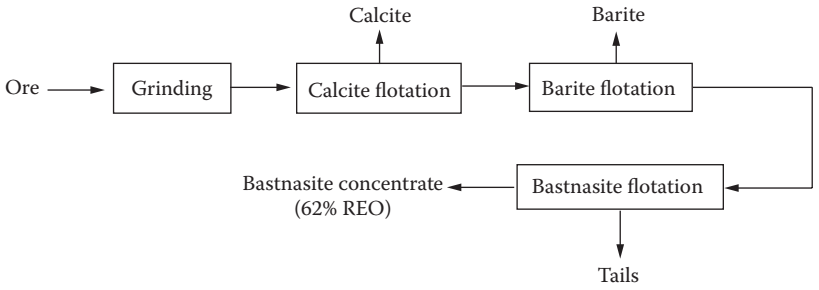


FIGURE 3.11 New scheme for the treatment of complex bastnasite ore. (From Ferron, C.J. et al., Beneficiation of rare earth oxide minerals. In Siribumrungsukha, B., Arrykul, S., Sanguan Sai, P., Pungrassami, T., Sikong, L., and Kooptarnon, K. (eds.), *Proc. Int. Conf. Rare Earth Minerals and Minerals for Electronic Uses*, Jan. 1991, Hat Yai, Thailand, pp. 251 –269, Prince of Songkla University, Thailand, 1991.)

the rare earths, magnetite, fluorite, hematite, and niobium oxide are recovered as valuable by-products. Three schemes for the processing flow sheet of Bayan Obo ore (Luo and Chen 1985, 1988; Houot et al. 1991) are shown in Figure 3.12. The initial bulk flotation is carried out after grinding the ore to 90% <74 μm, with Na_2CO_3 as a pH regulator, Na_2SiO_3 as a depressant of iron minerals and silicates, and sodium salt of oxidized petroleum (paraffin soap) as a collector. Depressed iron minerals and silicates remain at the bottom of the flotation cells and are taken for iron beneficiation and niobium recovery. After eliminating the surplus fatty acid collector by thickening and desliming, selective rare-earth flotation is carried out with Na_2CO_3 as a pH regulator, Na_2SiO_3 and Na_2SiF_6 as gangue depressants, and hydroxamic acid as a collector at a pH between 5 and 6. Depressed calcite, fluorite, and barite settle to the flotation cell bottom. After selective flotation, the rougher concentrate contains approximately 45% REO. It contains both monazite and bastnasite. The recovery of rare earth as the concentrate at this stage is ~80%. After the final treatment by cleaning or high-intensity magnetic separation, two concentrate fractions—the primary 68% REO concentrate and a secondary monazite concentrate containing 36% REO concentrate—are obtained at recoveries of 25% and 36%, respectively. The total recovery of rare earths from the ore is 61%.

Gravity separation (shaking tables, spiral concentrators, and conical separators) is used in combination with froth flotation at many rare-earth mineral processing operations throughout China (Chi et al. 2001). At Bayan Obo, gravity separation is used between the rougher and cleaner flotation circuits to efficiently separate monazite and bastnasite from the iron-bearing and silicate gangue material (Luo and Chen 1984). Here, the gangue minerals (e.g., barite) have specific gravities similar to the rare-earth minerals and collect in the concentrate stream. Besides, gravity separation is ineffective at separating very fine particles. This results in large losses of rare-earth values (Jordens et al. 2013).

Kul et al. (2008) summarized a complete processing scheme for the bastnasite ore in Beylikahir, Eskişehir, Turkey. The resource had an average grade of 3.14% REO and contains, apart from bastnasite ($LnFCO_3$) and thoro-bastnasite, fluorspar (CaF_2)

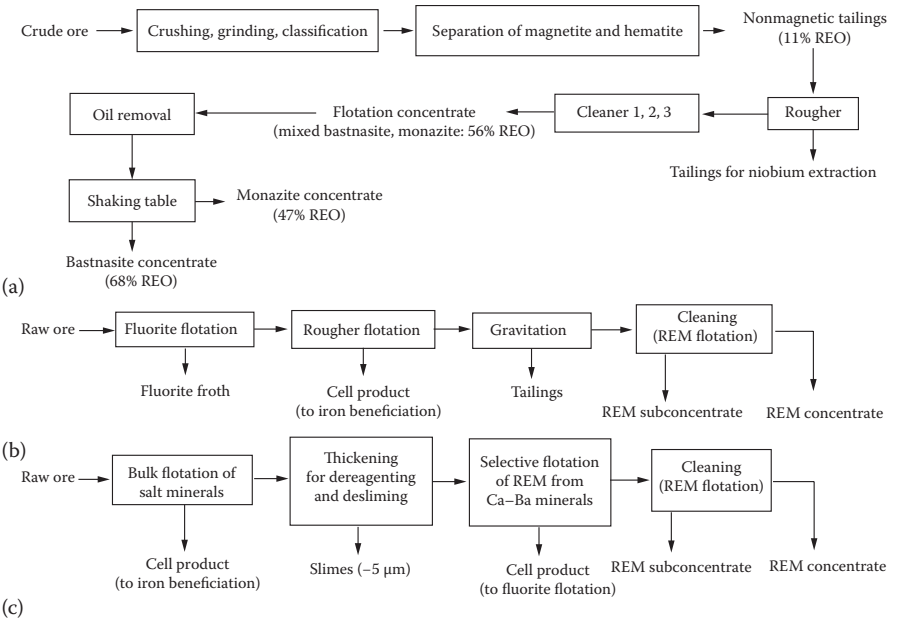


FIGURE 3.12 Schemes for the physical beneficiation of Bayan Obo ore. (From Anderson, L., *Erzmetall*, 39(4): 152–157, 1986; Houot, R. et al., Recovery of rare earth minerals with emphasis on flotation process. In Siribumrungsukha, B., Arrykul, S., Sanguan Sai, P., Pungrassami, T., Sikong, L., and Kooptarnon, K. (eds.), *Proc. Int. Conf. Rare Earth Minerals and Minerals for Electronic Uses,* Jan. 1991, Hat Yai, Thailand, Prince of Songkla University, Thailand, pp. 301–324, 1991.)

and barite ($BaSO_4$). Bastnasite occurs as very fine yellowish particles (1–2 μm), and physical beneficiation of the ore was very difficult by the usual mineral dressing processes. At best, the physical concentration methods, viz., attrition scrubbing, screening, and desliming by cyclones, could be applied to produce a low-grade concentrate, or preconcentrate, containing only 23.5% REO.

3.4 BENEFICIATION OF OTHER RARE-EARTH MINERALS

Jordens et al. (2013) reported results of physical beneficiation of ore from the Nechalacho deposit (Avalon Rare Metals, Inc.), Northwest Territories, Canada. The composition of the Nechalacho deposit is given in Table 3.1. Zircon is the most important RE mineral and hosts over 65% of all REEs in the deposit (Cox et al. 2011). The major gangue minerals are quartz, K-feldspar, plagioclase, biotite, and iron oxides.

The sequence of operations carried out in a laboratory scale is summarized in Figure 3.13 (Jordens et al. 2013). The ore was initially crushed to ≤850 μm using a jaw and cone crusher. A portion of the crushed ore was stage pulverized to 80% passing 53 μm and fed to a Knelson concentrator, and a second portion of the ore was ground dry in a rod mill before being stage pulverized to 80% passing 44 μm

TABLE 3.1
Mineralogical Composition of the Nechalacho Deposit Along with Specific Gravity and Magnetic Property Data

Mineral Component	Composition Weight %	Nominal Specific Gravity	Magnetic Properties
Quartz	35.1	2.63	Diamagnetic
K-feldspar	20.5	2.57	Diamagnetic
Plagioclase	10.5	2.68	Diamagnetic
Biotite	9.6	3.10	Paramagnetic
Fe oxides	8.3	5.30	Ferromagnetic
Zircon	4.1	4.65	Diamagnetic
Ankerite	3.7	3.05	Paramagnetic
Calcite	1.9	2.71	Diamagnetic
Dolomite	1.8	2.85	Diamagnetic
Bastnasite	1.3	4.98	Paramagnetic
Columbite (Fe)	0.5	6.30	Paramagnetic
Fluorite	0.3	3.18	Diamagnetic
Fergusonite	0.3	5.05	Paramagnetic
Monazite	0.2	5.15	Paramagnetic
Apatite	0.2	3.18	Diamagnetic
Synchysite	0.2	4.03	N/A
Allanite	0.1	3.75	Paramagnetic

Source: Long, K.R. et al., The principal rare earth elements deposits of the United States—A summary of domestic deposits and a global perspective, U.S. Geological Survey Scientific Investigations Report 2010–5220, available at http://pubs.usgs.gov/sir/2010/5220, 2010; Rosenblum, S. and Brownfield, I.K., Magnetic susceptibilities of minerals, report for US Geological Survey, 1999; Jordens, A. et al., *Miner. Eng.*, 41: 97–114, 2013.

and fed to the Falcon concentrator. Following gravity preconcentration, the material was processed using wet high intensity magnetic separator (WHIMS). Gravity preconcentration steps eliminated low-specific-gravity gangue minerals, and magnetic separation at varying magnetic field strengths removed unwanted ferromagnetic gangue minerals or concentrated valuable paramagnetic RE minerals.

Jordens et al. (2013) noted that for the Nechalacho ore, the combination of Falcon concentrator and WHIMS was more effective in concentrating the valuable heavy, magnetic minerals. Diamagnetic, low-specific-gravity gangue minerals in the RE ore such as K-feldspar and plagioclase are rejected into the tails of the Falcon concentration step, and when these tails are fed to a series of WHIMS steps, the same minerals report to the nonmagnetic fraction. The magnetic susceptibilities of fergusonite and allanite are of similar magnitude, both larger than the susceptibility of bastnasite. This would imply that fergusonite and allanite would require a lower applied magnetic field strength for magnetic recovery than bastnasite. Zircon in the ore behaves in a paramagnetic or ferromagnetic manner, possibly due to insufficient liberation resulting in many zircon grains associated with ferromagnetic iron oxides in locked

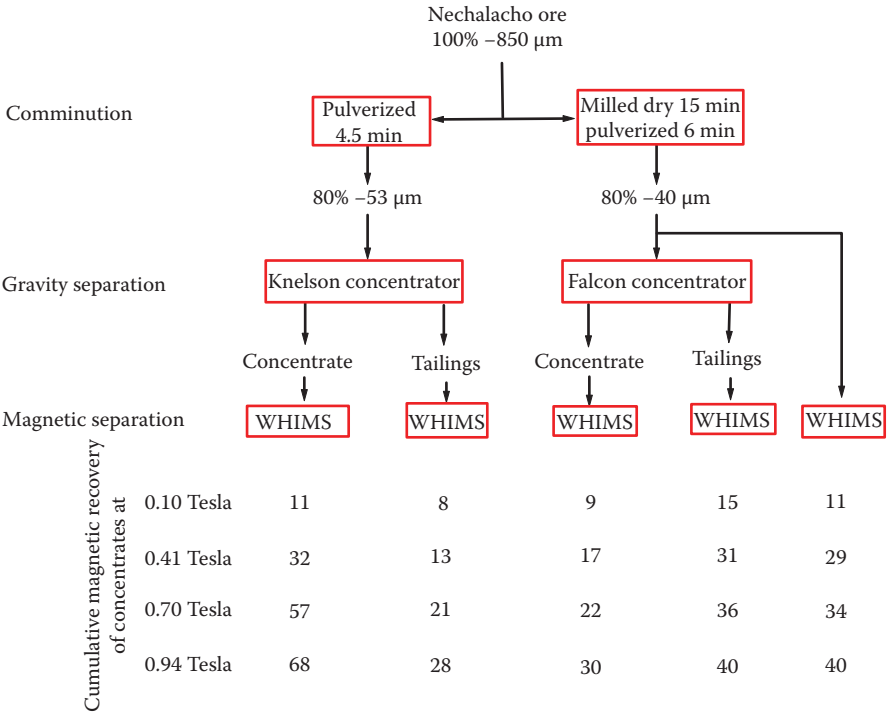


FIGURE 3.13 Flow sheet of WHIMS experiments with and without gravity preconcentration. (From Jordens, A. et al., *Miner. Eng.*, 62: 9–18, 2014.)

particles. The WHIMS first concentrate (lowest applied magnetic field strength) produced from the Falcon concentrate consisted of magnetite and hematite, indicating that the ferromagnetic iron oxide gangue minerals in the RE ore may potentially be removed from a future gravity concentrate using low-intensity magnetic separation. The removal of unwanted iron-bearing minerals from a potential flotation feed could be a critical process step depending on the selection of flotation collector.

Loparite occurs extensively in Russia's Kola Peninsula. This is concentrated by a combination of gravity and magnetic separation techniques (Hedrick et al. 1997), removing, in the process the gangue minerals aegirine, feldspar, nepheline, and ramsayite.

Raslan (2009) described the beneficiation, on a laboratory scale, of an HM resource (samarskite-[Y], columbite, and zircon from stream sediments of the Ras Baroud area, Central Eastern Desert, Egypt) containing approximately 1.5 wt.% samarskite-(Y). They used desliming, sieving, gravity separation (using a shaking table), and magnetic separation to produce a concentrate containing 73.8 wt.% samarskite. The operation sequence was as follows: (1) A feed consisting of samarskite-(Y), columbite, zircon, magnetite, garnet, goethite, ilmenite, hematite, and mica was deslimed and then sieved to 100% passing 1 mm. (2) The sieved material was sized, and the resultant size fractions were individually fed to a gravity shaking table. (3) The heavy fractions were then subjected to magnetic separation, first

to remove magnetite in a low-intensity process and then to produce a nonmagnetic concentrate containing predominantly samarskite-(Y) and zircon in a second, high-intensity step.

Gao and Chen (2010) studied the beneficiation of a rare-earth ore containing scandium, particularly the effect of feed fineness on the susceptibility of the ore to a series of high-gradient magnetic separations.

Reviewing the existing literature on the physical beneficiation of rare-earth minerals, Jordens et al. (2013) commented that the publications are mainly focused on the two major REE mineral deposits, Bayan Obo and Mountain Pass, with only a passing reference to other minor rare-earth minerals. A considerable amount of rare-earth research reported in Chinese journals does not usually provide background information (proper chemical names of collector molecules, detailed descriptions of processes, etc.) to help any significant insights into the development of separation processes for alternative rare-earth minerals. They concluded that each rare-earth mineral, no matter how widely investigated, presents significant opportunities for future research.

3.5 CHEMICAL TREATMENT

3.5.1 Monazite

The removal of thorium and recovery of mixed rare earths from monazite can be accomplished in many ways (Bril 1964), after chemically attacking the mineral with sulfuric acid or sodium hydroxide.

3.5.1.1 Acid Treatment

The sulfuric acid method had been used extensively in the United States (Parker and Baroch 1971). By this method (Shaw et al. 1954), depending on the acid–ore ratio, temperature, and concentration, either thorium or the rare earths can be selectively dissolved, or both thorium and rare earths are dissolved together. Rare earths and thorium are then recovered from the solution. The processes available are shown in Figure 3.14. The industrially used process of rare-earth recovery based on rare-earth double-sulfate precipitation was largely developed by Pilkington and Wylie (1952). Yttrium and the heavy rare-earth (HRE) double sulfates are quite soluble and go with thorium. Even in the stepwise neutralization procedure investigated at Ames (Smutz et al. 1954; Barghusen and Smutz 1958), yttrium and the HREs are precipitated along with thorium as a basic compound. The rare earths, however, are recoverable from the thorium fraction during solvent extraction for the purification of thorium and uranium. Solvent extraction with tributyl phosphate (TBP) from an 8N nitric acid solution of thorium and mixed rare earths permits the recovery of thorium, uranium, cerium, and cerium-free rare earths. Other commercially significant processes involve precipitation of thorium pyrophosphate or basic salts from the leach liquor and subsequent recovery of the rare earth in solution as double sulfates, fluorides, or hydroxides or even selective solubilization of thorium in the ore treatment stage itself, as originally developed by Société des Produits Chimiques des Terres Rares (Powell 1939). The sulfuric acid process does not yield pure products and is no longer in commercial use.

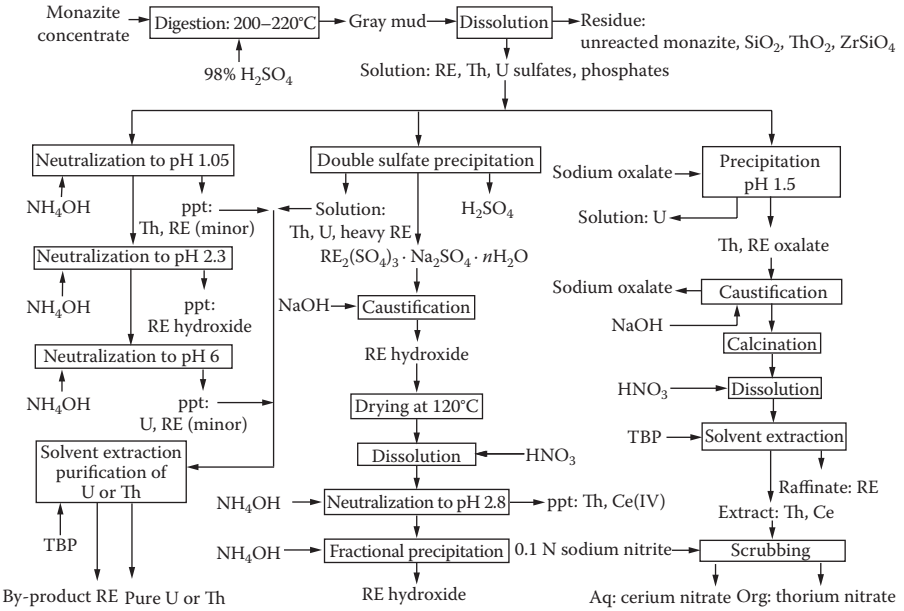


FIGURE 3.14 Monazite processing by acid treatment.

3.5.1.2 Alkali Treatment

The flow sheet for the present commercial process for monazite treatment using caustic soda is given in Figure 3.15. The phosphate content of the ore is recovered as a marketable by-product, trisodium phosphate, at the beginning of the flow sheet, and this has been a major attraction for the commercial use of this process. The practical development of caustic soda treatment for rare-earth processing is credited to de Rhoden and Peltier (1957), and considerable work on the process was carried out at the Battelle Memorial Institute. In the usual industrial practice, fine-ground monazite is attacked with a 60–70% sodium hydroxide solution at 140–150°C. In the Soviet practice, the grinding and caustic digestion are done in one step, and this leads to considerable (about 50%) savings in caustic soda consumption. Krumholz (1957) achieved a clean separation by digesting the ore with caustic soda at 170°C under a pressure of several atmospheres. The mixed rare-earth thorium hydroxide cake is processed for rare-earth and thorium recovery by a variety of methods.

The dissolution of the mixed rare-earth thorium hydroxide in nitric acid and separation of rare earths by extracting thorium and uranium with TBP is attractive but complicated because of interference arising from partial oxidation of cerium. An effective process for removing thorium completely and in a high state of purity is solvent extraction with higher amines. The amines function well with a sulfate solution (Kaczmarek 1981).

3.5.1.3 Indian Rare Earths Ltd. Practice

The Indian Rare Earths Ltd. (IRE) plant at Alwaye in Kerala uses the caustic soda treatment for the decomposition of monazite sands, and the process has four major

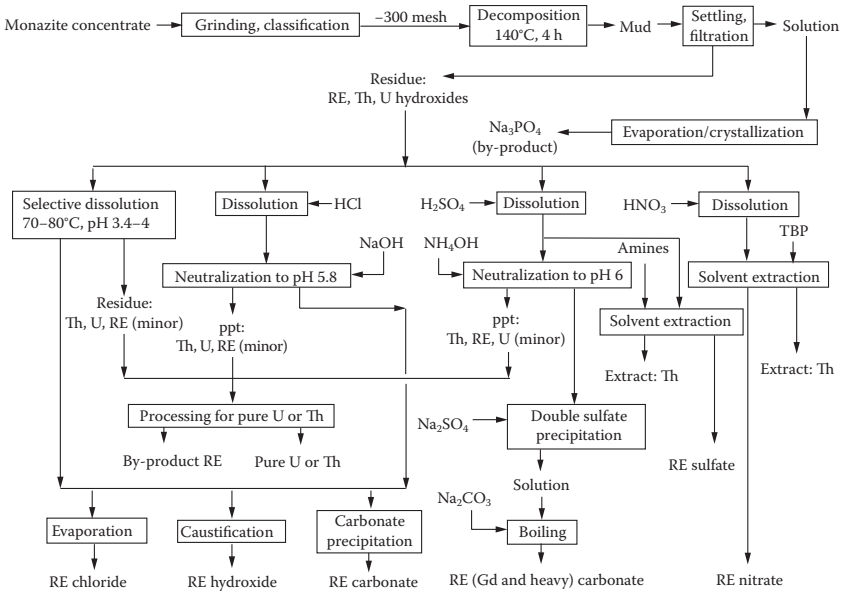


FIGURE 3.15 Monazite processing by alkali treatment.

stages: (1) reaction of finely ground monazite sand with a hot concentrated aqueous caustic soda solution, to convert the rare earth and thorium contained in the ore into their respective hydroxides; (2) separation of the insoluble hydroxides from the dissolved phosphate and excess caustic soda; (3) recovery of trisodium phosphate; and (4) separation of rare earths from thorium by leaching with hydrochloric acid. An outline of the flow sheet at the IRE plant is shown in Figure 3.16.

The monazite sand is ground in a ball mill to finer than 300 mesh size in a closed-circuit system using an air classifier. The ground sand in 0.5-ton batches is mixed with 50% caustic solution and fed to a conical mild steel tank and heated to approximately 150°C with the addition of fresh caustic soda at a ratio of about 1:1 monazite sand caustic soda. The final concentration of caustic soda to give is about 65–70%. The mixture is agitated during the reaction, which lasts for about 3–4 h. Most of the monazite is decomposed during this period.

The hydroxide–trisodium phosphate mixture is dumped into a tank containing dilute wash liquors from a previous decantation, and the slurry is heated to approximately 90°C and the density adjusted to about 30°Be. The slurry is allowed to settle for about 12 h when the supernatant liquid containing most of the trisodium phosphate and excess caustic soda is drawn off and sent to the trisodium phosphate recovery section. The hydroxides are washed once again with hot water and allowed to decant, and the supernatant liquid is drawn off to be reused for a subsequent extraction of trisodium phosphate.

By this means, the free alkalinity in the hydroxides is reduced from about 70 g/L (expressed as free NaOH) to about 15 g/L. The mixture of hydroxides is then fed to a vacuum leaf filter and washed to reduce the alkalinity before being treated for the separation of rare earths from thorium.

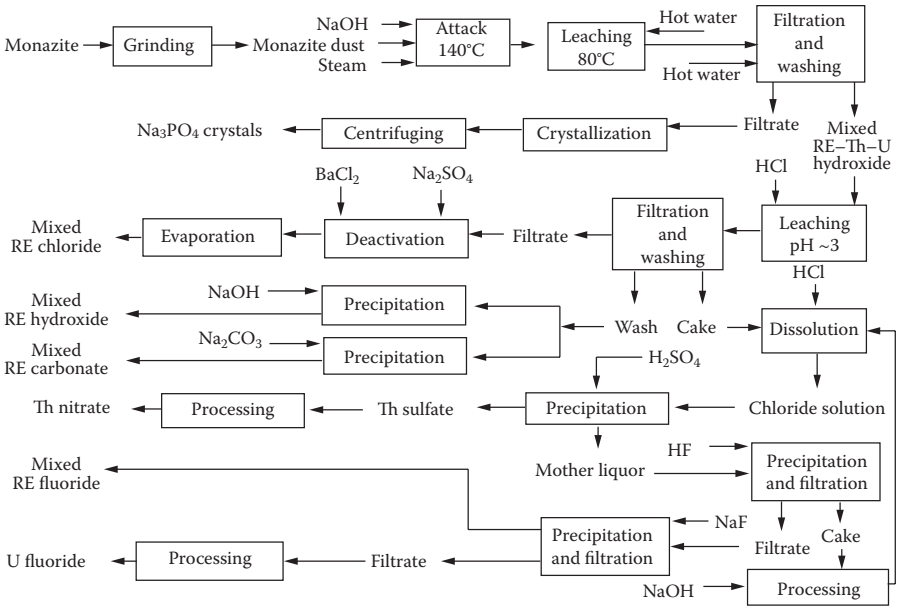


FIGURE 3.16 IRE process for caustic soda treatment of monazite.

The solution of trisodium phosphate and caustic soda from the decantation tanks is filtered and fed for crystallization. In the crystallizer, the solution is cooled in two stages from about 70°C to 20°C, at which temperature most of the trisodium phosphate crystallizes out. The mixture of trisodium phosphate crystals and dilute caustic soda solution is fed to a continuous centrifuge, and the centrifuged trisodium phosphate is dried in a hot-air conveyor drier. The dry trisodium phosphate contains approximately 19% P_2O_5 and is purer than the trisodium phosphate manufactured by the usual process of neutralization of phosphoric acid.

The washed hydroxide cake is treated in a rubber-lined tank with 21–22°Be hydrochloric acid. The quantity of hydrochloric acid added is sufficient to dissolve only the rare earths while the thorium remains undissolved. Iron is precipitated by oxidizing it to the ferric stage, and suitable precautions are taken to prevent oxidation of cerium to the ceric stage. The pH of this slurry is in the neighborhood of 3. The slurry is pumped to a plate and frame-type filter press using rubber-lined equipment.

The filtrate after removal of lead is converted to the fused mixed rare-earth chloride by heating it in an enameled cast iron vessel to the boiling point of approximately 145°C and then pouring it into steel drums, where it solidifies on cooling.

The thorium hydroxide is washed, and the rare earths in the wash waters are recovered as mixed rare-earth carbonate by the addition of sodium carbonate, or as the mixed rare-earth hydroxide by the addition of caustic soda. Both of these rare-earth compounds are dried in a rotary drier before being packed in steel drums. The cake contains all the thorium present in the monazite and most of the uranium. It also contains a certain percentage of rare earths and other insoluble impurities.

The crude thorium hydroxide cake is dissolved in an excess of hydrochloric acid, and the resulting chloride solution is filtered on a plate and frame-type filter press to remove insoluble impurities like ilmenite, zircon, etc. The clear filtrate is treated with an excess of 50% sulfuric acid. Most of the thorium is precipitated as a sulfate, while most of the rare earths and most of the uranium remain in solution. The thorium sulfate is centrifuged in a rubber-lined centrifuge, and the solution is sent for recovery of thorium, rare earths, and uranium that are in solution. The sulfate is not pure enough and is further purified by reprecipitating with 50% sulfuric acid to give a purer thorium sulfate.

The pure thorium sulfate is converted to hydroxide by reacting it with ammonium hydroxide. This is filtered and washed on filter presses to remove all the water-soluble impurities. The thorium hydroxide is then dissolved in chemically pure nitric acid to give a solution of thorium nitrate, which is filtered and evaporated to the required strength in a glass-lined evaporator. The molten nitrate is allowed to solidify in aluminum dishes and then packed in glass bottles or steel-lined drums.

The solution obtained from the precipitation of thorium sulfate is treated for the recovery of thorium, rare earths, and uranium by fractional precipitation with hydrofluoric acid.

3.5.1.4 Monazite Breakdown Practices

The conditions for monazite processing by alkali treatment have remained essentially unchanged for the past 40 years, except for minor variations. Summaries of alkali digestion practices (Mackey 1986; Koch 1987; Hart and Levins 1988) note that monazite can be very fine ground (to less than 10 μm) and cracked with a 70% NaOH solution under pressure for 2 h at 150°C to form an insoluble hydroxide residue of rare earths and thorium. Subsequently, the hydroxide residue is leached in nitric, sulfuric, or hydrochloric acid to prepare rare-earth solutions for solvent extraction. Studies on the decomposition of an Australian monazite concentrate (48.6% rare earths, 6% thoria, 31% phosphate, and 14% residue of mostly zircon) pointed out that the extraction reached 98% by digesting fine-ground (less than 45 μm) monazite concentrate in 80% w/v (NaOH–monazite weight ratio, 1.5:1) at 140°C for 3 h. Studies on Brazilian monazite have also confirmed the necessity of fine grinding (less than 45 μm) and high temperature (140–200°C) for effective decomposition. In their investigations on chemical treatment of Taiwanese black monazite, Miao and Horng (1988) used both "hydrothermal" and soda fusion methods. In the hydrothermal process, ground monazite (95% within 80–100 mesh) was cracked with 45 wt.% of aqueous alkali solution at 170°C and 5 atm in an autoclave for 3 h. As an alternative, they fed unground monazite into fused caustic soda at 400°C in an open cylindrical stainless steel tank and reacted the mass for 2.5 h with low-speed agitation. In each of these operations, 90% of the rare earths contained in the monazite were recovered in the product. Apparently, significantly higher temperature and the use of fused soda give an equivalent result to lower-temperature, high-pressure treatment with an alkali solution. The product was a rare-earth hydroxide slurry with sodium phosphate in the first case and a rare-earth hydrous oxide with a sodium phosphate hard mass rock in the second. In either case, the product was converted to the chloride by dissolving in HCl, and thorium was selectively precipitated as hydroxide from the RE chlorides by pH adjustment.

Caustic soda digestion is the process followed in the monazite cracking plant established in Malaysia in 1979, by Asian Rare Earth Sdn Bhd (ARE) at Bukit Merah in Perak State (Sulaiman 1991). Caustic soda digestion yields trisodium phosphate and the hydroxides of rare earths and thorium. The phosphate is separated from the hydroxides by dissolving it in water. From this solution, it is crystallized out or converted to tricalcium phosphate. Thorium and rare earths are separated by a selective dissolution method. Rare earths are dissolved in concentrated HCl, and the undissolved thorium is filtered and produced as thorium cake waste. The rare-earth fraction is separated into light rare earths (LREs) and HREs by solvent extraction with di-2-ethyl-hexyl phosphoric acid (HDEHP/D2EHPA), and the rare earths are finally precipitated as carbonates.

Rhône-Poulenc used caustic soda digestion for chemical treatment of monazite at its plants in La Rochelle (France) and Freeport (Texas, USA). Monazite concentrate is reacted with sodium hydroxide to break the phosphate matrix. The rare-earth hydroxides recovered in the process are leached with nitric acid to produce nitrate solutions for solvent extraction. Rhône-Poulenc separated all the rare earths by solvent extraction.

Amer et al. (2013) used an interesting combination of alkali and acid leaching to process Rosetta (Egypt) monazite. A schematic flow sheet is given in Figure 3.17. The objective was to avoid the direct breakdown of the concentrate with sulfuric acid, which results in impure products on the one hand, and also to recover the trisodium phosphate. The hydrous oxide cake from the alkali breakdown was dissolved by sulfuric acid, and from sulfate liquor, the REEs and thorium were precipitated as their insoluble oxalates, leaving uranium in solution. Instead of processing through the usual sequence of applying solvent extraction using TBP to extract Th

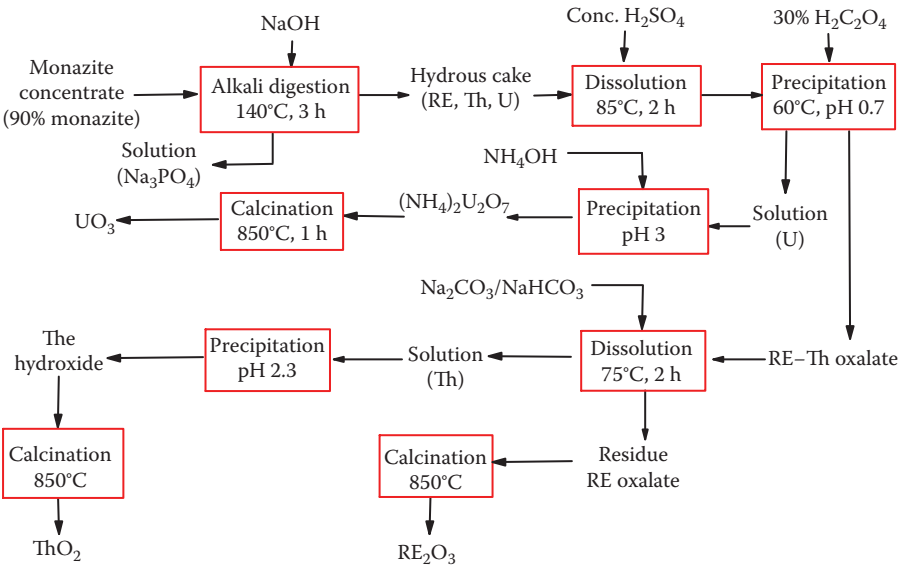


FIGURE 3.17 A schematic flow sheet for processing of Rosetta (Egypt) monazite. (From Amer, T.E. et al., *Int. J. Miner. Process.*, 125(10 December 2013): 106–111, 2013.)

and Ce(IV), a selective carbonate separation of thorium from the combined oxalate precipitate was attempted. The carbonate leaching was based on the observation by Cuthbert (1958) that Th and U can be separated from the rare earths by using the fact that both U and Th form soluble complex carbonates while the REEs form insoluble carbonates. Currently, only thorium is present in the cake apart from the rare earths, and on leaching with the carbonate, thorium alone enters the solution.

3.5.1.5 High-Temperature Process

A process based on high-temperature reaction of monazite with calcium chloride and calcium carbonate was suggested by Merritt (1990a). In this, monazite is decomposed by reacting it with calcium chloride and calcium carbonate in an environment that is both reducing and sulfidizing, at temperatures between 980°C and 1190°C. The products are rare-earth oxysulfides, oxychlorides, a thorium-rich oxide solid solution, and a calcium chlorophosphate (chloropatite). From the product, the REEs are leached out with 3% HCl, leaving gangue minerals and thorium-rich, oxide residue. The residue is resistant to acid attack and is probably suitable for disposal by burial. The process is attractive for the following reasons: (1) Effectively all the monazite is decomposed in 45 min compared to 3–4 h for the caustic digestion process. (2) Grinding of monazite to ~50 μm is not necessary. (3) The thorium oxide residue from the dilute acid leach is readily filtered, and, because it is more resistant to acid attack than thorium hydroxide, the residue is more suited for disposal by burial. The limitations are that (1) the maximum overall recovery of REEs is only 89% compared to 94.5% for the sodium hydroxide digestion process, (2) the recovery of phosphate value is not addressed, and (3) the method does not offer improved REE–thorium separation.

Another process (Merritt 1990b) used sodium carbonate as the reactant for attacking monazite in an environment that is both reducing and sulfidizing at 900°C. The products were REE oxysulfide, a thorium-rich oxide, and γ-trisodium phosphate and a mixed sodium–REE phosphate. From the reacted mass, most of the phosphate can be separated by leaching it with water at room temperature. From the water-leached residue, the REEs are selectively leached with 3.5% hydrochloric acid. In this process, decomposition of monazite is rapid (complete in only 2 h), grinding is not necessary, and the separation of rare earths from thorium is simple because unlike the present commercial process, careful control of pH is not necessary for separation. The better recovery of REEs, 94.5% in the sodium hydroxide digestion process, apparently makes it superior, but in that process, 10% of the original thorium remains with the REEs. In the sodium carbonate process, the corresponding figures are 91.5% recovery and only 6.6% of the original thorium left with the rare earths. Merritt (1990a,b) conducted the experiments for these investigations using very small changes in a tube furnace. It is probably too early to compare this process extensively with a process of multiton batch size. Another disadvantage of the present high-temperature process is the high temperature itself.

3.5.1.6 Chlorination

A method of preparing anhydrous rare-earth chlorides by high-temperature chlorination of monazite was investigated by Hartley (1952). Pelletized mixtures of monazite and charcoal were heated in chlorine at over 900°C in a silica reactor. Over 85% of the

rare earths in monazite were recovered as anhydrous rare-earth chlorides, virtually free of thorium chloride and phosphorus compounds. Later, Brugger and Greinacher (1967) proposed a process for the chlorination of bastnasite, which was also applicable.

3.5.2 Bastnasite

Chemical treatment of bastnasite can start with either crude ore or bastnasite concentrate. The methods available are summarized in Figure 3.18. The 60% REO bastnasite obtained after physical beneficiation can be upgraded to about 70% REO by leaching with hydrochloric acid to remove calcium and strontium carbonates. The 70% REO concentrate can be upgraded to 85–90% REO by calcination to remove the carbon dioxide.

The decomposition of bastnasite was extensively investigated at Ames and at the US Bureau of Mines (Rice 1959; Shaw 1959; Berber et al. 1960). A process was described, involving nitric acid digestion and solvent extraction, in which over 98% of the original rare-earth content was recovered starting from the crude bastnasite ore containing 7–10% REO. Shaw (1959) and Berber et al. (1960) described a process in which the bastnasite concentrate was dissolved in warm concentrated sulfuric acid and the rare earths were recovered as water-soluble sulfates. The sulfuric acid process has found commercial application (Kaczmarek 1981) for purifying rare earths from the common impurities Fe, Pb, Si, and Ba in the ore. Acid consumption is decreased when bastnasite concentrate is roasted to decompose the carbonate minerals before leaching with 30% HCI either hydrochloric or sulfuric acid.

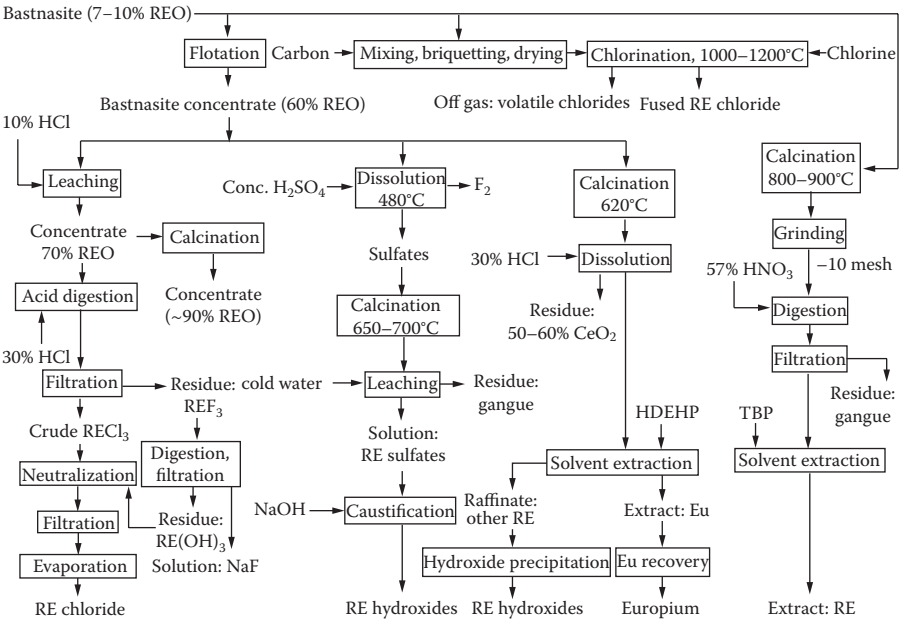


FIGURE 3.18 Chemical processing of bastnasite.

In the Molycorp process (World Mining 1966), the flotation concentrate, containing 60% REO, is roasted in air at 620°C to drive off carbon dioxide and oxidize cerium to a tetravalent state. The calcine is treated with 30% HCl to dissolve the non-cerium rare earths, yielding a marketable cerium concentrate containing 65–70% REO with 55–60% CeO_2. The solution is processed further for the recovery of europium and also to obtain other rare earths contained in it.

The ceria residue also contains mixed rare-earth fluorides. Leaching of bastnasite with hydrochloric acid (30% HCl) does not decompose the fluorides. The fluorides are, however, decomposed by treatment with caustic soda (Parker and Baroch 1971) to form rare-earth hydroxide. The rare-earth hydroxide is then leached with HCl.

Kruesi and Duker (1965) of Molycorp developed the process, shown in Figure 3.19, for the production of rare-earth chlorides from bastnasite. The process consists of three steps in which the following reactions occur.

$$REF_3–RE_2(CO_3)_3 + 9HCl \rightarrow REF_3 + 2RECl_3 + 3HCl + 3H_2O + 3CO_2$$

$$REF_3 + 3NaOH \rightarrow RE(OH)_3 + 3NaF$$

and

$$RE(OH)_3 + 3HCl \rightarrow RECl_3 + 3H_2O$$

The bastnasite concentrate (70% REO, 65% –325 mesh) was attacked with a minimum amount of hydrochloric acid (1.8 kg 20°Be acid/kg of ore or 2.5 kg/kg of RE_2O_3) for 4 h at 200°F. Solid–liquid separation of the leach liquor was done by decantation. In the next step, rare-earth fluoride in the solid residue was metathetically converted

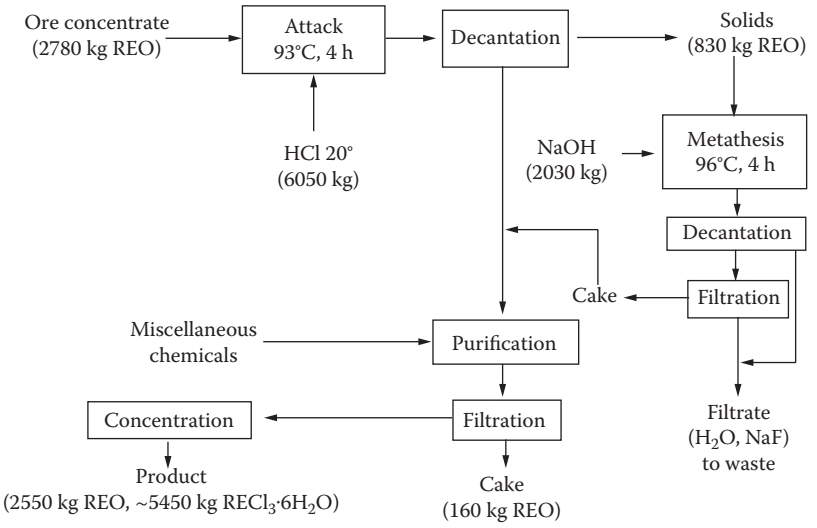


FIGURE 3.19 Production of rare-earth chlorides from bastnasite. (From Kruesi, P.R. and Duker, G., *J. Metals,* 17: 847–849, 1965.)

to rare-earth hydroxide using 500 kg NaOH/1000 kg of concentrate feed (or 0.73 kg NaOH/kg of REO feed). Reaction duration was 4 h. The metathesis cake was thoroughly washed with water to low sodium content.

The next step was neutralization and purification. Substantial amounts of free hydrochloric acid in the mother liquor were neutralized by addition of the rare-earth hydroxide obtained in the metathesis step, until a pH of about 3 was obtained. The pH control was necessary to remove impurities. Small amounts of hydroxide were added to the heated solution to completely precipitate iron hydroxide. A small amount of sulfuric acid was added to precipitate lead sulfate, and then barium chloride was added to precipitate excess sulfate and to act as a carrier in the removal of any thorium daughter product originally present in the ore. At this pH, thorium hydroxide is also insoluble, and traces of it were removed. On filtration, a sparkling clear solution of rare-earth chlorides was obtained, with all the impurities remaining in the cake. The cake was washed repeatedly to low rare-earth content and discarded. The rare-earth-chloride solution was concentrated by evaporation and cast into a solid form. The analyses of the bastnasite concentrate starting material and rare-earth-chloride end products are given in Table 3.2.

TABLE 3.2
Typical Analysis of Bastnasite Concentrate and the Rare-Earth Chlorides (Wt.%)

	Concentrate[a]		Chloride I[b]		Chloride II[c]
$BaSO_4$	1.0–0.5			$BaCl_2$	2.6–4.2
CaO	1.0–0.5	CaO	1.00	$CaCl_2$	3.4–3.6
F	5.0–5.5	MgO	1.00	Acid-insoluble fluoride	13–15
Fe_2O_3	0.5–0.3	Fe	0.005	Fe_2O_3	<0.01
SiO_2	1.0–0.5	SiO_2	0.05	$SrCl_2$	0.4–0.6
ThO_2	<0.01	Radioactivity	Absent	$MgCl_2$	0.1–0.2
REO	68–72	REO	46.0	REO	66.0
CeO_2	50.0			CeO_2	49–50
La_2O_3	31.0			La_2O_3 (including rare earths not listed)	32–35
Pr_6O_{11}	5.0			Pr_6O_{11}	3.8–4.3
Nd_2O_3	12.9			Nd_2O_3	11–12
Sm_2O_3	0.62			Sm_2O_3	0.6–1
Eu_2O_3	0.11				
Gd_2O_3	0.2				
Y_2O_3	0.05				
Other heavies	0.02				

[a] Mountain Pass bastnasite concentrate.

[b] Chloride I was obtained by the wet method (Kruesi and Duker 1965).

[c] Chloride II was obtained by the dry method (Brugger and Greinacher 1967).

In the process followed at the Thorium Ltd. plant in the United Kingdom, the bastnasite concentrate was treated with caustic soda to convert the fluoride component to hydroxide. Following this with dissolution in hydrochloric acid, a rare-earth-chloride solution was obtained from which the hexahydrate $RECl_3 \cdot 6H_2O$ was crystallized or the solution was processed further for recovering individual rare earths. This process entails high alkali consumption. In case monazite is present in the concentrate, the thorium will end up in both the leachate and the residue (Xie et al. 2014).

Direct alkaline roasting of the ore to convert the fluoride in the ore into soluble alkali fluoride, and then water leaching, followed by separation of unconverted barite by flotation was a process investigated by Kasey (1959).

The bastnasite concentrates are processed in China by heating with 98% sulfuric acid at 300–500°C in a rotary kiln. By this, the fluorocarbonate matrix is destroyed, carbon dioxide and hydrogen fluoride gases are released, and the rare earths are converted to their sulfates. The rare earths are precipitated as double sodium sulfate by leaching with water and adding sodium chloride. Subsequently, the rare-earth sulfates are converted to hydroxides by digestion in a strong caustic solution, and the hydroxides are then dissolved in hydrochloric acid. Separation and purification of the rare earths is done using solvent extraction (Koch 1987; Hart and Levins 1988).

Figure 3.20 shows the overall process used for treating Baotou rare-earth concentrates (Xie et al. 2014). The rare-earth sulfates formed during roasting are subsequently leached with water. Excess acid in the leach liquor is neutralized with magnesia and filtered. The clear solution is taken for solvent extraction. A mixed rare-earth-chloride product could be obtained by precipitation of the rare-earth values in the solution with ammonium carbonate, followed by redissolution in HCl and crystallization. Baotou concentrate contains some amount of monazite also. Thorium precipitates and collects in the leach residue. It can be neither recovered economically nor left in the residue, because of its radiotoxicity. HF and sulfur dioxide are

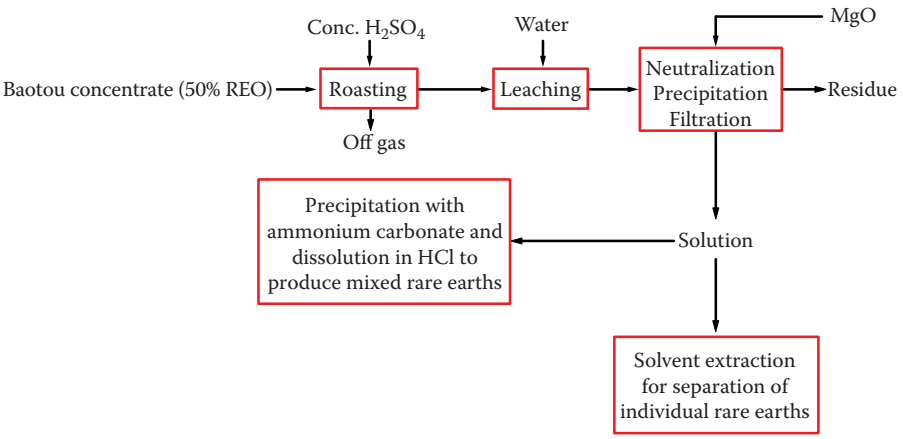


FIGURE 3.20 Overall process used for treating Baotou rare-earth concentrates. (From Huang, L.J. et al., *J. Alloys Compd.*, 421(1–2): 279–282, 2006.)

released into the off gas from roasting. They need to be washed with large amounts of water or alkaline solutions, resulting in large volumes of acidic effluents.

A variety of modifications have been listed by Xie et al. (2014) for the roasting procedure. MgO or CaO and NaCl have been added to the charge to stabilize fluorine in the leach residue and prevent its release to the waste gas stream. Ammonium chloride, added to bastnasite concentrate, decomposes to gaseous HCl, which forms rare-earth chlorides, readily leached with hot water (Chi et al. 2004). In another variant, the concentrate is first heated with sulfuric acid at 40–180°C for 2 to 4 h before roasting at 150–330°C. The decomposition of sulfuric acid is suppressed, resulting in a relatively high fraction of HF in the gas phase; this can be trapped as solid NH_4F by reacting with $(NH_4)_2CO_3$ in the off-gas line.

Kul et al. (2008) presented a working flow sheet for treating the Beylikahir bastnasite preconcentrate. Key elements of the flow sheet given in Figure 3.21 are that (1) the baking process releases hydrogen fluoride gas, which can be condensed to form HF acid; (2) most of the valuable elements were dissolved in the leach solution, except gypsum and barite compounds that remain in the leach residue and can be further separated; (3) leached REEs are almost selectively precipitated as $Ln_2(SO_4)_3{\cdot}Na_2SO_4{\cdot}2H_2O$ by addition of Na_2SO_4, to provide the main product; (4) the wastewater carried thorium, iron, aluminum, and other such impurities, from which thorium can be precipitated at pH 5 by the addition of NaOH; and (5) the solution may be recycled to the leach to precipitate more Y and Yb in the second cycle.

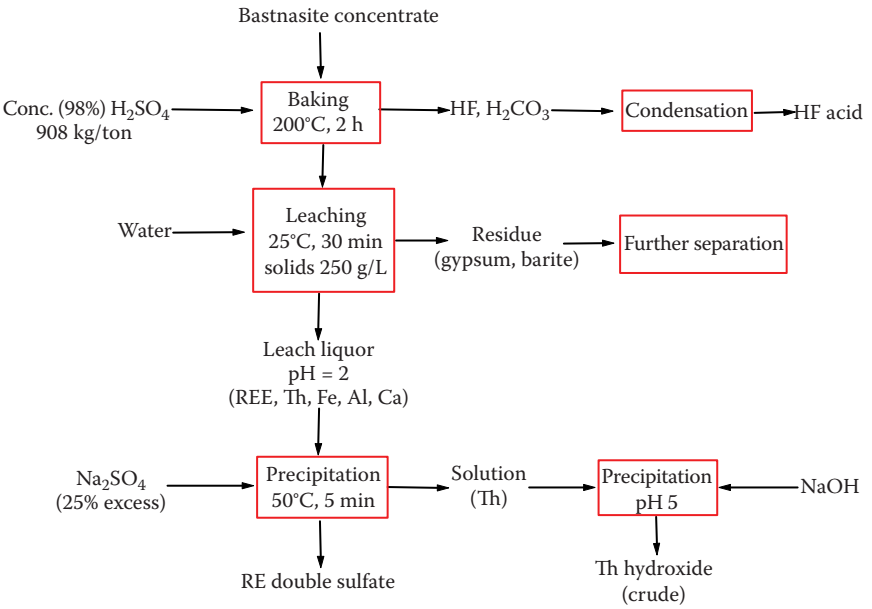


FIGURE 3.21 A working flow sheet for treating the Beylikahir bastnasite preconcentrate. (From Kul, M. et al., *Hydrometallurgy,* 93(3–4): 129–135, 2008.)

3.5.2.1 Processing Bear Lodge Ore

Even though Rare Element Resources Ltd. will refine the same REE-bearing mineral as Molycorp, a different refining process will most likely be used to extract REEs out of the ore from the Bear Lodge property. This highlights the unique refining methods employed at individual REE deposits. High-grade ores (>2.5%) recovered from carbonatite dikes will first be processed at the Bear Lodge property. On-site physical processing will include crushing and screening with water to mitigate dust pollution. Such processes are designed to concentrate the REE-bearing minerals and will overall resemble a gravel or mill operation. The low-grade ore (<2.5%) mined out of the pit will be stockpiled for future processing (Pickarts 2011). After the high-grade ores are milled at the physical processing plant, they will be transported by truck to Upton, Wyoming. At the Upton hydroprocessing plant, the milled ores will be leached in four individual vats of heated 15% hydrochloric acid, creating an REE oxide slurry. Soda ash or caustic soda will be introduced into the slurry to raise the pH to 3. This precipitates out the iron and hydroxides while keeping the REEs in solution. Other wastes including low levels of thorium, uranium, and metals will also be contained in this iron hydroxide precipitate and will be disposed of in a lined tailings facility. The pH of the remaining solution will then be further raised to around 6.5 to precipitate an REE-bearing carbonate for 90% REE recovery. The carbonate-bearing REEs will be shipped to another refinery to separate the individual REEs (Paul and Campbell 2011).

3.5.2.2 Goldschmidt Process

A high-temperature direct chlorination process was used by Goldschmidt AG in Germany (Brugger and Greinacher 1967) to directly obtain anhydrous rare-earth trichloride product directly from bastnasite ore. The chloride is well suited for the production of the corresponding metal. The flow sheet of a complete rare-earth chlorination process described by Brugger and Greinacher (1967) is shown in Figure 3.22.

Bastnasite ore was ground to less than 80 mesh. Regrinding was not necessary if the flotation concentrate was used. The ground ore was thoroughly mixed with a binder like sulfite liquor, sugar, starch, and some water. The relatively dry brew was compacted into pellets by a briquetting machine, and the pellets were passed through

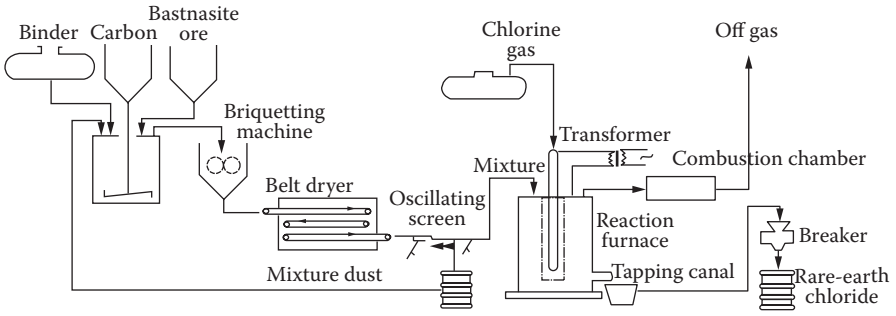


FIGURE 3.22 Goldschmidt process for bastnasite chlorination. (From Brugger, W. and Greinacher, H., *J. Metals*, 19(12): 32–35, 1967.)

a band drier. The fine fraction was screened off and reverted to the mixer because it would be blown out of the furnace due to high gas velocity. The pellet passed continuously or batchwise into the chlorination furnace.

The chlorination furnace is shown in Figure 3.23. The key requirement for complete chlorination is a temperature in the reaction zone of the furnace in the range of 1000–1200°C. Practically all metals and refractory materials react with chlorine and carbon and/or carbon monoxide. Natural graphite and amorphous carbon are resistant to the attack but not for a long time. Hence, special furnace inserts of amorphous carbon, which could be rapidly replaced, were used.

In the furnace, the ore–carbon mixture was completely converted to chlorides by chlorine gas. The chlorides were separated according to their volatility. The rare-earth chlorides were tapped from the bottom of the furnace periodically as a nonvolatile fluid melt. The tapped chloride was allowed to solidify. The alkali and alkaline earth chlorides likewise collected in the melt chamber. All other reaction products were carried off by the off-gas mixture. The important reactions occurring during chlorination are listed in Table 3.3. The analysis of the rare-earth-chloride product was given in Table 3.2.

The chlorination furnace was operated with alternating current at low voltage (10–20 V) and high current (2000–3000 A) with the loose layers of coke and of the ore–carbon briquettes functioning as the electrical resistance. The furnace was

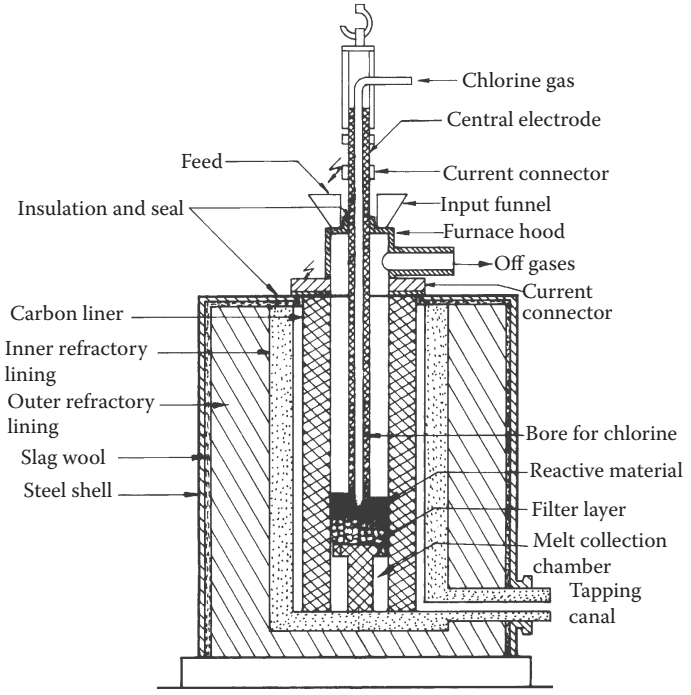


FIGURE 3.23 Diagram of chlorination furnace. (From Brugger, W. and Greinacher, H., *J. Metals*, 19(12): 32–35, 1967.)

TABLE 3.3
Important Reactions in the High-Temperature Chlorination of Bastnasite

Exothermic Reactions

$RE_2O_3 + 3C + 3Cl_2 = 2RECl_3 + 3CO$
$CeO_2 + 2C + 1.5Cl_2 = CeCl_3 + 2CO$
$CaO + C + Cl_2 = CaCl_2 + CO$
$Fe_2O_3 + 3C + 3Cl_2 = 2FeCl_3 + 3CO$
$FeO + 2C + 1.5Cl_2 = FeCl_3 + 2CO$

Endothermic Reactions

$SiO_2 + 2C + 2Cl_2 = SiCl_4 + 2CO$
$P_2O_5 + 3C + 1.5Cl_2 = POCl_3 + 3CO$
$P_2O_5 + 5C = 2P + 5CO$
$CO_2 + C = 2CO$

Source: Brugger, W. and Greinacher, H., *J. Metals*, 19(12): 32–35, 1967.

designed for high thermal loads and had a capacity of 100 tons/month of rare-earth chloride. It consumed chlorine at the rate of 0.9–1.0 kg/kg of $RECl_3$, and the energy consumption was 0.4–0.6 kWh/kg of $RECl_3$.

The process was described (Brugger and Greinacher 1967) as suitable for chlorination of not only bastnasite, but also monazite, allanite, cerite, xenotime, euxenite, fergusonite, and gadolinite. When monazite or xenotime is chlorinated, regrinding of the ore before mixing with carbon and compacting is not necessary. The required temperature of chlorination is higher for silicates and phosphates than for oxidic ores or niobates and tantalates.

Brugger and Greinacher (1967) mentioned many advantages of the chlorination process. The economic advantages include simplicity, low labor component, small space requirement, and low capital costs. Energy costs are also very small. The process yields anhydrous chlorides of the rare earths without oxide or oxychloride content, clearly separated from impurities, at a very high specific throughput.

A process essentially similar to that described by Brugger and Grenaicher (1967) was tested (Li et al. 1986) to chlorinate Baotau rare-earth concentrate on a laboratory scale. The concentrate consisted mainly of bastnasite, monazite, and certain other minerals that could be chlorinated in the presence of carbon at high temperatures. The mixture of rare-earth concentrate (60–70% REO) and charcoal (ratio of concentrate to fixed carbon in charcoal = 1:0.065–0.070) was pressed into briquettes, dried at 120–140°C, and then chlorinated in a long graphite reactor at 950–1100°C. The chlorides with lower boiling points, like $FeCl_3$, $SiCl_4$, and $ThCl_4$ were removed with the off gas, while the low-vapor-pressure chlorides like $CaCl_2$ and $BaCl_2$ remained with the rare-earth chloride. By this process, over 91% of the rare earths contained in the concentrate were obtained as the chloride. The chlorination product consisted of 60% REO, 4–5% Ca + Ba, <0.2% Fe, < 4% F, and <0.05% P. The rare-earth chlorides have been used for electrowinning of metals.

3.5.3 Xenotime

The process options for treating xenotime are shown in Figure 3.24. The acid process for xenotime breakdown (Banks et al. 1959; Powell and Spedding 1959b) involves attacking with concentrated (93%) sulfuric acid. The rare-earth phosphates are converted to water-soluble sulfates by leaching xenotime concentrates in concentrated H_2SO_4 at 250–300°C for 1–2 h. Such leaching was uneconomical for concentrates containing less than 10% xenotime. These are treated by wetting the solids with sufficient acid and heating the mass at 300°C followed by water leaching. About 80–90% of the rare earths are solubilized. The recovery of rare earths by processes such as double-sulfate precipitation is not possible, because yttrium and the HRE sulfates are quite soluble. The sulfate solution is directly taken for separation. In the alternative process, the fine-ground xenotime is treated by fusing it with molten caustic soda at 400°C (Topp 1965) or by mixing it with sodium carbonate and roasting at 900°C for several hours (Lever and Payne 1968). After leaching out the phosphates, the hydroxide residue is dissolved in a minimum amount of hydrochloric acid and filtered from impurities such as silica and cassiterite. The rare earths are recovered by precipitation as oxalates.

The xenotime processing plant of the Malaysian Rare Earth Corporation (MAREC) was located at Bukit Merah in Perak State, Malaysia. The acid leaching process used in the plant for the production of yttrium oxide concentrate from xenotime is outlined (Sulaiman 1991) in Figure 3.25. Xenotime is milled and then roasted in a furnace. These operations ensure that good recovery is obtained in the next stage, which is sulfuric acid digestion of the roasted material. Yttrium phosphate in the mineral is converted to water-soluble sulfate. Cold water is used as the leachant. Oxalic acid is added to the yttrium sulfate solution to precipitate yttrium oxalate, which is calcined to the oxide. The plant had a capacity to produce 200 tons of yttrium concentrate (60% Y_2O_3) per annum.

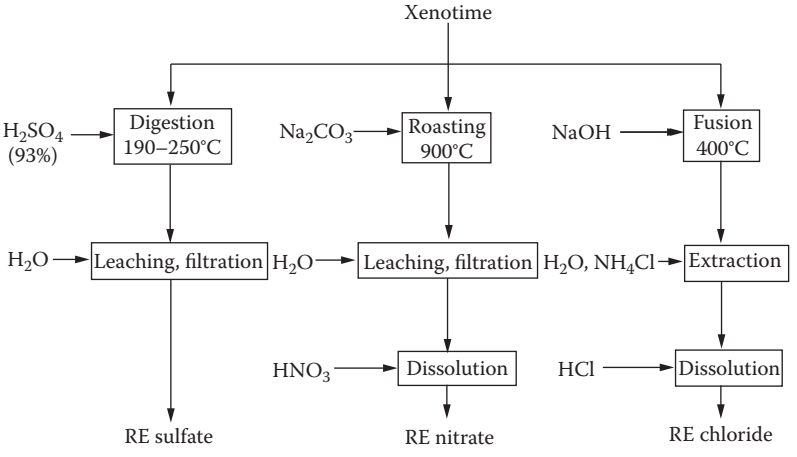


FIGURE 3.24 Chemical processing of xenotime.

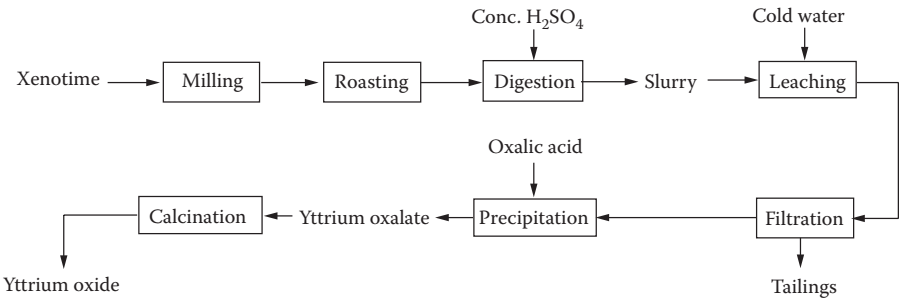


FIGURE 3.25 Xenotime processing in Malaysia.

3.5.4 Ion-Adsorption Ore

The chemical composition of an ore sample from the Zudong rare-earth mine area located in Longnan County (LN), Jiangxi Province, China, is given in Table 3.4. The LN rare-earth ore contains only 0.102% rare earth (Jun et al. 2010). The state of rare earths in the LN ore was determined to be (Chi et al. 2005) in the following four forms: (1) aqueous soluble-phase rare earth, where the aqueous soluble rare earth and rare-earth hydroxyl aqueous ions that were free or in individual form without being adsorbed by clay minerals during weathering and weathering–leaching processes; (2) ion-exchangeable-phase rare earth, where the rare earth exists as rare-earth ions adsorbed by clay minerals with aqueous soluble rare earth and rare-earth hydroxyl

TABLE 3.4
Features of Longnan Rare-Earth Ore

Main Chemical Composition of LN Rare-Earth Ore Sample (Mass Fraction %)

Element	RE	Al	Fe	Mn	Ca	Mg	SiO_2	Loss
Original rare-earth ore	0.102	14.66	3.24	0.04	0.32	0.57	60.4	20.37

Existing State of Rare Earth in the LN Rare-Earth Ore (Mass Fraction %)

Phase State	Aqueous Soluble	Ion Exchangeable	Colloidal Sediment	Mineral Phase
Distribution	6.15×10^{-3}	80.62	5.30	13.36

Partitioning of the LN Rare-Earth Ore (Mass Fraction %)

Element	La_2O_3	CeO_2	Pr_6O_{11}	Nd_2O_3	Sm_2O_3	Eu_2O_3	Gd_2O_3	Tb_4O_7
Content (%)	1.56	0.085	0.65	3.20	2.42	0.50	4.48	0.95
Element	Dy_2O_3	Ho_2O_3	Er_2O_3	Tm_2O_3	Yb_2O_3	Lu_2O_3	Y_2O_3	
Content (%)	6.90	1.56	4.33	0.55	3.48	0.50	68.94	

Source: Jun, T. et al., *Hydrometallurgy*, 101: 166–170, 2010.

cation states; (3) colloid sediment-phase rare earth, where the rare earth exists as insoluble rare-earth oxides or hydroxyl compounds bonding with or depositing on oxide minerals; and (4) mineral-phase rare earth, which includes rare-earth mineral crystals of ionic compounds as well as diffusion of rare-earth ions to displace mineral crystals in the ores. The rare earth exists predominantly in the ion-exchangeable phase, which accounts for 80.62%, less than 20% mineral phase (13.36%) and colloid sediment phase (5.3%), and hardly any aqueous soluble phase (6.15×10^{-3}%).

Although ion-adsorption clay deposits are of substantially lower grade than other lanthanide sources, the lower grade is largely offset by the easier mining and processing costs and the very low content of radioactive elements (normally associated with yttrium). These deposits are mined by open-pit methods, and no ore beneficiation is required. In fact, the rare earths adsorbed on the surface of clay minerals (P. Zhang et al. 1995; Wan and Liu 2005) and usual physical beneficiation methods such as magnetic separation, electrostatic separation, gravity concentration, and flotation were found to be ineffective in beneficiating the ion-adsorption ores (Kul et al. 2008; Jun et al. 2010).

Rare earths adsorbed on the surface of clay minerals can be recovered by a leaching process that exchanged and desorbed the rare-earth ion when encountering cations such as NH_4^+, K^+, Na^+, and H^+, which have more active chemical properties (Qiu et al. 2008). A simple leach using monovalent salt solutions at ambient temperature can produce a high-grade REO product (Ru'an 1988; Tran 1991). They are usually leached directly with inorganic acid, either in dumps or *in situ*.

Ion-adsorption clays are leached with concentrated inorganic salt solutions of monovalent cations (i.e., M_2SO_4 and MCl, where M = Na^+ or NH_4^+). During leaching, the physiosorbed REEs are relatively easily and selectively desorbed and substituted on the substrate by the monovalent ions and transfer into solution as soluble sulfates or chlorides (Equation 3.1).

$$\text{Clay–Ln} + 3\text{MX} = \text{Clay–M}_3 + \text{LnX}_3 \tag{3.1}$$

$$2\text{LnX}_3 + 3\text{H}_2\text{C}_2\text{O}_4 + 10\text{H}_2\text{O} = \text{Ln}_2(\text{C}_2\text{O}_4)_3 \cdot 10\text{H}_2\text{O} + 6\text{HX} \tag{3.2}$$

Equation 3.1 indicates a 3:1 stoichiometric ratio between the monovalent cation and the RE element. The permanently chemisorbed species can only be liberated (Moldoveanu and Papangelakis 2012) via more aggressive and nonselective acid leach.

Moldoveanu and Papangelakis (2012) studied the leaching efficiency of various salts at 0.5 M and 25°C as a function of monovalent cation type (i.e., Li^+, Na^+, Cs^+, and NH_4^+) and salt system (sulfates vs. chlorides). Leaching efficiency (in terms of the percentage of REE extracted) decreased in the order $Cs^+ > NH_4^+ > Na^+ > Li^+$, from 90% to ~60%, respectively, with sulfates exhibiting ~10% better extraction behavior than chlorides. $(NH_4^+)_2SO_4$ was identified as the lixiviant of choice. They also determined that terminal extraction levels of 80–90% are achievable under ambient temperature (25°C) and at a moderately acidic pH of 3 in less than 5 min regardless of lixiviant concentration, temperature, pH, and agitation.

Solubilized REEs are recovered/separated as high-purity end products either by solvent extraction (Li et al. 2006b; Preston et al. 1996c) or ion exchange

(Ochsenkühn-Petropoulou et al. 2002) as individual elements or selectively precipitated with oxalic acid to form oxalates (Equation 3.2) that are subsequently converted to REO via roasting at 900°C (Chi and Xu 1999; Liu et al. 2008).

In general, the rare-earth leach liquor of ion-adsorption ore contains various impurities in substantial amounts, such as $(NH_4)_2SO_4$ (~2000 mg/L), Al^{3+} (~1000 mg/L), Fe^{3+} (~100 mg/L), and Ca^{2+} (~1000 mg/L), along with a small amount of Fe^{2+}, Pb^{2+}, and Mn^{2+} (Yongxiu et al. 1999). Traditionally, rare earth from such leach liquor is recovered by chemical precipitation with oxalic acid or ammonium carbonate, forming rare-earth oxalate or carbonate, followed by washing, filtering, and calcining into rare-earth oxides (Chi et al. 2003; Chi and Xu 1999). Although they have been industry practice, these precipitation technologies are complicated, time consuming, and reagent consuming, and the impurities do not get removed to a sufficient extent, resulting in low product purity and, incidentally, low yield (Li 1995).

Jun et al. (2010) considered the extraction of rare earths from the leach liquor of the weathered-crust, elution-deposited rare-earth ore with nonprecipitation processes to have advantages and potential to reduce the amount of chemicals and energy consumed. The nonprecipitation processes include solvent extraction, ion exchange, and liquid membrane separation. Solvent extraction resulted in over 96% rare-earth recovery by multistage extraction and raffinate recycling for leaching the ore. In the ion-exchange method, an adsorption rate of 98.7% with a resin operation capacity of 77.4 g/L was possible. Using the liquid membrane process, there was over 98% rare-earth recovery, up to 95.2 g/L rare-earth concentration, 95% product purity, and about 70% impurity removal. Thus, for the processing of ion-adsorption ores, the nonprecipitation hydrometallurgical processes are anticipated to replace the existing precipitation technologies in industrial practice in the not-so-distant future.

A simplified flow diagram of the process possibly used for the ion-adsorption ores, is shown in Figure 3.26 (Ritcey 2006). The process not only concentrates the rare earths from the leach liquor but also separates rare earths from main impurities. The raffinate can be reverted, after topping up with some leaching agents, back to leaching new ores (Zhu 1991). Hence, no wastewater is generated. Leaching ores with the extraction raffinate solution gives pregnant leach solution (PLS). Extraction of rare earth from PLS with the barren organic solution (BO) gives the loaded organic phase (LO) and the extraction raffinate solution. Stripping the LO with hydrochloric acid solution (HCl) gives the barren organic and rare-earth loaded strip liquor.

With years of persistent mining of weathered-crust, elution-deposited rare earth, the amount of the rich ore has declined sharply, the ore resource became poorer and leaner, and the available rare-earth grade decreased to less than 0.05% (Jun et al. 2013). In the context of processing, the impurity in the ores has become more complicated, permeability of the rare-earth ores became worse, the leach liquor concentration of the rare-earth ore became lower, and leach selectivity became lower (Ghada et al. 2008; Jun et al. 2011). More critically, the consumption of reagent ammonium salt is high, and leaching recovery rate is low, leading to high concentration of ammonia–nitrogen $\left(NH_4^+ - N\right)$ in the discharge water (far higher than the wastewater discharge standard) when leaching these lean ores. There is a case for

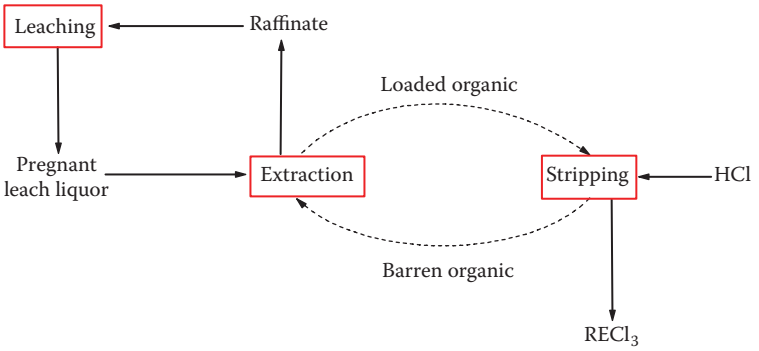


FIGURE 3.26 A simplified flow diagram of the process possibly used for the ion-adsorption ores. (From Ritcey, G.M., *Tsinghua Science and Technology* 11(2): 137–152, 2006; Jun, T. et al., *Int. J. Miner. Process.*, 98: 125–131, 2011.)

focused research on the optimization of the leach process for this important and increasingly challenging resource (Tian at al. 2013).

3.5.5 Elliot Lake Uranium Ore

The Elliot Lake uranium mines in Canada, upon demand, produce 60–70% REO concentrate from barren uranium leachate (Jackson and Christiansen 1993). A large volume of barren liquor, relatively free of uranium but containing lanthanides and thorium, is generated. The liquor is generated from sulfuric acid leaching of uranium ores followed by removal of uranium from the filtered leach liquor by ion exchange. The minerals brannerite, uraninite, and uranothorite from which uranium was leached contain lanthanum, yttrium, ytterbium, cerium, praseodymium, neodymium, samarium, thorium, and lesser quantities of dysprosium and erbium. In the leaching process currently used, even though only about 20% of total rare earths in the ore is leached, approximately 75% of yttrium in the ore is leached along with uranium and thorium. Thus, after the removal of uranium by ion exchange, the barren liquor contains considerable amounts of yttrium and other rare earths, which can be recovered (Ritcey and Ashbrook 1979).

The barren acid solutions are treated with lime and air in pachuka tanks to about 8.5 pH. The resultant oxidized slurry is thickened, and the clear overflow is sent to the tailings. The thickener underflow is recovered for further treatment. The underflow is acidified with H_2SO_4 to a pH of about 4.2 to redissolve yttrium and the rare earths and is filtered off from the iron, thorium, and aluminum in the solids. The rare earths are then precipitated with ammonia gas, thickened, and dried. The concentrate contains approximately 8–15% Y_2O_3 and 12–30% total REO, including yttrium.

3.5.6 Gadolinite

The processes for chemical treatment of gadolinite are outlined in Figure 3.27. The rare earths have been recovered from gadolinite by leaching the ground ore with

nitric or hydrochloric acid and precipitating the rare earths as oxalates, thus effecting the separation from associated iron and beryllium (Foos and Wilhelm 1954). Concentrated sulfuric acid or a mixture of sodium hydroxide and sodium peroxide has also been used to attack the ore.

3.5.7 Euxenite, Fergusonite, and Samarskite

Euxenite has been treated by reductive chlorination followed by distillation of the chlorides to separate rare earths, titanium, niobium, and tantalum fractions (Henderson et al. 1958). The processes for chemical treatment of euxenite are shown in Figure 3.27. Solvent extraction has also been used to remove tantalum–niobium chlorides and the rare-earth metals from the chlorination residue. Treatment of the ore by fusion with ammonium bisulfate or caustic soda; by digestion with hydrofluoric or sulfuric acid or mixtures of the two (Shaw 1959; Shaw and Bauer 1959); or by digestion in hot sodium hydroxide solution are the options available. The hydroxides of rare earths uranium, thorium, and iron formed are dissolved in dilute hydrochloric acid (Hedrick 1985b). Soda ash is added to this solution to form a complex carbonate

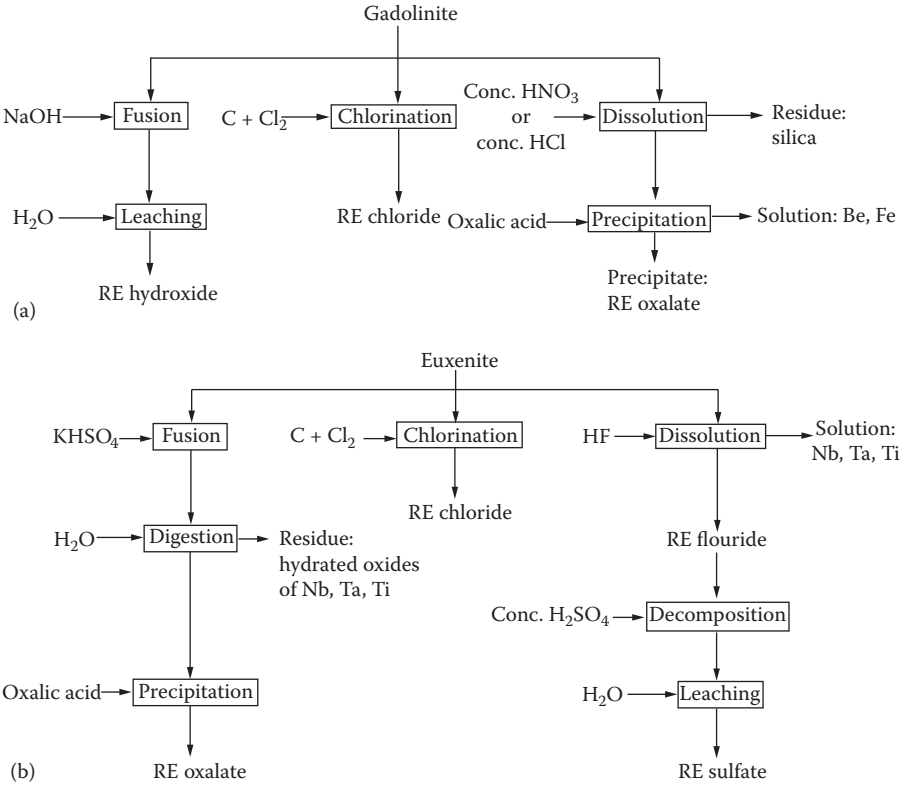


FIGURE 3.27 (a) Chemical processing of gadolinite. (b) Chemical processing of euxenite.

(*Continued*)

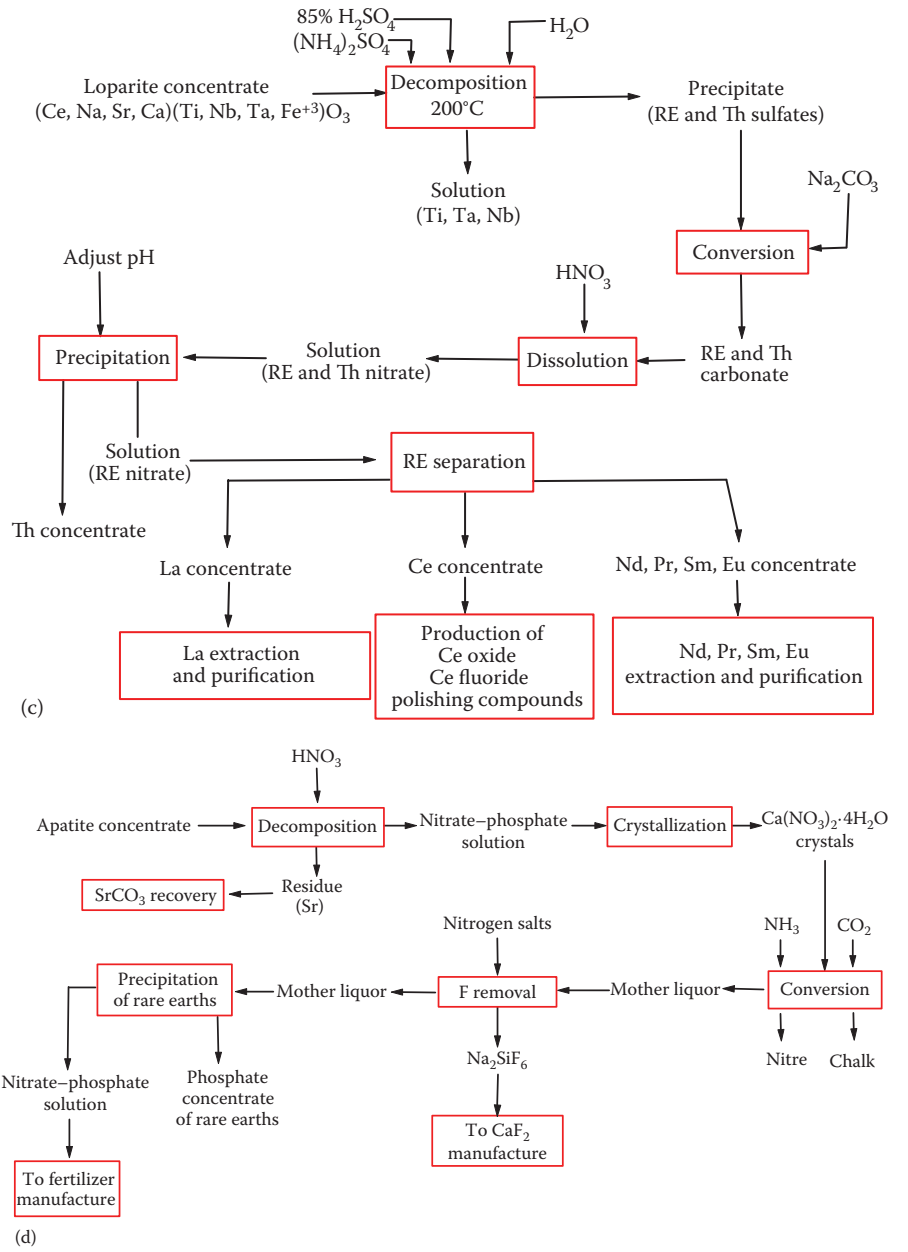


FIGURE 3.27 (CONTINUED) (c) Rare-earth extraction from loparite, acid process. (d) Complex nitric acid processing of apatite. (From Hedrick, J.B. et al., *J. Alloys Compd.*, 250(1–2): 467–470, 1997; From Skorovarov, J.I. et al., *J. Alloys Compd.*, 180(1–2): 71–76, 1992.)

(*Continued*)

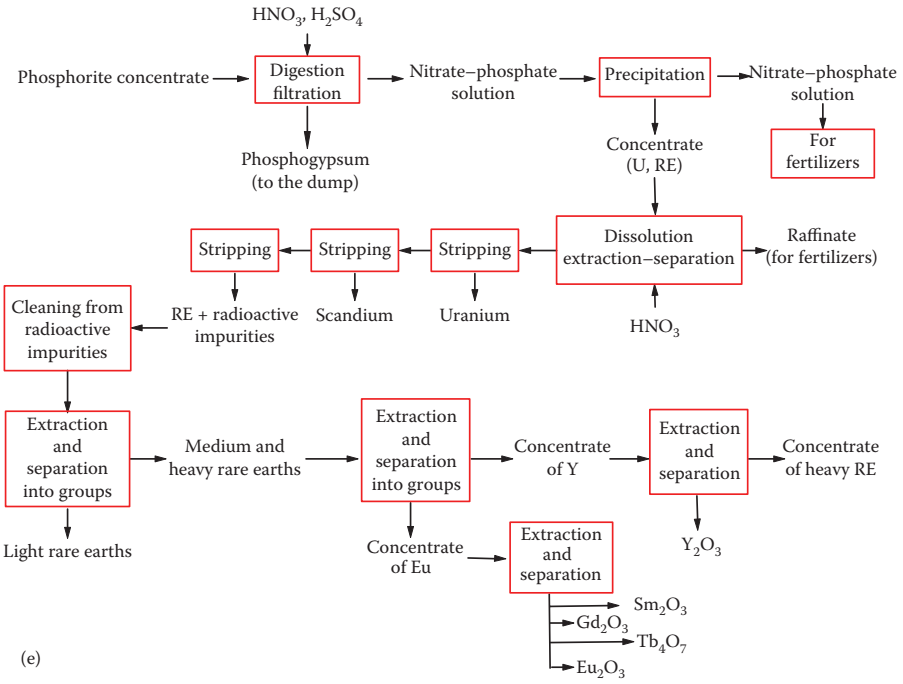


FIGURE 3.27 (CONTINUED) (e) Rare-earth recovery from phosphorites. (From Skorovarov, J.I. et al., *J. Alloys Compd.*, 180(1–2): 71–76, 1992.)

precipitate. The precipitate is leached with dilute sulfuric acid to selectively solubilize the rare earths. From the leach liquor, rare earths are precipitated as oxalates by adding oxalic acid. Euxenite was considered as a potential future source of rare earths (Jackson and Christiansen 1993). Rare earths are recoverable from fergusonite and samarskite by a hot caustic digestion followed by an acid dissolution process. The process is similar to that described for euxenite.

3.5.8 Loparite and Pyrochlore

Loparite was decomposed on an industrial scale by chlorination in the former Soviet Union, beginning in 1971 at the Solikamsk Magnesium Plant in Solikamsk, Perm Oblast, Russia. The solid product (rare earth-containing fusion cake) obtained after chlorination processing was treated further at Irtysh chemical-metallurgical plant in East Kazakhstan Oblast, in Kazakhstan, and at the Silmet plant (Sillamäe chemical-metallurgical united works) in Estonia.

Loparite is processed for its rare earth, titanium, and niobium contents. The overall processing involves chlorination and acid dissolution. Chlorination is the only process used to prepare feed for the acid stage (Hedrick et al. 1997). Loparite concentrate is chlorinated by elemental chlorine in the presence of reducing agent coke or charcoal, at 750–850°C. The chlorides of titanium, niobium, and tantalum, being more volatile, are transported away as vapor from the less volatile chlorides of rare

earths, calcium, iron, thorium, and uranium, which remain in the chlorinator as fusion cake. The fusion cake is leached with water to get the rare earths in solution, which are further separated and purified by the acid process.

The acid process is shown in Figure 3.27c. Loparite concentrate feed from the chlorination treatment is dissolved in an 85% solution of sulfuric acid in the presence of ammonium sulfate at 150–200°C. The sulfates of titanium, tantalum and niobium are soluble and remain in solution, while the double sulfates of rare earths and thorium are separated by filtration. Further processing of the double-sulfate cake is through conversion to carbonates, dissolution in nitric acid, precipitation of thorium hydroxide, and finally, solvent extraction with TBP.

Pyrochlore can be processed to yield a niobium-rich rare-earth concentrate. The process described by Villani (1980) begins with digestion of pyrochlore ore in hydrofluoric acid, followed by solvent extraction of niobium by methylisobutylketone (MIBK). In another process, the ore is first digested with hot concentrated sulfuric acid. Niobium and rare earths are then selectively precipitated by gradual reduction of acid concentration and temperature (Charlot 1976).

3.5.9 Apatite

Wet processing, using the digestion of phosphate rocks by sulfuric acid, is the most common process used to produce phosphoric acid. The simplified overall reaction between calcium phosphate minerals and sulfuric acid (Becker 1983) can be written as follows:

$$Ca_5F(PO_4)_3 + 5H_2SO_4 + 5xH_2O = 3H_3PO_4 + 5CaSO_4 \cdot x5H_2O + HF$$

where x is 0 for calcium sulfate anhydrate, 0.5 for hemihydrate, and 2 for dihydrate, i.e., gypsum. The process is described in detail by Preston et al. (1996a,b,c) for the Phalaborwa deposit.

The apatite deposit at Phalaborwa in South Africa contains significant amounts of rare-earth metals and is a feed material to a wet-process phosphoric acid plant in the same locality. In the process for phosphoric acid production, the apatite concentrate is dissolved in a mixture of sulfuric acid and recycled dilute phosphoric acid. The bulk of the rare-earth values, 70–85% of that contained in the feed, end up in the copious amount of phosphogypsum ($CaSO_4 \cdot 2H_2O$) formed in the dissolution reaction. The remainder of the rare-earth values dissolve in the crude dilute phosphoric acid (27% P_2O_5) but eventually precipitate as sludges that settle out when the dilute acid is concentrated to commercial grade (54% P_2O_5). These sludges consist mainly of calcium sulfate hemihydrate ($CaSO_4 \cdot 0.5H_2O$) but also 2–8% rare earths (REO). The amount of sludge produced is very substantial (~10,000 t/year) at the Phalaborwa plant alone, and it represents a valuable source of the rare-earth metals (Preston et al. 1996c).

The sludge is washed and leached with dilute nitric acid, to which calcium nitrate was added in a mechanically agitated flat-bottomed stainless steel pachuka, and over 85% of the rare earths contained in them were solubilized. From the leach liquor that contains nitric acid, calcium nitrate, and added ammonium nitrate, rare earths

are recovered by solvent extraction and finally precipitated from the strip solution as rare-earth oxalates. The oxalates were calcined in a rotary furnace to yield mixed rare-earth oxide of 89–94% purity. Rare-earth oxides have also been recovered from apatites in the former Soviet Union and Finland during the production of phosphoric acid for fertilizer. The ore is leached with nitric acid, and from the leach liquor, the silicic and fluorsilicic salts are precipitated by sodium nitrate. On partial neutralization of the leach liquor with ammonia, the rare-earth phosphates are precipitated. From the phosphates, the rare earths are redissolved in nitric acid and are precipitated in a purer form as oxalates by the addition of oxalic acid.

A greater part of apatite in the former Soviet Union was treated in the sulfuric acid circuit, and the rare earths ended up in the phosphogypsum, which was dumped. However, more than 1.5 million tons of apatite was processed every year using nitric acid, and the rare earths ended up in the nitrate–phosphate solution to be precipitated from there as phosphates. A flow sheet using nitric acid tor apatite processing is shown in Figure 3.27d. Nearly 85% of the rare earths contained in the apatite are recovered as a 24% REO concentrate.

The results reported for phosphorite deposits are as follows. In Poland, Jarosinski et al. (1993) found that 70% RE entered the calcium sulfate dihydrate ($CaSO_4 \cdot 2H_2O$, DH, or gypsum) during the dihydrate process for the Kola phosphorite, while almost all the rare earth was adsorbed by the calcium sulfate hemihydrate ($CaSO_4 \cdot 1/2H_2O$, HH) during the hemihydrate process. The rare earths had to be separately recovered from the phosphogypsum. The rare earths were precipitated with hydrofluoric acid or extracted with nonyl phenyl phosphoric acid (NPPA) to obtain a 40% concentrate from the phosphogypsum leaching solution (Jarosinski et al. 1993). In a Russian practice, the rare earths were leached out from phosphogypsum with sulfuric acid, and the leach liquor was evaporated to crystallize rare earths or was neutralized to precipitate the rare earths (Lokshin et al. 2004; Lededev and Lokshin 2000; Lededev et al. 2000). In any case, according to Wang et al. (2010), the process of the rare-earth recovery from phosphogypsum is complicated and uneconomical for industrialization.

In Russia, phosphorite concentrate (francolite) was processed for recovering, apart from the main products (fertilizers), uranium and rare earths as by-products (Skorovarov et al. 1992). The concentrate contains 25% P_2O_5, up to 1% REO, and a few tenths of a percent of uranium. The scheme used for phosphorite processing is given in Figure 3.27e. The extraction processes use esters of phosphoric organic acids and amines as extractants. The process yields oxides of individual REEs in 4 N purity.

The extraction of rare earths from Fanshan phosphorite ore was investigated by Wang et al. (2010). The ore consisted of 33.8% P_2O_5, 51.0% CaO, 0.55% REO, 0.8% MgO, 1.5% FeO, and 0.5% Al_2O_3. The REE content is shown in Table 2.7. More effective recovery of rare earths from phosphorite ores and RE enrichment in phosphoric acid was obtained by leaching at lower temperatures, with a larger liquid–solid ratio and higher concentration of phosphoric acid. Nonionic surfactant additives were found to result in a significant increase in RE leaching efficiency (up to 75%) due to enhanced gypsum crystal growth and less adsorption of RE. The impurity ions in wet-process phosphoric acid mainly include Al^{3+}, Fe^{3+}, Ca^{2+}, and Mg^{2+}. For rare-earth recovery, D2EHPA in kerosene was used to extract rare earths

from the phosphoric acid solution keeping a high concentration of extractant, large phase ratio, lower temperature, and relatively low concentration of phosphoric acid:

$$RE^{3+} + H_3PO_4 + 2(HL)_2 \rightleftharpoons RE(H_2PO_4)L_2(HL)_2 + 3H^+$$

where HL is D2EHPA (Wang et al. 2010). During the extraction of lanthanides from phosphoric acid, the impurities are also extracted into the organic phase. The degree of extraction of rare earths decreased very little with increasing Al^{3+}, Ca^{2+}, and Mg^{2+} concentration; however, Fe^{3+} has a great effect on RE extraction, and there is significant competitive extraction between Fe^{3+} and rare-earth-metal ions—the degree of RE extraction decreased when the amount of Fe^{3+} ions increased.

Apart from sulfuric acid, nitric and hydrochloric acids have been used as leaching agents for the extraction of REEs from apatite. When apatite is leached with HNO_3, all the rare earths substituted in the apatite lattice for calcium ions are dissolved, and several processes are available to recover them from the pregnant leach liquor (Li et al. 2006).

In all the processes described, the products (compounds) obtained after chemical processing of rare-earth minerals contain the rare earths in essentially the same ratio in which they were originally present in the ore. This is because of the similar chemical behavior of the various REEs in the reactions involved in these treatments. Operations such as double-sulfate precipitation used for separating thorium also result in partial rare-earth separations in the two fractions, one enriched in the cerium-group rare earths and the other enriched in the yttrium-group rare earths. The separation of cerium is also accomplished during chemical processes, involving its oxidation to Ce(IV). The subject of separation of rare earths is covered in the following section. Perhaps no other branch of rare-earth extractive metallurgy has attracted so much attention and research effort as the separation of naturally occurring mixed rare-earth compounds into pure individual rare-earth compounds.

3.6 SEPARATION PROCESSES

The processes for separating individual rare earths from naturally occurring rare-earth mixtures essentially utilize the small differences in basicity resulting from the decrease in ionic radius from lanthanum to lutetium. The basicity differences influence the solubility of salts, the hydrolysis of ions, and the formation of complex species, and these properties form the basis of separation procedures by fractional crystallization, fractional precipitation, ion exchange, and solvent extraction. In addition to a trivalent oxidation state, Ce, Pr, and Tb can also occur in the tetravalent state, and Sm, Eu, and Yb, in the divalent state. Selective oxidation or reduction of these elements is useful in effective separation because in the tetravalent and divalent states, the elements exhibit markedly different chemical behavior compared to that in the trivalent state.

3.6.1 Selective Oxidation

The most abundant rare earth, cerium, can be separated relatively easily and early in the separation sequence. This simplifies the subsequent separation of the less

abundant rare earths. Cerium is removed from the rare-earth mixture after oxidation of naturally occurring Ce(III) to Ce(IV). This valence change occurs, for example, when bastnasite is heated in air at 650°C or when the rare-earth hydroxides are dried in air at 120–130°C. In aqueous hydroxide suspensions, chlorination or electrolysis (Douglas and Bauer 1959; Bauer et al. 1960) can bring about the oxidation. An effective method of cerium removal from a complex lanthanide solution was suggested by an oxidation–precipitation process using ozone as the oxidizing agent. Once oxidized, Ce(IV) is separated (Bril 1964) from the trivalent components in the rare-earth hydroxide–oxide mixtures either by selective dissolution of trivalent species with dilute acid (Powell 1939) or by complete dissolution in concentrated acid followed by selective precipitation. Hydrochloric acid may be promoting reduction of Ce(IV). Hence, separation of Ce(III) from the other trivalent lanthanides may remain incomplete (Xie et al. 2014). The alternative, leaching all the rare earths, followed by precipitation of cerium by oxidizing it to Ce(IV) appears attractive. $Ce(OH)_4$ could be precipitated using ammonium carbonate and ammonium persulfate (Huang et al. 2005). Sodium hypochlorite can also be used for the oxidation of Ce(III).

The precipitation of even 99.8% pure ceric salts does not completely remove cerium from solution, and additional cerium removal steps are necessary to prepare rare earths free of cerium. A process considered particularly effective for cerium recovery from any acid leachate solution containing rare earths uses air oxidation (Figure 3.28), and, eventually, solvent extraction. A number of reagents have been studied for the solvent extraction of Ce(IV) nitrate, and TBP is preferred for large-scale operations (Douglas and Bauer 1959; Bauer et al. 1960).

Unlike Ce(IV), both Pr(IV) and Tb(IV) are not stable in aqueous solution. The higher oxides PrO_2 and Tb_4O_7 precipitate when a solution of rare-earth hydroxides in fused potassium hydroxide is oxidized either by anodic oxygen or by potassium chlorate. The oxides are recovered by decantation or by dissolving away the melt.

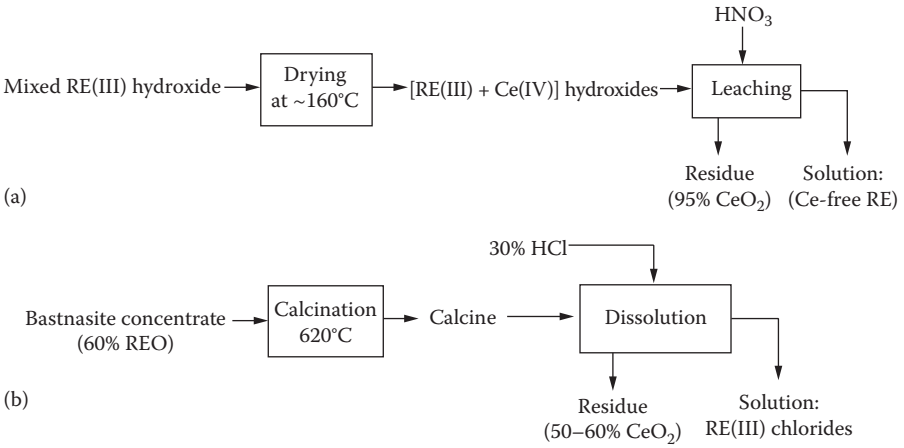


FIGURE 3.28 Separation of cerium by selective oxidation. (a) Low temperature drying of mixed RE hydroxide and (b) calcination of the rare earth concentrate.

3.6.2 Selective Reduction

Samarium, europium, and ytterbium can be easily separated from the trivalent rare-earth mixture after reducing them to the divalent state. Unlike cerium, these elements are much less abundant, and separation using reduction is carried out only after they have been enriched by other procedures. The first application of selective reduction for the separation of a rare earth was by Yntema (1930). Using a mercury cathode, he electrolytically reduced Eu(III) to Eu(II). Lithium amalgam electrodes were used for separation of Sm from Eu and Yb by selective reduction. Recently, the continuous electrolytic reduction of Eu(III) to Eu(II) in rare-earth-chloride solutions derived from monazite was demonstrated in a redox flow cell. Marsh (1942, 1943, 1957) had separated samarium, europium, and ytterbium from rare-earth mixtures in a buffered acetate solution by reductive extraction into a dilute sodium amalgam. The separation is clear and complete, and the method is amenable to counter-current operation. It has been used commercially (Lever and Payne 1968) for the recovery of samarium and ytterbium. The recovery of pure europium from such amalgams is achieved by treatment with cold concentrated hydrochloric acid, which causes precipitation of the sparingly soluble $EuCl_2 \cdot 2H_2O$. Both Sm and Yb are rapidly oxidized to very soluble trihalides, whereas the oxidation of Eu proceeds very slowly in the absence of oxygen.

On an industrial scale, the method developed by McCoy (1936, 1941) has found acceptance. In a chloride solution, Eu(III) is reduced to Eu(II) by zinc, and the divalent Eu is recovered as a sulfate. The process is shown in Figure 3.29. Zinc does not reduce Sm or Yb. When Eu is present only in a low concentration, $EuSO_4$ is recovered by coprecipitation with $BaSO_4$. The mixed sulfate precipitate is washed with an oxidizing acid solution to reoxidize and dissolve Eu(III), leaving $BaSO_4$ undissolved. The purity of Eu recovered in this process can be improved to 99.9% by precipitating $EuCl_2 \cdot 2H_2O$ from concentrated HCl. Recently, the separation of Eu has also been achieved by photochemical means.

Europium can be separated from other rare earths by a photochemical reduction to the divalent stage followed by precipitation of the divalent europium as sulfate or chloride (Shastri et al. 1988). The photochemical separation was investigated using a low-pressure mercury lamp with no filter at 185 nm, and with a Vycor filter at 254 nm and an ArF excimer laser operating at 193 nm. An equimolar mixture (0.01 M) of binary and ternary lanthanide perchlorates and 0.05 M K_2SO_4 in 10% isopropanol was irradiated. The separation factor for Eu–RE varied from 1 for Eu–Pr and >200 for Eu–Tm. Qiu et al. (1991) studied the separation of Eu from a solution mixture of $SmCl_3$, $EuCl_3$, and $GdCl_3$ in a rare earth–saturated ethanol–isopropanol system. The photo reduction of Eu was carried out with a high-pressure mercury lamp. From the alcohol mixture, $EuCl_2$ was produced by photoreduction and precipitation. The precipitated $EuCl_2$ was 92% pure, and the yield of Eu(II) was 95%.

A method of separating samarium, europium, and ytterbium is based on the fact that Sm, Eu, and Yb metals cannot be obtained by metallothermic reduction of their halides. During the reduction of a mixture of anhydrous rare-earth halides with calcium, the halides of Sm, Eu, and Yb are not reduced, and they remain in the slag from which they are subsequently separated.

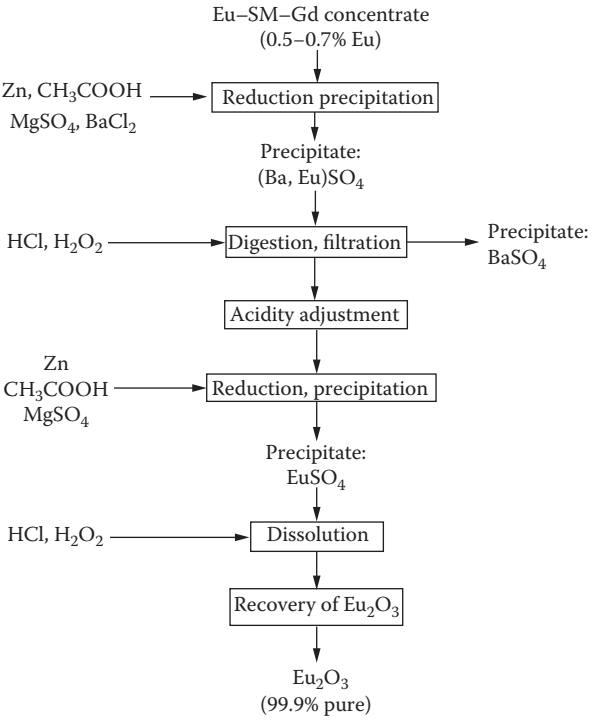


FIGURE 3.29 Separation of europium by selective reduction.

Samarium, which only reduces to the divalent state, also accumulates in the fused salt slag when the mixed rare-earth chloride is electrolytically reduced to misch metal. The slag has been an inexpensive source of samarium for some time (Gschneidner and Daane 1988).

Before 1950, in addition to the separation procedures based on selective oxidation or reduction, the methods based on fractional crystallization and fractional precipitation were widely used for rare-earth separations. The considerable effort spanning over 100 years that was applied to the problem of separation using these classical techniques has been extensively reviewed (Little 1921; Yost et al. 1947; Kremers 1953; Moeller 1963).

3.6.3 Fractional Crystallization

In fractional crystallization, a part of the salt in solution is precipitated by a change in temperature or by evaporation of a saturated solution. If the solubilities of various components in the solution differ, the composition of the crystal crop will be different from that of the original solution. While the crystal crop becomes enriched in the less soluble component, simultaneously, the more soluble components will be enriched in the liquor.

More than half a dozen salts and double salts have been used for the separation of REEs by fractional crystallization. This method was considered to be the best of the classical separation procedures for producing individual elements in high purity (Parker and Baroch 1971). The most suitable compounds have been the double ammonium nitrates $RE(NO_3)_3 \cdot 2NH_4NO_3 \cdot 4H_2O$ for the removal of lanthanum and separation of praseodymium and neodymium, and the double magnesium nitrates $2RE(NO_3)_3 \cdot 3Mg(NO_3)_2 \cdot 24H_2O$ for obtaining concentrates containing the middle rare earths (MREs) samarium, europium, and gadolinium. The double manganese nitrates $2RE(NO_3)_3 \cdot 3Mn(NO_3)_2 \cdot 24H_2O$ have also been used in the separation of the ceric group. In the separation of the yttric group, the bromates $RE(BrO_3)_3 \cdot 9H_2O$ and ethyl sulfates $RE(C_2H_5SO_4)_3 \cdot 9H_2O$ have been used.

Erbium, thulium, lutetium, and yttrium have been separated using a rare-earth hexa-antipyrine iodide salt. A sodium–rare-earth ethylenediaminetetraacetic acid (EDTA) salt has also been useful (Marsh 1955) for separating gadolinium, terbium, dysprosium, and yttrium by fractional crystallization. The separation by fractional crystallization of these salts has been used commercially (Lever and Payne 1968) to separate and raise to 99% purity oxides of Gd, Tb, and Dy.

The lanthanum end of the series, where the differences in cationic radius are the greatest, is the most amenable to separation by fractional crystallization. Lanthanum forms the least soluble double nitrate. Starting from a cerium-free rare-earth concentrate, a procedure for separating lanthanum in high purity involves the steps shown in Figure 3.30. From the rare-earth concentrate solution, 90% La_2O_3 can be precipitated out using an air–ammonia mixture. From this product, high-purity lanthanum is then obtained by purification using countercurrent crystallization of the double nitrates $RE(NO_3)_2 \cdot 2NH_4NO_3 \cdot 4H_2O$.

The fractional crystallization is particularly slow and tedious for the HREs and in the Sm(III)–Gd(III) region because the property difference between rare earths decreases as the atomic number increases. For example, a bromate salt of a thulium fraction recrystallized 15,000 times still contained ytterbium and erbium. The rare earth bromate had to be crystallized every day for 4 years to obtain good holmium.

3.6.4 Fractional Precipitation

Fractional precipitation denotes the removal of one or more of the rare earths from solution by the addition of a chemical reagent to form a new, less soluble compound. The rare earths still remaining in solution are recovered either by further precipitation as the same compound or by complete precipitation of all the rare earths as the oxalate, hydroxide, or other compound.

As with fractional crystallization, a number of compounds have been studied for the separation of rare earths by fractional precipitation. The hydroxides and double sulfates, in particular, have been widely used. Double-chromate precipitation has also been used to separate rare earths from yttrium. Among the REEs, hydrolysis occurs least extensively with lanthanum, which remains mostly in solution. For large-scale operations, ammonia is used for carrying out hydroxide precipitation from the nitrate or chloride (Berber et al. 1960) solutions. The preliminary enrichment of yttrium-group rare earths and the extraction of yttrium from yttrium concentrates are also

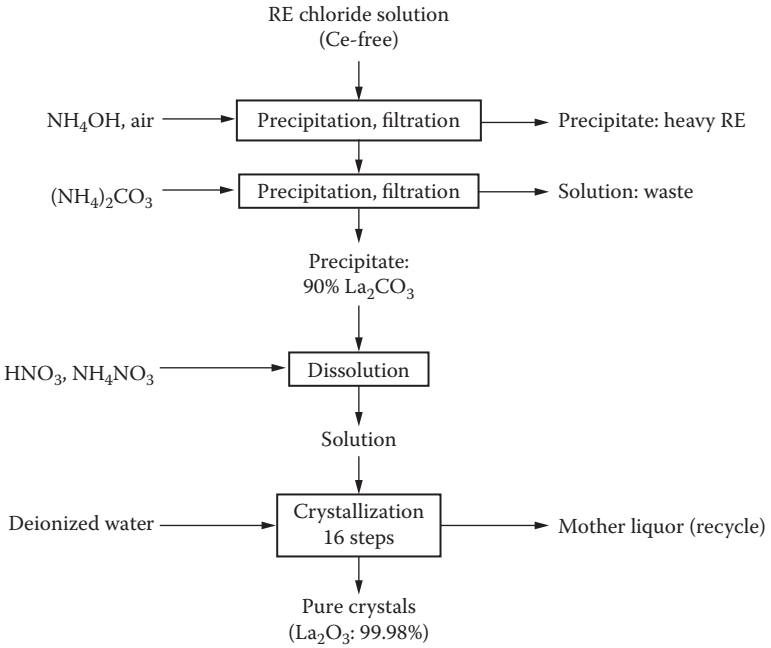


FIGURE 3.30 Separation of lanthanum by fractional crystallization.

possible by this method. Lever and Payne (1968) have used fractional precipitation of basic nitrates to separate a large fraction of yttrium from an HRE concentrate.

The double sulfates $RE_2(SO4)_3{\cdot}Na_2SO_4{\cdot}nH_2O$ are usually precipitated by the addition of sodium sulfate to the rare-earth solution. The elements La, Ce, Pr, Nd, and Sm form sparingly soluble double sulfates, whereas those of Ho, Er, Tm, Yb, Lu, and Y are soluble; Eu, Gd, and Dy form double sulfates of intermediate solubility. Generally, the use of this method is confined to crude separation of the rare-earth mixture into three groups. However, the elements La and Y could be readily separated.

Yttrium exhibits interesting behavior in fractional precipitation and is amenable to purification by a combination of hydroxide and double-sulfate precipitations (Powell 1961). The separation factor, however, is very small. In double-sulfate precipitation, yttrium behaves like holmium, and in basic precipitation, it behaves like neodymium. By the first method, the elements La–Dy can be removed, and in the second method, the elements Eu–Lu are removed.

A method in which the mixture to be separated was partially complexed with EDTA and the uncomplexed part was precipitated with sodium sulfate was also used. Earlier, a similar method had been proposed using oxalic acid as precipitating agent and nitrile-triacetic acid as the complexing agent.

Double chromates of rare earths with ammonium or potassium, precipitated from chloride solutions, have been found suitable for the industrial production of high-purity yttrium. For the separation of the HREs, a method based on fractional thermal decomposition of fused nitrates has also been investigated.

De Vasconcellos et al. (2006) described a "very simple, adequate and economical" method to separate yttrium from a low-cerium REE concentrate. The concentrate derived from monazite (NUCLEMON in São Paulo, Brazil) contained (in wt.%) 2.4 Y_2O_3, 0.6 Dy_2O_3, 2.7 Gd_2O_3, 2.5 CeO_2, 33.2 Nd_2O_3, 40.3 La_2O_3, 4.1 Sm_2O_3, and 7.5 Pr_6O_{11}. The separation is based on the fact that the REE solubility in ammonium carbonate varies progressively from element to element, the HRE elements being more soluble than the LRE elements. The concentrate is leached at room temperature (about 20–25°C), for a short time with 200 g/L ammonium carbonate to get a rich yttrium solution with about 60.3% Y_2O_3. This yttrium solution is treated with an excess of hydrogen peroxide (130 volumes), whereby cerium, praseodymium, and neodymium peroxides precipitated as an LRE–peroxycarbonate mixture completely and separated from yttrium. The filtered carbonate solution can be treated directly with oxalic acid to recover yttrium as the oxalate and finally as an oxide. The final product is 81% Y_2O_3. Dy and Ho have solubilities similar to yttrium. These elements will, therefore, collect with yttrium. In a later publication, de Vasconcellos et al. (2008) reported further on the behavior of the rare earths when treated with ammonium carbonate and with a binary mixture of ammonium carbonate plus ammonium hydroxide, and the possibility of using this information for separation of rare-earth mixtures, eventually on a plant scale.

In the years preceding 1947, the methods outlined thus far were the techniques available for separating the rare earths. For most of the REEs, these procedures were relatively inefficient and laborious. The purity of the end products obtained was also not comparable with that subsequently achieved in the modern methods of ion exchange and solvent extraction, which have dominated the commercial separation of rare earths starting in the 1950s.

3.6.5 Ion Exchange

3.6.5.1 Method

An ion-exchange resin or ion exchanger can be considered as an ionic salt in which one of the ions is attached to an insoluble organic matrix (Kleber and Love 1963). In an anion-exchange resin or anion exchanger, the charge on the ion is negative. Similarly, the charge on the ion is positive in a cation exchanger.

When the ion-exchange resin comes into contact with a salt solution, the mobile ion in the resin matrix may be displaced. Generally, (1) an ion of higher charge displaces an ion of lower charge; (2) between similarly charged ions, that with a larger radius displaces the one with the smaller radius; and (3) the displacement occurs according to the law of mass action.

The technique of ion exchange essentially involves the adsorption stage in which the ions from the solution get loaded or adsorbed on the exchanger and an elution stage during which, by a change of conditions, the ions desorb from the exchanger and enter into solution. In either step, an exchange between the ions in solution and those on the exchanger occurs. When more than one anion or cation is present in the solution and if certain selectivity is exhibited in these exchanges, the ion-exchange process becomes an ion-exchange separation.

According to the distribution law or partition law (Kleber and Love 1963), under equilibrium conditions, when a substance is distributed between two phases, the

ratio of the concentration of the substance in two phases will have a constant value. For instance, if the equilibrium concentration of the substance A in phase 1 is C_{A1} and that in phase 2 is C_{A2}, then D_A, called the distribution coefficient, is

$$D_A = \frac{C_{A1}}{C_{A2}}$$

If there is another substance B that is similarly distributed, then

$$D_B = \frac{C_{B1}}{C_{B2}}$$

Usually, the values of D_A and D_B are different. Comparison of D_A and D_B values gives information as to which of the two substances concentrates preferably, for example, in phase 1. In ion exchange, phase 1 can be taken as the resin phase, and in solvent extraction, phase 1 can be taken as the organic phase. The other phase, phase 2, is the aqueous phase in both techniques. The ratio of the distribution coefficients, α,

$$\alpha_B^A = \frac{D_A}{D_B}$$

is called the separation factor. If α is close to 1, no separation can be achieved, and separation is achievable if α is either >>1 or <<1.

The term *ion-exchange chromatography* was used (Powell 1961) to describe the technique for separating mixtures of ions based on sorption (adsorption) of the ions on a suitable ion exchanger followed by differential displacement of the individual ions with an eluant. Two kinds of behaviors were observed. One has been named *displacement chromatography*, and the other, *elution chromatography.*

The events in displacement chromatography are shown in Figure 3.31. Two ionic species B and C are sorbed on top of an exchange bed on which was loaded originally a third ionic species A, which has less affinity for the exchanger than either B or C. When this system is eluted with a simple salt solution containing ion D, which has greater affinity for the resin than even B and C, each ion tends to displace that having lesser affinity, and banding develops, as shown in Figure 3.31. The sequence in which the ions come out of the exchanger is shown (Powell 1961) in Figure 3.32. There is separation.

In elution chromatography, the ion sorbed initially and the eluant ion are usually the same. The eluant ion has a lesser affinity for the resin than the ions being separated. The equivalent concentration of the ions being eluted is less than the concentration of the eluant ion. Thus, the eluant ion displaces the sorbed ions inefficiently and overruns them. Under the influence of the eluant and having different affinities for the resin, the sorbed ions progress down the exchange beds at different rates. The type of elution curve (Powell 1961) shown in Figure 3.33 is then obtained.

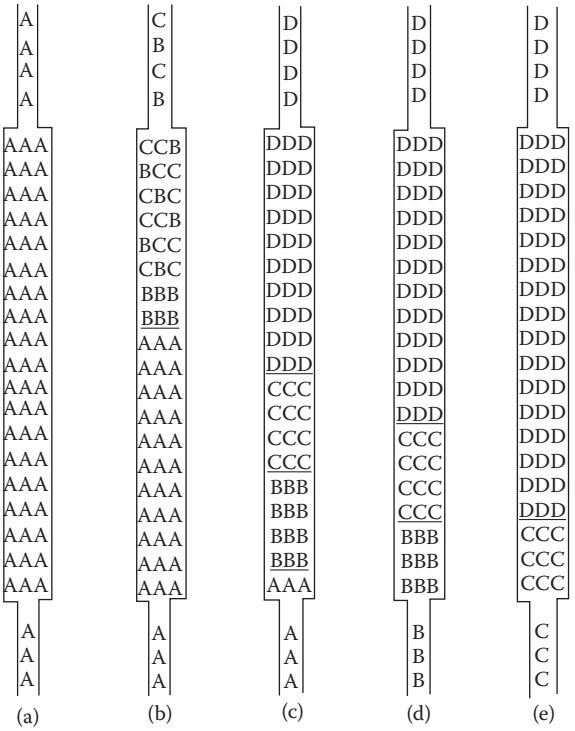


FIGURE 3.31 Simplified representation of events in displacement chromatography. (a) Column charged initially with A ions. (b) Column charged with a mixture of B and C ions—the order of increasing affinity is A, B, C; since C has greater affinity for the resin than B, some separation of B and C occurs during loading. (c) Bands of B and C being developed with an eluant containing D ions, which are more strongly attracted to the resin than A, B or C ions. (d) Developed band of B ions passing off the column. (e) Developed band of C ions passing off the column. (From Powell, J.E., Separation of rare earths by ion exchange. In Spedding, F.H. and Daane, A.H. (eds.). *The Rare Earths.* Chapter 6. 1961. Copyright Wiley-VCH Verlag GmbH & Co. KGaA. Reproduced with permission.)

3.6.5.2 Application

The first attempt at ion-exchange separation of rare earths dates back to the late nineteenth century, when in 1893, it was demonstrated that yttrium and gadolinium could be purified by adsorption on activated carbon. After a gap of over a half-century, it was shown that the simple procedure of adsorption of tripositive rare-earth ions on an ion exchanger and their removal by elution with sodium chloride effected no greater separation than fractional crystallization or precipitation. This was subsequently found true for most cation-exchange media. While there is a decrease in the affinity of the rare earths for the resin from La(III) to Lu(III), i.e., as the size of the hydrated ion is decreased, the affinities of the various REEs for the resin are not sufficiently different to result in satisfactory separation, because the separation factors for adjacent rare earths undergoing simple cation exchange are close to unity.

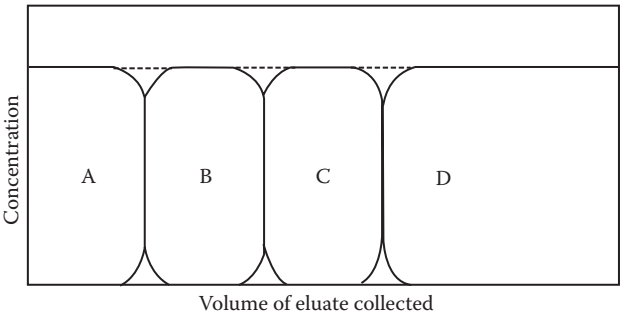


FIGURE 3.32 Typical elution plot in displacement chromatography. Some overlapping of bands is inherent, but regions of considerable extent are obtained within which the equivalent concentration of each ion is equal to the equivalent concentration of the driving ion in the eluant. (From Powell, J.E., Separation of rare earths by ion exchange. In Spedding, F.H. and Daane, A.H. (eds.). *The Rare Earths*. Chapter 6. 1961. Copyright Wiley-VCH Verlag GmbH & Co. KGaA. Reproduced with permission.)

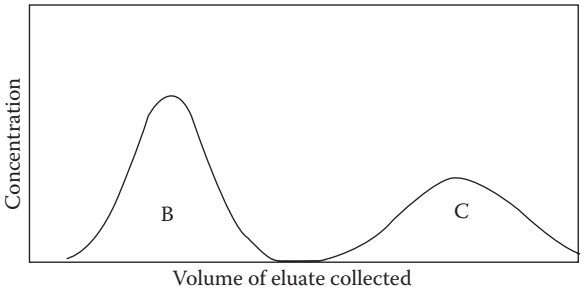


FIGURE 3.33 Typical elution plot obtained by elution chromatography. Eluent ions overrun and accompany the B band and the C band as they issue from the column. (From Powell, J.E., Separation of rare earths by ion exchange. In Spedding, F.H. and Daane, A.H. (eds.). *The Rare Earths*. Chapter 6. 1961. Copyright Wiley-VCH Verlag GmbH & Co. KGaA. Reproduced with permission.)

This situation was changed by the use of complexing agents to enhance separation factors. The successful separation of rare earths by ion exchange was subsequently demonstrated at Ames and at Oak Ridge National Laboratory by using a citric acid–ammonium citrate eluant at regulated pH and was reported in a series of papers in the *Journal of the American Chemical Society* (Ketelle and Boyd 1947). The separation was achieved as a result of the different stabilities of the citrate complexes formed by the individual rare earths in the mixture (Powell 1964, 1979; Powell and Spedding 1956, 1959b). The citrate elution has been performed successfully under a wide range of conditions (Powell 1964) and has proved effective for the separation of up to several hundred grams each of the LRE elements. The differences between complex formation constants of adjacent HREs are not as large as those between the LREs, and the citrate process has not

been very successful in separating bulk quantities of HREs. The extreme dilution of the eluant was also an economic disadvantage.

Besides the citrate, a number of eluting agents and process conditions were actively evaluated, and they have been reviewed by Powell (1961, 1964, 1979). The use of amino polyacetic acids such as Nitrilotriacetic acid (NTA) and EDTA as eluants was investigated but was unsuccessful due to the problem of aqueous insolubility. This and many other limitations of the elution process were solved in the band displacement technique developed by Spedding et al. (1954), using the resin in a special cation state. Compared with citrates, complexing agents such as EDTA and 2-hydroxy-ethylenediamine-triacetic acid (HEDTA) not only form 1:1 chelates of greater stability over wider pH ranges but also give greater differences in stability between adjacent rare earths and allow higher concentrations to be used. Commercially, the most useful complexing agents are EDTA and HEDTA. The acids diethylene triamine pentaacetic acid (DTPA) and 1,2-diamine cyclohexane tetraacetic acid (DCTA) also provide high separation factors (Powell 1964, 1979). Powell (1979) has discussed the separation potential of each of these chelating agents and ranks EDTA and HEDTA as the most useful. EDTA can effectively separate all of the rare earths and yttrium from each other with the exception of Eu–Gd and Yb–Lu pairs because of the small difference in the separation factor and adverse kinetic effects, respectively. The Dy–Y separation is also very slow with EDTA because of the small difference in the stability of the two complexes. There is, however, a large difference between the stabilities of HEDTA–Dy and HEDTA–Y complexes, so this pair can be separated by HEDTA. Besides, HEDTA is particularly useful in the separation of the Tm–Yb–Lu fraction, and good separations are possible with either La–Ce–Pr–Nd–Y–Sm or Ho–Er–Tm–Yb–Lu mixtures. The separation of an Sm–Eu–Gd–Tb–Dy–Ho mixture with HEDTA is poor because of small differences in chelate stabilities. An advantage of HEDTA elution is that hydrogen ion–retaining beds can be used because H_3(HEDTA) is considerably more soluble in cold water than H_4(EDTA). This permits easy recycling of reagent. The HEDTA complexes of HREs such as Tm, Yb, and Lu show only limited solubility and restrict the eluant concentration.

For the rapid separation of yttrium, a two-stage procedure that makes use of the different positions of yttrium in the elution sequence with different chelating agents was reported. In the EDTA system, yttrium elutes between Tb and Dy, whereas in HEDTA, it elutes between Nd and Sm. The HREs are first separated by elution with HEDTA, leaving yttrium in the Nd fraction. This fraction is then eluted with EDTA to separate yttrium from neodymium.

Temperature plays a crucial part in ion-exchange separations. Ketelle and Boyd (1947) first reported the shifting in the position of yttrium during elutions with 5% citrate. This was followed by investigations (Lindstrom and Winget 1962) on elutions at 87–90°C with citrate, lactate, and also EDTA, particularly for the separation of Y, Sm, Eu, and Tm. Lindstrom and Winget (1962) showed that the hydrogen ion could be used as retaining iron in rare-earth separations with EDTA if the system is operated at 90–95°C when H_4(EDTA) becomes more soluble. Powell (1964, 1979) pointed out several other advantages of operation at 92°C. These include improved height equivalent of a theoretical plate (HETP) values and an increase in Gd–Eu and

Eu–Sm separation factors. At all temperatures, with EDTA, Y elutes between Tb and Dy; however, with an increase in temperature to 92°C, Tb separation improves, and there is a decrease in Dy–Y separation. The rise in temperature also makes EDTA elution more effective for rare-earth separation from non-rare-earth impurities, as, for example, in the case of the Tb–Pb–Yb–Lu mixture, which is difficult to separate at room temperature.

As pointed out above, HEDTA gives poor separation of the elements Sm–Ho at room temperature. Much better separation becomes possible at 92°C because of improvement in the adjacent element separation factor with a rise in temperature (Powell 1979). The solubilities of species Tm(HEDTA), Yb(HEDTA), and Lu(HEDTA) increase with an increase in temperature, and eluant concentrations up to 0.072 M have been successfully used at 92°C compared with the maximum concentration of only 0.018 M at room temperature. In HEDTA elutions, there is a considerable shift in the position of yttrium with a change in temperature (Morton and James 1967). The isolation of yttrium on a large scale as a result of this shift has been studied. Powell (1979) has also pointed out that the poor kinetics observed in ion-exchange elution with DTPA could be countered to some extent by an increase in temperature.

The development of band displacement with ammonium ethylenediaminetetraacetate as the complexing agent established ion exchange as the main commercial process for rare-earth separation from the mid-1950s. The fact that it is feasible to separate a mixture of 15 rare earths into components exceeding 99.99% purity in one pass through the system and that the process can be scaled up to multiton quantities, with possibilities of recovering and recycling water, and retaining ion and complexant, has led to the continued commercial use of ion exchange even after the entry of solvent extraction in the field. A major limitation of the band displacement technique or displacement ion-exchange chromatography is that the technique is inherently a batch process. Taniguchi et al. (1988) have succeeded in adopting fixed column band displacement chromatography to the continuous annular chromatograph (CAC). This technique, called continuous displacement chromatography (CDC), combines the processing capabilities of fixed-column batch displacement chromatography with continuous operation of CAC and is applicable to any displacement chromatography separation that can be performed using conventional batch fixed-column chromatography.

3.6.6 Solvent Extraction

3.6.6.1 Method

The separation of rare earths by solvent extraction depends upon the preferential distribution of individual rare earths (in the cationic form, as complex anions, or as a neutral species) between two immiscible liquid phases that are in contact with each other. One of the liquid phases is an aqueous solution, and the other is a nonaqueous phase, i.e., the organic phase. The expressions given for the distribution coefficient and separation factor, earlier in connection with ion-exchange separation, can also be used for solvent extraction separation also. In ion exchange, phase 1 was taken as the resin phase, and in solvent extraction, phase 1 can be taken as the organic phase. Phase 2 is the aqueous phase in both cases.

There are many advantages to using solvent extraction as the process for rare-earth separation. One of them is that the rare-earth loading in the solvent/extractant can be very high (~180 g REO/L). Therefore, aqueous solutions with concentrations of 100–140 g REO/L can be used. These make the equipment required for the process very compact (McGill 1993).

The organic phase used in solvent extraction usually consists of two or more substances, the extractant, solvent, and modifier. The *extractant* proper is responsible for collecting the rare-earth species into the organic phase but is usually too viscous to be used in a practical system. It is dissolved in a suitable *solvent* to ensure good contact with the aqueous phase. Generally, the solvent is kerosene or any suitable hydrocarbon. A substance known as a *modifier* is also usually added to the organic phase to improve the hydrodynamics of the system.

The schematic of the solvent extraction process (Shibata 1991) is shown in Figure 3.34. Usually, the transfer of metal ions from the aqueous to the organic phase does not occur completely in one contact. Multiple contacts are necessary. This also holds true for scrubbing (contacting the LO with an aqueous solution to collect back the impurities extracted by the solvent) and stripping (contacting the scrubbed organic phase with an aqueous solution to recover the main extracted species from the organic phase, back to the aqueous phase).

The beginning of solvent extraction separation of rare earths was made in the 1930s through the observations of Hopkins and Quill (1933) and, a few years later, of Fischer et al. (1937). They found differences in the distribution of various rare-earth chlorides between water and partially miscible alcohols and ketones. Appleton and Selwood (1941) found a separation factor of 1.06 for the partition of lanthanum and neodymium thiocyanate between water and *n*-butyl alcohol and suggested that a

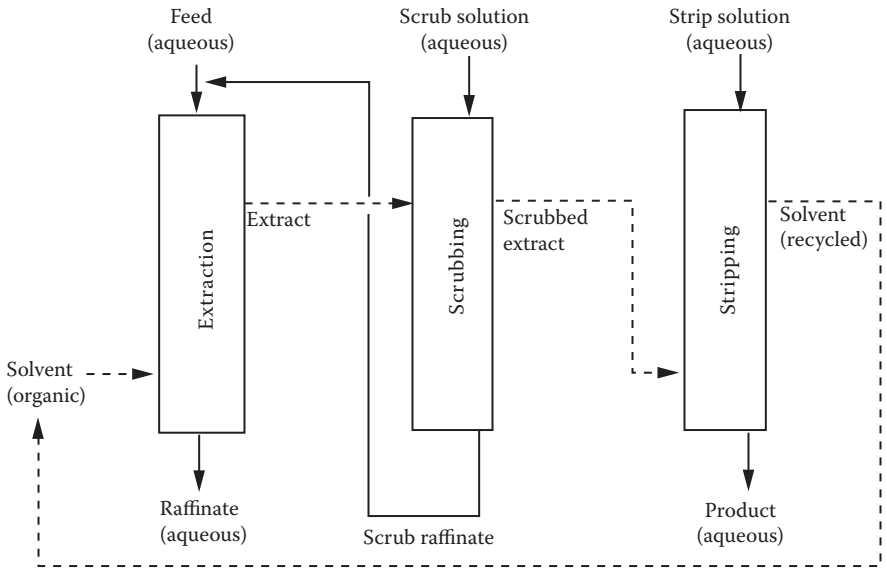


FIGURE 3.34 Typical solvent extraction flow sheet.

continuous counter-current extraction might be effective for separations. Higher separation factors of 1.29–1.55 depending on experimental conditions were obtained for the lanthanum–neodymium pair by Templeton and Peterson (1948) and Templeton (1949) for the distribution of the nitrates between water and *n*-hexyl alcohol. The important observation that Ce(IV) can be separated readily and completely from the trivalent cations in an aqueous nitric acid solution by extraction with TBP, first made by Warf (1949), marked the beginning of practical application of solvent extraction to rare-earth separations. The TBP extraction of Ce(IV) was later investigated by Bauer (1959). A flow sheet for the purification of cerium and recovery of cerium nitrate by TBP extraction is given in Figure 3.35. Cerium(IV) is stripped from the organic phase best by its reduction to cerium(III) using, for example, hydrogen peroxide (Warf 1949).

$$2[Ce(NO_3)_4(TBP)_2]_{org} + [H_2O_2]_{aq} = 2[Ce^{3+}]_{aq} + 8\left[NO_3^-\right]_{aq} + 2[H^+]_{aq} + O_2 + 4[TBP]_{org}$$

In such processes, cerium dioxide products of high purity (>99.99%) were obtained from the strip liquors. The extractability of rare earths with TBP from concentrated hydrochloric and nitric acid solutions has been studied at Argonne National Laboratory (Peppard et al. 1953, 1958). The studies showed that extractions with TBP are more effective in nitrate systems and that the TBP–nitric acid system could be used to separate the trivalent rare earths from one another. In 1953, Oak Ridge National Laboratory isolated the first kilogram of pure Gd_2O_3 (98% Gd_2O_3) by using TBP–nitric acid solvent extraction using a mixed rare-earth feed containing 25% Gd_2O_3 (Weaver et al. 1953). Using a similar technique, Weaver (1974) obtained better than 98% pure Sm_2O_3. The separation of rare earths from monazite using TBP (Ritcey and Pouskouleli 1987) was investigated by Bochinski et al. (1953, 1958).

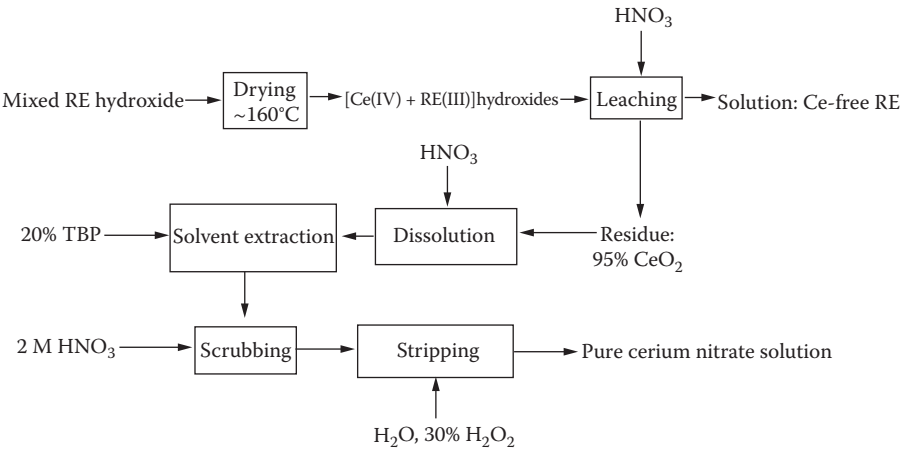


FIGURE 3.35 Separation and purification of cerium.

Foos and Wilhelm (1954) extended this work to study the separation of yttrium and HREs. A complete scheme for the separation of all the rare earths by solvent extraction was proposed by Callow (1967). However, the separation of rare earths beyond terbium with TBP has been difficult (Powell 1979).

Peppard et al. (1957a) first suggested the use of HDEHP for rare-earth separations. HDEHP may be used in either chloride or sulfate systems both for obtaining rare-earth concentrates from complex mixtures and to isolate individual rare earths in high purity. 99.8% pure lanthanum oxide was obtained using HDEHP in a 14-stage countercurrent extraction from a didymium chloride feed containing 45% La_2O_3, 35% Nd_2O_3, 10% Pr_6O_{11}, and 5% Sm_2O_3. By selective stripping of a preloaded solvent, Bauer and Lindstrom (1971) recovered >99% pure samarium oxide. The organic solvent (1 M HDEHP in kerosene) was loaded with an RE mixture 60% in Sm_2O_3, and the aqueous scrubbing solution contained 1.5% HCl and 20% NH_4Cl.

Many amines have also been examined for use in rare-earth separations. Of these, tertiary amine extraction has received particular attention. A euxenite concentrate containing 47% yttria was processed using tri-*n*-butyl-amine solvent in 3-methyl-2-butanone and an aqueous phase of 8 M HNO_3 (Gruzensky and Engel 1959). The product obtained was 83% yttrium oxide. Other amine types such as tri-isooctylamine (TIOA), methyl-dioctyl-amine (MDOA), dodecyl-amine (DDA), and alamine have also been used for the separation of rare earths (Rice and Stone 1962).

These early and experimental works were followed by many investigations in later years, and solvent extraction developed as a major technique for rare-earth separation. The solvent extraction of rare earths has been reviewed by Peppard (1964), Weaver (1974), Sherrington (1983), Preston and du Preez (1990), and Bautista (1995).

Numerous extractants have been used for analytical or laboratory-scale separation of rare earths from one another; however, only relatively few are used in industrial practice. They include cation-exchange extractants such as organophosphorus acids and carboxylic acids, neutral extractants such as tri-*n*-butyl phosphate (TBP), and anion-exchange extractants such as the amines. Among these, the primary industrial extractants used for the separation of rare earths by solvent extraction are HDEHP, 2-ethyl-hexyl-2-ethyl-hexyl phosphonic acid (EHEHPA), TBP, versatic acid, Versatic 10, and Aliquat 336. These and other commercially important extractants are listed in Table 3.5 (Ritcey and Ashbrook 1984; Rydberg et al. 2004; Xie et al. 2014). All three major classes of extractants, cation exchangers (or acidic extractants), solvation extractants (or neutral extractants), and anion exchangers (or basic extractants), have been used apart from some chelating extractants. Even though considerable published information is available on the extraction behavior of these solvents, the details of solvent extraction processes actually practiced in the industry are well-kept secrets.

3.6.6.2 Organophosphorus Acids

Monobasic organophosphorus acids include the well-known phosphoric, phosphonic, and phosphinic acids. HDEHP (D2EHPA) is the most investigated and most readily available organophosphorus acid. The organophosphorus acids are typical cation-exchange extractants. The extraction by cation exchange involves, most commonly,

TABLE 3.5
Some Commercial Extractants for Rare-Earth Solvent Extraction

Reagent Class	Molecular Formula	Extractant
		Cation Exchangers
Carboxylic acids	$(R_1{\cdot}R_2{\cdot}CH_3){\cdot}C{\cdot}COOH$	Versatic acids: $R_1 + R_2 = C_7$, Versatic 10 $R_1 + R_2 = C_6$–C_8, Versatic 911
	$(R_1{\cdot}R_2{\cdot}R_3{\cdot}R_4){\cdot}(CH_2)_n COOH$	Naphthenic acids R_1–R_4: varied alkyl groups
Phosphorous acids	$(R_1{\cdot}R_2){\cdot}POOH$	Phosphoric acids: $R_1 = R_2 = C_4H_9CH(C_2H_5)CH_2O$–, di-2-ethyl-hexyl phosphoric acid (D2EHPA) Phosphonic acids: $R_1 = C_4H_9CH(C_2H_5)CH_2O$–, $R_2 = C_4H_9CH(C_2H_5)CH_2$–, 2-ethyl-hexyl phosphonic acid mono-2-ethyl-hexyl ester (EHEHPA, HEHEHP, P507, PC88A) Phosphinic acids: $R_1 = R_2 = C_4H_9CH(C_2H_5)CH_2$–, di-2-ethyl-hexyl phosphinic acid (P229) $R_1 = R_2 = CH_3(CH_2)_3CH_2CH(CH_3)CH_2$–, di-2,4,4-trimethylpentyl-phosphinic acid (Cyanex 272)
	$(R_1{\cdot}R_2){\cdot}PSOH$	Monothiophosphorous acids: $R_1 = R_2 = CH_3(CH_2)_3CH_2CH(CH_3)CH_2$–, di-2,4,4-trimethylpentyl-monothiophosphinic acid (Cyanex 302)
	$(R_1{\cdot}R_2){\cdot}PSSH$	Dithiophosphorous acids: $R_1 = R_2 = CH_3(CH_2)_3CH_2CH(CH_3)CH_2$–, di-2,4,4-trimethylpentyl-dithiophosphinic acid (Cyanex 301)
Chelating exchangers	$R_1{\cdot}(CO){\cdot}CH_2{\cdot}(CO){\cdot}R_2$	β-diketones: $R_1 = R$–C_6H_5, $R_2 = CH_3(CH_2)_5$–, R: unknown side alkyl, (LIX 54)
Solvating extractants	$(R_1{\cdot}R_2{\cdot}R_3){\cdot}PO$	Phosphorous ester: $R_1 = R_2 = R_3 = CH_2(CH_2)_2CH_2O$–, tri-*n*-butyl phosphate (TBP) $R_1 = R_2 = CH_2(CH_2)_2CH_2O$–, $R_3 = CH_2(CH_2)_2CH_2$–, dibutyl-butyl phosphonate (DBBP) Phosphine oxides: $R_1 = R_2 = R_3 = CH_2(CH_2)_6CH_2$–, tri-*n*-octylphosphine oxide (TOPO, Cyanex 921)
Anion exchanger	$(R_1{\cdot}R_2{\cdot}R_3){\cdot}N{\cdot}CH_3Cl$	Primary amines: $R = (CH_3)_3C(CH)_2C(CH_3)_2)_4$ (Primene JM-T, N1923) Quaternary amines: $R_1 = R_2 = R_3 = C_8$–C_{10} mixture (Aliquat 336, Adogen 464)

Source: After Ritcey, G.M. and Ashbrook, A.W., *Solvent Extraction; Principles and Applications to Process Metallurgy*, Part I, Elsevier, Amsterdam, 1984; Rydberg, J. et al., *Solvent Extraction Principles and Practice*. Marcel Dekker, New York, 2004; Xie, F. et al., *Miner. Eng*., 56: 10–28, 2014.

the displacement of a hydrogen ion from the extractant by the extracted metal, resulting in the formation of an electrically neutral, organic soluble complex. In organic solvents of low polarity, the organophosphorus acids exist in the dimeric form H_2A_2, and the extraction is, therefore, represented (Mason et al. 1978) by

$$[RE^{3+}]_{aq} + 3[(HA)_2]_{org} \rightarrow [RE(HA_2)_3]_{org} + 3[H^+]_{aq}$$

As indicated by this reaction, the extraction is strongly pH dependent, inversely proportional to the third power of hydrogen ion concentration (Peppard et al. 1957a,b) in the aqueous phase apart from a third-power dependency on the extractant concentration in the organic phase. The extraction of rare earths with cation exchangers is promoted by increasing the pH of the aqueous phase, while the stripping, which reverses the extraction reaction, is promoted by increasing the acidity of the aqueous stripping solution (decreasing the pH). At high metal loading and low acidities, gel formation occurs in the organic phase, causing phase separation problems (Ferraro and Peppard 1963).

In nitric or hydrochloric acid solutions, the minimum value of the distribution coefficient is reached at an acid concentration of 3 N. For any given organophosphorus acid, the extraction efficiency of rare earths increases with an increase in atomic number. This could possibly result from the increase in the strength of the electrostatic attraction between the extractant anion $\left(HA_2^-\right)$ and the rare-earth cation, as the size of the cation decreases. The extraction of yttrium lies in the dysprosium–holmium–erbium region as could be anticipated on the basis of its cationic radius. On the same basis, it would also be anticipated that Ce(IV) is more preferentially extracted than the trivalent rare-earth ion, and Eu(II) is not extracted when RE^{3+} is present. These characteristics could be used to separate cerium and europium from the rare-earth mixture.

The distribution coefficient in HDEHP–rare earth systems increases with an increase in atomic number (and decreases in trivalent ionic radii), and the variation in the system HDEHP–perchloric acid is shown in Figure 3.36. HDEHP gives good separation factors for all REEs. The average separation factor for adjacent REEs is ~2.5. The separation factors in the system HDEHP–HCl are listed in Table 3.6.

HDEHP can extract from a variety of aqueous media, including nitrate, sulfate, chloride, and perchlorate, and the influence of the anion of the rare-earth salt on the separation is considered to be generally small. The anion, however, apparently plays a role in certain cases. Even though HDEHP can extract from both chloride and nitrate solutions, it is considered to extract better from the chloride than the nitrate medium. Chlorides or sulfates are preferred for the separation of neodymium and samarium. Besides, sulfates are preferred for better selectivity for the separation of cerium earths from the other REEs (McGill 1993).

Generally, the separation factor is neither greatly influenced by the total concentration of the REE nor by the relative concentrations of the various elements (McGill 1993). The distribution coefficients of rare earths decrease with an increase in temperature, and the effect of temperature is greater for the HREs. The distribution coefficient has been found to be dependent on the diluent for the organophosphorus

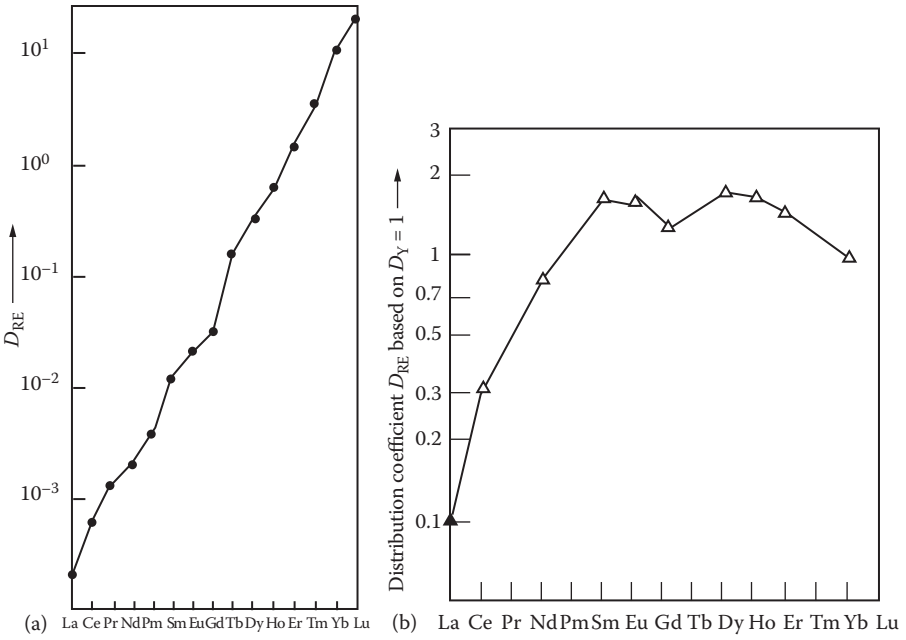


FIGURE 3.36 Distribution coefficient k_{RE} relative to $k_Y = 1$ in the system. (a) HDEHP–perchloric acid and (b) TBP with 50% kerosene/rare-earth nitrates (REO, 450 g/L). (From Pierce, T.B. and Peck, J.F., *Analyst,* 88: 217–221, 1963; McGill, I., Rare earth elements. In Elvers, B., Hawkins, S., Russy, W., and Schulz, G. (eds.), *Ullmann's Encyclopedia of Industrial Chemistry*, vol., A22, pp. 607–649, VCH, Weinheim, 1993.)

acid and decreases in the order kerosene > cyclohexane > CCl_4 > xylene > benzene. HDEHP in kerosene is usually chosen as the extractant.

In HDEHP extractions, there is also a possibility that separations can be enhanced by the use of scrubbing circuits in which exchange reactions, which are pH independent, like the following, occur:

$$[Sm^{3+}]_{aq} + [Nd(HA_2)_3]_{org} \rightarrow [Sm(HA_2)]_{org} + [Nd^{3+}]_{aq}$$

The extraction of rare earths by di-2-ethyl-hexylphosphinic acid (P229) in toluene was investigated by Preston and du Preez (1990). The distribution coefficient was found to increase in the order La < Ce < Pr < Nd < Sm < Eu < Gd < Tb < Dy < Ho < Y < Er < Tm < Yb < Lu. Based on these data, they concluded that the organophosphorus acids could be useful for separating the rare-earth mixture into light, middle, and heavy fractions. The light and middle fractions could be split between neodymium and samarium, and the separation of the middle and heavy fractions could be made between gadolinium and terbium. The results of Preston and du Preez are in tune with those obtained by Peppard and Mason (1961) when they reported the log of the distribution coefficient increasing linearly with the atomic number, *Z*, of the rare earth—lanthanum being the lowest and lutetium the greatest,

TABLE 3.6
Separation Factor $\left(\alpha_B^A\right)$ [a] of the Rare-Earth Elements in the Extraction Systems RE(III)–HCl–HDEHP

	B												
A	**Ce**	**Pr**	**Nd**	**Sm**	**Eu**	**Gd**	**Tb**	**Dy**	**Ho**	**Er**	**Tm**	**Yb**	**Lu**
La	2.14	2.28	2.43	11.8	26.3	44.6	71.1	101	125	212	319	414	425
Ce		1.07	1.14	5.2	12.3	20.9	33.3	47.2	58.4	99.1	149	193	199
Pr			1.06	5.16	11.5	19.5	31.1	41.1	54.7	92.7	139	181	186
Nd				4.86	10.8	18.3	29.2	41.5	51.3	87.1	131	170	175
Sm					2.23	3.75	6.02	8.55	10.6	17.9	27.0	35.1	36.0
Eu						1.69	2.70	3.83	4.74	8.04	12.0	15.7	16.2
Gd							1.60	2.26	2.80	4.75	7.15	9.30	9.55
Tb								1.42	1.76	2.98	4.48	5.83	5.90
Dy									1.24	2.10	3.16	4.11	4.22
Ho										1.70	2.55	3.31	3.41
Er											1.50	1.90	2.01
Tm												1.30	1.34
Yb													1.03

Source: Bautista, R.G., Separation chemistry, in Gschneidner, K.A. Jr. and Eyring, L. (eds.), *Handbook on the Physics and Chemistry of Rare Earths*, vol. 21, North Holland, Amsterdam, 1995.

[a] $\left(\alpha_B^A\right) = D_A / D_B$, in the extraction from 0.1 mol dm^{-3} hydrochloric acid solution with 0.2 mol dm^{-3} HDEHP in kerosene.

with yttrium appearing in between Tb and Tm, corresponding to a hypothetical atomic number 67.6. The average separation factor of two adjacent REEs was 2.5. The extraction behavior of the REEs with D2EHPA in toluene was similar for perchloric acid solutions (Pierce and Peck 1963) but poorer in nitrate media (Reddy et al. 1995). While the distribution coefficients of rare earths generally increased with increasing atomic number, the separation factors depend on both the acidity of the aqueous phase and nature of the anion (Xie et al. 2014).

In 1965, Molycorp first demonstrated the large-scale deployment of D2EHPA for preconcentrating europium from rare-earth-chloride feed derived from bastnasite (Kruesi and Schiff 1968). Later, Preston and du Preez (1996) preconcentrated europium from a chloride solution containing 0.22 M total rare earths (93% Eu, 3% Sm, 2% Nd, 1% Ce, 0.5% Pr, 0.5% and Gd) using 0.4 M D2EHPA in xylene; 99.98% Eu solutions were obtained in a single extraction stage at pH 2.7.

Starting from a didymium chloride feed solution containing 45% La, 35% Nd_2O_3, 10% Pr_6O_{11} and 5% Sm_2O_3, Nair and Smutz (1967) used extraction with 1 M D2EHPA to obtain a 99.8% La_2O_3 product. Two multistage countercurrent extraction circuits, a 12-stage cascade to concentrate La in the raffinate, and a 14-stage cascade for further purification were used with an overall La recovery of 60%.

Preston et al. (1996a,b,c) described a continuous solvent extraction process using 15% v/v of D2EHPA in Shellsol AB for separating the middle (Sm, Eu, Gd, and Tb) and the LRE fractions (La, Ce, Pr, and Nd) from a nitrate feed on a fairly extended scale. D2EHPA has also been used to separate Sm, Eu, and Gd from the other rare earths in a mixed nitrate–chloride leachate from Egyptian monazite (Rabie 2007).

The extraction of lanthanide chlorides by EHEHPA, also known as PC88A, in kerosene was also extensively investigated. The separation factors are listed in Table 3.7. The order of extraction of rare earths with 2-ethyl-hexyl phosphonic acid mono-2-ethyl-hexyl ester (HEHEHP) from chloride and nitrate media is La < Ce < Pr < Nd < Sm < Eu < Gd < Tb < Dy (_Y) < Ho < Er < Tm < Yb < Lu (Sato 1989). HEHEHP, marketed also as PC88A, SME 418, Ionquest 801, and P507, has been attractive for rare-earth separations because rare earths can be stripped at lower acidities than from D2EHPA (Reddy et al. 1995) and HEHEHP can be more heavily loaded with rare earth than D2EHPA before the onset of saturation effects. The extraction efficiency for the rare earths in EHEHPA also increases with atomic number but is lower in comparison with HDEHP under the same conditions. EHEHPA, however, is more selective for the separation of HREs from LREs. EHEHPA is preferred as an extractant for the separation of REEs due to the high separation factors between any two adjacent REEs compared to HDEHP. In the past decade, PC88A has practically replaced HDEHP in many of the applications where HDEHP was originally used for the industrial solvent extraction separation of rare earths. A process developed by Daihachi for separating rare earths using HEHEHP has been implemented in separation plants in Baotou, China (Zhu 1991).

As mentioned earlier, the organophosphorus acids are liquid cation exchangers and liberate hydrogen ion during the loading of the extractant with the rare-earth ions. This liberated hydrogen ion, i.e., the increase in the solution acidity, adversely affects metal extraction. This problem is circumvented by saponifying the extractant with NaOH. The degree of saponification is restricted, however, to avoid gel

TABLE 3.7
Separation Factor $\left(\alpha_B^A\right)$ [a] of the Rare-Earth Elements in the Extraction Systems RE(III)–HCl–EHEHPA

	B												
A	**Ce**	**Pr**	**Nd**	**Sm**	**Eu**	**Gd**	**Tb**	**Dy**	**Ho**	**Er**	**Tm**	**Yb**	**Lu**
La	1.30	1.42	1.67	3.33	6.52	9.52	22.5	36.4	93.9	117	156	175	199
Ce		1.09	1.28	2.57	5.02	7.36	17.3	28.0	72.3	90.5	120	135	152
Pr			1.17	2.35	4.59	6.72	15.8	64.2	66.0	82.7	110	123	140
Nd				2.00	3.94	5.74	13.5	21.8	56.3	70.5	93.7	105	119
Sm					1.96	2.87	6.74	10.9	28.2	35.3	46.8	52.6	59.5
Eu						1.46	3.45	6.39	14.4	18.0	24.0	26.9	30.4
Gd							2.35	3.81	9.82	12.3	16.3	18.3	20.7
Tb								1.62	4.18	5.23	6.95	7.81	8.83
Dy									2.58	3.23	4.29	4.82	5.45
Ho										1.25	1.66	1.87	2.11
Er											1.33	1.49	1.69
Tm												1.12	1.26
Yb													1.13

Source: Bautista, R.G., Separation chemistry, in Gschneidner, K.A. Jr. and Eyring, L. (eds.), *Handbook on the Physics and Chemistry of Rare Earths*, vol. 21, North Holland, Amsterdam, 1995.

[a] $\left(\alpha_B^A\right) = D_A / D_B$, in the extraction from 0.1 mol dm^{-3} hydrochloric acid solution with 0.2 mol dm^{-3} EHEHPA in kerosene.

formation due to excessive loading of rare earths and to avoid solubility of the saponified solvent in the aqueous phase. The organic phase typically containing 1.0 M PC88A in kerosene (mainly paraffinic and naphthenic hydrocarbon in the C_{10}–C_{14} range), containing 5% (v/v) isodecanol, after 20% saponification with NaOH, has been used for extraction of rare earths from a chloride aqueous solution (Thakur et al. 1990).

3.6.6.3 Carboxylic Acids

Carboxylic acids (C_7–C_{15}) are soluble in hydrocarbons and, like the organophosphorus acids, extract by cation exchange. The extraction, represented by

$$3[R_3C{\cdot}COOH]_{org} + [RE^{3+}]_{aq} \rightarrow [(REC{\cdot}COO)_3RE]_{org} + 3H^+$$

is conducted in a neutral or weakly acidic medium. Carboxylic acids are commercially available and are relatively inexpensive.

Among the carboxylic acids, the most widely used for rare-earth extraction (Bauer and Lindstrom 1964; Korpusov et al. 1974) are the versatic acids $R_1R_2(CH_3)C{\cdot}COOH$, where R_1 and R_2 are branched-chain alkyl groups. Versatic 911 has 9 to 11 carbon atoms, and Versatic 10 has 10 carbon atoms. The separation factors for Versatic 911 are listed in Table 3.8. The separation factors for La–Ce and Ce–Pr are 3 and 1.6, respectively, and these values are higher than those for TBP extraction. For Nd–Pr onward, the separation factors are similar to the TBP system (Brown and Sherrington 1979). Versatic acid extracts similarly from both nitrate and chloride media. This reagent also extracts the HREs.

Naphthenic acids are represented by the general formula RCOOH, where R is a radical derived predominantly from cyclopentane or a homolog of cyclopentane. Naphthenic acid with diethyl ether or *n*-hexanol as a diluent was used with some success as an extractant for rare-earth sulfates (Bauer and Lindstrom 1964). Rare-earth extraction was dependent on pH, naphthenic acid concentration, and the mole ratio of naphthenic acid to the rare earth. The separation factor was enhanced to 2.2 for adjacent yttrium-group elements by the addition of an aqueous phase chelating agent such as EDTA. Similarly, the addition of DTPA enhanced the separation factor to 3.5 for adjacent yttrium-group elements (Bautista 1995). In China, naphthenic acid has

TABLE 3.8
Separation Factors between Rare Earths for Extraction by Versatic 911/ Shellsol A from a Nitrate or Chloride Medium

Ce–La	Pr–Ce	Nd–Pr	Sm–Nd	Gd–Sm	Dy–Gd	Ho–Dy	Er–Ho	Yb	
3.00	1.60	1.32	2.20	1.96	1.94	1.17	1.28	1.49	
La–Y	**Ce–Y**	**Pr–Y**	**Nd–Y**	**Sm–Y**	**Gd–Y**	**Dy–Y**	**Ho–Y**	**Yb–Y**	**Er–Y**
0.028	0.085	0.14	0.18	0.39	0.77	1.50	1.75	2.25	3.35

Source: McGill, I., Rare earth elements, in Elvers, B. et al. (eds.), *Ullmann's Encyclopedia of Industrial Chemistry*, vol. A22, VCH, Weinheim, 1993.

been widely used for separating yttrium from other rare earths (Li et al. 1994). The aqueous solubility of naphthenic acids is high, and this leads to significant reagent losses. Certain novel carboxylic acids, such as sec-nonylphenoxy acetic acid (CA-100) and sec-octylphenoxy acetic acid (CA-12), used in China, have much lower aqueous solubilities than naphthenic acids.

The extraction behavior of yttrium differs for versatic and naphthenic acids. By Versatic 10, yttrium is extracted with the MREs (La < Ce < Nd < Gd < Y < Ho < Yb), whereas naphthenic acid extracts it with the LREs (La < Ce < Y < Nd < Gd < Ho < Yb). Preston and du Preez (1990) and du Preez and Preston (1992) attributed this alteration of order to steric reasons caused by the structure of the carboxylic acids and the atomic number of rare-earth-metal ions. With nonhindered acid and straight-chain acids, yttrium behaves like light lanthanides (e.g., Ce, or Pr), while with sterically hindered acids, it resembles the middle lanthanides (e.g., Gd or Tb). However, Zheng et al. (1991) noted a reason for the behavior of Y in the acidity of the extractant.

A study on the extraction of trivalent lanthanides (Sc, Y, Ln) and divalent transition metal ions (Cu, Zn, Ni, Mn, Cd, Co) from acidic chloride solutions with CA-100 in heptane revealed that CA-100 can extract rare-earth ions at lower pH values than Versatic 10. In CA-100, yttrium extracts with the HREs (Wang et al. 2002; Li et al. 2007a,b). The extraction behavior of rare earths has also been studied using cekanoic, neoheptanoic, and some 2-bromo alkanoic acids (Preston 1994; Singh et al. 2006). The introduction of the 2-bromo substitute in an alkanoic acid structure lowers the pK_a values and appears to enable the substituted acids to be effective extractants at a lower pH than the parent compounds (Xie et al. 2014).

Di-alkyl phosphinic acids have also been investigated for rare-earth separation, and Cyanex 272 [bis(2,4,4-trimethylpentyl)phosphinic acid] has been used commercially (Kolarik and Pankova 1966; Li and Frieser 1986; Banda et al. 2012). In laboratory investigations, Sabot and Rollat (1985) described the preparation of pure Yb_2O_3 (99.3%) from a mixture of ytterbium and lutetium oxides (87.5% Yb_2O_3 and 12.5% Lu_2O_3) using 1 mol/L Cyanex 272 in kerosene, Saleh et al. (2002) investigated the extraction of La(III) by Cyanex 272 in toluene from an acidic nitrate–acetato media, and El-Hefny et al. (2010) studied the extraction of samarium from chloride solutions with Cyanex 272. Studies on the extraction of La, Pr, Eu, Ho, and Yb into chloroform solutions containing dicyclohexyl phosphinic acid (DCHPA) showed that the extraction selectivity of DCHPA was inferior to that of other di-alkyl phosphinic acids (Cecconie and Frieser 1989).

3.6.6.4 Solvating Extractants

In an extraction by solvation, the extractant replaces some or all of the coordinated water molecules from the aquated metal ion to form a species that is soluble in the organic phase. The most important solvating extractant for rare-earth refining is TBP, and the extraction of a trivalent rare earth by TBP (Table 3.9) can be represented by the general reaction

$$[RE(NO_3)_3{\cdot}xH_2O]_{aq} + 3[TBP]_{org} \rightarrow [RE(NO_3)_3 3TBP]_{org} + xH_2O$$

TABLE 3.9
Separation Factors for Various Rare-Earth Pairs in TBP Extraction

REO Concentration in Aqueous Phase, g/L	Separation Factor							
	Ce–Y	**Nd–Y**	**Sm–Y**	**Gd–Y**	**Dy–Y**	**Ho–Y**	**Er–Y**	**Yb–Y**
60		4.08	5.71	4.44	3.96	3.03	2.13	
125	0.75	1.77	2.79	2.29	2.10	1.75	1.25	0.83
220	0.60	1.30	2.02	1.99	2.15	1.91	1.48	0.83
460		0.39	0.88	0.89	1.30	1.20	1.15	0.93
	Sm–Nd	**Gd–Sm**	**Dy–Gd**	**Ho–Dy**	**Er–Ho**	**Yb–Er**		
60	1.40	0.18	0.89	0.77	0.70	0.63		
125	1.58	0.82	0.92	0.83	0.72			
220	1.55	0.99	1.08	0.89	0.78			
460	2.26	1.01	1.45	0.92	0.96	0.81		

Source: McGill, I., Rare earth elements, in Elvers, B. et al. (eds.), *Ullmann's Encyclopedia of Industrial Chemistry*, vol. A22, VCH, Weinheim, 1993.

Under a given set of conditions, the lanthanide stabilities of the complexes and, hence, their extractabilities might be expected to increase through the series from La^{3+} to Lu^{3+}, as the cationic radius decreases because the electrostatic interaction between the cation and ligand should be proportional to the reciprocal of the cationic radius. Once the cationic radius is beyond a certain size, however, steric considerations overrule electrostatic effects. This is indicated by the existence of a maxima, as shown in Figure 3.37, in the extractions by neutral organophosphorus compounds. In the TBP system, the extraction of yttrium usually lies between that of erbium and thulium.

The separation of yttrium from lighter lanthanides, e.g., lanthanum, increases markedly with an increase in nitrate concentration; however, there is no such change on yttrium separation from the heavier rare earths, e.g., thulium.

Rare-earth nitrates up to a concentration of 0.5 mol/L (~170–190 g REO/L) can be loaded in pure TBP. The effect of temperature is small. REE salts such as perchlorates, chlorides, and thiocyanates have poor distribution coefficients and/or selectivities in TBP.

Peppard et al. (1957a,b) investigated the use of TBP for the extraction of trivalent rare earths from chloride and nitrate solutions. The extractability by TBP increased with increasing atomic number, but the distribution coefficients were much lower in chloride solutions than in nitrate solutions. Concentrated nitric systems appeared good for separating rare earths lighter than samarium.

It was observed by Preston and du Preez (1990) that TBP and other neutral organophosphorus compounds are useful in the bulk recovery of the rare-earth product from nitrate liquors, but they are less useful in separations among the trivalent lanthanides because the separation factors for adjacent rare-earth pairs are generally small, in the range of 1.2–2.2. This may be compared to the average separation factor of ~2.8 for HDEHP extraction from a nitrate medium.

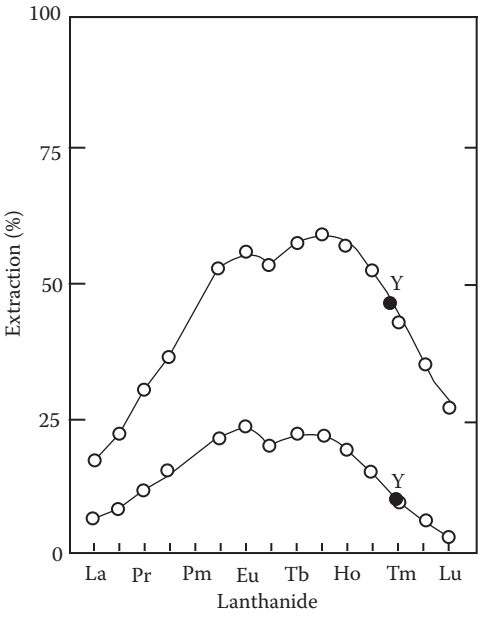


FIGURE 3.37 Extraction of trivalent lanthanides and yttrium from nitrate media by 2.0 M TBP in toluene at 20°C. Aqueous phases 0.01 M metal nitrates in 1 M HNO_3/2 M NH_4NO_3 (lower curve) and 1 M HNO_3/5 M NH_4NO_3 (upper curve). (Reprinted from *Solvent Extraction*, Sekine, T. (ed.), Preston, J.S. and Du Preez, A.C., Solvent extraction processes for the separation of rare earth metals, pp. 883–894, Copyright 1990, with permission from Elsevier; McGill, I., Rare earth elements. In Elvers, B., Hawkins, S., Russy, W., and Schulz, G. (eds.), *Ullmann's Encyclopedia of Industrial Chemistry*, vol., A22, pp. 607–649, VCH, Weinheim, 1993.)

3.6.6.5 Amines

Long-chain quaternary ammonium salts, $R_3CH_3N^+X^-$, in which R represents C_8–C_{12} groups and X represents nitrate or thiocyanate, are useful for the separation of rare earths (Preston and du Preez 1988). Amines extract by anion exchange. In an extraction by anion exchange, a simple inorganic anion from an ion pair-type extractant, such as a quaternary ammonium salt, is replaced by a complex metallic anion, in reactions such as

$$[R_4N{\cdot}NCS]_{org} + [RE^{3+}]_{aq} + 3[NCS^-]_{aq} \rightarrow [R_4N{\cdot}RE(NCS)_4]_{org}$$

$$[R_4N{\cdot}NO3]_{org} + [RE^{3+}]_{aq} + 3\left[NO_3^-\right] \rightarrow [R_4N{\cdot}RE(NO_3)_4]_{org}$$

The extraction of different rare earths in the thiocyanate and in the nitrate systems exhibits interesting results. This is shown in Figure 3.38. In the thiocyanate system, the extraction of a rare earth increases with its atomic number. In the nitrate system, on the other hand, the extraction decreases with an increase in atomic

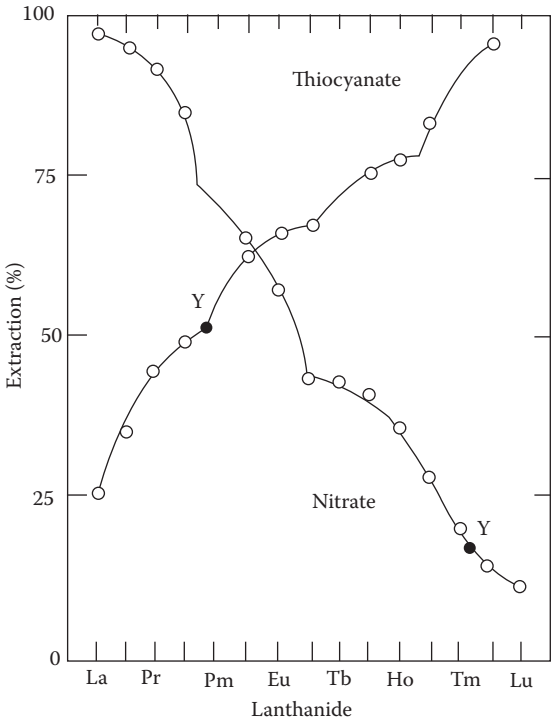


FIGURE 3.38 Extraction of trivalent lanthanides and yttrium (0.02 M as nitrates) from 4.0 M $NaNO_3$ by 0.5 M solutions of Aliquat 336 nitrate in xylene at 20°C and from 2.0 M KNCS by 0.25 M solutions of Aliquat 336–thiocyanate in toluene at 30°C. (Reprinted from *Solvent Extraction*, Sekine, T. (ed.), Preston, J.S. and Du Preez, A.C., Solvent extraction processes for the separation of rare earth metals, pp. 883–894, Copyright 1990, with permission from Elsevier.)

number. Preston and du Preez (1990) have attributed this behavior to the interplay of electrostatic and steric effects in the stability of the various complexes and, hence, their extractability. The extraction behavior of yttrium is particularly important. In the thiocyanate system, yttrium behaves as an LRE lying between neodymium and samarium. In the nitrate system, on the other hand, yttrium behaves like an HRE lying between thulium and ytterbium. This indicates the possibility of separation of the yttrium in thiocyanate media from the fraction containing dysprosium, holmium, and erbium to which it reports in extraction with organophosphorus acids (Preston and du Preez 1990). The separation factors for extraction with a typical anion-exchange extractant, Aliquat 336, are compared with the values for extraction with HDEHP and EHEHPA in Table 3.10.

Aliquat 336 (trioctyl methyl ammonium nitrate) extracts LREs more readily than the heavier ones in a nitrate media. This behavior is in contrast with that of most of the cation-exchange and solvating extractants, which extract the rare earths better as atomic number increases. Hence, quaternary ammonium salts provide a means

TABLE 3.10
Separation Factors for Aliquat 336 Compared with HDEHP and EHEHPA

Rare-Earth Metal		Separation Factor[a]		
A	B	Aliquat[b]	EHEHPA[c]	HDEHP
La	Ce	1.67	4.55	2.70
Ce	Pr	1.72	2.12	1.50
Pr	Nd	2.04	1.27	1.25
Nd	Sm	2.97	4.00	4.26
Sm	Eu	1.42	1.78	1.78
Eu	Gd	1.75	1.35	1.50
Gd	Tb	1.02	3.00	
Tb	Dy	1.08	1.94	
Dy	Ho	1.24	1.53	
Ho	Er	1.43	1.90	
Er	Tm	1.59	1.78	
Tm	Yb	1.47	2.12	
Yb	Lu	1.34	1.44	

Source: Preston, J.S., *Hydrometallurgy*, 42, 1996.

[a] Separation factors are expressed as $\alpha_B^A (= k_A / k_b)$ for Aliquat and as $\alpha_A^B (= k_b / k_A)$ for organophosphorus acids.

[b] For extraction of 0.02 M individual rare earths from 4.0 M sodium nitrate by 0.50 M Aliquat 336 nitrate in xylene.

[c] For extraction of 0.02 M individual rare earths from 4.0 M sodium nitrate by 0.20 M organophosphorus acid in toluene.

of removing LREs from process solutions, leaving the heavies to be removed by the other extractants.

Yttrium's anomalous behavior, as an HRE in the nitrate media and as a light in the thiocyanate media, has been utilized for treating xenotime, which contains 60% Y_2O_3 (Xie et al. 2014). The nitrate leach liquor from HNO_3 leaching of xenotime concentrate was freed of lighter rare earths by extraction with Aliquat 336 in an aromatic diluent. Yttrium and the HREs remained in the aqueous phase. Thiocyanate was added, and yttrium was then extracted by Aliquat 336, yielding 99.99% Y_2O_3, while other HREs remained in the raffinate (Gaudernack et al. 1973).

Neodymium is another rare earth, which has been extracted using quaternary amines. Lu et al. (1989) isolated >99% Nd_2O_3 from didymium nitrate solution (83% Nd, 15% Pr, and 2% other rare earths) with 95% Nd recovery using Aliquat 336 in a 45-stage extraction. Preston (1996) described a solvent extraction process for recovering neodymium oxide (95% Nd_2O_3) from an LRE nitrate solution using a 0.50 M solution of Aliquat 336 nitrate in Shellsol AB.

A large number of metal ions in the form of anionic complexes are extracted by long-chain amines. For REEs, however, primary and secondary amines are relatively

weak extractants and need high concentrations of salts and acids for a useful separation effect. These amines preferentially extract rare-earth sulfates (Bauer 1966; Rice and Stone 1962), and their poor selectivity is enhanced by the presence of EDTA and DTPA. In any case, these extractions are strongly dependent on pH and concentration and are difficult to control (McGill 1993). Tertiary amines are also poor extractants.

Amaral and Morais (2010) described the possibility of extracting, simultaneously, thorium and uranium from a liquor obtained by sulfuric acid treatment of monazite. A solvent containing a mixture of Primene JM-T and Alamine 336 was used, and the stripping was carried out with a hydrochloric acid solution. Under the best conditions, a continuous experiment was carried out in a mixer–settler circuit using four stages in the extraction step, five stages of stripping, and one stage of solvent regeneration. The loaded strip solution contained 29.3 g/L of ThO_2 and 1.27 g/L of U_3O_8, and the raffinate contained <0.001 g/L of thorium and uranium, indicating a thorium extraction of over 99.9% and a uranium extraction of 99.4%. The rare-earth content in the raffinate was 38 g/L of RE_2O_3.

Europium, gadolinium, and samarium are part of the MRE group. The separation of this Sm–Eu–Gd group into individual elements is usually done by the reduction of Eu(III) to Eu(II) and its precipitation as $EuSO_4$ (Preston et al. 1996b; Morais and Ciminelli 1998, 2001, 2002), followed by Sm–Gd separation by solvent extraction (Santos et al. 1999). Morais and Ciminelli (2007) experimented with an alternative route for the separation of the Sm–Eu–Gd mixture, removing samarium first and subsequently partitioning high-purity Gd and a Eu-enriched mixture by an amine solvent extraction that apparently gave a higher separation factor for the Eu–Gd pair.

3.6.6.6 Synergistic Effects

The distribution coefficient can be considerably more than the sum of the distribution coefficients of individual extraction agents when a mixture of extractants is used. Such systems, otherwise commonly used in hydrometallurgy practice, have not been developed to levels of industrial application for rare-earth extractions (McGill 1993).

On a laboratory experimental scale, numerous types of synergistic solvent extraction systems for extracting and separating rare earths have been evaluated and reported (Xie et al. 2014), including mixtures of acidic extractants (e.g., carboxylic or organophosphorus acids), mixtures of neutral extractants (e.g., TBP and tri-*n*-octylphosphine oxide [TOPO]), and combinations of these (Santhi et al. 1991; Tian et al. 2012, 2013; Tong et al. 2013; Wang et al. 2006b).

Preston and du Preez (1994) investigated the synergism upon addition of a series of trialkyl phosphates $(RO)_3PO$, di-alkyl alkylphosphonates $(RO)_2RPO$, alkyl di-alkylphosphinates $(RO)R_2PO$, and trialkylphosphine oxides R_3PO on the extraction of the trivalent lanthanides and yttrium from chloride media by 3,5-diisopropylsalicylic acid (DIPSA). Synergism was observed with all mixtures, to different extents. The effects were greater for lutetium(III) than for lanthanum(III). Mixtures of DIPSA and tri-isobutylphosphine oxide (TIBPO) resulted in separation factors between the light and the middle lanthanides ($\beta_{Sm/Nd} = 3.0$) better than Versatic 10 acid alone ($\beta_{Sm/Nd} = 2.6$). Between the HREs (thulium to lutetium), the separation factors were comparable to those with the versatic acid.

Zhang et al. (2008) reported studies of the solvent extraction of cerium(IV) and fluoride from sulfate solutions using a mixture of Cyanex 923 and D2EHPA in *n*-heptane. Ce(III) was not extracted by the mixture. The mixture exhibited strong separation ability (high separation factors) between Ce(IV), F, and RE(III), $\left[\mathrm{CE(IV)/Ce(III)} = 1321, \mathrm{CeF_2^{2+}/Ce(III)} = 36\right]$. A scheme was described by Zhang et al. for a new efficient method of separation and purification of Ce(IV), F from bastnasite. At first, Ce(IV) and F are separated and recovered from bastnasite by a Cyanex 923 + D2EHPA mixture system, and then, the other RE(III) in the aqueous phase can be effectively collected by HEHEHP.

Synergistic effect was reported by Ying et al. (2005) in the separation from a chloride solution of Yb–Tm and Lu–Yb but not for Tm–Er, Er–Ho, and Ho–Dy when a Cyanex 272 and P507 (HEHEHP) mixture was used. Synergism was also reported in the extraction of trivalent La, Nd, Sm, and Gd from sulfate media by a mixture of D2EHPA and HEHEHP at pH 2.0 and in the separation of Sm and Nd using a mixture of D2EHPA (40% v/v) and HEHEHP (60% v/v) (Li et al. 2007). Other systems where positive results of varying extents of synergism were observed include extraction of trivalent Sc, Y, La, Gd, and Yb from chloride media using a mixture of Cyanex 272 and sec-nonylphenoxy acetic acid (CA-100) in *n*-heptane (Sun et al. 2006) and extraction of REEs from chloride media by mixtures of CA-100 with Cyanex 301 or Cyanex 302 (Tong et al. 2009); separation of adjacent trivalent rare earths was better in a mixture of CA-12 and Cyanex 301 in *n*-heptane (Jia et al. 2009).

3.6.6.7 Industrial Processes

Rare-earth producers all over the world follow almost identical routes for solvent extraction separation of rare earths. These routes are based on the following overall scheme: (1) separation of rare earth generally in a trivalent state, (2) fractionation of the rare earths into three or four groups, (3) preferential separation of yttrium, (4) selective extraction of cerium and europium using their unique valence states Ce^{4+} and Eu^{2+}, and (5) separation of the desired individual rare earth of required purity. Mixer–settler assemblies are the standard contacting equipment. Typically, a modern rare earth-processing plant producing multiple single rare-earth products may contain hundreds of stages of mixers and settlers. Solvent extraction circuits usually resort to a countercurrent flow scheme. The actual equipment arrangement depends of the nature of the feed and product requirement. Various configurations, viz., simple countercurrent solvent extraction circuit, countercurrent solvent extraction circuit with optional scrub exit, and countercurrent solvent extraction circuit with reflux, have been mentioned by Xie et al. (2014).

For a solvent extraction system to be attractive for industrial application, there are several relevant factors (McGill 1993). The choice of the extractant and aqueous phase may be influenced by cost considerations of all the chemicals involved. In the extraction of rare-earth salts by neutral extraction media or when the rare earths are extracted as an anionic complex, the reactive chemical requirement is less. When the rare earths are extracted using cationic complexes, the reactive chemical requirement is more because a base is required for extraction from the aqueous phase and an acid is required for selective washing and re-extraction from the organic phase.

In other words, cationic extraction is considerably more expensive than anionic or neutral extraction. Cationic extraction is, however, more selective.

The first step in industrial solvent extraction is usually the separation of the REEs from other elements. A solvent whose distribution coefficient for the REEs as a group is markedly different from that of the other element in the aqueous solution (leach liquor) is chosen. HDEHP is a suitable extractant. This extractant is also suitable for concentrating the REEs because of its high extraction ability for them, which enables it to extract them from dilute and often acidic solutions. A classic example for industrial solvent extraction in rare-earth processing is the Molycorp process for the production of europium.

3.6.6.8 Molycorp

The schematic flow sheet for the Molycorp approach for the processing of Mountain Pass bastnasite (Harrah 1967) is shown in Figure 3.39. At the end of physical beneficiation and chemical treatment procedures, a chloride solution (100 g REO/L and 200 mg Eu_2O_3/L) containing all the rare earths (except Ce) originally contained in the ore is obtained. This solution is clarified, pH adjusted to 1.0 with soda ash, steam heated to 60°C, clarified again, and put through to the europium recovery circuit.

The chloride solution described in the previous paragraph contains 0.2 g Eu_2O_3/L. The solvent is 10% HDEHP in kerosene, and the extraction is performed in five mixer–settler stages. More than 98% of the europium in the solution is extracted. The loaded organic is stripped with 4 M HCl. The strip solution, which contains 10–20 g europium/L, also contains iron as an impurity, and this is precipitated out with soda ash at pH 3.5. Following iron removal, the Eu-bearing solution is subjected to a second solvent extraction with HDEHP in five mixer–settler stages. This second extraction further purifies europium, and the LRE fraction is left in the raffinate, which is reverted to the first solvent extraction (SX) circuit. Europium loaded in the organic is stripped with 5 M HCl. The aqueous strip solution is passed through a column of zinc amalgam to reduce Eu(III) to Eu(II). Sulfuric acid is added to the divalent europium solution to precipitate europium sulfate. Reduction and selective precipitation purify europium from the HREs. More than 99.99% pure Eu_2O_3 is obtained by calcination.

In the second SX circuit, along with europium, other HREs are loaded in the organic. After europium removal, the strip solution still contains samarium, the HREs, and yttrium. Gadolinium is extracted from the europium-barren solution by HDEHP in a 10-stage extraction circuit followed by 5 stages of stripping. The raffinate is neutralized with soda ash to precipitate samarium and the HREs. Raffinate from the europium (first solvent extraction) circuit contains La, Pr, and Nd, which are precipitated with ammonia and sodium hydrosulfide. Molycorp rare earth-processing facilities at Louviers, Colorado, produced Gd, Tb, Dy, Ho, Er, Tm, Tb, Lu, and Y.

The Molycorp process for the preparation of pure yttrium oxide is shown in Figure 3.40. Starting from a concentrate containing 52% Y_2O_3 in the REO mixture, pure yttrium is produced in two consecutive cycles. The rare earths are separated into La–Er and Y–Lu fractions by Aliqua–NO_3^- with recycling using $Mg(NO_3)_2$ for stripping. Yttrium is finally purified by extraction with versatic acid, including a double recycling.

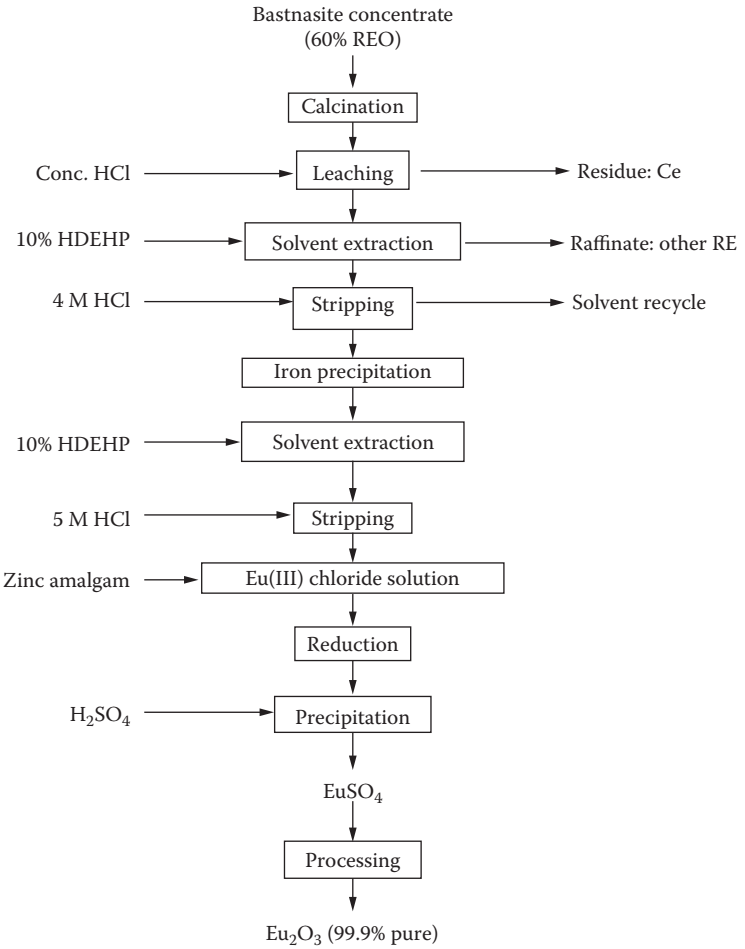


FIGURE 3.39 Molycorp process for europium oxide.

Xie et al. (2014) have emphasized the rationale to split and process the leach liquor in two streams, one carrying all the lighter rare earths (La–Nd) and the other loaded with Sm and the heavier rare earths. A split at Nd–Sm takes advantage of their separation factor being typically double that of any other consecutive rare-earth pair. Besides, the proportion of Sm and heavier rare earths being much less in bastnasite, they can be processed using smaller solution volumes and, hence, smaller equipment.

3.6.6.9 Denison Mines

The recovery of rare earths from sulfate solutions resulting from uranium processing at Denison Mines, Elliot Lake, Ontario, was done using solvent extraction with HDEHP. The flow sheet is shown in Figure 3.41. An yttrium-rich concentrate (~60% REO) is produced from sulfuric acid solutions containing 150 mg Y_2O_3/L.

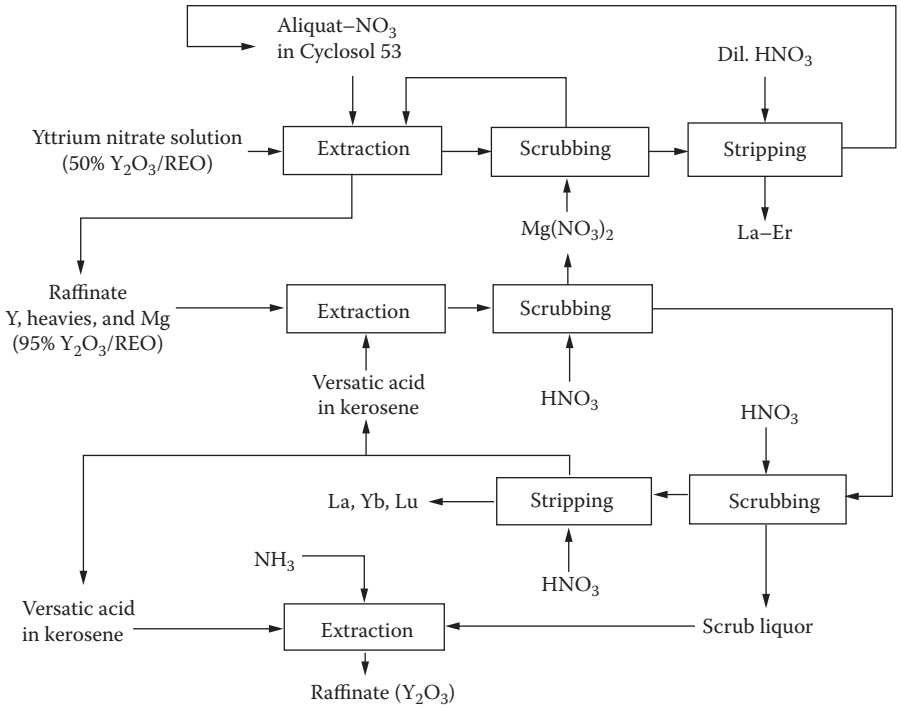


FIGURE 3.40 Molycorp process for pure yttrium oxide. (From McGill, I., Rare earth elements. In Elvers, B., Hawkins, S., Russy, W., and Schulz, G. (eds.), *Ullmann's Encyclopedia of Industrial Chemistry*, vol., A22, pp. 607–649, VCH, Weinheim, 1993.)

The uranium-barren solution at pH 2 from the ion-exchange circuit is treated with lime and air in pachuka tanks. The pH is controlled to precipitate iron, some amount of thorium, and other impurities. These are removed from solution using thickeners, filters, and clarifiers. The clarified solution is acidified with sulfuric acid and fed to the solvent extraction circuit. The solvent used is 10–12 vol.% HDEHP in kerosene with no modifier, and the extraction takes place in a countercurrent centrifugal extractor. Under extraction conditions used at present, all the rare earths and yttrium are loaded in the organic phase. The loaded solvent is stripped with nitric acid in a centrifugal contactor. The thorium and uranium present in the aqueous solution are loaded into the solvent together with the rare earths. The rare earths are separated from thorium and uranium during stripping. The nitric acid solution containing yttrium–rare earth is treated for precipitation. Slaked lime is added to the solution to consume all the free acid. Ammonia gas is then added to the solution to precipitate yttrium and other rare earths. The dried precipitate contains 30–35% Y_2O_3 and 60–70% RE_2O_3 including yttrium.

3.6.6.10 Indian Rare Earths

The mixed rare-earth-chloride solution obtained in the course of chemical treatment of monazite contains less than 1% of any of the HREs. At the Alwaye plant of IRE,

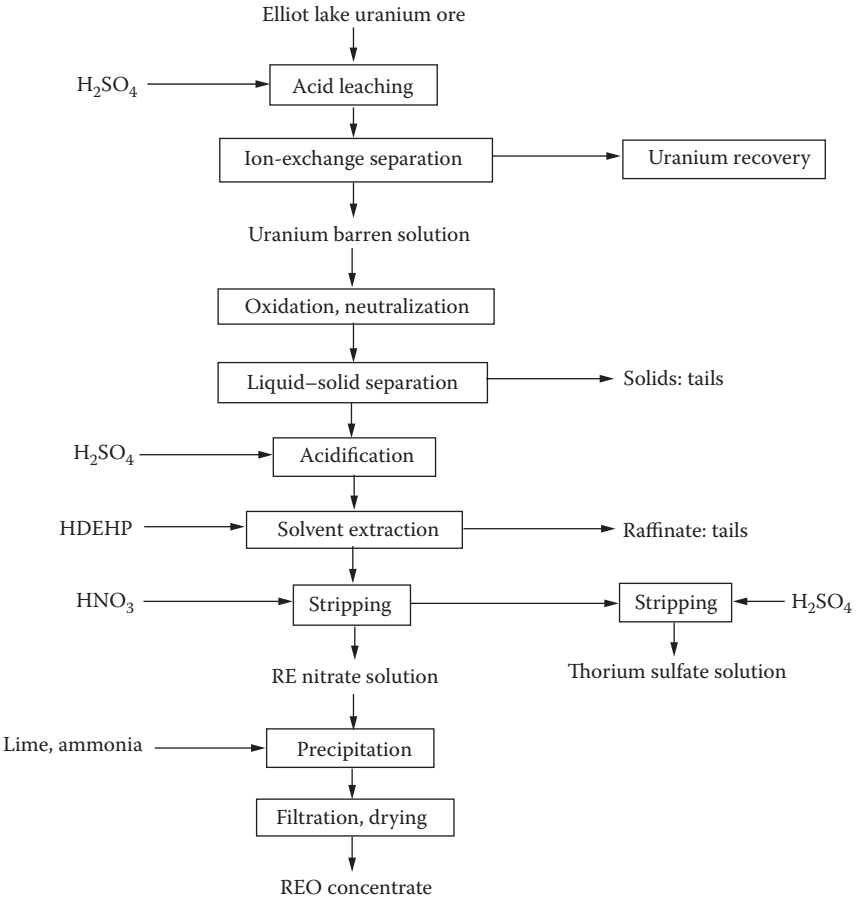


FIGURE 3.41 Denison Mines process for yttrium-rich rare-earth concentrates. (From Lucas, B.H. and Ritcey, G.M., *CIM Bull*., 68(753): 124–130, 1975; McGill, I., Rare earth elements. In Elvers, B., Hawkins, S., Russy, W., and Schulz, G. (eds.), *Ullmann's Encyclopedia of Industrial Chemistry*, vol., A22, pp. 607–649, VCH, Weinheim, 1993.)

solvent extraction with HDEHP was used for a quick initial concentration of the HREs and for the production of concentrates of various individual rare earths such as Sm, Eu, Gd, and Y with purities ranging from 60% to 95%. The schematic flow sheets are shown in Figures 3.42 and 3.43.

The flow sheets outlining the Indian practice for the fractionation of rare earths and for the separation of Nd and Pr using PC88A are shown in Figures 3.44 to 3.46. The flow sheets for the separation and purification of Sm, Eu, Dy, and Y are given in Figures 3.47 to 3.50 (Thakur et al. 2000).

In the Indian practice (Thakur et al. 1990), from the RE chloride solution containing 200–240 g REO/L and about 0.05 M HCl, the rare earths are extracted with 1 M PC88A in kerosene. Extraction parameters are so chosen that the solvent extracts Sm, other HREs, and also yttrium, leaving the LREs in the raffinate. The extract is

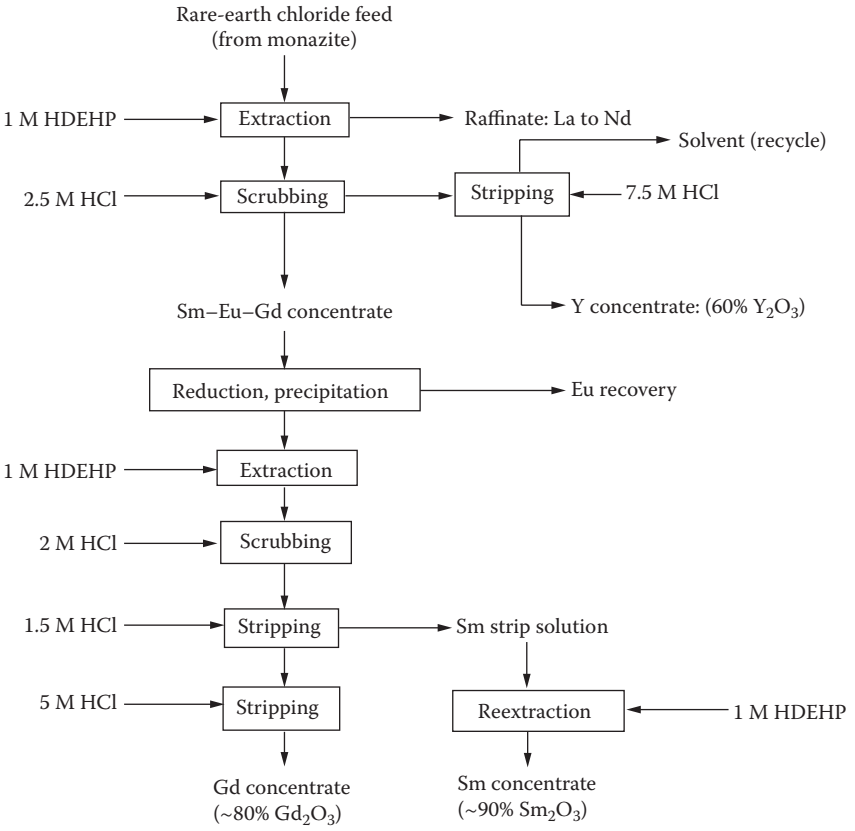


FIGURE 3.42 Flow sheet of rare-earth separations by solvent extraction at Indian Rare Earths I.

then selectively scrubbed with 3 M HCl at an organic to aqueous (O/A) phase ratio >20 to remove the LRE. From the scrubbed loaded solvent, Sm, Eu, and Gd (MREs) are selectively stripped with 1–1.5 M HCl. The extract, presently containing only the HREs, is then stripped with 3.5 M HCl.

The first strip solution containing the MRE fraction (40–50 g REO/L) is then processed to precipitate Eu as $EuSO_4$ after reduction with zinc dust. The Eu-free solution, now containing all Sm and Gd is put through one more cycle of solvent extraction with PC88A or HDEHP as extractant to produce >95% pure Sm_2O_3 and 80–90% pure Gd_2O_3.

The HRE fraction assaying around 60% Y_2O_3 and 15% Dy_2O_3 is treated further to obtain 93% Y_2O_3 in the first cycle of a two-cycle solvent extraction process. In the first cycle, the aqueous solution assaying ~25 g REO/L (60% Y_2O_3) and 0.4 M HCl is brought into contact with the solvent in eight stages. The solvent is 1.0 M PC88A in kerosene. The loaded solvent/extract is scrubbed with dilute HCl in six stages. Yttrium and HREs preferentially extracted by the solvent are finally stripped with strong HCl in four stages at a high phase ratio. The final strip solution would assay

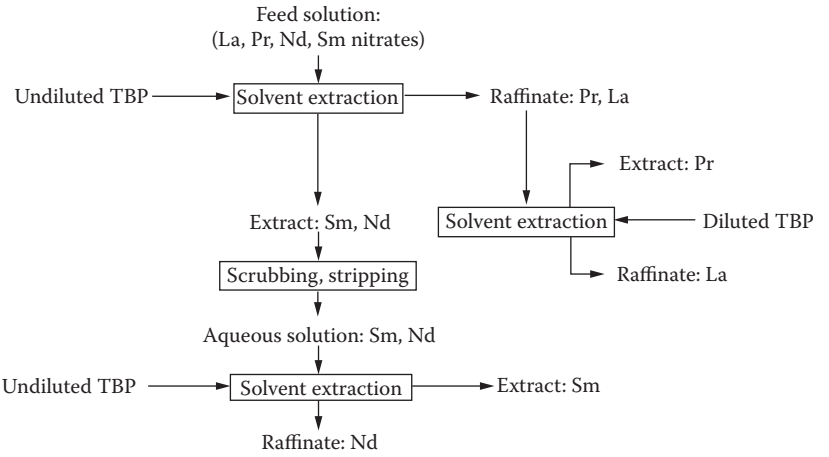


FIGURE 3.43 Flow sheet of rare-earth separations by solvent extraction at Indian Rare Earths II.

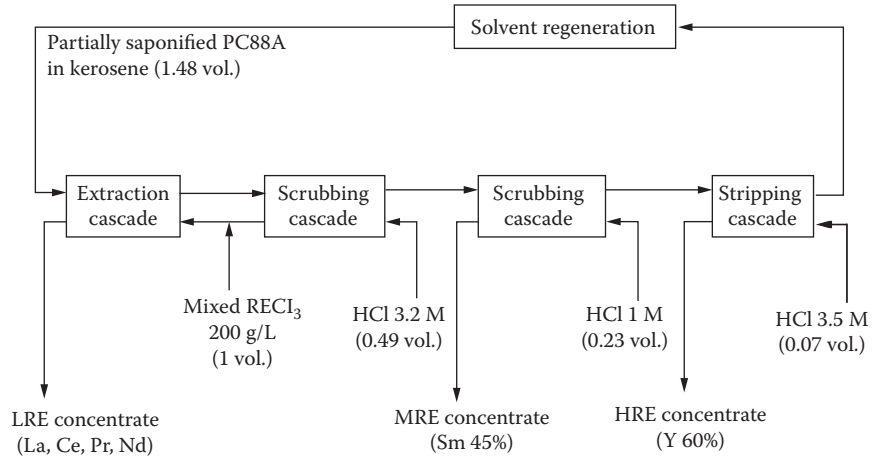


FIGURE 3.44 Flow sheet for the fractionation of rare earths using partially saponified PC88A. (From Thakur, N. V. *Mineral Process. Extractive Metal. Rev.*, 21(1–5): 277–306, 2000.)

about 40 g REO/L (93% Y_2O_3) and about 1.0 M HCl. This solution is neutralized with NH_4OH to a pH of 4.0, and NH_4CNS is added to make it 1 M NH_4CNS. The solution is put through the second cycle of solvent extraction with 50% TBP in kerosene. The treatment is done in 16–18 stages of extraction, 18–20 stages of scrubbing with water, and 8 stages of final stripping of the loaded extract with water. All rare earths other than Y are preferentially extracted by TBP, leaving Y in the aqueous raffinate as a high-purity product at above 90% recovery. The final strip solution containing HRE would assay about 50% Er_2O_3 and forms the source for further separation of Er_2O_3.

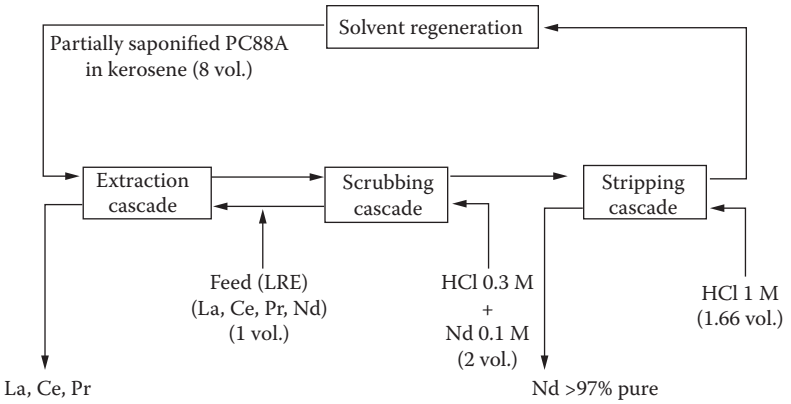


FIGURE 3.45 Flow sheet for the recovery of neodymium from LRE concentrate using partially saponified PC88A.

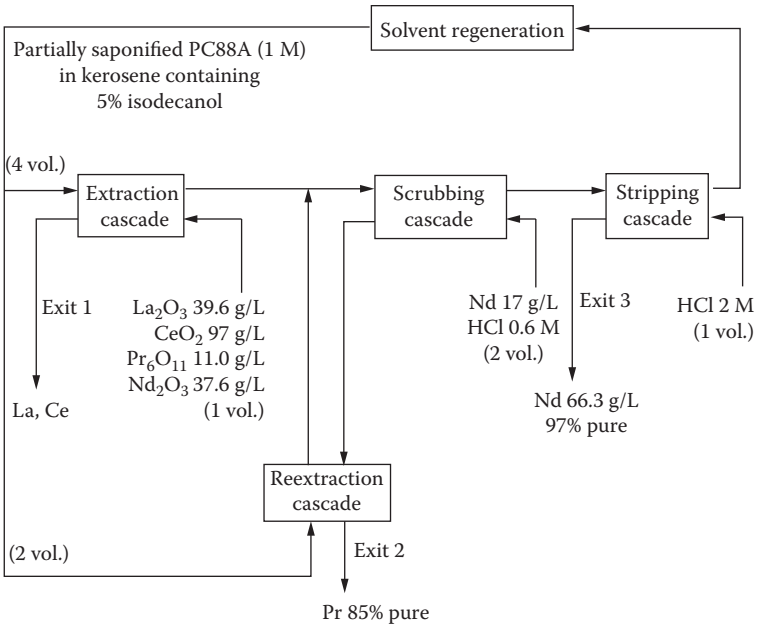


FIGURE 3.46 Flow sheet for three-exit solvent extraction process for simultaneous purification of neodymium and praseodymium by PC88A.

In the Indian practice, the 60% Y_2O_3 concentrate upgraded to 93% Y_2O_3 by PC88A extraction is also purified further to obtain 99.99% Y_2O_3 by extraction using the Aliquat 336–thiocyanate system in a chloride medium.

The aqueous raffinate obtained from the first cycle of SX for Y separation using PC88A assaying about 5 REO/L has the composition Dy_2O_3 (55–60%), Tb_4O_7 (15%), Gd_2O_3 (8–12%), Ho_2O_3 (1–2%), $Y_2O_3 < 10\%$ and is treated for the recovery of Dy and

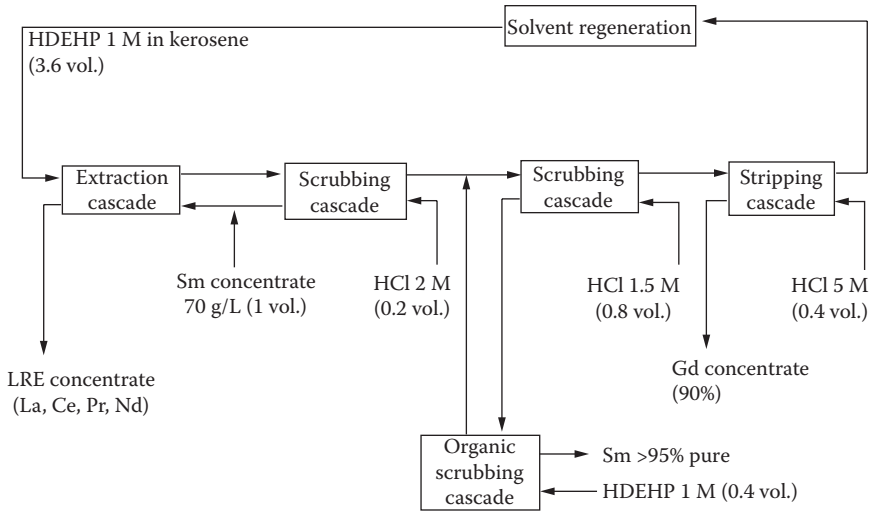


FIGURE 3.47 Flow sheet for the recovery of samarium from the MRE concentrate using HDEHP.

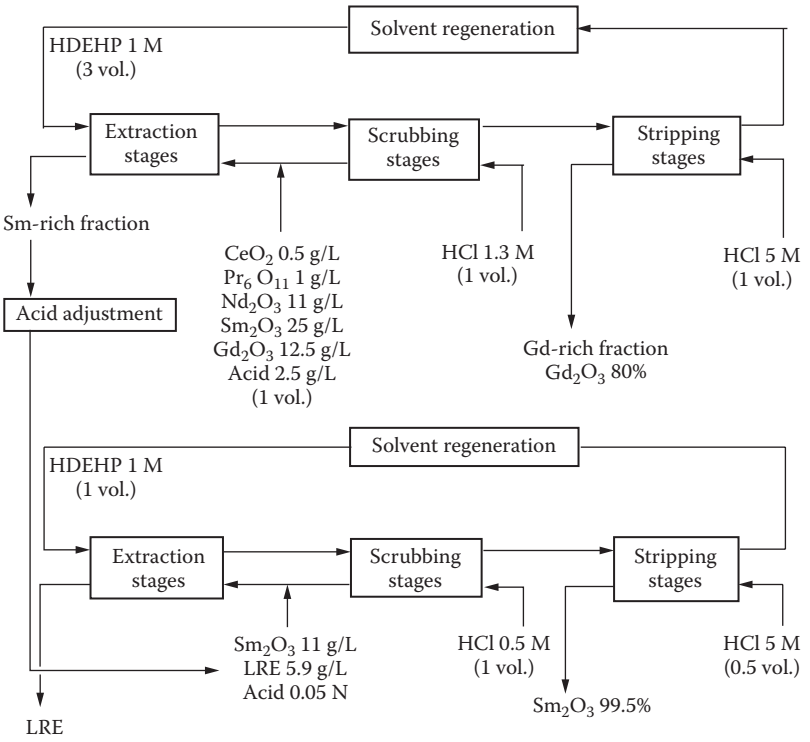


FIGURE 3.48 Flow sheet for the recovery of high-purity samarium.

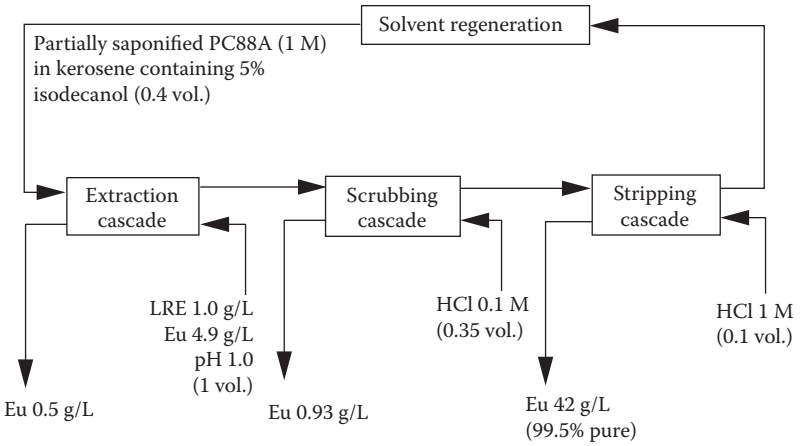


FIGURE 3.49 Flow sheet for the purification of europium by PC88A from the feed containing 83% Eu obtained after initial zinc reduction process. (From Thakur, N. V. *Mineral Process. Extractive Metal. Rev.*, 21(1–5): 277–306, 2000.)

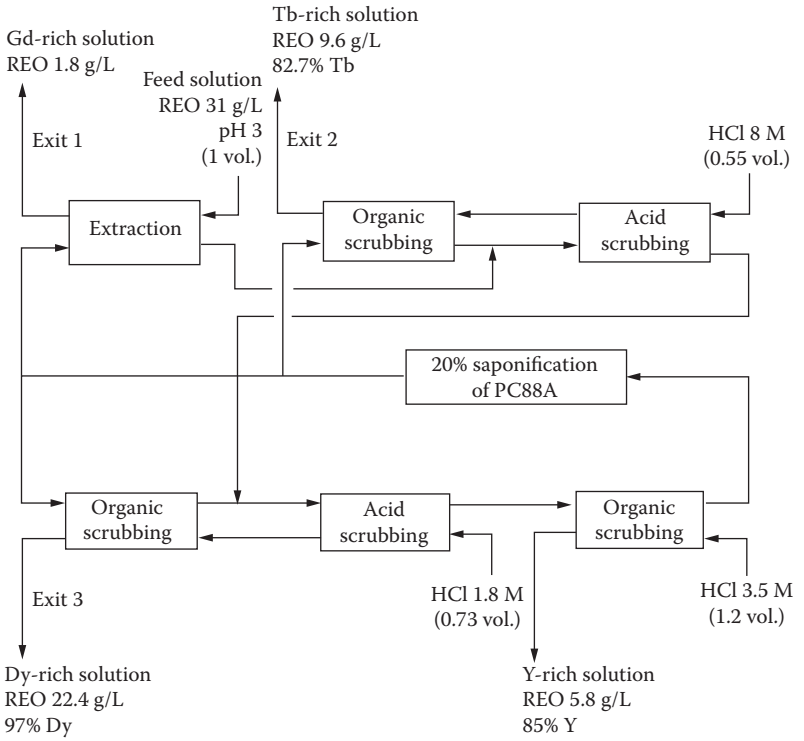


FIGURE 3.50 Flow sheet of the four-exit solvent extraction process for the simultaneous purification of dysprosium, terbium, gadolinium, and yttrium using PC88A.

Tb. This solution would have about 1 M HCl and is processed with 1 M HDEHP in kerosene. Keeping the phase ratio at 1 in extraction and 4 in scrubbing, the HREs are extracted preferentially and thus separated from LRE. Dy is then preferentially stripped with HCl from the loaded extract. The product Dy_2O_3 is about 97% pure.

In the processing of monazite ore at IRE, caustic digestion dissolves the phosphate and leaves a hydrated mixed metal-oxide cake containing thorium, uranium, and the rare earths. By leaching the cake with hydrochloric acid at pH 3.0, the bulk of the rare earths are preferentially removed and separated as mixed rare-earth chloride. The slurry after removal of the major portion of rare earths contains all the thorium and uranium present in the monazite feed. In addition, this slurry also contains recoverable quantities of rare earths. This rare-earth content is recovered by solvent extraction using PC88A as the extractant. The flow sheet is shown in Figure 3.51 (Narayanan et al. 1988). The RE–Th slurry obtained after decantation of the $RECl_3$ solution is dissolved in HCl, and after clarification, its acidity is adjusted to 1.5 M. The aqueous feed solution is contacted in the extraction circuit with the solvent PC88A (Ionquest 801) in two stages. During this step, uranium and all the thorium in the aqueous feed solution are completely picked up by the extractant,

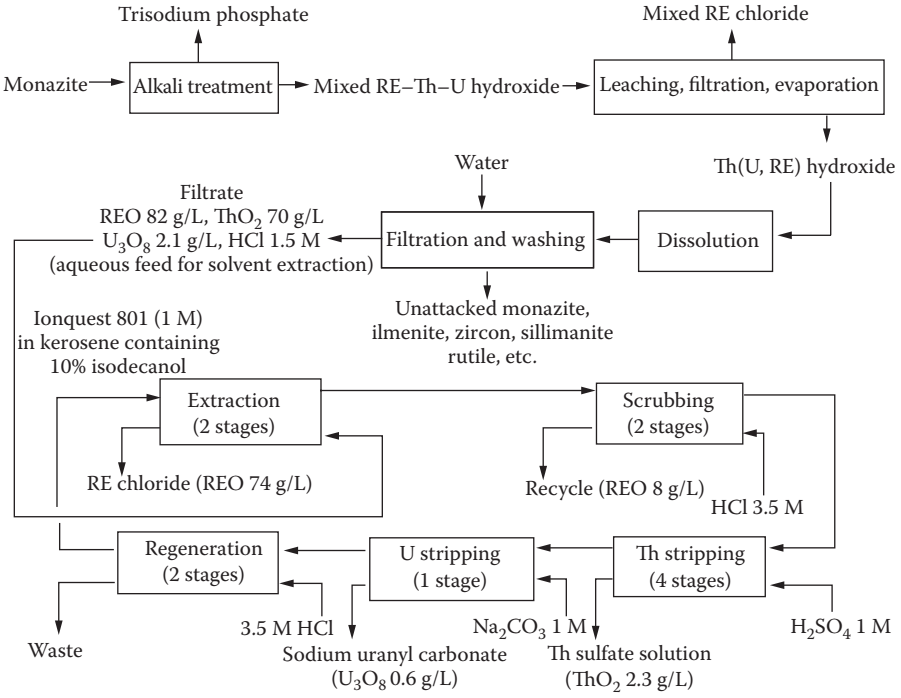


FIGURE 3.51 Process for the separation of rare earths, thorium, and uranium by solvent extraction using 2-ethyl-hexyl phosphonic acid mono-2-ethyl-hexyl ester (Ionquest 801). (From Narayanan, N.S. et al., Processing of monazite at the rare earths division, Udyogamandal. In Gupta, C.K. and Krishnan, T.S. (eds.), *Rare Earths—Applications and Technology*, pp. 45–56, Trans Tech Publications, Switzerland, 1988.)

leaving only the trivalent rare earths in the aqueous phase. Thorium and uranium are recovered separately from the loaded solvent, and the rare earths are recovered from the raffinate.

3.6.6.11 Mintek

Solvent extraction has been used for recovering rare earths from rare earth-carrying calcium sulfate sludge obtained in the manufacture of phosphoric acid from Phalaborwa apatite in South Africa (Preston et al. 1996a,b,c). The processing involved extensive application of solvent extraction using TBP, HDEHP, and Aliquat 336 to produce first a mixed rare-earth oxide concentrate, as shown in Figure 3.52, followed by separation of this mixed oxide into heavy, middle, and light fractions as well as preparation of pure cerium, europium, and neodymium oxides (Preston 1996).

As mentioned earlier, the rare-earth values were leached from the sludge by dilute nitric acid and calcium nitrate. From the leach liquor, the rare earths were recovered by solvent extraction using 33 vol.% dibutyl-butyl phosphonate (DBBP) in Shellsol 2325. The LO was stripped with water to yield a solution of mixed rare-earth nitrates from which mixed rare-earth oxide (98% pure) was obtained by the addition of oxalic acid and calcination of the oxalate precipitate. In later trials, the organic phase was

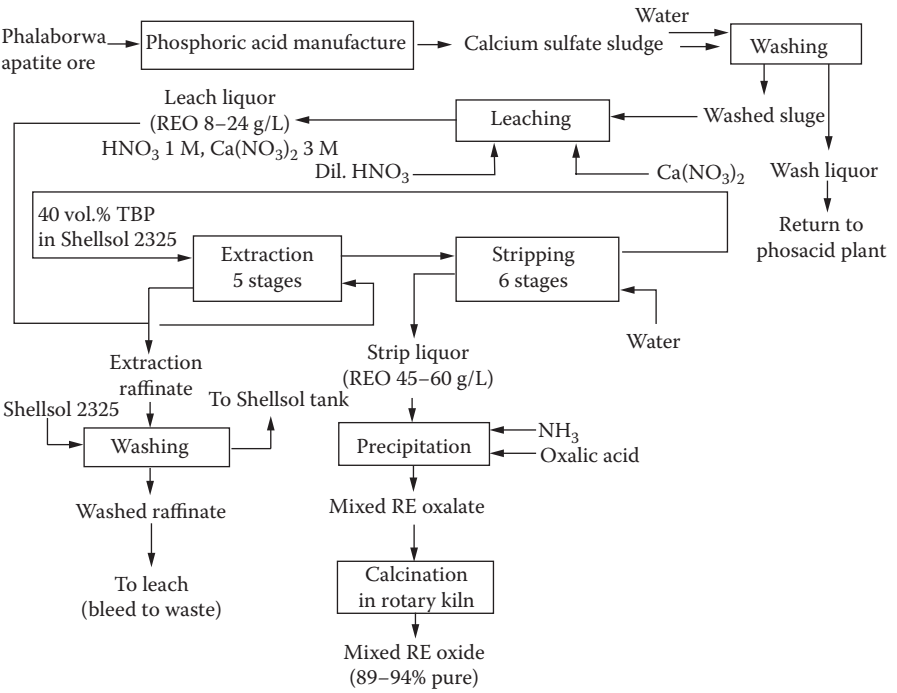


FIGURE 3.52 Schematic diagram of the pilot plant leaching and solvent extraction circuits for rare-earth recovery from Phalaborwa apatite source. (From Preston, J.S., *Hydrometallurgy*, 42: 151–167, 1996.)

changed to 40 vol.% TBP for an aqueous rare earth-bearing leach liquor containing 1 M nitric acid and 3 M calcium nitrate. The mixed rare-earth oxide obtained was 89–94% in purity and contained MREs, particularly neodymium, samarium, europium, and gadolinium, in considerably higher proportions than the commercially available mixed oxides from the usual commercial rare-earth resources.

Solvent extraction was used for the recovery of high-purity cerium dioxide and an HRE oxide concentrate from the mixed rare-earth oxide. The mixed oxide was dissolved in concentrated nitric acid to yield solutions in which up to 95% of the cerium was present as Ce(IV). From this solution, after dilution with water, Ce(IV) was extracted with high selectivity into a 15 vol.% solution of TBP in Shellsol K in four extraction stages. After four stages of scrubbing with 3 M nitric acid, stripping of the organic phase was accomplished by reduction of Ce(IV) to Ce(III) with dilute H_2O_2 in two stages. Oxalic acid was added to the strip solution, and the oxalate precipitated was calcined to 99.8% pure cerium dioxide, which was obtained in about 70% yield.

The raffinate from the cerium recovery circuit was extracted with 5 vol.% solution of HDEHP in Shellsol AB in six stages followed by stripping in four stages. From the strip liquor, oxalate precipitation and calcination yielded a mixed HRE oxide (99.4–99.8% REO). This contained 41–63% Y_2O_3, 17–31% Dy_2O_3, 4% HoO_3, and 4–5% Er_2O_3 together with smaller amounts of other rare earths.

The raffinate from HRE extraction was processed for the separation of MRE and LRE fractions. The processing consisted of extraction into a 15 wt.% solution of HDEHP in Shellsol AB in eight countercurrent stages, followed by scrubbing with 1 M nitric acid in two to four stages and stripping with 1.5 M hydrochloric acid in six to eight stages. Addition of oxalic acid to the strip liquors and calcination of the precipitated oxalate yielded a mixed MRE oxide product containing 45% Sm_2O_3, 29% Gd_2O_3, 13% Eu_2O_3, and 6% Nd_2O_3.

From the remaining LRE nitrate liquor containing Nd, Pr, Ce, and La, a 0.50 M solution of Aliquat 336 nitrate (tricaprylmethyl ammonium nitrate) in Shellsol AB was used to selectively extract La, Ce, and Pr in two extraction circuits. A purified neodymium solution was remaining as a raffinate. Extraction was carried out in eight extraction and six scrubbing stages. Loaded solvent was stripped with water in six stages. From the solutions thus obtained, rare-earth oxides were obtained by oxalate precipitation and calcination. From the raffinate, 75% of the neodymium present in the original feed was obtained as 95–96% pure (magnet grade) Nd_2O_3. The impurities were 2% Pr_6O_{11}, 1.5% Sm_2O_3, 0.7% CeO_3, and 0.2% La_2O_3. From the first circuit strip liquor, lanthanum concentrate (51% La_2O_3, 36% CeO_2, 7% Pr_6O_{11}, and 6% Nd_2O_3) and, from second circuit strip liquor, praseodymium concentrate (32% Pr_6O_{11}, 41% Nd_2O_3, 22% CeO_2, and 4% La_2O_3) were obtained.

3.6.6.12 Megon

The Megon Company in Norway, founded in 1969, processed xenotime to recover yttrium concentrate and high-purity yttrium oxide (Gaudernack et al. 1973). The flow sheet is shown in Figure 3.53. There are three extraction cycles (McGill 1993; Ritcey and Ashbrook 1979). From the rare-earth sulfate solution obtained after chemical treatment of xenotime concentrate, a 30% solution of HDEHP in Shellsol

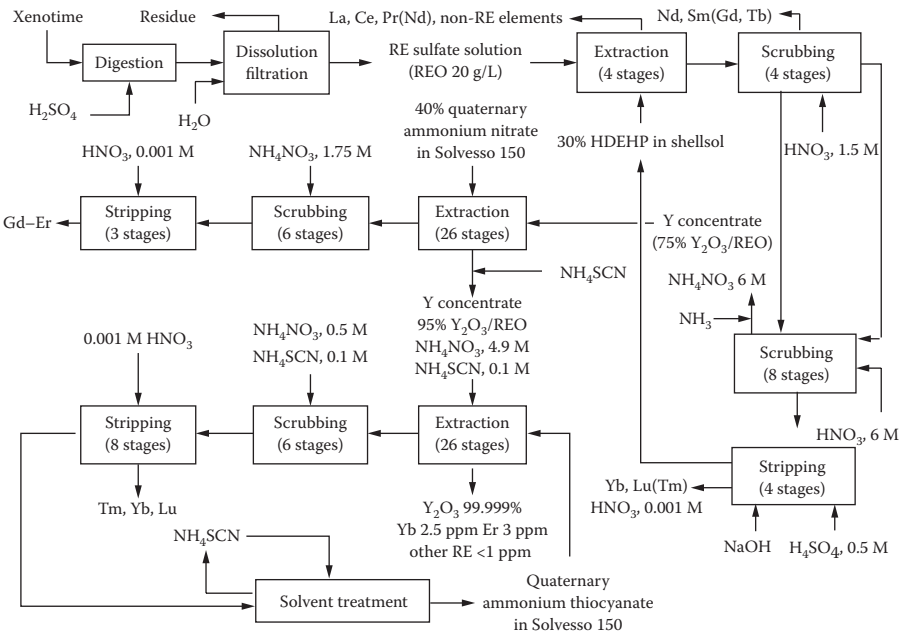


FIGURE 3.53 AS Megon process for high-purity yttrium oxide. (McGill, I.: Rare earth metals. In Habashi, F. (ed.), *Handbook of Extractive Metallurgy.* vol. III. 1997. pp. 1695–1741. Copyright Wiley-VCH Verlag GmbH & Co. KGaA. Reproduced with permission.)

T diluent is used to achieve an intermediate type of separation. In four mixer–settler stages, some Nd and all the heavier rare earths including yttrium are extracted, while La, Ce, and Pr remain in the raffinate. Stripping the extract with 1.5 N HNO_3 in four stages removes the Nd–Tb fraction, which includes large amounts of samarium and gadolinium. Stripping the extract with 6 N HNO_3 in eight stages of mixer–settlers removes yttrium with most of the heavy lanthanides. Ytterbium and lutetium are only partially stripped by HNO_3. They are, however, removed in a single stage with 10% NaOH. Instead of 10% NaOH, either 20% HF or 50% H_2SO_4 could also be used for an equally effective stripping. The caustic treatment also removes any Fe or Th present. The solvent phase is acidified with sulfuric acid and reverted to extraction.

The concentrated yttrium nitrate solution obtained by stripping with 6 N HNO_3 is processed to high purity in many stages of extraction using the quaternary ammonium compound, Aliquat 336. The separation of high-purity yttrium is based on the different extraction behavior of yttrium in nitrate and thiocyanate systems. Using 43% quaternary ammonium nitrate (nitrate of tricapryl-methylamine) in Solvesso 250, the lighter rare earths Gd–Er are extracted leaving yttrium in the raffinate along with thulium, ytterbium, and lutetium. The yttrium content of this rare-earth mixture is 95%. Ammonium thiocyanate was added to this raffinate, and using quaternary ammonium thiocyanate (tricaprylmethyl ammonium thiocyanate) in Solvesso 150, the rare earths Tm, Yb, and Lu were extracted, leaving yttrium in the raffinate. Yttrium is recovered from the raffinate by direct precipitation with oxalic acid and

calcination to an oxide product. To enhance the purity of the yttrium product further, an additional solvent extraction cycle is also carried out (mainly to separate yttrium from non-rare-earth impurities) ahead of the precipitation. From an aqueous solution containing ammonium thiocyanate, yttrium is extracted into the thiocyanate (SCN) form of Adogen 464. Yttrium is stripped from the solvent by water, and from the strip solution, yttrium is precipitated as oxalate. The above process was used by MCI-Megon, Norway, for commercial production of 99.995% purity Y_2O_3.

3.6.6.13 Rhône-Poulenc

In Rhône-Poulenc, all the REEs with purities of >99.999% were produced almost entirely by solvent extraction. For certain REEs, separation by solvent extraction alone would turn out to be very expensive. They were produced in kilogram quantities by ion exchange. The outline of the Rhône-Poulenc separation scheme is shown in Figure 3.54 (McGill 1993).

Monazite, which is the source mineral, is digested with NaOH, and from the mixed RE–Th hydroxide obtained after trisodium phosphate separation, a rare-earth-chloride solution and a rare-earth nitrate solution are produced. The unwanted elements are removed from each of these solutions. The solvent extraction stream in the chloride medium yielded nonseparated rare-earth compounds, such as dehydrated rare-earth chlorides, which are useful for electrolysis to misch metal. The solvent extraction stream in the nitrate medium is used to yield separated rare-earth oxides. Lanthanum (99.995% La_2O_5) is left in the aqueous phase, while the mixture

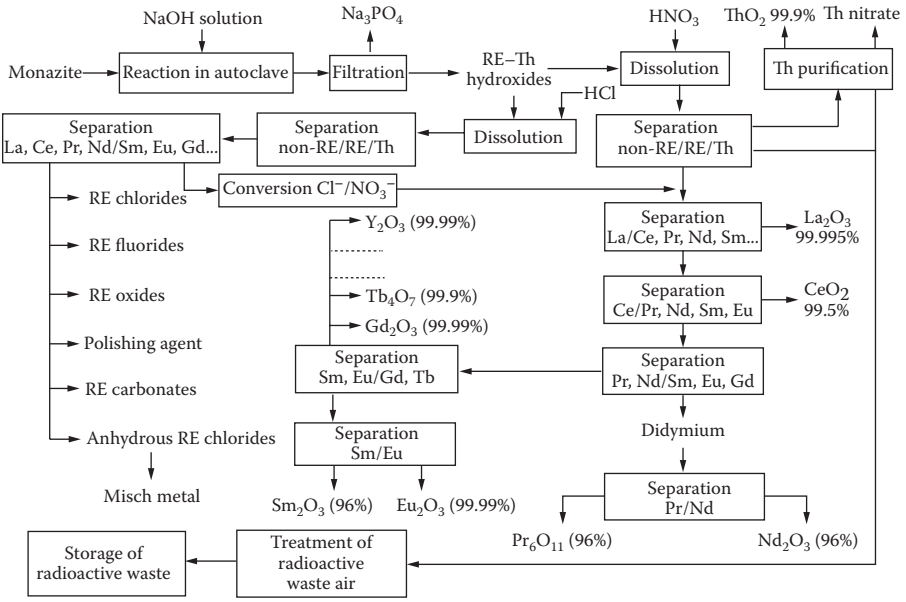


FIGURE 3.54 Rhône-Poulenc solvent extraction process for the separation of rare-earth elements. (From McGill, I., Rare earth elements. In Elvers, B., Hawkins, S., Russy, W., and Schulz, G. (eds.), *Ullmann's Encyclopedia of Industrial Chemistry*, vol., A22, pp. 607–649, VCH, Weinheim, 1993.)

of Ce, Pr, Nd, Sm, Eu, Gd, Tb, Y etc. goes into the organic phase. Similarly, CeO_2 (99.5%) is separated in the Nd–Sm stream. After primary Ce removal, following the sequence shown in Figure 3.54, Pr, Nd, Sm, Eu, Gd, Tb, and Y oxides are recovered. The purification and isolation of individual rare earths is carried out in a variety of extractants that include acidic and neutral organophosphorus compounds, amines, and carboxylic acids.

The solvent extraction separation of each REE was carried out in multistage batteries of mixer–settlers. At least 50 mixture settler stages per stream are needed to obtain a product with 99.99 to 99.9999% purity.

Rhône-Poulenc produced high-purity separated rare-earth oxides starting from not only monazite but also bastnasite or euxenite. The Rhône-Poulenc solvent extraction flow sheet was regarded as the standard for all industrial producers (Bautista 1995).

3.6.6.14 Thorium Ltd.

In the plant at the erstwhile Thorium Ltd. in the United Kingdom, a bastnasite concentrate was processed first by leaching the rare-earth carbonates by HCl followed by caustic treatment of the leached concentrate, to break the fluoride bond. The rare-earth hydroxides thus obtained were then leached with HCl. The mixed rare-earth-chloride solution was processed by solvent extraction. First, the rare earths samarium to yttrium were extracted by an unnamed extractant, and europium was reduced to the divalent state and recovered (Ritcey and Ashbrook 1979). Subsequently, gadolinium, samarium, and yttrium were recovered in a separate process. The raffinate contained La, Ce, Pr, and Nd. Sodium hypochlorite was used to oxidize Ce in the raffinate to Ce^{4+}, which precipitated as cerium hydroxide on the addition of ammonia. The solution, containing La, Pr, and Nd, was precipitated with sodium carbonate, and the precipitate was redissovled in nitric acid.

TBP was used as an extractant for the separation of individual rare earths from the nitrate solution (Sherrington 1966). The process was a batch extraction in which equilibrium was attained by total recycling (reflux) in the extraction stages as well as total recycling in the scrubbing stages until the desired solutes had been concentrated. Products of different composition were withdrawn from different stages. Water was used to strip the rare earths from the loaded solvent. The rare earths were precipitated as hydroxides or carbonates. The precipitates were dissolved once again in acid, and the solution was recycled. Even though this process finally yielded the desired product purity, it is costly relative to a continuous process and is also not attractive for use in large plant installations.

For the extraction and separation of yttrium, Thorium Ltd. used Versatic 911. They developed the technique of total recycling in two consecutive systems. The first was a 25-stage process operated with versatic acid, and the second was a 50-stage process operated with TBP as the extractant. By these, Y_2O_3 of 99.999% purity was obtained starting from a 47% Y_2O_3 concentrate (Brown and Sherrington 1979; McGill 1993).

3.6.6.15 Yao Lung Chemical Plant

The Yao Lung chemical plant in Shanghai was the first of the rare earth–processing plants in China. It went into production in 1964 and operated a similar process for

the digestion of monazite as Rhône-Poulenc. The simplified flow sheet of this plant for extraction and separation of rare-earth oxides from monazite (Zhang et al. 1982) is given in Figure 3.55. Following alkali digestion of Monazite, solid–liquid separation, and leaching of the hydroxide residue with HCl, a mixed rare-earth-chloride solution was obtained. The solution was purified by extraction with D2EHPA, and the rare earths recovered were split into three groups, from which mixed and pure oxides, carbonate, or chlorides were produced.

There are more than 60,000 to 80,000 t bastnasite or/and monazite separated every year in China, with 25,000 t coming from the Sichuan Province. Some of it is used directly to produce Si–Fe–RE alloys; the rest is converted to rare-earth chloride for separation. Normally, bastnasite in Baotou is decomposed with sulfuric acid to get the rare-earths as sulfates first, and then, the carbonates are precipitated. Finally, the carbonates are dissolved in hydrochloric acid to convert to rare-earth chlorides, as the feed for the solvent extraction process (Yan et al. 2006a).

The bastnasite ore or concentrates are typically roasted with H_2SO_4, followed by leaching with water or dilute sulfuric acid. Rare earths are recovered from the leach liquor by solvent extraction with P204 (D2EHPA). By selective stripping, two groups, La–Nd and Sm–Gd (the concentration of heavier rare earths is usually small), of rare earths are obtained. These are separated further into individual REEs if required (Huang et al. 2006). Alternative sequences and modified separation processes have been tested to reduce reagent consumption. In one approach, P204 or P507 is used to extract and remove Th and most of Ce first, before the raffinate containing the remaining rare earths undergo further solvent extraction to separate individual rare

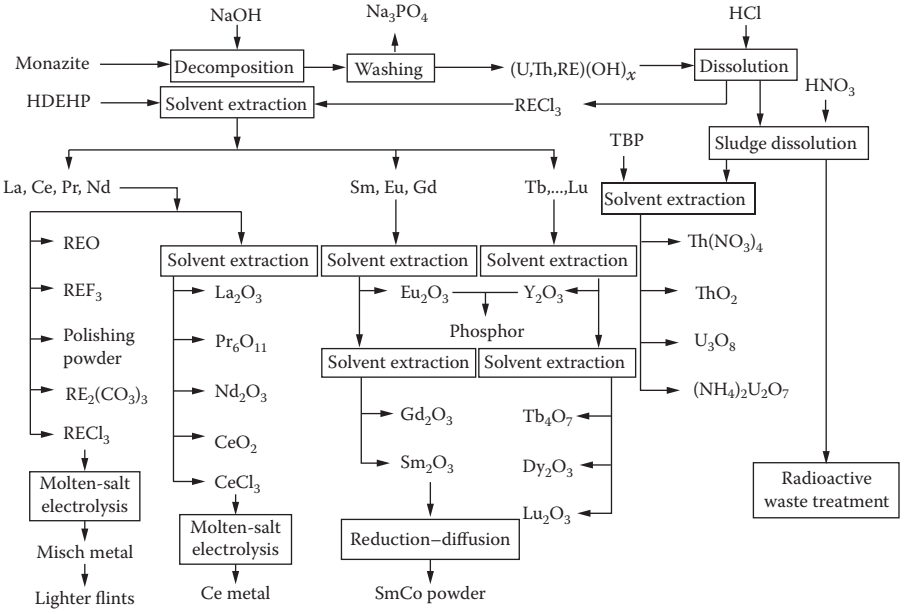


FIGURE 3.55 Simplified flow sheet of Yao Lung chemical plant. (From Zhang, B.Z. et al., *Hydrometallurgy*, 9: 205–210, 1982.)

earths, as indicated in Figure 3.56 (Huang et al. 2006). The F, Th, and Ce(IV) were selectively stripped from the organic phase.

Cyanex 923 (Dziwinski and Szymanowski 1998) has been used to separate and remove Ce(IV) from the leach liquor first. The raffinate containing thorium and other rare earths then underwent solvent extraction with N1923 (a primary amine) to separate Th, as shown in Figure 3.57 (Lu et al. 1998). Individual rare-earth compounds were produced from the Th-free raffinate in a third solvent extraction circuit.

From the leach liquor of the ion adsorption-type rare-earth ores, extractants such as HEHEHP and naphthenic acid are frequently used to extract the rare earths. Individual rare-earth compounds (oxides or chlorides) are recovered by controlled stripping (Huang et al. 2005, 2006).

Bastnasite (about 50% cerium) containing 0.2–0.3% Th and 8–10% F is processed in a plant in Sichuan Province, China, using a new extraction method to recover Ce(IV) and F from roasted bastnasite–sulfuric leach liquor with Cyanex 923 (Li et al. 2006). In this new method, Cyanex 923 is used to separate Ce(IV) from bastnasite, and F could be extracted into an organic phase with Ce(IV) and recovered as CeF_3 nanoparticles with a yield over 90%; the purity of the cerium product was over 99.99%. However, Cyanex 923 used in the extraction system is more difficult to manufacture than most common extractants such as D2EHPA and HEHEHP in China, which makes it difficult to use widely in industry.

There are rich rare-earth resources in China. Thorium minerals often coexist with rare-earth minerals, like monazite and bastnasite, which contain elements like U and Th. The main separation/recovery method for Th is solvent extraction.

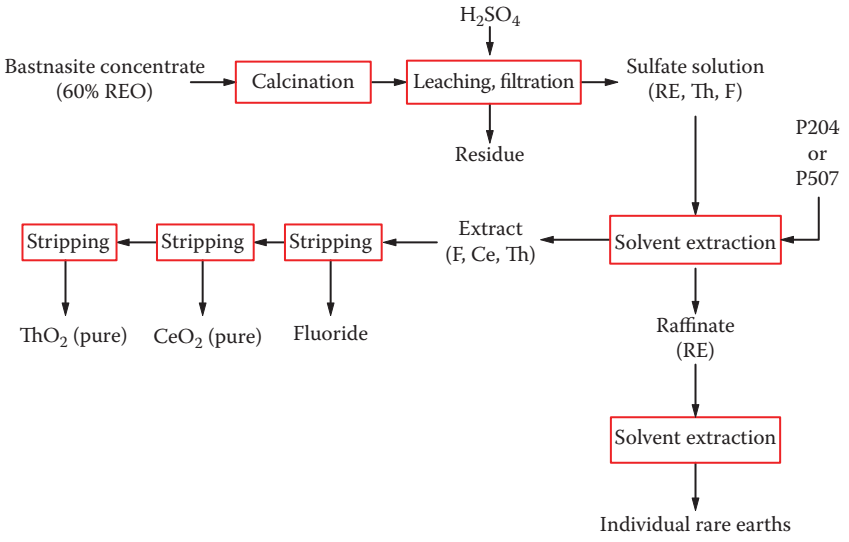


FIGURE 3.56 Simplified flow sheet for separating RE, F, and Th by solvent extraction with P204. (From Huang, L.J. et al., *J. Alloys Compd.*, 421(1–2): 279–282, 2006; Xie, F. et al., *Miner. Eng.*, 56: 10–28, 2014.)

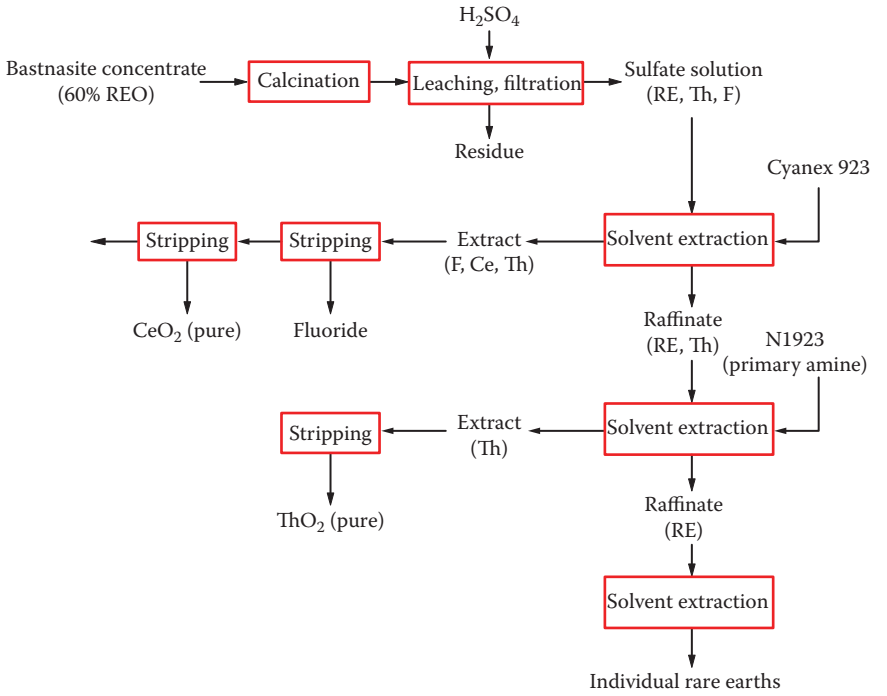


FIGURE 3.57 Simplified flow sheet for separating RE, F, and Th by solvent extraction with Cyanex 923. (From Lu, Y. et al., *J. Colloid Interface Sci.*, 202: 462–476, 1998; Xie, F. et al., *Miner. Eng.*, 56: 10–28, 2014.)

Grirem Advanced Materials Co., Ltd. (GRINM) has developed a new bastnasite treatment process, in which F^-, Th(IV), and Ce(IV) were directly extracted into HEHEHP. Ce(IV) was first reduced to Ce(III) by H_2O_2 and stripped with HCl, and then Th could be recovered by stripping, which not only simplified the treatment process but also increased the Th recovery. Th was usually stripped by Na_2CO_3; however, it was easily deposited and a lot of sodium carbonate was wasted in the stripping process. If Th is stripped directly using mineral acid, its recovery could be improved remarkably, and Th dispersion pollution could be avoided. Zhang et al. (2012) investigated the Th stripping behavior from HEHEHP with H_2SO_4, HCl, and HNO_3 and concluded that H_2SO_4 was the most effective stripping reagent compared with HCl and HNO_3. Based on the results, a pilot test for a new bastnasite treatment process was carried out, and the recovery of Ce, F, and Th was more than 99%, 98%, and 95% respectively.

In the newly developed process by Grirem, bastnasite concentrate is first decomposed by oxidation roasting and then leached with H_2SO_4, which contains F^-, Ce^{4+}, Th^{4+}, and RE^{3+}. The separation process is shown in Figure 3.58. When $[F^-] = 2$ g/L, the extraction rates of Ce^{4+}, F^-, and Th^{4+} are all beyond 98%. Then after 3 stages of extraction, 4 stages of RE^{3+} scrubbing, 10 stages of F scrubbing, and 5 stages of Ce^{4+} reduction stripping, Th^{4+} is stripped with 8.0 mol/L H_2SO_4 for 10 stages, and the phase ratio is 4:1. In the process, F and Ce could be totally stripped. The total Th

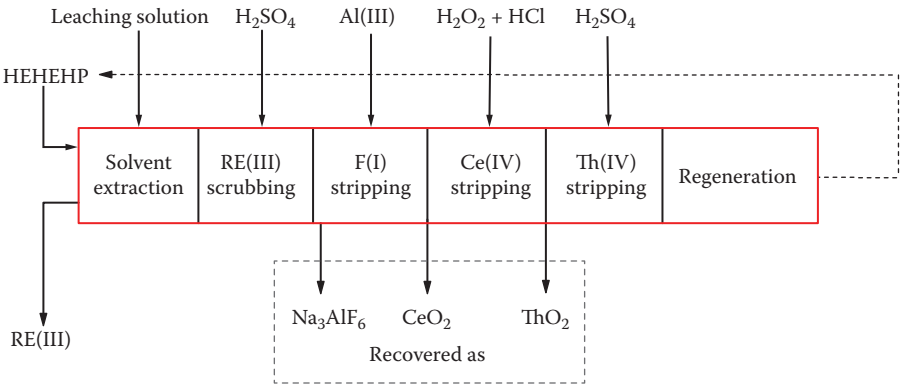


FIGURE 3.58 Extraction and separation of F^-, Ce^{4+}, Th^{4+}, and RE^{3+} from a bastnasite leaching solution. (From Zhang, Y. et al. *J. Rare Earths*, 30(4): 374–377, 2012.)

recovery is more than 95%. After further treatment, the purity of ThO_2 is more than 99%. The process could separate F–, Ce^{4+}, Th^{4+}, and RE^{3+} in one procedure by only one extractant with high efficiency and low cost.

A schematic flow sheet for the processing of an ionic adsorption RE deposit given by Yan et al. (2006a) is shown in Figure 3.59. P507 and naphthenic acid are the two main extractants. Naphthenic acid is diluted with kerosene, and isooctane alcohol is included as an additive to separate yttrium from other lanthanides. Almost all the aqueous phases are in the medium of hydrochloric acid, except that nitric acid is used in specific cases for the separation of other elements.

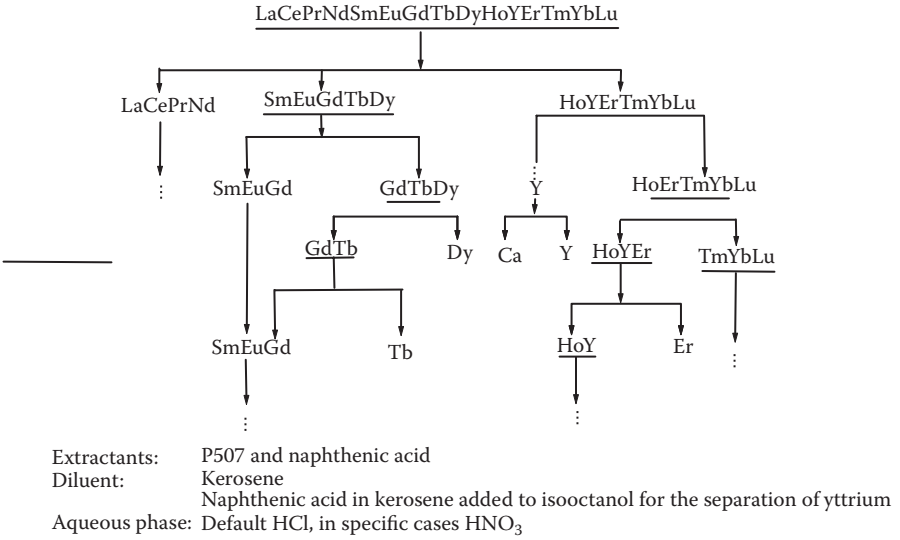


FIGURE 3.59 A schematic flow sheet for the processing of ionic adsorptive RE deposit. (From Yan, C. et al., *Tsinghua Sci. Technol.*, 11(2): 241–247, 2006.)

3.6.6.16 Spin-Off Processes

Beginning essentially as an analytical tool, developed further and used primarily for the processing of primary rare-earth resources, solvent extraction processing has grown to become an effective and versatile technique amenable to customizing for special needs. Foremost among these special purposes is the processing of secondary rare-earth resources or rare-earth materials for recycling. The application of solvent extraction in recycling is covered separately in a dedicated chapter later in the book. The processing of certain rare earth–bearing solutions not necessarily as a sequence in ore processing operations is looked at here.

A flow sheet for the simultaneous purification of yttrium and other HREs is shown in Figure 3.60. This flow sheet, believed to be used in Japan for commercial production (Thakur 2000), comprises solvent extraction operations with versatic acid, PC88A, and TBP.

Doyle et al. (2000) developed a novel solvent extraction configuration that yields a mixed Ce–Pr–Nd product (for magnet production) and pure Nd oxide simultaneously, with flexibility vto alter the relative proportions according to industry needs. The schematic flow sheet for this process is shown in Figure 3.61. A rare-earth-chloride solution generated by leaching oxide with HCl was extracted with P507 in kerosene. In the first circuit, Sm and heavier rare earths along with Y were loaded into the organic phase. The raffinate containing Nd and lighter rare earths was extracted with P507 in kerosene. By controlling the number of stages and reflux ratios, Pr, Nd, and part of the Ce were extracted into the organic phase, with the balance of Ce, and all the La remained in the aqueous phase. A marketable lanthanum product was produced from this raffinate. The loaded organic was selectively

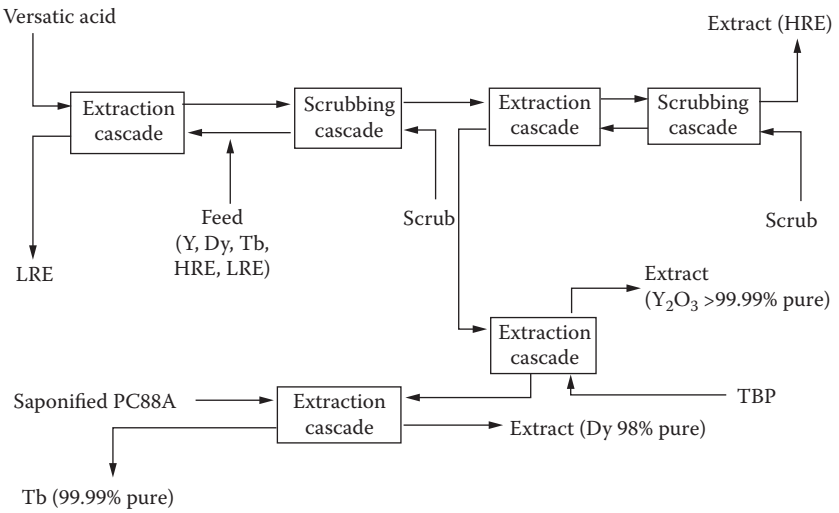


FIGURE 3.60 Flow sheet for the simultaneous purification of yttrium, terbium, and dysprosium using versatic acid, TBP, and PC88A. (From Thakur, N.V., *Mineral Process. Extractive Metal. Rev.*, 21(1–5): 277–306, 2000.)

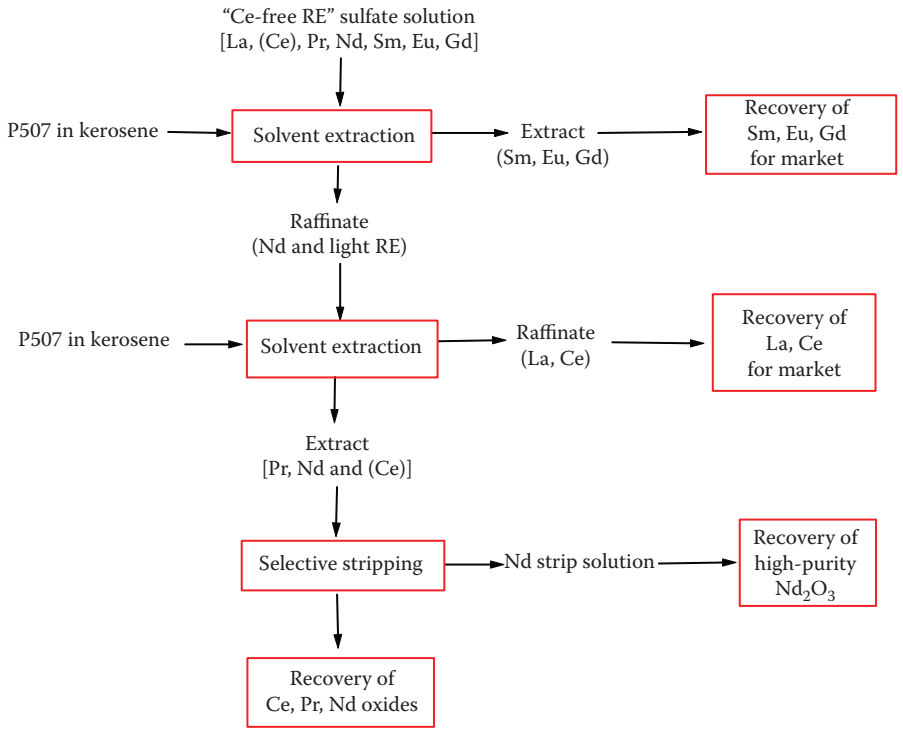


FIGURE 3.61 Simplified flow sheet for solvent extraction process for producing low-cost permanent magnet feed. (From Doyle, F.M. et al., Direct production of mixed, rare earth oxide feed for high energy-product magnets. In: Bautista, R.G., Mishra, B. (eds.), *Rare Earths and Actinides: Science, Technology and Applications IV*, pp. 31–44, TMS, Warrendale, PA, 2000; Xie, F. et al., *Miner. Eng.*, 56: 10–28, 2014.)

stripped to produce high-purity neodymium oxide and a mixture of Ce, Pr, and Nd oxides. Huang et al. (2008) used a synergistic extraction system to produce different rare-earth products from rare-earth sulfate solutions resulting from the leaching of bastnasite concentrates (Figure 3.62). A nonsaponified organic phase was used directly to extract rare earths from their sulfate or chloride solutions. By controlling operation conditions, five or even more commercial rare-earth products could be produced simultaneously.

3.6.6.17 Dry Processes

Murase et al. (1996) investigated a dry process for the separation of rare earths using a chemical vapor transport reaction. The reaction was mediated by metal halide vapor complexes $KRCl_4$,(g) and RAl_nCl_{3+3n}(g) (R = rare earths). Both KCl and $AlCl_3$ act as complex formers, i.e., transporting agents. Rare-earth concentrates or crude oxide mixtures were used as raw materials. The concentrates or crude oxides derived from monazite and xenotime, bastnasite, or ionic ores were chlorinated by chlorine gas at 1000°C. The resulting RCl_3 reacts with the complex

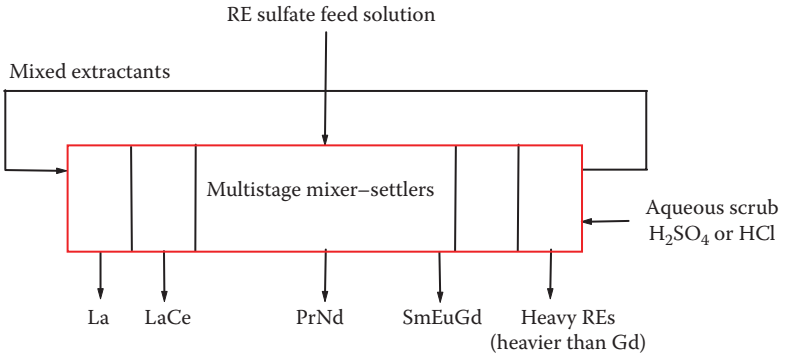


FIGURE 3.62 Simplified configuration of countercurrent separation of rare earths to produce various rare-earth products by solvent extraction. (From Huang X.W. et al., *Sichuan Rare Earth*, 4: 15–19, 2008; Xie, F. et al., *Miner. Eng.*, 56: 10–28, 2014.)

formers KC1 and $AlCl_3$ to form $KRCl_4$,(g) and RAl_nCl_{3+3n} vapor, which, while passing along a well-controlled temperature gradient, decompose to the rare-earth trichloride and collect as $RECl_3$. Heavier rare-earth chlorides including YCl_3 are generally more readily transported and concentrated in the deposit at temperatures around 600–700°C, and lighter ones, in higher temperature fractions at 800–900°C. There is a built-in selectivity in the process. Chlorides of other elements such as Th, U, and P in the raw materials were generally concentrated in lower temperature fractions. Yields of individual rare earths after reaction for 82 h increased with increasing atomic number or decreasing ionic radius of the rare-earth ion: 20–30% for La, 50–60% for Ce, 60–70% for Pr and Nd, and >80% for Gd–Lu and yttrium. Sun et al. (1998) also studied the possibility of mutual separation for the neighboring REEs Nd, Sm, Eu, and Gd from binary oxide mixtures Nd_2O_3–Sm_2O_3, Sm_2O_3–Eu_2O_3, and Eu_2O_3–Gd_2O_3 using a stepwise chlorination–chemical vapor transport reaction mediated by vapor complexes $LnAl_nCl_{3n+3}$, and computed the separation factors.

3.7 SCANDIUM

Solvent extraction has been the process used for the recovery and isolation of scandium from its resources, which are essentially non-rare-earth minerals. In the processing of uranium, during solvent extraction, scandium is extracted and concentrated together with uranium. In the subsequent purification of the uranium, the scandium is separated. Three processes for accomplishing this separation and recovery of 99% pure scandium were reviewed by Gschneidner (1975). The processes likely to be used for large-scale, high-purity scandium recovery from wolframite use solvent extraction for separation. The processes for opening thortveitite use chlorination (Iya 1953; Vickery 1955) or fluorination (Spedding et al. 1958) to obtain a scandium-rich material, which is subsequently dissolved, and the scandium is recovered in pure form by ion exchange and solvent extraction.

3.8 SUMMARY

The by-product status of one of the two principal minerals of rare earths, monazite, carries it through the processing steps from as-mined condition to the status of a mineral concentrate. Even though monazite mining and processing are carried out in different parts of the world, the processes applied for beneficiating the mineral are essentially the same: gravity, electrostatic, and electromagnetic separations, and flotation. For beneficiating the bastnasite ore from Mountain Pass and the iron–rare earth–niobium ore from Bayan Obo, flotation is the key process, and it works. Rare earth clay minerals (ion adsorption ores) cannot be beneficiated by processes, including flotation, used for monazite or bastnasite. Both acid and alkali digestion methods have been applied to monazite processing, and the alkali treatment technique that yields a trisodium phosphate by-product is used commercially. Chemical treatment of bastnasite is less extensive. Usually, the processes applied for chemical attack of monazite and bastnasite or their minor variations work well on the remaining resources such as xenotime, gadolinite, and euxenite. As regards the ion adsorption ores, the leaching is remarkably easy. They are usually leached directly with an inorganic acid either in dumps or *in situ*, or with a concentrated inorganic salt solution. Presently, all leaching procedures are evaluated considering their environmental impact. In this context, in the chemical treatment of bastnasite, the focus is increasingly on the trapping of fluorine either as a stable compound in the leach residue or collecting it suitably from the off gas stream as a fluoride or even condensing it as HF. As far as chemical treatment of rare-earth resources is concerned, direct chlorination in the presence of carbon has been a widely effective technique for every type of mineral.

The celebrated chemical similarity of the REEs has a built-in bug in the slow and steady change in basicity, as the elements lanthanum to lutetium and yttrium are considered. This difference has been exploited directly and indirectly in devising procedures for separating rare earths from one another, both by the classical methods of fractional crystallization and fractional precipitation and also by the modern methods of ion exchange and solvent extraction. Exploitation of multivalency, particularly in cerium and europium, is the basis of methods for effecting their separation. These techniques have remained timeless and continue to be used even in current procedures as part of the overall technique of separation either prior to or following ion exchange or solvent extraction. Ion exchange and solvent extraction rely on the availability of suitable complexing agents and solvents, respectively. EDTA and HEDTA are the mainstays for ion exchange. In solvent extraction TBP, DE2HPA, PC88A, versatic acid, and Aliquat 336 have been very useful.

In fact, every class of solvents–cation exchangers, anion exchangers, chelating exchangers, solvating extractants have been used, singly or in various synergistic combinations, for accomplishing rare earth separations.

Among the two modern separation techniques, ion exchange and solvent extraction, solvent extraction has the advantages of being fast and continuous and working on more concentrated solutions, and it is economical for handling large quantities of materials. Ion exchange is, on the other hand, regarded as superior for the production of extremely pure materials. However, commercial production of materials at 99.9%

or even 99.99% purity with solvent extraction has been possible (Bautista 1995). Although the details of actual procedures, sequence of various operations, and identities of certain organic solvents are usually not disclosed in publications, the solvent extraction technology has been expanded in the five decades starting from the mid-1960s to commercial-scale separation/purification of at least 11 of the 15 rare earths that occur in bastnasite, monazite, and xenotime ores. Solvent extraction would not be the method of choice in at least two instances: (1) when product purity exceeding 99.9% is required and (2) when the lesser abundant rare earths such as Tm, Yb, and Lu are to be isolated in a commercial solvent extraction circuit.

As mentioned for the leaching operations, separation processes would also be coming under increasing scrutiny for compliance with environmental regulations. A significant achievement this context is the process developed by Grirem for treatment of bastnasite, wherein, following a sulfuric acid leach, the key components F, Th, Ce(IV), and RE(III) are separately recovered. This is important from the point of F and Th waste management, which are serious issues.

Innovative processes and techniques that use ionic liquids, supported liquid membranes, supercritical systems have also been regularly explored for possible implementation in rare earths separation. When cost and throughput barriers have been crossed, these processes can be anticipated to enter the mainstream separation schemes. It is likely that they may first be proved to accomplish separation objectives in rear earth recycling before they graduate to primary ore processing operations.

4 Reduction

4.1 INTRODUCTION

The rare-earth oxides are the usual end products of the ore processing and separation operations. They are therefore the natural starting material for conversion to metal by reduction. Rare-earth oxides are extremely stable, and their reduction to metal is, therefore, very difficult. The difficulties are usually compounded but occasionally alleviated by the physical properties such as the melting point and vapor pressure of the rare-earth metals. In several instances, conversion of the rare-earth oxide to a rare-earth halide and reduction of the halide to the metal is a useful procedure because of certain inherent characteristics of the halide reduction method. Fused salt electrolysis as applied to the production of reactive refractory metals can also be effective for rare-earth-metal preparation. The relatively low melting point of many of the rare-earth metals is an advantage here. The preparation of rare-earth metals by a route in which an alloy is prepared first and the metal is then recovered from the alloy is another interesting possibility, being beneficial in both chemical and electrolyte methods of reduction.

Every method of rare-earth-metal preparation has certain advantages and limitations with respect to applicability to individual rare earths, purity of product, yield of the metal, batch size, operational convenience, and economy. In spite of their celebrated chemical similarity in their trivalent states, the rare earths do display considerable variation in properties like melting point and vapor pressure. This variation largely comes in the way of applying certain reduction methods uniformly for the preparation of all the rare-earth metals. Another factor is the possibility of a stable divalency in some of the rare-earth elements. This frustrates attempts to produce them by the usual chemical or electrolytic reduction processes. Special processes, however, can circumvent the limitation.

4.2 FUNDAMENTALS

The process of liberation of a metal from its compound or *reduction* is represented by the following general reaction:

$$MX_n + iR = M + iRX_{n/i} \tag{4.1}$$

where M is the metal to be obtained; X is oxygen, fluorine, or chlorine; and R is the reducing agent (or reductant), which, in general, may be hydrogen, carbon, or metals such as lithium, sodium, potassium, magnesium, calcium, or aluminum, in most of the cases. It is fundamental knowledge that metallurgical thermodynamics provides the answer to the question if reaction 4.1 can occur at all. The reaction is possible only when at a chosen reaction temperature the difference between the free energies

of formation, ΔG, of the compound formed by the reductant, $RX_{n/a}$, and of the starting compound, MX_n, is negative. In other words, if the condition

$$i\Delta G\,(RX_{n/i}) - \Delta G\,(MX_n) < 0 \tag{4.2}$$

is satisfied. Therefore, the free energies of formation of the compounds (oxides, fluorides, and chlorides) of the metal as well as the reductant and their dependence on temperature determine which element can function as R for a given compound MX_n to release the metal M. The data on the free energies of formation of compounds were presented as straight-line plots with temperature as the abscissa and standard free energy of formation as the ordinate first by Ellingham (1944) and later by Richardson and Jeffes (1948). The Ellingham diagrams of compounds relevant to the reduction of rare earths are given in Figures 4.1 to 4.5. Data from the US Bureau of Mines Publications (Pankratz et al. 1984) have been used in preparing these diagrams.

Even as the first approximation, the number of elements that can function as reducing agents for the rare earths is very limited. Under standard conditions, the order of stability, in the descending order, among the oxides is $CaO > RE_2O_3 > MgO > Al_2O_3 \gg SiO_2$. The situation is similar among the fluorides. Here again, the order of stability is $CaF_2 > REF_3 > LiF > NaF > MgF_2 > AlF_3$. There appears to be, however, a choice of many metals to reduce the rare-earth chlorides because the order of stability here is $KCl > NaCl \approx LiCl \approx CaCl_2 > RECl_3 > MgCl_2 \gg AlCl_3$. Thus, under standard conditions, which in effect means MX_n, R, M, and $RX_{n/i}$ given in Equation 4.1 are all pure

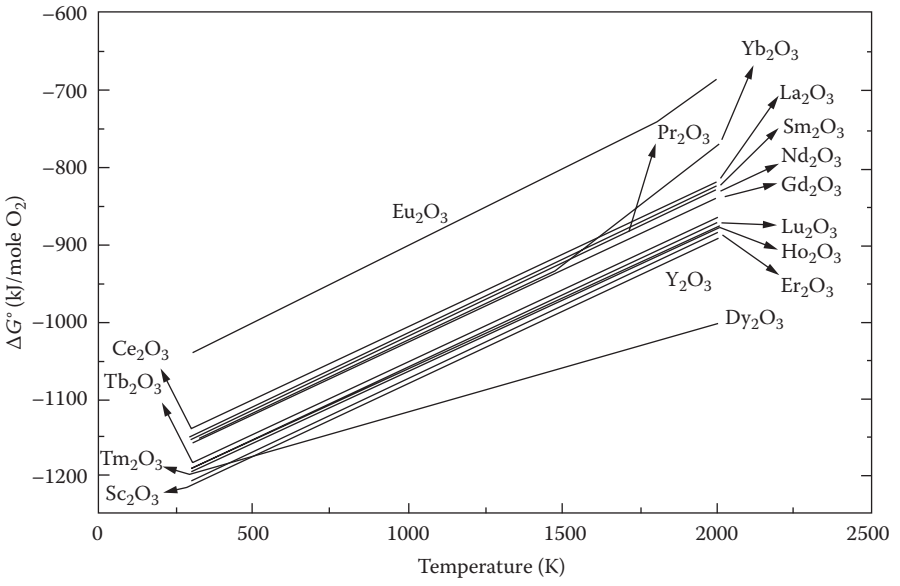


FIGURE 4.1 Standard free energy of formation of rare-earth oxides as a function of temperature.

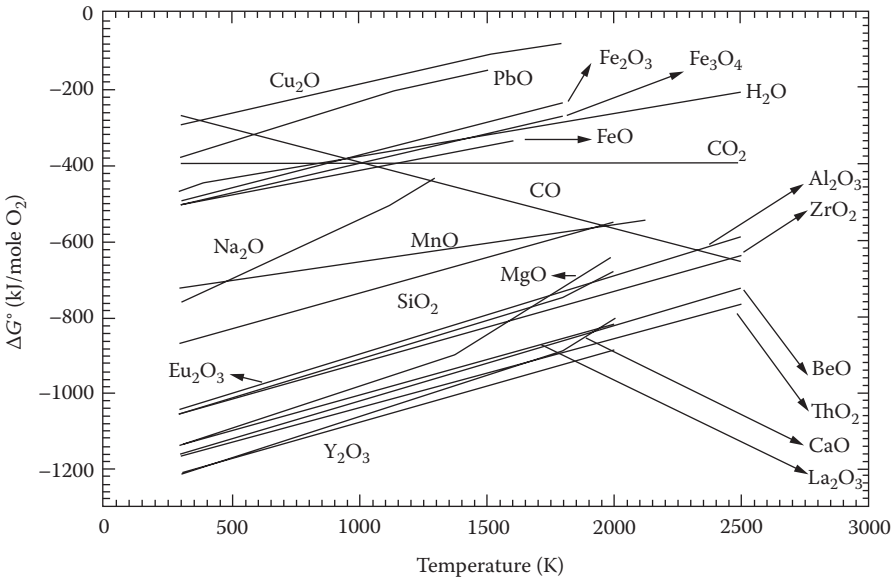


FIGURE 4.2 Standard free energy of formation of selected oxides of rare earths and certain common metals as a function of temperature.

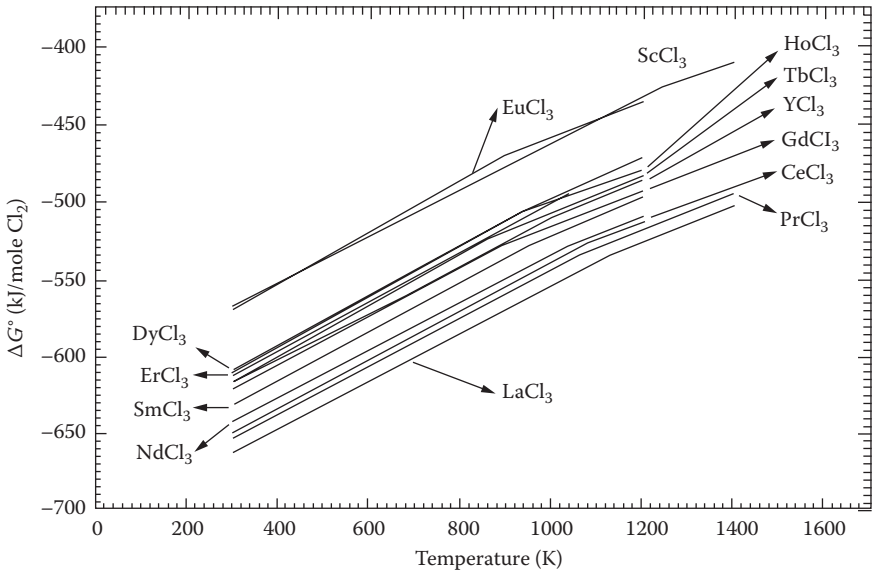


FIGURE 4.3 Standard free energy of formation of rare-earth chlorides as a function of temperature.

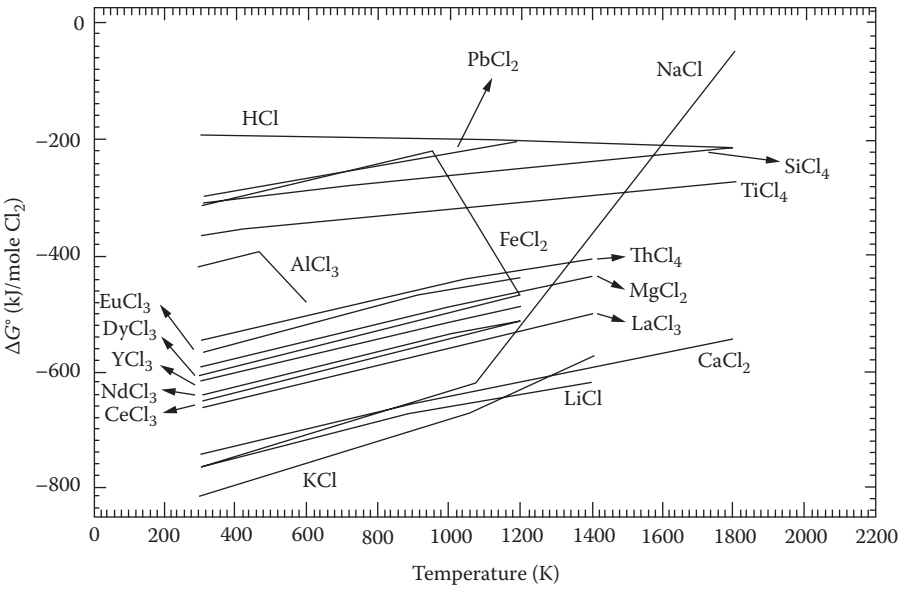


FIGURE 4.4 Standard free energy of formation of selected chlorides of rare earths and certain common metals as a function of temperature.

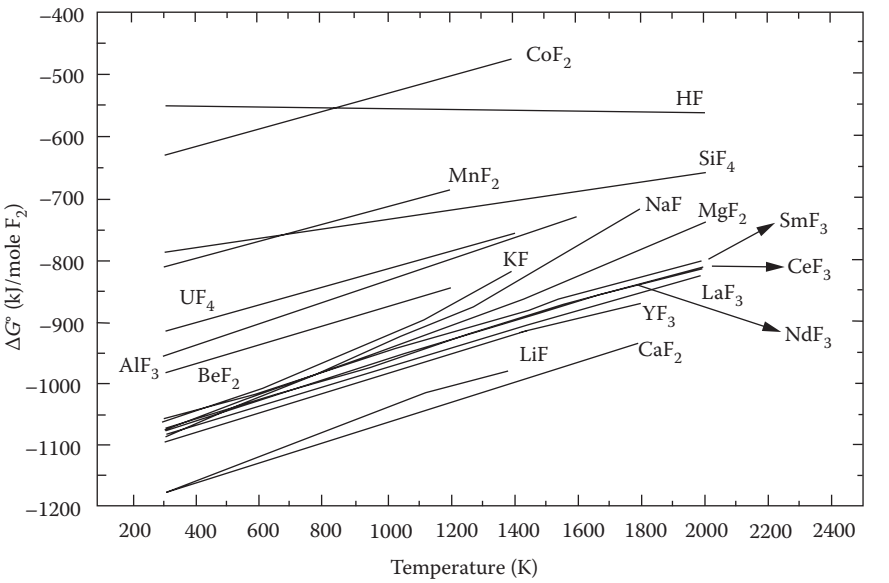


FIGURE 4.5 Standard free energy of formation of selected fluorides of rare earths and certain common metals as a function of temperature.

and at one atmosphere pressure, only calcium can reduce the rare-earth oxides and fluorides. However, the chlorides can be reduced by potassium, sodium, and lithium in addition to calcium. Among the nonmetals, hydrogen cannot reduce the rare-earth chlorides at temperatures normally used for conventional reduction. Carbon, forming carbon monoxide, can reduce the rare-earth oxide at high temperatures.

The picture under nonstandard conditions that, more often than not, more closely approximates the real reduction process condition is somewhat different. Here the reaction mixture need not be composed of only pure constituents R, M, and $RX_{n/i}$ under 1 atmosphere pressure. In other words, the activity, a, of each of the constituents, a_R, etc., need not be kept equal to 1. Consider the following thermodynamic expressions:

$$\Delta G = \Delta G^{o} + RT \ln Q$$

$$Q = \frac{a_{(M)} a^{i}_{(RX n/i)}}{a_{(MX n)} a^{i}_{(R)}}$$

To ensure a negative value for ΔG, even when ΔG^{o} is positive, Q can be appropriately varied, usually by decreasing the values of $a_{(M)}$ and/or $a_{(RX n/i)}$, and the variation amplified by a judicious choice of T.

The use of conditions where the activity "a" of one or more of the product components is made less than 1 alters the value of the free energy of the reaction and creates a more favorable tendency for the reaction to proceed. The typical methods to effect the activity change are the formation of a product metal having a low boiling point and hence vaporizing in the metallothermic reaction ($p_M < 1$ atm and $a_M < 1$), recovery of the reduced metal as an alloy ($a_M < 1$), and trapping the compound formed by the reductant in a complex slag ($a_{RX n/i} < 1$). It may also be mentioned here that carbothermic reduction under vacuum, which makes $p_{CO} \ll 1$ (or $a_{CO} \ll 1$), becomes an efficient method of reduction at high temperatures. Even after circumventing the reaction feasibility factor by tailoring the reaction component activities, there are other considerations that influence the practical implementation of the reduction process. In rare-earth-metal preparation, the choice of reducing agents being mainly metals, certain factors relating to the practicability of metallothermic reductions are given next.

4.3 METALLOTHERMY

The metallothermic reduction reaction may be generally represented by the equation

$$M(I)X_n + iM(II) = M(I) + iM(II)X_{n/i}$$

where M(I) is the metal to be produced, X is the anion, and i, n are the stoichiometric coefficients. While the feasibility of the metallothermic process is determined by the free energies of formation of the compounds involved in the above reaction, the practicability of the metallothermic reduction is determined by several other properties such as melting point, boiling point, vapor pressure, density, viscosity (for liquid components), and characteristics such as chemical reactivity and alloying behavior

of the various participants (reactants and products) of the reaction. The computation of the standard free energy of the reaction, therefore, presents only a limited picture on the reaction practicability. A more complete picture is obtained by considering the various properties of the reaction participants listed above.

The desirable characteristics of the metallothermic reduction have been summarized by Herget (1985) as follows: (1) the reaction should occur quickly and give product metal in high yields; (2) the reaction products must be obtained in compact forms—metal as an ingot and the slag as a well-separated layer; (3) the reaction should be self-sustaining and once initiated should proceed without the need for additional external heating; (4) the product metal must be of high purity; (5) the reaction proceeds in an open atmosphere; (6) the reaction should proceed safely without risk; and (7) the reaction should be amenable to being carried out in commercially available reactors using readily available refractories as containers.

Metallothermic reductions are generally exothermic reactions, and by a suitable choice of reactants, materials, and process conditions, it has been possible to realize many of the characteristics listed above and obtain the metal from its compound. The use of reactants in a powder or particulate form favors better reagent contact and, once initiated, a quicker reaction. If the heat generated during the reaction is sufficient to raise the temperature of both slag and metal to above their melting points, and if they remain molten for a sufficient length of time, so that the molten metal (denser) settles by gravity with the immiscible slag layer (lighter) remaining on its top, a metal ingot topped by a solidified slag results on cooling. Slag and metal are then separated mechanically. When the heat of reaction is insufficient to result in an all-liquid reaction mixture, other types of products can form. If the reduction occurs but neither the metal nor the slag melts, the metal is formed as a powder dispersed in the slag matrix. The slag in this case is leached away to separate the metal powder. Metal in the form of powder can result even if the slag melts when the melting point of the metal is very high and the metal is not sintered to any extent at the temperatures involved. When the reduction to metal occurs with only the slag melting but not the metal and the melting point of the metal is not very high, the metal particles may coalesce and undergo partial consolidation into what is called a sponge. Here the metal and sponge are separated either by aqueous leaching or by vacuum distillation.

By a suitable choice of reductants, reactors, and reaction conditions, the metal can usually be obtained in the chosen form. The rare-earth metals have been prepared by metallothermic reduction in the form of an ingot, sponge, or powder. Metal ingot has been prepared usually by metallothermic reduction of rare-earth fluorides as well as some of the rare-earth chlorides using calcium as the reductant. Rare-earth metal in the form of sponge has been obtained from the chloride using lithium as the reductant. Rare-earth-metal powder has been directly obtained by reducing rare-earth oxide with calcium. Instead of the elemental metal product, certain rare-earth alloys can also be directly prepared in ingot, sponge, or powder form. Metal can be subsequently obtained from the alloy by distillation in vacuum.

In the earliest successful attempt on rare-earth-metal preparation, metallothermic reduction was used and this technique, to date, remains the most widely used. The purity of the metallothermic reduction product depends, among other things, on the

purity of the starting materials, pure oxides, anhydrous chlorides and fluorides, and reductants. While the purity of rare-earth oxides is essentially determined by the separation step, the purities of chlorides and fluorides are determined by the method of their preparation, usually starting from the oxides.

4.4 PREPARATION OF RARE-EARTH CHLORIDES

The preparation of rare-earth chlorides for use as intermediate for reduction to metal has been accomplished by two routes (Block and Campbell 1961). One, known as the wet route, involves dehydration of hydrated rare-earth chloride, and in the other, the dry route, the oxide is directly converted to anhydrous chloride.

4.4.1 Preparation of Hydrated Rare-Earth Chlorides

The basic procedure was described by Spedding et al. (1952). The rare-earth oxide was dissolved in hydrochloric acid, and the solution was evaporated to syrup, which boiled at 128°C. This solution was then poured into a large porcelain disc and stirred while it cooled forming the hydrated chloride crystals.

Spedding and Daane (1952) also prepared hydrated cerium chloride by dissolving cerium ammonium nitrate in 6N hydrochloric acid and evaporating the resulting solution to a boiling point of 125–130°C. On cooling, the hydrated chlorides crystallized.

Nolting et al. (1960) prepared yttrium chloride by digesting yttrium oxide in concentrated hydrochloric acid and by evaporating the solvent until the yttrium chloride hexa-hydrate crystallized.

Mixed hydrated rare-earth chloride was produced in the past (Hirschhorn 1967) by wet chemical treatment of bastnasite and monazite. The process used for bastnasite at the York, Pennsylvania, plant of Molycorp (Kruesi and Duker 1965) was described in Chapter 3.

4.4.2 Dehydration of Hydrated Rare-Earth Chlorides

An old and popular method for the preparation of anhydrous rare-earth chlorides involves dehydration of the hydrated chloride under an atmosphere of dry HCl (Kleirheksal and Kremers 1928). Dehydration involves heating the hydrated chloride, and in many of the investigations (Block and Campbell 1961), it has been reported that the temperature should be below the melting point of partially dehydrated chloride to prevent it from reacting with the liberated water and forming oxychlorides. Harrison (1952), however, has observed that in the final stages of dehydration, temperatures above the melting point are necessary to prepare rare-earth chlorides free of oxychlorides. An increase in dehydration temperature can result in quicker dehydration. While several days are required to dehydrate a single batch of chloride when the temperature is kept at well below 100°C, complete dehydration could be affected in half a day if the hydrates were slowly heated to 250°C under a reduced pressure of approximately 3 kPa. During dehydration, a small flow of HCl is maintained over the salts to prevent hydrolysis.

The tendency to hydrolyze appears to depend on the temperature and the particular rare-earth chloride (Koch 1953). The stability of oxychlorides increases with the increase in temperature and in atomic number. Thus, heavier rare-earth chlorides would be more difficult to prepare by dehydration of hydrated chlorides.

The following overall procedure has been used at Ames laboratory to prepare anhydrous rare-earth chlorides on a fairly large scale (Block and Campbell 1961). Rare-earth oxides were dissolved in hydrochloric acid, and the solution was heated to drive off uncombined water. When the solution had been heated to about 130°C and had become viscous, it was poured into an evaporating dish and was allowed to cool. While cooling, the salt was stirred continuously to make it crystallize as a powder. The hydrated salt powder was then dehydrated by heating in a 75- to 100-mm-diameter pyrex tube through which purified HCl was passed while the pressure was maintained at 550–650 Pa. Heating was done gradually, raising the temperature from below 80°C up to 400°C over a period of 10 to 30 h. The product was anhydrous rare-earth trichloride free of any oxychloride.

Nolting et al. (1960) prepared anhydrous yttrium chloride in an apparatus shown schematically in Figure 4.6. The hydrated chloride was dehydrated by passing anhydrous hydrogen chloride gas under slight positive pressure downward through the dehydrating tower containing the yttrium chloride. Starting at 110°C, hydrogen chloride was passed (~0.5 L/min) through the column for 24 h by which time no more water was collecting downstream outside the tower. The water collected until it then corresponded to 80% of the water of hydration of the yttrium chloride. The

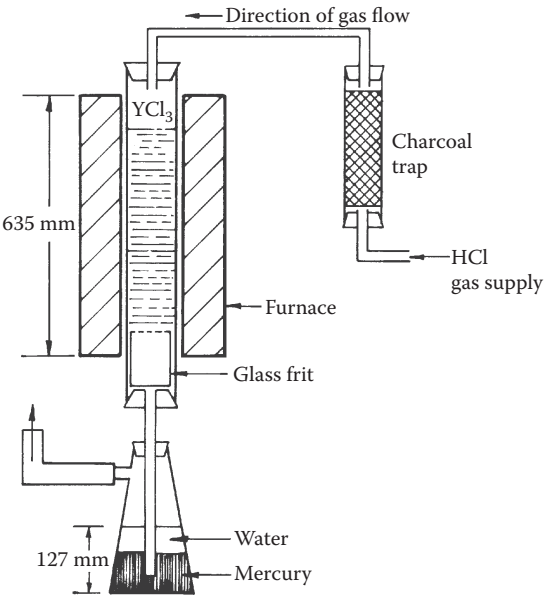


FIGURE 4.6 Setup for dehydrating yttrium chloride. (From Nolting, H.J. et al., *J. Inorg. Nucl. Chem.*, 14, 208–216, 1960.)

temperature was then raised to 350°C for another 24 h. Dehydrated yttrium chloride was removed from the tower after cooling. It was melted in a platinum crucible at 1000°C in an inert atmosphere to remove hydrogen chloride and cast into rods (25 mm diameter by 75 mm long) in a copper mold. The yield was quantitative.

In another method, the hydrated chloride was dehydrated in the presence of an excess of ammonium chloride (Gray 1951; Jantsch et al. 1930, 1931). The temperature of the salt was gradually raised keeping it under a stream of HCl or vacuum. As the heating continued, ammonium chloride was also evolved, and this helped to prevent the formation of oxychlorides. Block and Campbell (1961) have reported that better results were obtained when the hydrated salts were dehydrated in the presence of ammonium chloride at a very low pressure than when the hydrated salts were treated under a reduced pressure of HCl. This happens because ammonium chloride is a more effective chlorinating agent than HCl. The pressure during dehydration with ammonium chloride should be less than 60 Pa to minimize oxygen contamination. Such an operation, because of low ambient pressure, requires several days for completion. The following description given by Block and Campbell (1961) pertains to the preparation of anhydrous yttrium chloride in 20 kg batches.

Yttrium oxide was slowly dissolved in concentrated hydrochloric acid, and the insoluble matter was filtered out. Four moles of ammonium chloride per mole of yttrium was added to the filtrate. The solution was heated to evaporate water. Heating was continued until the normal boiling point of the solution reached 132°C, and at this point, the solution was a thick syrupy liquid. Upon cooling, this liquid solidified to a crystalline mass containing a mixture of ammonium chloride and hydrated yttrium chloride. This salt was dehydrated in a nickel vacuum retort (Block et al. 1960) shown in Figure 4.7.

The hydrated salt was loaded into a series of circular nickel trays to a depth of about 50 mm. Initially the retort was evacuated with a water aspirator and heated to 100–120°C. The bulk of the water was thus removed. After reaching 120°C and after the evolution of water had stopped, the valve to the aspirator was closed and the retort was connected to a rotary vacuum pump. A dry ice–acetone cold trap between the retort and the pump collected the water. The temperature of the retort was raised slowly to 350°C in such a way that the pressure within the retort remained at 3 to 70 Pa. During this operation, whatever water remained in the hydrated salt was removed and collected in the cold trap, and ammonium chloride was sublimed and collected by condensation on the water-cooled coils suspended from the top flange of the retort. Six to seven days of operation was required to handle a charge of 20 kg, and 95–98% of yttrium originally present in the yttria was converted to anhydrous yttrium chloride.

Croat (1969) used the apparatus shown in Figure 4.8 for vacuum dehydration of a mixture of NH_4Cl and the hydrated rare-earth trichloride. This apparatus consisted of an inconel furnace tube or retort (130 mm in diameter and 915 mm in length) in series with a dry ice and acetone trap and a pumping system. The faceplate of the retort contained a water-cooled cold finger made of inconel for freezing out part of the NH_4Cl. The chloride was contained in a platinum boat with a loose fitting lid. Croat (1969) used this apparatus to prepare anhydrous chlorides of dysprosium,

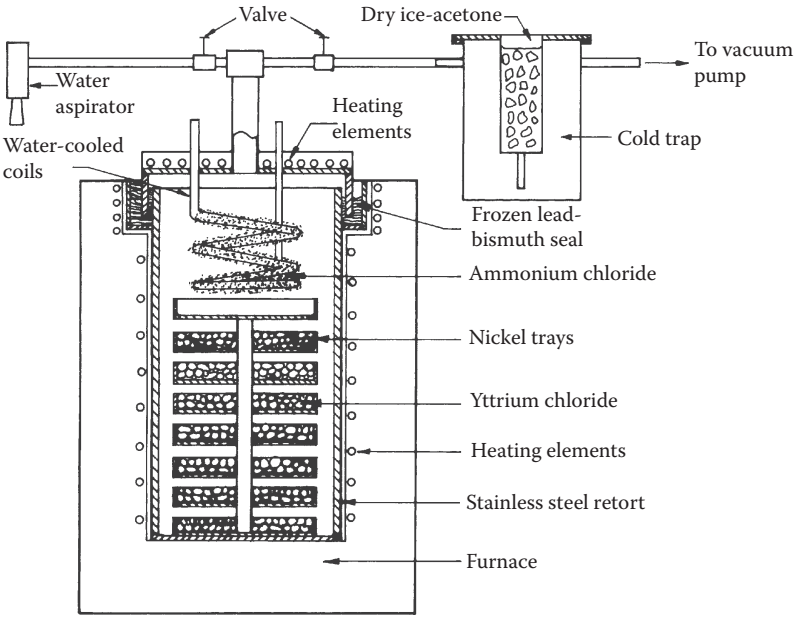


FIGURE 4.7 Yttrium chloride dehydration assembly. (From Block, F.E. et al., Preparation of high purity yttrium by metallic reduction of yttrium trichloride, Bureau of Mines Report of Investigations 5588, U.S. Department of the Interior, Washington, DC, 1960.)

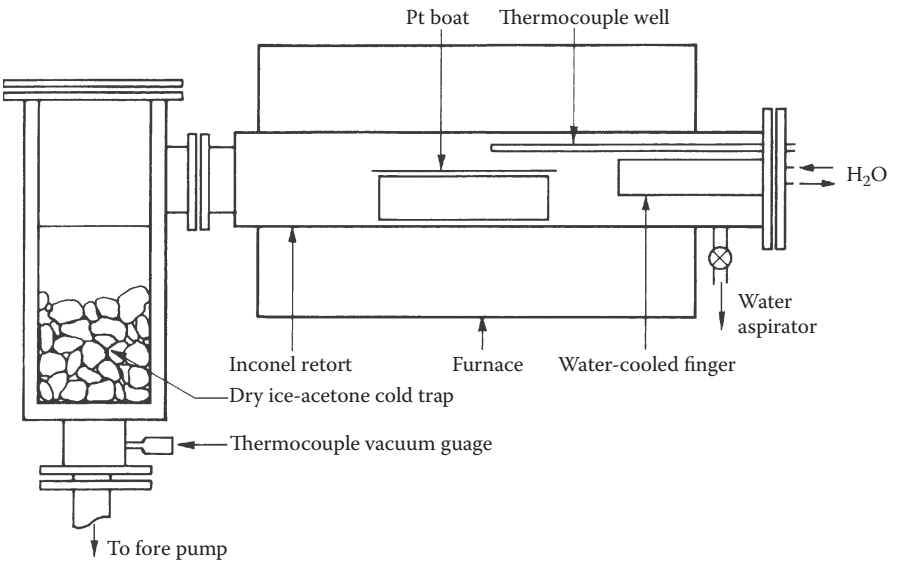


FIGURE 4.8 Schematic drawing of the apparatus for dehydrating hydrated rare-earth trichloride. (From Croat, J.J., *The preparation of high purity dysprosium, holmium and erbium by the lithium reduction of their trichloride salts*, Report No. IS-T-346, Ames Laboratory, ERDA, Iowa State University, Ames, IA, National Technical Information Service, Springfield, VA, 1969.)

holmium, and erbium. The hydrated chlorides were heated for 4 h at 90°C while evacuating the retort with a water aspirator. The bulk of the uncombined water was thus removed. The charge was then gradually heated to 335°C while evacuating to 1 Pa. The bulk of the removed NH_4Cl was collected on the water-cooled cold finger. The anhydrous chlorides were vacuum cast in the apparatus shown schematically in Figure 4.9. In the 62-mm-diameter and 250-mm-long tantalum crucible, approximately 600 g of the anhydrous chloride could be vacuum cast. The 6 mm tantalum tube extending upward from the bottom of the crucible was useful for venting volatile products during the casting process. The crucible lid made of a tantalum sheet was welded in place after the chlorides were loaded with the crucible. The chlorides were heated slowly under 0.001 Pa to approximately 100°C higher than their melting point and held for a few minutes only. The loss of chlorides by volatilization was negligible because the chloride vapor pressure at vacuum casting temperatures was less than about 10 Pa.

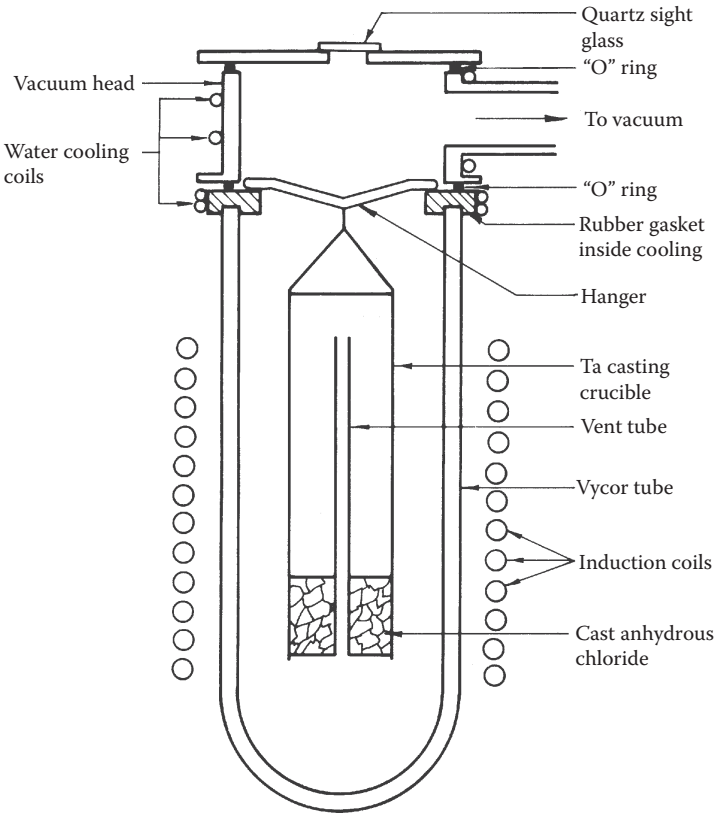


FIGURE 4.9 Apparatus for vacuum-casting the anhydrous rare-earth trichlorides. (From Croat, J.J., The preparation of high purity dysprosium, holmium and erbium by the lithium reduction of their trichloride salts, Report No. IS-T-346, Ames Laboratory, ERDA, Iowa State University, Ames, IA, National Technical Information Service, Springfield, VA, 1969.)

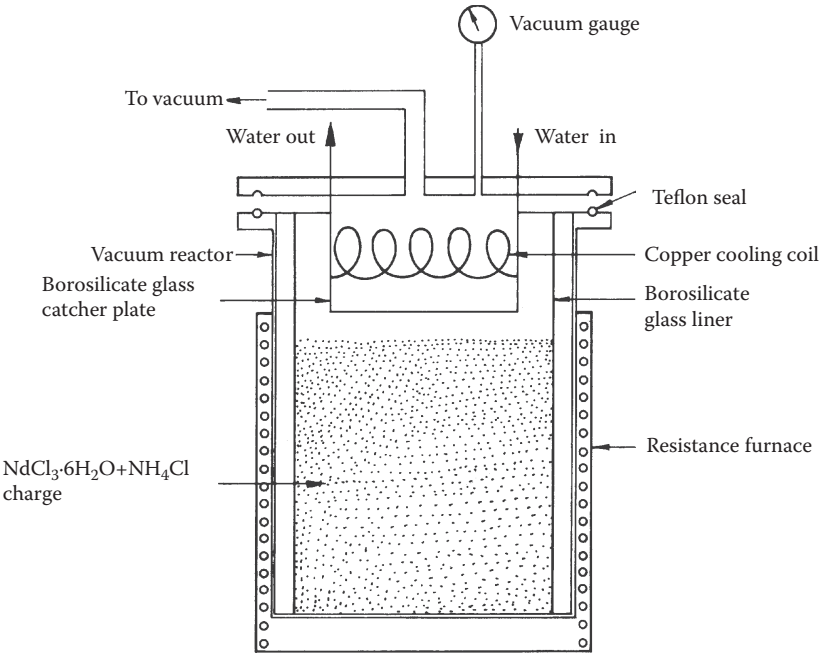


FIGURE 4.10 Apparatus for dehydrating neodymium chloride. (From Chambers, M.F. and Murphy, J.E., Molten salt electrolysis of neodymium from a chloride electrolyte. In Bautista, R.G. and Wong, M.M. (eds.), *Rare Earths*, pp. 369–376, The Minerals, Metals and Materials Society, Warrendale, PA, 1988.)

Chambers and Murphy (1988) used a glass-lined reactor, shown in Figure 4.10, for dehydration of neodymium chloride hexahydrate in a vacuum in the presence of ammonium chloride.

Hirschhorn (1967) has summarized the methods for dehydrating hydrated rare-earth chloride as used industrially in the 1940s. The hydrated chloride obtained by wet chemical treatment of monazite or bastnasite contained about 30% H_2O. It was dehydrated using methods that minimize oxidation or hydrolysis. The technique typically included heating in vacuum or heating in air with the admixture of a salt to reduce hydrolysis. The Auergesellschaft in Berlin used a rotary iron vacuum drum drier, steam-heated to 350°C at a vacuum of 90 kPa. The product had an oxychloride content of 1.5%. In Bavaria, Prometheus used a process involving heating a mixture of rare-earth chloride with $CaCl_2$ in air for 2–2.5 h. The yield was typically 62%, indicating that the dehydrated chloride contained substantial amounts of oxychloride. Treibacher Chemische Werke of Austria used a two-stage vacuum drying process in which the hydrate was heated first at 170°C and then at 350°C. While many dehydration techniques involve the addition of ammonium chloride to reverse hydrolysis, some commercial producers use sodium or calcium chloride to retard hydrolysis on the basis of common ion mass action effect.

4.4.3 Dry Methods

There are many dry methods to directly prepare anhydrous rare-earth chlorides. The method reported by Reed et al. (1935, 1939) involves the solid-state reaction of rare-earth oxide with ammonium chloride. By heating rare-earth oxide with twice the theoretically required quantity of ammonium chloride at about 190°C, complete conversion of the rare-earth oxide to rare-earth chloride occurred. Excess ammonium chloride was removed from the product by heating to 300–320°C under vacuum. About 85–95% of the rare earth present in the oxide was converted to anhydrous rare-earth chloride.

Another dry method involves the use of thionyl chloride in a sealed pressure vessel. Conversion was usually incomplete even after the temperature between 150°C and 300°C was maintained, and the treatment was continued for 3 days (Hecht et al. 1947).

Other dry methods for the preparation of anhydrous rare-earth trichloride used direct reaction of the metal carbide or the rare-earth oxide–carbon mixtures with a gaseous chlorinating agent, e.g., elemental chlorine. The method of directly chlorinating the rare-earth minerals–carbon mixture by chlorine was described earlier in Chapter 3 for monazite (Hartley 1952) and bastnasite (Brugger and Greinacher 1967). Actually, the process described for bastnasite by Brugger and Greinacher (1967) has been used on a production scale at Th. Goldschmidt AG. This process has also been useful for chlorinating other rare-earth ores like monazite, allanite, cerite, xenotime, euxenite, fergusonite, and gadolinite as well. The fused anhydrous chlorides of the rare earths obtained as final product are free from thorium chloride and any oxychloride and are suitable for the production of the corresponding metals. Using the same chlorinating procedure, one can convert pure rare-earth oxide to the corresponding anhydrous chloride.

Block and Campbell (1961) have described a method for chlorinating cerium and yttrium oxides, with a mixture of chlorine and carbon tetrachloride, in the presence of carbon. The oxides were mixed with an excess of carbon and a small amount of dextrin (binder) and were formed into pellets or nodules. The nodules were loaded into a vertical quartz tube in the apparatus shown in Figure 4.11 (Block et al. 1960) and heated to 600°C in the absence of air to decompose the dextrin. Either chlorine alone or carbon tetrachloride mixed with a small amount of chlorine was then passed up through the charge while it was heated to a temperature just below the melting point of the chloride. If the chlorides melt, they coat the unreacted particles of the charge. For cerium, temperatures between 750°C and 800°C were found to be optimum, and for yttrium, best results were obtained at 650°C. Approximately 95% of the rare earth present as the oxide was converted to the chloride in the above procedure. The product in these procedures was impure because of the presence of unreacted oxide and excess carbon and so needed a purification step.

Block et al. (1960) have also used yttrium oxalate in place of yttrium oxide–carbon mixture for chlorination. Yttrium oxalate was dried at 300°C for 8 h in the apparatus shown in Figure 4.11 and then was heated to 575°C while carbon tetrachloride was passed up through the charge. Chlorine was used as a carrier gas to sweep the carbon tetrachloride through the tube. Overall yttrium recoveries of only 75% were obtained

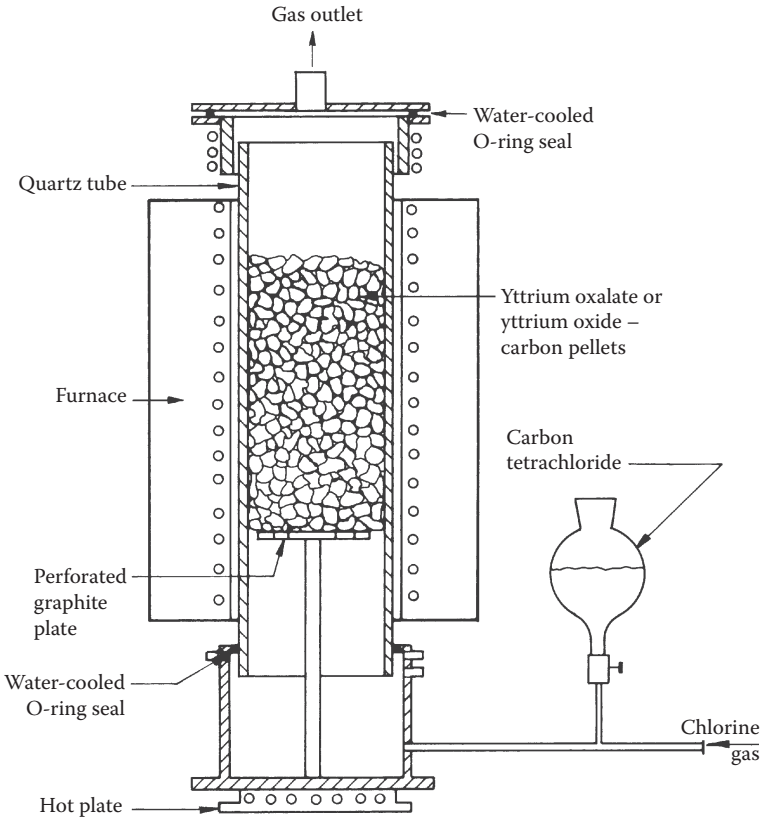


FIGURE 4.11 Yttrium chlorination apparatus. (From Block, F.E. and Campbell, T.T., Rare earth and yttrium halides for metal production—Chlorides, bromides and iodides. In Spedding, F.H. and Daane, A.H. (eds.), *The Rare Earths*, pp. 89–101, 1961. Wiley-VCH, Verlag. Reproduced with permission.)

by this procedure. Even though no carbon remained in the product from the reaction, it needed to be purified to separate it from unreacted yttrium compounds.

4.4.4 Purification of Rare-Earth Chlorides

The major impurity in rare-earth chloride is oxygen. It is present either as unconverted oxide or oxychloride. Carbon is another impurity, particularly when the chloride is prepared by a carbothermic reduction. Vacuum distillation and filtration are the two methods used for freeing the rare-earth chloride of oxygen-containing compounds, carbon, and several other impurities.

Purification by distillation was carried out by Block et al. (1960) in an apparatus shown in Figure 4.12. The raw yttrium chloride obtained after dehydration was loaded into the nickel container shown in the bottom of the retort. The pressure

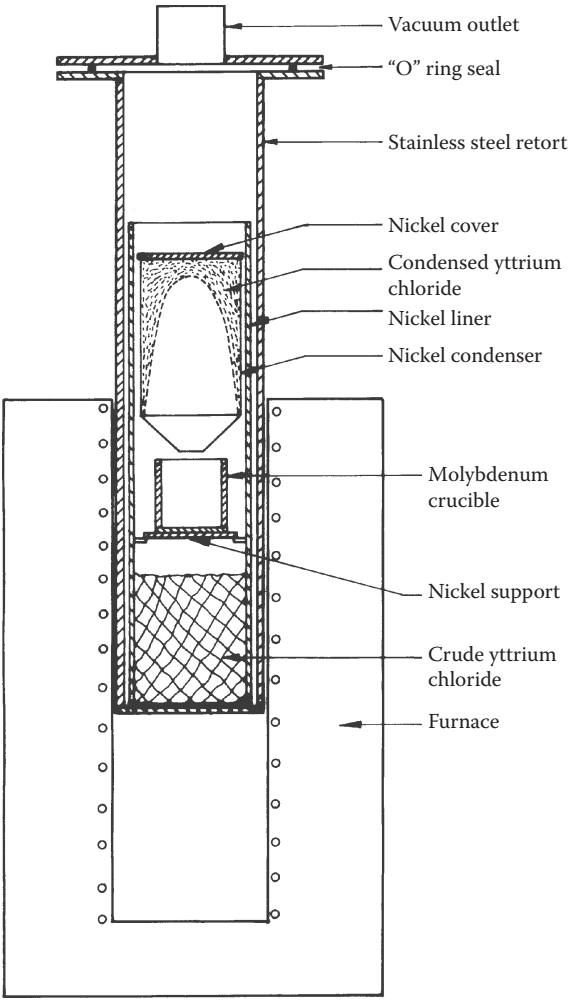


FIGURE 4.12 Yttrium chloride purification assembly. (From Block, F.E. and Campbell, T.T.: Rare earth and yttrium halides for metal production—chlorides, bromides and iodides. In Spedding, F.H. and Daane, A.H. (eds.), *The Rare Earths*. pp. 89–101. 1961. Copyright Wiley-VCH Verlag GmbH & Co. KGaA. Reproduced with permission.)

inside the retort was maintained between 5 and 50 mPa by continuous evacuation, while the lower end of the retort containing the charge was heated to between 850°C and 950°C. Yttrium chloride distilled and condensed in the upper cooler region of the retort. Distillation lasted 72 h to collect 20 kg of yttrium chloride. The retort was then backfilled with argon, and the furnace was repositioned to heat the upper section of the retort to 900°C. Heating was continued for 1 h to allow the yttrium chloride to melt and run down into the molybdenum crucible, which was placed midway between the charge container and condenser. Thus, yttrium chloride was cast

directly into the crucible, with minimum exposure to the atmosphere. Double distillation was done if an unusually large amount of impurities were present in the chloride. After the first distillation, the chloride was chipped off the nickel condensing shield and was loaded back into the lower container. The distillation was repeated. Between 90% and 95% of yttrium chloride charged to the retort was recovered in the purified product after vacuum distillation.

By vacuum distillation, not only the oxygen compounds are separated from the rare-earth chloride, but also the rare-earth chloride powder charge is converted into a dense crystalline mass. Even though the rare-earth chlorides are extremely hygroscopic, less hydration occurred when the crystalline mass was handled as it exposed considerably less surface to the atmosphere (Moriarty 1968).

It is more difficult to separate carbon than oxygen by vacuum distillation. A second distillation is usually necessary to bring down the carbon level to less than 0.2%. Repeated distillation is necessary if the rare-earth chloride is grossly contaminated. Solid impurities tend to entrain in the evaporating gas stream and are carried over to the condensate. Repeating the distillation results in their complete removal. As regards the overall recovery of rare-earth chloride after preparation and purification, Block et al. (1960) noted that better recoveries (~90%) were obtained when an initial wet procedure was followed by distillation.

Filtration of the molten chloride is another method useful for the purification of rare-earth chlorides (Block and Campbell 1961). This method was found to be especially effective for the separation of carbon from yttrium chloride. The molten chloride was allowed to drain through a pad of molybdenum wool, and the entire operation was carried out in an argon atmosphere. As long as there was no moisture in the system, molybdenum or nickel containers could be used to contain the molten chloride. Filtration was more effective than distillation for removing gross contamination. However, if the impurities were present in lower levels, distillation was more effective.

4.5 REDUCTION OF RARE-EARTH CHLORIDES

4.5.1 Early Attempts

The first recorded attempt at the preparation of a rare-earth metal is credited to C.G. Mosander (1827). As early as in 1826, he reduced cerium trichloride by heating it with potassium in a stream of hydrogen to obtain cerium metal powder. The product was, however, obtained in poor yield and was contaminated with excess reductant and reaction products. Following Mosander, several early attempts were made to reduce the rare-earth chlorides by sodium and other alkali metals (Trombe 1957). The product obtained was invariably a metal powder in poor yield, dispersed in alkali chloride slag. However, successful preparation of several light rare earths was reported by reduction of their chlorides with potassium and sodium vapor (Kremers 1925; Zintl and Neumayr 1933). To remove the excess reductant and its products, the as-reduced metal was vacuum annealed. Klemm and Bommer (1937) produced powder metals of all the rare earths except promethium. They carried out their reduction after sealing the rare-earth trichloride with potassium in quartz ampoules to avoid atmosphere contact. The ampoules were heated at 350–400°C, so that the rare-earth

chlorides would be reduced by potassium vapor. They succeeded in obtaining the rare-earth metals as small crystals intermixed with excess potassium reductant and potassium chloride slag. Even though they never compacted their metal into an ingot, the metals were pure and they measured fairly accurate lattice constants for most of the rare-earth metals.

The major investigations on the metallothermic reduction of rare-earth chlorides are summarized in Table 4.1. A powder product dispersed in slag results from insufficient heat of reaction to melt the reaction products. In the absence of an adequate supply of heat from an external source, (e.g., furnace heating), product melting and better slag–metal separation can be achieved primarily by (1) using a booster reaction to supplement the enthalpy of the main reaction and (2) forming a low melting reaction product such as the alloy and a multicomponent low melting slag. Cerium, neodymium, and gadolinium were obtained by reduction of their trichlorides with magnesium. As a result, a magnesium rare-earth alloy was obtained. On removal of magnesium by vacuum distillation, rare-earth metals with purities of 99.5–99.8% were obtained.

Following the earlier work of Moldenhauer (1914) and Karl (1934), calcium was also used to reduce cerium trichloride. Calcium in dolomite-lined steel bombs was used to reduce cerium trichloride securing kilogram levels of production of cerium metal. Here, additional heat necessary to melt and hence separate the reaction products was provided by using a calcium–iodine booster reaction. At the completion of the reduction, the slag was removed and the metal was vacuum-melted to remove any excess calcium or calcium chloride slag. The purity of cerium thus obtained

TABLE 4.1
Chloride Reduction Processes

Year	Reactants	Process	Results	Reference
1827	$CeCl_3$–K	Heated in hydrogen flow	Ce metal powder in slag matrix	Mosander 1827
1952	$RECl_3$–Ca; (La, Ce, Pr, Nd)	Heated in Ta crucible under vacuum	Consolidated RE separated from slag	Spedding and Daane 1952
1959	YCl_3–Na or Li	Heated in Mo/Ta crucible under inert gas	Y sponge; slag distilled off	Block and Campbell 1961
1960	YCl_3–Li	Li vapor reduction of YCl_3 in Ta crucible inside a steel bomb	Y crystals; slag distilled off	Nolting et al. 1960
1967	YCl_3–Ca, Mg	Heated to 950°C	Low-melting RE–Mg alloy; Mg distilled off	Carlson and Schmidt 1967
1968	$RECl_3$–Li; (La, Ce, Pr, Nd, Gd, Dy, Ho, Tb, Er, Lu, Y)	Li vapor reduction of $RECl_3$ in Ti crucibles inside steel bomb	RE crystals; slag distilled off	Moriarty 1968
1969	$RECl_3$–Li or Li–Ca; (Dy, Ho, Er)	Li vapor reduction of $RECl_3$	RE crystals; slag distilled off	Croat 1969

was greater than 98%, and the yields were approximately 95%. This technique was also used to prepare lanthanum, praseodymium, and neodymium metals apart from cerium metal.

4.5.2 Reduction in a Refractory Bomb

The schematic of the reactor used by Spedding et al. (1952) for carrying out the reduction is shown in Figure 4.13. The bomb (reactor) was constructed from standard black steel pipe by welding a bottom of 6 mm steel plate on one end and threading the top to receive a standard steel or cast iron pipe cap. To prevent contact of the reaction mixture with the steel wall of the bomb, a smooth surfaced refractory oxide liner was provided. The liner was a sintered lime or dolomitic oxide crucible inserted into the bomb and held in place by filling the narrow annular space between the crucible and the bomb walls with loose lime. On the top of the bomb, insulation was provided

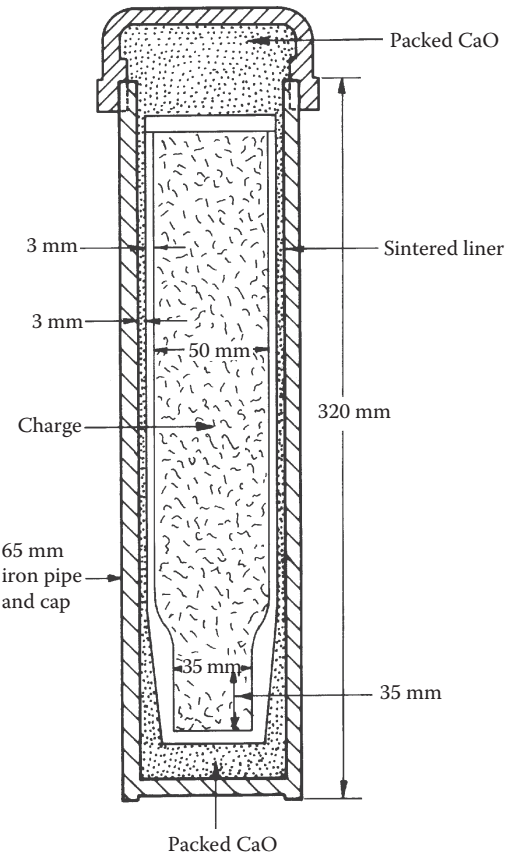


FIGURE 4.13 Loaded bomb for calciothermic reduction of rare-earth chloride. (From Spedding, F.H. et al., *Ind. Eng. Chem.*, 44: 553–556, 1952.)

by a layer of lime held in place by a sintered lime lid. The threads of the bomb were sealed effectively by plumber seal.

The bomb was filled with a thoroughly mixed charge of the powdered anhydrous rare-earth chloride, 20 mesh vacuum distilled calcium, and iodine in the ratio of 0.63 mol of iodine per mole of cerous chloride ($CeCl_3$) with 15% more calcium than the stoichiometric amount needed for the reaction. Reaction was initiated by placing the loaded and sealed bomb in a gas-fired furnace held at 650–750°C. As the bomb temperature reached about 400°C, the reaction began and was going to completion in a matter of seconds, which was indicated by the sudden rise of the bomb temperature. The heat of the reaction was found to be sufficient to melt both the slag and the metal and allow the metal to collect in the form of a massive cylinder in the bottom of the bomb. The bomb was removed from the furnace as soon as it fired and was allowed to cool before being opened.

The ingot obtained was invariably very clean with smooth sides and top and contained 1–5% calcium and 0.1–1% magnesium. The average yield of the metal in the ingot weighing 150–175 g per run was approximately 94%. The contaminants in the as-reduced metal were brought down to less than about 200 ppm each by remelting the metal in a magnesia or beryllia crucible in vacuum. Spedding et al. (1952) carried out much of the initial experiments with cerium but noted that, with respect to yields, contamination by calcium and magnesium, and quality of ingots, the results of cerium were duplicated by lanthanum, neodymium, and praseodymium. Kilogram quantities of these metals in high purity were prepared by this technique in addition to over 500 kg of 95–99% pure cerium on a 1.5 kg per batch scale.

Spedding and Daane (1954) noted that this method was capable of producing very pure metals if sufficient care was taken to introduce only pure rare-earth chloride, pure calcium, and pure iodine into a pure liner because, in the entire system, which was closed, no impurities could get into the metal other than calcium, magnesium, or oxygen. Both calcium and magnesium could be distilled out on remelting but oxygen remained. To prevent the introduction of oxygen, the calcium was handled in an inert atmosphere and the bomb was loaded in an argon atmosphere glove box. Considerable care had to be taken to ensure that the chlorides were completely anhydrous and free of oxychlorides because even small amounts of these materials could lead to high oxygen content in the metal and also poor yields. If too much moisture was present, it would invariably lead to explosions of the sealed bomb.

When only rare-earth chloride and calcium were used in the charge, the heat liberated by the reaction (on this scale, namely ~170 g) was not sufficient to heat the resulting rare-earth metal and calcium chloride slag to above their melting points. As a result, the rare-earth metal could not agglomerate into a massive ingot. Iodine was added as the booster, and the extra heat liberated by the Ca–I exothermic reaction was sufficient to heat the reaction products to beyond their melting temperatures and hence enabled the rare-earth metal to collect into a fused mass. Iodine also served to form a lower melting slag of $CaCl_2$–CaI_2. In an effort to find a substitute for the iodine, which was expensive, sulfur and potassium chlorate were also investigated as boosters (Spedding et al. 1952). The use of sulfur generated considerable heat, but no separation of the metal and slag occurred. Potassium chlorate, even under the best conditions, did not produce cerium metal in yields comparable to that obtained

with iodine, either externally with respect to adhering slag or internally with respect to inclusions.

The method described above for the preparation of cerium, lanthanum, praseodymium, and neodymium metals by reduction of their chlorides by calcium with iodine as a booster was also tried for yttrium (Spedding et al. 1952). Although the reaction proceeded vigorously enough to permit complete slag collection, apparently sufficient heat was not generated to fuse the metal, and the yttrium produced was intimately mixed with the slag. The unsuccessful attempt was attributed to the high melting point (1522°C) of yttrium. This procedure was not successful with even the relatively low melting gadolinium (1313°C). It turned out that the method could not be applied to metals melting at a temperature above the melting point of neodymium (1021°C).

4.5.3 Reduction in a Tantalum Crucible

Two major problems confronted the attempts made to prepare high melting rare-earth metals by chloride reduction. At high temperatures, the calcium chloride frothed and thus prevented clean slag–metal separation, and the oxide liners were attacked by the metal and impurities were introduced. Subsequently, Spedding and Daane (1952) attempted the reduction in a tantalum crucible. The procedure was as follows.

In a typical run, 70 g of rare-earth chloride and 18.5 g of calcium were thoroughly mixed in an inert atmosphere and either jolt packed into a tantalum crucible or compacted in a powder press into cylinders that were then placed in the tantalum crucible. This charge contained 10% more calcium than was required by the stoichiometry of the reaction

$$2MCl_3 + 3Ca \rightarrow 3CaCl_2 + 2M$$

in which M represents a rare-earth element. The loaded, outgassed crucible was covered with a tantalum lid, perforated to permit gas to enter or leave the vessel, and was placed inside a covered magnesia crucible (50 mm in diameter and 175 mm long). This was, in turn, placed inside a silica tube (58 mm diameter), one end of which was fused shut and the other end ground to serve as the inner half of a 55/50 standard taper joint. The silica tube was sealed onto a vacuum system evacuated to 0.1 Pa and then filled to 1 atm with argon, which was purified by passing it over hot uranium turnings. The tantalum crucible was heated by means of a 6 kW induction furnace. At 550–600°C, the exothermic reaction between calcium and the rare-earth chloride occurred as evidenced by the sudden increase in the temperature of the crucible. In about 5 min, the final holding temperature could be reached, and at this temperature, the crucible was held for 13 min to permit complete coalescence of the product metal. The final holding temperature was 1000°C for lanthanum, cerium, praseodymium, and neodymium and 1350°C for gadolinium. After cooling to room temperature, the tantalum crucible was soaked in water to remove the calcium chloride slag and most of the excess calcium, leaving in the crucible bottom a layer of fused rare-earth metal containing from 1% to 3% calcium. This impurity could be removed by remelting the metal under 0.1 Pa or better in the same crucible and

vacuum apparatus. The remelting temperature was 1200°C for lanthanum, cerium, praseodymium, and neodymium and 1350°C for gadolinium.

Lanthanum, cerium, praseodymium, and gadolinium metals were prepared by this technique in 40 g lots with yields consistently exceeding 99%. Calcium content in the remelted product metal was not over 150 ppm. The use of booster reaction was not necessary because external heating was used, and tantalum was more resistant to molten rare-earth-metal attack than any refractory material.

4.5.4 Intermediate Alloy Processes

The chloride reduction as described for the five metals could not be applied to the higher melting metals because of excessive chloride volatilization and decreased yields. The main problem was the need to use high temperatures so that the metal product would be molten at the reaction temperature. The need for high temperatures for reaction was overcome by preparing the metal as a low melting alloy. Carlson and Schmidt (1967) investigated the preparation of yttrium metal as an yttrium–magnesium alloy by calcium reduction of yttrium trichloride in the presence of magnesium. The excess calcium and magnesium were removed from the yttrium product by a subsequent heat treatment in vacuum.

A similar process was used by Schmidt and Carlson (1974) to prepare scandium metal by reducing scandium trichloride with calcium and/or magnesium. The calcium and magnesium from the as-reduced scandium were removed by vacuum heat treatment. Yttrium and scandium from alloys with magnesium will become molten at reaction temperatures that are considerably lower than the melting points of yttrium and scandium. Clean slag–metal separation was therefore possible.

4.5.5 Kroll-Type Processes

An effective method for rare-earth-metal preparation at reaction temperatures less than the metal's melting point is to obtain the metal in a sponge form, as in the Kroll process for titanium (Kroll 1959).

4.5.5.1 Lithium/Sodium Reduction of Yttrium Chloride

Block et al. (1960) prepared large quantities of high-purity yttrium metal by reducing the chloride with both lithium and sodium. The stainless-steel vacuum retort used for lithium reduction is shown in Figure 4.14. Both lithium and yttrium chloride react with moisture in the atmosphere. Hence, handling operations, as far as possible, were performed in an inert atmosphere glove box. High-purity lithium, 10–15% more than the stoichiometric amount required for reaction, was added to the molybdenum crucible containing yttrium chloride. The loaded crucible was transferred to the reduction distillation assembly. The retort was then evacuated to 0.01 Pa and backfilled to 35 kPa with argon. The charge was heated to 850°C for 1 h to complete the reaction, and thereafter, the retort was evacuated again while it was heated to 900°C for 16 h to remove the excess lithium and lithium chloride from the yttrium sponge. Block et al. (1960) used batch sizes of up to 1 kg of yttrium chloride in the assembly shown, and yttrium recoveries were between 95% and 100%.

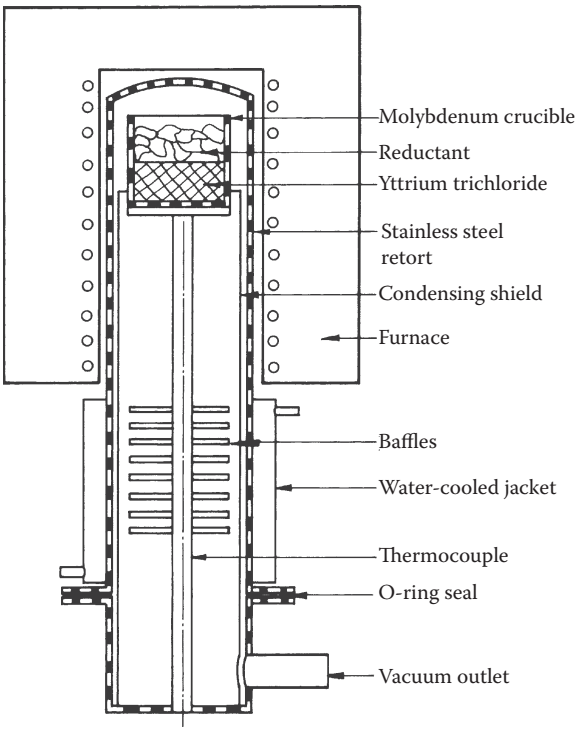


FIGURE 4.14 High vacuum reduction distillation assembly. (From Block, F.E. et al., Preparation of high purity yttrium by metallic reduction of yttrium trichloride, Bureau of Mines Report of Investigations 5588, U.S. Department of the Interior, Washington, DC, 1960.)

This procedure was also carried out in a larger assembly designed for preparing up to 9 kg of yttrium sponge per batch. The reduction temperature was 900°C, and holding time was maintained for 4 h and 45 min. After reduction, the crucible was inverted before the by-products were removed by vacuum distillation at 950°C for 24 h. Inverting the crucible allowed bulk of the excess lithium and lithium chloride to melt and run out of the crucible, thereby minimizing the time required for vacuum distillation.

The apparatus shown in Figure 4.15 was used by Block et al. (1960) for carrying out the sodium reduction of yttrium chloride. The batch size was 0.7 kg of yttrium chloride. Purified yttrium chloride was charged into a molybdenum crucible in the bottom of the stainless-steel retort, and excess sodium was placed in the steel container in the upper section of the retort. The loaded reduction retort was evacuated and filled with argon to between 7 and 15 kPa above atmospheric pressure. The lower section of the retort was heated to 850°C to melt the yttrium chloride, after which the section containing the sodium was heated at a temperature high enough to vaporize sodium, allowing the sodium vapors to react with the yttrium chloride until the reaction was complete, which took 5–7 h. This procedure, which is very similar to

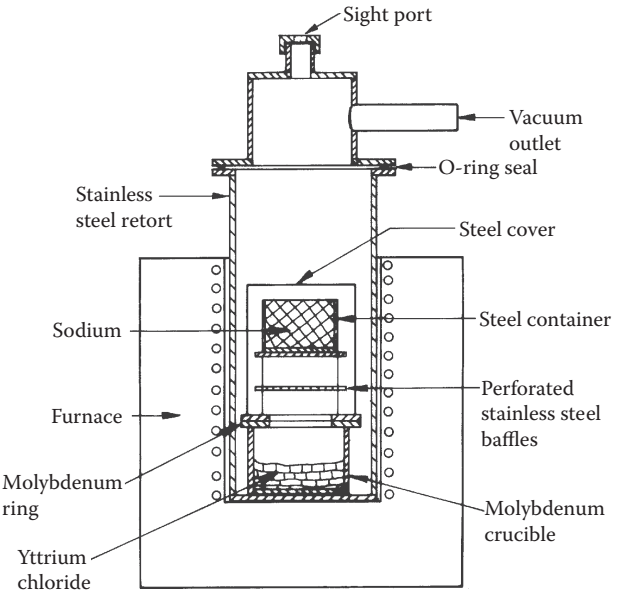


FIGURE 4.15 Metallic reduction assembly. (From Block, F.E. et al., Preparation of high purity yttrium by metallic reduction of yttrium trichloride, Bureau of Mines Report of Investigations 5588, U.S. Department of the Interior, Washington, DC, 1960.)

the Kroll process for zirconium, has the advantage of combining distillation purification of sodium with a facility for controlling the reaction. After the reaction was complete, the retort was rotated slightly beyond 90° from the vertical position, and the bulk of the excess sodium and sodium chloride were poured out of the crucible. The retort was then evacuated, and heating was continued to 850°C to remove the last traces of sodium and sodium chloride. Vacuum distillation without first pouring out the bulk of sodium invariably led to reverse reaction in which yttrium reduced the sodium chloride. As an alternative, after reduction, the retort could be cooled, the crucible inverted, and vacuum separation done as with the large-batch lithium reduction procedure.

Metal yields were between 95% and 99% in lithium reductions and between 61% and 85% in sodium reductions. The representative analysis of yttrium prepared by both lithium and sodium reduction is listed in Table 4.2. Yttrium produced by sodium reduction was lower in both carbon and oxygen impurities than that obtained by lithium reduction.

Nolting et al. (1960) and Moriarty (1968) have also used lithium vapor reduction of rare-earth trichloride to prepare yttrium and other high-melting rare-earth metals.

4.5.5.2 Lithium Reduction of Yttrium Chloride

Nolting et al. (1960) carried out the reductions in the reactor shown schematically in Figure 4.16. The stainless-steel reactor was 75 mm in diameter and 560 mm long. The reactor was lined with 0.25-mm-thick molybdenum foil. Two 100-mm tantalum

TABLE 4.2
Analysis of Arc-Melted Yttrium Buttons

	Impurity Content (ppm)										
Reductant	**O**	**N**	**C**	**Al**	**Na**	**Li**	**Fe**	**Cr**	**Ni**	**Si**	**Mo**
Lithium	270	40	260	80	150	<1	400	100	70	<10	90
Sodium	125	60	120	30	100	<1	200	100	200	10	62

Source: Block, F.E. et al., Preparation of high purity yttrium by metallic reduction of yttrium trichloride, Bureau of Mines Report of Investigations 5588, U.S. Department of the Interior, Washington, DC, 1960.

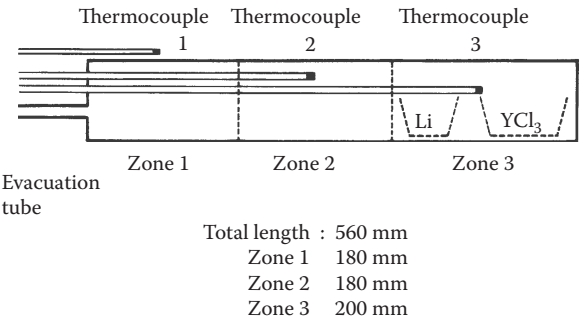


FIGURE 4.16 Reduction bomb assembly. (From Nolting, H.J. et al., *J. Inorg. Nucl. Chem.*, 14, 208–216, 1960.)

boats (reduction crucibles) containing lithium and yttrium chloride were placed as shown in the figure. The reduction crucibles were shaped to conform to chamber geometry, and they were placed on a tray constructed from 0.5 mm tantalum sheet. A 0.125 mm titanium foil was used as an additional liner and as a getter for gaseous contaminants.

Purified anhydrous yttrium chloride weighing 305 g and clean lithium weighing 40 g were placed in the respective containers and positioned adjacent to each other in zone 3 of the bomb chamber, after which the reactor was closed by welding the faceplate into position and the chamber was evacuated to 6 Pa. The reduction was initiated by placing the evacuated chamber in a preheated reduction furnace in a horizontal position. The bomb heated to 950°C in 15 min, and this temperature was maintained for 2 h over the entire length of the bomb. Within 5 min of exposure to temperature, the evacuation tube sealed due to condensation of lithium vapor. Lithium vapor reduced yttrium trichloride and the reduction was complete in 2 h. At the end of 2 h, the bomb was positioned so that the faceplate protruded out of the furnace opening and an airblast was directed at the faceplate. The furnace temperature was raised so that within 30 min, the temperature was steady at 1000°C in zone 3, 950°C in zone 2, and 400–500°C in zone 1. This gradient was maintained

for 12 h to ensure complete removal of lithium chloride slag and excess lithium from the as-reduced yttrium crystals. The slag and excess reductant distilled off to the cooler surface. The reactor was then removed from the furnace and cooled. The bomb chamber was cut open in zone 2 at the thermocouple position, and argon gas was flushed into the chamber. The product was 125 g of bright crystalline yttrium sponge, representing over 90% yield. Some of the crystals adhered to the tantalum crucible. Yttrium thus obtained was 99.8% pure with 0.16% oxygen as the major residual impurity. Nitrogen, carbon, and chloride contents were 0.006%, 0.007%, and 0.01%, respectively. The total nonmetallic content in the yttrium thus obtained was reported by Nolting et al. (1960) to be only 0.17%. The yttrium crystals were consolidated by arc melting.

4.5.5.3 Lithium Reduction of Rare-Earth Chlorides

Lithium reduction of rare-earth trichlorides was adopted on a commercial scale by Moriarty (1968). The reactor used for this purpose is shown (Beaudry and Gschneidner 1978) in Figure 4.17. Crude rare-earth chloride was placed in a titanium crucible with a tube down the center. A second titanium crucible was placed below it, and they were separated by a spacer. Both crucibles were placed on a pedestal inside a stainless-steel chamber. Chunks of commercial-grade lithium were placed around the pedestal. The chamber was evacuated and the upper titanium crucible

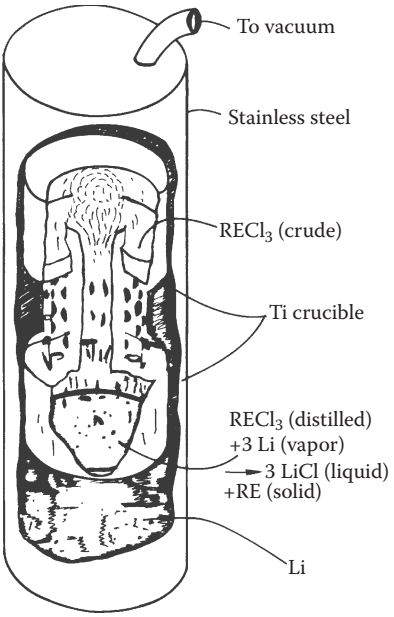


FIGURE 4.17 Reduction crucible used for lithium reduction of rare-earth chlorides. (From Beaudry, B.J. and Gschneidner, Jr., K.A., Preparation and basic properties of rare earth metals. In Gschneidner, Jr., K.A. and Eyring, L. (eds.), *Handbook on the Physics and Chemistry of Rare Earths*, vol. 1, pp. 173–232, North Holland, Amsterdam, 1978.)

was heated to distill the rare-earth trichloride into the lower crucible. After distilling the chloride, the entire steel chamber was heated to 800–1000°C. The lithium vapor filled the chamber, and some of the lithium condensed in the vacuum line, sealing the chamber. The lithium vapor reacted with the molten rare-earth chloride, reducing it to rare-earth metal and forming lithium chloride slag. After the reduction was complete, the steel chamber was partially removed from the furnace, and the lithium chloride slag was distilled from the reduction crucible to that part of the steel chamber that was outside the furnace and hence colder. After completing the distillation, the sealed steel chamber was opened and the rare-earth-metal crystals were consolidated by arc melting or induction melting. Moriarty (1968) reported the preparation of all of the rare-earth metals except promethium, samarium, europium, and ytterbium, using the lithium vapor reduction method described. The relatively low temperature of the reduction (800–1000°C) ensured that the contamination of the reduced rare-earth-metal crystal with the crucible material was very low. The major impurity in these metals was oxygen, which ranged from 225 ppm for holmium to 1600 ppm for terbium. The nitrogen content was below 40 ppm for all the metals. The yields of recoverable metals were between 77% and 86% after reduction at 1000°C.

4.5.5.4 Lithium Reduction of Dysprosium, Holmium, and Erbium Chlorides

The reduction of dysprosium, holmium, and erbium trichlorides with lithium was studied by Croat (1969). The anhydrous chlorides were reduced at 900°C using lithium–5% calcium or pure lithium as the reductant. The liquid–vapor reduction was carried out in two steps: (1) distillation of the lithium vapor into liquid rare-earth chloride at the reduction temperature and (2) distillation of the lithium chloride slag and excess reductant away from the product on completion of the reduction. Prior to reduction, the rare-earth chloride was purified by one or more distillation operations. As regards the lithium reductant, approximately 5% calcium was added to the reductant in order to make the lithium vapor purer during distillation. During the liquid–vapor reduction process, a certain amount of calcium also distilled and reduced the rare-earth chloride. Excess calcium and calcium chloride slag were easily removed along with the lithium chloride and excess lithium.

The reduction was entirely carried out in tantalum crucibles and retort. All operations beyond the initial preparation of the chlorides were carried out inside a controlled atmosphere glove box.

The reduction was carried out inside the glove box furnace as shown in Figure 4.18. The tantalum retort used both for distilling and reducing the rare-earth chloride is also shown positioned in the furnace in the figure. The retort measuring 300 mm in length and 83 mm in diameter was made of 0.75-mm-thick tantalum. The bottom and top ends of the retort were of 0.25-mm-thick tantalum and contained thermocouple wells for measuring the interior temperature. The retort lid also contained a tantalum vent tube extending up through a hole in the top radiation shielding. This tube allowed the retort to be welded shut in the glove box and then evacuated and maintained under a dynamic vacuum during the distillation of the chlorides. This vent tube sealed itself with lithium during reduction.

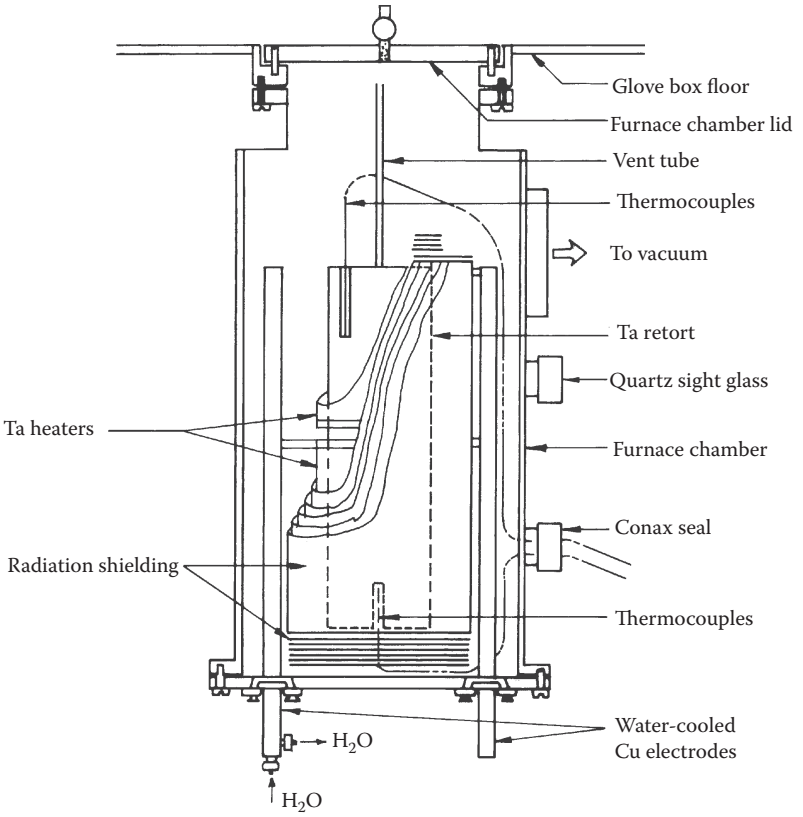


FIGURE 4.18 Schematic diagram of the glove box furnace used for rare-earth-metal reduction. (From Croat, J.J., The preparation of high purity dysprosium, holmium and erbium by the lithium reduction of their trichloride salts, Report No. IS-T-346, Ames Laboratory, ERDA, Iowa State University, Ames, IA, National Technical Information Service, Springfield, Virginia, 1969.)

The rare-earth chloride was purified by distillation, and only the purified chloride was used for reduction. The distillation assembly shown schematically in Figure 4.19 was made of tantalum and consisted of an inverted crucible, a spacer, and a reduction crucible resting on a pedestal at the bottom of the retort. During distillation, the chloride vapor passed from the inverted crucible by way of a tube welded in the bottom and extending upward to within 13 mm of the lid and downward to a point approximately 13 mm inside the reduction crucible.

The reduction apparatus, shown schematically in Figure 4.20, had a reduction crucible and a spacer placed on a pedestal at the bottom of the retort. Essentially, the distillation apparatus becomes the reduction apparatus by removing the distillation crucible and positioning the reduction crucible at the top rather than at the bottom of the retort.

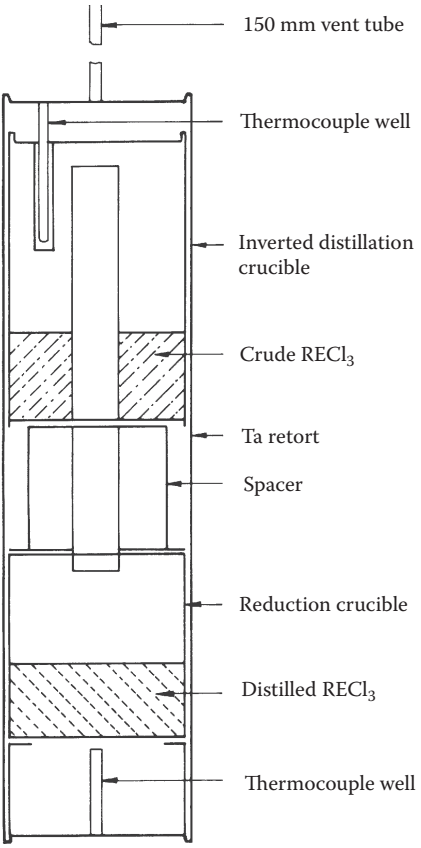


FIGURE 4.19 Schematic diagram of the distillation apparatus. (From Croat, J.J., The preparation of high purity dysprosium, holmium and erbium by the lithium reduction of their trichloride salts, Report No. IS-T-346, Ames Laboratory, ERDA, Iowa State University, Ames, IA, National Technical Information Service, Springfield, Virginia, 1969.)

Prior to reduction, the chlorides were purified by distilling them in the distillation assembly shown in Figure 4.19. The distillation crucible was loaded with cast chlorides and covered with a tight-fitting crucible lid. The loaded distillation crucible, reduction crucible, and spacer were loaded in the tantalum retort, and the lid of the retort was welded in place. The assembly was placed into the furnace, which was then evacuated to a maximum pressure of 10^{-4} Pa. The retort was evacuated simultaneously through the vent tube. The required temperature gradient for distillation was provided by heating only the top of the retort by the upper heating element of the furnace. Dysprosium chloride was distilled at 850°C, holmium chloride at 875°C, and erbium chloride at 910°C, and the distillation rate was 1 g/min. For some runs, the distillation was repeated once more and doubly distilled chloride was used for reduction.

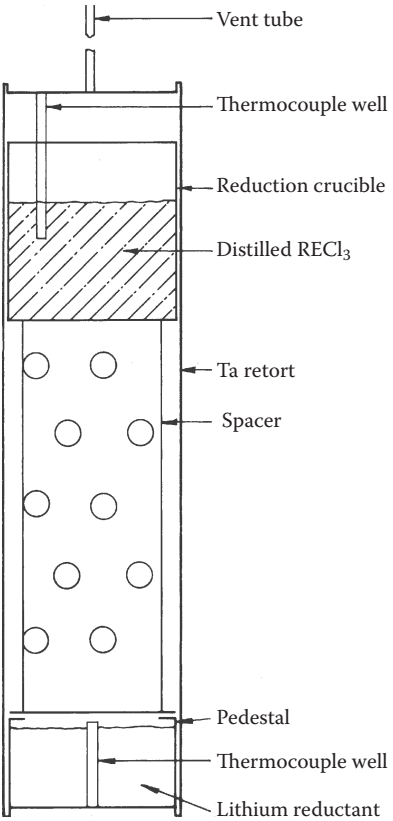


FIGURE 4.20 Schematic diagram of the reduction apparatus. (From Croat, J.J., The preparation of high purity dysprosium, holmium and erbium by the lithium reduction of their trichloride salts, Report No. IS-T-346, Ames Laboratory, ERDA, Iowa State University, Ames, IA, National Technical Information Service, Springfield, Virginia, 1969.)

The same retort in which the chlorides were distilled was also used for reduction. The reductant, lithium–5% calcium, was loaded into the bottom of the retort, the spacer was inserted, and the reduction crucible containing the distilled chlorides was loaded in the top as shown in Figure 4.20. The lid of the retort was rewelded, and the retort was positioned in the furnace. The bottom of the retort was first heated to 300°C to outgas the reductant and allow the formation of the less volatile CaO at the expense of volatile Li_2O. The entire retort was then heated to 900°C to carry out the reduction. The temperature was maintained for 2 h for every 100 g of chloride. After the reduction was complete, the bottom furnace was turned off and the top furnace was maintained at 900°C to distill the lithium chloride slag and any excess calcium out of the reduction crucible to the bottom of the retort. For every 100 g of rare-earth chloride reduced, the LiCl distillation temperature was maintained at 900°C for 1 h followed by 550°C for 2 h and 450°C for 2 h. The corresponding temperatures at the bottom of the retort were 640°C, 360°C, and 290°C, respectively. After completion

of the reduction schedule, the retort was opened by cutting off the welded flange, and the reduction crucible containing the as-reduced metal was removed from the retort and placed on a pedestal inside the vacuum furnace. It was then heated at 7×10^{-5} Pa and 950°C for several hours to ensure complete removal of any traces of lithium chloride and excess lithium reductant. The product, as reduced metal, was then recovered as bright, loosely packed crystals. The purity of as-reduced metals from singly distilled anhydrous chlorides averaged 99.94 wt.% or 99.2% atomic. Oxygen and hydrogen contents were quite high: approximately 500 and 15 ppm, respectively. The oxygen and hydrogen contents of metals prepared from doubly distilled chlorides are much lower, as shown in Table 4.3. The purity of a reduced metal prepared from doubly sublimed chlorides was 99.9% atomic. Less than 3 ppm each of F and Cl was present in the as-reduced metal, and no lithium was detected. The tantalum contents were below 30 ppm.

Croat (1969) carried out the reductions in batches ranging from 0.2 to 1 kg, and 20% excess reductant was used. The average yields of reduced metal from the chloride were approximately 96%, whereas the overall yields of oxide to as-reduced metal were approximately 79%.

The method of producing pure rare-earth metals by the chloride reduction route, though feasible for most of the metals, is usually an elaborate procedure requiring great procedural care and experimental facilities, particularly on account of their hygroscopicity and volatility. These two limitations are, to a large extent, circumvented by the use of fluorides in place of chlorides in the metal reduction procedures.

TABLE 4.3
Analysis of As-Reduced Dysprosium–Holmium and Erbium Obtained by Chloride Reduction

	Content, ppm		
Impurity	**Dysprosium**	**Holmium**	**Erbium**
H	6	5	10
Li	nd	nd	nd
C	39	17	11
N	7	3	7
O	135	81	109
F	<3	<3	<3
Cl	<3	<3	<3
Cr	2	<1	1.5
Fe	2	11	2
Ni	0.4	1	2

Source: Croat, J.J., The preparation of high purity dysprosium, holmium and erbium by the lithium reduction of their trichloride salts, Report No. IS-T-346, Ames Laboratory, ERDA, Iowa State University, Ames, Iowa, National Technical Information Service, Springfield, Virginia, 1969.

Note: Chlorides were doubly distilled before reduction; nd: not detected.

As will be seen shortly, it turned out that the fluoride reduction method is technically more perfect than the chloride route for most of the rare-earth metals in that the fluoride route satisfies more criteria as stated by Herget (1985) for a good metallothermic reduction method.

The preparation of rare-earth metals through the fluoride route essentially has two major steps. One is the preparation of anhydrous rare-earth fluoride starting from the oxide, and the other is the reduction of the fluoride to the metal.

4.6 PREPARATION OF RARE-EARTH FLUORIDES

The preparation of rare-earth fluorides for use as intermediates for reduction has been accomplished by two routes—the wet route and the dry route. The wet route involves the precipitation of fluoride from aqueous solution followed by dehydration of the hydrated rare-earth fluoride. In the dry route, the oxide is directly converted to anhydrous fluoride by reaction with HF or ammonium hydrogen fluoride.

4.6.1 Wet Method

This method consists of precipitation of hydrated rare-earth fluoride from an aqueous solution followed by a dehydration step. The reactions involved are as follows:

$$RE_2O_3 + 6HCl\ (aq) \rightarrow 2RECl_3 \cdot xH_2O$$

$$RECl_3 \cdot xH_2O + HF\ (48\%\ aq) \rightarrow REF_3 \cdot x'H_2O$$

$$REF_3 \cdot x'H_2O \xrightarrow[\text{or } 600°C \text{ in HF gas}]{300 \text{ in vacuum}} REF_3 + H_2O$$

In the above equations, x is usually 6 and x' is 1/2 or 1. The rare-earth oxide is dissolved in hydrochloric or nitric acid. Addition of aqueous hydrofluoric acid to this solution results in the precipitation of hydrated fluoride, which is recovered by decantation or filtration. The product is dried at 100–150°C in air to remove adhering moisture and then heated at 300°C in a vacuum or at 600° C in an anhydrous HF stream to thermally decompose the hydrate.

For the aqueous hydrofluorination of rare-earth solutions and to handle aqueous hydrofluoric acid and fluoride chloride solutions, plastic reaction vessels and filtration units are used. Carlson et al. (1956) have used this method of precipitation, filtration, and air-drying to prepare 50 kg lots of lanthanum, cerium, and yttrium fluorides. Treatment of the air-dried rare-earth fluoride in an anhydrous HF stream has been carried out in a piece of equipment normally used for the dry hydrofluorination.

Minor variations from the general procedure could be found in specific cases of rare-earth fluoride preparation by the aqueous route. In one approach, yttria was dissolved in hydrochloric acid, and the solution was concentrated by evaporation to obtain $YCl_3\ 6H_2O$ crystals. The addition of 70% HF to these crystals results in the formation of $YF_3\ 1/2H_2O$. In another approach, liquid anhydrous HF was used.

Liquid HF can be obtained by condensing the vapors in a copper coil immersed in a dry ice bath. Dripping of liquid HF into a YCl_3 solution at 100°C results in the precipitation of $YF_3 1/2\ H_2O$, which is readily filterable. In general, hydrated fluoride precipitates are gelatinous and difficult to filter from the aqueous solution.

Carlson et al. (1956) have noted that aqueous methods yield YF_3 with slightly more oxygen content than the dry methods. The oxygen content could be lowered in the purification step.

4.6.2 Dry Methods

4.6.2.1 Reaction of Rare-Earth Oxides with Anhydrous HF

The method consists of passing anhydrous HF gas directly over the oxide at elevated temperatures. The overall reaction is as follows:

$$RE_2O_3 + 6HF \rightarrow 2REF_3 + 3H_2O$$

For most of the rare earths, good conversion was obtained at 700°C in 8 h. A stationary bed type of furnace was quite adequate for preparing RF_3 in quantities of 500 to 1000 g (Carlson and Schmidt 1961a). The reactor consisted of a horizontal inconel tube having an inlet line for anhydrous HF and an outlet line for the gaseous products. The rare-earth oxide was placed in a platinum tray inside the inconel tube, which may also be lined with platinum. The tube was heated to 700°C by an electrical resistance furnace. At this temperature, to produce a high-quality product in an 8-h period, an excess of approximately 200% of HF gas was required. The product (fluoride) was allowed to cool, and any HF gas adhering to it was removed by vacuum/flushing with helium.

Lanthanum, cerium, neodymium, samarium, europium, gadolinium, terbium, dysprosium, holmium, erbium, thulium, ytterbium, lutetium, and yttrium fluorides have been prepared using this method. The fluoride conversion achieved in this process ranged from 99.90% to 99.98%.

The production of rare-earth fluorides on a larger scale by direct reaction of Y_2O_3 with HF gas has been carried out by (1) rotary batch method, (2) fluidized bed method, and (3) vibrating tray method.

4.6.2.1.1 Rotary Batch Method

A sketch of the unit used for large-scale hydrofluorination by the rotary batch method (Banks et al. 1959) is shown in Figure 4.21. High-purity yttrium oxide was loaded into the inconel inner tube, which was then inserted into another inconel tube that could be rotated. The tube was closed and the HF gas lines were connected to the system. The HF gas was turned on when the temperature of the furnace reached 150°C. The temperature was gradually raised to 750°C over a period of about 6 h. After a lapse of about 1 h at 750°C, the inconel tube was rotated for 5-min periods at 10-min intervals. This rotation sequence was continued for a 2 h period after which the furnace and HF flow were turned off. The fluoride was cooled in the furnace for 12 h after which the liner containing YF_3 was removed and flushed with helium.

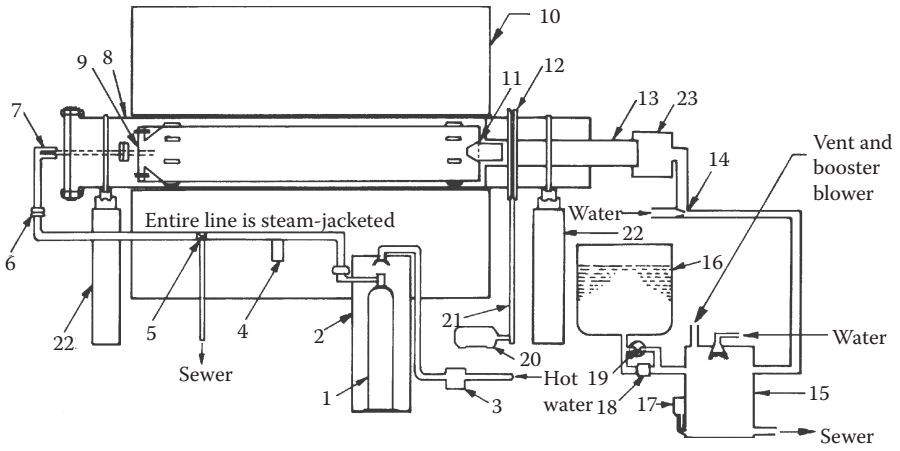


FIGURE 4.21 Furnace and rotary equipment for hydrofluorination of yttrium oxide. 1. Hydrogen fluoride cylinder; 2. spray chamber; 3. solenoid chamber; 4. manometer; 5. check valve; 6. union; 7. Teflon universal seal (inlet); 8. inconel outer tube; 9. inconel inner tube; 10. electric furnace; 11. dust trap; 12. chain sprocket; 13. nickel exit tube; 14. water aspirator; 15. neutralizing tank; 16. soda ash neutralizing solution; 17. Beckman pH meter; 18. valve to pH controller; 19. bypass valve; 20. AC motor (1 HP); 21. chain; 22. bearing supports; 23. Teflon universal seal (outer). (From Banks, C.V. et al., Studies on the preparation, properties and analysis of high purity yttrium oxide and yttrium metal at the Ames Laboratory, IS-1, National Technical Information Service, Springfield, Virginia, 1959.)

The fluoride was removed from the liner, evacuated, flushed, ground, and stored in polyethylene bags inside metal containers.

A critical parameter in the method described was the amount of draft on the fluoride bed produced by the exhaust system. This draft ensured adequate sweep of HF over the salt. The amount of HF used was approximately 250% over the stoichiometric amount. About 25 kg of high-purity Y_2O_3 was loaded in each batch in the reactor, and the yttrium fluoride product had an oxygen content in the range of 400–1000 ppm. Using this method, over 30,000 kg of high-quality YF_3 was prepared at Ames Laboratory over a 2-year period.

In the above method, the rotary motion of the reactor eliminates the problem of formation of yttrium fluoride crust on the surface of unreacted yttrium oxide. For example, in a static bed, if 25 kg or more of Y_2O_3 were hydrofluorinated, the increase in the depth of the oxide bed and formation of crust inhibit the diffusion of HF gas into the unreacted oxide and resulted in poor conversions.

4.6.2.1.2 Fluidized Bed Method

Fluidized beds offer advantages such as enhanced reactant contact, better heat transfer, and good temperature control and hence absence of local overheating and sintering in the charge. The use of a fluidized bed for the preparation of YF_3 by hydrofluorination was investigated by Knudsen and Levitz (1959) at Argonne National Laboratory. The reactor was a 75-mm-diameter and 1070-mm-high

monel column with a porous monel plate distributor. The reactor was heated externally.

The charge consisted of 1–2 kg of Y_2O_3. Nitrogen was used as the fluidizing gas initially, and the superficial gas velocities were kept at 0.15–0.2 m/s, about 50% more than the minimum fluidizing velocity of the bed. Anhydrous HF was combined with the nitrogen stream when the bed temperature reached 150°C. The gases were preheated in a packed tube inside a furnace. As the bed temperature rose, the rate of HF flow was adjusted to control the bed temperature and limit the reaction at a desired level. In runs of 7–10 h duration at 600–700°C, good conversion of Y_2O_3 to YF_3 was obtained. The nickel contamination in the product was less when the temperature was lower, e.g., 600°C. Even though scaling up the batch size from the small 2 kg charge might be feasible, this method was not used to prepare large quantities of fluorides (Carlson and Schmidt 1961a).

4.6.2.1.3 Vibrating Tray Method

The vibrating tray reactor (Fisher and Olson 1959) consisted of four inclined vibrating trays fixed in a cascade arrangement, so that Y_2O_3 would flow at a controlled rate countercurrent to the flow of HF gas. Conversions to >99% were obtained in a single pass at 700°C. Even though certain aspects of this unit appeared attractive, completely satisfactory performance was not achieved.

4.6.2.2 Reaction of Rare-Earth Oxides with Ammonium Bifluoride

Spedding and Daane (1956) developed a method in which ammonium hydrogen fluoride is used to convert the rare-earth oxide to rare-earth fluoride. The reaction is

$$RE_2O_3 + 6NH_4F\,HF \xrightarrow{300°C} 2REF_3 + 6NH_4F + 3H_2O$$

and the apparatus used for carrying out this reaction in batch sizes of 100–1000 g is shown in Figure 4.22.

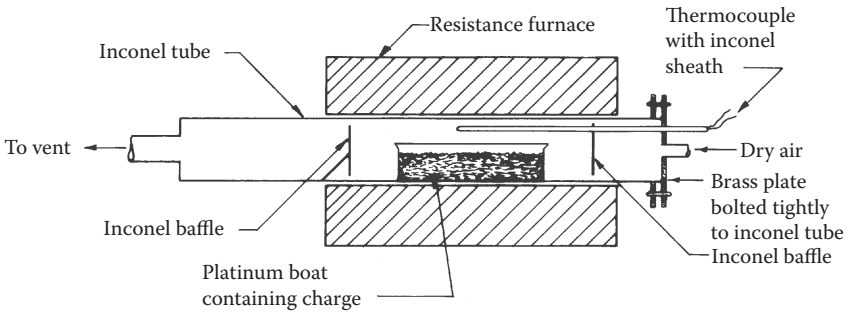


FIGURE 4.22 Apparatus used for the preparation of rare-earth trifluorides by the ammonium bifluoride process. (From Carlson, O.N. and Schmidt, F.A.: Preparation of the rare earth fluorides. In Spedding, F.H. and Daane, A.H. (eds.). *The Rare Earths*. pp. 79–88. 1961. Copyright Wiley-VCH Verlag GmbH & Co. KGaA. Reproduced with permission.)

The charge was a mixture of rare-earth oxide and high-purity ammonium bifluoride. The quantity of bifluoride was 30% more than the amount needed by the stoichiometry of the above equation. The charge was heated to 300°C for 12 h under a stream of dry air that swept away from the system volatile reaction products and excess NH_4F HF. The inconel baffles prevent plugging of the gas line because of condensation of NH_4F and NH_4F HF. The conversion of rare-earth oxide to the fluoride occurs quantitatively. Oxygen content in yttrium fluoride made by this process was approximately 400–1000 ppm.

4.6.3 Purification of Rare-Earth Fluorides

Rare-earth fluorides containing appreciable amounts of oxide or oxyfluoride could be purified by the following procedure in certain cases. The impure fluoride was combined with LiF (fluxing agent) to form a low-melting salt mixture. This mixture was contained in a platinum crucible and heated to 1000°C. Anhydrous HF was passed through the molten salt to effect purification. The purified fluoride mixture was used as feed for metallothermic reduction (Carlson and Schmidt 1961a). The fluorides of gadolinium, dysprosium, and yttrium have been purified by this method.

Another method applied mainly for the purification of yttrium fluoride (Carlson and Schmidt 1961a) is as follows. Yttrium–magnesium alloy is a suitable intermediate product in the preparation of yttrium metal. A mixture of YF_3 and MgF_2 is first prepared by direct hydrofluorination of their oxides at 600°C in a static bed. In this step, the conversions are usually 95–99%. For purification, LiF was added to the YF_3–MgF_2 mixture in a nickel vessel, degassed at room temperature, and then melted under an anhydrous HF atmosphere. Hydrogen was bubbled through the molten mixture for 1 h while its temperature was raised to 850°C. Anhydrous HF was then bubbled through the melt for 3 h, and then the mixture was again treated with hydrogen for approximately 16 h to decrease the contamination by iron, chromium, nickel, and sulfur. The molten salt was then transferred to a storage container through a sintered nickel filter. Oxygen content in the fluoride had decreased, and by extending the duration of hydrofluorination from 3 to 8 h, further decrease in oxygen content was achieved.

A process, known as topping, was extensively used at Ames to obtain purer rare-earth fluorides. This is the second part of the two-step process described by Spedding and Henderson (1971) for quantitative conversion of the rare-earth oxide to the fluoride. In the first step, a mixture of anhydrous HF and 60% Ar was passed over the rare-earth oxide at 700°C for 16 h. The inconel furnace tube was lined with platinum, and the oxide was contained in a platinum boat to prevent contamination of the fluoride. The oxygen content of the fluoride thus obtained was 300 ppm. This residual oxygen was lowered further to less than 20 ppm by topping. Topping involves heating the fluoride in a platinum crucible to approximately 50°C above its melting point under a dynamic HF–60% Ar atmosphere. Usually the time required for topping is 1 h at temperature for every 20 g of fluoride. A graphite resistance furnace is used.

In addition to lowering the oxygen content, topping also brings down the levels of impurity elements: aluminum, silicon, chromium, iron, nickel, and copper (Beaudry et al. 1983). The fluorides of these impurities have vapor pressures approximately 10^6 times greater than those of the rare-earth fluorides at their melting points.

4.7 REDUCTION OF RARE-EARTH FLUORIDES

Historically, the investigations on the metallothermic reduction of fluorides started much later than those using the chlorides. The important investigations on fluoride reduction methods for rare-earth-metal preparation are summarized in Table 4.4. In one of the earliest attempts of fluoride reduction, Eyring and Cunningham (1948) prepared metallic praseodymium by passing barium vapor over praseodymium fluoride at 1100°C under reduced pressure. Later, Gray (1951) developed a technique in which the rare-earth fluoride was reduced with lithium in a molybdenum crucible enclosed in a steel bomb. Iodine was added to lower the slag melting point. Reductions were conducted up to 1200°C, and cerium, lanthanum, and neodymium metals were prepared. Within a couple of years, the most enduring and successful process for the reduction of fluorides was developed at Ames. In the Ames process, calcium was used as the reducing agent, and the greater stability and lower vapor pressure of calcium fluoride permitted reduction temperatures as high as 1700°C, higher than the melting point of any rare-earth metal. It was thus possible to prepare all the rare-earth metals (except those exhibiting stable divalency) irrespective of their melting point.

The first major investigation on fluoride reduction for rare-earth-metal preparation, which was usable for commercial-level preparation of the metal, was by Gray

TABLE 4.4
Fluoride Reduction Processes

Year	Reactants	Process	Results	Reference
1951	REF_3–Li–I; (Ce, La, Nd)	Heated to 1200°C in a Mo crucible enclosed in a steel bomb	Consolidated Ce; separated from slag	Gray 1951
1953	REF_3–Ca; (Gd and all RE except Sm, Eu, Yb)	Heated in Ta crucible under argon	Consolidated RE metal well separated from slag	Daane and Spedding 1953
1956	YF_3–ZnF_2–Ca	Bomb reduction	Low-melting Y–Zn alloy; Zn distilled off	Carlson and Schmidt 1961a
1956	YF_3–$CaCl_2$–Ca–Mg	Heated in Zr or Ti crucible under argon	Low-melting Y–Mg alloy; Mg distilled off	Carlson and Schmidt 1961a
1961	YF_3–Li–Ca–Mg YF_3–Li–Mg	Heated in Ti crucible	Low-melting Y–Mg alloy; Mg distilled off	Haefling et al. 1961

(1951). The process was initially adopted by Johnson and Mathey (Lever and Payne 1968) for the production of lanthanum, cerium, and neodymium metals.

4.7.1 Lithium Reduction

Gray (1951) chose lithium as a suitable metal for reducing cerium trifluoride since it had a fairly high heat of reaction, produced the lowest melting fluoride, and did not alloy with cerium. However, as the heat of the reaction

$$CeF_3 + 3Li \rightarrow 3LiF + Ce$$

was not sufficient, in real conditions, to effect a rise in temperature sufficient for melting all the components, Gray provided iodine in the charge not only for Li–I booster reaction but also for the fluxing action of LiI on LiF slag.

The reactants cerium trifluoride, iodine, and lithium were loaded into the reactor shown in Figure 4.23. This reactor was constructed of mild steel and lined on the inside with molybdenum. The reactants were pressed into pellets only slightly smaller in diameter than the internal diameter of the crucible and loaded in the crucible in layers as shown at the bottom of the figure. A typical charge consisted of 110 g

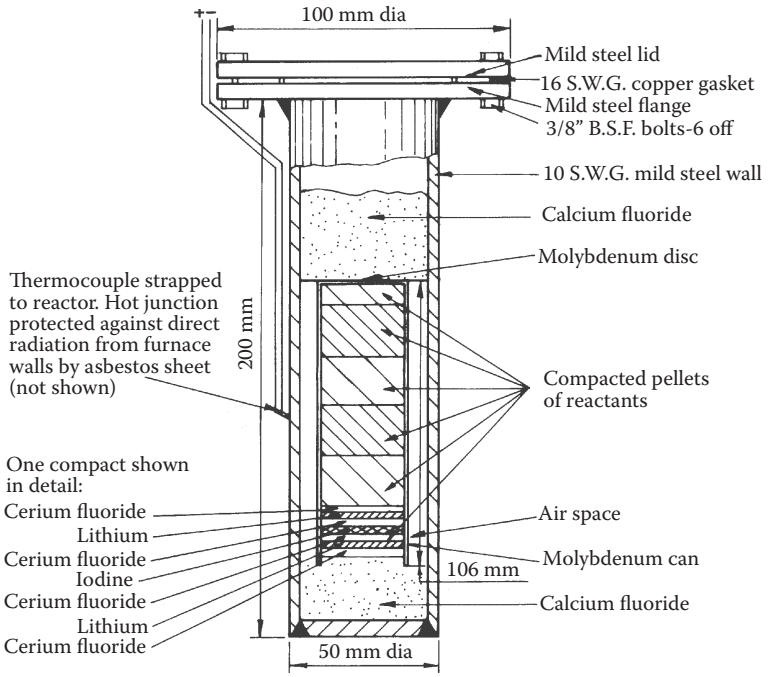


FIGURE 4.23 Reactor loaded for fluoride reduction. (From Gray, P.M.J., The production of pure cerium metal by electrolytic and thermal reduction processes, *Trans. Inst. Min. Met.*, 61 (Oct. 1951–Sept. 1952): 141–170, 1951.)

cerium trifluoride (=79 g cerium), 20 g iodine, and 14.1 g lithium (11.7 g to react with CeF_3, 1.1 g to react with iodine and 10% excess).

The loaded reactor was put in a pot furnace heated to 1300°C. When, after about 15 min, the outer wall of the reactor reached 1100°C, the furnace power was adjusted so that the reactor remained at 1100°C for 30 min, after which the reactor was removed from the furnace and allowed to cool.

In the reactor, cerium had collected at the bottom with the flux on top of it but cleanly separated from it. The metal yield was at best 82.5%, and the purity was consistently 99.92–99.93%. The main impurities were molybdenum (up to 0.06%) and iron (0.01–0.03%). Interstitial impurities were not analyzed, and, incidentally, no precautions were taken to exclude air from the reactor. The purity given was obtained by difference.

Small quantities of rare-earth metals, relatively low in oxygen content and also pure with respect to most nonmetallic impurities, have been prepared (Daane 1961b) using the apparatus shown in Figure 4.24. The rare-earth halide to be reduced and the reductant metal are placed in separate refractory metal crucibles in a tantalum container. The lid of the container is welded on, and it has a small-diameter tantalum tube that extends out of the furnace heating assembly. The system is evacuated while it is slowly heated to a temperature at which the reductant metal begins to volatilize and the vapors permeate the assembly. The metal vapors also condense in the cooler portions of the tantalum tube extending outside the furnace and seal off the system

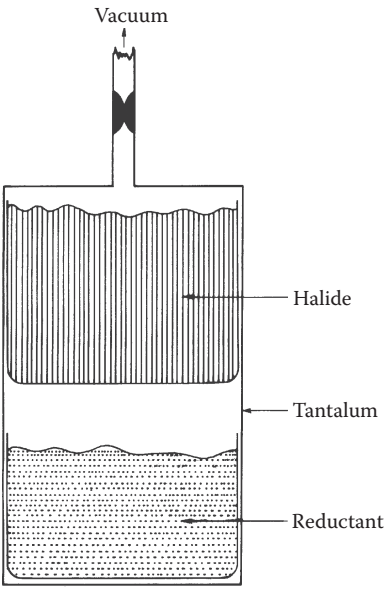


FIGURE 4.24 Rare-earth-metal reduction apparatus. (From Daane, A.H.: Metallothermic preparation of rare earth metals. In Spedding, F.H. and Daane, A.H. (eds.). *The Rare Earths.* pp. 102–112. 1961. Copyright Wiley-VCH Verlag GmbH & Co. KGaA. Reproduced with permission.)

by the time the system has been outgassed and gettered. During the reduction, which lasts several hours, the system thus remains free of gases that would have otherwise diffused back into the reaction chamber from the vacuum pumping system. Heating is done at such temperature that the salt phase in which the reduction takes place is liquid, and equilibrium is promoted between the reductant metal vapor and the halide undergoing reduction. The required temperature is less if sodium or potassium is used as the reductant or if a rare-earth chloride is being reduced than if calcium is the reductant and a rare-earth fluoride is being reduced.

4.7.2 Calcium Reduction (Ames Process)

In the Ames process (Daane and Spedding 1953), the reductions were carried out by mixing the calcium and rare-earth fluorides in a tantalum crucible in an argon environment. The fluorides were previously treated by vacuum sintering or fusion to remove the adsorbed gases from the very large surface area of the salt and also to reduce this surface area. Vacuum distilled calcium ground to 10 mesh particle size and stored in an inert atmosphere was used for these reductions. Mixing the reactants under inert gas cover decreases contamination by atmospheric gases. The quantity of calcium was 10% more than that required by the stoichiometry of the reaction.

$$3Ca + 2REF_3 = 3CaF_2 + 2RE$$

The charge was loaded into a vacuum-outgassed tantalum crucible that was then covered with a perforated tantalum lid. The arrangement is shown schematically in Figure 4.25. The crucible was placed in a silica tube vacuum induction furnace and heated slowly to 600°C to outgas the charge. Purified argon was admitted into the furnace at this temperature to a pressure of 70 kPa and the heating was continued further. The reaction started between 800°C and 1000°C, depending on the particular rare earth, and the exothermicity of the reaction resulted in a distinct increase in the temperature of the charge to above the temperature of the furnace. The reaction was not violent, and the external heating was continued to a temperature where both the products, slag and metal, were molten. The chosen temperature was 50°C above the melting point of calcium fluoride or 50°C above the melting point of the metal being prepared, whichever was higher. These reductions go to completion within a few minutes after reaching the chosen temperature, and holding for 15 min at the maximum temperature was sufficient to achieve good separation of metal and slag. Once the reductions had taken place and the furnace had cooled to room temperature, the crucible was removed from the furnace in air, and the slag layer that had formed on top of the metal ingot was knocked out of the crucible, leaving a clean ingot of rare-earth metal in a 97–99% yield with 0.1–2% calcium as the principal impurity. Daane (1961a) had described that in a 50-mm-diameter by 200-mm-high tantalum crucible, 300 g of the rare-earth metal could be made per batch. The crucibles were made of 0.25-mm-thick tantalum sheets for such a batch size, whereas 0.76-mm-thick tantalum crucibles were used in the semicontinuous operation, which

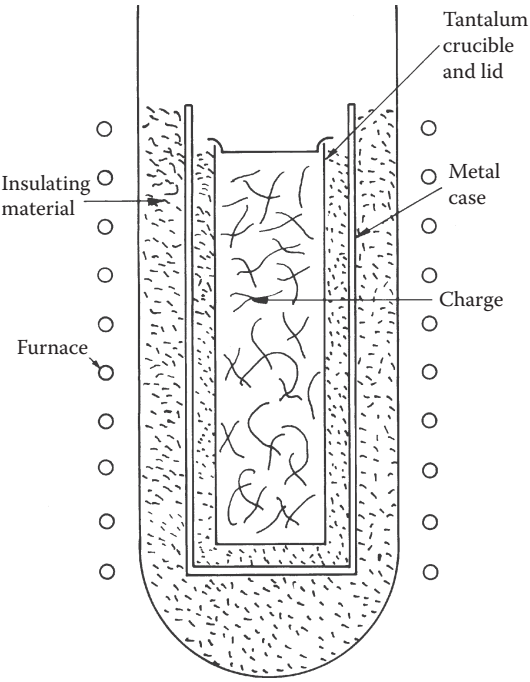


FIGURE 4.25 Schematic of the setup for the calciothermic reduction of rare-earth trifluorides. (Reprinted from *The Chemistry of Rare Earth Elements*, Topp, N.E., Copyright 1965, with permission from Elsevier.)

produced 9–14 kg of metal in each reduction. Higher thickness prevents erosion through the walls during repeated use of the crucible.

The cross section of a typical reduction crucible used (Spedding et al. 1970) for calciothermic reduction of rare-earth fluoride is shown in Figure 4.26. A large crucible is needed because of the low density of the starting materials. The volume occupied by the products of reaction is, however, much lower. Considering these, Daane (1961a) used the apparatus shown in Figure 4.27 to increase the amount of metal made in a heat. The charge was placed in the upper Pyrex hopper and held there while the tantalum crucible was vacuum outgassed. Required quantities of charge were then dropped into the tantalum reaction crucible by lifting the valve control tube, and as the charge reacted and melted down, more charge was added so that the crucible might be filled to near its top.

4.7.2.1 Semicontinuous Reduction

The calcium reduction of rare-earth fluoride could be carried out on a fairly large scale, as a semicontinuous process, using the reduction and pouring furnace described by Carlson and Schmidt (1961b) for the preparation of yttrium. The principal features of the furnace are shown in Figure 4.28. The charge, which consisted of YF_3 powder mixed with granular calcium (slightly in excess of the stoichiometric

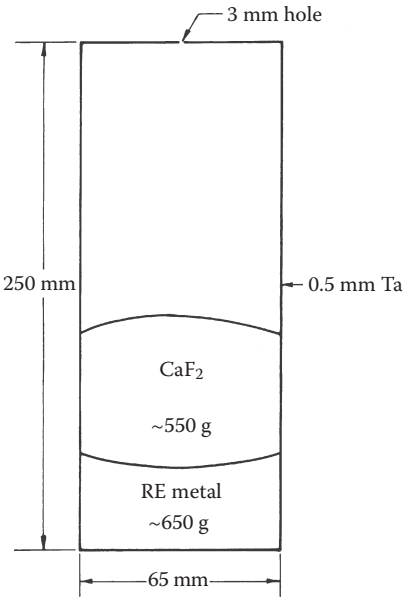


FIGURE 4.26 Cross section of a typical reduction crucible in calciothermic reduction of rare-earth trifluorides. (From Spedding, F.H. et al., The preparation and properties of ultrapure metals. In Les Elements Des Terres Rares 1, p. 25, Centre National de la Recherche Scientifique, Paris. Also R&D Report IS-2283, Ames Laboratory, USAEC, May 1970.)

amount), was introduced into the reduction crucible from a hopper through a sliding vacuum valve. The pouring spout below the hot zone of the graphite heater was sealed by a plug of yttrium metal that flowed into the tube and solidified at the beginning of reduction. Initial charge of the yttrium fluoride–calcium mixture was also placed in the reaction chamber. The system was evacuated and backfilled with argon. After the initial heating of the reaction chamber, to effect a reduction, additional reactants were introduced through the top vacuum valve from the hopper until the reaction chamber was filled with reduced metal and CaF_2 slag. The yttrium slug was then melted out by lowering the induction coil around a graphite focus inductor that heated the pouring spout. The metal and slag ran into the water-cooled mold below. After the pouring operation, a specially designed vacuum valve above the mold was closed so that the mold could be detached and emptied while the next reduction was in progress. The fresh charge of reactants was added to the tantalum crucible from the hopper, while the chamber was still hot. This procedure could be repeated until sufficient metal was obtained or a part of the equipment failed. The reduced yttrium ingot contained 0.15–0.5% Ca.

To remove calcium and also the residual fluoride, the as-reduced yttrium was melted into billets using a double-arc melting procedure. The analysis of yttrium thus obtained was 0.14–0.20% O, 0.05% F, 0.02% N, 0.01% C, 0.03% Fe, 0.001% Ca, and 0.4% Ta.

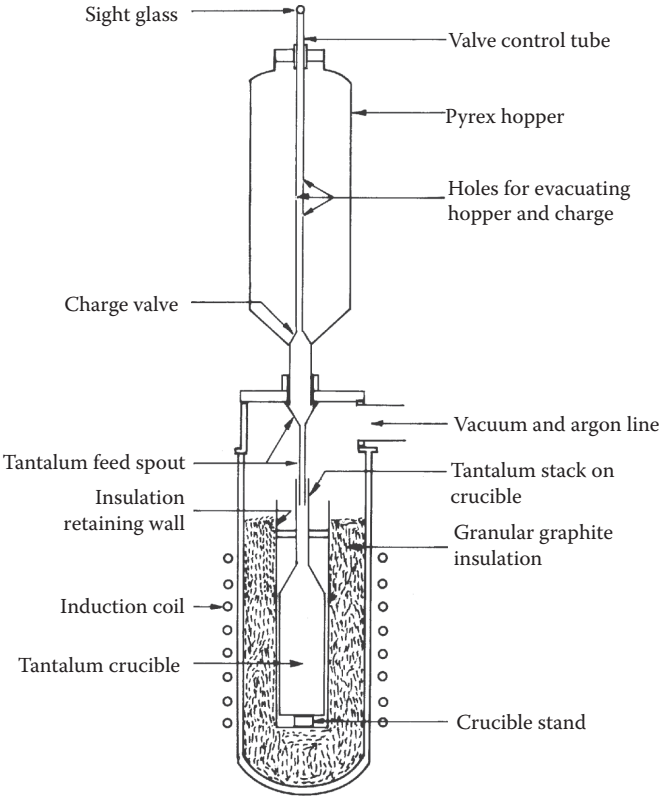


FIGURE 4.27 Apparatus for reducing rare-earth fluorides with calcium. (From Daane, A.H.: Metallothermic preparation of rare earth metals. In Spedding, F.H. and Daane, A.H. (eds.). *The Rare Earths*. pp. 102–112. 1961. Copyright Wiley-VCH Verlag GmbH & Co. KGaA. Reproduced with permission.)

4.7.2.2 Goldschmidt Process

In the industrial practice described by Herget (1985) for calcium reduction of rare-earth fluoride, the fluoride was mixed with granular calcium and the mixture was placed in a tablet form or as rammed material in a steel reactor. The reactor was lined on the inside with tantalum, which was coated with a layer of calcium fluoride. After evacuating the reactor, the metallothermic reduction was initiated by a spark discharge. The reduction proceeded to completion within minutes.

$$2REF_3 + 3Ca \xrightarrow[\text{vacuum}]{\text{up to } 2000^\circ C} 2RE + 3CaF_2$$

The rare-earth metal, collected as an ingot in the bottom part of the reactor, topped by solidified calcium fluoride slag.

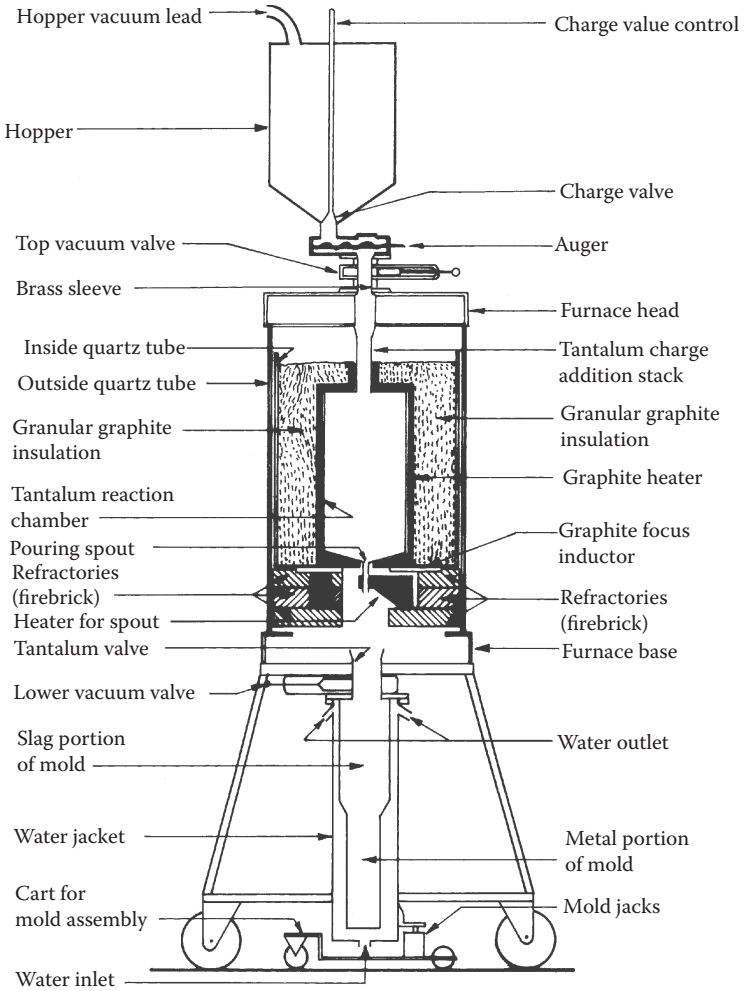


FIGURE 4.28 Reduction and pouring furnace for semicontinuous preparation of yttrium metal. (From Carlson, O.N. and Schmidt, F.A.: Metallothermic preparation of yttrium metal. In Spedding, F.H. and Daane, A.H. (eds.). *The Rare Earths*. pp. 113–125. 1961. Copyright Wiley-VCH Verlag GmbH & Co. KGaA. Reproduced with permission.)

The preparation of rare-earth metals by reduction of their trifluorides with calcium metal in tantalum crucibles leads to the introduction of up to 0.5% tantalum as impurity. This happens in particular in higher melting rare earths because higher temperatures are reached in their production, and solubility of tantalum in rare earths increases with temperature (Dennison et al. 1966a,b). In the case of scandium, the tantalum content ranges from 2% to 5%. A solution to this problem was in what is known as the intermediate alloy process.

4.7.3 Intermediate Alloy Process

The temperature necessary for fluoride reduction was lowered, and thus, the contamination of crucible material in the resulting rare-earth metal was decreased in the large-scale production of yttrium (Carlson and Schmidt 1961b) through a novel variant of the basic process. The process now proceeds through the formation of an intermediate low-melting alloy with zinc or more successfully with magnesium. A similar process was applied to scandium also (Spedding et al. 1960).

The first method using the intermediate alloy investigated by Carlson et al. (1956) involved the formation of yttrium–zinc alloy. The process was carried out in a bomb reactor, and yttrium trifluoride was reduced with calcium using ZnF_2 as a thermal booster. The product was a low melting Y–Zn alloy that was immiscible with the molten CaF_2 slag. The alloy was eventually heated in a vacuum to vaporize off zinc leaving behind yttrium. Even though the metal prepared was of satisfactory quality, difficulties were encountered in finding a suitable bomb liner in the reduction stage and also for the removal of zinc. This method was investigated no further (Carlson and Schmidt 1961b).

The yttrium–magnesium alloy method was also investigated by Carlson et al. (1960) and Carlson and Schmidt (1961b). Yttrium fluoride was reduced by calcium in the presence of magnesium and calcium chloride to form an Y–24% Mg intermediate alloy. The alloy and the slag formed in the reaction were both molten at 950°C. It was thus possible to carry out the reduction in a refractory metal crucible under an inert gas atmosphere. Calcium chloride not only forms a low-melting eutectic with CaF_2 but also decreases the density of the slag, which is an important factor for complete separation between the slag and the alloy phases.

A sketch of the apparatus used for the process is shown in Figure 4.29. Massive pieces of magnesium (290 g) and calcium (680 g) were transferred to the reduction crucible, and a mixture of YF_3 (1500 g) and $CaCl_2$ (1350 g) was loaded into the charging hopper. The unit was evacuated by a mechanical pump and then placed into a gas-fired furnace. When the retort temperature had reached 800°C, helium was admitted and a positive pressure of 7–35 kPa was maintained in the system throughout the remainder of the run. When calcium and magnesium were molten and reached a temperature of 900°C, the YF_3–$CaCl_2$ mixture was added slowly from the hopper into the molten metals at a rate required to maintain the temperature in the reacting mass above 800°C. The mass was then brought to a temperature of 960°C. At the completion of the run, the hot retort was raised from the furnace and allowed to cool in a slightly tilted position. Solidification occurring in this position resulted in easier slag–alloy separation.

The designed composition of the intermediate alloy was 24% magnesium, and a 10% excess calcium reductant gave a metal recovery of over 99% theoretical. The slag composition of 52% $CaCl_2$ gave the best slag metal separation and highest metal yields.

The alloy was crushed into approximately 12 mm pieces in a jaw crusher enclosed in a dry box. Magnesium removal was carried out by sublimation in a 150-mm-diameter stainless-steel retort equipped with a condenser. The alloy pieces were loaded in a titanium vessel in the vertical retort. The system was

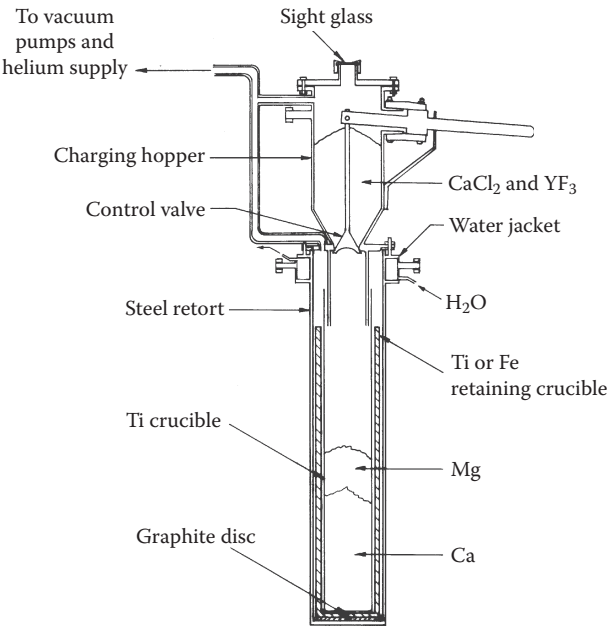


FIGURE 4.29 Schematic diagram of the reduction retort. (From Carlson, O.N. et al., *J. Electrochem. Soc.*, 107: 540–545, 1960.)

evacuated to 10^{-2} Pa at the outset, and this pressure was maintained throughout the run. The retort and contents were heated to 900°C in an electric furnace and held for 4 h after which the temperature was raised to 950°C and held for 20 h. Magnesium vapor collected on an air-cooled condenser. The yttrium obtained was in the form of bright porous sponge containing ~0.01% magnesium and calcium. The yttrium sponge obtained in the process was arc-melted in an inert atmosphere to form an ingot.

The intermediate alloy method has been used on a large scale for the preparation of yttrium (Carlson and Schmidt 1961b). A titanium or zirconium crucible (510 mm diameter, 1150 mm height, 6 mm wall thickness) was used as the reduction crucible. The crucible was reinforced with a mild steel outer jacket. A thin titanium sheet was inserted between the jacket and zirconium crucible to prevent alloying of steel and zirconium at the reduction temperature. In this process, granular calcium (37.6 kg, 10% excess) and granular magnesium (15.8 kg) were used to reduce yttrium trifluoride (82 kg) and $CaCl_2$ (37.6 kg) essentially following the procedure described above.

The analysis of yttrium produced by the above process is given in Table 4.5. The purer sample on the second column was lower in oxygen content because freshly distilled massive calcium was used and the crucible was titanium, which has a lower solubility in Y–Mg alloy than does zirconium.

Haefling et al. (1961) conducted experiments to find a reductant for YF_3 using an intermediate alloy process that is more economical than calcium, yet producing

TABLE 4.5
Chemical Analysis of Yttrium Produced by the Intermediate Y–Mg Alloy Process

Impurity	Content (%)	
Reductant	Calcium (Granules)	Calcium (Freshly Distilled Massive Metal)
Crucible	Zirconium	Titanium
Ca	0.001	0.001
Cu	0.010	0.010
Fe	0.015	0.015
Mg	0.003	0.003
Ni	0.035	0.020
N	0.015	0.015
O	0.25–0.40	0.12–0.25
Si	0.01	0.01
Ti	0.005	0.15
Zr	0.7	0.001

Source: Carlson, O.N. and Schmidt, F.A. Metallothermic preparation of yttrium metal. In Spedding, F.H. and Daane, A.H. (eds.). *The Rare Earths*. pp. 113–125. 1961. Copyright Wiley-VCH Verlag GmbH & Co. KGaA. Reproduced with permission.

yttrium metal of comparable quality. Lithium, calcium–lithium alloy, magnesium, aluminum sodium, and zinc were all evaluated.

Yttrium fluoride was reduced by lithium metal and by Ca–Li alloys in the presence of magnesium to form Y–24% Mg intermediate alloy. The apparatus used in these experiments was the same as that used by Carlson et al. (1960). A typical reaction mixture for lithium reduction of YF_3 consisted of 1500 g YF_3, 288 g Mg, and 235 g Li. The reactants were loaded into the reduction crucible, which was inserted into the steel retort. From then on, the run was conducted as described when calcium was used as the reductant, except that the reaction temperature was 975°C and duration was one-half hour. The alloy and slag formed were both molten at this temperature. Metal yields of 99% were obtained. The oxygen content was 0.12% in yttrium metal when distilled lithium was used, and it was 0.15–0.2% when filtered or ethanol pickled lithium was used.

Calcium–lithium alloys containing 15–60% lithium were also used as reductants for YF_3. In each experiment, 1500 g of YF_3 and 290 g of magnesium metal were added to form Y–24% Mg alloy. Lithium, calcium, and magnesium were all placed in the reduction crucible, and YF_3 was loaded in the feed hopper. The metals was heated to 975°C, as described earlier for runs using calcium as a reductant, and YF_3 was added in incremental amounts to the molten Li–Ca–Mg alloy. The reaction mixture was held at 975°C for one-half hour before it was cooled to room temperature, and the Y–24% Mg alloy obtained was processed to yttrium sponge. The yield of yttrium metal was greater than 99% when the reductant alloy contained at least 22% lithium. The oxygen content varied from 0.1% to 0.2%.

Using magnesium as a reducing agent, mixtures of Mg, YF_3, and anhydrous $CaCl_2$ were heated to 975°C in a tantalum crucible for various lengths of time. However, even after 4 h, the maximum yield was only 17%. The yield was only 18% when aluminum was used as a reducing agent at 1000°C, and the yield was only 7% with sodium after reduction at 900°C. No reaction occurred at 900°C with zinc as a reducing agent.

The advantage of using lithium as a reductant (Haefling et al. 1961) lies in the low-melting LiF slag (m.p. 870°C) that is formed. With the reduction temperature of 975°C, no fluxing agent was needed when LiF was formed. Lithium is costlier than calcium, but the cost difference, when the unit weight of yttrium produced is considered, is narrowed because calcium reactant needs a considerable quantity of $CaCl_2$ to flux the CaF_2 slag produced in the reaction. The use of Ca–Li alloy as a reductant for YF_3 offers all the advantages of lithium reductant because all compositions of CaF_2–LiF slag formed were fluid below 975°C. The use of Ca–22% Li alloy was economical because the cost savings for not having to use $CaCl_2$ more than offset the extra cost due to lithium in the reductant.

4.7.4 Preparation of Scandium

The use of an intermediate zinc alloy was not very successful with yttrium; however, zinc proved to be a suitable element for the intermediate alloy process to produce scandium (Spedding et al. 1960). The process is carried out as follows:

$$2ScF_3 + 3Ca + 3Zn + LiF \rightarrow Sc\text{–}60\%\ Zn\ alloy + 3CaF_2\text{–}LiF\ (eutectic\ composition)$$

The alloying of scandium (m.p. 1541°C) and formation of the low-melting slag made it possible to carry out the reduction and separation of the products into molten metal and slag layers at 1100°C. In a tantalum crucible, the reactants were sealed under a helium atmosphere by welding. The crucible was, in turn, sealed inside a stainless-steel bomb in a helium atmosphere. On heating the bomb in a muffle furnace to 1100°C, the reaction and subsequent separation of products into alloy and slag layers occurred. When cooled, the crucible was opened and the alloy layer was separated from the slag. The scandium–zinc alloy, which also contained 1–2% Ca, was brittle and was easily crushed into small pieces. These pieces were heated very slowly in an induction furnace under high vacuum whereby zinc and calcium sublimed off and a porous scandium sponge was obtained. This was consolidated by arc melting under 1 atmosphere argon. The metal was obtained with an overall yield of 90% and contained trace amounts of tantalum, magnesium, calcium, copper, lithium, iron, silicon, and zinc, less than 100 ppm of carbon, nitrogen, or hydrogen, and probably less than 1000 ppm of residual oxygen.

4.7.5 Reduction of Samarium, Europium, and Ytterbium Halides

The chloride and fluoride reduction methods described so far are applicable to all the rare-earth metals except samarium, europium, and ytterbium. This was realized as early as in 1937 by Klemm and Bommer (1937) and corroborated in later investigations

(Daane 1961a). When the chlorides or fluorides of samarium and europium or ytterbium reacted with calcium or barium, a very exothermic reaction occurred in which the trihalides were reduced to the dihalides but no metal was obtained.

4.7.5.1 Reduction of $SmCl_3$ by Mechanical Milling

Rare-earth metals that exhibit stable divalency cannot be prepared by the routine metallothermic reduction of halides. For example, calciothermic reduction of $SmCl_3$ results in the formation of $SmCl_2$, and the reduction stops there. This is true of other metallic reductants like Li and Na. Alonso et al. (1993) examined free energy change for the relevant reactions using the free energy change–temperature plots for the Sm and $SmCl_2$ formation reactions by sodium reduction of $SmCl_3$. They identified that the free energy of reaction plots cross at ~400 K, with the $SmCl_3$ reduction to Sm having the more negative free energy change at lower temperatures. The relatively low-temperature reaction possibility was investigated in a novel way—by mechanical milling.

Alonso et al. (1993) applied the mechanical alloying process for the synthesis. High-purity (99.9%) $SmCl_3$ powder (–325 mesh) and sodium (99.9% pure, 10–15 mm cubes, in 15% excess over stoichiometric requirement) were mechanically milled under an inert gas cover in a hardened steel equipment for 16 h. The reaction temperature was ensured to remain below 400 K by appropriate thermal insulation of the milling vessel. On observing the XRD patterns, Alonso et al. (1993) noted that the as-milled powder showed major peaks corresponding to Sm and NaCl—clear evidence of direct reduction of the trichloride to metal. They heated the product up to 823 K to observe possible reversal of the reduction reaction. Heating of the powder at 573 K for 2 h in vacuum resulted only in the sharpening of the diffraction peaks corresponding to Sm and NaCl. No evidence of reversal of reduction was observed, even though the temperature was 173 K above the cross over temperature. However, on treating at 823 K for 2 h, diffraction peaks corresponding to $SmCl_2$ and NaCl, were observed, clearly indicative of the reaction $Sm + 2NaCl \rightarrow SmCl_2 + 2Na$. Alonso et al. (1993) demonstrated that mechanical alloying can be used to induce reactions feasible only at lower temperatures but cannot be implemented in the conventional way due to possible kinetics limitations. Even normal reduction reactions like the reduction of $ErCl_3$ or $GdCl_3$ with Ca have been carried out in identical milling conditions in a short duration of 3 h (McCormik et al. 1992).

4.8 OXIDE REDUCTION PROCESSES

Rare earths form highly stable oxides. Among the popular metallic reducing agents, only calcium forms oxide stabler than that of the rare earths. The stability of magnesium oxide is only marginally higher than that of the heavy rare-earth oxides and comparable to those of the light rare-earth oxides. Apart from calcium, the only element that can reduce rare earths is carbon. In fact, at about 1700°C and a CO pressure below 100 Pa, carbon is the most efficient reducing agent. In the classical sense, therefore, the possibility of rare-earth oxide reduction appears restricted to the use of either calcium or carbon.

The important investigations on oxide reduction are listed in Table 4.6. Early attempts to produce rare-earth metals by reduction of their oxides were made between

TABLE 4.6
Oxide Reduction Processes

Year	Reactants	Process	Results	Reference
1950	RE_2O_3–Mg (Nd, Gd, Y)	Rare-earth oxide blocks dipped in molten magnesium heated to 1050°C	Mg–5%RE alloy	Mahn 1950
1953	RE_2O_3–La (Sm, Yb)	Reduction–distillation in Ta crucible and condenser	Pure RE metal condensate	Daane et al. 1953
1953	RE_2O_3–C	Carbothermic reduction	RE carbide formation	Trombe 1953
1957	Sm_2O_3–C	Reduction–distillation	Impure Sm condensate	Achard 1957
1959	RE_2O_3–Zr (Eu, Sm), La	Reduction–distillation in Mo crucible and condenser	Pure RE metal	Campbell and Block 1959
1959	Sm_2O_3–Ca	Reduction–distillation	Sm containing residual Ca in low yield	Onstatt 1959
1961	RE_2O_3–Ce	Reduction–distillation	Pure RE metal condensate	Daane 1961a
1966	RE_2O_3–La (Sm, Eu, Yb) RE_2O_3–Th (Nd, Gd, Dy, Er, Lu)	Reduction–distillation	Technique applied in the 1100–2400°C range; RE with limited volatility prepared	Westgaard and Bjornholm 1966
1968	RE_2O_3–La (Sm, Tm, Yb)	Reduction–distillation in Mo crucible and Ta condenser	Pure RE metal condensate	Moriarty 1968
1968	RE_2O_3–La (Dy, Ho)	Reduction–distillation	Residual La, O in condensate	Spedding and Daane 1968
1969	Dy_2O_3–Th	Reduction–distillation	Dy condensate purified by redistillation	Schiffmacher and Trombe 1969
1969	RE_2O_3–La (Sm, Eu, Yb) RE_2O_3–Th (Pr, Nd, Pm, Gd, Dy, Er)	Reduction–distillation Quartz collector	Technique applied in the 1125–2000°C range	Kobisk and Grisham 1969
1979	RE_2O_3–La RE_2O_3–Th All lanthanides except Ce, La	Reduction–distillation	High-purity, malleable products	Kobisk and Adair 1979
1987	Gd_2O_3–$CaCl_2$–Mg	Heated to reaction temperature and slag leached off	Gd metal powder	Okajima 1987

(*Continued*)

TABLE 4.6 (CONTINUED)
Oxide Reduction Processes

Year	Reactants	Process	Results	Reference
1987	Nd_2O_3–Ca	Reduction carried out in $CaCl_2$–NaCl bath and metal extracted by Nd–Zn or Nd–Fe alloy pool	Nd–Zn or Nd–Fe alloy	Sharma 1987
1988	Nd_2O_3–Na	Reduction carried out as with Ca	Nd–Zn or Nd–Fe alloy	Sharma and Seefurth 1988a,b
1991	RE_2O_3–Hf	Reduction–distillation Quartz dome collector	High-purity RE	Pengo et al. 1991

1890 and 1912 by Winckler (1890, 1891), Matignon (1900), and Hirsch (1912). Using magnesium or calcium as the reducing agent, they invariably ended up with a product mixture consisting of magnesium oxide or calcium oxide and the metal, which could not be separated. Several decades later, Mahn (1950) pursued the magnesium reduction route. Mahn dipped fused oxide blocks of neodymium, gadolinium, or yttrium group elements into molten magnesium heated to 1050°C. The oxide block was rapidly attacked by the magnesium metal, but the products obtained were dilute solutions (<5% RE) of rare earth in magnesium.

The simple and direct attempts to reduce rare-earth oxides by calcium and magnesium summarized above were destined to fail for many reasons. The stability of magnesium oxide is almost the same as that of the light rare earths at temperatures up to about 1100°C. Magnesia is stabler than yttrium and other heavy rare-earth oxides, but the difference in stability is not substantial enough for magnesium to function as a reducing agent for these oxides. Even though the considerable thermodynamic stability of calcia qualifies it as a reducing agent for rare-earth oxides, the high melting point of calcia (2600°C) is a definite disadvantage. During the calcium reduction, consolidated rare-earth metal is not produced because the enthalpy of reaction is not sufficient to melt the calcia slag and permit the metal separation by gravity. The reduction, at best, yields rare-earth metal dispersed in the slag matrix. Aqueous processing to recover the fine metal powder usually results in oxygen contamination.

The breakthrough in the development of methods for preparation of rare-earth metals by oxide reduction came in the 1950s when Daane, Dennison, and Spedding (1953) at Ames succeeded in devising the reduction–distillation process. This method, which is in a way similar to the Pidgeon process for magnesium, has been remarkably useful for the preparation of samarium, europium, and ytterbium, the three metals that could not be obtained by the normal halide reduction route.

4.8.1 Reduction–Distillation: Lanthanothermy

Systematic vapor pressure measurements of the rare-earth metals (Habermann and Daane 1961) had indicated that lanthanum was the least volatile of the rare-earth

metals and that dysprosium had a vapor pressure nearly 300 times that of lanthanum at the same temperature. The metals samarium and europium are also similarly very volatile. Besides, lanthanum oxide was known to have one of the highest (most negative) heat of formation among the rare-earth oxides. These observations led Daane et al. (1953) to devise a method for reacting the oxides of samarium, europium, or ytterbium with lanthanum metal and driving this reaction to completion by distilling away the volatile metals in vacuum. The method has since been called lanthanothermic reduction or lanthanothermy.

An important feature of the reduction distillation process is that it is forced to quantitatively yield the product required by removal (by vaporization) of the rare-earth metal formed from the reaction mixture. It was proved possible to perform reductions that have, to a certain extent, unfavorable thermodynamic characteristics at equilibrium. Thermodynamic basis for this process being that some reduction occurs at the temperature at which the desired metal product has the requisite vapor pressure (10 Pa is considered ideal). On continuous removal of the product metal from the reaction zone, the reaction is forced in the direction of complete reduction (Kobisk and Adair 1979).

4.8.1.1 Preparation of Samarium and Ytterbium

Samarium was the first metal to be prepared by the reduction distillation process. Daane et al. (1953) heated a mixture of 20 g of freshly prepared lanthanum turnings and 20 g of samarium oxide in a tantalum crucible to 1450°C under 0.1 Pa and held for about half an hour. The crucible was 200 mm long, 25 mm in diameter, and 0.6 mm thick. The upper half of the crucible protruded out of the furnace and had a perforated tantalum lid. On opening, the upper walls of the crucible and the bottom of the cap were found to be covered with a silvery crystalline metallic deposit, which analysis showed to be samarium of better than 99% purity with no lanthanum detectable (<0.02%). The yields were 80% from the original oxide. Several subsequent reductions obtained nearly 100 g of samarium of better than 99.9% purity each time, representing an overall 95% yield.

Preparation of ytterbium by the reduction–distillation process could be done at a lower temperature (Daane et al. 1953; Spedding and Daane 1954), due to its higher volatility compared to samarium, and the yield was similar.

4.8.1.2 Preparation of Europium

The first mention of the preparation of europium metal was made in 1954 by Spedding and Daane (1954). The details of europium preparation and handling appeared in a subsequent paper (Spedding et al. 1958). The schematic of the reduction system is shown in Figure 4.30. The reduction crucible was made from two concentric tantalum cylinders. A mixture of 86.5 g Eu_2O_3 and 73 g lanthanum turnings was charged in the annular space between two concentric tantalum cylinders welded together and shown as the reduction chamber. The chamber was heated to 1000°C, and the pressure was maintained at less than 0.01 Pa. The metal began to distill at 1100°C, and as the temperature reached 1200°C, droplets of europium began to reflux. The evaporated metal condensed in the lower part of the inner cylinder, and at intervals, the induction coil was lowered and the metal was melted down into the tantalum crucible below.

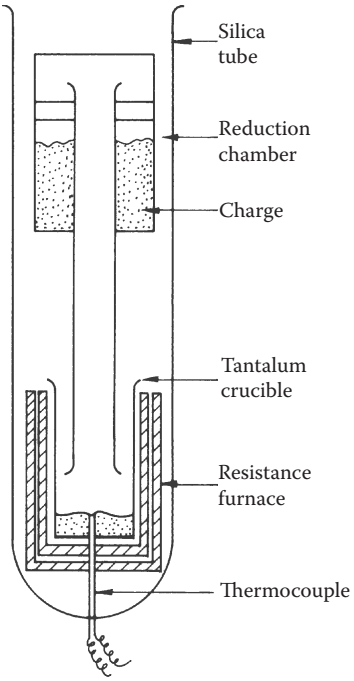


FIGURE 4.30 Schematic of the apparatus for the reduction of europium. (From Spedding, F.H. et al., *Trans. AIME*, 212: 379–383, 1958.)

An interesting feature of the above process is that the starting materials need not be extremely pure to get pure europium. Samarium is the usual impurity in europium oxide, but it is completely absent in the europium metal produced by the above process because samarium is less volatile than europium, and for the reduction of Sm_2O_3 to metal, a higher temperature is needed than that used for Eu_2O_3 reduction. Commercial lanthanum turnings can be used in place of the more expensive very pure lanthanum metal. Any calcium impurity in the charge would, however, be transported to europium.

4.8.1.3 Preparation of Samarium, Europium, Ytterbium, and Terbium

Daane (1961a) described the preparation of samarium, europium, and ytterbium. Lanthanum turnings in 10% excess were intimately mixed with the rare-earth oxide, and the mixture was heated in a tantalum crucible in a high vacuum to effect the reaction

$$2La + RE_2O_3 = La_2O_3 + 2RE$$

Two types of apparatus have been used for carrying out this reaction. One is a simple tantalum crucible, the upper portion of it acting as the condenser. The lower portion of the crucible was maintained at the highest possible temperature so that the volatile metals were recovered as bright crystalline condensates on the walls of the upper part of the crucible. Metal yields were greater than 98%. With a 50-mm-diameter reaction

chamber, 300–400 g metal could be obtained per batch. In another arrangement shown in Figure 4.31, an air-cooled copper condenser was fitted in the upper portion of the reaction chamber. This was first used for the preparation of samarium. The condenser was coated with an alcoholic wash of Sm_2O_3 to provide a barrier to prevent contamination of the metal deposit. A stream of air, controlled by a thermocouple attached to the condenser, was used to maintain the condenser temperature at 300–400°C. If the condenser temperature was too low, the metallic deposit was so powdery that it was pyrophoric and difficult to handle. Between 300°C and 400°C, good grain growth was maintained in the condensate, and a product that was stable in air was obtained. Ytterbium was also prepared under essentially similar conditions. Being a more reactive metal, europium needed to be always handled in an inert atmosphere.

Metals prepared by the above process were found to contain no detectable lanthanum or tantalum. This may be attributed to the great differences in volatility. The contents of other impurities such as carbon, nitrogen, oxygen, and hydrogen were less than 100 ppm.

Somewhat higher temperatures and a larger excess of reductant in the charge were recommended by Beaudry and Gschneidner (1978), who have outlined a procedure for the metallothermic reduction of the oxides of samarium, europium, thulium,

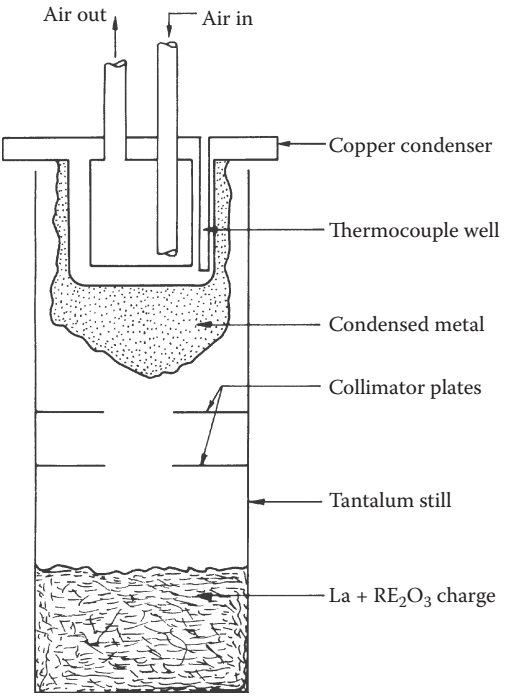


FIGURE 4.31 Apparatus for preparation of samarium, europium, and yttrium metals. (From Daane, A.H.: Metallothermic preparation of rare earth metals. In Spedding, F.H. and Daane, A.H. (eds.). *The Rare Earths*. pp. 102–112. 1961. Copyright Wiley-VCH Verlag GmbH & Co. KGaA. Reproduced with permission.)

and ytterbium. Thulium, like other metals in the group, is volatile and a candidate for preparation by reduction–distillation. The process described by Beaudry and Gschneidner (1978) is as follows. The rare-earth oxide was heated in air at 800°C for 15 h to drive off adsorbed compounds such as H_2O and CO_2. Freshly prepared chips or turnings of lanthanum that had been vacuum-melted at 1800°C or higher were mixed with freshly ignited oxide. The quantity of lanthanum was 15% more than that needed by the stoichiometry of the reaction

$$2La + RE_2O_3 = La_2O_3 + 2RE$$

The oxide–lanthanum turnings mixture was packed into a 6.4-cm-diameter by 25.4-cm-long tantalum crucible that was fitted with a 20-cm-long tantalum condenser and a tantalum optical baffle arrangement. The baffles prevent excessive entrainment of oxide particles in the vapor. The crucible and contents were evacuated and heated to a maximum of 1400°C for europium and ytterbium and 1600°C for samarium and held at that temperature for an additional 2 h. The temperature was raised slowly because a fast heating rate could cause lanthanum to melt and run to the bottom of the crucible. On the other hand, in slow heating, as lanthanum reacted with the rare-earth oxide, La–La_2O_3 solution was formed and this had a higher melting point than pure lanthanum metal. Once the melting point of the reducing medium was increased, the temperature could be raised to enhance the diffusion rate.

A typical charge for samarium preparation would consist of 550 g Sm_2O_3 and 540 g of lanthanum. The amount of lanthanum was about 15% more than the stoichiometric amount. After reduction–distillation, about 465 g of samarium was obtained representing a yield of 98%, which was usual in the process. The reduction crucible could be cleaned, loaded once again with lanthanum and samarium oxide, and reused for additional distillation runs.

4.8.2 Reduction–Distillation: Other Reductants

The basic criteria for a successful reduction–distillation process, that the product metal has an appreciable vapor pressure while all other components of the process possess negligible vapor pressure at the reaction temperature, are met in certain systems where, in place of lanthanum, metals like cerium or zirconium are used. Both cerium and zirconium have very stable oxides and low vapor pressure, and they can be obtained in very pure form. Campbell and Block (1959) investigated the use of cerium and zirconium as reductants for the preparation of europium and samarium.

The diagram of the apparatus used by Campbell and Block (1959) is shown in Figure 4.32. Samarium or europium oxides were mixed with the metal reductant (lanthanum, cerium, or zirconium) and compressed into pellets. The reductants were freshly prepared in a finely divided state as powder or lathe turnings. The pellets were loaded inside the closed end of a molybdenum thimble that was then placed inside a refractory vacuum retort. The evacuated retort was heated overnight at 200°C to remove adsorbed gases from the charge. The temperature was then gradually raised to the operating temperature while maintaining the pressure at less than 25 Pa. At the completion of the run, the pressures were approximately 0.5 Pa. The metal (samarium or europium)

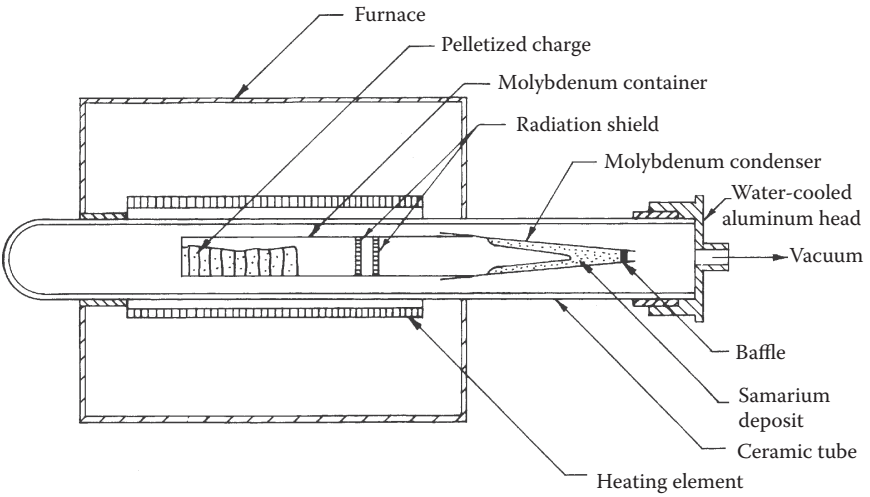


FIGURE 4.32 Reduction–distillation assembly.

collected as bright crystalline deposits in the tapered condenser that was fitted over the open end of the molybdenum thimble, as shown in Figure 4.32. Subsequent operations for collecting the metal deposit were performed under stringent atmosphere control to prevent air contamination. When cool, the condenser was transferred to an inert atmosphere handling chamber. The small end of the condenser was fitted into an expendable 0.125-mm-thick tantalum crucible. On heating the entire assembly under argon, the deposit was melted from the condenser surface and collected in the tantalum crucible, which was subsequently peeled from the cast metal ingot.

Using lanthanum as a reductant, high-purity europium was obtained in more than 90% yield at reduction temperatures as low as 900°C. This relatively low temperature is attractive for extending the technique to commercial practice. However, the yield was maximum, and time needed at maximum operating temperature was minimum when reduction was carried out at 1200°C.

Higher temperature was needed for preparing samarium from its oxide using zirconium as a reductant. Campbell and Block (1959) performed this reduction in a high-temperature apparatus shown in Figure 4.33. The entire assembly was mounted in a vertical position inside a vacuum furnace, and heat for the reaction was supplied by a hollow split graphite resistor mounted inside the water-cooled vacuum furnace shell. After degassing the furnace and reduction equipment at 1000°C until a vacuum of less than 0.1 Pa was obtained, the furnace was cooled under argon, and the molybdenum thimble containing the pelletized charge was introduced. The charge had pellets made from 85% Sm_2O_3 and –35 mesh zirconium sponge. The furnace temperature was raised to 1450°C over a 2-h period and maintained at this temperature for 1 h. The retort pressure during reduction was between 0.8 and 1.4 Pa. Crystalline metal deposit thus obtained was recovered from the condenser as described earlier.

Essentially the same operating procedures were adopted by Campbell and Block (1959) in the equipment for larger scale experiments, shown in Figure 4.34.

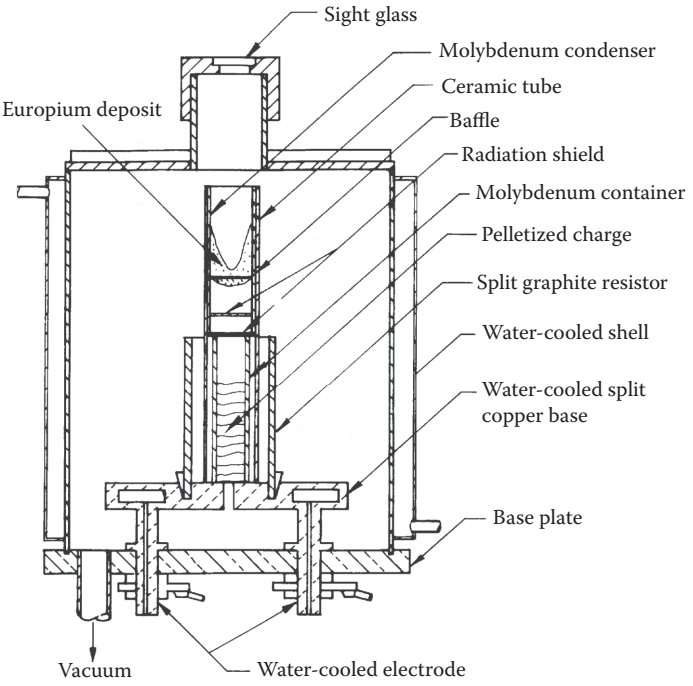


FIGURE 4.33 Split graphite resistor furnace assembly. (From Campbell, T.T. and Block, F.E., *J. Metals*, 11, 744–746, 1959.)

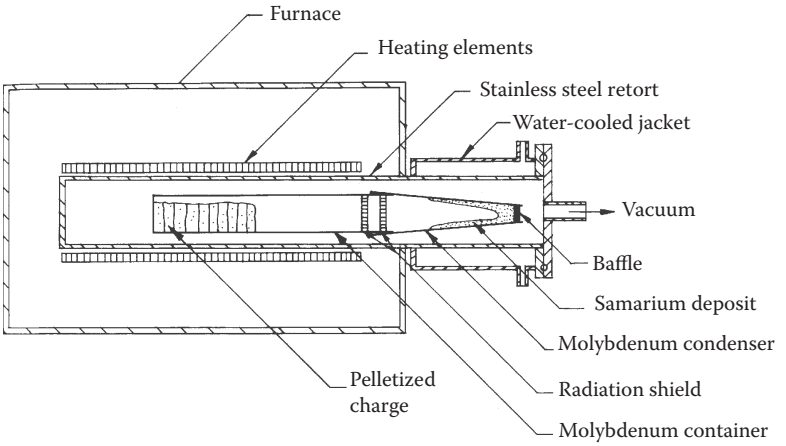


FIGURE 4.34 Larger-scale reduction–distillation assembly. (From Campbell, T.T. and Block, F.E., *J. Metals*, 11, 744–746, 1959.)

Apart from lanthanum, cerium, and zirconium, Campbell and Block (1959) tried aluminum also. It was observed that while both cerium and aluminum reduce samarium and europium oxides, they also exert appreciable vapor pressure at the operating temperature and tend to volatilize along with samarium or europium metals. Unlike cerium and aluminum, which tended to carry over into the crystalline deposit, neither lanthanum nor zirconium was detected in the rare-earth metals prepared with these reducing agents. Besides, the relatively low cost of zirconium makes it commercially more attractive.

The possibility of using cerium as the reductant in reduction–distillation was also mentioned by Daane (1961a). In addition, he also noted that good results were obtained with cheaper commercial misch metal; however, the commercial misch metal often contains volatile impurities such as magnesium, aluminum, and various halides. These impurities must be removed by vacuum melting before the use of misch metal for preparation of highly pure samarium, europium, or ytterbium. Thulium has also been prepared using misch metal as a reductant for thulium oxide, Tm_2O_3. However, the thulium metal prepared contained a few ppm of neodymium or volatile heavy lanthanides present in the misch metal. This can be attributed to the high temperature involved in the reduction. Lanthanum or cerium was used if high-purity thulium was desired.

In addition to the three metals (samarium, europium, and ytterbium) described in detail and the metal thulium mentioned earlier, heavy rare-earth metals that have vapor pressures significantly greater than lanthanum (but less than Sm, Eu, Tb, and Yb) have also been prepared by reduction distillation (Table 4.6).

Westgaard and Bjornholm (1966) prepared Yb, Sm, Dy, Er, Nd, Gd, and Lu metals, starting from their oxides, by the reduction–distillation process using lanthanum or thorium metal powder as the reducing agent. Among the listed metals, Yb, Eu, and Sm were prepared by La reduction and the remaining by thorium reduction. The vapor pressure of lanthanum is low enough to permit a clean separation only for Yb, Eu, and Sm. The reduction temperature for Sm was 1300°C. In the preparation of less volatile rare-earth metals Dy, Er, Nd, Gd, and Lu, the reduction temperatures were higher and the volatility of La could become unacceptable. In any case, Westgaard and Bjornholm (1966) studied lanthanothermic reduction of Yb, Sm, and Dy oxides also. Mixtures of scrupulously dried rare-earth oxide powder and lanthanum filings (1.2 times the stoichiometric requirement) were made and loaded into a tantalum crucible. A schematic of the reduction apparatus is shown in Figure 4.35. A tantalum stopper with a central hole is fitted on top of the crucible. The assembly is placed in an electron bombardment furnace. After further drying by evacuation to 10^{-3} to 10^{-4} Pa, the crucible was heated to temperatures ranging from 1100°C to 1750°C under high dynamic vacuum. The temperatures required for various metal reductions were as follows: Yb 1100–1200°C; Sm 1330–1400°C; and Dy 1650–1750°C. The reduction was tracked by observing the condensate growing on the W plate, which was initially placed at a distance of a few millimeters from the tantalum cap, and raised gradually as the condensate grew, to prevent shorting of the grounded tungsten plate and the crucible assembly. At the end of the experiment, after the system had cooled down, air/inert gas was let in, and the condensate easily retrieved from the tungsten plate by tapping/scrapping off.

On the basis of the vapor pressure of lanthanum and reduction temperatures used, certain amount of lanthanum contamination was to be expected in the distilled

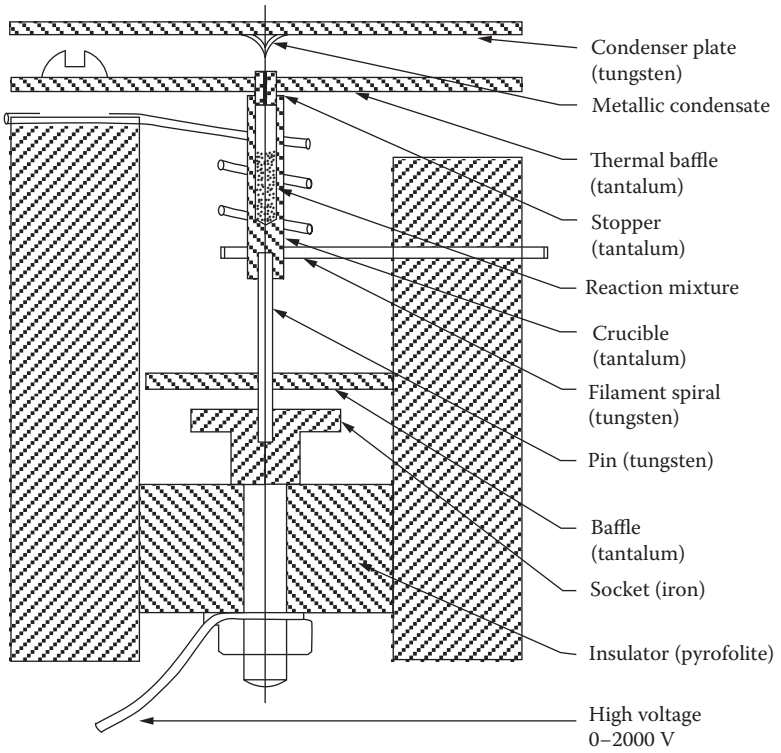


FIGURE 4.35 Schematic of the electron bombardment apparatus with crucible and condenser plate in place. (From Westgaard, L. and Bjornholm, S., *Nucl. Instrum. Methods*, 42: 77–80, 1966.)

metals. The values were as follows: Yb, Sm, < 1% La; and Dy, 5–10% La. Westgaard and Bjornholm (1966) redistilled the Dy and brought down its La content to <1%. The parameters for europium reduction were similar to those of Yb. The recovery of metallic europium from the plate had to be done under inert gas cover. The analytical values for residual impurities were obtained by neutron activation analysis.

Westgaard and Bjornholm (1966) prepared Dy, Er, Nd, Gd, and Lu metals, starting from their oxides, by reduction–distillation using thorium metal powder as the reductant. The technique was the same as described for the lanthanum reduction. The temperatures required were as follows—Dy: 1650–1750°C; Er: 1750–1850°C; Nd: 1750–1850°C; Gd: 2100–2200°C; Lu: 2300–2400°C. The distillate collected directly on a thin tantalum sheet. At the end of the experiment, the tantalum sheet along with the distillate was treated in a mixture of conc. HNO_3 and HF acids (1:1). Tantalum dissolved leaving behind the rare-earth metals that remained largely unaffected. The method is applicable for all rare earths with Z > 63 (Eu). The thorium contents in the distilled metals, as determined by NAA were as follows—Dy, Er, and Nd: <0.5%; Gd: 4%; and Lu: 12%. After a cycle of redistillation, the thorium content reduced in Gd to <1% and in Lu to 3–4%.

Westgaard and Bjornholm (1966) noted that metals could be redistilled at temperatures about 100–200°C lower than that required for the reduction–distillation. The metal yields in the process were typically 50–60% for all the metals except Gd and Lu, where the yields were only in the range 20–25%. The metals prepared were cold-worked using the pack rolling technique. The more ductile among the metals prepared—Yb and Sm—were rolled down to 0.5 mg/cm^2 and the hardest—Gd and Lu—to 1–1.5 mg/cm^2. The preparations described were for very small samples. The process should repeat without difficulty for larger configurations.

Spedding and Daane (1968) reduced a compacted mixture of the rare-earth oxide and lanthanum turnings at approximately 1500°C to prepare dysprosium and holmium metals. The yields were 85–94% in these reductions; however, the relatively low vapor pressure difference between lanthanum on the one hand and Dy and Ho on the other manifests in up to 1% lanthanum content in the condensate. The oxygen contents were also higher. Using zirconium in place of lanthanum, Spedding and Daane (1968) obtained a distillate of better quality, less than 1 ppm zirconium and approximately 150 ppm oxygen, but the yields were poor: 20–33%.

The preparation of dysprosium metal by reduction–distillation using thorium was also reported by Schiffmacher and Trombe (1969). Thorium filings were used to reduce dysprosium oxide at 1390–1750°C. The distillate was redistilled at 1600°C to obtain metal containing ppm levels of Th and O. The report did not mention the yield of the recoverable metal.

The Oak Ridge group (Kobisk and Grisham 1969) used the reduction–distillation process to prepare high-purity rare-earth metals (99.95%) that could be cold-rolled to ultrathin foils (0.00127–0.00051 mm thickness). Both lanthanum and thorium were used to produce high-purity Pr, Nd, Pm, Sm, Eu, Gd, Dy, Er, and Yb. The most volatile rare earths (Sm, Eu, and Yb) were reduced and distilled with lanthanum metal as a reductant. High-purity thorium metal was used to quantitatively reduce Pr, Pm, Dy, and Er oxides. The oxides of neodymium and gadolinium were also reduced with thorium, but reduction–distillation condensate had to be redistilled to decrease the residual thorium content. They noted that oxide reduction and product distillation proceeded best at temperatures close to or above the melting point of the reductant metal. Besides, a temperature where the vapor pressure of the product metal is approximately 10 Pa is considered ideal. The conditions for reduction–distillation for preparing various metals were determined by Kobisk and Grisham (1969) and listed in Table 4.7.

Kobisk and Grisham (1969) have listed various factors for ensuring efficient reduction–distillation. The oxide and reductant powder are mixed thoroughly and pelletized at ~10 MPa (1500 psi) to provide intimate contact between them. The pellets are so loaded in the reactor that there is good thermal conduction between the metal reactor, which is the heat source, and the reaction mixture. They estimated that the pellet is 100–200°C cooler than the reactor wall. The reactor and distillation column (Figure 4.36) are made of tantalum (Kobisk and Adair 1979). The reaction mixture is heated (by Joule heating, electron bombardment, or radio-frequency induction) to a temperature that exceeds the temperature at which the reduction reaction occurs. The process is carried out in a vacuum chamber pumped to 10^{-4} Pa or less. Maintaining a high level of dynamic vacuum ensures that the amount of

TABLE 4.7
Conditions for Reduction–Distillation Procedure for Rare-Earth Metals

Metal Oxide	Reductant	Reaction Temperature (°C)	Crucible Material	Heating Technique	Collection Efficiency
Pr	Th	1900–2000	Ta	Joule heating Electron bombardment heating Radiofrequency induction heating	75
Nd	Th	1950–2000	Ta	Joule heating Electron bombardment heating Radiofrequency induction heating	75
Pm	Th	1500–1700	W	Electron bombardment heating	75
Sm	La	1300–1350	Ta	Joule heating Radiofrequency induction heating	78
Eu	La	1150–1200	Ta	Joule heating Radiofrequency induction heating	92
Gd	Th	1900–1950	Ta	Joule heating Radiofrequency induction heating	75
Dy	Th	1750–1800	Ta	Joule heating Radiofrequency induction heating	80
Er	Th	1850–1900	Ta	Joule heating Radiofrequency induction heating	85
Yb	La	1125–1200	Ta	Joule heating Radiofrequency induction heating	90

Source: Kobisk, E.H. and Grisham, W.B., *Mater. Res. Bull.*, 4: 651–662, 1969.

reactive residual gas surrounding the reaction mixture is limited, and ultrahigh purity in the condensed metal is achieved.

The vapors streaming out of the still can, in principle, be collected by placing a cooled substrate a very short distance above the reduction chamber port. However, to condense rare-earth-metal vapors in conditions of high purity and maximum collection efficiency, Kobisk and Grisham (1969) used a thin quartz dome (hemisphere) shown schematically in Figure 4.36, on top of a distillation column (Ta). The figure illustrates the vacuum chamber assembly incorporating the induction-heated reactor still and a quartz (SiO_2) domelike receiver placed immediately over the vapor exit tube of the still. Internal baffling is used to condense lower vapor pressure impurities and to inhibit dusting during reaction. The quartz domes can be shaped into any geometry, and most metal condensates can be easily released from the quartz when cooled to room temperature. The typical analysis of rare-earth metals prepared by reduction–distillation at ORNL are listed in Table 4.8.

The lanthanothermic reduction procedure used by the Ames group (Beaudry and Gschneidner 1978) for the preparation of Sm, Eu, Tm, and Yb by oxide reduction was extended to all the 14 lanthanides by Pengo et al. (1991). They used 99.95% pure hafnium powder as the reducing agent mainly on the stated basis of its very low vapor pressure. The amount of hafnium used in the charge was twice the stoichiometric

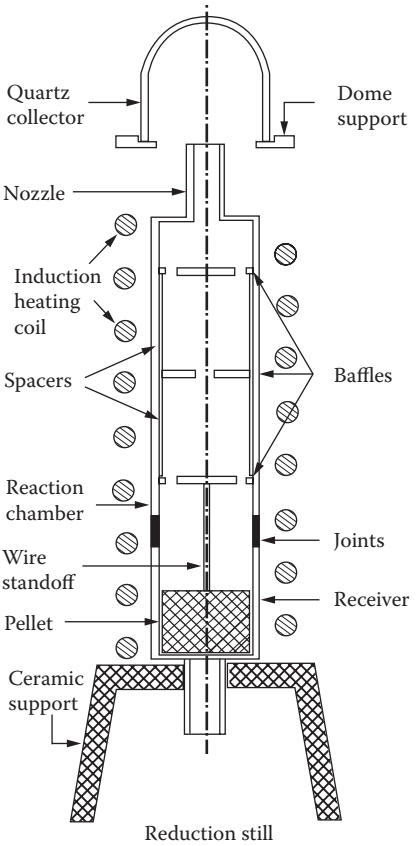


FIGURE 4.36 Schematic of the tantalum reduction still—with ceramic insulator mounting, internal tantalum baffles, and hemispherical quartz condenser in place. (From Kobisk, E.H. and Adair, H.L., *Nucl. Instrum. Methods*, 167: 153–160, 1979.)

requirement. The mixture was pressed in to a pellet and loaded in a tantalum crucible. In these experiments, the charge and the system were meticulously degassed by heating in vacuum, and the levels of vacuum used were better than 10^{-4} Pa. The distilled metal was collected in quartz dome maintained at room temperature. Pengo et al. (1991) carried out all the material handling operations under protective inert gas cover and obtained results summarized in Table 4.9. Except with europium, they succeeded in using reduction–distillation to obtain pure specimens of lanthanide metals from their oxides. The quality of metal produced is indicated by the size and weight of the rolled metal.

Clifford et al. (2002) investigated metallothermic oxide reduction–distillation as a means to prepare ultrahigh-pure metals including Sm, Eu, and Yb in addition to several non-rare-earth metals. Using an experimental system that consisted of a new design of vapor collector, they were able to consistently achieve collection efficiencies in excess of 90% for each of these three rare-earth metals. They used hafnium

TABLE 4.8
Analysis of Typical Rare-Earth Metals Prepared by Reduction Distillation

Impurity Element	Analyses (ppm)					
	Samarium		Erbium		Neodymium	
	Oxide	Metal	Oxide	Metal	Oxide	Metal
Al	20	20	50	50	60	20
Ca	300	80	2000	200	30	8
Fe	10	10	70	20	100	40
Si	40	40	100	100	1000	400
Ta	4	4	40	10	1	4
W	<0.4	<0.4	8	8	3	8
Pr	<0.1	<0.1	3	3	1	0.3
Eu	<2	<2	0.2	<0.2	<0.2	<0.2
Tm	<10	<10	300	100	1	1
Total	457	232	2758	722	1299	581

Source: Kobisk, E.H. and Grisham, W.B., *Mater. Res. Bull.*, 4: 651–662, 1969.

TABLE 4.9
Summary of the Results Obtained for the Reduction of the Different Rare-Earth Oxides

Element	Reduction Temperature (°C)	Collection Efficiency (%)	Rolled Film Thickness (μg/cm²)
Lanthanum	1750	72	700
Cerium	1750	65	600
Praseodymium	1650	50	1000
Neodymium	1800	60	1000
Samarium	1400	60	700
Europium	1200–1600	–	–
Gadolinium	1800	60	450
Terbium	1800	25	500
Dysprosium	1750	45	600
Holmium	1750	50	500
Erbium	1600	40	700
Thulium	1650	40	700
Ytterbium	1200	60	700
Lutetium	1750	25	750

Source: Pengo, R. et al., *Nucl. Instrum. Methods Phys. Res. A*, 303: 146–151, 1991.

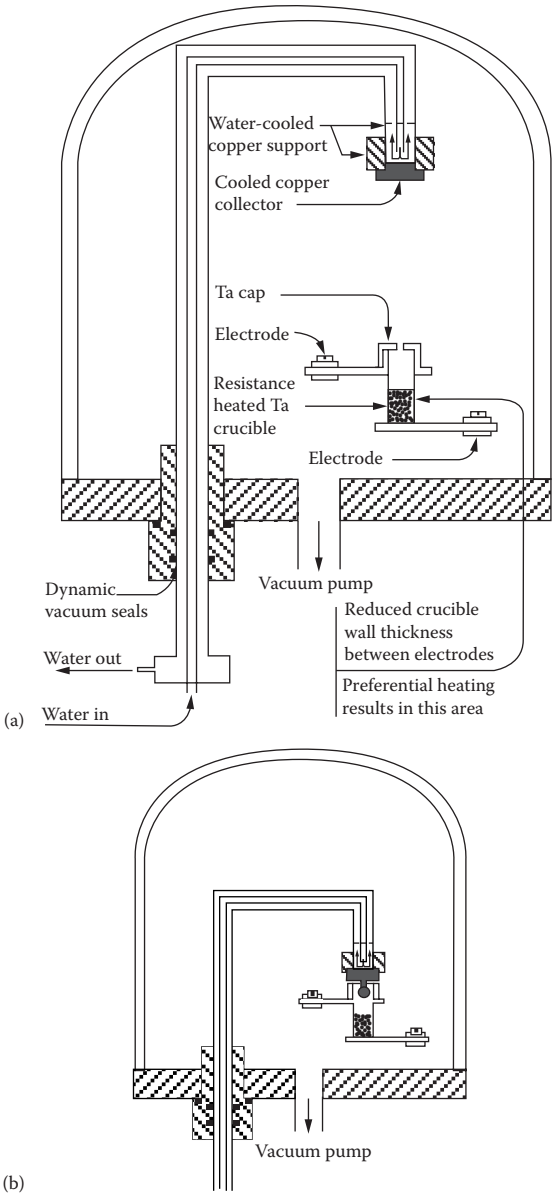


FIGURE 4.37 Metallothermic reduction system: (a) collector remote from crucible exit and (b) collector in position above reaction crucible. (From Clifford, S. et al., *Nucl. Instrum. Methods Phys. Res. A*, 480: 29–35, 2002.)

or lanthanum as the reductant. The systems used by Clifford et al. (2002) are shown schematically in Figures 4.37a, b and 4.38. Figure 4.37a is the diagram of the metallothermic reduction system provided with a water-cooled copper collector for the condensate (Clifford et al. 2002). During the mandatory degassing prior to reduction, the collector could be swiveled to a location away from the exit orifice of the tantalum crucible. After degassing is complete, the copper collector was moved into its collecting location immediately above the crucible cap (Figure 4.37b). The tantalum crucible and its contents (oxide + 50% molar excess of the reductant) were heated to the predetermined reduction temperature by resistance heating. The temperature and duration of heating for each of the three metals are listed in Table 4.10.

The schematic of the induction-heated vacuum distillation still used for purification is shown in Figure 4.38. Apart from the crucible and baffles, the water-cooled collector was also fabricated from tantalum. An example given by Clifford et al. (2002) related to how significant increases in metal purity could be achieved by vacuum distillation using the apparatus described above. Ytterbium obtained by reduction–distillation of ytterbium oxide with lanthanum contained 3–700 ppm lanthanum, depending on the reduction duration. After a single vacuum distillation of the contaminated ytterbium, the purified Yb contained only 3 ppm of lanthanum, thereby validating this technique to prepare highly pure metals.

Onstatt (1953) used calcium in place of lanthanum for reduction of Sm_2O_3, and the samarium metal was distilled. Calcium is more volatile than lanthanum. Distillation had to be repeated three to four times to reduce the calcium content in the reduced metal to less than 0.1%. The metal yield was only about 40%. The calcium reduction method turned out to be more laborious and less effective than the lanthanum reduction.

Achard (1957) used carbon in the reduction–distillation process for samarium preparation. The distilled product contained considerable oxygen; however, a second distillation in a Ta apparatus at 1–10 mPa yielded pure, malleable samarium. Europium and ytterbium were also prepared by the above process. Their purities were better.

The oxide reduction–distillation process, also called the direct reduction technique, has been in commercial use since 1959 to produce 99.9% pure (nuclear grade)

TABLE 4.10
Collection Efficiencies for Elements Obtained from Their Oxides by Metallothermic Reduction

Element	Oxide	Reduction Temperature (K)	Reduction Time (min)	Reductant	Collection Efficiency (%)
Sm	Sm_2O_3	1520–1820	80	Hf	90
Yb	Yb_2O_3	1470–1710	100	La	91
Eu	Eu_2O_3	1170–1410	80	La	92

Source: Clifford, S. et al., *Nucl. Instrum. Methods Phys. Res. A*, 480: 29–35, 2002.

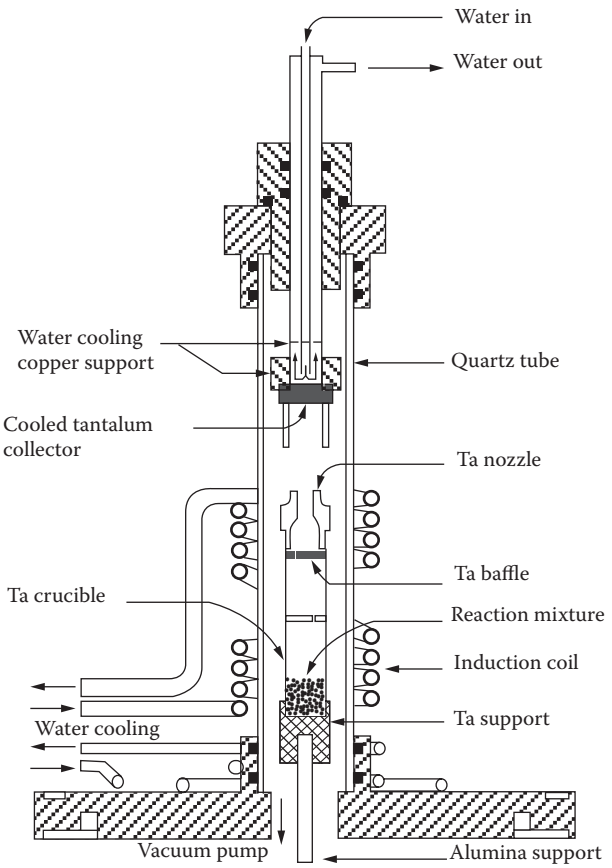


FIGURE 4.38 Diagram of the vacuum distillation still. (From Clifford, S. et al., *Nucl. Instrum. Methods Phys. Res. A*, 480: 29–35, 2002.)

rare-earth metals (Moriarty 1968). The reduction reactor consisted of a molybdenum crucible and a tantalum condenser. It took about 2–3 h of slow heating of a reaction mixture containing 1.4 kg of oxide to get about 1 kg of metal in the condensate. The condensate was consolidated by inert atmosphere melting and casting in an induction furnace. The direct reduction has been commercially used only for the preparation of samarium, europium, ytterbium, and thulium metals (Beaudry and Gschneidner 1978; Daane 1961a).

4.9 NEW REDUCTION PROCEDURES

Certain modified or new reduction procedures, using magnesium, calcium, or even sodium for reduction of the rare-earth oxides, have also been investigated. The rare-earth-metal product is obtained directly as a powder or as an intermediate alloy that has to be pyrovacuum-treated to obtain the metal.

4.9.1 Metallothermic Reduction in Molten Salt

A novel method for calciothermic reduction of rare-earth oxides was investigated at General Motors (Sharma 1987). The method has been applied to the reduction of neodymium oxide. Neodymium metal was produced by metallothermic reduction of Nd_2O_3 with calcium in a $CaCl_2$–NaCl melt, at temperatures between 710°C and 790°C by the overall reaction

$$Nd_2O_3 + 3Ca \rightarrow 3CaO + 2Nd$$

The metal was recovered from the salt melt by extraction into a molten Nd–Zn alloy pool. Later on, zinc was removed from the alloy by vacuum distillation. The basis of the technique and its application described by Sharma (1987) and Sharma and Seefurth (1988) are as follows.

Neodymium metal cannot be produced by the reduction of Nd_2O_3 with sodium by the reaction

$$Nd_2O_3 + 6Na \rightarrow 3Na_2O + 2Nd$$

But, calcium can reduce Nd_2O_3 according to

$$Nd_2O_3 + 3Ca \rightarrow 3CaO + 2Nd$$

and calcium can be generated by the reaction of $CaCl_2$ with sodium according to the reaction

$$CaCl_2 + 2Na \rightarrow Ca + 2NaCl$$

It therefore follows that Nd_2O_3 can be reduced to neodymium metal according to the reaction

$$Nd_2O_3 + 3CaCl_2 + 6Na \rightarrow 3CaO + 2Nd + 6NaCl$$

The above conclusions were arrived at from the standard free energy change data (Sharma and Seefurth 1988) for the various reactions plotted in Figure 4.39.

A metal in solution of its salt is more corrosive than when in its pure state. Thus, calcium in solution with $CaCl_2$ or $CaCl_2$–NaCl will react with Nd_2O_3 faster than pure calcium. According to Sharma and Seeforth (1988a), at temperatures between 710°C and 1100°C, $CaCl_2$–NaCl melts with greater than 70 wt.% $CaCl_2$ to provide a high-enough concentration of Ca for the reduction to occur at an appreciable rate. That the reduction of Nd_2O_3 is effected by calcium dissolved in the molten salt phase and that calcium metal is appreciably soluble in $CaCl_2$–NaCl melts are critical to the kinetics of the process. Carrying out the calciothermic reduction in $CaCl_2$–NaCl melts also facilitates separation of Nd from CaO and keeps CaO from interfering with the reaction. Nd_2O_3 can react with $CaCl_2$ to form the oxychloride, NdOCl. However, the neodymium oxychloride so formed is also reduced to the metal by calcium

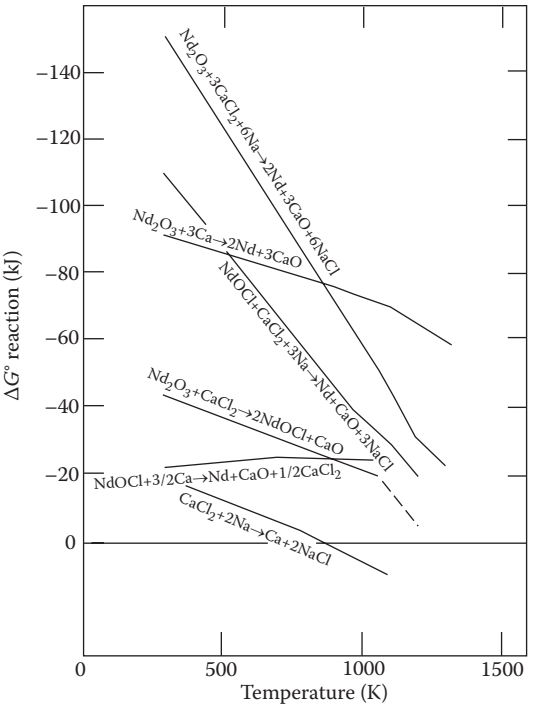


FIGURE 4.39 Standard free energy change of reactions as a function of temperature. (From Sharma, R.A. and Seefurth, R.N., *J. Electrochem. Soc.*, 135: 66–71, 1988.)

$$NdOCl + 1.5Ca \rightarrow Nd + CaO + 0.5\ CaCl_2$$

Complete separation of the neodymium metal from the salt phase is possible by dissolving neodymium in a liquid metallic pool, which can be a Nd–Zn or a Nd–Fe melt. With the density of the molten alloy being greater than that of the salt and CaO, there should be no difficulty in separating the metallic pool from the molten salt. Neodymium, which melts at 1021°C, can be separated from zinc that boils at 907°C by vacuum distillation; the vapor pressure of neodymium is negligible (~10^{-4} Pa) at this temperature. Extraction in Nd–Fe molten pool is preferred for the Nd–Fe alloy destined for magnetic alloy production.

Sharma (1987) carried out all experiments in a helium atmosphere (<1 ppm O_2, N_2, or H_2O) dry box that had a furnace (130 mm diameter by 550 mm depth) extending beneath its floor. A schematic of the apparatus in the furnace well is shown in Figure 4.40. The reduction was carried out in the tantalum crucible. Calculated quantities of neodymium (99% pure) and zinc (99.9+% pure) metals were first combined in the tantalum crucible to make the molten eutectic. At this stage, pre-weighed salt components (sodium chloride and anhydrous calcium chloride) were added to the crucible, and the temperature for reduction (700–725°C) was reached. Calculated quantities of Nd_2O_3, calcium metal granules, and sodium were added to the molten

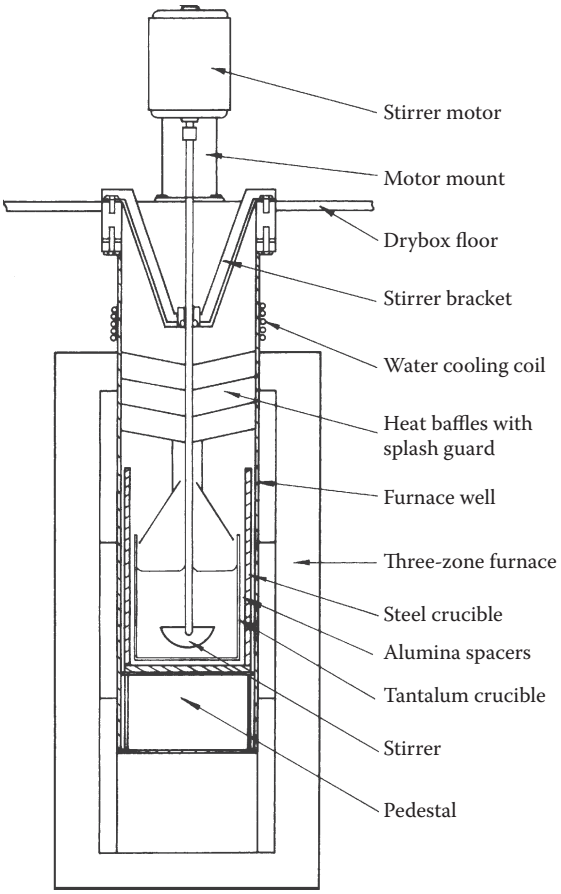


FIGURE 4.40 Schematic diagram of the reduction apparatus. (From Sharma, R.A. and Seefurth, R.N., *J. Electrochem. Soc*., 135: 66–71, 1988.)

bath. The salt bath and its contents were kept stirred till the reaction was complete. At the end of the reaction, the apparatus was pulled out from the furnace well and quenched. Completion of reaction was ascertained by taking radiographs of the reaction vessel to observe a clear, sharp interface between the salt and metal pool, and an increase in metal pool depth indicated completion of reaction. Salts were washed out of the crucible with warm running water, and the alloy product was recovered. A Nd–Zn alloy of nominal composition 90–10 was obtained in the reduction stage with nearly 98% recovery of Nd, and after vacuum distillation, +99% pure Nd was obtained. The reaction conditions and product details are given in Table 4.11.

Using a Nd–Fe pool instead of Nd–Zn pool, Sharma and Seefurth (1988) were able to extract reduced neodymium in the iron alloy using an essentially similar procedure. In another investigation, Sharma and Seefurth (1988) used sodium instead of Ca to reduce neodymium oxide and extract the metal in the iron alloy. Sodium

TABLE 4.11
Reduction Extraction of Neodymium from Nd_2O_3 in a Molten Salt with Sodium

Salt bath composition (g)	NaCl: 118, $CaCl_2$ 1060
Eutectic alloy Nd–Zn (g)	300
Reactants (g)	Nd_2O_3 233, Ca 91.8, Na 20
Reaction conditions	
Temperature (°C)	700–725
Duration (h)	4 h, with stirring (300 rpm)
	1 h, with stirring (60 rpm)
Product (g)	Nd 195.7
Recovery in alloy pool (%)	97.9
Vacuum distillation	
Temperature (°C)	1100

	Analysis (wt.%)						
Element	**Nd**	**Zn**	**Al**	**Si**	**Ca**	**Mg**	**Fe**
Alloy	90.2	9.9	0.5	0.1	0.03	0.05	0.05
Metal	99+	0.002	0.4	0.1	0.01	0.001	0.03

Source: Sharma, R.A., *J. Metals*, 39(2): 33–37, 1987.

reduction can also be used for obtaining the product first as Nd–Zn alloy and then the metal. This would be commercially more attractive than using calcium.

The molten salt oxide reduction process has not so far been reported for any other rare earth, except neodymium. Its applicability, however, appears wider.

4.10 CARBOTHERMIC REDUCTION

According to the Ellingham diagram, other than calcium, the only element that can reduce all the rare-earth oxides is carbon. In fact, at about 1750°C and with a CO pressure below 100 Pa, carbon is the most efficient reducing agent (Kruger 1971). Even the reduction of rare-earth oxides by carbon is, however, beset with problems. Carbides are formed during the reduction. The rare-earth carbides are high-melting and form extensive and stable solid solutions with oxygen and nitrogen. It is often possible, however, to avoid the formation of carbides in reactive metals reduction by choosing appropriate conditions of temperature, CO/CO_2 ratio, and high vacuum. These conditions are arrived at with the aid of Pourbaix–Ellingham diagrams. Neither these diagrams nor the complete set of thermodynamic data for constructing such diagrams are available for the rare earths. Besides, many of the rare earths are relatively low-melting and/or volatile at high temperatures, and the simultaneous vaporization of reduced metal and CO would lead to a reverse reaction occurring and also carbon contamination. These factors have made carbothermic reduction very difficult for rare-earth-metal production.

An interesting possibility of carbothermic reduction has emerged from the use of a suitable solvent (Anderson and Parlee 1976) to dissolve the reduced metal and lower its chemical activity to a level at which no carbides can form. In addition, high-temperature refractory attack and vaporization loss are also avoided. The technique is yet to be tried for the rare earths.

4.11 ELECTROLYTIC PRODUCTION OF RARE-EARTH METALS

Unlike the chemical reduction processes, all of which basically rely on the availability of reducing agents that form more stable chlorides, fluorides, and oxides than those of the rare-earth metals, the electrolytic reduction of compound intermediates for the preparation of metals is not limited by considerations of chemical stability. The standard free energy of formation of a compound, which is the measure of its chemical stability, is related to its decomposition potential by the equation $\Delta G^\circ = -n\mathrm{FE}^\circ$, and it can be calculated that an applied voltage as small as 4 V should be more than adequate to dissociate even the stablest chemical compound (Alcock 1976). However, in the same way as chemical stability is one of the many qualities of a reducing agent necessary for it to be used in practical processes, theoretical decomposition potential is but one of the several requirements of a compound intermediate for it to be electrolytically decomposed in practical processes. When the other requirements are also satisfied, electrolytic reduction offers an effective method for reducing stable rare-earth compounds to metals.

The electrolytic process for reducing metals from their salts or compound intermediates is basically simple. The salt of the metal is dissolved in another salt or a mixture of salts that are kept molten in an inert container. Two electrodes—a cathode and an anode—are inserted into the molten bath, and an electric current is passed through the circuit, with a voltage sufficient to reduce the salt. The molten salt, known as the carrier electrolyte, first of all, serves as a solvent for the metallic salt to be reduced, known as the functional electrolyte. The carrier electrolyte is so chosen to have a certain desirable solubility for the functional electrolyte, sufficient conductivity for the electric current, a melting point below the chosen operating temperature of the cell, low vapor pressure, and greater thermodynamic stability than the functional electrolyte. These properties are normally obtained by using an alkali or alkaline earth fluoride or chloride or a mixture of these fluorides and chlorides. Considerable variety is also observed in the cells used for electrolysis. These pertain to their size, shape, materials of construction, and disposition of the electrodes. Iron, graphite, ceramics such as firebrick and alumina, and refractory metals such as molybdenum and tungsten have all been used as cell materials. The anode is usually made of graphite, and the cathode is iron, molybdenum, or tungsten. Often the cell body itself serves as the anode or cathode. The temperature in the cell can be maintained in two ways, and on this basis, the electrowinning cells associated with rare-earth technology have been divided into two types. In one type, the electrolytic current is used to supply the heat necessary to keep the bath molten, and in the other type, supplemental thermal energy is provided to the bath by a furnace or by an arrangement in the cell independent of the electrolysis circuit.

The largest quantity of rare-earth metals commercially produced throughout the world is obtained by electrolytic methods. Lanthanum, cerium, praseodymium, and neodymium have melting points that permit their recovery in the liquid state by electrolysis of relatively inexpensive chlorides at temperatures less than 1100°C. Winning of rare-earth elements in the liquid state facilitates slag (electrolyte)–metal separation, minimizes contamination of the reduced metal, and enables continuous operation and high volume levels of production. The technical feasibility of preparing limited quantities of high-melting rare-earth metals such as gadolinium, dysprosium, and yttrium in consolidated form has also been demonstrated by using the fluorides as electrolytes in place of chlorides. These have been carried out in specially designed high-temperature cells. The advantages of liquid product recovery and low-temperature operation have been realized even in the case of high-melting rare-earth metals by using metals like cadmium, magnesium, zinc, manganese, chromium, and cobalt as cathode. These metals form liquid alloy with the rare-earth metal as it electrodeposits, and liquid product recovery is therefore facilitated.

In the beginning, rare-earth chlorides were electrolyzed in a fused salt to obtain the metal, and the direct electrolytic reduction of the rare-earth oxide dissolved in a mixture of rare earth and other fluorides was investigated later (Morrice and Wong 1979).

4.11.1 Chloride Electrolysis

The important investigations on the electrolysis of rare-earth chlorides are summarized in Table 4.12.

The possibility of electrolytic reduction of a molten salt for preparation of rare-earth metals was first demonstrated in 1875 by Hillebrand and Norton. They prepared a few grams of cerium, lanthanum, and didymium in a coherent form

TABLE 4.12
Electrolysis of Rare-Earth Chlorides

Year	Electrolyte	Electrodes[a]	Cell	Product	Reference
1902	$RECl_3$–NaCl–KCl	Carbon	Water-cooled copper	Several kilograms of Ce, La nodules	Muthmann et al. 1902
1912	$CeCl_3$–NaCl	Graphite (A) Cell (C)	Iron	Massive Ce	Hirsch 1912
1923	$LaCl_3$–KF–NaCl	Carbon (A) W (C)	Iron	La metal (0.77% Fe)	Kremers and Stevens 1923
1931	$CeCl_3$–CaF_2	Carbon (A) Mo (C)	Fluorspar	Ce ingot (99.8% pure)	Billy and Trombe 1931
1940	$RECl_3$–NaCl–KCl	Graphite (A) Fe (C)	Refractory lining	La, Ce, Di,[b] misch metal (99.5–99.9% pure)	Hirschhorn 1968

[a] A: anode; C: cathode.

[b] Di: Nd + Pr.

by the electrolysis of fused rare-earth chlorides using iron electrodes. The cell consisted of two porcelain crucibles, one of which was porous. The rare-earth chloride was melted in the porous crucible, which was then placed into the other porcelain crucible containing the sodium chloride–potassium chloride eutectic mixture. The cathode was placed in the rare-earth chloride melt, and the anode, which was an iron cylinder, was located in the sodium chloride–potassium chloride melt. The demonstration by Hillebrand and Norton was followed up by Frey (1876) and Muthmann et al. between 1902 and 1907. Frey (1876) reported that he had prepared rare-earth metals using the fused salt technique developed by Bunsen. Muthmann et al. (1902), Muthmann and Weiss (1904), and Muthmann and Scheidemandel (1907) reported the preparation of many metals in the cerium group (cerium, lanthanum, praseodymium, neodymium, and samarium) by electrolyzing fused rare-earth chlorides in a water-cooled copper vessel with carbon electrodes. The cell is shown schematically in Figure 4.41. The water-jacketed copper vessel used to hold the fused chloride bath was not part of the electrical circuit. Copper was protected from attack by molten rare-earth metal by a thin layer of frozen salt. Through the bottom of the copper vessel, the carbon rod cathode projected into the cell. This rod was electrically insulated from the vessel by porcelain rings. The anode, which was also a carbon rod, was introduced into the bath from the top of the cell. This cell arrangement was known as the Muthmann-type cell in the early literature. Several pounds of 99.92% pure cerium were prepared in one experiment in which a molten bath containing cerous chloride and sodium chloride–potassium chloride eutectic mixture was electrolyzed.

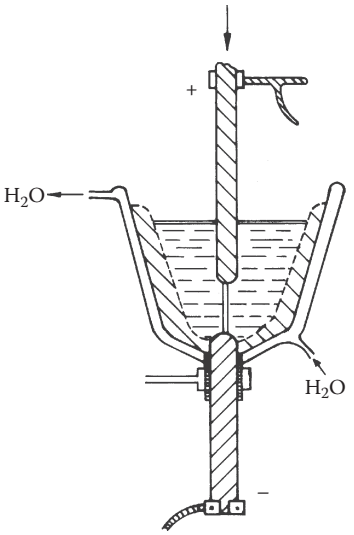


FIGURE 4.41 Schematic of Muthmann-type electrolysis cell. (From Trombe, F., Preparation of rare earth metals, In *Proc. Symp. Rare Metals, Bombay*, December 1957, pp. 402–444. The Indian Institute of Metals and Bhabha Atomic Research Center, 1957.)

Cerium and lanthanum were obtained in the form of large nodules. The metals contained some amount of carbon picked up from the cathode. Neodymium was recovered only in very small nodules, and praseodymium could not be electrowon in this cell. The failure was attributed to the formation of oxychlorides. As regards samarium, only a thin deposit of samarium metal was obtained on the cerium cathode from a fused bath of $SmCl_3$–$BaCl_2$.

A Muthmann-type cell, with graphite instead of copper as cell material, was used by Hirsch (1912) to electrolyze cerium and other rare-earth chlorides. This, however, resulted in the formation of carbides, which made the bath viscous and unsuitable for electrolysis. To circumvent this difficulty, Hirsch replaced the graphite container with a wrought iron crucible. Electrolysis of a molten mixture composed of 90% anhydrous $CeCl_3$ and 10% NaCl at 12–14 V with an average current of 200 A yielded 580 g of cerium ingot in 4 h. The current efficiency was 41.5%. Iron was the major impurity in the metal, which was 97.8% cerium.

Cerium was produced in good yield by Thompson (1917) who electrolyzed industrial-grade anhydrous fused rare-earth chloride in an iron crucible that served as the cathode, with a graphite anode. In addition to cerium chloride, the electrolyte consisted of sodium chloride, potassium chloride, and barium chloride added in small quantities to increase the resistance of the bath and check its decomposition.

Hicks (1918) reported the preparation of *yttrium mixed metal*, a mixture of yttrium and higher-melting rare-earth metals, in a powder form by electrolysis in a chloride bath at 900–1100°C. His cell consisted of a graphite container that was the cathode, and a graphite anode. He observed the formation of carbides. This was minimized in later experiments by lining the sides of the crucible with alumina.

Schumacher and Lucas (1924) electrolyzed fused anhydrous rare-earth chlorides in a cell consisting of a graphite crucible cathode and a graphite anode. On finding that much of the reduced metal was dispersed throughout the bath in the form of small particles, they raised the temperature of the bath at the end of each run by increasing the DC amperage. This was done to permit the metal particles coalescence at the bottom of the crucible in liquid form. The product was remelted in a magnesia crucible. The authors reported that the cerium prepared by the above procedure was 99.9% pure with only 0.03% carbon and 0.03% iron as impurities. Schumacher and Harris (1926) used the same procedure two years later to prepare small amounts of metallic cerium, lanthanum, praseodymium, neodymium, and samarium. The inclusion of samarium in the list is surprising because in a straight process, it is not amenable to electrolytic reduction to metal. The metals were remelted in magnesia crucible. The reported impurity contents in the metals were 0.03% carbon and 0.02% iron. Magnesium content was not, however, reported. Externally heated cells for electrolysis thus began to be used for rare-earth-metal preparation.

Beginning in 1923, a series of investigations on the electrowinning of rare-earth metals were carried out by Kremers and various coworkers (Kremers and Stevens 1923; Thompson and Kremers 1925). A graphite or iron crucible was used as the bath container and cathode, and the anode was carbon. The cell was heated in a resistance-type muffle furnace to the required temperature. During electrolysis, the bath temperature was kept below the melting point of the rare-earth metal. Toward

the end of electrolysis, however, the temperature was raised above the melting point to coalesce the cathode product. By electrolyzing the appropriate rare-earth chloride–sodium chloride mixtures in iron crucibles, cerium-free misch metal, lanthanum, cerium, and neodymium metals were prepared in quantities ranging up to 60 g. The metals were heavily contaminated with iron. Lanthanum and cerium contained up to 32% iron and neodymium up to 6.5% iron. Similar contamination resulted when lanthanum was prepared using a graphite crucible—lanthanum carbide was formed.

The metals obtained in the investigations described so far were generally not quite pure. The impurities resulted from cell material, electrodes, electrolyte, and also insufficiently separated rare-earth starting materials. Initially, attempts were made to find electrode and cell construction materials that were resistant to attack by both the molten electrolyte and molten metal. Later, as high-purity starting materials became available for the electrolysis, contamination from that source was also tackled.

The first directed attempt at reducing electrode contamination in rare-earth metals obtained by fused salt electrolysis was made by Kremers and Stevens (1923). They electrolyzed lanthanum chloride in a bath containing sodium chloride and potassium fluoride using a carbon anode and a tungsten cathode. The cell was an iron crucible, and this was not part of the electrical circuit. Lanthanum obtained did not contain any tungsten but contained 0.77% iron. Contamination from the electrode was circumvented.

Molybdenum was recognized as a suitable cathode material after Guertler (1923) reported that molybdenum is insoluble in the rare earths at red heat. Molybdenum was used as the cathode in the experiments for the preparation of high-purity rare-earth metals. A carbon crucible was used as the anode, and the cathode in the form of a rod was spinning. The cell arrangement is shown in Figure 4.42. A fluorspar

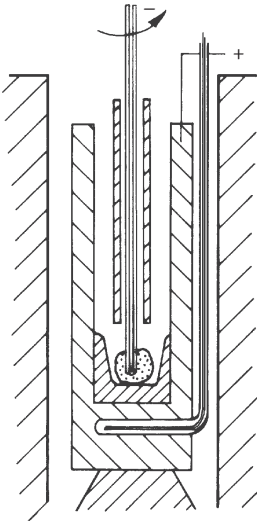


FIGURE 4.42 Schematic of Trombe-type electrolysis cell. (From Trombe, F., Preparation of rare earth metals, In *Proc. Symp. Rare Metals, Bombay*, December 1957, pp. 402–444. The Indian Institute of Metals and Bhabha Atomic Research Center, 1957.)

crucible was placed below the cathode in the melt to collect the product. The cell was heated externally to the required temperature. Fluorspar did not contaminate the rare-earth-metal product (unlike crucibles made of quartz, graphite, and certain ceramics that contaminated the product), but the chloride–fluoride melts dissolved fluorspar and became more viscous, making the in-cell operation difficult. Billy and Trombe (1931) conducted the electrolysis at 850°C using 25 g cerium trichloride and 16 g calcium fluoride as the electrolyte and obtained 9 g of cerium ingot in 90 min. The product contained only a small amount of molybdenum and no calcium. Lanthanum ingots were prepared by Trombe (1932) by electrolysis of $LaCl_3$–KCl–CaF_2 bath at 960–980°C. The ingot contained 0.05% silicon and 0.006% iron. Trombe (1932) also prepared neodymium by electrolyzing a mixture of $NdCl_3$–KCl–CaF_2 at 1040–1060°C. The neodymium product contained less than 0.05% silicon, 0.02% iron, and a trace of calcium. In this preparation, using a quartz crucible instead of fluorspar resulted in the silicon content in the product rising to 0.6%.

Weibke (1939) used the Trombe-type cell but with a crucible made of alumina instead of fluorspar to collect the metal. The molten salt was a fused mixture of $LaCl_3$–KCl–CaF_2, and molten lanthanum metal of 99.86% purity was collected in the alumina crucible. Gray (1951) essentially repeated Trombe's experiment with cerous chloride and obtained cerium metal that was up to 99.7% pure. His cell is shown schematically in Figure 4.43. He used crucibles made of beryllia, stabilized zirconia, and fluorspar to collect the molten cerium metal product. The use of beryllia resulted in 0.01–0.1% of beryllium impurity in the metal. Calcium, iron, and

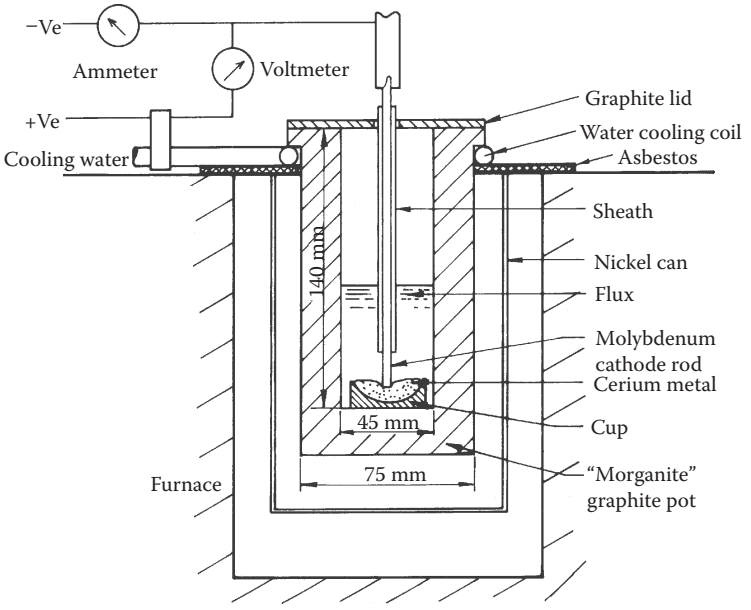


FIGURE 4.43 Gray's cell for electrolysis of cerium trichloride. (From Gray, P.M.J., *Trans. Inst. Min. Met.*, 61 (Oct. 1951–Sept. 1952): 141–170, 1951.)

magnesium oxides present in stabilized zirconia were found to react with molten cerium metal. Fluorspar was found to dissolve in molten chloride causing an increase in bath viscosity. The increasingly viscous bath rendered the electrolytic process unworkable beyond 30 min.

Kojima and Sato (1954) electrolyzed a molten mixture of 108 g of rare-earth chlorides and 99 g of KCl and obtained 22 g of misch metal in about 4 h. They purified their starting bath materials to remove oxygen and also prevented the surface of the melt from contacting air. They achieved current efficiency as high as 77% in some experiments. A LiCl–KCl eutectic containing $CeCl_3$ was electrolyzed at 850°C by Eastman et al. (1955). Cerium ingot weighing 15–100 g was obtained in each run at 80% current efficiency. The metal yield was found to improve from 82% to 97% with exclusion of air from the electrolyte cell. Eastman et al. (1955) used a beryllia or zirconia crucible below the tungsten cathode to collect the molten cerium metal. This cell arrangement was similar to that used by Trombe. The beryllia crucible was not attacked in the chloride system. A molten bath of $LaCl_3$–KCl at 900°C was electrolyzed by Kuroda (1957) to obtain lanthanum ingot. The metal contained 0.041% silicon, 0.034% aluminum, and 0.13% potassium. A high current efficiency of 91.7% was achieved. The effects of variables such as cathode current density, bath temperature, duration of electrolysis, addition of KCl, and distance between electrodes on the current efficiency were all investigated.

Ivanovskii and Ilyushchenko (1961) reported that rare-earth metals can be selectively electrodeposited from a melt consisting of mixed rare-earth chlorides and potassium chloride. Starting from a rare-earth chloride composition of 26% lanthanum, 53.9% cerium, and 21.1% other rare-earth elements, they electrodeposited alloys with low lanthanum content (≤3%) and a cerium content of ≤80%. The melt temperature was 560–700°C, and cathode current density was 0.25–1 A/cm^2.

4.11.2 Electrowinning at Room Temperature

Attempts have been made to prepare rare-earth metals at room temperature in both aqueous and nonaqueous media. In aqueous solutions, electrolysis is complicated by hydrogen formation even when the cathode displays a high hydrogen overvoltage, as in the case of mercury. The results of efforts in aqueous solutions, alcohols, ethylenediamine, pyridine, and other organic solvents have been discouraging. However, it was reported by McCoy (1941) that europium and ytterbium amalgams were prepared from potassium citrate solutions.

Starting in 1931, Audrieth, Hopkins, and others (Audrieth et al. 1931; Hopkins and Audrieth 1934; Jukkola et al. 1934; Meints et al. 1937) published a series of reports on the preparation of lanthanum, cerium, samarium, neodymium, and yttrium amalgams from their respective salts by electrolysis in aqueous solution as well as in organic solvents using a mercury cathode. Electrolysis of concentrated solutions of anhydrous chlorides dissolved in absolute ethyl alcohol yielded the best results. The amalgams were vacuum-distilled to remove mercury. The resulting rare-earth-metal powders were then heated in crucibles lined with the respective rare-earth oxides to result in small pellets of lanthanum, neodymium, and cerium.

Sklyarenko and Sakharov (1940) obtained amalgams reportedly containing 0.5–1.2 wt.% cerium by electrolysis of solutions of $CeCl_3$ in absolute ethyl alcohol, in methyl alcohol, and in mixtures of methyl and ethyl alcohols.

Hasegawa et al. (2003) reported the preparation of lanthanum and cerium metals by a two-step process comprising of electrolytic synthesis of amalgam in an aqueous solution followed by the thermal decomposition of the amalgam in a vacuum. The amalgamations of La(III), Ce(III)) were carried out from aqueous solutions of La(III), Ce(III) chloride buffered at pH 3.4–3.7 with 1.0 M acetic acid and 0.4 M sodium acetate, at the mercury cathode by the controlled current electrolysis. The amalgamation yields were almost quantitative. The resulting amalgam was rinsed by water and ethyl alcohol and then transferred to a magnesia crucible for pyrovacuum treatment. Most of the mercury was evaporated below 250°C, and the amalgam was decomposed completely by heating up to 900–1250°C under 10^{-5} Pa. The best purity and yield attained in the samples were given as follows—La: Hg 17 ppm, N 30 ppm, O 1100 ppm, C 130 ppm, best yield of metal 71%; Ce: Hg 31 ppm, N 31 ppm, O 360 ppm, C 180 ppm, best yield of metal 99%. Oxygen ingestion in to the metal could be due to magnesia crucible.

Moeller and Zimmerman (1954) reported indications of formation of yttrium, neodymium, and lanthanum metals from the electrolysis of anhydrous ethylenediamine solutions of $Y(OAc)_3$, $NdBr_3$, and $La(NO_3)_2$ using platinum electrodes.

4.11.3 Electrowinning Solid Metal Deposits

Molten rare-earth metals are markedly reactive, and problems due to this reactivity were sought to be circumvented by some investigators by conducting the electrolysis at temperatures below the melting point of the rare-earth metal. A mixture of $PrCl_3$, NaCl, and KCl, which melts at 535°C, was electrolyzed by Canneri and Rossi (1932) to obtain praseodymium (m.p. 931°C) sponge. The electrolysis temperature was below 600°C. A tungsten cathode and an Acheson graphite anode were used. Mazza (1939) obtained lanthanum (m.p. 918°C), cerium (m.p. 798°C), and praseodymium as solid metals by electrolyzing at 700°C and 750°C a bath of rare-earth chlorides dissolved in NaCl and KCl. The formation of oxychlorides was avoided by excluding oxygen. Relatively higher levels of purity, namely, 99.7% for lanthanum, 99.8–99.9% for cerium, and 99.6% for praseodymium, were reported for the product metals obtained.

4.11.4 *In Situ* Preparation of Electrolyte

A novel method of introducing rare earth into the molten chloride bath was described in a US Patent of 1959 (Merlub-Sobel 1959). The compacted rare-earth oxide–carbon mixture was placed in the hollow graphite anode of the electrolytic cell. Chlorine gas was passed through this mixture in the anode. Rare-earth chloride thus formed permeates into the molten bath to be electrolyzed. This method of generating metal chloride *in situ* in the fused salt electrolysis cell was extensively used in later years

by the US Bureau of Mines researchers for the electrolytic preparation of vanadium metal (Lei et al. 1967).

4.11.5 Commercial Electrowinning from Rare-Earth Chlorides

The rare-earth metals that have been produced by fused salt electrolysis of chlorides on a commercial scale (Morrice and Knickerbocker 1961; Hirschhorn 1968) are lanthanum, cerium, and didymium (Nd + Pr). Didymium metal is an alloy of neodymium and praseodymium with minor amounts of lanthanum and other rare earths. The cells had an iron, carbon, graphite, or refractory lined steel vessel to contain the molten bath. The cathode was the bath container itself or an iron or carbon block at the bottom of the container. The anodes were one or more graphite rods extending vertically into the cell through its top. Besides $RECl_3$, the electrolyte contained NaCl, KCl, $CaCl_2$, or other salts as preferred by the various producers, and the bath was molten even at 650°C. The cells were enclosed by steel covers to exclude air to prevent gas pickup in the metal produced.

After loading the mixture of rare-earth chloride and NaCl, KCl, or $CaCl_2$ into the cell, in one procedure, the charge was melted by external burners. In another practice, the anodes were lowered until they contacted broken pieces of cerium metal placed at the cell bottom. Solid bath was packed around the bottom of the anode, and DC was turned on to heat and melt the electrolyte. The anodes were then raised to their operating positions. The chloride bath was raised to a temperature between 800°C and 900°C by passage of DC, and external heating was normally not required during electrolysis.

During electrolysis, the metal collected at the bottom of the cell. The metal could be maintained in the molten state by resistance heating. Alternatively, the metal might be allowed to solidify by use of a cooled cathode, in which case it would be necessary to remelt the metal by internal resistance heating, sometimes supplemented by an external source of heat, prior to its removal from the cell.

The electrolysis was continued as long as the current efficiency or the metal quality was acceptable. The liquid metal product might be removed at fixed intervals by ladling, and additional chloride was introduced as needed to replace that used in the electrolysis. In one practice, the product was collected by pouring the entire contents of the cell, including the bath, into molds. After the metal had settled to the bottom of the mold, the liquid bath was returned to the cell, and electrolysis was started again.

Lanthanum, cerium, and didymium metals of better than 99% purity have been electrowon commercially from their anhydrous chlorides. The purities of metals obtained are listed in Table 4.13. Metals of high purity could be produced if carefully purified feed materials were used and if cell atmosphere composition was controlled. Current efficiencies of chloride cells were usually between 45% and 50%.

The maximum operating temperature of the chloride cell is 1100°C, and neodymium (m.p. 1021°C) is the highest-melting rare-earth metal that can be produced by chloride electrolysis. However, the yield of neodymium in such a cell is very low (Seon and Barthole 1986). At high temperatures in a chloride electrolyte bath, the volatility of bath constituents becomes unacceptable, the solubility of metals in their

TABLE 4.13
Analysis of Lanthanum, Cerium, and Didymium Metals Electrowon Commercially from Chloride Electrolytes

	Analysis (%)		
Element	**Lanthanum**	**Cerium**	**Didymium**
La	99.6		0.95
Ce	0.09		0.20
Nd	0.04		72.1
Pr	0.05		27.2
Sm	0.03		0.3
Other rare-earth elements	nd	0.10[a]	nd
Al	0.01	0	0.10
Ca	0.01	0.02	0.10
Fe	0.11	0.19	0.05
Mg	0.10	0.02	0.10
Si	0.04	0.002	0.07
Mn	nr	0.02	nr
P	nr	0.001	nr
C	nr	0.05	nr
O	nr	nr	nr
N	nr	nr	nr

Source: Morrice, E. et al., Electrowinning of cerium group and yttrium group metals, Bureau of Mines Report of Investigations 5868, U.S. Department of the Interior, Washington, DC, 1961.

Note: nd: not detected; nr: not reported.

[a] Includes all rare-earth elements other than cerium.

chlorides increases significantly, and the attack of cell wall materials by the rare-earth metals becomes severe. Considerably higher temperature operation, however, is possible in cells using fluoride electrolyte baths.

4.11.6 Oxide–Fluoride Electrolysis

Rare-earth-metal preparation by electrolysis of a fluoride–oxide bath was first reported 1907. This was followed by many other investigations listed in Table 4.14. Muthmann and Scheidemandel (1907), using a modification of the Muthmann-type cell described earlier for chloride electrolysis, prepared cerium ingot by electrolysis of CeF_3–CeO_2. The fluoride was prepared by precipitation with hydrofluoric acid and contained silicates. The cerium metal obtained was reported to be only 86.48% pure and contained 12.49% SiO_2 and 0.87% Fe. They also electrolyzed CeO_2 in mixtures of CeF_3, NaF, and KF in an attempt to have a lower melting electrolyte and conduct electrolysis at lower temperature. However, these electrolytes yielded only sodium and potassium metals. Electrolysis of rare-earth oxyfluoride baths using carbon and

TABLE 4.14
Electrolysis of Oxide–Fluoride Melts

Year	Electrolyte	Electrodes[a]	Collector	Product	Reference
1951	CeO_2–CeF_3–LiF–BaF_2	Graphite (A) Mo (C)	Mo crucible	Ce (99.7%)	Gray 1951
1960	CeO_2–CeF_3–LiF–BaF_2	Carbon (A) Mo (C)	Electrolyte skull	Ce (99.9%)	Morrice et al. 1960
1962	La2O_3–LaF_3–LiF–BaF2	Carbon (A) Mo (C)	Electrolyte skull	La (99.8%)	Morrice et al. 1962
1964	Ce_2O_3–CeF_3–LiF–BaF_2	Graphite (A) Mo (C)	Mo liner	Ce (99.8%), continuous electrowinning	Shedd et al. 1964
1966	La_2O_3–LaF_3–LiF–BaF_2	Graphite (A) Mo (C)	W crucible	La (99.8%), continuous electrowinning	Shedd et al. 1966
1967	RE_2O_3–REF_3–LiF	Graphite (A) W (C)	Electrolyte skull	Pr, Nd, Di nodules (99.83–98.85%)	Morrice and Henrie 1967

[a] A: anode; C: cathode.

graphite electrodes at temperatures of ~1400°C resulted in the formation of only carbides (Hirsch 1911). The bath melting temperature could not be lowered by addition of KF. In 1918, Hicks (1918) attempted to prepare a mixture of yttrium with other high-melting rare-earth metals by electrolyzing either a fused yttrium earth chloride bath or a solution of yttrium earth oxide in cryolite. The cell comprised a graphite container, which was the cathode, a graphite anode, and the molten bath, which was operated at temperatures up to 1300°C. The product was some black powder.

4.11.6.1 Gray's Cell

The most successful among the early experiments on oxide–fluoride electrolysis was reported by Gray (1951). In his experiments, CeO_2 was dissolved in a CeF_3–LiF–BaF_2 electrolyte contained in an externally heated 57-mm-inside-diameter carbon container. A schematic of the electrolysis cell used by Gray is shown in Figure 4.44. The cell pot was made of *Delanium* carbon, which was found to be quite impervious to the melt and protected the nickel can in which it was enclosed. The ash content of 2.3% of the Delanium carbon was high, and so it was lined on the inside with a high-purity (ash content < 0.01%), though somewhat porous, graphite. The anode was also made of high-purity graphite rod, and the cathode was a molybdenum rod; both were suspended from the top and immersed in the melt. The bath, cell materials, electrodes, and the product were all protected from the atmosphere by argon gas, which was continuously flowing around the cathode and over the top of the molten bath. A molybdenum crucible was kept below the cathode to collect the product. Gray chose molybdenum to contain molten cerium because he had found that unless

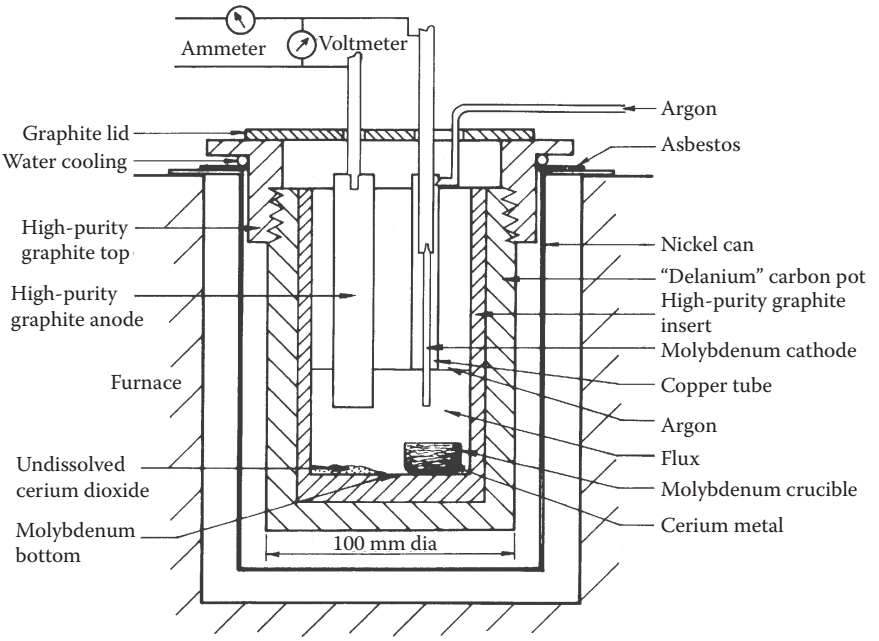


FIGURE 4.44 Gray's cell for electrolysis of cerium dioxide dissolved in fused fluorides. (From Gray, P.M.J., *Trans. Inst. Min. Met.*, 61 (Oct. 1951–Sept. 1952): 141–170, 1951.)

it is oxidized, molybdenum does not dissolve in cerium. The bottom of the cell was lined with a thin sheet of molybdenum to prevent any accidentally spilled cerium reacting with graphite to form cerium carbide. Cerium oxide was added to the bath on the side of the cell opposite to the cup.

The electrolyte, comprising 60.8% CeF_3, 26.9% LiF, and 12.3% BaF_2, was molten at 715°C and dissolved 3–5% CeO_2 at 850°C. Electrolysis was carried out at 880–900°C at cathode current density of 5.0–7.0 amp cm^{-2}. The normal cell voltage was 4.4 V. Molten cerium metal dropped off the cathode and collected in the molybdenum cup kept below. Yields of up to 77% were obtained, and the overall purity of the metal was 99.7–99.8% cerium. The product contained 0.1–0.6% calcium and up to 0.3% magnesium as major impurities. Much of the later work and further development of the oxide–fluoride electrolysis process was carried out at the Reno Metallurgy Center of the US Bureau of Mines during the 1960s (Morrice and Wong 1979).

4.11.6.2 Reno Cell Type 6

Many types of electrolytic cells were designed and used at Reno for carrying out oxide–fluoride electrolysis. The first was a 150 mm (6 in.) diameter electrowinning cell, known as cell type 6 (Morrice and Knickerbocker 1961; Morrice et al. 1961). The cell consisted of a 6-in.-diameter bath container made of graphite. Three

10-mm-diameter molybdenum cathodes and three 25-mm-diameter carbon anodes extended down into the container through its top. This electrode arrangement was first used to melt the bath with alternating current (AC) and later used for electrolysis with direct current (DC).

The cell was located within a controlled atmosphere temperature pressure (CATP) steel chamber in which atmosphere, temperature, and pressure were controlled. All cell operations, such as feeding, electrowinning, and raising and lowering electrodes, could be conducted while the electrolytic cell and its contents remained under the protected atmosphere within the chamber.

The standard procedure for the electrowinning of high-purity cerium using cell type 6 was as follows: first, the solvent phase electrolyte (73% CeF_3, 15% LiF, and 12% BaF_2 powders) was vacuum-dried at about 280°C and transferred to the cell chamber. The chamber was evacuated to 2 Pa and back-filled with high-purity argon or helium. The dried solvent powder was packed into the graphite cell container. A graphite resistor ring was placed on top of the powder, and the electrodes were lowered to make contact. On passing AC through the electrodes and the ring, the powder melted, and after sufficient melt had been obtained to carry the current, the graphite ring was removed and AC melting was continued until adequate quantity of the melt reached the temperature sufficient for electrolysis, 810–830°C. The solubility of ceria in the bath at the electrolysis temperature was in the range of 1–2%. One of the important features of the cell was the formation of a layer of frozen bath or skull on the interior surface of the graphite container. The skull prevents the molten electrowon rare-earth metals from contacting the graphite crucible. The thickness of the insulation on the sidewalls and bottom of the graphite cell, and the geometry of the electrode with respect to the sidewall and bottom of the cell were so chosen to maintain this electrolyte skull. An automatic vibrating screw feeder was used for continuous feeding of CeO_2 powder into the molten electrolyte. The feeder with hopper was located outside the cell chamber but was so arranged that it operates in the same controlled atmosphere as the cell. The feeder was also refillable without contaminating the cell atmosphere. After melting the bath, the feeder was turned on, and 10–20 g of previously vacuum-dried CeO_2 powder was added to the bath. The AC supply was disconnected, and DC was turned on for electrolysis to occur. During the electrolysis, CeO_2 was continuously fed to the molten bath at a rate of 7 g/min. Massive cerium nodules formed as a result of electrolysis, and in about 2 h, these nodules bridged the gaps between the electrodes, and electrolysis had to be stopped. After cooling the bath to room temperature within the cell atmosphere, the frozen mass was taken out in open air and broken up to recover the cerium nodules. Details of a sample electrowinning run and the product obtained are summarized in Table 4.15. In the process described, cerium was prepared as a liquid at temperatures very close to its melting point. This circumvented certain difficulties, such as entrapment of electrolyte, which is inherent in recovering the product as a solid, and also minimized contamination of metal with impurities present in molten bath. One major problem, however, was the excessive corrosion of both carbon and graphite anodes at or above the surface of the bath. This was caused by molecular oxygen, generated by the electrolytic reaction and present in the cell atmosphere (Morrice et al. 1961).

TABLE 4.15
Cell-Operating Data and Product Analysis in a Typical Type 6 Cell (USBM) Run for Electrowinning of Cerium Metal

Electrolysis parameters	
Electrolyte composition (%)	$73CeF_3$–15LiF–$12BaF_2$
Temperature (°C)	810–830
Cathode	10-mm-diameter Mo rods, 3 nos.
Anode	25-mm-diameter carbon rods, 3 nos.
Electrolysis	
Voltage (V)	11
Current (A)	249
Duration (min)	132
Initial cathode current density (A/cm^2)	10.23
Initial anode current density (A/cm^2)	4.10
Current efficiency (%)	
CeO_2 feed rate ($g\ min^{-1}$)	7
Cerium nodules recovered (g)	800
DC power consumption (kWh/kg of Ce)	7.5

Analysis of Cerium Nodules (%)

Element	**Content**	**Element**	**Content**
C	0.016	Li	0.002
N	nr	Ba	nd
O	0.036	Ca + Mg	<0.004
H	0.0003	Al	<0.01
Si	nd	Fe	0.0102
RE other than Ce	nd	Mo	nd

Source: Morrice, E. et al., Electrowinning of cerium group and yttrium group metals, Bureau of Mines Report of Investigations 5868, U.S. Department of the Interior, Washington, DC, 1961.
Note: nd: not detected; nr: not reported.

4.11.6.3 Reno Cell Type 12

These are electrolytic cells in which the electrolyte was contained in a ~300 mm (12 in.) diameter graphite crucible. These cells, called type 12 cells, were extensively used at Reno (Shedd et al. 1964). Initially experiments were conducted in which the metal product was collected in an electrolyte skull, and in later experiments, cells designed for continuous operation were used. As with the type 6 cell, the electrolyte cell components were all enclosed in a gas-tight chamber.

The arrangement of the type-12 cell components and the electrolyte skull is shown in Figures 4.45 and 4.46. The anode, which is a graphite tube (120 mm outside diameter, 75 mm inside diameter, 560 mm long) suspended vertically in the center of the crucible, also acted as a feed tube for adding electrolyte or cerium oxide to the

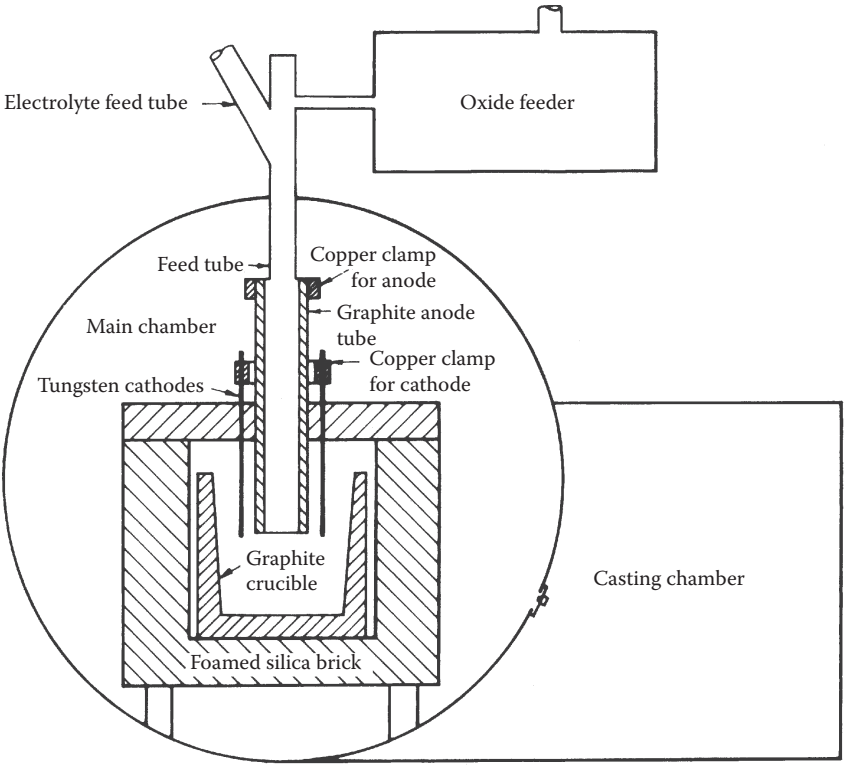


FIGURE 4.45 Electrolytic cell in protective atmosphere chamber. (From Shedd, E.S. et al., Continuous electrowinning of cerium metal from cerium oxides, Bureau of Mines Report of Investigations 6362, U.S. Department of the Interior, Washington, DC, 1964.)

cell. Molybdenum or tungsten rods 10 mm in diameter were used to make the nine cathodes that were arranged in a circle 30 mm from the anode surface.

The vacuum-dried electrolyte constituents, 73% CeF_3, 12% BaF_2, and 15% LiF, were fed and packed into the graphite crucible. Cerium was the metal electrowon. The bath was melted initially as described for the type 6 cell using AC. After the top portion of the electrolyte was liquid and the bottom 100–120 mm consisted of solidified electrolyte that provided a skull surface on which electrowon cerium collected, operating temperature of 850–900°C was maintained using AC current for 30–45 min to obtain a uniform melt temperature. The cerium oxide feeder was started at a predetermined controlled feed rate of 26–30 g/min for 5 min before the power was switched to DC. With an electrode immersion of 40 mm, the power requirement was 800–900 A and 7–8 V. This current was sufficient to maintain an operating temperature above 850°C. Cerium was deposited on and dripped from the cathodes and collected as nodules on the electrolyte skull initially in small pieces and then after 1 h, as temperature profile improved, in large massive pieces weighing 3–4.5 kg.

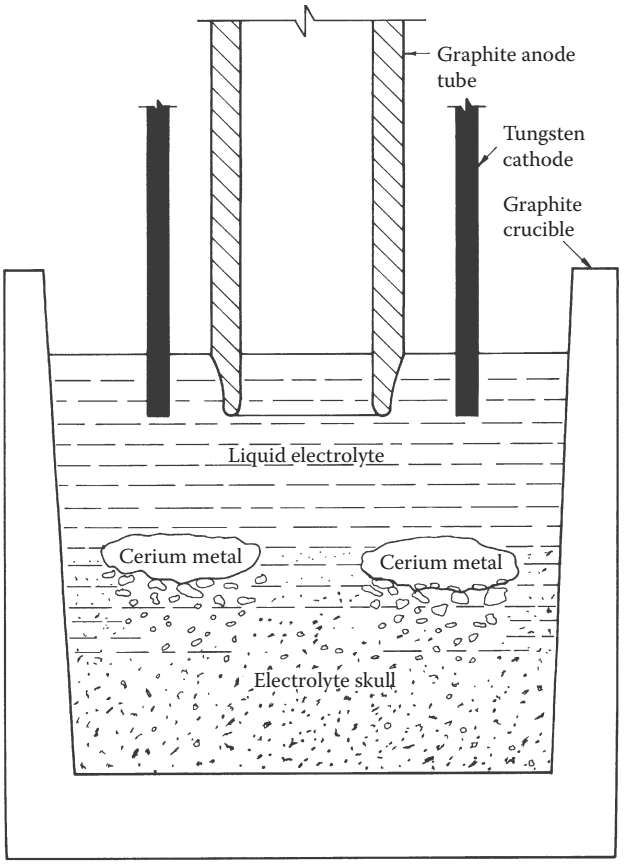


FIGURE 4.46 Electrolytic cell with electrolyte skull hearth. (From Shedd, E.S. et al., Continuous electrowinning of cerium metal from cerium oxides, Bureau of Mines Report of Investigations 6362, U.S. Department of the Interior, Washington, DC, 1964.)

The oxide content of the electrolyte was kept between 1% and 2% throughout the run, and electrolysis was continued for 15–20 min after termination of oxide feed. Analysis of the electrolyte after the run showed the oxide content to be 0.06–0.3%.

The metal produced by the above procedure, using an electrolyte skull, had a purity of at least 99.8%. Over 90% of the metal in the oxide feed was recovered at a current efficiency that ranged from 75% to 90%. The analysis of cerium obtained is shown in Table 4.16.

In electrolysis with CeO_2 as feed material, a major problem was excessive burning of the interior of the anode surface in a nonuniform manner. The nonuniform anode burning was eliminated using cerous oxide, Ce_2O_3, as feed. When Ce_2O_3 was fed to the cell, the corrosion was uniform and limited to the immersed portion. Otherwise the run was similar to that using CeO_2 as feed.

TABLE 4.16
Analysis of Cerium Metal Electrowon from an Oxide–Fluoride Melt (%)

Element	Cerium Collected in Electrolyte Skull	Tapped Cerium Metal
C	0.020	0.010
O	0.010	0.016
Al	0.012	0.040
Ba	nd	nd
Ca	0.001	nr
Cu	0.005	0.001
Fe	0.030	0.007
Li	0.002	nr
Mg	0.001	nr
Mo	0.035	0.076
Si	0.005	0.008
W	nr	0.002
Total impurities	0.121	0.160

Source: Shedd, E.S. et al., Continuous electrowinning of cerium metal from cerium oxides, Bureau of Mines Report of Investigations 6362, U.S. Department of the Interior, Washington, DC, 1964.
Note: nd: not detected; nr: not reported.

4.11.6.4 Reno Continuous Cell Type 12

Subsequent to the batch type 12 cell where metal was collected in a frozen electrolyte skull, a new cell design was developed at Reno for continuous electrolysis (Shedd et al. 1964).

The key feature in the cell shown in Figure 4.47 is that the bottom and sides of the graphite crucible were lined with a molybdenum sheet, and a tapping pipe was attached to the molybdenum hearth so that the molten metal could be tapped. The tapping pipe extended into an inert atmosphere casting chamber. When the molybdenum hearth or trough was nearly filled with cerium, an auxiliary AC heating circuit could be used to heat the tapping pipe without interrupting the electrowinning sequence. To serve as an electric probe for the AC circuit, a 19-mm-diameter molybdenum rod was submerged in the melt. An auxiliary carbon resistance heating unit was located beneath the cell.

The cell for continuous electrowinning of a rare-earth metal was first used for the preparation of cerium metal. The dry weight composition of the electrolyte was 63% CeF_3, 16% BaF_2, and 21% LiF, and the cell was operated at 900°C. Ce_2O_3 was the cell feed and was fed at a predetermined uniform rate of 30 g/min during electrowinning.

A typical continuous electrowinning run lasted over 3 days, during which metal was electrowon and several tappings of homogeneous cerium metal were made. The electrolyte was also tapped and recharged to the cell. The anode was changed as needed and electrowinning was resumed. A total of 12 kg of cerium was tapped.

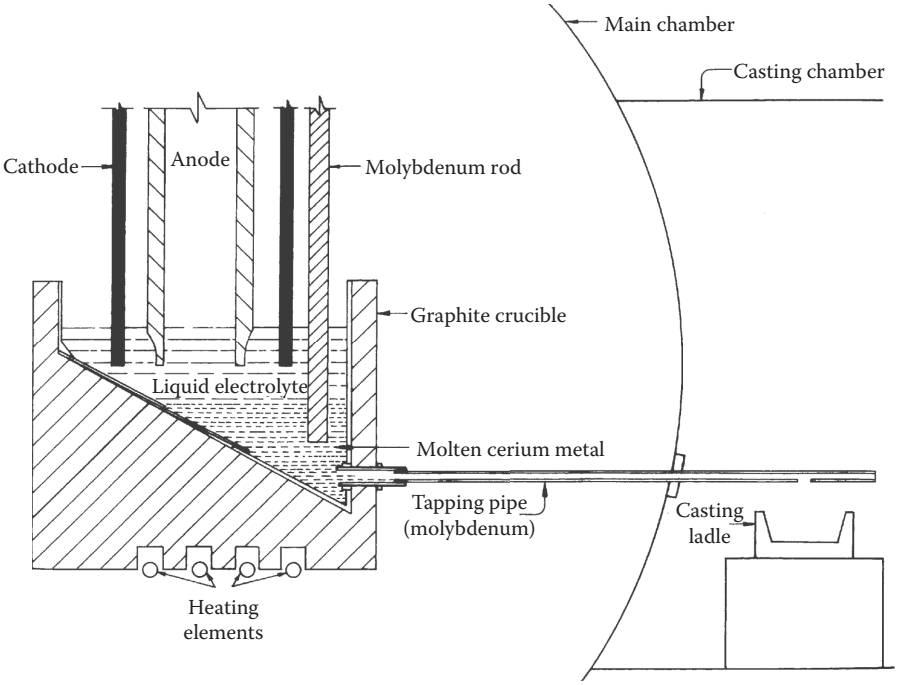


FIGURE 4.47 Design of cell used to study parameters for continuous operation. (From Shedd, E.S. et al., Continuous electrowinning of cerium metal from cerium oxides, Bureau of Mines Report of Investigations 6362, U.S. Department of the Interior, Washington, DC, 1964.)

The metal purity was 99.8%, and the impurities in the metal are listed in Table 4.16. Molybdenum figured as a major impurity. It was picked up by cerium during the extended contact with molybdenum hearth. Tungsten contamination, under similar circumstances, would be much less.

4.11.6.5 Cells for Electrowinning Lanthanum

Morrice et al. (1962) attempted to electrowin molten lanthanum metal from lanthanum oxide in a LaF_3–LiF–BaF_2 bath using the same electrode arrangement (Morrice et al. 1960) that worked well in the case of cerium (m.p. 798°C). The DC power that this cell could carry was not high enough to maintain the electrolyte temperature needed for the deposition of molten lanthanum (m.p. 918°C). This problem was solved by an improvement in the electrowinning cell as depicted in Figure 4.48. AC was used across the anodes as an auxiliary source of heat to maintain the required bath temperature. The lanthanum electrowinning cell was operated using an arrangement in which AC was imposed on the two anodes, and DC was imposed on one anode and the cathode. The operating data of the cell and analysis of the product obtained are listed in Table 4.17. This cell that operated with a current efficiency of about 60% yielded lanthanum nodules containing carbon and oxygen as major impurities. The total impurity content was, however, between 0.1% and 0.2%.

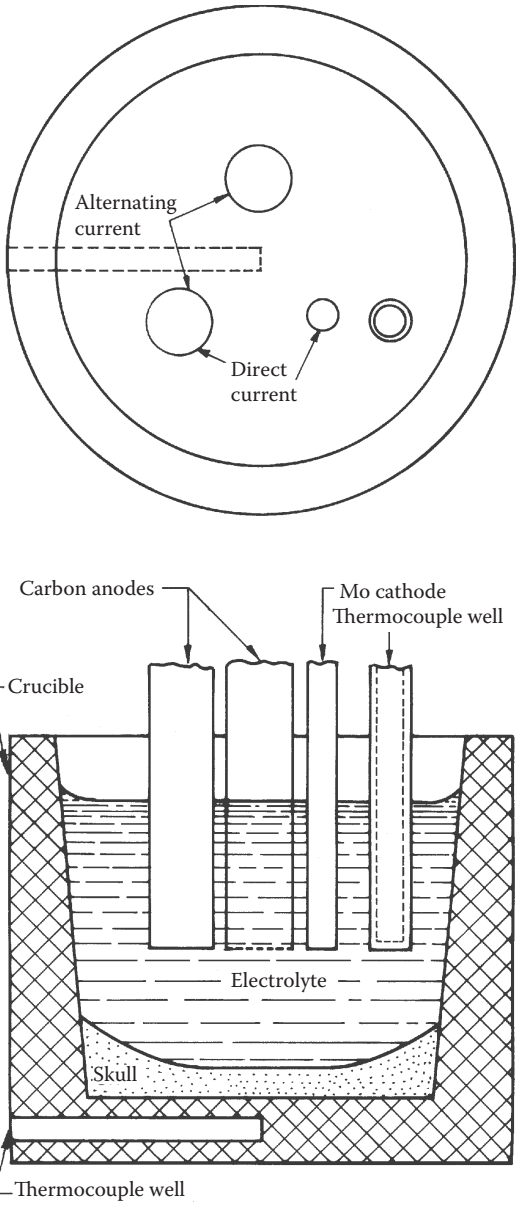


FIGURE 4.48 Imposed AC cell for electrowinning lanthanum. (From Morrice, E. et al., Electrowinning of molten lanthanum from lanthanum oxides, Bureau of Mines Report of Investigations 6075, U.S. Department of the Interior, Washington, DC, 1962.)

TABLE 4.17
Operational Data and Product Analysis in Lanthanum Electrowinning

Electrolyte composition (%)	$54.7LaF_3$–$30.3LiF$–$15BaF_2$
Temperature (9°C)	
Electrolyte	946
Cell bottom	711
Cathode	Molybdenum
Anode	Carbon
Electrolysis	
Voltage (V)	
Current (A)	12
Duration (h)	159
Initial anode current density (A/cm^2)	3
Cathode current density (A/cm^2)	6.2
Current efficiency (%)	1.5
La_2O_3 added to bath before electrolysis (g)	1320
La_2O_3 added during electrolysis (g)	886
Lanthanum metal recovered (g)	451
Metal recovery (%)	60
DC power consumed kWh/kg La	17.3
AC power consumed kWh/kg La	17.3

Analyses of Lanthanum Metal Nodules (%)

Al	Ba	Ca	Cu	Fe	Li	Mg	Mn	Mo	Si	C	O	N
0.001	<0.01	0.0009	0.004	0.04	0.016	0.015	<0.0008	0.019	0.01	0.03	0.04	<0.02

Source: Morrice, E. et al., Electrowinning of molten lanthanum from lanthanum oxides, Bureau of Mines Report of Investigations 6075, U.S. Department of the Interior, Washington, DC, 1962.

Note: Total impurities 0.19%.

A cell for continuous electrolysis was also developed at Reno (Shedd et al. 1966) for lanthanum metal. The electrode and hearth arrangement in this cell are different from those in the cell used for cerium. Shedd et al. (1966) stated that the ability of cerium to exist in +4 and +3 states permits sustenance of electrolysis even with a small anolyte volume provided by a single anode. For lanthanum, which has only the trivalent ion species, to achieve sustained electrolysis, a greater proportionate volume of the electrolyte is needed as an anolyte. This is possible in the different electrode arrangement shown in Figure 4.49, where the anodes are placed surrounding

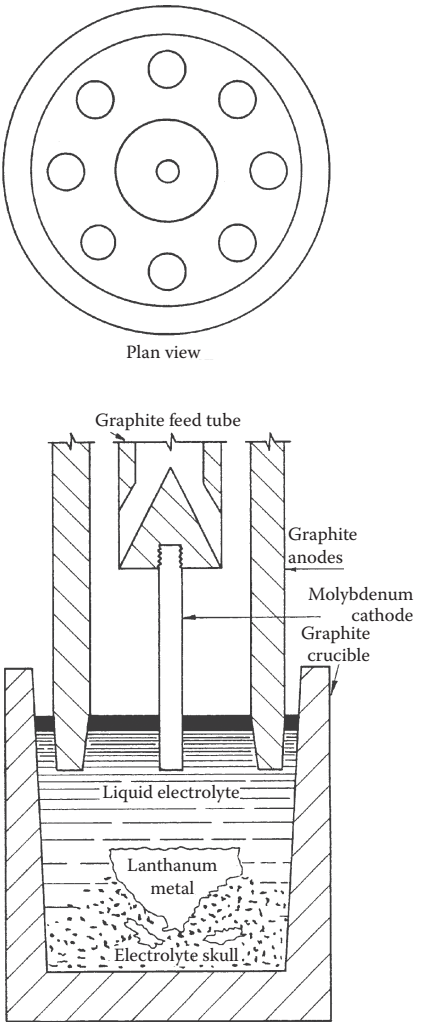


FIGURE 4.49 Special electrode arrangement in Reno cells for lanthanum electrowinning. (From Shedd, E.S. et al., Continuous electrowinning of cerium metal from cerium oxides, Bureau of Mines Report of Investigations 6362, U.S. Department of the Interior, Washington, DC, 1964.)

the cathode. Increased anolyte volume offered greater opportunity for the electrolyte to dissolve the oxide and make it available to the anode for reaction. Besides, the cerium cell arrangement could not support sufficient current to maintain the higher operating temperature required for molten lanthanum metal.

The cell had eight high-purity graphite rods, each 38 mm in diameter, functioning as anodes. There was, however, only a simple cathode made of a 25-mm-diameter arc cast molybdenum rod screwed into a graphite plug in the bottom of a central graphite tube. The cone-shaped plug had four holes drilled through the tube, and the momentum of the particles striking the cone deflected the oxide feed closer to the anode. The electrodes were suspended vertically from copper support clamps that also served as electrical contacts, as shown in Figure 4.50.

Shedd et al. (1966) used a batch type cell shown in Figure 4.50 to establish the electrode geometry, oxide feed rate, and optimum operating parameters. Subsequently, instead of collecting molten lanthanum in the electrolyte skull, a refractory metal crucible was placed in the bottom of the cell directly below the molybdenum cathode. Molten lanthanum was ladled from the tungsten hearth and cast into 2 lb. ingots. Both frozen electrolyte skulls and tungsten metal crucibles were found satisfactory

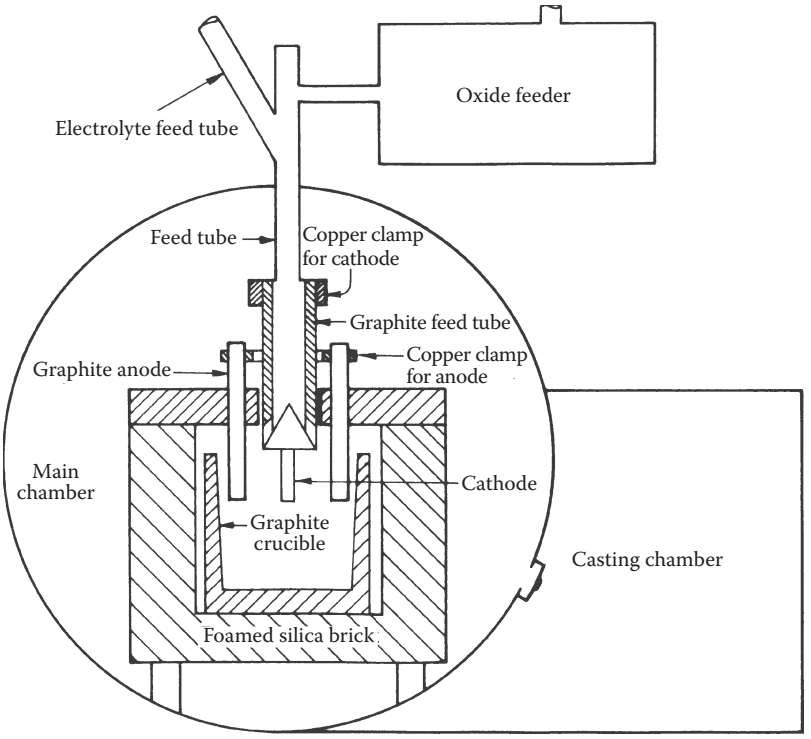


FIGURE 4.50 Lanthanum electrolysis cell in protective atmosphere chamber. (From Shedd, E.S. et al., Continuous electrowinning of cerium metal from cerium oxides, Bureau of Mines Report of Investigations 6362, U.S. Department of the Interior, Washington, DC, 1964.)

for collecting the metal and did not react with molten lanthanum. The chamber was maintained at a partial vacuum (10 kPa) by continuously discharging the carbon oxide gases during the electrowinning. The occurrence of anode effect was found to be markedly reduced under partial vacuum.

The electrolytic cell with tapping facilities for continuous electrowinning of lanthanum is shown in Figure 4.51. The hearth of the cell was a tungsten crucible 100 mm in diameter and 100 mm in depth. A molybdenum pipe was connected to the tungsten crucible through a 0.5-in.-diameter hole drilled in the side of the crucible. The pipe extended about 760 mm into the casting chamber. Electrical connections were

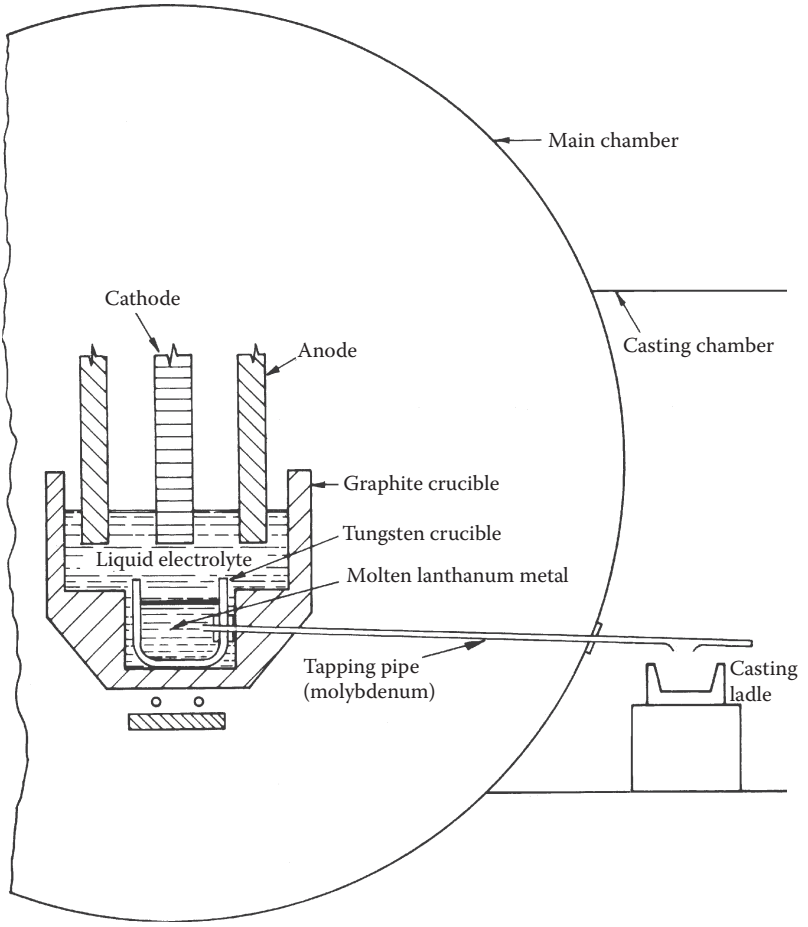


FIGURE 4.51 Electrolytic cell with tapping facilities for lanthanum electrowinning. (From Shedd, E.S. et al., Continuous electrowinning of cerium metal from cerium oxides, Bureau of Mines Report of Investigations 6362, U.S. Department of the Interior, Washington, DC, 1964.)

provided so that the pipe could be heated by passing AC through it and the submerged cathode.

The cell-operating parameters and product obtained in continuous electrowinning of lanthanum are listed in Table 4.18 (Shedd et al. 1966). The electrolyte containing 48% LaF_3, 27% BaF_2, and 25% LiF was loaded into the graphite crucible. The La_2O_3 solubility in this electrolyte was 2 wt.% at the cell-operating temperature. The cell-operating temperature of 1000°C was attained by AC. During electrolysis, oxides of carbon formed in the cell were continuously removed and flushed out with helium gas. The electrolysis sequence lasted about 2 h, and after every sequence, the AC was switched on through the tap pipe, auxiliary heat was supplied through the bottom heating elements to maintain the cell bottom at 1000°C, and the metal flowed from the cell through the pipe to the casting chamber where it collected in ladles.

TABLE 4.18
Operational Data and Product Analysis for Continuous Electrowinning of Lanthanum from Lanthanum Oxide

Electrolyte	$48LaF_3$–$27BaF_2$–25LiF
Temperature (°C)	975
Average current (A)	928
Average voltage (V)	11
Power requirement (DC) (kWh/kg)	8.8
Current efficiency (%)	76
Time of electrolysis (min)	220
Rate of feed of La_2O_3 (g/min)	29.5
Total amount of La_2O_3 (kg)	6.5
Efficiency of oxide utilization (%)	78
Rate of metal production (kg/h)	1.2
Anode carbon consumption/kg La (kg)	0.12
Analysis (%)	
Al	0.013
Ba	Not detected
Ca	0.002
C	0.500
Cu	0.001
Fe	0.018
Mo	0.017
O	0.009
Si	0.006
W	0.001
Total	0.567

Source: Shedd, E.S. et al., Electrowinning and tapping of lanthanum metal, Bureau of Mines Report of Investigations 6882, U.S. Department of the Interior, Washington, DC, 1966.

Several such tappings of homogeneous lanthanum metal could be made before it was time to tap the electrolyte itself from the cell. Lanthanum produced by the continuous electrowinning process was 99.81% pure. The impurities content (in %) in tapped lanthanum metal are Al 0.03, C 0.033, Fe 0.027, Mo 0.028, O 0.016, and Si 0.055. The elements tungsten, copper, calcium, and barium were not detected. The carbon content of the metal in the first tapping was very low but increased with successive ingots to 0.12% in the last ingot. The other impurities, however, showed a gradual decrease. The rise in the carbon content probably resulted from carbon spalling from the cell components, and this carbon collected on the melt surface contacting the nascent metal.

Continuous electrowinning has so far been applied to only two rare-earth metals: cerium and lanthanum; however, Sharma (1987) indicated the possibility of adopting such a cell to continuously produce neodymium metal. For neodymium, the operating temperature would be 1100°C, and the metal produced would probably have higher impurities than lanthanum or cerium because of higher operating temperature.

4.11.6.6 Cell for Electrowinning Neodymium, Praseodymium, and Didymium

The details of the cell used at Reno (Morrice and Henrie 1967) for electrowinning neodymium, praseodymium, and didymium metals are shown in Figures 4.52 through 4.54. As in the cases of cerium and lanthanum, these metals and the

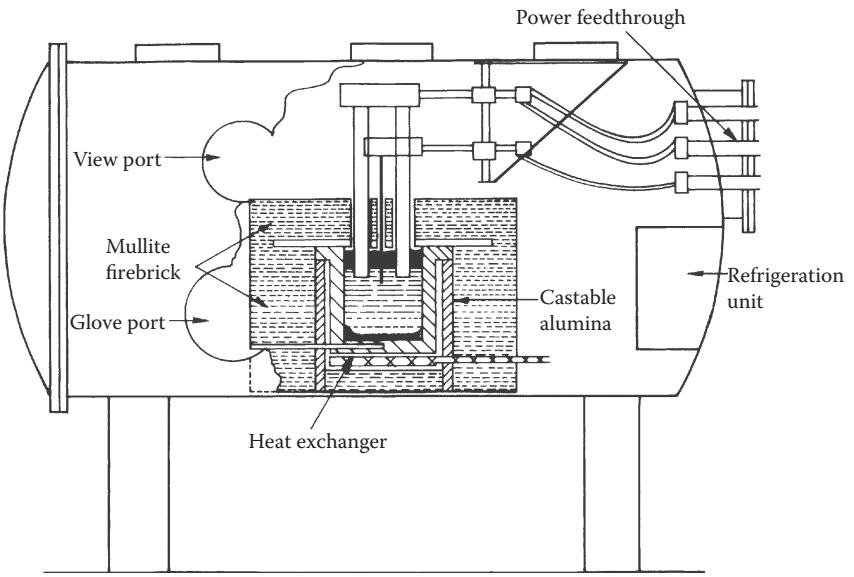


FIGURE 4.52 Protective atmosphere chamber. (From Morrice, E. and Henrie, T.A., Electrowinning of high purity neodymium, praseodymium and didymium metals from their oxides, Bureau of Mines Report of Investigations 6957, U.S. Department of the Interior, Washington, DC, 1967.)

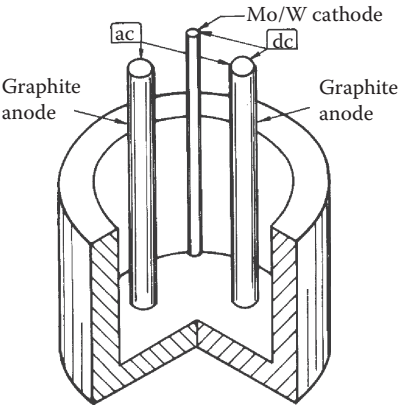


FIGURE 4.53 Basic features of Reno electrowinning cell. (Fom Morrice, E. et al., Direct electrolysis of rare earth oxides to metals and alloys in fluoride melts, Bureau of Mines Report of Investigations 7146, U.S. Department of the Interior, Washington, DC, 1968.)

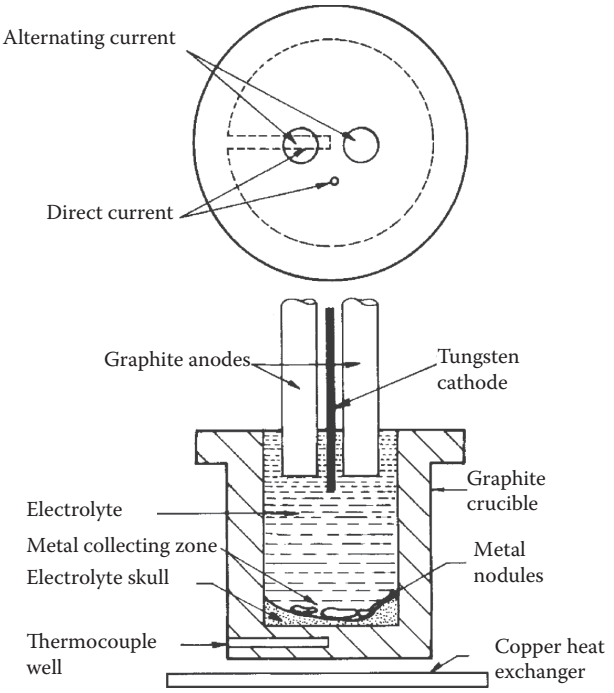


FIGURE 4.54 Electrowinning cell with AC applied to two anodes. (From Morrice, E. and Henrie, T.A., Electrowinning of high purity neodymium, praseodymium and didymium metals from their oxides, Bureau of Mines Report of Investigations 6957, U.S. Department of the Interior, Washington, DC, 1967.)

electrolyte constituents also react with air at the cell-operating temperatures. The cell was therefore enclosed in a gas-tight steel chamber as shown in Figure 4.52. The provision of glove and view ports made it possible to add electrolyte and feed and to adjust the electrodes during the electrowinning experiments. Heat lost from the exposed electrodes and molten bath could raise the ambient temperature within the chamber to >100°C. The refrigeration unit installed in the chamber, however, maintained the ambient temperature at <50°C.

The graphite crucible for holding the molten electrolyte had an inside diameter of 100–125 mm and a depth of 150 mm. The cathode was a 5-mm-diameter tungsten rod, and the anode was a graphite rod 19–25 mm in diameter. The cell was internally heated by applying AC between the two anodes. This design is indicated in Figure 4.53. To obtain a thermal gradient in the cell, for developing and maintaining a frozen electrolyte skull in the metal collection zone, while the cell was internally heated, the cell bottom was simultaneously cooled.

To start with, an inert atmosphere was obtained in the cell chamber by pumping down and backfilling with helium. The fluoride electrolyte powder was charged in the cell, and melt down was initiated by short-circuiting the AC between the anodes and crucible. After obtaining a molten pool of electrolyte, the anodes were raised to electrolysis position, additional electrolyte powder was charged, and heating continued until the required cell temperature was attained. Electrolysis was then started, and the appropriate oxide was intermittently fed to the cell. By a controlled flow of air or helium through the copper coil located beneath the crucible, the desired temperature gradient between the zones of metal deposition and collection was maintained. After completion of electrolysis, the electrolyte was allowed to cool to ambient temperature before the crucible was removed and crushed, metal nodules recovered, and crushed electrolyte returned for use as bath in the next experiment.

The operational parameters and analysis of product attained in typical electrowinning experiments for neodymium, praseodymium, and didymium (Morrice and Henrie 1967; Morrice et al. 1968) are summarized in Table 4.19.

The results at Reno show the possibility of preparing high-purity neodymium, praseodymium, and didymium by electrolysis of the oxides in a medium consisting of the respective rare-earth fluorides and lithium fluoride. The metals with overall 99.9% purity contained <0.02% each of carbon and oxygen and <0.025% tungsten as major impurities. Current efficiencies were up to 83%. In the electrowinning of didymium, the didymium metal product was enriched in neodymium and praseodymium and impoverished in lanthanum, samarium, and yttrium, as compared to the oxide fed to the cell.

4.11.6.7 High-Temperature Electrowinning Cell

A high-temperature electrowinning cell, also from Reno (Henrie and Morrice 1966), operating in the temperature range 1370–1700°C and used for preparation of liquid gadolinium, dysprosium, and yttrium is shown in Figure 4.55.

The electrolyte was contained in a graphite crucible 100–125 mm in diameter and 150 mm deep. The anodes were 19-mm-diameter graphite rods, and the cathode was a 5-mm-diameter tungsten rod. The cell was heated internally by DC, and the electrolysis current was supplemented by AC applied between the graphite

TABLE 4.19
Cell-Operating Data for Electrowinning of Neodymium, Praseodymium, and Didymium

Electrolysis Parameters	Neodymium	Praseodymium	Didymium
Electrolyte composition (mol%)	50NdF_3–50 LiF	50NdF_3–50 LiF	50NdF_3–50 LiF
Temperature (°C)			
Electrolyte	1098	1030	1115
Skull (cell bottom)	740	800	770
Cathode	5-mm-diameter W rod		
Anode	19-mm-diameter graphite (fluted)		
	Heating (AC)		
Voltage (V)	52	38	45
Current (A)	89	130	136
Anode current density (A/cm^2)	2	1.9	2.5
	Electrolysis		
Voltage (V)	27	19	24
Current (A)	55	50	60
Duration (h)	2	1.1	1.4
Initial cathode current density (A/cm^2)	6.9	6	9.6
Initial anode current density (A/cm^2)	0.6	0.3	0.6
Current efficiency (%)	77	88	55
REO added (g)	312	196	197
Metal recovered (g)	151	85	82

Analyses of Neodymium and Praseodymium Nodules[a] (%)

Impurity Element	Neodymium	Praseodymium
C	0.014	0.010
N	0.001	0.002
O	0.015	0.018
F	0.040	0.030
Si	0.005	0.003
Al	0.002	0.010
Ca	0.005	0.005
Fe	0.012	0.012
Li	0.013	Not determined
Mg	0.005	0.003
W	0.020	0.020
Other RE elements	0.020	0.060
Total	0.150	0.170

Source: Morrice, E. et al., Direct electrolysis of rare earth oxides to metals and alloys in fluoride melts, Bureau of Mines Report of Investigations 7146, U.S. Department of the Interior, Washington, DC, 1968.

[a] The impurity content in didymium was similar to neodymium and praseodymium.

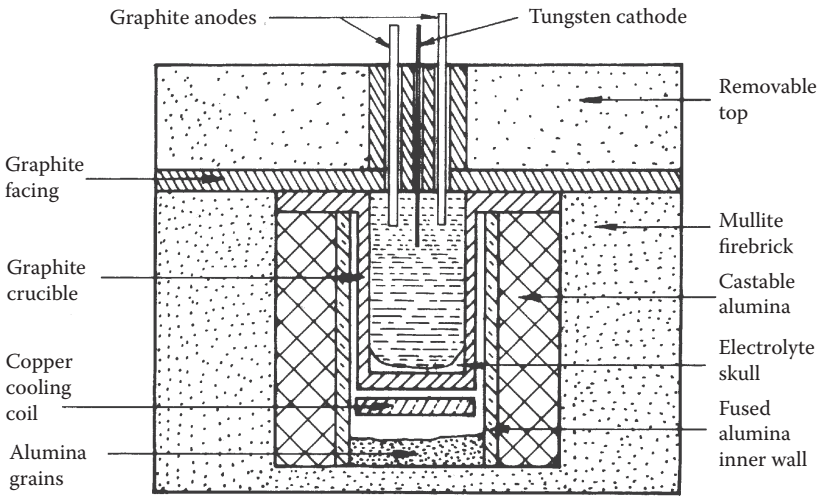


FIGURE 4.55 High-temperature electrowinning cell. (Fom Morrice, E. et al., Direct electrolysis of rare earth oxides to metals and alloys in fluoride melts, Bureau of Mines Report of Investigations 7146, U.S. Department of the Interior, Washington, DC, 1968.)

anodes, which supplied approximately 75% of the total power. The graphite anodes were fluted to provide the maximum possible surface area for the anode electrochemical reaction and decomposition of the rare-earth oxide to CO, which was the rate-controlling step in the cell operation. The cell bottom could be cooled by passing helium or air through the copper coil placed below the graphite crucible. The cell, like all the others from Reno, was enclosed in an inert atmosphere (CATP) chamber to prevent reaction of the cell components and chemicals with the atmosphere.

In the construction of the high-temperature cell, the materials were taxed to the extremes, and Morrice et al. (1968) used a judicious combination of materials to design a satisfactory cell. A shell fabricated from layers of various heat-insulating refractory materials surrounded the cell container to help maintain the required heat balance (see Figure 4.55). The inner wall of the shell was made from fused alumina. Castable alumina, 50 mm thick, was then placed around the inner wall. Then there was an outer wall, 100 mm thick, made from mullite brick. Granular alumina was placed below the graphite crucible to a depth of approximately 40 mm. The top of the cell was removable and was also made of mullite firebrick and had graphite facing to protect the bricks from erosion by the fluoride vapor and splashing electrolyte.

The electrolyte for gadolinium electrowinning consisted of an equimolar mixture of GdF_3 and LiF. Gadolinium oxide was fed to the molten electrolyte maintained at 1370°C. The metal was deposited as liquid at the cathode and dropped down to collect as modules in the frozen electrolyte skull at the bottom of the graphite crucible. The bottom was maintained at 810°C by cooling the bottom of the cell. Such a difference between the temperature of deposition and collection was essential to achieve high recovery and to ensure high purity of the metal product. A typical

gadolinium nodule contained 0.05% carbon, 0.01% oxygen, and 0.05% tungsten as major impurities.

Liquid yttrium and dysprosium were also electrowon from their oxides dissolved in melts composed of 50 mol.% LiF and 50 mol.% YF_3 or DYF_3. The metals were deposited on the cathode at 100–200°C above their melting points (m.p. of Dy 1412°C; m.p. of Y 1522°C) and collected at temperatures 400–500°C lower. Yttrium and dysprosium nodules thus recovered contained as little as 0.08% carbon and 0.10% oxygen.

The highest temperature at which an electrolysis cell operated was 1700°C for the preparation of liquid yttrium. Morrice et al. (1968) noted that at such temperatures, reactions are taking place with energies comparable to those found in arc furnaces. The 100- to 150-mm-diameter gadolinium and yttrium cells needed a power input of 12–15 kW, compared to the 9–10 kW power requirement in a typical 300-mm-diameter lanthanum or cerium cell (Henrie and Morrice 1966). Besides, the yttrium cell volume is only one-eighth the volume of the cerium cell. Operating at such high temperatures and power concentration severely stresses the construction materials of the cell, making the process challenging.

4.12 RECOVERY OF RARE-EARTH METALS AS ALLOYS

The earliest attempts at preparation of yttrium and the heavy rare-earth metals by chloride electrolysis was frustrated by the formation of metal powder dispersed in the electrolyte, rendering their separation in pure form difficult (Hicks 1918; Thompson et al. 1926). A novel way out of this difficulty appeared to be the recovery of rare-earth metal as an alloy that is molten at the electrolysis temperature. The alloy could thus be easily separated from the electrolyte. Metal was subsequently recovered from the alloy by pyrovacuum distillation. This approach attracted a number of investigations and considerable success was achieved. The important investigations are listed in Table 4.20.

TABLE 4.20
Electrolytic Preparation of Rare-Earth Alloys

Year	Electrolyte	Cathode	Product	Reference
1968	RE_2O_3–REF_3–LiF–BaF_2	Consumable metal rod: Cr, Fe, Co	Gd–4Cr Gd–15Fe Dy–18Co Sm–13Fe	Morrice et al. 1968
1969	RE_2O_3–REF_3–LiF	Consumable metal rod: Mn, Cr, Fe	Gd–34Mn Gd–6Cr Dy–16Fe Sm–13Fe Y–37Mn	Morrice et al. 1969
1973	Y_2O_3–YF_3–LiF	Liquid Mg	Y–46Mg alloy	Aamland et al. 1973
1988	$NdCl_3$–KCl	Liquid Mg–Cd Liquid Mg–Zn	Nd–Mg–Cd Nd–Mg–Zn	Chambers and Murphy (1988)

The process of recovering rare-earth metals as alloys that melt at temperatures far below the melting point of pure rare-earth metal has two major advantages. The direct benefit is that the product is recovered as a liquid that can be readily separated from the electrolyte, collected, and has superior product purity. The additional benefit is that the formation of solution and intermetallic between the rare-earth metal deposited and the cathode metal usually decreases the activity of the rare-earth metal to such an extent that the back reaction between the deposited metal and the electrolyte is eliminated. This improves the current efficiency and makes it feasible to electroreduce rare earths like Sm(III), Eu(III), and Yb(III) that have stable divalency as well and do not form metal electrodeposit in a straight process.

4.12.1 Electrolysis of Chlorides

Considerable pioneering work on the electrowinning of rare-earth metals from their molten chlorides using a liquid cadmium or zinc cathode was done by Trombe (1935, 1938, 1945) between 1935 and 1945. The cell arrangement for this purpose was similar to the one he had used for deposition of pure liquid metals except that the cathode was a liquid metal. An electrolyte composed of 44% $GdCl_3$, 44% KCl, and 12% LiCl with a liquid cadmium cathode was used. The bath temperature was held between 625°C and 725°C, and the electrolytic current was maintained for 15 min. A cadmium alloy containing 6% gadolinium was obtained. This alloy was heated in a vacuum to distill away cadmium. Gadolinium thus obtained was melted in a molybdenum crucible at 1240°C to form a semi-agglomerated mass, which was analyzed at 98.4% gadolinium and 0.7% silicon and cadmium. It was a small-scale experiment that used only a total of 4 g of electrolyte. Besides gadolinium, europium (Trombe 1938) and dysprosium (Trombe 1945) were also prepared using cadmium as the liquid cathode. A molten alkali chloride bath was used at 750°C to which praseodymium, yttrium, or samarium chlorides were added. The cathode was a liquid alloy of Mg–Cd. On electrolysis, the liquid cathode collected the rare-earth metal. The resulting alloy, which contained up to 35% rare-earth metal, was vacuum-distilled to remove magnesium and cadmium. Of the three rare earths investigated, only samarium tended to distill together with magnesium.

A scandium–zinc alloy was obtained at the cathode of an electrolysis cell with eutectic KCl–LiCl containing dissolved scandium chloride as the electrolyte and molten zinc as the cathode (Fischer et al. 1937). Scandium was recovered after distilling off zinc. An equimolar mixture of $SmCl_3$–NaCl was electrolyzed at 500°C using a liquid zinc cathode, and a $SmZn_{12}$ alloy was obtained (Ishikawa et al. 1974).

Chambers and Murphy (1988) investigated the fused salt electrolysis of neodymium from a chloride electrolyte using a liquid metal cathode. Even though it was possible to electrodeposit neodymium into a liquid zinc cathode, the current efficiencies averaged only 50%, and zinc was dispersed throughout the electrolyte at all current densities. The mobility of zinc in the electrolyte decreased during electrowinning between 500°C and 600°C, but current efficiencies averaged only 40%. Using a temperature between 600°C and 700°C also did not yield satisfactory results. At above 700°C, zinc readily mixed with the electrolyte leading to a very

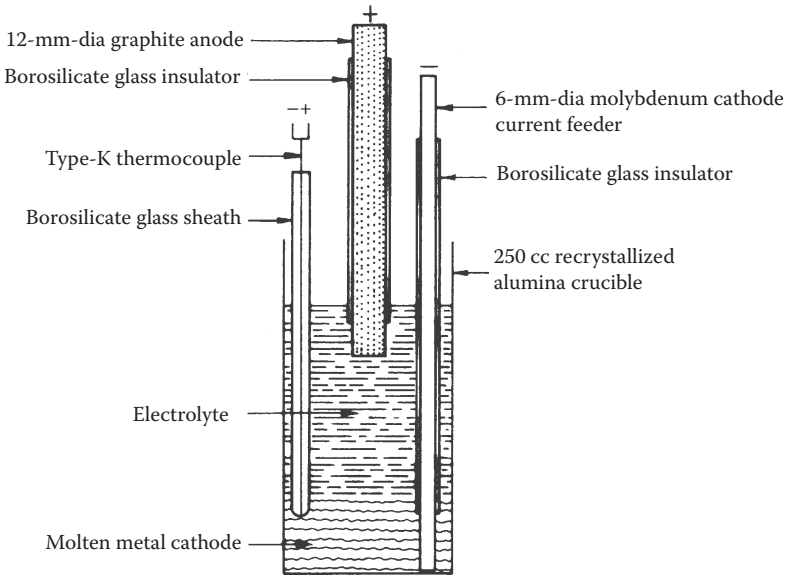


FIGURE 4.56 Electrolysis cell for reduction of neodymium. (From Chambers, M.F. and Murphy, J.E., Molten salt electrolysis of neodymium from a chloride electrolyte. In Bautista, R.G. and Wong, M.M. (eds.), *Rare Earths*, pp. 369–376, The Minerals, Metals and Materials Society, Warrendale, PA, 1988.)

poor metal–salt separation at the end of electrolysis. These problems were circumvented by Chambers and Murphy (1988) by the use of Mg–Zn and Mg–Cd cathodes. The intermetallic compounds MgZn and Mg_3Cd_2 melt between 500°C and 550°C, and these were used as cathodes. They used an electrolytic cell shown schematically in Figure 4.56. A recrystallized alumina crucible (55 mm diameter and 105 mm height) was the electrolyte container. The anode was a 12-mm-diameter graphite rod, and an electrical connection to the liquid metal cathode was made with a 6-mm-diameter molybdenum rod. Sheathing the anode and the molybdenum current feeder with borosilicate glass tubes fixed the electrode surface area and enabled accurate control of the current density. The cell was heated externally by a furnace, and temperature was measured by a thermocouple sheathed with borosilicate glass and immersed in the molten metal cathode. The electrolyte was a 50:50 mole ratio mixture of $NdCl_3$ and KCl eutectic composition, and its melting point was 480°C. The cell was operated at 650°C and electrolysis lasted for 4 h. In the end, the cell contents were allowed to cool in the alumina crucible, after which the crucible was broken and the alloy was separated from the solidified electrolyte.

Neodymium was recovered from the cathode alloy by distillation. The apparatus used is shown in Figure 4.57. The alloy was contained in a molybdenum crucible placed inside a graphite condenser column. The column was placed in a bell jar that was evacuated. Distillation was carried out at 900°C and 0.1 Pa for 15 min followed by heating at 1100°C and 0.1 Pa for up to 30 min. Magnesium and zinc or cadmium were distilled off leaving behind neodymium in the molybdenum crucible. This was

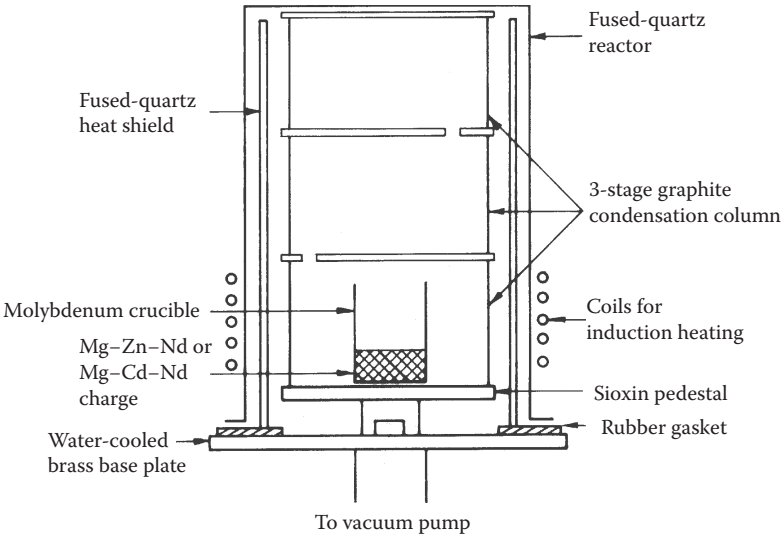


FIGURE 4.57 Vacuum distillation apparatus. (From Chambers, M.F. and Murphy, J.E., Molten salt electrolysis of neodymium from a chloride electrolyte. In Bautista, R.G. and Wong, M.M. (eds.), *Rare Earths*, pp. 369–376, The Minerals, Metals and Materials Society, Warrendale, PA, 1988.)

recovered by inverting the crucible and heating under a vacuum, allowing the molten neodymium to drip onto a cold copper hearth.

Between the two liquid alloy cathodes Mg–Zn and Mg–Cd, Chambers and Murphy (1988) considered the Mg–Cd cathode better, even though the current efficiency was only 80% as compared to 90% current efficiency when the Mg–Zn cathode was used. The Mg–Cd–Nd alloy yielded purer neodymium product on vacuum distillation. Neodymium metal of purity 99.9+% was recovered from the Mg–Cd alloy cathode, whereas about 2% zinc persisted in the neodymium recovered from the Mg–Zn alloy. Besides, the residual chlorine, carbon, and oxygen contents of the neodymium product from vacuum distillation of the zinc alloy cathode were 100, 300, and 180 ppm, respectively, while the corresponding values for the product from the cadmium alloy cathode were 30, 80, and 110 ppm. The Mg–Cd alloy resulted in a cleaner metal–salt separation than did the Mg–Zn alloy. The separation of the Mg–Cd alloy from neodymium by vacuum distillation was achieved more readily than when zinc was involved.

The feasibility of electroreduction of Sm(III) to metal [SM(0)] in a molten eutectic of LiCl–KCl was investigated by Castrillejo et al. (2011). They carried out electrochemical measurements using tungsten, aluminum, and aluminum-coated tungsten as the cathode. They found that, on a W cathode, electroreduction of Sm(III) takes place only to Sm(II). No further reduction, i.e., Sm(II)/Sm(0), was observed prior to reduction of Li(I) ions from the solvent. The electrolytic extraction of samarium from the molten salt is not conceivable on an inert electrode. Cyclic voltammetry and open-circuit chronopotentiometry showed that solutions of Sm ions can be reduced

on an aluminum electrode forming different samarium–aluminum alloys. It was also possible to form these alloys by codeposition of samarium and aluminum at the surface of a W electrode. Deposition of Sm on Al coated on W was also feasible. Potentiostatic electrolysis was used to form the alloys (Al_3Sm and Al_2Sm) depending on the applied potential using Al plates. The potential shift of the redox couple is caused by the decrease in Sm activity in the metal phase due to the formation of Sm–Al alloys at the interface. This is the second advantage mentioned previously.

4.12.2 Electrolysis of Oxide–Fluoride Melts

The electrolytic reduction of rare-earth oxide dissolved in a fluoride melt to yield the alloy directly has also been investigated. In many cases, the alloy can be distilled in vacuum to yield the pure metal as the condensate or as the residue. Two types of cathodes were used. In one type, the cathode was solid at the electrolysis temperature but formed a liquid alloy when the rare-earth metal was deposited on it. In the other, the cathode was a metal or alloy that was already molten at the electrolysis temperature and formed a molten alloy with the electrodeposited rare-earth metal. When the cathode was solid, the temperature of electrolysis was higher than the melting point of the eutectic between the cathode and the rare-earth metal but lower than the melting point of the cathode metal (Morrice et al. 1968, 1969). The combinations of rare earth and consumable cathodes investigated at Reno are shown in Figure 4.58 (Morrice 1985). The electrolyte comprised rare-earth oxide dissolved in REF_3–LiF–BaF_2, and the cell arrangement is the same as that used for high-purity metal preparation. Instead of Mo, a consumable rod of Fe, Ni, Cr, or Co is used as the cathode. Low-melting near-eutectic alloys of the rare earth and the cathode metal formed and dripped off during electrolysis at the working temperature of 850–1000°C and were collected at the cooled bottom of the cell in

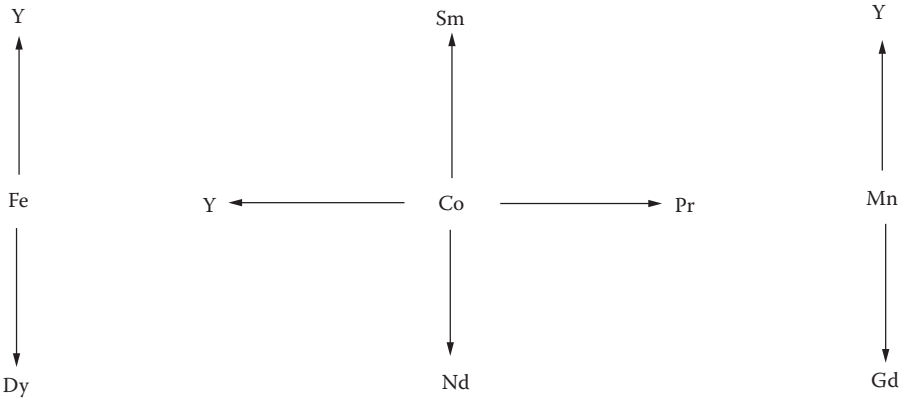


FIGURE 4.58 Combinations of rare earths and consumable anodes in the electrolytic preparation of alloys. (From Morrice, E., Molten, Salt electrowinning of rare earth and yttrium metals and alloys. In Xu Guangxian and Xiao Jimei (eds.), *New Frontiers in Rare Earth Science and Application*, vol. II, pp. 1099–1106, Science Press, Beijing, 1985.)

a solid form. The consumable cathode rod was lowered into the bath at a controlled rate, and semicontinuous operation of the cell was achieved. The alloy could be tapped from the bottom spout after heating the cell to sufficient temperature. The alloys contained about 80–90% REM. Even the difficult-to-reduce samarium was obtained as Sm–13Fe alloy with about 46% current efficiency, principally because alloy formation effectively prevented back reaction of samarium with the fluoride, which results in the formation of Sm(II).

Morrice et al. (1969) investigated the electrodeposition–vacuum distillation process for the preparation of gadolinium, dysprosium, yttrium, and samarium. As high-purity liquid metals, the first three are difficult to electrowin because of their high melting points (>1300°C). At the requisite cell-operating temperatures (~1400°C), there will be increased carbon contamination of the product. Even though samarium has a comparatively low melting point (1072°C), direct electrowinning of the metal was unsatisfactory because of its reactivity with the electrolyte (Morrice et al. 1968). Electrowinning of these metals as alloys circumvented these problems. Morrice et al. (1969) chose manganese and chromium as alloying elements for gadolinium, manganese for yttrium, and iron for samarium and dysprosium, on the basis of phase diagram information of the corresponding binary alloys and the vapor pressures. The eutectics of the binary systems contain about 75–95% of the rare-earth metal, and, except in the case of gadolinium–chromium, the eutectic temperatures were low enough to permit cell operation in the temperature range of 900–1000°C.

The cell used by Morrice et al. (1969) for the electrodeposition of gadolinium, dysprosium, samarium, and yttrium with manganese, chromium, or iron is shown in Figure 4.59. The graphite crucible for holding the molten electrolyte had an inside diameter of 100 mm and a depth of 100 mm. The anodes were two 18-mm-diameter fluted graphite rods. The cathode was a 5- to 6.5-mm-diameter iron or chromium metal rod or a 15-mm-diameter as-melted manganese metal bar. The cell was enclosed in an inert gas chamber to avoid atmosphere contamination. Glove and view ports in the chamber permitted addition of cell feed and allowed the raising and lowering of the electrodes during operation.

The electrolytes for the electrodeposition of gadolinium–manganese, gadolinium–chromium, dysprosium–iron, and yttrium manganese alloys contained 50 mol.% rare-earth fluoride and 50 mol.% lithium fluoride. The electrolyte for the electrodeposition of samarium–iron alloy contained 25 mol.% SmF_3 and 75 mol.% LiF. The solubilities of rare-earth oxides in the electrolyte are between 2 and 4 wt.%.

In the beginning, melting of the electrolyte was started from the top by striking an arc between two tungsten rods. Subsequently, the cell was internally heated by applying AC between the graphite anodes. For electrolysis, DC was applied to the anode and cathode. The rare-earth metal was electrodeposited on the manganese, chromium, and iron cathode to form a low-melting alloy. The alloy, as it formed, dripped off, the cathode penciled down, and a new section of the cathode was lowered into the electrolyte. The molten alloy descended and collected at the bottom of the cell, where a skull of frozen electrolyte prevented graphite contamination of the alloy. After completion of the experiment, the electrolyte was allowed to freeze, and alloy nodules weighing 2–75 g each were recovered. The operational data for electrodeposition of the various alloys are given in Table 4.21.

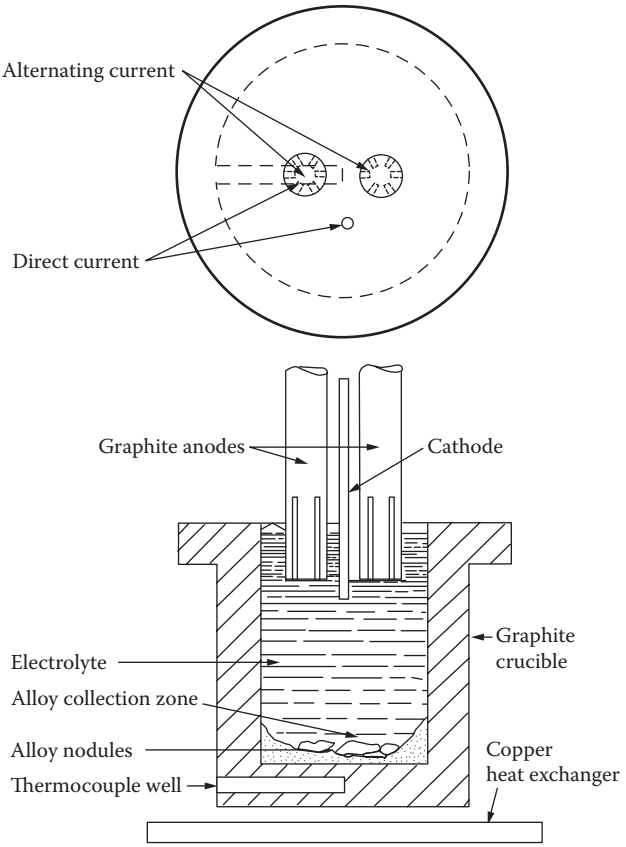


FIGURE 4.59 Rare earth–ferroalloy electrodeposition cell. (From Morrice, E. et al., *J. Metals*, 21(1): 34–37, 1969.)

The next step of the process, vacuum distillation, was carried out by Morrice et al. (1969) in the apparatus shown in Figure 4.60. In the distillation apparatus, the alloy sample was contained in a 25-mm-diameter by 25-mm-deep tungsten crucible having a wall thickness of 1.6 mm. To collect the distilled metal, a tantalum condenser was placed above the crucible. The apparatus including the induction furnace for heating the sample was enclosed in a Pyrex bell jar chamber that could be evacuated to 6.6×10^{-5} Pa. The crucible and condenser temperatures were measured using thermocouples.

Distillation was carried out by slowly heating the electrodeposited alloy nodules, about 30 g in each experiment, while maintaining the vacuum at 1.3×10^{-4} Pa. Pure samarium and dysprosium metals distilled off from the iron alloy and collected in the condenser. They were separated from the collector by peeling away the tantalum. Gadolinium and yttrium, being less volatile than the alloying components chromium or manganese, remained as residue in the crucible while the alloying constituent distilled off. After completion of experiment, the crucible containing these metals

TABLE 4.21
Operational Data for Electrodeposition of Alloys

	Values for Specific Alloys				
Operational Parameters	**Gd–Mn**	**Gd–Cr**	**Dy–Fe**	**Sm–Fe**	**Y–Mn**
Electrolyte composition (mol%)	$50GdF_3$–50LiF	$50GdF_3$–50LiF	$50DyF_3$–50LiF	$25SmF_3$–75LiF	$50YF_3$–50LiF
Average direct current (A)	63	71	70	45	64
Average direct current voltage (V)	22	27	25	26	30
Initial anode current density (A/cm^2)	0.7	0.7	0.7	1.1	0.9
Initial cathode current density (A/cm^2)		18	14	10.1	
Average electrolyte temperature (°C)	964	1339	1056	887	1048
Average cell bottom temperature (°C)	677	834	707	719	700
Duration of electrolysis (h)	0.4	0.8	1.0	1.5	1.0
Alloy recovered (g)	58	79	122	67	85
Rare earth metal content (%)	66	94	84	87	63
Current efficiency (%)	78	67	73	46	76

Source: Morrice, E. et al., *J. Metals*, 21(1): 34–37, 1969.

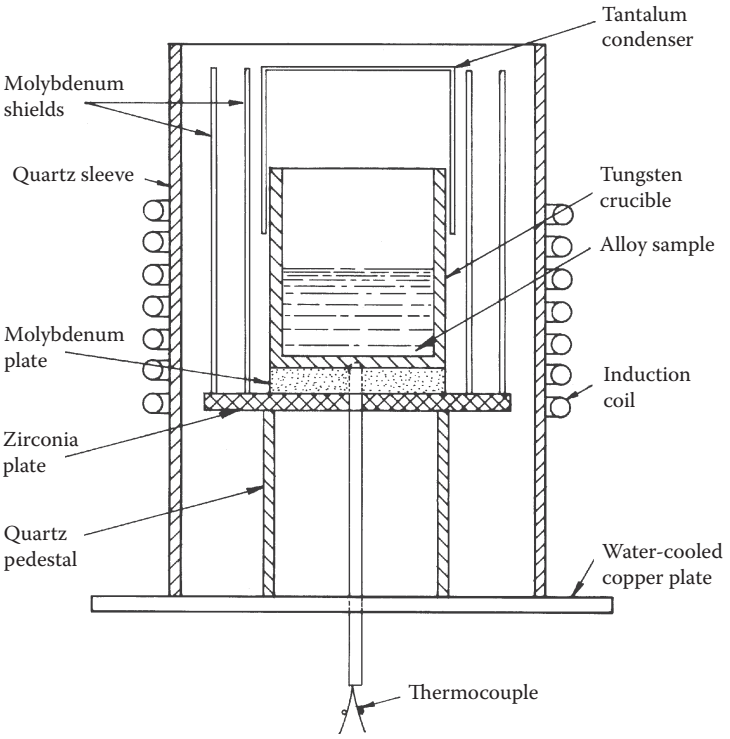


FIGURE 4.60 Rare earth–ferroalloy distillation apparatus. (From Morrice, E. et al., *J. Metals,* 21(1): 34–37, 1969.)

was inverted, and the metals melted under vacuum onto water-cooled copper hearth. The details of distillation, starting alloy, and final product analyses are summarized in Table 4.22. After distillation, gadolinium, samarium, and yttrium contained less than 0.02% of ferrous metal. Distillation did not effectively separate dysprosium from iron, and high-purity dysprosium was not obtained. The difference in vapor pressure between Dy and DyF_3 was not sufficient for effective separation of dysprosium from the fluoride impurity, either.

The method described previously for a consumable solid cathode cannot be used to prepare alloys composed of yttrium and low-melting constituents such as magnesium, aluminum, or zinc. A suitable method for these was described by Aamland et al. (1973). The method consisted of electroreduction of Y_2O_3 dissolved in molten YF_3–LiF electrolyte and subsequent deposition of yttrium in a floating magnesium cathode. The process was carried out in a specially designed MgO diaphragm cell at a temperature ranging from 780°C to 970°C. The product alloys, prepared in batches of ~20 g, contained up to 55% yttrium. The cathode current efficiencies were 21–60%. The purity of the alloy was comparable to that obtained by metallothermic reduction. On distillation in vacuum, these alloys yielded yttrium metal comparable in purity (0.1–0.2% oxygen content) to that obtained by distillation of metallothermic alloys.

TABLE 4.22
Operational Data for Distillation of Alloys Containing Rare Earth and Ferrous Metals, and Analysis of Starting Alloys and Final Products

	Distillation Parameters											
Alloy	Duration (h)	Distillation Temperature (°C)	Condenser Temperature (°C)	RE Recovered (%)		Analyses (%)								
						Al	Ca	C	F	Fe	Mg	O	Si	Ta
Dy–16Fe	2	1300	1095	75	Alloy	<0.01	<0.003	0.024	0.26	16.2	0.003	0.030	0.005	<0.02
					Distillate	<0.01	<0.003	0.002	0.21	0.008	<0.001	0.021	<0.005	<0.02
Sm–13 Fe	3	1000	700	85	Alloy	<0.01	<0.003	0.049	0.58	13.0	0.030	0.050	0.010	<0.02
					Distillate	<0.01	<0.003	0.010	0.03	0.005	0.001	0.015	<0.002	<0.02
						Al	Ca	C	Cr	F	Mn	O	Si	W
Gd–6Cr	3	1350	*	95	Alloy	<0.01	<0.003	0.025	6.2	0.48	<0.003	0.027	0.004	<0.01
					Residue	<0.01	<0.003	0.020	0.1	<0.002	<0.003	0.030	0.008	<0.01
Gd–34Mn	0.5	1350	*	96	Alloy	<0.01	<0.003	0.030	0.005	0.39	33.7	0.019	0.004	<0.01
					Residue	<0.01	<0.003	0.050	0.004	0.018	<0.003	0.020	0.010	<0.01
Y–37Mn	0.1	1550	*	93	Alloy	<0.01	<0.003	0.045	0.004	0.35	37.0	0.020	0.005	<0.01
					Residue	<0.01	<0.003	0.050	0.004	0.003	0.003	0.060	0.003	0.35

Source: Morrice, E. et al., *J. Metals*, 21(1): 34–37, 1969.
Note: * means not given or not mentioned.

Besides Mg, molten aluminum was also used as the cathode in the preparation of yttrium–aluminum alloy (Al–20Y) using an electrolyte of Y_2O_3 in YF_3–LiF (Bratland et al. 1972, 1973). Yttrium–aluminum alloy of approximately eutectic composition (91% Y) was electrowon from a mixture of yttria and alumina dissolved in a YF_3–LiF melt (Morrice et al. 1968). This cell used liquid Y–Al cathode and a graphite anode.

4.12.2.1 Electrodeposition of Europium from Molten Fluoride

Gibilaro et al. (2009) studied the electrodeposition of europium from molten fluoride (LiF–CaF_2) media by (1) the use of a reactive cathode made of copper and (2) the codeposition with aluminum on an inert electrode, leading to the formation of europium–copper and europium–aluminum alloys. The authors had earlier demonstrated that Eu (III) is reduced in two steps in the LiF–CaF_2 eutectic on a Mo inert electrode at 840°C according to (Massot et al. 2009)

$$\mathrm{Eu(III)} + \mathrm{e}- \Leftrightarrow \mathrm{Eu(II)}$$

$$\mathrm{Eu(II)} + 2\mathrm{e}- \Leftrightarrow \mathrm{Eu}$$

The conclusion of this earlier investigation was that the electroreduction of Eu(II) to Eu metal takes place at a more cathodic potential than the solvent ion reduction Li(I). Consequently, the extraction of Eu ions from the molten salt was not feasible on an inert electrode. An elegant and effective alternative is decreasing the activity of electrodeposited metal at the cathode. The effectiveness of this approach was demonstrated in two different electrochemical processes—the use of a reactive cathode made of copper (Nourry et al. 2009) or the coreduction of europium and aluminum ions (Gibilaro et al. 2008), both yielding Eu-based alloys as the cathode products. Both copper and aluminum readily form stable inermetallics with europium and result in the crucially required decrease in europium activity in the cathode. This is the key to the success of the process route. Cyclic voltammetry and square wave voltammetry were used to identify the reduction pathway and to characterize the steps of Cu–Eu and Al–Eu alloy formation. Then, electrochemical extractions using the two methodologies have been implemented with an extraction efficiency of around 92% for copper electrode and 99.7% for coreduction with aluminum ions.

4.12.2.2 Electrochemical Reduction of Cerium Oxide to Metal

The Fray Farthing and Chen (FFC) and Ono and Suzuki (OS) processes originally developed for the reduction of titanium oxide to titanium metal by electrolysis in high-temperature molten alkali chloride salts (Chen et al. 2000; Ono and Suzuki 2002) were used by Claux et al. (2011) for the reduction of CeO_2 to cerium metal. A ceria pellet attached to a tungsten wire was used as an electrode for the study of the reduction mechanism. They set out to elucidate by electroanalytical techniques the reduction pathway leading to the metal and concluded that the reduction of CeO_2 was feasible via an indirect mechanism. Calcium metal was electrodeposited at the cathode from $CaCl_2$–KCl solvent and reacted chemically with ceria to form not only metallic cerium, but also cerium oxychloride. The electroreduction process has a poor current efficiency—only 10% of the current was used to convert CeO_2 into cerium metal.

4.13 CURRENT EFFICIENCY

Current efficiency in the electrolytic cells described here is determined by several factors. The current efficiency of commercial chloride cells is low, usually below 50%. At the temperature of electrolysis (~900°C), the rare-earth metals can react with O_2, H_2, CO_2, and graphite, forming products with low electrical conductivity and a high melting point. The presence of oxychlorides, either from the starting material or by reaction between the trichloride and moisture, is detrimental to the electrolytic process. Oxychlorides have higher melting points than the anhydrous halides and limited solubility in the latter. Their existence causes an increase in viscosity in the molten salt leading to current losses because of lower ionic mobility and a higher temperature for bath operation.

The presence and accumulation of multivalent elements such as Sm, Eu, and other nonreducible components in the electrolyte also lead to lower current efficiency. $SmCl_3$ can easily react with Sm, more readily at higher temperatures, to form soluble divalent chlorides. During electrolysis, the oxidation–reduction reaction of Sm^{3+}–Sm^{2+} can occur cyclically at anode and cathode and cause high current consumption and low efficiency.

The current efficiencies of molten fluoride systems are better and range from 75% to 95% (Hirschhorn 1968). The fluoride electrolysis investigations, however, have been conducted using high pure starting materials in inert atmosphere electrolytic cells.

Morrice (1985) has commented that low cathode current efficiency could result from reaction of the metal product with the electrolyte and poor coalescence of the electrowon metals. More efficient cell designs to provide cathodic protection and prevent metal products from being contaminated, and the determination of the effects of electrolysis temperature and melt composition, have also been suggested by him as a means of improving current efficiency. In addition to low current efficiency, Morrice (1985) had listed anode effect, metal and alloy product contamination, corrosion of cell components, and efficient heat utilization in the cell as areas that need research attention in the molten salt electrowinning of rare earth metals and alloys.

4.14 SUMMARY

Rare-earth metals are among those metals that are considered to be most difficult to produce in pure form. Several processes have been developed for the production of rare-earth metals of different purities. These include (1) reduction of anhydrous chlorides or fluorides, (2) reduction of rare-earth oxides, and (3) fused salt electrolysis of rare-earth chlorides or oxide–fluoride mixtures. A qualitative picture as to which reactive element is usable as a reducing agent for rare-earth-metal preparation is obtained from the free energies of formation of the oxides, fluorides, and chlorides and their dependence on temperature. The data for rare earths and some potential reducing agents indicate that in the oxide systems, the order of stability is $CaO > RE_2O_3 > MgO > Al_2O_3 \gg SiO_2$; whereas among the fluorides, it is $CaF_2 > REF_3 > LiF > NaF > MgF_2 \gg AlF_3$; and among the chlorides, $KCl > NaCl \approx CaCl_2 > RECl_3 > MgCl_2 \gg AlCl_3$. The indicated order of stabilities, however, can be changed in real systems by changing the activities of one or more of the reactants or products. When

no such change is effected, the above data indicate that calcium is the only choice for the reduction of rare-earth oxides and fluorides, whereas the chlorides can be reduced by lithium, sodium, or potassium. Thermodynamic feasibility is at best the first of many factors that determine the practicability of the reduction process. Consideration of the other factors, including the melting point of calcia slag and exothermicity of the reaction, indicated that calciothermic reduction of rare-earth oxides is not a suitable process for rare-earth-metal preparation. It had to be the halide route.

Rare-earth metals are highly reactive, particularly at the high temperatures required for their preparation. The halide reduction, which usually involves the metallothermic reduction of pure anhydrous halides with pure metallic reductants, is a standard method of reactive metal preparation and is meant to be an oxygen free process. However, oxygen and other interstitial impurities such as carbon and nitrogen do find entry into the reduced metal in various ways. This is traceable to the extreme stability of the solutions and compounds formed by these elements with rare-earth metals. While this cannot be avoided, it can certainly be minimized by suitable choice of materials and procedures.

The methods for producing rare-earth metals by chloride reduction processes are summarized in Figure 4.61. Starting from rare-earth oxide, the process basically involves two stages. In the first, anhydrous rare-earth trichloride is prepared, and in the second stage, the trichloride is reduced to the metal. The oldest and most widely used process for chloride preparation is the wet route. Rare-earth trichloride hexahydrate is crystallized from a HCl solution of rare-earth oxide. The hydrated chloride is then dehydrated by heating under dry HCl flow under reduced pressure. Alternatively, dry methods such as chlorination of the oxide by heating with ammonium chloride or chlorination of the oxide or even the rare-earth ore concentrate by heating with carbon under chlorine flow have also been used. The chloride can be purified by distillation. The principal reducing agents for rare-earth trichloride are calcium and lithium. Calcium reduction has been used at Ames for the production of low-melting lanthanides La, Ca, Pr, and also Nd and Gd. For gadolinium and higher-melting rare earths, using a higher reaction temperature was complicated by $CaCl_2$ slag frothing and bomb liner attack. Tantalum crucibles were useful. Reduction of rare-earth chloride with lithium has been successfully used for most of the rare earths. In the USBM process, chloride and lithium were heated together in a molybdenum crucible under inert atmosphere. In the Ames process as well as in the commercial process, lithium vapor reduction of rare-earth trichloride could yield yttrium and other high-melting rare-earth metals. Tantalum was used as a container. The LiCl slag was removed by vacuum distillation.

The use of rare-earth fluorides as intermediates for reduction to metal circumvents the problems associated with the use of hygroscopic and volatile chlorides. Purer metals are obtained in this elegant process. The methods are summarized in Figure 4.62. Out of the three major alternatives for converting the rare-earth oxide to rare-earth fluoride, hydrofluorination at 700°C has been used to prepare the purest fluorides. The Ames process is the technically perfect method for conversion of the fluoride to metal. In this method, the rare-earth fluoride and calcium loaded in a tantalum crucible are externally heated in an argon atmosphere to about 50°C above the melting point of the highest melting component of the reaction mixture. The

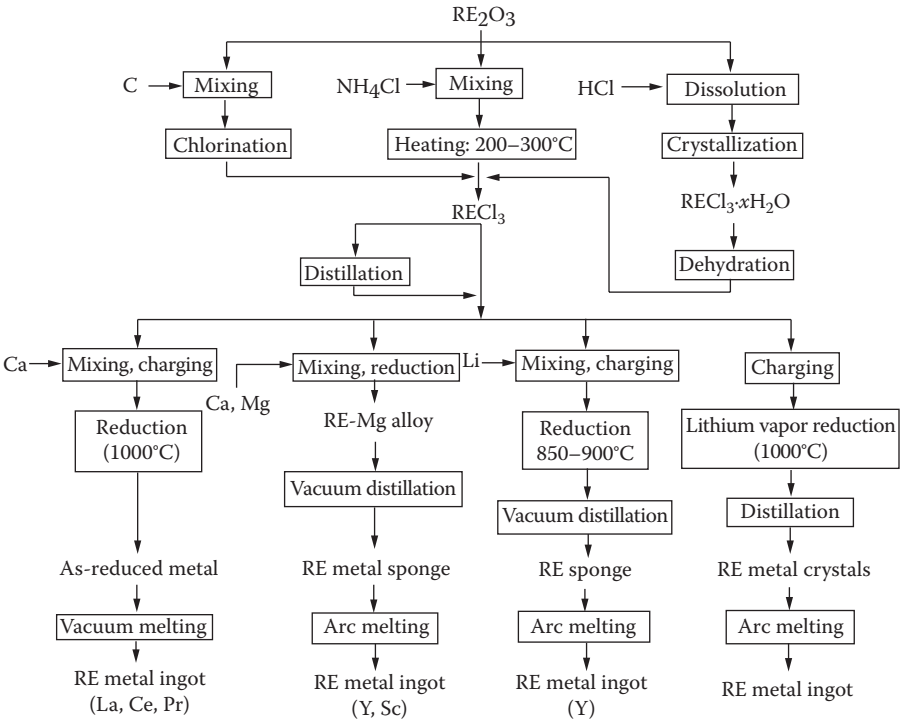


FIGURE 4.61 Processes for the preparation of rare-earth metals through the chlorides.

reaction goes to completion in a few minutes resulting in good slag–metal separation. The excess calcium and adhering slag are removed from the metal by vacuum melting, and high-purity metal is obtained in 97–99% yield. Any rare-earth metal, independent of its melting point, except Sm, Eu, and Yb, which form stable divalent halides, can be reduced to metal by this process. Lithium is the only other reductant that has been found to be quite as effective, but less than calcium. An important variant of the process, particularly for yttrium, is to conduct the reduction in the presence of magnesium at a lower temperature. Magnesium is removed from the Y–Mg alloy by vacuum distillation and the yttrium sponge vacuum melted. A limitation of the fluoride route is the high cost of fluorine chemicals, which end up as low-value calcium fluoride.

Even though samarium, europium, and ytterbium cannot be produced by halide reduction, their oxides can be directly reduced to metal in a process that exploits the pronounced volatility of these metals. The technique is quite similar to that used by Pidgeon for magnesium. Lanthanum is among the least volatile of the rare-earth metals. Besides, La_2O_3 has one of the most negative values for its heat of formation. In the process, an intimate mixture of lanthanum chips and rare-earth oxide is heated in a tantalum crucible fitted with a long tantalum condenser. Lanthanum reduces the rare-earth oxide, and the rare-earth metal produced, being volatile, escapes and collects in the condenser. Certain metals such as cerium, misch metal, zirconium,

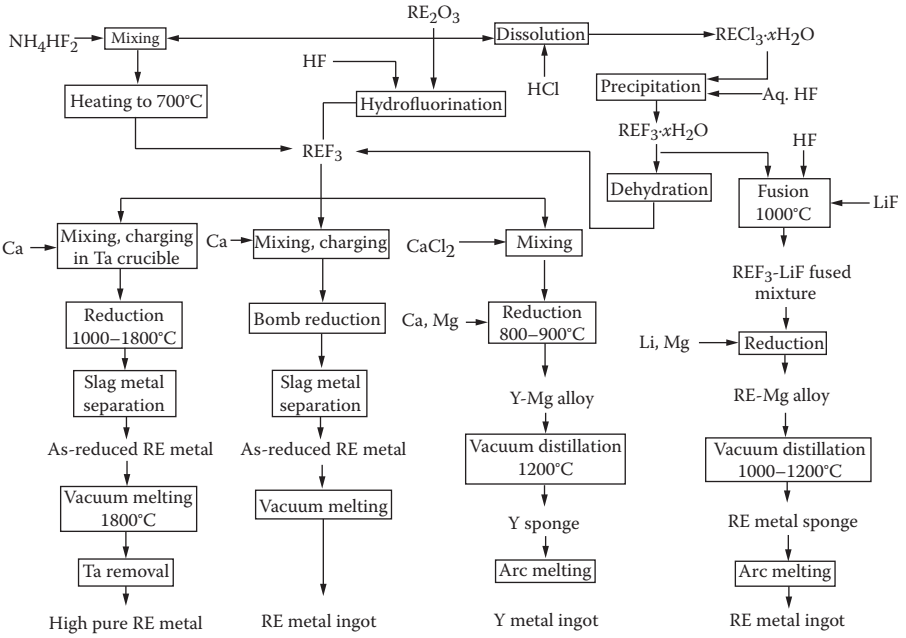


FIGURE 4.62 Processes for the preparation of rare-earth metals through the fluorides.

hafnium, and thorium, which are similar in the relevant characteristics to lanthanum, have also been used in its place. The process is shown in Figure 4.63 along with certain other specific oxide reduction methods. The reduction–distillation process has been shown to be applicable to all the rare-earth metals except lanthanum and cerium. High-purity metals have been obtained in what are essentially low throughput experiments. Many innovations can be incorporated in the process to improve throughput and possibly economy.

A relatively new entrant to the field of metallothermic rare-earth production methods is the process of molten salt reduction extraction, developed at General Motors. The reduction is carried out by reacting the Nd_2O_3 with calcium generated *in situ* in a molten salt bath ($CaCl_2$–NaCl) and simultaneously extracting the reduced metal into a molten Nd–Zn or Nd–Fe alloy. The Nd–Zn alloy product is treated in a vacuum to remove zinc and produce Nd metal. The process has been made commercially more attractive by the use of sodium instead of calcium as the reducing agent.

The electrolytic methods currently account for the largest volume fraction of rare-earth metals commercially produced throughout the world. Lanthanum, cerium, and praseodymium have melting points that permit their recovery in a liquid state by electrolysis of inexpensive fused chlorides at temperatures less than 1100°C. Winning of the rare-earth elements in the liquid state facilitates slag (electrolyte)–metal separation, minimizes contamination of the reduced metal, and enables continuous operation and high volume levels of production. Such electrolytic processes are inherently simpler and cheaper compared to complex metallothermic reduction procedures. The technical feasibility of preparing limited quantities of high-melting rare-earth

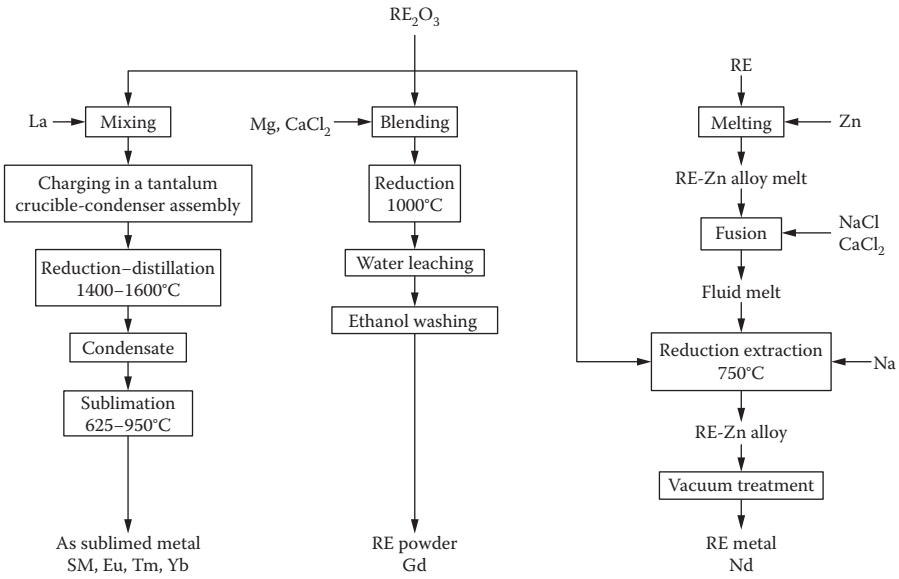


FIGURE 4.63 Processes for the preparation of rare-earth metals by oxide reduction.

metals such as gadolinium, dysprosium, and yttrium in addition to neodymium, praseodymium, and didymium (Nd + Pr) in a consolidated form has also been demonstrated by using the fluorides as electrolytes in place of chlorides. These studies have been carried out in specially designed high-temperature cells that can operate up to 1700°C. For cerium and lanthanum, cells have been designed and operated at US Bureau of Mines for continuous production of these metals by oxide–fluoride electrolysis. Instead of as pure metals, if the rare-earth metals are recovered as binary alloys having melting points in the range 600–1000°C, the electrolytic process has been found applicable to all the rare-earth metals with the added advantages of liquid metal recovery and low-temperature operation. Besides, by this process, all the rare-earth metals, including those with stable divalency, could be recovered as alloys. If a relatively more volatile metal such as cadmium, zinc, or magnesium is used as the alloying component with a relatively less-volatile high melting rare earth, e.g., neodymium, gadolinium, and yttrium, the alloy can be vacuum distilled to pure metal.

The question of a technically perfect reduction process for rare-earth-metal preparation was answered as early as the 1950s and 1960s with the development of the fluoride reduction process and the lanthanothermic direct reduction process at Ames. But these processes are expensive because of the high cost of chemicals, the expense of the reactor, and the batch nature of the process. The same may be said of electrolytic processes except those for the recovery of lanthanum, cerium, and praseodymium in a chloride bath. The highly effective oxide–fluoride electrolysis has problems of high-temperature operation, corrosion, low solubility of oxides in molten fluoride, and limitations on current density. The field remains open for improvement and new processes that are easy on costs and procedure yet provide adequate purity in the final metal product.

5 Refining

5.1 INTRODUCTION

As-reduced rare-earth metals, whether produced metallothermically or by fused-salt electrowinning, are generally 98–99% pure. It is usually possible in certain cases, if care is taken to use pure raw materials and adopt controlled environment processing, to restrict the total impurities in the as-reduced metals to about 0.5%. More often than not, this additional gain in purity either is not technically possible or involves a great increase in process cost, especially in commercial-scale operations. The general alternative to improving or modifying the reduction technique itself is first to prepare even a relatively impure metal by a commercially viable reduction method and follow it by a suitable refining procedure. This is important because fairly good-grade rare-earth metals with purity adequate for many application requirements are usually available at reasonable prices, and the metal that qualifies as pure for one application could be impure for another application. This also highlights the need for customizing the refining procedure for a particular application, with commercial metals as the source material. The refining step is, therefore, a necessary and important operation in the extractive flow sheet of the rare-earth metals.

A number of processes are used for refining the as-reduced rare-earth metals to different levels of purity. The nature and concentration of the impurity to be removed and the final purity level desired in the refined metal generally govern the refining technique that should be used. In the case of rare-earth metals, the applicable processes are strongly influenced by the melting points of the metals and their vapor pressure at the melting point. This influence is clearly brought out in Figure 5.1, which depicts the generalized sequence of processes for purification of rare-earth metals (Gupta and Krishnamurthy 1992). Complete purification is not achieved by any one refining technique, and as a rule, a sequence of processes has to be applied to remove all the impurities (Jones et al. 1982).

The usefulness of a given technique for the near-complete removal of one or more impurities from rare earths is a necessary but not a sufficient criterion for its adoption for large-scale or commercial operations. The technique has to be compatible with other demands such as product form, metal yield, batch size, operational simplicity, and economics. On the other hand, in the choice of a technique for small-volume metal refining for research purposes, major emphasis is placed on the ultimate purity achievable, and considerations such as yield and economics become secondary.

This chapter covers postreduction rare-earth-metal purification processes, beginning with a reference to the origin of various impurities usually associated with as-reduced rare-earth metals. The underlying processes of impurity removal during refining by pyrovacuum treatments like vacuum melting, vacuum distillation, and sublimation are then covered along with the techniques that have been used and results that were achieved. Fused-salt electrorefining has been applied to

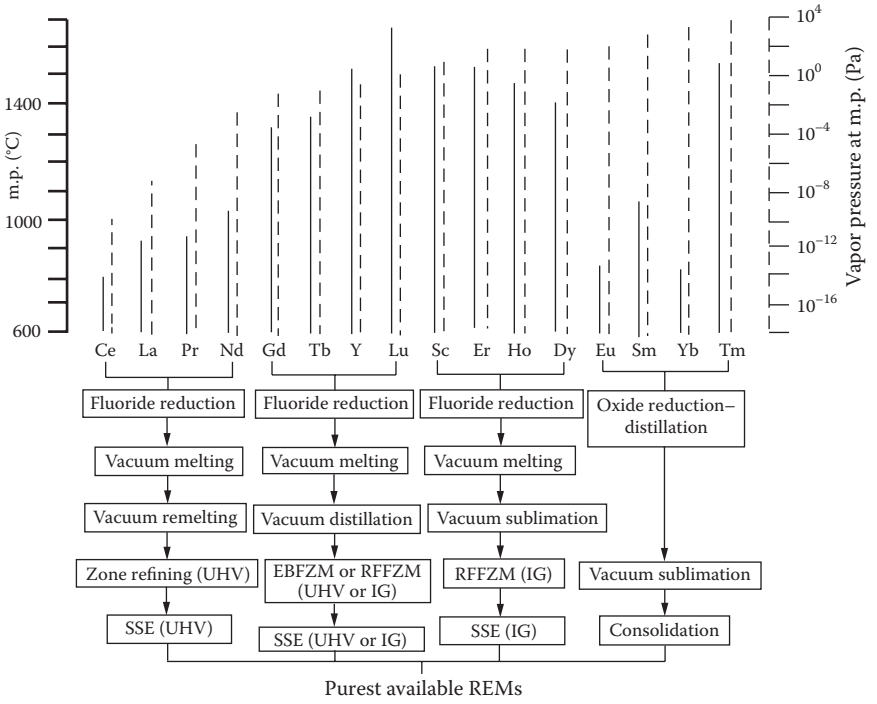


FIGURE 5.1 Processes for the purification of rare-earth metals. m.p., melting point.

rare-earth-metal refining in a limited way, particularly as a complement in areas where the pyrovacuum techniques meet roadblocks. The iodide refining or the Van Arkel–de Boer process has not been especially valuable for the rare earths. Ultrapurification of rare-earth metals has been important not only for obtaining the purest specimens for property measurements but also to prepare high-purity rare earth-bearing products. This is usually carried out by zone refining and its many variations as well as by solid-state electrotransport and its variations. The choice of a particular technique, as mentioned earlier, is strongly determined not only by the impurity to be removed but also by the physical properties of the rare-earth metal, particularly its melting point and vapor pressure. Unlike the chemical properties of rare earths, which are well known for their close similarity, the physical properties vary significantly among the rare earths (Gschneidner et al. 1995). This is reflected in the applicable techniques for rare-earth-metal refining and ultrapurification.

5.2 ORIGIN OF IMPURITIES

It may be recalled and briefly referred to here that the methods useful for rare-earth-metal production are high-temperature controlled-atmosphere reduction of halides, either the anhydrous chlorides or fluorides, by reductants such as calcium or lithium; fused-salt electrolysis of chlorides or oxide–fluoride mixtures; direct reduction of

oxides by lanthanum, cerium, zirconium, hafnium, thorium, or even misch metal; and finally, certain special reduction procedures in molten salts. As-reduced rare-earth metals obtained by the above processes are pure enough for certain applications but need further purification for many other applications. Depending on the raw material used and the process adopted, the type and level of impurities in the rare earths vary. Besides, the rare-earth metals themselves, because of their inherent characteristics, are selective in picking up certain impurities more avidly than others.

While the careful control of raw materials' purity and process variables will enable preparation of metal that is 99.99+% pure in respect to other metallic elements, the situation is very different for nonmetallic impurities such as oxygen, nitrogen, carbon, hydrogen, and the halides. To get metal that is better than 99.9% by weight pure with regard to all elements is an extremely challenging task. The rare earths getter nonmetallic elements, and they end up in the metal at all stages of manufacture or handling. In addition, these elements, even in small quantities, influence to a significant extent the properties of rare-earth metals.

In the as-reduced rare-earth metals, the impurities principally come from the starting materials and the environment in which the process is carried out. The best way to produce the pure metals is to prepare them in such a manner that the impurities do not get into the system. This is best done by using the reactants in a pure form and keeping the system free from atmospheric gases and adsorbed impurities at all times—a task not always feasible because of technical and/or economic reasons. Any loose nonmetallic element present in the container materials or on the inner surfaces of the reactor will invariably end up in the metal.

5.2.1 Starting Materials

In the as-reduced metals, the metallic impurities to be considered first are the metallic reductant and any metal added to the charge to form a low-melting alloy. A reaction constituent, when used in excess of the stoichiometric amount, can end up as an impurity. Calcium, lithium, and lanthanum impurities are all examples in this context. Magnesium and zinc impurities originate from adding an alloy constituent. A reaction constituent also ends up as an impurity in the event of incomplete reduction. The presence of residual fluorine or chlorine and residual oxygen in the metal is an example. The amount of fluorine that remains in the as-reduced metal prepared by fluoride reduction, however, is not the same as the amount of residual chlorine when the metal is obtained by chloride reduction. For example, when Dy, Ho, and Er are prepared by calcium reduction of rare-earth fluorides, the metal invariably contains 25–75 parts per million (ppm) fluorine impurity. On the other hand, when these metals are prepared by lithium reduction of their anhydrous chlorides, the chlorine contents in the as-reduced metals are very low, namely, <3 ppm (Croat 1969). In electrolytic reduction of rare-earth metals, for example, the impurities to be anticipated are lithium, fluorine, and oxygen. Lithium and fluorine result from the melt, and oxygen comes from the rare-earth-oxide starting material. Reaction constituents can be the source of impurities in another way also. The impurities present in the compound intermediate or reductant are often quantitatively transferred to the as-reduced metal.

For a long time and until the modern separation methods of ion exchange and solvent extraction were developed for effectively separating the rare earths from one another, one of the difficult problems was to get the rare-earth oxide that is pure with respect to all the other rare earths. Using ion exchange, it is possible to get one rare earth so pure that all other rare earths together amount to less than 10 ppm (Spedding et al. 1970). Solvent extraction methods also can provide such purity in many cases. It should, however, be pointed out that once a certain amount of other rare-earth impurity is allowed to be present in the rare-earth oxide, it will end up in the metal; usually, none of the postreduction purification techniques is particularly effective in removing these impurities, and they will persist in the purified metal.

Commercial chemicals frequently used in solvent extraction and ion exchange can be the source of certain metallic impurities found in the rare-earth oxides. Lead and calcium are examples. Impurities such as iron, cobalt, nickel, and copper enter the process stream as a result of a chemical attack on reactor materials, such as stainless steel, and end up in the rare-earth oxide. Redissolution of this oxide and reprecipitation using very pure chemicals and very pure water usually lead to substantial purification of the oxide from these impurities.

Conversion of highly purified oxides to anhydrous fluorides or chlorides is another stage where impurities can get easily introduced. Hydrogen fluoride (HF) is a very corrosive gas, and it can attack the metals of construction, forming volatile fluorides. These lead to the introduction of impurities such as molybdenum or iron into the rare-earth fluorides. Oxyfluorides and oxychlorides are readily formed by the fluorides and chlorides, and a good part of whatever oxygen is there in the halides will end up in the metal.

Among the many methods used for fluoride preparation, hydrofluorination by reaction between the rare-earth oxide and HF can yield the purest product. After preparing the fluoride in the powder form by passing HF over the oxide, in a practice followed at Ames, the fluoride was subjected to a process known as topping to get rid of any trace oxy compounds (Beaudry and Gschneidner 1978). It was subsequently found (Beaudry et al. 1983) that the oxygen contents of metals prepared from topped and untopped fluorides were nearly the same, particularly for light rare earths. Metallic impurities such as Cu, Ni, Fe, Cr, and Si, which remain in the fluoride after low-temperature hydrofluorination, were reduced in the topping process. Topping is not done in commercial practices. The fluorides prepared by the aqueous methods have been found to have slightly higher oxygen contents than the fluorides prepared by hydrofluorination. However, the preparation of fluoride by precipitation of REF_3 from an aqueous solution using 48% HF and by the reaction of RE_2O_3 with NH_4HF_2 are simpler methods and also are useful if certain impurities can be tolerated in the final product. Impurities such as Al, Fe, and Cu are introduced from the NH_4HF_2 (Beaudry and Gschneidner 1978).

Once very pure fluorides have been prepared, they must not be exposed to air, because they will react with moisture in the air and form oxyfluoride and will also pick up some carbon dioxide. The hygroscopicity of chlorides is more than that of the fluorides, and they also have a strong tendency to form oxychlorides. The best fluorides prepared at Ames contain considerably less than 20 ppm oxygen and less than 10 ppm metallic impurities (Spedding et al. 1970).

The impurity levels in the interprocess intermediate, for example, the rare-earth fluoride, that can be tolerated for producing metal of certain purity also depend on

the process used for reduction. For restricting impurity levels in the product, the method of preparing fluoride for use in the electrolytic reduction is not as critical as for the calcium reduction technique (Beaudry and Gschneidner 1978). Similar observations were made by Gray (1951) concerning cerium chloride for metallothermic reduction and cerium chloride for electrolytic reduction. In a calcium reduction, the oxygen content of fluoride is quite critical because any oxide present in the fluoride will end up in the metal. It is not so in electrolytic reduction. In oxide–fluoride electrolysis, CeO_2 or Ce_2O_3, for example, is added to the fluoride melt, and it is the oxide that undergoes reduction to the metal. The fluoride melt can actually extract oxygen and certain impurities such as C, N, F, Mg, and Ni (Carlson et al. 1960). Thus, in the electrolytic preparation, it may be anticipated that the long contact time of the metal with the fluoride flux may decrease the level of some impurities in the metal. However, a fluoride flux well loaded or saturated with impurities from the previous runs can also pass on some impurities to the metal.

In the electrolytic preparation of cerium, the method of preparation of CeF_3 influences the purity of the metal obtained. Preparation of the fluoride using NH_4HF_2 introduced impurities such as Al, Fe, and Cu from the bifluoride, and these impurities showed up in the metal. The preparation of CeF_3 by reaction of the oxide with anhydrous HF might lower the levels of these impurities in the metal.

In the same way as impurities in the interprocess intermediates can end up in the metal, impurities contained in the reductant can also find themselves in the as-reduced metal. Calcium is the most important reducing agent for metallothermic reduction of fluorides, and its purity is an important parameter (Spedding et al. 1968). Even the triply distilled commercial calcium invariably contains several hundred ppm of oxygen, and when this calcium is exposed to air even for a very short period of time, the oxygen content in it will increase to several thousand ppm. It is therefore very necessary to reprocess (distill) calcium just before using and keep it sealed from the atmosphere until use. At Ames, for best results, calcium is sublimed at a low temperature (825°C) under a few millimeters of helium. With such care, calcium containing 10–30 ppm oxygen could be produced. Another impurity in calcium is carbon. About 100 ppm carbon persists in the distilled calcium, and a part of this carbon will ultimately come into the metal (Spedding et al. 1970).

Even while using lithium as a reductant, great care has to be taken, as was done for calcium, because commercial lithium invariably contains more oxygen than what is acceptable.

5.2.2 Crucible

The materials of construction of the crucible and the reactor in which the metal is prepared come into close contact with the metal and can end up as impurities. A reduction carried out in a tantalum crucible results in an average of 0.05% tantalum in the as-reduced metal (Huffine and Williams 1961). This concentration can be much higher if reduction is carried out at higher temperatures or for longer periods of time. A tantalum crucible was used by Croat (1969) in the preparation of Dy, Ho, and Er. These metals were prepared, as described in the previous chapter, by the reduction of their anhydrous chlorides with lithium as a reductant. The temperature of reduction

was 900°C, which was well below the melting point of these metals. The tantalum contamination of as-reduced Dy, Ho, and Er was quite low, i.e., <30 ppm. This can be contrasted with the tantalum content of 0.1–0.2% that Dy, Ho, and Er have in their as-reduced from when they are obtained by calcium reduction of their fluorides in tantalum crucibles. These reductions are carried out at high temperatures, above the melting point of the rare-earth metals.

Daane (1961a,b) stated that because the solubility of tantalum in liquid rare-earth metals increased measurably with increasing temperature, the lowest possible temperature is used in the processes wherein the rare-earth metal is processed in contact with tantalum, in order to keep the tantalum impurity as low as possible. In the reduction of the light rare-earth metals (lanthanum through neodymium), the amount of tantalum in the metal is approximately 200–300 ppm. For higher-melting heavy rare earths and yttrium, this figure increases to about 1000–5000 ppm. Among the rare-earth metals, tantalum is the most soluble in scandium. As much as 3% tantalum is present in scandium melted in tantalum. As far as dissolution is concerned, tungsten is better as a crucible material. In the liquid rare-earth metals, less tungsten dissolves than does tantalum at any temperature (Dennison et al. 1966a,b). The refractory metals molybdenum, niobium, titanium, and zirconium are distinctly more soluble in molten rare-earth metals than are tantalum and tungsten.

In reduction procedures, where an alloying element is used to lower the melting point of the as-reduced metal (e.g., magnesium in yttrium reduction), titanium or zirconium may be used as crucibles. When an yttrium–magnesium alloy was reduced in titanium crucibles, the alloy picked up an average of 0.15% titanium, and when zirconium was used, the pickup was 0.58% zirconium (Huffine and Williams 1961).

In the electrolytic preparation of the rare-earth metals, cell corrosion can occur extensively, and the corrosion products can end up in the metal produced. Carbon impurity in the electrolytically produced metals usually comes from graphite anodes and/or cell walls (Beaudry and Gschneidner 1978). Besides carbon, depending on the materials used for cell construction, the metals may be contaminated with iron, silicon, and other metallic impurities. The use of Mo as a liner or for the crucible in the cell leads to pickup of the element in the electrolytic metal. Electrolytic cerium metal obtained using Mo as cell material showed a Mo level of >750 ppm. The use of Ta in place of Mo lowered Mo contamination in the metal, and Ta was also not picked up significantly (Shedd et al. 1964).

Experiments at Ames have indicated that even tantalum can be a source of certain interstitial impurities (Beaudry and Palmer 1974). Gadolinium prepared using topped fluoride and high-purity calcium, with the reactants and products handled in an inert atmosphere, showed less C, O, and N contents when W was used as a crucible than when Ta was used as the crucible.

5.2.3 Environment

A major source of interstitial impurities in the rare-earth metals can be the atmosphere used to handle the starting materials and products. This was clearly brought out by the results given by Beaudry and Palmer (1974) for cerium. A batch of cerium was prepared from topped fluoride and high-purity calcium, with the reactants and products handled

under purified helium. The residual impurity content was (in ppm) O, 15; N, 40; H, 3; C, 15; and F, 14. When the metal was prepared from topped fluorides and high-purity calcium but handled in air, it contained O, 350; N, 20; H, 10; C, 75; and F, 20. Many nonmetallic interstitial impurities have their origin in the processing atmosphere, which, incidentally, is the factor to be closely monitored and controlled even during the refining processes designed for elimination of impurities from the as-reduced metals.

5.3 METHODS FOR IMPURITY REMOVAL

Impurities once present in the metal can be removed by a variety of techniques (Beaudry and Gschneidner 1978). Two major types of processes can be distinguished. In one, the impurities and the metal are separated from each other, and in the other type, the impurities are not completely separated from the metal but are only redistributed so that one physical portion of the metal is substantially purer than the other portion. Impurity separation is accomplished usually in the conventional first-level purification processes, and starting from an as-reduced metal, which may be rather crude, a pure metal is produced, eliminating in the process several key impurities. Impurity redistribution is resorted to in the ultrapurification methods, and starting from a pure metal, an ultrapure metal is produced. Often, the ultrapurification methods work to remove certain impurities introduced into the metal during the purification process. Both in purification and ultrapurification, a high vacuum or ultrahigh vacuum (UHV) is used as the environment, not only for preventing atmospheric impurities from coming into contact with the metal undergoing refining but also to effect removal of impurities from the metal. In ultrapurification, an inert gas effectively equal in purity to high or UHV is used for certain metals for specific reasons. Generally, however, a vacuum is the natural accompaniment to high temperature in metal purification processes, broadly termed pyrovacuum treatments, which begin with vacuum melting as the first and major step for all but the four most volatile rare-earth metals. Purification of the volatile rare-earth metals is effected by another pyrovacuum treatment, vacuum sublimation.

5.4 PYROVACUUM TREATMENTS

Pyrovacuum treatment is the most important and effective means available for the purification of rare-earth metals with respect to most of the impurities. The process essentially involves heating of the rare-earth metal to temperatures up to or above its melting point, under high vacuum. Heating under vacuum at high temperatures is also necessary in certain purification procedures where the purification occurs not exclusively because of high temperature and low pressure but because of other reasons. Examples are the techniques of zone melting and solid-state electrotransport. These are generally not grouped as pyrovacuum treatments. Techniques that are called *pyrovacuum refining treatments* or simply *pyrovacuum treatments* are those where purification occurs because the impurity vaporizes, leaving behind the metal, or the metal itself vaporizes, leaving behind the impurity. In rare-earth refining, the first process occurs in techniques grouped as vacuum melting even though the impurities are distilled off. The second process occurs in techniques grouped as vacuum sublimation or vacuum distillation. The term *vacuum distillation* appears to

be specifically reserved for processes involving the distillation of the desired metal. During vacuum melting, a variety of processes occur that contribute to rare-earth refining. The principal mechanisms are simple distillation (of the impurity), degassing, and certain complex deoxidation reactions.

5.4.1 Distillation

Metallic impurities usually present in as-reduced rare-earth metals are calcium, magnesium, iron, nickel, silicon, aluminum, chromium, copper, titanium, molybdenum, tantalum, tungsten, and zirconium. When the rare-earth metal is heated/melted under high vacuum, some of these elements simply distill away, while others do not. Which of the elements will distill and to what extent they would be so removed depend upon the partial pressures of the impurity metals over the metal/melt. The vapor pressures of pure rare-earth metals and also of the impurity metals (Hultgren et al. 1973) are plotted in Figure 5.2. Even at the highest temperature (1850°C) used for vacuum melting of the rare-earth metal (Spedding et al. 1968; Beaudry and Gschneidner 1978), among the impurity metals listed, only Ca, Mg, Fe, Si, and Al are more volatile than the least volatile rare-earth metals. Nickel and all the refractory metals are substantially less volatile than the rare-earth metals. Because impurities are usually present as a dilute solution in the rare-earth metals, their partial pressure over the rare-earth metals will be considerably less. Taking this into account, the vaporization rate of the impurity element, i, G_i, may be approximated by the following free evaporation equation (Alcock 1976):

$$G_i = 44.32 S_i p_i^0 \sqrt{M_A/T}\ g\,\mathrm{cm}^{-2}\,\mathrm{s}^{-1}$$

When the impurity i is vaporizing from a solution in which its mole fraction is X_i and activity coefficient is γ_i, G_i is given by

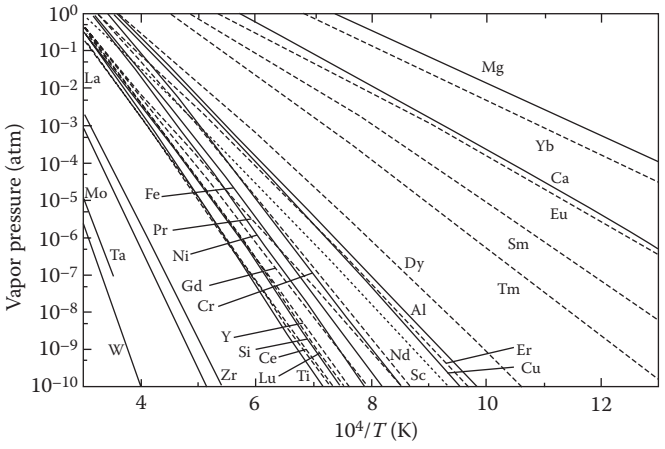


FIGURE 5.2 Vapor pressures of rare-earth and certain impurity elements.

$$G_i = 44.32 S_i \gamma_i X_i p_i^0 \sqrt{M_A/T}\ g\,cm^{-2}\,s^{-1}$$

Here, p_i^0 is the vapor pressure of the pure impurity element *i* in atmospheres, at the temperature considered; S_i is the vaporization coefficient, which may be equated to 1 as a first approximation, M is the molecular weight of the evaporating species, and T is the temperature in Kelvin at which the evaporation is considered. Even though p_i^0 is higher, a low value of X_i and γ_i would seriously limit the vaporization rate. So, unless the vapor pressure of the impurity element is very high, so that $p_i = \left(\gamma_i X_i p_i^0\right)$ and hence G_i will be substantial at the vacuum-melting temperature, no significant refining with respect to the impurity will occur by vacuum melting. These criteria restrict the metallic elements removable from rare-earth metals by vacuum melting to Fe, Cu, Al, Mg, and Ca.

The vapor pressures of the rare-earth metals are higher or, at best, of the same order of magnitude as those of the refractory metal impurities. Hence, the separation of rare-earth metals from these impurities by distilling off the impurities is ruled out. Instead, there is a good possibility of the rare-earth metal being distilled off, leaving behind the impurities in the residue. This situation arises because of high p_{RE}^0 and hence G_{RE}, forming the basis of rare-earth-metal purification by distillation.

It is entirely possible that the more volatile impurities are first removed from the rare-earth metal by distilling them off by vacuum melting, after which the rare earths are themselves distilled off next from the less volatile impurities. When the vapor pressure of the rare earths is very high, e.g., Sc, Dy, Ho, Er, and Lu, even distillation is not necessary. They can be purified by subliming them off from the impurity elements. This applies also to the most volatile of the rare-earth metals, Sm, Eu, Tm, and Yb.

5.4.2 Removal of Halogens/Halides

Fluorine and chlorine are the two elements usually found in as-reduced rare-earth metals, and their removal by degassing is important (Croat 1969). They may be present in the rare earth either as unreduced trihalide salt or unremoved reductant salt. Both could either be dissolved in the metal or exist as a second phase adhering to the metal–slag interface or possibly even trapped in pockets beneath the surface of the ingot. For complete removal of these impurities to be possible, their vapor pressures relative to that of the rare-earth metal must be sufficiently different.

Dysprosium, holmium, and erbium are the most volatile among all the rare earths prepared by a fluoride or chloride reduction process. The vapor pressures of pure Dy, Ho, and Er relative to the vapor pressure of their pure trifluoride salts and CaF_2 are plotted in Figure 5.3 (Croat 1969). The vapor pressure curves of the metal and the fluoride salts are closely bunched almost at all temperatures, and if the fluorine content removal occurs by fluoride salt evaporation, the chances of metal purification with respect to fluorine impurity do not appear very good.

It must, however, be borne in mind that the relative vapor pressure of components in solution cannot be compared using vapor pressure data for pure components unless the activity coefficients of the components in the system are known. Since the

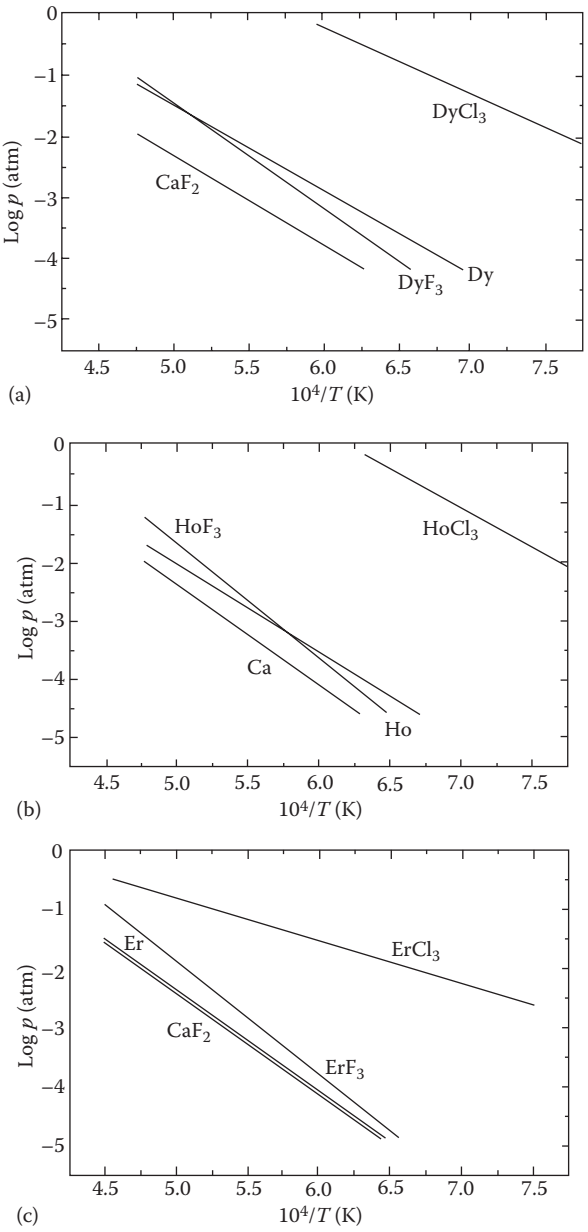


FIGURE 5.3 Vapor pressures of calcium fluoride, metals, and the trifluoride and trichloride of (a) dysprosium, (b) holmium, and (c) erbium. (From Croat, J.J., The preparation of high purity dysprosium, holmium and erbium by the lithium reduction of their trichloride salts, Report No. IS-T-346, Ames Laboratory, ERDA, Iowa State University, Ames, IA, National Technical Information Service, Springfield, VA, 1969.)

solutions considered in a purification situation are dilute (<0.1%), as a first approximation, they may be assumed to follow Henry's law, and the partial pressure of the solute or impurity may be considered to be proportional to its mole fraction.

In contrast to the trifluoride salts, the trichlorides exhibit considerable vapor pressure, as also shown in Figure 5.3 (Croat 1969). The trichlorides are more volatile, by a factor of 1000, than the trifluorides, and the separation of chlorides from the metal should not pose serious problems. The situation is similar regarding the volatility of calcium chloride and lithium chloride vis-à-vis the rare-earth metals.

5.4.3 Degassing

Among the nonmetallic impurities present in as-reduced rare-earth metals, the most critical ones are the gaseous elements hydrogen, nitrogen, and oxygen. Their removal from the rare earths can be termed degassing, and this is one of the most important and also most difficult tasks carried out during pyrovacuum treatment.

The reaction of hydrogen, nitrogen, and oxygen with the rare-earth metal can be represented by

$$\frac{1}{2}X_2(g) \leftrightarrow [X]_{\mathrm{RE}}$$

where X stands for H, N, or O and $[X]_{\mathrm{RE}}$ stands for the solution of the gas in the rare-earth metal. If these gases have to be removed from solid or liquid rare earths at a useful rate by pyrovacuum treatments, the equilibrium pressure of the gas species over the solution at the degassing temperature must be high. In other words, the following conditions should be satisfied: $p_{X_2} \gg p_{\mathrm{RE}}$ and $p_{X_2} \gg 1$ mPa.

The first condition is necessary for purification to occur by degassing. The second condition ensures that the degassing occurs at a practically useful rate. Hydrogen, nitrogen, and oxygen behave differently with respect to the above requirements.

5.4.3.1 Dehydrogenation

According to the rare-earth metal–hydrogen phase diagrams (Lundin 1961), the composition range of the terminal solid solution between the rare-earth metal and hydrogen is considerable, up to ~40 at.% hydrogen. In the range of hydrogen concentration usually encountered in as-reduced metals, the hydrogen will invariably be present in the solid solution. Hydrogen elimination will therefore be determined by the pressure–compositional isotherm of the solid solution. These data point to near-complete elimination of dissolved hydrogen from the rare-earth metals during vacuum melting (Goldschmidt 1967).

5.4.3.2 Denitrogenation

When considering nitrogen removal in as-reduced rare-earth metals, it should be noted that the nitrogen content is usually in the range of a few hundred ppm and seldom exceeds 1000 ppm. In this concentration range, nitrogen is present in the rare earths as a solid solution. For example, the solubility limit of nitrogen in cerium at 750°C is 0.3%. Data giving nitrogen pressure in equilibrium with a rare-earth

metal–nitrogen solid solution are sparse. The data on the free energy of formation of rare-earth nitrides (Pankratz et al. 1984) indicate that the mononitrides of rare earths are more stable than the lowest nitrides (M_2N) formed by the group V metals vanadium, niobium, and tantalum but are not quite as stable as those formed by the group IV metals titanium and zirconium. The decomposition pressures of these nitrides are low. The equilibrium nitrogen pressure over the rare-earth metal–nitrogen solid solutions would be considerably lower. The rare earth would not easily degas with respect to nitrogen during vacuum melting (Goldschmidt 1967). Incidentally, the equilibrium nitrogen pressure over the RE–N solid would equal or exceed the vapor pressure of the metal itself for most of the rare-earth metals.

5.4.3.3 Deoxidation

Among the nonmetallic impurities in rare-earth metals, oxygen is the most important and, invariably, the nonmetallic element present in greatest concentration in the as-reduced metal. Concentration of a few thousand ppm of oxygen in as-reduced metal is not uncommon, and the higher limit of the oxygen content may extend to 1% (Kremers 1961). The solution between the rare-earth metal and oxygen has a large range (Massalski et al. 1990), and deoxidation ultimately involves removal of oxygen from the rare-earth metal–oxygen solid solution. Even in metal–oxygen solutions of much lower stability than those of the rare earths (e.g., V–O, Nb–O, Ta–O system), equilibrium oxygen pressures over the solution are very low. Apart from the general information gathered by analogy and occasional experimental observation of the great stability (very low activity coefficient) of oxygen in the RE–O primary solid solution, Okabe et al. (1996) have actually determined the activity–composition relations in the Y–O system, and the results are summarized in Figure 5.4. The expectations are confirmed. Equilibrium pressures of oxygen over Y–O solid solutions are extremely low. They are lower than the corresponding values of even other rare earths and also group IV and V reactive refractory metals. However, an examination of the response of the refractory metal systems to pyrovacuum treatments is rather revealing even for the rare earths as regards the behavior of oxygen. It is apparent from the oxygen partial pressure data of the V–O, Nb–O, or Ta–O solid solutions (and similar systems) that deoxidation of these metals by evolution of gaseous oxygen is not possible, because at all temperatures, the partial pressure of oxygen over the solution is considerably lower than the partial pressure of the metal itself (Fromm and Horz 1980). The concentration of oxygen in these metals, however, decreases considerably during pyrovacuum treatments. This has been explained (Smith 1958; Brewer and Rosenblatt 1962; Garg and Sundaram 1974) as due to the formation and evaporation of certain complex oxide species.

5.4.3.4 Sacrificial Deoxidation

The formation of volatile suboxides of several reactive and refractory metals and their evaporation from metal–oxygen systems was postulated and experimentally verified by mass spectrometric investigations in the 1950s and 1960s (Smith 1958; Ingraham and Drowart 1960). Smith (1958), in his original paper on sacrificial deoxidation, listed yttrium as one of the metals that will deoxidize by suboxide

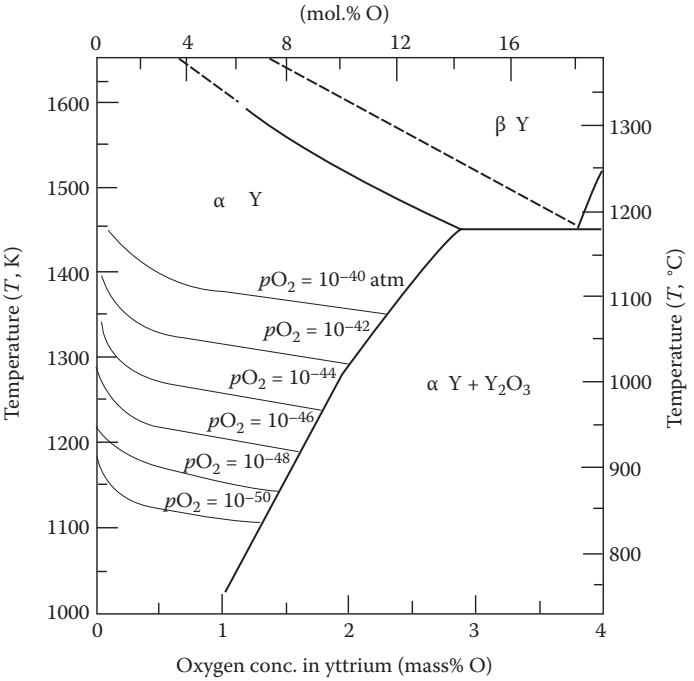


FIGURE 5.4 Phase diagram of the yttrium end of Y–O binary. Calculated iso-oxygen potential lines in the primary solid solution field. (From Okabe, T.H. et al., *J. Alloys Compd*., 237: 150–154, 1996.)

vaporization. It has been verified from experimental observations that several rare-earth elements do form suboxides. The formation and evaporation of volatile suboxides of a metal is, by itself, not a sufficient criterion for a metal to deoxidize. There are other factors, as described below.

The formation of a rare-earth-metal suboxide (REO) may be represented as follows:

$$[O]_{RE} + RE = (REO)$$

The square brackets represent the solution, and the parentheses represent the gas phase. The standard free energy of formation of the gaseous suboxide becomes more negative with an increase in temperature in the same way as the stability of CO increases with an increase in temperature (Pankratz et al. 1984). When the volatile suboxide forms and evaporates, not only an oxygen atom is removed from the metal, but a metal atom is also lost (or sacrificed). This process of deoxidation came to be known as sacrificial deoxidation. Initially, Smith (1958) concluded that in all metal–oxygen systems where the ratio of the vapor pressure of the suboxides to that of the metal, p_{MO}/p_M, is more than 1, sacrificial deoxidation can lead to purification of the metal with respect to oxygen. In his original paper, he listed yttrium also as

one of the metals amenable to sacrificial deoxidation because p_{yo}/p_y was 103 at the vacuum treatment temperature. Several exceptions were subsequently found to this conclusion, and the ability to refine the metal by sacrificial deoxidation was found to depend on the R ratio value as defined (Brewer and Rosenblatt 1962) below:

$$R = \frac{[C_O/C_M]_{vapor}}{[C_O/C_M]_{metal}}$$

where C_O and C_M are the concentration (in at.%) of oxygen and metal in the phases indicated by subscript. The R value essentially gives the relative concentration of oxygen in the vapor phase to that in the condensed phase. At a given temperature, the R value changes with a change in the oxygen content. However, Garg and Sundaram (1974) have pointed out that if the monoxide and monatomic metal are the only species in the vapor phase, and if the oxygen is in the concentration range where it obeys Henry's law, the R factor approaches a limiting value independent of concentration at any temperature. The magnitude of the limiting R value determines the possibility of sacrificial deoxidation. If this value is more than 1, then the metal can be purified by sacrificial deoxidation.

The R values for rare-earth metal–oxygen systems have not been computed. The requisite data, namely, the vapor pressure of suboxide as a function of oxygen content, are not available. Certain conclusions, however, may be derived from experimental observations on deoxidation during pyrovacuum treatment of oxygen-containing rare-earth metals.

There are two other pyrovacuum deoxidation processes that might be useful for residual oxygen removal from the rare-earth metals. These are called carbon deoxidation and silicon deoxidation.

5.4.3.5 Carbon Deoxidation

Carbon deoxidation is based on the occurrence of the reaction

$$[O]_{RE} + [C]_{RE} = (CO)$$

between oxygen and carbon dissolved in rare-earth metals. Oxygen is present in the metal, and a suitable quantity of carbon may be purposely added to encourage carbon deoxidation.

The occurrence of carbon deoxidation basically depends on the reaction above leading to the establishment of a sufficient CO partial pressure over the RE–C–O system. The partial pressure of CO is related to the thermodynamic properties of the RE–C–O system by the following equation:

$$p_{CO} = \gamma_c X_c \gamma_o X_o \exp\left(-\Delta G^o_{CO}/RT\right)$$

where γ_c, γ_o and X_c, X_o are the activity coefficients and atom fractions of carbon and oxygen in the rare-earth metals, respectively. If the values of these parameters are

such that a sufficient CO pressure is established at the vacuum-melting temperatures even at low oxygen contents, oxygen is removable by carbon deoxidation. Here again, to estimate the feasibility of carbon deoxidation, the thermodynamic parameters γ_c and γ_o must be known. Data are not available currently for the rare-earth systems. The feasibility of carbon deoxidation in RE–C–O systems has to be assessed from experimental observations on deoxidation during pyrovacuum treatments of carbon-doped rare earth–oxygen alloys.

5.4.3.6 Silicon Deoxidation

The deoxidation by silicon occurs in certain refractory metal–oxygen–silicon systems through the formation and evaporation of silicon monoxide (Awasthi et al. 1998). The possible occurrence of silicon deoxidation in rare earth–oxygen alloys containing silicon may be represented by

$$[O]_{RE} + [Si]_{RE} = (SiO)$$

The calculation of silicon monoxide pressure and the estimation of silicon deoxidation tendency in the rare-earth systems rely on the activity coefficient values for oxygen and silicon being available. The development of good SiO pressure even at low Si and O content in rare earths is key to the silicon deoxidation's usefulness. In the deoxidation of group V metals, silicon deoxidation is proving to be more efficient than carbon deoxidation. In the case of rare-earth metals, the lack of thermodynamic data on the activity of silicon and oxygen in the metals precludes estimation of silicon deoxidation tendencies. Experimental observations on the pyrovacuum treatment of rare-earth metal containing oxygen and doped with silicon form the basis, presently, for assessing the silicon deoxidation tendencies of rare-earth metals.

The success of sacrificial, carbon, and silicon deoxidation processes for oxygen removal from the refractory metals like niobium is not only due to favorable values for the activity coefficients of oxygen, carbon, silicon, and also the free energy of formation of niobium monoxide, but also due to the metal's high melting point and low vapor pressure. The last two properties enable the deoxidation treatments to be conducted at high temperatures under conditions of enhanced suboxide stability. Solid-state processing enhances the more desirable carbon and silicon deoxidation at the expense of the sacrificial mode of oxygen removal, which, incidentally, is more favored when the metal is molten (Kruger 1971; Garg and Sundaram 1975). Rare-earth metals, in comparison, are low melting and are also more volatile. These two factors limit the extent to which carbon and silicon deoxidation processes can be useful for oxygen removal.

The high volatility of many of the rare-earth metals puts the spotlight on another method of refining for freeing the rare-earth metal from oxygen. This option is to distill off the rare-earth metal while leaving behind an oxygen-enriched residue. Unlike in the deoxidation procedures discussed above where a high volatility of the suboxide and other oxides is desired, when the metal is distilled off from an oxide-enriched residue, the volatility of oxygen-containing vapors is unwelcome. However, the enrichment of oxygen in the melt actually encourages the evaporation of the oxygen-containing vapors.

5.4.3.6.1 Removal of Carbon and Silicon

Carbon is very much less volatile than even the least volatile of the rare-earth metals. So when a rare-earth metal containing only carbon as an impurity is pyrovacuum treated, an increase in carbon concentration in the metal will result because of the preferential removal of the metal as vapor. The only method by which carbon can be removed in such a situation is by forming a volatile compound, and carbon monoxide is the compound formed in many refractory metal systems that contain residual carbon impurity to be removed. Carbon deoxidation, when feasible, is useful not only for deoxidizing a metal but also for decarburizing it. By introducing oxygen in carbon-contaminated rare-earth metal, the system becomes RE–C–O, and under pyrovacuum conditions, the evolution of carbon monoxide can ultimately bring down the level of residual carbon. The ideal situation exists when carbon and oxygen are removed only by CO evolution, i.e., exclusive carbon deoxidation, because in such a situation, a precise quantity of oxygen doping will result in a predictable extent of carbon removal. As mentioned, however, the key factor is the occurrence of carbon deoxidation in RE–C–O solid solutions, which has yet to be established. Pure silicon is more volatile than carbon and also some of the rare earths. However, when present in low concentrations, silicon will not distill from the rare-earth metals. In the same way that carbon removal can be attempted through the formation of CO, silicon removal can occur through SiO vaporization. The feasibility of silicon removal by this reaction depends on the feasibility of silicon deoxidation from RE–Si–O solid solutions.

The process of carbon and silicon removal from rare earth is not so easy as described above; therefore, the alternative of distilling off the rare-earth metal and leaving behind a carbon- and/or silicon-enriched residue may be considered. The workability of this approach depends on the rare-earth metal's vapor pressure. As noted elsewhere, many of the rare-earth metals are rather volatile, and in those cases, distillation of the rare-earth metal from the carbon and silicon impurities becomes the practically useful approach.

5.5 PYROVACUUM TECHNIQUES

The metallothermic reduction of a rare-earth metal is usually completed by pyrovacuum treatment that essentially comprises vacuum melting and/or vacuum distillation. The rare-earth metals often contain many impurities that do not volatilize off during vacuum melting. Except perhaps oxygen, however, all these impurities will remain in the residue and possibly not interfere when the metal is distilled off and collected. Thus, both the options of pyrovacuum treatment—vacuum melting, which relies on the distilling off of the impurities either in elemental form or as certain compounds, and vacuum distillation, which relies on distilling off of the metal and leaving the impurities behind in the residue—are useful in pyrovacuum refining of the rare-earth metals. As may be anticipated, vacuum melting and vacuum distillation are serially combined in the overall process sequence.

The rare-earth metals could be divided into four groups primarily on the basis of their volatility. In the postreduction vacuum treatment, each group is processed somewhat differently (Beaudry and Gschneidner 1978).

5.5.1 Lanthanum, Cerium, Praseodymium, and Neodymium

These four light rare earths are characterized by relatively low melting points, very high boiling points, and hence, extremely low vapor pressures at the melting point. High-temperature vacuum melting is the only process by which they are purified. Distillation is ruled out on account of their low vapor pressure.

As-reduced La, Ce, Pr, and Nd from the fluoride process just separated from the CaF_2 slag contain Ca, CaF_2 and F, and H. The rare-earth metal containing these impurities readily reacts with moisture, and the as-reduced metal should always be handled under an inert atmosphere. All these impurities are more volatile than the rare-earth metals and are removed by melting the metals in a vacuum. Melting at pressures less than 0.1 Pa was adequate for removing calcium. Calcium content thereby decreased from over 1% to less than 150 ppm. Although removal of Ca and H occurs by heating the metal to just above its melting point, the quantitative removal of fluorine, which can be as high as 500 ppm in the as-reduced metal, required heating to at least 1800°C for 30 min.

In the Ames practice (Beaudry and Gschneidner 1978), vacuum melting of La and Ce was carried out at 1850°C; for Pr, the temperature was 1750°C, and for Nd, it was 1650°C. The melting lasted at these temperatures for 10 min. Heating was done in an induction furnace, and a tantalum crucible was used. At the high temperatures used for vacuum melting, the rare-earth metals dissolve a considerable amount of tantalum (Dennison et al. 1966a,b). However, the solubility of tantalum in these metals decreases with temperature, and it is very low at the metals' melting point. This information was utilized in restricting the amount of tantalum impurity in the rare-earth metal.

After vacuum melting the metals at high temperature, the furnace was slowly cooled to about 10°C above the melting point of the metal to allow the Ta to precipitate out of the solution and settle to the bottom of the crucible. Empirically, the time needed for complete settling of the tantalum was estimated at 24 min/cm height of the liquid metal column (Beaudry and Gschneidner 1978). Later, when the ingot was removed from the furnace, the thin tantalum crucible and the dendrites that had settled to the bottom of the crucible were machined off.

A typical analysis of La, Ce, Pr, and Nd prepared by calcium reduction of topped rare-earth fluoride, followed by vacuum melting, is given in Table 5.1. During these processes, the reactants and products were handled under an inert gas cover.

5.5.2 Yttrium, Gadolinium, Terbium, and Lutetium

The complete pyrovacuum purification sequence for these metals consists of a high-temperature vacuum treatment followed by distillation. The volatile impurities calcium, magnesium, and the fluorides do not pose a serious problem with these metals, because they are distilled off during the high-temperature vacuum melting.

An analysis of yttrium metal produced by direct calciothermic reduction of YF_3 in the as-reduced form, just separated from CaF_2 slag, is given in Table 5.2. An analysis of the metal produced by the Y–Mg intermediate alloy process after removal of Mg but before any refining treatment is also listed in the table. A variety

TABLE 5.1
Preparation Method and Major Impurities in Lanthanum, Cerium, Praseodymium, and Neodymium

	Major Impurities			
Impurity Element	Content (ppm)			
	Lanthanum	Cerium	Praseodymium	Neodymium
C	11	4	7	9
O	35	44	43	35
N	5	7	5	6
H	2	2	1	2
F	10	15	5	3
Ca	<0.1	<0.1	0.1	<0.1
Pt	<0.1	<1	<1	<1
Ta	5	8	12	25

Source: Beaudry, B.J. and Gschneidner, K.A. Jr., Preparation and basic properties of rare earth metals, in Gschneidner, K.A. Jr. and Eyring, L. (eds.), *Handbook on the Physics and Chemistry of Rare Earths*, vol. 1, North Holland, Amsterdam, 1978.

Note: Method: Ames process. Calciothermic reduction of rare-earth trifluoride in a tantalum crucible. As-reduced metal was purified by vacuum melting in a tantalum crucible, and the tantalum ingested into the metal was removed by precipitating it out in the molten metal and machining off the precipitate from the solidified rare-earth metal ingot. The entire process was carried out in a protected atmosphere of purified inert gas.

of pyrovacuum treatments have been investigated for refining as-reduced yttrium. In addition to melting in tantalum crucibles in an induction furnace, other methods of vacuum melting have also been used. An yttrium metal sponge obtained after "demagging" an Y–Mg alloy has been purified by consumable electrode arc melting (Daane 1961b). The demagged metal sponge has a calcium and magnesium content of 100 ppm each. To arc melt, these granular sponge particles were pressed into sticks that were welded end to end to make the electrode, and this electrode was consumable arc melted into a 100-mm-diameter ingot in a vacuum. The 100-mm-diameter ingots so obtained were welded together to make a 1525-mm-long electrode, which was arc melted in a vacuum into 150-mm-diameter ingots. A typical analysis of a 150-mm-diameter ingot thus obtained was as follows: Ca less than 10 ppm, Mg 30 ppm, and O 500–1650 ppm. This ingot had a titanium content of 0.5–1.5%, derived mainly from the titanium crucible in which it was demagged. Titanium was not removed from yttrium by arc melting. Consumable electrode arc melting of yttrium, the first melt in an argon atmosphere and the second in a vacuum at a nominal pressure of 0.1 Pa, typically yields a metal with the analysis listed in Table 5.2. There is a decrease in the residual calcium content in the metal to about 5 ppm and that of magnesium to about 20 ppm (Huffine and Williams 1961). Arc melting caused little change as far as other impurities in yttrium are concerned.

TABLE 5.2
Typical Analysis of as-Reduced Yttrium Metal[a]

Impurity	Metal Produced by Direct Ca Reduction of YF_3	Metal Produced by Ca Reduction of YF_3 through the Y–Mg Alloy Process	Arc-Melted Yttrium Metal Ingot
O	1400–2000	1500–2000	2750
N	200	150	190
F	500	800	750
C	100	200	110
Ta	4000	–	–
Ti	–	1500	–
Zr	–	–	5800
Ca	10	10	5
Mg	–	30	20
Fe	300	–	620

Source: Daane, A.H., Metallothermic preparation of rare earth metals, in Spedding, F.H. and Daane, A.H. (eds.), *The Rare Earths*, Wiley, New York, 1961; Huffine, C.L. and Williams, J.M., Refining and purification of rare earth metals, in Spedding, F.H. and Daane, A.H. (eds.), *The Rare Earths*, Wiley, New York, 1961.

[a] These analyses refer to different batches of metals. The metal in column 1 was produced in a tantalum crucible; for the metal in column 2, the crucible was titanium; and the reduction of metal in column 3 was carried out in a zirconium crucible.

One of the major improvements in the vacuum-melting process has been the use of electron bombardment as a method of heating (Smith et al. 1959). Temescal Metallurgical Corporation developed the electron bombardment furnaces for conducting vacuum metallurgical processes, and the process was more often referred to as electron beam melting. This technique was considered a great improvement over arc melting in a vacuum because in electron beam melting, it was possible to maintain pressures of about 0.01 Pa or less in the immediate vicinity of the melting metal. Such pressures led to volatilization processes proceeding more rapidly and to a greater degree of completion. As the melting metal would be made to drop off the feedstock, a large surface of the material, was exposed and this also enhanced the purification reactions.

The results of electron bombardment melting of yttrium (Huffine and Williams 1961) are given in Table 5.3. The purpose was to decrease the considerable oxygen content in yttrium by electron beam melting, but the results were not encouraging.

A more detailed investigation of electron-beam-melt refining of yttrium was carried out by Anable and Beall (1965) at the Albany Metallurgy Research Center of the US Bureau of Mines. Their purpose was to investigate the purification of commercially available yttrium by melting it in an electron bombardment furnace. Segments of yttrium weighing about 50 g were melted on a water-cooled copper hearth in the electron beam melting furnace. The samples were melted at power levels corresponding to temperatures in the range of 1730–1770°C at low pressure (7×10^{-3} to

TABLE 5.3
Analyses of Yttrium Ingot before and after Electron Bombardment Melting

	Content (ppm)	
Impurity	**Before Melting**	**After Melting[a]**
O	3250	3470
N	200	310
Zr	5000	4000
Cr	150	100
Fe	1000	190
Ni	2000	2000
Cu	–	100

Source: Huffine, C.L. and Williams, J.M., Refining and purification of rare earth metals, in Spedding, F.H. and Daane, A.H. (eds.), *The Rare Earths*, Wiley, New York, 1961.

[a] In the section of the electron bombardment-melted ingot having the highest overall purity.

13×10^{-3} Pa) for 1–120 min. The samples were cooled in vacuum before they were removed from the furnace and analyzed.

The results of yttrium purification are listed in Table 5.4. On electron beam melting, except for nickel, silicon, and zirconium, the concentration of all other listed metallic impurities lowered significantly. The aluminum content decreased from 50 to 30 ppm within a few minutes of exposure at all power levels except the lowest power level used. After exposure for 2 h, the Al content decreased to 10 ppm. The iron and copper were removed slowly throughout the 2 hours of exposure. The iron content came down from 100 to less than 50 ppm, and the copper content was lowered from 40 to 5 ppm. In the minimum exposure period of 20 min, the concentrations of magnesium and manganese decreased from 420 and 30 ppm, respectively, to <5 ppm. No change occurred in the nickel and zirconium contents, which were originally at 100 and 3000 ppm, respectively.

The silicon contents of all the samples decreased initially, in the first 20 min, from 100 to about 50 ppm. The silicon content increased slightly to 60 ppm after 2 h of exposure.

The changes in the oxygen, carbon, and nitrogen content in yttrium during electron beam melting at various power levels (temperatures) are shown in Figure 5.5. The oxygen content increased only by electron beam melting. The increase in oxygen content came about partly from the rapid loss of yttrium and partly from oxygen pickup, probably resulting from degassing of the furnace and from the small amount of oxygen that constantly leaked into the furnace. These data do not point to the occurrence of sacrificial deoxidation of yttrium.

The carbon content of yttrium decreased initially from 545 to 220 ppm during electron beam melting at 1770°C but, on continued melting, increased to a maximum

TABLE 5.4
Purification of Yttrium by Electron Beam Melting

Temperature (°C)	Duration of Melt (min)	Weight Loss (%)	Analysis (ppm)									
			Al	Cu	C	Fe	H	Mg	Mn	N	O	Si
Start material			50	40	545	100	50	420	36	178	5860	100
1730	20	6.2	50	30	310	90	<0.5	<5	<5	220	8000	50
1730	120	24.4	50	5	440	<50	<0.5	<5	<5	240	10,000	60
1745	20	10.0	30	30	230	90	<0.5	<5	<5	170	7500	80
1745	120	28.1	10	5	440	50	<0.5	<5	<5	210	12,000	90
1760	20	11.1	30	30	240	90	<0.5	<5	<5	190	6000	50
1760	120	37.3	10	5	470	<50	<0.5	8	<5	250	11,000	80
1770	20	10.3	30	30	220	90	<0.5	<5	<5	210	5500	50
1770	120	37.5	10	5	510	<50	<0.5	<5	<5	240	12,000	60

Source: Anable, W.E. and Beall, R.A., Electron beam melting of yttrium, U.S. Bureau of Mines Report of Investigations 6661, US Department of the Interior, Washington, DC, 1965.

Note: The nickel and zirconium content remained constant at 100 and 3000 ppm, respectively.

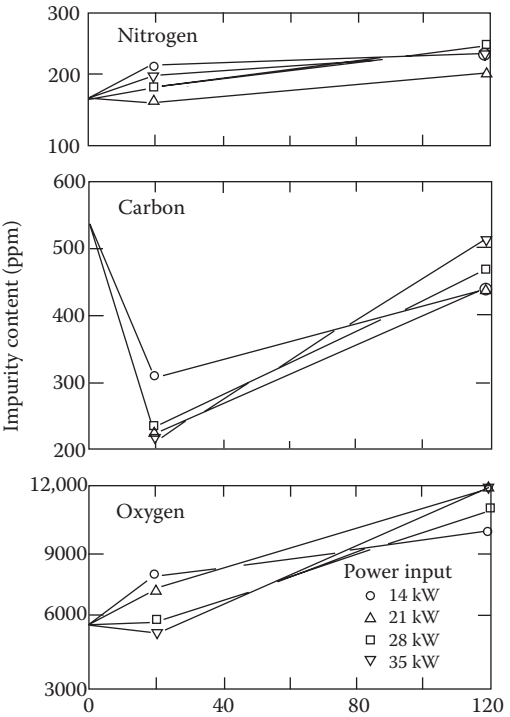


FIGURE 5.5 Oxygen, carbon, and nitrogen contents in electron beam–melted yttrium. (From Anable, W.E. and Beall, R.A., Electron beam melting of yttrium, U.S. Bureau of Mines Report of Investigations 6661, U.S. Department of the Interior, Washington, DC, 1965.)

of 510 ppm. This trend points to the possible occurrence of carbon deoxidation in the initial stages of melting. Specific experiments by Anable and Beall (1965), where the duration of melting was up to 5 min (Table 5.5) and samples were analyzed every minute suggested the possibility of a carbon deoxidation in the early phase of the operation: the carbon level came down from 545 to 330 ppm in the first minute, and the oxygen content decreased from 5860 to 4950 ppm during this period. A minimum level of oxygen was attained when yttrium was held molten for 1 min. Interestingly, the oxygen content of yttrium during the first 5 min of melting was lower than any value observed between 20 and 120 min. In contrast, the lowest carbon values were consistently obtained after 20 min rather than after 1–5 min. Anable and Beall (1965) concluded that a carbon reduction of oxygen was not involved, because the oxygen loss is an order of magnitude greater than the carbon loss and the oxygen loss occurred considerably earlier in the operation. It must be noted, however, that the only way carbon can be removed at ~1750°C in vacuum from the yttrium considered here is by forming CO. Secondly, carbon deoxidation need not occur exclusively and thus can result in the removal of only a part of the oxygen. The other part of the oxygen removed may be accounted for by loss occurring due to

TABLE 5.5
Behavior of Carbon, Oxygen, and Nitrogen during Electron Beam Melting of Yttrium

Temperature (°C)	Duration of Melt (min)	Weight Loss (%)	Analysis (ppm)		
			Carbon	Nitrogen	Oxygen
Start material			545	178	5860
1745	1	7.5	330	190	4950
1745	2	4.0	330	290	5200
1745	3	5.5	350	180	5150
1745	4	6.2	380	270	5100
1745	5	6.5	430	300	5300

Source: Anable, W.E. and Beall, R.A., Electron beam melting of yttrium, U.S. Bureau of Mines Report of Investigations 6661, US Department of the Interior, Washington, DC, 1965.

suboxide, YO, vaporizing. The possibility of CO and YO vaporizing from the alloy cannot be ruled out. A mass spectrometric work, similar to the one carried out by Anable (1970) for vanadium, could possibly clarify the picture.

The nitrogen content of yttrium remained nearly constant during electron beam melting. Some of the samples showed higher nitrogen content than the original metal. These observations are consistent with the expected behavior of no degassing of nitrogen from yttrium during pyrovacuum treatment. The increased nitrogen content may have the same explanation as the increased oxygen content observed in the sample, on a minor scale.

Having concluded that yttrium does not undergo sacrificial deoxidation during electron beam melting, Anable and Beall (1965) attempted doping of oxygen-contaminated yttrium with a small amount of a second metal or compound, so that a volatile compound that could be removed by evaporation might form. They investigated as many as 17 metallic additives and 3 compounds in addition to carbon. Among the metals investigated, titanium and zirconium are known to form volatile suboxides that can be used for refining refractory metals (Garg and Sundaram 1975). Carbon and silicon are already the well-known deoxidizing agents in pyrovacuum treatments. Electron beam melting of doped yttrium was carried out at 1745°C, and the metal was held molten for 5 min. The results of doping experiments did not show any decrease in oxygen content. Apparently, yttrium did not deoxidize by the sacrificial mode, nor did it undergo carbon or silicon deoxidation. Other pyrovacuum deoxidants like titanium and zirconium also failed with yttrium. Electron beam melting of yttrium decreased the residual fluorine content. The fall in fluorine content in yttrium from 0.06% to 0.002% was attributed to the evaporation of volatile oxyfluorides during electron beam melting (Carlson et al. 1960).

Electron beam melting has also been used for the purification of electrorefined gadolinium (Nagai et al. 1978; Zwilling and Gschneidner 1978). On electron beam

melting, the fluorine content decreased from about 0.2% to less than 10 ppm. The hydrogen content also decreased to low levels.

The removal of Ca, Mg, and fluorine has not been a serious problem in these metals, and it is achieved by pyrovacuum treatment by induction melting or electron beam melting. The real challenge is posed by oxygen in these metals. In yttrium and gadolinium, the oxygen content is not significantly decreased by induction or electron beam melting.

In the same manner as in the first group of metals (La, Ce, Pr, and Nd) discussed, the use of a tantalum crucible in vacuum melting at ~1800°C leads to the dissolution of a certain amount of tantalum in the metals Y, Gd, Tb, and Lu. Unlike in the four light rare earths, however, the tantalum solubility in Y, Gd, Tb, and Lu does not decrease much on lowering the temperature to the melting point, and therefore, the tantalum in the solution does not precipitate out. The only pyrovacuum way to remove tantalum is by distilling off the rare-earth metals, leaving tantalum in the residue. However, under certain circumstances, distillation can be avoided. If tungsten crucibles were used instead of tantalum in reduction and vacuum melting, tungsten would dissolve in the rare earth. But after vacuum melting in these metals, tungsten could be precipitated out in exactly the same way as Ta was allowed to settle in La, Ce, Pr and Nd. This alternative is available if the 0.012 at.% W that would persist in the Gd after precipitation can be tolerated. Similarly, at the end of precipitation, 0.03 at.% W will remain in Tb and 0.07 at.% W in yttrium (Dennison et al. 1966a; Beaudry and Gschneidner 1978).

The distillation of Y, Gd, Tb, and Lu was carried out at Ames in tungsten crucibles because refluxing of some of the distilled metals eroded the tantalum crucibles, causing them to leak. A tungsten-lined condenser was used since tantalum diffuses into the hot condensate more readily than tungsten. The distillation unit at Ames (Spedding et al. 1970; Beaudry and Gschneidner 1978) is shown in Figure 5.6. The distillation column was prepared from 0.76 mm tantalum and measured 125 mm in length and 40 mm in diameter. The condensers were prepared from 0.127 mm tantalum and were lined, leaving the lid, with 0.025 mm tungsten foil. The furnace used for distillation was a split-tube tantalum resistance furnace 175 mm long and 65 mm in diameter. The heater was made from 0.05 mm tantalum and was surrounded by five cylindrical radiation shields spaced approximately 6 mm apart. The sublimation column was suspended inside the heater by flaring the mouth of the column and dropping it through a tight-fitting hole in the top radiation shielding.

The reactor chamber housing the furnace system was a stainless steel ball jar, which was double walled for water cooling and had a quartz sight glass for optical temperature measurement. The vacuum system for this chamber consisted of a 400 L/s ion pump and a 4000 L/s titanium sublimator pump, and these pumps evacuated the system to 1.3×10^{-6} to 1.3×10^{-7} Pa after it was initially evacuated to <0.6 Pa with a 425 L/min forepump.

The details of pyrovacuum treatment, such as (1) temperature of vacuum melting and distillation, (2) impurities that usually remained, (3) temperature of the condenser, (4) typical size of the run, and (5) distillation rate, are all summarized in Table 5.6 (Beaudry and Gschneidner 1978). The distillation rate was quite slow (~1 g/h), and in a week, only 168 g of metal was purified. However, a slow rate of

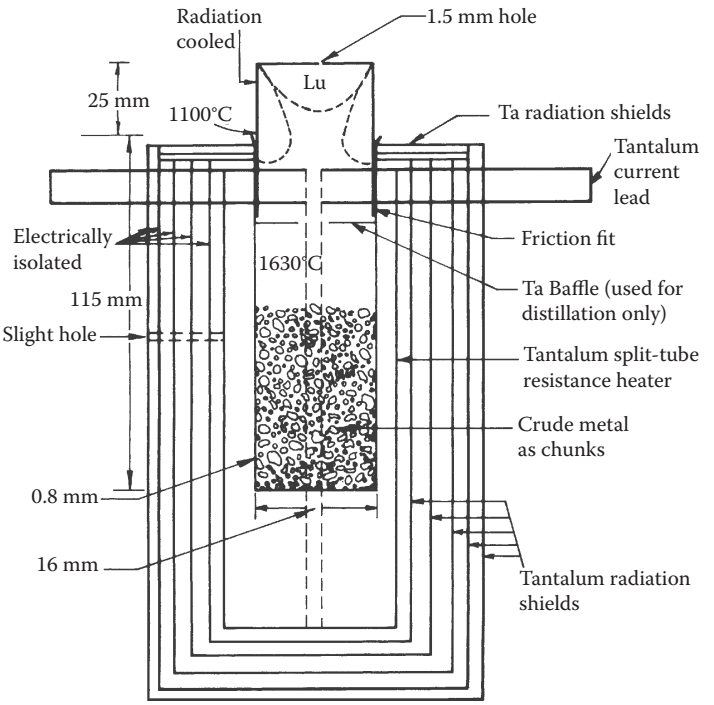


FIGURE 5.6 Tantalum split resistance furnace used in 1.3×10^{-6} Pa vacuum system to sublime rare-earth metals. The temperatures shown are typical for lutetium sublimation. (From Spedding, F.H. et al., The preparation and properties of ultrapure metals. In Les Elements Des Terres Rares 1, p. 25, Centre National de la Recherche Scientifique, Paris. Also R&D Report IS-2283, Ames Laboratory, USAEC, May 1970.)

distillation helped minimize the impurity transfer from the crucible to the distillate. In commercial practices, a much higher distillation rate was used. The vacuum required in the distillation assembly was better than 1.3×10^{-6} Pa so that contamination of the distillate was prevented.

The oxygen contents of Y, Gd, and Tb were not decreased even by distillation. This has been reasoned by Spedding et al. (1968) as due to the codistillation of the volatile oxides YO, GdO, and TbO. The vapor pressure of these volatile oxides is high enough in the rare-earth matrix that they distill along with the metals. According to Spedding et al. (1968), for each metal at a given temperature of distillation, a constant boiling mixture is apparently reached where the two species, metal and suboxide, come over in the same ratio and repeated distillations lead to very little improvement. This points to the possibility that the R value of the sacrificial deoxidation is 1 for these metals. In this situation, volatile metal suboxides vaporize, but there will be no decrease in the oxygen content.

Among all the rare-earth metals, yttrium is especially troublesome with oxygen impurity (Spedding et al. 1968). It is the most difficult element from the standpoint that under similar conditions of preparation, the oxygen content of the final metal is likely to

TABLE 5.6
Preparation Method and Major Impurities in Yttrium, Gadolinium, Terbium, and Lutetium

Process Conditions	Yttrium	Gadolinium	Terbium	Lutetium
		Vacuum Melting		
Temperature, °C	1850	1800	1750	1800
Vacuum, Pa	1.3×10^{-4}	1.3×10^{-4}	1.3×10^{-4}	1.3×10^{-4}
		Vacuum Distillation		
Crucible temperature, °C	1725	1725	1575	1645
Condenser temperature, °C	900	900	800	850
Vacuum, Pa	1.3×10^{-6}	1.3×10^{-6}	1.3×10^{-6}	1.3×10^{-6}
Distillation rate, g/h	1	1.5	1.5	1
Run size, g	150	250	225	250
		Major Impurities		
		Content (ppm)		
Impurity	**Yttrium**	**Gadolinium**	**Terbium**	**Lutetium**
C	20	18	10	16
O	58	48	67	100
N	3	1	8	4
H	4	2	6	3
F	<3	<3	<3	<3
Ca	0.5	<0.5	0.1	<0.1
Pt	<0.1	<0.1	<0.1	<0.2
Ta	2	4	14	<3
W	24	<0.4	7	<24

Source: Beaudry, B.J. and Gschneidner, K.A. Jr., Preparation and basic properties of rare earth metals, in Gschneidner, K.A. Jr. and Eyring, L. (eds.), *Handbook on the Physics and Chemistry of Rare Earths*, vol. 1, North Holland, Amsterdam, 1978.

Note: Method: Ames process. Calciothermic reduction of rare-earth trifluoride in a tantalum crucible. As-reduced metal was purified by vacuum melting in a tantalum crucible, and the tantalum ingested into the metal was removed by a vacuum distillation step. For vacuum distillation of yttrium, gadolinium, and terbium, tungsten crucibles and tungsten-lined tantalum condensers were used, whereas for lutetium, which could be purified by vacuum sublimation, a tantalum crucible and tungsten-lined condenser were used. Pure metal was collected as the condensate. Tantalum impurity remained in the residue. The entire process was carried out in a protected atmosphere of purified inert gas or under high vacuum as appropriate.

run the highest of all the rare earths or even rare earth–like elements. This is supported by the results of the thermodynamic investigations mentioned earlier for the Y–O solid solution (Okabe et al. 1996, 1998). The only way out seems to be in preparing the original metal with as little oxygen as possible by starting with very pure raw materials and by taking great pains to carry out all operations in a highly purified inert atmosphere.

5.5.3 Scandium, Dysprosium, Holmium, Erbium, and Lutetium

These metals have appreciable vapor pressure at their melting points. The vacuum melting, therefore, had to be relatively brief, or much of the metal would be lost by distillation. The temperature and duration of vacuum melting normally practiced (Beaudry and Gschneidner 1978) are listed in Table 5.7.

Fluorine impurity, which was removed relatively easily in the two groups of rare-earth metals described earlier, was particularly difficult to remove from this group of metals.

When these metals were vacuum melted for the length of time given (time necessary for quantitative removal of the fluorine impurity), there was substantial metal loss by vaporization, 30% for Sc and Dy, 20% for Ho, and 10% for Er. The evaporated metal and the volatilized impurities were, however, collected in a Ta cylinder placed above the crucible to facilitate easy recovery of the metal. The duration of vacuum melting could be shortened and, hence, metal loss decreased if several-hundred-ppm impurities can be tolerated in the final product.

The removal of fluorine from Dy, Ho, and Er was also investigated by Croat (1969). A single batch of 1070 g of as-reduced Dy was vacuum melted at approximately 1450°C for 5 min. In the process, 345 g (approximately 30%) of the metal distilled out of the crucible but was collected. This distillate contained 6500 ppm fluorine and 3000 ppm Ca. The remaining undistilled metal was found to contain 119 ppm fluorine and 20 ppm Ca. Similar results were obtained for Er. During vacuum melting, 20% of the metal was removed. The distillate contained 1300 ppm fluorine, and the melt had only 32 ppm.

The other part of pyrovacuum treatment in the refining of Sc, Dy, Ho, and Er is sublimation. The high volatility of these metals is an advantage here, and purification of metals by sublimation is comparatively easy. Tantalum introduced in the metals during the vacuum-melting step was removed by subliming off the metal. The common interstitial impurities N, C, and O formed stable compounds and remained in the residue when these metals were sublimed at a slow rate. Because this operation was so effective, the great care taken to remove oxygen from fluoride and to prevent the introduction of it and other interstitial impurities in the first two groups of metals was not necessary here. Sc, Dy, Ho, and Er metals were purified with respect to these three interstitial impurities during the sublimation step. The major problem on purification of these metals by sublimation is the carryover of fluorine impurity into the condensate. If any fluorides are present, either dissolved in the metal or in the slag trapped in the metal or even attached to the surface, the fluorides distill along with the metal, and these metals were analyzed as high in fluoride contamination (Spedding et al. 1968). The solution to this problem is either preparing the metals fairly free from fluoride impurities or following a reduction process, such as the vapor-phase rare-earth-chloride reduction technique (Croat 1969).

Croat (1969) has compared the purity of Dy, Ho, and Er obtained by the chloride process as well as by the fluoride process. He stated that in terms of metal purity, the as-reduced Dy, Ho, and Er from the chloride process are better because the low temperature (900°C) of reduction results in quite low (<30 ppm) tantalum pickup.

TABLE 5.7
Preparation Method and Major Impurities in Scandium, Dysprosium, Holmium, and Erbium

Process Conditions	Scandium	Dysprosium	Holmium	Erbium
		Vacuum Melting		
Temperature, °C	1550	1440	1480	1540
Time, min	10	45	45	30
		Vacuum Sublimation		
Crucible temperature, °C	1425	1175	1220	1300
Condenser temperature, °C	900	700	725	825
Sublimation rate, g/h	1	2.5	2.1	2.1
Run size, g	100	1000	600	1000
		Major Impurities		
		Content (ppm)		
Impurity	**Scandium**	**Dysprosium**	**Holmium**	**Erbium**
C	15	8	4	11
O	95	39	30	22
N	8	1	3	1
H	8	6	4	1
F	8	14	6	5
Ca	0.5	<1	0.5	<0.1
Pt	<0.2	<0.3	<0.1	<0.5
Ta	2	25	<0.8	7
W	77	<1	1	9

Source: Beaudry, B.J. and Gschneidner, K.A. Jr., Preparation and basic properties of rare earth metals, in Gschneidner, K.A. Jr. and Eyring, L. (eds.), *Handbook on the Physics and Chemistry of Rare Earths*, vol. 1, North Holland, Amsterdam, 1978.

Note: Method: Ames process. Calciothermic reduction of rare-earth trifluoride in a tantalum crucible. As-reduced metal was purified by vacuum melting in a tantalum crucible, and the tantalum ingested into the metal was removed by a vacuum distillation step. Tantalum crucibles and tantalum condensers were used. Pure metal was collected as the condensate. Tantalum impurity remained in the residue. The entire process was carried out in a protected atmosphere of purified inert gas or under high vacuum as appropriate.

This may be compared with 0.1–0.2% Ta in the as-fluoride-reduced metal. Also, the chloride process eliminates F as an impurity without at the same time introducing characteristic impurities such as Cl and Li. Comparing Dy, Ho, and Er prepared from both chloride and fluoride methods and sublimed under the same conditions, Croat (1969) concluded that the metals were identical in purity with the exception of 25–75 ppm F in the metal prepared from the fluoride. The analysis data of Beaudry

and Gschneidner (1978) show that the fluorine content, even in the fluoride-reduced and sublimed metal, is only 10 ppm or less (Table 5.7). The sublimation temperatures given in the table are about 100°C lower than the temperatures used by Croat (1969), and the sublimation rates in the table are also only one-fifth of the rate used by Croat (1969).

Lutetium had been purified by distillation as well as by sublimation (Spedding et al. 1968). When distillation was carried out at 1850°C in tantalum crucibles, tantalum dissolved in the refluxing liquid lutetium, and the liquid metal often eroded a hole through the tantalum crucible. At such high temperatures, oxygen also apparently distilled along with lutetium. Sublimation of lutetium at a temperature slightly below its melting point seemed the better alternative. However, the use of a tungsten crucible and tungsten-lined condenser enabled distillation of lutetium without extensive crucible attack (Beaudry and Gschneidner 1978).

5.5.4 Samarium, Europium, Thulium, and Ytterbium

These four metals are prepared by the lanthanothermic or reduction–distillation method. Tantalum is not the major impurity with the metals Sm, Eu, Tm, and Yb, because they do not undergo the high-temperature vacuum-melting step. The reduced–distilled metals usually contain several hundred ppm La in addition to O and H. These impurities are removed by sublimation. The details of this sublimation and the levels to which the impurities are removed are given in Table 5.8 (Beaudry and Gschneidner 1978).

The sublimation is carried out in the same crucible in which the reduction–distillation is done. A tantalum optical baffle arrangement is provided in the condenser during reduction–distillation to prevent excessive entrainment of oxide particles. The baffles are removed, and the crucible is leached with acid and then vacuum degassed at 1800°C to remove any volatile impurities before carrying out the low-temperature sublimation.

The metals in the as-sublimed condition are composed of many small crystals and possess a large surface area. They are then prone to react with air and pick up impurities. The metal crystals are therefore consolidated as soon as possible. One method is to seal them in a tantalum crucible in an inert gas welder and then heat the crucible in a vacuum to above the melting point of the metal. The high reactivity of europium necessitates that the as-sublimed metal be handled under an inert atmosphere. Hydrogen remains as an impurity in the as-sublimed metal. This can be removed quantitatively in the consolidation step by holding the temperature above the metals' melting point for 24 h in a dynamic vacuum. Hydrogen diffuses through the tantalum and is pumped away.

5.5.4.1 Purification of Europium by Distillation

Busch et al. (1971) carried out the purification of europium by UHV distillation of the commercial metal in a simple quartz apparatus. The europium was obtained in such purity that would exceed the levels attained by the Ames group later (Beaudry and Gschneidner 1978).

TABLE 5.8
Preparation Method and Major Impurities in Samarium, Europium, Thulium, and Ytterbium

Process Conditions	Samarium	Europium	Thulium	Ytterbium
		Vacuum Melting		
Temperature, °C	1600	1400	1600	1400
Total time, min	4	4	4	4
		Vacuum Sublimation		
Crucible temperature, °C	800	700	950	625
Condenser temperature, °C	500	400	550	350
Sublimation rate, g/h	3	3	3	4
Run size, g	1000	500	500	800
		Major Impurities		
		Content (ppm)		
Impurity	**Samarium**	**Europium**	**Thulium**	**Ytterbium**
C	6	100	14	10
O	33	70	8	38
N	20	Not detected	<1	9
H	4	13	9	4
Ca	2	10	0.2	<13
La	3	1	5	4
Ta	30	<0.6	<1	<1
W	<2	<3	<3	<1

Source: Beaudry, B.J. and Gschneidner, K.A. Jr., Preparation and basic properties of rare earth metals, in Gschneidner, K.A. Jr. and Eyring, L. (eds.), *Handbook on the Physics and Chemistry of Rare Earths*, vol. 1, North Holland, Amsterdam, 1978.

Note: Method: Ames process: Direct reduction or reduction–distillation. Lanthanothermic reduction of rare-earth oxide in a tantalum crucible–tantalum condenser assembly. As-reduced metal distills off simultaneously and collects in the condenser. The condensate was purified with respect to major impurities—lanthanum, oxygen, and hydrogen—by vacuum sublimation in a tantalum crucible. The entire process was carried out in a protected atmosphere of purified inert gas or under high vacuum as appropriate.

Busch et al. (1971) attempted to replicate the capabilities of a piece of elaborate equipment with large UHV pumps in a simpler system, by exploiting the gettering action of europium. Both degassing and distillation were carried out in a simple, homemade, quartz–Pyrex, UHV system using mercury pumps. The system could be evacuated down to a pressure of 10^{-7} Pa. Figure 5.7 shows two different distillation columns used by Busch et al. (1971). They were assembled from a molybdenum crucible, a Mo tube, and a baffle made from 0.10 mm Mo foil.

After loading the crucible with lumps of europium metal, assembling the system, and performing the mandatory baking and degassing procedures, the temperature of

the charge was raised to and kept at 1000°C, the distillation being completed in a few hours under 1.3×10^{-3} Pa. The distillate collected in the two upper baffles is shown in Figure 5.7a. Column b (Figure 5.7b) had no baffle. Following the same procedure as described above, the distillation was performed at 1000°C under 2.5×10^{-4} to 6.6×10^{-5} Pa. No condensation took place on the water-cooled lid. The europium atoms were reflected by the lid and condensed on the walls of the tube, which was cooled, as in the first experiment, from outside by a water curtain. They formed a soft metal foil, which could be easily detached eventually from the wall. Part of the metal that condensed on the walls lying within the HF coil did heat up due to coupling with the high-frequency power and became an excellent getter for the gases emerging from the crucible. This metal was not pure and adhered strongly to the quartz.

Busch et al. (1971) analyzed of the condensates in a spark-source mass spectrometer. The photographically detected mass spectra were evaluated by means of a densitometer. The results are summarized in Table 5.9. The high concentration of impurities in the commercial europium is clearly eliminated in the process. Europium condensed at a higher temperature (B1) is purer. Calcium, on account of its almost identical melting point (Eu, 826°C; Ca, 848°C) and similar boiling point (Eu, 1439°C; Ca, 1240°C), ends up in the condensate, but the content is least in the high-temperature condensate. The calcium concentration on the lid (B2) was 92 ppm, and in the baffle (B1), it was only 6 ppm. Busch et al. (1971) concluded that

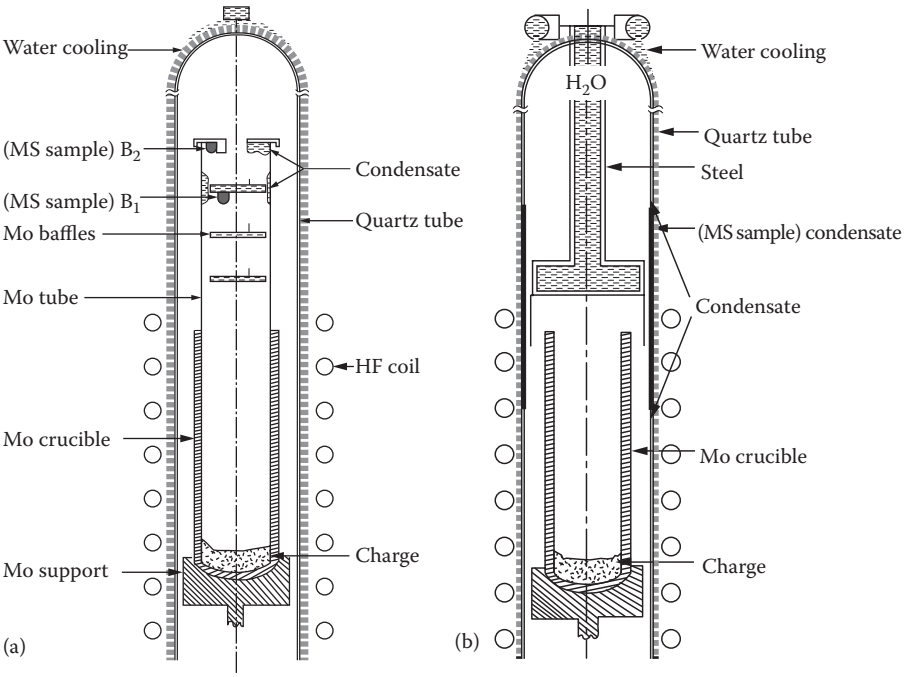


FIGURE 5.7 Apparatus for the UHV distillation of europium. (a and b) Different column designs. (From Busch, G. et al., *J. Less Common Metals*, 24: 456–457, 1971.)

TABLE 5.9
Purification of Europium by Distillation

				Purified Europium		
Impurity	**Commercial Europium**			**B1**	**B2**	**C**
C	105	19	300	2.2	8.9	4.2
O	1700	48	300	5.6	27	8
N	6.3	1.3	100	0.2	0.5	0.5
H	8000	nd	300	140	nd	nd
Ca	80	3.6	30	5.9	92	50

Source: Busch, G. et al., *J. Less Common Metals*, 24, 1971.
Note: nd, not detected.

distillation of commercial europium with a simple column such as that shown in Figure 5.7 can produce high-purity europium containing only H, C, O, Ca, and Ba in concentrations greater than 1 ppm.

While the pyrovacuum treatments of vacuum melting and vacuum distillation/sublimation have been the most important methods of as-reduced metal refining, several other methods have been explored for this purification. Electrorefining in a fused salt is one among these methods. This method has been applied particularly to yttrium and gadolinium.

5.6 ELECTROREFINING

Electrorefining as a process for rare-earth-metal purification has been applied for the purification of yttrium and gadolinium. These are the two metals that are most difficult to obtain in pure form by the exclusive pyrometallurgy route unless great pains are taken to choose very pure materials and carry out all operations in a highly purified inert atmosphere. With gadolinium, there is the additional problem of removing dissolved tantalum. Gadolinium has both a low melting point and a low vapor pressure. There is a good amount of refluxing during the distillation process, and this causes considerable attack on the W or Ta crucible used (Beaudry and Gschneidner 1978).

5.6.1 Yttrium

Electrorefining of yttrium was investigated by Merrill and Wong (1967) at the Reno Metallurgy Center of the US Bureau of Mines. The starting material was an ingot of yttrium containing about 0.57% oxygen, 2.25% zirconium, 0.08% tantalum, and several hundred ppm each of carbon, nitrogen, and many other metallic impurities. They used a LiCl–YCl_3 electrolyte at 710°C. Adhering electrolyte salt was removed from the electrodeposited metal by vacuum distillation. In their study, the affinity of yttrium for oxygen was given major consideration, and emphasis was placed on

selecting equipment and a procedure that would minimize the contact of the product with air and moisture.

The apparatus shown schematically in Figure 5.8 was used by Merrill and Wong (1967). This system permitted electrorefining and vacuum distillation of the product to be performed under an inert gas, thus minimizing atmosphere contamination. In the cell, a 12-mm-diameter mild steel rod was used as the cathode, and the anode was the electrolyte chamber with crude yttrium charged in the bottom. The

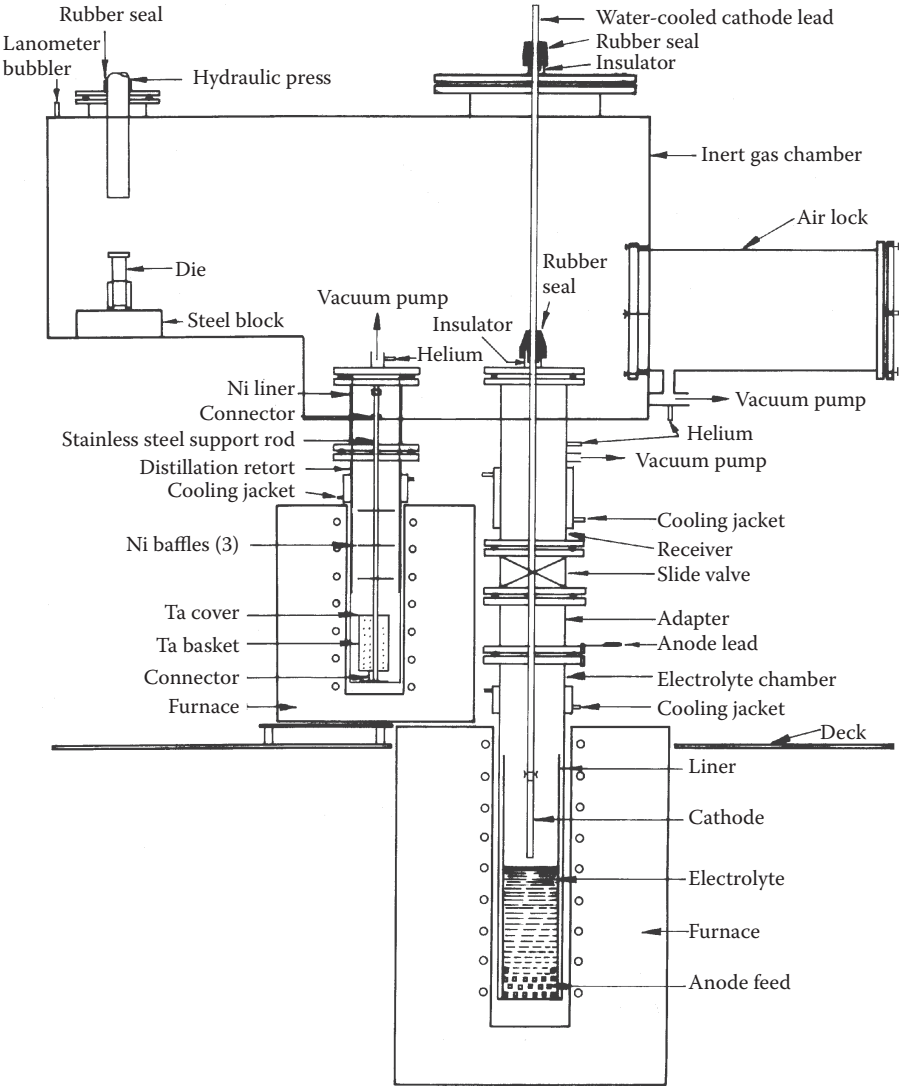


FIGURE 5.8 Schematic of the electrorefining apparatus. (From Merrill, C.C. and Wong, M.M., Electrorefining yttrium, U.S. Bureau of Mines Report of Investigations 7018, U.S. Department of the Interior, Washington, DC, 1967.)

distillation retort, 75 mm in diameter and 430 mm long, was made of mild steel and had a nickel liner. The charge was contained in a tantalum basket.

At the start of the electrolysis, approximately 1200 g of freshly cut pieces of yttrium metal (50 × 50 × 25 mm) were loaded in the chamber and degassed. Then 1600 g of LiCl was also charged. After evacuating and backfilling with helium, the cell was heated to 710°C. The YCl_3 component in the electrolyte was made *in situ* by reacting HCl gas with yttrium metal, using an *in situ* chlorination apparatus. After the desired concentration of YCl_3 in the electrolyte was attained, chlorination was stopped, the cathode was installed, and electrolysis was started. Details of the electrolysis and analysis of the product obtained are listed in Table 5.10.

At the end of each deposition cycle, the cathode deposit was lifted above the electrolyte, allowed to drain, sealed in the receiver, and cooled to room temperature. The deposit was then stripped from the cathode, loaded into a tantalum basket, and sealed in the distillation retort. Distillation of the salt from the cathode deposit was carried out at 880°C for 3 h with a final pressure of less than 1.3 Pa. The salt condensed in a ring inside the liner at a level slightly below the external cooling jacket. There was a facility to compact the product metal by a press inside the inert gas chamber before it was sealed in a bottle prior to removal from the chamber.

The results given in Table 5.10 indicate that the electrolysis was effective in lowering all metallic impurities but not the interstitial elements. The nitrogen content in the refined metal was higher than that of the anode feed even though the oxygen content was appreciably lower. Above 5.4 mol.% YCl_3 in the electrolyte, the oxygen content in the electrorefined metal increased sharply (to values much more than that in the anode feed) with an increase in the proportion of YCl_3 in the electrolyte. For example, when the YCl_3 content was 13.4 mol.%, the oxygen content of the electrorefined metal was approximately 13,000 ppm, whereas it was only about 5700 ppm in the anode feed. However, an increase in the YCl_3 concentration in electrolyte did not markedly affect the metallic impurity levels. Cathode current efficiency was excellent, always above 90%, and in some tests, it was 100%. No noticeable effect of the impurity content of the electrorefined metal was observed with variation in initial cathode current density.

The efforts on electrorefining of yttrium were continued at Reno, with Fleck et al. (1973) using selected low-melting yttrium base alloys as anodes in addition to crude yttrium. Electrolysis in electrolytes other than LiCl–YCl_3 was also tried to possibly achieve the difficult refining with respect to oxygen.

The electrorefining apparatus used by Fleck et al. (1973) is shown in Figure 5.9. All the experiments were conducted in a helium atmosphere. The electrolyte consisted of LiCl and YCl_3. A variety of yttrium-containing materials were used as anodes. They are listed in Table 5.11.

The results demonstrated that the process causes a substantial decrease in the levels of metallic impurities in the cathode deposit when anodes of yttrium alloys with iron, nickel, and manganese were used. Yttrium–copper and yttrium–magnesium, however, were not satisfactorily electrorefined, because the copper and magnesium transferred to the cathode products in appreciable quantities. No refining with respect

TABLE 5.10
Fused-Salt Electrorefining of Yttrium

Electrolysis Parameters	
Electrolyte composition, %	(1) 1.7 YCl_3 – 98.3 LiCl, (2) 5.4 YCl_3 – 94.6 LiCl
Temperature, °C	710
Cathode	12.5-mm-diameter mild steel rod
Anode	Crude yttrium
Container	Mild steel
Cell	Mild steel
Voltage, V	(1) 0.35, (2) 0.67
Current, A	(1) 5, (2) 20
Initial cathode current density, A/cm	(1) 0.44, (2) 1.76
Cathode current efficiency, %	(1) 99, (2) 98
Weight of metal deposited, g	(1) 32.9, (2) 32.6

	Analysis (ppm)		
Impurity	**Anode Feed**	**Electrorefined Metal (1)**	**Electrorefined Metal (2)**
Al	60	25	bl
C	135	40	10
Ca	250	<10	10
Cl	nr	1800	2100
Cu	55	15	<10
Fe	360	25	35
Li	<10	25	100
N	140	240	200
Ni	210	<10	bl
O	5750	2400	3400
Si	110	<45	130
Ta	800	<300	<300
Ti	460	<250	<250
Zr	22,500	<250	<250

Source: Merrill, C.C. and Wong, M.M., Electrorefining yttrium, U.S. Bureau of Mines Report of Investigations 7018, US Department of the Interior, Washington, DC, 1967.

Note: bl, below detection level; nr, not reported.

to oxygen occurred in electrolysis conducted using LiCl–YCl_3. Fleck et al. (1973) also evaluated electrolytes composed of bromides and fluorides, and the results are summarized in Table 5.12. In these systems, the refining of the metallic impurities was the same as that achieved in the LiCl–YCl_3 melt. There is very little, if any, refining with respect to oxygen in the NaBr–KBr–YBr_3 melt. The oxygen content was significantly reduced when yttrium was electrorefined in a LiF–YF_3 or LiCl–LiF–YF_3 system. The main problem, however, in most of these electrolytes was that it was impossible to completely remove the adhering salts from the metal crystals in the cathode deposit.

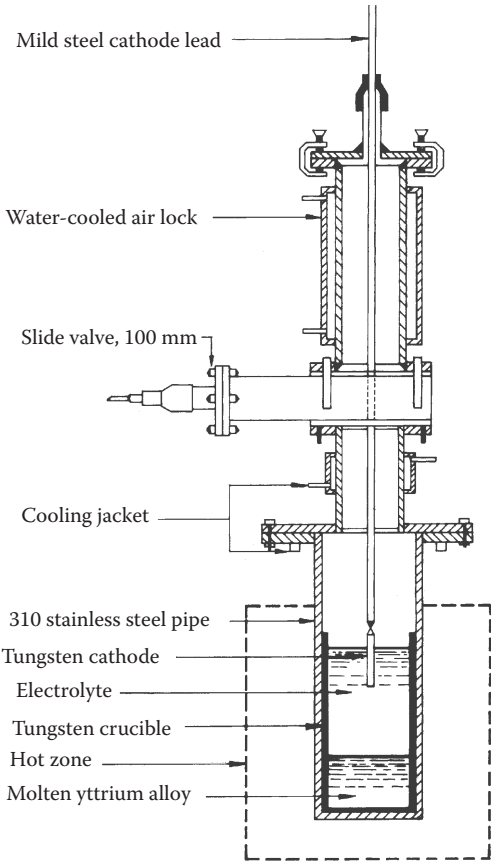


FIGURE 5.9 Electrorefining apparatus. (From Fleck, D.C. et al., Purification of yttrium by electrorefining, U.S. Bureau of Mines Report of Investigations 7710, U.S. Department of the Interior, Washington, DC, 1973.)

5.6.2 Gadolinium

The purification of crude gadolinium by fused-salt electrorefining was investigated by Nagai et al. (1978) and also by Bratland and Gschneidner (1980).

Nagai et al. (1978) used a fluoride–chloride electrolyte composed of 77.6% LiCl, 11.2% LiF, and 11.2% GdF_3. The function of LiF was primarily to increase conductivity and also to lower the melting temperature of GdF_3 (GdF_3–27% LiF melts at ~625°C). LiCl lowers the melting temperature of the mixture even further. The cathode was pure gadolinium, prepared from distilled gadolinium, in the form of a rod 1.6 mm diameter × 15 cm long. The anode, which was the impure gadolinium to be refined, was prepared from gadolinium made by the calcium reduction of untopped GdF_3 followed by vacuum melting. The anode was in the form of a cylinder 13 mm in diameter and 150 mm long.

TABLE 5.11
Fused-Salt Electrorefining of Yttrium—Metallic Element Transfer

Electrolysis Parameters

Electrolyte composition, wt.%: LiCl–(7 to 12)YCl_3
Temperature, 900–1000°C, 825 for 60Y–40Mg alloy
Cathode: 6-mm-diameter tungsten rod
Anode: Crude yttrium
Container: Tungsten crucible (75 mm in diameter and 150 mm in height)
Cell: United States Bureau of Mines (USBM) inert atmosphere electrorefining apparatus
Voltage, V: 0.35
Initial cathode current density, A/cm^2: 0.27

Result Summary: Analysis Values in ppm

	80Y–20Ni			80Y–20Fe			80Y–20Cu			60Y–40Mg		
Element	Anode	Initial Run	Final Run	Anode	Initial Run	Final Run	Anode	Initial Run	Final Run	Anode	Initial Run	Final Run
Al	70	22	<20	40	<20	<20	40	<15	15	60	<15	<15
Ca	<20	nd	nd	<20	nd	nd	<20	nd	nd	<20	nd	nd
Cr	150	<3	3	<3	<3	<3						
Co	<30	nd	nd	<30	nd	nd				30	50	nd
Cu	240	27	25	180	18	21	20%	7	2100	120	<20	<20
Fe	220	<15	<15	20%	<15	18	110	<20	<20	180	1800	1800
Mg	14	14	<10	<10	<10	<10	10	25	160	40%	1000	11%

(*Continued*)

TABLE 5.11 (CONTINUED)
Fused-Salt Electrorefining of Yttrium—Metallic Element Transfer

Result Summary: Analysis Values in ppm

	80Y–20Ni			80Y–20Fe			80Y–20Cu			60Y–40Mg		
		Initial	Final		Initial	Final		Initial	Final		Initial	Final
Element	Anode	Run	Run	Anode	Run	Run	Anode	Run	Run	Anode	Run	Run
Mn	740	<6	21	120	<6	<6	120	<10	15	200	160	400
Mo	30	<7	<7	30	<7	<7	35	nd	nd	20	10	10
Ni	20%	<10	20	1200	<10	<10	1200	nd	500	900	nd	nd
Si	120	<45	<45	50	<45	<45	50	<10	<10	50	<20	<20
CCE, %		98	69		99	70		88	65		68	13
Y yield, %		95			70			80			nr	

Source: Fleck, D.C. et al., Purification of yttrium by electrorefining, U.S. Bureau of Mines Report of Investigations 7710, US Department of the Interior, Washington, DC, 1973.

Note: CCE, cathode current efficiency; nd, not detected; nr, not reported.

TABLE 5.12
Deoxidation in the Electrorefining of Yttrium

Electrolyte Composition (%)	LiCl–(7 to 12) YCl_3	50.9KBr–29.3NaBr–19.8YBr_3	66YF_3–35LiF	70LiCl–14LiF–16YF_3
Temperature, °C	900–1000	750–800	825–925	725–825
Cathode current density, A/cm^2	0.027	0.027–0.32	0.027–0.11	0.027–0.11
Oxygen content in the anode material, %	0.4	0.4	0.4	0.4
Oxygen content in the cathode product, %	0.52	0.36	0.11	0.06

Source: Fleck, D.C. et al., Purification of yttrium by electrorefining, U.S. Bureau of Mines Report of Investigations 7710, US Department of the Interior, Washington, DC, 1973.

A tantalum crucible, 65 mm in diameter and 130 mm long, was used to contain the electrolyte. A schematic diagram of the apparatus used for electrolysis is given in Figure 5.10. The 88-mm-diameter and 600-mm-long stainless steel tube in which electrolysis was carried out was lined with tantalum to prevent attack by the LiCl and LiF vapors from the electrolyte. After electrolysis, the cleaned cathode deposit was

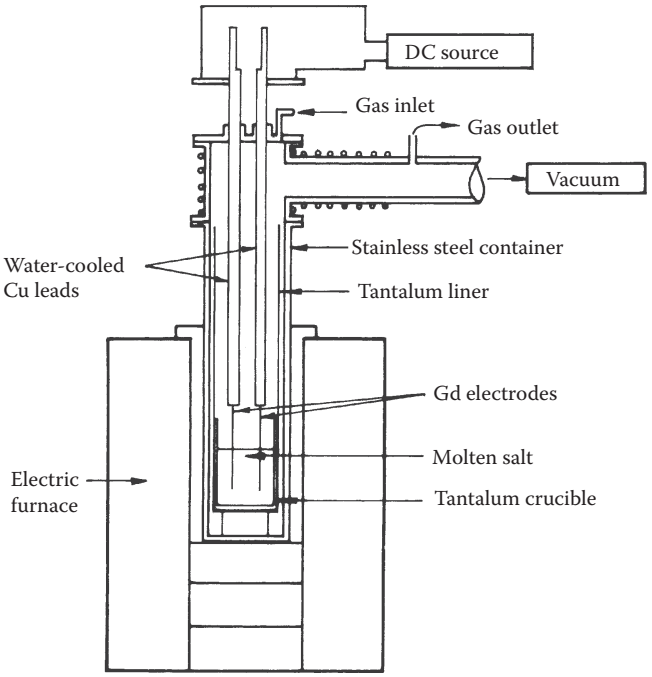


FIGURE 5.10 Schematic of the electrolysis system. (From Nagai, H. et al., *Metall. Mater. Trans.*, 9B: 25–28, 1978.)

heated in a vacuum induction furnace to 800°C and held for 30 min at 1.3×10^{-4} Pa to remove the adhering electrolyte. The crystals were then arc melted to consolidate them.

The details of electrolysis parameters and purity achieved by Nagai et al. (1978) are summarized in Table 5.13. The purest deposit of Gd was obtained when LiCl and LiF were purified by distillation. The H and F impurities were rather high in the as-arc-melted Gd. Electron beam melting removed both fluorine and hydrogen. The fluorine content in the deposit probably came from entrapment of fluoride salt from the electrolyte during the growth of the dendrites.

Gadolinium was electrorefined in an all-fluoride electrolyte by Bratland and Gschneidner (1980). The electrolysis cell was essentially the same as that used by Nagai et al. (1978), shown in Figure 5.10. The only difference was that a swing gate valve was mounted in the stainless steel container where the electrolysis cell was located. The advantage, like in the Reno cells, is that with the furnace still hot, the electrode could be removed from the system without admitting air to the hot part of the container, which was kept under an argon atmosphere at all times. A viewing glass was provided in the top lid to observe the cell.

The electrolyte consisted of 65 mol.% LiF and 35 mol.% GdF_3. Commercially available gadolinium metal was used as the starting material for electrowinning. A graphite crucible, with 90 mm inside diameter and 100 mm deep, was used to contain the 1.6 kg electrolyte.

TABLE 5.13
Fused-Salt Electrorefining of Gadolinium

Electrolysis Parameters

Electrolyte composition, %	77.6LiCl–11.2LiF–11.2GdF_3
Temperature, °C	700
Current, mA	600
Current density, A/cm^2	0.15
Current efficiency, %	70
Deposition rate, g/h	0.8

Analysis (ppm)

		Refined Metal		
Element	**Crude Metal**	**1**	**2**	**3**
O	490	85	180	180
N	89	43	87	98
H	3	60	95	8
F	200	1500	1500	7

Source: Nagai, H. et al., *Metall. Trans.*, 9B, 1978.

Note: (1) Arc-melted metal; electrolyte prepared from distilled LiCl, topped GdF_3, and distilled LiF. (2) Electrolyte prepared from distilled LiCl, topped GdF_3, and reagent-grade LiF. (3) Metal obtained by electron beam melting of the electrorefined metal in column 2.

The gadolinium to be electrorefined was made in the form of a rod and used as the anode. The cathode was a 6-mm-diameter tantalum rod. The electrolysis temperature was 900°C. These and other details of electrolysis are summarized in Table 5.14.

The electrolyte was not subjected to any special purification procedure before charging. It was, however, subjected to pre-electrolysis. The pre-electrolysis was carried out at a constant voltage of 2.7 V and a temperature of 900°C. This step was for removal of dissolved oxide and hydroxide. Bratland and Gschneidner (1980) found that in 2.5 h of electrolysis, a 90% decrease in the oxide concentration was achieved, and continued pre-electrolysis of the melt for 6 h decreased the terminal oxide concentration further. At this stage, the electrolyte was considered ready for electrorefining the gadolinium metal.

In the electrorefining experiments, two cathode arrangements were tried by Bratland and Gschneidner (1980). In one, the cathode was inserted 6 mm into the electrolyte for the entire run. In the second, the cathode barely touched the surface in the beginning of the experiment, and as the metal formed on the cathode, it was gradually pulled upward in increments of 5 mm for a total of 35 mm. This was primarily tried to improve the salt drainage of the cathode deposit, which is a problem in all molten-salt electrorefining where crystalline deposits are obtained.

TABLE 5.14
Purification of Gadolinium by Electrorefining with Pre-Electrolysis

Electrolysis Parameters	
Electrolyte composition, mol.%	65LiF–35GdF_3
Temperature, °C	900
Cathode	Pure gadolinium rod
Anode	Crude gadolinium
Container	Graphite crucible
Pre-electrolysis	
Voltage, V	2.7
Duration, h	8
Electrolysis	
Current, A	4
Duration, Ah	5
Cathode current density	
Current efficiency, %	84

	Analysis (ppm)		
Element	**Impure Anode**	**Stationary Cathode**	**Retractable Cathode**
O	1100	50	34
H	88	50	21
N	400	140	43
C	209	Not detected	253

Source: Bratland, D. and Gschneidner, K.A. Jr., *Acta Chemica Scandinavica*, A34, 1980.

The electrorefined gadolinium was consolidated by arc melting. The current efficiency, calculated on the basis of the amount of metal recovered after arc melting two times, was 69.2% and 84.0%, respectively, for the stationary cathode and the retracting cathode. Higher current efficiency in the latter case can be reasoned as due to the more efficient removal of the gadolinium deposit when only the tip of the cathode or metal was exposed to the bath. Besides, when the metal was exposed to the bath for a shorter time, redissolution of the metal was minimized. However, there was no improvement as far as salt drainage was concerned when the cathode was gradually pulled out of the bath.

In addition to higher current efficiency, the product obtained with the retractable cathode was purer, as shown in Table 5.14, indicating that the contaminations originate from the bath and/or the anode metal and not from the furnace atmosphere.

The oxygen content of the metal electrorefined with a retracted cathode was lower than any previously electrowon or electrorefined gadolinium metal. This implies that pre-electrolysis of the electrolyte was at least as effective as other methods of purification, such as treating molten gadolinium fluoride under a dynamic HF–60% Ar atmosphere. Between the two alternatives, pre-electrolysis appears more attractive because it can be performed *in situ*.

Bratland and Gschneidner (1980) observed that the oxygen contamination of the metal was reduced with decreasing oxide concentration in the bath. Electrolysis of an oxide-deficient melt, which probably still contained some oxide, yielded a minimum concentration of about 80 ppm oxygen. Zwilling and Gschneidner (1978) used purified lithium fluoride and gadolinium fluoride containing less than 20 ppm oxygen and, adding no oxide, electrolyzed the melt to obtain gadolinium dendrites that still contained a minimum of 40 ppm oxygen. Comparing these results with those obtained by Bratland and Gschneidner (1980) using pre-electrolysis indicated that pre-electrolysis was attractive not only because it was convenient but also because it was very effective in decreasing the oxygen content of the bath and, hence, in the electrorefined metal.

The carbon content of electrorefined gadolinium was more than that of the impure anode. The source was a graphite cell. A small immersed graphite anode might reduce the contamination and eliminate the need for a graphite cell. Zwilling and Gschneidner (1978), however, found that the carbon contamination of gadolinium electrorefined in a Ta crucible was lower (60–100 ppm) but still considered more. This resulted from carbon impurity in the lithium fluoride. It was apparently not true after all that the carbon anode was the principal source of carbon contamination in electrorefined gadolinium.

The nitrogen content of the gadolinium electrolyzed by the above procedure was more than what was normally found in gadolinium electrowon in a similar cell. It appeared that nitrogen was very effectively transferred through the electrolyte from anode to cathode. Hydrogen and oxygen were also transferred to the electrolyte by anodic dissolution. The a priori concentration of these elements as oxide and hydroxide impurities in the electrolyte, however, determined the hydrogen and oxygen contamination of the electrorefined metal.

In their experiments, Bratland and Gschneidner (1980) found that pre-electrolysis was at least as efficient as any other purification method known. While most of the

oxygen and hydrogen were removed, the last traces of oxygen and hydrogen were virtually impossible to remove. Besides yttrium and gadolinium, electrorefining was tried for cerium also. The experiments, mainly to see feasibility, were conducted at Reno by Shedd et al. (1964).

5.6.3 Cerium

The electrorefining of relatively impure cerium metal in a chloride electrolyte was demonstrated by Shedd et al. (1964) at Reno. The electrolysis parameters and results are summarized in Table 5.15. An electrolyte composed of 64% $BaCl_2$, 17% KCl, and 19% LiCl was melted in a graphite-lined 100-mm-diameter inert-atmosphere electrorefining cell. Cerium chloride was generated *in situ* in the electrolyte by chlorinating a cerium bar with HCl gas. When the electrolyte contained 1% $CeCl_3$, the chlorination was stopped, and the cerium bar was removed. A 5-mm-diameter tantalum cathode and a 12-mm-diameter cerium anode were inserted 75 mm into the bath. Electrorefining was conducted at 0.17 V and 2.5 A, and the operating temperature was 700°C (about 100° lower than the melting point of cerium). Very fine crystals of cerium were deposited on the cathode. This deposit and adhered salt were melted at 900°C under an inert atmosphere in a boron nitride crucible. After melting,

TABLE 5.15
Fused-Salt Electrorefining of Cerium

	Electrolysis Parameters
Electrolyte composition, wt.%	1 $CeCl_3$–63$BaCl_2$–17KCl–19LiCl
Temperature, °C	700
Cathode	5-mm-diameter tantalum rod
Anode	12-mm-diameter cerium rod
Cell	Graphite
Current, mA	2.5
Voltage, V	0.17

	Analysis (ppm)	
Impurity	**Before Refining**	**After Refining**
C	350	190
O	40	30
Si	30	50
Fe	340	40
Mo	600	80
Al	250	20
Total impurities	1610	410

Source: Shedd, E.S. et al., Continuous electrowinning of cerium metal from cerium oxides, Bureau of Mines Report of Investigations 6362, US Department of the Interior, Washington, DC, 1964.

the contents were poured on a tungsten crucible, and the cerium button and salt were readily separated.

The analysis of the starting material and refined metal is given in Table 5.15. Shedd et al. (1964) noted that the anode was made by consolidating the small, impure, pea-size cerium nodules obtained during electrowinning. After refining this material, a purer product than the electrowon metal was obtained.

5.7 ULTRAPURIFICATION METHODS

After the pyrovacuum or electrorefining treatments for removing a variety of metallic and nonmetallic impurities from as-reduced rare-earth metals, certain purification techniques may be applied to the purified metals for several reasons: (1) to further decrease the contents of impurities that have already been removed by the purification techniques, (2) to remove impurities whose concentration had not decreased by the purification techniques, and (3) to remove impurities that have inevitably been introduced by the purification techniques. These methods are known as ultrapurification methods. Two techniques of ultrapurification have been widely applied for the rare-earth metals. They are zone refining and solid-state electrotransport.

5.8 ZONE REFINING

The process of zone refining involves generating a thin molten zone of the metal by localized melting and passing the zone slowly along the length of the metal rod to be purified in one direction several times. Purification takes place at the traveling solid–liquid interface. The solubility of an impurity element in the coexisting solid and liquid phases is usually different. Impurities more soluble in the molten metal will move in the direction in which the molten zone is moved and therefore concentrate in the zone to solidify last and accumulate in the finishing end of the rod. On the other hand, impurities more soluble in the solid phase concentrate in the crystallizing solid and so ultimately accumulate in the starting end of the rod. The liquid-soluble and solid-soluble impurities apparently move in opposite directions. Zone refining is essentially a technique for impurity redistribution within the sample rather than impurity removal (Pfann 1966), and only a portion of the rod ends up as pure metal in the process. Since the extent of purification depends on the solubility of the impurities in the solid metal, those impurities that are soluble in the solid cannot be removed to below the equilibrium concentration. As a result, the interstitial impurities that are quite soluble in the solid rare-earth metal just below its melting point cannot be removed completely. Generally, zone refining is more useful for substitutional impurity removal and less effective for the interstitial impurities. The use of a vacuum in the process combines the benefits of conventional zone refining with those of pyrovacuum treatments. In the zone refining of rare-earth metals, the use of a high vacuum or an equally pure inert atmosphere is mandatory to prevent the metal from picking up impurities from the gaseous atmosphere.

Basically, two techniques are used for the passage of molten zones. The simpler technique involves the use of a crucible to hold the metal. The metal is contained in a long horizontal trough or crucible, and the zone is moved in a horizontal direction.

As mentioned earlier, the rare-earth metals are so reactive that they reduce ceramic container materials at their melting points and get contaminated. Attempts have been made to overcome this problem by using a water-cooled container in which an unmolten skin of the metal being purified is maintained, and this thin skin acts as the true container of the molten metal. The other technique is the vertical floating zone technique, in which the metal is supported vertically from the ends without a container, the narrow molten zone being maintained because of the surface tension of the metal. Heating in either method is by induction, and this mode of heating can have either an inert atmosphere or a vacuum. Better control and narrower zones are obtained by electron beam heating, but this requires a high vacuum.

5.8.1 Preliminary Studies

At the time of the first review on zone refining of rare earths by Huffine and Williams (1961), zone refining had been reported on only two metals. Kendall in General Electric had purified gadolinium by using the conventional horizontal induction heating technique with a tantalum crucible in a purified argon atmosphere (Huffine and Williams 1961). He made 10 passes of a 45-mm-wide zone at a rate of 38 mm/h. The product was evaluated only by metallography. The purified ingot showed substantial concentration of impurities at the ingot ends with corresponding purification of the middle of the ingot.

Yttrium was subjected to purification by zone melting at the General Electric Company's Aircraft Nuclear Propulsion Department (GE-ANPD), and the results were summarized by Huffine and Williams (1961). The refining was done by the floating zone technique with induction heating, and a 9.5-mm-diameter rod was processed in a continuously pumped vacuum. Three heating passes were made (below the melting point) in order to remove the volatile impurities sufficiently to prevent the arcing of the heating coil. The main impurity, magnesium, and a considerable amount of yttrium oxyfluoride were vaporized. Following this, six zone passes were made at the rate of 64 mm/h, and the analysis of the purified metal is given in Table 5.16.

The results given in Table 5.16 indicate no significant change in O, N, Ni, and Ti contents and only a marginal movement of the metallic impurities Cr, Cu, Fe, and Zr. Other indicators of purity such as microstructure and hardness also did not reveal any significant variation with location in the zone-refined rod. It appeared that zone refining was not a useful purification process for yttrium.

Two other early attempts at zone refining of yttrium were reported. An yttrium rod containing 0.052% oxygen and 0.065% fluorine was zone refined in two passes by Carlson et al. (1960). However, no significant change in oxygen content was observed, although there was a decrease in the fluorine content. The decrease in fluorine was attributed to the evaporation of oxyfluoride.

Necker (1961) zone refined yttrium and observed that metallic impurities could be decreased from 4300 to 1800 ppm after six zone passes. This observation did not agree with that of Huffine and Williams (1961).

Revel et al. (1974) carried out the zone refining of cerium in an induction-heated cold crucible. They found that 12 passes of a molten zone decreased a number of

TABLE 5.16
Purification of Yttrium by Zone Refining

	Content (ppm)			
	Before	After Processing		
Impurity	Processing	Beginning	Middle	End
O	5800	7600	6170	5310
N	270	280	250	250
Fe	500	500	300	100
Cr	10	10	<1	<1
Cu	10	2	0.5	0.5
Ni	50	50	50	50
Ti	100	100	100	100
Zr	4700	4300	3100	2750

Source: Huffine, C.L. and Williams, J.M., Refining and purification of rare earth metals, in Spedding, F.H. and Daane, A.H. (eds.), *The Rare Earths*, Wiley, New York, 1961.

metallic impurities to the part-per-billion range. The purification with respect to interstitial impurities during the zone refining was not determined. Beaudry and Gschneidner (1978) noted that it was not likely that purification with respect to interstitial impurities was attained during the experiments of Revel et al. (1974), because the vacuum used was inadequate and the interstitial impurities exhibit high solubility in solid cerium. They, however, stated that from impure cerium, many metallic impurities could be decreased by zone refining.

Two years later, Hukin and Jones (1976) zone refined terbium under an atmosphere of pure argon in a horizontal cold crucible with induction heating. They observed that O, N, and C moved in the direction opposite to that of the molten zone. Significant purification with respect to the interstitial impurities as well as the metallic impurities was reported.

Jones et al. (1978) reported that in much of the earlier work on zone melting, the ingot underwent degradation during processing, particularly by oxygen and nitrogen, rather than undergoing any possible improvement from the treatment. In fact, they were corroborating the statement of Revel et al. (1974) that zone refining of cerium would fail to remove nonmetallic elements (N, O) and that one should be satisfied not to increase their amount during the treatment. This state of affairs was changed by the work of groups at the University of Birmingham and at the Ames Laboratory (Jones et al. 1978; Fort et al. 1981).

Making use of technological developments associated with cold boat crucibles together with advances in vacuum technology, particularly the use of UHV equipment, the groups of D. Fort at the University of Birmingham and K.A. Gschneidner Jr. at Ames were able to handle molten rare earth without degradation during processing and contributed to much of the current knowledge on zone refining of rare-earth metals.

5.8.2 Lanthanum, Gadolinium, and Terbium

Commercially available lanthanum, gadolinium, and terbium metals were zone refined by Jones et al. (1978) in water-cooled boats using radio-frequency heating. The lanthanum was zone refined in UHV (working pressure, ~10^{-8} Pa), while purified argon of equivalent purity was used for gadolinium and terbium. The use of argon moderated the vaporization problems, particularly with terbium. The configuration of the boats was such that melting occurred right through the ingot.

In the zone melting of lanthanum, ~15 g pieces of the metal were consolidated in the cold boat by a general melting. The start material outgassed badly, and outgassing was considered complete when the whole rod could be held molten in a vacuum better than 10^{-7} Pa. The ingot length was 120 mm, zone width was ~15 mm, and the zoning speed was 180 mm/h. After 33 zone passes, the ends were cropped for mass spectrographic analysis, and the remaining rod (now 104 mm long) was treated further. The rod was replaced inverted and subjected to a further 30 zone passes at an average speed of 150 mm/h, while the vacuum remained better than 10^{-7} Pa during the whole zoning procedure.

At the completion of zoning, samples were removed from the beginning, end, and middle portions of the refined rod. The beginning and end samples were actually cut 10 cm from the extremities of the ingots. The analysis of the zone-refined lanthanum is given in Table 5.17.

In the refining of gadolinium and terbium, 120 g start material was consolidated and outgassed to a constant vacuum better than 1.3×10^{-5} Pa, as described for lanthanum. The ingots were then zone refined under static high-purity argon. The zoning width was 15 mm, zoning speed was 250 mm/h, and the number of passes in each case was 25. The analysis after zone refining appears in Table 5.17.

The results in the table show that in lanthanum, gadolinium, and terbium, zone refining results in redistribution of oxygen and nitrogen. After zoning, in each of the three cases, the maximum impurity concentration occurred at the *start* end, thus indicating that these impurities had moved in the opposite direction to that of zone travel. The hydrogen content showed no consistent segregation effects, possibly because of the reversible nature of the rare earth–hydrogen reaction. Most of the metallic impurities had moved in the direction of the zone. The results indicated that zone refining can result in a greatly improved product, perhaps even on a commercial scale.

5.8.3 Lanthanum, Cerium, and Gadolinium

In experiments jointly conducted by groups from the University of Birmingham and the Ames Laboratory (Fort et al. 1981), a zone-refining apparatus constructed to UHV standards was used to ultrapurify high pure Ames metals. The metals were lanthanum, cerium, and gadolinium. Only three rare earths—lanthanum, cerium, and praseodymium—have vapor pressures that are low enough at the melting points of the metals to allow conventional cold-boat zone refining in vacuum, and all other rare-earth elements require an inert gas environment to suppress volatilization. The use of inert gas can result in contaminant introduction, but such contamination could

TABLE 5.17
Analysis of Zone-Refined Lanthanum, Gadolinium, and Terbium

	Analysis (ppm)		
Impurity	**Beginning**	**Middle**	**End**
		Lanthanum	
H	900	759	526
O	11,829	7450	5248
N	690	776	204
Tb	15		3
Y	30		10
Ni	75		160
S	31		100
Na	5		0.3
Li	30		10
		Gadolinium	
H	17	17	17
O	933	593	341
N	39	24	14
Tb	10	27	60
La	6	7.5	20
Cu	4	6.5	65
Ni	2	3	30
Fe	40	49	190
Ti	1.5	3	8
Si	32	49	65
Al	15	95	450
S	7	20	26
		Terbium	
H	13	10	13
O	1999	640	348
N	140	69	29
Pb	0.4	1	1.5
Cu	6.5	7	32
Ni	0.5	2.5	4.5
Fe	6.5	27	75
Ti	5	3	4
Al	6	50	170

Source: Jones, D.W. et al., Zone refining of rare earth metals, in McCarthy, G.J. and Rhyne, J.J. (eds.), *The Rare Earths in Modern Science and Technology*, vol. 1, Plenum Press, New York, 1978.

be kept to acceptable levels provided that no gaseous impurities leaked into the system during refining and that negligible degassing from the system walls into the argon occurred. The use of UHV-rated equipment and pumping the system to a high vacuum before admitting argon help in keeping contamination to acceptable levels.

A schematic diagram of the cold-boat zone-refining assembly used by Fort et al. (1981) is given in Figure 5.11.

The assemblies were constructed using stainless steel UHV components and copper gaskets throughout. One assembly was evacuated using ion and sublimation pumps, and the whole system was bakeable to 400°C. It had a base pressure of 2.6×10^{-8} Pa. This system was used for zone refining both in vacuum and under argon. Another cold-boat assembly was evacuated by a diffusion-pumped vacuum system with a cryogenic trap. The assembly was leak tested initially to 2.6×10^{-8} Pa, but the actual pumps had a base pressure of only 6.6×10^{-6} Pa. This assembly was used for zoning runs under argon. For zoning runs under inert gas, the systems were filled with argon (to 1 atm) via an inert gas purifier specified to reduce the total amount of impurities to less than 1 vol. ppm. To induce the molten zone, induction heating at 350 kHz was used. A "double pancake"-type coil with six turns in two layers was used. The radio-frequency power output was regulated to keep the molten zone lengths at approximately 10% of the total bar length.

Cerium has the lowest vapor pressure of all the rare-earth metals and would therefore exhibit the optimum potential for purification with respect to oxygen, nitrogen, or hydrogen when zone refined under UHV conditions. During UHV zone refining of cerium, Fort et al. (1981) experienced severe trouble in stabilizing the molten zone. The zone kept vibrating and touching the cold boat, where it would freeze, then remelt, touch the boat, and freeze again. This stability problem was overcome when the cerium rod was zone refined under 1 atm pressure argon. The rod was loaded into the diffusion-pumped cold boat, the rod was degassed by melting in a vacuum (initially 6.6×10^{-6} Pa but rising to 5×10^{-4} Pa during melting), and then purified argon was admitted to a pressure of 1 atm. The molten zone became well defined (the

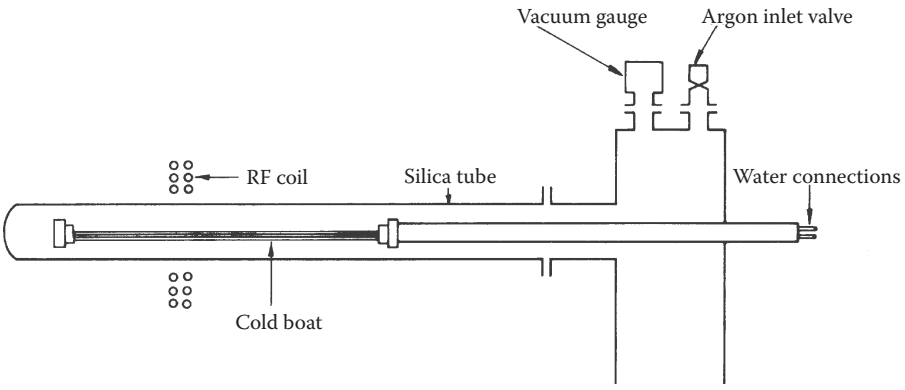


FIGURE 5.11 Schematic drawing of the cold-boat zone-refining assembly. (From Fort, D. et al., *J. Less Common Metals*, 81: 273–292, 1981.)

melting–freezing cycles ceased), and a constant length and controlled zone refining were possible. At the rate of 12.7 cm/h, a total of 15 zones were passed.

The zone stability problem exhibited by cerium in UHV was also displayed by lanthanum (Fort et al. 1981) experiments. However, previously commercial-purity lanthanum had been zone refined (Jones et al. 1978) in UHV without problems in stabilizing the molten zone. Stability of the molten zone appeared to be connected to material purity. The impurities in the metal influence the surface tension of the molten metal and hence affect the molten zone stability. An inert gas atmosphere may stabilize the molten zone by making the temperature profile across the zone much sharper by increasing the heat losses from the nonheated parts of the bar and also by altering the surface characteristics of the molten metal.

Fort et al. (1981) proceeded with zone refining of lanthanum in UHV in spite of not achieving a stable molten zone. The refining run was composed of 14 zone passes at 18.7 cm/h and then 11 zone passes at 11.7 cm/h. During zoning, the vacuum improved from 1.3×10^{-5} Pa during the initial pass to 5.3×10^{-7} Pa for the final 10 passes.

Gadolinium could not be cold-boat zone refined in UHV because of the metal's high vapor pressure and hence its excessive volatilization. Fort et al. (1981) zone refined Gd under inert gas. Two different vacuum treatments were given to Gd before argon was let in. In one, the starting material was degassed at red heat (~800°C) to a vacuum of 2.6×10^{-5} Pa before it was cooled to room temperature and purified argon was admitted, and at 25.2 cm/h, 20 zone passes were made. In the other treatment, the starting material was degassed to a vacuum of 2.6×10^{-7} Pa before admission of argon. Nine zones were run at 18.7 cm/h followed by 11 passes at 11.7 cm/h. In another run, gadolinium containing 190 atomic (at.) ppm tungsten was zone refined, principally to redistribute this impurity. The diffusion-pumped cold-boat system was used. After degassing the starting metal (to 6.6×10^{-6} Pa), purified argon was filled to 1 atm, and first, 20 zones were passed at 12.7 cm/h, followed by 1 zone pass at 2.5 cm/h. The last pass was to promote grain growth.

The analyses of cerium, lanthanum, and gadolinium before and after zone refining are listed in Table 5.18. The results show that in cerium and gadolinium, under the conditions used, the impurity levels rise or fall progressively from the beginning of the bar to the end. The results for lanthanum and cerium are shown in Figure 5.12. Unlike cerium, the results for lanthanum do not show a consistent trend, and this is traceable to the unstable molten zone. A stable molten zone is necessary for worthwhile refining.

5.8.3.1 Redistribution of Interstitial Impurities

Fort et al. (1981) observed that in the zone refining of gadolinium, terbium, and lanthanum, the impurities oxygen, hydrogen, and nitrogen moved against the zone directions. The impurity profiles for oxygen and carbon are shown in Figure 5.13. It is seen that unlike oxygen, carbon was found to move in the zone direction in gadolinium. It is thus not possible to decrease the levels of all four major interstitial impurities at one end of a gadolinium bar by zone refining. Also, the lowest levels of oxygen, hydrogen, carbon, and nitrogen achieved by Fort et al. (1981) did not represent significant improvements over the starting concentrations. They also observed

TABLE 5.18
Analysis of Ce, La, and Gd before and after Zone Refining

		After Zone Refining				
Element	**Start**	**Beginning**	**1/4**	**1/2**	**3/4**	**End**
			Lanthanum			
O	295	434	434	1215	564	174
H	275	965	1100	2338	2062	688
N	30	30	20	80	50	20
Ta	3.4	41	40	33	36	220
Cu	10	37	20	16	15	120
Fe	10	5	4	4	9	66
Ni	2	2	1	1	2	10
Co	<0.2	2	1	1	7	15
Cl	3	10	10	7	7	5
			Cerium			
O	395	1226	683	823	455	341
H	556	1668	973	1112	417	139
N	260	260	240	230	130	60
			Gadolinium			
O	864	1770	894	648	432	304
H	1092	780	780	780	468	312
N	34	190	101	101	45	56
C	367	262	367	524	616	1087
W	190	<1	<1	55	33	1433
Fe	38	3	10	20	5	160
Al	10	<0.04	1	4	8	100
Ta	11	<0.03	1	24	23	10
Si	5	<0.03	10	10	2	20
Co	2	<0.03	<0.05	<0.1	0.2	5
Ni	3.2	<0.3	<0.3	3	0.8	10

Source: Fort, D. et al., *J. Less Common Metals*, 81, 1981.
Note: Values in at. ppm.

in the zone refining of gadolinium that UHV degassing was advantageous before zoning under vacuum.

5.8.3.2 Redistribution of Metallic Impurities

Metallic impurities were found to be markedly redistributed in gadolinium by zone refining (Fort et al. 1981). The impurity profile in gadolinium after zone refining is shown in Figure 5.14. All three metallic impurities shown—aluminum, iron, and tungsten—have undergone redistribution by zone refining and have concentrated at the end, leaving the portion from the beginning to three-fourths of the bar enhanced

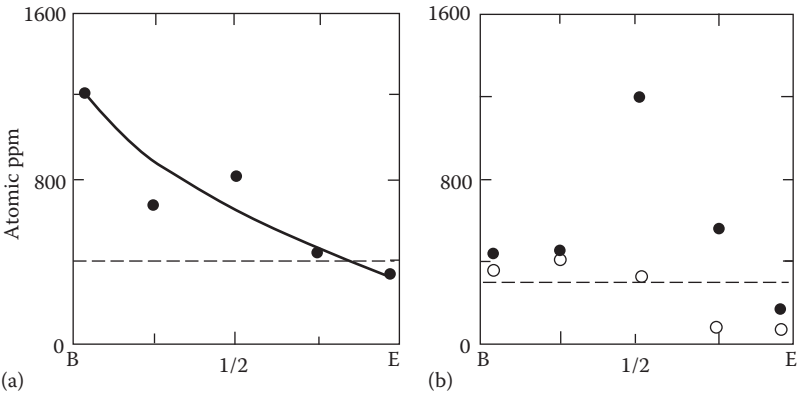


FIGURE 5.12 Oxygen concentration profiles along the zone-refined bar from beginning B to end E for (a) cerium and (b) lanthanum. Dashed horizontal line indicates starting concentrations. In (b), solid circles represent values at the top of the bar, and hollow circles represent the values at the bottom of the bar. (From Fort, D. et al., *J. Less Common Metals*, 81: 273–292, 1981.)

in purity. Tungsten, iron, and aluminum move well, but zone refining has not been particularly effective for zirconium. In fact, the metallic impurities were so effectively redistributed by zone refining of gadolinium that Fort et al. (1981) achieved the total metallic impurity level in the beginning section—the lowest ever recorded in a rare-earth metal. From a starting concentration of 190 at. ppm, zone refining left at least one-quarter of the bar with a tungsten content of less than 1 at. ppm. In lanthanum, despite the instability of the molten zone, useful transport of metallic impurities was observed (Fort et al. 1981).

In the zone refining of rare-earth metals, Fort et al. (1981) observed that the majority of the metallic contaminants were transported in the zone direction. This was observed for iron, copper, cobalt, nickel, tantalum, tungsten, and aluminum. Such behavior can be anticipated because the binary phase diagrams of each of these metals with the rare earths showed eutectics adjacent to the pure rare earths due partly to the low solubility of most of these elements within the matrix of the large rare-earth atoms. The lowering of the melting point of the host rare-earth metal by small amounts of impurities led to the distribution coefficient (k_{eff}) becoming less than 1 and, as a consequence, movement of impurity in the zoning direction.

In gadolinium, many of the common metallic impurities have been amenable to considerable transportation by zone refining. Interestingly, the direction of transport of oxygen, hydrogen, and nitrogen, which are present in considerable concentrations besides not transporting very effectively, is opposite to the direction of transport of common metallic impurities, which are present in relatively low concentrations but transport very efficiently. As a result, no part of the zone-refined bar is of greatly improved overall purity compared to the starting metal. This was stated clearly by Fort et al. (1981); see Figure 5.15. The inevitable conclusion is that zone refining is not a particularly viable method of refining rare-earth metals with respect to all impurities.

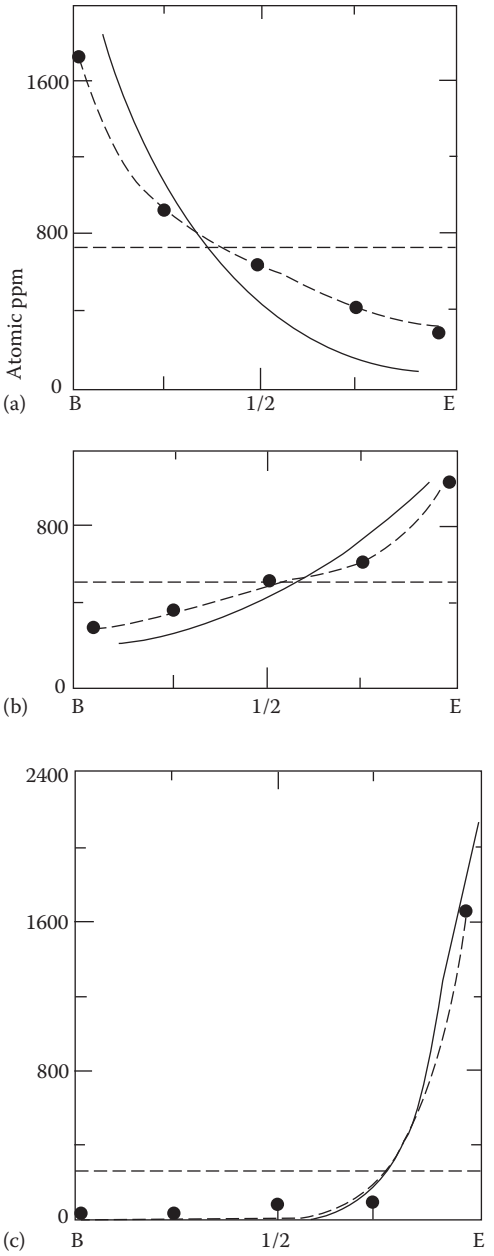


FIGURE 5.13 Impurity profiles in zone-refined gadolinium after 20 passes. (a) oxygen, (b) carbon, and (c) tungsten + iron + aluminum. Dashed horizontal line, starting concentrations; solid line, calculated ultimate concentration distribution profile. Dashed curve connects experimental data points. (From Fort, D. et al., *J. Less Common Metals*, 81: 273–292, 1981.)

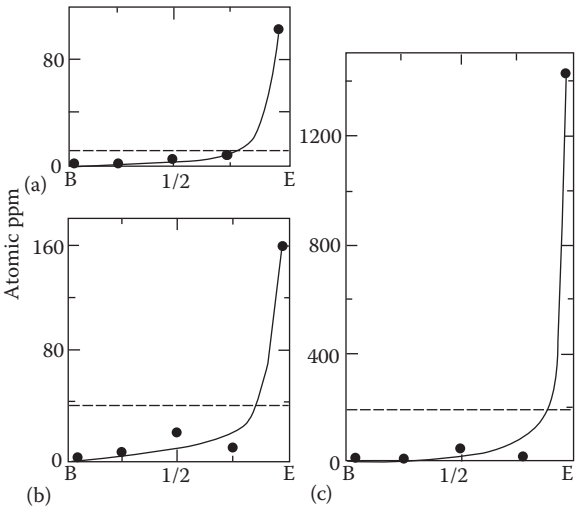


FIGURE 5.14 Profile of metallic impurities (a) aluminum, (b) iron, and (c) tungsten in zone-refined gadolinium. Dashed horizontal line, starting levels. (From Fort, D. et al., *J. Less Common Metals*, 81: 273–292, 1981.)

The ability of zone refining to refine rapidly with respect to metallic impurities makes the technique still useful, particularly in combination with another technique that can refine with respect to the interstitial impurities. Zone refining in combination with solid-state electrotransport should enable production of very pure rare-earth metals.

5.9 SOLID-STATE ELECTROTRANSPORT

It has been known for many years that foreign ions in a metal lattice that is subjected to a direct current field display mobility (Jost 1952). The mobility is more pronounced for the nonmetallic atoms, which can possibly migrate interstitially in the metal, even though metallic impurities also move (Seith and Wever 1953). The remarkable mobility of oxygen in zirconium was reported as early as 1940 by de Boer and Fast (1940). Inspired by this fact, Williams and Huffine (1959) at GE-ANPD examined the technique in 1959 for the purification of yttrium.

Williams and Huffine (1959) electrolyzed yttrium bars of 9.5 mm and 19 mm in diameter in static argon using the vacuum chamber of an arc-melting furnace. The temperatures were 1370°C and 1270°C, respectively, and the electrolysis lasted for 200 h. Water-cooled electrodes were fixed to the bars, and the bars were heated by the passage of direct currents of approximately 300–700 A.

The results of electrolysis at the two temperatures were similar, but the overall transport of impurities was better at the higher temperature. This could be anticipated for a diffusional process. Data obtained at 1230°C are shown in Table 5.19. The movement of oxygen toward the anode was very marked. The movement of nitrogen, though in the same direction, was less pronounced. Many metallic impurities also moved toward the anode.

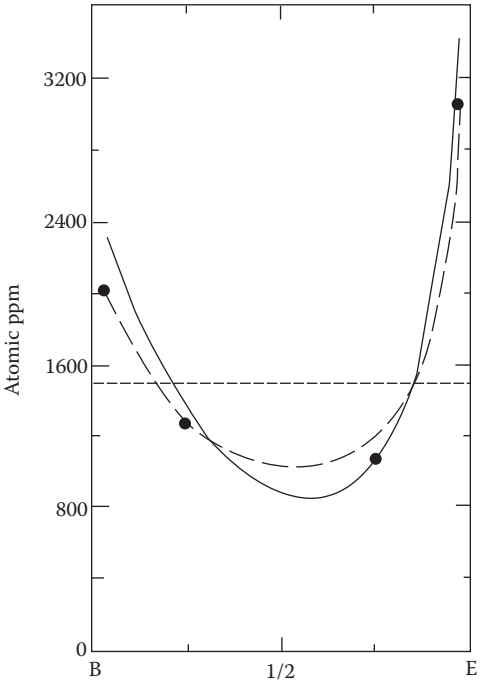


FIGURE 5.15 Sum of the oxygen, carbon, tungsten, iron, and aluminum impurity levels in zone-refined gadolinium after 20 passes. Dashed horizontal line, starting concentrations; solid line, calculated ultimate concentration distribution profile. Dashed curve connects experimental data points. (From Fort, D. et al., *J. Less Common Metals*, 81: 273–292, 1981.)

The solubility of oxygen in yttrium is low; however, the mobility of what is dissolved is quite high. This leads to the situation where the high mobility of dissolved oxygen results in dissolution of oxygen from the insoluble inclusion, resulting finally in the removal of the inclusion itself. The inclusions completely removed near the cathode appeared near the anode.

These encouraging initial observations of Williams and Huffine (1959) laid the foundation of future work on this technique of purification of rare-earth metals at Ames by Verhoeven, Carlson, Schmidt, Beaudry, and Gschneidner and at the University of Birmingham by Fort and Jones (Fort 1987; Fort et al. 1987, 1990; Jones et al. 1982).

The solid-state electrolysis (SSE) described by Huffine and Williams (1961) is more popularly known by the name solid-state electrotransport. In solid-state electrotransport, a direct current is passed through a rod or strip of metal held between two electrodes in an appropriate container. Those impurities are amenable to transport and migrate to one end of the rod, leaving the remainder enhanced in purity.

During electrotransport, the impurities move under the influence of the electric field to one end of the bar. A greater electric field makes the impurities move faster. Jones et al. (1982) describe this as the electron flow sweeping the impurities

TABLE 5.19
Electrotransport Purification of Yttrium

Impurity	Content before Processing (ppm)	Content after Processing (ppm)		
		Near Cathode	Center	Near Anode
O	3330	665	3100	10,900
N	510	366	570	700
Si	55	100	10	140
Fe	150	60	50	600
Mn	9	<1	<1	6
Mg	5	10	<5	6
Zr	9000	9000	9000	7000
Ni	250	50	100	10,000
Cr	80	20	20	30
B	7	3	6	15
Ti	9	<3	<3	30
Co	1	<1	<1	6

Source: Williams, J.M. and Huffine, C.L., *Nucl. Sci. Eng.*, 9, 1961.

(particularly the interstitial impurities O, H, N, and C) toward the anode end. The same electric current also (resistance) heats the metal rod (to near the melting point), enhancing the impurity transport rates. Since the passage of the electric current heats the rod, however, the maximum field becomes limited by the rate at which the heat can be removed from the bar. The use of a higher electric field without leading to a rise in temperature to unacceptable levels is favorable for SSE. The maximum temperature that can be acceptable for using a higher electric field is limited by two factors. One is the melting point of the metal. The other is the vapor pressure of the metal being purified. When SSE is carried out under high vacuum, the heat is lost by radiation. When an inert atmosphere is used, cooling also occurs by conduction. When the rod is of a smaller diameter, the surface-to-volume ratio is greater, and this increases the cooling per unit length and permits an increase in the electric field. A rod of smaller diameter also means processing less material.

The extent of purification is often determined by the surroundings. A vacuum of 1.3×10^{-7} Pa or an equally pure inert gas is the minimum requirement for realizing the movement of gaseous impurities to one end of the metal by electrotransport faster than they enter the metal from the surroundings.

The ends of the rod being purified by electrotransport are usually cooler, and in this portion, the transport would be slower. As a result, there is a danger that the cooler end, from which the impurities are removed, will release or feed the impurities at a rate slower than the rate at which the impurities are transported through the rest of the material. This end can continue to act as an impurity source even after other portions have been purified. This limitation has been circumvented by butt welding a previously electrotransport-purified rod to the end from which impurities are being removed.

A concentration and chemical potential gradient is established along the length of the rod during electrotransport. This gradient will encourage back diffusion, and this is another source of impurity.

Verhoeven (1966) derived a theoretical expression to estimate the degree of purification attainable in SSE for a specified set of conditions. There are major limitations, however, as described above, in achieving experimentally what has been predicted by theory. In any case, purification by electrotransport can be enhanced by maximizing transport by an electric field, thereby minimizing contamination from the surroundings and the cold end and finally minimizing diffusion of impurities. Another item is that solute mobilities are considerably higher in the body centered cubic (bcc) phase, and when possible, it is preferable to process the metal in the bcc phase.

Following the initial work of Huffine and Williams (1961), many investigations have been carried out on the electrotransport purification of rare-earth metals. A summary of electrotransport purification studies presented by Carlson and Schmidt (1976) has been updated with later works and is given in Table 5.20.

SSE has emerged as one of the major methods for purifying rare-earth metals to the highest levels. It is practically indispensable in this role because the major contaminants in rare-earth metals are invariably oxygen, hydrogen, carbon, and nitrogen. These four elements usually account for more than 95% of the impurities found in commercially obtainable rare-earth metals. These interstitial impurities are exactly those that are most amenable to electrotransport purification. Table 5.20 also summarizes purification achieved with respect to these impurities.

5.9.1 SSE System

In SSE, UHV-rated equipment is always used to reduce environmental contamination risks even when processing under inert gas. Fort et al. (1987) used the hot chuck technique to maintain the sample at a uniform temperature throughout its length. Here, the sample holders were at a temperature similar to the sample. While the basic UHV chambers and power generators used for SSE have not changed much since the early days of SSE, the electrodes (or clamps, chucks, or adaptors) that provide electrical contact between the sample and the main power feed through the chamber have become more sophisticated. The section of chuck adjoining the sample should operate within 100 K of the sample temperature, should not contaminate the sample, should allow for length changes in the sample while heating and cooling, and should also carry high currents (~300 A). Tantalum is the preferred chuck material because, among other things, in this metal, oxygen, hydrogen, and nitrogen electromigrate from anode to cathode in the opposite direction to that of the rare earths. So, electromigration of these impurities from the chucks into the purer (cathode) ends of the rare-earth samples is ruled out.

The sample for solid-state electrorefining was prepared by induction melting in a cold boat either under vacuum or in purified argon followed by mechanical swaging. Single-crystal rods grown by electron beam float zoning (EBFZ) in a vacuum (for Gd, Tb, and Y) or radio-frequency float zoning (RFFZ) under argon (for Gd, Tb, Y, Ho, and Dy) were also used.

TABLE 5.20
Electrotransport Purification of Rare-Earth Metals

Rare-Earth	Atmosphere	Temperature (°C)	Time (h)	Initial Concentration (ppm)			Initial RRR	Final Concentration (ppm)			Final RRR	Reference
				C	N	O		C	N	O		
Pr	UHV				Ames metal						400	Fort 1987
Nd	UHV	860	1237	13	54	45			1	16	116	Carlson and Schmidt 1976
Nd	Ar	800–863	1250	7	2	40		5		20	40	Fort et al. 1987
Gd	UHV	1000–1050	2600	21	2	51		5	2	3	800	Fort et al. 1987
Tb	UHV	1050	350		30	380	17.5		15	25	60	Jordan et al. 1975
Tb	UHV	985–1075	900	Ames metal					400			Fort 1987
Dy	Ar	1050–1100	500	Ames metal					125			Fort 1987
Ho	Ar	1100	200	Ames metal					90			Fort 1987
Lu	UHV	1150	168	70	15	475	21	60	6	42	150	Peterson and Schmidt 1969
Y	Ar	1230–1370	200		510	3330			90	340		Williams and Huffine 1961

When SSE processing was to be carried out under purified argon, the procedure (Fort 1987) involved (1) pumping and backing the system and sample assembly until the base pressure was 10^{-5} Pa; (2) outgassing the sample and electrodes by passing a current through them, the temperature designed to be attained being determined by the volatility of the element; (3) admitting argon into the system to a pressure of about 70 kPa via an inert gas purifier designed to reduce the total of all gaseous impurities to below 1 vol. ppm; (4) performing the SSE processing; and (5) evacuating the system to make sure no leaks had developed during processing.

5.9.2 Residual Resistivity Ratio

The electrical resistivity, ρ, of metals at low temperatures is an excellent tool to determine impurity concentration in them (Schulze 1981). The residual resistivity ratio, RRR, is calculated as

$$\mathrm{RRR} = (\rho_{298\,\mathrm{K}} - \rho_{4.2\,\mathrm{K}})/\rho_{4.2\,\mathrm{K}}$$

where ρ is the resistivity at the temperature given as subscript. RRR is related to the impurity concentration, C_i, by

$$C_i = K/\mathrm{RRR}$$

where K is a constant of proportionality. A high value of RRR is seen to indicate a low value of C_i and vice versa.

5.9.3 Lanthanum

The solute mobilities are high in the bcc phase, and this phase is stable in lanthanum above 1138 K. Fort (1987) conducted SSE processing of lanthanum above this temperature. To achieve steady-state distribution of C and N, processing for 500 h was necessary. Oxygen distributes relatively more quickly in lanthanum. It is interesting to note that an attempt to SSE process a relatively impure lanthanum start material led to run failure because a buildup of impurities at the anode end led to a decrease in the melting temperature of the region. After 120 h of SSE, the anode portion melted even at 1033 K.

In an earlier investigation, Ames lanthanum metal was SSE refined by Pan et al. (1980). The metal was refined to a resistance ratio of 260.

5.9.4 Praseodymium

SSE processing has been carried out on praseodymium by Fort (1987) using commercial metal as well as Ames metal as the start material. When refining standard-grade commercial praseodymium, impurity transport and precipitation resulted in failure by melting at that point. On the other hand, high-purity commercial metal as

well as Ames metal could be refined to RRR values of approximately 250 and over 400, respectively.

5.9.5 Neodymium

The vapor pressure of neodymium at SSE processing temperatures is about two orders of magnitude higher than that of praseodymium. At temperatures approaching 1150 K, however, losses by volatilization were still not too high. In an SSE-refined material starting from commercially available neodymium, analytical and metallographic evidence indicated impurity transport by SSE, but the RRR values showed no gradient along the length of the sample. The flat RRR profile was attributed to a minor substitutional impurity that had a disproportionate effect on RRR and that was not significantly transported during SSE. If the same material were zone refined and the substitutional impurity removed prior to electrotransport, an RRR gradient appeared. As could be anticipated, SSE processing of Ames neodymium resulted in a product having RRR gradients with or without preliminary zone refining (Fort 1987).

5.9.6 Gadolinium

Early work on successful purification of gadolinium by the electrotransport technique was carried out by groups at the Ames Laboratory and the Materials Science Center, University of Birmingham. Using a purified helium atmosphere at 1245°C, Peterson and Schmidt (1972) obtained metal with a resistance ratio ($R_{300\ K}/R_{4.2\ K}$) of 405. A somewhat lower temperature and a UHV were used by Jordan et al. (1975), and the metal refined had a resistance ratio of 175.

Fort (1987) noted that in the SSE purification of gadolinium, two of its properties had to be allowed for. One is its comparatively high volatility, and the other is the closeness of the hexagonal close packed (hcp)-hcp-to-bcc transformation temperature to the melting point. He estimated that several hundred hours of SSE at 1320 K would be required for oxygen to approach steady-state conditions. Typically, the SSE program for gadolinium consisted of 500–1000 h at 1273–1323 K followed by slow cooling to room temperature over about 100 h. Starting with a previously zone-refined Ames metal, the highest RRR value of 800 was obtained.

5.9.7 Terbium

Jordan et al. (1975) refined terbium by SSE under UHV at 1050°C for 350 h. They prepared terbium of better than 99.9 at.% purity from metal of commercial purity. The highest resistivity ratio obtained for the refined metal was 60 after a double processing treatment and 90 for the triple-processed metal.

Fort (1987) used single-crystal rods grown by electron beam float-zone melting (EBFZ) and radio-frequency float-zone melting (RFFZ) of Ames metals as starting material. For terbium, the highest RRR attained was more than 400 with initial SSE processing at 1348 K for 200 h followed by approximately 600 h at 1273–1283 K and 100 h at 1258 K. At these temperatures, volatilization rates were controllable.

5.9.8 Yttrium

As described earlier, the technique of electrotransport was first used by Williams and Huffine (1959) for a rare-earth metal to refine yttrium. A purer grade of yttrium containing lower interstitial impurity resulted from refining at a lower temperature under nearly 10^{-5} Pa vacuum, as compared to the product obtained from the first attempt (Carlson et al. 1966). Murphy et al. (1975) performed an interesting experiment in electrotransport purification with a Y–2% Fe alloy. The alloy was electron transport–purified at 1200°C for only 60 h. Even by this, the iron content of the entire cathode section decreased to below 0.01%. Carlson and Schmidt (1976) stated that electrotransport should be a feasible method for purifying yttrium with respect to silver, nickel, and other fast-diffusing metallic elements besides iron. The interstitial impurities carbon, nitrogen, and oxygen also have favorable mobilities in yttrium and are removable to very low concentrations if a UHV was used and end effects and surface reactions were minimized.

Fort (1987) considered 1390–1420 K as the temperature at which the volatilization rates in a vacuum were acceptable for the processing time of 1000 h required for carbon and nitrogen impurities to closely approach steady state. Oxygen reached this state quickly. The highest RRR value of 800 (extrapolating to well over 1000 at the cathode end) was obtained with a high-purity metal initially grown into a single-crystal rod using RFFZ. The RFFZ processing program, in turn, consisted of 750 h at 1373–1423 K, 300 h at 1273–1373 K, and cooling to room temperature over 240 h.

5.9.9 Dysprosium and Holmium

Both dysprosium and holmium have moderately high vapor pressures. Fort (1987) noted that in processing them by SSE, an inert gas environment is necessary. However, even with 100 kPa gas pressure, problems due to volatilization did not disappear. One problem is whisker formation. During SSE, vaporization and recondensation onto the samples resulted in the formation of dendritic whiskers on the sample surface. The 2- to 4-mm-long whiskers form in dense clusters on parts of the sample, and in these parts, marked reduction in temperature was noticeable because of the cooling effect of the large surface area. Such whiskering, usually most severe toward the top of the sample, could be greatly reduced by slanting the sample about 45° to the vertical, so that the vapor originating at the sample bottom rose away from the rest of the rod. Holding the sample horizontal was suspected to induce grain boundary sliding and was hence not attempted.

SSE processing of dysprosium, under 70 kPa argon pressure, was carried out by Fort (1987), keeping the temperature between 1323 and 1373 K and processing time to 500 h. Prior to and after the main processing under argon, the sample and clamps were degassed at 1073–1173 K in vacuum. A commercially pure start metal, resublimed under UHV conditions, was refined by SSE as above to obtain the lightest RRR of 125.

In the case of holmium, an Ames metal, SSE processed at 1373 K for 200 h refined to an RRR of 90.

5.9.10 Erbium

The SSE of erbium has been described in detail by Fort et al. (1990). Ames metal was used as the start material. The metal was cast into a crude rod in a cold boat using arc melting. The rod was mechanically swaged to a uniform diameter of 7.1 mm except for one end, which was left slightly thicker. This thicker section, which would run cooler during SSE and was less likely to melt in the event of excessive impurity buildup, was intended to be the anode. The swaged rod was thoroughly cleaned, degassed, and stress relieved at 850°C and mounted in the SSE equipment. To prevent whisker formation, as explained in dysprosium processing, the sample was held at a 45° angle to the vertical.

The entire SSE processing was carried out in six stages. Some of these stages were carried out in UHV, and some, under argon.

By SSE purification, the total impurity content in erbium decreased from 921 at. ppm in the start material to 338 at. ppm in the purest (cathode) section. This represents a 63% decrease in the overall impurity level. The resultant purity in the cathode end was 99.97 at.% or 99.996 wt.% compared to the start-level purity of 99.91 at.% or 99.988 wt.%. In fact, the cathode end of the SSE-refined rod represents the lowest impurity concentration ever reported for erbium.

Oxygen, nitrogen, and hydrogen electromigrated in erbium, as expected, toward the anode. Oxygen was the main contaminant at 640 at. ppm in the start material. This level decreased in the cathode end to 200 at. ppm after three stages of processing and to 168 ppm after six stages. The start value of nitrogen was 48 at. ppm (4 wt. ppm); after six stages of processing, the N content at the cathode was below the limit of detection (1 wt. ppm), and there was a progressive increase along the length of the sample from the cathode to the anode. In the start metal, the H content was below the detection limit. But at the end of SSE, the H level was 1500 at. ppm (9 wt. ppm) at the anode end, while the H contents at other positions were below the detection limit. Some H contamination had occurred during SSE, and H had then migrated toward the anode. Carbon concentration in the start metal was 97 at. ppm, but at the end of SSE, the value at the cathode was 111 at. ppm. Carbon did not show a progressive increase in concentration from cathode to anode even though the level was lowest at the anode. Some carbon contamination of the sample had occurred during the SSE procedure, most likely during the preparation of the SSE rod and by the degassing of carbonaceous gases from the furnace walls. The final high carbon value was 306 at. ppm in the center section and 195 at. ppm at the anode.

Fluorine is another intractable impurity in erbium, and its content in the SSE-refined erbium rod showed no constant trend along the rod length. This, most probably, is connected with possible inhomogeneous distribution of fluorine in the start metal. Fluorine contamination is a factor in erbium because the vapor pressures of ErF_3 and Er are comparable. Therefore, during pyrovacuum refining, the fluoride tends to cosublime, and the sublimate collected first will have a higher F content than the one collected later.

For the metallic impurities, no consistent trend was generally apparent, possibly due to their presence in relatively low concentrations. Overall, SSE is significant as the final step in the preparation of high-purity erbium.

5.9.11 Lutetium

Carlson et al. (1973) purified lutetium by SSE. A rod of lutetium, 2.5 mm in diameter and 153.5 mm long, was SSE purified at 1150°C for 168 h in an all-metal UHV chamber under 3.3×10^{-8} Pa. The impurity profile of the rod and corresponding resistance ratios obtained by Carlson et al. (1973) are shown in Figure 5.16. They noted that there is a correlation between the resistance ratio and oxygen content of lutetium because the carbon and nitrogen content remained constant along the length of the rod. Peterson and Schmidt (1969) had predicted a favorable purification factor but low mobility for carbon at a temperature of 1150°C, resulting in a long time for carbon to reach steady state. Even though conditions for the removal of oxygen and nitrogen were stated to be favorable, as shown in Figure 5.16, only the redistribution of oxygen was actually observed.

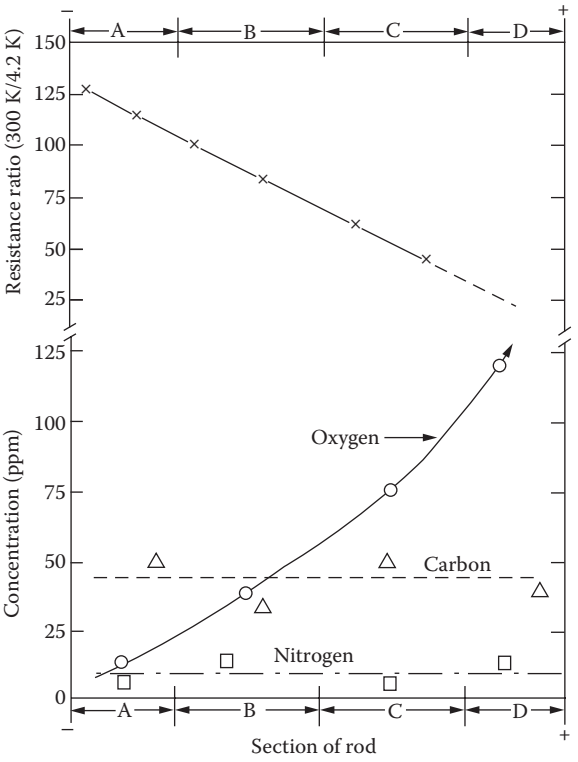


FIGURE 5.16 Concentration profile and resistance ratio of lutetium rod after purification by electrotransport at 1175°C for 160 h. (From Carlson, O.N. et al., Purification of rare earth metals by electro-transport. In Kevane, C.J. and Moeller, T. (eds.) *Proc. 10th Rare Earth Research Conf.*, pp. 701–710, Carefree, AZ, May 1973, Conf-730402, P2, National Technical Information Service, Springfield, Virginia, 1973.)

5.9.12 Samarium

Samarium is volatile. Its vapor pressure at its melting point is approximately two orders of magnitude higher than dysprosium and holmium. Even under 70 kPa argon, the maximum temperature at which SSE processing of Sm could be carried out was 710–720°C, more than 350°C below its melting point. At these relatively low temperatures, whisker formation was a problem, and even after 200 h, no significant purification was detected by Fort (1987). In other words, SSE was not successfully applied to samarium, because volatilization could not be sufficiently suppressed.

Electrotransport refined the maximum number of rare-earth metals and, in the process, obtained some of the rare earths in their purest known states. However, Fort (1987) stated that SSE was a viable method of turning good-quality metal into very good-quality metal but was not a successful method for improving the purity of poorer-quality start metals, because the buildup of impurities resulted in melt-through. While commenting on the potential of SSE processing for rare-earth elements in the context of vaporization problems encountered, Fort (1987) observed that the vapor pressure should be 10^{-4} Pa or less when processing under vacuum and 0.5 Pa or less when processing under 70 kPa of argon, at the chosen SSE processing temperature. Among the rare-earth elements not covered above, cerium and possibly scandium should be amenable to SSE processing in vacuum. Refining of scandium and europium under 70 kPa argon should be possible. It is not possible to SSE refine thulium and ytterbium.

5.10 ZONE REFINING AND ELECTROTRANSPORT

Electrotransport is the ultrapurification method effective for redistribution of interstitial impurities, and zone refining redistributes substitutional or metallic impurities effectively. In the ultrapurification of rare-earth metals, refining has to be accomplished with respect to both the metallic and nonmetallic (interstitial) impurities. For this, in the overall sequence of ultrapurification, zone refining is followed by electrotransport. This sequence has been extensively investigated by Fort et al. (1987) for neodymium and gadolinium metals.

5.10.1 Neodymium

Fort et al. (1987) have described the ultrapurification of neodymium by zone refining followed by electrotransport. A bar of neodymium weighing about 92 g was degassed in the cold boat (of zone-refining equipment) at red heat and 2.6×10^{-7} Pa. The system was then filled with purified argon and subjected to zone refining (25 molten zones were passed at the rate of 11.7 cm/h). Matter transport also occurred during the process, and the beginning of the rod became significantly thicker than the end. It was removed and swaged to a diameter of 8 mm, and its ends were cropped because zone transported impurities would have accumulated in the ends. The rod was then cleaned, placed in the cold boat, degassed in a vacuum to red heat, backfilled with argon, and zone refined (14 molten zones were passed at 11.7 cm/h). It was again removed, swaged to a diameter of 6.4 mm, its ends cut off because impurities

had accumulated there, and the remaining (middle) portion of the rod was subjected to SSE.

The *beginning* end from zone refining was made the cathode in SSE because during zone refining, most metallic impurities would have transported to the *end* end. Moreover, interstitial impurities would migrate from the cathode end to the anode end during SSE. Purification of neodymium by SSE was done under purified argon. The SSE processing consisted of an initial outgassing of the sample in a vacuum at 830°C for 144 h followed by the main run in 50×10^3 Pa purified argon at >863°C, 820–863°C, and 800°C, for a total of 755 h SSE under argon. The processing did not result in any dramatic increase of RRR. After cropping the anode end where impurities had accumulated, Fort et al. (1987) processed the sample by SSE in a vacuum. The run lasted for a total of 1060 h, of which for 412 h, the sample temperature was above 863°C. The analysis is given in Table 5.21.

Among the metallic impurities, iron migrated to the anode end, while tantalum had also distributed. The tantalum content of the start material was 88 at. ppm. This content decreased to 60 at. ppm at the cathode and to progressively lower levels in the center and the anode end. The indication is that tantalum was transported against the zone direction during zone refining. The decrease in iron content from an initial

TABLE 5.21
Analysis of Zone-Refined and Electrotransported Neodymium

		After Zone Refining and SSE (at. ppm)		
Element	**Start (at. ppm)**	**Cathode**	**Center**	**Anode**
O	360	180	239	360
H	571	bl	bl	143
N	21	bl	31	165
C	84	64	312	480
Ta	88	60	40	21
Fe	11	<0.6	1	16
Cu	3	2	3	0.7
Cr	2.6	<0.5	<0.06	<0.4
Se	4.3	8	5.4	8.2
Ce	3.6	4.7	6.3	5
Tb	<2	4	5	4
Si	<6	4	2	4
Gd	<3	<2	3	1.6
Cl	6	10	4	4
All impurities	<1166	<336	<652	<1212
Metallic impurities	<124	<82	<66	<60
O + H + N + C	1036	244	582	1148
Atomic percentage	99.88	99.97	99.93	99.88

Source: Fort, D. et al., *J. Less Common Metals*, 134, 1987.
Note: bl, below limits of detection.

11 at. ppm to a final 0.6 at. ppm at the cathode could have occurred by zone refining, but this conclusion could not be stated with certainty, because iron is known to electromigrate rather quickly for a substitutional solute in many rare-earth metals.

The interstitial impurities migrated toward the anode, as expected, during SSE. The carbon content indicated possible pickup of carbon from swaging and cleaning operations involving the use of hydrocarbons as lubricants or solvents. The overall impurity content decreased from about 1160 at. ppm in the start material to approximately 330 at. ppm at the cathode section after SSE. This corresponds to an improvement in purity from 99.88 at.% to 99.97 at.%. Much of the impurity content was as interstitial impurities O, H, N, and C. They together constituted 1036 at. ppm, and by combined zone refining and SSE, principally the latter, their content decreased to 244 at. ppm at the cathode end. As pointed out earlier, the low impurity content of neodymium is not reflected in the RRRs of the purified samples, values that probably remain low because of reasons other than impurity concentration.

5.10.2 Gadolinium

Fort et al. (1987) have purified gadolinium by zone refining followed by electrotransport, enhancing, in the process, the purity from 99.75 at.% to 99.94 at.%. The procedure adopted is similar to that used for neodymium, using UHV-rated equipment.

A bar of gadolinium (Ames metal) weighing 110 g was degassed at red heat in a cold boat to a vacuum of 2.6×10^{-7} Pa. The system was backfilled with pure Ar to 100 kPa, and zone refining was conducted with nine successive molten zone passes at a rate of 18.7 cm/h followed by nine passes at 11.7 cm/h. A significant amount of material transport back toward the beginning of the bar occurred during zone refining, and this is shown schematically in Figure 5.17. Portions marked *A* in the figure accumulated impurities transported to the *beginning* end of the zone-refined bar and had the highest O and N levels. Those sections were discarded. Virtually all iron, tungsten, aluminum, and copper impurities accumulated in sections D and E, and these were also discarded. Parts marked *B* and *C* had the lowest overall impurity contents after zone refining. Those portions were cut, remelted into a rod about 100 mm long, swaged to a diameter of 6.4 mm, cleaned, degassed, and again remelted in one quick zone pass. This rod was taken for refining by SSE.

Gadolinium is a relatively volatile metal that restricts the temperature and/or duration of SSE refining in a vacuum. The electromigration velocities of oxygen, carbon, and nitrogen are higher in the bcc phases (above 1235°C), but at such temperatures, vaporization of gadolinium would severely curtail run duration. Hence, processing has to be done in the a hcp phase, and the temperature chosen by Fort et al. (1987) was 1030–1040°C. The total processing time for the entire run, which was done in two parts, including initial degassing, warming up, and cooling down, was 2600 h.

The RRR profile of the SSE-refined gadolinium rod is given in Figure 5.18. The measured best value of RRR near the cathode was 730, and the extrapolated value at the extreme cathode end was 800, the highest resistance ratios reported for gadolinium. The purest portion was the cathode end. The analysis of gadolinium purified by zone refining followed by SSE is given in Table 5.22.

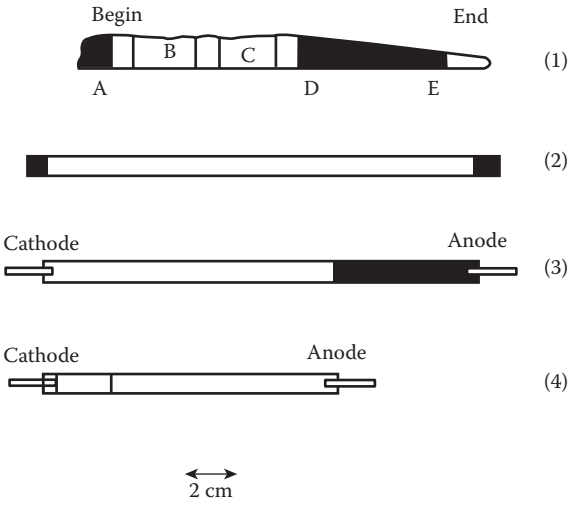


FIGURE 5.17 Schematic diagrams showing the size and shape changes of the gadolinium sample (1) after zone refining, (2) after remelting parts B and C and swaging, (3) after first stage of SSE, and (4) after final stage of SSE. Sections marked black were discarded before the next stage of processing. The tantalum end rods screwed onto the sample to act as current carriers during SSE are also shown. (From Fort, D. et al., *J. Less Common Metals*, 134: 27–44, 1987.)

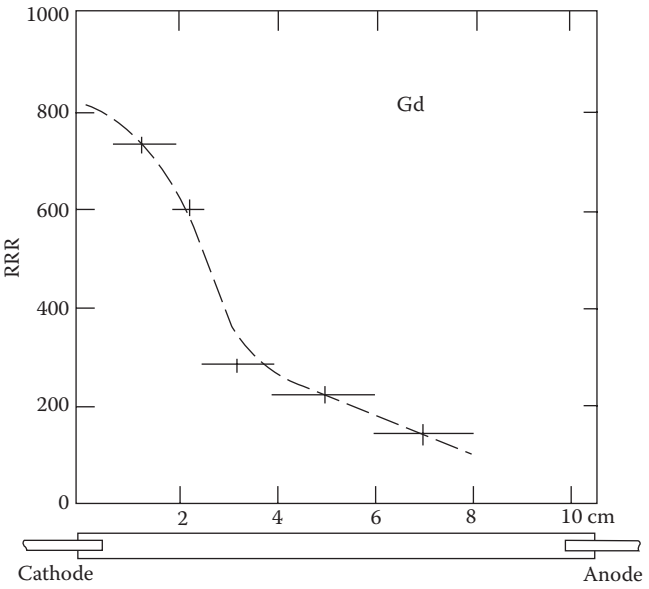


FIGURE 5.18 The final resistance ratio ($\rho_{293\ K}/\rho_{4.2\ K}$) profile along the zone-refined and electrotransport-purified gadolinium. (From Fort, D. et al., *J. Less Common Metals*, 134: 27–44, 1987.)

TABLE 5.22
Analysis of Gadolinium Purified by Zone Refining and Electrotransport

		After Zone Refining					After SSE
Element	**Start**	**Begin**	**1/4**	**1/2**	**3/4**	**End**	**Cathode End**
O	550	658	457	378	304	363	29
H	1560	468	390	468	390	780	468
N	11	39	17	11	11	11	22
C	320	210	288	341	419	563	60
Fe	10	1	0.3	2.5	68	900	0.22
W	5	<2	<1	<1	8	140	4.3
Al	4	<0.2	0.6	1	6	50	<0.07
Si	2	<0.5	<0.4	<0.4	2	40	0.84
Ti	2	<0.2	<0.1	0.9	7	18	<0.08
Cr	2	<0.5	<0.6	<0.6	4	10	0.37
Ni	8	0.3	0.03	0.1	<0.4	20	0.17
Zr	9	12	9	15	60	60	5.7
Cu	2	0.4	0.2	0.3	10	200	0.13
Ce	0.4	0.4	0.1	0.2	0.6	0.6	1.7
Hg	1	2	<0.02	<0.05	<0.3	1	2.1
Ta	2	<0.4	<0.3	<0.3	3	6	1.9
Cl	nd	5	6	4	20	9	0.63
All impurities	2481	<1398	<1171	<1224	1318	3171	597
Metallic impurities	40	<18	<13	<22	169	1445	18
O + H + N + C	2441	1375	1152	1198	1129	1717	579
Atomic percentage	99.75	99.86	99.88	99.88	99.87	99.68	99.94

Source: Fort, D. et al., *J. Less Common Metals*, 134, 1987.
Note: Values in at. ppm. nd, not detected.

By zone refining followed by SSE, the overall impurity level in gadolinium decreased from 2480 at. ppm (in the start metal) to 597 at. ppm at the cathode section. In other words, the gadolinium purity improved from 99.75 at.% to 99.94 at.%. Much of the impurity content given above is due to hydrogen, which, in the start material, was 1560 at. ppm (10 wt. ppm) and decreased to 468 at. ppm (3 wt. ppm). If impurities other than hydrogen are considered, the initial value was 921 at. ppm, and after zone refining and after SSE, it was 129 at. ppm.

The oxygen content was 550 at. ppm in the start material. It decreased marginally to 500 at. ppm in the purest region after zone refining and came down to as low as 29 at. ppm at the cathode end after SSE. Carbon zone refined in the zoning direction and electromigrated toward the anode. The effects of both these techniques worked in the same direction. Yet the content decreased from 320 at. ppm in the start material to only 60 at. ppm at the cathode end. Maximum purification with respect to carbon occurred during SSE. If metallic impurities alone were considered, the improvement was from 40 at. ppm to less than 17 at. ppm. Iron was transported by both these techniques and decreased from 10 at. ppm in the start material to 0.22 at. ppm at the

cathode end. Zirconium moved in both zone refining and electrotransport, but these did not markedly decrease its content.

5.11 IODIDE REFINING

The iodide refining process, developed in 1925 by Van Arkel and de Boer (1925), has been successfully applied to the refining of several reactive and refractory metals. The process is carried out by heating the impure metal with iodine in a closed system. A volatile iodide of the metal is formed, and this iodide is decomposed on contact with a hot wire whereby the pure metal deposits on the wire and the released iodine returns to react with more of the crude metal.

Two general criteria must be met before a metal is considered for iodide refining (Loonam 1959). One is that the metal must be capable of existing as a condensed phase (solid or liquid) at some temperature and pressure in equilibrium with a gas (gaseous iodide) of high atomic ratio of iodine to metal. The second criterion is the capability of the metal to react readily with the gaseous product of the deposition reaction at the same pressure but a different temperature to yield a gaseous product of low atomic ratio of iodine to metal. It is also desirable that the metal have a high melting point and low vapor pressure. These aid in the deposition of the metal as a solid. The iodide refining is most likely to be feasible with metals that form triiodide and tetraiodide because the large positive entropy changes on dissociation lead to an overall decrease in the free energy of dissociation with increasing temperature. In other words, the metals least likely to be amenable to refining are those that form monoiodides that remain monomeric and stable in the vapor phase. According to Loonam (1959), the monoiodides of rare-earth metals would be sufficiently stable to prevent dissociation, and this observation has been confirmed by the data of Scaife and Wylie (1958). In addition, the generally high volatilities of rare-earth metals are not very favorable for iodide refining, because at the high temperature needed for the dissociation of the iodide, the deposited metal would vaporize.

Foster et al. (1952) used a modified Van Arkel–de Boer process for the deposition of lanthanum, the least volatile of the rare earths. The iodide was formed by reaction of iodine and aluminum on lanthanum oxide. At 1000°C, the dissociation of iodide was negligible and only slightly improved at 1800°C. Only small amounts of lanthanum were detected on the wire, and even this deposit was contaminated with aluminum.

The deposition of yttrium from both bromide and iodide was also attempted by Frazier (Huffine and Williams 1961). The bulb temperature (iodide formation) was between 300°C and 350°C, and the molybdenum filament temperature (iodide decomposition) was between 600°C and 1600°C. No deposit was formed, which suggested that it was not possible to deposit rare-earth metals by the Van Arkel–de Boer process.

5.12 MISCELLANEOUS PROCESSES

Many techniques, not covered above, have been applied for the purification of one or more rare-earth metals. One is based on amalgamation of rare-earth metals or

the hydrides. This technique has been used by Schumacher and Harris (1926) and Audrieth (1939). While mercury wets the rare-earth metals and hydrides and forms amalgams, the oxides, carbides, and halides remain insoluble in mercury and could be separated by underpouring or filtration. Warf and Kerst (1953) and Warf et al. (1957) have shown that the hydrides of lanthanum, cerium, and ytterbium were wetted by mercury, whereas the oxide and other impurity inclusions floated on the amalgam. The metal has to be in a finely divided form for efficient amalgamation, which can be accomplished by forming the brittle hydride and grinding. After the flotation, mercury and hydrogen were removed by vacuum distillation, and pure rare-earth-metal powder was obtained.

In the refining and ultrapurification of rare-earth metals, the issue of oxygen removal has been attracting more investigation resources than any other aspect of purification, The reason being that (1) rare-earth metals are avid getters of oxygen and (2) once present in the metal matrix, oxygen is amenable to neither easy nor complete elimination. In addition to the host of purification pathways that have been summarized so far for the removal of oxygen along with various other impurities, two specialized and effective techniques for deoxidation have been investigated by the groups at Ames and at Tohoku University.

5.12.1 Deoxidation by Oxyhalide Formation

At Ames, Corbett et al. (1986) investigated the following reaction as a means of removing traces of oxygen from the rare-earth metals.

$$R_2O_3 \text{ (in R)} + RX_3(s,1) \rightarrow 3ROX(s)$$

The aim was to extract dissolved oxygen (1–5 at.%) in yttrium, lanthanum, neodymium, and gadolinium metals as ROCl by reaction between the oxygen contained in the metal and the metal trichloride. The equilibration was carried out by heating the metal (containing oxygen) and the corresponding trichloride in a sealed niobium or tantalum container encased, in turn, in a quartz jacket at 730–850°C for 1–2 weeks' duration. The oxygen transfers from the metal matrix to the metal oxychloride, and the oxygen concentration in the metal decreased to 0.1–0.2 at.%. The results were reportedly (Corbett et al. 1986) consistent with thermodynamic estimates or the reaction limits. In the case of lanthanum, after annealing at 850°C for the time duration applied to other metals, the oxygen removal does not proceed beyond 0.5 at.% from the original concentration of 2–5 at.% oxygen. However, this limit was decreased to about 0.27 at.% by longer reactions at 760–775°C. Corbett et al. (1986) observed that these types of reactions appeared general for the selective removal of oxygen from nearly all the rare-earth metals. They provided a detailed thermodynamic description of the process and indicated the possibility of other halides to be used for such deoxygenation. With reference to the general expression given above, it should be noted that the deoxygenation by oxychloride formation usually proceeds beyond the reaction with precipitated oxides, removing the oxygen in solid solution as well.

5.12.2 Electrochemical Deoxidation of Rare-Earth Metals

At Tohoku University, Hirota et al. (1999) have investigated the removal of oxygen from rare-earth metals (Gd, Tb, Dy, Er) down to very low levels by an electrochemical deoxidation method. The process is essentially carried out in an electrolysis cell, where, in the $CaCl_2$ electrolyte, calcium generated by electrolysis at the cathode deoxidizes the rare-earth metal there. The calcium oxide thus formed dissolves in the electrolyte, and the oxygen is eventually released as CO and CO_2 at the graphite anode. The entire process is represented as follows:

$$Ca^{2+}(CaCl_2) + 2e^- = Ca \text{ (RE cathode)}$$

$$O(RE) + Ca = Ca^{2+}(CaCl_2) + O^{2-}(CaCl_2)$$

$$O^{2-}(CaCl_2) + C \text{ (anode)} = CO(g) + 2e^-$$

$$2O^{2-}(CaCl_2) + C \text{ (anode)} = CO_2(g) + 4e^-$$

During electrolysis, calcium is continuously produced at the cathode, and oxygen ions are discharged at the anode. There is no accumulation of oxygen in the melt, and the activity of CaO in the melt does not change during electrolysis.

In their experiments, Hirota et al. (1999) used a titanium wire mesh basket containing the rare-earth metal as the cathode and a high-purity graphite rod as the anode. The cathode was submerged in molten $CaCl_2$ electrolyte. Rare-earth metals containing more than 2000 ppm oxygen were deoxidized to a 10–50 ppm level by electrolysis at 1189 K for 10 h. There was a concurrent removal of nitrogen also (but to a lesser extent) from the rare-earth metal during the process possibly due to the formation of nitride ions:

$$N(RE) + 3e^- = N^{3-}(CaCl_2)$$

The calcium concentration of RE metals was found to increase by about 50–200 ppm from the initial value possibly due to the increase in the activity of calcium metal at the cathode. Electrochemical deoxidation is suitable for producing extremely low-oxygen RE metals in a relatively short time compared to other purification methods.

Hirota et al. (1999) also compared the new electrochemical techniques with the conventional deoxidation methods reported in the literature. Their comparison is given in Table 5.23.

Earlier, Okabe et al. (1996) have succeeded in reducing oxygen concentration in Y from 5700 ppm to below 100 ppm by the electrochemical deoxidation technique. It may be recalled that the yttrium–oxygen solid solution is the most stable among the rare earth–oxygen solid solutions. The effectiveness of the electrochemical deoxidation technique with the other rare-earth metals is apparent. The very low level of oxygen partial pressure achieved in electrochemical deoxidation is shown in Figure 5.19.

TABLE 5.23
Summary of the Results of Deoxidation of RE–O Solid Solutions by Various Processes

Sample	Method	Temperature (K)	Holding Time (h)	Oxygen Concentration (mass ppm)		Reference
				Initial	After Deoxidation	
Gd	SSE	1518	150	50	6	Peterson and Schmidt 1972
	SSE	1373	310	511	11	Jordan et al. 1975
	(Zone refining)			56	25	Fort et al. 1981
	Oxyhalide	1123	240	758	49	Corbett et al. 1986
	SSE	1303	1272	56	3	Fort et al. 1987
	Ca/CaO	1143	18	2780	2260	Kamihara et al. 1993
	Ca halide flux	1233	72	200	100	Okabe et al. 1998
	Elec. deox.	1189	10	2200	10	Hirota et al. 1999
Tb	SSE	1323	350	381	26	Jordan et al. 1975
	Ca/CaO	1143	18	1360	1520	Kamihara et al. 1993
	Ca halide flux	1118	192	540	140	Okabe et al. 1998
	Elec. deox.	1189	10	2500	20	Hirota et al. 1999
Dy	Ca/CaO	1143	18	4020	3750	Kamihara et al. 1993
	SSE	1303	750	33	13	Fort et al. 1995
	Ca halide flux	1137	168	590	140	Okabe et al. 1998
	Elec. deox.	1189	10	2300	20	Hirota et al. 1999

(*Continued*)

TABLE 5.23 (CONTINUED)
Summary of the Results of Deoxidation of RE–O Solid Solutions by Various Processes

Sample	Method	Temperature (K)	Holding Time (h)	Oxygen Concentration (mass ppm)		Reference
				Initial	After Deoxidation	
Er	Ca halide flux	1118	192	1500	170	Okabe et al. 1998
	Elec. deox.	1189	10	2900	20	Hirota et al. 1999
Y	SSE	1643	200	3379	340	Williams and Huffine 1961
	SSE	1448	190	782	90	Carlson et al. 1966
	SSE	1433	500	613	40	Volkov et al. 1981
	Oxyhalide	1004	336	3379	342	Corbett et al. 1986
	Elec. deox	1223	8	5700	50	Okabe et al. 1996
	SSE	1373	48	5100	1800	Kuroda 1997
	Ca halide flux	1118	191	9700	1150	Okabe et al. 1998
	Elec. deox.	1189	10	11,100	340	Hirota et al. 1999

Source: Hirota, K. et al., *J. Alloys Compounds*, 282, 1999.

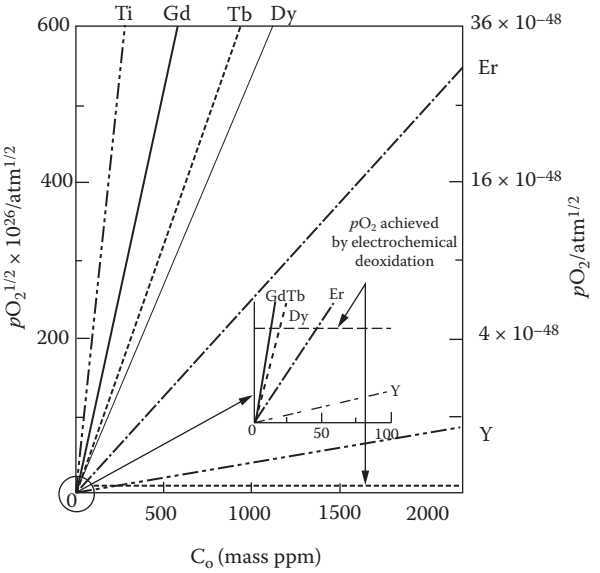


FIGURE 5.19 Sievert's law plot for rare-earth metal–oxygen solid solutions at 1173 K. (From Hirota, K. et al., *J. Alloys Compd*., 282(1–2): 101–108, 1999.)

5.13 SUMMARY

As-reduced rare-earth metals are usually 98–99%, or at best 99.5%, pure. A number of processes may be used to refine and ultrarefine these metals to as high as 99.99 at.% purity. The nature and concentration of impurity to be removed, the final purity level desired in the refined metal, and the physical properties of the metal itself determine the refining techniques to be used. Complete purification is not achieved by any one refining technique, and as a rule, a sequence of processes has to be applied to remove all the impurities.

Impurities in the as-reduced rare-earth metals originate from many sources. The most important sources are the starting materials, namely, the rare-earth compound intermediate and the reductant. Also important is the environment in which reduction is carried out, namely, the gaseous atmosphere, or the residual gases in the atmosphere if the process is conducted in a vacuum, as well as the container for reduction. Any other rare earth present in the rare earth that is currently processed is also an impurity, but the presence of such impurity rare earths in a given rare-earth metal has to be controlled in the separation stage itself before the metal reduction. The impurities originating from the starting materials are calcium, lithium, magnesium, cerium, zirconium, thorium, zinc, iron, cobalt, nickel, copper, fluorine, chlorine, and oxygen. The impurity content of the final metal is determined by the purity of the raw materials, the processes used for converting raw materials to interprocess intermediates for reduction, and the reduction process itself. The impurities oxygen, nitrogen, hydrogen, and carbon usually originate from the atmosphere in which the

processes are carried out. Crucibles for reduction come into intimate contact with the metal being reduced, undergo corrosion or dissolution, and end up as an impurity in the metal. Iron, silicon, carbon, titanium, zirconium, molybdenum, and tantalum are examples of impurities that end up in the metal this way.

There are two major methods of impurity removal from as-reduced metals. In the first type, to which most of the conventional purification techniques belong, the impurities are eliminated from the metal. In the second type, to which most of the ultrapurification techniques belong, the impurities are not completely separated from the metal but are redistributed so that one physical portion of the metal is substantially purer than the other portion. In both purification and ultrapurification, a high vacuum or UHV is used as the environment not only for preventing atmospheric impurities from coming into contact with the metal undergoing refining but also to effect removal of impurities from the metal.

Pyrovacuum treatment, in which the metal is heated to temperatures up to and above its melting point under high vacuum in a tantalum crucible, is the most important and effective means available for the purification of rare-earth metals. In vacuum melting, purification occurs because the impurities vaporize, leaving behind the purer metal. In vacuum distillation or sublimation, the metal itself is vaporized off to condense as a purer product, leaving behind impurities in the residue. The rare earths lanthanum, cerium, praseodymium, and neodymium all have very low vapor pressures, and vacuum melting and vacuum remelting complete the purification operation. In the case of gadolinium, terbium, yttrium, and lutetium, the vapor pressures are relatively higher, and vacuum melting is followed by vacuum distillation. The metals scandium, erbium, holmium, and dysprosium are more volatile and can be purified by vacuum melting followed by vacuum sublimation. In the case of the four most volatile rare-earth metals, europium, samarium, ytterbium, and thulium, no vacuum melting is done, and purification is effected exclusively by vacuum sublimation. The pyrovacuum treatments are carried out in induction- or resistance-heated furnaces using tungsten or tantalum as a container for most of the metals and also in electron beam melting furnaces for yttrium.

Electrorefining in an inert-atmosphere electrolysis cell, as a process for rare-earth-metal purification, has been applied for the purification of yttrium and gadolinium, the two metals that are most difficult to completely purify by exclusive pyrometallurgy routes. When refined in a $LiCl–YCl_3$ bath, the metallic impurities were removed, whereas refining in a $LiF–YF_3$ bath led to the removal of oxygen in addition to the metallic impurities. In the electrorefining of gadolinium, the electrolyte invariably contained GdF_3 in addition to LiF. The electrorefined metal contained less oxygen, but the final oxygen concentration is determined by the oxide and hydroxide impurities in the electrolyte.

Further removal of impurities, the bulk of which have already been eliminated in pyrovacuum treatments, is achieved by the ultrapurification techniques of zone refining and electrotransport. Zone refining is useful for bringing down the levels of metallic impurities, particularly tantalum and tungsten picked up by the metals during pyrovacuum refining. In zone refining of rare-earth metals, the use of a high vacuum or an equally pure inert atmosphere is mandatory to prevent the metal from picking up impurities from the gaseous atmosphere. Two techniques have been used. In one,

the metal is contained in a long horizontal trough or crucible, and the zone is moved in a horizontal direction. In the other, the metal is supported vertically from the ends without a container, the narrow molten zone being maintained because of the surface tension of the metal. Heating is by induction or preferably by an electron beam.

Much of the early work on zone refining was done on yttrium, but later works focused attention on lanthanum, cerium, gadolinium, and terbium. Metallic impurities such as iron, copper, cobalt, nickel, tantalum, tungsten, and aluminum are transported efficiently in the zone direction. As it is, these elements are not originally present in high concentrations. The direction of transport of oxygen, hydrogen, and nitrogen is opposite to the direction of transport of common metallic impurities. These three impurities are usually present in considerable concentration and also do not transport efficiently. As a result, no part of the zone-refined bar is of greatly improved overall purity compared to the starting metal. The ability of zone refining to refine rapidly with respect to metallic impurities, however, makes the technique useful, particularly in combination with another technique that can refine with respect to the interstitial impurities. Zone refining in combination with solid-state electrotransport enabled production of rare-earth metals with the lowest possible impurity content.

In solid-state electrotransport, a direct current is passed through a rod or strip of metal held between two electrodes in a UHV-rated container. During electrotransport, the impurities move under the influence of the electric field and, when held for sufficient time, accumulate at one end or another of the bar, leaving the remainder enhanced in purity. The electric current also heats the metal rod to near the melting point, and the high temperature enhances the impurity transport rates. The vapor pressure of the metal at the electrotransport temperature determines whether the process is carried out in UHV or under an equivalently pure inert gas cover. The technique was first applied to purify yttrium and subsequently to purify lanthanum, praseodymium, neodymium, gadolinium, terbium, erbium, lutetium, cerium, and scandium. Purification by this technique is very difficult for samarium and europium and impossible for thulium and ytterbium.

Oxygen, hydrogen, carbon, and nitrogen account for more than 95% of the impurities found in commercially obtainable rare-earth metals, and these are the elements most amenable to electrotransport purification. It is a slow process and works on relatively small samples, and only a portion of the sample is left in a highly purified condition. Zone refining is also a process of refining by impurity redistribution, particularly of substitutional impurities, and the combined zone-refining electrotransport operation finally results in only a small portion of the metal in a highly purified state with respect to all impurities. Such very high-purity metals have been invaluable for research.

Some more techniques, including iodide refining, have been attempted for rare-earth metals, but the results were unsuccessful or inconclusive. Innovative techniques to deal with stubborn oxygen impurity in rare-earth metals work by oxygen extraction by rare-earth chloride–oxychloride equilibria and electrochemical deoxidation using calcium as the active species. The sequence of vacuum melting, vacuum distillation/vacuum sublimation, zone refining, and electrotransport remains by far the most technically perfect route for the conversion of as-reduced rare-earth metals to the purest possible rare-earth metals. The technically wiser route, however, would seek to avoid, if in any way possible, the entry itself of impurity in the metal.

6 Rare-Earth Materials

6.1 INTRODUCTION

Rare earths containing end-product materials for commercial use or for research applications are numerous. A complete description of the most popular among these materials was given in the section on applications of rare earths in Chapter 1. These materials can be basically divided into two groups. One group comprises commercially used rare-earth compounds, alloys, and metals, while the other group comprises rare earth-bearing products obtained using rare-earth compounds, alloys, and metals as the interprocess intermediates. This chapter focuses on the preparation of the commercially used rare-earth compounds, alloys, and metals. Several materials, for example, rare-earth compounds such as the chloride, hydroxide, fluoride, oxide, and carbonates, figure as intermediates obtained during routine ore processing or by processes branched readily from the regular flow sheet. The preparation of these compounds was therefore included in the chapter on resource processing. Preparation of elemental rare earths was covered in the preceding two chapters, which also included certain references to the preparation of rare-earth alloys, either because the processes used were very similar or because the alloys were interprocess intermediates for the preparation of pure metals.

The materials covered in this chapter are specific specialty alloys of rare earths, starting from misch metal and including rare earth–iron–silicon alloys, yttrium–aluminum alloys, lanthanum–nickel alloys, permanent magnet materials based on samarium and neodymium, and magnetostrictive and magnetocaloric materials. Many rare-earth compounds have emerged as special performance materials in a range of new technology areas. Their preparative aspects have also been described.

6.2 MISCH METAL

Misch metal is the material containing, in metallic form, the mixed light rare earths in the same or slightly modified ratio as found in the minerals monazite and bastnasite. The composition of the misch metal depends on the source from which it is derived. Misch metal obtained from monazite is relatively high in neodymium and praseodymium, whereas the misch metal from bastnasite is high in lanthanum but low in neodymium and praseodymium.

Traditionally, monazite was the source of rare earths (Morrice and Knickerbocker 1961). In the 1890s, monazite was processed for the extraction of thorium as thorium nitrate, which was used in Auer gas mantles. The residue after thorium extraction contained cerium, lanthanum, neodymium, praseodymium, and other rare-earth compounds in minor amounts and was discarded. Auer Von Welsbach discovered that a pyrophoric metal (misch metal) could be prepared from this residue. In 1908, he founded the Treibacher Chemical Works in Austria and started commercial

production of misch metal. The pyrophoric properties of misch metal was used in making lighter flints. Soon, monazite was processed principally as a source for misch metal. Starting in 1949, when a large bastnasite deposit was discovered in Mountain Pass, California, bastnasite was also processed as a source for misch metal. Presently, misch metal is obtained from both monazite and bastnasite sources. The processes used are fused salt electrolysis or thermal reduction. More recently, the declining use of monazite as a rare earth resource point to the predominant availability of bastnasite derived misch metal.

Misch metal is commercially produced in tonnage quantities principally by fused salt electrolysis of anhydrous chlorides (Hirschhorn 1968). Specific details of these commercial operations are seldom revealed, but several descriptions of procedures and equipment have been published. Recent regulations in China (the predominant producer) do not permit the use of chloride electrolysis (Schuler et al. 2011) and insist that fluoride electrolytes must be used.

6.2.1 Preparation of Mixed Rare-Earth Chlorides

Commercially, misch metal is produced from mixed rare-earth chloride, $RECl_3$. In the past, all of mixed rare-earth chloride was obtained by wet chemical treatment of monazite and bastnasite in the form of a hydrated product. This hydrated product contained about 30% H_2O and was treated to yield an anhydrous product with low oxychloride content for electrowinning. Dehydration was accomplished using methods that minimize oxidation and hydrolysis.

Typically, dehydration techniques involved the use of vacuum heating of hydrated mixed rare-earth chloride or heating them in air with an admixture of certain non-rare-earth salts. The additives were meant to reduce hydrolysis. During World War II, one supplier to the German misch metal industry (the Auergesellschaft in Berlin) used rotary iron vacuum drum dryers that were steam-heated to 350°C at a vacuum level of 93×10^3 Pa. The anhydrous chloride was reported to contain 1.5% oxychlorides (Livingston and Kent 1946).

In another method, the chloride was melted in a cast iron, steel, or ceramic vessel from which air was largely excluded (Kremers 1954). Heating was carried on until a porous, solid, nearly anhydrous product was obtained. The product had up to 10% of water-insoluble basic chloride content.

Heating a mixture of rare-earth chloride with $CaCl_2$ in air for 2 to 2 1/2 h was practiced at Prometheus in Bavaria (Hirschhorn 1968). The yield was usually 62%. This indicates that there was obviously substantial oxychloride content in the product. A two-stage vacuum-drying process was used at Treibacher Chemische Werke in Austria. The hydrate was heated first at 170°C and then at 350°C (Livingston and Kent 1946).

In certain commercially adopted dehydration procedures (Hirschhorn 1968), ammonium chloride was added to the hydrated chloride to reverse the hydrolysis, according to the following reactions:

$$RECl_3 + 3H_2O \rightarrow RE(OH)_3 + 3HCl$$

$$RE(OH)_3 + 3NH_4Cl \rightarrow RECl_3 + 3NH_3 + 3H_2O$$

In industrial practice, to carry out dehydration, $RECl_3 \cdot 6H_2O$ was quickly heated to 400–500°C with NH_4Cl in an inert atmosphere.

Some producers used sodium or calcium chloride to retard hydrolysis on the basis of the common chloride ion mass action effect. The addition of NaCl and/or $CaCl_2$ to the electrolyte was usually desirable, and their incorporation into the feed during dehydration was convenient.

Apart from the route that involves preparation of a hydrated chloride and its subsequent dehydration, there are other processes for obtaining the anhydrous chlorides directly from the mineral. Th. Goldschmidt AG at Essen in Germany used chlorination of monazite or bastnasite to produce anhydrous rare-earth chlorides (Brugger and Greinacher 1967). The product is suitable, without any further processing, for electrolysis to misch metal. The analysis of this chloride (Hirschhorn 1967) is given in Table 6.1 along with the analysis of chlorides from the wet processing of both monazite and bastnasite.

TABLE 6.1
Typical Analysis of Rare-Earth Chlorides

Component	Hydrated Chloride from Monazite	Hydrated Chloride from Bastnasite	Anhydrous Chloride from Chlorination of Bastnasite
Total RE oxide[a]	46.2	46.0	66
CeO_2	47.6	50.3	49.1
Pr_6O_{11}	5.0	4.2	4.7
Nd_2O_3	17.3	11.2	12.7
Sm_2O_3	2.9	1.3	1.6
La_2O_3 and other RE oxides	27.1	32.8	29.5
H_2O	28.5	29.0	0.5
Fe_2O_3	0.04	0.002	<0.01
P_2O_5	<0.04	<0.03	<0.01
Na_2O	0.1	0.15	0.16
MgO	0.1	0.1	0.09
CaO	0.9	0.19	1.3
SrO		0.2	0.3
BaO		0.24	1.1
Insoluble residue	0.05	0.04	5.4[b]

Source: Hirschhorn, I.S., Commercial production of rare earth metals by fused salt electrolysis. In Koehler, W.C. (ed.), *Proc. 6th Rare Earth Research Conf.*, May 3–5, 1965, Gatlinberg, TN, Available on Report AFOSR–67–1214, National Technical Information Service, Springfield, Virginia, pp. 728–738, 1967.

[a] The individual REO contents are given as the percentage of total REO present. The contents of other components are in percentage.

[b] Mainly rare-earth fluoride.

6.2.2 Electrolysis of Chlorides

Two types of cells have been used for the production of misch metal by chloride electrolysis (Singer et al. 1945; Livingston and Kent 1946). Details of these cells are given in Figures 6.1 and 6.2 and listed in Table 6.2.

The cells shown in Figure 6.1 are ceramic cells. The container for the molten electrolyte and for the molten misch metal cathode is made of firebrick. The electrical connection to the cathode was given through two water-cooled steel blocks inserted in the cell walls. The anode was 50 cm in diameter and 1 m long and was made of

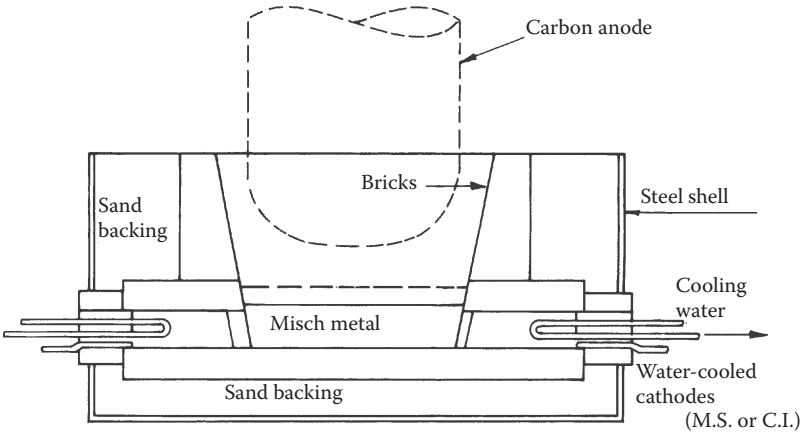


FIGURE 6.1 Electrolysis cell at Treibacher Chemische Werke, Austria. M.S., mild steel; C.I., cast iron. (From Morrice, E. and Wong, M.M., *Minerals Science and Engineering*, 11(3): 125–136, 1979.)

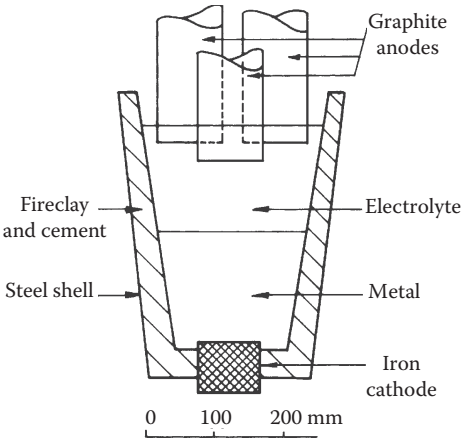


FIGURE 6.2 Electrolysis cell at Prometheus, Bavaria. (From Hirschhorn, I.S., Commercial production of rare earth metals by fused salt electrolysis. In Koehler, W.C. (ed.), *Proc. 6th Rare Earth Research Conf.*, May 3–5, 1965, Gatlinberg, TN, Available on Report AFOSR–67–1214, National Technical Information Service, Springfield, Virginia, pp. 728–738, 1967.)

TABLE 6.2
Characteristics of Some Fused Salt Electrolytic Cells for Preparation of Misch Metal

	Treibacher Cell	Prometheus Cell
Electrolyte	$RECl_3$–NaCl	$RECl_3$–$CaCl_2$
Anode	Carbon	Graphite
Cathode	Iron	Iron
Bath temperature (°C)	850	850
Cell atmosphere	Cell gases + air	Cell gases + air
Average DC current (A)	2300	1500
Average DC voltage (V)	14	12
DC power consumption (kWh/kg)	15.6	13.6
Current efficiency (%)	45	50
$RECl_3$/Metal ratio	2.3	2.8
Capacity (kg metal/h)	1.86	1.32

Source: Hirschhorn, I.S., Commercial production of rare earth metals by fused salt electrolysis. In Koehler, W.C. (ed.), *Proc. 6th Rare Earth Research Conf.*, May 3–5, 1965, Gatlinberg, TN, Available on Report AFOSR–67–1214, National Technical Information Service, Springfield, Virginia, pp. 728–738, 1967.

amorphous carbon. The anode could be raised and lowered into the electrolyte. The cells were usually operated in series to facilitate semicontinuous production. Molten electrolyte was transferred from one cell to another for rapid start-up. During operation, misch metal collected at the bottom of the cell where it was kept in the molten state by the flow of direct current (DC) through it to the cathode. At suitable intervals, the metal that was covered with a layer of molten electrolyte was ladled out and poured into molds. The metal solidified in the mold under the protective layer of electrolyte. After cooling, the solidified electrolyte was broken off, and the metal was separated and washed.

The cell shown in Figure 6.2 also has a refractory lined steel vessel to contain the molten bath (Hirschhorn 1967). The cathode was an iron block at the bottom of the container. Several graphite rods extended vertically into the cell through its top and served as anodes. Unlike the cell shown in Figure 6.1, the cell in Figure 6.2 was tiltable (Livingston and Kent 1946). This arrangement simplified pouring of the product into molds.

Contamination of the product, misch metal, due to iron and silica could be decreased by constructing cells of graphite. When misch metal contaminated with iron was acceptable, as for example, misch metal for ferrous alloy applications, iron pots could be used instead of graphite (Greinacher 1970).

Before electrolysis, a mixture of anhydrous rare-earth chloride, NaCl, KCl, or $CaCl_2$, was charged into the pot. In one procedure, the charge was melted by external burners. In another procedure, the anodes were lowered into the cell until they contacted broken pieces of cerium kept at the bottom of the pot. The solid bath constituents were then packed around the bottom of the anodes. DC was turned on, and after

sufficient electrolyte had melted, the anodes were raised to begin electrolysis. The bath temperature was raised to 800–900°C by passage of electric current. During electrolysis, additional external heating was not required.

The cells could be enclosed by steel covers to exclude air and thus decrease gas content in the misch metal produced. The gaseous products of electrolysis, mainly chlorine mixed with gaseous carbon compounds, were drawn off and treated by absorption in a suitable off-gas treatment system to decrease air pollution.

The electrolysis was usually continued as long as the current efficiency remained high and metal quality was satisfactory. Generally, the current efficiencies of the commercial cells described for misch metal production are low. This is in part due to the energy consumption for maintenance of cell temperature and also due to the accumulation of compounds of samarium, europium, and other nonreducible rare-earth compounds in the electrolyte (Hirschhorn 1967). The product was collected at the bottom of the cell where it could be maintained in the molten state by resistance heating or allowed to solidify by using a cooled cathode. In the latter case, the solidified metal was melted again by internal resistance heating, supplemented, if needed, by an external source of heat before it was removed from the cell. The misch metal was recovered from the cell in many ways. One was to scoop the liquid metal with a ladle. The other was to pour the entire contents of the cell, electrolyte bath included, into molds in which it was kept molten. After the misch metal had settled to the bottom of the mold, the liquid bath was returned to the electrowinning cell and the electrolysis was started again. The analysis of misch metal commercially produced by chloride electrolysis is given in Table 6.3.

Commercial misch metal was produced primarily by chloride electrolysis. In the United States and Japan (Kudo 1988; Thomas 1977), and now in China also, an oxide feed to the electrolytic cell and a mixed fluoride electrolyte were used. This procedure was developed by the US Bureau of Mines (USBM) at the Reno Metallurgy Research Center. The USBM process of electrowinning misch metal directly from mixed rare-earth oxides (REOs) dissolved in a fluoride electrolyte was adopted by the Rare Earth Metal Corp. of America, a joint venture of Alcoa and Molycorp in the United States and by Santoku Metal Industry Co. in Japan. As early as in 1977, the Rare Earth Metal Corp. successfully completed operation of a pilot electrolytic cell using mixed REO and began construction of a 20,000 amp cell for a production rate of about 100,000 kg of misch metal per year. Santoku switched over from chloride electrolysis to the USBM process and operates several 20,000 amp cells for misch metal production (Thomas 1977).

6.2.3 Electrolysis of Oxide–Fluoride Melts

The electrolysis of a mixed REO feed obtained by processing of bastnasite concentrate in a REF_3–LiF–BaF_2 electrolyte was investigated at the Reno Center of the US Bureau of Mines for preparing misch metal (Shedd et al. 1970). The process was carried out in a 300-mm-diameter cell for continuous electrolysis, shown in Figure 6.3.

The cell had a 300 mm inside diameter with a 50-mm-diameter molybdenum cathode surrounded by eight 50-mm-diameter graphite rod anodes. The spacing between the cathode and anode was 65 mm. The feed material was added to the cell

TABLE 6.3
Analysis of Commercially Produced Misch Metal

Element	Content in MM (%)
Ce	53
La	23
Nd	16
Pr	5
Dy	Trace
Gd	2
Y	Trace
Other RE	Not detected
Cr	0.034
Fe	0.035
Mg	0.032
Mn	0.006
Si	0.010
C	0.008
O	0.002
N	0.003

Source: Hirschhorn, I.S., Commercial production of rare earth metals by fused salt electrolysis. In Koehler, W.C. (ed.), *Proc. 6th Rare Earth Research Conf.*, May 3–5, 1965, Gatlinberg, TN, Available on Report AFOSR–67–1214, National Technical Information Service, Springfield, Virginia, pp. 728–738, 1967.

through a 25-mm-diameter tube positioned between two anodes. A molybdenum crucible was placed below the cathode to collect the misch metal product. A molybdenum pipe attached to the molybdenum collecting crucible extended out of the cell 760 mm into a casting chamber where a mold was kept to collect the molten misch metal.

The cell was internally heated. Initial melting of the bath and heating to electrolysis temperature were done by applying alternating current (AC) to a graphite resistor positioned between the cathode and the two anodes. Once the electrolyte reached 950°C, the resistor was removed and the DC used for electrolysis provided sufficient heat to maintain the cell at 950°C.

The cell was insulated by refractory bricks and was enclosed in a gas-tight steel chamber, 1220 mm in diameter and 1220 mm long. The chamber was equipped with a glove and view and access ports. It was evacuated and back-filled with helium four times before the start of each operation.

The feed material for electrolysis was derived from bastnasite. It was prepared as follows. The bastnasite concentrate was leached with dilute hydrochloric acid to

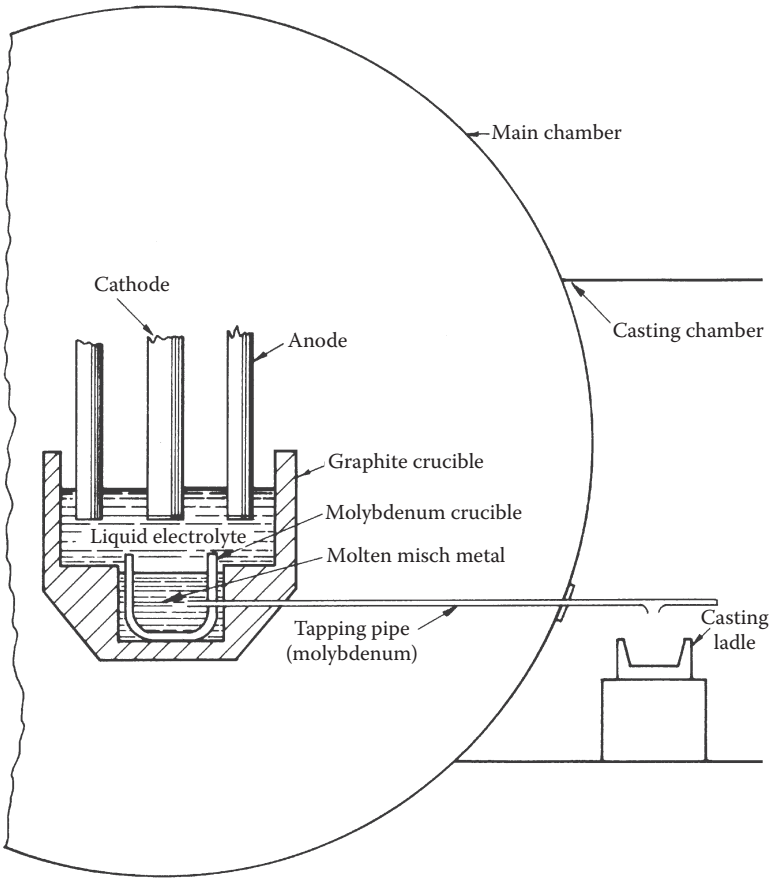


FIGURE 6.3 Electrolytic cell with provision for tapping metal product. (From Shedd, E.S. et al., Electrowinning misch metal from a treated bastnasite concentrate, Bureau of Mines Report of Investigations 7398, U.S. Department of the Interior, Washington, DC, 1970.)

remove $CaCO_3$ and $SrCO_3$. The leach residue was roasted with Na_2CO_3 at 700°C to convert the barite impurity to $BaCO_3$ and to decompose the carbonate. The material was then leached in water to remove Na_2SO_4 and dried at 400°C. The bastnasite concentrate thus treated was a mixture of oxides with a small amount of fluorides. The analysis is given in Table 6.4.

The electrolyte was composed of REF_3, LiF (99.6% pure), and BaF_2 (98.2% pure). The mixed rare-earth fluoride was prepared from the treated bastnasite concentrate by hydrofluorination. The oxygen content of the fluoride was 0.64% and the sulfur content was 0.04%. All the electrolyte components were dried at 300°C for 24 h before use. Based on preliminary experiments in a 75-mm-diameter experimental cell, Shedd et al. (1970) chose an electrolyte containing 50% REF_3, 20% BaF_2, and 30% LiF. Forty-five kilograms of electrolyte was used. The cell-operating data are listed in Table 6.5. The cell was maintained at the operating temperature throughout

TABLE 6.4
Analysis of Treated Bastnasite Concentrate

Element	Content (%)
Ba	4.7
Ca	0.3
C	0.6
Ce	42.3
Eu	Not detected
F	2.0
Gd	0.01
Fe	0.7
La	23.9
Nd	9.8
Pr	3.2
Sm	0.6
Si	1.0
S	0.07
Th	Not detected
Y	0.2

Source: Shedd, E.S. et al., Electrowinning misch metal from a treated bastnasite concentrate, Bureau of Mines Report of Investigations 7398, U.S. Department of the Interior, Washington, DC, 1970.

the duration of electrolysis during which many electrodepositions were carried out. At times when electrolysis was not conducted, the electrolyte was kept molten by passing AC through the electrodes.

After electrolysis, the metal product was tapped. To tap the metal, the cathode was raised out of the electrolyte, and an AC of 1500 A at 9 V was passed between the anode and the molybdenum tapping pipe. Metal flowing from the pipe was collected in the iron mold in the casting chamber. Tapping lasted until all the metal had drained and electrolyte began to flow through the pipe. The AC was then turned off, and the electrolyte was allowed to freeze in the tapping pipe. The analysis of the tapped metal is also given in Table 6.5.

Shedd et al. (1970) noted that several electrodepositions could be conducted in the electrolyte, and the electrolyte system would sustain prolonged use if periodic additions of salts were made to readjust the electrolyte composition.

Even though misch metal is commercially prepared by the fused salt electrolysis methods described above, and the product is suitable for most of its applications such as alloying additive for ductile iron and steels and as a lighter flint, there are a number of applications where misch metal can be potentially useful as a replacement for the relatively more expensive individual rare-earth metals, and a purer misch metal

TABLE 6.5
Data for Operation of Electrowinning and Tapping of Misch Metal

Electrolyte composition (%)	50 REF_3–20 BaF_2–30 LiF
Temperature (°C)	950
Anode	50-mm-diameter graphite rods, 8 nos.
Cathode	50-mm-diameter molybdenum rod, 1 no.
Average voltage (V)	8,5
Current (A)	980
Initial anode current density (A/cm^2)	1.04
Cathode current density (A/cm^2)	8.32
Treated bastnasite concentrate fed (g)	8630[a]
Feed rate of treated bastnasite concentrate (g/min)	14.4
Duration of electrolysis (h)	10
Misch metal product (g)	6359
Current efficiency (%)	37
REO utilization (%)	98

Analysis of Tapped Misch Metal Product

Element	Al	C	Fe	Mo	O	Si	S	Ce
Content (%)	0.17	0.15	0.56	0.38	0.02	0.20	0.005	60.0
Element	La	Nd	Pr	Sm, Gd, Y, Th				
Content (%)	18.4	15.2	6.0	not detected				

Source: Shedd, E.S. et al., Electrowinning misch metal from a treated bastnasite concentrate, Bureau of Mines Report of Investigations 7398, U.S. Department of the Interior, Washington, DC, 1970.

[a] Contained rare-earth value as RE_2O_3 6481 g.

is desirable. A method based on metallothermic reduction of the fluoride has been described by Palmer et al. (1982) of the Ames group for preparation of pure misch metal.

6.2.4 Ames Process

The flow sheet for the production of pure misch metal starting from mixed rare-earth carbonate obtained from bastnasite or monazite processing (Palmer et al. 1982) is shown in Figure 6.4. The term *purity* here refers to the absence of the non-rare-earth elements in this mixed rare-earth alloy. The purity in the product was achieved by using purified start materials. As-received mixed rare-earth carbonates from bastnasite and monazite origin were first purified by dissolution in HCl and precipitation of the rare earths as oxalate. The oxalate was calcined to the oxide in fused silica trays. This treatment brought down the levels of almost all the impurities originally present in the rare-earth carbonate and resulted in purer mixed REO. The values are given in Table 6.6.

Oxalate precipitation is a well-known analytical procedure to recover pure rare earths from solution. Along with thorium and the alkaline earths, calcium, strontium,

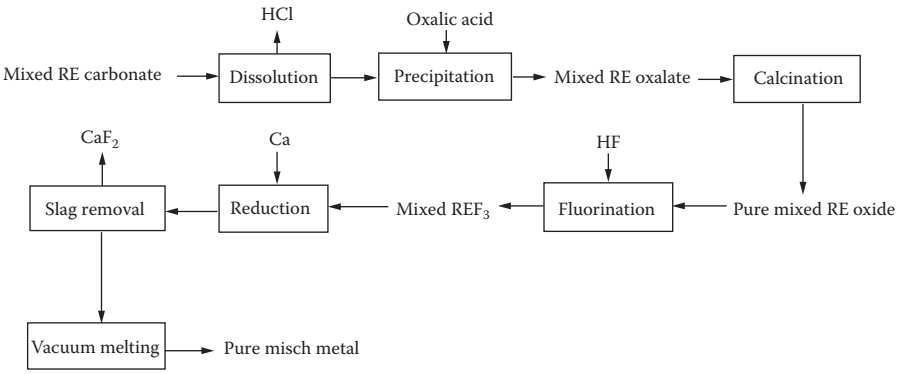


FIGURE 6.4 Flow sheet for the preparation of pure misch metal.

TABLE 6.6
Analyses of REO from Bastnasite and Monazite before and after Purification

	Bastnasite		Monazite	
Impurity	**As-Received**	**Purified**	**As-Received**	**Purified**
Si	50	7	20	<2
Ca	22,000	1400	820	100
Mn	3	<0.5	1000	1
Fe	500	20	400	20
Cu	800	<0.1	400	<0.1
Zn	60	<2	60	<1
Sr	7000	20	2	<2
Ba	200	<0.4	10	<0.4
Th	6.5	<4	120	50
U	1.4	<0.2	100	6

Source: Palmer, P.E. et al., *J. Less Common Metals*, 87: 135–148, 1982.

and barium, the rare earths also form the most insoluble oxalates. Oxalates of most of the non-rare-earth metals are not precipitated from dilute acid solutions. As a result, oxalate precipitation, using oxalic acid, leads to complete partition between the rare earths on the one hand and silicon, manganese, iron, copper, and zinc on the other (Palmer et al. 1982). Use of strongly acidic media will result in some calcium, strontium, barium, thorium, and uranium being left behind in the aqueous phase.

The oxides were converted to fluorides in 300 g batches. The oxide loaded in a platinum tray was heated to 650°C under a flow of 8 L/h anhydrous HF and 20 L/h argon for 24 h. The fluorides were then reduced with high-purity calcium in tantalum crucibles as described in Chapter 4 for metal preparation. From the reduced mass, CaF_2 slag was removed and the misch metal was vacuum-melted at 1000°C. The misch metal thus obtained contained H 1 ppm, C < 10 ppm, N < 6 ppm, and O ≤ 30 ppm. The

residual fluorine content varied from ~60 to ~250 ppm. Vacuum melting at 1700°C, instead of 1000°C, brought down the residual fluorine content drastically to ~10 ppm.

As regards the composition of the misch metal with respect to constituent rare earths, Palmer et al. (1982) anticipated and also observed certain composition changes between the mixed REO/fluoride, the as-reduced metal, and the vacuum cast metal. In the reduction step, the samarium trifluoride SmF_3 will at best reduce to SmF_2, and this very stable difluoride will remain with CaF_2 slag. Samarium metal is thus lost as it does not end up in the misch metal. Even in the electrolytic production of misch metal, samarium content in the mixed rare-earth-chloride feed was found to concentrate in the slag, and this slag, incidentally, was one of the prime sources of samarium for use in $SmCo_5$ permanent magnets. Another significant composition change, regarding the proportion of the various rare-earth metals in misch metal, occurs during vacuum melting. Vacuum melting at 1700°C leads to the loss of a quarter to half of the neodymium contained in the as-reduced or 1000°C vacuum cast metal. The analysis of misch metals prepared at Ames and commercially available from Ronson are listed in Table 6.7 (Palmer et al. 1982).

The Ames experiment of thermal reduction as a method for preparation of misch metal is the second, highly refined, implementation of the process. The first attempt was made by Decroly et al. (1953) in Brussels, Belgium in 1952 using a thermite-type reaction.

6.2.5 Thermal Reduction Process

Starting from mixed REOs prepared by processing of bastnasite and monazite ores from the Belgian Congo, Decroly et al. (1953) at the University of Brussels prepared mixed rare-earth fluoride and reduced it by calcium to misch metal.

The mixed oxide was converted to fluoride by using ammonium bifluoride. The reaction was carried out in the apparatus shown in Figure 6.5. An intimate mixture of REO and excess ammonium bifluoride was loaded in a crucible made of aluminum but lined on the inside with slightly sintered CaF_2. The crucible was placed in an electric furnace, and a copper or aluminum collector was put over the crucible to recover the gases that evolved in the reaction. The collector was connected with a silica tube where some volatilized ammonium bifluoride could be condensed and recovered. The charge was heated at 150°C for several hours, and a solid double fluoride product was obtained.

$$RE_2O_3 + 4NH_4HF \rightarrow 2REF_3{\cdot}NH_4F + 2NH_3 + 3H_2O$$

In the second step, the double fluoride was decomposed by heating to 400°C.

$$REF_3{\cdot}NH_4F \rightarrow REF_3 + NH_4F$$

The decomposition was carried out in the apparatus shown in Figure 6.6. A silica tube placed in an electric furnace was the decomposition vessel. This vessel was connected to another silica tube by a rubber connection. The second tube was cooled by a copper coil in which water was circulated. To sweep away the ammonium fluoride

TABLE 6.7
Composition (at.%) of Various Misch Metals

Source	Vacuum Casting Temperature (°C)	La	Ce	Pr	Nd	Sm	Gd	Y	Fe	Mg	Si	C	N	O	F
Monazite	1000	20.1	49.7	6.4	20.4	<0.5	1.8	1.6	0.009	<0.0001	<0.0001	7	4	21	86
Monazite	1700	22.5	52.2	6.2	15.5	<0.5	2.0	1.6	0.008	<0.0001	<0.0001	7	6	22	8
Bastnasite	1000	39.8	37.5	6.2	16.5	<0.5	<0.2	<0.05	0.006	<0.0001	<0.0001	23	1	15	132
Bastnasite	1700	42.1	40.8	6.5	10.6	<0.5	<0.2	<0.05	0.006	<0.0001	<0.0001	<2	3	29	13
Ronson	As-received	23.6	54.4	5.4	12.1	0.5	0.4	0.1	4.3	2.8	0.2				
Ronson	1700	24.4	53.3	5.3	11.9	0.5	0.4	0.1	2.6	0.01	0.2	13	55	740	20

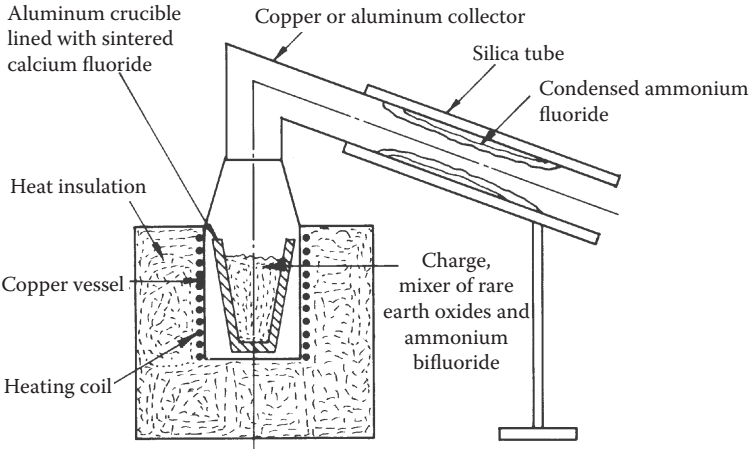


FIGURE 6.5 Apparatus for the fluorination of mixed REO. (From Decroly, C. et al., *J. Electrochem. Soc.*, 100: 388–391, 1953.)

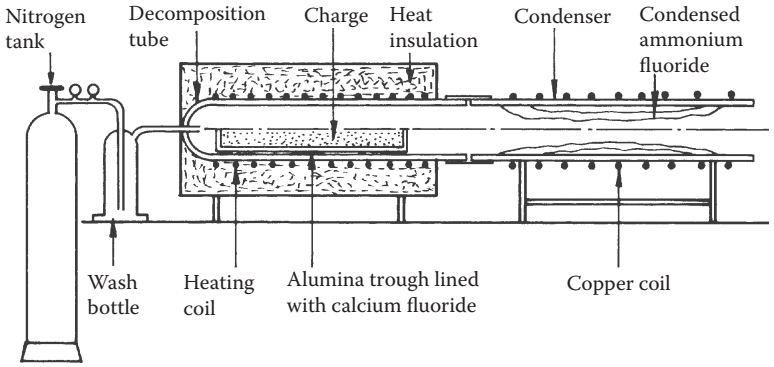


FIGURE 6.6 Apparatus for the decomposition of ammonium rare-earth double fluoride. (From Decroly, C. et al., *J. Electrochem. Soc.*, 100: 388–391, 1953.)

vapors and to keep an inert atmosphere in the reactor, dry nitrogen was introduced into the decomposition vessel. Ammonium fluoride collected in the condensation tube and was easily recovered.

The double fluoride was loaded in a calcium fluoride-lined alumina trough, and the trough was placed in the decomposition vessel. Keeping a nitrogen flow, the temperature was raised to 400°C. The double fluoride decomposed. The decomposition of 1000 g of double fluoride took 10–12 h. The completion of the double fluoride decomposition was checked by determining the nitrogen content of the residue, and decomposition was considered complete when the nitrogen content was 10 ppm. Chemical analysis for fluorine confirmed the quantitative formation of rare-earth trifluoride.

Calcium was used as the reducing agent for the mixed rare-earth trifluorides, but the heat available from the heat of reaction alone for $2REF_3 + 3Ca \rightarrow 2RE + 3CaF_2$

was not sufficient to heat and melt the reduced metals and slag in a typical thermit-type reduction. The use of iodine as booster was necessary.

The apparatus used by Decroly et al. (1953) to carry out the reduction of mixed rare-earth fluoride with calcium is shown schematically in Figure 6.7. It comprised a steel pot with a removable lid. To obtain air tightness when the lid was closed, a water-cooled circular rubber gasket was used. This gasket was placed in a circular trough welded at the top of the steel pot. The wall of the reaction chamber was made of packed CaF_2 powder, and the chamber was conical in shape. At the bottom of this chamber was a cylindrical crucible of sintered CaF_2. An electric heating coil provided in the pot was used for drying the lining and crucible. The use of pure calcium fluoride as refractory material eliminated the possibility of contamination of the produced metal except by elements already present in the charge.

The reaction mixture had 150 g of mixed fluorides, 70 g of iodine, and an amount of calcium chips 15% in excess of the quantity theoretically needed to reduce the fluorides and combine with iodine. After loading this mixture, the reaction was started by a burning magnesium ribbon. The reaction proceeded very smoothly and lasted only a few seconds. When the reduction was through, the vessel was closed with the lid, which had a tube that allowed pumping off all the air present in the reactor and replacing it with pure argon. The product was cooled under a positive pressure of argon. After cooling, the slag was easily separated, and the metal collected in the lower crucible as a small ingot, which was recovered.

The analysis of the misch metal obtained is given in Table 6.8. It was not quite pure but good enough for preparing pyrophoric alloy. Even in the small-scale experiments, the yield of misch metal was 78–80%.

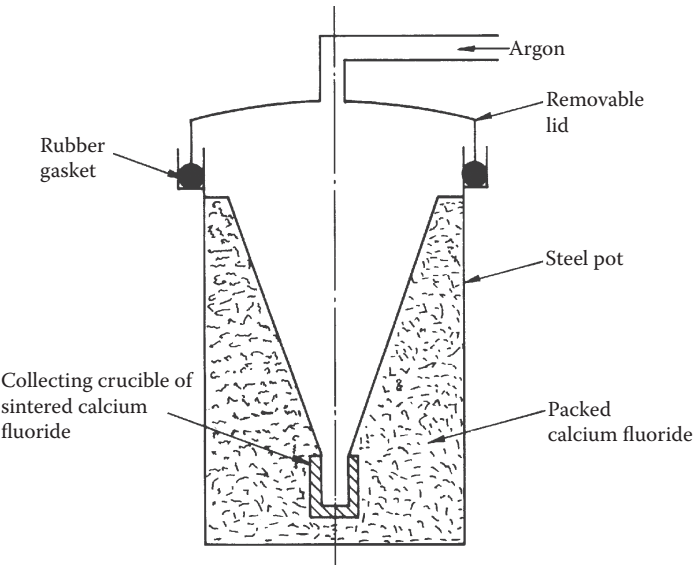


FIGURE 6.7 Apparatus for thermit-type reduction of rare-earth trifluoride by calcium. (From Decroly, C. et al., *J. Electrochem. Soc.*, 100: 388–391, 1953.)

TABLE 6.8
Analysis of Misch Metal Prepared by Thermit Reduction

Element	Content (%)
RE metals	98.2[a]
Ca	0.32
Si	0.09
Fe	1.04
Cu	0.28
Not determined	0.07

Source: Decroly, C. et al., *J. Electrochem. Soc.*, 100: 388–391, 1953.

[a] 47.9% Ce, 50.3% La, Nd, etc.

6.3 RARE EARTH–SILICON–IRON ALLOYS

Rare earths are added to steel mostly in the form of rare earth–silicon–iron alloy or as misch metal. The alloy is often preferred over misch metal because of its low cost.

Commercially, the rare earth–silicon–iron alloy is prepared by carbothermic reduction of a mixture of rare-earth compounds, silica, and iron at above 1930°C (Staggers 1977). An alloy composed of misch metal, silicon, and iron in approximately equal proportions by mass, was obtained in a submerged electric arc furnace by the direct reduction of bastnasite ore concentrate, iron ore, and quartz. In the commercial production process, the rare-earth recovery is not more than 60%.

Many other techniques have been reported (Marchant et al. 1980) for the preparation of rare earth–silicon–iron alloys. They rely on the use of calcium–silicon (~30% Ca) alloy or calcium silicide as reducing agents for mixed REOs prepared from monazite or bastnasite sources. Many variations of the reduction technique have been patented. In one, up to 50% of the calcium–silicon alloy was replaced by either calcium or silicon (Krismer and Smetana 1968). Calcium carbide was also used as a partial replacement of the calcium–silicon alloy (Kallenbach and Bungardt 1969). In yet another process, mixed REOs were reduced with calcium silicide at 1500°C, and iron scrap was added to the molten charge to get a product containing 30% RE, 29% Si, 40% Fe, and 1% Ca (Hirschhorn and Klein 1969). The use of calcium silicide, ferrosilicon, silicon, and aluminum as reductants for mixed REOs prepared from bastnasite flotation concentrate was investigated at the Reno Center of USBM to obtain rare earth–silicon–iron–aluminum alloys (Marchant et al. 1980).

6.3.1 Reno (USBM) Process

The flow sheet of the process is shown schematically in Figure 6.8. The start materials were mixed rare-earth oxide, aluminum turnings, and ferrosilicon. The mixed

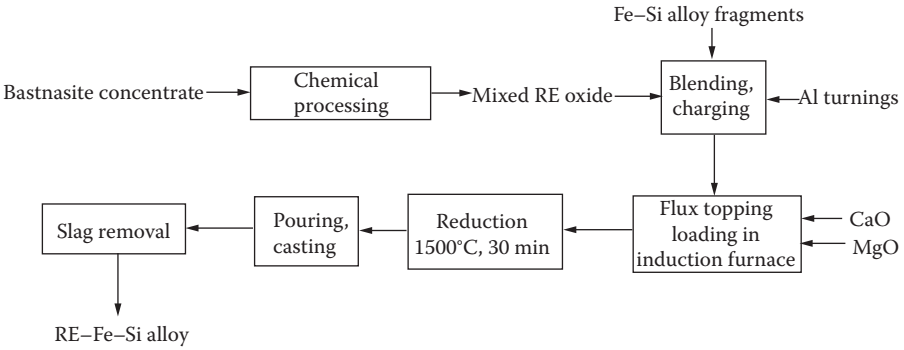


FIGURE 6.8 Schematic flow sheet for the preparation of rare earth–iron–silicon alloy.

REO was a commercially available leached and calcined bastnasite concentrate (78.6% TREO: 40.5 Ce, 25.1 La, 9.3 Nd, 3.25 Pr, and <0.4% other REOs). The ferrosilicon was also a commercially available product with a nominal composition of 25% Fe–75% Si. The reduction procedure involved blending the mixed REO with aluminum turnings and 6 mm pieces of ferrosilicon and loading the mixture in a densified silicon carbide crucible. A flux of lime (CaO) and magnesia (MgO) was added on top of the reduction charge. The flux was necessary, because if it were absent, a significant amount of rare earth–silicon–iron alloy became entrapped in a viscous slag. As a result, complete separation of slag from the alloy became difficult when attempts were made to pour the molten product. The reduction was carried out in an induction furnace. The charge and flux were melted and held at 1500°C for 30 min to complete the reaction. The melt was then poured into an iron mold. The rare earth–silicon–iron alloy was recovered by allowing the melt to freeze and breaking the slag away. The product analysis is given in Table 6.9.

The following reactions were also investigated by Marchant et al. (1980) for preparing rare earth–silicon, rare earth–silicon–aluminum, and rare earth–silicon–aluminum–iron alloys.

$$RE_2O_3 + 3CaSi_2 \rightarrow 2RESi_2 + 2Si + 3CaO$$

$$2RE_2O_3 + 11Si \rightarrow 4RESi_2 + 3SiO_2$$

The use of ferrosilicon in place of silicon resulted in iron reporting to the alloy product. The rare-earth recovery was highest (98%) when 120% of the stoichiometric amount of calcium silicide was used. For industrial use, calcium silicide is not very suitable because of its limited availability and high cost. The rare-earth recovery in the alloy was very low (~40%) when silicon or ferrosilicon was used even at 120% of the stoichiometric amount. The use of aluminum in addition to silicon or ferrosilicon improved the rare-earth recovery to ~70%; however, ~600% of the stoichiometric amount of aluminum had to be used.

$$3RE_2O_3 + 15Si + 2Al \rightarrow 6RESi_2 + 3SiO_2 + Al_2O_3$$

TABLE 6.9
Results for Ferrosilicon–Aluminum Reduction of Mixed REO in an Induction-Heated Reactor

Charge weight (g)	1170
Reactants	
Mixed REO (g)	681
Fe–78 Si alloy (g)	309
Aluminum	182
Flux	
CaO (g)	681
MgO (g)	45
Alloy product weight (g)	812
Slag weight (g)	1100

Analysis

Alloy			Slag	
Components	**Content (wt.%)**	**Recovery (%)**	**Component**	**Content (wt.%)**
RE	52.6	80	RE_2O_3	12.7
Si	27.6	93	SiO_2	4.7
Fe	10.7	85	FeO	1.2
Al	3.8	16	Al_2O_3	28.9
Ca	5.0		CaO	49.3
P	0.05		MgO	2.3
S	0.003		P	0.15
O	0.28		S	0.24

Source: Marchant, J.D. et al., Preparing rare earth–silicon–iron–aluminum alloys, Bureau of Mines Report of Investigations 8445, U.S. Department of the Interior, Washington, DC, 1980.

The resulting alloy contained ~18% aluminum. When silicon was used in the above reaction, the product was a rare earth–silicon–aluminum alloy. The rare earth–silicon–aluminum alloy disintegrates into powder even after a short time exposure to air. On the other hand, when ferrosilicon was used in place of silicon, the resulting rare earth–silicon–aluminum–iron alloys remained stable in air. The rare-earth alloy in the disintegrated form would be undesirable as a ladle addition because of dusting problem.

The major advantages of the USBM process are the higher rare-earth content in their alloy product (53% RE, 28% Si, 11% Fe, and 4% Al) and higher (80%) rare-earth recovery. This compares favorably with the commercial process figures of 30% rare earth in alloy and 60% rare-earth recovery. Functionally, the USBM alloys were as good as the commercial rare earth–silicon–iron alloys (Marchant et al. 1980).

6.3.2 BARC Process

The preparation of rare earth–silicon–iron alloy by metallothermic reduction was also investigated at the Metallurgy Division of Bhabha Atomic Research Centre (BARC) (Bose et al. 1985). A mixed REO concentrate of monazite origin, obtained from Indian Rare Earths in Alwaye, was used. The RE_2O_3 content of the mixed oxide was 95%, and the ratio of CeO_2 to RE_2O_3 in the oxide was about 48%. Commercially available 80% grade ferrosilicon and aluminum rod scrap (>99% Al) were used as the reactants. Two types of fluxes were used. One was a CaO–MgO flux, and the other was a CaO–CaF_2 flux. The details of charge and products are listed in Table 6.10.

The charge comprising mixed REO, 25 mm pieces of ferrosilicon, and aluminum was loaded in a 250-mm-diameter graphite crucible and covered on top with the CaO–MgO flux mixture.

The reduction was carried out by heating the charge to 1550°C in an induction furnace and keeping it at that temperature for 30 min. The molten RE–Si–Fe alloy that was formed was tilt-poured and cast in cast iron molds.

When CaO–CaF_2 flux was used, the procedure was different. Calcium fluoride was first melted in the crucible. Mixed REO and then CaO were added to the melt to form a molten bath of REO–CaO–CaF_2. Ferrosilicon and aluminum in lump form were added to the bath at 1500°C, and the reaction was allowed to proceed for 30 min. The alloy product was finally cast.

The rare earths loading in the rare earth–silicon–iron alloy and the recovery of rare earths in the alloy were similar in the experiments conducted at USBM and at BARC. The mixed REO derived from monazite was used at BARC and a bastnasite source material at USBM. The product obtained at BARC was higher in Si content and relatively low in iron. CaO–CaF_2 is the more favorable flux mixture in view of better slag fluidity, lower temperature of operation, and better rare-earth recovery in the alloy. The REO losses into the slag phase were also limited to below 10%.

6.3.3 Baotou Process

Li et al. (1985) used the rare earth containing blast furnace slag, obtained on smelting of the Bayan Obo iron–rare earth ore at the Baotou blast furnaces, as the source of rare earths for reduction to the rare earth–silicon–iron alloy. The composition of the slag and the alloy obtained from it are both given in Table 6.11.

The alloy was obtained by reduction of the blast furnace REO slag in an arc furnace using lime as the flux and ferrosilicon as the reductant. The recovery of REM was in the 60–70% range, and many different grades of alloys, including 30% RE–Si–Fe alloy, could be prepared.

6.4 RARE EARTH–MAGNESIUM–SILICON ALLOYS

The rare earth–Mg–Si alloys have been used as additives in the making of nodular iron. The conventional methods for production of these alloys have disadvantages such as consumption of large amounts of metallic magnesium and the loss of

TABLE 6.10
Metallothermic Reduction of Mixed REO

Charge			Flux				Product				
REO	Fe–80Si	Al	CaO	MgO	CaF_2	RE–Si–Fe Alloy Recovered	REM	Si	Fe	Al	REM Recovered (%)
5000	2670	1336	5000	330	–	5610	54.2	33.2	5.5	4.0	76
4000	2600	1070	5050	–	7000	5000	55.0	33.0	5.0	4.0	82

Source: Bose, D.K. et al., *J. Less Common Metals*, 110: 239–242, 1985.

TABLE 6.11
Composition of the Baotou Slag and RE FeSi Alloy Obtained

Baotou Slag								
Elements	REO	Fe	P	F	CaO	SiO_2	MnO	Alkalinity
Content (%)	10–16	<1	<0.1	10–16	38–42	20–24	<2	1.0

RE–Si–Fe Alloy						
Elements	RE	Si	Mn	Ca	Ti	Fe
Content (%)	18–47	45–50	5–2	6–2	3–0.5	Balance

Source: Caiquan, L. et al., Rare earth ferrosilicon alloy, in Xu, G. and Xiao, J. (eds.), *New Frontiers in Rare Earth Science and Application*, vol. II, Science Press, Beijing, 1985.

magnesium due to vaporization. Xu et al. (1985) carried out direct preparation of rare earth–Mg–Si alloys by a silicothermic reduction process.

The rare earth-bearing raw materials were from the Bayan Obo deposit. One of the two materials is the Baotou blast furnace slag containing >10% REO, and the other is the rare-earth concentrate containing about 30% REO. The other components of the charge were calcined dolomite containing 34% MgO and reducing agents such as ferrosilicon, calcium, and silicon. Reductions were carried out in an electric arc furnace. The optimum smelting conditions were temperature >1550°C, CaO + MgO ≈ 35–45%, and silicon content of the reducing agent >85%. The composition of the alloy obtained was Mg 3–5%, (Ca + Mg) > 10%, RE 6–17%, and Si 50–55%, and the balance was Fe. Xu et al. (1985) noted that controlling the voltage and current in the operation and timely tapping of the alloy were necessary for the success of the process.

6.5 RARE EARTH–ALUMINUM–ZINC ALLOYS

A galvanizing zinc alloy containing 5% aluminum and small amounts of lanthanum and cerium has been considered to offer much better protection to underlying steel than does normal zinc cover (Radtke and Herrschaft 1983). Xujun et al. (1985) have investigated molten salt electrolysis as an alternative to conventional methods of melting together the components or thermal reduction of compound intermediates.

The electrolyte consisted of 20–30% $RECl_3$ in an equimolar mixture of KCl–NaCl, with CaF_2 1% and NaF 1% as additives. A cylindrical graphite crucible, which was also the anode, was used to contain the molten salt. The cathode was molten Al–Zn alloy (Al/Zn = 60:40) contained in a porcelain crucible and placed in the cell. Electrolysis was conducted at 650–680°C, and the bath was continuously stirred. Cathode current density was kept at 2–2.5 A/cm^2. After electrolysis was completed, the cathode product was removed and cooled, and the electrolyte on the alloy surface was washed away.

Under the conditions mentioned, an alloy containing 8% RE was obtained. The current efficiency was as high as 81%, and the rare-earth recovery was quantitative. In their experiments, Xujun et al. (1985) produced up to 375 g of the alloy per batch.

6.6 YTTRIUM–ALUMINUM ALLOYS

Both yttrium and aluminum are constituents in several oxidation-resistant alloys useful for high-temperature service. Yttrium–aluminum master alloy is convenient for introducing these elements in the high-temperature alloys. Methods mainly based on fused salt electrolysis have been used for the production of these alloys (Morrice et al. 1973).

In one method (Bratland et al. 1972), yttrium–aluminum alloys were made by electrolysis of yttrium oxide in yttrium fluoride–lithium fluoride melts using floating cathodes of liquid aluminum. By this arrangement, the maximum concentration of yttrium recovered in the alloy was only 22%.

Yttrium–aluminum alloys of higher yttrium content were prepared at Reno by electrolyzing mixtures of yttrium oxide and aluminum oxide dissolved in yttrium fluoride–lithium fluoride melts and codepositing the metals to form liquid alloys. The 120-mm-diameter cell used at Reno for electrowinning Y–Al alloy using a liquid Y–Al alloy cathode is shown in Figure 6.9 (Morrice et al. 1973). The anode and the crucible used to contain the molten electrolyte were made of graphite. The cell was placed inside a shell of mullite bricks to provide thermal insulation. To furnish heat to melt the electrolyte and to maintain the desired operating temperature, a graphite resistance heater was located below the graphite crucible. To protect cell components, the alloy product, and the graphite resistor from air oxidation at the operating temperature, the entire assembly was placed inside a chamber under helium. As usual, glove ports and view ports were provided in the chamber to facilitate the cell operation.

Yttrium fluoride was prepared by fluorinating 99.9% pure Y_2O_3 powder with ammonium bifluoride (Carlson and Schmidt 1961b). The rare-earth fluoride contained 0.1–0.2% residual oxygen. Lithium fluoride, yttrium oxide, aluminum oxide, yttrium metal, and aluminum metal used by Morrice et al. (1973) were all 99.9% pure.

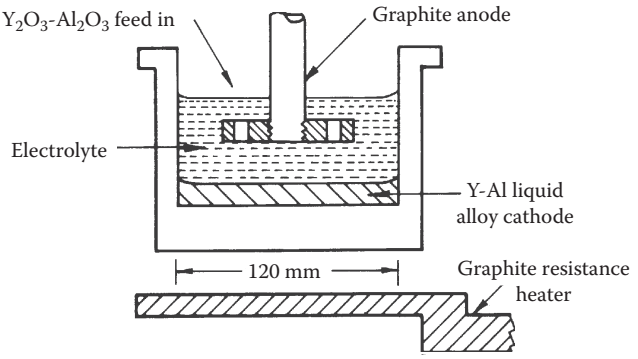


FIGURE 6.9 Electrolytic cell for production of Y–Al alloy at a Y–Al liquid cathode. (From Morrice, E. et al., Electrowinning of yttrium–aluminium alloy from yttria alumina mixtures. In Kevane, C.J. and Moeller, T. (eds.), *Proc. 10th Rare Earth Research Conf.*, Carefree, AZ, May 1973, Conf-730402, P1 and P2, pp. 682–691, National Technical Information Service, Springfield, Virginia, 1973.)

The starting alloy pool was a 91% Y–9% Al liquid alloy (at the operating temperature), and it covered the bottom of the graphite crucible. This alloy was obtained by arc-melting the alloy components together. This liquid alloy pool was the cathode. The anode, a 75-mm-diameter, 12-mm-thick horizontal graphite disk, was immersed into the electrolyte, and it was 12–19 mm above the alloy pool surface. The electrolyte was prepared by mechanically mixing the required amounts of yttrium fluoride and lithium fluoride to obtain the composition 80% YF_3–20% LiF. The electrolyte temperature was 1025°C. An oxide mixture comprising 87% Y_2O_3–13% Al_2O_3 (this mixture has the same Y/Al ratio as that of the eutectic alloy) was fed to the cell, and electrolysis was conducted at 4 V and 70–80 A for 3 h. Yttria and alumina were electrolytically reduced, and the resulting metals formed alloy in the alloy pool, which increased in quantity without major change in composition, as the electrolysis progressed.

The composition of the alloy formed needed to be closely controlled because if the aluminum content of the cathode pool increased, it would tend to float and interfere in electrolysis. On the other hand, if the yttrium content in the cathode pool increased, the melting point of the alloy pool would rise and the pool would solidify.

The operation of the liquid cathode has been investigated for 12–15 h (Morrice et al. 1973). The current efficiency and Y–Al alloy recovery were maximum at 68% and 89%, respectively, when 85% Y_2O_3–15% Al_2O_3 oxide mixture was fed to the cell. The electrowon alloy was approximately of eutectic composition (91% Y).

6.7 RE–TM–Mg ALLOYS

Rare earth–transition metal–magnesium intermetallics are important alloy additives in modern lightweight alloys and also host materials for hydrogen storage applications.

The rare earth–transition metal–magnesium compounds can be prepared directly from the pure elements (Rodewald et al. 2007). On account of the reactivity and volatility of the components, surface-cleaned elemental constituents are loaded in ampoules made of niobium or tantalum and melted in a water-cooled chamber of an induction furnace (Kussmann et al. 1998). In certain small-scale experiments, silver ampoules have also been used in place of the refractory metals. The light-gray polycrystalline samples are quite brittle and stable in air. Finely ground powders are dark gray; single crystals exhibit metallic luster. Apart from comelting, these intermetallics may also be produced by mechanical alloying (Orimo et al. 1997; Zaluski et al. 1997; Zhu et al. 2006). Amorphous and nanocrystalline magnesium-based alloys and intermetallics can also be obtained by melt spinning (Spassov et al. 2002; Huang et al. 2006).

6.8 FCC CATALYSTS

In the early 1960s, the petroleum refining industry underwent a sort of technical revolution with the introduction of zeolite-based cracking catalysts that enabled significant improvement in the performance of the FCC process. Cracking catalysts are multicomponent systems comprising an active component, zeolite; an active matrix,

alumina; a binder, generally a silica sol or gel; and an inert matrix, the clay. The faujasite, or zeolite Y, is the usual active component in FCC catalysts. Y zeolites are used in FCC catalysts in the form of hydrogen Y or exchanged with rare earth (HY or REHY, respectively). The NaY zeolite is a parent catalyst in catalytic cracking of hydrocarbons and petrochemical processes. Y zeolites are traditionally prepared from NaY zeolites by ion exchange with ammonium and or rare-earth salts, followed by calcination. The rare-earth precursors used are a mixture of lanthanum, cerium, neodymium, and praseodymium salts, in which the first two elements usually occur in larger quantities (Sousa-Aguiar et al. 2013).

Mixed rare-earth chloride obtained in the primary rare-earth ore processing flow sheet is the usual raw material for the synthesis of FCC catalysts. Considering the high demand for neodymium, it would be profitable to remove all of it from the mixed rare-earth chloride before it is sent for FCC catalyst manufacture. This is currently the practice in the case of misch metal. By about 2007, the high demand for neodymium has made it profitable to remove all of the heavier lanthanides and neodymium (and sometimes all of the praseodymium as well) from the natural-abundance lanthanide mixture for separate sale, and to include only La–Ce–Pr or La–Ce in the most economical forms of misch metal. The light lanthanides are so similar in their metallurgical properties that any application for which the original composition would have been suitable would be equally well served by these truncated mixtures.

6.9 PERMANENT MAGNET MATERIALS

There are numerous permanent magnet materials, and those that have been commercially important are listed in Table 6.12 (Strnat 1985). Permanent magnets are rated on the basis of several key properties, for example, the energy product and coercivity. The attractive characteristics of good permanent magnet materials are high coercivity (resistance to demagnetization) and high-energy product. The energy product $(BH)_{max}$ is a measure of the useful strength of a permanent magnet and is the most often quoted figure of merit for comparing permanent magnets. The progression of the maximum energy product in various permanent magnet materials during this century (Strnat 1985; Constantinides 2012a) is shown in Figure 6.10. The figure illustrates the 10-fold increase in the magnetic energy that can be stored in a volume unit. The enhancement of the coercivity is by an even larger factor. Many of these enhancements began in the late 1960s with the discovery and development of rare earth-based permanent magnet materials. These materials are based on either the rare earth–cobalt system or the neodymium–iron–boron system.

6.10 RARE EARTH–Co PERMANENT MAGNETS

About 5% of the rare-earth magnets produced belong to the Sm–Co family, which has been developed since the mid-1960s (Strnat 1970; Liu et al. 1999).

During the past four decades, the rare-earth transition metal (RE-TM)-based magnets have evolved into a family of commercial products of considerable variety and constantly growing technological importance. The first group of rare-earth magnets developed in the 1960s and commercially produced in the 1970s was based

TABLE 6.12
Important Permanent Magnet Materials

Magnet	Energy Product $(BH)_{max}$ (kJ/m³)	Remanence, B_r (mT)	Coercivity at 20°C (kA/m)		Temperature Coefficient of Remanence (%/°C)	Curie Temperature (°C)	Maximum Temperature for Practical Use (°C)	Density (g/cm³)
			B^HC	J^HC				
BaFe, plastic bonded anisotropic	17.9	245	175	207	–0.20	450	100	3.7
BaFe anisotropic	25.5	365	175	180	–0.20	450	~200	5.0
AINiCo 500 precision casting	36	1150	48	50	–0.20	860	450	7.4
Sm–Co plastic bonded	56–64	550–590	360–416	600	–0.04	725	80	5.1
Sm–Co	180	950	720	1800	–0.04 (20–1000°C)	725	~250	8.3
Sm_2Co_{17}	195–225	1000–1100	690–820	1200–2070	–0.03 (20–100°C)	750–800	~300	8.4
NdFeB plastic bonded	80	680	460	820	–0.10 (25–90)	340	150	6.0
NdFeB	225–800	1100–1250	720–930	800–1120	–0.10	310	100–150	7.4

Source: Strnat, K.J., A review of rare earth permanent magnets, applications and prospects, in Xu, G. and Xiao, J. (eds.), *New Frontiers in Rare Earth Science and Application*, vol. II, Science Press, Beijing, 1985.

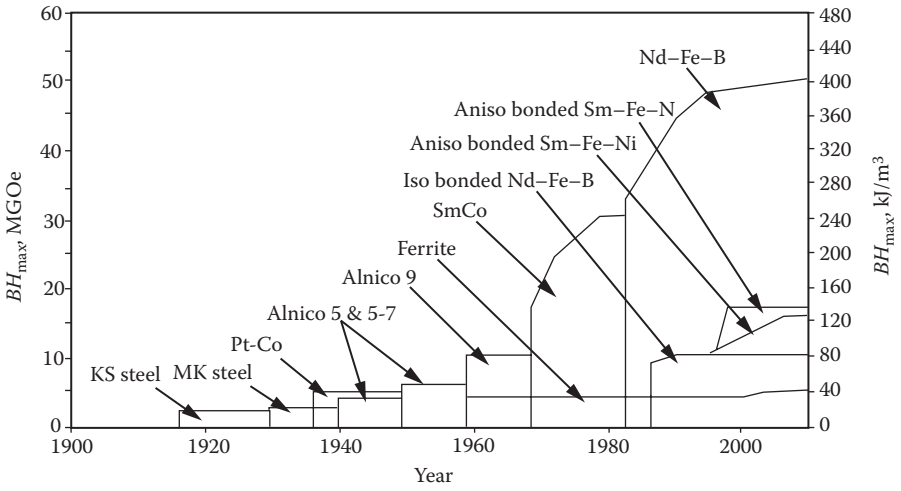


FIGURE 6.10 Permanent magnet development since the beginning of the last century. (From Constantinides, S., *Material matters.* Available at http://www.northeastern.edu/nanomagnetism/downloads/EAM2012_Arnold_120711_mod120802.pdf, 2012.)

on the intermetallic compounds $RECo_5$ and RE_2Co_{17}. These intermetallic compounds possess a good combination of magnetic and structural properties for magnet applications. The first important magnet of this type was $SmCo_5$. The structure of $SmCo_5$ is hexagonal ($CaCu_5$ structure), its saturation induction is moderate, and it has extremely large positive values of magnetocrystalline anisotropy. The magnets based on $SmCo_5$ are single phase, and magnetic property values achieved in the laboratory are B_r = 1 T, H_{cj} = 3200 kA/m, and $(BH)_{max}$ = 200 kJ/m^3. The $(BH)_{max}$ in commercial $SmCo_5$ magnets are in the range 130–160 kJ/m^3. In other words, $SmCo_5$ magnets offer energy per unit volume 2 to 3 times more than that of the old-generation magnets such as PtCo and AlNiCo and also exhibit 5 to 20 times greater resistance to demagnetization. In single-phase $SmCo_5$ magnets, the mechanism of coercivity is based on nucleation and/or pinning of domain walls at surfaces or grain boundaries. To achieve large values of coercivities, it is necessary to have particle form (1–10 μm) or fine-grained sintered magnets prepared from such powders. Magnet production techniques are, therefore, based on powder metallurgical procedures and include field pressing, i.e., alignment in a magnetic field during the pressing operation as a key process.

Less expensive alternatives to $SmCo_5$ have also been widely investigated (Wernick 1995). These include the use of Pr, Ce, and Ce–MM in combination with samarium. (Pr, Sm)Co_5 have higher values of saturation induction than $SmCo_5$. The Sm–Ce and Sm–MM combinations are cheaper, but the magnetic properties are also inferior.

The addition of copper to certain $RECo_5$ alloy (partial substitution of Cu for Co) and proper heat treatment can result in a finely distributed two-phase structure and high coercive force, even in bulk (Nesbitt and Wernick 1973). Low copper Sm or $SmCo_5$-based alloys are magnetically hardened by a Cu-rich 1–5 phase precipitated

TABLE 6.13
Magnetic Data of Selected 1–7 or 2–17 Alloys

Alloy Type	Production Method	$(BH)_{max}$ (kJ/m^3)	B_r (T)	$_mH_c$ (kA/m)	α (%/°C [Temp. Range])
$SmCo_5$	Sintering	192	0.98	955	–0.04 (–50 to +100)
$(MM_{0.8}Sm_{0.2})Co_5$	Sintering	128	0.82	1194	–0.055 (–50 to +100)
$Sm(Co,Fe,Cu)_7$	Sintering, precipitation annealing	211	1.04	494	–0.03 (20 to 120)
$Sm_2(Co,Fe,Cu,Zr)_{17}$	Sintering, precipitation annealing	242	1.12	533	–0.03 (–50 to +150)
$(Sm,Ho)Co_5$	Sintering	99	0.71	>200	~0 (–90 to +50)
$SmCo_5$	Polymer bonding	112	0.75	>1195	–0.04 (–35 to +100)

Source: Strnat, K.J., *J. Magn. Magn. Mater.*, 7: 351–360, 1978.
Note: α is the approximate value of the temperature coefficient of remanence per 1°C.

within the grain. The precipitate impedes domain wall motion and gives $_mH_c$ in the range 400–560 kA/m. Copper additions strongly broaden the high-temperature homogeneity range of the 1–5 phase toward 2–17 and permit incorporation of iron into the lattice. It has therefore been possible to prepare precipitation-hardened magnet alloys (Sm, Ce) $(Co, Cu, Fe)_z$ up to $z = 6.8$ and (Sm, Y) $(Co, Cu, Fe)_z$ up to $z = 7.2$ with excellent properties. These may be considered as 1–7 alloys. The magnetic data for selected magnets are listed in Table 6.13.

The RE_2TM_{17} compositions have basic properties that could lead to magnets of energy products of 480 kJ/m^3 or more (Strnat 1990). Sm_2Co_{17} ($SmCo_{8.5}$) has the highest anisotropy and best potential. Commercial magnets based on $SmCo_{8.5}$ contain, in addition to Co, the metals Cu, Fe, and Zr to replace some of the Co. The preparation of sintered magnets very close to the 2–17 stoichiometry, having energy products exceeding the highest for the 1–5 composition, has been reported (Strnat 1978). For example, $Sm_2(Co,Fe,Mn,Cr)_{17}$ and $Sm_2(Co,Fe,Cu,Nb)_{17}$ have an energy product of 225 kJ/m^3, while $Sm_2(Co,Fe,Cu,Zr)_{17}$ have energy products of 240 kJ/m^3 each. The attractive hard magnetic properties of these materials arise from microstructural precipitates that pin domain walls.

6.10.1 Preparation of Magnet Material

The preparation of RE–Co magnets involves two major stages. The first is the preparation of the RECo alloy, and the next is the production of the magnets from the alloy. The RECo alloy has been prepared by many routes. They are (1) direct melting of the alloy components, (2) coreduction or reduction–diffusion using the metal oxides as start materials, and (3) direct production of the alloy by fused salt electrolysis using cobalt as the consumable anode.

6.10.1.1 Direct Melting

Rare earth–cobalt alloys for magnets can be prepared by melting together the alloy components. The melting can be carried out by high-frequency induction heating either in crucibles such as boron nitride and alumina (Kirchmayr and Poldy 1979) or in a cold crucible arrangement. The latter, however, is slowly attacked by the melt. A survey of the various techniques for preparing RE–Co alloys has been given by Herget and Domazer (1975). For melting a mixture of samarium or other rare earth and cobalt, either small ready-made crucibles or crucibles that are rammed and fired *in situ* using an inner graphite core have been used. Vacuum induction melting is a particularly clean method for preparing these alloys. If small quantities of alloys are to be prepared, the components can be melted in an arc furnace. Walkiewicz et al. (1973) prepared Sm–Co compounds by nonconsumable arc melting of 99.9% pure metals. About 80 g charges of these metals were melted under helium. To achieve homogeneity, the arc-melted buttons were inverted and remelted a total of five times. An excess of samarium was provided in the charge to compensate for samarium loss due to vaporization. To obtain the stoichiometric $SmCo_5$ composition of 33.8% samarium, a charge composition of 37% samarium and 63% cobalt was used. A blending method was also used as an alternative to the above approach, which essentially involved obtaining a particular alloy composition by adding controlled amounts of Sm and Co to the charge before melting. In this method, two separate compounds, near stoichiometric $SmCo_5$ and Sm_2Co_{17}, were first prepared. These compounds were then blended in the required ratio and melted to obtain the optimum composition of 36.7 ± 0.3% samarium. Walkiewicz et al. (1973) found the blending method to be superior to the direct melting method in which samarium content was directly controlled during melting.

At the beginning of the 1970s when alloys of the type $RECo_5$, particularly $SmCo_5$, were becoming important, development of new economic methods of alloy preparation began apart from the direct melting route. It was discovered that calciothermic reduction of Sm_2O_3 in the presence of cobalt powder, and eventually of additional alloy components, yielded the required alloy directly in the powder form. There are two variants of this method, and they are known as reduction–diffusion and coreduction.

6.10.1.2 Reduction–Diffusion

The process was invented in 1969 by Cech (1974) working at the General Electric Corporate R&D Center in Schenectady, New York. The flow sheet of the process is given in Figure 6.11. Cobalt powder, REO, and calcium hydride were used as the starting materials. They were first pretreated. The pretreatment sequence consisted of removal of residual oxygen from the cobalt powder, removal of moisture from the REO, and conversion of metallic calcium to the hydride form. As an alternative, Cech (1974) suggested that cobalt oxide and REO could be mixed first, and then the dispersed cobalt oxide could be reduced to the metallic state with hydrogen. The pretreated starting materials were then intimately mixed under an inert atmosphere and subjected to a programmed thermal treatment in a hydrogen atmosphere furnace.

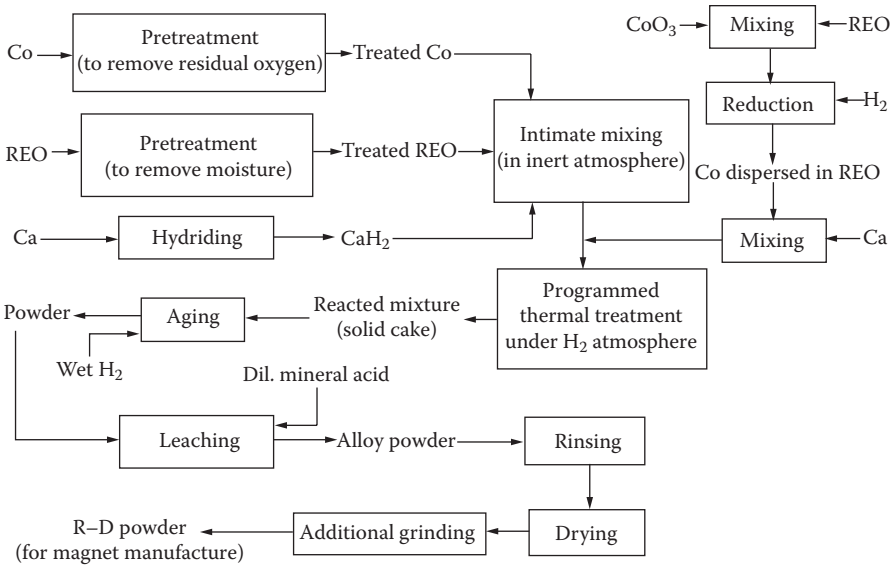


FIGURE 6.11 Schematic of the reduction–diffusion process.

The reacted mixture, which was in the form of a solid cake, was aged in wet nitrogen. This treatment permitted excess calcium dispersed in the product to react with moisture and led to the spontaneous disintegration of the product cake into powder. The powder was treated with a dilute mineral acid to leach out calcium oxide. The powder was then rinsed, dried, and subjected to additional grinding to refine the particle size to that needed for the fabrication of magnets.

In his experiments, Cech (1974) prepared the cobalt powder by hydrogen reduction of the cobalt oxide after it was first dispersed in the REO. He also prepared calcium hydride *in-house* from commercial-grade calcium nodules. He dispersed calcium nodules in the cobalt metal–REO mixture before converting them to hydride. Hydriding of calcium required only a brief furnacing treatment. The mixture was then homogenized by passing through a double-disk pulverizer and then repacked in a covered iron boat for the chemical reduction treatment.

The chemical reduction treatment consisted of heating the charge at 850°C for 2 h followed by three 30-min holding periods at 900°C, 950°C, and 1000°C and finally a 2 h holding at 1050°C. The charge was then drawn into a water-cooled chamber to facilitate rapid cooling. Slow cooling, in a hydrogen atmosphere, it was observed, led to the formation of Sm_5CoO-type material by the reversal of the second reaction given below.

Cech (1974) suggested that the following reactions closely describe the reduction–diffusion process for $RECo_5$ alloy formation.

$$10Co + RE_2O_3 + CaH_2 \rightarrow 2RECo_5O + CaO + H_2\ (850°C)$$

$$2RECo_5O + 2CaH_2 \rightarrow 2RECo_5 + 2CaO + 2H_2\ (1050°C)$$

According to Cech (1974), carrying out the reduction step directly at 1050°C led to undesirable complications arising out of formation of low-melting rare earth-rich intermetallic phases. The reduction should occur at such a rate that the rare earth formed should at the same time be removed by solid-state diffusion into cobalt.

The maximum overall yield of rare earth in the alloy obtained by Cech (1974) was at least 97% using the following stoichiometry:

$$10Co + Sm_2O_3 + 12(3CaH_2) \rightarrow 2SmCo_5 + 3CaO + 0.6CaH_2$$

The yield decreased both at lower and higher proportions of CaH_2. The batch size of the experiments was 2.7 kg of $SmCo_5$.

In addition to $SmCo_5$, other alloys containing 75% Pr and 25% Sm in the rare-earth part of the alloy have been prepared by the reduction–diffusion. This fine powder alloy was processed to magnets that were as good as or superior to those made from conventional melt cast powder.

The original reduction–diffusion developed by Cech (1974) at General Electric was modified by McFarland (1973) from the same laboratory, and the schematics of both processes are shown in Figure 6.12.

Cech (1974) was attempting to generate a powder in the 5–10 μ size range to avoid an expensive fluid energy-milling step. The work on magnet fabrication by Cech

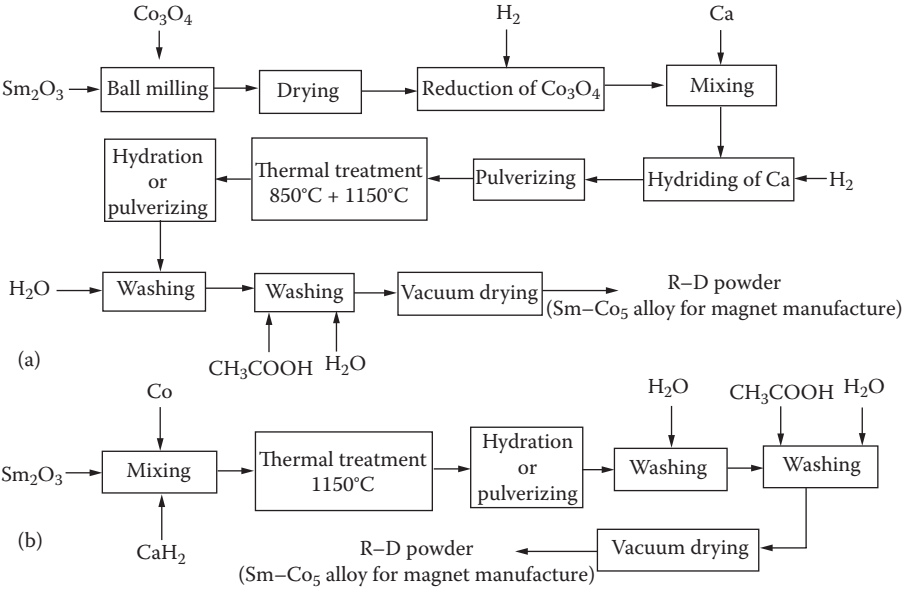


FIGURE 6.12 Original (a) and modified (b) reduction–diffusion processes. (From McFarland, C.M., Cobalt–rare earth powders by the reduction–diffusion process. In Kevane, C.J. and Moeller, T. (eds.), *Proc. 10th Rare Earth Research Conf.*, Carefree, AZ, May 1973, Conf–730402, P2, pp. 701–710, National Technical Information Service, Springfield, Virginia, 1973.)

as well as by Benz and Martin (1970) had indicated that superior magnets could be made with powders of 6–8 μ size, and this size was not achieved without milling. McFarland (1973) therefore decided to do away with particle size controlling features in the Cech process and to mill the final powder to the desired size. This led to process simplification by eliminating the initial wet ball-milling step, the subsequent drying step, and a final screening step for removing oversize particles. In addition, cobalt oxide (Co_3O_4), which was chosen by Cech (1974) as the source of cobalt and also to provide many nuclei for the formation of fine particle Co–RE alloy, was replaced by commercially available cobalt metal powder. Commercially available CaH_2 was used instead of generating it *in situ*. These changes eliminated the four steps following the first drier, namely, the steps that required careful handling of freshly reduced, pyrophoric cobalt, and a complicated heating, cooling, and grinding schedule to generate and blend in the CaH_2. Thus, all the early steps are telescoped into one step in McFarland's modification. The modified process, which was also scaled up, was carried out as follows.

The starting materials were weighed and loaded into a blender. Cobalt and REOs, in stoichiometric quantities, were mixed first, and then the calcium or calcium hydride up to 1.5 times the theoretically required quantity was added. The blending continued until a uniform mixture was obtained. The mixture was loaded into boats with loose-fitting covers. A glove box flushed with nitrogen gas was routinely used for the CaH_2 addition and boat-filling operations.

The loaded boats were introduced into an electrically heated retort with a hydrogen atmosphere. The retort was initially heated at 850°C for 2–3 h, and the temperature was then raised to 1150°C and maintained for 2–3 h before the boats were moved to the cooling zone, still under hydrogen atmosphere.

After cooling to room temperature, the medium-hard lumpy product material in the boat was transferred to a glove bag containing a moist hydrogen atmosphere. The material decrepitated, following the exothermic reactions,

$$CaH_2 + H_2O \rightarrow CaO + 2H_2$$

$$CaO + H_2O \rightarrow Ca(OH)_2$$

to a fine powder. Depending primarily on the excess CaH_2 present, this hydration treatment required 1–5 days.

The bulk of the slaked lime was removed from the hydrated material by purely mechanical means. The hydrated powder was slurried in water, the alloy was allowed to settle, and suspended lime was removed by decanting. An AC magnetic field was found to be useful to agitate the magnetic powder but to hold it in the bottom of the container for easy separation. Finally, the powder was rinsed with water and then with alcohol and transferred to a vacuum filter. The moist powder with about 3–5% alcohol was placed in trays in a vacuum oven drier and dried overnight at 50°C. The dry powder was stored in a sealed container preparatory to magnet manufacture. Following the above procedure, McFarland (1973) produced several compositions—from near stoichiometric $SmCo_5$ to $(Sm_{0.5}Pr_{0.5})Co_5$ and $(Sm_{0.6}MM_{0.25}Pr_{0.15})Co_5$.

Jones et al. (1976) have described a scaled-up reduction–diffusion process for the production of $RECo_5$ and RE_2Co_7, followed at Hitachi Magnetics Corporation MI, since 1973.

The general reaction of the reduction–diffusion process

$$x\mathrm{Co} + \frac{y}{2}\mathrm{RE_2O_3} + \frac{3y}{2}\mathrm{Ca} \rightarrow \mathrm{Co}_x\mathrm{R}_y + \frac{3y}{2}\mathrm{CaO}$$

was adopted for the production of the stoichiometric samarium compounds $SmCo_5$ and Sm_2Co_7 as per the reactions

$$5\mathrm{Co} + \frac{1}{2}\mathrm{Sm_2O_3} + \frac{3}{2}\mathrm{Ca} \rightarrow \mathrm{SmCo_5} + \frac{3}{2}\mathrm{CaO}$$

$$7\mathrm{Co} + \mathrm{Sm_2O_3} + 3\mathrm{Ca} \rightarrow \mathrm{Sm_2Co_7} + 3\mathrm{CaO}$$

An excess of calcium, about 1.2–1.4 times the theoretically needed amount, was used in carrying out the reactions in practice.

Calculated quantities of cobalt powder, samarium oxide, and calcium granules (the raw materials) were mechanically mixed to form a uniform charge. The charge was heated in dry hydrogen at 1160°C for 4 h to complete the calcium reduction and rare-earth diffusion. The reacted mass, which consisted of the Sm–Co alloy, CaO, and CaH_2, was placed in a high-humidity environment to slack the lime and decompose the CaH_2. The resulting $Ca(OH)_2$ was separated by magnetic and gravimetric means. The alloy powder was washed with dilute acetic acid to remove remaining traces of hydroxide, vacuum filtered, and dried. It was then sealed in metal cans and stored.

Two compositions for the final alloy were selected for production. One was the stoichiometric alloy with 33.8% Sm. This was the base alloy powder. The other was an alloy with 42.2% Sm. This was used as the additive. The base alloy powder and additive were used for magnet fabrication. The additive powder being richer in rare-earth content, a blend of the two resulted in an overall composition hyperstoichiometric to the $RECo_5$ after correction for the oxygen content (as RE_2O_3). The particle size and particle size distribution of these alloy powders depend upon the cobalt powder used.

Magnets made entirely from reduction–diffusion powder display permanent magnetic properties, which are equivalent to those of magnets made from ingot material. In either case, the properties attained were strongly dependent upon the unit processes used to make the magnets. In this context, excellent reproducibility was possible for the products from reduction–diffusion powders.

Jones et al. (1976) refer to the impact of the reduction–diffusion process on the cost of producing the rare earth–cobalt magnet alloys. Even though calcium metal used as a reductant in the process is expensive, it is at least cheaper by a factor of 2 than the alternative misch metal used to produce the samarium metal. Besides, a costly controlled atmosphere-melting step was also eliminated. Overall, the raw material and process cost reductions associated with the reduction–diffusion process

resulted in an eightfold reduction in the published price of Sm–Co magnet alloys between 1971 and 1976.

6.10.1.3 Coreduction

The coreduction process developed at Th. Goldschmidt AG (Domazer 1976; Herget 1982) also leads to the direct preparation of samarium–cobalt alloy from the metal oxides. Calcium was used as the reductant, a part of the cobalt in the final alloy was derived from cobalt oxide used to function as thermal booster in the reaction mixture, and the process was carried out in a vacuum at 1100–1200°C according to the overall reaction

$$Sm_2O_3 + Co_3O_4 + 7Co + 7Ca \xrightarrow[\text{vacuum}]{1100-1200^\circ C} 2SmCo_5 + 7CaO$$

The schematic flow sheet of the process is shown in Figure 6.13. A pelletized mixture of Sm_2O_3, Co_3O_4, Co, and Ca in stoichiometric quantities was heated at 1100–1200°C. Coreduction, like reduction–diffusion, occurred rather quickly after initiation at high temperatures. However, it was necessary to keep the charge at the temperature indicated for about 2–4 h to permit full alloy formation between just formed but still partly isolated Sm and Co particles. Solid CaO product particles form very early in the reaction, and by remaining interspersed between the metal particles, they slowed down alloy formation by diffusion. The high melting point of CaO precluded the formation of a molten slag and hence metal–slag separation. As a result, the alloy came out as a powder and not as an ingot. This was desirable

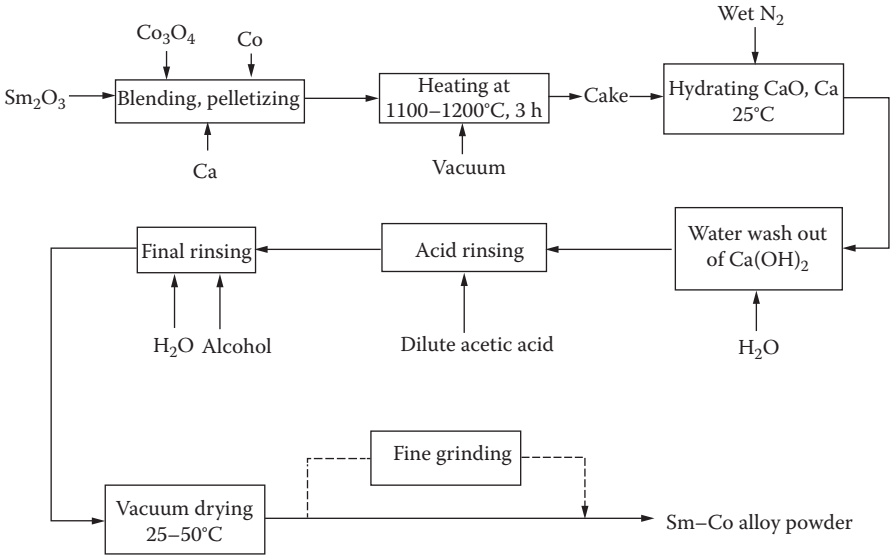


FIGURE 6.13 Schematic flow sheet of the coreduction process. (From Strnat, K.J., R–Co permanent magnets. In Buschow, K.H.J. (ed.), *Ferromagnetic Materials*, vol. 4, pp. 131–209, North Holland, Amsterdam, 1988.)

because all the rare earth–transition metal alloys were being processed into magnets by powder metallurgical methods, and even if an ingot were first produced, it would have to be pulverized to obtain the alloy as powder.

As metal did not coalesce and thus did not collect separately from the slag during the above process, a separation step for powder product collection was necessary. This was carried out by first reacting the CaO and excess calcium metal with moist nitrogen, mechanically removing most of the $Ca(OH)_2$, and leaching the remainder away with a mild acid (acetic acid).

6.10.1.4 Electrolysis

Apart from the reduction–diffusion and coreduction methods described so far, electrolytic methods have been investigated at the US Bureau of Mines, Reno Center (Morrice et al. 1969) for the preparation of rare earth–cobalt alloys for magnet use. Morrice et al. (1969) have described the following process for preparing high-purity cobalt alloys containing individually samarium, yttrium, praseodymium, cerium, lanthanum, gadolinium, dysprosium, neodymium, didymium mixture, mixed yttrium group metals, and mixed cerium group metals. Because the relatively high prices of high-purity rare-earth metals are an important factor for producing rare earth–cobalt magnet materials, the electrolytic process uses oxides, a relatively cheap source of high-purity rare-earth metals, as feed materials.

Two internally heated thermal gradient cells were used for electrolysis. They are shown in Figures 6.14 and 6.15. The cells were enclosed in inert gas chambers to prevent atmospheric contamination. In both cells, the electrolyte was contained in a graphite crucible, and the crucible was placed inside a shell fabricated from insulating bricks to enable it to maintain the requisite heat balance. The cathode in each cell was a 6-mm-diameter cobalt rod.

The first cell, shown in Figure 6.14, used a 150-mm-diameter and 175-mm-deep graphite crucible. The anode was a fluted 38-mm-diameter graphite rod. For supplementary heating, AC was applied between two 32-mm-diameter graphite rods. Approximately 9 kg of electrolyte was used in the cell. The cell was used to prepare cobalt alloys of cerium, praseodymium, lanthanum, neodymium, didymium mixture, and the mixed cerium group metals.

The second cell, shown in Figure 6.15, used a 100-mm-diameter and 125-mm-deep graphite crucible. For supplementary heating, AC was applied between two 19-mm-diameter fluted graphite rods. These fluted graphite rods were also connected to a DC source and functioned as anodes during electrolysis. Generally 4 kg of electrolyte was contained in the cell. This cell was used to prepare cobalt alloys of samarium, yttrium, gadolinium, dysprosium, and mixed yttrium group metals.

The electrolytes used comprised LiF and the respective rare-earth fluoride. The electrolyte for cobalt–didymium alloy preparation contained BaF_2 as an additional component. This was necessary for increasing the resistance of the electrolyte so that the desired electrolyte temperature could be maintained. For the preparation of mixed rare earth–cobalt alloys, the proportion of individual rare-earth fluorides in the electrolytes corresponded approximately to the proportions in the respective mixed oxides used as cell feed.

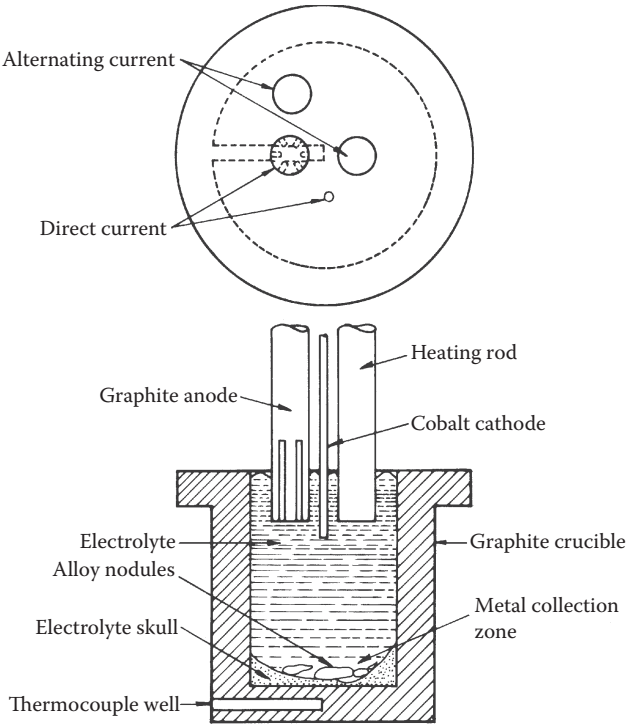


FIGURE 6.14 Electrolysis cell for RE–Co alloy preparation—I (6-in.-diameter cell). (From Morrice, E. et al., *J. Metals*, 21(1): 34–37, 1969.)

Before commencing electrolysis, the inert atmosphere chamber was evacuated and backfilled with helium. The required electrolyte temperature was attained by applying AC to the heater rods. Once the bath reaches the required electrolysis temperature, electrolysis was started, and the REO was intermittently fed to the cell at a rate determined by the rate of rare-earth metal production. At the cathode zone, the temperature was maintained at above the melting temperature of the eutectic formed between cobalt and rare-earth metals. The cathode was consumed as the molten alloy formed and dripped off, and successive new sections of the cathode were lowered into the electrolyte. The alloy was collected in the form of nodules in a skull of frozen electrolyte at the bottom of the cell. At the conclusion of electrolysis, the cell was allowed to cool in the inert atmosphere chamber. The solidified electrolytic cake was then removed from the crucible and broken to recover the alloy nodules. The adhering electrolyte on the nodules was cleaned off by grinding. The summary of operating data for preparing all the cobalt alloys is listed in Table 6.14.

There are two major benefits in using this cell arrangement. The electrolysis takes place at a temperature above the melting temperature of the eutectic between cobalt and the rare earth but below the melting point of cobalt, and the low-melting alloy formed dripped off the cathode to the cell bottom, which is at a lower temperature than the cathode zone. One benefit is that the reaction between the rare-earth alloy

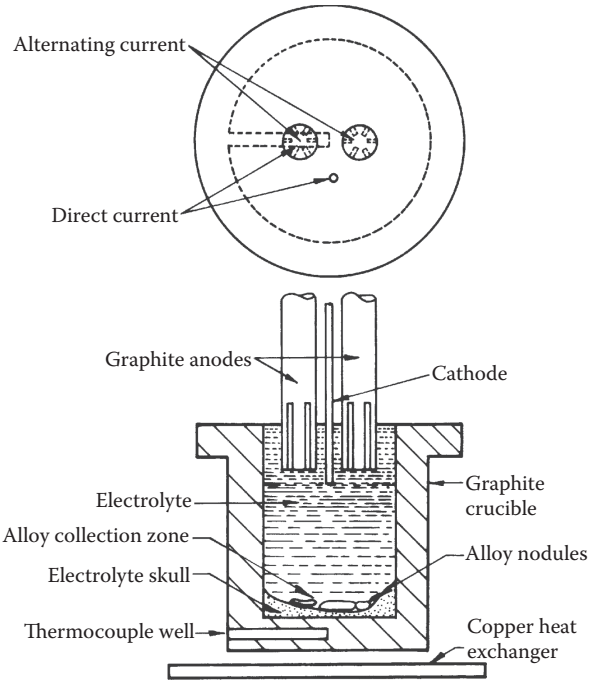


FIGURE 6.15 Electrolysis cell for RE–Co alloy preparation—II (4-in.-diameter cell). (From Morrice, E. et al., *J. Metals*, 21(1): 34–37, 1969.)

and the electrolyte is minimized; the other benefit is that the frozen electrolyte skull prevents contact between the product and graphite crucible.

During electrolysis, the alloy product coalesced well and nodules weighing as much as 60 g each were formed. The compositions of the alloys formed are also given in Table 6.14. The proportions of cobalt and rare-earth metals in the alloy products corresponded to the lowest melting eutectics in the RE–Co system, and in any given experiment, the concentration of cobalt usually varied by less than 3% among the nodules. In the products obtained using mixed oxide feed, the concentrations of certain rare-earth metals contained in the alloy products did not correspond to their proportions in the oxide feed. The reason may be traceable to the difference in the concentrations of the individual rare earths in the electrolyte, the difference in their readiness to form alloys with cobalt at a given temperature, and the difference in their reaction rates with the electrolyte.

The rare earth–cobalt alloys directly produced by electrolysis were relatively low in impurities. They were rich in rare-earth metals and were found to be suitable for the preparation of rare earth–cobalt compounds with the addition of more cobalt by melting. Then the compounds can be processed into fine particle permanent magnets by pulverization and consolidation.

It is seen in Table 6.14 that the cathode current efficiency varied widely among the various rare-earth alloys. Low current efficiency is probably caused by reactions between the rare-earth metals and the electrolytes. This was rather prevalent in the

TABLE 6.14
Cell Operating Data and Product Analyses for Electrolytic Preparation of Selected Rare-Earth Cobalt Alloys

	Co–Ce	Co–Pr	Co–Sm	Co–Y
Electrolyte composition (%)	35LiF–65CeF_3	32LiF–68PrF_3	27LiF–73SmF_3	15LiF–85YF_3
Current (A)	50	39	53	59
Voltage (V)	6	7.5	31	26
Anode current density[a] (A/cm^2)	0.6	0.5	0.7	0.8
Cathode current density[a] (A/cm^2)	5.1	4.0	10	11
Electrolyte temperature (°C)	775	875	945	910
Cell bottom temperature (°C)	685	835	660	715
Duration of electrolysis (h)	3.2	2.0	1.4	1.6
Alloy recovered (g)	174	175	50	135
Rare-earth content (%)	89	69	74	67
Cathode current efficiency (%)	74	88	27	87
Major impurities (%)				
Al	0.020	0.010	0.010	0.003
C	0.002	0.010	0.014	0.008
Fe	0.010	0.015	0.030	0.030
O	0.003	0.002	0.028	0.020
Ni	0.010	0.015	0.015	0.040
Si	0.005	0.010	0.010	0.010

Source: Morrice, E. et al., *J. Metals*, 21(1): 34–37, 1969.

[a] Based on initial electrode area.

electrolytic preparation of samarium–cobalt alloy. Samarium metal reacts with the SmF_3–LiF electrolyte

$$2SmF_3 + Sm \rightarrow 3SmF_2$$

resulting in not only low yield but also a coating of dark red salt that was rich in SmF_2, on the alloy nodules. In some experiments, BaF_2 was added to the electrolyte for improving the product recovery, but it was found that Sm also reacted with SmF_3–LiF–BaF_2 electrolyte. Morrice and Wong (1978) found that the rate of reaction of electrowon samarium with the electrolyte (SmF_3–LiF eutectic) increased markedly with the increase in the temperature of the electrolyte. To reduce the amount of back reaction, it was desirable to deposit samarium on the consumable cobalt cathode and to collect the samarium–cobalt alloy product at as low a temperature as possible. However, high temperature increases the solubility of Sm_2O_3 in the electrolyte and augments the formation of samarium–cobalt alloy at the cathode. It therefore follows that to obtain the best cell operation for Sm–Co alloy preparation, the cell will have to be a thermal gradient cell.

Morrice and Wong (1978) obtained samarium–cobalt alloy by fused salt electrolysis in a thermal gradient cell. The electrolyte was a SmF_3–LiF eutectic with a

composition of 25 mol.% (73%) SmF_3 and 75 mol.% (27%) LiF, and a eutectic temperature of 690°C. The cell enabled the following conditions to be realized:

1. At the Sm_2O_3 feed zone, the temperature of the electrolyte was such that (high) sufficient dissolved Sm_2O_3 was available for electrolysis.
2. At the cathode zone, the temperature was such that the liquid samarium–cobalt alloy formed and dripped off the cathode.
3. At the alloy collection zone, the temperature was such that the reaction rate between samarium–cobalt alloy product and the electrolyte was minimum.

A schematic of the thermal gradient cell is shown in Figure 6.16. The electrolyte was contained in a 125-mm-diameter by 150-mm-deep graphite crucible. The cell was heated internally by passing AC between two fluted 19-mm-diameter anodes. As much as 6 kW of AC power could be applied to the upper 25–38 mm of the molten electrolyte, and this arrangement enabled maintaining a temperature difference of 300°C between the upper and lower portions of the bath. A 6-mm-diameter cobalt rod was used as the cathode. The cathode rod was electrically insulated from the top or anolyte portion of the bath by a boron nitride sleeve. To collect the samarium–cobalt alloy product, a perforated molybdenum basket was suspended in the electrolyte directly below the cathode. The temperature at which the samarium–cobalt alloy was prepared and collected could thus be selected by raising or lowering the cathode and the product collection basket. After electrolysis, the basket containing

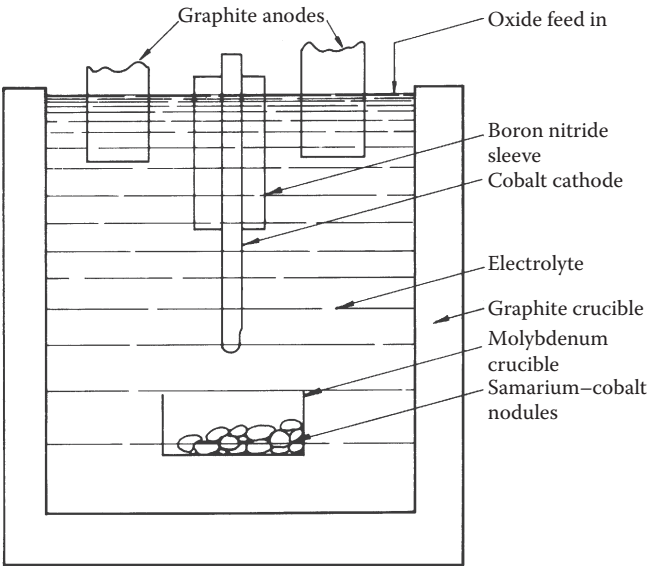


FIGURE 6.16 Schematic of the thermal gradient electrolytic cell for Sm–Co alloy preparation. (From Morrice, E. and Wong, M.M., Effect of temperature on the electrolytic preparation and recovery of samarium–cobalt alloy, Bureau of Mines Report of Investigations, 7556, U.S. Department of the Interior, Washington, DC, 1978.)

TABLE 6.15
Operating Data and Product Analysis for Sm–Co Alloy Preparation in the Thermal Gradient Cell

Electrolyte composition (%)	73 SmF_3–27 LiF
Direct current (A)	40
Direct current (V)	36
Alternating current[a] (A)	66
Alternating current[a] (V)	55
Initial anode current density[b] (A/cm^2)	0.6
Initial cathode current density[b] (A/cm^2)	5.2
Oxide feed zone temperature (°C)	953
Cathode zone temperature (°C)	720
Time of electrolysis (min)	50
Cobalt cathode consumed (g)	13
Samarium–cobalt recovered	42
Samarium content (%)	79
Cathode current efficiency (%)	53

Analysis of Remelted Samarium–Cobalt Alloy Product

Element	Al	C	Cr	Co	Cu	Fe	Mg	Mo	Mn	Ni	O	Sm
Content	0.04	0.17	0.003	43.5	0.04	0.02	0.003	0.46	0.07	0.15	0.05	55.6

Source: Morrice, E. and Wong, M.M., Effect of temperature on the electrolytic preparation and recovery of samarium–cobalt alloy, Bureau of Mines Report of Investigations, 7556, U.S. Department of the Interior, Washington, DC, 1978.

[a] Supplemental powder applied to anode.

[b] Calculated using the initial cathode surface area.

the alloy product as nodules would be lifted off the molten bath to drain out the excess electrolyte.

The optimum cell-operating data for the thermal gradient cell and product analysis are given in Table 6.15. The current efficiency achieved was at least 50%, which is approximately double the current efficiency achieved for Sm–Co alloy in a usual oxide fluoride electrolysis cell.

6.10.2 Preparation of Magnets

In the attempts, beginning in 1968, to produce usable high-density permanent magnets from $RECo_5$ alloys, the initial approach was to grind the alloys, $SmCo_5$, $La_{1-x}RE_xCo_5$, and $MMCo_5$, which was followed by alignment and pressing of the powders mixed with chemical binders (Buschow et al. 1968; Strnat et al. 1968; Velge and Buschow 1968; Westendorp and Buschow 1969). However, the interest in the plastic bonded magnets decreased after the first successful preparation of sintered magnets in 1969. In the mid-1970s, the plastic bonded magnets attracted attention once again (Menth et al. 1978) because they are not brittle and are easy to handle and

machine. There are essentially two types of magnets sintered and bonded, which are made from $RECo_5$ magnetic materials.

6.10.2.1 Sintered Magnets

The sintered magnets were first reported by Das (1969). Several subsequent investigations focused on sintering, and the sintering technology was eventually optimized for $SmCo_5$ as well as for other $RECo_5$ alloys (Menth et al. 1978). A schematic representation of the production steps involved is given in Figure 6.17. The starting alloy may be obtained either by direct melting or by the direct alloy production processes of reduction–diffusion or coreduction.

In general, the major steps in the preparation of these magnets are blending of the starting alloys, milling of the mixture, aligning and pressing to a compact, sintering of the green powder compact, and the post-sintering heat treatment.

6.10.2.1.1 Blending

During the blending (mixing of the alloy components, melting, and casting), samarium loss can occur due to evaporation and oxidation; therefore, the process should begin with a starting composition having an excess of Sm. This is done either by starting with an alloy of composition $SmCo_{5-x}$ or by starting with a mixture of two alloys with different Sm contents, for example, $SmCo_5$ and a Sm-rich sinter additive (e.g., 60% Sm–40% Co). As another alternative, a mixture of two alloys, $SmCo_{5+x}$ and $SmCo_{5-x}$, may be used (Naastepad et al. 1973). The important point is that the

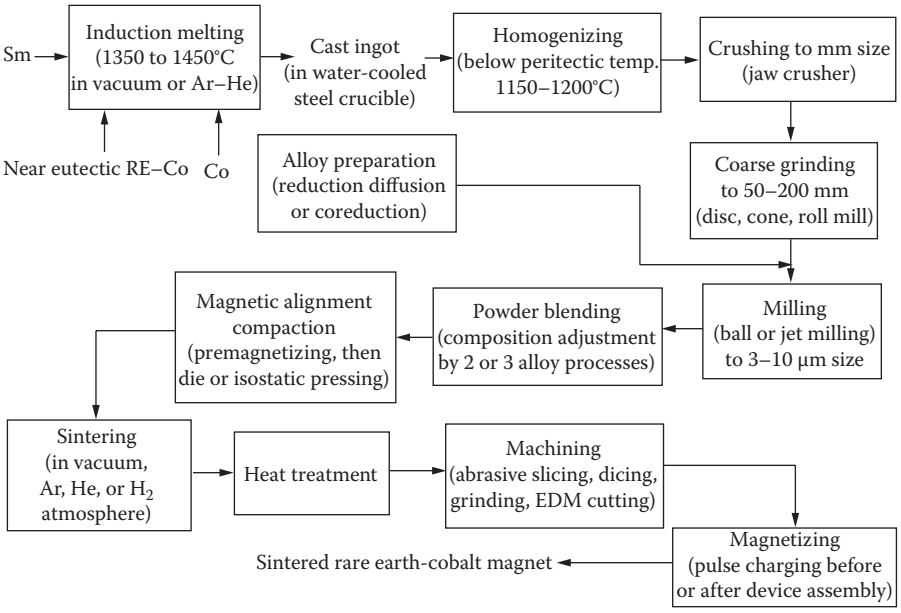


FIGURE 6.17 Flow sheet for sintered rare earth-cobalt permanent magnet production. (From Strnat, K.J., R–Co permanent magnets. In Buschow, K.H.J. (ed.), *Ferromagnetic Materials*, vol. 4, pp. 131–209, North Holland, Amsterdam, 1988.)

samarium content must be so chosen that no Sm_2Co_{17} phase is present in the final $SmCo_5$ magnets. Similarly, in the production of Sm_2Co_{17} magnets, the starting composition must ensure that no Co phase is present in the final sintered magnet. Inclusions of such a second phase would adversely affect the coercivity.

6.10.2.1.2 Milling

Many critical parameters need to be controlled during the milling process. They are grain size, grain size distribution, damage to crystal structure, and the loss of Sm due to oxidation. The loss of Sm is kept low by exclusion of air and water vapor. The techniques of milling that fulfill the stated conditions are ball milling under toluene or petroleum ether, and jet milling with dry nitrogen as the working gas. The resulting average grain size of the powder should be comparable to the initial diameter for a single-domain particle. Usually the alloys are milled into particles of about 3–7 pm average size. In the final magnets, a good magnetic homogeneity is achieved if the grain size distribution is narrow. Grains that are too small have a high structural defect density and an unfavorable surface-to-volume ratio giving rise to a high oxidation rate. Grains that are too large no longer exhibit single-domain character and may not be single crystals, resulting in poor magnetic alignment of the powder.

6.10.2.1.3 Aligning and Pressing

The powder is compacted in a die to 60–70% of bulk density, usually with an ~800–2400 kA/m magnetic field applied to achieve grain orientation. Sometimes the die pressing is followed by further isostatic compaction.

6.10.2.1.4 Sintering

The aligned green compacts are sintered under an atmosphere of argon, helium, or vacuum. The objective is to obtain an optimum combination of high-density (i.e., high remanence) and high-coercive field. It is necessary to have a constant and well-defined sintering temperature to ensure that the magnet has no open porosity, and that no grain growth occurs that would have a detrimental effect on the coercive field. For $SmCo_5$, the sintering temperature is 1120°C, and for $MM_{0.85}Sm_{0.15}Co_5$, it is 1050°C. Sintering usually lasts for 30 min to 1 h. Sintering in H_2 above 1100°C is also possible if suitable precautions are taken to avoid hydride formation (Jones et al. 1977). Hot pressing has also been used to prepare good magnets (Strnat 1978).

6.10.2.1.5 Heat Treatment

A post-sintering heat treatment is used to increase the coercive field of $RECo_5$ as well as RE_2Co_{17} magnets. For $SmCo_5$, the optimum annealing temperature is 900°C, and for $MM_{0.85}Sm_{0.15}Co_5$, it is 950°C. The beneficial effects of annealing $RECo_5$ magnets include (1) gradual removal of the lattice defects that determine the nucleation of the reversed domains, (2) decrease in local inhomogeneities in composition, and (3) partial precipitation in the grain boundaries of the oxygen that is dissolved in the magnetic phase during sintering.

Following annealing, the magnet has to be cooled to room temperature at a carefully controlled rate depending on its mass and shape. Cooling too slowly can result in the eutectoidal decomposition of the 1:5 phase to the 2:17 phase and associated

lattice defects, adversely affecting the coercive field. Cooling too fast, on the other hand, can create microscopic cracks and internal stresses that adversely influence both the stability of the magnets against oxidation and the coercivity.

The magnetic properties of the products obtained in the above procedure depend greatly on many parameters, including composition, particle size, alignment, sintering conditions, and the final heat treatment. Close quality control for all the processing steps is important as its presence or absence is made obvious by the product magnet's hysteresis loop shape, the spread of properties in a production lot, the magnitude of irreversible flux losses on heating, and the long-term stability of the magnets (Strnat 1978). A well-sintered magnet at high mass density and a high H_k (the reverse field that reduces the flux density to 0.9 B_r) displays low irreversible losses during short-term heating and good long-term aging stability, especially at elevated temperatures in air.

6.10.2.2 Precipitation-Hardened Magnets

The copper containing rare-earth magnets can in principle be produced by casting (Naastepad et al. 1973) followed by processing by zone melting or recrystallization to promote directional grain growth. Such magnets are brittle and are not in commercial use. All commercial magnets of the copper type, near the 1–5, 1–7, or 2–17 compositions, are made by the powder metallurgical route shown in Figure 6.18. Only a single powder (no Sm–Co additive or sintering aid) is used. For these magnets, milling and sintering are less critical compared to the procedure for fine particle magnets. The powder particles have to be single crystals so that they can be aligned easily in a magnetic field; however, they need not be single-domain particles as is necessary for nucleation-type magnets. The choice of grain size can be based on requirements of minimal oxidation and optimum sintering kinetics. No negative influence on the hard magnetic properties comes from grain growth during sintering. The sintering temperature of the $Sm(Co,Cu,TM)_{5<z<7.5}$ alloys must be below the peritectic temperature. TM here represents a transition metal. For example, for $Sm(Co_{0.84},Cu_{0.16})_{7.2}$, the sintering temperature of 1180°C (peritectic temperature ≈ 1220°C) results in an almost 100% theoretical density for the magnet. The coercive

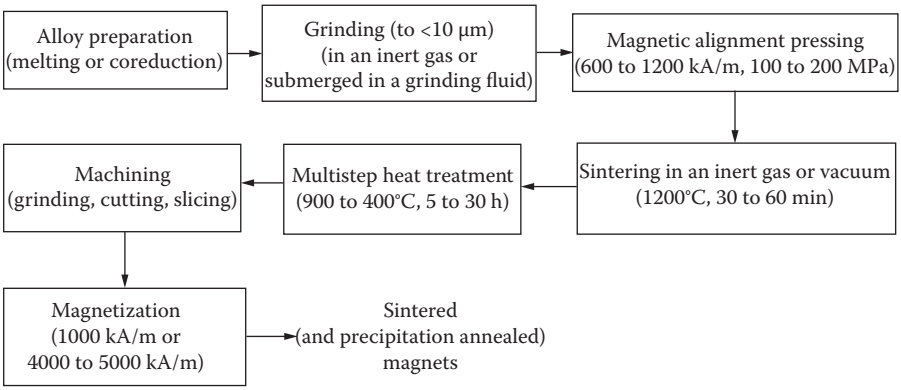


FIGURE 6.18 Flow sheet for the preparation of precipitation-hardened magnets.

field in these alloys is relatively low, at about 72 kA/m, after sintering. The coercive field can be improved by up to a factor of 6 by an appropriate annealing that results in an optimum density and precipitate size.

Machining, handling, and magnetizing: Sintered RE–Co magnets present certain problems in machining, handling, and magnetizing. They are hard and brittle. Machining them involves slicing with diamond blades, and surface grinding or cutting on spark erosion machines in a demagnetized state. The high H_c and low recoil permeability of rare-earth permanent magnets (REPMs) allows precharging and manipulation in an open circuit, and they will not self-demagnetize. For larger high-energy magnets, however, machining, shipping, and handling in the magnetized state are difficult. It is therefore often necessary to magnetize after partial assembly of a device. This can be problematic. High H_c 2–17 magnets and $SmCo_5$, first charged and then field demagnetized, need up to 4 MA/m for saturation. This demands expensive magnetizing equipment and may not be at all possible for larger assemblies. Incompletely magnetized $SmCo_5$ magnets can display severe thermal instabilities of the flux. Some of these limitations are circumvented in the bonded magnets, which are also attractive for many more reasons.

6.10.2.3 Bonded Magnets

The RE–TM-based bonded or matrix magnets were first introduced in the late 1960s, but their commercial development was slow. There were issues relating to chemical reactivity of the powder and inexpensive manufacturing methods. Earlier products were made from 5 to 20 μm particles of $SmCo_5$ bonded with epoxy, polyethylene chloride, or ethylene vinyl acetate. These deteriorated very quickly at temperatures above 50°C and were not magnetically very stable even at room temperature (Strnat et al. 1976). Much improvement was brought about by coating the particles with metallic or organic diffusion barriers and with careful selection of compatible polymeric binders. The most important development was the introduction of alloys bulk-hardened with copper. Used as coarse powders (≈20–200 μm), these did not suffer the severe sensitivity of H_c to the particle surface condition. They were, therefore, much more stable. Another way of improving the elevated temperature stability was to use a soft metal matrix. Alloys with compositions close to the 2–17 stoichiometry and with higher Fe content were developed particularly for bonded magnets. Methods developed for producing ingots with a coarse columnar grain structure obviated the need for presintered blocks for making bonded magnets. Moreover, the adaptation of inexpensive molding methods such as extrusion and injection molding in an orienting field encouraged large-scale production and industrial applications of the bonded REPMs.

The schematic flow sheet for the production of polymer-bonded RE–Co magnets is given in Figure 6.19 (Strnat et al. 1976). The RE–Co alloy was converted to a powder comprising mostly single crystal particles of sufficiently high coercive force. The powder was stabilized and/or magnetically hardened before sizing and blending with a binder. Then the blend was exposed to a magnetic field that magnetizes and orients the particles, the mass was compacted, and the binder was hardened. In an alternative procedure, the magnetic powder alone was compressed into a porous body that was then infiltrated with a liquid binder that subsequently

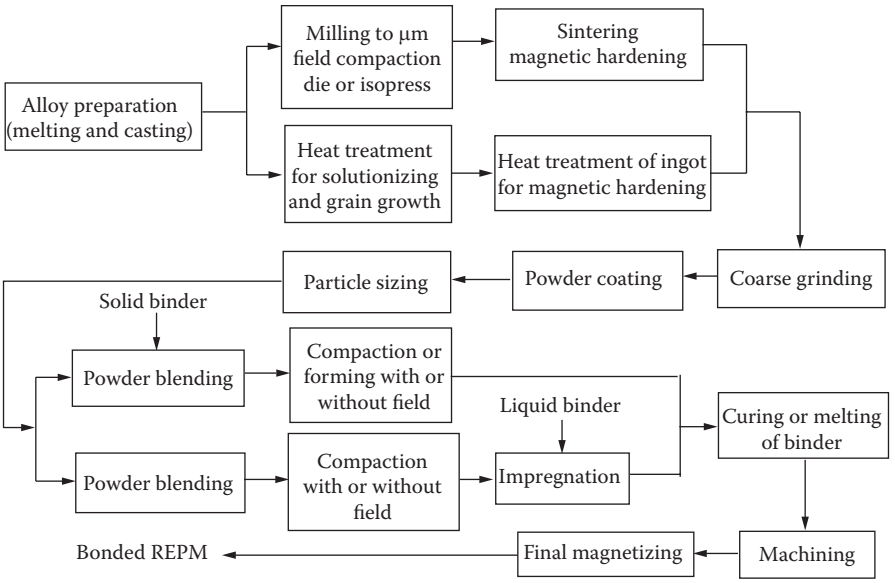


FIGURE 6.19 Schematic flow sheet for the production of bonded RE–Co magnets.

solidified. The polymer-bonded magnets were produced in two basic forms. One form was as rigid bodies with thermosetting or chemically hardened resin binder, and the other was as flexible sheets or strips with a thermoplastic or rubber binder (Strnat et al. 1976). Such magnets were generally made from $SmCo_5$ powder and were anisotropic by field alignment of the particles. The energy products of plastic-bonded magnets ranged from 25 to >135 kJ/m^3. The 2–17 alloys were used in the upper end, $SmCo_5$ in the middle, and alloys with MM substitution in the low B_r region. As regards the magnetic properties of the bonded magnets, the best compression molded 2–17 matrix magnets offer room-temperature properties equivalent to medium-grade sintered $SmCo_5$. They are, however, far superior to any non-RE magnet type. Injection-molded magnets are commercially attractive because of the low cost of processing, but they had significantly poorer B_r, H_{ci}, and loop shape. Metal matrix magnets with 2–17 alloy, a Sn–Pb binder, and Cu filler have been prepared to obtain magnet sets with precisely controlled variable saturation (Strnat and Strnat 1991).

The most important advantage of matrix bonding is inexpensive mass production. This comes about because of the possibility of molding magnets or even subassemblies to final shapes with close tolerances. There is little cutting scrap or grinding loss, and machining, when necessary, can be done with conventional machine tools. Compared to sintered magnets, there are fewer handling problems with bonded magnets. As regards mechanical behavior, the bonded magnets are somewhat ductile (metal matrix) and elastic or even flexible (plastic or rubber binders). At dense packing, they are moderately brittle. The bonded magnets can be conveniently produced in much larger sizes than the sintered ones without ending up with property

inhomogeneities, or cracking and warping by uneven shrinkage, which are size-limiting factors for the sintered bodies.

The samarium–cobalt magnets proved to be attractive replacements for the older ferrites, for Pt–Co and Alnico permanent magnets, and also for electromagnets in many applications. Their use has all along been constrained by economic disadvantages. Among the light rare earths, samarium is the least abundant and hence most expensive, and this unfavorable situation is aggravated by the fact that the price and availability of cobalt are subject to largely unpredictable excursions. The bulk of the world's cobalt is mined in Zaire, and the 1978 civil war there dried up the supplies. This drastically intensified the worldwide search for alternative RE–TM systems having economically more acceptable elemental constituents. Neodymium–iron–boron magnets were discovered and developed as a consequence.

6.11 NEODYMIUM–IRON–BORON MAGNETS

Even though iron-based materials having the characteristics of samarium–cobalt had long been desired, no suitable compounds were known. RE–Fe phases having $CaCu_5$ structure do not exist, and $REFe_{17}$ compounds in which RE is a light rare earth have an unusually low Curie temperature. Two lines of research, one relying on the rapid solidification by melt-spinning of rare earth–iron–metalloid alloys and the other based on conventional powder metallurgy, gave encouraging results by the early 1980s. Croat et al. (1984a,b) reported energy products as large as 112 kJ/m^3 in melt-spun ribbons of $Nd_{0.135}Fe_{0.817}B_{0.048}$. Sagawa et al. (1984a,b) applied traditional sintering methods to ternary light rare earth–iron systems and obtained $(BH)_{max}$ ~ 288 kJ/m^3 for $Nd_{0.15}Fe_{0.77}B_{0.08}$. Both of these high $(BH)_{max}$ materials, rapidly solidified as well as sintered, contained an iron-rich tetragonal phase $Nd_2Fe_{14}B$. The larger energy product reported by Sagawa et al. (1984a) came from the crystalline orientation provided by the powder metallurgy procedure. $Nd_2Fe_{14}B$ immediately attracted considerable technological interest because of its excellent intrinsic magnetic properties [$(BH)_{max}$ ~ 512 kJ/m^3, H_a ~ 5840 kA/m] as well as cost advantages over samarium–cobalt materials. The best laboratory Nd–Fe–B magnets have energy products as high as 470 kJ/m^3, close to the theoretical maximum of $|BH|MAX$ = 512 kJ/m^3. Practical magnets with energy products in the range of 320–400 kJ/m^3, values that are significantly larger than any attained previously, were prepared from melt-spun (Lee 1985; Croat 1989) and sintered (Sagawa et al. 1987b) alloys. Large-scale production programs following both the approaches have been subsequently implemented. Production of NdFeB magnets in 2010 was 80,000 t. The demand for superior grades with improved performance at elevated temperatures for energy-related applications such as electric vehicles and direct-drive wind turbines (Gutfleisch et al. 2011) has been growing. Replacing some of the Nd by a heavy rare earth, Dy or Tb (3–10 wt.%), helps maintain adequate hysteresis at temperatures up to 200°C (Coey 2012).

The overall process for the production of Nd–Fe–B magnets has two major stages. One is the production of magnetic alloy, and the other is processing of the Nd–Fe–B alloy into permanent magnets.

6.11.1 Production of Nd–Fe–B Alloys

Many methods have been developed for the production of neodymium–iron–boron (Nd–Fe–B) alloys (Agarwal et al. 1988). They include direct melting, coreduction, and several special techniques that make use of reduction extraction or thermit-type processes for directly making the Nd–Fe or Nd–Fe–B alloys.

6.11.1.1 Direct Melting

The direct melting method was used by Ormerod (1985) at Philips Electronic Components and Materials Division, The Netherlands, to prepare the Nd–Fe–B alloy. The target composition in their vacuum induction melting was 15 at.% Nd, 77 at.% Fe, and 8 at.% B, which was the composition reported by Sagawa et al. (1984a) as giving the optimum magnetic properties. The alloy was prepared from 99.9% Fe, 99.9% Nd, and 99.8% B. The iron and boron were initially melted in an alumina crucible under argon. After degassing under vacuum, the melt temperature was allowed to come down to just above the liquidus, and neodymium was added. Corrections were made for any anticipated melting losses. The melt was then cast in a thick-walled copper mold with a 5 mm cavity. The advantage of vacuum induction melting is that it can yield a wide range of alloy compositions with very low (<200 ppm) oxygen contents; however, pure elemental starting materials and oxygen-free environment are needed.

Kaneko and Ishigaki (1994) have used ferroboron as the source of boron in the preparation of Nd–Fe–B alloy by direct melting. Using 99.5% pure rare-earth metals, 99.9% pure electrolytic iron, and ferroboron, as raw materials, the $(Nd,Pr,Dy)_{12.5–15}Fe_{77–815}B_{6–8}$ alloys were prepared by induction melting in an argon atmosphere. The as-cast alloy was subsequently put through a homogenization treatment by heating for 5 h at 1000°C before it was converted to powder.

Nd–Fe–B alloys have also been made by arc melting. For example, an alloy of 81.5 at.% Fe, 13 at.% Nd, and 5.5 at.% B was prepared by arc melting Nd–17.5% Fe master alloy, electrolytic iron, and crystalline boron under a continuous flow of ultrapure argon. To minimize segregation and achieve compositional homogeneity in the alloy, the arc-melted ingot was remelted four times. The arc-melted alloy was subsequently induction-melted before processing by rapid solidification.

6.11.1.2 Coreduction

In continuation of their earlier work on Sm–Co alloys, efforts were on at Th. Goldschmidt AG in Germany to make the Nd–Fe–B type of materials by the calciothermic reduction technique soon after the first announcement of the Nd–Fe–B magnets at the 29th MMM Conference in Pittsburgh in November 1983 (Sagawa et al. 1984a). The technique was successfully developed by October 1984 (Herget 1985). Coreduction was based on the following overall reaction:

$$7.5Nd_2O_3 + 50.7Fe + Fe_2O_3 + 0.143Fe_{44}B_{56} + 52.5Ca$$

$$\xrightarrow[\text{vacuum, 4 h}]{1100–1200°C} Nd_{15}Fe_{77}B_8 + 52.5\,Cao$$

The source of boron used in the above reaction was commercially available ferroboron powder containing 20% boron. The conditions for carrying out the above reaction were essentially similar to those used for coreduction of Sm_2O_3 and Co_3O_4 because the differences of the free energies of formation between Sm_2O_3 and CaO on the one hand and between Nd_2O_3 and CaO on the other are similar. Calculated quantities of the starting materials were thoroughly mixed, pressed into pellets, and loaded in crucibles made of high-temperature-resistant steel. The crucibles were closed by welding except for an opening for evacuation and put in a vertical position into electric furnaces. These furnaces were evacuated and heated to reaction temperature.

The Nd–Fe–B alloy exhibits a much greater tendency for oxidation compared to $SmCo_5$ (Herget 1985), and this introduces differences in the process used for separation of the alloy powder from the CaO slag. A new and proprietary leaching procedure was developed and used by Th. Goldschmidt AG for the separation of alloy and CaO, and this process kept the oxygen content at 0.20% or even less in alloys with >40% Nd.

The coreduction process has been used by Herget (1985) not only to achieve a neodymium content of above 40% in the Nd–Fe–B alloy but also to add/incorporate rare earth or alloying elements such as Dy, Al, Nb, or Co in the product. The alloy powders produced typically contained O 0.12–0.25%, C 0.03–0.04%, Ca 0.03–0.06%, and Al 0.01–0.20% as residual impurities. The Al impurity was derived from the aluminum content of ferroboron, which was itself produced by an aluminothermic reduction process. If elemental boron were used instead of the aluminothermic ferroboron, the Al content could have been avoided.

Herget (1985) noted that the alloy powder picked up oxygen, and its oxygen content tended to increase even when stored in sealed plastic bags.

The calciothermic production of Nd–Fe–B alloys has also been used by a group at the Beijing University of Iron and Steel Technology (Herget 1985). The reduction process was carried out at ambient pressure under argon. The details of the procedure for aqueous treatments for alloy–CaO separation were not disclosed in these investigations.

The advantages of the calciothermic technique are high alloy yields, immediate production of powder that is so fine that it can be directly fed into the fine milling stage without prior crushing, flexibility regarding the number of components as well as alloy compositions, and cost benefits because of using commercial oxide as the starting materials. There are certain disadvantages also. They are the high cost of the reducing agent—calcium, the batch nature of the reduction operation, and interestingly, the powder form of the product. Alloy in the form of powder hampers its use for the magnet manufacturing process originally adopted by General Motors. The neodymium alloy powders with their high surface area and hence possibility of quick oxidation are not very suitable to melting, and melting precedes melt spinning and quenching as practiced by the General Motors process. Metals in the form of lumps are preferred.

6.11.1.3 Production of Consolidated Alloys

There are two basic routes to production of metallic rare-earth alloys, and several companies have developed their own proprietary modifications of these basic routes

to make neodymium alloys for magnets (Agarwal et al. 1988). The two major routes are based on oxide as the starting material but differ in the reduction step. Oxide reduction can be carried out by using calcium as the reductant for the oxide or after converting the oxide to fluoride, or the reduction is achieved by a fused salt electrolysis technique. The modifications and the major unit operations involved are summarized in Figure 6.20. The processes shown and their modifications have been used for making neodymium alloys by Molycorp, Research Chemicals, Comurhex, Goldschmidt, General Motors, Ronson, and Santoku.

6.11.1.3.1 Molycorp

The schematic flow sheet of the Molycorp process is shown in Figure 6.20a. The process used was calciothermic reduction of neodymium fluoride prepared from the carbonate by a wet process.

Neodymium nitrate was made from the carbonate by an aqueous process. The nitrate was fed to a batch precipitation reactor at a controlled rate with excess hydrofluoric acid. The solution pH was controlled by adding sodium hydroxide solution. At the end of the reaction, the reactor contents were passed through a continuous filter where the neodymium fluoride precipitate was removed and thoroughly washed. The filtrate was neutralized, and excess fluoride was precipitated from it by the addition of lime.

Water was removed from the neodymium fluoride precipitate by first feeding it to a dryer for removal of adhering moisture and then feeding it to a calciner for removing water of hydration. Calcination was carried out in an atmosphere of hydrogen fluoride, which was obtained from an HF still. The off-gases were scrubbed and neutralized. The calcined product was stored under nitrogen.

Anhydrous neodymium fluoride was blended batchwise with an excess of calcium granules. The mixture was loaded in tantalum crucibles and reduced in an induction furnace under a nitrogen atmosphere. The furnace was provided with a charging system for solids and a crucible tilting mechanism. Thus, portions of calcium fluoride/calcium slag could be poured off, and the crucible recharged twice during the course of reduction. The decanted slag was solidified and disposed of, and the reduced neodymium was cast into molds for purification.

As-reduced neodymium metal was purified by vacuum-melting in an induction furnace. Purification needed high vacuum and a long duration. The purified neodymium was cast into molds for alloying. Alloying was carried out by adding iron and ferroboron in controlled amounts to pure neodymium metal, and alloy melting was carried out in a nitrogen atmosphere. The alloy was cast in molds and analyzed. *Off-spec* material was recycled, and acceptable material was sent for magnet manufacturing.

6.11.1.3.2 Research Chemicals

The route followed is calciothermic reduction of neodymium fluoride, and the fluoride was prepared from the oxide by a dry process. The schematic flow sheet is shown in Figure 6.20b as the Ames process. Neodymium oxide was blended with a large excess (100%) of ammonium bifluoride, and the mixture was charged to a drum-type fluorinating reactor. This batch reactor was operated with a programmed

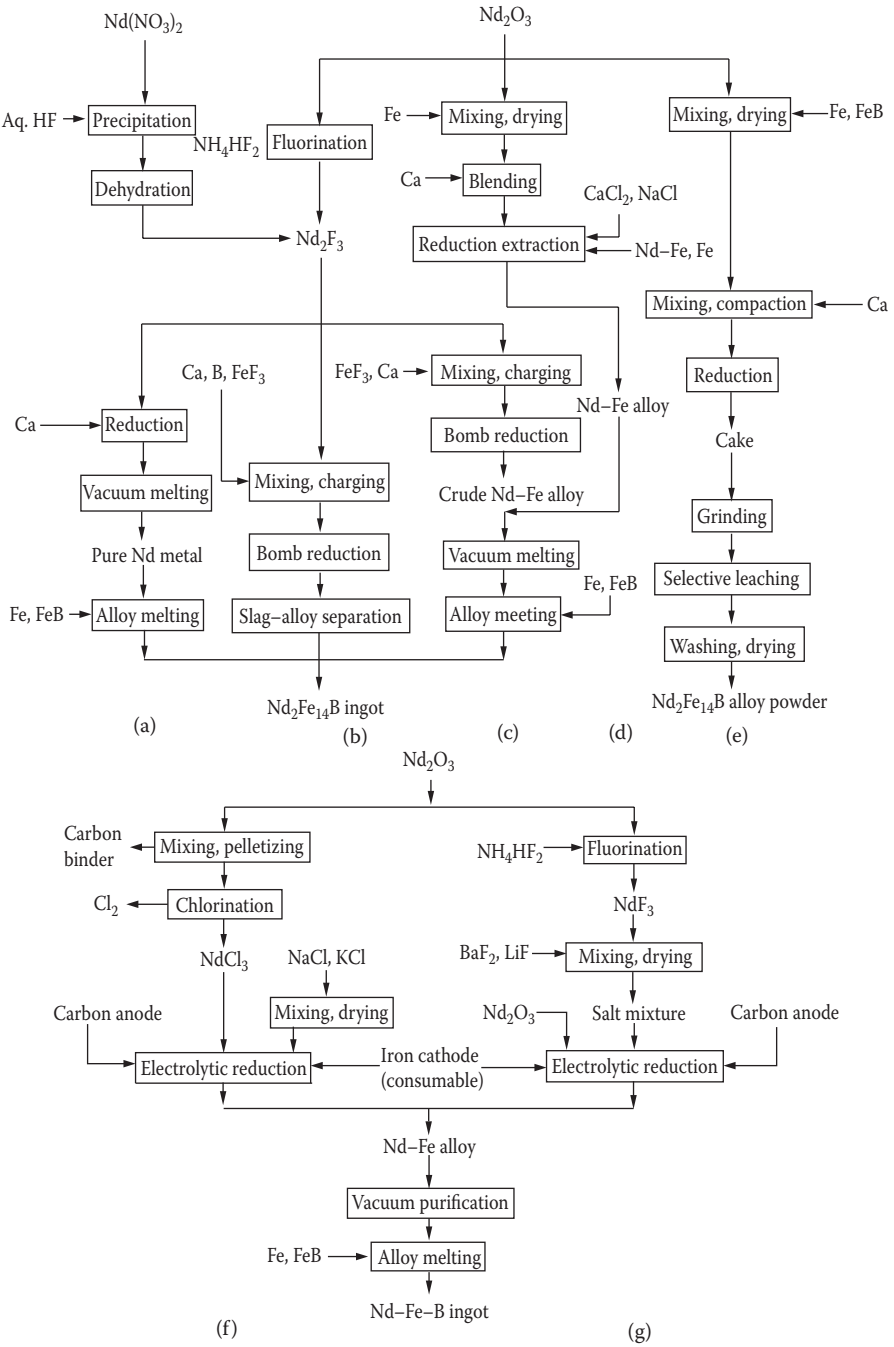


FIGURE 6.20 Preparation of Nd–Fe–B alloys: (a) Molycorp process, (b) Ames process, (c) Comurhex process, (d) General Motors process, (e) Goldschmidt process, (f) Ronson process, and (g) Santoku process.

temperature cycle. The charge was heated to first convert the oxide to the complex fluoride and then to remove the unreacted excess bifluoride. The complex fluoride was then decomposed by heating in vacuum, and the fluoride product was calcined. The drum was rotated during the reaction period to effect mixing of the phases. The calcined fluoride was cooled, removed from the reactor, and stored under nitrogen. The fluoride was processed to the magnet alloy using the same equipment and procedure as that described for the Molycorp process.

During fluorination, initially, the reaction products, ammonium fluoride, water, and unreacted hydrogen fluoride, were removed from the reactor in a stream of nitrogen and were scrubbed with water for disposal. At the time of excess bifluoride removal, the off gases passed through switching condensers where the bifluoride was collected as a solid. This was scrubbed, and the scrub solution was treated with sufficient lime to bring the pH to near neutral. The solution was then clarified, the overflow discharged, and the sludge disposed.

The condensers that had collected the bifluoride were heated sequentially to above the solid's (ammonium bifluoride) melting point, and the liquid was pumped to a scrapped surface heat exchanger for solidification. The bifluoride was recycled.

6.11.1.3.3 Comurhex

The schematic flow sheet of the Comurhex process is shown in Figure 6.20c. The key step was an adiabatic calciothermic reduction of a mixture of neodymium and iron fluorides.

The wet process described earlier for the Molycorp flow sheet was used for the preparation of neodymium fluoride. Iron fluoride was prepared by reaction of iron chloride with gaseous hydrogen fluoride that was obtained by stripping a portion of the hydrofluoric acid used in neodymium nitrate precipitation. Hot and dry iron chloride, obtained by feeding iron chloride continuously to a dryer/preheater, was fed to a fluoridizing reactor in which excess hydrogen fluoride was fed countercurrently. The reactor was staged and cooled to control the temperature profile. The reactor off-gas contained hydrogen chloride, excess hydrogen fluoride, and some iron chloride. It was scrubbed with water and then disposed. The scrub solution was discharged after fluoride removal by liming and clarification. The iron fluoride was cooled in the final reactor stage and collected warm for storage. It was stored under nitrogen.

Neodymium fluoride, iron fluoride, and excess calcium were mixed in a proportion sufficient to produce a reaction product mass at a temperature between 1100°C and 1200°C adiabatically. The mixture was loaded around a mandrel and compressed into steel reactor vessels. These vessels were jacketed and were designed to withstand an internal pressure of 7 MPa. A tantalum cup was fitted below the charge to collect the alloy product. An ignitor charge comprising calcium and iron fluoride was placed over the top of the charge.

After loading the reactor, it was purged with nitrogen and the charge was ignited. The reaction proceeded rapidly from the core to the outside where it was quenched by the cold material in contact with the wall. The reduced iron–neodymium alloy has a relatively low melting point and drained through the calcium fluoride slag into the tantalum cup. After cooling, the reactor was opened, the alloy was retrieved from the tantalum cup, and the slag was removed from the reactor for disposal. The

unreacted charge adhering to the wall was separately collected and recycled for blending with fresh material.

The crude NdFe alloy was purified by vacuum-melting and adjusted to the required final composition in alloy-melting furnaces by the procedure described for the Molycorp process.

6.11.1.3.4 Th. Goldschmidt

The schematic flow sheet of the Th. Goldschmidt process for producing neodymium–iron–boron alloy is shown in Figure 6.20e. Neodymium alloy powder of desired composition was directly produced by a calciothermic reduction of a proportionate mixture of neodymium oxide, iron, and ferroboron.

Neodymium oxide was mixed with a slight excess of iron and ferroboron, and the mixture was heated to remove traces of moisture and kept in a nitrogen atmosphere. Calcium, in a suitable excess quantity, was blended with this mixture, and the charge was fed to the press for compaction. The pellets were loaded into holding vessels, and the vessels were closed and purged with nitrogen and then with argon. These vessels were then transported to electrically heated furnaces, where they were heated to the reaction temperature. After completion of the reaction, the vessels were removed from the furnace and allowed to cool, and the contents were discharged into holding bins under an argon atmosphere.

The reduced alloy was liberated from the slag by grinding the reaction product in a closed-circuit ball mill under liquid hexane. From the finely ground material, hexane was removed by evaporation in a wiped surface evaporator, and the ground material was transferred to surge bins under argon atmosphere. The material now contained unreduced reactant, excess calcium, and calcium oxide in addition to the product alloy. The other materials were separated from the alloy by a proprietary leaching process in which pH and E_h were carefully controlled, and nitric acid, a chelating agent, or other chemicals were probably used for selective leaching. The leach effluent was filtered to recover the solid product. The product was washed with deoxygenated water, dried, and stored under argon. The filtrate was treated with lime to neutralize excess acid and precipitate dissolved neodymium and iron as hydrous oxides. The effluent was clarified and the overflow discharged. The sludge was also disposed.

The product was quality controlled, and *on-spec* material was stored in lined containers under inert gas. The off-spec material was either used for blending or converted to ingot in an alloy furnace after the addition of required boron or ferroboron.

6.11.1.3.5 General Motors

The schematic flow sheet of the General Motors process is shown in Figure 6.20d. The key process is the calciothermic reduction of a mixture of neodymium oxide and iron that takes place in a molten salt mixture in a stirred tank reactor.

Neodymium oxide was blended with iron, and the mixture was heated to remove traces of moisture. The dried material was stored under an inert atmosphere. The quantities of neodymium oxide and iron were chosen so that on reduction of the oxide, neodymium and iron would form an alloy of eutectic composition. Calcium and sodium chlorides were also blended and heated before loading them into the

reduction reactor as makeup. The iron–neodymium mixture was blended with excess calcium, and the charge was kept in surge bins under an inert atmosphere for feeding to the reactor.

The reduction was carried out in a tantalum-lined electrically heated stirred tank reactor. The reactor was charged with the required amount of salt mixture, and a heel of eutectic alloy and solids was melted. The temperature was raised to ~750°C, and the neodymium oxide–iron charge was fed to the reactor at a controlled rate with high agitation for a predetermined period. Charge feeding was then interrupted, agitation was decreased and then stopped to permit the phases to settle, and the molten alloy product was removed by bottom tapping. This cycle was repeated many times while the unreacted calcium and neodymium oxide and the calcium oxide slag were being retained within the reactor. At the conclusion of the cycles, all of the eutectic was removed, and the salt, which contained large amounts of solids, was discharged for disposal. The NdFe eutectic was vacuum-purified and alloyed to the final composition by the same procedure as described for Molycorp.

6.11.1.3.6 Ronson

The schematic flow sheet of the process used by Ronson is shown in Figure 6.20f. The process is an electrochemical reduction of neodymium chloride by electrolysis of a mixture of fused chloride salts using a consumable iron cathode.

Neodymium chloride was prepared from neodymium oxide by chlorination in the presence of carbon. The oxide was mixed with excess carbon and a binder, and the mixture was compacted into pellets. The green pellets were dried and screened. The undersize pellets were recycled and the others held in surge. Chlorination was carried out in a shaft furnace. The pellets fed to the top of the shaft furnace descend against a countercurrent flow of heated chlorine gas. The neodymium chloride formed is molten at the prevailing temperature. It drained from the reactor into a heated enclosed receiver. Unreacted oxide and excess carbon were settled and skimmed in the receiver. The furnace off-gas containing excess chlorine and carbon oxides was scrubbed with off-gas from the electrolytic cells to remove chlorine.

The liquid neodymium chloride from the chlorination furnace was transferred under inert atmosphere to an exchanger for solidification. The solid chloride was held warm under nitrogen for charging to the electrolytic cells. The electrolyte components, sodium chloride, and potassium chloride were mixed, heated under an inert atmosphere to remove moisture, and held for changing to the cell. Electrolysis was carried out in cells with carbon anodes and a consumable iron cathode. Neodymium–iron alloy formed at the cathode was collected at the cell bottom and tapped periodically. Chlorine was evolved at the anode. The gas was scrubbed in an oxidizing solution of calcium hydroxide, and the resulting solution of soluble chloride salt was released. During electrolysis, impurities in the charge materials, especially the oxychlorides, accumulated in the electrolyte, and the electrolyte must be purged to remove them.

The crude alloy obtained from the electrolytic cell was purified by vacuum-melting to remove volatile chlorides and was then alloyed with iron and ferroboron as in the Molycorp process.

6.11.1.3.7 Santoku

The schematic flow sheet of the Santoku process is given in Figure 6.20g. The process involves electrolytic reduction of the neodymium oxide in a fused fluoride electrolyte and recovery of the metal as the iron alloy.

Neodymium oxide was dried by heating to remove the moisture, and the dry oxide was stored under an inert atmosphere for charging to the cell. A portion of the oxide was converted to the fluoride using ammonium bifluoride as the fluorinating agent under conditions described for the Research Chemicals/Ames flow sheet. Neodymium fluoride was mixed with barium fluoride and lithium fluoride, and the mixture was dried by heating to remove the trace amounts of water. The dry fluoride mixture was stored under inert gas cover for charging to the cells.

Electrolysis was carried out in cells equipped with carbon anodes and iron cathodes. The cathode was consumable as the reduced neodymium metal alloys with the iron forming a low-melting eutectic that was collected in tantalum liners at the cell bottom. Oxides of carbon were formed at the carbon anode. These gases were vented and scrubbed for discharge.

The cells were loaded with the fluoride electrolyte mixture and heated to melt the electrolyte and attain the cell operating temperature. The oxide was charged at a controlled rate, and the molten alloy product was bottom-tapped periodically. Unreacted oxide and other impurities collected in the electrolyte and they were purged. The neodymium–iron alloy obtained from the cell was first purified mechanically to remove adhering electrolyte and then charged to the alloy-melting furnace. This furnace was equipped with a vacuum system and was used first to purify the alloy from volatile impurities by vacuum-melting, after which alloying additions were introduced to obtain the final composition.

Among the processes listed above, neodymium recovery of about 90% was possible when calcium was the reducing agent, and neodymium fluoride was the intermediate starting compound. The yield was only about 70–75% in the electrolytic processes because of losses caused by bleeding of the electrolyte to control its chemical composition. The primary alloy product contained about 30–32% neodymium. This neodymium was actually 96% neodymium and 4% other rare-earth metals.

The processes for alloy production of rare-earth metals are considered fairly straightforward up to the primary alloy stage. Both the yield and quality control become major concerns when these primary alloys are processed to fabricate the final magnet product.

6.11.2 Production of Nd–Fe–B Magnets

Commercial sintered $Nd_2Fe_{14}B$ magnets are produced by one of two methods: a powder metallurgy liquid-phase sintering method (a process also used to manufacture $SmCo_5$ magnets) or a rapid solidification method, similar to the melt-spinning process used to produce glassy metals (Cook and Rossiter 1989). Once the magnet material is ready, there are many ways by which the magnet can be fabricated.

Prior to the production of Nd–Fe–B magnets, the Nd–Fe–B alloys that have been prepared by one or another of the above methods are first processed to a metallurgical

or physical form suitable for further conversion to magnets. One process is melt spinning. The molten alloy is rapidly cooled to a thin flake before it is processed further as it is or after milling to a powder. In the other route, the cast alloy ingot is converted to fine powder before a modified powder metallurgical consolidation to magnets. The second is known as the sintering route.

6.11.2.1 Melt Spinning

In melt spinning, Nd–Fe–B alloy is melted, and a fine jet or stream of molten alloy is directed onto the surface of the rapidly spinning large copper wheel. The apparatus is shown schematically in Figure 6.21. The disc is usually made of copper because of its high thermal conductivity, and it rotates with surface velocity v_s. While the jet feeds a pool of liquid metal, at its point of contact with the spinning wheel, the molten alloy is rapidly quenched with the heat being taken away by the wheel. The solidified (quenched) metal is obtained in the form of a thin ribbon or flake. The process is carried out in an inert atmosphere, usually argon, because the rare earths are very reactive chemically and need to be protected from oxidation during high-temperature processing. In melt spinning, the cooling or quench rate attained is of the order of 10^5°C/s, and this rate can be varied by changing v_s. The cooling rate is directly proportional to v_s. The quenched material is inherently brittle, and the flakes are obtained in dimensions typically 30–50 μm thick, 1–3 mm wide and having lengths on the millimeter or centimeter scale, depending on v_s.

The microstructure and magnetic properties of melt-spun Nd–Fe–B ribbons are sensitively dependent upon the quench rate (Herbst and Croat 1991), which in turn depends upon v_s. Plotted as a function of v_s, H_{ci} and $(BH)_{max}$ each exhibits a maximum. At high quench rates ($v_s \geq 30$ m/s), essentially amorphous, *overquenched* materials with negligible H_{ci} and $(BH)_{max}$ are obtained. At quench rates $v_s = 19$ m/s, ribbons consisting of spheroidal $Nd_2Fe_{14}B$ grains with an average diameter of 30 nm are obtained. These ribbons have the highest coercivities (H_{ci} « 1120 kA/m) and

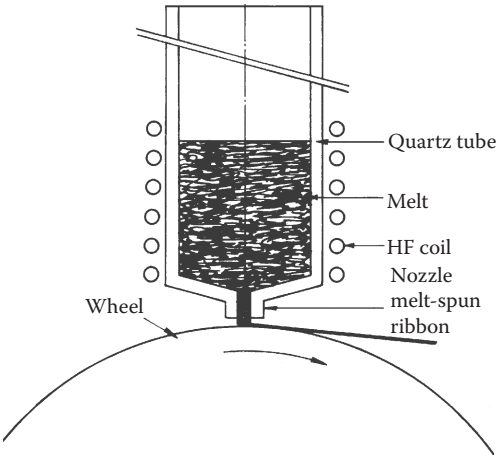


FIGURE 6.21 Schematic of the melt-spinning apparatus. (From Ormerod, J., *J. Less Common Metals*, 111: 49–69, 1985.)

energy products [$(BH)_{max}$ ~ 112 kJ/m^3]. These are optimally quenched ribbons. At v_s below the value resulting in optimally quenched ribbons, ribbons composed of progressively larger $Nd_2Fe_{14}B$ crystallites and characterized by decreasing H_{ci} and $(BH)_{max}$ are formed. The melt-spun ribbons may be heat-treated in an argon atmosphere to generate hard magnetic properties (Ishii et al. 2007). It is interesting and technologically significant that the largely amorphous, overquenched ribbons melt-spun at quench rates required only to exceed a minimum value instead of confining to a narrow interval can be suitably annealed to nearly duplicate the properties of optimally quenched materials obtained directly. The quenched ribbon or flake is usually ground down to a fine powder before processing to consolidated magnets.

6.11.2.2 Strip Casting

The excellent glass-forming ability of Nd–Fe–B–Ti–C-based alloys allows adoption of a high-throughput rapid solidification technique called *strip-casting* (SC), which has been used increasingly in production of high-end Nd–Fe–B sintered magnets. SC is basically a process to obtain a continuous strip by extracting a molten alloy from a pool of liquid by using a moving surface of a chilled drum. Upon contact with the drum surface, the alloy quickly solidifies and is extracted from the melt pool as strips. The SC process differs from the melt-spinning process in that the molten alloys are simply poured upon a guide and lead to a chilled roll whereas in the melt spinning (MS) process, the alloys are ejected from a small orifice by applying pressure.

The SC is one of the major turning points to improve the microstructure of NdFeB sintered magnet. A SC alloy has finer dendrites with scattered rare earth-rich phase. The rare earth-rich phase easily generates a liquid phase because of the uniformly surrounding 2–14–1 dendrites. Furthermore, as the jet-milling process improved almost twice in efficiency in comparison with the conventional method of comminution, the resultant particle size distribution is also easily controlled to be fine with an increase in the productivity (Kaneko et al. 2006).

Chen et al. (2012) studied the influence of substitution of Nd with Pr on the magnetic properties of sintered permanent magnets. Strip casting technique was used to prepare the alloys strips with nominal compositions of $(Nd_{1-x}Pr_x)_{29}Dy_{1.3}R_{3.1}Fe$ bal (wt.%, R = $Al_{0.3}Cu_{0.2}Co_{1.5}B_1Zr_{0.1}$) with x varying from 0 to 1. The strips were crushed by hydrogen decrepitating (HD) treatment and then jet-milled (JM) under N_2 gas flow. The powder was pressed and simultaneously aligned in a magnetic field of 2 T and then isostatic-pressed under a pressure of 300 MPa for 60 s.

6.11.2.3 Hydrogenation–Disproportionation–Desorption–Recombination

The hydrogenation–disproportionation–desorption–recombination (HDDR) process is a unique method for achieving a submicron-textured microstructure within initially monocrystalline $Nd_2Fe_{14}B$ powders through a simple heat treatment in hydrogen gas (Nakayama and Takeshita 1993; Takeshita and Nakayama 1990). The resultant microstructure is very similar to that observed in sintered Nd–Fe–B magnets except that the grain size is one order of magnitude smaller (Nozawa et al. 2011).

The HDDR-processed powders have a unique microstructure. They consist of fine crystalline grains with the size distribution from 100 to 900 nm. The size of

most grains is about 300 nm, which is comparable with the single-domain size of the $Nd_2Fe_{14}B$ phase. There are no grain boundary phases between grains, which is quite different from the powder prepared by melt-spinning route where very small grains of about 50 nm diameter are surrounded by a thin layer of amorphous boundary phase. Coercivity and the magnetization reversal mechanism in HDDR-processed bonded magnets originate from their unique microstructure (Plusa et al. 2006).

The HDDR process involves hydrogenation of the alloy at relatively low temperatures (less than 500°C) and disproportionation of the alloy into a fine-scaled mixture of a rare-earth hydride and α-Fe. The fine-scaled mixture is heated under vacuum (typically at 700–800°C) to desorb the hydrogen and recombine the rare-earth and α-Fe to form an intermetallic with submicron grain structure. Most often, HDDR processing produces an isotropic magnet powder, and, as a consequence, the remanence and the maximum energy product of the bonded magnets made from them are not too high. Through elemental additions, it is possible to produce an anisotropic powder. Magnets with better properties can be produced from anisotropic powder, which can be obtained by employing the HDDR process on the Nd–Fe–Co–B alloys with small anisotropy-inducing additions of Ga, Zr, Nb, or Hf (Chen et al. 2003; Takeshita and Morimoto 1996). Morimoto et al. (2012) have shown that with proper Al and Nd contents, the slow hydrogen desorption of the HDDR treatment can remarkably improve the coercivity of the Dy-free Nd–Fe–Co–B–Ga–Zr–Al powders. The process is outlined as follows by Nozawa et al. (2011). A cast alloy of $Nd_{13.5}Fe_{72.0}Co_{8.0}B_{6.5}$ was homogenized at 1110°C for 16 h and subjected to hydrogen decrepitation prior to the HDDR process. The alloy was then crushed into powder with particle sizes ranging from 50 to 300 μm. The HDDR process consisted of heating the powder under hydrogen gas flow at an atmospheric pressure at 840°C for 3 h and subsequent heating under Ar gas flow of about 5 kPa for 1 h. The powder had a remanence (B_r) of 0.99 T and an intrinsic coercivity (H_{cj}) of 824 kA/m at room temperature. Another description is from Morimoto et al. (2012). The $Nd_xFe_{bal}Co_{5.8}B_{6.3}Ga_{0.50}Zr_{0.1}Al_y$ (x = 12.9–15.0, y = 0–2.5) alloy ingots were prepared by induction melting of constituent elements in argon atmosphere. They were subjected to homogenization heat treatment at 1140°C for 20 h in argon and then crushed into powder of particle sizes of <150 μm. The alloy powder thus obtained were HDDR-treated as schematically shown in Figure 6.22. The hydrogenation–decomposition (HD) process was carried out by heating the powder up to 840°C in an atmospheric hydrogen–argon mixture and keeping them at this temperature for 180 min. In the desorption–recombination (DR) process, the powders were desorbed under a constant hydrogen partial pressure of 3 kPa at 840°C C for 90 min (DR-Step 1), and subsequently evacuated to a high vacuum of 1 Pa at the same temperature (DR-Step 2). This two-step desorption process can induce high coercivity in the powder without causing a decrease in residual induction. The time period of DR-Step 2 was set to 45 min (hereafter designated as fast desorption) or 90 min (slow desorption) by adjusting a vacuum valve. After this processing, the powder was quenched using argon to room temperature.

The HDDR process is the main method for the production of the anisotropic Nd–Fe–B powder (Zhang et al. 2006a). It is the HDDR process that is being used to produce anisotropic $Nd_2Fe_{14}B$ powder for use in polymer-bonded magnets. With industrialization of anisotropic Nd–Fe–B magnetic powder, the requirements for good

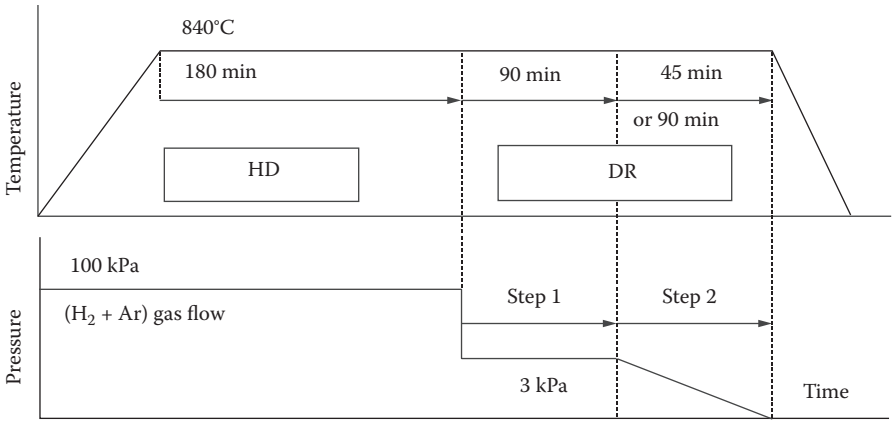


FIGURE 6.22 Schematic HDDR treatment pattern. (From Morimoto, K. et al., *Journal of Magnetism and Magnetic Materials*, 324(22):3723–3726, 2012.)

magnetic properties provided by anisotropic bonded magnets have increased. The next step in the sequence for the of making of magnets is consolidation of the magnet material powder into a suitable form. A summary of the variety of consolidation techniques used in the production of rare-earth magnets and their features are listed in Table 6.16.

TABLE 6.16
Structural Comparison of the PMs

Method	Advantages	Limitations
Sintering	Maximum energy product for a given magnet size and weight	Limited to simple geometries
	Maximum output	Brittle
Injection Molding	Complex geometries	Lower $(BH)_{max}$
	Relatively tough	
	Lower assembly costs	
	Allows high volume manufacturing	
	Shaping flexibility	
Pressure Bonding	Greater volumetric loading of magnetic phase	Limited to simple geometries
	Brittle	Complex magnetizing patterns
	Tight geometric tolerances	
	Low-cost manufacturing	
Casting	Allows relatively complex shapes	Difficult to machine
	Higher $(BH)_{max}$	Lower mechanical resistance
	Extremely hard and brittle	
	Shaping flexibility	
Calendering and extruding	Complex geometries	Lower $(BH)_{max}$
	Easy to tool and machine	
	Shaping flexibility	

6.11.2.4 Consolidation

The production of bulk magnets by consolidation of melt-spun ribbons (Lee 1985; Lee et al. 1985) is accomplished by the procedures outlined in Figure 6.23. The first procedure yields *bonded magnets*, and the second procedure yields *hot-pressed magnets*.

There are benefits in loading the magnet powder in a polymer matrix to make moldable or flexible magnets (Coey 2012). Bonded magnets with complex geometries can be produced using injection-molding techniques. A variety of polymer binders and polymer additives provide flexibility for production and meet the needs of various applications including use in electric machines (Gundogdu and Komurgoz 2013).

6.11.2.4.1 Bonded Magnets

Bonded Nd–Fe–B magnets are manufactured from the rapidly solidified magnetic powder (Lee 1985; Lee et al. 1985; Croat 1998). This is done in many ways. Melt-spun ribbons are very desirable for bonded magnet production. Due to the extremely fine particle size, no degradation of the properties accompanies pulverization. The flat geometry of the ribbon fragments (~0.5 mm × 0.5 mm × 40 μm) facilitates efficient packing so that densities of approximately 85% with respect to $Nd_2Fe_{14}B$ can be obtained even with modest pressures of 600–700 MPa. The bonded magnet, like its constituent ribbons, is magnetically isotropic. The melt-spun ribbon or flake is typically ground down into a finer powder before being processed into bonded magnets. Bonded Nd–Fe–B magnets are prepared by mixing the hard magnetic powder with polymer binder, followed by compression or injection-molding techniques. The magnetic properties of compression-molded elements are higher than the magnetic properties of injection-molded elements due to the larger loading magnetic powder in compression molding (95–98%) compared to injection-molded elements (50–60%). At present, nearly 90% of the bonded neodymium magnets are produced using a compression (compaction) molding process. Compression molding is based on pressing a mixture of magnetic powder and resin powder in a die and then curing green compact in the furnace. The magnetic powder is blended with an epoxy dissolved in a suitable organic solvent. While blending of the mixture is continuing, the solvent is drawn off resulting in a coating or encapsulation of the magnetic powder particles. The encapsulated powder is dried and then fed into a conventional powder metal press and compacted into the required shape. After compaction, the parts are heated in an oven to cure the epoxy. The energy products obtained in magnets made by compaction molding are usually in the range of 80–88 kJ/m^3. Tailoring of magnetic and mechanical properties of compression-molded magnets can be done by adding to the mixture Nd–Fe–B powder and resin powder, powder of different metals or alloys such as powder of iron (Slusarek et al. 2005, 2007).

The polymer-bonded magnets containing silane-coated NdFeB magnetic filler with high loading (about 62 vol.%) show zero irreversible loss in magnetic flux density after exposure to temperatures up to 180°C. The silane-coating treatment alters the magnetic properties by increasing the remanence of polymer-bonded magnets via increasing the interparticle coupling coefficient. The coating avoids deterioration

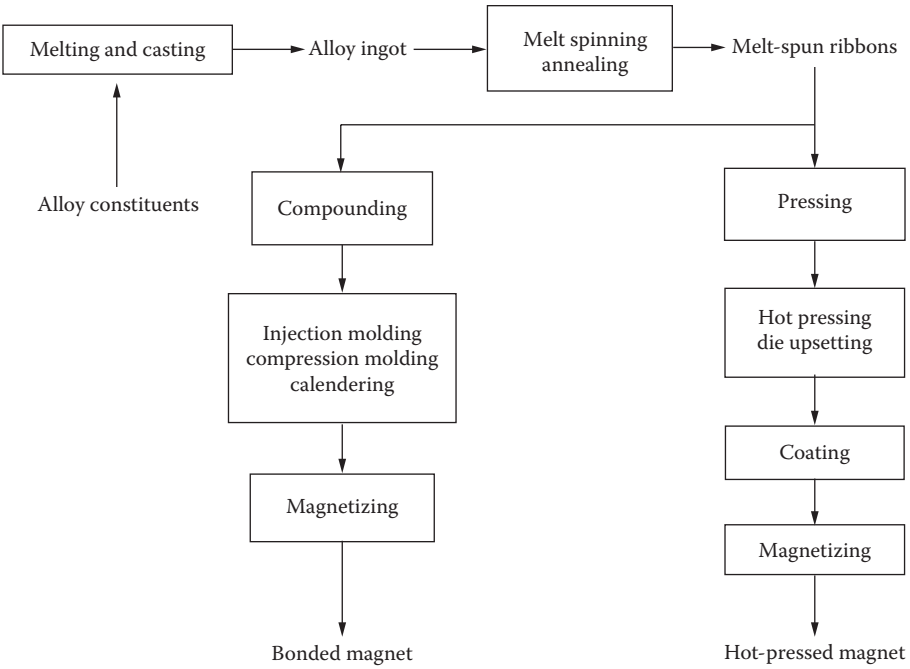


FIGURE 6.23 Processes for magnets from melt-spun ribbons. (From Tourre, J.M., Rare earths 1998 market update. In *Preprints of the Conference, China Magnets*, held on 18–21 October 1998 at Beijing, PR China, 1998.)

of magnetic performance at elevated temperatures, and these materials may be suitable for applications in humid and high temperature environments where common untreated permanent (NdFeB) magnets are not usable.

The details of the compression-molding method after silane coating, used by Xiao et al. (2000), are as follows. The commercial NdFeB magnetic powder (MQP-O, Magnequench International, Inc.) used was a multimodal mixture of plate-like particles. The surface modification of the NdFeB is performed using an organometallic compound such as c-aminopropyltriethoxysilane (referred to as silane) as the coating agent. The silane coating is done by simple immersion of the $Nd_2Fe_{14}B$ particles in an aqueous solution of the silane under ultrasonic agitation for 5 min. The excess silane solution is decanted, and the powders are dried to constant weight in a vacuum oven at 85°C. The silane reacts readily with the rare earth–bearing particles to form a protective monolayer. Silanes can chemically bond organic polymers to inorganic substrates such as $Nd_2Fe_{14}B$ particles. Zhang et al. (2009) described the production of bonded magnets from magnequench powder. The samples were produced from a mixture of isotropic Magnequench MQP-B powder and binder combined through a compression-molding technique. The magnetic powder was coupled with the acetone solution containing a silane-coupling agent and was dried in an oven with argon protection before further processing.

Ishii et al. (2007) prepared a high-coercivity Nd–Fe–B–Ti–C–Cr nanocomposite magnet with uniform grain sizes having excellent thermal resistance. The rapidly solidified ribbons of the $Nd_{4.5}Fe_{73}Co_2B_{18.5}Cr_2$ alloy containing a few atom percent each of Ti and C were prepared by the melt-spinning technique in an argon atmosphere onto a copper wheel rotating at a surface speed of 5–20 m/s. Elemental metals of purity higher than 99.8% were used. The ribbons were then annealed between 873 and 1073 K for 0.36 ks in argon. Resin-bonded magnets were processed from pulverized powder of the optimally heat-treated ribbons by compression molding. No coating was applied on the magnets. The addition of Cr was found to enhance coercivity of Nd–Fe–B–Ti–C dramatically. A large coercivity (H_{cj} = 1609 kA/m) was obtained by adjusting Nd, B, and C contents in the Nd–Fe–B–Ti–C–Cr system. H_{cj} increased with refinement of grain sizes that was realized by increasing the total amount of B and C.

Anisotropic bonded NdFeB magnets have magnetic properties better than those of conventional isotropic bonded NdFeB magnets and have been used to make devices with special oriented magnetization, such as radially oriented rings. Anisotropic magnet powder (210 μm average size and BH_{max} 310 kJ/m^3) made by d-HDDR process (dynamic HDDR) is commercially available and used by Tao et al. (2009) to make the radial magnets. A starting mixture of 97 wt.% alloy powder and 3 wt.% thermosetting epoxy resin was used. The anisotropic bonded NdFeB magnets with radially oriented magnetization were prepared by two-step warm compaction molding. In the first (aligning) step, the magnetic powder particles aligned along the radial direction of the magnetic field (1.0 T) and are compressed under 143 MPa at 393 K. $(BH)_{max}$ and density of the magnets were 146 kJ/m^3 and 5.7 g/cm^3, respectively. Then the ring compacts were recompressed under 800 MPa at 420 K in the second (densifying) step. The density increased to 6.2 g/cm^3 and magnetic properties were B_r = 0.92 T, H_{cj} = 1020 kA/m, and $(BH)_{max}$ = 168 kJ/m^3. That the magnets had excellent microstructure and the magnetic particles were evenly coated by a binder was confirmed by SEM results.

Bonded neodymium magnets are also produced from melt-spun powders by injection molding. This is the second most common method. The powder is first mixed or *compounded* with a thermoplastic material such as nylon. It is then fed to a conventional injection-molding machine. The energy products of injection-molded magnets are lower (due to lower loading of the magnet material), in the range of 40–48 kJ/m^3, because these magnets have a higher percentage of resin. The properties were enhanced by using anisotropic powder.

Injection molding has been used for low-cost, high-volume production of magnets with complicated geometry (Garrell et al. 2003), usually with isotropic magnet powder. Zhang et al. (2006b) investigated production of anisotropic injection bonded Nd–Fe–B magnets prepared from HDDR anisotropic Nd–Fe–B powder. Magnetic powder (70–106 μm) was mixed (60% powder, 40% binder and additive) with a binder and an additive, prilled for 5–6 min at 205–215°C, and injected through channels and mold cavities under the injection pressure of 5–6 MPa and the press time of 5 s at 265°C. Molding temperature was 80°C. Figure 6.24 shows the process sequence.

The magnetic properties of anisotropic bonded Nd–Fe–B magnets made in the above conditions from d-HDDR powder were B_r = 0.72 T, H_{Ci} = 983 kA/m, and $(BH)_{max}$ = 75 kJ/m^3.

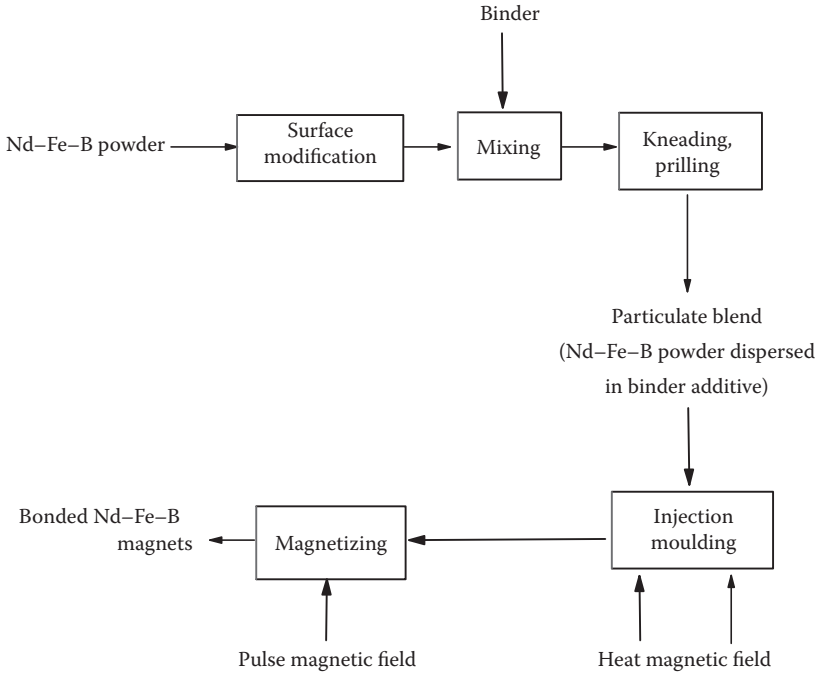


FIGURE 6.24 Process of bonded Nd–Fe–B magnets by injection molding. (From Zhang, X. et al., Study on fabrication process of anisotropic injection bonded Nd–Fe–B magnets, In Wei Li, Yang Luo, Zhongguo-Jinshu-Xuehui (eds.), *Proceedings of 19th International Workshop on Rare Earth Permanent Magnets & Their Applications* (Workshop on REPM'06), August 30–September 2, 2006, pp. 286–288, Chinese Society for Metals, Friendship Hotel Beijing, China, 2006.)

The bonded neodymium magnets are given a coating before the final assembly. The coating prevents surface oxidation and also loss of magnetic particles.

6.11.2.4.2 Hot-Pressed Magnets

The procedure based on hot pressing permits complete densification of melt-spun ribbons. The temperatures and pressures needed for hot pressing depend on the starting alloy composition. For composition near $Nd_{0.135}Fe_{0.817}B_{0.048}$, full density was achieved using $p \sim 100$ MPa and $T \sim 700°C$. The most desirable grain size was developed by hot-pressing *overquenched* ribbons. Energy products of the hot-pressed magnets were in the range of 80–160 kJ/m^3. Only a slight (~10%) crystallographic alignment of the easy C axis parallel to the press direction was introduced by the uniaxial hot pressing.

Another variant of the hot-pressing method, called die upsetting, results in a greater (~75%) crystallographic alignment of the easy C axis and consequently much larger energy products. In this method, an initial hot press is followed by another in a die cavity of larger diameter. The second hot press in the larger die, called die upsetting, causes bulk lateral plastic flow and an accompanying reduction in ribbon thickness. It has been found (Nozawa et al. 1988; Tokunaga et al. 1989) that the greatest magnetic alignment was achieved only if the original sample height was reduced by at least a factor of 4 during die upsetting. Like their hot-pressed precursors, the die upset magnets are fully dense and possess energy products as high as 360 kJ/m^3. Rapid solidification produces an isotropic magnet material, which may be hot-pressed and die-upset in subsequent processing stages to produce the anisotropic material.

In the matter of nanocrystalline NdFeB magnet powders, one of the issues during the densification and deformation process by conventional method (Huang et al. 2012; Song et al. 2013; Xu et al. 2012) is excessive grain growth and consequent properties degradation. Spark plasma sintering (SPS), with its high sintering speed, can effectively restrain the grain growth and allow the preparation of high-density fine crystalline materials.

The procedure adopted by Hu et al. (2012) involved melt quenching, SPS, and die upsetting. The alloy ingot with nominal composition of $Nd_{11.5}Dy_3Fe_{78.5}Nb_{0.75}Al_{0.23}Cu_{0.02}B_6$ was cast using vacuum induction furnace, and following melt-quenching at a wheel speed of 20 m/s under Ar atmosphere, the as-spun flakes were then crushed to 150–200 μm. Isotropic bulk magnets were prepared by SPS at 700°C under 300 MPa with a diameter of 13 mm in a tungsten carbide mold, and then these magnets were die-upset. The composition modification and optimization of the die-upsetting process led to further improvement of the remanence (B_r) and intrinsic coercivity (H_{ci}) of die-upset Nd–Fe–B magnets.

Using SPS, Song et al. (2013) fast consolidated commercial RS magnet powders in a tungsten carbide (WC) die (15 mm diameter × 40 mm height) at 650°C for 3 min under 300 MPa. The hot-pressed magnets were then hot-deformed (die upset) with height reduction of 60% at 750°C to obtain the best properties of $B_r = 1.36$ T, $H_{ci} = 1143$ kA/m, and $(BH)_{max} = 370$ kJ/m^3. In the hot-pressed condition (before the deformation), the $(BH)_{max}$ of the magnet was 128 kJ/m^3. Microstructure observation revealed

that good magnetic properties of both the hot-pressed and hot-deformed magnets are due to uniform microstructures.

Apart from the more widely available sintered forms, fully dense anisotropic Nd–Fe–B magnets have also been commercially produced by melt-spinning followed by hot-pressing. Yi et al. (2010) blended commercial rapidly quenched Nd–Fe–B ribbons with nominal composition $Nd_{13.34}Fe_{74.74}Co_{5.5}Ga_{0.42}B_6$ and fine Cu powders 0.2–0.5 wt.% (10–30 μm) before hot pressing. They made isotropic hot-pressed magnets at 893 K and 150 MPa in vacuum. Anisotropic magnets were produced by die-upsetting the hot-pressed precursors in an oversized die at 1133 K and 100 MPa under high pure argon until their height reduced by 70%. The incorporation of Cu powder was effective in improving both the magnetic properties and the bending strength of the die-upset magnets. The increase in H_{cj} for magnet, which contains 0.4 wt.% Cu, is modest from the Cu-free magnet. The addition of Cu significantly increases the B_r of the hot-deformed magnets to 14.11 kG and $(BH)_{max}$ to 49.07 MGOe.

Compositional modifications in magnet materials offer opportunities for altering the intrinsic properties of the major component and/or the nature of secondary phases and their influence on coercivity. The Curie temperature increases monotonically with x in the stoichiometric $RE_2Fe_{14-x}Co_xB$ compounds, and melt-spun Nd–(Fe,Co)–B materials containing $Nd_2Fe_{14-x}Co_xB$ as the principal constituent have been prepared (Wecker and Schultz 1990). In $Nd_2Fe_{14-x}Co_xB$, the Curie temperature increases from 312°C for $x = 0$, through 427°C for $x = 2$, to 727°C, which is the T_c of $SmCo_5$, when $x = 14$, i.e., for $Nd_2Co_{14}B$. For $x > 9$ in the $Nd_2Fe_{14-x}Co_xB$ system, however, B_r, H_{ci}, and $(BH)_{max}$ all vanish as T approaches a temperature T_s (which is less than T_c), and this intrinsic behavior limits the practical magnets (Herbst and Croat 1991).

The coercivity of melt-spun Nd–Fe–B materials is significantly increased by doping (at concentrations <5 at.%) with other elements (Herbst and Croat 1991). Niobium and zirconium are known to improve H_{ci} of melt-spun ribbons (Kohmoto et al. 1987; Wecker and Schultz 1990). Enhancement of H_{ci} by 10–90% has been found (Fuerst and Brewer 1990, 1991) in hot-pressed and die-upset magnets containing Ag, Au, Cd, Cu, Ir, Mg, Ni, Pd, Pt, Ru, or Zn.

New technologies, without the use of dysprosium, to enhance coercivity of Nd–Fe–B magnet materials have become important, because substituting Dy for Nd faces the Dy supply limitations. The HDDR process is a good method to produce anisotropic Nd–Fe–B magnet powders with high coercivity (Harris and McGuiness 1990; Takeshita and Nakayama 1989), and coercivity of HDDR-treated Nd–Fe–B powders without Dy can be improved by the diffusion of Nd–Cu or Nd–Al eutectic alloys, i.e., mixing the HDDR powder with the Nd-rich alloy powder, and then heat treating them to diffuse Nd-rich liquid into the magnet powder particles (Mishima et al. 2012; Sepehri-Amin et al. 2010). Morimoto et al. (2012) have shown that with proper Al and Nd contents, the slow hydrogen desorption of the HDDR treatment can remarkably improve the coercivity of the Dy-free Nd–Fe–Co–B–Ga–Zr–Al powders. Coercivity enhancement of the powders might be ascribed to the formation of continuous Nd-rich grain boundary phase. Al addition and slow desorption promote the uniform growth of this phase by distributing excess of Nd over the $Nd_2Fe_{14}B$ stoichiometry.

6.11.2.5 Sintered Magnets

Processed magnets are frequently fully dense sintered, oriented blocks produced by power metallurgy or ceramic methods. An alignment step to orient the easy axes of all the crystallites is highly beneficial as, without it, the remanent magnetization is decreased by more than a factor of 2 and the energy product by a factor of 4 (Coey 2012).

The magnets prepared through the sequence of orient, press, sinter operations on finely divided alloy powders are designated as *sintered*. Sagawa et al. (1984a) were the first to apply this method to Nd–Fe–B. Their procedure was as follows. Neodymium–iron–boron alloy having the composition $Nd_{0.15}Fe_{0.77}B_{0.08}$ was prepared by induction melting. It may be noted that this composition was substantially enriched in Nd and B relative to both stoichiometric $Nd_2Fe_{14}B$ (corresponding to $\approx Nd_{0.12}Fe_{0.82}B_{0.06}$) as well as the optimum melt-spinning composition of $\approx Nd_{0.13}Fe_{0.82}B_{0.05}$. The ingot was crushed, milled, and pulverized to powder with a particle size of ~3 μm. The powder was aligned in a magnetic field (800 kA/m) and pressed ($P \sim 200$ MPa) perpendicular to the alignment direction. The compact obtained was sintered in argon gas at ~1100°C for 1 h and cooled quickly. It was then subjected to a post-sinter anneal at ~625°C under argon to improve the coercivity to its maximum value. By the sintering route, which is quite similar to the process for preparing $SmCo_5$ magnets, Nd–Fe–B magnets with energy products up to 360 kJ/m^3 have been prepared (Kirchmayr 1985).

In general, the steps for the production of sintered REPMs are as given in Figure 6.25. The Nd–Fe–B alloy, after vacuum-melting and casting, is in the form of chill cast lumps. These are crushed, under a nitrogen atmosphere, in a high-energy hammer mill to <500 μm particles. The premilled (crushed) magnet alloy is milled to produce a narrow size distribution of single crystal particles. Milling is carried out, for example, by vibration ball milling in an organic liquid under an inert atmosphere. In the next step, the powder particles are magnetically aligned and pressed such that the easy axes of magnetization of the particles are parallel. The compaction is done by die pressing or isostatic pressing. The applied field is either DC or some combination of DC and pulsed. The compaction pressure is kept sufficient to give the powder

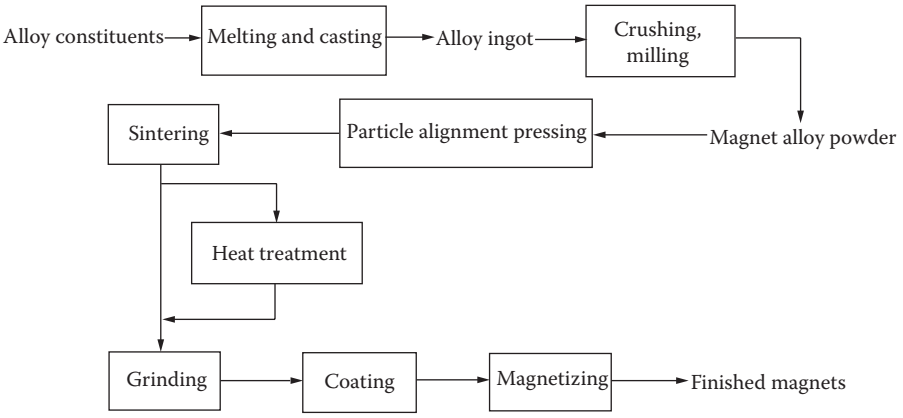


FIGURE 6.25 Process steps for the production of sintered REPMs.

compact enough mechanical strength for handling but not high enough to cause particle misorientation. The compacted magnets are sintered in the region of 1100°C in inert gas atmospheres or under vacuum to over 95% of theoretical density. The optimum sintering temperature range for Nd–Fe–B magnets (Sagawa et al. 1984a) is much wider (approximately 120°C) than that for $SmCo_5$ magnets. In the as-sintered form itself, the properties obtained with a Nd–Fe–B magnet are such that the material forms a useful permanent magnet.

A post-sintering heat treatment, usually an isothermal heat treatment in the region of 630°C for 1 h, was reported by Sagawa et al. (1984a) to increase the coercivity of the Nd–Fe–B magnets. However, heat treatment does not appear as a necessary procedure in the overall process scheme for making the sintered Nd–Fe–B magnets.

Over the years, the basic procedure for the preparation of sintered NdFeB magnets has not undergone any significant alteration. The procedure appearing in recent publications is outlined next.

NdFeB sintered magnets are mass-produced through a powder metallurgical process as shown in Figure 6.25. Rare-earth elements such as Nd, Pr, Dy, and Fe, Fe–B are melted in a vacuum furnace. Nonconsumable electrode arc melting (Wang et al. 2006a) or induction melting (Yu et al. 2008) in an inert atmosphere has been used for obtaining homogeneous alloys with as many as four to seven components. The cast ingots were first crushed and pulverized ~250 μm under the argon atmosphere, and then through jet milling, the coarse powders were milled to fine powders with an average particle size of ~4.0 μm. Hydriding of the cast alloy before crushing may or may not be used. The fine powders are compacted in a magnetic field (1.5–1.65 T), and the compacts are finally sintered (1100–1200°C). Sintering may be followed by an annealing treatment (600–900°C).

A detailed treatment schedule is provided by Pan et al. (2010). They prepared the magnet alloys $Nd_{14.63}Fe_{77.48}Cu_{0.16}Al_{1.47}Nb_{0.21}B_{6.03}$ and $Nd_{14.63}Fe_{76.98}Cu_{0.16}Al_{1.47}Nb_{0.21}Tb_{0.5}B_{6.03}$. Metals of Nd, Fe, Tb, Cu, and Al with purity of 99.9%, FeB (B 19.3 at.%), and NbFe (Nb 66.3 at.%) were used. The alloys were melted in an induction furnace, and then the ingots were dumped into rectangular water-cooled copper molds. In order to eliminate the α-Fe phase, these alloys were annealed at 1000°C for 10 h under vacuum (>10^{-3} Pa). The annealed ingot was crushed into powder and heated at 850°C for 1 h in a high-purity hydrogen atmosphere of 1.2 atm. After cooling to room temperature, the powder was placed in a spiral-type jet mill to produce the powder (average particle size = 4.8 μm) under a high-purity nitrogen atmosphere. The powders were aligned magnetically in an external field of 1.8 T, then pressed isostatically, and vacuum-sintered at 1180°C for 3 h to form single-phase sintered NdFeB magnets.

Generally the rare-earth magnets, particularly the SmCo magnets, are hard and brittle. The Nd–Fe–B magnets, however, are tougher and less prone to breakage and chipping. After sintering and heat treatment, the magnets are ground, and, in the case of large blocks, they are divided into even, very small magnets by cutting and slicing. The sintered pieces are ground on conventional grinding machines fitted with silicon carbide or diamond grinding wheels.

The Nd–Fe–B magnets combine relative recoil permeability close to unity and high coercivity and may be magnetized prior to assembly without flux loss. Because

of the difficulty in handling magnetized and brittle material, it is usual that magnetization is carried out during system assembly.

RE magnets are, in general, prone to corrosion. In service, they get exposed to aggressive media such as acids, alkalis, salts, lubricants, and gases. They need to be protected. High humidity or dew formation is sufficient to cause corrosion in the case of Nd–Fe–B. The magnets are protected from corrosion by coating them. Metallic coatings, for example, of nickel or tin, are applied by galvanic processes. Coating also ensures that the magnets can be cleaned thoroughly free of all magnet dust.

After the magnet is put into its final shape, it is magnetized to saturation. This is done using very high magnetic fields, using capacitor discharge magnetizers. Magnetization is done only parallel to the magnetic orientation set during particle alignment pressing.

The powder metallurgical fabrication of Nd–Fe–B magnets is facilitated not only by the superior intrinsic properties of $Nd_2Fe_{14}B$ but also by the fact that $Nd_2Fe_{14}B$, Nd, and the tetragonal compound $Nd_{1+\varepsilon}Fe_4B_4$ form a ternary eutectic that makes possible liquid-phase sintering resulting in high densification without significant grain growth (Sagawa et al. 1987b). The highest energy product $(BH)_{max}$ ~ 405 kJ/m^3 for a sintered Nd–Fe–B magnet was reported by Sagawa et al. (1987b). The composition was $Nd_{0.15}Fe_{0.82}B_{0.05}$. Ge et al. (1998) have noted that an improved method for casting molten Nd–Fe–B alloy can help in making better magnets. One of the key factors is to bring down the Nd content in the alloy to as close to 27% (stoichiometric composition of $Nd_2Fe_{14}B$: 26.69% Nd, 72.31% Fe, 1.00% B) without at the same time precipitating the α-Fe phase.

Sintered RE–Fe–B magnets with $(BH)_{max}$ ~ 320 kJ/m^3 have been obtained (Kirchmayr 1985) by using 5Ce–didymium (Nd–15% Pr–5% Ce). Many investigations (Herbst and Croat 1991) have been directed at finding substitutions in additives to sintered Nd–Fe–B magnets essentially to extend their useful operating temperature range. This is achievable via enhancement of T_c and H_{ci}, decrease in the temperature coefficients of B_r and H_{ci}, and diminution of the irreversible flux losses accompanying high-temperature exposure. Sagawa et al. (1984b) demonstrated that cobalt substitution increases T_c and decreases the temperature coefficient of B_r; however, cobalt substitution is accompanied by a loss of coercivity. Partial replacement of Nd by Dy substantially enhances H_{ci} and then decreases the temperature coefficient of H_{ci}, although it lowers B_r somewhat. The largest room temperature coercivity ever observed in a neodymium-based sintered magnet was achieved in $(Nd_{0.53}Dy_{0.47})_{a15}Fe_{a77}B_{a08}$ by Sagawa et al. (1987a). The $(BH)_{max}$ was 160 kJ/m^3 and H_{ci} = 3980 kA/m. Combined Dy and Co substitution has been found to be effective in raising T_c and H_{ci} and in decreasing the temperature coefficient of B_r and the irreversible flux losses. Other elements that have been found to have beneficial effects on coercivity and thermal stability are Al, Ga, and Nb. By a process described by Liang et al. (1998), Nd–Fe–B magnets with $(BH)_{max}$ = 334–358 kJ/m^3, H_{cj} > 1114 kA/m, and B_r = 1.33–1.37 T were produced starting from a magnet alloy of composition $Nd_{9.5}Pr_{3.4}Dy_{0.4}Tb_{0.4}B_{6.1}Al_{0.7}Fe_{79.5}$. The process outline as given by them is shown in Figure 6.26. The authors, however, did not present details of the *treatments* given to the magnet powder before pressing.

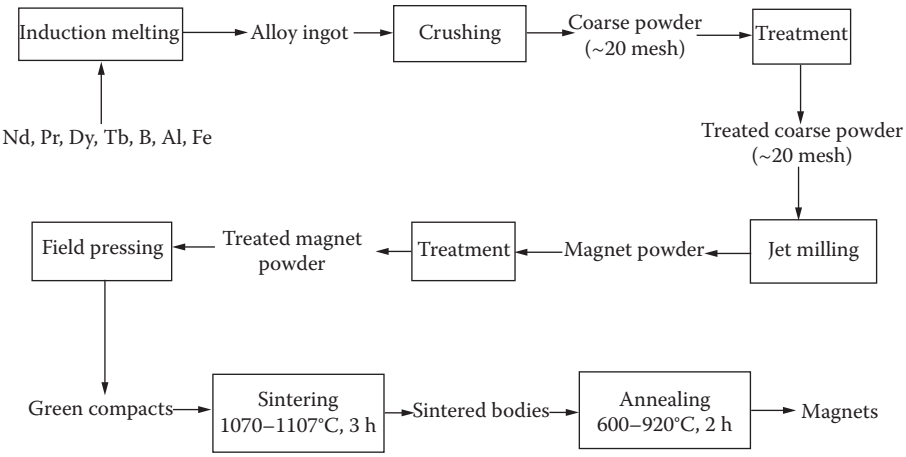


FIGURE 6.26 Process steps for sintered Nd–Fe–B magnets with additives. (From Liang, S. et al., High performance NdFeB magnets. In *Preprints of the Conference*, China Magnets, held on 18–21 October 1998 at Beijing, 1998.)

Nd–Fe–B magnets are exemplary as regards the swift progress from the laboratory discovery to commercialization. The largest energy products realized so far, ~400 kJ/m^3, are substantially short of $(BH)_{max}$ ~ 512 kJ/m^3. Alloy modification and alternate preparation methods are being explored to bridge this gap. New preparation methods include mechanical alloying (Schultz et al. 1989), hot deformation of ingots (Shimoda et al. 1988), and the hydrogenation, disproportionation, and desorption process (McGuiness et al. 1990).

6.11.3 Preservation and Enhancement of Magnetic Properties

Nanocrystalline Nd–Fe–B-type magnetic materials display enhanced remanence and coercivity, leading higher energy products, compared to the conventional microcrystalline counterparts. This has been attributed to the exchange coupling across the grain boundaries and the fact that the grain size is well below the threshold for a single domain (Liu et al. 2013). Nanocomposite magnets based on $Fe_3B/Nd_2Fe_{14}B$ in the vicinity of $Nd_{4.5}Fe_{73}Co_2B_{18.5}Cr_2$ have large remanence (>1 T) but low resistance to thermal flux losses. This limitation was improved by alloying Ti and C simultaneously (Ishii et al. 2007).

The mechanical properties of sintered NdFeB magnets were basically poor and sought to be improved by the use of additives. Jiang et al. (2000) and Liu et al. (2005) found that Al, Cu, Co, and Nb additions improved the strength of sintered NdFeB magnets. Dy substitution for Nd was found to improve also the impact resistance of sintered NdFeB magnets (Wang et al. 2006a).

The theoretical value of the maximum energy product of NdFeB magnets is calculated to be 512 kJ/m^3 (64 MGOe) (Sagawa et al. 1985). The key factors to improve magnetic properties of real magnets towards this value are (1) compositional control, (2) densification, (3) grain size control, and (4) alignment of the 2–14–1 grains

(Kaneko and Ishigaki 1994). In order to increase the volume fraction of 2–14–1 phase, it is important to maintain the composition close to the stoichiometric 2–14–1 phase with keeping a required volume of the Nd-rich phase. Kaneko et al. (2006) have obtained by strip casting the microstructure of the alloy that has finer dendrites keeping an excellent orientation without the primary Fe phase. The rare-earth content of the alloy is only 12.3 at.%, which is close to the stoichiometric 2–14–1 phase. As a result, not only the compositional and microstructural uniformity of magnets but also the size and morphology of 2–14–1 grains are improved after sintering. Kaneko et al. (2006) have succeeded in developing the 460 kJ/m^3 magnets (Kuniyoshi et al. 2004). In this, the volume fraction of 2–14–1 phase is improved to 97.8%, and the degree of alignment of 2–14–1 grains is improved to 98.5%. Further improvements of the powder-making and -aligning method can enhance properties further. Dy improves coercivity. In order to improve coercive force with minimal content of Dy, it is required to control to a known limit not only the grain size and morphology but also the grain boundary phase (Hirosawa 1989). One of the solutions is to reduce oxygen impurity.

In the manufacturing of magnets, controlling residual oxygen has been a highly challenging task. Neodymium oxidizes readily and degrades the magnet performance. HITACHI invented the HILOP technology in the 1990s, which reduced the oxygen content to below 2000 ppm (1000–2000 ppm), and improved the performance of NdFeB in mass production. Xie et al. (2006) mentioned a *Zhenghai Oxygen-Free Process*, which is based on a *dry method* for the manufacture of NdFeB magnets containing oxygen not more than 100–400 ppm. The resulting high performance of the magnet was considered good enough to meet the severe requirements of motor field, on account of its good consistency, equality, corrosion resistance, and temperature stability, even as a replacement for SmCo at 200°C. The details of oxygen control procedures have not been disclosed.

Magnetic properties of Nd–Fe–B sintered magnets were improved in two ways. One was the improvement of B_r and the other was the improvement of H_{cj}. Improvement of B_r was achieved by the following method: (a) increase in the volume ratio of the $Nd_2Fe_{14}B$ main phase; (b) improvement of grain orientation in the pressing process; and (c) realization of the full density in the sintering process. Nd–Fe–B sintered magnets are mainly composed of three phases. The main phase in the Nd–Fe–B sintered magnet is $Nd_2Fe_{14}B$. The other two phases are $Nd_{1+\varepsilon}Fe_4B_4$ and an Nd-rich phase. An increase in the volume ratio of the main phase is one of the important factors to improve residual magnetization (B_r). The volume ratio of the main phase also decreases by inclusion of impurities such as nitrogen and carbon, apart from oxygen which come from magnet manufacturing processes (Matsuura 2006).

Grain orientation is an important factor for high-performance magnets. The coercive force (H_{cj}) of the Nd–Fe–B sintered magnet is also affected by grain orientation (Matsuura 2006). In a magnet manufacturing process, a raw material that is made by induction furnace is crushed into powder 3–5 μm in grain diameter. In this process, almost every grain is crushed into a single crystal. This powder is aligned in the magnetic field before pressing. In the pressing process, pressing pressure and the friction exerted between grains disturb grain orientation to be oblique from the magnetic field direction. Many methods such as cold isostatic press (CIP),

rubber isostatic press (RIP) (Sagawa and Nagata 1993), inclined magnetic pulse field method (Kuniyoshi et al. 2004), and a wet press, which is called the HILOP process, were applied to improve the degree of grain orientations in the pressing process. The highest grain orientation achieved was 0.991 using the improved inclined magnetic field method (Matsuura 2006).

Various additives such as V, Mo, and W were applied to improve the H_{cj} of Nd–Fe–B sintered magnets (Sagawa and Hirosawa 1988), but B_r decreases with increasing additive content. Improvement of H_{cj} is still mainly dependent on heavy rare earths such as Dy or Tb. A heavy rare-earth sputtering method was applied onto as-sintered Nd–Fe–B magnets to reduce heavy rare-earth content (Ishigaki et al. 2005). Magnet was heat-treated after sputtering. In this magnet, heavy rare earth was observed in the grain boundary after heat treatment, and coercive force increases to 30–50% compared to the case without a sputtering treatment. The coercive force (H_{cj}) of the Nd–Fe–B sintered magnet is also affected by grain orientation (Matsuura 2006).

A new world record of magnetic properties with B_r = 1.555 T, $(BH)_{max}$ = 474 kJ/m^3, and H_{cj} = 653 kA/m was established by NEOMAX Co. Ltd. in 2005 (Matsuura 2006). In this magnet, the main phase volume ratio was 0.982, oxygen content 600 ppm, and grain orientation 0.991.

Plusa et al. (2006) determined that magnets with better properties can be produced from anisotropic powder, which can be obtained by employing the HDDR process on the Nd–Fe–Co–B alloys, with small anisotropy-inducing additions of Ga, Zr, Nb, or Hf (Chen et al. 2003; Takeshita and Morimoto 1996). Based on the results of initial magnetization curve shape and the field dependence of coercivity, they attributed the coercivity of the anisotropic resin-bonded magnets based on Nd–Fe–Co–B to the pinning of domain walls at the grain boundaries.

The Ames group, Iver Anderson, Bill McCallum, and Matthew Kramer, have developed a high-performance permanent magnet alloy that operates with good magnetic strength at 200°C, suitable for making electric drive motors. Using gas atomized alloy powder, instead of only neodymium, the rare-earth magnets are manufactured by metal injection molding (MIM). Neodymium, yttrium, and dysprosium all form the 2–14–1 crystal, and the rare-earth part of the alloy comprises all three of these metals. Due to the influence of yttrium and dysprosium, there is much less degradation of their magnetic properties with temperature.

In Nd–Fe–B permanent magnets, both the coercivity and corrosion resistance are sensitive to the character of the intergranular phase. Therefore, the addition of intergranular modifiers is of importance for simultaneously improving the coercivity and corrosion resistance of magnets. Element alloying (with additions such as Al, Ga, Cu, Mg, and Sn) during the melting stage is effective in improving the coercivity and corrosion resistance, but the remanence decreases due to the magnetic dilution effect (Cui et al. 2008). Copper is a popular additive. Sintered permanent magnets have been prepared by blending Nd–Fe–B jet-milled powders with Cu nanopowders before pressing in a perpendicular magnetic field. Results showed that the grain size of the $Nd_2Fe_{14}B$ phase was refined and more homogeneous, and the grain boundaries became clear and smooth, resulting in the improvement of coercivity H_{cj}; the corrosion resistance of Nd–Fe–B magnets improved while T_c remained nearly unchanged. Cu was not detected in the matrix phase $Nd_2Fe_{14}B$ but was found concentrated in the

intergranular region. The effect of Cu additions on the electrochemical potential of the intergranular phase, and the increase in the magnet density improved the corrosion resistance (Cui et al. 2008).

There have been many efforts and much progress through alloy modifications and heat treatments to enhance the thermal stability of Nd magnets while balancing other magnetic properties. Usually, alloy modifications improve some characteristics and impair some other characteristics. Addition of Co increases the Curie temperature, but B_r and H_{ci} are reduced. Addition of Dy, Co, and Al improved the coercivity and thermal stability but decreased B_r and $(BH)_{max}$. But copper improves coercivity without loss of remanence (Hirosawa and Kaneko 1998). Yan et al. (2006b) reported a continuous/uniform distribution of the grain boundary phase obtained through right annealing treatment with Cu addition. The temperature coefficient α improved with the addition of Gd, but the remanence and maximum energy product linearly decreased. As Cu was added, the remanence, maximum energy product, and coercivity increased due to the density improvement, and main-phase grains were well isolated. By combined addition of Gd (0.8%) and Cu (0.2%), optimum magnetic properties with temperature coefficient $\alpha = -0.05\%/°C$ and $(BH)_{max} = 339$ kJ/m^3 could be obtained (Yu et al. 2008).

Results similar to copper nanopowder addition were obtained by Cui et al. (2009) with the addition of chemically precipitated silica nanopowder for essentially the same reasons. The addition of SiO_2 nanopowders (20–25 nm) is effective in improving the magnetic properties and corrosion resistance of the sintered magnets. Optimum H_{cj}, B_r, $(BH)_{max}$, and corrosion resistance are simultaneously obtained when 0.01 wt.% SiO_2 is added.

As known, the coercivity of NdFeB magnets can be improved significantly by adding a small amount of dopants, such as Co, Ga, Zn, and Al, or some other refractory elements. For example, Kanekiyo et al. (1994) reported that the addition of 3 at.% V to NdFeB alloys can increase the coercivity significantly. Also Harrison et al. (2006) found that the addition of Ti and C into magnetic alloys could modify the microstructure and subsequently resulted in the improvement of the coercivity. Generally, the main reason for the enhanced coercivity is attributed to the refinement of the microstructure of the sintered magnets by adding these elements (Pan et al. 2010).

6.11.3.1 Super High-Energy Magnets

Many groups have attempted to achieve the theoretical limit of maximum energy product $(BH)_{max}$ for Nd–Fe–B magnets, 512 kJ/m^3, calculated on the basis of saturation magnetization of the $Nd_2Fe_{14}B$ single crystal (Sagawa et al. 1985). In 1987, Sagawa et al. (1987b) obtained, as mentioned above, 405 kJ/m^3 for $Nd_{128}Fe_{80.7}B_{6.5}$ (in wt.%: 27.4 Nd–70.17 Fe–1.08 B) by controlling the oxygen content to less than 1000 ppm. In 1990, Otsuki et al. (1990) achieved a higher value of 416 kJ/m^3 by a special procedure in which they added neodymium-rich alloy powder prepared by the rapid solidification technique to the alloy powder having a stoichiometric composition ($Nd_2Fe_{14}B$), and then sintered the powders. In 1994, Kaneko and Ishigaki (1994) succeeded in developing Nd–Fe–B sintered magnets, having the highest magnetic properties of $B_r = 1.495$ T, $(BH)_{max} = 431$ kJ/m^3, and $H_{ci} = 845$ kA/m. The procedure

they adopted aimed at densification of magnets up to a theoretical value, increasing the volume fraction of the $Nd_2Fe_{14}B$ (T_1) phase and achieving a high degree of alignment of the T_1 grains. It was carried out as follows. The alloy corresponding to the overall composition 29.2% Nd–69.80% Fe–1.00% B ($Nd_{13.1}Fe_{80.9}B_{6.0}$) was made by induction melting of 99.5% pure rare-earth metal, 99.9% pure electrolytic iron, and ferroboron. As-cast alloys were homogenized by heating in vacuum at 1000°C for 5 h; the cast alloys were crushed using a jaw crusher and a disc mill to coarse powder (<200 μm). Fine powders of about 3 μm mean particle size were then obtained by pulverizing the coarse powder in a jet mill. The particle size distribution of the resulting powder was more uniform than those found in currently mass-produced magnets. A new compacting method for fine powder was used to improve the degree of alignment of the T_1 grains up to 95% or more. The isostatic press was carried out in three steps: (1) filling powders into a cylindrical mold in which the packing density was 2000 kg/m^3, (2) aligning with a pulse magnetic field of 6400 kA/m, and finally (3) compacting by isostatic pressing at a pressure of 200 MPa. The compacts thus obtained were sintered at about 1060–1080°C for 3 h in an argon atmosphere and were subsequently annealed at about 500–600°C for 1 h, also in argon.

The mean particle size measured by a Fisher subsieve sizer is the same, i.e., 3 μm for the alloy powders obtained by Kaneko and Ishigaki (1994) and for the commercially used alloy powders. The particle size distribution of the former, however, is more uniform; as a result, the microstructure of the sintered magnet obtained under the improved pulverizing conditions became finer and the grain size became smaller than under conventional conditions. This finer microstructure results in an increase in H_{ci}. The degree of alignment of T_1 grains improves with the strength of the pulse magnetic field and exceeds 95% for a magnetic field of 6400 kA/m. The improvement of B_r and $(BH)_{max}$ in the new magnets is due to the high degree of orientation of T_1 crystals.

Kaneko and Ishigaki (1994) state that the making of a super high-energy product magnet is dependent upon controlling the chemical composition, increasing the volume fraction of the $Nd_2Fe_{14}B$ matrix phase, improving the particle size distribution, and adopting the isostatic pressing method to get better alignment of fine particles. As pointed out earlier, Kaneko's group (Kaneko et al. 2006; Kuniyoshi et al. 2004) have already succeeded in developing the 460 kJ/m^3 magnets, wherein the volume fraction of the 2–14–1 phase is improved to 97.8% and the degree of alignment of 2–14–1 grains to 98.5%.

In the 1990s, the highest grade sintered Nd magnets in large-scale production had an energy product of 320 kJ/m^3, and the coercivity was also insufficient. To be able to obtain a higher residual magnetization (B_r), iron-rich composition close to a 2–14–1 compound is necessary. There are, however, difficulties in achieving this composition at the production level. The problems are powder oxidation and a decrease in B_r. The Nd–Fe–B alloys in the form of fine powders with diameters of 3–4 μm easily oxidize in air to form Nd_2O_3. The oxygen content in sintered Nd magnets ranges from 0.5% to 0.7%. Oxidation consumes neodymium, and the nonmagnetic Nd_2O_3 lowers the magnetic property of the material. In sintered Nd–Fe–B magnets, additions used to increase coercivity decrease residual magnetization. To obtain a high-performance Nd magnet, a balance between oxidation protection and decreased use of additives is necessary. The poor corrosion resistance of sintered Nd magnets necessitates the use

of coating for actual use. Honshima and Ohashi (1994) developed a two-alloy method for producing sintered neodymium–iron–boron magnets. Their method addresses the twin problems of oxidation resistance and minimum use of additives.

6.11.3.2 Two-Alloy Process

The process flow sheet of the two-alloy method of Honshima and Ohashi (1994) is shown in Figure 6.27. This is a powder metallurgy procedure that used two alloys as the starting material. One alloy, the main alloy, had a composition closely approximating the 2–14–1 compound, and the other alloy, called the suballoy, had a composition rich in rare-earth elements and cobalt. The main alloy was responsible for the intrinsic magnetic properties. The suballoy was a sintering aid and was responsible for the densification of the sintered body and the cleaning of sintered particle grain boundaries during the sintering process. The two alloys were melted and cast individually and crushed to 200 μm size. After the coarse pulverization, they were mixed and processed further. In the present process, the pressing of fine powder in a homogeneous magnetic field was accomplished in air.

The main alloy composition was $Nd_{12.3}Fe_{81.8}B_{5.9}$. In the as-cast alloy, a large amount of primary iron exists, and a solid solution heat treatment was necessary to obtain the single 2–14–1 phase. The suballoy was rich in cobalt, and this improved the corrosion resistance of the fine powder and the sintered body. Dysprosium, praseodymium, and gallium added via the suballoy enhanced coercivity. The main and suballoy mixing ratio was approximately 90:10, and after sintering, the final composition of the magnet was $Nd_{11.3}Pr_{1.6}Dy_{0.8}Fe_{76.9}Co_{3.1}B_{5.9}Ga_{0.3}$.

The magnet produced by the two-alloy method was superior to that produced by the conventional (one-alloy) method. Using the two-alloy method, sintered Nd magnets with energy products of 360 kJ/m^3 and moderate coercivity were mass-produced. The oxidation stability of fine powder of two-alloy magnets was excellent. For example,

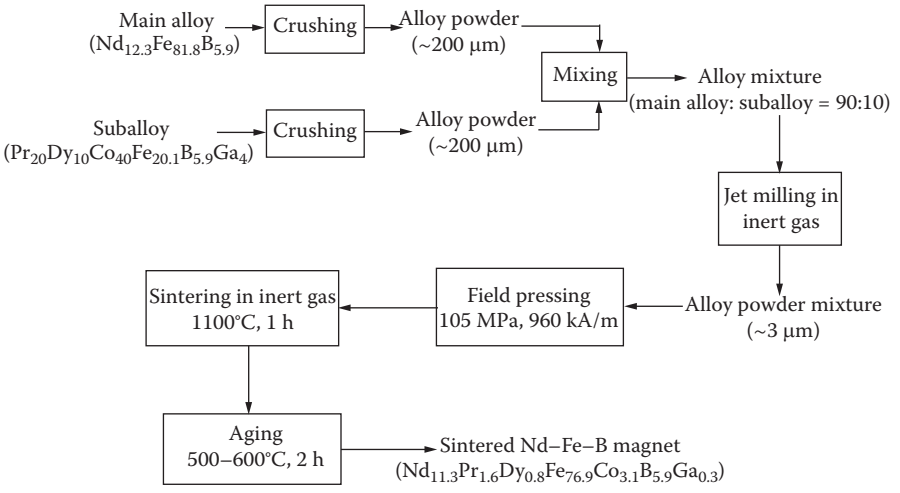


FIGURE 6.27 Flow sheet of the two-alloy method for making Nd–Fe–B magnets. (From Honshima, M. and Ohashi, K., *J. Materials Engineering Performance*, 3(2): 218–222, 1994.)

after exposure of the powder to air at 24°C and 40% relative humidity for 3 days, the coercive force of the sintered magnet produced by the two-alloy method remained almost constant. In contrast, even after 1 day of exposure, the coercive force of the conventionally produced sintered magnet decreased considerably (to less than half of the original value). The low oxidation level of the fine powder is attributed to cobalt base compounds. The two-alloy method thus allows the fine powder to be handled in air during the pressing process, obviating the need for special processing under vacuum or inert gas. The method is therefore attractive for use in mass production. The two alloy method also resulted in less oxygen in the sintered body and improved its corrosion resistance. The cobalt addition to the 2–14–1 alloy suppressed oxidation further.

Improved magnetic properties of the two-alloy product were attributed primarily to the dysprosium distribution and partially to praseodymium distribution. Even though dysprosium increased coercivity, it decreased saturation magnetization. In the processing method described, however, dysprosium was distributed mainly near the grain boundaries of the sintered 2–14–1 particles. Its presence near grain boundaries increased coercivity, and its absence in the center region reduced the decrease in saturation magnetization, thus yielding a high-performance Nd magnet. Companies such as Shin-Etsu and Hitachi are working to reduce the need for dysprosium by a process of heavy rare-earth element (HREE) diffusion (S. Constantinides, private communication, 2015).

Even though fine powder oxidation and corrosion resistance of the sintered magnet body were improved by the two-alloy process, the improvement in corrosion resistance was not sufficient. Thus, like in the case of conventional sintered Nd magnets, a coating was necessary for corrosion protection (Minowa et al. 1989). An electroless copper layer, which has good contact with the Nd magnet, was first provided, and over this copper underlayer, an electroless nickel upper layer was provided. The total thickness was about 10 μm. While coating adhesion was ensured by the copper underlayer, the electroless plating method ensured that film thickness was uniform throughout, including the magnet edges (Honshima and Ohashi 1994).

The sintered NdFeB permanent magnets are characterized with a complex multiphase microstructure. Electrochemically these phases have different potentials, and hence this structure is susceptible to galvanic corrosion. The minor phase at the grain boundary is anodic with respect to the major phase, and accelerated corrosion at the grain boundary ensues. Intergranular corrosion eventually leads to disintegration of the structure.

Two remedial approaches have been followed. One is to alter the electrochemical potential of the Nd-rich grain boundary phase through alloying additions, and the other is to stop corrosion through barrier coatings (Ali 2011). Partial substitutions for the rare-earth element and/or the transition metal have been attempted. Some elements marginally improve the corrosion resistance at a sacrifice of magnetic properties. Dy may be substituted for Nd and Al, Cu, Co, Ga, Nb, W, and Mo for Fe. The resulting protection, if any, being insufficient, barrier coatings are necessary.

6.11.4 Corrosion Control by Coatings on Magnets

With the tendency of NdFeB magnets to corrode, the consequences and attempts to tackle corrosion were alluded to in an earlier section. Corrosion protection of

sintered NdFeB magnets is necessary and effectively achieved with a barrier coating. Both organic and metallic coatings have been developed, but each has an application space. The organic coatings, which may comprise mainly epoxy and/or urethanes, provide a barrier between the magnet and the environment but do not seal the magnet completely from the environment. The metallic coatings, such as Al and Ni, show excellent ability to prevent the corrosion of this magnet from occurring under severe conditions of high temperature and humidity even for a long-term operation. Aluminum can be deposited to a uniform thickness in all portions of a magnet, and it also has a superior adhesion. A thin-type Al, which is less than 5 μm thick, is widely applied for IT devices and compressor motors of the air-conditioner. In place of chromate passivated aluminum coating, a new Al coating named EAC does not use chromic acid as a final treatment for the Al film.

Aluminum may be plated by hot dip aluminizing method. At lower temperature, the coating may not adhere to the magnet, and at too high temperatures, the coating may react with the magnet. Aluminum plating is also nonhermetic and needs additional (conversion) coating to fully seal off from the environment. Together the coating layer might become too thick and expensive.

A Zn–Cr coating that can be applied through dipping samples in (or brushing samples with) paint containing zinc flakes and chromium oxides, followed by baking and sintering at a temperature below the melting point of zinc, has been developed. Yu and Chen (2006) studied the 12-μm-thick Zn–Cr coating, which was prepared on an NdFeB magnet through dipping in the Zn–Cr–B solution, followed by baking at 80°C and sintering at 300°C. Zn–Cr coating provides both passivated anode-type and mechanical barrier protection for NdFeB magnets. Besides, the coating has no significant adverse effect on the magnetic performance of NdFeB magnets. Zinc is anodic to the NdFeB magnet and provides galvanic protection to the substrate. Zinc plating is also nonhermetic. A conversion coating is again needed with the zinc plating to seal the substrate from the air and moisture.

Electrolytic nickel coating provides a hermetic seal. Electroless nickel is slightly inferior to electrolytic Ni coating. Nickel is cathodic to the NdFeB substrate; any damage or discontinuity in the nickel coating will expose the anodic NdFeB magnet to the air and moisture, and corrosion of the magnet will be rapid. Dual-layer or multiple-layer coatings are therefore necessary. The most successful one is the Ni–Cu–Ni triple-layer coating for the NdFeB permanent magnet. The magnetic properties of Ni/Cu/Ni-coated NdFeB magnets remained unchanged, and this coating is considered the benchmark for rating other coatings. Electrolytic, electroless, spray, and dip coatings are the methods commonly used. Sol-gel, thermally evaporated, and/or PVD techniques have also been used for providing the coating.

Nickel coating is not very stable in salt and acidic environmental conditions. An organic overcoat offers improved resistance to salt spray and better protection from air and moisture. Nickel is less resistant against the sulfate ions compared to the chloride ions. Certain organic coatings, electrodeposited nickel or zinc, electroless nickel, electroless nickel–phosphide or nickel–cobalt–phosphide, hot dip zinc, aluminizing, electrophoresis, and chromate passivated aluminum coating are known corrosion-proofing options for neo magnets, but each has its own limitations particularly in moist and humid environments. Ceramic and composite coatings like

TiO_2, Ni–P/Ti_2O, and cathodic arc physical vapor deposition (CAPVD) Ti_2N coatings (Song et al. 2008; Ali et al. 2010) are emerging as new alternatives especially as a layer in a composite coating (Yu and Chen 2006). A summary of various coating options is given in Table 6.17.

The electrodeposition of nickel onto the polished and cleaned substrate (sintered NdFeB) is straightforward and done in Watt's solution. The coating variables like current density, pH, coating time, and bath temperature are so chosen to deposit a dense 2–5 μm layer of nickel. First, a nickel strike layer is electrodeposited followed

TABLE 6.17
Features of Typical Surface-Coating Technologies for NdFeB Sintered Magnets

Coating	Contents	Thickness (μm)	Features	Applications
Aluminum	Aluminum–chromate	7–19	Excellent adhesive strength Uniform thickness of Al film	Motors, generators, sensors pick-ups for CD, DVD, automobile applications
	Eco-aluminum	7–19	Non-chromic acid	
	Thin-type aluminum	~5	Thin type	Speakers, etc.
	Pure-type aluminum	~5	Compressors usage	
Nickel	Direct electro Ni plating	10–20	Ni only electroplating	VCM
	High corrosion resistance	15–25	System electroplating with some special elements	Motors, sensors
	Electroless Ni plating	~5	Electroless plating	Two-pole cylindrical motors
Epoxy	Electrodeposition	20–30	High electrical insulating	Pick-ups for CD
	Spray coating	10–20	Uniform thickness of film	Rodless cylinder
Simple treatment	V coating	~3	Simple chemical treatment	Motors
	M treatment	~2	Simple stabilized treatment	
Special treatment	TiN coating	5–10	Available in high vac. (10−10 Pa)	Undulator
	Polyimide coating	5–10	High electrical insulating	Pick-ups for CD

Source: Kaneko, Y. et al. Proven technologies on high-performance Nd–Fe–B sintered magnets, *J. Alloys Compd.*, 408–412: 1344–1349, 2006.

by electrodeposition of a layer of copper and then an electrodeposit of nickel as an overcoat.

Ti_2N is a chemically resistant, thermally stable (oxidizes at 800°C under normal atmospheric conditions), and excellent diffusion barrier that is electrically conductive. It forms a molecular bond with the substrate. The technique used for its deposition is CAPVD. Here, an electric arc struck to a solid Ti cathode (target) vaporizes it, and as the vapor is transported across the nitrogen-filled chamber, it deposits material on the substrate forming a Ti_2N coating. Deposition parameters are chosen to deposit a thick and dense coating with low density of open pores. Multiple layers are coated by repeating the process. A strike layer of nickel and Ni/Ti_2N composite coating provides superior protection and better electrochemical impedance than Ti_2N ceramic coating alone.

6.12 Sm–Fe–N MAGNETS

Coey and Sun (1990) discovered the interstitial compound $Sm_2Fe_{17}N_x$ as a permanent magnetic material. $Sm_2Fe_{17}N_x$ exhibits fairly high saturation magnetization (1.54 T), high anisotropy field (14 T) under room temperature, and high Curie temperature (476°C), intrinsic magnetic properties that are comparable with or better than those of $Nd_2Fe_{14}B$. However, $Sm_2Fe_{17}N_x$ decompose into SmN and α-Fe phases at 650°C or above (Schnitzke et al. 1990), and the conventional sintering route is not suitable for processing of compacted magnets. The present applications of the $Sm_2Fe_{17}N_x$ compounds are limited to bonded magnets, wherein due to the additional polymer or metal, the magnetic properties of $Sm_2Fe_{17}N_x$ magnets will be decreased (Ye et al. 2007).

Permanent magnet materials belonging to the 2:17 phase intermetallic with the rhombohedral Th_2Zn_{17}-type structure include RE_2Fe_{17} binary alloys (Sm_2Fe_{17}) and $RE_2(Fe,TM)_{17}$ ternary alloys. The intrinsic properties of these binary and ternary alloys can be changed markedly by the incorporation of nitrogen or carbon onto the interstitial sites surrounding the rare-earth ion (Coey and Skomski 1993; Coey and Sun 1990). The addition of N, C, or B atom into Sm_2Fe_{17} changes magnetization from in-plane to perpendicular with increasing concentration of the interstitial atoms (Horiuchi et al. 1995). Interstitial modification results in an increase in the Curie temperature and an expansion in the lattice, and it may induce hard magnetic properties such as coercivity. For example, on nitriding Sm_2Fe_{17} to obtain $Sm_2Fe_{17}N_x$, there is an increase in the Curie temperature from 116°C to 476°C and expansion of the lattice (about 6 vol.%), and the magnetic easy axis changes from being in the basal plane to the *c*-axis, inducing coercivity.

$Sm_2Fe_{17}N_x$ has excellent intrinsic magnetic properties with high Curie temperature, but it is difficult to make into bulk magnets by conventional sintering process, as $Sm_2Fe_{17}N_x$ decomposes into SmN, α-Fe, and N_2 above 600°C. Even the use of novel high-temperature consolidation methods like SPS (Coey et al. 1991a,b; Omori 2000; Zhang et al. 2006a) or field-activated pressure-assisted synthesis (Ye et al. 2007) involving the simultaneous application of an electrical field and pressure during combustion synthesis was not entirely successful.

Sm_2Fe_{17} alloys are made by induction melting of 99.9% pure start materials in an argon atmosphere. The ingot was annealed in argon atmosphere at 1050–1100°C

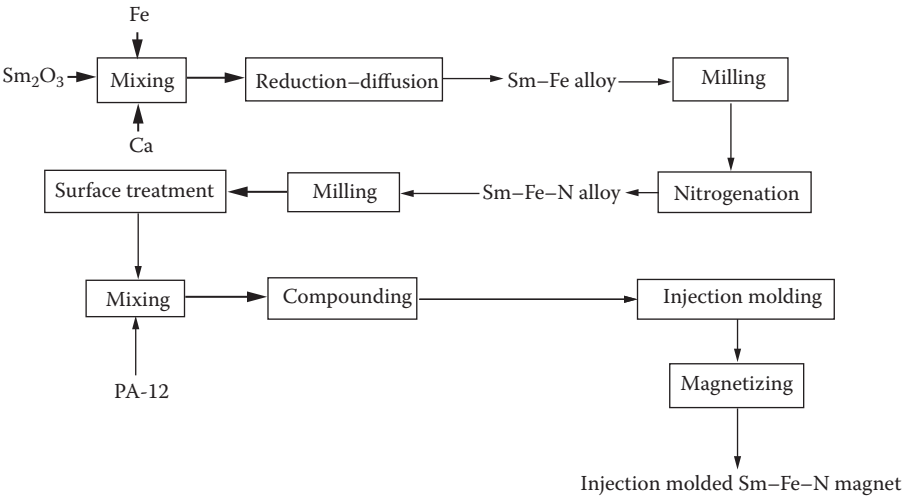


FIGURE 6.28 Production process for injection-molded Sm–Fe–N magnet. (From Ohmori, K., The use of reduction–diffusion process (R/D) in magnet industry. In *Preprints of the Conference, China Magnets*, held on 18–21 October 1998 at Beijing, PR China, 1998.)

for 12–24 h and then crushed and milled into powder of less than 10–30 μm in size. Zhang et al. (2006a) nitrided the powder at this stage. The nitridation was done at 500°C for 5 h in nitrogen gas. $Sm_2Fe_{17}N_x$ powders with nitrogen content up to 2.8 atoms per formula were further pulverized by ball milling into fine powders of 1–3 μm. Ye et al. (2007) carried out the preparation of $Sm_2Fe_{17}N_x$ after an HDDR treatment of the original alloy powder. The HDDR process was carried out as follows: the alloy powder was placed in a furnace and heated to 775°C at a rate of 5°C/min in high-purity hydrogen (0.1 MPa), held for 1 h, and then the furnace was evacuated to 10^{-4} Pa, held in vacuum for 2 h. There is a small fraction volume of H atom left in the sample after the HDDR process at 775°C. After cooling to room temperature, the powders were nitrided at 500°C for 5 h in pure nitrogen (0.3 MPa). The product powder is nearly composed of single $Sm_2Fe_{17}N_x$ phase. It was isotropic Sm–Fe–N permanent magnetic powder.

The Sm–Fe alloy has been prepared by reduction–diffusion, and the bonded magnet has been made by injection molding. The production process followed at Sumitomo is shown in Figure 6.28. The properties of bonded Sm–Fe–N (Ohmori 1998) are shown in Figure 6.29.

6.13 LANTHANUM SUBSTITUTION IN FERRITES

Presently, two families of magnets are produced on a large scale. One is the ferrite family (Stablein 1982), which was developed in the Netherlands 60 years ago (Coey 2010). The common phases are $BaFe_{12}O_{19}$ and $SrFe_{12}O_{19}$, which have the hexagonal magnetoplumbite structure. The energy product of these magnets does not exceed 38 kJ/m^3, but they are inexpensive and relatively easy to produce. Ferrites represent

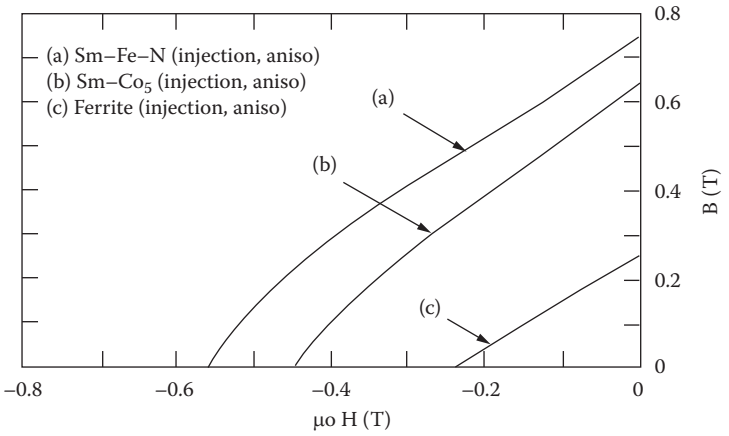


FIGURE 6.29 Comparison between injection-molded Sm–Fe–N and other bonded magnets. (From Ohmori, K., The use of reduction–diffusion process (R/D) in magnet industry. In *Preprints of the Conference, China Magnets*, held on 18–21 October 1998 at Beijing, PR China, 1998.)

about one-third of the permanent magnet market and the lion's share by mass of the million tonnes of magnets shipped each year (Coey 2012).

Since their discovery in the 1950s, hexagonal ferrites have been widely used as permanent magnets due to their reasonably good energy product and the best performance-to-cost ratio. Efforts have been made to improve their magnetic properties by using different synthesis methods involving elemental substitution. Liu et al. (2006) have reported remarkable improvement in the magnetic properties of M-type strontium ferrites with substitution of Sr^{2+} by rare-earth La^{3+}, and a little amount of Fe^{3+} by Co^{2+} according to the formula $Sr_{1-x}La_xFe_{12-y}Co_yO_{19}$. In the process described by Liu et al. (2006), the starting materials used were $SrCO_3$ (98%, industry purity), La_2O_3 (98%), Fe_2O_3 (99%), and Co_2O_3 (98.5%) mixed together in the composition of Sr+La:Fe+Co = 1:12. Mixtures of these raw materials were milled in water in a centrifugal planetary ball mill using hardened steel balls. The mixed powder was dried, crushed, and sifted. These samples were made into balls of about 8 mm diameter and calcined for 2 h in air at 1250–1300°C in a muffle. The precalcined samples were dry-milled using a vibration mill and then wet-milled with additives ($CaCO_3$, SiO_2, Al_2O_3, or Cr_2O_3) by using an attritor. The finely milled slurry with a mean particle diameter of about 0.8 μm was pressed into disk-shaped compacts in the magnetic field of 800 kA/m, which was parallel to the pressing direction. The pressed compacts were sintered in a muffle from 1207 to 1231°C in air.

Based on the information on crystal structure, magnetic properties, and Curie temperature, Liu et al. (2006) concluded that La^{3+}–Co^{2+} ions partially substituted the Sr^{2+}–Fe^{3+} ions. The ferrite ($Sr_{1-x}La_xFe_{12-y}Co_yO_{19}$ compounds) obtained had a higher saturation magnetization and excellent coercive force (H_{cj}) and residual flux density (B_r). The coercive force is remarkably increased without significant decrease in residual flux density by La^{3+}–Co^{2+} substitution that was effected.

6.14 MAGNETOSTRICTIVE MATERIAL (TERFENOL-D)

When a magnetic field is applied to a magnetostrictive material, it will expand or contract. Similarly, when stress is applied to the material, a magnetic pulse is generated. (Tb, Dy)Fe_2 Laves compound possesses excellent magnetostrictive and magnetomechanical properties pointing to high conversion efficiency from magnetic to mechanical energy or vice versa. It is an important functional material for actuators and transducers (Clark 1980).

Investigations carried out in the mid-1960s on the magnetic properties of pure rare-earth metals revealed that some of them exhibited large magnetostriction at low temperatures (Clark 1979). In 1971, Clark and Belson (1972) from the Naval Ordnance Laboratory announced that $TbFe_2$ exhibited magnetically induced strains at room temperature that were larger, by a factor of 10, than that of any other magnetostrictive materials like Ni, ferrites, known until then. This was almost simultaneously confirmed by Koon et al. (1971). It was subsequently found that dysprosium added to the $TbFe_2$ compound allowed the use of lower magnetic fields to produce the strain, but this led to some degradation in the total strain. Magnetostrictive materials need to have characteristics of higher magnetostrictions and lower magnetic anisotropy. The high magnetic anisotropy of $TbFe_2$ was compensated by alloying $DyFe_2$, and resulting in an optimized composition $Tb_{0.27}Dy_{0.73}Fe_2$, which exhibits for a single crystal bulk form a high magnetostriction over 1200 ppm at room temperature. The giant magnetostriction (GM) exhibited by the optimum composition, known as *terfenol-D* is ~100 times larger than that by nickel alloys. Much of the work on developing the optimum properties of the $TbFe_2$ materials was carried out by Clark and coworkers at the Naval Ordnance Laboratory, and the name *terfenol* was derived from terbium–iron (Fe) and the initials of the Naval Ordnance Laboratory. *D* stands for dysprosium.

Schmidt et al. (1986) prepared terfenol-D by a thermit reduction process. Appropriate amounts of TbF_3, DyF_3, and FeF_3 plus 10% excess calcium were mixed together and loaded into a heavily-walled iron crucible lined with CaF_2. The crucible was closed, and the reaction was triggered electrically using a hot iron filament. The exothermic reaction proceeded quickly, and with the alloy and slag forming immiscible liquids, they settled giving terfenol-D, which was well separated from the CaF_2 slag on cooling. The yield of terfenol-D was 94%. This method is a less expensive alternative to the conventional method of preparation of the material by arc melting.

In arc melting, the high-purity metals, Fe 99.98%, Dy 99.97%, and Tb 99.97%, were alloyed together. Initial alloying by arc melting in a water-cooled copper hearth is followed by several meltings to prepare homogeneous alloys (Verhoeven et al. 1987).

Experiments on the growing of terfenol-D crystals and directionally solidified polycrystalline materials were carried out at the Ames Laboratory by McMasters et al. (1986). To achieve the optimum magnetostrictive characteristics, attempts were directed to obtain (1) single crystals oriented with ⟨111⟩ along the crystal axis, (2) a minimum amount of defect structure and impurity content, and (3) a constant stoichiometry along the crystal axis.

Bai and Jiang (2010) have prepared ⟨110⟩ oriented $Tb_{0.3}Dy_{0.7}Fe_{1.90}$ polycrystalline rods that exhibited excellent magnetostrictive properties. Starting with 99.99%

purity metals, $Tb_{0.3}Dy_{0.7}Fe_{1.90}$ alloys are arc-melted under high-purity argon, and rods of 6.8 mm diameter are cast. In a high-temperature gradient furnace, oriented rods are obtained by zone melting with unidirectional solidification in alumina tubes with an inner diameter of 7.2 mm. Rods were grown from the melt with a growth velocity of 240 mm/h to form cellular morphologies along the growth direction.

C15 Laves phase compounds $REFe_2$ form through a single or double peritectic transformation(s). The production of a single phase of $REFe_2$ is a difficult process, and the single crystal forms of giant magnetostrictive actuator (GMA) (Uchida et al. 1996) are expensive. Thin films of GMA are made relatively easily with the single $REFe_2$ phase without a peritectic transformation. Uchida et al. (2002) have prepared thin films of GMA—$TbFe_2$, $DyFe_2$, and (Tb, Dy)Fe_2 compounds—using vacuum flash evaporation (FE) (Uchida et al. 1992), ion beam sputter (Wada et al. 1996), ion plating and electron beam evaporation (Matsumura et al. 2000), and DC–magnetron sputter (MS) (Nakazato et al. 2000).

6.15 MAGNETIC REFRIGERANTS (MAGNETOCALORIC MATERIALS)

The magnetocaloric effect was discovered by Warburg in 1881. The heating or cooling of a magnetic material when it is placed in or removed from a magnetic field is known as the magnetocaloric effect. It results in a temperature change (ΔT_{ad}) in an adiabatic process and in an entropy change (ΔS_{iso}) in an isothermal process (de Oliveira and von Ranke 2010).

The magnetocaloric effect has potential for technological applications, for instance, in magnetic refrigeration. The materials with the larger magnetocaloric effect are needed to use in magnetic refrigeration.

The interest on the near-room-temperature magnetic refrigerator is attributed to Brown's work in 1976 (Brown 1976) and Pecharsky and Gschneidner's discovery of the giant magnetocaloric effect (GMA) near room temperature in $Gd_5Si_2Ge_2$ (Pecharsky and Gschneidner 1997a,b,c). However, the underlying physics of magnetocaloric effect is not yet completely understood. Magnetic refrigeration is an environment-friendly technology, and magnetic refrigerators are expected to operate with an energy saving of up to 30% as compared to the conventional vapor cycle refrigerators.

Brown obtained a temperature reduction from 319 to 272 K for a magnetic field variation from 0 to 7 T using gadolinium as a magnetic refrigerant in his prototype magnetic refrigerator. In gadolinium, at around 292 K, the magnetocaloric potentials ΔS_{iso} and ΔT_{ad} are approximately 10 J/(kg K) and 10 K, respectively, upon magnetic field variation from 0 to 5 T. In 1997, Pecharsky and Gschneidner (1997a,b,c) discovered in $Gd_5Si_2Ge_2$ at around 273 K that the isothermal entropy change upon magnetic field variation from 0 to 5 T is about 20 J/(kg K). Since the discovery of the giant magnetocaloric effect in $Gd_5Si_2Ge_2$, Pecharsky and Gschneidner showed that the series of compounds $Gd_5(Si_xGe_{1-x})_4$ for $x < 0.5$ also exhibit the giant magnetocaloric effect. The compounds with the $Gd_5Si_2Ge_2$-type monoclinic structure at room temperature undergo a first-order phase transition to the orthorhombic Gd_5Si_4-type structure when the temperature decreases. The structural and magnetic transitions in these compounds are coupled and induce the giant magnetocaloric effect (Yuzuak et al. 2010).

Starting from commercially available metals (gadolinium 99.8 wt.%, silicon 99.995 wt.%, germanium 99.999 wt.%, and manganese 99.99 wt.%), Yuzuak et al. (2010) obtained the $Gd_5Si_{2.05-x}Ge_{1.95-x}Mn_{2x}$ ($2x = 0$, 0.03, and 0.08) compounds in the monoclinic phase by arc-melting to good homogeneity, stoichiometric amounts of the elements in an argon atmosphere on a water-cooled copper hearth. The arc-melted compounds were heat-treated at 900°C for 1 week in an evacuated quartz tube. The heat treatments were in argon atmosphere, and all compounds were quenched in ice water.

6.15.1 Magnetic Refrigeration

In principle, magnetic cooling is analogous to gas compression cooling. For continuous refrigeration, the heat generated in the magnetic material when the magnetic field is increased must be rejected to the ambient. This is equivalent to the compression stage of gas cycle refrigeration. During the demagnetization step, a thermal link cools the load, which is equivalent to the gas expansion stage of a compressor. By continued repetition of these two steps, the load temperature is maintained at a desired low level (Gschneidner and Pecharsky 2006).

The simultaneous use of the magnetic refrigerant as a regenerator considerably enhances the performance of the magnetic cooling device, especially if the volumetric heat capacity of the regenerator material is large. The regenerator is constructed of either a bed of tightly packed spheres (100–300 μm or irregularly shaped powders), or a set of closely spaced parallel thin plates (foils), or a wire mesh. In the active magnetic regenerator (AMR) cycle, a porous bed of a magnetic refrigerant material acts as both the refrigerant (coolant) and the regenerator for the heat transfer fluid. Gschneidner and Pecharsky (2006) have described the operation.

Apart from having good to excellent ΔS_{iso} and ΔT_{ad} values, there are many other criteria for selection of a refrigerant for a real magnetic cooling device. These include the raw material cost, the preparation of tons per day quantities, the vapor pressure of the components, the fabrication costs to develop the material into a useful form for the regenerator, the refrigeration capacity (i.e., the amount of heat transferred per cycle), hysteresis, time dependence of ΔT_{ad}, environmental concerns, and corrosion. Considering all available options, Gschneidner and Pecharsky (2006) declare that Gd will be the material of choice as the magnetic refrigerant.

Several other materials have been considered for magnetic refrigeration in different temperature regimes, especially for research purposes. Initially, GdPd and later the intermetallics $(Dy_{0.5}Er)Al_2$ and $TbNi_2$ have been found useful as magnetic refrigeration materials used for cooling gases or systems to temperatures as low as 4 K. Magnetic refrigerators have been considered more efficient than most cryogenic cooling systems particularly below liquid nitrogen temperature (Anon 1989).

The magnetic refrigerant rotates through a magnetic field, and while doing so warms or cools itself. As the refrigerant enters the magnetic field, it warms up, and when it leaves the magnetic field, it cools down. This behavior permits heat exchange and cooling of a gas or a system. The gadolinium refrigerant, for example, is rotated at ~5 rpm.

A design (Gschneidner et al. 1994a) of the AMR-MR refrigerator for the liquefaction of hydrogen gas is based on a modified Joule–Brayton cycle and uses GdPd as

the active component for the low temperature range. The problems associated with GdPd are the cost of Pd and the ductility of the compound, which makes crushing the intermetallic to a fine powder difficult. The refrigerant in the form of a fine powder is necessary for efficient heat transfer during various heating and cooling cycles. A detailed analysis of the state of the art of magnetic refrigeration is given by Houssem Rafik El-Hana Bouchekara and Mouaaz Nahas (2012).

The intermetallic $(Dy_{0.5}Er_{0.5})Al_2$ is not only cheaper and more brittle than GdPd but also has a much larger (30% more than GdPd) magnetocaloric effect. It is an excellent replacement for GdPd (Gschneidner et al. 1994a). The magnetocaloric effect of $TbNi_2$ is also 15% larger than GdPd (Gschneidner et al. 1994b).

For attaining extremely low temperatures, the intermetallic compound $PrNi_5$ has been used as the key material in an adiabatic demagnetization refrigerator, in conjunction with the nuclear magnetic cooling of copper (Gschneidner et al. 1995). In the two-stage adiabatic demagnetization unit, $PrNi_5$ was used as the first stage and copper as the second stage. In the presence of two magnetic fields, one around the $PrNi_5$ stage and the second around the copper, the entire unit was cooled down by a dilution refrigerator to ~25 mK. Then as the ~6 T field was slowly removed from the $PrNi_5$ stage, the entire unit cooled down to ~5 mK. A temperature of ~30 μK could then be reached when the field around copper in the second stage was reduced.

The preparation of magnetic refrigeration materials is usually accomplished by arc melting 99.8 at.% pure rare-earth metals and >99.99% pure nickel or aluminum in correct proportions on a water-cooled copper hearth (Gschneidner et al. 1994b). When more than one rare-earth metal was in the alloy, the rare earths were melted first, and then in the second step, the non-rare-earth-metal component was melted in. The methods described earlier for rare-earth intermetallics and metals or the atomization technique described below for making cryogenic cooler materials could be used for powder preparation.

Cryogenic coolers used for applications in present and emerging technologies such as magnetic resonance imaging, Josephson circuitry, and magnetic levitation utilize packed bed heat exchangers for transferring heat from a load to a sink. The packed beds are composed of rare-earth-metal compounds (RE_xM_y) such as Er_3Ni, DyCo, and $(Er_{0.9}Yb_{0.1})Ni$ or pure rare-earth metals such as Nd. The diameter of the particles used in the packed beds is ~200 μm.

Osborne et al. (1993) have used centrifugal atomization with a rotating disk to produce high-quality spherical particles of RE_xM_y compounds and pure metals. In the process used by Osborne et al. (1993) for the preparation of Er_3Ni powder, the starting Er_3Ni compound was first prepared. Stoichiometric amounts of Er and Ni were alloyed by arc melting in a water-cooled copper hearth. The Er_3Ni intermetallic thus obtained contained 89.5% Er, 10.5% Ni, 45 ppm O, 4 ppm N, and 18 ppm C.

Alumina crucibles were used to contain molten Er_3Ni prior to atomizing. The alumina crucible had a 3.2 mm hole drilled in it for bottom pouring. The charge (Er_3Ni) was melted under ultrahigh-pure Ar atmosphere, heated to 50–100°C above the melting point, held for 5 min for complete homogenization, and then poured onto a rotating 50-mm-diameter atomization disk made of low-density alumina with an erosion-resistant coating. A schematic of the system is shown in Figure 6.30. The atomized particles were quenched in a 2 L volume of a low-viscosity (100 centistokes) silicone oil. The oil was held in a container, and the container was also

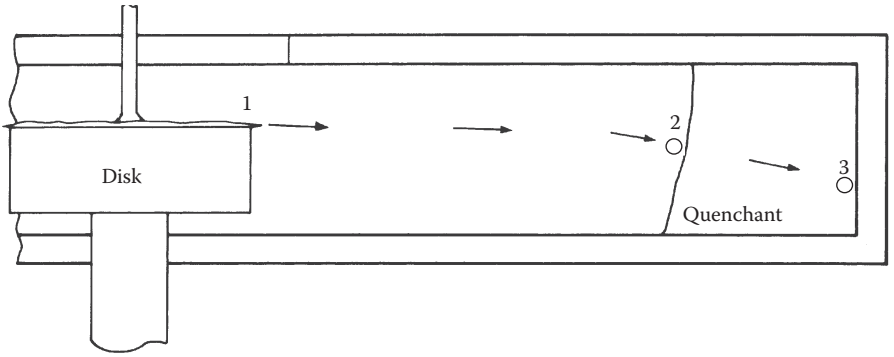


FIGURE 6.30 Schematic diagram of the rotating disc atomizer. Cross section of the quench bath. 1, Atomization skull; 2, a particle before contacting the quenchant; and 3, a particle before contacting the container. (From Osborne, M.G. et al., Centrifugal atomization of rare earth metal and intermetallic compounds. In Lawley, A. and Swanson, A. (eds.), *Advances in Powder Metallurgy and Particulate Materials—1993 Powder Characterization, Testing and Quality Control*, vol. 1, pp. 65–73, Metal Powder Industries Federation—American Powder Metallurgy Institute, Princeton, NJ, 1993.)

rotating concentrically at a lower rpm in the same direction as the atomization disk. The oil was preheated to 170°C in air to improve dehydration of the quenchant.

The particles were collected from the quenchant by filtration. They were cleaned with heptane and methyl alcohol. Even though the purity of the powder obtained was high and its shape was spherical, Osborne et al. (1993) did not consider the particle shape optimal. In the ideal case, the superheat must be so high that the particles have time to respherodize in the quenchant, yet low enough that complete solidification occurs before contacting the container wall.

Particles of Nd metal were also prepared by a similar technique. The important difference was that in place of alumina as the container, tantalum was used, and prior to use, it was baked at 1300°C for 8 h under 10^{-4} Pa.

Prior to the development of the centrifugal atomization technique for making $ErNi_5$ powder, the Ames group (Anderson et al. 1993) had investigated a high-pressure gas atomization approach to produce uniform spherical powders of high-purity $ErNi_3$. The average yield of high-quality spherical powders was only about 16% of the initial atomizer charge weight.

Other techniques for obtaining rare-earth metals and intermetallic compounds in powder form are (1) mechanical grinding of cast ingots into powder, (2) spark erosion, and (3) rotating electrode processing. These techniques have one or more limitations relating to powder shape, purity, and composition. Among all the techniques, centrifugal and high-pressure gas atomization procedures appear better.

6.16 THIN FILM DEPOSITION PROCESSES

For many applications, rare earth–bearing materials are required in the form of a thin film deposited on a suitable substrate. The preparation of terfenol as thin films

has been already mentioned (Uchida et al. 2002). Historically, the techniques used for the preparation of bubble domain memory materials and magneto-optic storage media serve as typical illustrations.

6.16.1 Bubble Domain Memory Materials

In 1970, Bobeck et al. (1970) discovered that many rare-earth garnet crystals grown from fluxes possess sufficient uniaxial anisotropy to maintain bubble domain stability. Subsequently, it was shown that films of magnetic garnets could be readily deposited by liquid phase epitaxy from molten $PbO–B_2O_3$ solutions onto gadolinium gallium garnet (GGG), $Gd_3Ga_5O_{12}$, substrates. A large number of substrates, 30 at a time, can be simultaneously dipped into the melt under near isothermal conditions at temperatures ranging from 750°C to 1100°C, and melt compositions can be adjusted to yield garnet films of required specifications. The substrate GGG is prepared as follows.

The GGG melts congruently at 1740°C and is grown by the well-known Czochralski or pulling technique. Crystals are grown from melts contained in indium crucibles in an atmosphere of nitrogen containing 2% O_2 (Brandle and Valentino 1972; Brandle et al. 1972). Large crystals of GGG, 75 mm diameter and weighing up to 75 g, are grown routinely (Nielsen 1981). The crystals are sewed, lapped, and polished to prepare substrates onto which the magnetic garnet films are deposited.

6.16.2 Magneto-Optic Storage Media

Magneto-optic storage media (Buschow 1988; Kryder 1993) consist of a thin film of magnetic material deposited on a transparent substrate, usually glass or plastic. The thin film is made in such a way that it is energetically most favorable for the magnetization to lie perpendicular to the plane. The most common magneto-optic storage media consist of amorphous alloys of the rare-earth elements gadolinium and terbium and the transition metal elements iron and cobalt. The amorphous alloys, e.g., $Tb_{25}(Fe_{0.9}Co_{0.1})_{75}$, are deposited onto substrates by some form of sputtering process (to a thickness of 500 μm).

A sputtering system typically consists of a vacuum chamber in which a target and the substrates to be coated are located. The target consists of the magnetic material to be deposited onto the substrates. The target is biased with a strong negative voltage (about 1000 V) relative to the ground potential of the vacuum chamber itself. When an inert gas, such as argon, is leaked into the chamber at a low pressure, the large voltage potential in the system causes the electrons to be stripped from the argon atoms, and a plasma is formed. Then the positive argon ions are accelerated toward the negatively biased target and strike it with high energy. The ensuing transfer of momentum from the argon ions causes atoms or clusters of atoms of the target material to be sputtered away from the target. These sputtered atoms diffuse away from the target. If a substrate is in close proximity to the target, it gets coated with a thin film of the target material.

The rare-earth transition metal thin films deposited by such a sputtering method are typically amorphous. This fact has proved to be important to their performance as low-noise recording media. In spite of their amorphous structure, the rare-earth

transition metal thin films exhibit anisotropic properties such that the lowest energy orientation for magnetization is perpendicular to the film plane. This is necessary for a good magneto-optic storage medium.

Rare-earth transition metal alloys are prone to corrosion and must be protected from the environment. This is done in magneto-optic media by using a thin dielectric that is impervious to both water vapor and oxygen, between the substrate and the magnetic film. Suitable materials are Si_3N_4 or AlN. The top surface of the film is protected by a similar dielectric and a reflective metal overcoat, such as aluminum. The rare-earth transition metal media manufactured this way have design lifetimes of over 10 years.

The rare-earth transition metal thin films used as storage medium in magneto-optic disks include GdTbFe and TbFeCo with the total rare-earth content of about 20%.

6.17 NiMH BATTERY AND HYDROGEN STORAGE MATERIALS

6.17.1 $LaNi_5$–Hydrogen System

The hydrogen absorption characteristics of $LaNi_5$-type compounds were first revealed by Zijlstra and Westendorp (1969) and elaborated further by Van Vucht et al. (1970) at the Philips Research Laboratories in Eindhoven, The Netherlands. $LaNi_5$ behaves like a hydrogen sponge. When hydrogen is introduced into a finely divided alloy of $LaNi_5$, it will be absorbed resulting in the formation of lanthanum nickel hydride:

$$LaNi_5 + 3H_2 = LaNi_5H_6$$

The absorption reaction is exothermic, and this will limit the reaction rate at a fixed H_2 pressure if heat is not removed. When heat is removed, the hydrogen adsorption rate remains high, and the quantity that could be absorbed is remarkable. Because the hydrogen is actually chemically bound within the hydride crystal lattice, when fully loaded, $LaNi_5H_6$ has a volumetric density of hydrogen that is significantly greater than even liquid hydrogen. $LaNi_5$ hydride is more attractive as a hydrogen storage system than many alternatives because (1) it operates at ambient temperature; (2) it stores H_2 at low pressure, comparable to liquid; (3) it is comparable in weight efficiency to compressed gas; and (4) it is comparable in volumetric efficiency to cryogenic liquid. The only disadvantage of $LaNi_5$ is the high cost compared to, for example, FeTi.

In the $LaNi_5$–H system, the hysteresis of the adsorption–desorption cycle is small. Like adsorption, the desorption kinetics is also fast. There is a 25% increase in volume in $LaNi_5$ on full hydrogen loading. Desorption at a comfortable rate can be accomplished at temperatures around 150°C.

6.17.2 Preparation of the Alloys

For an actual application, the $LaNi_5$ alloy was prepared by arc melting to the proper stoichiometry lanthanum and nickel metals of at least 99.5% purity (Lundin 1973).

The arc-melted alloy ingot was broken to granule size in a hardened steel mortar and pestle. The grinding operation could be conducted in air. The size of the granules was approximately 0.75–3 mm. The Ce, Nd, and Pr substituted La–Ni alloys have also been prepared by arc melting using a water-cooled copper crucible, using elements of high purity (from Johnson Matthey and Treibacher) (La 99.99%; Ce 99.12%; Pr 99.12%; Nd 99.7%; Ni 99.951%). The alloys were melted under argon at least five times to ensure homogeneity.

Rare earth-containing alloys for nickel metal hydride (NiMH) battery applications are prepared invariably starting from the constituent elemental metals by a melting process. No report of direct alloy synthesis from compound intermediates has appeared. Induction melting, arc melting as mentioned above, and in one case rapid solidification have been used to prepare the homogeneous multicomponent alloys required for various battery configurations. Contamination of the alloy is controlled by using appropriate crucibles and melting environments, and volatilization issues with high vapor pressure components are tackled by providing required overage in the charge or by other ingenious procedures.

Genshi et al. (1985) prepared $MMNi_5$ compound by chemical synthesis. The chlorides of $Ni(NiCl_2)$ and $MM(MMCl_3)$ were dissolved in water and then precipitated as $MM_2(CO_3)_25Ni_2(OH)_2CO_3{\cdot}xH_2O$. The precipitate was dried and heated under H_2 at about 750°C to reduce Ni^{2+} to Ni and obtain misch metal carbonate–nickel mixture. This powder was reduced with Ca at 1000°C to yield misch metal nickel intermetallic compounds. As regards hydrogen adsorption–desorption, the behavior of (La, Ce) Ni_5 and $MMNi_5$ alloys is basically similar to that of $LaNi_5$.

One of the problems with the use of rare earth–nickel hydride-forming materials is pulverization of alloys into a very fine powder upon repetitive hydriding–dehydriding cycles and very poor thermal conductivity of the powdered alloys. To prevent such disintegration and also improve thermal conductivity, Ishikawa et al. (1985) proposed a microcapsulation method. In this method, fine particles of hydride forming alloys such as $LaNi_5$ and $MMNi_{4.5}Mn_{0.5}$ were coated with a thin layer of metallic copper by a chemical plating method. Hydrogen storage capacities of alloys were not appreciably affected due to the plating. The encapsulated alloy powders was easily pressed into pellets. The pellets had high thermal conductivity and sufficient porosity to permeate hydrogen leading to fast reaction kinetics. The encapsulation is done as follows.

As-cast $LaNi_5$ and $MMNi_{4.5}Mn_{0.5}$ were crushed and then pulverized by repeating the hydrogen adsorption–desorption cycle up to 10 times. After the final dehydrogenation, the powders were ground and screened to 20 μm average particle size in air. The surfaces of alloy particles were activated by treating with the aqueous $SnCl_2$ and HCl solution and then with $PdCl_2$ + HCl aqueous solution. The powders were then immersed in the Cu^{2+}–tartaric acid complex + CH_2O + NaOH aqueous solution to form a metallic copper layer of ~1 μm thick. The coated alloy powders were pressed into pellets at 100 MPa at room temperature. The encapsulated alloy powder in the pellets was easily reactivated by evacuating and then heating at ~100°C under 10 atm hydrogen pressure. The encapsulated particles were able to withstand more than 5000 repeated hydriding–dehydriding cycles without disintegrating.

6.17.3 Alloys for Hydride Compressor

The AB_5 alloys consisting of Lanthanum (A) and nickel (B), as well as a series of compositions where Ce progressively substitutes for lanthanum in the alloy, were prepared by Odysseos et al. (2013) by induction melting of the constituent elements. These alloys were not destined for a NiMH battery but for a hydride compressor.

The equilibrium hydrogen pressure over AB_5 alloys, where A is La or a mixture of La and Ce and B is Ni, increases with an increase in the Ce content. Extensive absorption–desorption experiments (Van't Hoff diagrams) have shown that $La_{1-x}Ce_xNi_5$ alloys can be used to build a metal hydride compressor, compressing H_2 gas from 0.2 to 4.2 MPa operating between 20°C and 80°C. By combining four different alloys, starting from pure $LaNi_5$ (AB_5) and progressively substituting 0.2, 0.3, 0.4, and 0.5 Ce, hydrogen delivery pressure (equilibrium pressure at the relevant temperature) was raised from 0.2 to 4.2 MPa in a staged system, yielding a global compression ratio as high as 21 (Odysseos et al. 2013).

6.17.4 Preparation of Multicomponent RE–Ni–Mg Intermetallics

The AB_5 alloy in the NiMH battery electrode is seldom only a rare earth and nickel. There are invariable additives to modify/improve one property or another, and partial substitutions are always there for the rare-earth part and for the nickel part. This is evident from the compositions of some of the alloys narrated here.

High hydrogen storage capacity (7.60 wt.%), abundant natural existence, and the low density (1.74 g/cm^3) make magnesium a candidate for the hydrogen storage applications, in the form of intermetallics of magnesium with lanthanum and nickel. A comparison of the isothermal pressure-hydrogen absorption curve for La_2Mg_{17} and $LaNi_5$ shows that both in the absorption and desorption of hydrogen of the pressure of hydrogen gas is larger than that of temperature for the magnesium alloys. There was no change in the dimensions of the sample of La-Mg even after 70 absorption desorption cycles. The hydrogen absorbing power per mole of La-Mg, is about double that of La-Ni but the variation in hydrogen absorption with temperature is also larger for LaNi. Typically La-Mg absorbs-desorbs at a higher temperature–higher pressure regime. The addition of Ni decreased the hydrogen desorption temperature. The lowest temperature for hydrogen desorption was 274°C and 257°C for Mg_3La and $Mg_3LaNi_{0.1}$, respectively. La_2Mg_{17} alloy could absorb hydrogen at about 350°C to ~6.0 wt.%. The temperature is still too high for its practical applications (Yajima and Toma 1977). Slow kinetics and high desorption temperature apparently limit the industrial application of $LaMg_{3.93}Ni_{0.21}$ and the Mg–Ni alloys containing rare earths in immediate industrial hydrogen management applications. $LaMg_{3.93}Ni_{0.21}$ alloy ingot was prepared by inductive melting of La, Mg, and Ni (purity more than 99.9%) in a magnesia crucible under argon atmosphere. A slight excess of Mg was added to compensate for evaporative Mg loss during the melting procedure. Then the ingot was annealed at 738 K for 6 h (Pei et al. 2012). Induction melting was also used (Shi et al. 2013) to prepare $LaMg_{8.52}Ni_{2.23}M_{0.15}$ (M = Ni, Cu, Cr) alloys with La, Mg, Ni, Cu and Cr (purity more than 99.9%). The melting and heat treatment was conducted exactly as above for the ternary alloy.

As a typical AB_5-type alloy, $MmNi_{3.55}Co_{0.75}Mn_{0.4}Al_{0.3}$ demonstrates high discharge capacity and durable cycle life by restraining alloy pulverization during charge/discharge cycling with only about 10% Co by weight (Zhou et al. 2010). However, the cost of Co accounts for almost half of the total raw material cost. Therefore, in order to reduce the cost, focus in recent years has been on the several low-Co and Co-free alloys.

For use in hydride batteries as a substitute for $MmNi_{4.05}Co_{0.45}Mn_{0.4}Al_{0.3}$ alloy, Zhou et al. (2010) prepared $MmNi_{4.2}Co_{0.3}Mn_{0.4}Al_{0.3}Mg_{0.03}$ hydrogen storage alloy by single-roll rapid quenching followed by annealing for 8 h at 1213 K. The objective was to reduce consumption of expensive cobalt. Electrochemical experiments by Zhou et al. (2010) indicated that the annealing treatment at 1213 K extends cycle life from 193 to 358 cycles, increases the maximum discharge capacity, and also slightly decreases the activation behavior. Mg-added low-Co alloy annealed at 1213 K would be a promising substitution for the $MmNi_{4.05}\,Co_{0.45}\,Mn_{0.4}Al_{0.3}$ alloy product. Zhou et al. (2010) prepared Mg-added low-Co AB5-type over-stoichiometric alloy $MmNi_{4.2}Co_{0.3}Mn_{0.4}Al_{0.3}Mg_{0.03}$ (Mm comprises 62 at.% La, 27 at.% Ce, 3 at.% Pr, and 8 at.% Nd) by induction melting and subsequent single-roll rapid quenching. The gross weight of raw materials was about 5000 g, and the purity of that is higher than 99%. Because of its extremely high vapor pressure, magnesium element was added in the form of nickel–magnesium alloy when all the other elements apart from Mg in the form of pure elements were molten in order to prevent magnesium from evaporating. The alloy flakes were annealed at 1213 K for 8 h and air-cooled under an argon atmosphere. These alloy flakes with the thickness between 0.1 and 0.3 mm were ground and sieved to less than 74 μm.

In the realm of high-power output, long cycle life, and low-cost Ni-MH batteries, Takasaki et al. (2013) reported a cobalt-free (Co-free) $RE_{0.9}Mg_{0.1}Ni_{3.9}Al_{0.2}$ alloy (RE: rare earth) negative electrode of the Ni–MH battery, which effectively improved the high-rate discharge and suppressed the self-discharge compared to the conventional AB5-type alloy. A carbon-coated $Ni(OH)_2$ was also used to produce a Co-free Ni–MH battery. A 205 Ah Co-free Ni–MH battery cell was constructed using the Co-free materials, and this cell reportedly exhibited a good high-rate discharge performance.

6.18 SPECIAL RARE-EARTH CERAMICS

6.18.1 Yttrium Aluminum Garnet, Nd:YAG Ceramics

For nearly half a century, yttrium aluminum garnet (YAG) crystal made by the Czochralski method has been the most widely used solid-state laser host (Giesen et al. 1994; Ikesue and Aung 2006). Its fabrication needs expensive equipment and crucible materials. High ion-doping concentration or large-diameter crystals are difficult to obtain (Yagi et al. 2007). Polycrystalline YAG ceramic is a substitute for single-crystal YAG due to its excellent optical properties, mutilayer doping design, large-size and high ion-doping concentration, high-temperature mechanical properties, and far lower production cost (Chen et al. 2008; Huang et al. 2013). In 1995, Ikesue et al. (1995) reported highly transparent YAG ceramics by solid-state reaction (SSR) sintering method. Doped with Nd^{3+}, its laser slope efficiency was similar to

Czochralski-grown single crystals. This was followed by numerous investigations on SSR sintering, hot isostatic pressing, and SPS with various degrees of success.

Chaim et al. (2006) described the synthesis of YAG nanopowders by a modified coprecipitation method. Well-dispersed 50 nm particles were obtained by this method. They used a two-step sintering method with tetraethyl orthosilicate (TEOS) as the sintering additive to sinter nanocrystalline YAG particles to transparency (43% transmittance).

YAG transparent ceramics were fabricated by sintering in oxygen atmosphere using 0.5 wt.% tetraethyl orthosilicate (TEOS) as the sintering additive to control the grain growth and densification. The process outlined by Huang et al. (2013) is as follows. Stoichiometric quantities of high-purity α-Al_2O_3, Y_2O_3 (50 μm) were mixed and milled with ZrO_2 balls for 12 h with ethanol and 0.5 wt.% TEOS. After drying and sieving, the −200 mesh powder mixture was dry-pressed at 5 MPa and then isostatically pressed at 250 MPa to ~56% theoretical density. The compacts were sintered in an oxygen atmosphere in an alumina tube furnace. Pores were eliminated clearly at a temperature lower than 1700°C, while grain size was around 3 μm. The samples were transparent (in-line transmittance was 80% at 1064 nm) when samples were sintered at 1710°C (the grain size was 4.95 μm).

6.18.2 Gadolinium Gallium Garnet

Phase-pure, cubic gadolinium gallium oxide ($Gd_3Ga_5O_{12}$, GGG) nanopowders are the starting material for the growth of single-crystal GGG—well-known laser matrix, as well as for fabrication of rare-earth ion-doped polycrystalline transparent GGG ceramics, the latest solid-state laser materials.

Methods for synthesis of nanosized GGG powders are coprecipitation (Luo et al. 2005), sol-gel (Sun et al. 2005; Yao and Lin 2006), modified sol-gel (Lipiska et al. 2009), and solid-state synthesis (Hellstrom et al. 1989). All these methods require calcination up to 1350°C for phase-pure GGG formation. Mann et al. (2012) used solution combustion for synthesis of GG oxide nanopowders. In solution synthesis, a solution containing metal nitrates with a suitable fuel such as amino, hydroxyl, or carboxyl group is allowed to undergo a rapid combustion in a preheated furnace or oven. Due to the very short reaction time and sudden evolution of large amount of gases, the process always yields very fine nanosized powders.

Urea is a good fuel for gallium oxide synthesis and glycine for gadolinium oxide synthesis. A fuel mixture of urea and glycine was used for the synthesis of mixed oxides. In the process carried out by Mann et al. (2012), gallium oxide, Ga_2O_3 (99.99%), and gadolinium oxide, Gd_2O_3 (99.999%), were dissolved in nitric acid corresponding to a stoichiometric ratio Gd^{3+}/Ga^{3+} of 3:5. Glycine and urea were added to the solution. The mixture was placed in an alumina crucible and treated for 10 min in a furnace preheated at 500°C. Very porous white powder was obtained on combustion with mixed fuel. Combustion product was found to be phase-pure cubic GGG.

6.18.3 Scandia Ceramics

Wang et al. (2007) synthesized Sc_2O_3 nanopowder from scandium sulfate and hexamethylenetetramine [$(CH_2)_6N_4$] using a precipitation method. The precursor

precipitate $[Sc(OH)_{2.2}\cdot(SO_4)_{0.4}]\cdot 0.4H_2O]$ on calcination at 1100°C for 4 h in a corundum crucible yielded Sc_2O_3 nanopowder with good dispersion and a mean particle size of 80 nm. The Sc_2O_3 nanopowder was cold-compacted (300 MPa, steel die) and sintered to transparent Sc_2O_3 ceramic (58% transmittance) by vacuum (1 mPa) sintering at 1700°C for 5 h without any additives.

Scandium oxide (Sc_2O_3) is a specialty ceramic used in multifunctional laser crystals, solid electrolytes, transparent ceramic scintillators, infrared laser windows, high-temperature windows, infrared guided missile domes, and optical components for high-temperature and strong radiation environments. Compared to some other ceramics (alumina, yttria, YAG), scandium oxide has comparatively high bulk refractive index, high band gap, high melting point (2430°C), and high thermal conductivity (17 Wm/K).

6.18.4 Rare-Earth Sulfides

Rare-earth sulfides are among the critically important materials for special service. Apart from other uses, they are excellent refractory materials for containment of reactive liquid metals. A method for their preparation is given by Yuan et al (2009). The commercial REO powder was placed on a graphite crucible and inserted into a corundum tube furnace. After flushing with argon gas at room temperature, the tube furnace was heated to the preset temperature while under argon flow. Then, CS_2 gas was introduced into the reaction tube by passing Ar carrier gas through a bubbler that contained liquid CS_2. The sulfurization reaction was carried out for 3 h. At the end of the reaction, the tube furnace was cooled down to room temperature under argon flow. The preparation conditions for various sulfides are listed in Table 6.18 (Yuan et al. 2009). In the preparation of some γ-phase rare-earth sulfides, the synthetic rare-earth sulfide powder was placed on a graphite crucible and inserted into a corundum tube furnace. The sample was annealed at 1500°C for 1 h at nitrogen atmosphere.

6.19 PREPARATION OF RARE-EARTH PHOSPHORS

A selection of techniques used in phosphor preparation is given next. Highest purity ingredients are invariably used. The process description may at best be taken as a general method because commercial manufacturing practices are seldom revealed for the open literature.

6.19.1 Homogeneous Precipitation

In 1993, Nichia Chemical Company developed the GaN-LED with blue emission. Semiconductor diode solid lighting was thus possible for the first time. Three years later, the company prepared a series of Ce-doped YAG phosphors. Ce:YAG phosphors were combined with GaN-LED to fabricate highly efficient white LED (W-LED). A highly efficient lighting resource, which can replace daylight lamp, became available.

TABLE 6.18
Appropriate Preparation Conditions of Single-Phase Rare-Earth Sulfides and Their Colors

Starting Materials	Sulfurization Conditions	Synthesized Products	Color
La_2O_3	800°C, 3 h	β-La_2S_3	Light yellow
CeO_2	800°C, 3 h	β-Ce_2S_3	Red
Pr_6O_1	1950°C, 3 h	β-Pr_2S_3	Lime green
Nd_2O_3	850°C, 3 h	α-Nd_2S_3	Maroon
Sm_2O_3	800°C, 3 h	α-Sm_2S_3	Maroon
Gd_2O_3	1100°C, 3 h	α-Gd_2S_3	Maroon
Tb_4O_7	1050°C, 3 h	α-Tb_2S_3	Maroon
Dy_2O_3	1050°C, 3 h	α-Dy_2S_3	Maroon
Eu_2O_3	1000°C, 3 h	EuS	Dark brown
CeO_2	1250°C, 3 h	γ-Ce_2S_3	Red
Pr_6O_{11}	1200°C, 3 h	γ-Pr_2S_3	Lime green
Nd_2O_3	1150°C, 3 h	γ-Nd_2S_3	Green
Sm_2O_3	1250°C, 3 h	γ-Sm_2S_3	Orange
Gd_2O_3	1250°C, 3 h sulfurized + 1500°C, 1 h annealed	γ-Gd_2S_3	Yellow
Tb_4O_7	1250°C, 3 h sulfurized + 1500°C, 1 h annealed	γ-Tb_2S_3	Yellow
Dy_2O_3	1250°C, 3 h sulfurized + 1500°C, 1 h annealed	γ-Dy_2S_3	Yellow
Y_2O_3	1250°C, 3 h	δ-Y_2S_3	Light yellow
Dy_2O_3	1250°C, 3 h	δ-Dy_2S_3	Yellow
Ho_2O_3	1200°C, 3 h	δ-Ho_2S_3	Yellow
Er_2O_3	1200°C, 3 h	δ-Er_2S_3	Tan
Tm_2O_3	1200°C, 3 h	δ-Tm_2S_3	Light yellow
Yb_2O_3	1250°C, 3 h	ε-Yb_2S_3	Yellow
Lu_2O_3	1200°C, 3 h	ε-Lu_2S_3	White

Source: Yuan, H. et al., *J. Rare Earths*, 27(2): 308, 2009.

SSR is the primary method to produce Ce:YAG phosphor, but the method needs long reaction time and high reaction temperature, and yields product with a large particle size. Postprocessing of the large particles will reduce the luminescent properties.

The wet chemical methods could improve homogeneity, decrease calcining temperature and time, and also decrease particle size. Microwave technique has been recognized as widely useful in inorganic synthesis. A wet chemical method using the microwave technique, i.e., homogeneous precipitation under microwave irradiation, yields ultrafine (80 nm) Ce:YAG phosphors.

The staring materials were REOs and nitrates. Y_2O_3 (>99.99%) was dissolved in reagent-grade nitric acid. As determined by the stoichiometric requirement,

$Al(NO_3)_3{\cdot}9H_2O$ (>99.0%) and $Ce(NO_3)_3{\cdot}6H_2O$ (> 99.0%) were added into the yttrium nitrate solution under agitation. Urea was added to solution followed by ammonium sulfate, and the solution was heated for 30 min in microwave oven by 2.45 GHz microwave irradiation under 900 W output power. An amorphous precursor, which is a carbonate of aluminum, yttrium, and cerium, was precipitated.

The precursor was washed in water and ethanol, and dried at 80°C for 12 h in air. Subsequently, it was calcined from 900°C to 1200°C for 4 h in air. Upon calcination at 1100°C, the amorphous precursor transformed into phase-pure YAG (particle size 80 nm) directly. On calcination at 1200°C, the particle size was 150 nm.

Presently, white LEDs comprise GaN-based blue LED as the excitation source and coating with $Y_3Al_5O_{12}:Ce^{3+}$ phosphors. This arrangement is attractive because of easy fabrication, low cost, and high brightness. However, LEDs with $Y_3Al_5O_{12}:Ce^{3+}$ phosphors generate cool white, and search has been on for phosphors emitting at longer wavelength.

6.19.2 Solid-State Reaction

Silicates, with a stable crystal structure and high thermal stability, are considered excellent luminescent hosts. Cheng et al. (2010) reported on the fabrication of $Sr_3SiO_5:Eu^{2+}$ phosphor by high-temperature SSR using analytically pure raw materials—$SrCO_3$, ultrafine SiO_2, BaF_2, CaF_2, MgF_2, $BaCl_2$, and 99.99% Eu_2O_3 powder.

Stoichiometric amounts of the raw materials were thoroughly blended, and the mixture was pre-sintered at 1100°C for 2 h in an ambient air. The prefired products were then ground and calcined at 1400°C for 6 h with some amount of fluxing agents in a reducing atmosphere (95%N_2–5%H_2). $Sr_3SiO_5:Eu^{2+}$ phosphors with various fluxing agents and Eu^{2+} ion concentration were thus obtained. The phosphor showed a broad excitation band from 300 to 500 nm and a broadband emission peaking at 561 nm. Park et al. (2006) noted that $Sr_3SiO_5:Eu^{2+}$ phosphors provide warm white light and possibly a better alternative to $Y_3Al_5O_{12}:Ce^{3+}$.

SSR at high temperature was also used to prepare the phosphors $LaNbO_4:Eu^{3+}$. In an appropriate stoichiometric ratio, the start materials La_2O_3 (99.99%), Nb_2O_5 (99.5%), and Eu_2O_3 (99.99%) were weighed in and ground finely in an agate mortar. Next, the homogeneous mixture was calcined in an alumina crucible at 1200°C for 5 h (Huang et al. 2010). Upon excitation with 395 nm UV irradiation, the phosphors $La_{0.75}Eu_{0.25}NbO_4$ ($LaNbO_4:Eu^{3+}$) and $La_{0.65}Eu_{0.25}Bi_{0.10}NbO_4$ show strong red-emission lines at 615 nm, and the International Commission on Illumination (CIE) chromaticity coordinates were close to the standard of NTSC. They are considered as potential competitors to the present commercial red-emitting Y_2O_2S:0.05 Eu^{3+} for near-UV InGaN-based LED applications.

In phosphors, using double activation, energy could be transferred from one luminescent activator to the other one, resulting in more efficient or brighter device operation. Coactivators could be added to a host material to change the color of the emitted light. Nazarov and Noh (2010) described the preparation of some efficient phosphors with improved luminescence properties. They are $CaWO_4:Eu^{3+}$, Tb^{3+}; $(Y, M)NbO_4:Eu^{3+}$ (M: Al, Ga) and $Tb_3Al_5O_{12}:Ce^{3+}$, Eu^{3+}.

$CaWO_4$:RE phosphor was prepared by SSR from homogeneous mixtures consisting of luminescent-grade $CaWO_4$ as host lattice; WO_3, Eu_2O_3 (99.99%), and/or Tb_4O_7 (*Specpure*) as the activating system, and alkaline salts as the flux. $CaWO_4$ used as a precursor in phosphor synthesis was obtained from highly purified $CaCl_2$ and Na_2WO_4 solutions. The starting mixture containing flux and equivalent amounts of WO_3 and Eu_2O_3 or Tb_4O_7 was homogenized, fired at 900°C, cooled, washed, dried, and sieved. The incorporation of trivalent RE ions into the $CaWO_4$ proceeds in two ways—either $2RE^{3+}$ replace $3Ca^{2+}$ ions, or a pair of RE^{3+} and M^+ replaces $2Ca^{2+}$ ions (where M^+ = alkali ion). The alkali salt acts as a mineralizing agent and also as a source of compensating ion. A series of mixtures was synthesized according to the general phosphor formula $Ca_{1-2x-2y}Eu_xTb_yM_{x+y}WO_4$. The double activation of $CaWO_4$ with Tb^{3+} and Eu^{3+}, in the presence of alkaline salts as flux, opens the possibility to synthesize phosphors with variable chromatic emissions.

The phosphor $Tb_3Al_5O_{12}:Ce^{3+}$, Eu^{3+} is designated TAG:Ce, Eu. Application of TAG:Ce, Eu in the LED showed the better chromaticity coordinates of luminescence and color rendering index of LEDs. The TAG:Ce, Eu powder is prepared by a conventional SSR. According to the nominal composition of $Tb_3Al_5O_{12}:Ce^{3+}$, Eu^{3+}, the starting materials Tb_4O_7, Al_2O_3, CeO_2, and Eu_2O_3 (99% for Al_2O_3, 99.9% for all other oxides) are weighed and milled. Synthesis was carried out at 1500°C for 2 h in a furnace heated by induction using a sealed alumina tube in a reducing atmosphere of H_2/N_2 to stabilize the Tb^{3+} state. The crucible was made out of alumina. BaF_2, LiF, and H_3BO_3 were used as flux materials.

Apart from the presently used, (Y, Gd)$BO_3:Eu^{3+}$ or $Y_2O_3:Eu^{3+}$ for red, Zn_2SiO_4:Mn^{2+} or $BaAl_{12}O_{19}:Mn^{2+}$ for green, and $BaMgAl_{14}O_{23}:Eu^{2+}$ or $BaMgAl_{12}O_{17}:Eu^{2+}$ for blue phosphors for plasma display panel (PDP) (Y, Gd, Lu)$BO_3:Eu^{3+}$ is also as an improved alternative red phosphor.

The phosphor was synthesized with Y_2O_3 (99.99%), Gd_2O_3 (99.99%), Lu_2O_3 (99.99%), Eu_2O_3 (99.99%), and H_3BO_3 (99.5%) as raw materials. Stoichiometric Y_2O_3, Gd_2O_3, Lu_2O_3, Eu_2O_3, and 10 mol.% excess H_3BO_3 were thoroughly ground by adding ethanol to mix homogeneously and then sintered at 800°C for 120 min. The mixtures were re-ground thoroughly and sintered at 1150°C for another 180 min. Then the fired products were ground and washed with 80–100°C distilled water for several times to remove the excess B_2O_3 and dried at 120°C.

6.19.3 Sol-Gel Synthesis

A typical process for the preparation of a phosphor, $MgTiO_3:Eu^{3+}$, by the sol-gel method has been described by Zhang et al. (2012). Titanates are a good matrix for rare-earth ion-activated phosphors because of their easy preparation and high luminescence efficiency. $MgTiO_3:Eu^{3+}$ has also been reported as a promising red-emitting phosphor by Kominami et al. (2006).

Eu_2O_3 (99.99%) was dissolved in nitric acid, $Mg(NO_3)_2{\cdot}6H_2O$, $Al(NO_3)_3{\cdot}9H_2O$, and adequate amount of citric acid was dissolved in distilled water. The above solutions were mixed to form solution A. $Ti(C_4H_9O)_4$ was dissolved in anhydrous ethanol to get solution B. Stoichiometric amount of solution A was added to solution B under vigorous stirring to form a sol, then a transparent viscous gel was obtained after the

sol was heated at 90°C for 8 h. The gel was calcined in a muffle furnace at 700°C for 4 h after pretreatment at 400°C for 2 h to yield the phosphor powder. The phosphor product was found to emit strong red light under the 465 nm excitation, which matched well with the output wavelength of commercial GaN-based blue LEDs.

Silicate-based phosphors, for example, YPS ($Y_2Si_2O_7$), have excellent photoluminescence properties and a crystal structure conducive to getting higher CRI (Sokolnicki 2013). In the YPS lattice, Eu^{3+} can be reduced to a 2^+ oxidation state, whose bluish–greenish emission, together with the red one of Eu^{3+} and the green luminescence of Tb^{3+}, contributes to the white light.

The preparation of YPS:Eu^{3+}, YPS:Eu^{3+}, Tb3$^+$ and YPS:Ce^{3+}, Eu^{3+}, Tb^{3+} nanocrystalline phosphors by the combination of combustion and sol-gel techniques were described by Sokolnicki (2013). Y_2O_3:Ln^{3+} (Ln^{3+} = Ce^{3+}, Eu^{3+}, and Tb^{3+}) was prepared using the solution combustion synthesis with mixed fuel containing glutamic acid and glycine. Stoichiometric quantities of the metal nitrates and fuel (glycine/glutamic acid) were dissolved in a small amount of water. Subsequently, the solution was dried at 150°C for about 3 h. The dry mixture was fired at 600°C for 2 h in air to decompose residual nitrate ions. Silica sol was obtained by the acid-catalyzed hydrolysis of tetraethoxysilane (TEOS) with deionized water, and C_2H_5OH was added to dissolve the TEOS. The pH was adjusted to 2 using diluted nitric acid. The molar ratio of (TEOS):(H_2O):(ethanol) was 1:4:8. The sol was mixed with Y_2O_3:Ln^{3+} in a stoichiometric amount directly after the hydrolysis had been completed. The samples containing Ce^{3+}, Eu^{3+}, and Tb^{3+} were heated at up to 1200°C in air or in the reducing atmosphere for 5 h. Nanocrystalline samples of YPS, Y_2O_3:Ln^{3+} (Ln^{3+} = Ce^{3+}, Eu^{3+}, and Tb^{3+}) were thus successfully obtained by the reaction of Y_2O_3:Ln^{3+} and colloidal silica at 1200°C.

Yerpude and Dhoble (2013) described a simple combustion synthesis of trivalent rare-earth (RE^{3+} = Dy, Eu, and Ce) activated $Sr_4Al_2O_7$ phosphor. $Sr(NO_3)_2$, $Al(NO_3)_3{\cdot}9H_2O$, Eu_2O_3, Dy_2O_3, urea (NH_2CONH_2), and $(NH_4)_2Ce(NO_3)_6$ were the start materials and urea was the fuel. The product was obtained as a foamy powder.

6.19.4 Melt Synthesis

In contrast to SSRs, reactions in a melt are extremely rapid and homogeneous because of liquid mixing and rapid diffusion in the liquid phase. These melt-synthesis techniques are therefore suitable for synthesizing multicomponent compounds and solid solutions where homogeneous cation mixing is required.

6.19.4.1 Molten Salt Synthesis

Compared with the other synthesis methods: precipitation, sol-gel, combustion, spray pyrolysis, and hydrothermal, molten salt synthesis method has advantages such as low sintering temperature, smooth surface, special morphology for product, low cost, and efficient mass production (Wu et al. 2010a). Y_2O_3 and Eu_2O_3 were converted into their nitrates by dissolving in a minimum amount of dilute nitric acid. Then rare-earth nitrates were homogeneously mixed with eutectic mixtures of KNO_3–$NaNO_3$ or KCl–NaCl by milling in an agate mortar. Finally, the homogenously

mixed materials were annealed at appropriate temperatures, and after repeatedly washing and drying, the as-expected Y_2O_3:Eu products were obtained.

6.19.4.2 Flux Method

(Y, M)NbO_4:Eu^{3+} (M: Al, Ga) powders were synthesized by a flux method. The start material was a stoichiometric mixture of Y_2O_3, Nb_2O_5, Al_2O_3, Ga_2O_3, and Eu_2O_3 powders. All the powders were 99.99% pure. The amount of Eu_2O_3 was in the range of 0–45 mol.% and LiCl (7 wt.%) was added as a flux to promote a SSR. After ball milling the mixtures for 24 h, they were fired at 1300°C for 12 h in an electric tube furnace flowing N_2 gas. Phosphors based on $YNbO_4$ and doped with Eu^{3+}, Ga^{3+}, and Al^{3+} showed higher intensity under nUV and x-ray excitation in comparison with $YNbO_4$:Eu^{3+} phosphors.

6.20 SUPERCONDUCTORS

Superconductivity was discovered in 1911 by Kammerlingh Onnes who showed that mercury loses all of its electrical resistance (becomes superconducting) when cooled to liquid helium temperature (4 K). Between that time and 1986, a variety of materials were found to be superconducting, but the highest known critical temperature, T_c, was 23.3 K for Nb_3Ge. The critical temperature is the upper limit of the temperature range in which the material is still superconducting. The critical current and critical magnetic field are similarly defined because superconductivity is destroyed by too much current and too great a field, and these three critical variables characterize the superconductor. It is technologically and commercially advantageous to have materials that have high critical values.

In 1986, a new group of materials known as high-temperature superconductors was discovered by Bednorz and Muller (1986). They originally reported work on a multiphase Ba–La–Cu–O compound with a T_c below 30 K. As work continued in several groups, it was revealed that the superconducting phase had a perovskite-like structure, and that T_c could be pushed up to 40 K by replacing barium ions in the compound with strontium. The widely accepted BCS (Bardeen, Cooper and Schrieffer) theory of superconductivity had predicted a maximum possible T_c of about 40 K. As shown in Figure 6.31, this limit as well as the liquid nitrogen temperature of 77 K was quickly crossed with the discovery of newer ceramic superconducting compounds (Fisher 1988; Alford 1992; Fox 1996). The Most significant of these was the discovery in February 1987 by Chu's group at Houston that a multiphase Y–Ba–Cu–O compound (YBCO) had a T_c of 92 K. It was subsequently shown that the YBCO phase responsible for superconductivity was perovskite-like with a composition of $Y_1Ba_2Cu_3O_{7-x}$ (commonly referred to as the 1–2–3 phase).

The Ginzburg and Landau (known as GL) theory explains many features of high-temperature superconductivity. One conclusion from the GL theory, particularly relevant to the processing of superconductors, is that all high-T_c superconductors, already discovered and yet to be discovered, should have very short coherence lengths of typically atomic-scale dimensions. Coherence length is the distance over which paired electrons (carrying supercurrent) interact. In high-temperature

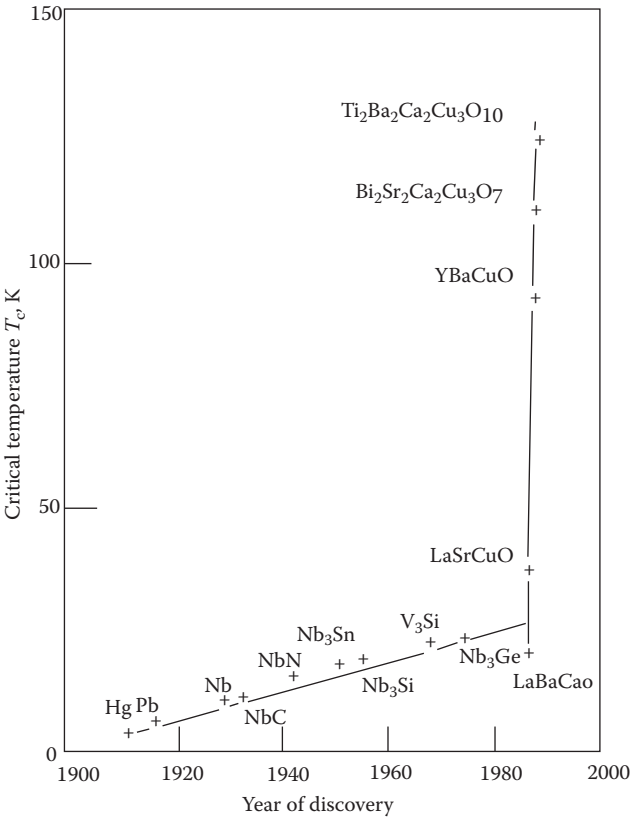


FIGURE 6.31 Development of high-temperature superconducting alloys.

superconductors, the coherence length is about 1–3 nm, which is less than that for a conventional superconductor.

The very short coherence length of the electron pair in all high-T_c superconductors implies that, in polycrystalline material, grain boundaries must be sharp and contain no amorphous phases. If the grain boundary width exceeds the coherence length, the electron pairs will be strongly scattered. Generally, the crystalline defects, other than those that pin fluxoids without scattering electron pairs, must be minimized. The coherence length is comparable with the spacings of the copper–oxygen layers in YBCO. Thus, the critical current in a direction perpendicular to these layers will be low. This is confirmed in that high J_c is obtained in directions parallel to *a*–*b* planes but not parallel to the *c*-axis. Texturing, therefore, becomes essential to obtain high critical current densities in polycrystalline materials. Besides, to obtain ceramic superconductors with sufficient strength for winding, for example, into coils and to withstand the Lorentz force originating from a high current in a high magnetic field, the size of pores and cracks must be minimized.

In $YBa_2Cu_3O_{7-x}$, the highest critical density is achieved when $x = 0$, but the material remains superconducting down to $YBa_2Ca_3O_{6.5}$. In the production of bulk $YBa_2Cu_3O_7$, the tetragonal phase $YBa_2Cu_3O_6$ is formed first and then annealed in oxygen to produce the tetragonal to orthorhombic phase transformation to $YBa_2Cu_3O_7$.

These are three main techniques for making high-T_c superconductors. In the first, the materials can be deposited onto a single-crystal structure by methods such as evaporation, laser ablation, or sputtering so that epitaxial growth occurs. In the second, thick films can be made by mixing the powder with various polymers and solvents and applying it to a suitable polycrystalline ceramic or metallic substrate. In the third method, bulk materials can be made by sintering a powder of right stoichiometry, for example, Y_2O_3, $BaCO_3$, and CuO mixed in the molar proportions 1:2:3. The fracture toughness of superconducting ceramics is so low that making bulk ceramics in complex shapes requires rather sophisticated processing techniques.

Thin films of high-T_c superconductors are produced because they have major potential application in electronic devices, and for basic scientific measurements, single-crystal thin films are relatively easy to grow. The best superconducting thin films have been obtained by growing them epitaxially on substrates closely lattice-matched to the superconductor. As regards methods for producing the thin films, if $Y_1Ba_2Cu_3O_7$ is used as a target, it can be sputter-deposited onto a substrate held at about 400°C. The YBCO layer will be oxygen-deficient and in amorphous or polycrystalline form. Subsequent annealing in oxygen results in epitaxial growth that nucleates at the substrate–film interface. Alternatively, the materials can be directly sputtered onto a single-crystal substrate held at 650°C. A tetragonal epitaxial film of approximate composition $YBa_2Cu_3O_6$ is formed, and oxygen annealing leads to orthorhombic superconducting $YBa_2Cu_3O_{7-x}$. Thin film deposition can also be done by laser ablation, molecular beam epitaxy, metal organic chemical vapor deposition, and metallorganic molecular beam epitaxy. Thin film (0.5 μm) superconductors are capable of carrying large amounts of current (10 million A/cm^2), but they are not suitable for many practical applications because of their fragility. Bending of the thin film material can damage the YBCO grain structure, and misalignment in the grain structure hampers the flow of current.

Thick film tapes (1–2 μm thickness) conduct 1 million A/cm^2 and can retain half of their current-carrying ability in magnetic fields as high as 9 T. In a process developed in 1995 at the Superconductivity Technology Center of the Los Alamos National Laboratory, a three-layer tape made of YBCO compound and zirconium oxide placed in a pliable nickel alloy tape was made. The zirconium oxide layer prevents interaction between the YBCO compound and nickel and also forces the YBCO into a regular crystalline order that promotes superconductivity. Ion beam deposition is used to apply the zirconium dioxide layer. One beam of ions lays down a few hundred thousandths of an inch of zirconium oxide, while the second beam orients the crystals as they form on nickel. This results in an orderly symmetrical surface on which the YBCO layer can be affixed.

By pulsed layer deposition of thick films (6–10 μm) of Y-123, researchers at Los Alamos National Laboratory have reported J_c values greater than 1 MA/cm^2 at 77 K (Foltyn et al. 1993). This potentially scalable technique may be used to prepare a

superconductor coated continuously on long lengths of metal or ceramic substrates with suitable buffer layers.

Bulk superconducting YBaCuO can be made by sintering Y_2O_3, CuO, and BaO and annealing in oxygen. However, careful control is needed in the annealing temperature and cooling rate, in reducing the particle size, and in eliminating impurities. It is then possible to produce a material that is 99% pure superconducting $Y_1Ba_2Cu_3O_{7-x}$, having 99% of grain boundaries atomically sharp with no traces of impurities. Critical current values in the pure polycrystalline materials typically exceed 10^7 A/m^2.

To obtain $YBa_2Cu_3O_{7-x}$ that has sufficient strength to be fabricated into wires and coils, the density must be above 85% and the larger the better, and crack size should be less than 10 μm. The critical current density increases with an increase in the density of the material. In addition to good mechanical properties, high-density materials also have longer life and do not degrade.

Typically, the density of a sintered body can be increased by raising the sintering temperature. In the Y-123 system, if special precautions such as vacuum calcination are not taken during powder preparation, often a low melting (~900°C) Ba–Cu–O liquid forms. While sintering above this temperature leads to more rapid liquid phase sintering resulting in improved density and increased grain size, it also results in an insulating phase along the grain boundaries thereby decreasing the critical current density (McGinn 1994).

To obtain a bulk superconductor with good mechanical properties, high-purity starting material in the form of submicrometer powder is essential (Masur et al. 1994). Using viscous processing routes, coils and shapes can then be fabricated.

To achieve high current densities in polycrystalline wires and thick films of ceramic superconductors, texturing is essential. Texturing or texture processing leads to improved J_c in polycrystalline Y-123 by avoiding or minimizing many of the weak link limitations to J_c. Some of the primary causes of weak link behavior can be minimized by having a microstructure where the current flow is directed primarily in the basal plane and by minimizing the occurrence of high-angle grain boundaries. In bulk Y-123, formation of texture has been achieved by a number of different techniques, including compaction processes, magnetic alignment of particles, and directional solidification of particles. Transport J_c values exceeding 10 kA/cm^2 in applied fields of several teslas have been achieved by solidification routes described by the term *melt texturing* (Jin et al. 1988, 1989). In the case of Y-123, melt texturing describes directional solidification from the melt or partially melted state. Texturing is achieved in various ways such as melt texturing, rolling, and solidification in high magnetic fields.

A process known as the metallic precursor (MP) approach has been used to prepare long lengths of high T_c ceramic superconducting wires (Sandhage 1990). The MP approach is particularly attractive for fabrication of high filament count, fine filamentary composite conductors because most of the wire-forming process is performed while the material is in its metallic state. In the process described by Masur et al. (1994) of the American Superconductor Corporation, high filament count silver-sheathed composite wires of $YBa_2Cu_4O_8$ were prepared. The process starts with the preparation of homogeneous alloy powder by mechanical alloying of the metallic

elements. The alloy powder is packed into a silver can that is sealed and extruded into a hexagonal rod. Cut pieces of the rod are stacked into a multirod bundle that is again packed into a can and extruded into a hexagonal rod. This process is repeated many times. In the final step, the can is extruded with a reduction ratio of up to 300:1 into a rectangular tape or round wire. The extruded metal tapes were internally oxidized to form silver–suboxide composites. The suboxides consisted of Y_2O_3, BaO, CuO, and $Ba_2Cu_3O_x$. They were then reacted to form the Y-124 phase. The finely divided suboxides that form from the oxidation process react quickly to form Y-124 even at ambient oxygen pressure. Following oxidation, the tapes were subjected to thermomechanical treatments (TMTs) to convert the suboxides into textured polycrystalline Y-124 grains. The TMT involved multiple iterations of heat treatment in the range of 600–825°C followed by uniaxial pressings of up to 2 GPa and a final heat treatment at 750°C for 100 h in 1 atm of oxygen. Tapes containing up to 962,407 filaments with filament dimensions as fine as 0.25 μm thick and 1 μm wide with significant biaxial crystallographic texture were thus made. These wires exhibited transport current densities in the oxide filament of 69,500 A/cm^2 at 4.2 K in self-field with decreased weak link behavior in applied field, better critical current retention during binding, and in general some of the best properties for a polycrystalline, sintered wire of YBCO in an applied magnetic field.

6.21 SUMMARY

There are numerous rare earth-containing end-product materials suitable for commercial applications or research uses. Many of these are compounds, alloys, and metals that are produced either as end products of ore processing or as interprocess intermediates in the preparation of rare-earth metals. Many rare-earth materials, however, have to be produced specifically starting from interprocess intermediates or metals. These processes have been covered in this chapter.

The first commercial rare-earth material was the gas mantle produced by Carl Auer von Welsbach. The production method was mentioned in Chapter 1. To light the gas mantles, a lighter flint based on misch metal was also invented by Welsbach. As early as 1908, he used fused salt electrolysis of mixed rare-earth chloride as the method to obtain misch metal. This method to date remains the most important process for misch metal production. In the United States, Japan, and China, the USBM process of oxide–fluoride electrolysis has also been adopted for commercial production of misch metal. Thermal reduction processes based on calcium reduction of mixed rare-earth fluoride have been investigated in Brussels and at Ames.

The addition of rare earths to steel results in several advantages. Rare earths are added in the form of misch metal or as rare earth–iron–silicon–iron alloys. The rare earth–iron–silicon alloys are commercially prepared by a carbothermic reduction of a mixture of rare-earth compounds or ore concentrate, iron or iron ore, and silica in a submerged electric arc furnace. Many other processes that result in higher rare-earth loading in the alloy and better rare-earth recovery have also been developed. These include the USBM process in which a mixed REO of bastnasite origin was reduced by calcium silicide, ferrosilicon, silicon, and aluminum, and the BARC process in which a mixed REO of monazite origin was reduced with ferrosilicon and aluminum

scrap. In the Chinese practice, rare earth-containing blast furnace slag from Baotou was reduced with ferrosilicon using lime as flux in an arc furnace. Electric arc furnace reductions have also been used to produce rare earth–magnesium–silicon alloy starting from rare earth–containing blast furnace slag, calcined dolomite–ferrosilicon, calcium, and silicon. Electrolytic processes have been used to prepare rare earth–aluminum–zinc and yttrium–aluminum alloys.

Rare-earth transition metal-based magnets are a family of commercial products of considerable variety and constantly growing major technical importance. The first group of rare-earth magnets developed in the 1960s and 1970s were based on the intermetallic compounds $RECo_5$ and RE_2Co_{17}. These compounds possess an ideal combination of magnetic and structural properties for high-performance magnet applications. They were prepared by the simple technique of direct melting of alloy components or by using more sophisticated methods such as coreduction or reduction–diffusion using metal oxides as start materials. The technique of direct production of alloy by fused salt electrolysis using cobalt as the consumable anode was also used. The alloys were ground to a powder, mixed with a chemical binder, and pressed under a magnetizing field to produce the plastic-bonded magnets. The adoption of inexpensive molding methods such as extrusion and injection molding in an orienting field facilitated large-scale production and industrial application of the bonded REPMs. Instead of plastic, a soft metal matrix has also been used as the binder, and metal matrix bonded magnets have better elevated temperature stability. Sintered magnets were prepared by following the sequence of blending, milling, aligning and pressing, sintering, and finally a postsintering heat treatment. As regards the magnetic properties, the sintered magnets are superior, but bonded magnets also have numerous practical advantages.

Cost and supply problems of samarium and cobalt were serious disadvantages of the samarium–cobalt magnets, and the search for suitable alternatives culminated in the development of neodymium–iron–boron magnets in the 1980s. Like in the case of the samarium–cobalt, the overall process for the production of Nd–Fe–B magnets comprises two major stages. One is the production of magnetic alloy, and the other is the processing of the Nd–Fe–B-type alloys into permanent magnets.

Many methods have been developed for the production of Nd–Fe–B alloys. They include direct melting, coreduction, and certain special techniques that make use of reduction extraction or thermit-type processes for directly making the Nd–Fe or Nd–Fe–B alloys. The alloys are converted to magnets by two basically distinct routes. One route involves the rapid solidification technique of melt spinning, and the other follows the traditional pressing and sintering route. The melt-spinning procedure involves ejection of molten Nd–Fe–B alloy through a crucible orifice onto the surface of a spinning substrate disc. The product so obtained is in the form of ribbons typically 30–50 μm thick and 1–3 mm wide. The melt-spun ribbons are consolidated into a dense form to produce either a bonded magnet or a hot-pressed magnet. Fine-tuning of magnetic properties to desired values is also achieved by doping the magnet alloy with elements such as niobium, zirconium, and many others.

The *sintered Nd–Fe–B magnets* are prepared starting from finely divided alloy powders obtained from pulverizing of cast ingots or directly reduced powders, and following the sequence of orient, press, sinter operations. In spite of the numerous

cost and magnetic property advantages of the Nd–Fe–B magnets over the rare earths–cobalt magnets, the Nd–Fe–B magnets have one major limitation—their Curie temperature is low. Attempts have been made to overcome this problem through partial replacement of neodymium by dysprosium and/or iron by cobalt. Other beneficial elemental additives are aluminum and gallium, copper, and even silica. On the processing side, significant improvements in magnet properties have been realized by the use of HDDR treatment of the magnet material to produce anisotropic Nd–Fe–B magnet powders with high coercivity and resorting to die upsetting process during fabrication.

Attempts have been on to realize in practical magnets the theoretical maximum energy product for Nd–Fe–B magnets, namely, 512 kJ/m^3. The key factors to improve magnetic properties of real magnets towards this value are (1) compositional control, (2) densification, (3) grain size control, and (4) alignment of the 2–14–1 grains. One of the solutions is to reduce oxygen impurity. In the manufacturing of magnets, controlling of residual oxygen has been a highly challenging task. A new world record of magnetic properties with B_r = 1.555 T, $(BH)_{max}$ = 474 kJ/m^3, and H_{cj} = 653 kA/m was established by NEOMAX Co. Ltd. in 2005. In this magnet, the main phase volume ratio was 0.982, oxygen content 600 ppm, and grain orientation 0.991. There have been many efforts and much progress through alloy modifications and heat treatments to enhance the thermal stability of Nd magnets while balancing other magnetic properties.

The sintered NdFeB permanent magnets are characterized with a complex multiphase microstructure. Electrochemically these phases have different potentials, and hence this structure is susceptible to galvanic corrosion. Corrosion control has been attempted by the use of additives with certain positive results. Corrosion protection of sintered NdFeB magnets is necessary and effectively achieved with a barrier coating. The most successful one is the Ni–Cu–Ni triple layer coating for the NdFeB permanent magnet. The magnetic properties Ni/Cu/Ni coated NdFeB magnets remained unchanged, and this coating is considered the benchmark for rating other coatings. Many other coatings including organic and ceramic coatings have been found more appropriate and/or superior depending on the service environment.

The interstitial compound $Sm_2Fe_{17}N_x$ exhibits fairly high saturation magnetization (1.54 T), high anisotropy field (14 T) under room temperature, and high Curie temperature (476°C), intrinsic magnetic properties that are comparable with or better than those of $Nd_2Fe_{14}B$. The material can be readily prepared. However, $Sm_2Fe_{17}N_x$ decomposes into SmN and α-Fe phases at 650°C or above, and the conventional sintering route is not suitable for processing of compacted magnets. The present applications of the $Sm_2Fe_{17}N_x$ compounds are limited to bonded magnets, wherein due to the additional polymer or metal, the magnetic properties of $Sm_2Fe_{17}N_x$ magnets are diluted.

Rare earths are not only important materials for permanent magnets but also versatile magnetic materials. The alloy $Tb_{0.3}Dy_{0.7}Fe_{1.90}$, called *terfenol-D*, is a remarkable magnetostrictive material. Terfenol-D has been produced either by the conventional method of direct melting of the constituents in an arc furnace or by a thermit-type reduction of appropriate amounts of TbF_3, DyF_3, and FeF_3 with calcium, in a crucible lined with CaF_2. Initially, GdPd and later the intermetallics $(Dy_{0.5}Er_{0.5})$

Al_2 and $TbNi_2$ were identified as magnetic refrigeration materials for cooling gases and systems to as low as 4 K. These materials have been usually prepared by arc melting of 99.8 at.% pure rare-earth metals and >99.99% pure nickel or aluminum in correct proportion. A process known as centrifugal atomization has been used to produce ~200-μm-size fine particles of cryocooler materials such as Er_3Ni, DyCo, and $(Er_{0.9}Yb_{0.1})Ni$. High-pressure gas atomization has also been used to produce uniform spherical powders of high-purity Er_3Ni. Both these techniques are superior in powder shape, purity, and composition to methods such as mechanical grinding of cast ingots into powder, spark erosion, and rotating electrode pressing.

The work of Brown and of Gschneidner's team at Ames brought up the possibility of room temperature magnetic refrigeration, using essentially gadonlinium alloys. These alloys are usually synthesized from elemental constituents by co-melting under contamination-free conditions that are now commercially feasible.

The intermetallic $LaNi_5$ behaves like a hydrogen sponge. When hydrogen is introduced into a finely divided alloy of $LaNi_5$, it will be absorbed at room temperature and bound in the lanthanum nickel hydride $LaNi_5H_6$ that is formed. At a higher temperature, e.g., 150°C, the hydrogen is desorbed at a comfortable rate. This property of $LaNi_5$ has led to numerous applications. Apart from the original $LaNi_5$, a variety of modified compositions have been investigated with technically and/or commercially positive results to perform the hydrogen absorption–desorption activity in devices ranging from simple gas purification systems, through nickel–metal hydride batteries to hydride compressors. Rare earth-containing alloys for NiMH battery applications are prepared invariably starting from the constituent elemental metals by a melting process. Induction melting, arc melting as mentioned above, and in one case rapid solidification have been used to prepare the homogeneous multicomponent alloys required for various battery configurations. Contamination of the alloy is controlled by using appropriate crucibles and melting environments, and volatilization issues with high vapor pressure components are tackled by providing required overage in the charge or by other ingenious procedures.

Rare earths are key components in several special ceramics that have applications as laser and phosphor hosts, electronic components, fuel cell parts, and also crucibles for reactive metal melting and evaporation. They are usually prepared by standard chemical procedures of ceramic material synthesis.

Rare-earth phosphors are critically important materials for myriad lighting applications. Highest purity ingredients are invariably used in their preparation. The process description may at best be taken as a general method because commercial manufacturing practices are seldom revealed for the open literature. The techniques used are homogeneous precipitation, SSR, sol-gel synthesis, melt synthesis, molten salt synthesis, and flux method apart from certain thin film deposition techniques.

One of the most remarkable applications of rare earths is in the new generation high-T_c superconductors. High T_c was first reported in a multiphase Ba–La–Cu–O compound, and one of the most important compositions that has T_c above liquid nitrogen temperatures is an Y–Ba–Cu–O (YBCO) compound. The YBCO phase responsible for superconductivity is perovskite-like with a composition of $Y_1Ba_2Cu_3O_{7-x}$ (commonly referred to as the 1–2–3 phase). There are three main techniques for making high-T_c superconductors. First, the materials can be deposited

onto a single-crystal structure by methods such as evaporation, laser ablation, or sputtering so that epitaxial growth occurs. Second, thick films can be made by mixing the powder with various polymers and solvents and applying it to a suitable polycrystalline ceramic or metallic substrate. Third, bulk materials can be made by sintering a powder of right stoichiometry.

Thin film (0.5 μm) superconductors are capable of carrying large amounts of current (10 million A/cm^2), but they are not suitable for many applications because of their fragility. Thick film tapes (1–2 μm thick) conduct 1 million A/cm^2 and can retain half of its current-carrying ability in magnetic fields as high as 9 T. In one process developed at the Los Alamos National Laboratory, a three-layer tape comprising YBCO compound and zirconium oxide placed on a pliable nickel alloy tape was made. By pulsed layer deposition of thick films (6–10 μm) of Y-123, Los Alamos researchers have obtained J_c values greater than 1 MA/cm^2 at 77 K. This potentially scalable technique may be used to prepare superconductor coated continuously on long lengths of metal or ceramic substrates with suitable buffer layers. Bulk superconducting YBaCuO can be made by sintering Y_2O_3, CuO, and BaO under carefully controlled conditions. To obtain a bulk superconductor with good mechanical properties, high-purity starting materials in the form of submicrometer-size powder is essential. Using various processing routes, coils and shapes can then be fabricated. To achieve high current densities in polycrystalline wires and thick films of ceramic superconductors, texturing is essential. Texturing is achieved in various ways such as melt texturing, rolling, and solidification in high magnetic fields. A process known as the MP approach has been used to prepare long lengths of high-T_c ceramic superconducting wires. The process proceeds through the stages of mechanical alloying of MP elements, repeated extrusion and compound forming by internal oxidation, and thermomechanical treatments.

A great variety in applications and an equally wide range of methods for processing mark the role of rare-earth materials in modern technology. Materials synthesis and materials processing are both very important. Purity of components and products and management of material form and microstructure and their disposition are usually the key to realizing the performance levels that the rare earths are intrinsically capable of delivering.

7 Recycling

7.1 INTRODUCTION

The term recycling covers the process of collection, treatment, and use of material that was, in the first place, put aside as currently unusable and/or waste for disposal. Recycling entails tangible benefits in the matters of resource conservation, energy expenditure, and environmental damage. The recycling of rare earths, it will be seen, is a narration of these basic precepts in action.

Waste streams containing rare earths that could be the feed for recycling are generated at different independent stages in the overall life cycle of rare-earth elements (REEs). As the rare earth undergoes metamorphosis from its disposition in the ore to its final place in a functioning device, a part of it can and invariably does enter into a waste stream before the device is made (manufacturing scrap). At the end of the device's useful life, all the rare earths in that can, and in the best-case scenario will, end up in a waste stream for recycling (end-of-life [EOL] scrap).

Recycling of manufacturing scrap is far easier than the processing of EOL scrap. The practice of recycling in the rare-earth industry did begin with the processing of manufacturing scrap. Manufacturing scrap works with a captive collection system, the chemical and material history of the scrap is known, and generally, these are "pure" scraps that need minimum processing. The challenge with EOL scrap begins with the collection, and then comes physical dislodging of the required component from the frame of the device. Usually, the components have been manufactured by a different entity than the recycler, and the technical history of the component may not become known. Chemically these components are more complex (than the manufacturing scrap), and in usage, they could have undergone further degradation.

Reports of investigations on processes that have potential for recycling of rare earths from waste streams (Oakdene Hollins Research & Consulting 2010) began to appear as early as the early 1990s (Table 7.1), but the activity was confined mostly to the United States and Japan and to magnets and batteries. In 2011, Oeko-Institut e.V. (Schuler et al. 2011) brought out its report dealing with the matter of rare-earth recycling in industrialized countries. It focused on recycling activities essentially on recyclable materials of preconsumer origin. Recycling of postconsumer rare earth–containing products was apparently of minor importance. The situation could have arisen due to one or more of the following factors: (1) rare earths being used in quite dissipative applications (relevant for EOL products), (2) low price of rare earths, (3) the absence of any supply shortage or looming uncertainty on their long-term availability, and (4) the chemical tendency of rare earths to move into slags of smelter plants.

A major reason for the absence of industry-level practice of rare-earth recycling has been the unfavorable economics. A precondition for an economically viable recycling process is the long-term stability of adequate prices for the rare earths.

TABLE 7.1
Summary of Rare-Earth Recycling Efforts

Material Recycled	Process	Key Reagents, Reaction Components	Recycling Goal	Reference
Nd–Fe–B magnet sludge	Arc melting/induction melting, melt spinning	NdFeB, Ti, Si	NdFeB bonded magnets, Fe–Si, FeTi for microwave absorbers	Horikawa et al. 2006
Sm–Co swarf	Acid dissolution, precipitation, solvent extraction	HCl, HNO_3, H_2SO_4, $Sm_2(C_2O_4)_3$, $SmCl_3$, $Na_2SO_4Sm_2(SO_4)_3$, TBP, D2EHPA	Sm_2O_3	Bounds 1994
Sm–Co magnet scrap	H_2SO_4 leaching, double sulfate precipitation	H_2SO_4, Na_2SO_4, $Na_2SO_4Sm_2(SO_4)_3{\cdot}2H_2O$	Sm_2O_3	Koshimura 1988
$Sm_{1-x}Pr_xCo_5$ scrap	HCl leaching, D2EHPA extraction	HCl, D2EHPA, $SmCl_3$, $PrCl_3$, $CoCl_2$	Sm_2O_3	Koshimura and Yamamoto 1983, 1984
$SmCo_5$, Sm_2Co_{17} scrap	Acid leaching, fractional crystallization	HNO_3, H_2SO_4, $Sm_2(SO_4)_3{\cdot}8H_2O$	Sm_2O_3	Sato et al. 1997
$SmCo_5$, Sm_2Co_{17} scrap	HNO_3(2M) leaching, solvent extraction	HNO_3, D2EHPA, LIX65N, H_2SO_4, oxalic acid, oxalates	Sm, Co	Sanuki et al. 1995
NdFeB scrap	Acid leaching, fractional crystallization	HNO_3, H_2SO_4, $Nd_2(SO_4)_3{\cdot}8H_2O$	Nd_2O_3	Sato et al. 1997
NdFeB scrap	H_2SO_4 dissolution, precipitation	H_2SO_4, alkali–Nd double sulfate, Fe–jarosite	30% Nd contained in the magnet	Lyman and Palmer 1993a
NdFeB scrap	Roasting–magnetic separation/ selective leaching	H_2–water vapor mixture (pO_2 control), H_2SO_4	Separation of Nd_2O_3 from iron	Lyman and Palmer 1993b
NdFeB scrap	Oxidative roasting–leaching–double salt precipitation	H_2SO_4, $Na_2SO_4Nd_2(SO_4)_3$	Nd recovery from sintered and bonded scrap	Yoon et al. 2003; Lee et al. 1998

(*Continued*)

TABLE 7.1 (CONTINUED)
Summary of Rare-Earth Recycling Efforts

Material Recycled	Process	Key Reagents, Reaction Components	Recycling Goal	Reference
NdFeB scrap	Oxidative roasting–selective leaching	Fe_2O_3, 0.01–02M HCl	Selective dissolution of Nd(III)	Koyama and Tanaka 2011a,b
NdFeB sintered magnet	Hydrothermal method–leaching precipitation	HCl, oxalic acid, $Nd_2(C_2O_4)_3$	Pure Nd oxalate recovery	Itakura et al. 2006
NdFeB magnet	Selective leaching–solvent extraction	Chloride leach liquor, $DyCl_3$, $NdCl_3$ PC88A, HCl	Dy–Nd separation	Tanaka et al. 2009
Mixed $SmCo_5$–NdFeB swarf	Flotation–leaching	H_2SO_4, flotation reagents	$SmCo_5$ in the froth, NdFeB in solution and grinding medium in tailing	Lyman and Palmer 1993b
Mixed $SmCo_5$–NdFeB scrap	Roast–leach–solvent extraction (many solvents), HCl	HCl, many solvents (EHPNA, TOPO, versatic acid 9/10)	Sm, Nd, Co, Cu, Fe separation	Niinae et al. 1994
Sludges of Sm_2Co_{17}, NdFeB, $LaNi_5$	Chemical vapor transport (CVT) of chloride complexes	Cl_2, $AlCl_3$, $REAl_nCl_{3+3n}$	$RECl_3$	Murase et al. 1995
NdFeB	CVT via carbonylation	CO, $Fe(CO)_5$	RE concentrate	Miura et al. 2008
NdFeB	Chlorination of magnet sludge by $FeCl_2$	$FeCl_2$, $NdCl_3$, $DyCl_3$, HCl	>99.2% pure $NdCl_3$–$DyCl_3$ mixture, closed-cycle operation	Uda 2002
Sm–Nd, Nd–Pr scrap	Selective reduction–vacuum distillation	$SmCl_3$, $NdCl_3$, $PrCl_3$	Separation of Sm from Nd, and Nd from Pr	Uda et al. 2000
NdFeB magnet waste	Nd, Dy extraction into molten $MgCl_2$, separation of $MgCl_2$(v) from $RECl_3$	$MgCl_2$, $NdCl_3$, $DyCl_3$	Nd and Dy recovery, $MgCl_2$ recycle	Shirayama and Okabe 2008

(*Continued*)

TABLE 7.1 (CONTINUED)
Summary of Rare-Earth Recycling Efforts

Material Recycled	Process	Key Reagents, Reaction Components	Recycling Goal	Reference
NdFeB magnet powder	Chlorination RE content by NH_4Cl, water leaching to dissolve $RECl_3$, Fe, Fe–B in solid residue	NH_4Cl, $NdCl_3$, Fe, Fe–B	RE recovery	Itoh 2009
NdFeB	Extraction of Nd into molten Mg, Fe, Fe–B in solid residue	NdFeB, Mg, Nd(Mg), Fe, Fe–B	Nd recovery as metal	Xu et al. 2000; Okabe et al. 2003a; Takeda et al. 2006
NdFeB magnet scrap	Extraction of Nd into molten Ag, selective oxidation of Nd, Ag recycle	Nd(Ag), Ag, Fe, Fe–B, Nd_2O_3, O_2	Nd recovery as oxide	Takeda et al. 2004
Magnet scrap (oxidized), sludge containing oxides	Oxidation at 800°C; H_2 reduction at 980°C; Ca reduction at 950°C; water leaching of Ca, CaO, and $CaCl_2$	Air, H_2, Ca, Fe_2O_3, RE_2O_3, CaO, $CaCl_2$	Removal of residual carbon and oxygen in the magnet to <0.001% C and 0.1% oxygen, refabrication of magnets	Suzuki et al. 2001; Saguchi et al. 2006
In-plant Nd magnet scrap	Hydrometallurgy treatment (leaching–SX and/or precipitation)–molten salt electrolysis (MSE)		Recovery of Nd and Di(Nd–Pr)	Tanaka et al. 2013
NdFeB magnet scrap	MSE using bifunctional electrode geometries	Chloride melt Fluoride melt	Selectivity in anodic dissolution (dealloying) and cathodic reduction to metal/alloy	Tanaka et al. 2013

(*Continued*)

TABLE 7.1 (CONTINUED)
Summary of Rare-Earth Recycling Efforts

Material Recycled	Process	Key Reagents, Reaction Components	Recycling Goal	Reference
Magnet alloy scrap (oxidized)	Extraction of REO into a molten fluoride flux	REO (in the scrap), LiF–NdF_3, LiF–DyF_3	REO in the scrap cleaned out by washing with molten fluoride flux	Takeda et al. 2009; Takeda and Okabe 2011
Magnet scrap: NdFeB, Sm–Fe, Sm–Fe–N	Glass-slag process: oxidation of rare earths in the scrap and their extraction into a glass-slag phase	B_2O_3, Nd_2O_3 in glass-slag; Sm_2O_3 in glass-slag		Saito et al. 2003c, 2005a,b
Magnet alloy scrap	Glass-slag process with carbon	Fe (unattacked—remains in metallic form), two liquid slag phases: Nd_2O_3–B_2O_3 and B_2O_3		Kubo et al. 2011
In-plant waste sludge	Thermal treatment under controlled oxygen potential: 1550°C under Ar $pO_2 = 10^{-10}$ to 10^{-15} atm	Sludge molten and separates into liquids: iron–solid REO phases	(Quantitative collection of RE in oxide phase)	Tanaka et al. 2013; Katayama et al. 2010
In-plant Nd magnet scrap	Electroslag refining	$CaCl_2$–CaF_2–REF_3	Magnet alloy cleaned of impurities	Ellis et al. 1994
NdFeB magnet scrap	Acid dissolution–solvent extraction of Fe, Nd, Dy, and Co		Recovery of individual metal values	Chen 2004
Sm–Co magnet scrap	Acid dissolution–precipitation	H_2SO_4, oxalic acid, NaOH	REO concentrate and Co concentrate	Ferron and Henry 2013
Scrap Sm–Co, NdFeB magnets	Leaching–ionic liquid extraction		REE (Nd, Dy, Sm) separation from impurities (Fe, Co, Mn, Cu, Zn)	Ferron and Henry 2013

(*Continued*)

TABLE 7.1 (CONTINUED)
Summary of Rare-Earth Recycling Efforts

Material Recycled	Process	Key Reagents, Reaction Components	Recycling Goal	Reference
Scrap Sm–Co, NdFeB magnets	Hydrogen decrepitation		Recycling magnet material	Pearson (Ferron and Henry 2013); Zakotnik 2009
NiMH batteries	Ultrahigh temperature (UHT) smelting to get REE in slag	Shaft furnace or DC arc smelting		Umicore (Ferron and Henry 2013)
NiMH batteries	Acid leaching–solvent extraction		RE concentrate, Co oxalate, Ni oxalate	Zhang et al. 1998
NiMH batteries	Acid leaching–RE precipitation–MSE		Ni–Co alloy, RE metals	Ferron and Henry 2013
Red phosphor waste (Y_2O_3, Gd_2O_3, Eu_2O_3)	Leaching–precipitation		REO concentrate	Okabayashi and Otsuka 1970
Fluorescent lamp waste	Thermal treatment (Hg removal), leaching–SX/IX		REE recovery	Otto and Kasprzak 2011
Polishing sludge	Leaching–precipitation		REO concentrate	Henry et al. 2013

This is necessary to support a flow sheet involving complex dismantling and treatment processes with the attendant high-energy input. The turnaround time for post-consumer items also needs to be considered because many of the recyclable devices containing rare earths have a long service life. Electric motors in vehicles and wind turbines will function for 10–20 years and only then will enter the recycling loop. However, beginning in 2010, the sharp increase of rare-earth prices and spotlight on the possibility of supply shortages triggered by mining and export regulations by the dominant supplier China have changed the scenario. The issue of rare-earth recycling began attracting attention in the industry. The situation was becoming critical because several of the REEs are key ingredients for the sustenance and growth of cutting edge technologies. They are also essential for the continuity of device mix and production practices that either have been started already or are on the verge of being taken up. A significant share of the new demand for rare earths is based on and caused by what are known as *green technologies*, which are designed for environmental protection through reduction in energy consumption and development of renewable energy carriers apart from a decrease in the direct pollution of air, water, and land. In recent times, major changes have occurred on a global scale in the application of rare earths. Technology innovations and improvisation have expanded the scope and volume of rare-earth applications, and the reach of these applications has gone beyond the boundaries of industrialized societies into developing economies. The net result is a steep increase in the demand for rare earths that is neither temporary nor stagnant. For the foreseeable future, there is going to be a steadily accelerating demand for rare earths and hence sustained pressure on the resources.

This is a serious situation and goes beyond the ripples caused by the events originating from, and the disposition of, the People's Republic of China. The demand for several of the REEs such as neodymium, praseodymium, dysprosium, terbium, lanthanum, yttrium, and europium would probably exceed the current supply within the next few years. Most importantly, even if China imposes no export restrictions, the new demand can only be met if more mines are brought on stream and supported by measures such as substitution of rare earths with non-rare-earth materials and efficient and widespread recycling of rare earth-containing materials. There will also be increased relevance of rare-earth recycling.

It is widely accepted that recycling of metals, in general, has several irrefutable advantages compared to the use of primary resources. The advantages in the case of rare earths are tremendously more due to the unique issues in the nature of primary resources and the technology involved in their processing.

When recycling is practiced for the supply of rare earths, the dependence on external resources is reduced, and reliability/stability of supply is enhanced. The amount of recyclable material available from EOL products is directly related to the quantities consumed. If a recycling scheme is implemented by the consumer, the larger the consumer, the more viable is the process whereby the secondary resources are returned to the industrial metabolism by urban mining.

Processes for recycling share many features and also details with the processes for the treatment of primary resources. A major advantage of rare-earth recycling is the freedom from radioactive material handling. In most cases, natural rare-earth deposits are associated with radioactive elements, and primary rare-earth resource processing

produces radioactive wastes that require specialized (and expensive) management. In general, the chemicals and energy carriers required for recycling are the same as in primary processing but in lesser quantities. This translates to a net gain in air emissions, groundwater protection, acidification, eutrophication, and climate protection.

In this chapter, the opportunities and challenges of rare-earth recycling are presented, beginning with the list of rare-earth materials that can undergo recycling (Table 7.2) and proceeding to a case history-type coverage of individual recycling options. That there have been four major technical reviews on the recycling of rare earths (Binnemans et al. 2013; Ferron and Henry 2013; Schüler et al. 2011; Tanaka et al. 2013) in three years, highlights the importance of the topic. Notwithstanding the growing number of investigations that deal with the techniques of recycling, the number of industries engaged in recycling focused on actual rare-earth recovery have been noticeably few (Table 7.3) and the quantity involved very limited.

TABLE 7.2
Rare Earth-Bearing Materials for Recycling

Materials Stream and Application	Quantity Set to Enter Recycle Stream (Increasing, ↑; Stable, ↔; Decreasing, ↓)	REEs/Typical Composition of Recycling Feeds, %
1. Preconsumer production scrap and residues		
Magnet swarf and rejected magnets	↑	Nd, Dy, Tb, Pr
REE-containing residues arising during metal production/recycling		All
Post smelter and electric arc furnace residues		Ce, La, critical REEs
Industrial residues (phosphogypsum, red mud, etc.)	↔	All
2. End-of-life products containing		
Phosphors		Red $60Y_2O_3$ + $3Eu_2O_3$, green 30Tb, blue 10Eu
Fluorescent lamps (straight/curved)	↔	Eu, Tb, Y (Ce, Gd, La)
Compact fluorescent lamps (CFLs)	↑	Eu, Tb, Y (Ce, Gd, La)
LEDs	↑	Ce, Y
LCD backlights	↔	Eu, Tb, Y (Ce, Gd, La)
Plasma screens	↔	Eu, Tb, Y (Ce, Gd, La)
Cathode ray tubes (CRTs)	↓	Eu, Y
Others (specialty applications)		Also Tm
Permanent NdFeB magnets		Fe 50–60, Dy 1–2, Nd 20–30, B 1, Co 4, Pr <7
Automobiles (small magnets as motors, switches, sensors, actuators, etc.)	↔	

(*Continued*)

TABLE 7.2 (CONTINUED)
Rare Earth-Bearing Materials for Recycling

Materials Stream and Application	Quantity Set to Enter Recycle Stream (Increasing, ↑; Stable, ↔; Decreasing, ↓)	REEs/Typical Composition of Recycling Feeds, %
Mobile phones (loudspeakers, switches, microphones, etc.)	↔	
Hard disk drives (HDDs)	↓	
Computers and peripherals (cooling fans, switches, drive motors, scanner head motors, small HDDs, etc.)	↔	
Consumer electric and electronic devices (kitchen utensils, handheld tools, electric shavers, etc.)	↔	
Electric bicycles (motor)	↑	Higher Dy level
Electric vehicle and hybrid electric vehicle motors	↑	Higher Dy level
Wind turbine generators	↑	
Permanent SmCo magnets	↔	Sm 18–30, Co 50, Fe <20, Cu 8, Zr 4, Gd <9
Other magnet applications	↔	Sm (in SmCo magnets)
Nickel–metal hydride batteries		Ni 48, Co 3.5, Fe 13, La 15, Ce 1, Pr 3, Nd 10, Sm 0.3
Rechargeable batteries	↑	
Electric vehicle and hybrid electric vehicle batteries	↑	
CRT phosphors		
Glass-polishing powders	↔	Ce 40–50, La 1–6, Nd 0.1–0.7, Si 5–10, Pb 1–2, Fe 1–2
Fluid cracking catalysts	↑	3.5 REE (mostly La + Ce, Pr, Sm)
Auto converter	↑	<3.5 REO (mostly Ce)
Optical glass		Decol 0.65CeO_2, stabil <2.5CeO_2, color <5 RE, camera <40 La_2O_3
3. Landfilled REE-containing residues		
Industrial residues (phosphogypsum, red mud, etc.)		All

Source: Binnemans, K. et al., *J. Clean. Prod.*, 51, 2013; Ferron, C.J. and Henry, P., A review of the recycling of rare earth metals, in London, I.M. et al. *Rare Earth Elements*, Canadian Institute of Mining, Metallurgy and Petroleum, Quebec, 2013.

TABLE 7.3
Industrial RE Recycling Activities

Company/ Researcher	Feed for Recycling	Product	Reference[a]
Hitachi, Japan	Magnet from air conditioners, hard disks, and compressors; capacity, 120 units/h	60 T RE/year Nd, Dy	Baba et al. 2013
Mitsubishi	Magnets from air conditioners and washing machines; capacity, 120 units/h	Dismantled permanent magnets for direct recycle (reuse) of RE magnet	
Honda, Toyota	NiMH batteries from hybrid car; rate, 400 T/year	24 T RE/year with a recovery of 80% Nd, La, Ce, MM	Honda 2012
Rhodia/Solway in partnership with Umicore in St. Fons and La Rochelle	NiMH batteries, low-energy lightbulbs, 1000 T/year of batteries (Li ion plus NiMH)	RE component	Rhodia 2011
TU Bergakade mie Freiberg	Slag of the pyrometallurgical treatment of used Ni–MH BATTERIES	RE metal	Heegn 2009
OSRAM	EOL lamps	Yttrium and europium from discharge lamps	OSRAM 2009
Resende and Morais	TV tubes and computer monitors	Yttrium and europium	Resende and Morais 2010
Kosaka Smelting	Waste electrical and electronic equipment (WEEE)	Neodymium and dysprosium from used electronics	Tabuchi 2010
Ganzhou Recycle Hi-Tech Co. Ltd.	Magnet scrap, 8000 T/year	2000 T REO/year	
Hydrometal SA Engis, Belgium	Glass-polishing sludges and magnet sludges	~1200 T REO since 2011 (till 2013)	
Showa Denko KK Vietnam	Permanent magnet scraps	800 T RE/year	

Source: Ferron, C.J. and Henry, P., A review of the recycling of rare earth metals, in London, I.M. et al. *Rare Earth Elements*, Canadian Institute of Mining, Metallurgy and Petroleum, Quebec, 2013; Bongaerts, J.C. and Liu, J., *IMRE J.*, 7, 2013.

[a] Recycling activities reference year.

7.2 MATERIALS FOR RECYCLING

A list of rare-earth materials that can, in principle, be feed for recycling is given in Table 7.2. In the life cycle of rare earths, as mentioned already, waste for recycling becomes available at two levels: waste streams on the preconsumer level

and the postconsumer waste. Waste streams on the preconsumer level (waste arising during manufacturing) is relevant in magnet production, the lighting industry, upstream rare-earth processing plants, polishing-powder manufacturing, and the units for the production of devices for information technology and electronics. Postconsumer waste (products that have been used and are no longer usable) includes magnets from electric motors and generators (arising in wind power plants, hybrid and electric vehicles, hard disks, and e-bikes); lamps (fluorescent lamp); displays (plasma displays and LCD, LED); and catalysts (automotive catalysts and industrial catalysts).

Out of the three major components of recycling for rare earths—collection, treatment, and use—the second one witnessed more directed efforts first. The list included sludge from shaping and grinding magnet alloys in Japan, small quantities of yttrium from laser crystals and synthetic garnets, and reuse of magnets from MRI machines (Shirayama and Okabe 2009; UNEP 2011). It was specifically noted by Schuler et al. (2011) that, in the beginning, there was no large-scale recycling of rare earths from magnets, batteries, lighting, and catalysts.

In the recycling scenario, the foremost requirement is the building up and implementation of an efficient collection system for accessing all recyclable rare earth–containing materials. A special challenge here is to access postconsumer goods such as EOL vehicles and electronic scrap that end up in developing countries. As another challenge, there is dismantling of rare earth-containing components from various machines and devices. Presently done manually, at least in part, full automation would be needed here, sooner rather than later (Clenfield and Shiraki 2010).

7.3 POTENTIAL FOR RECYCLING

As shown in Table 7.1, from the beginning in the 1990s, almost all efforts of recycling apparently have been made in the United States, Japan, and Germany. The United States and Japan are also the major end-product manufacturers of rare-earth materials. Incidentally, 1990 is also the period when the People's Republic of China emerged as the major producer of rare earths from primary sources. No recycling effort has been reported from China even though they are now the predominant end-product manufacturer and hence also generate huge quantities of rare-earth scrap.

Recycling of rare earths has not been sufficiently investigated, in the sense that regular industrial-level recycling is not apparent. There are no answers already available to questions and problems that might arise when considering waste-containing rare-earth materials. Rare earth-containing end products that are commercially used are numerous. However, the recycling is focused on only a few of them, particularly the magnets and NiMH batteries. Work has also been reported on rare earth-containing glass compositions and lamp phosphors. While consolidated global figures are hard to get, the nature of the quantities involved in recycling can be appreciated by considering figures available for certain individual countries. The amount of NdFeB magnets produced is estimated to be 6000 t in Japan (Itoh et al. 2004a,b). For the NdFeB sintered magnets, 20–30% of the raw magnet gets wasted

as scrap powder (sludge) while cutting and grinding to desired shapes (Horikawa et al. 2006), and approximately 2000–2500 t of sludge powder is generated every year in Japan alone. Since their launch in 1991, the amount of NiMH batteries sold increased steadily up to 10,000 t in the European Union, through 2003. Even though the battery life is between 6 and 8 years, it is estimated that over 65% of spent batteries are not disposed of. In Germany alone, over 97 t of NiMH was recycled in 2003, and by 2007, the figure was expected to reach 1000 t/year (Muller and Friedrich 2006). By 2020, it has been projected that nearly 14,000 tons of NiMH batteries from hybrid electric vehicles (HEVs) will become available annually for recycling and can provide 3350 tons of rare earths, 9500 tons Ni, and 1150 tons Co (Itoh and Machida 2011). A more formal estimate of the recycling potential for REEs is given by Binnemans et al. (2013).

Binnemans et al. (2013) provided a first, very rough estimation of the global REE recycling potential for the year 2020, focusing on the possible EOL recycling rates (EOL-RRs) for the REEs embedded in the key applications, i.e., magnets, nickel–metal hydride batteries and lamp phosphors. Bongaerts and Liu (2013) agree with this stand when they present a summary of current recycling activities. The recycling potential is basically determined by three main factors (UNEP 2011). Aside from technical feasibility, the cost of recycling must be less than the value of elements to be recycled and availability of the logistic system for collecting EOL products containing REEs. The largest rare-earth recycling potential, therefore, involves end products containing high levels of REEs and a tangible collection and recycling infrastructure, viz., fluorescent lamps, magnets, car batteries, and catalytic converters. According to UNEP (2011), only a small amount of magnetic scrap containing neodymium, praseodymium, dysprosium, and laser materials scrap containing yttrium are recycled. It is likely that many countries and companies are in the process of developing recycling technologies. Table 7.3 provides examples of the main reported recycling activities, even though details of processes and quantities handled are not readily made public (Bongaerts and Liu 2013). Binnemans et al. (2013) estimated the overall recycling rate of a single metal by taking the product of collection rate and the recycling process efficiency rate. Interestingly, they gave a pessimistic and an optimistic scenario for the year 2020. For example, for the magnets, assuming the global collection rate to be 30% (pessimistic) and 60% (optimistic), with the recycling process efficiency rate estimated to be 55%, the EOL-RR would be 16.5–33%. In the case of nickel–metal hydride batteries, global collection rates were assumed to be 40% (pessimistic) and 70% (optimistic), with the recycling process efficiency rate estimated at 50%. This would result in an EOL-RR of 20–35% in 2020. For lamp phosphors, global collection rates were assumed to range between 40% (pessimistic) and 70% (optimistic), while the recycling process efficiency rate is estimated to be 80%. This would result in an EOL-RR of 32–56% in 2020. The implication is very clear. Immediate enhancement in the EOL-RR can be realized by working on the collection logistics.

In Table 7.4, the recycling potential for REEs from the three key applications (magnets, nickel–metal hydride batteries, and phosphors) calculated by Binnemans et al. (2013) is given. They used values of in-use stocks of the REEs in 2007

TABLE 7.4
Recycling Potentials for (Quantities Processed by Recycling of) REE from Magnets, Nickel–Metal Hydride Batteries, and Phosphors

REE Application	Estimated REE Stocks in 2020, tons	Estimated Average Lifetime, years	Estimated REE Old Scrap in 2020, tons	Pessimistic Scenario: Recycled REE in 2020, tons	Optimistic Scenario: Recycled REE in 2020, tons
Magnets	300,000	15	20,000	3300	6600
Lamp phosphors	25,000	6	4167	1333	2333
Nickel–metal hydride batteries	50,000	10	5000	1000	1750
Total	375,000		29,167	5633	10,683

Source: Binnemans, K. et al., *J. Clean. Prod.*, 51: 1–22, 2013.

current growth rates for the different applications, and assumed average lifetimes of the goods to arrive at the final values. The estimates for the average lifetimes are 15 years for magnets, 6 years for lamp phosphors, and 10 years for nickel–metal hydride batteries.

The values arrived at by Binnemans et al. (2013) indicate that the total REE recycling potential ranges between about 5600 and about 10,700 tons in 2020. For the individual REEs, the best case scenario figures for the recycling are 4755 tons of Nd, 1600 tons of Pr, 1070 tons of La, 840 tons of Ce, 1615 tons of Y, 330 tons of Dy, 121 tons of Tb and 115 tons of Eu. These estimates, which in US dollar value amount to several hundred millions per year, highlight the stakes and that REE urban mining can be sufficiently attractive besides making a significant contribution to the overall REE supply, especially for regions without primary REE production. Binnemans et al. (2013) included a note of caution in their comments stating that EOL REE recycling should not be regarded as low-hanging fruits and that hard work would be necessary.

7.4 PROCESSES FOR RECYCLING

Several processes, similar to those used in primary rare-earth mineral treatment, are useful for rare-earth recycling. These include physical processes (gravity separation, flotation, and magnetic separation); chemical processes (leaching and precipitation/crystallization); and halogenation, which have been found to be effective in meeting many of the processing objectives for preparing the interprocess intermediates. Techniques for the separation of individual rare earths, even from a pure mixture of rare earths that are used for primary resource processing, are also useful in rare-earth recycling. Then there are certain pyrometallurgical processes that are relevant to and effective for scrap reclamation. A summary of all these processes and the zone of their applicability appears in Table 7.5 (Binnemans et al. 2013; Tanaka et al. 2013).

7.5 PYROMETALLURGICAL PROCESSES

7.5.1 Smelting

It is interesting to note that nickel was all along considered as the most worthy element for recovery from spent NiMH batteries (Muller and Friedrich 2006). Spent NiMH batteries contain 36–42% nickel, 3–4% cobalt, and 8–10% misch metal. Presently, the discarded batteries are used in the steel industry as a cheap source of nickel. In this case, cobalt is not recovered, and the rare-earth content is also lost. Pointing this out, Muller and Friedrich (2006) have described a process, conducted trials on a large scale, and provided detailed information on their assessment of the recycling process for NiMH batteries. Their scheme outline is given in Figure 7.1. The key feature is melting the dismantled and processed NiMH in a direct-current (DC) electric arc furnace to produce a nickel–cobalt alloy and a slag phase highly enriched with the rare-earth oxide. To achieve this, the choice of a suitable slag is important. They evaluated both $CaO–CaF_2$ and $CaO–SiO_2$ and found that $CaO–CaF_2$

TABLE 7.5
Overview of Different Recycling Methods for REE Magnets, NiMH Batteries, and Phosphors

Method	Features	Issues
	REE Magnets	
Direct reuse in current form/ shape	Most economical way of recycling (low energy input, no consumption of chemicals) No waste generated	Only for large, easily accessible magnets (wind turbines, large electric motors and generators in hybrid and electric vehicles) Not available in large quantities in scrap today
Reprocessing of alloys to magnets after hydrogen decrepitation	Less energy input required than for hydrometallurgical and pyrometallurgical routes No waste generated Especially suited for hard disk drives (little compositional change over the years)	Not applicable to mixed scrap feed, which contains magnetswith large compositional variations Not applicable to oxidized magnets
Hydrometallurgical methods	Generally applicable to all types of magnet compositions Applicable to nonoxidized and oxidized alloys Same processing steps as those for extraction of rare earths from primary ores	Many process steps required before obtaining new magnets Consumption of large amounts of chemicals Generation of large amounts of wastewater Loss of value addition
Pyrometallurgical methods	Generally applicable to all types of magnet compositions No generation of wastewater Fewer processing steps than hydrometallurgical methods Direct melting allows obtaining master alloys Liquid metal extraction allows obtaining REEs in metallic state Value addition preserved	Larger energy input required Direct smelting and liquid metal extraction cannot be applied to oxidized magnets Electroslag refining and the glass-slag method generate large amounts of solid waste
Gas-phase extraction	Generally applicable to all types of magnet compositions Applicable to nonoxidized and oxidized alloys No generation of wastewater	Challenging technology Consumption of large amounts of chlorine gas Aluminum chloride is very corrosive
	NiMH Batteries	
Hydrometallurgical routes	Low investment costs Recycling possible of different waste fractions (cathode and anode materials, metals from casing) that can be marketed separately	Many manual operations are required for dismantling of batteries and separating the different components Large consumption of chemicals

(*Continued*)

TABLE 7.5 (CONTINUED)
Overview of Different Recycling Methods for REE Magnets, NiMH Batteries, and Phosphors

Method	Features	Issues
Pyrometallurgical routes	Well-developed technology Energy recovery from plastic casings and other organic components Same processing steps used for extracting REEs from slags as from primary ores	High investment cost for furnace REEs, which need to be extracted from slags REEs are obtained as mixtures, and further separation is required
	Lamp Phosphors	
Direct reuse	Very simple method No chemical processing required Value addition preserved	Only applicable to one type of fluorescent lamp because different lamps make use of different phosphor mixtures Phosphors deteriorate over the lifetime of the lamp
Separation of phosphors in individual components	Relatively simple process No or limited amounts of chemicals are consumed Value addition preserved	Very difficult to obtain very pure phosphor fractions Separation process may change the phosphor particle size Phosphors deteriorate over the lifetime of the lamp
Recovery of REE content	Generally applicable to all types of phosphor mixtures Same processing steps as those for extraction of rare earths from primary ores Gives very pure rare-earth oxides that can also be used for other applications	Many process steps required before obtaining new lamp phosphors Consumption of large amounts of chemicals Generation of large amounts of wastewater

Source: Binnemans, K. et al., *J. Clean. Prod.*, 51: 1–22, 2013.

is better. Nickel and cobalt were found completely in the metal phase, while the rare earths transferred completely to the slag phase as oxides. Pyrometallurgical refining of the nickel–cobalt alloy using a top-blown oxygen lance to remove Fe and Mn by selective oxidation was suggested by theoretical calculations but presented difficulties in actual trials.

An industrial-scale flow sheet (Cheret and Santen 2007) for the recycling of rare earths from EOL NiMH batteries uses an ultrahigh–temperature smelting technology. The batteries are fed in a vertical shaft furnace together with coke and a slag former. Oxygen-enriched air is injected into the furnace at the bottom. Much of the energy needed for smelting is provided by the combustion of plastics and organic electrolytes in the charge. Nickel, cobalt, copper, and iron concentrate as alloy, and the slag consists of oxides of calcium, aluminum, silicon, iron,

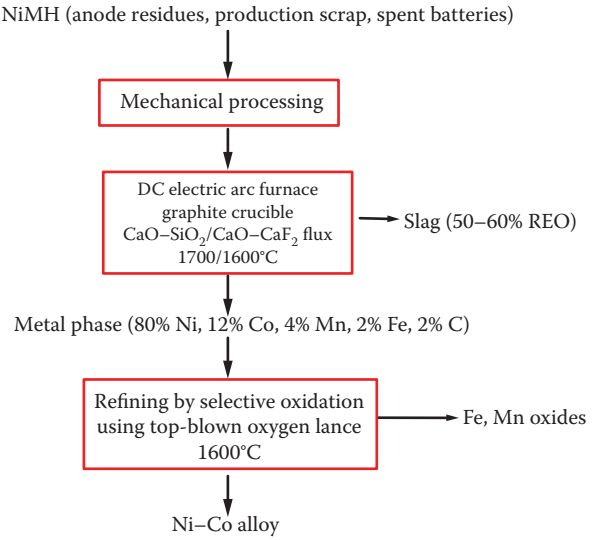


FIGURE 7.1 Processing of NiMH battery scrap by smelting in a DC electric arc furnace.

lithium, and the rare earths (Verhaeghe et al. 2011). The rare earths, in keeping with their chemical nature, concentrate into the slag (oxide) and are usually lost. However, the oxide slag is amenable to processing to recover lithium and the rare earths as concentrates. A hydrometallurgical process to recover RE metal from slag generated in the pyrometallurgical treatment of used NiMH batteries has been reported (Heegn 2009) by researchers from TU Bergakade mie Freiberg, Germany.

7.5.2 Melt Spinning

The nickel-coated sintered NdFeB magnets are recyclable by a melt-spinning process. The possibilities are outlined in Figure 7.2. If the chemical contamination levels are not too high, the (usually EOL) magnets can be simply melted for reuse. It is generally processed by melt spinning, wherein, as described earlier in Chapter 6, the molten alloy is rapidly cooled to thin ribbons by pouring it on an internally cooled rotating wheel (Itoh et al. 2004a,b). The alloy was melted together with whatever nickel was present as coating. In such amounts, nickel has no effect on the magnetic properties of newly prepared magnets.

The recycling of Ni-coated sintered NdFeB magnet waste to produce isotropic bonded NdFeB magnets was investigated by Itoh et al. (2004b). The process is shown in Figure 7.2a. From the waste, NdFeB ribbons of 1.5 mm width were prepared in the single-copper-roller melt-spinning apparatus. The oxygen content of the recycled magnet ribbons was less than in the waste because during the sample preparation by RF melting, the oxide slag separated from the molten alloy. The alloy ribbons were

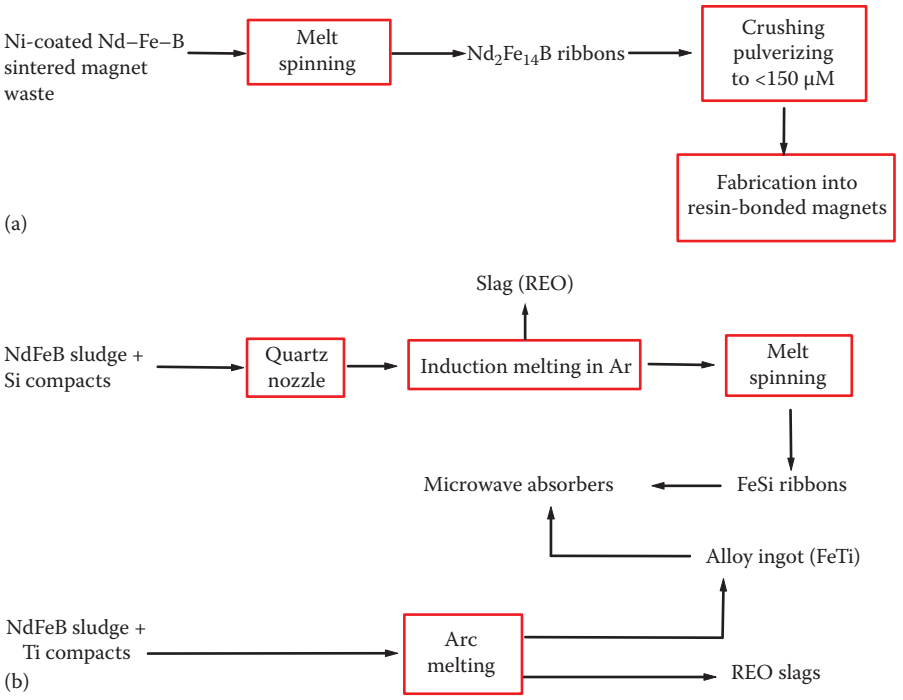


FIGURE 7.2 (a) Recycling of nickel-coated sintered NdFeB magnets to isotropic bonded magnets. (b) Processing of magnet sludge to microwave absorbers. (From Itoh, M. et al., *J. Rare Earths* 22: 168–171, 2004; Itoh, M. et al., *J. Alloys Compd*., 374: 393–396, 2004.)

crushed and pulverized into powder of <150 μm size. The bonded magnet prepared from this powder was comparable in properties to the bonded magnets prepared from a commercial source of powder for bonded magnets.

Horikawa et al. (2006) investigated a recycling route for both NdFeB sintered magnet scrap and silicon and titanium metal scrap generated as industrial waste in device fabrication for aerospace and biomedical industries. They converted the scrap into FeSi and Fe_2Ti intermetallic compounds that possess efficient microwave absorbing properties in the GHz range. The overall process is outlined in Figure 7.2b.

The NdFeB sintered magnet scrap was compressed with/without Fe powder into cube compacts using a steel die under 20 MPa pressure. For the preparation of FeSi, the sludge–Fe cubes and Si were charged into a quartz nozzle, inductively melted in argon, and rapidly quenched on a melt-spin apparatus at a roll surface velocity of 25 m/s. The FeSi intermetallic was obtained as ribbons, and the rare-earth component of the sludge remained in the quartz nozzle as a rare-earth-oxide slag. The FeSi was ground to a fine size by ball milling and processed further.

To prepare Fe_2Ti, the sludge cubes and Ti were arc melted into homogeneous ingots. The resulting product was mechanically separated into main alloy ingot portions of the Fe_2Ti intermetallic and coproduct rare-earth-oxide slags. The intermetallic was ground further in a tungsten carbide lined (WC) mortar and processed further.

Epoxy resin composites with 80% FeSi or 83% Fe_2Ti were prepared, processed, and evaluated for microwave absorption properties by Horikawa et al. (2006). Over 60% of the neodymium contained in the raw sludge was efficiently collected as rare-earth-oxide slags.

7.5.3 Chlorination

Chlorination has been used in various formats to achieve value recovery from rare earth-containing scraps. One is to operate with all components in the condensed phases. The other alternative is to get some components in the vapor phase and separate them for recovery.

At a relatively low temperature (~1000°C), molten magnesium chloride not only chlorinates the constituents of the magnet alloy scrap but also extracts the chlorides into the melt (Shirayama and Okabe 2008). From the melt, now comprising magnesium chloride, magnesium, and rare-earth chlorides (Nd and Dy), magnesium chloride could be distilled off as the vapor phase and reused for more extractions.

Ammonium chloride was also used for chlorinating neodymium magnet alloy scrap (Itoh et al. 2008; Ito et al. 2009). The chlorination was selective, and at 300–350°C in 3 h, 90% of neodymium in the scrap was converted to the chloride. The product was leached with water to dissolve $NdCl_3$, leaving α-iron and FeB in the solid residue.

A scheme for the selective chlorination of magnet swarf that permits recycling of much of the chlorine was outlined by Uda and Hirasawa (2003) and Uda (2002). The process scheme operates with the net consumption of only carbon and water. Oxygen-contaminated magnet swarf was selectively chlorinated by $FeCl_2$ to yield $RECl_3$. The reaction is aided by the presence of activated carbon, which was added to the charge. After complete chlorination, the rare-earth chlorides were separated from the residue (iron alloy and excess $FeCl_2$) by sublimation in a vacuum. As the next step, the rare-earth chlorides were subjected to pyrohydrolysis, wherein they react with moisture, convert to the oxide, and release HCl, which was used to chlorinate iron to $FeCl_2$. The ferrous chloride, in turn, was used to chlorinate the scrap.

The possibility of accomplishing rare-earth separation by combining selective reduction and vacuum distillation was also indicated by Uda et al. (2000). The rare-earth pairs investigated were samarium–neodymium and neodymium–praseodymium.

One or more elements in the rare earth-bearing scrap may be selectively converted to vapor and carried away from the residue scrap, for recovery. This is a more effective and economical alternative to the conversion of all the elements in the scrap to the vapor state for processing.

7.5.4 Chemical Vapor Transport

One of the earliest attempts at magnet scrap recycling by pyrometallurgy is based on chemical vapor transport. Rare-earth chlorides ($RECl_3$) are not particularly volatile, but they can form highly volatile complex chlorides with alkali metal chlorides ($KRECl_4$) and with aluminum chloride ($REAl_nCl_{3+3n}$ with $n = 1–4$) (Jiang et al. 1997). Most of the other metals that are present with the rare earths in the magnet (Fe, Cu, Zr, Al, Co, Ni) also readily form volatile chlorides or volatile complex chlorides. There are differences in the temperature-dependent stability and volatility of various chloride and complex chloride species that form, and these differences can be exploited to effect separation and recovery.

In devising processes based on chemical vapor transport, Adachi et al. (1991) and Murase et al. (1995) used temperature-dependent stability ($\Delta G° - T$) of the various chloride and complex chloride species formed and the differences in the volatility of the constituent chlorides and their complexes, to separate and collect them along a temperature gradient. The rare-earth scrap is first heated in a stream of chlorine gas and nitrogen whereby the metallic constituents convert to the corresponding chlorides. Aluminum chloride is generated by chlorination of ϒ-alumina, and this chloride vapor is then swept over the chlorinated scrap by a nitrogen carrier gas whereby volatile complex adducts form. The vapor stream is swept along the length of the reactor tube, where a temperature gradient is maintained. Driven by the temperature-dependent stability, various constituents of the vapor decompose, and depending on the volatility of the decomposition products, they deposit in various temperature zones. The rare earths deposit as anhydrous chlorides in the 800–900°C zone; cobalt and nickel chlorides in the 500–700°C zone; and chlorides of the metals Fe, Cu, Zr, and Al in the zone below 350°C. The purity of the chlorides in these deposits is very high (>99%). The process has been used by Adachi et al. (1991) and Murase et al. (1995) for the treatment of Sm–Co and NdFeB scraps. The process is more general and has been used for the treatment of other rare earth-bearing scrap materials as well as certain primary resources (Binnemans et al. 2013; Tanaka et al. 2013).

This elegant process has its share of challenges. Aluminum chloride is highly corrosive and very sensitive to moisture. Almost all the components in the scrap are converted to chlorides, and this entails huge consumption of chlorine gas. Variants that work around these limitations have been attempted. Some of these are described later.

The formation of a carbonyl has also been exploited for chemical vapor transport processing of rare-earth scrap. Itoh et al. (2009) and Miura et al. (2008) reacted neodymium magnet scrap with carbon monoxide to form volatile $Fe(CO)_5$. Sulfur is a catalyst for this reaction. Over 90% of iron was recovered subsequently by a hydrogenation–disproportionation treatment.

7.5.5 Liquid Metal Extraction

Certain liquid metals can be used as solvents to selectively extract rare-earth metals in elemental form from rare earth-containing scrap. The extracted rare-earth

metal can be released to a different solvent or media, from where the rare earth can be retrieved/collected in a pure form. The process works like conventional solvent extraction of hydrometallurgy.

In the 1960s, Bayanov et al. noted that the rare-earth metals lanthanum to lutetium can distribute between two immiscible liquid metal phases, lead and zinc. They also determined the distribution coefficient for each of the rare-earth metals. The rare-earth metals have a strong tendency to dissolve into the zinc phase, and the distribution coefficient $K_d = C_{Zn}/C_{Pb}$ at 500°C ranged from 5000 for lanthanum 4000 for Nd and 3000 for Sm (Bayanov and Serebrennikov 1964; Bayanov et al. 1966). In principle, therefore, from a rare-earth magnet scrap, the REEs can be trapped into a lead–zinc melt. After saturation, the zinc-rich and lead-rich liquid layers are separated by the density difference, and the dissolved metals are removed by sublimation or distillation. In practice, however, there are difficulties.

In the recycling of REE scraps, it is often necessary to separate rare earths from transition metals. In the Pb–Zn system, iron, cobalt, and nickel have distribution coefficients (K_d) that exceed 10,000. The lead–zinc system is, therefore, not really useful for separating rare earths from transition metals. The idea/concept remains very attractive especially because all the value addition done to the rare earths to get them in pure elemental state is retained if a suitable melt is identified to effect the separation.

7.5.5.1 Ames Process

Recycling of the rare-earth materials using the liquid–liquid extraction technology based on liquid metal solvents has been investigated at the Ames Laboratory as the technique for recycling that (1) has the ability to handle a wide variety of scrap feed materials, i.e., swarfs to ingots; (2) allows production of very clean material, i.e., low C, N, O, and unwanted metallics; and (3) eliminates having to return to primary metal reduction from a metal compound. The process essentially consists of dissolution of the rare-earth alloy in a molten metal system in which the rare earths and other transition metals distribute themselves between the liquid phases, where the liquid phases are not miscible in any proportions.

The Ames Laboratory process for $Nd_2Fe_{14}B$ is based on selective dissolution/extraction of neodymium from the alloy scrap (Xu 1999; Xu et al. 2000). It was, in fact, a liquid–solid system. Magnesium melts at 649°C. Neodymium dissolves in liquid magnesium, and the equilibrium solubility is 65 at.% at 800°C (Okamoto 1991). Iron is practically insoluble in liquid magnesium (solubility < 0.035 at.% at 800°C) (Nayeb-Hashemi et al. 1985), and so is boron.

In the process, the NdFeB particles are degreased and then immersed in liquid magnesium at 800°C. As an alternative, magnesium can also be melted over the degreased magnet scrap particles. After equilibration, the neodymium-saturated liquid magnesium is poured off or otherwise separated from the iron–boron residue. Neodymium is recovered subsequently from the magnesium alloy by distilling off magnesium in a vacuum. Magnesium can be recycled. Taking advantage of the high vapor pressure of magnesium, Japanese researchers devised a method to recirculate magnesium and made this liquid–solid separation process continuous (Okabe et al. 2003a,b; Takeda et al. 2005, 2006). In addition to neodymium metal,

even the Nd–Mg alloy and Fe–B residue are marketable products. The process cannot handle partially oxidized scrap and, as developed at Ames, was relatively slow (2–3 days).

The Ames process can be used to recycle not only Nd from $Nd_2Fe_{14}B$ alloys but also La from $LaNi_5$ alloys. The same technique has also been applied for the recycling of $LaNi_5$ alloy. Here, separation of La from nickel is not desired, and reclaiming the alloy for reuse is the goal. Vacuum sublimation or distillation is used to remove excess magnesium. Magnesium is recycled in the process.

Silver can be used instead of magnesium in the liquid metal extraction process for recycling NbFeB scrap (Takeda et al. 2004). Molten silver (melting point, 962°C) dissolves Nd but not Fe or B. By oxidizing dissolved Nd to Nd_2O_3, all Nd can be completely recovered from silver. Molten silver has no solubility for Nd_2O_3. Silver is easier to handle, recycle, and reuse. The process, outlined in Figure 7.3, relies on the fact that when a NdFeB alloy is contacted with molten silver, Nd selectively dissolves in silver, leaving behind FeB. Molten silver dissolves up to 57–59 wt.% Nd at 1363 K. After solid–liquid separation, on exposure to oxygen at 1409–1445 K, Nd in Ag selectively oxidizes and separates as a solid phase. The silver is recycled.

Apart from being more expensive than Mg, the main disadvantage of using silver appears to be that Nd product is recovered as Nd_2O_3 and not as elemental Nd like in the case of the Mg process.

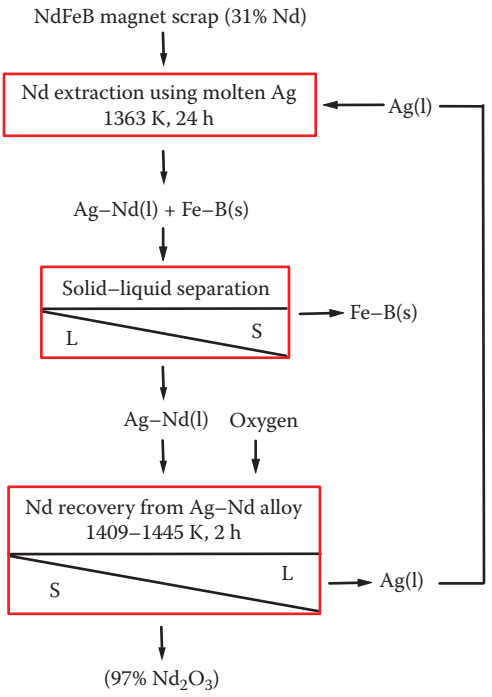


FIGURE 7.3 Processing of NdFeB scrap by liquid metal (Ag) extraction. (From Takeda, O. et al., *J. Alloys Compd*., 379: 305–313, 2004.)

7.5.6 Flux-Based Processes

7.5.6.1 Electroslag Refining

Electroslag refining (ESR) is suitable for the recycling of partly oxidized REE magnet alloys available as relatively clean and large pieces (e.g., magnet broken during manufacture) and not for swarf or fine particulate materials. The process does not accomplish separation of rare earths from transition metals.

The ESR process (Ellis et al. 1994) is shown schematically in Figure 7.4. The cleanup of the scrap is accomplished by a reactive flux, which can remove carbon, hydrogen, nitrogen, and oxygen as well as metallic impurities such as Li, Na, Al, Zn, Mg, Ca, and Si. The flux is made by melting a mixture of $CaCl_2$ and CaF_2, to which a rare-earth fluoride is added. The scrap is rendered molten either by using it as the consumable electrode in arc melting or by addition to a molten bath at a sufficiently high temperature. In the case of arc melting, as the scrap is melted, the molten material from the electrode descends through the slag layer into a shallow pool in a water-cooled chill mold, where it solidifies. As the molten metal droplets travel through the molten slag, the impurities are picked up from the droplets and are trapped in and by the slag. When the scrap material is added to the molten slag bath, the material must be held molten long enough to allow the impurities in the metal to react with the slag and get trapped in it. At the end of this process, the cleaned metal is transferred and cast into molds.

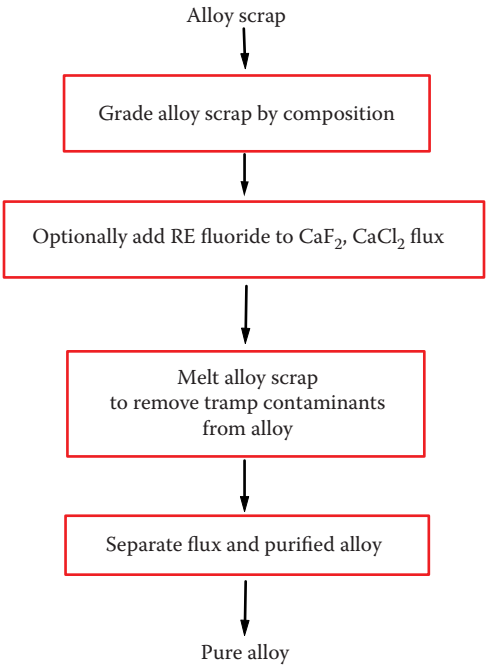


FIGURE 7.4 The ESR process for RE alloy scrap recycling. (From Ellis, T.W. et al., Methods and opportunities in the recycling of rare earth based materials, Report No. IS-M 796, Ames Laboratory, Iowa, 1994.)

7.5.6.2 Molten Flux Process

Takeda et al. (2009) proposed another flux-based process, similar to ESR, to remove rare-earth oxide formed in the magnet alloy, which had gotten oxidized during the manufacturing of magnets. Molten fluorides like LiF–DyF_3 and LiF–NdF_3 are used as the flux. Rare-earth oxides dissolve in molten fluoride media. Remelting the magnet alloy in the flux leads to the dissolution of RE oxide in the molten fluoride. After separating the cleaned metal from the molten flux, the NdFeB is usable as a master alloy for magnet production. The oxygen content decreased from 5000 ppm in the scrap to 200 ppm in the cleaned master alloy. Interestingly, the REO trapped in the molten salt becomes the source of RE metal if the salt is electrolyzed in a conventional oxide–fluoride set up for rare-earth production (Morrice et al. 1968).

7.5.6.3 Glass-Slag Method

A process known as the glass-slag method has been used by Saito et al. (2005a,b) for the extraction of samarium from Sm–Fe–N magnets. The process is outlined in Figure 7.5. First, the Sm–Fe–N magnet alloy compact is heated with B_2O_3 in an argon atmosphere until the oxide melts and encapsulates the alloy. The composite

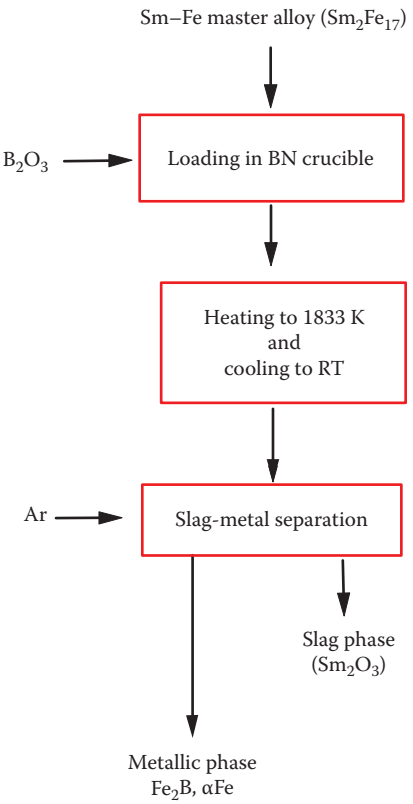


FIGURE 7.5 Extraction of samarium from Sm–Fe alloy by the glass-slag method.

(B_2O_3-encapsulated alloy) is then heated to 1560°C (100°C above the melting temperature of Sm_2Fe_{14}) for 1 h and cooled to room temperature. This heating and cooling was also done under argon cover. At the end of this treatment, almost all the samarium from the alloy has been transferred to B_2O_3. Earlier work by the same group on Sm–Co (Saito et al. 2003a,b) and Sm–Fe (Saito et al. 2005a) alloys had revealed that Sm–Co could be separated into Sm containing B_2O_3 and a Co–B alloy, and that an Sm–Fe alloy could be separated into Sm containing B_2O_3 and a Fe–B alloy. Saito and Motegi (2004) have reported on the extraction of Tb from Tb–Fe alloys by the glass-slag method. The metallic specimen produced from the $TbFe_2$ alloy by the glass-slag process consisted of the Fe_2B phase, and the slag component was $TbBO_3$.

In the glass-slag method of Saito et al. (2003b,c), when the REE magnet scrap and B_2O_3 are heated together, boric oxide functions both as the oxidizing agent as well as the extraction medium. The rare-earth content in the scrap is oxidized, and this oxide dissolves in B_2O_3. Boric oxide is an excellent glass former, and the RE_2O_3–B_2O_3 solution solidifies into a glass. Neither Fe nor B is attacked, but the extraction of Nd is so complete that the α-Fe and Fe_2B phases that remain in the scrap contain residual Nd less than 0.01 wt.% (Saito et al. 2003c). The process is fairly versatile and has also been applied to Sm–Fe–N (Saito et al. 2005b) and La–Ni alloys (Saito et al. 2003a). Only the rare-earth content is extracted as oxide, and the other components are left intact. Sulfuric acid can dissolve the glass slag, and the rare earths now in solution can be precipitated as double sulfate or hydroxide (Saito et al. 2006). This effective process for recycling also generates a considerable amount of inorganic/mineral waste.

7.5.7 Oxidation–Reduction and Other Options

It so happens that the only issue in the recycling of relatively new and clean magnet scrap to produce a new magnet alloy is the residual nonmetallic content of the scrap, particularly oxygen and carbon. Carbon-containing alloys have inferior magnetic properties, and oxygen, if present, will result in slag formation, loss of rare earths in the slag, and degradation of magnetic properties. The removal of carbon and oxygen from magnet scrap to make it suitable for direct magnet alloy melting has been studied by Suzuki et al. (2001) and Saguchi et al. (2006). Carbon can only be removed by oxidation at 800°C, but the alloy also oxidizes. Oxygen is then removed by a two-stage reduction. The first stage is hydrogen reduction of Fe_2O_3 at 980°C. In the second stage, residual rare-earth oxides are reduced by calcium. The products of reduction are removed by water leaching. Thus, the carbon content in the alloy was decreased to <0.001% and oxygen to ~0.1%. Effectively, the reduction step in the primary alloy-making flow sheet is reenacted as follows.

The process for recycling grinding sludge generated in the making of NdFeB magnets is outlined in Figure 7.6 (Saguchi et al. 2006). The grinding sludge is sifted through a screen to remove foreign bodies, and the slurry is squeezed through a conventional filter press to obtain claylike compacts. The free carbon in the scrap is oxidized by heating the compacts in the air, and carbon content decreases to less than 0.001%. Iron in the compact also oxidizes to iron oxide. The decarburized but

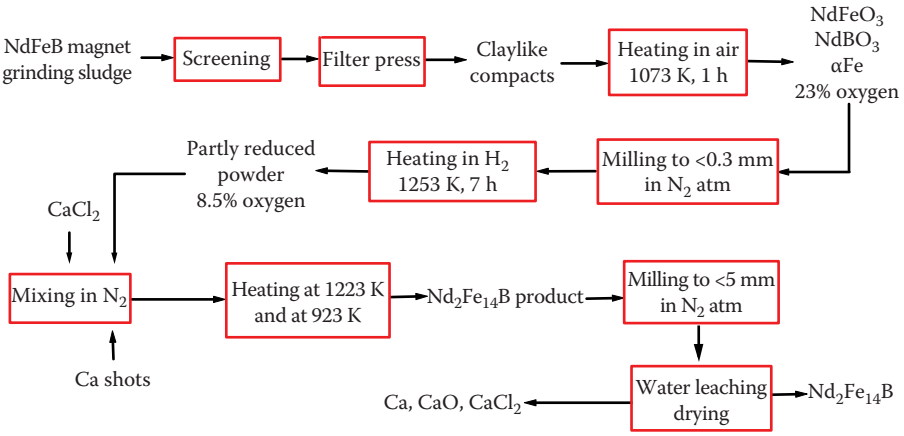


FIGURE 7.6 Recycling of magnet grinding sludge to magnet alloy. (From Saguchi, A. et al., *J. Alloys Compd.*, 408: 1377–1381, 2006.)

oxidized scrap is milled, classified in a nitrogen atmosphere, and heated in a hydrogen atmosphere to reduce the iron oxides. Hydrogen-reduced scrap powder is mixed with anhydrous calcium chloride and calcium shots, and the mixture is charged into stainless steel vessels and heated at 950°C under argon followed by heating at 650°C for alloying. The product of calcium reduction was milled to 5 mm under nitrogen. Residual calcium, byproduct calcia, and the solvent calcium chloride are leached out with water; the alloy powder is squeezed in a filter press and dried in a vacuum. It is then ready for use in magnet manufacture.

An example of recycled NdFeB magnet material values put to use, not once again as permanent magnets but as efficient microwave absorbers, has been reported by Miura et al. (2006).

The NdFeB bonded magnet scrap powder is first ground to a coarse powder (several hundred micrometers) under an argon atmosphere in a WC mortar and then ball milled to a fine size. The fine magnet scrap powder is subjected to hydrogenation–disproportionation treatment at 150–650°C in a hydrogen stream. The products are NdH_2, Fe_xB, and α-Fe. On exposure of the hydride powder to air at room temperature, NdH_2 converted to fine particles of Nd_2O_3. Resin-bonded disks prepared from the composite powders of Nd_2O_3–Fe_xB–α-Fe (mean diameter, 20 nm), Fe_xB (amorphous), and Nd_2O_3 particles showed excellent electromagnetic (EM) wave absorption ability in a frequency range of 4–6.7 GHz. This is a higher frequency range, and spinel-type ferrites are no longer effective. Rare earth-bonded magnet scrap has been effectively recycled as EM wave absorption materials to suppress electromagnetic interference (EMI) problems in devices.

7.6 HYDROMETALLURGY

In hydrometallurgy processes, much of the value addition to the rare-earth material in the final product is lost during recycling because, more often than not, the values

are processed by routing through an aqueous solution. Two major process variants are used. One relies on leaching of the scrap material with or without pretreatment followed by recovery of values essentially by a precipitation method. The other is to treat the scrap leach liquor by precipitation and/or solvent extraction.

7.6.1 Leaching and Precipitation

In the overall process for recovery of rare earths by recycling, pyrometallurgical treatments often need to be complemented by hydrometallurgy. Rare earths, in quantities suitable for recycling, are frequently available in the form of slags and sludges. Oxides containing REEs are used in glass formulations and polishing powders. An oxide slag (Nd_2O_3–B_2O_3) is generated as interprocess intermediate in the recycling of NdFeB and SmFeN magnet scrap. A chemical recycling process has been proposed for recovering neodymium values from neodymium-containing boron trioxide (Saito et al. 2006). The flow sheet is shown in Figure 7.7.

Neodymium-containing boron trioxide was first dissolved in sulfuric acid and heated. From the solution, neodymium was precipitated either as sodium–neodymium sulfate hydrate or as neodymium hydroxide. Of the two, neodymium hydroxide is not a complex compound and is preferred as the final product over sodium–neodymium sulfate. However, in the process outlined, approximately 75% of the neodymium present in the oxide slag can be recovered as the complex compound, whereas the recovery is only 57% when the neodymium is precipitated as neodymium hydroxide. Saito et al. (2006) have, however, noted that further work on improving process conditions could lead to better recovery and that the process could be applied to other rare earth–containing sludges by improving the process conditions.

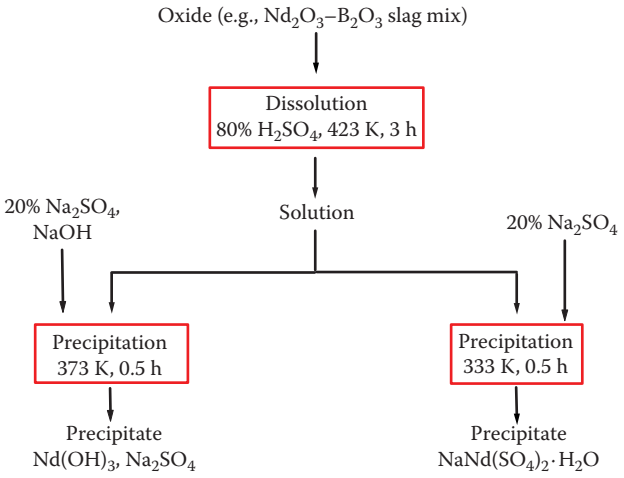


FIGURE 7.7 Chemical treatment process for recycling of neodymium-containing oxides. (From Saito, T. et al., *J. Alloys Compd.*, 425: 145–147, 2006.)

Bounds (1994) proposed a general flow sheet for the recovery of both samarium and cobalt in the form of oxides. The flow sheet is given in Figure 7.8 for $SmCo_5$ and $Sm_2(Co,Fe,Cu,Zr)_{17}$ swarf. The steps are as follows. (1) Dissolution: The rare earths and most of the other metals in the swarf dissolve in common mineral acids like HNO_3, HCl, and H_2SO_4. The choice of a particular acid is dictated by the route for subsequent processing. (2) Precipitation: If the precipitation route is to be followed, sulfuric acid is chosen for dissolution. From the sulfuric acid solution, samarium can be selectively and quantitatively precipitated as the oxalate $Sm_2(C_2O_4)_3$ or double sulfate $Na_2SO_4 \cdot Sm_2(SO_4)_3 \cdot 2H_2O$ or $(NH_4)_2SO_4 \cdot Sm_2(SO_4)_3$. The transition metals remain in solution. (3) Fractional crystallization: Detailed investigations on the fractional crystallization from sulfate solutions were reported (Sato et al. 1997; Tanaka et al. 2013; Wei et al. 1989) for the of processing $SmCo_5$ and $Sm_2(Co,Fe,Cu,Zr)_{17}$ scrap. Sato and Nanja's group extended their basic investigations on fractional crystallization on Sm–Co recovery to the Nd alloy as well (Sato et al. 1997; Wei et al. 1989).

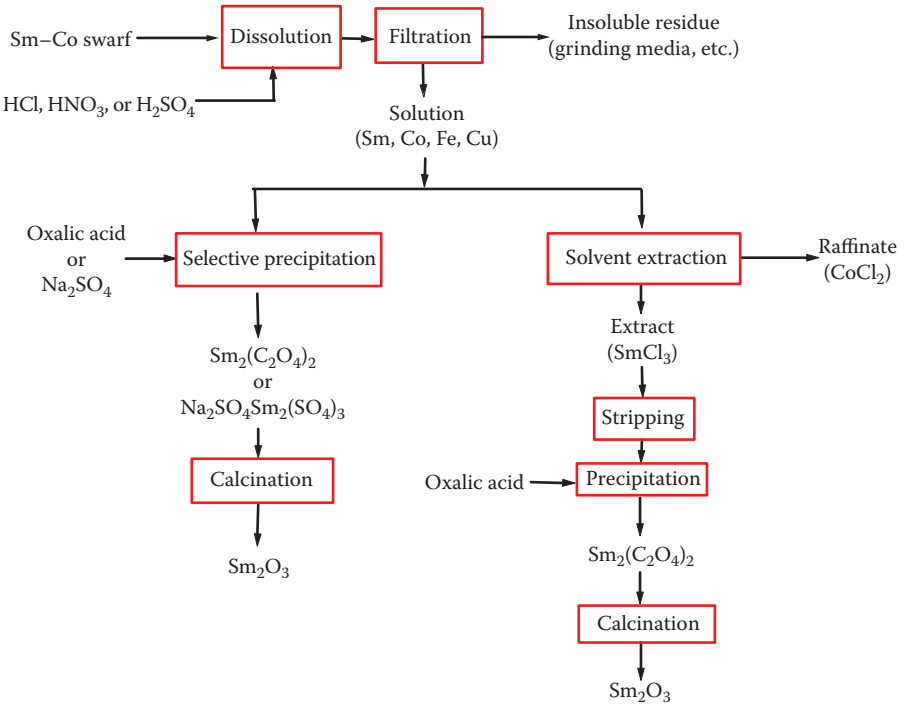


FIGURE 7.8 General flow sheet for the recovery of both samarium and cobalt from magnet swarf. (From Bounds C.O., The recycle of sintered magnet swarf, In: Liddell, K.C., Bautista, R.G., Orth, R.J. (Eds.), *Symposium on Metals and Materials Waste Reduction, Recovery and Remediation*, at the 1994 Materials Week Meeting Location: Rosemont, IL, October 3–6., pp. 173–186, The Minerals Metals & Materials Society, Warrendale, Pennsylvania, 1994.)

They obtained correlations on the solubility of Nd and Fe in aqueous solutions as a function of SO_4^- concentration and temperature. Working on these data, the group recovered neodymium sulfate hydrate of nearly 97% purity in over 97% yield by processing NdeB magnet scrap by fractional crystallization of metal sulfates (Tanaka et al. 2013).

The processing of NdFeB scrap by roasting in air, sulfuric acid leaching, and sulfate precipitation was investigated by Lee et al. (1998). Selectivity in leaching (maximum dissolution of Nd and minimum dissolution of Fe) was found to be influenced by the temperature of roasting, H_2SO_4 concentration, temperature of leaching, and time. Considerable selectivity was achieved when the roasting temperature is higher, sulfuric acid concentration lower, leaching temperature lower, and leaching time shorter.

At USBM, Lyman and Palmer (1992, 1993a,b) developed a process for treating NdFeB scrap by acid dissolution and precipitation. The overall scheme is outlined in Figure 7.9. The scrap is completely dissolved in sulfuric acid. By maintaining the pH (0.2) and molarity of various solutes within predetermined limits, the dissolution of all components is ensured. Sodium–neodymium double

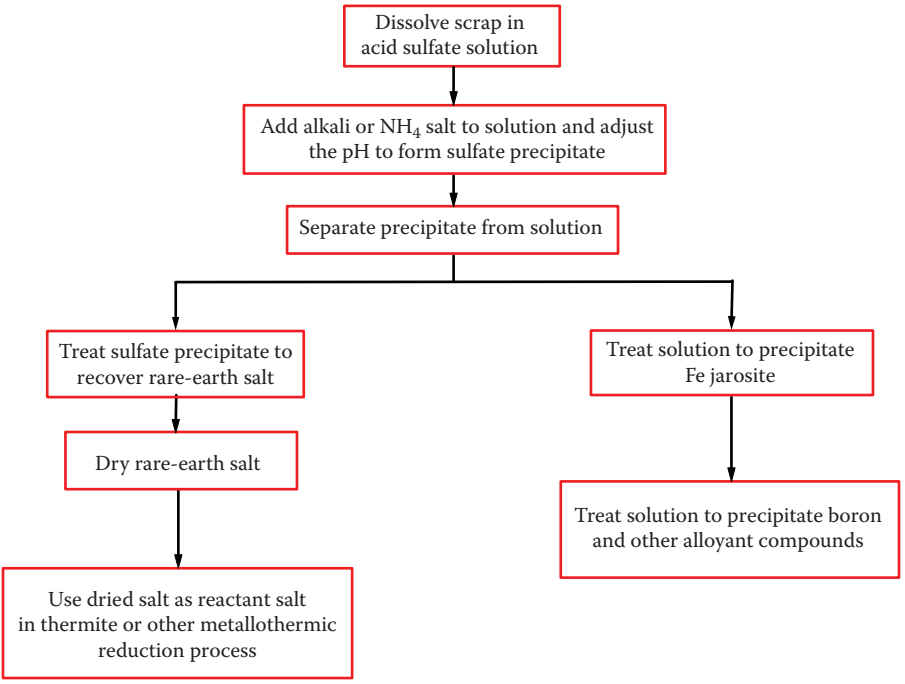


FIGURE 7.9 USBM process for treating NdFeB scrap by acid dissolution and precipitation. (From Lyman, J.W. and Palmer, G.R., *High Temp. Mater. Process.* 11: 175, 1993a; Lyman, J.W. and Palmer, G.R., Recycling of neodymium iron boron magnet scrap, Report of Investigations 9481, United States Bureau of Mines, 1993b.)

sulfate [$Na_2SO_4 \cdot Nd_2(SO_4)_3 \cdot 6H_2O$] is precipitated by raising the pH of the solution to 1.5 by the addition of NaOH. The precipitate is filtered. The filtrate is heated to 90°C, and oxygen is bubbled through it to fully oxidize Fe^{2+} to Fe^{3+} and remove it as a jarosite [$NaFe(SO_4)_2(OH)_6$], which is easier to filter than $Fe(OH)_3$. Through all these treatments, boron in the original scrap remains in solution. A useful fire retardant compound, zinc borate hydrate, can be produced by separately precipitating boron from the solution by adding zinc and raising the pH of the solution.

The precipitation of sodium double sulfate results in the best yield (98%) of rare earths. Potassium and ammonium double sulfates can also be precipitated by adding KOH and NH_4OH, respectively. The yield is lower (70%) for the ammonium salt. Praseodymium, terbium, and dysprosium, if present, respond like neodymium. At the jarosite precipitation stage, instead of oxygen gas, hydrogen peroxide solution may be added to oxidize iron. Cobalt, if present, does not precipitate with iron. It may be extracted using Cyanex 272 as the solvent.

The USBM process is effective but open to improvement. The beginning on this also was made by Lyman and Palmer (1993b). To avoid the processing of the major component in the scrap, iron, they explored alternatives based on roasting under a controlled oxygen potential (partial pressure). The scrap was roasted in a hydrogen–water vapor mixture (pO_2 is controlled by the ratio pH_2/pH_2O and the temperature) to selectively oxidize Nd to Nd_2O_3 while the iron remains as Fe. This step, which was carried out under conditions dictated by the Nd_2O_3–Fe coexistence region of the stability diagram of the Nd–Fe–O ternary, was successful. However, the roasted product had extremely fine grain size and was not much amenable to subsequent processing by magnetic separation or acid leaching to yield the separated products Nd_2O_3 and Fe.

Koyama et al. (2009) chose the conditions on the basis of the Pourbaix diagram of the Fe–H_2O and Nd–H_2O systems for selective leaching of Nd^{3+}, leaving iron as Fe_2O_3 from an oxidized Nd magnet alloy scrap. Commercial Nd magnets were thermally demagnetized, crushed, and roasted in air at 900°C for 6 h and leached in an autoclave with 0.02 M HCl at 180°C for 2 h. By this, more that 99% of the rare earths in the roasted scrap entered into solution, whereas less than 0.5% of the iron from the scrap dissolved. The roasting as specified is critical prior to leaching in order to restrict the dissolution of iron to <0.5% (Tanaka et al. 2013).

7.6.1.1 Rhône Poulenc Process

A process investigated at Rhône Poulenc for recycling NdFeB swarf (Bounds 1994) comprises low-temperature oxidation followed by leaching oxidized material at atmospheric pressure with HCl, H_2SO_4, or HNO_3. In the oxidation step, the temperature is kept low so that no sintering of oxidized material occurs and granular nature of oxide is preserved. Leaching dissolved all except iron oxide. After separation of the insoluble residue, the leach liquor is routed to an RE separation circuit for processing along with materials from the primary mineral concentrate leaching operations. The report by Bounds (1994) does not hint on how the processing limitations indicated by USBM were circumvented at Rhône Poulenc.

Lyman and Palmer (1995) also investigated the leaching of NiMH scrap in different mineral acids (HCl, H_2SO_4, and HNO_3) to solubilize the rare earths. The best results were obtained with 4 M HCl. From the leach liquor, rare earths were precipitated as rare-earth phosphates by the addition of phosphoric acid. Another hydrometallurgy scheme was suggested by Pietrelli et al. (2002). Their approach consisted of producing a leach liquor from the spent NiMH batteries and obtaining selective separation of RE by precipitation in sulfuric acid media before processing the solution for separation and recovery of the other components, which included iron, nickel, cobalt, and zinc. In the process, the electrodes, both positive and negative, were mechanically crumbled and leached with 2 M sulfuric acid for 2 h at 20°C. From the leach liquor, mixed rare earths are precipitated as double sulfates by pH adjustment by addition of NaOH. Some of the metals contained in the leach liquor could also be precipitated effectively by pH adjustment or by coprecipitation. The authors note that from 1 ton of spent batteries (all materials), 37.5 kg of rare earth (as metal) at about 80% purity can be obtained.

Kanamori et al. (2009) treated NiMH battery waste with 2 M HCl. The metals, now in solution, were precipitated at room temperature at pH 12 by addition of 2 M NaOH. The precipitate was calcined to a mixture of oxides: NiO, CeO_2, and $LaCoO_3$. The chemical treatments outlined in Figure 7.10 yielded the final product.

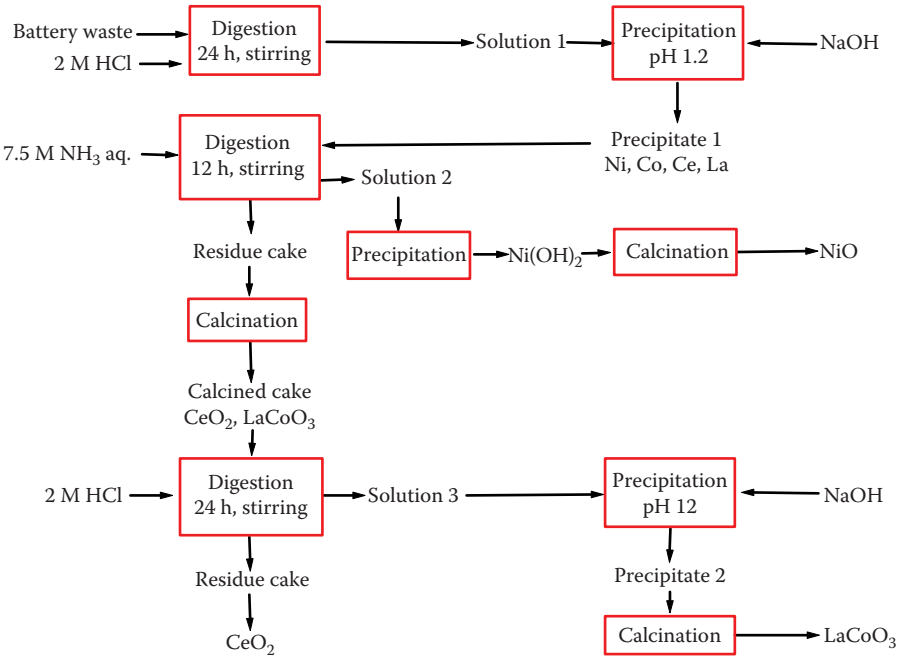


FIGURE 7.10 Procedure for the separation of NiO, CeO_2, and $LaCoO_3$ from Ni–MH battery waste. (From Kanamori, T. et al., *J. Hazard. Mater.*, 169: 240–245, 2009.)

7.6.1.2 Hydrothermal Process

In yet another process called *hydrothermal process*, which relies on leaching and precipitation to achieve REE recycling, Itakura et al. (2006) treated a commercially available nickel-coated NdFeB magnet alloy at 110°C for 6 h in an aqueous solution of 3 M HCl and 0.2 N oxalic acid. The neodymium from the magnet dissolved and precipitated out as neodymium oxalate. Almost all neodymium (over 99%) present in the magnet was recovered as oxalate. The remaining elements in the solution were also recovered as follows: boron as parasibirskite $CaB_2O_5 \cdot H_2O$ by addition of $Ca(OH)_2$ (Itakura et al. 2006; Itoh et al. 2010) and iron and nickel as oxalates at less acidic conditions (at an higher pH) than neodymium.

Ellis et al. (1994) outlined a process to recycle both neodymium and iron from NdFeB magnet alloy scrap following a chemical treatment. The scrap was dissolved in nitric acid, and the solution was treated with HF to precipitate an iron–neodymium double salt. This double salt could be used to directly produce a NdFeB master alloy by calciothermic reduction. The process steps for the recovery of rare-earth components as a fluoride salt or as an oxalate can be readily incorporated in the recycle schemes outlined. The sulfate double salt can be converted to the rare-earth trifluoride by leaching in a HF solution. Alternatively, on treating the sulfate double-salt solution with an aqueous oxalic acid solution, the rare-earth oxalate is selectively precipitated. None of the process steps outlined so far in this section led to any separation among the multiple rare earths if present in the scrap. All the rare earths precipitate together as the double sulfate, fluoride, or oxalate. They may be processed separately by solvent extraction or its variants if individual rare earths are needed.

Any recycling operation involving chemical attack by acids has certain universality in that it is effective and can accept, as feed, scrap in a variety of forms and wide range of compositions. The disadvantages are also quite a few. One is that the rare-earth value is reverted from being a *finished product* to almost become a *mineral concentrate*. This is a major loss of all the value addition in the original processing. The acid leaching is slow and hence time consuming. Large amounts of chemicals (acids, alkalis) are used for once-through operation, and relatively large volumes of waste are generated. Several alternatives to the existing process, or if not, at least improvements in existing processes, are being constantly researched to keep the operating processes in the realm of industrial and commercial viability.

Leaching has been practiced extensively in rare-earth scrap recycling. It is a slow process. An interesting and significant improvement in leaching rate has been reported by the use of ultrasound for different acids and with different rare-earth metals (Gasgnier et al. 1994; Tanaka et al. 2002).

7.6.2 Leaching, Precipitation, Solvent Extraction

Several alternatives to aqueous-based technology for rare-earth recycling have been investigated at the Ames Laboratory (Ellis et al. 1994). The outline of one the processes appears in Figure 7.11. The process begins with the dissolution of rare-earth scrap using HNO_3, H_2SO_4, or HCl in an aqueous solution and removal of the insoluble fraction by filtration. From the filtrate, complete separation of all the elements can be accomplished by using solvent extraction or ion-exchange technology—the

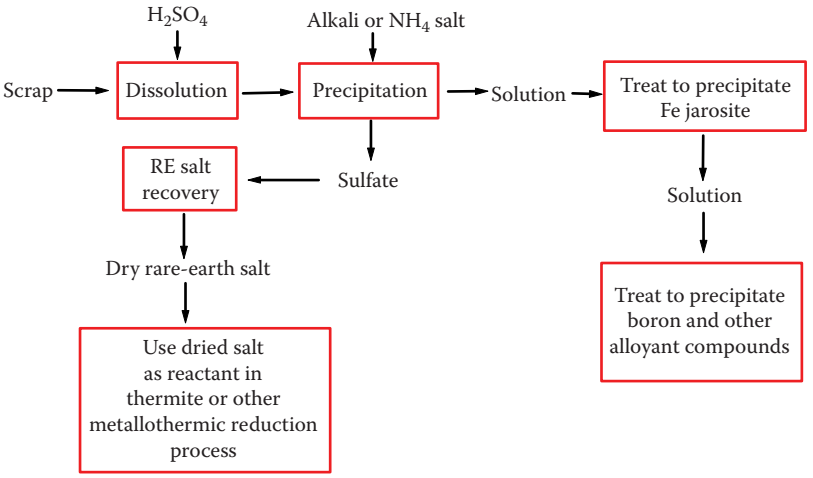


FIGURE 7.11 Aqueous processing for recycling of rare-earth scrap. (From Ellis, T.W. et al., Methods and opportunities in the recycling of rare earth based materials, Report No. IS-M 796, Ames Laboratory, Iowa, 1994.)

same processes that are currently used for producing rare-earth oxide from natural ores. The REEs are then precipitated by the addition of HF. Direct precipitation of rare earths from solution as fluorides alleviates the additional energy-consuming steps involved if the oxalate is precipitated, calcined to oxide, and converted to fluoride. Aqueous-based technology, appropriately chosen, has proved to be versatile and produces high-quality material. It is especially relevant with swarf materials and cutting, grinding, and machining wastes that are highly contaminated and oxidized.

If solvent extraction using tributyl phosphate (TBP) or di-2-ethyl-hexyl phosphoric acid (D2EHPA) is to be followed, the Sm–Co magnet scrap is dissolved in nitric or hydrochloric acid. Samarium can be selectively extracted from the solution. Sanuki et al. (1995) explored the option of leaching out all component metals from $SmCo_5$ and Sm_2Co_{17} scrap using 2 M HNO_3 and processing the leach liquor to separate and recover Fe(III), Zr(IV), Sm(III), Cu(II), and Co(II) with a sequence of extractions using D2EHPA, LIX65N. For leaching, they found HCl and H_2SO_4 to be less effective, and nitric acid leaching left copper in the leach residue. From the nitric acid leach liquor, iron(II) and zirconium(IV) are first extracted into D2EHPA, and after pH adjustment, Sm(III) is also extracted into the same extractant. Using oxalic acid, Sm(III) is recovered from the organic by precipitation stripping, and this procedure effectively prevents coprecipitation of other metals. Iron(III) and Zr(IV) are then stripped from D2EHPA with oxalic acid. In the strip solution, Fe(III) is selectively reduced to the divalent state photochemically and precipitated as Fe(II), leaving Zr(IV) oxalate in the solution. Divalent copper and cobalt in the raffinate are extracted by LIX65N and stripped using sulfuric acid (Tanaka et al. 2013).

A flow sheet (Figure 7.12) involving the leaching of battery scrap with 3 M H_2SO_4, solvent extraction with D2EHPA, evaporation, and crystallization to recover nickel,

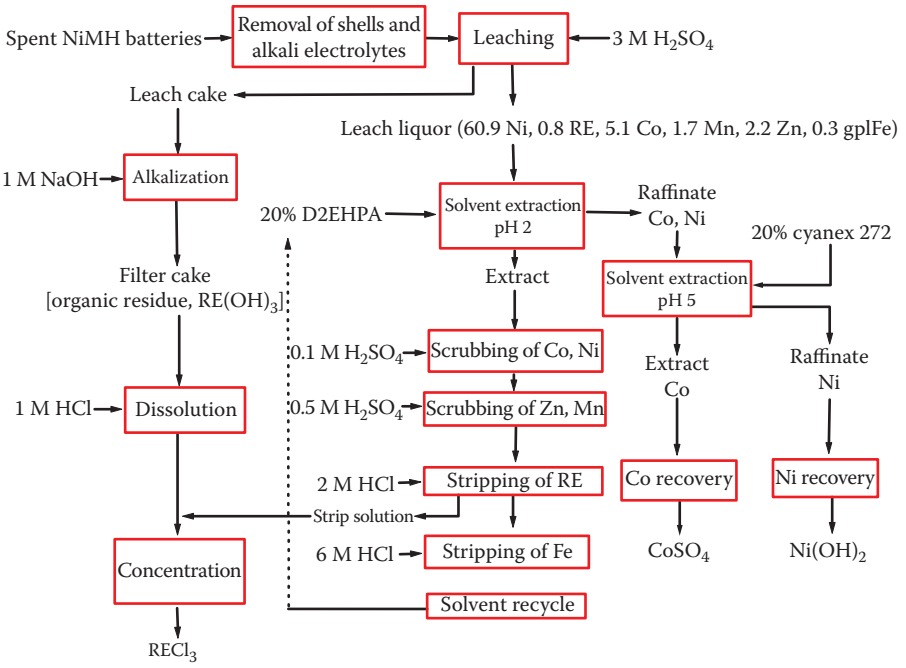


FIGURE 7.12 Overall flow sheet for recovery of Ni, Co, and RE from spent Ni–MH batteries. (From Li, L. et al., *Hydrometallurgy*, 100(December): 41–46, 2009.)

cobalt, and the rare-earth contents from the solution was proposed by Li et al. (2009). The rare earths were finally obtained as chlorides, with an overall recovery of nearly 98%.

The recovery of Ni, Co, and the rare earths (La, Ce, Nd, and Pd) from used NiMH batteries can be done by an acid (H_2SO_4) leaching process. The recovery of RE from NiMH batteries was also investigated by Gao and Tang (2009). Ekberg et al. (Larsson et al. 2011a,b, 2012) described a flow sheet for recycling that consisted of selective dissolution of electrode materials from dismantled NiMH batteries, followed by separation of metals by solvent extraction. The solvating extractant trialkyl phosphine oxide mixture, Cyanex 923, was used on leach liquors from nickel–metal hydride batteries dissolved in 8 M hydrochloric acid. They have given separation routes for leach liquors from individual electrode materials and a mixed material (Figures 7.13 through 7.15). The batteries used contained 13 metals, and the developed separation schemes separate them in up to four fractions, with the rare-earth fraction containing all the rare earths and aluminum. The main fraction in each case contains nickel, and part of the nickel raffinate is refluxed to the dissolution step in order to reduce the amount of metals to be extracted into the organic phase. A nitrate strip step separates the cobalt and manganese from the coextracted rare earths.

The recycling of metals from a mixture of different types of popular household batteries was investigated by Provazi et al. (2011). The overall scheme used

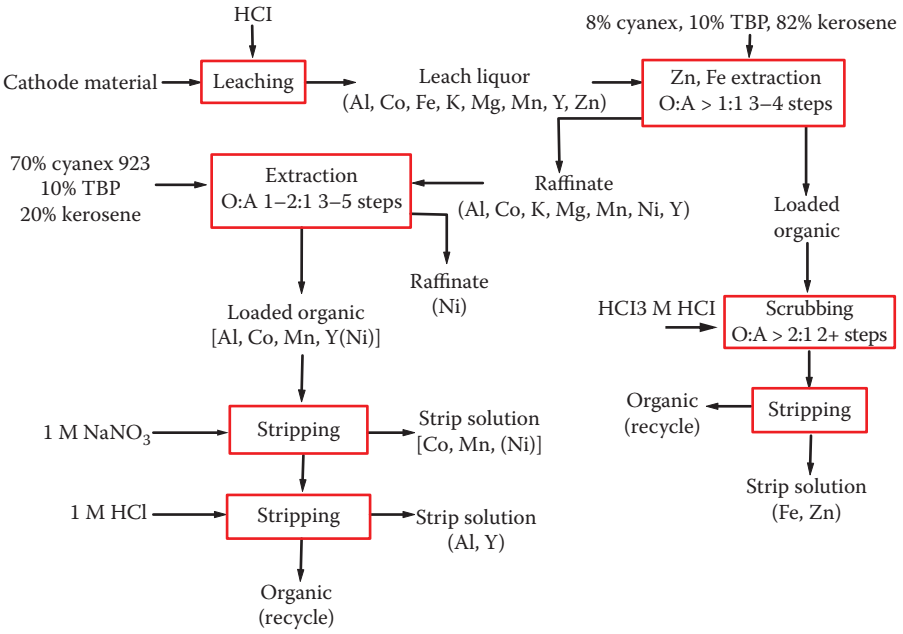


FIGURE 7.13 A potential process for a system based on cathode leach liquors. The number of steps is calculated based on ideal systems requiring more than 99% purity. (From Larsson, K. et al., *Hydrometallurgy*, 129–130: 35–42, 2012.)

a hydrometallurgical route, comprising selective precipitation and liquid–liquid extraction separation techniques. The metal values were obtained in the solution by grinding the waste of mixed batteries (Zn–C alkaline, Zn–C dry cell, NiCd, NiMH, and Li ion), reduction, and elimination of volatile metals using an electric furnace. The battery waste was pretreated and heated to 1000°C for 4 h under an inert atmosphere to eliminate volatile metals such as Cd, Zn, and Hg. Manganese oxides present in the waste get reduced to MnO, which is soluble in H_2SO_4. The material was then treated by acid leaching. The solution was processed by selective precipitation with sodium hydroxide and liquid–liquid extraction using Cyanex 272 [bis(2,4,4-trimethylpentyl) phosphoric acid] the as extracting agent. By liquid–liquid extraction, at a pH of 2.5, Zn had a 99% extraction rate, and at pH 7.0, more than 95% Fe and more than 90% Ce were extracted. Mn, Cr, Co Ni, Cd, and La were also extracted with good efficiency at different pH values.

Honda Motor Corporation and Japan Metals & Chemicals Co. Ltd. had plans to set up a plant to recycle used NiMH batteries collected through the Honda dealers from Honda hybrid vehicles. The process and technology used for recycling are, however, not disclosed.

In the recycling of rare earths from NiMH batteries, the rare-earth concentrated residue obtained at the end of physical separation is leached with sulfuric

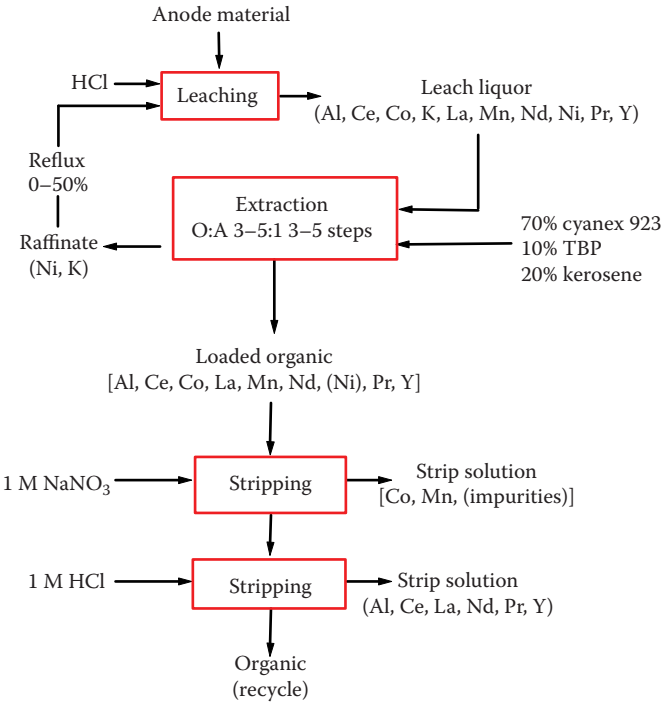


FIGURE 7.14 A potential process for a system based on anode leach liquors. The number of steps is calculated based on ideal systems requiring more than 99% purity. (From Larsson, K. et al., *Hydrometallurgy*, 129–130: 35–42, 2012.)

acid (Yoshida et al. 1995). Parameters such as temperature, H_2SO_4 concentration, and reaction time that affect the extracted metal (RE) yield have been extensively investigated (Heegn and Rutz 2009; Li et al. 2009; Lupi et al. 2000; Nan et al. 2006a,b; Provazi et al. 2011; Rodrigue and Mansur 2010; Yoshida et al. 1995). From the sulfate leach liquor, much of the rare-earth content is recovered by precipitation as double sulfate. This is shown schematically in Figure 7.16. Over 94% of the rare earth (La, Lu, Pr, Nd) precipitate as double sulfate at pH 1.6, separating clearly from Fe, Mn, and other elements in the solution. Whatever rare earths remain in solution after double sulfate precipitation (~5.2% of the original content) was separated by solvent extraction with D2EHPA (Li et al. 2009). The rare earths along with iron, zinc, and manganese are extracted into the organic containing 20% D2EHPA, leaving behind all the Ni and Co in the raffinate. The organic is first scrubbed with 0.5 M H_2SO_4 for removing Zn and Mn and then stripped with 2 M HCl to recover the rare earths.

The rare-earth sulfates are transformed to rare-earth chlorides (Heegn and Rutz 2009; Li et al. 2009) by a simple chemical process. The sulfates are treated with NaOH to form the hydroxides, and the hydroxides, in turn, are dissolved in

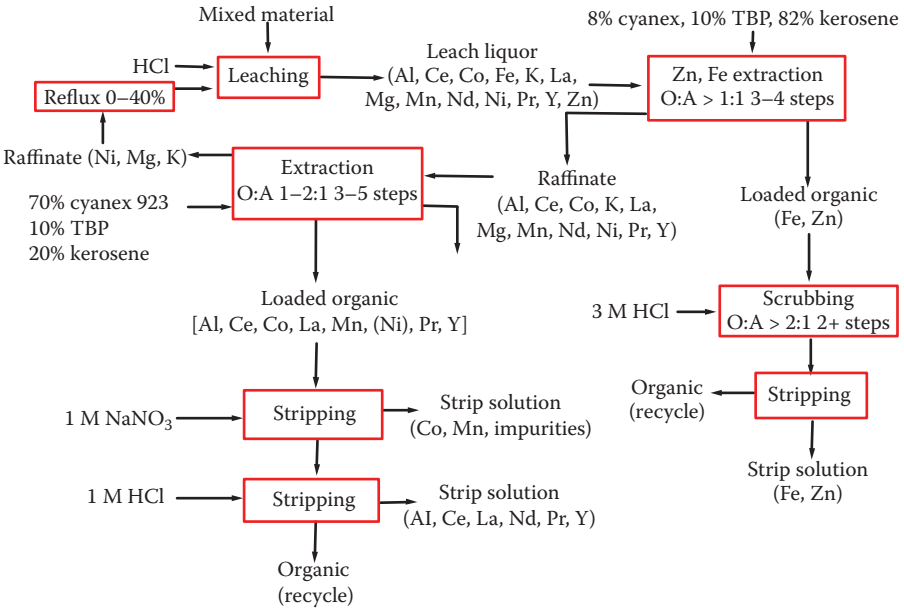


FIGURE 7.15 A potential process for the solution based on a mixed material. The number of steps is calculated based on ideal systems requiring more than 99% purity. (From Larsson, K. et al., *Hydrometallurgy*, 129–130: 35–42, 2012.)

concentrated HCl to form rare-earth chlorides, which are eventually separated by crystallization.

Another process for recovering rare earths from concentrated battery waste residue also uses a combination of acid leaching and solvent extraction. The completely hydrometallurgical process was developed in Japan (Zhang et al. 1998) for the recovery of metal values such as cobalt, nickel, and rare earths from spent NiMH batteries. An outline of the process flow sheet is given in Figure 7.17. The process consists of (1) total leaching of the electrode materials of the battery with hydrochloric acid, (2) separation of rare earths and impurity elements from nickel and cobalt by solvent extraction with D2EHPA, (3) separation of rare earths from impurity elements by selective precipitation of rare-earth oxalates, (4) separation of cobalt and nickel from each other by extraction with trioctylamine (TOA), and (5) recovery of separated nickel and cobalt by precipitation of nickel oxalate and cobalt oxalate, respectively. As the battery residue is leached with HCl, nearly 99% of the rare earths contained in the residue along with all other metals (Ni, Co, Zn, Al, Fe, Mn) enter the solution (Tzanetakis and Scott 2004a; Zhang et al. 1998). Using 25% D2EHPA in kerosene, the rare earths are quantitatively extracted at pH 2. All metals in the solution other than Ni and Co track rare earths to the extract. Traces of Co also get extracted but could be scrubbed with 0.3 M HCl. The rare earths along with Zn, Mn, and some Al are stripped with 2 M HCl. Addition of oxalic acid to the strip solution selectively precipitates the rare earths as oxalate. The overall yield of rare earths in this process was

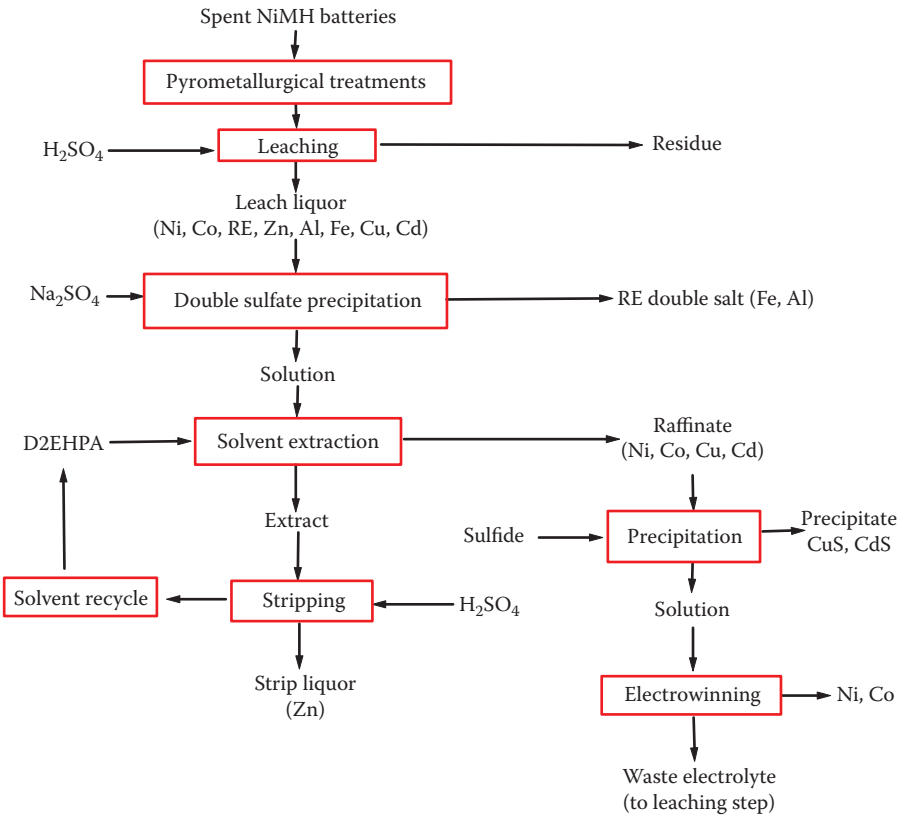


FIGURE 7.16 Metal recovery from spent NiMH batteries by sulfuric acid leaching. (From Yoshida, T. et al., *Recycling of Used Ni–MH Rechargeable Batteries*, pp. 145–152, Minerals Metals & Materials Society, 1995; Reprinted from Bunzli, J.C.G., Pecharsky, V.K. (Eds.), *Handbook on the Physics and Chemistry of Rare Earths*, vol. 43, Chapter 255, Tanaka, M., Oki, T., Koyama, K., Narita, H. and Oishi, T., Recycling of rare earths from scrap, pp. 159–212, Copyright 2013, with permission from Elsevier.)

98% (Zhang et al. 1998). Nickel and cobalt were also recovered from the raffinate after D2EHPA extraction. Cobalt was selectively extracted by 25% TOA. Following TOA extraction, nickel from the raffinate and cobalt from the strip solution were separately precipitated as oxalates and calcined to oxides (Tzanetakis and Scott 2004b; Zhang et al. 1998). Approximately 98% of rare earths contained in the batteries are recovered as REO with <1% impurities. The total yield of nickel and cobalt are approximately 96% and 98%, and the nickel and cobalt oxalates were over 99.9% pure.

7.7 SEPARATION OF INDIVIDUAL RARE EARTHS

Solvent extraction is relevant and useful in the recycling of rare earths from scrap materials in two situations: to isolate the rare earths from non-rare-earth constituents

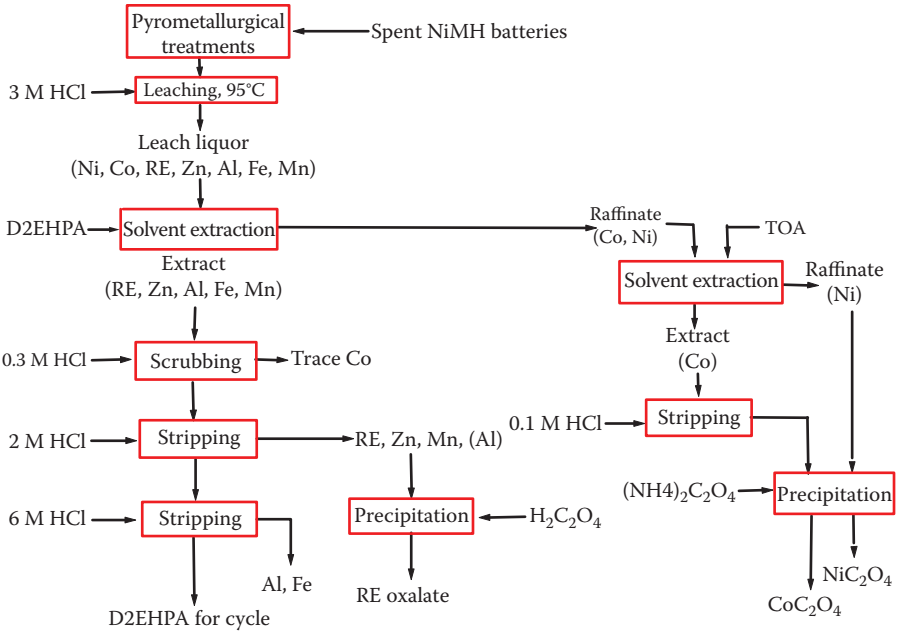


FIGURE 7.17 Metal recovery from spent NiMH batteries by hydrochloric acid leaching and solvent extraction. (From Zhang, P.W. et al., *Hydrometallurgy*, 50: 61–75, 1998.)

in the leach liquor and to separate rare earths from one another. The challenge to solvent extraction is much less in scrap recycling compared to primary ore processing in that the number of entities that need to be separated is smaller. In effect, the rare earth-bearing solution from the scrap circuit either can be processed separately in a solvent extraction sequence or can feed at an appropriate stage into an existing rare-earth processing circuit tackling a primary resource.

The application of solvent extraction to Sm–Co scrap processing comes up for the separation of samarium from the elements cobalt, iron, and copper in the leach liquor. From a leach liquor obtained by HCl dissolution of Sm–Co scrap, samarium is extracted completely by D2EHPA, effectively separating it from the non-REEs. Praseodymium (if present, as in the case of $Sm_{1-x}Pr_xCo_5$ magnet scrap) coextracts with samarium. It can be removed from the loaded organic by scrubbing with a solution containing samarium and HCl (Koshimura 1988).

Among the commercially available solvents, acidic organophosphorous reagents such as PC88A provide larger separation factors for intragroup separation of rare earths (Nash 1994). Instead of PC88A, the use of partially neutralized (~40%) PC88A significantly increases the distribution coefficient of Nd (Lee et al. 2005) when the metal concentration and pH of the aqueous solution are higher, such as in the solution obtained by dissolution of NdFeB scrap. In the Nd magnet alloy, Dy is almost always present. The latest estimate of dysprosium usage is given in Table 7.6

(S. Constantinides, private communication, 2015). Whenever a magnet alloy containing dysprosium is processed for recycling, solvent extraction separation of dysprosium from neodymium is carried out. Tanaka et al. (2009) have shown that the operation is best carried out using PC88A from solutions obtained by the selective leaching of rare earths from roasted scrap. The distribution coefficient of dysprosium is higher, and the Dy–Nd separation factor is also large. However, due to its large concentration in the leach liquor, a small amount of Nd does get extracted into the organic. On scrubbing with an aqueous solution of $DyCl_3$ or HCl, this Nd reverts to the aqueous phase.

The acid dissolution–precipitation/solvent extraction route for scrap Sm–Co magnets was also investigated by Koshimura and Yamamoto (Tanaka et al. 2013). Praseodymium, when present in the magnet alloy scrap ($Sm_{1-x}Pr_xCo_5$), is coextracted with samarium but could be separated from the loaded organic by scrubbing with a

TABLE 7.6
NdFeB Magnets for Different Applications

		Percentage of Mix	
Applications	**Typical Dy%**	**2008**	**2014**
Motors, industrial, general auto, etc.	4.14	26.0	23.0
HDD, CD, DVD	2.76	14.8	18.0
Electric bicycles	4.14	9.2	11.4
Transducers, loudspeakers	2.76	9.0	6.0
Unidentified and all others	1.38	7.2	6.0
Magnetic separation	2.76	5.0	3.5
MRI	1.38	4.0	1.5
Torque-coupled drives	4.14	3.0	2.5
Sensors	1.38	3.0	1.5
Hybrid and electric traction drive	8.74	3.0	6.1
Hysteresis clutch	2.76	2.5	1.5
Generators	6.44	2.5	1.0
Energy storage systems	4.14	2.0	2.5
Gauges	2.76	1.5	0.8
Magnetic braking	4.14	1.5	0.8
Relays and switches	4.14	1.2	0.2
Pipe inspection systems	4.14	1.0	1.0
Wave guides: TWT, undulators, wigglers	6.44	1.0	1.0
Magnetically levitated transportation	4.14	1.0	1.0
Reprographics	4.14	0.7	0.5
Wind power generators	4.14	0.5	9.6
Magnetic refrigeration	1.38	0.3	0.5
Advertising	0.00	0.1	0.0

Source: Constantinides, S., Private communication, 2015.

solution containing samarium chloride and hydrochloric acid, resulting in the process yielding highly pure samarium oxide.

New solvents (extractants) and newer techniques have also been investigated for neodymium–dysprosium separation and recovery. The Nd–Dy separation will be a persistent requirement in the recycling of neodymium magnets, and dysprosium is a critical rare-earth metal. Many of these investigations have been carried out on a small scale in laboratories. A novel extractant, N,N-dioctyldiglycolamic acid (DODGAA), has been considered for the processing of rare earths (Naganawa et al. 2007; Shimojo et al. 2007). The possible advantages of DODGAA over the established solvents D2EHPA, PC88A, and Cyanex 272 include high selectivity of rare earths over Fe(III) and Zn(II) and higher ability to achieve intragroup separation among the light rare earths—possibly between Nd and Pr also. Apart from the possible use of this new solvent as a stand-alone extractant in conventional solvent extraction separation, it was proposed (Baba et al. 2011; Kubota et al. 2010) to be used together with a new class of chemicals known as ionic liquids in a separation arrangement called supported liquid membranes (SLMs) for implementing rare-earth separations.

Ionic liquids, as the name implies, are liquids composed entirely of ions even at room temperature. They have characteristics that could lead to their replacing the conventional organic phase, partly or entirely, in the liquid–liquid extraction process. Besides, unlike the usual solvents, the ionic liquids have very low vapor pressure and are safer from a fire hazard point of view. The potential of ionic liquids to make solvent extraction separation of rare earths more efficient has been indicated by Binnemans (2007) and Wellens et al. (2012).

SLMs are configurations found useful for achieving separations that have been traditionally implemented in an ion-exchange or solvent extraction system. SLMs have been using a conventional organic solvent as the liquid membrane phase. Ionic liquid-based SLMs have been found to offer superior performance. The solvent DODGAA shows good selectivity to the rare earths and efficient stripping behavior. The selective permeation of Dy and Nd ions against ferric ions in an ionic liquid-based SLM using DODGAA as the mobile career was studied by Kubota and Goto's group (Baba et al. 2011). The ionic liquid was 1-octyl-3-methyl imidazoliumbis (trifluoromethylsulfonyl) imide $[C_8mim][Tf_2N]$. Stable transport of Dy and Nd was reportedly achieved, and these two rare earths were quantitatively recovered in the receiving phase. The results point to the possible use of an SLM system for the recovery of rare earths from the leach liquor of Nd magnet scrap.

While every rare earth-bearing material that is prepared is, in principle, recyclable, much of the research and development and industrial effort in recycling has been directed principally toward rare-earth magnets, nickel–metal hydride batteries, phosphors, and, to a lesser extent on polishing powders, glass and catalysts. As has been pointed out elsewhere, most of the effort has been in the R&D space for over two decades, and industrial activity has remained much less in proportion. Table 7.3 (Binnemans et al. 2013) provided an overview of the current direction of these activities.

7.8 MAGNETS

The most important application of the rare earths and also the most vulnerable to supply shortages is their use in high-performance magnets. The major types of rare-earth magnets are listed in Table 7.7 (Tanaka et al. 2013).

Investigations on the recycling of rare-earth permanent magnets began in the early 1990s with processes aimed at $SmCo_5$. At that time, neodymium was a much cheaper material compared to both samarium and cobalt. Apart from environmental reasons, there was really no pressing need to process waste neodymium magnets. The scenario changed post 2005, when the specter of REE supply shortages and restrictions began to emerge. It is now firmly established that recycling of neodymium magnets is a necessity and establishment of a closed cycle for the REEs in the neodymium magnets can ensure stability of supply for these materials. Neodymium magnets are used in a wide variety of devices, much of which are listed in Table 7.6 (Binnemans et al. 2013; Constantinides 2011a). The issues of collection, dismantling,

TABLE 7.7
Major Types of Rare-Earth Magnets and Their Composition (Nominal)

	Chemical Composition of Magnet, Mass%				
Elements	**$SmCo_5$**	**Sm_2Co_{17}**	**$Nd_2Fe_{14}B$**	**Sm_2Co_{17} Magnet Swarf**	**$Nd_2Fe_{14}B$ Magnet Swarf**
Sm	35.3	29.7		24.1	
Co	64.7	46.3		46.9	
Fe		14.9	69	15.5	56.2
Cu		7.5		3.8	
Zr		1.3		3.0	
Nd			25		32.4
Dy			4		1.5
B			1		1.04
Al				0.08	0.35
Mg				0.03	
Ca				0.18	0.08
C				0.75	0.90
N				0.15	0.15
O				5.3	7.12
Si				0.18	0.26
Others			1		
Reference	Sanuki et al. 1995		Minowa 2011	Bounds 1994	Bounds 1994

Source: Tanaka, M. et al., Recycling of rare earths from scrap, in Bunzli, J.C.G. and Pecharsky, V.K. (eds.), *Handbook on the Physics and Chemistry of Rare Earths*, vol. 43, Chapter 255, Elsevier, Amsterdam, 2013.

and processing of rare-earth magnets are exemplary of the issues that could be anticipated for recycling of every other major rare-earth product.

7.8.1 In-Plant or Preconsumer Scrap

Magnet scrap is generated in substantial quantities during production; 20–30% of rare-earth magnets are scrapped during manufacturing. Recovery of rare earths from production waste was not industrially practiced, even till 2009 (Shirayama and Okabe 2009). This indicates the dominant role played by cost and resource availability factors in determining the viability of industrial recycling operations. For recycling, there are a number of technology options (Table 7.5): (1) remelting of scrap to recover metallic values in an unoxidized state (the yield would be low); (2) recovery of the rare-earth content of the scrap as oxide; (3) reuse of the magnetic materials without separation of the material mix for new magnets (usually of lower quality); and (4) selective extraction of neodymium and dysprosium from the magnet scrap (molten $MgCl_2$ is a suitable extracting agent) (Shirayama and Okabe 2009).

7.8.2 End-of-Life Scrap

Much of the current stock of the recyclable NdFeB material is in waste electronics and electrical equipment (WEEE). These include electronic goods such as loudspeakers, mobile phones, and hard drives, and appliance components such as air conditioner compressors and direct drive motors of laundry machines. Among these, the HDDs are very important because (1) they are produced in large numbers (~600 million each year) (Walton and Williams 2011), (2) they have rapid turnaround time (~5 years), and (3) they are relatively more amenable to mechanized/automated dismantling (separation of magnets from the device). The mass flow in this source of recyclable NdFeB amounts to between 6000 and 12,000 tons of alloy—approximately 600 million HDDs to process and 10–20 g NdFeB per HDD (Binnemans et al. 2013).

7.8.2.1 Collection

This is probably the most challenging step in the overall scheme, not only for magnets but also for other recyclable rare-earth commodities, especially when these materials have become part of consumer goods and become dispersed over wide geographical, cultural, and ethnic landscapes, to millions of owners. Interestingly, these millions would need to be convinced that each of these devices has lived its life and needs to be returned to a stream that will enable its recycling with ultimate direct and indirect benefits to them. Once the owners have decided to part with them, then come the logistics of actually collecting them. Local bodies, companies, and the government would need to work together. Embedded innocuously in the collection step is the transportation of the EOL scrap to the recycler. Magnets need to be handled with care. Devices that have magnets have to be demagnetized before transportation to avoid unwarranted complications in handling. For example, because of their field, these materials can interfere with aircraft instruments. Options are

other transport modes or regional recycling activities (Oakdene Hollins Research & Consulting 2010).

7.8.2.2 Dismantling

Recycling of magnets from consumer devices usually requires a costly and extensive dismantling. The magnet, usually quite small, is to be demagnetized before separation from iron parts, if possible. When the magnet is embedded in plastic, there is extra work.

There are two types of NdFeB magnets, for example, in an HDD. The spindle motor uses a resin-bonded magnet, and the voice coil motor (VCM) uses a sintered magnet. Shredding is the process currently used to destroy the data in HDDs. While shredding, the magnets break up into tiny pieces. However, being strongly magnetic, the granules stick to whatever iron part they contact in the waste and in the shredder. Additional process steps become necessary to isolate the metal fractions. Demagnetization of the magnets before they are put through any type of dismantling operation simplifies the whole process.

Industrial demagnetization is carried out by either heating the magnets to above the Curie temperature or treating the magnets in a strong magnetic field (Miura 2011) applied opposite to the original magnetizing direction. The thermal method uses simple equipment but involves heating a large device along with, usually, a small magnet. The demagnetizing apparatus is, on the other hand, expensive and treats only small amounts of wastes at a time.

The present industrial processes for treating the shredder residues are based on smelting. The rare earths, if present in the smelter, charge oxidize and always end up in the slag phase in a diluted form. The rare earths are either recovered from the smelter slag or, better still, removed from the waste stream before they are smelted.

The removal of rare-earth magnets from EOL products before they are shredded or smelted has been a serious issue in the overall recycling operation. Besides, the resin-bonded magnets generate a weaker magnetic field and do not reveal themselves easily.

Machines for dismantling magnets from various devices have been developed (Baba et al. 2013; Tanaka et al. 2013). The dismantling apparatus for HDDs relies on impact and vibration and is described by Nemoto et al. (2011). More elaborate actions are required for retrieving magnets from compressors and laundry machines (Arai 2010; Arai et al. 2011). Even explosives are used to remove the magnets from the rotor of alternating-current (AC) compressors (Wang et al. 2011). The recovery of high-purity (95–97% pure) magnet powder from VCMs of HDDs has been described by Oki et al. (2011) and Oki (2011).

A method to separate sintered NdFeB magnets from HDDs using hydride decrepitating was investigated at the University of Birmingham (Walton and Williams 2011; Walton et al. 2012). On exposure to hydrogen at atmospheric pressure, NdFeB absorbs hydrogen exothermically, and the material disintegrates to a coarse powder. The nickel coating on NdFeB also flakes away from the surface during hydrogen treatment. However, before exposure to hydrogen, the HDDs are sectioned to remove

the VCM corner. After hydriding, the cut section of the HDDs is rotated in a porous drum to liberate the hydride magnet alloy powder and nickel flakes. Nickel flakes are separated from the magnet alloy hydride by physical processing, and the residual nickel content in the magnet alloy powder could be brought down to <325 ppm. The powder so obtained from HDDs can be directly used to make sintered magnets or resin-bonded magnets.

In the best-case scenario, properties of magnets from reprocessed alloy powders could match the properties of magnets made from powder from primary processing (Harris et al. 2012; Shriden et al. 2012; Walton and Williams 2011; Walton et al. 2012; Zakotnik et al. 2006, 2008a, 2009). This is more likely in the reprocessing of HDD materials because the composition of these magnets has changed little, if at all, over the years and also because the various manufacturers use alloys of more or less the same composition for making magnets for HDDs.

Methods involving chemical attack for processing can handle mixed scraps that contain magnets with a large compositional range. There are a number of electronic devices that contain very small quantities of NdFeB incorporated in a complicated physical framework. The retrieval of magnets here almost always involves shredding. Removal of magnets from shredded waste is a challenging operation, and the compositional range of magnet material recovered therefrom would make them unsuitable for direct remaking of magnets. Chemical treatment by hydrometallurgical and/or pyrometallurgical processing, described in detail earlier, would be needed.

7.8.2.3 Samarium–Cobalt

The processing of samarium magnets is simpler because, (1) there is no protective coating on the magnet, (2) there is essentially one rare earth in the magnet, and (3) the elements in the magnet material are separable by simple chemical operations.

7.8.2.4 NdFeB

Hydrometallurgical treatments for NdFeB have been more elaborately investigated than Sm–Co, and the initial approaches were extensions of processes that worked for samarium–cobalt scrap. The issues with NdFeB are the 72% iron content (not an attractive recyclable component), the presence of nickel protective coating, and the rare-earth portion comprising Dy, Tb, and Pr in addition to Nd.

7.8.2.5 Mixed Sm–Co and Nd–Fe–B Scrap

The feasibility of recycling a mixed $SmCo_5$ and NdFeB swarf was investigated by Lyman and Palmer (1992, 1993b). A flotation leaching process was used. $SmCo_5$ concentrates in the froth, NdFeB swarf is dissolved by H_2SO_4, and the grinding medium contaminant sinks. Solvent extraction processing of mixed scrap was investigated by Niinae et al. (1994) as a part of an oxidative roasting–hydrochloric acid leaching–solvent extraction scheme. The solvent combinations of PC88A/tri-*n*-octylphosphine oxide (TOPO) and PC88A/TOA were found more suitable for the extraction of Nd and Sm compared to PC88A alone.

7.9 NICKEL–METAL HYDRIDE BATTERIES

The starting material for rare-earth recovery from batteries is almost always used (postconsumer) NiMH batteries. The objective of recycling here (JOGMEC 2011) is efficient recovery of Ni, Co, and rare earths/misch metal from waste NiMH batteries and refining of the recovered metals for reuse in new batteries.

Rechargeable batteries of the Ni–MH type were developed in 1989 and commercialized within a year in Japan and eventually all over the world. Presently, they have replaced, almost totally, the Ni–Cd batteries on account of higher capacity, reliability, safety, and cost-effectiveness (Itoh and Machida 2011), and they even score over the technically superior lithium-ion batteries in terms of cost and safety in heavy-duty applications. One of the important and emerging uses of Ni–MH batteries is in HEVs. Nearly 60% of the use of NiMH batteries is accounted for by the HEVs. The market of NiMH batteries for HEVs is projected to be worth USD 2.3 billion by 2015 (Rodrigue and Mansur 2010).

The NiMH battery has for a positive electrode a porous nickel plate, and the negative electrode is a porous nickel plate and a hydrogen-absorbing alloy. The alloy is an AB_5 type intermetallic where A is lanthanum and B is nickel. Nickel may be partially substituted in the alloy with cobalt, and lanthanum is substituted with the cheaper misch metal, with some performance penalty. The hydrogen absorber alloy has compositions like $La_{0.8}Nd_{0.2}Ni_{2.5}Co_{2.4}Si_{0.1}$, $La_{0.8}Nd_{0.2}Ni_{2.5}Co_{2.4}A_{l0.1}$, $MMNi_{3.55}Co_{0.75}Mn_{0.4}A_{l0.3}$, and $MMNi_{3.5}Co_{0.7}A_{l0.8}$. The misch metal composition (in wt.%) is also variable, e.g., (1) 50–55Ce, 18–28La, 12–18Nd, or 4–6Pr; (2) 50La, 30Ce, or 14Nd (Heegn and Rutz 2009); or (3) 40La, 38Nd, 12Ce, or 11Pr (Rodrigue and Mansur 2010).

The rare earth-containing portion of the Ni–MH batteries, i.e., the hydrogen-absorbing alloys from the negative electrode, can be concentrated by physical methods. Batteries subjected to cooling, crushing, grinding, and wet classification yield portions of fine rare earth-enriched particles (Lupi et al. 2000). Alternatively, the crushed material (<75 μm in size) was also enriched by magnetic separation (Ito et al. 2009, 2010).

Processes described earlier on in the sections on both pyrometallurgical and hydrometallurgical options in recycling NiMH batteries are useful (Table 7.5). Actual recycle volumes resulting in rare-earth recovery are very modest even as of now.

7.10 PHOSPHORS

An overview of the recovery and recycling methods for rare earths from fluorescent powder containing Y, Eu, La, and Ce has been provided by Mei et al. (2007). The recovery of yttrium and europium from lamps, TV tubes, and computer monitors was investigated by Rabah (2008) and Resende and Morais (2010). The recycling of yttrium and europium from discharge lamps and fluorescent lamps was investigated by OSRAM (2009) and Kasprzak (2007). The management and recycling of waste fluorescent lamps for recovery of rare earths was studied by Guarde et al. (2010).

There are five major rare earths used in phosphors. They are cerium, europium, terbium, yttrium, and lanthanum. The first three are optically active due to their 4*f* electrons, and the last two are optically inactive. Rare-earth phosphors are used in large fluorescent lamps and compact fluorescent lamps (CFLs) for general illumination, and in a variety of displays—cathode ray tubes (CRTs), small fluorescent lamps used in LCD backlights, and white LEDs and plasma display panels.

Originally, fluorescent lamps used for general illumination used calcium halophosphate [$Ca_{10}(PO_4)_6FCl$:Sb,Mn] as the fluorescent material. In recent times, there has been an increase in the use of three-band phosphor tubes that provide better color purity and luminous efficiency (Horikawa and Machida 2011). Halophosphate phosphors do not contain rare earths, and the three-band phosphors are rare earth based. While the straight-tube fluorescent lamps can have phosphors of the halophosphate or three-band types, CFLs have only three-band–type phosphors. The issue with CFLs, which come in different sizes and shapes, is to disassemble them and recover the three-band phosphors completely. A mechanical process makes it possible to remove 100% of three-band phosphors with a quality of 96% (Tanaka et al. 2013).

The recycling of rare-earth phosphors is challenging. The emission characteristics are sensitive to the concentration and purity of the rare earths in the phosphors. There is variety in the types of fluorescent tubes; the type of phosphor and its content depend on the type of fluorescent tube. Phosphors undergo degradation during use (Horikawa and Machida 2011).

As regards the quantity of rare earths used in phosphors and the extent of their recycling, data are available in Germany and Japan for two different years. The data are relatively old but do highlight the quantities one deals with when considering rare earth-containing phosphors for use and for recycle.

As of 1998, in Germany alone, 200 tons of fluorescent lamps were disposed, of which 80 tons were three-band tubes (Radeke et al. 1998). These tubes (three band) contained 20 tons of yttrium oxide and 600 kg europium. In 2005, in Japan, 140 tons of Y_2O_3 and 8.5 tons of terbium oxide (Tb_4O_7) were consumed for making lamps for illumination. About 20% of this quantity could be recycled material (Tanaka et al. 2013).

The phosphors in EOL fluorescent lamps are a rich source of scarce rare earths europium and terbium apart from yttrium. In the overall scheme of recycling of scrap phosphors, there are many possibilities: (1) the lamp phosphors may be directly reused in new lamps, (2) the individual phosphor components may be separated from the scrap phosphor for separate reuse, and (3) they may be chemically processed to get back their rare-earth content.

7.10.1 Composition of Recycled Lamp Phosphor

The rare-earth phosphors used in fluorescent lamps are listed in Table 7.8 (Justel et al. 1998; Ronda 1995; Yu and Chen 1995). The chloroapatite blue phosphor is less common, and the halophosphate phosphor is usually mixed with Y_2O_3:Eu^{3+} for good color rendering. Scrap lamp phosphors for recycling also contain significant quantities of alumina and silica. These are materials of a barrier layer that is always present

TABLE 7.8
Commercially Used Fluorescent Lamp Phosphors

Name	Composition	Color
YOX	$Y_2O_3:Eu^{3+}$	Red
LAP	$LaPO_4:Ce^{3+}, Tb^{3+}$	Green
CBT	$(Gd,Mg)B_5O_{12}:Ce^{3+}, Tb^{3+}$	Green
CAT	$(Ce,Tb)MgAl_{11}O_{19}$	Green
BAM	$BaAl_{10}O_{17}:Eu^{2+}$	Blue
Chloroapatite	$(Sr,Ca,Ba,Mg)_5(PO_4)_3Cl:Eu^{2+}$	Blue
Halophosphate	$(Sr,Ca)_{10}(PO_4)$, $(F,Cl)_2:Sb^{3+}$, Mn^{2+} {check}	Broadband white

Source: Justel, T. et al., *Angew. Chem. Int. Ed*., 37, 1998; Yu, Z.S. and Chen, M.B., *Rare Earth Elements and Their Applications*, Metallurgical Industry Press, Beijing, 1995; Ronda, C.R., *J. Alloys Compd.*, 225, 1995.

between the phosphor layer and glass surface. The barrier layer prevents attack of the glass envelope by mercury and also reflects ultraviolet (UV) radiation back into the lamp (Binnemans et al. 2013).

At the end of their useful life, the fluorescent lamps are collected in many countries because they are not only recyclable but also considered hazardous waste due to the presence of mercury. Almost all the components—glass, metal, plastics, phosphor powder, and mercury—are recycled. It is relatively easy to remove phosphors from straight fluorescent lamps. The ends are cut off, and phosphor is removed by air blowing. Since a large fraction of phosphor used in straight fluorescent lamps is the halophosphate type, the phosphor recovered from fluorescent lamp wastes would be a mixture of halophosphates and the three-band phosphors. Removing phosphors from CFL is more complex. Used CFLs are crushed and shredded, and the broken glass pieces are separated from phosphor powder by sieving. It is usually not easy to completely separate phosphor powder from glass particles. Glass, if present, is likely to add impurities in subsequent chemical processing.

In countries where REEs are not recovered from phosphors, they are stored in containers or landfilled after ensuring that mercury is in a nonleachable form. In such a situation, the chemistry of the phosphor for recycling can become progressively more complex as phosphors from various sources and devices such as CRTs of old TVs and computer monitors also find their way to the storage.

Considering various lamp phosphors and the country-wise variations possible in the products, the lamp phosphor fraction available for recycling may contain the following elements: the six phosphor-relevant REEs (La, Ce, Eu, Gd, Tb, and Y); elements like Al, Si, P, and Ca in relatively large concentrations; and Ba, Sr, Mg, Mn, Sb, Cl, F, Hg, Pb, and Cd in relatively minor amounts. Iron, notably, is not expected (Binnemans et al. 2013).

Mercury is invariably present in fluorescent lamps and in CFLs. The amount varies depending on the type of lamp and the year of manufacture, from as much

as an average of 33 mg per lamp in older units to as low as 2.5 mg per lamp in the recently manufactured CFLs. During prolonged use, part of mercury gets permanently bound to the phosphor. The removal of mercury is an issue in the recycling/reprocessing of lamp phosphors. Vacuum treatment at 400–600°C will work, but the mercury will not be fully removed, especially the portion that got incorporated as an inorganic mercury compound. An effective method is to leach out the mercury during the dissolution of the lamp phosphor and trap the mercury from the leach liquor using resins with mercury-binding functional groups (Binnemans et al. 2013).

7.10.2 Physical Separation

In the recycling of lamp phosphors, separation of three-band phosphors from the halophosphates is an important step. This is done by a dry separation process. Takahashi et al. (1999, 2001a,b) used a centrifugal pneumatic separator to process the phosphor mixture. A phosphor sludge comprising a rare-earth phosphor, halophosphate-type phosphor, and glass was separated into components with a 70% recovery of the rare-earth phosphor in the sludge for further processing. The rare-earth content of this component was about 30%, which was 100% more than the rare-earth content of the phosphor sludge.

The original phosphor sludge could also be separated into components by more efficient wet methods. The difference in the specific gravities of halophosphate-type phosphors (3.07) and rare-earth phosphors (4.34–5.23) is used in a heavy media separation (CH_2I_2; specific gravity, 3.3). In Japan, studies have been carried out with waste phosphors collected during the recycling of EOL fluorescent lamps to obtain a highly enriched phosphor product as starting material for better extraction of REEs. The work was aimed at separating low-density calcium halophosphate phosphors from the high-density rare earth-activated phosphors through dense-medium centrifugation (with diiodomethane as the organic dense medium). The outline of the overall process is given in Figure 7.18. Using diiodomethane, heavy media separation by centrifugal treatment also gave improved-grade RE phosphor as a sediment. During the investigations, a product assaying approximately 49% rare earth-activated phosphor was collected with over 97% recovery. Besides, nearly all of the diiodomethane used as a dense medium could be recovered and reused. The authors, Hirajima et al. (2005a), noted that the cost of the chemical process for rare-earth recovery could be lessened, and its efficiency could be improved with such a highly enriched (49% RE-activated phosphor) product as starting material. The halophosphate was recovered as the floated component, and the rare-earth phosphors sank. There was a fourfold to fivefold increase in the concentration of the rare-earth phosphors (Takahashi et al. 1999, 2001a,b). As of now, heavy media separation remains too expensive for industrial-scale use. To ensure cost-effectiveness, Hirajima et al. (2005a) attempted gravity separation using water as the medium in a hydrocyclone. Even though separation was achieved, it did not meet the standards of industrial feasibility. Hirajima et al. (2005b) also attempted a separation of phosphors by flotation.

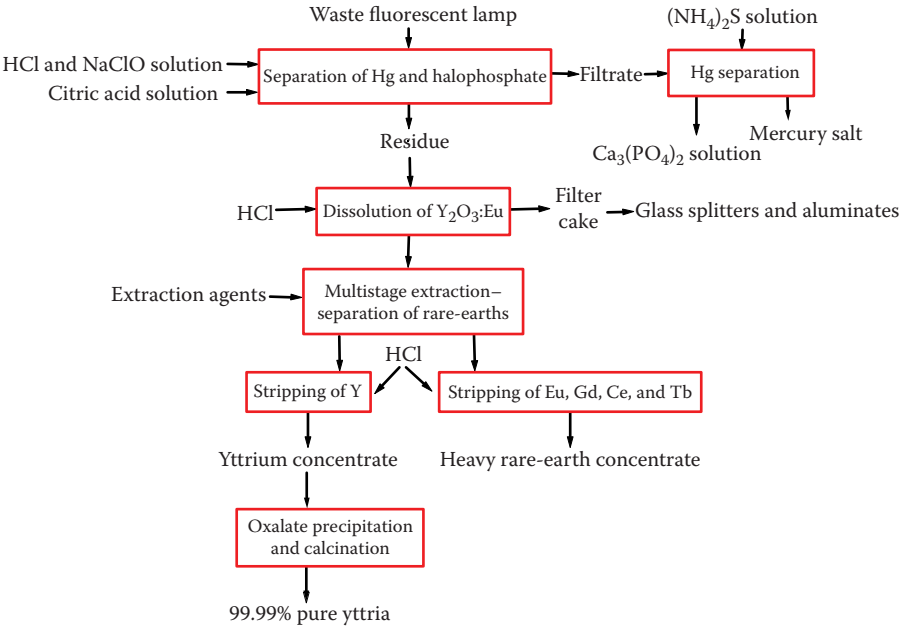


FIGURE 7.18 Extraction processes for fluorescent lamp waste. (From Radeke, K.H. et al., *Chem. Technik* 50(3): 126, 1998; Reprinted from Bunzli, J.C.G., Pecharsky, V.K. (Eds.), *Handbook on the Physics and Chemistry of Rare Earths*, vol. 43, Chapter 255, Tanaka, M., Oki, T., Koyama, K., Narita, H. and Oishi, T., Recycling of rare earths from scrap, pp. 159–212, Copyright 2013, with permission from Elsevier.)

7.10.3 Separation of Individual Phosphors

The particle size of phosphors is <10 μm, which is less than the typical particle size (~50 μm) of ground minerals. Hence, mineral processing techniques like gravity separation using bulk properties are not particularly effective. The way out could be to use a separation technique based on surface properties.

Froth flotation was attempted by Hirajima et al. (2005a) for separating rare-earth phosphor from halophosphate phosphor from an actual phosphor mixture provided by a recycler. The results obtained were strongly dependent on both the type of collector used and the pH. The possibility of totally removing halophosphate phosphor from the mixture by flotation was indicated at pH values below 4.5. Rare-earth phosphors were left behind. Conventional froth flotation was not effective for further separating the phosphors of individual rare earths from the mixture.

In order to separate the mixture of three lamp phosphors Y_2O_3:Eu^{3+}, $LaPO_4$:Ce^{3+},Tb^{3+}, and $(Sr,Ca,Be,Mg)_5(PO_4)_3Cl$:$Eu^{2+}$, a two-step, two-liquid flotation process using N,N-dimethyl formamide (DMF) as the polar phase and heptane as the nonpolar phase was used by Otsuki et al. (2008). The two liquids are immiscible.

In the first step, using dodecyl ammonium acetate as the surfactant, the green phosphor $LaPO_4$: Ce^{3+},Tb^{3+} could be collected at the interface of the two liquids,

while the mixture of other two phosphors was in the polar phase. In the second step, using the surfactant sodium 1-octane sulfonate, the blue phosphor $(Sr,Ca,Be,Mg)_5(PO_4)_3Cl:Eu^{2+}$ was collected at the interface, while the red phosphor $Y_2O_3:Eu^{3+}$ remained in the DMF phase. The recovery and purity of each of the three phosphors were more than 90%. The separation of this mixture of three phosphors using other surfactants has also been reported (Mei et al. 2009a,b; Otsuki et al. 2008).

Another possibility to separate the phosphor particles relies on the differences in magnetic susceptibility (Horikawa and Machida 2011). Phosphors with high terbium content [$LaPO_4$: Ce^{3+},Tb^{3+}, $(Gd,Mg)B_5O_{12}:Ce^{3+}$,Tb^{3+}, and $(Ce,Tb)MgAl_{11}O_{19}$] are substantially more paramagnetic compared to europium-based phosphors or halophosphate phosphors. A magnetic separation could be used for them. Akai et al. (2011) achieved color separation of three-band phosphors using strong magnetic fields in in-plant recycling trials during the production of phosphors. A high-gradient (2T) magnetic separator (HGMS) was used, and the separation was performed in a column on a phosphor mixture dispersed in deionized water. The feasibility of separating BAM ($BaAl_{10}O_{17}:Eu^{2+}$) and YOX ($Y_2O_3:Eu^{3+}$), even though their magnetic susceptibilities are close to each other, was demonstrated by applying a combination of several surfactants and repeating the separation procedure.

Radeke et al. (1998) have suggested a process for the separation of mercury, calcium, yttrium, and heavy rare earths in fluorescent lamp waste containing both halophosphate and three-band phosphors. The process outline is shown in Figure 7.18. The separation of mercury and the halophosphate components from the three-band phosphor is done by chemical treatment. The residue containing rare-earth phosphor (Y_2O_3:Eu) is dissolved in hydrochloric acid followed by further processing by a multistage extraction separation of rare earths. The purity of yttrium obtained as an end product was 99.99%. Radeke et al. (1998) noted that the cost–benefit estimations point to a profitable operation of the process.

Although reuse in new lamps is an attractive option for the separated phosphor compounds, it is not practical except in very special circumstances (Binnemans et al. 2013). The physicochemical methods of separation of phosphor mixtures do not yield pure enough product for direct reuse. More importantly, the phosphors, during use, have undergone various types of degradation and are no longer equivalent to the new phosphors, even if they could be physicochemically separated in pure enough form. The separation methods can also introduce changes in particle size distribution. There could also be variations in the original phosphors from different manufacturers with respect to the purity of rare-earth oxides. In general, physicochemical separation methods can, at best, be considered pretreatment processes for phosphor mixtures before they are put through processes for the recovery of their rare-earth content.

Reclaimed lamp phosphor mixtures are a reliable source of the rare earths Eu, Tb, and Y. The total REO content in lamp phosphors could be as high as 28 wt.%, but in the recycled fractions available for REE recovery, the REO content is usually about 10% (Wang et al. 2011). Chemical compounds of rare earths constituting the phosphors are quite resistant to normal leaching media, but leaching/dissolution is necessary for the separation and recovery of the rare earths contained.

Various phosphor components respond differently to attempts of chemical attack/dissolution, and this has resulted in a number of processes for rare-earth recovery in this source. The range of chemical attacks investigated for solubilizing the REE value in phosphors is listed in Table 7.9. Once in solution, the rare earths are separated and recovered by the solvent extraction and selective precipitation processes.

Dilute acids are good enough for the dissolution of halophosphates and YOX. The phosphate and aluminate phosphors are difficult to dissolve and need harsh conditions. Novelties such as mechanochemical treatments and supercritical fluid extraction ensure/enhance complete dissolution under milder conditions (Zhang and Saito 1998; Zhang et al. 2000). Mechanochemical treatment using a planetary mill was shown to cause disordering of the crystal structures of the phosphor and thus enables leaching under mild conditions: yttrium, europium, terbium, lanthanum, and cerium were dissolved in 1 kmol/m^3 HCl at room temperature after the mechanochemical treatment for 2 h with more than 80% efficiency (Zhang et al. 2000). The green phosphor ($LaPO_3$:Ce,Tb) is much less soluble than the red and blue phosphors. Even with several kilomoles per cubic meter of acid concentration, the green phosphor is not leached at all, while other phosphors are dissolved. Takahashi et al. (1996) used concentrated sulfuric acid, and Zhang et al. (2000) applied mechanochemical treatment in order to improve leaching of the green phosphor. In a project of recycling phosphor waste managed by JOGMEC (2011), alkaline fusion followed by HCl leaching is used to dissolve all the rare earths in the waste phosphor. A basic flow sheet is shown in Figure 7.19. Solvent extraction is then used to separately recover yttrium, terbium, and europium. Nitric acid dissolution of alumina from a barrier layer in fluorescent tubes, along with phosphors, has been shown to be advantageous by Yang et al. (2012). Subsequently, in solvent extraction, $Al(NO_3)_3$ can function as a salting-out agent for the extraction of rare earths from the aqueous to an organic phase.

Takahashi et al. (2001a) proposed a flow sheet, given in Figure 7.20, for the recovery of yttrium and europium oxides from fluorescent lamp waste. Under the leaching conditions given, 92% of yttrium and 98% of europium from the powder dissolved. Some other rare earths remained as the phosphate residue. The sequence of chemical dissolution and precipitation finally yielded an over 98% pure rare-earth oxide mixture that contained both yttrium and europium. The yield of each of these two rare earths in the oxide mixture was about 65%. Several variants of this flow sheet were also reported by Takahashi et al. (1999). The liquor obtained after sulfuric acid leaching was subjected to solvent extraction with PC88A. Separation of Y and Eu was accomplished, resulting in 99.3% Y_2O_3 and 97% Eu_2O_3 in the end. Total rare-earth yield remained at 65%.

As another alternative, from the same leach liquor, yttrium was first extracted at pH 1.5, and then europium was extracted at pH 2. None of the impurities listed in the flow sheet was extracted at these pH conditions. The assay of the oxides obtained was (in wt.%) 99.7 Y_2O_3, 0.2 CaO, 0.05 Sb_2O_3, and 90 Eu_2O_3, 1.95 CaO and 0.40 Sb_2O_3 (Takahashi et al. 2003).

Chelating resins were also found useful for the separation of rare earths in phosphor waste. In the sequence investigated by Takahashi et al. (1996), the phosphor powder was leached in two steps. Leaching with 1.5 kmol/m^3 sulfuric acid got Y

TABLE 7.9
Options for the Leaching of Lamp Phosphors

Phosphor	Leachant	Conditions	Results	Reference
$Y_2O_3:Eu^{3+}$	Dilute acids			Binnemans et al. 2013
$LaPO_4:Ce^{3+}, Tb^{3+}$	Molten Na_2CO_3	1000°C		Porob et al. 2012
$(Ce,Tb)MgAl_{11}O_{19}$	Molten Na_2CO_3	1000°C		Porob et al. 2012
$BaAl_{10}O_{17}:Eu^{2+}$	Molten Na_2CO_3	1000°C		Porob et al. 2012
Three-band phosphor mixture	HCl (4 mol/L) + H_2O_2 (4.2 g/L)		Strong leachant	Wang et al. 2011
$Y_2O_3:Eu^{3+}$	Acids	Mechanical activation (ball milling)	Readily dissolved	Mio et al. 2001
Spent fluorescent lamps ($Y_2O_3:Eu^{3+}$ and halophosphate mixture)	H_2SO_4–HNO_3 mixture	Pressure leaching, 125°C, 5 MPa	96.4% Y and 92.8% Eu dissolved	Rabah 2008; Shimizu et al. 2005
Lamp phosphors	Supercritical CO_2 containing TBP complexes of HNO_3 and water	15 MPa, 60°C, 2 h	>99.5% Y and Eu present in the phosphor mixture leached	Shimizu et al. 2005
Lamp phosphors	TBP–HNO_3–H_2O	At atmospheric pressure	<40% Y and Eu extracted	

(*Continued*)

TABLE 7.9 (CONTINUED)
Options for the Leaching of Lamp Phosphors

Phosphor	Leachant	Conditions	Results	Reference
Phosphor powder	HCl, HNO_3, H_2SO_4, and ammonia		HNO_3 dissolves largest % yttrium; HCl and HNO_3 dissolve similar percentage of yttrium; ammonia gives very low yttrium recovery; H_2SO_4 preferred because of less codissolution of Ca, Pb, and Ba	De Michelis et al. 2011
Y_2O_3:Eu^{3+} and halophosphate mixture	Dilute HCl Dilute H_2SO_4/HCl	<30°C 60–90°C	Only halophosphate dissolves Y_2O_3:Eu^{3+} dissolved	
$LaPO_4$:Ce^{3+}, Tb^{3+}	H_2SO_4	Hot concentrated, 120–230°C	Dissolved	Otto and Kasprzac 2012
(Ce,Tb)$MgAl_{11}O_{19}$	NaOH	35% NaOH at 150°C in an autoclave	Attacked	Otto and Kasprzac 2012
$BaAl_{10}O_{17}$:Eu^{2+}	NaOH	35% NaOH at 150°C in an autoclave	Attacked	Otto and Kasprzac 2012
(Ce,Tb)$MgAl_{11}O_{19}$	NaOH	Molten alkali	Attacked	Otto and Kasprzac 2012
$BaAl_{10}O_{17}$:Eu^{2+}	NaOH	Molten alkali	Attacked	Otto and Kasprzac 2012

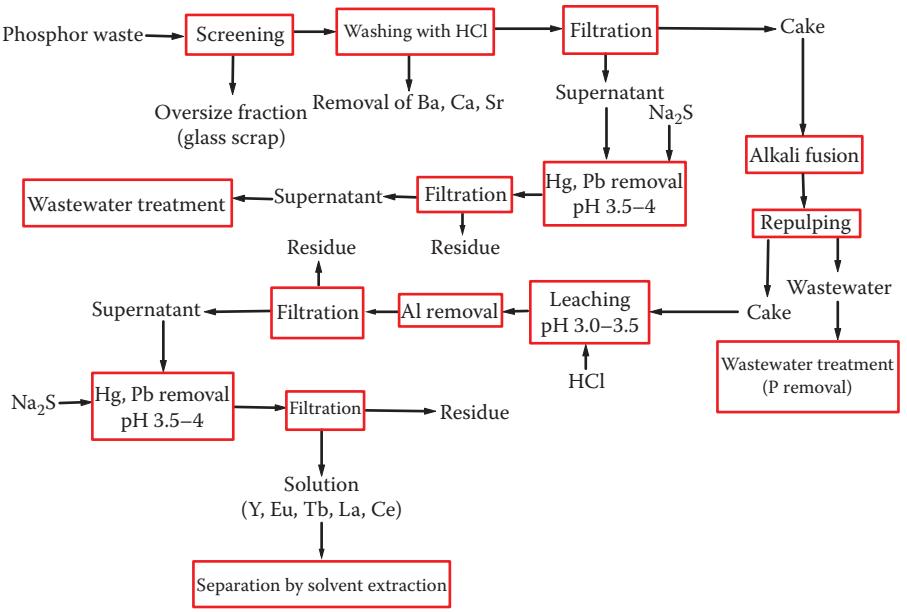


FIGURE 7.19 Pretreatment process for phosphor waste. (Reprinted from Bunzli, J.C.G., Pecharsky, V.K. (Eds.), *Handbook on the Physics and Chemistry of Rare Earths*, vol. 43, Chapter 255, Tanaka, M., Oki, T., Koyama, K., Narita, H. and Oishi, T., Recycling of rare earths from scrap, pp. 159–212, Copyright 2013, with permission from Elsevier.)

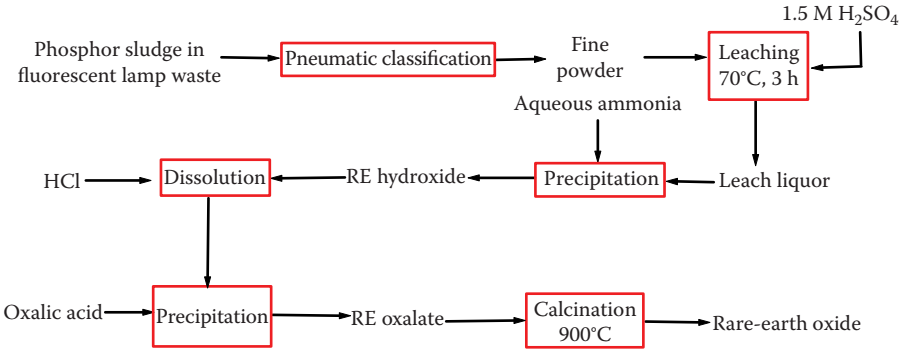


FIGURE 7.20 Recovery of europium and yttrium oxides from fluorescent lamp wastes. (From Takahashi, T. et al., *J. MMIJ* 117: 579, 2001; Reprinted from Bunzli, J.C.G., Pecharsky, V.K. (Eds.), *Handbook on the Physics and Chemistry of Rare Earths*, vol. 43, Chapter 255, Tanaka, M., Oki, T., Koyama, K., Narita, H. and Oishi, T., Recycling of rare earths from scrap, pp. 159–212, Copyright 2013, with permission from Elsevier.)

and Eu in solution, and then leaching the residue with 18 kmol/m^3 sulfuric acid solubilized the rare earths La, Ce, and Tb. To accomplish the separation of rare earths, iminodiacetic acid-type resin was used for the Y–Eu fraction and nitrilotriacetic acid-type resin for the La, Ce, and Tb fraction. The separated rare earths were precipitated as oxalates and calcined to oxides. The yield and purity of each of the oxides were 50% and 99.8% Y_2O_3, 50% and 98.3% Eu_2O_3, 30% and 96% La_2O_3, 30% and 87.3% Ce_2O_3, and 90% and 91.8% Tb_4O_7.

In CRTs, used until recently for color television and computer monitors, only the red phosphor contains rare earths. The major component in the phosphor is zinc, present as the compound ZnS. The CRT typically had $Y_2O_2S.Eu^{3+}$ for red, ZnS:Cu for green, and ZnS:Ag for blue. In the beginning, $YVO_4:Eu^{3+}$ was used as the red phosphor, but it was eventually replaced by $Y_2O_2S \cdot Eu^{3+}$. As regards processes for recycling, any acid treatment of this phosphor mixture released H_2S. This may be avoided by roasting the phosphor in air at 900°C to convert ZnS to ZnO, before acid dissolution. In a process investigated by Resende and Morais (2010) for recycling the phosphor coating powder collected from computer monitors, leaching with H_2SO_4 at room temperature dissolved over 95% of Y and Eu, and the solution was directly processed further by solvent extraction.

According to Dexpert-Ghys et al. (2009), alkali treatment of CRT phosphor was better than an acid attack. Interestingly, commercial-scale operations for the recycling of CRTs were focusing on the recycling of lead-containing glass and whatever metal values were there, but they did not recover rare earths from phosphor powder (Menad 1999).

7.11 GLASS-POLISHING POWDER

A large quantity of cerium oxide (CeO_2) is used as a glass-polishing compound. This is a localized bulk application, and almost all of the nearly 10,000 tons of ceria used annually in this application can be tracked (Sato and Kato 2010; Xu and Peng 2009) and recycled. In this application, which has been in vogue for several decades, slurry (10%) of CeO_2 in water is used as the polishing agent. The polishing occurs due to a combination of mechanical abrasion and chemical etching of the glass surface. The polishing powder gets contaminated by small silica particles picked up from the glass surface that was polished. At present, a flocculent containing aluminum chloride is added to the spent slurry to precipitate the powder, which is then dehydrated in a filter press and discarded as landfill. Hydrolysis of aluminum chloride in the flocculent results in the formation of alumina that also contaminates the polishing powder (Table 7.10). Recycling of spent polishing powder needs to take care of these impurities and also ensure that the recycled product conforms to the strict specifications with respect to particle size distribution, which is essential for high-quality polishing action.

A method developed by Terziev and Minkova (1997) for the recycling yielded 0.8 kg of fresh material from every kilogram of spent cerium oxide polishing powder. The polishing-powder waste was dissolved in a HNO_3–H_2O_2 mixture, and the rare-earth content of the resulting solution was precipitated as carbonate. The carbonate was calcined to the oxide.

TABLE 7.10
Typical Composition of the Polishing Powder and Its Waste

	Content, Weight%	
Component	**Polishing Powder**	**Spent Polishing Powder**
La_2O_3	34.2	17.8
CeO_2	43.8	22.1
Pr_6O_{11}	3.4	2.3
Nd_2O_3	10.9	5.1
BaO	2.62	0.67
SiO_2		12.6
Al_2O_3		24.8

Source: Kato, K. et al., Nippon Kagaku Kaishi, 725–731, 2000; Tanaka, M. et al., Recycling of rare earths from scrap, in Bunzli, J.C.G. and Pecharsky, V.K. (eds.), *Handbook on the Physics and Chemistry of Rare Earths*, vol. 43, Chapter 255, Elsevier, Amsterdam, 2013.

Kato et al. (2000a,b), removed silica and alumina impurities from the spent polishing powder by treating with a concentrated (4 mol/kg) sodium hydroxide solution at 50–60°C for 1 h. Cerium oxide remains unattacked and could be filtered out from the solution that now contains all the alumina and silica. Kim et al. (2011) separated silica and alumina from spent polishing powder by froth flotation and by dissolution in a concentrated sodium hydroxide solution. The separated cerium oxide met the particle size standards of the original powder and was suitable for polishing applications. Earlier, Liang et al. (2009) had attempted flotation recovery of REO from a real sludge. Purity of the powder recycled was also only marginally better than the feed, and the yield was only 40%.

Recycling of polishing powder by a combination of acid leaching and solvent extraction has also been investigated (JOGMEC 2011; Yamada et al. 2010, 2011). Adachi et al. (Ozaki et al. 1999a,b) studied the chlorination–dry chemical vapor transport process to recycle REE from polishing powder.

7.12 CATALYSTS

7.12.1 Fluid Cracking Catalysts

In the past, the recycling of REEs from spent catalysts of both industrial and automotive origin was not practiced, possibly due to the low price of REEs. This is strikingly evident from a report from Germany (Hassan 2001) that all of the 9100 tons of spent fluid cracking catalyst (FCC) from catalytic cracking processes in German oil refineries (in 1998) were used as cement additives. In fact, the annual mass flow of approximately 600,000 t FCC catalysts that typically contain at least 2% REE point to a sizable potential for REE recycling from this particular application. Apart from technical process issues in recovering REE from catalysts, the

advantages of a robust and live business-to-business relationship between the catalyst suppliers and oil refineries augurs well for a nearly 100% collection rate of the spent catalysts for recycling. Such a scenario already exists for the platinum-group metals.

The rare-earth content of FCCs is about 3.5 wt.% REO. Lanthanum is the predominant component. Smaller amounts of cerium, praseodymium, and neodymium are also present (Yu and Chen 1995). Approximately 50% of the world production of lanthanum is consumed in this application. However, there has been hardly any industrial-scale recycling of rare earths from the spent FCC. Studies on recycling have mainly focused on leaching with acidic solutions (He and Meng 2011; Vierheilig 2012).

7.12.2 Automotive Exhaust Catalysts

In automotive exhaust catalysts, rare earths (mainly cerium) are present along with the precious metals Pt, Rh, and Pd. Presently, the focus worldwide is on the recovery of platinum-group metals from recycling of automotive catalysts. These are recycled by a pyrometallurgical processing (smelting) route whereby the precious metals are recovered (Felix and Vanriet 1994; Hageluken 1999, 2001). The rare earths accumulate in the slag and are not presently processed further for recovery.

As in the case of other recyclable rare earth–containing devices, processes have been investigated for dismantling of the EOL exhaust gas catalytic converters of automobiles and concentrating the rare earth in the feed for recycling. Kim et al. (2010) have reported a two-step crushing procedure that increases the concentration of rare-earth metals in the feed by a factor of five.

7.13 OPTICAL GLASS

The addition of lanthanum to glass imparts to it a high refractive index and low dispersion, making it very suitable for the making of lenses (Yu and Chen 1995) for cameras, microscopes, and binoculars. The La_2O_3 content of the glass can exceed 40%, and only very high-purity rare-earth oxide devoid of any coloring rare earth or transition metal impurity can be used. Apart from lanthanum oxide, and in addition to it, Y_2O_3 and Gd_2O_3 are also used as additives to glass. Annual world production of optical glass is 20,000 tons, pointing to a potential of nearly 2000 tons of REO from recycling. However, till recently, there has been no commercial level recycling of REO from this source.

A hydrometallurgical process to treat spent borosilicate optical glass for recovery of rare earths has been described by Jiang et al. (2004, 2005). The rare-earth content of the glass is converted to (water-insoluble) rare-earth hydroxide by treatment with hot (140°C), concentrated (53 wt.%) NaOH. The hydroxide is then leached with 6 M HCl at 90°C to produce a rare-earth chloride solution for further processing. The schematic flow sheet is given in Figure 7.21. From a glass containing 43.12% La_2O_3, 9.37% Y_2O_3, and 4.60 wt.% Gd_2O_3, by this process, all of the yttrium and gadolinium and over 99% of the lanthanum could be recovered.

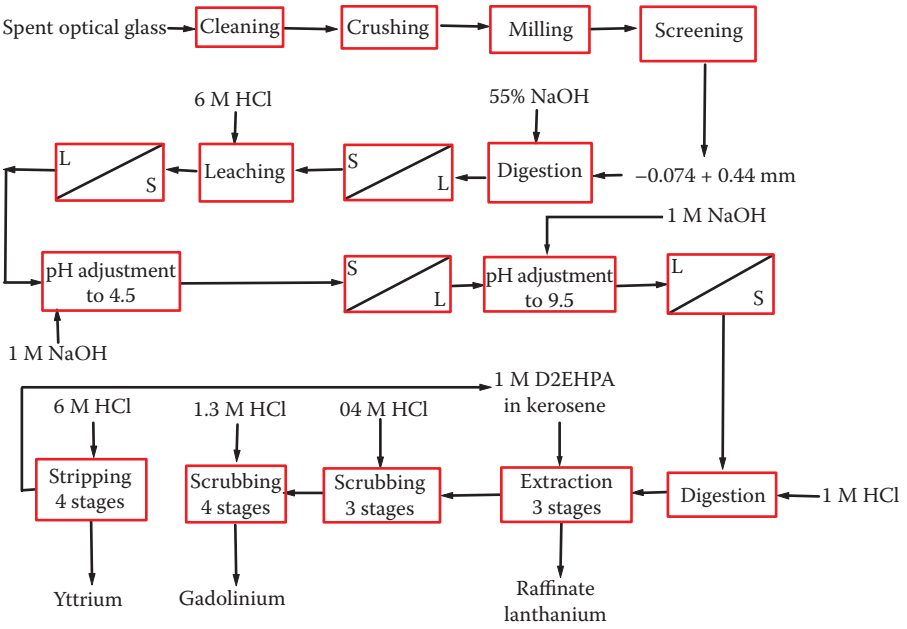


FIGURE 7.21 A hydrometallurgical process to treat spent borosilicate optical glass for recovery of rare earths. (From Jiang, Y.R. et al., *Can. Metall. Q.*, 43: 431–438, 2004; Jiang, Y.R. et al., *Hydrometallurgy*, 76: 1–9, 2005; Reprinted from Bunzli, J.C.G., and Pecharsky, V.K. (Eds.), *Handbook on the Physics and Chemistry of Rare Earths*, vol. 43, Chapter 255, Tanaka, M., Oki, T., Koyama, K., Narita, H. and Oishi, T., Recycling of rare earths from scrap, pp. 159–212, Copyright 2013, with permission from Elsevier.)

7.14 MISCELLANEOUS MATERIALS

Red mud is the solid waste generated from aluminum production. It could have accumulated rare earths that are often occurring in bauxite. An investigation on recovering REE from red mud was reported by Wang et al. (2005). The process broadly consists of roasting the red mud followed by leaching the roasted material with HCl. From the leach liquor, scandium and other rare-earth oxides are separated.

Electronic scrap is often processed for recovery of many metals in pyrometallurgical plants. Due to their great affinity for oxygen, the REEs undergo oxidation and become part of the slag. Presently, the slag is not processed for rare-earth recovery.

7.15 SUMMARY

The advantages and necessity of recycling of rare earths are irrefutable, real, and also urgent. Almost all of the major rare earth-bearing devices are technologically amenable to recycling. The sheer number of processes that have been developed for recycling not only speak of the many possibilities of recycling but also highlight the prevailing uncertainty as to the best process.

One of the advantages of recycling is the preservation of value addition to the rare earths. Value addition to rare earths occurs at two major stages. One is when the individual rare earth is separated from other co-occurring rare earths, and the other is when the pure separated rare-earth compound is reduced to the metal or alloy. The best recycling routine will preserve both these stages of value addition. Liquid metal extraction processes operating in a closed loop are an example of such a possibility. In this route, there is no possibility of separating co-occurring rare earths into individual members.

The separation of co-occurring rare earths into individual members is necessarily accomplished by hydrometallurgical routes after taking the rare-earth values from the scrap into solution. Here, the emphasis is to conserve the resources and stabilize the supply of critical elements like Dy, Tb, Nd, and Eu rather than preserving value addition. Many of the rare earth-containing devices have characteristically long device lives. Thus, the establishment of a comprehensive rare-earth cycle (like the water cycle and nitrogen cycle in nature) wherein the rare-earth inventory in the industrial stream is closely controlled by human intervention may take time but remains within the realm of technological possibility. There may be no escaping this coordination because, as of now, primary supply of critical rare earths from natural resources may not be sufficient to meet the growth of demand in the not-too-distant future, even if China eases all the restrictions. Recycling is here to stay, forever.

The development of a technically efficient, commercially viable, and environmentally benign recycling system for rare earths needs to be complemented by (1) possibly more efficient use of rare earths and (2) the substitution for critical rare earths in their many applications by material and process changes. This aspect of the rare-earth technology has slowly and surely moved to center stage in informed discourses on the future direction of the world rare-earth industry. Beyond the immediate corrections at the consumer level, necessitated by the production controls the dominant rare-earth producer, China, is implementing, it needs to be recognized that the long-term reliable and sustained supply of rare earths to meet the rapidly escalating world demand is everyone's, including China's, problem. Sooner, rather than later, the REE cycle will need to attain and maintain a situation like that of aluminum in that approximately 85% of all aluminum ever produced is still in use.

8 Analysis

8.1 INTRODUCTION

The importance of accurate and reliable techniques for the chemical characterization of rare-earth materials at various stages of their extraction processing cannot be overemphasized. The analysis of rare-earth materials is carried out for (1) the determination of total rare earths in materials like minerals, concentrates, compounds, alloys, and metals as well as process solutions; (2) the determination of individual rare-earth contents in a mixture of various rare earths; and (3) the determination of non-rare-earth metallic and nonmetallic impurities in rare earths. Until the early 1940s, routine rare-earth analysis was essentially confined to category (1) above (Banks and Klingman 1961). The rare earths were isolated from materials that hosted them and determined as a group by gravimetric methods. Much of the developments in the analytical characterization of rare earths—as with many other branches of rare-earth extractive metallurgy—have occurred since the 1940s.

8.2 CHEMICAL METHODS

The classical chemical methods, gravimetry and volumetry, are used for analysis of rare earths in certain instances. Gravimetry is useful essentially for the determination of rare earths as a group. Volumetry has been often used for the determination of individual concentrations of cerium and europium.

8.2.1 Gravimetry

For their determination, the rare earths may be precipitated from an aqueous solution as an oxalate, hydroxide, or fluoride. When precipitated as an oxalate, the rare earths get separated from Na, Al, Fe, Be, Ti, P, Ca, Mg, Mn, and Co if these elements are present in the solution. The precipitation of rare-earth oxalates is a simple and very effective method for the separation and determination of rare earths, but the conditions of precipitation demand careful attention (O'Laughlin 1979; Woyski and Harris 1963). On precipitation as hydroxides (by adding ammonia), the rare earths are separated from Ca, Mg, Mn, Co, and Na if these elements are present in solution. Rare earths, as a group, can also be precipitated as the fluorides. By this, there is separation from Al, Be, Si, Ti, P, Na, Nb, and Ta, if these elements are present in the solution.

Apart from the compounds mentioned for precipitation, the rare earths as a group can also be precipitated by organic precipitants (Hassan and Mahmoud 1982; Woyski and Harris 1963). Cerium(IV) also can be precipitated for analytical determination from a thorium-free rare-earth solution. The suitable compounds are Ce(IV) iodate or Ce(IV) periodate (Venugopalan and George 1956).

Amongst all the compounds, the precipitation as oxalate is most preferred. Ammonia precipitation is resorted to for separating the rare earths from an excess of alkali salts like NaCl and Na_2SO_4 present in the solution, before eventually determining the rare earths by oxalate precipitation. To ensure complete separation of rare earths from a substantial amount of impurities in solution, a double oxalate precipitation (a sequence of two oxalate precipitations), or a combination of ammonia and oxalate precipitation or fluoride and hydroxide precipitation, may be required.

The precipitated oxalate is ignited in air to the oxide. From the weight of the oxide, the rare-earth content in the original sample is calculated. If many rare-earth elements (REEs) are present in the solution, all of them precipitate together as oxalate. If only a particular rare earth is present in the solution, only its oxalate will precipitate. The precipitate is filtered, washed, and ignited in a platinum crucible at 800–900°C to the pure oxide, and its rare-earth content is calculated. Oxalic acid is the preferred reagent for precipitation. It is always added in excess in any analytical procedure. The conditions for analytical oxalate precipitation have been summarized by Broadhead and Heady (1960). Most of the rare-earth oxalates are converted to the sesquioxides (RE_2O_3), cerium oxidizes to CeO_2, praseodymium to Pr_6O_{11}, and terbium to Tb_4O_7.

The procedure for the analysis of total rare-earth content in gadolinite, monazite, fergusonite, euxenite, and samarskite, by chemical dissolution and precipitation of oxalate, has been outlined by Furman (1939). Any thorium present in the mineral also gets precipitated along with the rare earths and should be corrected for. Bastnasite can also be assayed similarly after chemical decomposition with sulfuric acid.

8.2.2 Volumetry

As regards the determination of individual rare earths, this method is usable only for cerium and europium. The determination of rare earths as a group is also possible volumetrically, taking advantage of the complex formation between the rare earths and ethylenediaminetetraacetic acid (EDTA).

The rare earths form very stable complexes with EDTA. Even though the titration of individual rare earths in a mixture is not possible with this reagent, titration of rare earths as a group is widely practiced (Welcher 1958). Before titration, the free acid in the solution is neutralized, and a small amount of triethanolamine or hexamine is added to maintain the desired pH. Xylenol orange or Arsenazo I is used as a metallochromic indicator (O'Laughlin 1979).

Typically, the RE^{3+} contents in the ore/concentrate leach liquor can be determined by volumetric titration methods using EDTA. α-Benzoin oxime is used to precipitate the heavy metal ions, acetylacetone to mask aluminum ions, ascorbic acid to reduce ferric iron to ferrous iron, and sulfosalicylic acid to mask the ferrous iron. Using hexamethylenetetramine as a buffer and xylenol orange as an indicator, titration analyzes the rare-earth concentration with EDTA (Tian et al. 2013).

8.2.2.1 Determination of Cerium

Cerium exists in a stable tetravalent state in aqueous solutions (H_2SO_4, HNO_3). The potential of the Ce^{+4}/Ce^{+3} couple varies from 1.3 to 1.9 V in an aqueous solution, depending on the anion. The volumetric method for cerium relies on the quantitative

oxidation of cerium from +3 to the +4 state using a strong oxidizing agent, like ammonium persulfate with a silver catalyst or sodium bismuthate. The oxidized cerium is estimated by titration with ferrous ion (usually as ferrous ammonium sulfate). O-phenanthroline or N-phenyl anthranilic acid has been used as an indicator in the titration. Willard and Young (1928) have outlined the volumetric procedure for cerium estimation.

When analyzing ores and minerals for cerium, the rare earths are first isolated as a group by oxalate precipitation and ignited to oxide. The (mixed) oxide is digested with concentrated HCl until fully dissolved. Concentrated sulfuric acid is added, and the mixture is evaporated to copious fumes to expel all HCl. After cooling, the sulfates are dissolved in cold water. Cerium oxidation and titration are then carried out.

8.2.2.2 Determination of Europium

Europium is the only rare earth that can be reduced to the divalent state by moderately strong reducing agents in a mildly acidic medium. Amalgamated zinc is one such reducing agent and is commonly known as Jones reductor. Foster and Kremers (1953) described the following procedure for the determination of europium in rare-earth mixtures.

The rare-earth chloride solution containing europium [Eu(III) in HCl] is passed through a column packed with Jones reductor into an excess of ferric chloride. Eu(III) in the original solution gets reduced to Eu(II) in the column by Jones reductor. Eu(II) now flowing in to FeCl3 oxidizes itself back to Eu(III) at the same time reducing an equivalent amount of Fe(III) in the chloride to Fe(II). This Fe(II), present as ferrous chloride is determined by titration with a standard solution of potassium dichromate.

Even though Sm and Yb can exist in the divalent state, they are not reduced by zinc, and hence, there is no interference from them in the determination of europium.

8.3 ANALYTICAL SEPARATION OF RARE EARTHS

The separation of rare earths as a group from a matrix or from impurities is often necessary for their accurate analytical determination. In some cases, separation has to be carried out to isolate the individual rare earths also.

Simple chemical procedures with or without an added carrier, involving oxalate precipitation or a repeated hydroxide–fluoride precipitation, are usually sufficient. For rigorous separation, chromatographic methods are used. Cation exchange, anion exchange, extraction chromatography, high-performance liquid chromatography (HPLC), and ion chromatography are all used.

8.4 INSTRUMENTAL METHODS

Accuracy is strongly influenced by the sensitivity of the analytical method, reproducibility of the result, and its freedom from significant determinate errors. The most serious determinate error arises from the co-constituents of a sample. The chemical methods have serious limitations on this account, particularly as regards the rare earths due to their inherent chemical nature. The exceptions in the cases of cerium and europium have already been indicated.

Several instrumental methods have been developed for rare-earth analyses. They permit highly sensitive determination of individual rare earths, in many cases, in an unprocessed or partially separated mixture. Among the instrumental methods, the widely used techniques rely on optical absorption and emission spectroscopy, x-ray fluorescence (XRF), mass spectrometry, and neutron activation analysis (NAA).

8.5 SPECTROSCOPY

8.5.1 Spectrophotometry

Spectrophotometric analyses of rare earths are well covered in the classics (Banks and Klingman 1956; Moeller and Brantley 1950; O'Laughlin 1979; Stewart and Kato 1958).

The spectrophotometric methods of rare-earth determination are based on the absorption spectra of rare-earth ions in solution. All the rare earths absorb in the spectral range 200–1000 nm with the exception of scandium, yttrium, lanthanum, and lutetium. The absorption bands of the rare-earth ions are sharp even in solution because they arise from electronic transitions in the shielded 4*f* subshell and they are characteristic of the individual cations. However, their molar absorptivity, which is an indicator of the possible sensitivity of their determination, is low—the highest being about 12 L/mol cm. Subject to this limitation, the absorption bands can be used to determine the individual rare earths in mixtures in chloride and perchlorate solutions. The molar absorptivity of rare-earth ions at analytical wavelengths was compiled and given by O'Laughlin (1979) and reproduced in Table 8.1. It is apparent that in each of the wavelengths, many ions show absorptivity, and to the extent that the absorptivity values are closer to each other, interference is anticipated and observed.

Among the 12 naturally occurring REEs that have absorption bands in the 200–1000 nm range, Ce(III), Gd, and Tb absorb in the ultraviolet (UV) region. They are not used for determination, due to interference issues. The molar absorptivities of rare-earth ions at analytically useful wavelengths are listed by O'Laughlin (1979). However, λ_{max} and molar absorptivity need to be checked for the instrument used.

Each of the REEs has a characteristic absorption spectrum, and this has been useful in the analysis of rare-earth mixtures. The rare earths are determined in moderately acidic solutions of the chlorides or perchlorates. Any cerium present is reduced to the trivalent state. The absorption peak of an REE usually coincides with the background absorption by other REEs. The absorbance of the solution at any analytical peak is the sum of the absorbance of each element at that wavelength. When complex mixtures are examined, the concentration of individual elements may be obtained by the solution of simultaneous equations set up from absorbance measurements, which is now done by software-based systems.

The sensitivity of spectrophotometric determination is enhanced by complexing of the analyte with a chromogenic reagent. The molar absorptivity of such colored complexes is a thousand times more, in the range 10^3–10^5 L/mol cm. Very low concentrations of rare earths can be determined. The absorption spectra of complexes formed by different REEs are not significantly different. It is therefore possible only to determine the total rare earths with enhanced sensitivity and not the individual

TABLE 8.1
Molar Absorptivity of Rare-Earth Ions at Analytical Wavelengths

	Molar Absorptivity, ε (l/mole cm)					
λ (Å)	4–12	3–4	2–3	1–2	0.1–1	0.025–0.1
272.8	Gd			Pr	Er, Tm, Yb, Eu, Ho, Nd, Dy, Sm	
287.9		Ho		Nd	Tm, Pr, Er, Yb, Dy, Eu	
350.4			Nd, Dy		Tm	Er, Ho, Sm
361.1			Ho		Tm, Sm, Er, Dy	Eu, Nd
365.0			Dy	Er	Ho, Sm, Tm	Eu, Nd
379.6	Er				Eu, Dy	Nd, Sm, Ho
394.2		Eu			Dy, Sm, Ho	Er, Nd
401.5		Sm			Dy	Eu, Er, Ho
444.2	Pr				Ho, Er	Dy, Sm
450.8	Ho			Pr	Er, Dy	Nd
521.6	Nd		Er			Ho
523.5		Er		Nd		Ho
537.9	Ho					Er
575.5	Nd				Pr	
640.4		Ho			Er	
683.0			Tm		Nd	
739.5	Nd					Tm
794.0	Nd				Tm, Er	Dy
974.0			Yb	Er		Sm, Dy

Source: O'Laughlin, J.W., Chemical spectrophotometric and polarographic methods, in Gschneidner, K.A. Jr. and Eyring, L. (eds.), *Handbook on the Physics and Chemistry of Rare Earths*, vol. 4, North Holland, Amsterdam, 1979.

Note: The sample solutions contained 20 mg of oxide in 1 ml of 1 M $HClO_4$ (except for erbium 10 mg/ml).

components of a mixture. Even the complexes of several non-REEs have absorption spectra similar to those of the rare earths. Chemical separation of the rare earths as a group and from one another is necessary prior to their determination by forming colored complexes with the chromogenic reagents.

Some of the chromogenic reagents used for the spectrophotometric determination of rare earths are known by the names thoron, Arsenazo I, and Arsenazo III. They are listed in Table 8.2. As regards Arsenazo III, it does not show a color reaction with cations with a radius less than approximately 0.7 A (0.07 nm). Such cations are Al, Be, Ge, Ti, and Sn. Thorium, U, and Zr at a low pH, and Fe, apart from a few other elements at a higher pH, form colored complexes. The rare earths are determined at pH 1.5–3.5. Rare-earth complexes show two absorption maxima—one at 655 nm and the other at 610 nm.

Several metal ions such as trivalent iron, aluminum, chromium, quadrivalent titanium, and zirconium strongly interfere with the spectrophotometric

TABLE 8.2
Important Chromogenic Reagents Used for REE and Thorium

Element	Reagent	Reaction Conditions, pH	Molar Absorptivity, L/mol cm	Selectivity
Lanthanides	Arsenazo III	1–4	$5.5–6.5 \times 10^4$	Low
	Arsenazo I	1–4	1×10^4	Low
	Antipyrine S	2–5	1×10^4	Low
	Alizarin Red S		1×10^4	
	Carboxynitrazo (Ce)	2–4	1.6×10^5	High
Thorium	Thoron I	0.7–1.2	1.2×10^4	High
			1.2×10^5	High

Source: Kantipuly, C.J. and Westland, A.D., *Talanta*, 35(1): 1–13, 1988.

determination of rare earths with organic reagents. Ligand buffer masking of metal chelates has been used in such cases to increase the tolerance of various interfering elements from microgram to milligram quantities, and this, in certain cases, eliminated the need for a separation procedure (Cheng et al. 1982). Hassan and Mahmoud (1982) have suggested the use of chromogenic reagent peridihydroxynaphthindenone for the spectrophotometric determination of rare earths. Many impurity ions, naturally occurring or commonly associated with the rare earths, do not interfere in these determinations. Dual- and three-wavelength spectrophotometry techniques have been applied in the analysis of rare-earth mixtures by a method involving the formation of asymmetrical diazo derivatives of chromotropic acid (Zeng et al. 1983).

Iron has been determined in pure rare-earth oxides and metals by a spectrophotometric procedure based on the colored complex bathophananthroline forms with Fe(II). Many of the non-rare-earth impurities such as Al, Co, Cr, Fe, Ni, Si, Ta, and Ti have also been determined by spectrophotometry. Fluorine has also been determined by this technique based on the bleaching effect of fluoride on a zirconium SPADNS complex (Carlson and Schmidt 1961b). SPADNS [4,5 Dihydroxyl-3-(p-Sulfophenylazo)-2,7-Naphthalene-Disulfonic Acid Trisodium Salt] is a popular reagent for fluoride determination.

A highly sensitive spectrophotometric determination of rare earths after their extraction into di(2-ethylhexyl) phosphoric acid and trioctylamine was described by Vilímec and Jakubec (1987). A sample of the extract is diluted with *n*-butanol, and a solution of chlorophosphonazo III in *n*-butanol is added before absorbance is measured at 660–665 nm against a reagent blank. The method is suitable for the study of the extraction of individual rare earths by different organic reagents.

The total rare-earth content of the rare-earth ores can be determined by acidifying and purifying the ore sample after fusion with sodium peroxide and sodium hydroxide. And then, the rare-earth content can be determined by Arsenazo III spectrophosphorimetry (Tian et al. 2013; Vilímec and Jakubec 1987).

8.5.2 Emission and Absorption Spectroscopy

Emission spectroscopy is the primary analytical tool for the chemical analysis of rare-earth materials and for the determination of rare-earth impurities in other materials. The famous chemical similarity of the REEs does not extend to their spectra. The spectrum of an REE is unique and the most useful property available to the analytical chemist.

The spectra of many of the REEs are complex. The elements Ce, Pr, and Nd have the most complex spectra. The spectra of Sm, Tb, Dy, Ho, Er, and Tm are only a little less complex. Relatively simple spectra are given by Y, La, Eu, Gd, Tb, and Lu. Detection limits are better (lower) for elements with simpler spectra. Instrumental resources also determine limits of analytical determination. A reciprocal linear dispersion of 2.5 A/mm is considered adequate for most analytical determination involving rare earths. When the spectra are more complex, a more perfect optical system is needed.

Optical emission spectroscopy has been used for the determination of rare earths in mixtures at the trace, minor. and major constituent levels. Flame, alternating current (AC) or direct current (DC) arc, and spark discharge have all been used as excitation sources of the emission spectra. The methods developed at Ames by Fassel et al. (DeKalb and Fassel 1979; Fassel et al. 1973a,b) have been widely adopted. The rare-earth oxide is mixed with graphite and subjected to DC arc excitation in a graphite electrode. At the prevailing electrode temperature, the oxide is at least partially reduced to the volatile metal, undergoes excitation, and emits the radiation containing the elemental fingerprint in the spectra. The intensity of the emitted radiation is measured and related to elemental concentration. Although DC arc is considered an uncontrolled type of excitation, this simple method has been yielding good analyses for the rare earths. The internal standard principle could be utilized to full advantage. Detection limits as low as a few tenths of a part per million (ppm) have been possible if the impurity and matrix elements have relatively simple spectra. Generally, the detection limits are in the range 10–1000 ppm. Fassel's basic method has also been used with modifications such as (1) the use of a controlled atmosphere to eliminate interference from cyanogen bands; (2) variations in the arcing current, sample electrode dimensions, and sample weight; (3) addition of carriers to the sample that selectively enhance transport of the analyte to the arc; and (4) use of an AC arc instead of a DC arc, with the resultant payoffs in terms of better detection limits and precision. In the complex spectra of REE, Ozumi et al. (1971) achieved impurity detection limits of 2–40 ppm. Other modifications were spark excitation, a rotating disk electrode, and a controlled atmosphere.

Table 8.3 reproduces the listing by DeKalb and Fassel (1979) of the best detection limits obtainable for direct spectral determination without preconcentration. Separation and preconcentration could improve the detection limits.

Flame emission spectra are strikingly simple compared to the arc or spark spectra, which are characterized by an extremely large number of lines. Besides, interelement interference is virtually absent in the flame spectra. All the rare earths exhibit line spectra of sufficient intensity to possess analytical utility. The REEs that evade detection by spectrophotometry are readily observed in the flame spectra. The importance of flame chemistry in the production of free atoms, and thus the

TABLE 8.3
Detection Limits for Rare Earths in Rare Earth Matrices

Method: Atomic Emission Spectroscopy, Arc or Spark Excitation without Preconcentration

Rare-earth impurity	Sc	Y	La	Ce	Pr	Nd	Sm	Eu	Gd	Tb	Dy	Ho	Er	Tm	Yb	Lu
Detection limit, ppm	0.5	2	3	10	5	6	3	0.5	0.5	5	1	5	0.5	0.5	0.01	0.1
Matrix	Y_2O_3	Sm_2O_3	Y_2O_3	Y_2O_3, Sm_2O_3	Y_2O_3	Sm_2O_3	Y_2O_3	Y_2O_3	Y_2O_3	Y_2O_3	Y_2O_3, Sm_2O_3	Y_2O_3	Y_2O_3	Y_2O_3	Y_2O_3	Y_2O_3

Method: XRF

Matrix	Detection Limit, % for														
	La	Ce	Pr	Nd	Sm	Eu	Gd	Tb	Dy	Ho	Er	Tm	Yb	Lu	Y
La		0.005	.01	0.005	0.005										
Ce	0.01		0.02	0.02	0.01										
Pr	0.01	0.01		0.01	0.01										
Nd		0.01	0.01		0.01	0.005	0.01								
Sm		0.005	0.01	0.005		0.01	0.005								

(*Continued*)

TABLE 8.3 (CONTINUED)
Detection Limits for Rare Earths in Rare Earth Matrices

	Method: XRF														
	Detection Limit, % for														
Matrix	**La**	**Ce**	**Pr**	**Nd**	**Sm**	**Eu**	**Gd**	**Tb**	**Dy**	**Ho**	**Er**	**Tm**	**Yb**	**Lu**	**Y**
Eu			0.01	0.02	0.01		0.01	0.01							
Gd					0.005	0.005		0.005	0.02	0.01					
Tb					0.01	0.01	0.01		0.005	0.01					
Dy						0.005	0.005	0.005		0.01	0.005				
Ho							0.005	0.005	0.01		0.01	0.01	0.02		
Er								0.005	0.005	0.005		0.005	0.01	0.005	0.005
Tm									0.002	0.002	0.005		0.01	0.002	0.002
Yb									0.005	0.005	0.005	0.005		0.01	0.005
Lu											0.002	0.005	0.002		0.002
Y							0.01	0.005	0.005	0.01	0.01		0.01		

Source: DeKalb, E.L. and Fassel, V.A., Optical atomic emission and absorption methods, in Gschneidner, K.A. Jr. and Eyring, L. (eds.), *Handbook on the Physics and Chemistry of Rare Earths*, vol. 4., North-Holland, Amsterdam, 1979; Chandola, L.C. et al., X-ray flourescence analysis of cerium-dioxide for rare earth opportunities, Bhaba Atomic Research Centre, Bombay, India, 1975.

atomic line spectra, has been emphasized by Fassel et al. (1962, 1979). The technique has been reviewed by Fassel et al. (1973b) and DeKalb and Fassel (1979). Once the free atoms are formed, they can be detected and determined quantitatively even at the trace level by atomic flame emission [flame emission spectroscopy (FES)] and atomic absorption spectrometry (AAS). DeKalb and Fassel (1979) have listed analytically useful spectral wavelengths for AES and AAS. Flame emission spectrometry detection limits are generally superior to those observed in AAS. Flame emission spectrometry (AES with flame as the excitation source) techniques can be used in the analysis of rare-earth mixtures and the determination of low concentration of the REEs. The detection limits feasible in FES are listed along with the limits in other spectroscopic techniques in Table 8.4.

AAS is based on quantification of the absorption of the radiation by the ground-state analyte (element to be analyzed) atoms generated from the sample by a suitable atomization method. The technique makes use of the wavelengths of light specifically absorbed by an analyte. The radiation to which the analyte is exposed is the same that the analyte would emit on its transition from an excited to the ground state. It is generated, normally, by a hollow cathode lamp. Two methods are commonly used to produce atoms from the sample. Aspiration involves sucking a solution of the sample into a flame, and electrothermal atomization is where a drop of a sample is placed into a graphite tube that is then heated electrically. Electrothermal vaporization provides better sensitivity. In some instruments, both atomization systems are used, but they share one set of hollow cathode lamps. The applications of AAS to rare-earth analysis have been described by Ooghe and Verbeek (1974), Van Loon et al. (1971), Sen Gupta (1976, 1984), and Joworowski et al. (1967). The possible instrumental, process, and procedure modifications in AAS to enhance the sensitivity have been indicated by Sen Gupta (1985).

All lanthanides, with the exception of cerium and promethium, were determined by AAS by Ooghe and Verbeek (1974). They used an 80% methanol solution of the sample, with sodium and potassium chlorides added to suppress ionization. Samples of monazite, bastnasite, and gadolinite were all analyzed by them. In general, AAS methods are less sensitive for the REEs than for the majority of metals. Among the rare earths, AAS is least sensitive for La and Nd, but these are rare earths that are abundant in most natural samples. Yttrium, europium, and the elements Tb–Lu were determined in minerals by AAS using aqueous sample solutions by Van Loon et al. (1971). The lowest values determined were around 0.05%. Sen Gupta (1985) determined Y, Nd, and the elements Dy to Yb by AAS using ethanol sample solutions adopting microsample injection and flame emission. Europium was determined at concentrations less than 10 μg/g. In the best cases, the sensitivity of AAS can approach those achieved by NAA.

8.5.3 Induction-Coupled Plasma Excitation

The generation and excitation of free atoms to obtain their spectra by heating the sample aerosol in a plasma was conceived by Reed (1961) and has evolved into an analytical tool of extraordinary capability. High-frequency electric current flowing in a coil inductively heats a stream of argon inside the coil space to generate the

TABLE 8.4
Comparison of Experimentally Measured Dissolved Sample Detection Limits

Element	Sc	Y	La	Ce	Pr	Nd	Sm	Eu	Gd	Tb	Dy	Ho	Er	Tm	Yb	Lu
FES	0.03	0.03	0.01	10	0.07	0.7	0.2	0.0005	2	0.03	0.05	0.02	0.04	0.02	0.002	1
AAS	0.1	0.3	2		4	2	0.6	0.04		2	0.2	0.1	0.1	0.08	0.02	3
ICP	0.003	0.0002	0.003	0.007	0.06	0.05	0.02	0.001	0.007	0.2	0.004	0.01	0.001	0.007	0.0009	0.008

Source: DeKalb, E.L. and Fassel, V.A., Optical atomic emission and absorption methods, in Gschneidner, K.A. Jr. and Eyring, L. (eds.), *Handbook on the Physics and Chemistry of Rare Earths*, vol. 4., North-Holland, Amsterdam, 1979.

Note: AAS, atomic absorption spectroscopy; Band emission observed in the cases of La, Tb, and Y in FES; Detection limit = concentration (μg/mL) required to produce a signal at least twice as large as the standard deviation of the total background noise fluctuations; FES, flame emission spectroscopy; ICP, induction-coupled plasma technique.

plasma. The sample, introduced into the plasma as an aerosol by a nebulizer system, experiences high temperature (4000–6000 K). Free atoms are formed and also excited. Usually, the spectra of free atoms generated are observed in the tail flame, where the temperature is about 4000 K. If the emitted light is analyzed, the technique is called induction-coupled plasma atomic-emission spectrometry (ICP-AES), and if the generated particles are analyzed by a mass spectrometer, the technique is called induction-coupled plasma mass spectrometry (ICP-MS). Both techniques are extensively used for rare-earth analysis.

8.5.4 ICP-AES

The commercial development of atomic-emission spectrometry using argon plasma as the excitation source (ICP-AES) has permitted detection limits up to three orders of magnitude lower than those obtained by other methods (e.g., flame emission), provided a linear response over a concentration range of several orders of magnitude, reduced matrix effects, good precision, and also rapid analysis. Broekaert et al. (1979) have determined all the REEs in standard mineral samples using this technique.

Among the spectrometric methods, ICP-AES is the least prone to interferences. The sources of error usually are interelement effects of various types as well as spectral interferences. ICP excitation leads to freedom from interelement effects, and analytical calibration for the determination of REE in any RE matrix can be used for any other matrix of RE, however complex, if there is no spectral line interference. The limits of detection for rare earths using this technique are also listed in Table 8.4.

ICP-AES is usually preceded by separation and concentration of rare earths using, for example, solvent extraction or ion exchange to overcome some of these problems with spectral line interferences. Yoshida and Haraguchi (1984) used ICP-AES interfaced with high performance liquid chromatography (HPLC) for the determination of REEs. ICP-AES was used as an element-sensitive detector for HPLC. The separation of rare earths by HPLC helps to avoid erroneous analytical results arising from spectral interferences and greatly enhances the analytical limits of ICP-AES. Using such a combination, Li et al. (1987) have determined 13 rare-earth trace impurities in 99.9999% pure Gd_2O_3. A similar sequence was adopted by Roy Choudhuri (1995) to analyze RE in silicate rocks. Djingova and Ivanova (2002) determined REEs in soils and sediments by ICP-AES after cation-exchange separation, typically carried out as follows.

One gram of sample was weighed into a polytetrafluoroethylene (PTFE) beaker and heated with 5 mL of 70% $HClO_4$ and 10 mL of 48% HF in a sand bath to incipient dryness. The acid attack with $HClO_4$ and HF (1 + 2) was repeated three times to complete digestion of the silicate matrix. Then the samples were transferred into flasks and diluted to 50 mL with 0.2% HCl. Ten milliliters of the sample solution was passed through a column (14 × 1 cm) with 100–200 mesh Dowex 50WX8 cation resin pre-equilibrated with 1 M HCl. The matrix elements, Al, Ca, Fe, K, Na, Mg, etc., were eluted with 60 mL of 1.7 M HCl (Merck). This eluate was discarded. Then the REEs were eluted with 45 mL 6 M HCl (Merck). The eluate was evaporated on a hot plate to 1 mL. The solution was transferred into a flask, diluted to 10 mL with 0.2% HCl, and analyzed for the REEs. Most analytical lines of REEs are interfered

with by matrix elements. A method for calibration leading to minimization of these effects is applied. Djingova and Ivanova (2002) compared instrumental determination after calibration with pure rare-earth solutions and IAEA Soil-5 to conclude that a higher number of REEs could be reliably determined by the second approach.

Murthy et al. (1995) used ICP-AES for determining REs in apatites. The major constituents of apatite rock, calcium and phosphate, cause no serious interference. Neither do the minor metals present in the mineral sample. The rare earths could be determined by directly nebulizing the sample solution into the plasma. ICP-AES was used by Grossman et al. (1990) to analyze the rare-earth contents in alloy steels.

Ayranov et al. (2009) described a procedure for the determination of REEs U, Th, Ba, Hf, and Zr in solutions with high iron content by ICP-AES. A substantial part of the detection power of ICP-AES may be lost if the sample contains a major element with a rich line spectrum. Iron exhibits a very rich line spectrum in ICP-AES, which interferes very strongly with most analytes' lines. A number of separation procedures including Ion exchange (IX), Solvent extraction (SX), and coprecipitation have been generally applied for group separation and determination of REE. None of these methods is suitable for selective separation as a group of REE, Th, U, Ba, and Zr from iron in the leach liquor. It was determined by Ayranov et al. (2009) that iron could be selectively separated by solvent extraction with diethyl ether from an HCl media. From a 6 mol/L HCl acid solution, Fe(III) was extracted into diethyl ether as an ion-pair complex. REE, U, Th, Ba, and Zr are not extractable under these conditions and the separation between them and iron was complete.

Apart from the ICP source, another plasma source—the direct current plasma (DCP) jet—has been used for analytical work. Johnson and Sisneros (1982) demonstrated accurate determination of rare-earth distribution in ore concentrate samples using a DCP–echelle spectrometer system. Zang et al. (1985) determined trace amounts of RE in geological samples by DCP-source spectrometry. After sample dissolution, the REs were separated from most other elements by a process involving adsorption on a cation-exchange resin. The adsorbed REs were eluted with HCl, and the chloride was analyzed by DCP spectrometry, whereby a detection limit in the range of 0.02–0.30 ppm was achieved.

Laser has also been used as the excitation source. In laser-induced breakdown spectroscopy (LIBS), a high-power pulsed laser beam is focused onto the sample to generate a high-temperature transient plasma, and a high-resolution spectrometer in conjunction with a gated intensified charge coupled device (ICCD) is used to analyze the spectra emitted by the sample. It is considered a versatile technique for rapid and efficient elemental analysis. Abedin et al. (2011) have analyzed, using the LIBS technique, raw monazite sands from the monazite-rich beach sands (Cox's Bazar area) from Bangladesh and identified a number of rare earths in the presence of strongly interfering elements such as iron and titanium. In fact, the technique is very versatile and has been used for applications ranging from determination of carbon in molten steel to trace contaminants in water. Alamelu et al. (2008) have used it for simultaneous determination of Sm, Eu, and Gd in aqueous solution.

Another variation is the use of microwave plasma. Zhao et al. (2010) used a combination of online preconcentration by di(2-ethylhexyl) phosphoric acid resin in the presence of a complexing agent with microwave plasma atomic-emission

spectrometry for the determination of rare earths. All the four light rare earths La–Nd were determined with detection limits of 1.09 μg/L for lanthanum, 3.31 μg/L for cerium, 2.05 μg/L for neodymium, and 1.25 μg/L for yttrium. The method was applied to the determination of the rare earths in water samples.

8.6 ICP-MS

Lichte et al. (1987) developed a method of analysis called ICP-MS for the determination of REEs in geological materials. Samples are analyzed directly following acid digestion without any need for preconcentration or separation. ICP-MS is being routinely used for determining the partitioning (composition) of rare-earth ore samples (Tian et al. 2013).

As mentioned earlier, ions of the analyte are generated from the sample aerosol introduced into the plasma created by an induction coupling of an argon gas stream. A fraction of the positive ions generated in the inductively coupled ion source is extracted into a quadrupole mass spectrometer attached to the system to be analyzed for their charge-to-mass (e/M) ratio. The ions travel through successive vacuum stages from the Ar plasma source operating at a very high temperature (8000 K) at atmospheric pressure to the quadrupole mass analyzer operating in a moderately high vacuum at close to room temperature.

The spectra obtained by ICP-MS are fairly simple, with a smaller number of spectral interferences compared to ICP-AES. The detection limits are in the range 0.01–0.2 ng/mL. Relatively simple spectra (mass spectra) and high sensitivity make this technique very suitable for trace RE determination.

Isobaric interference (Isobars are atoms of different chemical elements that have the same number of nucleons [protons + neutrons]. So, isobars differ in atomic number [or number of protons] but have the same mass number) is a common problem in ICP-MS. The RE isotopes span the mass range 139–176 amu. Five of the rare earths, Pr, Tb, Ho, Y, and Tm, are monoisotopic. A knowledge of isotopic abundance of elements present in a sample is essential to evaluate possible isotopic mass overlaps and isobaric interferences. In many cases, it is possible to choose isotopes without overlap. A more serious problem comes up when the monoxides of light RE interfere with the determination of relatively less abundant heavy REEs. The possibility is brought out in Table 8.5. Different ways of correcting these errors have been explored.

Over the past two decades, ICP-MS has increasingly become the preferred method for determination of REE, Sc, and Y abundances in meteoritic and geological materials (Balaram 1996; Bayon et al. 2009; Eggins et al. 1997; Jarvis 1988; Pin and Joannon 1997; Potts 1997; Robinson et al. 1999; Yu et al. 2001). Akinlua et al. (2008) determined the rare-earth content in crude oils—from both onshore and offshore wells—of the Niger Delta by ICP-MS. The analytical method was based on acid digestion of oil samples into a colorless aqueous solution that was suitable for ICP-MS instrumentation. The contents of La, Ce, Pr, Nd, Sm, Eu, Gd, Dy, Er, and Yb were all determined to range between a low of 0.01 ppb to a high of 1.58 ppb.

Zhang et al. (1995, 2007) outlined the methods to overcome potential problems encountered in ICP-MS when applied to the trace and ultratrace RE impurity determination in high-purity Sm_2O_3 and Eu_2O_3. They showed that matrix suppression

TABLE 8.5
Interferences in ICP-MS

Nuclide	Abundance, %	Oxide Interference
^{139}La	99.91	^{123}SbO, ^{123}TeO
^{140}Ce	88.48	^{124}SnO, ^{124}TeO
^{141}Pr	100.00	^{125}TeO
^{145}Nd	8.30	
^{147}Sm	15.00	
^{151}Eu	47.8	^{135}BaO
^{157}Gd	15.65	^{141}PrO
^{159}Tb	100.00	^{143}NdO
^{163}Dy	24.9	^{147}SmO
^{165}Ho	100.00	^{149}SmO
^{167}Er	22.95	^{151}EuO
^{169}Tm	100.00	^{153}EuO
^{173}Yb	16.12	^{157}GdO
^{175}Lu	97.40	^{159}TbO

Source: Kantipuly, C.J. and Westland, A.D., *Talanta*, 35(1): 1–13, 1988.

could be compensated for by adding an internal standard. The intensities of internal standard elements and the analyte of interest decreased at the same time as the matrix concentration increasing. In the analysis of samarium oxide, indium was used as the internal standard. However, isobaric interferences may only be removed by chemical separation of elements responsible for interference. An attempt to overcome isobaric interference by tracking double-charged ions in the analysis of 4 N pure Gd_2O_3, was shown to lead to the problem of insufficient sensitivity (Takaku et al. 1993). Zhang et al. (2007) noted that the determination of Dy, Ho, Er, Tm, and Yb (all these elements suffered from isobaric interference) without separation of the samarium matrix would have pointed to an oxide purity of only 99.0%, while the actual purity of samarium oxide was 99.999–99.9999%.

In an attempt to determine 14 REEs present as trace impurities in high-purity samarium oxide (Sm_2O_3) using ICP-MS, the elements La, Ce, Pr, Nd, Eu, Gd, Tb, Lu, and Y could be measured without a need for Sm matrix separation because of no interference problems occurring that could affect the analysis of these elements. On the other hand, as mentioned above, the five elements Dy–Yb could be determined only after Sm matrix is removed completely by means of an extraction-chromatographic separation using 2-ethylhexyl hydrogen ethylhexyl phosphonate (EHEHP). The limits of quantitations (LOQs) for 14 REEs' impurities were from 0.01 to 0.07 μg/g. Thus, the ICP-MS methodology was found to be suitable for the determination of a trace of the 14 REEs in 99.999–99.9999% high-purity Sm_2O_3 (Zhang et al. 2007).

Kawabata et al. (1991) carried out the analysis of high-purity La_2O_3 and Gd_2O_3 using ICP-MS after removing the matrix completely using an online

ion-chromatography unit. An analytical procedure using capillary electrophoresis coupled online to a double-focusing sector-field ICP-MS (CE-ICP-MS) has been described by Day et al. (2000) for the analysis of REE mixtures in aqueous samples. ICP-MS coupled online to a liquid chromatographic unit (LC-ICP-MS) has also been used in the analytical procedures for high-purity RE samples Pedreira et al. (2001). Isobaric interferences of atomic and molecular ions arising from matrix were reported to be completely eliminated in the analysis of Gd_2O_3 and Yb, when extraction-chromatographic separation using EHEHP preceded ICP-MS (Cao et al. 1999; Zhang et al. 2004).

Vargaa et al. (2010) described a simple analytical procedure for the trace-level determination of lanthanides (REEs) in uranium-bearing materials by inductively-coupled-plasma sector-field mass spectrometry (ICP-SFMS). The method involves a selective extraction-chromatographic separation of lanthanides followed by ICP-SFMS analysis. The limits of detection of the method proposed are in the low picogram (the picogram is equal to one trillionth of a gram [10^{-12}g]) per gram range, are approximately two orders of magnitude better than that without chemical separation.

During the past decade and half, ICP-MS techniques have generally utilized single-collector, sector-field, or quadrupole mass spectrometers (Pourmand et al. 2012). Multicollector ICP-MS (MC-ICP-MS) in conjunction with isotope dilution mass spectrometry (IDMS) has only been recently explored for REE measurements (Baker et al. 2002; Kent et al. 2004). Simultaneous measurement of multiple isotopes with MC-ICP-MS allows techniques such as isotope dilution and standard-sample bracketing to achieve enhanced precision and accuracy in the determination of elemental concentrations. The influence of fluctuations inherent in the plasma source and sample introduction systems that limits the precision and accuracy of the analysis with single-collector ICP-MS is circumvented in the concurrent measurement of multiple isotopes. Baker et al. (2002) described a method, developed essentially for geological and ore samples, for the rapid chemical separation and highly reproducible analysis of the REE by isotope dilution analysis by means of a multiple collector MC-ICP-MS. Compared to quadrupole ICP-MS or thermal-ionization mass-spectrometric isotope dilution techniques, the MC-ICP-MS technique is stated to be superior in terms of the analytical reproducibility and rapidity of analysis. Samples are digested by standard hydrofluoric-nitric acid-based methods and spiked with two mixed spikes. The bulk REEs are separated from the sample on a cation-exchange column, collecting as two groups—the middle–heavy and light REEs, which provides a middle–heavy REE cut with sufficient separation of the light from the heavier REEs to render (isobaric) oxide interferences trivial, and a Ba-free light REE cut. The heavy (Er–Lu), middle (Eu–Gd), and light REE (La–Eu) concentrations are determined by three short (1–2 min) analyses with a CETAC Aridus desolvating nebulizer introduction system. Comparison to standards established that concentrations can be reproduced to <1%. This technique consumes very small amounts (subnanograms) of the REE and will allow precise REE determinations to be made on much smaller samples than hitherto possible.

Pourmand et al. (2012) listed several conditions to improve the accuracy and precision of REE, Sc, and Y measurements by MC-ICP-MS: (1) complete digestion of refractory phases and minerals in the samples; (2) low procedural blanks;

(3) separation of interfering matrix, and (4) elimination of molecular (i.e., oxides and hydrides) and direct isobaric interferences on the mass of the analytes of interest. They described an analytical protocol to reduce REE, Sc, and Y concentrations in commercial $LiBO_2$ flux, which facilitates processing small aliquots (~15–50 mg) of samples with concentrations as low as 10 ng/g. Extraction chromatography using a resin, N,N,NN′tetraoctyl-1,5-diglycolamide ligand (TODGA); purified REE; Sc; and Y. The exceptional affinity of TODGA for these elements has made this resin an effective medium for separating the rock matrix that interferes with REE, Sc, and Y measurements during ICP-MS analysis (Connelly et al. 2006; Horwitz et al. 2005; Pourmand and Dauphas 2010; Sasaki et al. 2007). Improved sample digestion with low-blank, high-temperature $LiBO_2$ fusion; a single TODGA extraction chromatography step for quantitative matrix separation; and a dynamic multicollector cup configuration method that allows the measurement of REE, Sc, and Y by MC-ICP-MS in a single sample solution enabled measurement of elemental concentrations with high precision at very low levels of concentration.

8.7 XRF

In the electromagnetic spectrum, x-rays cover the wavelength range 0.01 nm to 10 nm. Atoms may emit x-rays when exposed to electrons or even x-ray photons of energy sufficient to dislodge an electron from an inner orbital. The vacancy thus formed triggers electron transitions across energy levels of the atoms, resulting in the emission of x-rays from the atoms. XRF or x-ray secondary emission refers to the phenomenon when the original incident radiation is an x-ray. If an electron was ejected from the K shell, the vacancy can be filled by electrons from the L, M, and N shells, and the resulting spectral lines are K lines. An electron knocked off from the L shell and transitions occurring to this L vacancy from the M and N shells lead to L spectral lines. The x-ray spectra of elements are simpler than the optical spectra. Since only the inner electronic orbitals are involved in the absorption and emission of x-rays, the variation of the wavelength of the emitted x-rays with the atomic number of the atom is a uniformly progressive function. Thus, the wavelength of the emitted (fluorescent) x-ray carries the information of the elemental identity, and the intensity of the fluorescent radiation carries information on the quantity of the element, giving rise to the x-ray. Essentially, the issue of rare-earth analysis becomes the same as analyzing any group of consecutive elements. For the rare earths, the K spectra are used only for yttrium, whereas for all other REEs, the L spectra are used in the determinations.

XRF has been a rapidly developing analytical technique based on the measurement of the intensities of fluorescent x-rays emitted when a sample is irradiated with hard x-rays. Apart from a simpler spectrum, minimal sample preparation is an advantage of XRF. The technique has been used for the determination of individual REEs in almost any material that contains rare earths—rocks, minerals, rare-earth concentrates, process solutions, and pure products (Bonnevie-Svendsen and Follo 1973; DeKalb and Fassel 1979). Samples can be in the form of solid pieces, powder, pressed compact, liquid, and solution, and in a supported state. Minimal sample preparation is needed. XRF analysis is usually limited to concentrations greater than

100 ppm (Chandola et al. 1975) and is applicable to the whole concentration range up to 100%. Instruments that permit determinations at concentrations as low as a few ppm for many metals are also available. It is a rapid and precise method and easily automated.

Commercially available instruments are limited to the determination of elements with $Z > 11$ in most natural materials. Different isotopes of an element cannot be distinguished by XRF, and neither can different valence states. The application of XRF to rare-earth analysis, the problems that arise, and the solutions that are available have been discussed by Bonnevie-Svendsen and Follo (1973) and DeKalb and Fassel (1979).

Even though x-ray spectra are simple, line interferences can occur for elements with close Z values. Absorption of the exciting (incident) radiation and a decrease of its effectiveness in exciting fluorescence in deeper layers, as well as absorption of fluorescent radiation generated beneath the surface of other atoms, are sources of errors. The techniques available in dealing with these errors include the use of internal standards, synthetic standards for calibration, spike and standard addition, dilution of a sample with a matrix, and validation of XRF results with the results obtained on the same sample by ICP-AES and neutron activation. The detection limits for various rare earths in different rare-earth matrices are summarized in Table 8.3. XRF has also been used to determine the overall chemical composition of clays; the samples were analyzed using pressed powder pellets, with the calibration refined using both standard reference materials (SRMs) and synthetic ones (Moldoveanu and Papangelakis 2012).

Wu et al. (2010b) summarized the applications of XRF analysis in China's rare-earth industry during the last 20 years. The technique has been applied to the analysis of REEs in ores and soil, concentrates, compounds, metals, alloys, and functional materials, and for fast and online information in the separation process. The analytical method has been used for materials in the form of pressed powders, fused beads, and liquid thin films, apart from solid pieces. The matrices included iron and steel, nonferrous metals, and materials in the petrochemical, geology, biology, electronics, and other fields. Presently, XRF spectrometry can be used to analyze various sample forms, types, and elements in a wide range of concentrations, rapidly, stably, and in a highly automated manner. The detection limit of REEs can reach 10^{-6} level. XRF analysis can complement ICP-AES in the matters of major element content, poor repeatability, and elements such as F and O, and provide an alternative to the chemical methods of analyses that are time consuming, involve high reagent consumption, labor-intensive, and relatively ineffective at the trace levels.

Yan et al. (2006a) described a ^{241}Am-excited energy-dispersive XRF spectrometry as an online analysis method. The 59.6 keV γ-ray acts as an excitation source for rare-earth samples in both aqueous and organic phases collected from the solvent extraction process. Characteristic K-series XRF of the rare earths is emitted and detected by a high-purity planar Ge detector after transmission through a Be window. The whole energy spectrum is recorded by a multichannel board and processed by a personal computer. All the REEs, from La to Tm, including Y, are analyzed. The results compare well with those obtained from ICP spectrometry techniques, and the method is said to be rapid, accurate, and nondestructive.

8.8 NAA

Neutron activation analysis (NAA) is a very sensitive technique for the quantitative determination of REEs even when they are present in extremely low concentrations. For example, using this technique, as little as 1.6×10^{-17} g of europium, i.e., just about 60,000 atoms of europium, has been determined in a matrix (Boynton 1979). In certain cases, NAA may also be the quickest and most convenient technique. The sample preparation requirements are generally minimal.

In NAA, the sample is irradiated in a flux of thermal neutrons, usually in a nuclear reactor. Atoms of elements that have a propensity to absorb neutrons and may undergo activation. Propensity is quantified by mentioning the cross section, e.g., in this case, the neutron absorption cross section. A large numerical value for the neutron absorption cross section indicates a great propensity to absorb neutrons to form isotopes, some of which could be radioactive. The radioactivity of these isotopes is then measured and related to the quantity of elements responsible for the radioactivity, present in the sample. The radioactivity is quickly quantified (identified and measured) by looking at the value for the half-life, $t_{1/2}$ which is the time needed for exactly half of the present number of a particular radioactive isotope to decay/transform by a radioactive process. The detection limits and other issues pertaining to the applicability of NAA are given in Table 8.6.

If, for example, a sample containing dysprosium is so irradiated, ^{164}Dy absorbs a neutron and promptly emits a γ-ray to form ^{165}Dy, which in turn decays to ^{165}Ho by emitting a β particle and associated γ-ray with a $t_{1/2}$ of 141 min. The decay or disintegration rate or activity of ^{165}Dy is proportional to the amount of Dy present in the sample. Measurement of the radioactivity (usually γ, and sometimes β also) leads to the determination of the quantity of the isotope causing radioactivity present in the sample.

In the same manner that a spectral line bears the signature of the element responsible for the spectra, the type and energy of radioactivity bear the signature of the isotope causing it. With the use of suitable instrumentation, it has been possible to simultaneously track, identify, and quantify numerous radioactivities coming from a sample, and this, in short, has been the unique value of NAA. NAA for rare earths has been reviewed by Beranznai (1971), Boynton (1979), Haskin and Korotev (1973), and Steinnes (1973).

The sensitivity of NAA is governed by the neutron flux during irradiation, activation cross section of the nuclides, irradiation duration, $t_{1/2}$ of the activated nuclide, energy of the associated radiation, sensitivity, and resolution of the counting equipment. In practice, for analysis, the relative method of experimentation is used. The sample is weighed into a quartz or polythene container, which is then wrapped in an Al foil. Standards containing known amounts of the elements of interest are irradiated with the samples, and finally, the induced activity of both is measured under the same conditions. The specific activity (count rate per unit mass of the element) of a particular nuclide in the sample is then identical to the specific activity of the standard. Hence, the mass of the element in the sample can be calculated.

The post-irradiation steps in NAA are handling of irradiated samples and measurement of induced activity. There are two routes, radiochemical neutron activation

TABLE 8.6
Detection Limit, Nuclear Properties, and Interferences in the NAA Determination of Rare Earths

Element	Product Isotope	Half-Life	Analytical γ-ray, keV	Detection Limit, Separated Elements, $\times 10^{-15}$ g	Detection Limit, Group Separation, $\times 10^{-12}$ g	Interferences from γ-ray, keV
Sc	^{46}Sc	83.8 days	889.26	2.8	25	^{160}Tb(879.4); ^{110m}Ag(884.7); ^{192}Ir(884.5); ^{46}Ti(n,p)^{46}Sc
Y	^{90}Y	64.0 h	–	6.5		
La	^{140}La	40.23 h	329, 487, 1596	1.1	11	^{235}U(n,f); ^{24}Na, ^{239}Np(334.3); ^{152}Eu(488)
Ce	^{141}Ce	32.53 days	145	180	550	^{125}Yb(145); ^{235}U(n,f); ^{59}Fe(142.4); ^{133}Pa(145.4); ^{182}Ta(152.4)
Ce	^{143}Ce	33.0 h	293	93	580	–
Pr	^{142}Pr	19.16 h	1576	0.83	360	–
Nd	^{147}Nd	10.99 days	91, 531	160	520	^{235}U(n,f); ^{169}Yb(93.6); ^{140}Ba(537.2)
Nd	^{149}Nd	1.73 h	211	420	3600	^{171}Er(211)
Sm	^{153}Sm	46.5 h	103	0.21	1.1	^{235}U(n,f); ^{239}Np(99.6, 103.8); ^{153}Gd(103); ^{182}Ta(100.1)
Eu	^{152}Eu	13.2 years	122, 344, 1408	5.0	18	^{169}Yb(118.2, 130.53); ^{133}Ba(123.7); ^{134}Cs(1400.4)

(*Continued*)

TABLE 8.6 (CONTINUED)
Detection Limit, Nuclear Properties, and Interferences in the NAA Determination of Rare Earths

Element	Product Isotope	Half-Life	Analytical γ-ray, keV	Detection Limit, Separated Elements, $\times 10^{-15}$ g	Detection Limit, Group Separation, $\times 10^{-12}$ g	Interferences from γ-ray, keV
Gd	^{153}Gd	241.5 days	98, 103			^{153}Sm(98, 103)
	^{159}Gd	18.6 h	363	18	570	
Tb	^{160}Tb	72.3 days	87, 879	9	57	
Dy	^{165}Dy	2.35 h	94, 546	0.05	1.1	^{169}Yb(94)
Ho	^{167}Ho	26.8 h	81	0.1	2.3	
Er	^{171}Er	7.52 h	296	35	160	^{152}Eu(296)
Tm	^{170}Tm	129 days	84	4.0	35	
Yb	^{169}Yb	31 days	110, 177	22	76	
	^{175}Yb	4.10 days	396	0.96	59	^{233}Pa(398.5); ^{160}Tb(392.5); ^{131}Ba(404.3)
Lu	^{177}Lu	6.71 days	208	0.52	9.8	^{239}Np(209.8); ^{131}Ba(216)

Source: Boynton, W.V., Neutron activation analysis, in Gschneidner, K.A. Jr. and Eyring, L. (eds.), *Handbook on the Physics and Chemistry of Rare Earths*, vol. 4, North-Holland, Amsterdam, 1979; Kantipuly, C.J. and Westland, A.D., *Talanta*, 35(1): 1–13, 1988.

Note: f, fission; n, neutron; p, proton.

analysis (RNAA), which involves chemical separation of various elements after irradiation prior to measurement of the radioactivity, and instrumental neutron activation analysis (INAA), which determines the radioactivity of the irradiated sample without subjecting it to any chemical processing.

The chemical separation in NAA has been necessary for two reasons. The rare earths Sm, Eu, Gd, and Dy have a large absorption cross section for thermal neutrons. Hence, the trace impurities in such REE matrices, experience a decreased neutron flux and this lowers their analytical value. This is called the self-shielding effect. The solution for this problem is chemical separation of the trace rare earths either as a group or individually from such matrices prior to irradiation. One method of minimizing the self-shielding is to dissolve the sample and maintain it in solution for irradiation and subsequent processing and counting.

An illustrative example on the conditions when a chemical separation becomes necessary along with NAA is the work of Mossart and Hoste (1968) on *spec. pure* Gd_2O_3 for determining RE impurities. The contents of Sm and Eu were 31 and 316 ppm respectively. Europium (capture and activation cross section both high) could be determined in Gd without chemical separation, but samarium (high capture and lower activation cross section) could not, the issue being the huge neutron absorption cross section of Gd (46,000 barns) and the self-shielding effect resulting from this property, even in solution samples. When the impurity contents are very low, irrespective of the nuclear properties of the impurities, a separation of the impurity from the matrix is necessary. A typical example is the determination of trace impurities in europium oxide by NAA (Alimarin et al. 1970). The capture and activation cross sections of europium are high. A preliminary separation of the total amount of RE impurities present in Eu_2O_3 was necessary to determine their concentrations, which were 1 ppm Yb, 8 ppm Dy, 4.2 ppm Ho, 6.4 ppm Sm, and 5.7 ppm lanthanum.

It has been known for long that the heavy RE contents in Indian monazite are very low. Parthasarathy et al. (1986) determined individual RE contents in Indian monazite by a radiochemical neutron activation procedure. Monazite was decomposed and taken into solution in H_2SO_4. A small amount of this solution, along with mixed rare-earth standards, was irradiated. Counting was done on a 1024-channel analyzer using a Ge(Li) detector after different decay intervals. A broad separation of heavy and light RE up to gadolinium was carried out using a Dowex 1 resin column. The contents of all RE, lanthanum to lutetium in Indian monazite, were determined.

NAA is highly specific, and interference effects are fewer compared to other trace analysis techniques for REE. With the advent of superior γ detectors and multichannel analyzers, the need for chemical separation after irradiation has been obviated in many cases. However, the combination of pre-irradiation and post-irradiation chemical separation and superior detectors and instrumentation provides the complete solution to the issue of accurate results in any matrix even at very low concentration levels. Most of the technical limitations can be circumvented by proper selection of procedures. NAA, in one configuration or another, has been successfully used for the determination of rare earths in different types of matrices, in various physical forms, and in a range of concentrations: rock samples of interest in geological studies, rare earth–bearing ores and concentrates, purified rare-earth products in which

other rare earths may be present as impurities, and rare earths as impurities in other materials. A list indicating this versatility is given in Table 8.7.

Graber et al. (1970) determined by RNAA all the stable lanthanides in silicate rocks. The finely ground sample along with standards were irradiated for 30 min in a neutron flux of 1.8×10^{12} n/cm^2 s. The irradiated sample was subjected to chemical

TABLE 8.7
Application of Neutron Activation Analysis of Rare Earths

Material	Elements Analyzed	Reference
	Instrumental Neutron Activation Analysis	
Aerosols (atmospheric pollutants)	Sc, La, Ce, Sm, Eu, Yb, Lu	Zoller and Gorden 1970
Coal and fly ash	Various elements including rare earths	Nadkarni 1975; Ondov et al. 1977
Crude oil	29 elements, 5 rare earths	Al-Shahristani and Al-Atyia 1973
Geological and extraterrestrial materials	10 rare-earth elements	Haskin and Korotev 1973; Nadkarni 1976
Glass	Sc, Eu, Tb, Yb	Kudo et al. 1975
Rare-earth minerals	Y and 12 rare-earth elements	Mantel and Amiel 1973
Lanthanum oxide	Oxygen	Volborth et al. 1974
Yttrium oxide (99.99% pure)	Ppm–ppb levels of RE impurities	Bruijs 1973
Alloy steel	La, Ce, Nd, Sm	Burianová and Frána 1976
Titanium alloys	Y, Nd, Sm, Tb, Er	Broadhead et al. 1965
Aluminum	Sc	Blouri et al. 1973
	Radiochemical Neutron Activation Analysis	
Uranium	All 14 lanthanides	Bachmann and Lieser 1970
Geologic and extraterrestrial materials	La–Nd, Sm–Tb, Yb–Lu	Brunfelt et al. 1974
	La–Tb, Ho–Lu	Higuchi et al. 1970
Geologic and extraterrestrial materials	All 16 rare earths	Mosen et al. 1961
Geologic and extraterrestrial materials	14 lanthanides	Graber et al. 1970
Glass	13 rare-earth elements	McClendon and LaFleur 1973
Rare-earth concentrates	La, Ce, Pr, Nd, Sm, Eu, Gd, Tb, Dy, Yb, Lu, and Th	Van den Bergh et al. 1970
Europium oxide	Yb, Dy, Ho, Sm, and La	Alimarin et al. 1970b
Terbium oxide	Gd, Dy, Ho, Er	Kubota 1974
Holmium oxide	Dy, Er, Yb	
Ytterbium oxide	Sc, Eu, Tb, Tm	
Steel	La, Ce, Pr, Nd	Dogadkin et al. 1976
Uranium	La as low as 1 pg/g	Alimarin et al. 1970a

Source: Boynton, W.V., Neutron activation analysis, in Gschneidner, K.A. Jr. and Eyring, L. (eds.), *Handbook on the Physics and Chemistry of Rare Earths*, vol. 4, North-Holland, Amsterdam, 1979.

separation to concentrate the rare earths. Counting was carried out over a period of 26 days (on day of irradiation for Dy and Er; after 1 day for Eu, Gd, La, Pr, and Ho; after 3 days for Ce, Lu, Yb, and Sm; after 8 days for Nd and Tb; after 26 days for Tm) to establish that the RE contents in the silicate rocks varied from 0.95 ppm for Lu to 150 ppm for Ce.

Two separate investigations were carried out for REE assay in the same standard silicate rock samples. Desai et al. (1964) determined Sc, Y, Sm, and La in the irradiated samples by a procedure consisting of chemical separation and β activity counting using a Geiger-Muller (GM) counter, and γ was counted using a NaI(Tl) scintillation detector. Later, Melsom (1970) used the INAA technique with the Ge(Li) detector and a 400-channel analyzer. Good agreement was found between the two sets of results.

NAA is a great technique for determination of rare earths especially at low concentrations. All rare earths, with the exception of Dy and Er, activate to nuclides with long-enough half-lives that an on-site nuclear reactor is not required. INAA is amenable to automated procedures and nondestructive, and many elements can be determined simultaneously. The limitations of NAA are (1) nuclear reactors not being easily accessible to all analytical laboratories, (2) equipment necessary being complex and expensive, (3) having to work with a certain (considerable) level of radioactivity, and (4) experiments and data collection possibly having to go on for a long time before results can be obtained. Results comparable to NAA are possible in many cases by optical emission and ICP techniques when preceded by preliminary separation/concentration of rare earths.

8.9 OTHER INSTRUMENTAL TECHNIQUES

8.9.1 Cathode Ray–Excited Emission Spectroscopy

Cathode ray-excited emission spectroscopy (CREE) can be used for the analysis of many rare earths in trace levels in any matrix that will support cathodoluminescence, i.e., luminescence excited by cathode rays (electron beam). Larach (1973) reviewed the potential of this technique. Yttrium and gadolinium oxides and phosphor-grade zinc sulfide are useful matrix materials. Comparison standards consisting of rare earths in the chosen matrix (Y_2O_3, Gd_2O_3, or ZnS) are required as in the case of other spectroscopic methods. A CREE spectrometer consists of a high-voltage (8–16 keV) electron source, a sample rack that can be loaded with a number of samples and/or standards, and an analyzer for the luminescent optical beam given out by the sample.

Rare-earth impurities in phosphor host Y_2O_3, Gd_2O_3, or ZnS are determined with greatest sensitivity by CREE—for example, 0.1 ppm of Eu in yttria, 0.005 ppm Eu in gadolinia, and 0.01 ppb Tm in zinc sulfide. CREE has certain inherent limitations, and except for some suitable matrices, it may not have much advantage over ICP-AES or XRF.

8.9.2 X-ray–Excited Optical Luminescence Spectroscopy

For the determination of rare earths in trace and ultratrace levels, a method known as x-ray–excited optical luminescence (XEOL) spectroscopy was used at Ames by

Fassel et al. (1973a,b) and D'Silva and Fassel (1979). Optical luminescence is exhibited by some of the rare-earth complexes and ions in solids and has been used for both detection and determination of rare earths. Although optical luminescence can also be excited by flame, UV or visible radiation, electron beam, or accelerated protons, XEOL of the rare-earth ions has been used more extensively than other methods.

8.9.3 Spark Source Mass Spectrometry

Spark source mass spectrometry (SSMS) is a technique to detect and determine all REEs at trace and ultratrace levels (Conzemius 1979; Taylor 1979). This technique is characterized by a wide elemental coverage in a variety of matrices along with high sensitivity and does not require chemical separation operations on the sample. Taylor (1979) used SSMS for trace-element analysis (down to 0.01 ppm) of REEs in geological samples. Conzemius (1979) used SSMS for the analysis of rare-earth metals, oxides, fluorides, and other salts and alloys.

8.9.4 Secondary Ion Mass Spectrometry

Quantitative ion microprobe analysis or secondary ion mass spectrometry (SIMS) is a highly sensitive technique (Zinner and Crozaz 1986; Reed 1984) for the determination of rare-earth abundances in most minerals. SIMS basically analyzes the composition of solid surfaces by sputtering the surface of the specimen with a focused primary ion beam and collecting and analyzing ejected secondary ions. For example, in allanite, the europium and heavy rare-earth concentrations are below the electron probe micro analysis (EPMA) detection limits, but ion microprobe analysis has enabled the complete REE abundance pattern to be determined (Reed 1984). Ion microprobe analysis enables determination of all the REEs down to the level of 100 ppb. However, this method does not appear to have been used for ultratrace impurity determination in purified rare-earth intermediates and finished products.

8.10 DETERMINATION OF INTERSTITIALS

Analysis of rare-earth metals, alloys, and intermetallics for substitutional impurities can be carried out in the same way as analysis of the compounds after getting the material into a solution.

In rare-earth metals, carbon, oxygen and nitrogen are major, frequent, and important impurities. The determination of carbon in rare earths is by combustion of the sample in a stream of oxygen. The carbon dioxide liberated is determined by a conductometric method, infrared (IR) radiation absorption, or thermal conductivity measurement. Reliable and sensitive automated instruments are commercially available.

Oxygen, hydrogen, and nitrogen are determined by vacuum or inert gas fusion (Carlson and Schmidt 1961b). Highly sensitive instruments are commercially available for these determinations. The basis of the techniques for the determination of gases in metals is the inert gas fusion method developed by Singer in 1940 for the determination of oxygen in steel. The vacuum fusion or inert gas fusion techniques

involve high-temperature fusion of the metal specimen in a graphite crucible so that oxygen is reduced by carbon to form carbon monoxide and carbon dioxide, and thermal decomposition of the nitrides and hydrides occurs. Under the analysis conditions, even the nitrogen and hydrogen held in solution in the metals are evolved. The collected gases are analyzed by conductivity (for CO, via its conversion to CO_2), gas chromatography, or mass spectrometry.

TABLE 8.8
Determination of Oxygen in Rare-Earth Metals

Method	Flux	Temperature, °C	REM Analyzed	Reference
Vacuum fusion	Platinum	1800–1850	All	Guhathakurta and Singh 2000
	Platinum–tin	1650–1725	Gd, Tb, Dy, Ho, Er, Lu, Y, Sc	Fassel et al. 1966; Dallman and Fassel 1967
	Nickel	1600–1900	La	Peterson and Beernsten 1957
	Platinum	2000	Tb, Gd	Shigeta et al. 1986
	Graphite	2000	Tb, Gd	Shigeta et al. 1986
Inert gas fusion	Platinum	1800	Y, La, Nd, Gd, Dy, Ho, Er, Yb	Smiley 1958
	Platinum	1950	Er, Gd	Holt and Goodspeed 1963
	Platinum	2100–2200	Y	Banks et al. 1960
	Pt–Sn	2275–2325	Sc, Y, Gd, Tb, Dy, Ho, Er, Lu	Fassel et al. 1966; Dallman and Fassel 1967
	Fe–Sn		Tb, Gd	Shigeta et al. 1986
Neutron activation analysis	$^{16}O(n,\gamma)^{13}N$		Sm, Yb	Clark and Stensland 1970
Arc discharge extraction–gas chromatography			La–Y	Fassel and Goetzinger 1965; Winge and Fassel 1965

	Difficulty Level	
Rare Earths	**Sample Preparation**	**Amenability to Analysis**
Sc, Y, Gd, Tb, Dy, Ho, Er, Lu	Relatively easy	Relatively easy
La, Ce, Pr, Nd	Need care	Relatively easy
Sm, Tm	Relatively easy	Need attention
Eu, Yb	Challenging	Problematic

Source: Guhathakurta and Singh, H., *Rare Earths*, Rare Earth Association of India, Indian Rare Earths Ltd., Mumbai, 2000.

In the vacuum fusion and inert gas fusion procedures, a variety of alloying metals (fluxes) have been used to generate a molten bath that ensure the complete release of the analyte to the detector system. Platinum and platinum–tin are common fluxes. The complete list is given in Table 8.8. Experimental details and nuances are provided by Peterson and Beernsten (1957), Banks et al. (1960), Fassel et al. (1966), and Dallmann and Fassel (1967). Oxygen has also been determined by NAA and arc-discharge gas chromatography methods, and nitrogen, by Kjeldahl's method (Block et al. 1960).

8.11 SUMMARY

Noyes and Bray (1927) described classical chemical methods for the qualitative analysis (detection) of REEs. The methods are, at present, only of historical value because the presence of REE in a material is readily confirmed by spectroscopic methods. The elements Ce and Eu could be regarded as exceptions to the above statement. There are a large number of qualitative reactions fairly selective to these two elements (O'Laughlin 1979). The determination of individual members of the rare-earth group by chemical methods is exceedingly difficult because of their unique chemical similarity in their default trivalent state. Cerium and europium, on account of their multivalency, are amenable to determination by electrochemical methods that are also sensitive. Except lanthanum and lutetium, the lanthanides can be determined on the basis of characteristic sharp line absorption spectra in aqueous solution. Europium and terbium exhibit unique fluorescence spectra in aqueous solution, and this can be used for their determination. Generally, for the determination of individual rare earths in a mixture of REEs, separation on an ion-exchange column or other chromatographic methods were used, but these lengthy procedures are not always needed now. If the REEs are present in extremely low concentrations, they can be preconcentrated by solvent extraction prior to their determination. It is also generally possible, without much difficulty, to roughly separate the rare-earth mixture into the light and heavy fractions. A popular and important procedure in rare-earth determination is the precipitation of rare-earth oxalates and their ignition to oxides. This not only is useful for the determination of total rare earths in some matrices but also serves to separate the rare-earth group from other elements present in the solution. The individual rare earths are then determined by other methods.

As mentioned above, the rare earths are selectively precipitated as oxalates by, for example, oxalic acid. Scandium is an exception in that in the presence of excess oxalate ion, scandium forms a water-soluble oxalate complex, and the heavy lanthanides are also not completely precipitated (O'Laughlin 1979).

The first step in the chemical analysis of rare earths is the dissolution of the sample. Even the chemically resistant ore samples (monazite, xenotime) are put into solution completely by heating with concentrated sulfuric acid. Digestion with nitric, perchloric, or even hydrofluoric acids is also used in certain instances. Many other fusion and acid digestion–fusion procedures have also been used. In fusion, Na_2CO_3, Na_2O_2, Na_2F_2, NaHF, $NaHF_2$, and KHF_2 have all been used (Aladjem 1970).

In gravimetry, apart from the popular oxalate precipitation, the rare earths can be precipitated as hydroxides, fluorides, iodate or periodate, or several organic precipitants (Aladjem 1970).

The most useful volumetric methods for rare earths are for the determination of cerium by the titration of Ce(IV) with a standard solution of a reducing agent Fe(II) and the titration of rare earths as a group with a complexing agent like EDTA. Many metallochromic indicators have been used for the detection of end points of the titration of rare earth with EDTA and other polydentate ligands.

The separation of rare earths as a group and the separation of individual rare earths from one another by ion-exchange and solvent extraction procedures, for analytical purposes, is important but very selectively used because it is time consuming and cumbersome.

The absorption spectra of the lanthanide ions are the most valuable tool available for their determination. The spectra are quite characteristic of individual lanthanides. All the rare earths except scandium, yttrium, lanthanum, and lutetium absorb in the spectral region from 200 to 1000 nm. The molar absorptivities are characteristically low, but a good spectrometer can do the job. The lanthanides are usually determined in chlorides or perchlorates in moderately acidic solutions (Banks et al. 1956). The method is particularly useful for the precise determination of selected rare earths in alloys when the approximate composition is known and for the direct determination of the purity of the oxides. This is due to compensation for any errors introduced in the measurement itself because the standard and unknown solutions are affected to almost the same extent.

The molar absorptivities of rare-earth complexes with some chromogenic reagents are on the order of 7×10^4 L/mol cm (compared to 12 L/mol cm or less of rare-earth ion at analytical wavelengths). The colorimetric determinations can be very sensitive. A number of chromogenic reagents have been reported for the rare earths.

Atomic absorption and emission spectroscopy methods are superior to spectrophotometric techniques for the determination of trace amounts of individual rare earths. However, enhancements to the spectrophotometric techniques like more sensitive and selective reagents, extraction–photometric methods, and the use of competing ligands have kept spectrophotometry a workable low-cost alternative for trace-level determination of rare earths (O'Laughlin 1979). Very sensitive methods for the determination of several rare earths (Pr, Sm, Eu, Gd, Tb, Dy) based on the fluorescence of these elements in sold matrices have also been developed.

Optical atomic-emission and absorption methods provide several of the most useful and specific means for the determination of the REEs at the trace, minor, and major constituent levels (DeKalb and Fassel 1979). Hundreds of papers describing atomic emission, absorption, or fluorescence methods of determination of individual rare earths have appeared in the scientific literature. The arc and spark spectra of many of the REEs contain thousands of lines of rather uniform intensity, making information extraction a challenging task. Combustion flames have potential for producing simple and analytically more useful spectra if the flame chemistry is controlled to ensure production of free atoms of REEs (Fassel et al. 1962).

DC arc discharge is a widely used technique for the excitation of nonmetallic samples. The powdered oxide is vaporized in a high-current DC arc. This is an uncontrolled source in which the excitation temperature varies continuously. Analytical spectroscopists usually provide internal compensation by measuring the intensity ratio of the analytical line with respect to the line of another element

(a rare-earth matrix) present in the arc column. Detection limits are usually in the range of 10–1000 ppm with ±5% precision.

Spark, flame, and plasma excitation can be applied for the direct excitation of solution samples. Flame emission methods (FES) for the determination of REE in an essentially pure rare earth have been carried out by many analysts. Flame atomic absorption spectroscopy (AAS), involves systematic study of absorption spectra of the REEs in a fuel-rich oxy-acetylene flame. The high-temperature flame serves as the absorption cell. The emission detection limits are equal to or better than those obtained by the absorption methods. "Electrical flames" or electrically generated flame-like plasmas (ICP) have physical and spectroscopic properties that make them highly effective free atom generators and excitation sources for the determination of rare earths. The possible detection limits are two to three orders of magnitude lower than the lowest values achieved by flame emission. ICP is the near-ideal excitation source for the spectroscopic determination of rare earths (DeKalb and Fassel 1979).

For the determination of other impurities in rare earths, DeKalb and Fassel (1979) note that the issue is the very different volatilization rate of the impurities to be determined and the rare-earth matrix. This affects precision. They have noted the use of four different approaches to improve precision. One is adding reference elements with similar volatilization rates as the impurities, another is a spark-type excitation, the third is the carrier distillation technique, and the fourth is separation of most non-rare-earth impurities from the rare-earth matrix and their separate determination. The detection limits for impurities range from less than 1 ppm for most of the elements to 10–100 ppm for the refractory metals, thorium and strontium, when arc and spark excitation is used. A summary of these limits given by DeKalb and Fassel (1979) is reproduced in Table 8.9.

As regards the determination of rare-earth mixtures, when arc or spark excitation is used, an internal standard is invariably used, and ceria was preferred by Fassel (1949). Lanthanum and also yttrium have also been used instead of ceria. Flame analysis techniques are applicable to the determination of REEs in a complex mixture of these elements. Adequate precision is usually obtained by net absorbance or

TABLE 8.9
Detection Limits for the Determination of Non-Rare-Earth Impurities in Various Rare-Earth Oxides

Detection Limits	Elements
1 ppm or less	Ag, Al, As, B, Ba, Bi, Ca, Cd, Co, Cr, Cu, Fe, K, Li, Mg, Mn, Na, Ni, Pb, Si, Sn, Ti, V, Zn
2–10 ppm	Be, Ge, Mo, Sb, Zr
11–100 ppm	Hf, Nb, Sr, Ta, Th, W

Source: DeKalb, E.L. and Fassel, V.A., Optical atomic emission and absorption methods, in Gschneidner, K.A. Jr. and Eyring, L. (eds.), *Handbook on the Physics and Chemistry of Rare Earths*, vol. 4., North-Holland, Amsterdam, 1979.

Note: Method: arc or spark excitation without any preconcentration.

intensity measurements. Addition of a reference element is not needed. Interelement effects and line interferences are not a problem. Apart from the freedom from interelement effects, ICP excitation also has the advantage of linear analytical calibration curves that cover a change in concentration of up to five orders of magnitude.

When it comes to the determination of rare-earth materials in other substances, separation of the rare earths as a group precedes the analysis. This enables lower detection limits and simplifies the analytical problem, particularly for geological samples of varying compositions. The rare earths are separated with the aid of a carrier, yttrium. Other carriers have also been tried.

XRF has been a popular technique, extensively used, for the determination of rare earths in rocks, minerals, rare-earth concentrates, complex rare-earth mixtures, essentially pure rare earths, and other diverse materials such as alloys and nuclear reactor fuel. Minimal sample preparation and simpler spectra are among the attractions of this technique.

Mass spectrometry techniques are used in two formats for rare-earth analysis, named depending on the method of sample excitation and ion generation: ICP-MS and SSMS. The MS techniques have several inherent advantages, with an unparalleled range of elements amenable to analysis, small sample and rapid analysis, and very high sensitivity. The major issue is isobaric interference, and this usually can be resolved by a preconcentration procedure. The technique has been the favorite for the analysis of geological samples.

When facilities are accessible for neutron irradiation, handling of activated samples, and measurement of induced radioactivity, NAA is the preferred technique for quantitative determination of rare earths, particularly at low concentrations. Minimal sample preparation, high sensitivity, and absence of interference issues make the technique attractive. This technique is also used for the determination of residual oxygen in rare-earth metals.

The determination of interstitial impurities in rare-earth metals and alloys is done by well-standardized methods—the same as those used for refractory metals like niobium: carbon by combustion, and oxygen, nitrogen, and hydrogen by vacuum and/or inert gas fusion. Kjeldahl's method is still preferred for nitrogen and, as mentioned above, neutron activation for oxygen, in certain specific cases.

9 Environmental Aspects

9.1 INTRODUCTION

Among the current major rare earths consumers, United States, Japan, and the European Union are concerned about the rare-earth element (REE) supply, considering that the elements are vital input to materials and devices that support and sustain industrial economy apart from military technology and clean energy initiatives. The US Department of Energy (DOE) commissioned a study to determine which periodic elements are essential to maintaining the integrity of the United States, where key and critical materials were identified (USDOE 2010). Nine of the 14 key elements are REEs. The European Union undertook a similar exercise, and the results are the same. The REEs receiving "key" designations include lanthanum, cerium, praseodymium, neodymium, samarium, europium, terbium, dysprosium, and yttrium. The five other key elements are elements scattered throughout the periodic table and include lithium, cobalt, gallium, indium, and tellurium. "Critical elements" are a selection of the key elements that are necessary for clean energy technology production and have even greater supply risks than the key elements. The key elements conferred with the critical designation in the short term (0–5 years) were dysprosium, neodymium, terbium, europium, yttrium, and indium. Critical materials in the medium term (6–15 years) include dysprosium, neodymium, terbium, europium, and yttrium. All of them are REEs. The same US DOE report has even outlined a strategic plan to explore substitution of key and critical elements in future technologies, recycling from waste electronics, and development of a globally diverse supply of these elements. Out of these three options, the last one will provide a lasting solution if adequately supported by the first two options.

Countries need REEs. By an interesting turn of events that lasted about two decades, the world production and supply of REEs came to be completely controlled by China. The rare-earth prices shot up steeply in 2010, and supply became restricted at about the same time. The message became clear. Many countries had exploitable rare-earth resources but no active industrial infrastructure for processing these resources. There was another factor. Rare-earth processing had gained a reputation as being environmentally problematic. Record-high REE prices and uncertainty in long-term supply from China's primary resources have already resulted in increased investments for exploration and development of REE deposits in the United States and elsewhere in the world. Companies began rediscovering the mining potential of REE deposits across the nation from the Bokan Mountains in Alaska to the Bear Lodge Mountains in Wyoming; from the Northwest Territories, Canada, through Greenland to the deserts of Western Australia. Favorable market conditions and a promising deposit could result in a geographically distributed and rapidly developing REE mining in various countries, which will eventually lead to an era of price stability and supply reliability (Chen 2011).

As with any mine or refinery, REE production (mining and processing) could contaminate the environment if the best technology and management practices are not used and the operations are not closely monitored. Companies in their own wisdom as well as federal and state agencies must determine how to best oversee the projects to ensure that the operations do not put human health and the environment at risk. Many potential contaminants reside within REE-bearing rocks and minerals. The possible contaminants include, but are not limited to, radionuclides, REEs, metals such as barium, beryllium, copper, lead, manganese, and zinc, sulfide minerals, carbonate minerals, and other potential contaminants such as fluorine and asbestos minerals. Mining exposes these possible contaminants, while refining isolates and concentrates the possible contaminants. REE mining is hard-rock mining, so any of the environmental concerns associated with hard-rock mining could be a concern with REE production (Castor and Hedrick 2006).

The possible contaminants cause negative effects toward aquatic and terrestrial organisms in addition to humans. Some of the radionuclides and metal contaminants are even classified as human carcinogens by international and federal health agencies. Other possible contaminants increase the mortality rates of aquatic and terrestrial organisms. Apart from such direct effects, a variety of indirect consequences can arise due to the reagents and production practices that have not been carefully screened and rated high in benignity index toward the earth and its environment. The past two decades have revealed what can go wrong environmentally when there is unrestrained processing on rare-earth resources for maximizing output. The corrective actions in China's facilities and the new and revised practices in Mountain Pass and Mount Weld present valuable lessons to potential miners and processors all over the world. It is now possible to design and implement enlightened methods of rare-earth mining and extractions from resources that are basically plentiful and widely distributed all over the world.

9.2 CONTAMINANT ELEMENTS IN RARE-EARTH ORES

9.2.1 Radioactive Contaminants

One special type of contaminant associated with REE ores is radionuclides. REE-bearing minerals such as monazite, xenotime, and bastnasite usually contain low but varying levels of primordial thorium-232 and uranium-238, along with their decay products. Uranium-235 is also present but in very low quantities. Thorium-232 and uranium-238 are rather benign by themselves, but some of their decay series products can represent a danger to the environment due to the energetic particles and gamma rays released during radioactive decay. Therefore, uranium-238, thorium-232, and their decay products, if they get into the environment, could present a threat to human health. Radium-226 in the uranium-238 decay chain produces radon-222 gas, with $t_{1/2}$ = 3.8 days and bismuth-214, which are intensely radioactive (Argonne National Laboratory 2005). Due to the short half-lives of radon-222 (gas and prone to be inhaled and to decay in the lungs) and bismuth-214 ($t_{1/2}$ = 20 minutes) from the radioactive decay of radium-226, these isotopes exhibit accelerated decay rates than their parents, which have very long half-lives. This is the reason that

radium-226 is often regulated as opposed to uranium-238. Nuclear radiation have the potential to dislodge electrons from important biological molecules including water, protein, and DNA.

Radionuclides released into the atmosphere can be carried by wind and travel long distances before settling in soil or water. Uranium is very soluble in water, which can result in groundwater contamination. Radium is less soluble. Thorium is generally insoluble and seldom a groundwater concern. The radioactive materials reaching the ground can become incorporated by plants, which can then bioaccumulate in organisms eating the plants, including humans. Various studies have shown that low doses of radiation cause humans no harm, but beyond a threshold can cause seriously detrimental health effects. Ionizing radiation from radioactive decay is generally known to be a human carcinogen. The decay products of radon-222 gas in air represent the greatest risk to developing cancer. The energetic particles can be inhaled and can harm lung tissue to the extent that cancerous cells can develop. These carcinogenic effects can be observed in all living organisms.

9.2.2 Contaminants from Hard-Rock Mining

Radioactivity is not the only concern from REE production. As many as 15 different REEs could make their way into the environment during production from carbonate mineral dissolution. However, the toxicity of REEs in the environment is not completely understood. REE mining is hard-rock mining, so any metal of concern associated with hard-rock mining should be a concern with REE mining as well. Such metals as aluminum, arsenic, cadmium, cobalt, copper, gold, iron, lead, manganese, silver, and zinc are often associated with hard-rock mining. The dangers of these metals, if any, in the environment are well documented. Many of the potential metal contaminants also occur within sulfide minerals that often accompany REE ores. The dissolution of sulfide minerals, such as pyrite and chalcopyrite, can release these metals into the environment.

Sulfide mineral dissolution also creates a reaction where sulfuric acid is formed and causes acid mine drainage. Sulfuric acid lowers the pH of water resources aiding in further sulfide mineral dissolution, releasing more metals and acid into the environment. It initiates a positive feedback loop that is not good for the environment. However, with the REE ores, sulfide minerals are usually not the main mineral constituents. Carbonate minerals are often the dominant minerals present in REE ores. These minerals help neutralize acid that is generated during sulfide mineral dissolution. The dissolution of carbonate minerals can raise the pH of the aqueous system and limit sulfide mineral dissolution, preventing acid generation and the ingestion of metals into water.

Excessive carbonate mineral dissolution is equally undesirable as sulfide mineral dissolution. Carbonate mineral dissolution introduces alkaline materials into water, where they can raise the pH of water and introduce contaminants into the environment similar to how sulfide mineral dissolution does. Bastnasite is one of the carbonate minerals that can undergo dissolution. Another contaminant to be concerned about in carbonate mineral dissolution is fluorine. Fluorine is also a constituent of bastnasite. The dangers of fluorine in the environment are well documented. One last

geochemical consideration associated with REE ores is the presence of the mineral riebeckite. Some REE deposits contain known occurrences of this asbestos mineral. This highlights the chemical uniqueness of every REE deposit and the importance of extensive chemical characterization to determine likely environmental concerns at individual deposits (Castor and Hedrick 2006).

9.2.3 Rare-Earth Elements

The threats to human health and the environment from radionuclides are well recognized, but the threats from REEs are equally unknown. Information on the pattern of movement of REEs in the environment is generally lacking. The toxicology of REEs to aquatic, human, and other terrestrial organisms is not well understood either.

9.3 MAIN PROCESS STEPS IN MINING AND PROCESSING

The United States is one of the three countries where mining for rare earths started in the closing years of the nineteenth century. The other two countries are Brazil and Sweden. Historically, mining activities in the American West, in an unregulated environment, have created numerous ecosystem disturbances. Mining activities basically expose previously unexposed rocks to bacteria, oxygen, water, and wind. The collective action of these weathering forces chemically and physically alters the chemical-laden rocks that have been below the surface for millions of years (EPA 1995). Chemical and physical alteration of natural constituents in rocks during mining can lead to dispersal in the environment and its contamination. In any case, mining and milling itself are not the only means of contaminating the environment. Refining processes that accompany hard-rock mining also do the same and can be dangerous to the environment. While mining exposes contaminant-laden rocks and increases the surface area of minerals, refining isolates and concentrates the waste materials also. The chemicals and compounds used during refining contaminate the environment too.

Rare-earth deposits are diverse, and hence a wide variety of mining and processing technologies are used for the production of rare earths. Usually, rare earths are recovered as a by-product of other metals. The prime example is the largest rare-earth mining at Bayan Obo, where the main output is iron and rare earths are obtained as a by-product. Another by-product from this mine is niobium. Many smaller REE extractions are by-products from titanium or uranium mining operations (BGS 2010). The most frequently practiced processing technique of the crude ore after mining is the concentration (also called beneficiation) by milling and flotation or other physical beneficiation methods. This technique—milling and flotation—is used at Bayan Obo, at the Sichuan mine, at Mountain Pass, and also at Mt. Weld. The main process steps in REE mining and beneficiation are shown schematically in Figure 9.1.

Rare earths are most frequently mined by open-pit methods. There are also deposits, like the Canadian deposit at the Thor Lake, which require underground mining. In open-pit mining, before accessing the ore that is rich in metals to be extracted, the soil and vegetation above the bedrock (overburden material) as well as the waste rock (not ore-bearing or having a too low concentration of the ore) are removed and kept aside.

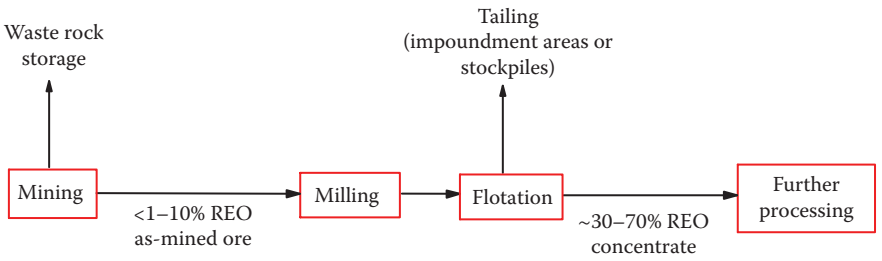


FIGURE 9.1 Main process steps in REE mining and processing. (From Schuler, D. et al., *Study on Rare Earths and Their Recycling*, Oeko-Institut e.V, Darmstadt, Germany, 2011.)

The next step after mining of the crude ore is milling. The ore is crushed and subsequently ground to fine powder in the mill. Further processing/separation of ore is done by exploiting surface properties of minerals, and milling is done with the aim of creating a high surface area. The third step is the separation of the valuable metals from the milled ore by physical methods. The popular method for major rare-earth mineral is flotation, which consumes a lot of water and chemicals (flotation agents) as well as a high amount of energy. The input into the flotation is the milled crude ore in which concentrations (grades) of REO are often between 1% and 10%. The product of the flotation is a concentrate with an REE percentage in the range of 30–70%. The large waste streams, called tailings, are a mixture of water, process chemicals, and finely ground minerals. Usually, the tailings are collected in impoundment areas, which can be either artificial reservoirs or even natural water bodies (e.g., lakes). They are surrounded by dams (Schuler et al. 2011).

Eventually, the concentrate undergoes further processing after transportation to a refinery, usually off-site. The REEs are progressively purified, further extracted, and separated into the different elements as required. This separation of individual REEs is a particularly challenging task and is difficult due to their chemical similarity. Certain ore deposits have characteristics that permit *in situ* leaching (ISL) technology, wherein, without actually mining the ore, the rare-earth values contained in it are obtained in the solution, and the solution is recovered from the mine site for further processing in a refinery. A well-known example of this technology in use is the Chinese *heavy rare-earth element (HREE) mining* from ion-adsorption deposits. The process details were given earlier in Chapter 3.

9.4 CONTAMINANT RELEASE POINTS

An overview of the potential dangers to the environment if mining and processing are carried out without specific regard to possible effects on the environment is depicted in Figure 9.2. An indication of the gravity of the damage (or severity of risk) is denoted by the number of ">" sign that appears in the loop. The severity is more if the sign appears many times. These factors are also listed in Table 9.1. The radionuclides, REEs, metals, sulfides, carbonates, and other contaminants may get

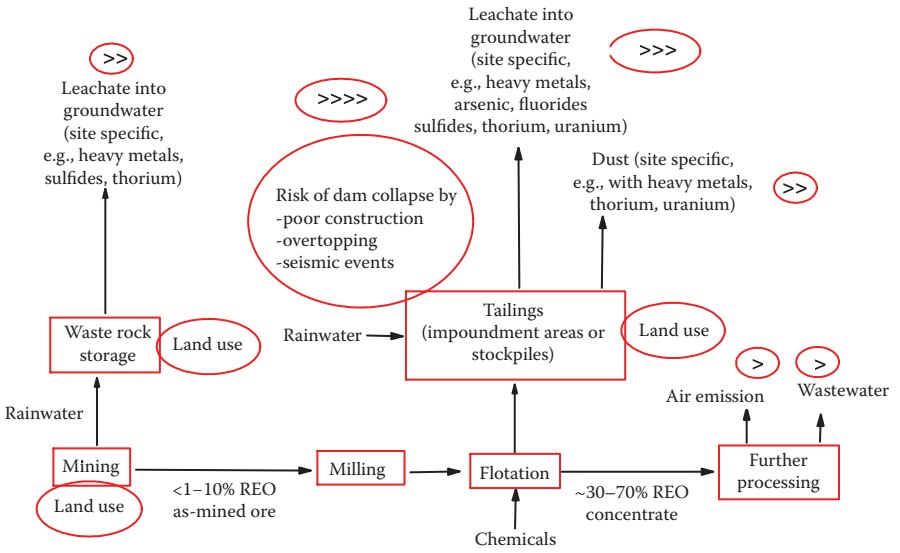


FIGURE 9.2 Risks of rare-earth mining without or with insufficient environmental protection systems. (From Schuler, D. et al., *Study on Rare Earths and Their Recycling*, Oeko-Institut e.V, Darmstadt, Germany, 2011.)

TABLE 9.1
Summary of Issues and Risks in the Head-End Operations of Rare-Earth Mining and Processing

Issue/Risk	Affected Compartments	Relevant Toxic Compounds
Overtopping of tailing dam	Groundwater, surface water, soil	Water emissions: in most cases, radionuclides, mainly thorium and uranium; heavy metals; acids; fluorides
Collapse of tailing dam by poor construction	Groundwater, surface water, soil	
Collapse of tailing dam by seismic event	Groundwater, surface water, soil	
Pipe leakage	Groundwater, surface water, soil	
Ground of tailing pond not leakproof	Groundwater	
Waste rock stockpiles exposed to rainwater	Groundwater, surface water, soil	Air emissions: in most cases, radionuclides, mainly thorium and uranium; heavy metals; HF; HCl; SO_2; etc.
Dusts from waste rock and tailings	Air, soil	
No site rehabilitation after ceasing of mining operation	Land use, long-term contaminated land	
Processing without flue gas filters	Air, soil	
Processing without wastewater treatment	Surface water	

Source: Schuler, D. et al., *Study on Rare Earths and Their Recycling*, Oeko-Institut e.V., Darmstadt, Germany, 2011.

released into the environment at the mine site and refinery. The route by which the possible contaminants could be introduced into the environment represents likely *waste streams*.

Apart from the impacts mining has on the environment, mining also entails social issues in and around the facility location, and this will have to be carefully considered when planning and implementing mining projects.

9.4.1 Mine Pit

All contaminants, if they exist at a mine, will be exposed in the bottom and walls of an open pit, where they will interact with bacteria, oxygen, water, and wind. These contaminants remain exposed to these weathering conditions over the life of the mine. The longer the pit remains open, the more these possible contaminants can be released into the environment. The *open pit* itself continues to remain an environmental risk, particularly after the closure of the mine. It will be exposed to rainwater, which will dissolve the contents of exposed areas in the mine, which might include toxic and radioactive substances. The concern is more of the solution so formed percolating down through the mine base into the water table below.

9.4.2 Tailing Impoundment

The *tailings* are a major short- and long-term risk. The tailings comprise fine particles (hence large surfaces), wastewater, and flotation chemicals. Usually, they are left to remain forever in the impoundment areas. Over time, they are likely to be exposed to rainwater and storm water runoff, and by this continuous exposure to water, contents of the tailings including the toxic substances are likely to be washed out. Unless the ground of the impoundment areas is leakproof there will be steady emissions to groundwater. Another serious risk, acute in nature, is the storm water runoff. During heavy rainfall, the impoundment areas may not be able to store the huge amounts of storm water. Then, large amounts of untreated toxic water will mix with and pollute surrounding water bodies and soils. The extent of this damage is site specific as the composition of polluting water depends on the composition of the host minerals and flotation agents used. In most cases, the tailings include radioactive substances, fluorides, sulfides, acids, and heavy metals. Most of the rare-earth deposits contain uranium, thorium, and their decay-chain products. The storage of radioactive substances in the tailing pond and possible dispersal into the environment along with other toxic substances need to be separately quantified to assess the real risk in a disaster scenario wherein the dam collapses and the highly toxic water and sludge flood the surroundings. There are several factors that might lead to a dam collapse: overtopping from storm water, poor construction, and seismic events. These risks require long-term monitoring as the dams must not only remain stable during the mining operation but also stay intact over really long periods after the closure of the mine.

9.4.3 Waste Rock Stockpiles

A similar risk is also posed by the contaminants residing in waste rock stockpiles at a mine site. In fact, it is more likely that the contaminants from waste rock piles will be introduced into the environment considering that these are not contained in a pit and that only man-made barriers can prevent them from being dispersed into the environment. They are also exposed to rainwater, and chemically toxic substances, such as fluorides, sulfides, acids, and heavy metals, as well as radioactive substances may be washed out and spread into water bodies and soil. In reality, this is of much lower consequence because of the form and composition of the waste rock heap. On the whole, the potential release is anticipated to be much lower than in the tailings, as the rock consists of coarse minerals, whereas the tailings consist of finely milled particles, and process chemicals are not mixed up with waste rock stockpiles.

9.4.4 Mill

The mill itself represents a waste stream. Some REE ores may unintentionally be lost during the milling process. Planned wastes will also be piled on-site. Unless the ores and wastes are carefully collected and monitored, contaminants could easily end up in the environment.

9.4.5 Air Emissions

Apart from the leaching of toxic substances by rainwater and associated risks of this solution and sludge spreading to the surrounding areas and water, there are emissions into air that need to be addressed. A risk factor for the workers and the neighborhood are windblown dust particles containing toxic (heavy metals) and possibly radioactive substances. Here again, the concentration and quantity are important. The dusts originate from the mine and the mining operations, the milling, the transportation, and finally, the storage. The windblown dust particles from the tailings and waste rock stockpiles are also to be considered. Dust emissions are particularly serious in dry operations involving fine particles. Wet matter does not contribute much to this problem.

9.4.6 Mine Site

Technically, the land use for mining also constitutes environmental interference. It covers the mine proper, the storage of the waste rocks, the tailings, the entire infrastructure, and the immediately surrounding areas that are occupied by the mine and related activities during the mining operation as well as after the mine closure. Another environmental issue is the large water and power consumption, particularly if the mining is carried out in dry areas. Restoring the mining area per se to the original ecosystem has been successfully implemented in certain instances but not yet for any major rare-earth mine.

9.4.7 Head-End Processing

The refining of the rare-earth concentrate is a very energy-intensive process and has potential for direct and indirect air emissions (e.g., SO_2, HCl, dust, toxic substances, and CO_2) if no abatement technologies are in place. Various acids and bases are used to refine the REE ores into marketable products. The chemicals and compounds used to isolate and concentrate possible contaminants become their carriers and should be of concern too.

Majority of the rare-earth deposits also contain certain amounts of thorium and/or uranium, making it necessary to track them through the entire processing sequence and take appropriate remedial measures if there are real issues as determined by the objective quantification of the radioactivity involved in emissions at various stages. The major environmental issues are listed in Table 9.1.

9.5 ENVIRONMENTAL ASPECTS OF MINING AND PROCESSING IN CHINA

9.5.1 Overview

Much (nearly all) of the world's rare-earth mining and processing activities during the past decade and a half have been confined to China. It is generally believed that most of this mining and processing was carried out without any strict adherence to industry regulations that are in place to minimize the direct and consequential damage to the environment. In such a situation, data collected could point to the worst-case scenario as regards environmental damage in rare-earth mining. It may be kept in mind that no mining of the placer monazite is involved here. Approximately four-fifths of the ore mined and processed is bastnasite, and one-fifth, the ion-adsorption ore. The data pertain essentially to bastnasite. According to the Chinese Society of Rare Earths, every ton of REEs produced generates approximately 8.5 kg of fluorine and 13 kg of flue dust. Additionally, sulfuric acid refining techniques used to produce 1 ton of REEs generates 9600–12,000 m^3 of gas laden with flue dust concentrate, hydrofluoric acid, sulfur dioxide, and sulfuric acid. Not only are large quantities of harmful gas produced; huge amounts of liquid and solid waste also resulted from the refining processes. The estimate is that at the completion of refining 1 ton of REEs, approximately 75 m^3 of acidic wastewater and about 1 ton of radioactivity containing waste residue are produced. In 2008, for example, China produced over 130,000 t of REEs. It is estimated that total production yields extreme amounts of waste. The industry in China and elsewhere in the world can learn a lot from China's environmental issues related to REE production. Unless monitored and controlled, mining and refining processes can introduce REEs, metals, radionuclides, and other potential contaminants into the environment at unnaturally high rates.

There are several large mines and a large number of small mines in China. Some of the mines, especially the small ones, are known to be partly unregulated. The environmental problems associated with all these mines have been the stated reason for China implementing the quota system for rare-earth exports is environmental protection.

9.5.2 Bayan Obo Facilities

The largest rare-earth mine in the world, the Bayan Obo mine, is located in Inner Mongolia. It is essentially an iron ore mine. The main product is iron ore; light rare earths and niobium are by-products. Surface mining is practiced. The rare earths are recovered from a bastnasite–monazite mix containing light rare-earth elements (LREEs) and also thorium. Considerable environmental problems and health hazards in mining, concentration, and further processing are known to exist.

Mining at Bayan Obo has been going on for more than 40 years. Nearly one-third of the main and east ore bodies have been already exploited. For nearly 30 years, since the beginning, the recovery rate of mineral resources remained less than 10%, and the present recovery rates are between 40% and 60% (Schuler et al. 2011). The thorium resource at Bayan Obo has not been utilized.

The tailings are transported to the tailing impoundment/reservoir in nearby territories and collected. The impoundment of the whole mining operations (iron ore and rare-earth concentration plants) covers an area of 11 km^2, and is 12 km in length. Incidentally, this reservoir is about 100 times the size of the alumina factory waste pond that collapsed in Hungary on August 4, 2010, which released 600,000–700,000 m^3 of toxic red sludge into its surroundings (Bradsher 2010; WISE-Uranium 2010). The amount of tailings from the iron and rare-earth mining in Bayan Obo has already reached 150 million tons (MEP 2009). This contained in tailings and residues.

According to the data available with the Baotou Radiation and Environmental Management Institute, the average Th content in the Bayan Obo ore bodies is 0.0135%. This is reflected in the gamma radiation dose rates of the ore bodies exceeding the background values. Besides, plants and soils in the area have higher contents of ^{232}Th, ^{238}U, ^{226}Ra, and ^{40}K (Schuler et al. 2011).

Thorium-containing dust is emitted at about 61.8 t/year during the ore crushing process. Adverse health effects attributable to these dusts in Baotou has been observed (Schuler et al. 2011). Besides, groundwater pollution, possibly caused by the tailings pond has also been reported in the area.

Here are some numbers to present the magnitude of the problem. Processing 100,000 tons of rare-earth concentrates per year during the extraction phase leaves behind approximately 200 tons of ThO_2 contained in sludge. Using the sulfuric acid roasting method, the production of every ton of rare-earth concentrate causes the release of between 9600 and 12,000 m^3 of waste gas containing fluoride, SO_2, SO_3, and dust. Furthermore, 75 m^3 of acid-washing wastewater and 1 ton of radioactive residues are also generated (MEP 2009).

9.5.3 Sichuan Mine

The Sichuan mine is another large open-pit mine for LREE based on bastnasite. The thorium content of bastnasite is higher (MEP 2009). Very limited information is available on the environmental load due to operations at the Sichuan mine. According to Cheng and Che (2010), the recovery rate of the mining and concentration plant of the Sichuan mine has remained below 50%. The present ore (Sichuan bastnasite)

processing practice involving oxidizing roasting–hydrochloric acid leaching not only yields low-purity cerium but also disperses fluorine and thorium into waste residues and wastewater.

9.5.4 Ion-Adsorption Deposits

Heavy rare earths are mined from the famous ion-adsorption deposits in southern China. Significantly, these are rare-earth deposits that are essentially thorium-free. There is no uranium either. Nevertheless, there are serious environmental problems associated with their exploitation. On account of their low RE grade but amenability to easy release of rare-earth values into somewhat milder leachants, the mining is carried out with *in situ* leaching (ISL), a technique that requires no surface and no underground mining (Cheng and Che 2010).

ISL is carried out by drilling holes into the ore deposit and pumping the leaching solution into the deposit, where it makes contact with the ore. The solution bearing the dissolved ore content is then pumped out to the surface and processed. In comparison to other leaching technologies such as pond and heap leaching that can be practiced for these ores, the ISL technology is regarded as more environmentally sound by the Chinese government (MIIT 2010). The ISL procedure is not controllable hydrogeologically, and this may cause problems.

Presently, the scarce ion-adsorption deposits are processed with an average recovery rate of 75% by applying the ISL method. Beginning in 1970, for nearly 30 years, the pond leaching method was used, and the recovery rate was only about 26% (Cheng and Che 2010).

9.5.5 Processing

In the course of the elaborate extracting, separating, and refining processes, for the rare earths, a large number of chemicals in considerable quantities are used, leading to a huge amount of waste gas, wastewater, and solid waste. An overview of the present mining as well as refining methods in China's rare earth industry for three dominant minerals is given in Table 9.2. According to Chen (2010), most of the facilities in the country do not have sufficiently elaborate waste stream treatment systems. Some small rare-earth smelting–separation facilities do not even have any system for monitoring or controlling the discharges at all. In recent times, the Chinese government has taken note of this state of affairs and is disposed to raise the environmental standards.

9.5.6 Wastewater from REE Separation and Refining

Saponification with ammonia has been widely used (as of 2011) for rare-earth refining in China. For the separation of every ton of rare-earth concentrate (with an REE content of 92% REO), 1–1.2 tons of ammonium bicarbonate are needed (MEP 2009). A large quantity of wastewater is also produced. According to an estimate, in the entire rare earth-refining industry, approximately 20,000–25,000 t

TABLE 9.2
Overview of Mining, Extraction, and Separation Methods Adopted in China's Rare-Earth Industry

Minerals	Mining and Beneficiation	Decomposition of Rare-Earth Concentrate	Separation and Refining of REO	Extraction of Rare-Earth Metal
Bastnasite–monazite mixed type (Bayan Obo mine, Inner Mongolia)	Surface mining: the ore is iron–niobium–REE deposit. The ore is crushed into gravel size and transported to the mill factory. Through low-intensity magnetic separation to high-intensity magnetic separation up to flotation process, rare-earth concentrates (with 30–60% grade of REO) are produced as coproducts by the main product, iron.	The two following methods are used: 1. Acidic method: REOs are roasted at 400°C and 500°C in concentrated sulphuric acid to remove fluoride and CO_2. Then the solution is leached in water and filtered to remove the impurities. REEs are then leached in extraction agents like ammonium bicarbonate $(NH_4)HCO_3$ precipitation and hydrochloric acid. REE chlorides ($RECl_3$) are achieved. This method is used for 90% of products. 2. Alkaline method.	For successive separation, liquid–liquid extraction is adopted mainly based on P507 ($C_{16}H_{35}O_3P$) and HCl. Then the solvent is precipitated by ammonium bicarbonate, $(NH_4)HCO_3$, or oxalic acid, $C_2H_2O_4$. The precipitate [$RE_2(C_2O_4)_3$ or $RE_2(CO_2)_3$] is heated, and REOs are formed by oxidation.	Light rare-earth metals are extracted by molten-salt electrolysis based on chloride or oxide. The middle and heavy rare metals such as Sm, Eu, Tb, and Dy are obtained by metallothermic reduction in vacuum. The reaction is carried out at 1450–1750°C and needs an inert gas like argon.
Bastnasite (Sichuan)	Surface mining: the ore is an alkali granite–type rare-earth element deposit. The ore is crushed into gravel size and transported to the mill factory. Two methods are adopted: – From gravity separation to magnetic separation – From gravity separation to flotation separation	The rare-earth concentrates achieved a grade of 70% REO. The present treatment process of Sichuan bastnasite in the industry is an oxidating roasting–hydrochloric leaching process. The roast is carried out at 600°C to remove CO_2. The RE concentrates are leached in hydrochloric acid, precipitated by sodium hydroxide solution, and leached in hydrochloric acid again. REE chlorides ($RECl_3$) are achieved.		

(*Continued*)

TABLE 9.2 (CONTINUED)
Overview of Mining, Extraction, and Separation Methods Adopted in China's Rare-Earth Industry

Minerals	Mining and Beneficiation	Decomposition of Rare-Earth Concentrate	Separation and Refining of REO	Extraction of Rare-Earth Metal
Ion-adsorption deposits (seven provinces in the south of China)	Currently used mining method is *in situ* leaching (ISL), which is a typical flow process coupled with chemical reaction and solute transport. Heap leaching and ponding leaching have been banned due to massive vegetation damage. The minerals are firstly leached in ammonium sulfate $(NH_4)_2SO_4$ through an ion-exchanging reaction. Then rare-earth concentrates are obtained by precipitation with ammonium bicarbonate, $(NH_4)HCO_3$, or oxalic acid, $C_2H_2O_4$. Rare-earth concentrates with a grade of 92% REO are achieved.		Concentrates are leached in hydrochloric acid (HCl). Extraction is carried out in a P507 ($C_{16}H_{35}O_3P$) system. This extraction reagent, 2-ethylhexyl 2-ethylhexyl phosphate (P507), is widely used to extract and separate rare-earth metals.	

Source: Schuler, D. et al., *Study on Rare Earths and Their Recycling*, Oeko-Institut e.V., Darmstadt, Germany, 2011. Compiled based on MEP, The explanation of compiling emission standards of pollutants from the rare earth industry 2009, Ministry of Environmental Protection, 2009.

of wastewater was generated for the production of 103,900 t REO in 2005. The NH_3/NH_4^+ content of wastewater is in the range of 300–5000 mg/L, which is 10 to 200 times (MEP 2009) the limit set by the government. This and many other characteristics of China's rare-earth industry were set to change with the Ministry of Industry and Information Technology of China issuing in May 2010 the notice on the consultative draft of "Entry Criterions for Rare Earth Industry" (MIIT 2010).

9.6 ENTRY CRITERIA FOR RARE-EARTH INDUSTRY (CHINA)

Issued in May 2010 by Ministry of Industry and Information Technology, China, the notice on the consultative draft of "Entry Criterions for Rare Earth Industry" (MIIT 2010) clearly stipulates thresholds and requirements in terms of environment protection to assist the rare-earth industry in sustainable development. It also foresees a restructuring of the rare-earth industry. The major environment related issues appearing in the report of Schuler et al. (2011) are

1. Mining of pure monazite minerals is banned due to the high-level of radioactive elements in them and the resulting environmental damage.
2. The facilities for the processing of bastnasite and mixed minerals must be installed with a complete treatment system for waste water, waste gas, and solid waste.
3. As regards the ion-adsorption deposits, ponding and heap leaching are banned due to possibility of massive environmental damage. The ISL (in-situ leaching) method is recommended.
4. Saponification with ammonia is banned in rare-earth refining.
5. Elemental metal refining should not adopt fused chloride electrolysis. When using molten fluoride electrolytes, a treatment system capable of dealing with fluorine-containing wastewater and waste gas should be in place.
6. Fluorine-containing solid waste should be disposed of separately and must not be mixed with other industry residues.
7. The maximum electrical energy demand per ton of rare earths produced must be indicated.
8. The mining-loss rate for mixed rare-earth minerals and bastnasite should not be more than 10%, while the ore-dressing recovery rate of these ores should exceed 72%.
9. The ore-dressing recovery rate of ion-adsorption deposits should not be less than 70%.
10. The recycling rate of ore-dressing wastewater of mixed rare-earth minerals and bastnasite should exceed 85%, while the figure for ion-adsorption deposits should exceed 90%.
11. The rehabilitation of plants and vegetation after mining of ion-adsorption deposits should cover at least 90% of the affected area.
12. The yield of refined rare-earth metal should be more than 92%.

In addition these, the Ministry of Environmental Protection of China revised the Emission Standards of Pollutants from Rare Earths Industry in July 2010. The new standard set specific thresholds (differentiated between existing enterprises and newly established enterprises) for the amount of pollutants including wastewater, waste gas, and radioactive elements, especially thorium. Certain thresholds in these emission standards were even more stringent than those in industrialized nations (Schuler et al. 2011).

9.7 RESEARCH AND DEVELOPMENT ON CLEANER PRODUCTION IN CHINA

Spurred by the renewed emphasis on environmental consciousness, the research community in China responded with a series of ideas and processes for cleaner production of rare earths (Schuler et al. 2011), addressing issues including tailings from Bayan Obo, full recycling and clean production in the rare-earth leaching process, and an oxidizing roasting–sulfuric acid leaching extraction process as a promising alternative green process that not only produces high-purity cerium but also realizes the separation of fluorine and thorium (Luo et al. 2008). Grirem Advanced Materials Co., Ltd., developed an environmentally friendly hydrometallurgical separation process—a nonsaponification solvent extraction process based on hydrochloric acid and sulfuric acid to separate neodymium and samarium. This method eliminated the generation of ammonia–nitrogen wastewater. The consumption of other extraction agents is decreased by 20% due to a reduced number of process steps (MEP 2009). Besides, according to a patent by the Beijing General Research Institute for Nonferrous Metals, a method for extracting and separating quadrivalent cerium, thorium, and fluorine, as well as, to a small extent, trivalent cerium, from a rare-earth-sulfate solution has been developed. The synergistic extraction agents are based on P507 (2-ethyl-hexyl-2-ethyl-hexyl phosphate) or P204 (di-2-ethyl-hexyl phosphoric acid [D2EHPA]). The advantages of this method are listed as high separation ratio of thorium; no emulsion generated during the process; and all elements (cerium, thorium, fluorine, and iron) being extracted into an organic phase and separated by step-by-step back extraction (stripping). As regards the environment, since no ammonia saponification agent is adopted, there is no wastewater containing ammonia–nitrogen, and fluorine and thorium are recovered (Beijing Nonferrous Metal 2008).

9.7.1 Technology Solutions to Environmental Problems

9.7.1.1 Fluorine Emission and Mitigation

The World Health Organization (WHO) has classified fluoride as one of the contaminants of water that causes large-scale health problems (Bhatnagara et al. 2011) on human consumption. Among the environmental issues relating to the common processes of bastnasite treatment, the release of fluorine via waste liquid or waste solid is considered important. Fluorine accounts for up to 10 wt.% of bastnasite concentrate, and the treatment of thousands of tons of bastnasite concentrate would lead to the release of a few thousand tons of fluorine to the environment. The discharge

of such quantities of wastes leads to the fluoride contamination of surface water and groundwater (Wang et al. 2012).

In order to treat bastnasite in a more environment-friendly way, Li's group (Zhang et al. 2008, 2010) invented a new method to recover RE and fluorine with Cyanex 923 from roasted bastnasite sulfuric acid leaching liquor. Cyanex 923 is more expensive than other common extractants, such as D2EHPA and 2-ethyl-hexyl phosphonic mono-2-ethyl-hexyl ester (HEHEHP), resulting in the high cost of commercialization. Furthermore, the solid CeF_3 formed in the mixer–settler equipment during stripping causes organic losses and difficult operation.

Fluoride ion is coordinated with Ce(IV) to form CeF_2^- complex, which can be extracted into the organic phase easily with D2EHPA by the following reaction: $Ce^{4+} + 2F^- + 2(HA)_2 = CeF_2 2(HA_2) + 2H^+$. It is known that Al^{3+} can form a complex with F^- strongly (Martin 1996). A solution of aluminum salt can be used as the coordination reagent of fluoride ions to scrub the fluoride from the loaded organic phase into the aqueous phase and thus separate it from cerium. The resultant scrubbing solution containing aluminum fluoride complexes was subjected to a subsequent step to produce cryolite. Cryolite (Na_3AlF_6) is an important industrial chemical, which is widely applied in industry, especially in the Hall–Héroult process (a process for production of aluminum). Recovery of the fluoride in the form of synthetic cryolite from the bastnasite could increase the economical value of the bastnasite and also mitigate the environmental concerns by reducing the discharge of waste containing fluoride.

Wang et al. (2013) describe a novel process for conducting the extraction and recovery of cerium, fluorine, and thorium from a bastnasite sulfuric leaching solution using HEHEHP as the solvent. Analysis of the process shows that Ce(III) extraction capacity with HEHEHP is negligible, and extraction efficiency for the elements is in the order of Ce(IV) > F(I) > Th(IV) > Ce(III). After coordination scrubbing of F(I) with Al(III), Ce(IV) is reductively stripped with H_2O_2 and HCl, allowing recovery of CeO_2 with a purity of 99.95%. This process provides a more environmentally sound integrated separation and recovery flow of rare earths from bastnasite. The flow sheets for bastnasite treatment and recovery of fluorine as cryolite (Wang et al. 2012, 2013) are given in Figures 9.3 through 9.5.

9.7.1.2 Eco-Friendly RE/Th Separation

Bastnasite in Sichuan was discovered in the 1980s. Besides the rare earth, there are approximately 0.2 wt.% thorium and 9 wt.% fluoride. The former is radioactive, and the latter, harmful. Li and his coworkers (Zhang et al. 2008, 2010) developed an eco-friendly process with a new extractant to separate cerium from thorium and RE, and then, N1923 was used to separate thorium from RE. In this process, F^- is recovered. This process is also valuable to solve a similar problem in Baotou RE metallurgy (Yan et al. 2006a).

9.7.1.3 Wastewater Treatment

In China, high NH_3–N and high-salt wastewater generated in the rare-earth manufacture process caused serious environment pollution, especially in the surrounding water bodies. Traditional water treatment processes were either incapable of reducing pollutant concentration to the regulation levels or prohibitively expensive and

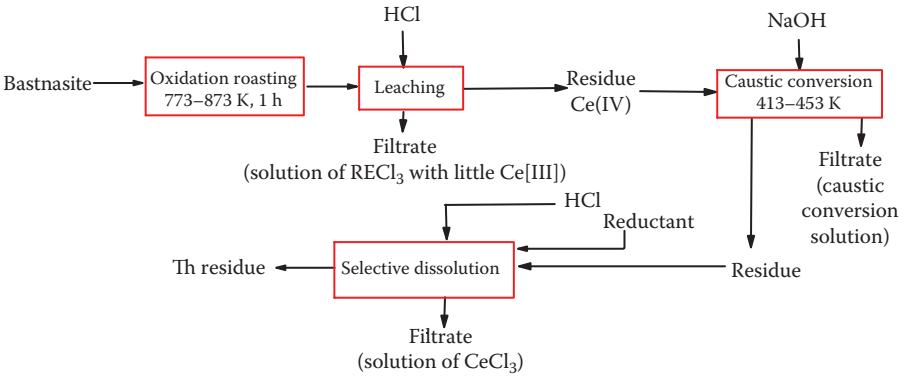


FIGURE 9.3 Schematic flow chart of bastnasite treatment by oxidization roasting, hydrochloric acid leaching, and caustic conversion. (From Wang, L. et al., *J. Hazard. Mater.*, 209–210: 77–83, 2012; Wang, L. et al., *Chem. Eng. J.*, 215–216: 162–167, 2013.)

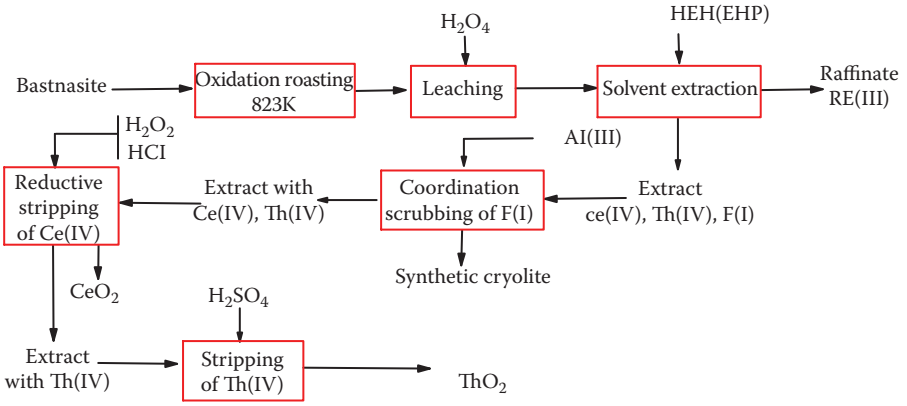


FIGURE 9.4 Schematic flow chart for the separation and recovery of RE(III), Ce(IV), Th(IV), and F(I) from bastnasite. (From Wang, L. et al., *Chem. Eng. J.*, 215–216: 162–167, 2013.)

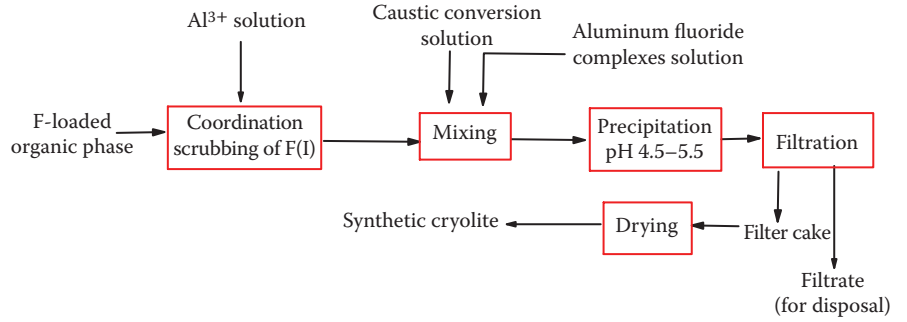


FIGURE 9.5 Schematic flow sheet of the formation of synthetic cryolite. (From Wang, L. et al., *J. Hazard. Mater.*, 209–210: 77–83, 2012.)

difficult to operate. Zhang et al. (2010a) proposed a hybrid process that integrated air stripping pretreatment and low-pressure reverse osmosis (LPRO) to treat this wastewater containing high ammonia and salt. The removal ratio of ammonia after the LPRO desalination process could reach up to 98%, fluoride amounted to more than 99%, desalt efficiencies reached up to 95%, and stripped gas ammonia could be effectively recovered. The resultant water quality was good enough for reuse or discharge standards (Zhang et al. 2010a).

9.8 ENVIRONMENT-FRIENDLY PROCESSING OUTSIDE CHINA

9.8.1 General Outlook

9.8.1.1 Monazite and Xenotime

In the past, xenotime from Malaysian placer deposits with very high contents of uranium (2%) and thorium (0.7%) was processed in Malaysia. Due to this high radioactivity level, the Malaysian processing industry failed, and the plants were closed (Yusoff and Latifah 2002, cited in BGS 2010). High levels of radioactivity in thoria—a product of monazite processing—is an issue in monazite processing. The processing of beach sands containing monazite has been banned in Australia, China, and Europe due to environmental concerns (Curtis 2009a,b, cited in BGS 2010). However, nearly all deposits that are currently under exploration also have certain amount of thorium and uranium that occur with products of their natural radioactive decay chain. The two outstanding exceptions are the ion-adsorption clay deposits in southern China as well as the Douglas River deposit in Saskatchewan, Canada (GWMG 2010; Kanazawa and Kamitani 2006).

Against the background of the severe concerns of dealing with ores containing any amount of radioactive elements, Kanazawa and Kamitani (2006) proposed that countries should examine geological structures similar to the ion-adsorption clay deposits in China in order to discover other radioactivity-free rare-earth sources. Parallel to this, research and development for mineral separation, smelting, and recovery should be focused on, including processing and appropriate disposal of radioactive wastes in a commercially manageable way.

The presence of thorium and/or uranium in the rare-earth ores is of concern not only for mining and concentration but also for refining and further processing. In all process steps, waste that arises tends to be considered radioactive and has to be handled differently. An example of this situation is the French company Rhodia Electronics and Catalysts handling its interprocess intermediates and wastes in the processing of rare earths (ANDRA 2009). In addition, the refining of rare-earth concentrate is a very energy-intensive process and has associated air and water emission concerns in common with similar industrial endeavors.

9.8.2 Recovery Rates

The specific environmental burden of mined and processed rare earths could be reduced directly and significantly by higher efficiencies in all stages of production. The first losses occur in the mining process when the cutoff grade chosen is too

high. This means that minerals with lower REO contents are not further processed. The cutoff grade is mine specific as it depends on the kinds of minerals and their response in the concentration process.

Further losses arise in the concentration process. The mines show quite different recovery rates (ratio between REO output and REO input of the concentration plant). The Mountain Pass concentration plant operates with a high recovery rate of about 90% due to very fine grinding of the minerals. Lynas (2009, 2010) states that the plant at Mt. Weld will have a recovery rate of 63%. The recovery of Chinese mines is reported to have been very low in the past. Currently, it ranges from 40% to 60% for flotation and is about 75% for the ISL method. The issue appears to be mainly technoeconomic. Environmental pressures will push recovery rates toward higher values. Further losses arise in all stages of further refining and processing. The trend and pressure will be to maximize recovery, if not for anything else but the environment.

9.8.3 Mine Planning and Management

Mining, and the industries it supports, is the bedrock of modern society. The benefits of mining have been many, but they may be coming at a great cost to the environment. Over the past century, there has been an increasing recognition that the environment needs to be protected by conscious human effort and that such protection is fundamental not only to a healthy society but also to a prosperous economy. As mines have increased in size and complexity, environmental controls, too, have become increasingly sophisticated and more effective. Modern mines are required to comprehensively evaluate environmental concerns at the earliest stages of mine planning and design and implement them all through their lifetime and usually beyond that too. Environmental controls are now considered as an integral part of overall mine management (EPA 1997). Mining and refining of REEs, like many other metals, can present considerable threats to human health and the environment. They can also be mitigated by technology and management. This situation is dramatically evident in the nation dominating REE production today, China. In the rare-earth industry, as regards the environmental load, the status is that there are fairly comprehensive hard data from the industry on all that can go wrong, and there is also a comprehensive knowledge base on how the environmental challenges can be mitigated or circumvented, not only in existing operations but also in the numerous operations planned worldwide for exploiting these wonderfully useful elements. No one group among the nearly hundred-odd chemical elements can claim to build and sustain a worldwide green industrial economy more than the rare earths. The expectation everywhere is that if these elements are going to build and sustain a green economy, they cannot be produced by technology and practices that destroy the environment.

9.9 MOUNTAIN PASS

The Mountain Pass mine and refinery began operation in 1952, when historically, few environmental controls existed, and reigned as the largest and most important rare-earth producer in the world for nearly four decades. As a consequence of

sustained competition from lower-cost China-sourced rare earths beginning in the mid-1980s, and weakened by regulatory pressures triggered by pipeline leakage of radioactive liquids, the Mountain Pass facility of Molycorp scaled down and eventually stopped production in 2002. Between 2002 and 2012, the mine site was held by Chevron Mining Inc. and later by Molycorp Minerals, which was only generating revenue from products manufactured from its relatively small stockpile of rare earths. On September 30, 2008, Molycorp Minerals LLC acquired the Mountain Pass, California, rare-earth deposit and associated assets from Chevron Mining Inc. through Rare Earth Acquisitions LLC (which was later renamed Molycorp Minerals LLC). Molycorp Minerals recommenced rare-earth mining in 2012 after modernization of its production facilities were completed, and it has plans to continue mining till 2042 with a steady annual production of approximately 20,000 t.

Molycorp proposes to expand the open-pit mine both laterally to the west, southwest, and north as well as deepening it. In addition to the existing overburden stockpile located west of the pit, which will serve as the initial overburden stockpile when mining recommences, additional overburden stockpiles will be constructed to the north or east of the pit to provide additional storage capacity sufficient to accommodate the remaining overburden material for the existing permitted life of the mine (Paul and Campbell 2011).

When mining activities ceased, the open pit was 1500 ft. wide by 400 ft. deep. It is estimated that the REE reserves (relative to a 5% cutoff grade) remaining at the Mountain Pass mine exceed 20 million tons. The average REE content in the bastnasite mineral ore is approximately 9%, and the gangue minerals (calcite, barite, and dolomite) in the carbonatite igneous rock body make up approximately 91% of the ore-containing rock. The expected overburden produced is estimated to be 104 million tons, which will be stored at two existing storage piles. These storage piles will, together, cover approximately 315 acres within 30 years of the proposed period of operation through 2042 and represent approximately a 120% change over current stockpiles accumulated between 1950 and 2002 (EPA 2012). The concentrate shall contain 68% rare earths, and recovery rate shall be around 90% (Molycorp 2010a). The site contains, apart from the open-pit mine and overburden stockpiles, a crusher and mill/flotation plant, a separation plant, a mineral recovery plant tailing storage area, on-site evaporation ponds, and off-site evaporation ponds. Groundwater and soil contamination is known to exist around the facility. Contaminants include barium, gross alpha, gross beta, nitrate, sodium lignin sulfonate, strontium, total dissolved solids, total lanthanides, total petroleum hydrocarbons (kerosene/diesel), total radium, total thorium, and total uranium. Claims have already been brought under environmental laws, regulations, and permits for toxic torts, natural resource damages, and other liabilities, as well as for the investigation and remediation of soil, surface water, groundwater, and other environmental media (Paul and Campbell 2011).

The planned reopening of the Molycorp facility required an elaborate approval procedure, which resulted in an approval in 2004. Considering the background of the recommencement of mining in Mountain Pass, it is to be expected that the plant operation will run on an environmentally advanced standard, which will translate to significantly reduced environmental load compared to facilities elsewhere in the world. It may well be anticipated that Mountain Pass will provide a benchmark for

future environmentally benign rare-earth mining and processing facilities (Molycorp 2010c).

For Molycorp Minerals (Molycorp 2010a,b), the major issues in terms of the environment and the arrangement to address them are as follows: The Mountain Pass ore contains 0.02% thorium and 0.002% uranium by weight, as uranium and thorium occur in the bastnasite mineral. Following mining, the ore is crushed and milled to produce a bastnasite concentrate. These radionuclides will partition and persist in the tailings (average, 0.022% Th and 0.0022% U) and the concentrate (0.12% U + Th). When the bastnasite concentrate is leached, U and REO dissolve, but Th remains in solid form. Subsequent to leaching, the uranium is selectively precipitated from the leach liquor, and thorium is filtered off along with the insoluble fraction of the ore. The uranium precipitate and the thorium solids are codisposed with the tailings generated during the milling step. During the milling, approximately 10% of the mined ore mass is recovered as the concentrate, and 90% of the mass ends up as the tailings. A number of non-rare-earth-bearing minerals—barite, calcite, dolomite, strontianite, and silicates—constitute the bulk of the tailings. The removal of rare-earth values from the ore and the addition of Th residue and U precipitate from the processing steps to the tailings for codisposal result in an average tailing concentration of U and Th that is somewhat higher than that of the original ore. The permission of the new plant operation allows facility personnel to conduct the day-to-day management of radioactive materials under the supervision of a radiation safety officer and a radiation safety committee. Other aspects that are environmentally relevant in the approval include the following:

1. Salt recovery (recovery of hydrochloric acid, sodium hydroxide, sodium hypochlorite) and water recycling facilities will be installed in order to reduce the freshwater consumption to approximately 10% of the water consumption of the mid-1990s (when the mine had an output of 20,000 t REO per year).
2. The wastewater generated from the mineral recovery operations as well as wastewater from the treatment of pit water and groundwater remediation systems will be evaporated in a series of on-site ponds. A groundwater remediation system will be operated.
3. The open-pit water will be pumped, treated, and reused. The facility is constructed with a series of storm water diversion ditches and settling ponds, along with a series of check dams and silt fencing to minimize erosion.
4. The hazardous waste (mainly containing lead) shall be disposed of on exterior landfills.
5. Flue gas treatment plants will be installed in order to reduce air emissions.
6. Finally, the remediation of the area after mine closure is also part of the approval.

At Mountain Pass, tailing management uses *paste technology*. Most of the water that is present during rare-earth recovery operations is filtered away from the tailings and recycled, resulting in a thick, viscous material that looks and feels like toothpaste or wet cement (Park et al. 2012). This material is conveyed by pipeline to

a lined impoundment and laid out in thin layers to facilitate rapid drying. More layers are periodically deposited, producing a pile of tailings. As the pile is developed, the side slopes are covered with soil and vegetated. At the end of the impoundment's life, the remaining surfaces of the pile are covered with soil and vegetated, resulting in a permanent repository that meets local regulations.

9.10 BEAR LODGE

9.10.1 Water Contamination

The Bear Lodge and Mountain Pass properties exhibit somewhat similar geology and contain the same dominant REE-bearing mineral, bastnasite. Analyzing the environmental issues associated with REE production at Mountain Pass provides the model for identifying potential risks at the Bear Lodge property (Paul and Campbell 2011). Any of the environmental concerns at Mountain Pass should be a concern at the Bear Lodge property along with some unique concerns specific to the Bear Lodge property. Some of possible contaminants associated with mining at Bear Lodge include, but are not limited to, radionuclides, REEs, metals, sulfides, carbonates, and other elements, such as fluorine.

Water represents the environmental medium of overall greatest concern at Bear Lodge. Not only can the possible contaminants go into solution, but also, a great deal of water is consumed during REE mining and processing. Such issues generate both water quality and quantity concerns that will heavily depend on what management practices are put into place. Pit lake water represents a potential environmental concern; however, Rare Element Resources does not intend for a pit lake to develop, because the pit will be above the water table and surface water will be diverted away from the pit. Even though the company is taking these measures, the environmental concerns of pit lake water must be analyzed because it remains a possibility until the mine is opened and it is proven not to be an issue. This could be the most dangerous water issue at the mine if the pit is opened to depths where sulfide minerals are present, considering the constant contact water would have with sulfides at depth. Water will also be in constant contact with carbonate minerals in the carbonatite dikes. Meteoric water will come into contact with stockpiled rare-earth ores while being saved for future production. How much ore is piled, how long it remains piled, and what management practices are put in place will determine the extent of contaminant release into the environment. To prevent contamination from these likely waste streams, the runoff needs to be captured and storm water controls put in place. The waters produced from the physical processing plant may pose an environmental threat as well.

The Madison formation is the prominent aquifer in the Bear Lodge area, which is often hundreds of feet from the surface (Wyoming State Geological Survey 2008). The Bear Lodge area is a recharge zone for the regional aquifer that provides drinking water to people in Sundance and the surrounding areas of northeastern Wyoming and western South Dakota. Northeastern Wyoming receives 15–20 in. of rain every year, and the streams in the area are predominantly ephemeral, with some surface springs present. The lack of surface water compels Rare Element Resources

to use water from the Madison formation in REE production at the property, and they plan to recycle 100% of water used during physical processing and collect runoff from tailing piles to be used at the mill. In such a scenario, Rare Element Resources believes that the aquifer can handle the company's planned water extraction. It is not known how aquifer usage will affect surface spring behavior at the Bear Lodge property, which provides the most reliable water source for animals in the area. Elevated water extraction from the Madison could dry the springs, or they may not be affected.

Water is a dominant concern at most mine sites, including the Bear Lodge property. REE mining presents various water issues of concern, including contamination of groundwater, surface water, and surface water runoff from the chemical constituents of the REE ores. Processes leading to contamination are accelerated by increasing the surface area of the rock by crushing, milling, and processing. This is especially true in REE ores that often contain greater amounts of minerals that can undergo dissolution. No acid drainage issues are anticipated at the Bear Lodge property, but acid mine drainage is a concern at many mine sites and needs to be monitored for the long term at the Bear Lodge property as well, where the natural buffer in the carbonatite may help mitigate acid concerns. The natural buffer in carbonatite is the reason why the miner, Rare Element Resources, will leave at least a 30 ft. reaction front directly above the sulfide-rich zone. The reaction front ensures that enough carbonate is present to prevent an acid lake from forming in the pit.

9.10.2 Air Contamination

Air quality issues are invariably associated with mining and processing. Dust can be created during physical processing, and fumes are generated from chemical processing. This will also be the case at the Bear Lodge property and Upton processing plant. The mining and milling processes at Bear Lodge may also cause deposition of particulates off-site. Alarming concentrations of radionuclides do not exist at Bear Lodge, but the physical processing of the ores on-site could cause radionuclides present in the ore to become airborne. Rare Element Resources plans to use water to ensure that excess dust is not created during the crushing and grinding of rare-earth ores and plans to establish four air monitoring stations around the property to record possible airborne radionuclide. Fumes bound to be created by chemical refining of the REE ores will be similarly addressed.

Another important issue is to ensure that soil quality and quantity are maintained during and after mining.

9.11 MOUNT WELD

In 2007, Lynas started mining (open pit) and the installation of a concentration plant at the Mt. Weld deposit. Mining was planned for a period of 11 years. About 800,000 t of ore with an average grade of 15% REO (cutoff, 2.5%) was mined and stored in 2008. The concentration plant was to start operation in 2011 and to produce a concentrate of around 40%. The concentration plant shall operate for 18 years. The production of REO concentrate at Mt. Weld shall start with 11,000 t REO per year and increase up

to 20,000 t REO per year (Lynas Corporation Ltd. 2010), with an average recovery rate of around 63%. Further processing will be carried out at the Lynas Advanced Materials Plant in Malaysia (Lynas 2009).

In 2006, the Environmental Protection Authority of the Government of Western Australia and later, in 2008, the Department of Environment and Conservation granted approvals for mining and beneficiation project at Mt. Weld, with the following key regulations (Schuler et al. 2011).

1. Dust suppression techniques are required to ensure that dust emissions are of low significance.
2. The tailings are stored in the tailing ponds equipped with an impervious layer on the base and on the walls with a high standard of seepage management design. A groundwater monitoring system will be in place.
3. Around 14% of the water input to the tailing pond will be returned to the process plant.
4. The tailing ponds will be deemed contaminated sites after plant closure.
5. The pipelines will be controlled by electronic supervisory devices as well as by daily sight inspections.
6. The tailings contain 500 ppm thorium oxide and 30 ppm uranium oxide. The management of the radioactivity shall be as per Radiation Safety Act 1999.
7. The rehabilitation works of the overburden stockpiles are to be carried out.

The further processing of the concentrate, with an output of up to 22,000 t REO per year, will be carried out in Malaysia by the 100% subsidiary of Lynas called Lynas Malaysia. The approval from the Malaysian authorities was obtained in 2008, and the construction of the plant started in 2008. The construction having been completed, startup is stalled by environmental groups in Malaysia. Lynas chose the Malaysian site in an existing industrial estate because of the good infrastructure, the skilled labor force with experience in the chemical industry, and the nearby supply of the required chemicals.

9.12 DUBBO ZIRCONIA PROJECT

The Dubbo Zirconia Project, located in the central west region of New South Wales, is owned by Alkane Resources Ltd. The project will yield zirconium, niobium, and tantalum in addition to rare earths. The primary ore feed contains about 100 ppm uranium (0.01% U) and 450 ppm thorium (0.045% Th). The process to be adopted does not involve any mineral processing operation, and hence there will be no tailings from mineral beneficiation steps. The process will be a "whole-of-rock" sulfuric acid leach whereby uranium and thorium will also enter the solution along with zirconium, niobium, and the REEs.

In subsequent chemical processing, uranium tracks zirconium. It is removed by a solvent extraction process step and is sent to waste as an acidic steam. This stream, on neutralization with limestone, forms uranium precipitate, which is mixed with other waste streams for disposal. The final U concentration in the stream is 60 ppm.

Thorium in the leach liquor tracks both niobium and HREE products. It is removed by a combination of water washing and chemical precipitation. The waste streams are neutralized with limestone, bringing down the thorium content to about 300 ppm, and sent for storage along with zirconium process waste.

The storage facility will be a typical mine-type dam, which will have an impervious base and walls to prevent any solution escape. Uranium and thorium remain insoluble as long as the pH of the waste remains above 7. In the long term, the dam will be covered with waste rock (to about 0.5 m thickness) and then with topsoil and will be revegetated. This cover will eliminate any future radioactive element emissions (Park et al. 2012).

9.13 KVANEFJELD

Large resources of rare earths with a high content of HREE of about 14% occur in the Kvanefjeld region in southern Greenland, which is currently considered for the joint mining of uranium and rare earths. The very large size of this deposit and its significant HREE contents (the Kvanefjeld deposits contain 7.7% Y, 0.2% Tb, 1.1% Dy, 0.2% Ho, 0.6% Er, 0.1% Tm, and 0.5% Yb, according to GMEL [2010]), in comparison to other deposits where premining activities also take place, are the main attractions. The mining company Greenland Minerals and Energy Ltd. (GMEL) with its head office in Perth, Australia, had plans to start construction work in 2013 and to initiate production in 2015 (Schuler et al. 2011).

An important environmental issue in this project is the tailing's management. GMEL favors tailing disposal in the nearby natural lake Taseq (GMEL 2009). However, following an extensive study, Risø (1990) concluded that the outlet from contaminated water from Taseq would cause pollution of the whole fluvial system (from the lake, via rivers, into the ocean) with radioactive substances, fluorine, and heavy metals. The wastewater treatment installations at the outlet of the lake may not be able to manage the large amounts of water, particularly in times of heavy rain or snow melting.

The extensive work on the Kvanefjeld deposit conducted by the Danish authorities concluded that apart from the tailing impoundment, the open pit and the waste dump are the most important sources of pollution. In the long term (>100 years), the tailing pond will be the most critical point. Risø (1990) compared two options: the direct inlet of the tailings into the sea and tailing disposal in the nearby natural lake Taseq (see above). The latter was considered even worse than the former in terms of environmental impacts. Though waste disposal in oceans was frequently practiced in the past, the procedure is not acceptable at all either. Equally, an inlet of toxic tailings into natural water bodies does not meet any environmental standards. The situation in Greenland seems particularly critical when considering the fact that the expected climate change—linked to the melting of glaciers and unfreezing of permafrost soils—might considerably alter water bodies and the stability of soils.

By way of a short overview of the planned technologies for the GMEL Kvanefjeld project and the progress of the (pre)feasibility studies and approval issues, the following is the status. Mining shall be by conventional open pit followed by uranium extraction with the carbonate pressure leach (CPL) technology. The CPL residue will

then be processed and the REO concentrated by froth flotation, leached with acid, and then refined to produce rare-earth carbonate. The nominal forecast annual production will be 44,000 t REO and nearly 4000 t of uranium oxide; the overall plant recovery rates are 34% and 84%, respectively (GMEL 2009).

The present stand (2010) by the Greenland government appears to be that although radioactive elements may now be surveyed, their extraction is still not permitted. There is a cooperation agreement between the government of Greenland and the European Environment Agency on environmental issues (EEA 2010) that might lead to an exchange of expertise and contribute to a sustainable course of action concerning the Kvanefjeld deposit and mining activities in Greenland in general (Paul and Campbell 2011).

9.14 STEENKAMPSKRALL MINE

The Steenkampskrall mine in Western Cape, South Africa, belonging to the Great Western Minerals Group, Canada, is an underground hard-rock monazite mine, operated earlier for thorium. It is being revived for the production of rare earths.

The ore contains 17% REO, 3.7% ThO_2, and 150–200 ppm U_3O_8. The mined ore is crushed, screened, milled, and deslimed. Further beneficiation treatments consist of gravity and magnetic separation and flotation. At the end of flotation, the monazite concentrate contains approximately 60% REO, 10% ThO_2, and 800 ppm U_3O_8. The tails from gravity and flotation treatments contain approximately 1% ThO_2. This thoria is in the mineral monazite, which is considered environmentally immobile and good for use as backfill in the underground workings.

The monazite concentrate is treated further by the caustic digestion process, whereby rare-earth and thorium contents are converted to hydroxide. Acid leaching of the hydroxide cake selectively dissolves the rare earths (and any radium present in the hydroxide), while thorium and uranium are left in the residue. The acid leach liquor is treated with barium chloride solution to clean up any radium in the solution. The rare-earth-chloride solution is now sufficiently freed of radioactive contaminants (Park et al. 2012). Two waste streams, the thorium stream and the radium stream, have thus been produced. They are combined and sent to underground storage.

Thus, radioactive material has been removed in three stages from the Steenkampskrall monazite ore. In the first stage, monazite tailings containing approximately 1% Th in the beneficiation process are generated. The second and third stages are the generation of thorium and radium streams in hydrometallurgical processing. All these are destined for underground storage under the prevailing nuclear authorization for the mine site. Such sequestering of all radioactive products underground, including those from historical waste rock and tailings at the surface, facilitate surface remediation at the mine site.

9.15 NECHALACHO PROJECT

The ore body at Avalon Rare Metals' Nechalacho rare-earth deposit, in Northwest Territory, Canada, contains an average of only 114 ppm (0.01%) thorium and 23 ppm

(0.002%) uranium. These concentrations are approximately 10 times the naturally occurring average background abundance of thorium (10 ppm) and uranium (2.5 ppm). At these low concentrations, the use of standard risk mitigation procedures such as ventilation should ensure exposures to radiation from mining activities at below thresholds of concern (Park et al. 2012).

9.16 SUMMARY

The attention to REEs, particularly the key and critical elements, will only increase as governments around the world work to address serious supply issues as a result of the continued increase in global usage and decreased accessibility of REEs from China over the past few years. In particular, the United States government is concerned about REE supply considering that the elements are vital to military technology production apart from the electronic and clean energy industries. The US DOE commissioned a study and generated an assessment of the periodic elements vital for maintaining the industrial and security interests of the United States. Several key and critical materials were clearly identified. Nine of the 14 key elements are REEs. The REEs receiving key designation include lanthanum, cerium, praseodymium, neodymium, samarium, europium, terbium, dysprosium, and yttrium. The five other key elements are lithium, cobalt, gallium, indium, and tellurium. A selection of key elements that are necessary for clean energy technology production and have supply risks greater than the average key elements are designated critical elements. The key elements receiving critical designation in the short term (0–5 years) were dysprosium, neodymium, terbium, europium, yttrium, and indium. Critical materials in the medium term (6–15 years) include dysprosium, neodymium, terbium, europium, and yttrium. All are REEs.

Record-high REE prices and accessibility issues, especially for the critical elements, have already resulted in increased investments for exploration and development of REE deposits in the United States and other locations outside China. Companies are rediscovering the mining potential of REE deposits across the nations and across continents. Location of deposits with good potential for extraction is only a small part of the journey toward critical material independence. The difficult part is in the processing—the technology, the fallouts (environmental), and hence the cost.

As with any mine or refinery, REE production could contaminate the environment if best management practices are not used and the operation is not closely monitored. Companies as well as federal and state agencies must determine how to best oversee the projects to ensure that this operation does not put human health and the environment at risk. There may be no shortcuts or routes that circumvent the possibility of environmental audit—scheduled or surprise. The REE-bearing rocks and minerals are also home to many potential environmental contaminants. These include, but are not limited to, radionuclides, REEs; metals such as barium, beryllium, copper, lead, manganese, and zinc; sulfide minerals; carbonate minerals; and other potential contaminants such as fluorine and asbestos minerals. Mining exposes these possible contaminants, while refining isolates and concentrates the possible contaminants. REE mining is hard-rock mining, so any of the environmental concerns associated with hard-rock mining could be a concern with REE production.

Environmental challenges abound in processing as well. The main risks are the tailings, which are a mixture of small-size particles, wastewater, and flotation chemicals and arise at the concentration of the mined ore. They are stored in impoundment areas. The tailing dam is exposed to manifold risks such as overtopping due to storm water, poor construction, or seismic events. A failing dam leads to site-specific emissions such as thorium, uranium, heavy metals, and fluorides, and can contaminate land and water resources in the vicinity with chemicals and radioactive residues in an uncontrolled manner. Even from the concentrate onward, rare-earth metallurgy entails heavy consumption of industrial solvents (organic) and chemicals including a variety of acids and alkalis. Only a small fraction of these are recycled in current plant practices. Much of these materials, loaded with contaminants, may end up as waste streams, demanding expensive management to meet regulations.

China has been the most important rare-earth producer for the past two decades and will continue to dominate world rare-earth production in the immediate future as well. There has been serious environmental damage in the Chinese rare-earth mines and their surroundings. The Chinese government stepped in to reduce the environmental harm by installing environmental technologies in the large mines and by reducing the numerous small illegal mines, which probably have no environmental technologies at all. China also aims at higher efficiencies in mining and processing and is running some research projects on a sustainable rare-earth economy. China's experience has provided valuable hard data to the industry on the hazards in an environmentally unregulated rare-earth processing scenario. Incidentally, the ores processed did not include placer monazite, which has the highest radioactivity loading and therefore should be the most problematic resource. Rendered wiser by the Chinese experience, rare-earth producers with projects in an advanced stage of implementation have taken to comprehensive environmental monitoring and controls. The most advanced mines outside of China, at Mountain Pass in the United States and at Mt. Weld in Australia, will provide environmental protection systems, which will significantly reduce the environmental damage compared to old outdated techniques. However, the global pressure for a steady rare-earth supply might lead to further new mines outside of China with major challenges to meet environmental prescription. One example of potential concern about environmental damage is the plan for joint mining of uranium and rare earths in Greenland. The interested mining company intends to store the tailings in a natural lake with a connection to maritime waters, which is widely perceived as an unacceptable solution. Similarly, there are challenges as regards water management in the Bear Lodge project. All these aspects of interplay between rare-earth processing and environmental conservation come up in different formats in the industry. The industry is, at the same time, under huge pressure to provide critical elements to satisfy the fast-expanding world demand. These conflicting situations have been alluded to in various sections of the book but are dealt with more explicitly in this chapter, in the context of resource availability for and technology practices of current rare-earth production and the future challenges.

References

Aamland, E., MacDonald, D.J. and Kerterke, D.G. (1973) Molten salt electrowinning of magnesium–yttrium alloys, Bureau of Mines Report of Investigations 7722, U.S. Department of the Interior, Washington, DC.

Abedin, K.M., Haider, A.F.M.Y., Rony, M.A. and Khan, Z.H. (2011) Identification of multiple rare earths and associated elements in raw monazite sands by laser-induced breakdown spectroscopy, *Opt. Laser Technol.*, 43: 45–49.

Abeidu, A.M. (1972) The separation of monazite from zircon by flotation, *J. Less Common Metals*, 29: 113–119.

Achard, J.C. (1957) Separation de certains elements des terres rares par voie seche. Application au samarium et a l'europium, *C. R. Acad. Sci.*, 245: 1064–1066.

Adachi, G., Shinozaki, K., Hirashima, Y. and Machida, K. (1991) Rare-earth separation using chemical vapor transport with $LnCl_3$–$AlCl_3$ gas-phase complexes, *J. Less Common Metals*, 169: L1–L4.

Adams, J.W. (1971) Resources. In Parker, J.G. and Baroch, C.T. (eds.), *The Rare Earth Elements, Yttrium and Thorium—A Materials Survey*, pp. 22–39, Bureau of Mines Information Circular 8476, U.S. Department of the Interior, Washington, DC.

Adams, J.W. and Staatz, M.H. (1973) Rare earth elements, United States mineral researches, U.S. Geol. Survey Prof. Paper 820, pp. 547–556.

Agarwal, J.C., Loreth, J.M. and Katrak, F.E. (1988) Economics of production of rare earth metals alloys. In Bautista, R.G. and Wong, M.M. (eds.), *Rare Earths*, pp. 281–289, The Minerals, Metals and Materials Society, Warrendale, PA.

Akai, T., Yamashita, M. and Oki, T. (2011) Phosphor separation by high magnetic field gradient magnetic separation, *Rare Earths*, 58: 14–15.

Akinlua, A., Torto, N. and Ajayi, T.R. (2008) Determination of rare earth elements in Niger Delta crude oils by inductively coupled plasma–mass spectrometry, *Fuel*, 87: 1469–1477.

Al-Shahristani, H. and Al-Atyia, M. (1973) Determination and geochemical significance of trace elements in Iraqi crude oils using instrumental neutron activation analysis. *Journal of Radioanalytical and Nuclear Chemistry*, 14(2): 401–413.

Aladjem, A. (1970) *Analytical Chemistry of Yttrium and the Lanthanide Elements*, pp. 197–205, Ann Arbor–Humphery Science Publishers, Ann Arbor, MI.

Alamelu, D., Sarkar, A. and Aggarwal, S.K. (2008) Laser-induced breakdown spectroscopy for simultaneous determination of Sm, Eu and Gd in aqueous solution, *Talanta* 77(1): 256–261.

Alcock, C.B. (1976) *Principles of Pyrometallurgy*, pp. 239–240, Academic Press, New York.

Alford, N.M. (1992) Applications of high temperature superconductors, *Chem. Ind.* (21): 809–812.

Ali, A. (2011) Magnetic properties and corrosion resistance of uncoated and coated rare-earth based permanent magnets, Thesis, Department of Metallurgical and Materials Engineering, University of Engineering & Technology, Lahore.

Ali, A., Ahmad, A. and Deen, K.M. (2010) Impeding corrosion of sintered NdFeB magnets with titanium nitride coating, *J. Mater. Corr.*, 61(2): 130–135.

Alimarin, I.P., Miklishanskii, A.Z. and Yakovlev, Y.V. (1970a) Neutron activation analysis of rare earth impurities in metallic uranium. *Journal of Radioanalytical Chemistry*, 4(1): 45–51.

Alimarin, I.P., Miklishanskii, A.Z. and Yakovlev, Y.V. (1970b) Neutron activation analysis of rare earth impurities in europium oxide, *J. Radioanal. Chem.*, 4: 75–80.

Alonso, T., Liu, Y., Dallimore, M.P. and McCormick, P.G. (1993) Low temperature reduction of $SmCl_3$ during mechanical milling. *Scripta Metallurgica et Materialia*, 29(1): 55–58.

Altschuler, Z.S., Berman, S. and Cuttitta, F. (1966) Rare earths in phosphorite—Geochemistry and potential recovery, U.S. Geological Survey Open-File Report 66–3, Arlington, VA.

Altschuler, Z.S., Berman, S. and Cuttitta, F. (1967) Rare earths in phosphorites—Geochemistry and potential recovery, U.S. Geol. Survey Prof. Paper 575B, pp. B1–B9.

Amaral, J.C.B.S. and Morais, C.A. (2010) Thorium and uranium extraction from rare earth elements in monazite sulfuric acid liquor through solvent extraction, *Miner. Eng.*, 23(6): 498–503.

Amer, T.E., Abdella, W.M., Abdel Wahab, G.M. and El-Sheikh, E.M. (2013) A suggested alternative procedure for processing of monazite mineral concentrate, *Int. J. Miner. Process.*, 125: 106–111.

Anable, W.E. (1970) Purification of vanadium by vacuum melting, *J. Vac. Sci. Technol.*, 7(6): 574–581.

Anable, W.E. and Beall, R.A. (1965) Electron beam melting of yttrium, U.S. Bureau of Mines Report of Investigations 6661, U.S. Department of the Interior, Washington, DC.

Anderson, L. (1986) Occurrence and processing of rare earth minerals, *Erzmetall*, 39(4): 152–157.

Anderson, R.N. and Parlee, N.A.D. (1976) Carbothermic reduction of refractory metals, *J. Vac. Sci. Technol.*, 13: 526–529.

Anderson, I.E., Osborne, M.G., Takeya, H. and Gschneidner, Jr., K.A. (1993) Gas atomized ErNi3 powder for cryocooler applications. In *Proceedings of the 7th International Cryocooler Conference, Santa Fe, NM*, November 17–19, 1992, pp. 1120–1132, Phillips Laboratory, Air Force Material Command, Kirtland Air Force Base, NM.

ANDRA (2009) Agence Nationale pour la Gestion des Déchets radioactifs (ANDRA): L'Édition 2009 de l'inventaire Nationale des Matières et Déchets Radioactifs. Available at http://www.andra.fr.

Anon (1989) Magnetic refrigeration, *Supercond. Ind.*, 2: 34–41.

Anon (2010) Rare earth elements. Enablers of high tech applications and green energy technologies. Available at http://www.amrmineralmetal.com/download/corporate/REE_Industry.pdf (accessed July 1, 2015).

Aplan, F.F. (1988) The processing of rare earth minerals. In Bautista, R.G. and Wong, M.M. (eds.), *Rare Earths*, pp. 15–34, The Minerals, Metals and Materials Society, Warrendale, PA.

Appleton, D.B. and Selwood, P.W. (1941) Fractional partition of the rare earths, *J. Am. Chem. Soc.*, 63: 2029.

Arai, Y. (2010) Recycling of rare earth magnets from used home appliances. In *Symposium on Recycling of Rare Metals*, July 9, Japan Society of Material Cycles and Waste Management, Tokyo, Japan. Available at http://jsmcwm.ur.jplrecycle/7_Arai_MMC.pdf.

Arai, Y., Koga, S., Hoshina, H., Yamaguchi, S. and Kondo, H. (2011) Recycling of rare earth magnets from used home appliances, *Mater. Cycl. Waste Manag. Res.*, 22: 41–48.

Argall, Jr., G.O. (1980) Three iron ore bodies of Bayan Obo, *World Min.*, 33(1): 38–46.

Argonne National Laboratory (2005) Investigating rare earth element mine development in EPA region 8 and potential environmental impacts, USEPA EPA Document-908R11003, p. 15, USEPA, Washington, DC.

Armbrustmacher, T.J. (1988) Geology and resources of thorium and associated elements in the Wet Mountains Area, Fremont and Custer Counties, Colorado, US Geological Survey, Professional paper. No. 1049-F, U.S. Geological Survey, Reston, Virginia.

Armbrustmacher, T.J. (1989) Minor element content, including radioactive elements and rare-earth elements, in rocks from the syenite complex at Roy Creek, Mount Prindel area, Alaska, U.S. Geological Survey Open-File Report 89–146, 11 pp, U.S. Geological Survey, Reston, VA.

Audrieth, L.F. (1939) Preparation of amalgams. In Booth, H.S. (ed.), *Inorganic Syntheses*, Vol. 1, McGraw Hill, New York.

Audrieth, L.F., Jukkola, E.E., Meints, R.E. and Hopkins, B.S. (1931) Observations on the rare earths XXXVII. Electrolytic preparation of rare earth amalgams—Preparation of amalgam of lanthanum and neodymium, *J. Am. Chem. Soc.*, 53: 1805–1809.

Auzel, F. and Goldner, P. (1999) Rare earth ions in the glass amplifying medium: A proposal for new doping precursors, *Mater. Sci. Forum*, 315–317: 34–41.

Awasthi, A., Krishnamurthy, N., Bhatt, Y.J., Venkataramani, R. and Garg, S.P. (1998) Refining of tantalum by silicon deoxidation, *J. Alloys Compd.*, 265: 190–195.

Ayranov, M., Cobos, J., Popa, K. and Rondinells, V. (2009) Determination of REE, U, Th, Ba, and Zr in simulated hydrogeological leachates by ICP-AES after matrix solvent extraction, *J. Rare Earths*, 27(1): 123–127.

Baba, K., Hiroshige, Y. and Nemoto, T. (2013) Rare earth magnet recycling, *Hitachi Rev.*, 62(8): 452–455.

Baba, Y., Kubota, F., Kamiya, N. and Goto, M. (2011) Selective recovery of dysprosium and neodymium ions by a supported liquid membrane base on ionic liquids, *Solv. Extr. Res. Dev. Japan*, 18(10): 193–198.

Bachmann, K. and Lieser, K. (1970) Activation Analysis Rare Earths In Nuclear Reactor Fuels. *Zeitschrift Fur Analytische Chemie Fresenius* 250(3): 172.

Bagchi, D.C. (1988) The use of rare earths in cinema arc carbons. In Gupta, C.K. and Krishnan, T.S. (eds.), *Rare Earths—Applications and Technology*, pp. 265–268, Trans Tech Publications, Switzerland.

Bai, X. and Jiang, C. (2010) Dynamic parameters of Tb–Dy–Fe giant magnetostrictive alloy, *J. Rare Earths*, 28(1): 104–108.

Baker, J., Waight, T. and Ulfbeck, D. (2002) Rapid and highly reproducible analysis of rare earth elements by multiple collector inductively coupled plasma mass spectrometry, *Geochim. Cosmochim. Acta*, 66(20): 3635–3646.

Balaram, V. (1996) Recent trends in the instrumental analysis of rare earth elements in geological and industrial materials, *TrAC Trends Anal. Chem.*, 15(9): 475–486.

Banda, R., Jeon, H.S. and Lee, M.S. (2012) Solvent extraction separation of La from chloride solution containing Pr and Nd with Cyanex 272, *Hydrometallurgy*, 121–124: 74–80.

Banks, C.V. and Klingman, D.W. (1956) Spectrophotometric determination of rare earth mixtures, *Anal. Chim. Acta.*, 15: 356–363.

Banks, C.V. and Klingman, D.W. (1961) Analytical chemistry of the rare earths. In Spedding, F.H. and Daane, A.H. (eds.), *The Rare Earths*, pp. 571–593, Wiley, New York.

Banks, C.V., Spooner, J.L. and O'Laughlin, J.W. (1956) Differential spectrophotometric determination of neodymium in neodymium-yttrium mixtures, *Anal. Chem.*, 28(12): 1894–1897.

Banks, C.V., Carlson, O.N., Daane, A.H., Fassel, V.A., Fisher, D.W., Olsen, E.H., Powell, J.E. and Spedding, F.H. (1959) Studies on the preparation, properties and analysis of high purity yttrium oxide and yttrium metal at the Ames Laboratory, IS-1, National Technical Information Service, Springfield, VA.

Banks, C.V., O'Laughlin, J.W. and Kamin, G.J. (1960) Determination of oxygen in yttrium and yttrium fluoride by the inert gas fusion method, *Anal. Chem.*, 32(12): 1613–1616.

Barchevtsev, V., Artisyuk, V. and Ninokata, H. (2002) Concept of erbium doped uranium oxide fuel cycle in light water reactors, *J Nuclear Sci. Technol.*, 39(5): 506–513.

Barghusen, J.J. and Smutz, M. (1958) Processing of monazite sands, *Ind. Eng. Chem.*, 50: 1754–1755.

Bashir, V.S. (1988) Monazite, the basic raw material for rare earths beneficiation from beach sands. In Gupta, C.K. and Krishnan, T.S. (eds.), *Rare Earths—Applications and Technology*, pp. 33–44, Trans Tech Publications, Switzerland.

Bauer, D., Diamond, D., Li, J., Sandalow, D., Telleen, P. and Wanner, B. (2010) Critical Materials Strategy, U.S. Department of Energy, Washington, DC.

Bauer, D.J. (1959) Development of equipment and processes for extracting cerium (IV), Bureau of Mines Report of Investigations 5536, U.S. Department of the Interior, Washington, DC.

Bauer, D.J. (1966) Extraction and separation of selected lanthanides with a tertiary amine, U.S. Bureau of Mines, R.I., 6809, U.S. Department of the Interior, Washington, DC.

Bauer, D.J. and Lindstrom, R.E. (1964) Naphthenic acid solvent extraction of rare earth sulphates, Bureau of Mines Report of Investigations 6396, U.S. Department of the Interior, Washington, DC.

Bauer, D.J. and Lindstrom, R.E. (1971) Differential extraction of rare earth elements in quaternary ammonium salt chelating agent systems, Bureau of Mines Report of Investigations 7524, U.S. Department of the Interior, Washington, DC.

Bauer, D.J., Rice, A.C. and Berber, J.S. (1960) Liquid–liquid extraction of rare earth elements, Bureau of Mines Report of Investigations 5570, U.S. Department of the Interior, Washington, DC.

Bauer, D., Diamond, D., Li, J., Mckittrick, M., Sandalow, D. and Telleen, P. (2011) Critical materials strategy, December, U.S. Department of Energy, Washington, DC. Available at http://energy.gov/sites/prod/files/edg/news/documents/criticalmaterialsstrategy.pdf.

Bautista, R.G. (1995) Separation chemistry. In Gschneidner, Jr., K.A. and Eyring, L. (eds.), *Handbook on the Physics and Chemistry of Rare Earths*, Vol. 21, pp. 1–28, North Holland, Amsterdam.

Bayanov, A.P. and Serebrennikov, V.V. (1964) Distribution of some rare earth elements between two molten metals, *Zh. Neorg. Khim.*, 9: 1658–1661.

Bayanov, A.P., Gurskaya, S.F. and Serebrennikov, V.V. (1966) Distribution of the rare-earth metals and of yttrium during the crystallization of zinc from a lead melt, *Zh. Prikl. Khim. (S.-Petersburg, Russ. Fed.)*, 39: 447–448.

Bayon, G., Barrat, J.A., Etoubleau, J., Benoit, M., Bollinger, C. and Révillon, S. (2009) Determination of rare-earth elements, Sc, Y, Zr, Ba, Hf and Th in geological samples by ICPMS after Tm addition and alkaline fusion, *Geostand. Geoanal. Res.*, 33(1): 51–62.

Beaudry, B.J. and Gschneidner, Jr., K.A. (1978) Preparation and basic properties of rare earth metals. In Gschneidner, Jr., K.A. and Eyring, L. (eds.), *Handbook on the Physics and Chemistry of Rare Earths*, Vol. 1, pp. 173–232, North Holland, Amsterdam.

Beaudry, B.J. and Palmer, P.E. (1974) The use of inert atmospheres in the preparation and handling of high purity rare earth metals. In Haschke, J.M. and Eick, H.A. (eds.), *Proc. 11th Rare Earth Research Conf., Traverse City, MI*, Conf-741002, Part 2, pp. 612–620, National Technical Information Service, Springfield, VA.

Beaudry, B.J., Palmer, P.E. and Gschneidner, Jr., K.A. (1983) The effect of fluoride preparation on the purity of the rare earth metals, *J. Less Common Metals*, 93: 277.

Becker, P. (1983) *Phosphates and Phosphoric Acid: Raw Materials, Technology, and Economics of the Wet Process*, Marcel Dekker, New York.

Bednorz, J.G. and Muller, K.A. (1986) Possible high-T_c superconductivity in the Ba–La–Cu–O system, *Z. Phys. B Condensed Matter*, B64: 189–193.

Beijing Nonferrous Metal (2008) Technique for extraction separation of quadravalence cerium, thorium, fluorine and cerium less tervalence rare earth from sulphuric acid rare earth solution, Patent CN 200710098732.

Benz, M.G. and Martin, D.L. (1970) Cobalt–samarium permanent magnets prepared by liquid phase sintering, *Appl. Phys. Lett.*, 17(4): 176–177.

Beranznai, T. (1971) Activation analysis of rare earth elements, *J. Radioanal. Chem.*, 9: 81–100.

Berber, J.S., Shaw, V.E., Rice, A.C., Lindstrom, R.E. and Bauer, D.J. (1960) Technology of bastnasite, Bureau of Mines Report of Investigations 5599, U.S. Department of the Interior, Washington, DC.

Bernardes, A.M., Espinosa, D.C.R. and Tenório, J.A.S. (2004) Recycling of batteries: A review of current processes and technologies, *J. Power Sources*, 130: 291–298.

Bhatnagara, A., Kumara, E. and Sillanpää, M. (2011) Fluoride removal from water by adsorption—A review, *Chem. Eng. J.*, 171: 811–840.

Billy, M. and Trombe, F. (1931) Préparation de cerium pur, *Compt. Rend.*, 193: 421–423.

Binnemans, K. (2007) Lanthanides and actinides in ionic liquids, *Chem. Rev.*, 107: 2592–2614.

Binnemans, K., Jones, P.T., Blanpain, B., Gerven, T.V., Yang, Y., Walton, A. and Buchert, M. (2013) Recycling of rare earths: A critical review, *J. Cleaner Prod.*, 51: 1–22.

Block, F.E. and Campbell, T.T. (1961) Rare earth and yttrium halides for metal production—Chlorides, bromides and iodides. In Spedding, F.H. and Daane, A.H. (eds.), *The Rare Earths*, pp. 89–101, John Wiley, New York.

Block, F.E., Campbell, T.T., Mussler, R.E. and Robidart, G.B. (1960) Preparation of high purity yttrium by metallic reduction of yttrium trichloride, Bureau of Mines Report of Investigations 5588, U.S. Department of the Interior, Washington, DC.

Blouri, J., Fedoroff, M. and Revel, G. (1973) Application of a Semiconductor Detector to the Systematic Analysis of Aluminum. *J. Radioanal. Chem.*, 17(1): 185–194.

Bobeck, A.H., Spencer, E.G., Van Vitiert, L.G., Abrahams, S.C., Barns, R.L., Grodkiewicz, H., Sherwood, R.C., Schmidt, P.H., Smith, D.H. and Walters, E.M. (1970) Uniaxial magnetic garnets for domain wall "bubble" devices, *Appl. Phys. Lett.*, 17: 131–134.

Bochinski, J., Smutz, M. and Spedding, F.H. (1953) Separation of individual rare earths by liquid–liquid extraction from multicomponent monazite rare earth nitrates I. Undiluted TBP and concentrated aqueous rare earth nitrate systems at low acid concentrations, U.S. Atomic Energy Commission Report ISC-348, National Technical Information Service, Springfield, Virginia.

Bochinski, J., Smutz, M. and Spedding, F.H. (1958) Separation of monazite rare earths by solvent extraction, *Ind. Eng. Chem.*, 50: 157–160.

Bongaerts, J.C. and Liu, J. (2013) Production process and recycling of rare earth elements, *IMRE J.*, 7(2): 1–9.

Bonnevie-Svendsen, M. and Follo, A. (1973) X-ray fluorescence analysis of rare earth elements. In Michelsen, O.B. (ed.), *Analysis and Application of Rare Earth Materials*, pp. 87–107, Universitetforlaget, Oslo.

Bose, D.K., Mehra, O.K. and Gupta, C.K. (1985) Preparation of rare earth–iron–silicon alloys by metallothermic reduction, *J. Less Common Metals*, 110: 239–242.

Bouchekara, H.R.E. and Nahas, M. (2012) Magnetic refrigeration technology at room temperature. In Barsan, V. and Lungu, R.P. (eds.), *Trends in Electromagnetism—From Fundamentals to Applications*, Chapter 10, InTech, Rijeka, Croatia. Available at http://www.intechopen.com/books/trends-in-electromagnetism-from-fundamentals-to-applications/magnetic-refrigeration-technology-at-room-temperature.

Bounds, C.O. (1994) The recycle of sintered magnet swarf. In Liddell, K.C., Bautista, R.G. and Orth, R.J. (eds.), *Symposium on Metals and Materials Waste Reduction, Recovery and Remediation, at the 1994 Materials Week Meeting Location: Rosemont, IL*, October 3–6, pp. 173–186, The Minerals Metals & Materials Society, Warrendale, PA.

Boynton, W.V. (1979) Neutron activation analysis. In Gschneidner, Jr., K.A. and Eyring, L. (eds.), *Handbook on the Physics and Chemistry of Rare Earths*, Vol. 4, pp. 457–470, North-Holland, Amsterdam.

Bradsher, K. (2010) After China's rare earth embargo, a new calculus, *New York Times*, October 29.

Brandle, C.D. and Valentino, A.J. (1972) Czochralski growth of rare earth–gallium garnets, *J. Cryst. Growth*, 12: 3–8.

Brandle, C.D., Miller, D.C. and Nielsen, J.W. (1972) The elimination of defects in Czochralski grown rare earth–gallium garnets, *J. Cryst. Growth*, 12: 195–200.

Bratland, D. and Gschneidner, Jr., K.A. (1980) Electrorefining and electrowinning of gadolinium in a molten fluoride electrolyte purified by pre-electrolysis, *Acta Chem. Scand.*, A34, 683–686.

Bratland, D., Boe, G.H., Grjotheim, K., Rensvik, H. and Aamland, E. (1972) Some introductory investigations on electrolytic deposition of Y–Al and Y–Mg alloys, *Rev. Roum. Chim.*, 17(1–2): 41–48.

Bratland, D.G., Boe, H. and Grjotheim, K. (1973) On electrowinning of yttrium–aluminium and yttrium–magnesium alloys from molten fluorides, *Rev. Chim. Miner.*, 10: 347–353.

Brewer, L. and Rosenblatt, G.M. (1962) Thermodynamics of suboxide vaporization, *Trans. AIME*, 224: 1268–1271.

Bril, K.J. (1964) Mass extraction and separation. In Eyring, L. (ed.), *Progress in the Science and Technology of Rare Earths*, Vol. 1, pp. 30–61, Pergamon, Oxford.

Broadhead, K.G. and Heady, H.H. (1960) Radiochemical precipitation studies of rare earth oxalates, *Anal. Chem.*, 32(12): 1603–1606.

Broadhead, K.G., Shanks, D.E. and Heady, H.H. (1965) 14-MeV-neutron production of isomeric states for several rare-earth elements. *Physical Review*, 139(6B): B1525.

Broekaert, J.A.C., Leis, F. and Laqua, K. (1979) Application of an inductively coupled plasma to the emission spectroscopic determination of rare earths in mineralogical samples, *Spectrochim. Acta*, 34B: 73–84.

Brown, G.V. (1976) Magnetic heat pumping near room temperature, *J. Appl. Phys.*, 47: 3673–3680.

Brown, C.G. and Sherrington, L.G. (1979) Solvent extraction used in industrial separation of rare earths, *J. Chem. Technol. Biotechnol.*, 29: 193–209.

Brown, J.S., Emery, J.A. and Meyer, Jr., P.A. (1954) Explosion pipe in test well on Hicks Dome, Hardin County, Illinois. *Econ. Geol.*, 49(8): 891–902.

Brugger, W. and Greinacher, H. (1967) A cracking process for rare earth ores by direct chlorination at high temperature on a production scale, *J. Metals*, 19(12): 32–35.

Bruijs, P.C.M.N. (1973) The determination of rare earths in yttrium oxide by means of a preconcentration technique and Ge (Li) gamma-spectrometry. *Journal of Radioanalytical and Nuclear Chemistry*, 16(1): 115–122.

Brunfelt, A.O., Roelandts, I. and Steinnes, E. (1974) Determination of rubidium, caesium, barium and eight rare earth elements in ultramafic rocks by neutron-activation analysis. *Analyst*, 99(1178): 277–284.

Bruno, A. (2013). Kingsnorth believes Rare Earth Element demand and prices to increase. Available at http://investorintel.com/technology-metals-intel/dudley-kingsnorth-believes-that-ree-demand-and-prices-will-double-by-2015/.

Buckingham, S., Maheswaren, J., Meehan, B. and Peverill, K. (1999) The role of applications of rare earth elements in enhancement of crop and pasture production, *Mater. Sci. Forum*, 315–317: 339–347.

Bulatovic, S. (2007) Flotation of sulfide ores. In *Handbook of Flotation Reagents: Chemistry, Theory and Practice*, Vol. 1, Flotation of sulfides ores, pp. 5–42, Elsevier, Amsterdam.

Bulatovic, S. (2010) Handbook of Flotation Reagents: Chemistry, Theory and Practice, Vol. 2, Flotation of gold, PGM and oxide minerals, pp. 151–173, Elsevier Science, Amsterdam.

Bureau of Mines Staff (1975) Classification of resources. In *Mineral Facts and Problems* (edn.), pp. 16–17, Bureau of Mines, U.S. Department of the Interior, Washington, DC.

Burianová, M. and Frána, J. (1976) Determination of residual content of rare earth elements in the steel deoxidated by ferroalloy "silicon-cerium." inis.iaea.org.

Busch, G., Kaldis, E., Muheim, J. and Bischof, R. (1971) The purification of europium, *J. Less Common Metals*, 24: 456–457.

Buschow, K.H.J. (1984) Hydrogen absorption in intermetallic compounds. In Gschneidner, Jr., K.A. and Eyring, L. (eds.), *Handbook on the Physics and Chemistry of Rare Earths*, Vol. 6, pp. 1–112, North Holland, Amsterdam.

Burton, J.P. and Fralick, P. (2003) Depositional placer accumulations in coarse-grained alluvial braided river systems. *Economic Geology*, 98(5): 985–1001.

Buschow, K.H.J. (1988) Magnetooptical properties of alloys and intermetallic compounds. In Wohlforth, E.P. and Buschow, K.H.J. (eds.), *Ferromagnetic Materials*, Vol. 4, p. 595, North Holland, Amsterdam.

Buschow, K.H.J., Luiten, W., Nastepad, P.A. and Westendorp, F.F. (1968) Magnet material with $(BH)_{max}$ of 18 million Gauss Oersteds, *Philips Tech. Rev.*, 29: 336.

Callow, R.J. (1967) *The Industrial Chemistry of Lanthanum, Yttrium, Thorium and Uranium*, Pergamon, New York.

Campbell, P. (2012) Performance and cost assessment for motors using alternative rare earth free magnets, Rare Earth Alternatives in Critical Technologies ("REACT") program, Advanced Research Projects Agency—Energy, U.S. Department of Energy, Washington, DC.

Campbell, T.T. and Block, F.E. (1959) Europium and samarium reduction, *J. Metals*, 11: 744–746.

Canneri, G. and Rossi, A. (1932) On the preparation of metallic praseodymium, *Gazz. Chim. Ital.*, 62: 1160–1163.

Cannon, J.G. (1974) Rare earth elements and metals. In Considine, D.M. (ed.), *Chemical and Process Technology Encyclopedia*, pp. 961–969, McGraw Hill, New York.

Cao, X.D., Yin, M. and Li, B. (1999) Determination of rare earth impurities in high purity gadolinium oxide by inductively coupled plasma mass spectrometry after 2-ethylhexyl-hydrogen-ethylhexy phosphonate extraction chromatographic separation, *Talanta*, 48: 517–525.

Carbonneau, C. and Carbon, J.C. (1965) The production of pyrochlore concentrates at St. Lawrence Columbium and Metals Corporation, *CIM Trans.*, 68: 71–79.

Carlson, O.N. and Schmidt, F.A. (1961a) Metallothermic preparation of yttrium metal. In Spedding, F.H. and Daane, A.H. (eds.), *The Rare Earths*, pp. 113–125, John Wiley, New York.

Carlson, O.N. and Schmidt, F.A. (1961b) Preparation of the rare earth fluorides. In Spedding, F.H. and Daane, A.H. (eds.), *The Rare Earths*, pp. 79–88, John Wiley, New York.

Carlson, O.N. and Schmidt, F.A. (1967) Metallurgy Division Research and Development Report IS-1600, p. M-10, Ames Laboratory, USAEC, Iowa State University, Ames, IA, National Technical Information Service, Springfield, VA.

Carlson, O.N. and Schmidt, F.A. (1976) Electrotransport of solutes in rare earth metals. In Lundin, C.E. (ed.), *Proc. 12th Rare Earth Research Conference*, July 18–22, pp. 460–469, University of Denver, Denver Research Institute, Vail, CO.

Carlson, O.N., Schmidt, F.A. and Spedding, F.H. (1956) Preparation of yttrium metal by reduction of yttrium trifluoride with calcium, Report ISC-744, U.S. Atomic Energy Commission, National Technical Information Service, Springfield, VA.

Carlson, O.N., Haefling, T.A., Schmidt, F.A. and Spedding, F.H. (1960) Preparation and refining of yttrium metal by Y–Mg intermediate alloy process, *J. Electrochem. Soc.*, 107: 540–545.

Carlson, O.N., Schmidt, F.A. and Peterson, D.T. (1966) Electrotransport of interstitial atoms in yttrium, *J. Less Common Metals*, 10: 1–11.

Carlson, O.N., Schmidt, F.A. and Peterson, D.T. (1973) Purification of rare earth metals by electro-transport. In Kevane, C.J. and Moeller, T. (eds.), *Proc. 10th Rare Earth Research Conf., Carefree, AZ*, May, Conf-730402, P2, pp. 701–710, National Technical Information Service, Springfield, VA.

Castor, S.B. (2008a) The Mountain Pass rare-earth carbonatite and associated ultrapotassic rocks, California, *Can. Mineral.*, 46(4): 779–806.

Castor, S.B. (2008b) Rare earth deposits of North America, *Resour. Geol.*, 58(4): 337–347.

Castor, S.B. and Hedrick, J.B. (2006) Rare earth elements. In Kogel, J.E., Tivedi, N.C., Barker, J.M. and Krukowski, S.T. (eds), *Industrial Minerals and Rocks—Commodities, Markets and Uses*, 7th edn., pp. 769–792, Society for Mining, Metallurgy and Exploration, Littleton, CO.

Castor, S.B. and Nason, G.W. (2004) Mountain Pass rare earth deposit, California. In Castor, S.B., Papke, K.G. and Meeuwig, R.O. (eds.), *Betting on Industrial Minerals—Proceedings of the 39th Forum on the Geology of Industrial Minerals, Reno/Sparks, NV*, May 18–24, 2003, pp. 68–81, Special Publication 33, Nevada Bureau of Mines and Geology.

Castrillejo, Y., Fernández, P., Medina, J., Hernández, P. and Barrado, E. (2011) Electrochemical extraction of samarium from molten chlorides in pyrochemical processes, *Electrochim. Acta*, 56: 8638–8644.

Cecconie, T. and Frieser, H. (1989) Extraction of selected tervalent lanthanides using dicyclohexylphosphinic acid, *Solvent Extr. Ion Exc.*, 7(1): 15–29.

Cech, R.E. (1974) Cobalt–rare earth intermetallic compounds produced by calcium hydride reduction of oxides, *J. Metals*, 26(2): 32–35.

CEN (1965) Rare earths—The lean and hungry industry, *Chem. Eng. News* 43(19): 78.

Chaim, R., Marder-Jaeckel, R. and Shen, J.Z. (2006) Transparent YAG ceramics by surface softening of nanoparticles in spark plasma sintering, *Mater. Sci. Eng. A*, 429: 74–78.

Chambers, M.F. and Murphy, J.E. (1988) Molten salt electrolysis of neodymium from a chloride electrolyte. In Bautista, R.G. and Wong, M.M. (eds.), *Rare Earths*, pp. 369–376, The Minerals, Metals and Materials Society, Warrendale, PA.

Chan, T.N. (1992) A new beneficiation process for the treatment of supergene monazite ore. In *Rare Earths: Extraction. Preparation and Applications*, pp. 77–94, TMS and AusIMM, San Diego, CA.

Chandola, L.C., Machado, I.J. and Mohile, A.N. (1975) X-ray fluorescence analysis of cerium dioxide for rare earth impurities, Bhabha Atomic Research Centre, Bombay, India.

Chang, W.C. and Hsing, D.M. (1996) Magnetic properties and transmission electron microscopy microstructures of exchange coupled $Nd_{12-x}Fe_{82+x}B_6$ melt spun ribbons, *J. Appl. Phys.*, 79(8 Pt. 2A): 4843–4845.

Chao, E.C.T., Back, J.M., Minkin, J.A., Tatsumoto, M., Wang, J., Conrad, J.E., McKee, E.H., Meng, Q. and Huang, S. (1997) The sedimentary carbonate-hosted giant Bayan Obo REE–Fe–Nb ore deposit of inner Mongolia, China; A cornerstone example for giant polymetallic ore deposits of hydrothermal origin, Bulletin 2143, USGS, Reston, VA.

Charlot, G. (1976) Process for treatment of pyrochlore concentrates, U.S. Patent 3,947,542.

Chem. Eng. (1953) Rare earths now medium rare, *Chem. Eng.*, 60(1): 120–124.

Chen, Y. (2004) A complete solvent extraction flowsheet for the recovery of rare earth elements and cobalt from NdFeB scrap, China Resources *Comprehensive Utilization*, (6): 10–12.

Chen, Z. (2011) Global rare earth resources and scenarios of future rare earth industry, *J. Rare Earths*, 29(1): 1–6.

Chen, G.Z., Fray, D.J. and Farthing, T.W. (2000) Direct electrochemical reduction of titanium dioxide to titanium in molten calcium chloride, *Nature*, 407: 361–364.

Chen, W., Gao, R.W., Zhu, M.G., Pan, W., Li, W., Li, X.M., Han, G.B., Feng, W.C. and Wang, B. (2003) Magnetic properties and coercivity mechanism of isotropic HDDR NdFeB bonded magnets with Co and Dy addition, *J. Magn. Magn. Mater.*, 261: 222–227.

Chen, Z., Li, J., Xu, J. and Hu, Z. (2008) Fabrication of YAG transparent ceramics by two-step sintering, *Ceram. Int.*, 34(7): 1709–1712.

Chen, L., Jiang, Y., Yang, G., Zhang, G., Xin, X. and Kong, D. (2009) New red phosphor (Y, Gd, Lu)BO_3: Eu^{3+} for PDP applications, *J. Rare Earths*, 27(2): 312–315.

Chen, B., Liu, X., Chen, R., Guo, S., Lee, D. and Yan, A. (2012) The mechanism of enhanced magnetic properties of sintered permanent magnets by substitution of Pr for Nd, *J. Alloys Compd.*, 516(5): 73–77.

Cheng, J. and Che, L. (2010) Current mining situation and potential development of rare earth in China, Baogang Research Institute of Mine, Baotou, Iron & Steel Co., China, *J. Chin. Rare Earths*, 31(2): 65–69.

Cheng, T., Luo, Q., Cai, R., Li, X. and Tseng, Y. (1982) Spectrophotometric determination of rare earths in ligand buffer masking systems. In McCarthy, G.J., Silber, H.B. and Rhyne, J.J. (eds.), *The Rare Earths in Modern Science and Technology*, Vol. 3, pp. 513–516, Plenum, New York.

Cheng, J., Hou, Y. and Che, L. (2007) Flotation separation on rare earth minerals and gangues, J. Rare Earths, 25(1): 62–66.

Cheng, G., Liu, Q., Cheng, L., Lu, L., Sun, H., Wu, Y., Bai, Z., Zhang, X. and Qiu, G. (2010) Synthesis and luminescence property of $Sr_3SiO_5:Eu^{2+}$ phosphors for white LED, *J. Rare Earths*, 28(4): 526–528.

Cheret, D. and Santen, S. (2007) Battery recycling, US Patent 7,169,206.

Chi, R. and Tian, J. (2008) *Weathered Crust Elution–Deposited Rare Earth Ores*, pp. 1–29, Nova Science Publishers, New York.

Chi, R. and Xu, Z. (1999) A solution-chemistry approach to the study of rare earth precipitation by oxalic acid, *Metall. Mater. Trans. B*, 30B: 189–195.

Chi, R., Xu, S., Zhu, G., Xu, J. and Qiu, X. (2001) Beneficiation of rare earth ore in China. In *Light Metals 2001, Technical Sessions at the 130th TMS Annual Meeting*, pp. 1159–1165, TMS Aluminum Committee, New Orleans, LA.

Chi, R., Zhu, H.G., Xu, S., Zhou, Z. and Xu, Z. (2003) Solution-chemistry analysis of ammonium bicarbonate consumption in rare-earth element precipitation, *Metall. Mater. Trans. B*, 34B: 611–617.

Chi, R., Zhang, X., Zhu, G., Zhou, Z.A., Wu, Y., Wang, C. and Yu, F. (2004) Recovery of rare earth from bastnasite by ammonium chloride roasting with fluorine deactivation, *Miner. Eng.*, 17: 1037–1043.

Chi, R., Tian, Y., Li, Z., Peng, C., Wu, Y., Li, S., Wang, C. and Zhou, Z. (2005) Existing state and partitioning of rare earth on weathered ores, *J. Rare Earths*, 23(6): 756–759.

Chistov, L., Barsukova, N., Georgiadi, E., Monastyrskii, I., Ratnikov, E. and Yufryakov, V. (1995) Effect of microwave treatment on physical and technological parameters of niobium/rare earth ores, *J. Mining Sci.*, 31(1): 69–74.

Cioroianu, T.M., Bunus, F., Filip, D. and Filip, G. (2001) Environmental considerations on uranium and radium from phosphate fertilizers. *Impact of new environmental and safety regulations on uranium exploration, mining, milling and management of its waste*, IAEA-TECDOC, Vol. 1244, pp. 215–224, International Atomic Energy Agency, Vienna.

Clark, A.E. (1979) Magnetostrictive RFe_2 intermetallic compounds. In Gschneidner, Jr., K.A. and Eyring, L. (eds.), *Handbook on the Physics and Chemistry of Rare Earths*, Vol. 2, pp. 231–258, North Holland, Amsterdam.

Clark, A.E. (1980) Magnetostrictive rare earth-Fe_2 compounds. In Wohlfarth, E. (ed.), *Ferromagnetic Materials*, Vol. 1, pp. 531–590, North-Holland, Amsterdam.

Clark, R.G. and Stensland, W.A. (1970) Service oxygen analyses with 14 MeV neutrons at Iowa State University, *Journal of Radioanalytical Chemistry*, 4(2): 365–373.

Clark, A.E. and Belson, H.S. (1972) Giant room temperature magnetostriction in $TbFe_2$ and $DyFe_2$, *Phys. Rev. B*, 5: 3642–3644.

Clark, A.L. and Zheng, S. (1991a) China's rare earth potential, industry and policy. In Siribumrungsukha, B., Arrykul, S., Sanguan Sai, P., Pungrassami, T., Sikong, L. and Kooptarnon, K. (eds.), *Proc. Int. Conf. Rare Earth Minerals and Minerals for Electronic Uses, Hat Yai, Thailand*, January, pp. 577–662, Prince of Songkla University, Thailand.

Clark, A.L. and Zheng, S. (1991b) China's rare earth potential, industry and policy, *Mater. Sci. Forum*, 8: 577–602.

Claux, B., Serp, J. and Fouletier, J. (2011) Electrochemical reduction of cerium oxide into metal, *Electrochim. Acta*, 56: 2771–2780.

Clay, A.N., Machowski, R., Jones, I., Marra, G.L., Duke, V., Harper, F. and de Klerk, A.J. (2014) National Instrument 43-101 Independent Technical Report on the Results of a Feasibility Study for the Steenkampskraal Rare Earth Element Project in the Western Cape, South Africa for Great Western Minerals Group Ltd., VMD1445, June 20, Venmyn Deloitte.

Clenfield, J. and Shiraki, M. (2010) Hitachi develops machine to recycle rare earths to cut reliance on China, December 6. Available at http://www.bloomberg.com/news/2010-12-06/hitachi-says-itdeveloped-machine-to-recycle-rare-earths.html.

Clifford, S., Xu, G., Ingelbrechtc, C. and Pomeroya, M.J. (2002) Processes for the production of ultra-pure metals from oxide and their cold rolling to ultra-thin foils for use as targets and as reference materials, *Nucl. Instrum. Methods Phys. Res. A*, 480: 29–35.

Coehoorn, R., Duchateau, J.P.W.B. and Denissen, C.J.M. (1989) Permanent magnet materials based on neodymium iron carbide ($Nd_2Fe_{14}C$) prepared by melt spinning, *J. Appl. Phys.*, 65(2): 704–709.

Coey, J.M.D. (2010) *Magnetism and Magnetic Materials*, Cambridge University Press, Cambridge.

Coey, J.M.D. (2012) Permanent magnets: Plugging the gap, *Scripta Mater.*, 67(6): 524–529.

Coey, J.M.D. and Skomski, R. (1993) New magnets from interstitial intermetallics, *Phys. Scripta*, T49: 315–321.

Coey, J.M.D. and Sun, H.J. (1990) Improved magnetic properties by treatment of iron based rare earth intermetallic compounds in ammonia, *J. Magn. Magn. Mater.*, 87: L251–L254.

Coey, J.M.D., Lawler, J.F., Sun, H. and Allan, J.E.M. (1991a) Nitrogenation of R_2Fe_{17} compounds: R = rare earth, *J. Appl. Phys.*, 69(5): 3007–3010.

Coey, J.M.D., Sun, H. and Hurley, D.P.F. (1991b) Intrinsic magnetic properties of new rare earth iron intermetallic series, *J. Magn. Magn. Mater.*, 101: 310–316.

Collins, J.F., Calkins, V.P. and McGurty, J.A. (1961) Applications of rare earths to ferrous and non-ferrous alloys. In Spedding, F.H. and Daane, A.H. (eds.), *The Rare Earths*, pp. 499–511, John Wiley, New York.

Collocott, S.J., Dunlop, J.B., Lovatt, H.C. and Ramsden, V.S. (1999) Rare earth permanent magnets: New magnet materials and applications, *Mater. Sci. Forum*, 315–317: 77–83.

Connelly, N.G., Hartshorn, R.M., Damhus, T. and Hutton, A.T. (2005) *Nomenclature of Inorganic Chemistry IUPAC Recommendations 2005*, International Union of Pure and Applied Chemistry, The Royal Society of Chemistry, Cambridge.

Connelly, J.N., Ulfbeck, D.G., Thrane, K., Bizzarro, M. and Housh, T. (2006) A method for purifying Lu and Hf for analyses by MC-ICP-MS using TODGA resin. *Chem. Geol*, 233(1–2): 126–136.

Constantinides, S. (2011a) Rare earth science community help needed for clean energy initiatives. Presented at the 26th Rare Earth Research Conference (RERC 2011), June 19–23, Santa Fe, NM.

Constantinides, S. (2011b) Rare earth materials. In *SMMA Management Conference*, Spring, May 10–12, San Diego, CA, 2011.

Constantinides, S. (2012a) Material matters. Available at http://www.northeastern.edu/nanomagnetism/downloads/EAM2012_Arnold_120711_mod120802.pdf.

Constantinides, S. (2012b) The demand for rare earth materials in permanent magnets. In *51st Annual Conference of Metallurgists*, Niagara Falls, September 30–October 3, COM 2012, Met. Soc. of CIM.

Conzemius, R.J. (1979) Analysis of rare earth matrices by spark source mass spectrometry. In Gschneidner, Jr., K.A. and Eyring, L. (eds.), *Handbook on the Physics and Chemistry of Rare Earths*, Vol. 4, pp. 377–404, North-Holland, Amsterdam.

Cook, J.S. and Rossiter, P.L. (1989) Rare-earth boron supermagnets, *Crit. Rev. Solid State Mater. Sci.*, 15: 509–550.

Coon, V.T., Wallace, W.E. and Craig, R.S. (1978) Methanation by rare earth intermetallic catalysts. In McCarthy, G.J. and Rhyne, J.J. (eds.), *The Rare Earths in Modern Science and Technology*, Vol. 1, Plenum, New York.

Corbett, J.D., Smith, J.D. and Garcia, E. (1986) The selective removal of oxygen from rare earth and thorium metals through oxyhalide formation, *J. Less Common Metals*, 115: 343–355.

Cordier, D.J. (2009) *Rare Earths. U.S. Geological Survey Minerals Yearbook 2009*, pp. 60.1–60.15, U.S. Department of the Interior, Washington, DC.

Cordier, D.J. (2011) *Rare Earths, Mineral Commodity Summaries*, U.S. Geological Survey, Reston, VA.

Cordier, D.J. (2012) *Rare Earths, Mineral Commodity Summaries*, U.S. Geological Survey, Reston, VA.

Cordier, D.J. and Hedrick, J.B. (2008) *Rare Earths. U.S. Geological Survey Minerals Yearbook 2008*, pp. 60.1–60.15, U.S. Department of the Interior, Washington, DC.

Cornelis, J., Groenenboom, G.J. and Wieringa, P.A. (1989) Cracking catalyst of sepiolite, zeolite Y, clay and matrix, U.S. Patent 4840724.

Cox, J.J., Ciuculescu, T., Goode, J.R. and Hains, D.H. (2011) Avalon Rare Metals—Technical Report on the Thor Lake Project, NI 43-101 Report, August 25, Toronto, ON, CA.

Crawford, M.K. and Brixner, L.M. (1991) Phospholuminable phosphorus for x-ray imaging: Applications and mechanisms, *J. Lumin.*, 488(49): 37.

CREI (1998) Rare earth industry in Baotou, *China Rare Earth Inf.*, 4(5).

Croat, J.J. (1969) The preparation of high purity dysprosium, holmium and erbium by the lithium reduction of their trichloride salts, Report No. IS-T-346, Ames Laboratory, ERDA, Iowa State University, Ames, IA, National Technical Information Service, Springfield, VA.

Croat, J.J. (1989) Manufacture of Nd–Fe–B permanent magnets by rapid solidification, *J. Less Common Metals*, 148: 7–15.

Croat, J.J. (1998) The current status of bonded NdFeB permanent magnets. In Preprints of the Conference, China Magnets, held on October 18–21, 1998 at Beijing, PR China.

Croat, J.J., Herbst, J.F., Lee, R.W. and Pinkerton, F.E. (1984a) Pr–Fe and Nd–Fe based materials: A new class of high performance permanent magnets, *J. Appl. Phys.*, 55: 2078–2082.

Croat, J.J., Herbst, J.F., Lee, R.W. and Pinkerton, F.E. (1984b) High energy product Nd–Fe–B permanent magnets, *Appl. Phys. Lett.*, 44: 148–149.

Cross, W.M. and Miller, J.D. (1988) Bubble attachment time measurements for selected rare earth phosphate minerals in oleate solutions. In Bautista, R.G. and Wong, M.M. (eds.), *Rare Earths*, pp. 45–55, The Minerals, Metals and Materials Society, Warrendale, PA.

CSRE (2002) Chinese Society of Rare Earth: Annual Report 2002.

Cui, X.G., Yan, M., Ma, T.Y. and Yu, L.Q. (2008) Effects of Cu nanopowders addition on magnetic properties and corrosion resistance of sintered Nd–Fe–B magnets, *Phys. B Condens. Matter*, 403(23–24): 4182–4185.

Cui, X.G., Yan, M., Ma, T.Y., Luo, W. and Tu, S.J. (2009) Effect of SiO_2 nanopowders on magnetic properties and corrosion resistance of sintered Nd–Fe–B magnets, *J. Magn. Magn. Mater.*, 321(5): 392–395.

Curtis, N. (2009a) Lynas Corporation presentation—Mount weld rare earths latest developments. In *5th International Rare Earths Conference*, November, Hong Kong.

Curtis, N. (2009b) Lynas Corporation presentation—Observations of an emerging producer. In *5th International Rare Earths Conference*, November, Hong Kong.

Cuthbertson, R.E. (1952) Froth flotation of monazite from heavy gravity minerals, U.S. Patent 2,610,738.

Cuthbert, F.L. (1958) Production of Uranium Metal. In *Australian Atomic Energy Symposium, 1958: Proceedings* (p. 102). Published by Melbourne University Press on behalf of the Australian Atomic Energy Commission.

D'Silva, A.P. and Fassel, V.A. (1979) X-ray excited optical luminescence of the rare earths. In Gschneidner, Jr., K.A. and Eyring, L. (eds.), *Handbook on the Physics and Chemistry of Rare Earths*, Vol. 4., pp. 441–456, North-Holland, Amsterdam.

Daane, A.H. (1961a) Yttrium. In Hampel, C.A. (ed.), *Rare Metals Handbook*, pp. 653–666, Reinhold, New York.

Daane, A.H. (1961b) Metallothermic preparation of rare earth metals. In Spedding, F.H. and Daane, A.H. (eds.), *The Rare Earths*, pp. 102–112, Wiley, New York.

Daane, A.H. and Spedding, F.H. (1953) Preparation of yttrium and some heavy rare earth metals, *J. Electrochem. Soc.*, 100: 442–444.

Daane, A.H., Dennison, D.H. and Spedding, F.H. (1953) The preparation of samarium and ytterbium metals, *J. Am. Chem. Soc.*, 75: 2272–2273.

Dallmann, W.E. and Fassel, V.A. (1967) Simultaneous determination of oxygen and nitrogen in metals by carrier gas fusion extraction, *Anal. Chem.*, 39(5): 133–142.

Das, D.K. (1969) Twenty million energy product samarium–cobalt magnet, *IEEE Trans. Magn.*, MAG-5: 214–216.

Davies, K.E. (1981) Industrial applications of pure rare earth metals and related alloys. In Gschneidner, Jr., K.A. (ed.), *Industrial Applications of Rare Earth Elements*, pp. 165–175, ACS Symposium Series 164, American Chemical Society, Washington, DC.

Day, J.A., Caruso, J.A. Becker, J.S. and Dietze, H.-J. (2000) Application of interfaced to double focusing sector field ICP-MS for nuclide abundance determination of lanthanides produced via spallation reactions in an irradiated tantalum target, *J. Anal. Atomic Spectrom.*, 15: 1343–1348.

Dayton, S.H. (1958) Radioactive black sand is yielding columbite concentrate at Idaho Mill, *Min. World*, 20(5): 36–41.

de Boer, J.H. and Fast, J.D. (1940) Electrolysis of solid solutions of oxygen in metallic zirconium, *Rec. Trav. Chim.*, 59: 161–167.

de Oliveira, N.A. and von Ranke, P.J. (2010) Theoretical aspects of the magnetocaloric effect, *Phys. Rep.*, 489: 89–159.

de Rhoden, C. and Peltier, M. (1957) Treatment of monazite, U.S. Patent 2,783,125.

de Vasconcellos, M.E., da Rocha, S.M.R., Pedreira, W.R., Queiroz, C.A.d.S. and Abrão, A. (2006) Enrichment of yttrium from rare earth concentrate by ammonium carbonate leaching and peroxide precipitation, *J. Alloys Compd.*, 418(1–2): 200–203.

de Vasconcellos, M.E., da Rocha, S.M.R., Pedreira, W.R., Queiroz, C.A.d.S. and Abrão, A. (2008) Solubility behavior of rare earths with ammonium carbonate and ammonium carbonate plus ammonium hydroxide: Precipitation of their peroxicarbonates, *J. Alloys Compd.*, 451: 426–428.

Decroly, C., Tytgat, D. and van Impe, J. (1953) Preparation of misch metal by thermal reduction, *J. Electrochem. Soc.*, 100: 388–391.

DeGuire, E. (2012) Large deposit of rare earth neodymium discovered in Brazil, *Ceramic Tech. Today*, April 11.

DeKalb, E.L. (1973) Emission spectroscopy for rare earth analyses, and for the determination of impurities in rare earth materials. In Michelsen, O.B. (ed.). *Analysis and Application of Rare Earth Materials: Lectures Given at the NATO Advanced Study Institute*, Kjeller, Norway, August 23–29, 1972. Universitetsforlaget.

DeKalb, E.L. and Fassel, V.A. (1979) Optical atomic emission and absorption methods. In Gschneidner, Jr., K.A. and Eyring, L. (eds.), *Handbook on the Physics and Chemistry of Rare Earths*, Vol. 4., pp. 405–440, North-Holland, Amsterdam.

De Michelis, I., Ferella, F., Varelli, E.F. and Veglio, F. (2011) Treatment of exhaust fluorescent lamps to recover yttrium: Experimental and process analyses. *Waste Manage*, 31: 2559–2568.
Dennison, D.H., Tschetter, M.J. and Gschneidner, Jr., K.A. (1966a) The solubility of tantalum in eight liquid rare earth metals, *J. Less Common Metals*, 10: 108–115.
Dennison, D.H., Tschetter, M.J. and Gschneidner, Jr., K.A. (1966b) The solubility of Ta and W in liquid rare earth metals, *J. Less Common Metals*, 11: 423–435.
Dent, P.C. (2012) Rare earth permanent magnets (Invited), *J. Appl. Phys.*,111: 07A721.
Derry, D.R. (1960) Evidence of the origin of the Blind River uranium deposits. *Economic Geology*, 55(5): 906–927.
Desai, G.C. (1988) Use of rare earths in paints and pigments, *Mater. Sci. Forum*, 30: 259–264.
Desai, H.B., Krishnamurthy Iyer, R. and Shankar Das, M. (1964) Determination of scandium, yttrium, samarium and lanthanum in standard silicate rocks G-1 and W-1, by neutron activation analysis, *Talanta*, 11: 1249–1255.
Dexpert-Ghys, J., Regnier, S., Canac, S., Beaudette, T., Guillot, P., Caillier, B., Mauricot, R., Navarro, J. and Sekhri, S. (2009) Re-processing CRT phosphors for mercury-free applications, *J. Lumin.*, 129: 1968–1972.
Diatloff, E., Asher, C.J. and Smith, F.W. (1999) The effect of rare earth elements on the growth and nutrition of plants, *Mater. Sci. Forum*, 315–317: 354–360.
DiFrancesco, C.A., Hedrick, J.B., Cordier, D.J. and Gambogi, J. (2014) *Rare Earth Statistics*, U.S. Geological Survey, Reston, VA.
Djingova, R. and Ivanova, J. (2002) Determination of rare earth elements in soils and sediments by inductively coupled plasma atomic emission spectrometry after cation-exchange separation, *Talanta*, 57: 821–829.
Dobretsov, N.L. and Pokhilenko, N.P. (2010) Mineral resources and development in the Russian Arctic, *Russ. Geol. Geophys.*, 51: 98–111.
Dogadkin, N., Kychinskaya, O., Tustanovsky, V. and Yakovlev, Y. (1976) The determination of rare earth alloying additives in special steels by neutron activation analysis. *Journal of Radioanalytical and Nuclear Chemistry*, 29(2): 251–258.
Domazer, H.G. and Strnat, K.J. (1976) New substituted Sm-Co alloys—Preparation and magnetic properties. In Strnat, K.J. (ed.), *Proc. 2nd Int. Workshop on R–Co Permanent Magnets*, pp. 348–363, University of Dayton, Dayton.
Douglas, D.A. and Bauer, D.J. (1959) Liquid–liquid extraction of cerium, Bureau of Mines Report of Investigations 5513, U.S. Department of the Interior, Washington, DC.
Doyle, F.M., Benz, M.G., Shei, J.C., Bao, D.S., Ku, H.X. and Zhen, N.D. (2000) Direct production of mixed, rare earth oxide feed for high energy-product magnets. In Bautista, R.G. and Mishra, B. (eds.), *Rare Earths and Actinides: Science, Technology and Applications IV*, pp. 31–44, TMS, Warrendale, PA.
Drew, L.J., Qingrun, M. and Weijun, S. (1991) The geology of Bayan Obo iron–rare earth–niobium deposits, Inner Mongolia, China. In Siribumrungsukha, B., Arrykul, S., Sanguan Sai, P., Pungrassami, T., Sikong, L. and Kooptarnon, K. (eds.), *Proc. Int. Conf. Rare Earth Minerals and Minerals for Electronic Uses, Hat Yai, Thailand*, January, pp. 13–31, Prince of Songkla University, Thailand.
Du Preez, A.C. and Preston, J.S. (1992) The solvent extraction of rare earths metals by carboxylic acids, *Solvent Extr. Ion Exc.*, 10(2): 207–230.
Duncan, L.K. (1970) Cerium oxide for glass polishing, *Glass Ind.*, 41: 387–393.
Dziwinski, E. and Szymanowski, J. (1998) Composition of Cyanex® 923, Cyanex® 925, Cyanex® 921 and TOPO. *Solvent Extraction Ion Exchange*, 16(6): 1515–1525.
Eastman, E., Fontana, B., Thurmond, C. and Wilmarth, W. (1955) The preparation of cerium by electrolysis of molten salts, U.S. Atomic Energy Commission Report TID-5212, National Technical Information Service, Springfield, VA.
Eggins, S.M., Woodhead, J.D., Kinsley, L.P.J., Mortimer, G.E., Sylvester, P., McCulloch, M.T., Hergt, J.M. and Handler, M.R. (1997) A simple method for the precise determination of

N = 40 trace elements in geological samples by ICPMS using enriched isotope internal standardization, *Chem. Geol.*, 134(4): 311–326.

El-Hefny, N.E., El-Nadi, Y.A. and Daoud, J.A. (2010) Equilibrium and mechanism of samarium extraction from chloride medium using sodium salt of CYANEX 272, *Sep. Purif. Technol.*, 75: 310–315.

Ellingham, H.J.T. (1944) Reducibility of oxides and sulphides in metallurgical processes, *J. Soc. Chem. Ind.*, 63: 125–133.

Elliott, J. (2012) IM global rare earths roundup, *Industrial Minerals*, February 24.

Ellis, T.W., Schmidt, F.A. and Jones, L.L. (1994) Methods and opportunities in the recycling of rare earth based materials, Report No. IS-M 796, Ames Laboratory, Ames, IA.

Emley, E.F. (1966) *Principles of Magnesium Technology*, Pergamon, Oxford.

EPA (1992) Proposed rare earths mining and beneficiation at Mt Weld, Laverton and secondary processing at Meenaar, near Northam, Ashton Rare Earths Ltd, Bulletin 646, August, Environmental Protection Authority, Perth, Western Australia.

EPA (1995) Historic hardrock mining: The West's toxic legacy, EPA 908-F-95-002, United States Environmental Protection Agency, Washington, DC.

EPA (1997) Hardrock mining framework, United States Environmental Protection Agency, Washington, DC.

EPA (2012) Rare earth elements: A review of production, processing, recycling, and associated environmental issues, EPA 600/R-12/572, December. Available at http://www.epa.gov/ord.

Evans, J.R. (1964) Xenotime mineralization in the Southern Music Valley Area Riverside County, California, Special Report 79 California Division of Mines and Geology Ferry Building, San Francisco.

Evans, J.R. (1966) California's Mountain Pass mine now producing europium oxide, *Miner. Inf. Serv.*, 18(2): 23–32.

Eyring, L. and Cunningham, B. (1948) Chemistry Division Quarterly Report for September, October and November 1948, US Atomic Energy Commission Report UCRL-264, National Technical Information Service, Springfield, VA.

Falconer, A. (2003) Gravity separation: Old technique/new methods, *Phys. Sep. Sci. Eng.*, 12(1): 31–48.

Falconnet, P. (1993). The rare earth industry: A world of rapid change. *Journal of Alloys and Compounds*, 192(1): 114–117.

Falconnet, P.G. (1988) Rare earths production and marketing opportunities. In Gupta, C.K. and Krishnan, T.S. (eds.), *Rare Earths—Applications and Technology*, pp. 1–12, Trans Tech Publications, Switzerland.

Farr, M.B. (1982) Rare earths, *Min. Ann. Rev.*, 94–95.

Fassel, V.A. (1949) The quantitative spectrographic analysis of the rare earth elements, *JOSA*, 39(2): 187–192.

Fassel, V.A. and Goetzinger, J.W. (1965) Emission spectrometric determination of the gaseous elements in metals—VIII. Establishment of a master analytical curve for oxygen without standard samples. *Spectrochimica Acta*, 21(2): 289–293.

Fassel, V.A., Curry, R.H. and Kinseley, R.N. (1962) Flame spectra of the rare-earth elements, *Spectrochim. Acta*, 18: 1127–1153.

Fassel, V.A., Dallmann, W.E. and Hill, C. (1966) A critical study of carbon reduction techniques for the determination of oxygen in thorium and yttrium metals, *Anal Chem.*, 38(3): 421–425.

Fassel, V.A., DeKalb, E.L. and D'Silva, A.P. (1973a) Trace level rare earth determinations by x-ray excited optical fluorescence (XEOF) spectroscopy. In Michelsen, O.B. (ed.), *Analysis and Application of Rare Earth Materials*, pp. 109–122, Universitetsforlaget, Oslo.

Fassel, V.A., Kinseley, R.N. and Butler, C.C. (1973b) Flame and atomic absorption, emission and fluorescence spectroscopy of the rare earth elements. In Michelsen, O.B. (ed.), *Analysis and Application of Rare Earth Materials*, pp. 71–86, Universitetsforlaget, Oslo.

Fassel, V.A., Katzenberger, J.M. and Winge, R.K. (1979) Effectiveness of Interference Filters for Reduction of Stray Light Effects in Atomic Emission Spectrometry, *Applied Spectroscopy*, 33(1): 1–5.

Felix, N. and Vanriet, C. (1994) Recycling of electronic scrap at UMS Hoboken Smelter. In *Precious Metals 1994—Proceedings of the 18th International Precious Metals Conference*, June, pp. 159–169, Vancouver, Canada.

Ferraro, J.R. and Peppard, D.F. (1963) Structural Aspects of Organophosphorus Extractants and Their Metallic Complexes as Deduced from Spectral and Molecular Weight Studies, *Nucl. Sci. Eng.*, 16(4): 389–400.

Ferron, C.J. and Henry, P. (2013) A review of the recycling of rare earth metals. In London, I.M., Goode, J.R., Moldoveanu, G. and Rayat, M.S. (eds.), *Rare Earth Elements*, pp. 517–532, Canadian Institute of Mining, Metallurgy and Petroleum, Quebec.

Ferron, C.J., Bulatovic, S.M. and Slater, R.S. (1991) Beneficiation of rare earth oxide minerals. In Siribumrungsukha, B., Arrykul, S., Sanguan Sai, P., Pungrassami, T., Sikong, L. and Kooptarnon, K. (eds.), *Proc. Int. Conf. Rare Earth Minerals and Minerals for Electronic Uses, Hat Yai, Thailand*, January, pp. 251–269, Prince of Songkla University, Thailand.

Fischer, W., Dietz, W. and Jubermann, O. (1937) Ein neues Verfahren zur Trennung der seltenen Erden, *Naturwissenschaften*, 25: 348.

Fisher, G. (1988) Superconductor mysteries unravel as developments proceed, *Am. Ceram. Soc. Bull.*, 67: 725–735.

Fisher, R.W. and Olson, D.G. (1959) Vibrating tray hydrofluorination furnace, AEC Document IS-2, July, National Technical Information Service, Springfield, VA.

Fitzgibbon, K. and Veasy, T.J. (1990) Thermally assisted liberation—A review, *Miner. Eng.*, 3(1): 181–185.

Fjellvag, H., Karen, P., Kjekshus, A., Lyng, S. and Bratten, O. (1988) Is mutual separation of rare earth elements crucial for preparation of high T_c materials?, *Physica C*, 153–155: 1421–1422.

Fleck, D.C., Kleespies, E.K. and Kesterke, D.G. (1973) Purification of yttrium by electrorefining, U.S. Bureau of Mines Report of Investigations 7710, U.S. Department of the Interior, Washington, DC.

Foltyn, S.R., Tiwari, P., Dye, R.C., Le, M.Q. and Wu, X.D. (1993) Pulsed laser deposition of thick $YBa_2Cu_3O_{7-5}$ films with $J_c > 1$ MA/cm^2, *Appl. Phys. Lett.*, 63: 1848–1850.

Foos, R.A. and Wilhelm, H.A. (1954) Separation of yttrium and some rare earths by liquid–liquid extraction, U.S. Atomic Energy Commission Report ISC-695, National Technical Information Service, Springfield, VA.

Fort, D. (1987) The purification and crystal growth of rare earth metals using solid state electrotransport, *J. Less Common Metals*, 134: 45–65.

Fort, D., Jones, D.W., Beaudry, B.J. and Gschneidner, Jr., K.A. (1981) Zone refining of rare earth metals: Lanthanum, cerium and gadolinium, *J. Less Common Metals*, 81: 273–292.

Fort, D., Beaudry, B.J. and Gschneidner, Jr., K.A. (1987) The ultrapurification of rare earth metals, gadolinium and neodymium, *J. Less Common Metals*, 134: 27–44.

Fort, D., Beaudry, B.J. and Gschneidner, K.A. (1990) Solid state electrotransport of erbium, *J. Less Common Metals*, 166(1): 173–188.

Foster, D.C. and Kremers, H.E. (1953) Europium determination in rare earth mixtures, *Anal. Chem.*, 25: 1921–1922.

Foster, K.W., Pish, G., Schamp, H.W., Goode, J.M. and Eyles, T.E. (1952) Preparation of lanthanum metal by the de Boer process, Mound Laboratory, AEC Report MLM-686, National Technical Information Service, Springfield, VA.

Fox, G.J. (1996) High temperature superconductors open door to advanced technology, *Elements*, August/September: 22–26.

Frey, E. (1876) Notice of the preparation of the earth metals in the chemical plant of Dr. Schuchardt in Gorlitz, *Ann.*, 183: 367–368.

Fromm, E. and Horz, G. (1980) Hydrogen, nitrogen, oxygen and carbon in metals, *Int. Mater. Rev.*, 25: 269–311.

Fuerst, C.D. and Brewer, E.G. (1990) Enhanced coercivities in die-upset Nd–Fe–B magnets with diffusion alloyed additives (Zn, Cu, and Ni), *Appl. Phys. Lett.*, 56: 2252–2254.

Fuerst, C.D. and Brewer, E.G. (1991) Diffusion alloyed additives in die-upset Nd–Fe–B magnets, *J. Appl. Phys.*, 69: 5826–5828.

Fuerstenau, D.W. and Pradip, K. (1986) The role of inorganic and organic additives in bastnasite ore flotation. In *Flotation Heute, Heft 48*, pp. 19–38, GDMB, Clausthal-Zellerfeld, Germany.

Fuerstenau, D.W. and Pradip, K. (1991) The role of inorganic and organic reagents in the flotation separation of rare-earth ores, *Int. J. Min. Proc.*, 32: 1–22.

Fujita, M. and Leepawpanth, Q. (1991) Thai–Japan research cooperation on the recovery of rare metals from tin tailings. In Siribumrungsukha, B., Arrykul, S., Sanguan Sai, P., Pungrassami, T., Sikong, L. and Kooptarnon, K. (eds.), *Proc. Int. Conf. Rare Earth Minerals and Minerals for Electronic Uses, Hat Yai, Thailand*, January, pp. 537–556, Prince of Songkla University, Thailand.

Fullam, M. and Grewal, I. (2001) *The Knelson Continuous Variable Discharge (CVD) Concentrator*, pp. 1–6, The Knelson Group, Langley, BC. Available at http://knelsongravity.xplorex.com/sites/knelsongravity/files/reports/report30s.pdf.

Furman, N.H. (ed.) (1939) *Scott's Standard Methods of Chemical Analysis*, 5th edn., Vol. 1, pp. 247–250, D. Van Nostrand Co, Inc., New York.

Gambogi, J. (2011) *Rare Earths. U.S. Geological Survey Minerals Yearbook 2010*, pp. 60.1–60.12, U.S. Department of the Interior, Washington, DC.

Gambogi, J. (2013) Rare earths, Mineral Commodity Summaries, U.S. Geological Survey, U.S. Department of the Interior, Washington, DC.

Gambogi, J. and Cordier, D.J. (2010) *Rare Earths. U.S. Geological Survey Minerals Yearbook 2010*, pp. 60.1–60.13, U.S. Department of the Interior, Washington, DC.

Gao, H. and Tang, Y. (2009) Recovery of Rare Earth from Spent Metal Hydride–Nickel Batteries*, Trans. Shenyang Ligong University,* 2: 004.

Gao, L. and Chen, Y. (2010) A study on the rare earth ore containing scandium by high gradient magnetic separation, *J. Rare Earths*, 28(4): 622–626.

Garg, S.P. and Sundaram, C.V. (1974) Thermodynamics of sacrificial deoxidation, BARC Report 777, Bhabha Atomic Research Center, Bombay.

Garg, S.P. and Sundaram, C.V. (1975) Thermodynamics of C- and Al-deoxidation of refractory metals, BARC Report, 822, Bhabha Atomic Research Center, Bombay.

Garg, S.P., Venkataraman, M., Krishnamurthy, N. and Krishnan, R. (1996) *Phase Diagrams of Binary Tantalum Alloys*, pp. 173–189, Indian Institute of Metals, Calcutta.

Garrell, M.G., Shih, A.J., Ma, B.M., Curzio, E.L. and Scattergood, R.O. (2003) Mechanical properties of nylon bonded Nd–Fe–B permanent magnets, *J. Magn. Magn. Mater.*, 257: 32–43.

Gasgnier, M., Albert, L., Derouet, J., Beaury, L. and Caro, P. (1994) Selective leaching of rare earth oxide powders LnO_x (Ln = Pr and Tb) in acetic acid: Ultrasonic irradiation effects and acoustic emission, *C. R. Acad. Sci., Ser. II: Mec., Phys. Chim. Astron.*, 318: 915–920.

Gaudernack, B., Hannestad, G. and Hundere, I. (1973) Process for separating yttrium values from the lanthanides. *U.S. Patent No. 3,751,553*. Washington, DC: U.S. Patent and Trademark Office.

Ge, Z., Sun, C. and Luo, Y. (1998) Progress in preparing magnet alloy. In Preprints of the Conference, China Magnets, held on October 18–21, 1998 at Beijing, PR China.

Gee, B., Holtham, P., Dunne, R. and Gregory, S. (2005) Recovery of fine gold particles using a Falcon 'B' separator. In Deschenes, G., Hodouin, D., Lorenzen, L. (eds.), *International Symposium on the Treatment of Gold Ores*, pp. 3–15, CIM, Calgary, AB, CA.

Genshi, W., Daxin, Z., Deying, S., Xianglong, W. and Panwan, S. (1985) Chemical synthesis and hydrogen storage characteristics of misch metal–nickel compounds. In Xu, G. and Xiao, J. (eds.), *New Frontiers in Rare Earth Science and Application*, Vol. II, pp. 1062–1065, Science Press, Beijing.

Ghada, M.M., Nabil, T.E.H., Ahmad, M.F. and Omneya, M.E.H. (2008) Separation of rare earth elements from sulfate leach liquor by heterocyclic nitrogen compound. *Journal of Rare Earths*, 26(4), 544–551.

Gibilaro, M., Massot, L., Chamelot, P. and Taxil, P. (2008) Study of neodymium extraction in molten fluorides by electrochemical co-reduction with aluminium, *J. Nucl. Mater.*, 382(1): 39–45.

Gibilaro, M., Massot, L., Chamelot, P., Cassayre, L. and Taxil, P. (2009) Electrochemical extraction of europium from molten fluoride media, *Electrochim. Acta*, 55: 281–287.

Giesen, A., Hugel, H., Voss, A., Wittig, K., Brauch, U. and Opower, H. (1994) Scalable concept for diode-pumped high-power solid state lasers, *Appl. Phys. B-Lasers Opt.*, 58(5): 365–372.

GMEL (2009) Kvanefjeld Multi-Element Project, Pre-Feasibility Study—Interim Report Section 2, Executive Summary, December, Greenland Minerals and Energy Ltd.

GMEL (2010) Building the foundations of a world-class mining project, October, Greenland Minerals and Energy Ltd. Avalable at http://www.ggg.gl/userfiles/Greenland_Presentation_Oct_2010.pdf.

Goldschmidt, H.J. (1967) *Interstitial Alloys*, Plenum, New York.

Goonan, T.G. (2011) *Rare Earth Elements—End Use and Recyclability*, Scientific Investigations Report 2011–5094, US Department of the Interior, US Geological Survey, U.S. Geological Survey, Reston, Virginia.

Graber, F.M., Lukens, H.R. and Mackenzie, J.K. (1970) Neutron activation analysis determination of all 14 stable rare earth elements with group separation and Ge(Li) spectrometry, *J. Radioanal. Chem.*, 4(2): 229–239.

Grasso, V.B. (2013) Rare earth elements in national defence: Background, oversight issues, options for congress, Congressional Research Service (CRS) Report R41744. Available at http://www.crs.gov.

Gray, P.M.J. (1951) The production of pure cerium metal by electrolytic and thermal reduction processes, *Trans. Inst. Min. Met.*, 61: 141–170.

Greenland minerals (2011) Kvanefjeld Multielement Project. Available at http://www.ggg.gl/projects/kvanefjeld-rees-uranium-zinc/

Greinacher, E. (1970) *Seltene Erden. Chemische Technologie Vol. 2, Anorganische Technologie II*, pp. 218–222, Hanser Verlag, Munich.

Greinacher, E. (1981) History of rare earth applications, rare earth market today: Overview. In Gschneidner, Jr., K.A. (ed.), *Industrial Applications of Rare Earth Elements*, pp. 3–18, ACS Symposium Series 164, American Chemical Society, Washington, DC.

Greskovich, C. and Duclos, S. (1997) Ceramic scintillators, *Ann. Rev. Mater. Sci.*, 27: 69–88.

Greskovich, C.D., Cusano, D.A., Riedner, R.J. and Hoffman, D. (1992) Ceramic scintillators for advanced X-ray detectors, *Am. Ceram. Soc. Bull.*, 71(7): 1120–1130.

Groenenboom, C.J. and Wieringa, P.A. (1989) Cracking catalyst of sepiolite, zeolite y, clay and matrix. *U.S. Patent No. 4,840,724*. Washington, DC: U.S. Patent and Trademark Office.

Grossman, A.M., Ciba, J., Jurczyk, J. and Spiewok, W. (1990) Determination of lanthanum, cerium, prasedodymium and neodymium in alloy steels by inductively coupled plasma—Atomic emission spectrometry, *Talanta*, 37(8): 815–818.

Gruzensky, W.G. and Engel, G.T. (1959) Separation of yttrium and rare earth nitrates with the solvent extraction system tri-N-butylamine-3-methyl-2-butanone, *Trans. Met. Soc. AIME*, 215: 738–742.

Gschneidner, Jr., K.A. (1975) Derivation, extraction and preparation. In Horovitz, C.T. (ed.), *Scandium*, pp. 66–75, Academic Press, London.

Gschneidner, Jr., K.A. (1980) Rare earth speciality inorganic chemicals. In *Proceedings, Symposium on Speciality Inorganic Chemicals, Salford*, pp. 403–443, The Royal Society of Chemistry, London.

Gschneidner, Jr., K.A. (1981) *Industrial Applications of Rare Earth Elements*, ACS Symp. Ser. 164, American Chemical Society, Washington, DC.

Gschneidner, Jr., K.A. (1990) Physical properties of rare earth metals, *Bull. Alloy Phase Diagrams*, 11: 216–224.

Gschneidner, Jr., K.A. (2011a) Globalization and the Sustainability of the Rare Earths, Presentation, March 25, Materials Engineering 220, Iowa State University, Ames, IA.

Gschneidner, Jr., K.A. (2011b) The rare earth crisis—The supply and demand situation for 2010–2015, *Mater. Matters*, 6(2).

Gschneidner, Jr., K.A. and Daane, A.H. (1988) Physical metallurgy. In Gschneidner, Jr., K.A. and Eyring, L. (eds.), *Handbook on the Physics and Chemistry of Rare Earths*, Vol. 11, pp. 409–484, North Holland, Amsterdam.

Gschneidner, Jr., K.A. and Pecharsky, V.K. (2006) Rare earths and magnetic refrigeration, *J. Rare Earths*, 24: 641–647.

Gschneidner, Jr., K.A., Takeya, H., Moorman, J.O. and Pecharsky, V.K. (1994a) $(Dy_{0.5}\ Er_{0.5})\ Al_2$: A large magnetocaloric effect material for low temperature magnetic refrigeration, *Appl. Phys. Lett.*, 64(2): 253–255.

Gschneidner, Jr., K.A., Takeya, H., Moorman, J.O., Pecharsky, V.K., Malik, S.K. and Zimm, C.B. (1994b) New magnetic refrigeration materials for the liquefaction of hydrogen. In Kittel, P. (ed.), *Advances in Cryogenic Engineering*, Vol. 39, pp. 1457–1465, Plenum, New York.

Gschneidner, Jr., K.A., Beaudry, B.J. and Capellen, J. (1995) Rare earth metals. In *ASM Metals Handbook*, pp. 720–732, ASM International, Metals Park, OH.

Gschneidner, Jr., K.A., Pecharsky, V.K., Pecharsky, A.O. and Zimm, C.B. (1999) Recent developments in magnetic refrigeration, *Mater. Sci. Forum*, 315–317: 69–76.

Guarde, D., von Heeren, C., Sanchez, J.C., Arnaiz, S., Iribarnegaray, D. and Castillo, B. (2010) Improved management and recycling of waste fluorescent lamps, The Prolux Project; Care Innovation 2010, November 8–11, Vienna, Austria.

Guertler, W. (1923) Molybdenum as a constituent in alloys, *Z. Metallkd.*, 15: 151–154.

Guhathakurta, S. and Singh, H. (2000) Rare Earths, Rare Earth Association of India, Indian Rare Earths Ltd, Mumbai.

Gunasekaran, N. (1988) Mixed rare earth oxides and their catalytic applications. In Gupta, C.K. and Krishnan, T.S. (eds.), *Rare Earths—Applications and Technology*, pp. 117–124, Trans Tech Publications, Switzerland.

Gundogdu, T. and Komurgoz, G. (2013) The impact of the selection of permanent magnets on the design of permanent magnet machines—A case study: Permanent magnet synchronous machine design with high efficiency, Istanbul Technical University, Department of Electrical Engineering Przegląd Elektrotechniczny, R. 89 NR 3a/2013, pp. 104–108.

Guo, A.H., Yu, X.J. and Li, W. (1998) Rare earth permanent magnets with low temperature coefficients. In Preprints of the Conference, China Magnets, October 18–21, 1998, Beijing.

Gupta, C.K. and Krishnamurthy, N. (1992) Extractive metallurgy of rare earths, *Int. Mater. Rev.*, 37(5): 197–248.

Gutfleisch, O., Willard, M.A., Bruck, E., Chen, C.H., Sankar, S.G. and Liu, J.P. (2011) Magnetic materials and devices for the 21st century: Stronger, lighter, and more energy efficient, *Adv. Mater.*, 23: 821–842.

Guy, P.J., Bruckard, W.J. and Vaisey, M.J. (2000) Beneficiation of Mt Weld rare earth oxides by gravity concentration, flotation, and magnetic separation. In *Seventh Mill Operators' Conference*, pp. 197–205, AusIMM, Kalgoorlie.

GWMG (2010) Great Western Minerals Group, Available at http://www.starminerals.ca/s/Diane_Lake.asp.

Habermann, C.E. and Daane, A.H. (1961) Vapour pressure of rare earth metals, *J. Chem. Phys.*, 41: 2818–2827.

Haefling, J.A., Schmidt, F.A. and Carlson, O.N. (1961) A study of several metals as reductants for yttrium fluoride, Research and Development Report ISC-374, Ames Laboratory, USAEC, National Technical Information Service, Springfield, VA.

Hageluken, C. (1999) Recycling of spent noble metal catalysts with emphasis on pyrometallurgical processing, *Oil Gas—Eur. Mag.*, 25: 36–39.

Hageluken, C. (2001) Securing the supply for tomorrow: Precious metals recycling from automotive catalysts, *Metall*, 55: 104–111.

Hagelüken, C., Buchert, M. and Stahl, H. (2005) *Materials Flow of Platinum Group Metals—Systems Analysis and Measures for Sustainable Optimization of the Materials Flow of Platinum Group Metals*, GFMS Ltd, Umicore Precious Metals Refining and Öko-Institut, e.V., London.

Halpin, K.M. (2010) The characteristics and origin of the Hoidas Lake REE deposit, MSc Thesis, Department of Geological Sciences, University of Saskatchewan, Saskatoon.

Hampel, C.A. (ed.) (1961) *Rare Metals Handbook*, 2nd ed., Reinhold, London.

Harrah, H.W. (1967) Rare earth concentration at Molybdenum Corporation of America, Part 2, Solvent extraction plant, *Deco Trefoil*, 31(5): 9–16.

Harris, I.R. and McGuiness, P.J. (1991) Hydrogen: Its use in the processing of NdFeB magnets, *J. Less Common Metals*, 172–174 (Part 3): 1273–1284.

Harris, R.I., Williams, A., Walton, A. and Speight, J. (2012) Magnet recycling, U.S. Patent 2012/0137829.

Harrison, E.E. (1952) Vapour pressure of some rare earth halides, *J. Appl. Chem.*, 2: 601–602.

Harrison, N.J., Davies, H.A. and Todd, I. (2006) $Nd_2Fe_{14}B$-based nanocomposite magnets with transition metal and carbon additions, *J. Appl. Phys.*, 99: 08B504.

Hart, K.P. and Levins, D.M. (1988) Management of wastes from the processing of rare earth minerals, *Chemeca 88: Australia's Bicentennial International Conference for the Process Industries;* Preprints of Papers. Institution of Engineers, Barton, ACT, Australia, pp. 82–88.

Hartley, F.R. (1952) The preparation of anhydrous lanthanum chlorides by high temperature chlorination of monazite, *J. Appl. Chem.*, 2: 24–31.

Hasegawa, K., Sano, Y., Aoshima, A. and Shiokawa, Y. (2003) Preparation of lanthanum and cerium metals by hydrometallurgy. *Journal of Alloys and Compounds*, 352(1): 246–249.

Hashimoto, T., Numasawa, T., Shino, M. and Okada, T. (1981) Magnetic refrigeration in the temperature range from 10K to room temperature: The ferromagnetic refrigerants, *Cryogenics*, 21: 647–653.

Haskin, L.A. and Korotev, R.L. (1973) Determination of rare earths in geological samples and raw materials. In Michelsen, O.B. (ed.), *Analysis and Application of Rare Earth Materials*, pp. 183–211, Universitetsforlaget, Oslo.

Haskin, L.A. and Paster, T.P. (1979) Geochemistry and mineralogy of rare earths. In Gschneidner, Jr., K.A. and Eyring, L. (eds.), *Handbook on the Physics and Chemistry of Rare Earths*, Vol. 3, pp. 1–80, North Holland, Amsterdam.

Hassan, A. (2001) Raw material savings through recycling of spent catalysts from the chemical industry, UBA texts 21/01 March, TU Berlin, Berlin.

Hassan, S.S. and Mahmoud, W.H. (1982) Spectrophotometric, potentiometric and gravimetric determination of lanthanides with peri-dihydroxynaphthindenone, *Anal. Chem.*, 54(20): 228–231.

Hatfield, W.E. and Miller, J.H. (1988) *High Temperature Superconducting Materials Preparation, Properties and Processing*, Marcel Dekker, New York.

Haughton, J.L. and Prytherch, W.E. (1937) *Magnesium and Its Alloys*, HMSO, London.

Haxel, G.B., Hedrick, J.B. and Orris, G.J. (2002) Rare earth elements—Critical resources for high technology, USGS Fact Sheet 087-02, U.S. Geological Survey, Washington, DC. Available at http://minerals.usgs.gov/minerals/pubs/commodity/rare_earths.

He, H. and Meng, J. (2011) Recycling rare earth from spent FCC catalyst using P507 (HEHEHP) as extractant, *Zhongnan Daxue Xuebao, Ziran Kexueban*, 42: 2651–2657.

Heartling, G.H. (1981) PLZT electrooptic ceramics and devices. In Gschneidner, Jr., K.A. (ed.), *Industrial Applications of Rare Earth Elements*, pp. 3–18, 265–283, ACS Symposium Series 164, American Chemical Society, Washington, DC.

Heartling, G.H. and Land, C.E. (1971) Hot pressed (Pb,La)(Zr,Ti)O_3 ferroelectric ceramics for optoelectronic applications, *J. Am. Ceram. Soc.*, 54: 1–11.

Hecht, H., Jander, G. and Schlapmann, H. (1947) The influence of thionyl chloride on oxides, *Z. Anorg. Chem.*, 254: 259–264.

Hedrick, J.B. (1985a) Rare earth minerals and metals. In *Minerals Yearbook*, Vol. 1, pp. 791–803, U.S. Department of the Interior, Washington, DC.

Hedrick, J.B. (1985b) Rare earth elements and yttrium. In *Minerals Facts and Problems, Bureau of Mines Bull. 675*, pp. 647–664, U.S. Department of the Interior, Washington, DC.

Hedrick, J.B. (1986) Rare earth minerals and metals. In *Minerals Yearbook*, Vol. 1, pp. 771–782, U.S. Department of the Interior, Washington, DC.

Hedrick, J.B. (1988) Availability of rare earths, *Ceram. Bull.*, 67(5): 858–861.

Hedrick, J.B. (1991) Rare earths: The lanthanides, yttrium and scandium. In *Minerals Yearbook 1991*, Vol. 1, pp. 1211–1237, Bureau of Mines, U.S. Department of the Interior, Washington, DC.

Hedrick, J.B. (1992) Rare earths: The lanthanides, yttrium and scandium. In *Minerals Yearbook 1992*, pp. 1035–1061, Bureau of Mines, U.S. Department of the Interior, Washington, DC.

Hedrick, J.B. (1995) *Rare Earths. Minerals Yearbook 1995*, Vol. 1, pp. 1–11, Bureau of Mines, U.S. Department of the Interior, Washington, DC.

Hedrick, J.B. (1997) Rare earth metal prices in the U.S. ca. 1960 to 1994, *J. Alloys Compd.*, 250: 471–481.

Hedrick, J.B. (1998) *Rare Earths. Minerals Yearbook 1998*, Vol. 1, pp. 61.1–61.14, U.S. Geological Survey, U.S. Department of the Interior, Washington, DC.

Hedrick, J.B. (2000) *Rare Earths. U.S. Geological Survey Minerals Yearbook 2000*, Vol. 1, pp. 62.1–62.17, U.S. Department of the Interior, Washington, DC.

Hedrick, J.B. (2001) *Rare Earths. U.S. Geological Survey Minerals Yearbook 2001*, Vol. 1, pp. 61.1–61.17, U.S. Department of the Interior, Washington, DC.

Hedrick, J.B. (2002) *Rare Earths. U.S. Geological Survey Minerals Yearbook 2002*, Vol. 1, pp. 61.1–61.16, U.S. Department of the Interior, Washington, DC.

Hedrick, J.B. (2003) *Rare Earths. U.S. Geological Survey Minerals Yearbook 2003*, pp. 60.1–60.15, U.S. Department of the Interior, Washington, DC.

Hedrick, J.B. (2004) *Rare Earths. U.S. Geological Survey Minerals Yearbook 2004*, pp. 60.1–60.15, U.S. Department of the Interior, Washington, DC.

Hedrick, J.B. (2005) *Rare Earths. U.S. Geological Survey Minerals Yearbook 2005*, pp. 60.1–60.14, U.S. Department of the Interior, Washington, DC.

Hedrick, J.B. (2006) *Rare Earths. U.S. Geological Survey Minerals Yearbook 2006*, pp. 60.1–60.14, U.S. Department of the Interior, Washington, DC.

Hedrick, J.B. (2007) *Rare Earths. U.S. Geological Survey Minerals Yearbook 2007*, pp. 60.1–60.18, U.S. Department of the Interior, Washington, DC.

Hedrick, J.B. (2009) *Rare Earths, Mineral Commodity Summaries*, U.S. Geological Survey, Reston, VA.

Hedrick, J.B. (2010) *Rare Earths, Mineral Commodity Summaries*, U.S. Geological Survey, Reston, VA.

Hedrick, J.B., Sinha, S.P. and Kosynkin, V.D. (1997) Loparite, a rare-earth ore (Ce,Na,Sr,Ca)(Ti,Nb,Ta,Fe^{+3})O_3, *J. Alloys Compd.*, 250(1–2): 467–470.

Heegn, H. (2009) Recycling moderner Batterien, Teil 1: Aufbereitung von Nickel-Metallhydrid-Batterien, *Aufbereitungstechnik*, 50(6): 48–61.

Heegn, H. and Rutz, M. (2009) Technical Solutions-Gut getrennt/Well separated-Recycling moderner Batterien, Teil 1: Aufbereitung von Nickel-Metallhydrid-Batterien [Well separated/well separated recycling modern batteries, Part 1: Preparation of nickel-metal hydride batteries.] *Aufbereitungs-Technik (Mineral Processing Technology)*, 50(6): 48.

Hellstrom, E.E., Ray, R.D. and Zhang, C. (1989) Preparation of gadolinium gallium garnet by solid-state reaction of the oxides, *J. Am. Ceram. Soc.*, 72: 1376–1389.

Henderson, A.W., May, S.C. and Higbie, K.B. (1958) Chlorination of euxenite concentrates, *Ind. Eng. Chem.*, 50: 611–612.

Henrie, T.A. (1964) Electrowinning of rare earth and uranium metals from their oxides, *J. Metals*, 16: 978–981.

Henrie, T.A. and Morrice, E. (1966) A high temperature electrowinning cell for rare earths, *J. Metals*, 18: 1207–1208.

Henry, P., Lamotte, S. and Bier, J-M. (2013) Recycling of rare earth materials at Hydrometal (Belgium), In London, I.M., Goode, J.R., Moldoveanu, G. and Rayat, M.S. (eds.), *Rare Earth Elements*, pp. 537–542, Canadian Institute of Mining, Metallurgy and Petroleum, Quebec.

Herbst, J.F. and Croat, J.J. (1991) Neodymium–iron–boron permanent magnets, *J. Magn. Magn. Mater*, 100: 57–78.

Herget, C. (1982) Production and properties of rare earth–cobalt permanent magnet alloy powders, *Met. Powder. Rep.*, 37(1): 34–36.

Herget, C. (1985) Metallurgical ways to NdFeB alloys, permanent magnets from coreduced NdFeB. In Strnat, K.J. (ed.), *Proc. 8th International Workshop on Rare Earth Magnets and their Applications*, May 6–8, pp. 407–422, University of Dayton, Magnetics, KL-365, Dayton, OH.

Herget, C. and Domazer, H.G. (1975) Methods for the production of rare earth–3d metal alloys with particular emphasis on the cobalt alloys, *Goldschmidt Informiert*, 4/75(35): 13–22.

Hicks, J.F.G. (1918) The preparation and properties of yttrium mixed metal, *J. Am. Chem. Soc.*, 40: 1619–1626.

Higashiyama, Y. and Asano, K. (2007) Recent progress in electrostatic separation technology, *Particul. Sci. Technol.*, 16(1): 77–90.

Highley, D.E., Slater, D. and Chapman, G.R. (1988) Geological occurrence of elements consumed in the electronics industry, *Trans. Instn. Min. Metall.*, 97(Section C): C34–C41.

Higuchi, H., Tomura, K. and Hamaguchi, H. (1970) Determination of rare-earth elements in rock samples by neutron activation analysis. *Journal of Radioanalytical Chemistry*, 5(2): 207–222.

Hill, W.H. (1951) Rare Earth Inc. redredges Idaho gold placer for monazite, *Min. World*, 13(2): 12–14.

Hillebrand, W.F. and Norton, T.H. (1875) Electrolytic deposition of cerium, lanthanum and didymium, *Ann. Phys. U. Chem.*, 155: 633–639.

Hirajima, T., Sasaki, K., Bissombolo, A., Hirai, H., Hamada, M. and Tsunekawa, M. (2005a) Feasibility of an efficient recovery of rare earth-activated phosphors from waste fluorescent lamps through dense-medium centrifugation, *Sep. Purif. Technol.*, 44(3): 197–204.

Hirajima, T., Bissombolo, A., Sasaki, K., Nakayama, K., Hirai, H. and Tsunekawa, M. (2005b) Floatability of rare earth phosphors from waste fluorescent lamps, *Int. J. Miner. Process.*, 77(4): 187–198.

Hirosawa, S. (1989) On the dependence of intrinsic coercivity on grain size in the nucleation-controlled rare earth–iron–born sintered magnets, *IEEE Trans. Magn.*, MAG-25: 3437.

Hirosawa, S. and Kaneko, Y. (1998) Rare earth magnets with high energy products. In Schulz, L. and Mueller, K.D. (eds.), *Proceedings of the 15th International Workshop on Rare-Earth Magnets and Their Applications*, Vol. 1, pp. 43–54, Werkstoff–Informationsgesellschaft, Dresden.

Hirota, K., Okabe, T.H., Saito, F., Waseda, Y. and Jacob, K.T. (1999) Electrochemical deoxidation of RE–O (RE = Gd, Tb, Dy, Er) solid solutions, *J. Alloys Compd.*, 282(1–2): 101–108.

Hirsch, A. (1911) The preparation and properties of metallic cerium, *Ind. Eng. Chem.*, 3: 880–896.

Hirsch, A. (1912) The preparation of metallic cerium, *J. Electrochem. Soc.*, 20: 57–102.

Hirschhorn, I.S. (1967) Commercial production of rare earth metals by fused salt electrolysis. In Koehler, W.C. (ed.), *Proc. 6th Rare Earth Research Conf., Gatlinberg, TN*, May 3–5, 1965, pp. 728–738, Available on Report AFOSR-67-1214, National Technical Information Service, Springfield, VA.

Hirschhorn, I.S. (1968) Commercial production of rare earth metals by fused salt electrolysis, *J. Metals*, 20(3): 19–22.

Hirschhorn, I.S. and Klein, E.A. (1969) Rare earth metal and silicon alloys, German Patent 1,800,701 (April 30).

Hoatson, D.M., Jaireth, S. and Miezitis, Y. (2011) The Major Rare-Earth-Element Deposits of Australia: Geological Setting, Exploration, and Resources, Geoscience Australia, Canberra.

Holocombe, C.E. and Kovach, L. (1982) Stable materials for fluorine rich environments, *Ind. Eng. Chem. Prod. Res. Dev.*, 21(4): 673–677.

Honshima, M. and Ohashi, K. (1994) High energy NdFeB magnets and their applications, *J. Mater. Eng. Perform.*, 3(2): 218–222.

Holt, B.D. and Goodspeed, H.T. (1963) Determination of Nitrogen, Oxygen, and Hydrogen in Metals by Inert Gas Fusion. A Manometric Method. *Analytical Chemistry*, 35(10): 1510–1513.

Hopkins, B.S. and Audrieth, L.F. (1934) The electrolysis of rare earth metal salts in nonaqueous solvents, *J. Electrochem. Soc.*, 66: 135–142.

Hopkins, B.S. and Quill, L.L. (1933) Use of non-aqueous solvents in the study of the rare earth group, *Proc. Natl. Acad. Sci. U.S.A.*, 19: 64–68.

Horikawa, T. and Machida, K. (2011) Reuse and recycle processing for rare earth phosphors, *Mater. Integr.*, 24: 37–43.

Horikawa, T., Miura, K., Itoh, M. and Machida, M. (2006) Effective recycling of Nd–Fe–B sintered magnet scraps, *J. Alloys Compd.*, 408–412: 1386–1390.

Horiuchi, H., Koike, U., Kaneko, H., Kurino, T. and Uchida, H. (1995) Effects of N, C and B additions on the Sm_2Fe_{17} crystal structure and magnetic properties, *J. Alloys Compd.*, 222(1–2): 131–135.

Horrigan, R.V. (1981) Rare earth polishing compounds. In Gschneidner, Jr., K.A. (ed.), *Industrial Applications of Rare Earth Elements*, pp. 95–100, ACS Symposium Series 164, American Chemical Society, Washington, DC.

Horwitz, E.P., McAlister, D.R., Bond, A.H. and Barrans, R.E. (2005) Novel extraction of chromatographic resins based on tetraalkyldiglycolamides: Characterization and potential applications, *Solvent Extr. Ion Exc.*, 23(3): 319–344.

Houot, R. (1982) Beneficiation of phosphatic ores through flotation, *Int. J. Miner. Process.*, 9(4): 353–384.

Houot, R., Cuif, J.P., Mottot, Y. and Samama, J.C. (1991) Recovery of rare earth minerals with emphasis on flotation process. In Siribumrungsukha, B., Arrykul, S., Sanguan Sai, P., Pungrassami, T., Sikong, L. and Kooptarnon, K. (eds.), *Proc. Int. Conf. Rare Earth Minerals and Minerals for Electronic Uses, Hat Yai, Thailand*, January, pp. 301–324, Prince of Songkla University, Thailand.

Hu, Z., Qu, H., Zhao, J., Luo, C., Li, J. and Liu, Y. (2012) Enhanced mechanical properties in die-upset Nd–Fe–B magnets via die-upsetting process, *J. Rare Earth*, 30(11): 1112–1115.

Huang, X., Long, Z., Li, H., Ying, W., Zhang, G. and Xue, X. (2005) Development of rare earth hydrometallurgy technology in China, *J. Rare Earths*, 23(1): 1–5.

Huang, L.J., Liang, G.Y. and Sun, Z.B. (2006) Hydrogen-storage properties of amorphous Mg–Ni–Nd alloys, *J. Alloys and Compounds*, 421(1–2): 279–282.

Huang, X.W., Li, H.W., Long, Z.Q., Peng, X.L., Li, J.N., Zhang, Y.Q., Cui, D.L. and Yang, G.L. (2008) Research and development on green rare earth metallurgy, *Sichuan Rare Earth*, 4: 15–19.

Huang, J., Zhou, L., Liang, Z., Gong, F., Han, J. and Wang, R. (2010) Promising red phosphors $LaNbO_4$: Eu^{3+}, Bi^{3+} for LED solid-state lighting application, *J. Rare Earths*, 28(3): 356–360.

Huang, Y.L., Liu, Z.W., Zhong, X.C., Yu, H.Y., Gao, X.X., Zhu, J. and Zeng, D.C. (2012) Diffusion of Nd-rich phase in the spark plasma sintered and hot deformed nanocrystalline NdFeB magnets, *J. Appl. Phys.*, 111: 033913.

Huang, Y., Jiang, D., Zhang, J., Lin, Q. and Huang, Z. (2013) Sintering of transparent Nd:YAG ceramics in oxygen atmosphere, *J. Rare Earths*, 31(2): 153–157.

Huffine, C.L. and Williams, J.M. (1961) Refining and purification of rare earth metals. In Spedding, F.H. and Daane, A.H. (eds.), *The Rare Earths*, pp. 145–162, Wiley, New York.

Hukin, D.A. and Jones, D.W. (1976) Rare earths—A growth industry. In Lundin, C.E. (ed.), *Proc. 12th Rare Earth Research Conference, Vail, CO*, July 18–22, pp. 891–904, University of Denver, Denver Research Institute, Denver, CO.

Hultgren, R., Desai, P.D., Hawkins, D.I., Gleiser, M. and Kelley, K.K. (1973) *Selected Values of the Thermodynamic Properties of Binary Alloys*, American Society for Metals, Metals Park, OH.

Hurst, C. (2010) China's Rare Earth Elements Industry: What Can the West Learn? *Institute for the Analysis of Global Security (IAGS)*, p. 18, U.S. Army's Foreign Military Studies Office, Fort Leavenworth, Kansas.

Hussin, K., Aziz, A., Ibrahim, M. and Sulaiman, M.Y. (1991) The content of rare earth elements in amang from selected mines in Malaysia. In Siribumrungsukha, B., Arrykul, S., Sanguan Sai, P., Pungrassami, T., Sikong, L. and Kooptarnon, K. (eds.), *Proc. Int. Conf. Rare Earth Minerals and Minerals for Electronic Uses, Hat Yai, Thailand*, January, pp. 81–89, Prince of Songkla University, Thailand.

Huston, E.L. and Sheridan, J.J. (1981) Applications for rechargeable metal hydrides. In Gschneidner, Jr., K.A. (ed.), *Industrial Applications of Rare Earth Elements*, pp. 223–250, ACS Symposium Series 164, American Chemical Society, Washington, DC.

Ikesue, A. and Aung, Y.L. (2006) Synthesis and performance of advanced ceramic lasers. In *9th International Ceramic Processing Science Symposium, Coral Spring, FL*, January 8–11, p. 1936, Coral Spring, FL.

Ikesue, A., Furusato, I. and Kamata, K. (1995) Fabrication of polycrystalline, transparent YAG ceramics by a solid-state reaction method, *J. Am. Ceram. Soc.*, 78(1): 225–228.

Ilyin, A.V. (1998) Phosphorites of the Russian Craton, *Earth-Sci. Rev.*, 45(1–2): 89–101.

Ingraham, M.G. and Drowart, J. (1960) Mass spectrometry applied to high temperature chemistry. In *Proc. Symp. on High Temperature Technology*, pp. 219–240, McGraw Hill, New York.

Ishigaki, N., Suzuki, S. and Machida, K. (2005) Surface improvements on magnetic properties for small-sized Nd–Fe–B sintered magnets, *Neomax Tech. Rep.*, 15: 15–19.

Ishii, R., Miyoshi, T., Kanekiyo, H. and Hirosawa, S. (2007) High-coercivity nanocomposite permanent magnet based on Nd–Fe–B–Ti–C with Cr addition for high-temperature applications, *J. Magn. Magn. Mater.*, 312(2): 410–413.

Ishikawa, H., Utsunomiya, T., Hatano, T., Hoshino, Y. and Sato, M. (1974) Preparation of samarium metal by molten salt electrolysis with a fused zinc cathode, *Bull. Tokyo Inst. Technol.*, 20: 103–118.

Ishikawa, H., Oguro, K., Kato, A., Suzuki, H. and Ishii, E. (1985) Microcapsulated rare earth–nickel hydride forming materials. In Xu, G. and Xiao, J. (eds.), *New Frontiers in Rare Earth Science and Application*, Vol. II, pp. 1058–1061, Science Press, Beijing.

Itakura, T., Sasai, R. and Itoh, H. (2006) Resource recovery from Nd–Fe–B sintered magnet by hydrothermal treatment. *J. Alloys and Compounds*, 408: 1382–1385.

Ito, T. (1991) The MMAJ rare earth R&D project. In Siribumrungsukha, B., Arrykul, S., Sanguan Sai, P., Pungrassami, T., Sikong, L. and Kooptarnon, K. (eds.), *Proc. Int. Conf. Rare Earth Minerals and Minerals for Electronic Uses, Hat Yai, Thailand*, pp. 325–336, Prince of Songkla University, Thailand.

Ito, S., Yotsumoto, H. and Sakamoto, H. (1991) Magnetic separation of monazite and xenotime. In *Proceedings of the International Conference on Rare Earth Minerals and Minerals for Electronic Uses, Hat Yai, Thailand*, pp. 279–299, Prince Songkla University, Thailand.

Ito, M., Kashiwaya, K., Sumiya, N., Hiroyoshi, N. and Tsunekawa, M. (2009) Anode activating agent recovery by magnetic separation from the < 0.075 mm fraction of crushed nickel metal hydride batteries from hybrid vehicles, *Sep. Purif. Technol.*, 69(2): 149–152.

Ito, M., Kashiwaya, K., Sumiya, N., Furuya, H., Hiroyoshi, N. and Tsunekawa, M. (2010) Estimating the size distribution of anode and cathode activating agents in the crushed products of nickel metal hydride batteries from hybrid vehicles and its classification, *Int. J. Miner. Process.*, 97(1–4): 92–95.

Itoh, H., Sasai, R. and Itakura, T. (2010) Consolidation recovery of rare/hazardous elements from polluted water by the hydrothermal mineralization process. In Popov, V., Itoh, H., Mander, U. and Brebbia, C.A. (eds.), *Waste Management and the Environment V*, pp. 369–378, WIT Press, Southampton.

Itoh, M. and Machida, K. (2011) *Mater. Integr.*, 24(2): 32.

Itoh, M., Masuda, M., Suzuki, S. and Machida, K.I. (2004a) Recycle for sludge scrap of Nd–Fe–B sintered magnet as isotropic bonded magnet, *J. Rare Earths*, 22: 168–171.

Itoh, M., Masuda, M., Suzuki, S. and Machida, K.I. (2004b) Recycling of rare earth sintered magnets as isotropic bonded magnets by melt-spinning, *J. Alloys Compd.*, 374: 393–396.

Itoh, M., Miura, K. and Machida, K.I. (2007) A novel process of resource recovery from rare earth magnet scrap using carbonylation reaction and recycle as electromagnetic wave absorber, *J. Ceramic Soc. Jpn.*, 115(1346): 628–632.

Itoh, M., Miura, K. and Machida, K.I. (2008) Extraction of rare-earth elements from Nd–Fe–B magnet scraps by NH_4Cl, *Chem. Lett.*, 37: 372–373.

Itoh, M., Miura, K. and Machida, K. (2009) Novel rare earth recovery process on Nd–Fe–B magnet scrap by selective chlorination using NH_4Cl, *J. Alloys Compd.*, 477: 484–487.

Ivanovskii, L.E. and Ilyushchenko, E.G. (1961) Separation of rare earth metals by electrolysis of fused salt, *Trudy Inst. Elektrokhim. Uralskogo Filiala Akad. Nauk SSSR*, 2: 131–134.

Iya, V.K. (1953) Preparation of pure scandium, *C. R. Acad. Sci.*, 236: 608–610.

Jackson, W.D. and Christiansen, G. (1993) International strategic minerals inventory summary report—Rare earth oxides, U.S. Geological Survey Circular 930-N, U.S. Geological Survey, Map Distribution, Denver, CO.

Jacobs, J., Korotev, R., Blanchard, D. and Haskin, L. (1977) A well-tested procedure for instrumental neutron activation analysis of silicate rocks and minerals. *Journal of Radioanalytical and Nuclear Chemistry*, 40(1–2): 93–114.

Jantsch, G., Jawurek, H., Skalla, N. and Ganalouski, H. (1930) Halides of the rare earths VI. Halides of the terbium and erbium earth groups, *Z. Anorg. Allgem. Chem.*, 193: 391–405.

Jantsch, G., Skalla, N. and Jawurek, H. (1931) Halides of the rare earths V. The halides of ytterbium, *Z. Anorg. Allgem. Chem.*, 201: 207.

Jarosiński, A., Kowalczyk, J. and Mazanek, C. (1993) Development of the Polish wasteless technology of apatite phosphogypsum utilization with recovery of rare earths. *Journal of Alloys and Compounds*, 200(1): 147–150.

Jarvis, K.E. (1988) Inductively coupled plasma mass-spectrometry—A new technique for the rapid or ultra-trace level determination of the rare-earth elements in geological materials, *Chem. Geol.*, 68(1–2): 31–39.

Jia, Q., Tong, S., Li, Z., Zhou, W., Li, H. and Meng, S. (2009) Solvent extraction of rare earth elements with mixtures of sec-octylphenoxy acetic acid and bis(2,4,4-trimethylpentyl) dithiophosphinic acid, *Sep. Purif. Technol.*, 64: 345–350.

Jiang, J.Z., Ozaki, T., Machida, K. and Adachi, G. (1997) Separation and recovery of rare earths via a dry chemical vapour transport based on halide gaseous complexes, *J. Alloys Compd.*, 260: 222–235.

Jiang, J.H., Zeng, Z.P., Wu, J.S. and Tokunaga, M.J. (2000) Influence of alloying elements on mechanical properties and microstructures of sintered Nd–Fe–Co–B magnet, *J. Magn. Magn. Mater*, 214: 61–68.

Jiang, Y.R., Shibayama, A., Liu, K. and Fujita, T. (2004) Recovery of rare earths from the spent optical glass by hydrometallurgical process, *Can. Metall. Q.*, 43: 431–438.

Jiang, Y.R., Shibayama, A., Liu, K.J. and Fujita, T. (2005) A hydrometallurgical process for extraction of lanthanum, yttrium and gadolinium from spent optical glass, *Hydrometallurgy*, 76: 1–9.

Jiles, D.C. (1994) The development of highly magnetostrictive rare earth iron alloys, *J. Phys. D., Appl. Phys.*, 27: 1–11.

Jin, S., Tiefel, T.H., Sherwood, R.C., Davies, M.E., van Dover, R.B., Kammlott, G.W. and Fastnacht, R.A. (1988) High critical currents in Y–Ba–Cu–O superconductors, *Appl. Phys. Lett.*, 52: 2074–2076.

Jin, S., Sherwood, R.C., Gyorgy, E.M., Tiefel, T.H., van Dover, R.B., Nakahara, S., Schneemeyer, L.F., Fastnacht, R.A. and Davies, M.E. (1989) Large magnetic hysteresis in a melt textured Y–Ba–Cu–O superconductor, *Appl. Phys. Lett.*, 54: 584–586.

JOGMEC (2008) *Material Flow of Mineral Resources 2007*, 2008, pp. 227–234.

JOGMEC (2011) *Material Flow of Mineral Resources 2010*, pp. 383–403, Japan Oil Gas and Metals National Corporation, Tokyo.

Johnson, G.W. and Sisneros, T.E. (1982) Analysis of rare earth elements in ore concentrate samples using direct current plasma spectrometry. In McCarthy, G.J., Silber, H.B. and Rhyne, J.J. (eds.), *The Rare Earths in Modern Science and Technology*, Vol. 3, pp. 525–529, Plenum, New York.

Jones, F.G., Thoe, J.H., Lehman, H.E. and Downs, R.B. (1976) Production of RCo_5 and R_2Co_7 powders by the R/D process. In Lundin, C.E. (ed.), *Proc. 12th Rare Earth Research Conference, Vail, CO*, July 18–22, pp. 1054–1062, University of Denver, Denver Research Institute, Denver, CO.

Jones, F.G., Doser, M. and Nezu, T. (1977) Hydrogen atmosphere sintering of cobalt–samarium magnets, *IEEE Trans. Magn.*, 13: 1320–1322.

Jones, D.W., Fort, D. and Hukin, D.A. (1978) Zone refining of rare earth metals. In McCarthy, G.J. and Rhyne, J.J. (eds.), *The Rare Earths in Modern Science and Technology*, Vol. 1, pp. 309–314, Plenum Press, New York.

Jones, D.W., Abell, J.S., Fort, D. and Hulbert, J.K. (1982) Preparation of rare earth materials, crystals and specimens, *J. Magn. Magn. Mater.*, 29: 20–30.

Jonsson, A., Harris, D.R., Chang, R.Y. and Thomsen, O.J. (1992) Analysis of critical experiments with erbia–urania fuel, *Trans. Am. Nucl. Soc.*, 65: 415–417.

JORC (2012) *Australasian Code for Reporting of Exploration Results, Mineral Resources and Ore Reserves*, The JORC Code 2012 edn., The Australisian Institute of Mining and Metallurgy (Aus IMM), Available at http://www.jorc.org/docs/JORC_code_2012.pdf.

Jordan, R.G., Jones, D.W. and Hems, V.J. (1975) The purification of rare earth metals II. Solid state electrotransport purification of terbium, *J. Less Common Metals*, 42: 101–110.

Jordens, A., Cheng, Y.P. and Waters, K.E. (2013) A review of the beneficiation of rare earth element bearing minerals, *Miner. Eng.*, 41: 97–114.

Jordens, A., Sheridan, R.S., Rowson, N.A. and Waters, K.E. (2014) Processing a rare earth mineral deposit using gravity and magnetic separation, *Miner. Eng.*, 62: 9–18.

Jorjani, E., Bagherieh, A.H. and Rezai, B. (2007) Determination of rare earth elements in products of Chadormalu iron ore concentrator plant (Iran) from beneficiation point of view, *Iran J. Chem. Chem. Eng. (Int. Engl. Ed.)*, 26(4): 11–18.

Jost, W. (1952) *Diffusion in Solids, Liquids and Gases*, Academic Press, New York.

Joworowski, R.J., Weberling, R.P. and Bracco, D.J. (1967) Atomic absorption studies on rare earth and refractory metals, *Anal. Chim. Acta*, 37: 284–294.

Jukkola, E.E., Audrieth, L.F. and Hopkins, B.S. (1934) Observations on the rare earths XLI. Electrolytic preparation of rare earth amalgams. 3. Amalgam of lanthanum, neodymium, cerium, samarium, and yttrium. Metallic lanthanum, neodymium and cerium by thermal decomposition of their amalgams, *J. Am. Chem. Soc.*, 56: 303–304.

Jun, R., Wenmei, W., Jiake, L., Gaoyun, Z. and Fangqiong, T. (2003) Progress of flotation reagents of rare earth minerals in China. *Journal of Rare Earths* 21 (1): 1–8.

Jun, T., Jingquin, Y., Ruan, C., Guohua, R., Mintao, J. and Kexian, O. (2010) Kinetics of leaching rare earth from weathered crust elution deposited rare earth ores with ammonium sulphate solution, *Hydrometallurgy*, 101: 166–170.

Jun, T., Jingqun, Y., Kaihong, G., Guohua, R., Mintao, J. and Ruan, C. (2011) Extraction of rare earths from leach liquor of the weathered crust elution-deposited rare earth ore with non precipitation, *Int. J. Miner. Process.*, 98: 125–131.

Jun, T., Xuekun, T., Jingqun, Y., Xianping, L., Guohua, R. and Mintao, J. (2013) Process optimization on leaching of a lean weathered crust elution deposited rare earth ores, *Int. J. Miner. Process.*, 119: 83–88.

Justel, T., Nikol, H. and Ronda, C. (1998) New developments in the field of luminescent materials for lighting and displays, *Angew. Chem. Int. Ed.*, 37: 3085–3103.

Kaczmarek, J. (1981) Discovery and commercial separations. In Gschneidner, Jr., K.A. (ed.), *Industrial Applications of Rare Earth Elements*, ACS Symp. Ser. 164, American Chemical Soc., Washington, DC, 135–166.

Kallenbach, R. and Bungardt, W. (1969) Low phosphorus alloys of silicon with rare earth metals, German Patent 1,274,801 (March 13).

Kamihira, K., Hasegawa, R. and Ogawa, O. (1993) Solid state deoxidation of some rare earth metals and reduction of their interstitial impurity concentrations by electron beam melting. *Materials Transactions, JIM*, 34(3): 243–247.

Kanamori, T., Matsuda, M. and Miyake, M. (2009) Recovery of rare metal compounds from nickel–metal hydride battery waste and their application to CH_4 dry reforming catalyst, *J. Hazard. Mater.*, 169: 240–245.

Kanazawa, Y. and Miyawaki, R. (1991) Rare earth minerals and their crystal structures. In Siribumrungsukha, B., Arrykul, S., Sanguan Sai, P., Pungrassami, T., Sikong, L. and Kooptarnon, K. (eds.), *Proc. Int. Conf. Rare Earth Minerals and Minerals for Electronic Uses, Hat Yai, Thailand*, January, pp. 43–79, Prince of Songkla University, Thailand.

Kanazawa, Y. and Kamitani, M. (2006) Rare earth minerals and resources in the world, *J. Alloys Compd.*, 408–412: 1339–1343.

Kandil, A.T., Aly, M.M., Moussa, E.M., Kamel, A.M., Gouda, M.M. and Kouraim, M.N. (2010) Column leaching of lanthanides from Abu Tartur phosphate ore with kinetic study, *J. Rare Earths*, 28(4): 576–580.

Kanekiyo, H., Uehara, M. and Hirosawa, S. (1994) Magnetic properties and microstructure of V-and-M-added, Fe_3B-based, Nd–Fe–B nanocrystalline permanent magnets (M = Al, Si), *Mater. Sci. Eng. A.*, 181–182: 868–870.

Kaneko, Y. and Ishigaki, N. (1994) Recent developments of high performance NEOMAX magnets, *J. Mater. Eng. Perform.*, 3: 228–233.
Kaneko, Y., Kuniyoshi, F. and Ishigaki, N. (2006) Proven technologies on high-performance Nd–Fe–B sintered magnets, *J. Alloys Compd.*, 408–412: 1344–1349.
Kantipuly, C.J. and Westland, A.D. (1988) Review of methods for the determination of lanthanides in geological samples, *Talanta*, 35(1): 1–13.
Karl, A. (1934) Chemical preparation of cerium and its alloys, *Bull. Soc. Chim.*, 1: 871–877.
Kaschuk, V.A. and Svetlov, M.B. (1982) Investigation of some properties of VT5L alloy with rare earth additions. In Williams, J.C. and Belov, A.F. (eds.), *Titanium and Titanium Alloys—Scientific and Technological Aspects*, Vol. III, pp. 2201–2208, Plenum Press, New York.
Kasey, J.B. (1956) Method of treating rare earth ores, U.S. Patent 2735747, pp. 1–5.
Kasey, J.B. (1959) Process for recovering rare earth oxides, British Patent 825,305.
Kasprzak, W. (2007) Production of synthetic rare earth concentrate from fluorescent waste, Dissertation at the Technical University of Clausthal, Clausthal Zellerfeld, Germany.
Kato, K., Yoshioka, T. and Okuwaki, A. (2000a) Recycle of ceria-based glass polishing powder using NaOH solution, *Nippon Kagaku Kaishi*, 10: 725–731.
Kato, K., Yoshioka, T. and Okuwaki, A. (2000b) Study for recycling of ceria-based glass polishing powder, *Ind. Eng. Chem. Res.*, 39: 943–947.
Kato, Y., Fujinaga, K., Nakamura, K., Takaya, Y., Kitamura, K.,Ohta, J., Toda, R., Nakashima, T. and Iwamori, H. (2011) Deep-sea mud in the Pacific Ocean as a potential resource for rare-earth elements, *Nat. Geosci.*, 4(8): 535–539.
Kawabata, K., Kishi, Y., Kawaguchi, O., Watanabe, Y. and Inoue, Y. (1991) Determination of rare-earth elements by inductively coupled plasma mass spectrometry with ion chromatography, *Anal. Chem.*, 63: 2137–2140.
Kelly, E.G. and Spottiswood, D.J. (1989a) The theory of electrostatic separations: A review—Part I. Fundamentals, *Miner. Eng.*, 2(1): 33–46.
Kelly, E.G. and Spottiswood, D.J. (1989b) The theory of electrostatic separations: A review—Part II. Particle charging, *Miner. Eng.*, 2(2): 193–205.
Kelly, E.G. and Spottiswood, D.J. (1989c) The theory of electrostatic separations: A review—Part III. The separation of particles, *Miner. Eng.*, 2(3): 337–349.
Kennard, F.L. (1981) Oxygen sensors. In Gschneidner, Jr., K.A. (ed.), *Industrial Applications of Rare Earth Elements*, pp. 251–263, ACS Symposium Series 164, American Chemical Society, Washington, DC.
Kent, A.J., Jacobsen, B., Peate, D.W., Waight, T.E. and Baker, J.A. (2004) Isotope dilution MC-ICP-MS rare earth element analysis of geochemical reference materials NIST SRM 610, NIST SRM 612, NIST SRM 614, BHVO-2G, BHVO-2, BCR-2G, JB-2, WS-E, W-2, AGV-1 and AGV-2, *Geostandards Geoanalytic. Res.*, 28(3): 417–429.
Ketelle, B.H. and Boyd, G.E. (1947) The exchange absorption of ions from aqueous solutions by organic zeolites IV. The separation of yttrium group rare earths, *J. Am Chem. Soc.*, 69: 2800–2812.
Kilbourn, B.T. (1988) Metallurgical applications of yttrium and the lanthanides, *J. Metals*, 40(5): 22–25.
Kilbourn, B.T. (1990) Rare earths: Lanthanides and yttrium, *Am. Ceram. Soc. Bull.*, 69: 874–877.
Kim, W.-T., Kim, B., Choi, D., Oki, T. and Kim, S. (2010) Selective recovery of catalyst layer from supporting matrix of ceramic-honeycomb-type automobile catalyst, *J. Hazard. Mater.*, 183: 29–34.
Kim, J.Y., Kim, U.S., Byeon, M.S., Kang, W.K., Hwang, K.T. and Cho, W.S. (2011) Recovery of cerium from glass polishing slurry, *J. Rare Earths*, 29: 1075–1078.
King, A. (2012) *Rare Earth Magnet R&D*, The Ames Laboratory, USDOE Iowa State University of Science and Technology, National Technical Information Service, Alexandria, VA.

Kingsnorth, D.J. (2010) Rare earths: Facing new challenges in the new decade. In *SME Annual Meeting*, February 28–March 3, Phoenix, AZ.

Kirchmayr, H.R. (1985) Magnetic properties of rare earth intermetallics. In Xu, G. and Xiao, J. (eds.), *New Frontiers in Rare Earth Science and Applications*, pp. 879–886, Science Press, Beijing.

Kirchmayr, H.R. and Poldy, C.A. (1979) Magnetic properties of intermetallic compounds of rare earth metals. In Gschneidner, Jr., K.A. and Eyring, L. (eds.), *Handbook on the Physics and Chemistry of Rare Earths*, Vol. 2, pp. 55–230, North Holland, Amsterdam.

Kleber, E.V. and Love, B. (1963) *The Technology of Scandium, Yttrium and the Rare Earth Metals*, Pergamon, Oxford.

Kleirheksal, J.H. and Kremers, H.E. (1928) Observations on the rare earths XXIX: The preparation and properties of anhydrous rare earth chlorides, *J. Am. Chem. Soc.*, 50: 959–967.

Klemm, W. and Bommer, H. (1937) Contribution to the knowledge of the rare earths, *Z. Anorg. Allg. Chem.*, 231: 138–171.

Knelson, B. (1992) The Knelson concentrator. Metamorphosis from crude beginning to sophisticated world wide acceptance, *Miner. Eng.*, 5(10–12): 1091–1097.

Knudsen, I.E. and Levitz, N.M. (1959) Preparation of yttrium fluoride in fluidized beds, AEC Document ANL-6011, National Technical Information Service, Alexandria, VA.

Kobayashi, M. and Oki, T. (2009) Method and device for selectively crushing waste fluorescent lamp, Int. Patent Appl. No. PCT/JP2008/066961; Publ. No. WO/2009/038163, March 26.

Kobisk, E.H. and Adair, H.L. (1979) Conversion of isotope compounds to metals by reduction–distillation methods, Part IV General target preparation methods, *Nucl. Instrum. Methods*, 167: 153–160.

Kobisk, E.H. and Grisham, W.B. (1969) Application of reduction–Distillation method for preparing high purity rare earth isotope metals, *Mat. Res. Bull.*, 4: 651–662.

Koch, C.W. (1953) Thermodynamics of the trichlorides and oxychlorides of some of the lanthanide and actinide elements, Thesis, UCRL-2286, National Technical Information Service, Alexandria, VA.

Koch, D.F.A. (1987) Rare earth extraction and separation. In *Rare Earth Horizon 1987, Proceedings of a Conference at National Measurement Laboratory*, April, pp. 73–85, Lindfield.

Kohmoto, O., Yoneyama, T. and Yajima, K. (1987) Magnetic properties of rapidly quenched $Nd_{10}Fe_{85-x}T_xB_5$ (T = Zr, Nb) alloys, *Jap. J. Appl. Phys.*, 26(Pt. 1): 1804–1805.

Kojima, T. and Sato, M. (1954) Metallurgical research on cerium metal (part 10), Application: On the fused salt electrolysis of $CeCl_3$·2KCL–KCl eutectic mixture, *J. Electrochem. Soc. Japan*, 22: 303–306.

Kolařík, Z. and Pankova, H. (1966) Acidic organophosphorus extractants—I Extraction of lanthanides by means of dialkyl phosphoric acids—Effect of structure and size of alkyl group. *Journal of Inorganic and Nuclear Chemistry*, 28(10): 2325–2333.

Kominami, H., Tanaka, M., Hara, K., Nakanishi, Y. and Hatanaka, Y. (2006) Synthesis and luminescence properties of Mg–Ti–O:Eu red emitting phosphors, *Phys. Status Solidi C*, 8: 2758–2761.

Koon, N.C., Schindler, A.I. and Carter, F.L. (1971) Giant magnetostriction in cubic rare earth iron compounds of the type RFe_2, *Phys. Lett.*, 37A: 413–414.

Koopman, C. and Witkamp, G.J. (2000). Extraction of lanthanides from the phosphoric acid production process to gain a purified gypsum and a valuable lanthanide by-product. *Hydrometallurgy*, 58(1): 51–60.

Korpusov, G.V., Danilov, N.A., Krylov, Y.S., Korpusova, R.D., Drygin, A.I. and Shvartsman, V.Y. (1974) Investigation of rare-elements extraction with different carboxylic acids. In *Solvent Extraction Proceedings of the International Solvent Extraction Conference, ISEC 74, Lyon*, September 8–14.

Koshimura, H. (1988) Recovery of samarium from scrap of samarium–cobalt alloy by a batch countercurrent extractor. In Report of Tokyo Metropolitan Industrial Technology Center, No. 17, pp. 83–88.

Koshimura, H., Yamamoto, S. (1983) In *Proceedings of Symposium of Solvent Extraction*, December 9–10, 1983. Japanese Association of Solvent Extraction, Hamamatsu, pp. 155–162.

Koshimura, H., Yamamoto, S. (1984) In *Proceedings of Symposium of Solvent Extraction*, December 7–8, 1984. Japanese Association of Solvent Extraction, Hamamatsu, pp. 115–120.

Kosynkin, V.D., Moiseev, S.D., Peterson, C.H. and Nikepelov, B.V. (1993) Rare earth industry in the Commonwealth of Independent States, *J. Alloys Compd.*, 192: 118–120.

Koyama, K., Kitajima, A. and Tanaka, M. (2009) Selective leaching of rare-earth elements from an Nd–Fe–B magnet, *Kidorui*, 54: 36–37.

Koyama, K. and Tanaka, M., (2011a) In Machida, K. (ed.), *The Latest Technology Trend and Resource Strategy of Rare Earths*, pp. 127–131, CMC Press, Tokyo.

Koyama, K. and Tanaka, M. (2011b) In *Proceedings of MMIJ Annual Meeting 2011*, No. 2411, The Mining and Materials Processing Institute of Japan, Tokyo.

Krahulec. K. (2011) Rare Earth Element Prospects and Occurrences in Utah, Utah Geological Survey, Utah Department of Natural Resources, Utah.

Kramer, M.J., McCallum, R.W., Anderson, I.A. and Constantinides, S. (2012) Prospects for non-rare earth permanent magnets for traction motors and generators, *JOM*, 64(7): 752–763.

Krea, M. and Khalaf, H. (2000) Liquid–liquid extraction of uranium and lanthanides from phosphoric acid using a synergistic DOPPA–TOPO mixture. *Hydrometallurgy*, 58(3): 215–225.

Kremers, H.E. (1925) The preparation and some properties of metallic neodymium, *Trans. Am. Electrochem. Soc.*, 47: 365–371.

Kremers, H.E. (1953) Rare earth metals. In Kirk, R.E. and Othmer, D.F. (eds.), *Encyclopedia of Chemical Technology*, Vol. 11, pp. 503–521, Interscience, New York.

Kremers, H.E. (1954) Rare earth metals. In Hampel, C.A. (ed.), *Rare Metals Handbook*, pp. 329–346, Reinhold, New York.

Kremers, H.E. (1961) Rare earth metals. In Hampel, C.A. (ed.), *Rare Metals Handbook*, 2nd edn., pp. 393–417, Reinhold, New York.

Kremers, H.E. and Stevens, R.G. (1923) Observations on the rare earths XIV. The preparation and properties of metallic lanthanum, *J. Am. Chem. Soc.*, 45: 614–617.

Krikorian, O.H. and Curtis, P.G. (1988) Synthesis of CaS and interaction with molten metals, *High Temp. High. Proc.*, 20: 9.

Krishnamurthy, N., Kundu, T., Awasthi, A. and Garg, S.P. (2000) Derived thermodynamic properties and phase diagrams of the rare earth–tungsten systems, *Z. Metallkd.*, 91(3): 234–240.

Krismer, B. and Smetana, O. (1968) Alloys of silicon with scandium, yttrium, rare earth metals and thorium, Austrian Patent 259,881 (February 12).

Kroll, W.J. (1959) The present status of titanium extractive metallurgy, *Trans. Met. Soc. AIME*, 275: 546.

Kruesi, P.R. and Duker, G. (1965) Production of rare earth chloride from bastnasite, *J. Metals*, 17: 847–849.

Kruesi, P.R. and Schiff, N.N. (1968) Molybdenum Corporation of America's Mountain Pass Europium Process. 19 pp., In *AIME Annual Meeting*, February, New York.

Kruger, J. (1971) Extractive metallurgy. In Winkler, O. and Bakish, R. (eds.), *Vacuum Metallurgy*, pp. 145–335, Elsevier, Amsterdam.

Krumholz, P. (1957) Brazilian practice for monazite treatment. In *Proc. Symp. Rare Metals, Bombay*, December, pp. 78–82, The Indian Institute of Metals and Bhabha Atomic Research Centre.

Kryder, M.H. (1993) Magnetooptical storage media. In Cahn, R.W. and Bever, M.B. (eds.), *Encyclopedia of Materials Science and Engineering*, Suppl. Vol. 3, pp. 1773–1778, Pergamon, Oxford.

Kubo, T., Sekimoto, H., Kon, T. and Yamaguchi, K. (2011) In *Proceedings of MMIJ Fall Meeting*, September 26–29, PY-35, The Mining and Materials Processing Institute of Japan, Tokyo.

Kubota, M. (1974) Separation of rare earths by an ion-exchange method: Determination of impurities in high-purity rare earth oxides. *Journal of Radioanalytical and Nuclear Chemistry*, 23(1–2): 73–82.

Kubota, F., Shimobori, Y., Koyanagi, Y., Shimojo, K., Kamiya, N. and Goto, M. (2010) Uphill transport of rare-earth metals through a highly stable supported liquid membrane based on an ionic liquid, *Anal. Sci.*, 26(3): 289–290.

Kudo, K., Kobayashi, K. and Shigematsu, T. (1975) Substoichiometric and non-destructive determination of trace impurities in high-purity optical glasses by neutron activation analysis. *Journal of Radioanalytical and Nuclear Chemistry*, 27(2): 329–344.

Kudo, Y. (1988) Industrial applications of rare earths in Japan. In Gupta, C.K. and Krishnan, T.S. (eds.), *Rare Earths—Applications and Technology*, pp. 243–258, Trans Tech Publications, Switzerland.

Kul, M., Topkaya, Y. and Karakaya, I. (2008) Rare earth double sulfates from pre-concentrated bastnasite, *Hydrometallurgy*, 93(3–4): 129–135.

Kuniyoshi, F., Nakahara, K. and Kaneko, Y. (2004) Developing 4k0kJm^{-3} Nd–Fe–B magnets, *J. Jpn. Soc. Powder Powder Metall.*, 51: 698–702.

Kuroda, T. (1957) The preparation of lanthanum by fused salt electrolysis and its application, *Denki Shikenjo Kenkyu Hokoku*, 561: 103.

Kušnír, I. (2000) Mineral resources of Vietnam, *Acta Montanistica Slovaca Ročník* 5(2): 165–172.

Kussmann, D., Hoffmann, R.-D. and Pöttgen, R. (1998) Syntheses and crystal structures of CaCuGe, CaAuIn, and CaAuSn—Three different superstructures of the KHg_2 type, *Z. Anorg. Allg. Chem.*, 624: 1727.

Kuzmin, V.I., Lomayev, V.G. and Pashkov, G.L. (2006) Processing of the ores weathered carbonatite crusts is the future of the rare metal industry of Russia, *Non-Ferrous Metals*, 12: 62–68 (in Russian).

Kuzmin, V.I., Pashkov, G.L., Lomaev, V.G., Voskresenskaya, E.N. and Kuzmina, V.N. (2012) Combined approaches for comprehensive processing of rare earth metal ores, *Hydrometallurgy*, 129–130: 1–6.

Laferty, J.M. (1951) Boride cathodes, *J. Appl. Phys.*, 22: 299–309.

Larach, S. (1973) Cathode-ray-excited-emission spectroscopic analysis of trace rare earths. In Kevane, C.J. and Moeller, T. (eds.), *Proc. 10th Rare Earth Research Conf., Carefree, AZ*, May, Conf-730402, P2, pp. 799–812, National Technical Information Service, Springfield, VA.

Larsson, K., Aneheim, E., Ekberg, C. and Odegaard-Jensen, A. (2011a) Exotic reagents for separation of metals from nickel metal hydride batteries. In *19th International Solvent Extraction Conference (ISEC2011)*, October 3–7, pp. 201–208, Santiago, Chile.

Larsson, K., Ekberg, C. and Odegaard-Jensen, A. (2011b) Metal separation after selective dissolution of nickel metal hydride batteries. In *19th International Solvent Extraction Conference (ISEC2011)*, October 3–7, pp. 38–45, Santiago, Chile.

Larsson, K., Ekberg, C. and Odegaard-Jensen, A. (2012) Using Cyanex 923 for selective extraction in a high concentration chloride medium on nickel metal hydride battery waste, *Hydrometallurgy*, 129–130: 35–42.

Lededev, V.N. and Lokshin, E.H.P. (2000) Method of isolation of rare earth elements from Phosphogypsum, RU Patent 2158317 (in Russian).

Lededev, V.N., Masloboev, V.A., Lokshin, E.H.P., Popova, L.A. and Sergeeva, S.D. (2000) Method of extraction of rare earth element phosphates from apatite concentrate, RU Patent 2120408 (in Russian).

Lee, R.W. (1985) Hot pressed neodymium–iron–boron magnets, *Appl. Phys. Lett.*, 46: 790–791.

Lee, R.W., Brewer, E.G. and Schaffel, N.A. (1985) Processing of neodymium–iron–boron melt spun ribbons to fully dense magnets, *IEEE Trans. Magn.*, MAG-21: 1958–1963.
Lee, J., Kim, W., Jeong, J. and Yoon, I.J. (1998) Extraction of neodymium from Nd-Fe-B magnet scraps by sulfuric acid, *J. Korean Inst. Met. Mater.*, 36: 967.
Lee, M.S., Lee, J.Y., Kim, J.S. and Lee, G.S. (2005) Solvent extraction of neodymium ions from hydrochloric acid solution using PC88A and saponified PC88A, *Sep. Purif. Technol.*, 46: 72–78.
Lei, K.P.V., Cattoir, F.R. and Sullivan, T.A. (1967) Electrolytic process for producing ductile vanadium, Bureau of Mines Bulletin 6972, U.S. Dept. of the Interior, Washington, DC.
Lever, F.M. and Payne, J.B. (1968) Separation of the rare earth and production of the metals. In *Advances in Extractive Metallurgy*, pp. 789–804, The Institution of Mining and Metallurgy, London.
Levine, A.K. and Palilla, F.G. (1965) YVO_4Eu, A new red emitting phosphor for colour television, *Trans. N.Y. Acad. Sci., Ser. II*, 27: 517–529.
Li, K. and Frieser, H. (1986) Extraction of Lanthanide metals with bis(2,4,4-trimethylpentyl) phosphinic acid, *Solvent Extr. Ion Exc.*, 4: 739–755.
Li, C., Tang, Z. and Lu, Z. (1985) Rare earth ferrosilicon alloy. In Xu, G. and Xiao, J. (eds.), *New Frontiers in Rare Earth Science and Application*, Vol. II, pp. 1190–1193, Science Press, Beijing.
Li, W., Jiang, L., Wang, D., Sun, T. and Zhu, J. (1986) Rare-earth–transition-metal–boron permanent magnets with smaller temperature coefficients, *J. Less Common Metals*, 126: 95–100.
Li, L., Ma, J. and Jin, G. (1987) *Xi You Jin Shu*, 6(4): 284–289.
Li, F., Wang, J. and Zeng, X. (1988) A process for the recovery of RE minerals with a chelating collector. In Bautista, R.G. and Wong, M.M. (eds.), *Rare Earths*, pp. 71–79, The Minerals, Metals and Materials Society, Warrendale, PA.
Li, D.Q. (1995) Chemical engineering problems in hydrometallurgical industry of rare earths. *Progress in Chemistry (in Chin.)*, 7(3): 209–213.
Li, D.Q., Wang, Z.H. and Meng, S.L. (1994) Recommended separation processes for ion-adsorbed rare earth minerals. In *Hydrometallurgy '94*, pp. 627–634, Chapman Hall, London.
Li, D.Q., Li, H.F., Guo, F.Q. and Zhang, Z.F. (2006a) A new method to prepare high pure CeF3 nanoparticles, Chinese Patent CN200410010618.2.
Li, H., Guo, F., Zhang, Z., Li, D. and Wang, Z. (2006b) A new hydrometallurgical process for extracting rare earths from apatite using solvent extraction with P350, *J. Alloys Compd.*, 408–412: 995–998.
Li, J., Huang, X., Zhu, Z., Long, Z., Peng, X. and Cui, D. (2007) Extracting rare earth from D2EHPA-HEHEHP-H_2SO_4 system, *J. Chin. Rare Earth Soc.*, 25(1): 55–58.
Li, W., Wang, X., Meng, S., Li, D. and Xiong, Y. (2007a) Extraction and separation of yttrium from the rare earths with sec-octylphenoxy acetic acid in chloride media, *Hydrometallurgy*, 54: 164–169.
Li, W., Wang, X., Zhang, H., Meng, S. and Li, D. (2007b) Solvent extraction of lanthanides and yttrium from nitrate medium with CYANEX 925 in heptane, *J. Chem. Technol. Biotechnol.*, 82: 376–381.
Li, L., Xu, S., Ju, Z. and Wu, F. (2009) Recovery of Ni, Co and rare earths from spent Ni–metal hydride batteries and preparation of spherical $Ni(OH)_2$, *Hydrometallurgy*, 100: 41–46.
Liang, S., Hui, Y., Chen, F., Li, W. and Zhong, X. (1998) High performance NdFeB magnets. In Preprints of the Conference, China Magnets, held on October 18–21, 1998, Beijing.
Liang, R., Yamada, T., Kikuchi, E., Kawashima, H. and Soma, T. (2009) In *Proceedings of MMIJ Annual Meeting*, March 26–28, Vol. II, pp. 181–182, The Mining and Materials Processing Institute of Japan, Tokyo.

Lichte, F.E., Meier, A.L. and Croak, J.G. (1987) Determination of the rare-earth elements in geological materials by inductively coupled plasma mass spectrometry, *Anal. Chem.*, 59(8): 1150–1157.

Lide, D.R. (1997) Abundance of elements in the earth's crust and sea. In Lide, D.R. (ed.) *CRC Handbook of Physics and Chemistry*, 78th edn, p. 14, CRC Press, Boca Raton, FL.

Liedtke, M. and Elsner, H. (2009) Bundesanstalt für Geowissenschaften und Rohstoffe, Seltene Erden, Commodity Top News Nr. 31.

Lifton, J. (2013) Counterpoint: Supply and demand in the rare-earths market 2015–2020, Technology Materials Research, August 1, 2013. Available at http://www.techmetalsresearch.com/2013/08/counterpoint.

Lifton, J. and Hatch, G.P. (2012) Recent dynamics in the rare earth sector, Presented at the *International Symposium on Rare Earths, The Academy of Sciences Malaysia (ASM) and The National Professors Council (NPC)*, May 7–9, Kuala Lumpur. Available at http://asmic.akademisains.gov.my/download/RareEarth/symposium/Lifton.pdf.

Lin, H. (2009) The development and prospect of China's rare earth production, *J. Rare Earth*, 1: 11–17.

Lindstrom, R.E. and Winget, J.O. (1962) Hydrogen as retaining ion for rare earth separation by ion exchange, Bureau of Mines Report of Investigations 6131, U.S. Department of the Interior, Washington, DC.

Linebarger, H.F. and McCluhan, T.K. (1981) The role of rare earth elements in the production of nodular iron. In Gschneidner, Jr., K.A. (ed.), *Industrial Applications of Rare Earth Elements*, pp. 19–42, ACS Symposium Series 164, American Chemical Society, Washington, DC.

Lipiska, L., Ryba-Romanowski, W., Rzepka, A., Ganschow, S., Lisiecki, R., Diduszko, R. and Pajczkowska, A. (2009) Preparation and characterization of Nd doped gadolinium gallium garnet nanopowders and crystals, *Cryst. Res. Technol.*, 44(5): 477–483.

Little, H.F.V. (1921) In Friend, J.N. (ed.), *A Textbook of Inorganic Chemistry*, Chaps. 10–14, Charles Griffini, London.

Liu, J.F., Zhang, Y., Dimitrov, D. and Hadjipanayis, G. (1999) Microstructure and high temperature magnetic properties of Sm (Co, Cu, Fe, Zr) z (z = 6.7–9.1) permanent magnets, *J. Appl. Phys.*, 85(5): 2800–2804.

Liu, J.F., Vora, P., Walmer, M.H., Kottcamp, E., Bauser, S.A., Higgins, A. and Liu, S. (2005) Microstructure and magnetic properties of sintered NdFeB magnets with improved impact toughness, *J. Appl. Phys.*, 97(10): 10H101.

Liu, X., Gómez, P.H., Huang, K., Zhou, S., Wang, Y., Cai, X., Sun, H. and Ma, B. (2006) Research on La^{3+}–Co^{2+}-substituted strontium ferrite magnets for high intrinsic coercive force, *J. Magn. Magn. Mater.*, 305(2): 524–528.

Liu, Z., Li, M., Hu, Y., Wang, M. and Shi, Z. (2008) Preparation of large particle rare earth oxide by precipitation with oxalic acid, *J. Rare Earths*, 26(2): 158–162.

Liu, X., Hu, L. and Wang, E. (2013) Cold compaction behavior of nano-structured Nd–Fe–B alloy powders prepared by different processes, *J. Alloys Compd.*, 551: 682–687.

Livingston, J. and Kent, H. (1946) The cerium metal and light flint industry in Germany and Austria, Final Report No. 909, Office of the Military Government for Germany, Field Information Agency, Technical, pp. 5–18.

Lokshin, E.H.P., Vershkova, J.U.A., Kalinnikov, V.T., Tareeva, O.A., Ivlev, K.G. and Fedorov, S.G. (2004) Method of recovering rare earth minerals from phosphogypsum, RU Patent 2225892 (in Russian).

Long, K.R., Van Gosen, B.S., Foley, N.K. and Cordier, D. (2010) The principal rare earth elements deposits of the United States—A summary of domestic deposits and a global perspective: U.S. Geological Survey Scientific Investigations Report 2010–5220, Arlington, VA. Available at http://pubs.usgs.gov/sir/2010/5220.

Loonam, A.C. (1959) Principles and application of the iodide process, *J. Electrochem. Soc.*, 106(3): 238–244.

Love, B. and Kleber, E.V. (1960) Rare earths: Sixteen new metals are ready to use, *Mater. Des. Eng.*, 52(5): 134–137.

Lu, D., Horing, J.S. and Hoh, Y.C. (1989) The separation of neodymium by quaternary amine form didymium nitrate solution, *J. Less Common Metals*, 149: 219–224.

Lu, Y., Drelich, J. and Miller, J.D. (1998) Oleate adsorption at an apatite surface studied by ex-situ FTIR internal reflection spectroscopy, *J. Colloid Interface Sci.*, 202: 462–476.

Lucas, B.H. and Ritcey, G.M. (1975) Examination of a rare earth solvent extraction circuit for possible upgrading of the thorium product, *CIM Bull.*, 68(753): 124–130.

Lundin, C.E. (1961) Rare earth metal phase diagrams. In Spedding, F.H. and Daane, A.H. (eds.), *The Rare Earths*, pp. 224–385, Wiley, New York.

Lundin, C.E. (1973) The use of LaNi5 as a hydrogen source for fuelling a nonpolluting internal combustion engine. In Kevane, C.J. and Moeller, T. (eds.), *Proc. 10th Rare Earth Research Conf., Carefree, AZ*, May, Conf-730402, P1 and P2, pp. 662–669, National Technical Information Service, Springfield, VA.

Luo, J. and Chen, X. (1984) Research into the recovery of high-grade rare-earth concentrate from Baotou complex iron ore, China. In *Processing, Mineral and Metallurgy, Extractive*, pp. 663–675, IMM and Chinese Society of Metals, Kunming, Yunnan Province.

Luo, J. and Chen, X. (1985) *A New Development of Mineral Processing Flowsheet for the Treatment of a Complex Ore Containing Fe, Rare Earths, Nb and F, XVth ZMPC*, Vol. 3, pp. 474–485, Cannes, France.

Luo, J. and Chen, X. (1988) Selective flotation of fluorite, barite and calcite. In Xu, G. (ed.), *Proc. Int. Conf. Rare Earth Dev. & Appl.*, Vol. 1, pp. 67–70. Metallurgical Industry Press, Beijing.

Luo, X.-P., Qiu, T.-S., Yan, Q. and Fang, X.-H. (2002) Research progress and developing orientation of chemical extraction technology of weathering crust strain amass-type rare earth ore, *J. South. Inst. Metall.*, 23(5): 1–6.

Luo, Z.L., Lu, M.L., Bao, J., Liu, W.H. and Gao, C. (2005) Co-precipitation synthesis of gadolinium gallium garnet powders using ammonium hydrogen carbonate as the precipitant, *Mater. Lett.*, 59: 1188–1191.

Lupi, C., Pilone, D., Cannavale, G. and Pescetelli, A. (2000) Metal recovery from Ni-MH batteries. In Taylor, P.R. (ed.), *EPD Congress 2000*, pp. 257–270, The Minerals, Metals & Materials Society, Warrendale, PA.

Luyckx, L.A. (1981) The rare earth metals in steel. In Gschneidner, Jr., K.A. (ed.), *Industrial Applications of Rare Earth Elements*, pp. 43–78, ACS Symposium Series 164, American Chemical Society, Washington, DC.

Lyman, J.W. and Palmer, G.R. (1992) Scrap treatment method for rare earth transition metal alloys, US Patent 5,129,945.

Lyman, J.W. and Palmer, G.R. (1993a) Recycling of rare earths and iron from NdFeB magnet scrap, *High Temp. Mater. Process.*, 11(1–4): 175–188.

Lyman, J.W. and Palmer, G.R. (1993b) Recycling of neodymium iron boron magnet scrap, Report of Investigations 9481, United States Bureau of Mines, U.S. Department of the Interior, Washington, DC.

Lyman, J.W. and Palmer, G.R. (1995) Hydrometallurgical treatment of nickel–metal hydride battery electrodes. In *Third International Symposium on Recycling of Metals and Engineered Materials*, November 12–15, pp. 131–144, Point Clear, Alabama.

Lynas (2008) *Annual Report 2007*, 76 pp., Lynas Corporation Ltd., Sydney.

Lynas (2009) *Annual Report 2009*, Lynas Corporation Ltd., Sydney. Available at http://www.lynascorp.com/Annual Reports/Annual_Report_2009_778195.pdf.

Lynas (2010) *Rare Earths*, Lynas Corporation Ltd., Australia Corporate Access Days, September 27–28. J.P. Morgan, New York.

Mackey, T.S. (1986) Recent developments in U.S. rare earth technology. In Somasundaram, P. (ed.), *Advances in Mineral Processing*, pp. 509–534, Society of Mining Engineers Inc., Littletown, CO.

Mahajan, Y.R. and Rama Rao, P. (1988) Rare earths in new materials. In Gupta, C.K. and Krishnan, T.S. (eds.), *Rare Earths—Applications and Technology*, pp. 125–146, Trans Tech Publications, Switzerland.

Mahn, F. (1950) *J. Recher. CNRS*, 10: 28–31.

Maksimović, Z.J. and Pantó, G. (1996) Authigenic rare earth minerals in karst-bauxite and karstic nickel deposits. In Jones, A.P., Wall, F. and Williams, T. (eds.), *Rare Earth Minerals—Chemistry, Origin and Ore Deposits*, pp. 257–279, Chapman and Hall, London.

Malunga, G.W.P., Samama, J.C. and Houot, R. (1991) Rare earth potential in Malawi. In Siribumrungsukha, B., Arrykul, S., Sanguan Sai, P., Pungrassami, T., Sikong, L. and Kooptarnon, K. (eds.), *Proc. Int. Conf. Rare Earth Minerals and Minerals for Electronic Uses, Hat Yai, Thailand*, January, pp. 193–203, Prince of Songkla University, Thailand.

Mann, R., Laishram, L. and Malhan, N. (2012) Single step low temperature synthesis of gadolinium gallium garnet nanopowders, *J. Rare Earths*, 30(6): 545–547.

Mantel, M. and Amiel, S. (1973) Determination of rare earths by high-resolution X-ray spectrometry following neutron activation. *Journal of Radioanalytical and Nuclear Chemistry*, 16(1): 127–137.

Marchant, J.D., Morrice, E., Herve, B.P. and Wong, M.M. (1980) Preparing rare earth–silicon–iron–aluminum alloys, Bureau of Mines Report of Investigations 8445, U.S. Department of the Interior, Washington, DC.

Marinsky, J.A., Glendenin, L.E. and Coryell, C.D. (1947) The chemical identification of radioisotopes of neodymium and element 61, *J. Am. Chem. Soc.*, 69: 2781–2785.

Marsh, J.K. (1942) Rare earth metal amalgams. Part I: The reaction between sodium amalgam and rare earth acetate and chloride solutions, *J. Chem. Soc.*, 398–401.

Marsh, J.K. (1943) Rare earth metal amalgams. Part IV: The isolation of europium, *J. Chem. Soc.*, 531–535.

Marsh, J.K. (1955) Separation of lanthanons with the aid of ethylene diamine NNN'N' tetraacetic acid ('Enta' acid). Part V: The solubilities of some alkali lanthanon enta salts, *J. Chem. Soc.*, 451–452.

Marsh, J.K. (1957) Isolation of samarium, europium and ytterbium materials by means of sodium amalgam, *Inorg. Syn.*, 5: 32–37.

Martin, B.R. (1996) Ternary complexes of Al^{3+} and F^- with a third ligand, *Coord. Chem. Rev.*, 141: 23–32.

Mason, B. and Moore, C.B. (1982) *Principles of Geochemistry*, 4th edn., Wiley, New York.

Mason, G.W., Bilobron, I. and Peppard, D.F. (1978) Extraction of U(VI), Th, (IV), Am (III) and Eu(III) by bis para-octyl phosphoric acid in benzene diluent, *J. Inorg. Nucl. Chem.*, 40: 1807–1810.

Massalski, T., Okamoto, H. and Subramanyam, R. (eds.) (1990) *Binary Alloy Phase Diagrams*, 2nd edn., Vols. 1–2, American Society for Metals, Materials Park, OH.

Massot, L., Chamelot, P., Cassayre, L. and Taxil, P. (2009) Electrochemical study of the Eu(III)/Eu(II) system in molten fluoride media, *Electrochim. Acta*, 54(26): 6361–6366.

Masur, L.J., Podtburg, E.R., Craven, C.A., Otto, A., Wang, Z.L. and Kroeger, D.M. (1994) Advances in the processing and properties of $YBa2Cu4O_8$, *J. Metals*, 46(12): 28–30.

Matignon, C. (1900) *C. R. Acad. Sci.*, 131: 837–839, 891–892.

Matsumura, Y., Uchida, H., Ono, M. and Kaneko, H. (2000) Preparation of $TbFe_2$ thin film by ion plating process. In *Proceedings of the Sixth International Workshop on RE Magnets and Their Applications*, pp. 985–994, Japan Institute of Metals, Sendai.

Matsuura, Y. (2006) Recent development of Nd–Fe–B sintered magnets and their applications, *J. Magn. Magn. Mater.*, 303(2): 344–347.

Mazza, I. (1939) On the electrometallurgy of lanthanum, cerium and praseodymium, *Atti Congr. Intern. Chim., 10th Congr., Rome*, 1938, 3, 604–609.

McCallum, R.W. (1998) New or novel applications of rare earth materials. In *Rare Earths '98*, Abstracts, p. 26, Freemantle, Western Australia.

McColl, J.R. and Palilla, F.C. (1981) Use of rare earths in television and cathode ray phosphors. In Gschneidner, Jr., K.A. (ed.), *Industrial Applications of Rare Earth Elements*, pp. 177–193, ACS Symposium Series 164, American Chemical Society, Washington, DC.

McClendon, L.T. and LaFleur, P.D. (1973) Determination of rare earths in standard reference material glass using neutron activation analysis and reversed-phase chromatography. *Journal of Radioanalytical Chemistry*, 16(1): 123–126.

McCormick, P.G., Alonso, T., Liu, Y., Lincoln, F.J., Parks, T.C., Schaffer, G.B., Bautista, R.G. and Jackson, N. (1992) Rare Earths Resources. *Science, Technology and Applications, TMS*.

McCoy, H.N. (1936) Contribution to the chemistry of europium, *J. Am. Chem. Soc.*, 58: 1577–1580.

McCoy, H.N. (1941) Europium and ytterbium amalgams, *J. Am. Chem. Soc.*, 63: 1622–1624.

McFarland, C.M. (1973) Cobalt–rare earth powders by the reduction–diffusion process. In Kevane, C.J. and Moeller, T. (eds.), *Proc. 10th Rare Earth Research Conf., Carefree, AZ*, May, Conf-730402, P2, pp. 701–710, National Technical Information Service, Springfield, VA.

McGill, I. (1993) Rare earth elements. In Elvers, B., Hawkins, S., Russy, W. and Schulz, G. (eds.), *Ullmann's Encyclopedia of Industrial Chemistry*, Vol., A22, pp. 607–649, VCH, Weinheim.

McGill, I. (1997) Rare earth metals. In Habashi, F. (ed.), *Handbook of Extractive Metallurgy*, Vol. III, pp. 1695–1741, Wiley-VCH, Weinheim.

McGinn, P.J. (1994) Progress in the melt texturing of RE-123 superconductors, *J. Metals* 46(12): 31–33.

McGuiness, P.J., Zhang, X.J., Forsyth, H. and Harris, I.R. (1990) Disproportionation in $Nd_{16}Fe_{76}B_8$-type hydrides, *J. Less Common Metals*, 162: 379–387.

McKeown, F.A. and Klamic, H. (1959) Rare earth bearing apatite, at Mineville, Essex Co., N.Y., *U.S. Geol. Survey Bull.*, 1046B: 9–23.

McLemore, V.T. (1990) Background and perspectives on the Pajarito Mountains yttrium - zirconium deposit, Mescalero Apache Indian Reservation, Otero County, New Mexico, *New Mexico Geology*, 12: 22.

McLemore, V.T. (2011) Rare Earth Elements for Emerging Technologies, New Mexico Earth Matters, 11(2): 1–4.

McMasters, O.D., Verhoeven, J.D. and Gibson, E.D. (1986) Preparation of terfenol-D by float zone solidification, *J. Magn. Magn. Mater.*, 54–57(2): 849–850.

Meechumna, P. (1991) Separation of microlite from cassiterite and zircon. In Siribumrungsukha, B., Arrykul, S., Sanguan Sai, P., Pungrassami, T., Sikong, L. and Kooptarnon, K. (eds.), *Proc. Int. Conf. Rare Earth Minerals and Minerals for Electronic Uses, Hat Yai, Thailand*, January, pp. 211–220, Prince of Songkla University, Thailand.

Mei, G., Xie, K. and Li, G. (2007) *Progress in Study on Spent Fluorescent Lamps' Harmless Disposal and Resource Utilization*, College of Resources and Environmental Engineering, Wuhan University of Technology, China.

Mei, G.J., Rao, P., Matsuda, M. and Fujita, T. (2009a) Separation of red (Y_2O_3:Eu^{3+}), blue ((Sr, Ca, Ba)10(PO_4)6Cl_2:Eu^{2+}) and green ($LaPO_4$:Tb^{3+}, Ce^{3+}) rare earth phosphors by liquid/liquid extraction, *J. Wuhan Univ. Technol.–Mat. Sci. Ed.*, 24: 418–423.

Mei, G.J., Rao, P., Matsuda, M. and Fujita, T. (2009b) Separation of red (Y_2O_3:Eu^{3+}), blue ($BaMgAl_{10}O_{17}$:Eu^{2+}) and green ($CeMgAl_{10}O_{17}$:Tb^{3+}) rare earth phosphors by liquid/liquid extraction, *J. Wuhan Univ. Technol.–Mat. Sci. Ed.*, 24: 603–607.

Meints, R.E., Hopkins, B.S. and Audrieth, L.F. (1937) Electrolytic preparation of rare earth amalgams II, Decomposition of lanthanum amalgam for the preparation of the free metals, *Z. Anorg. Allgem. Chem.*, 231: 54–62.

Melsom, S. (1970) Precision and accuracy of rare earth determinations in rock samples using instrumental neutron activation analysis and a Ge(Li) detector, *J. Radioanal. Chem.*, 4: 355–363.

Menad, N. (1999) Cathode ray tube recycling, *Resour. Conserv. Recy.*, 26: 143–154.

Menth, A., Nagel, H. and Perkins, R.S. (1978) New high performance magnets based on rare earth transition metal compounds, *Ann. Rev. Mater. Sci.*, 8: 21–47.

Merlub-Sobel, M. (1959) Preparation of fused salt electrolytes, U.S. Patent 2,870,072, U.S. Patent and Trademark Office, Washington, DC.

Merrill, C.C. and Wong, M.M. (1967) Electrorefining yttrium, U.S. Bureau of Mines Report of Investigations 7018, U.S. Department of the Interior, Washington, DC.

Merritt, R.R. (1990a) High temperature methods for processing monazite: I. Reaction with calcium chloride and calcium carbonate, *J. Less Common Metals*, 166: 197–210.

Merritt, R.R. (1990b) High temperature methods for processing monazite. II. Reaction with sodium carbonate, *J. Less Common Metals*, 166: 211–219.

Mertie, Jr., J.B. (1953) Monazite deposits of the southeastern Atlantic States, U.S. Geological Survey Circular 237, Arlington, VA.

Metal Powder Report (2009) New PM magnetic developments, MPR, June. Available at http://www.metal-powder.net.

Mialki, W. (1965) Seltene Erden in der Kerntechnik, *Metall*, 19: 16–21.

Miao, M.W. and Horng, J.S. (1988) Decomposition of Taiwan black monazite by hydrothermal and sodium fusion methods. In Bautista, R.G. and Wong, M.M. (eds.), *Rare Earths*, pp. 195–206, The Minerals, Metals, and Materials Society, Warrendale, PA.

Mineral Facts and Problems (1985) "Resource reserve definitions," minerals facts and problems 1985, Bureau of Mines Bulletin 675, pp. 2–7, U.S. Department of the Interior, Washington, DC.

Minh, N.Q. (1993) Ceramic fuel cells, *J. Am. Ceram. Soc.*, 76(3): 563–588.

Mining Journal (1994) Malaysian rare earth plants to close, *Mining J.* (London), 322(8262): 106, February 11.

MIIT (Ministry of Industry and Information Technology of China) (2010) Notice on the consultative draft of "Entry Criterions for Rare Earth Industry," May.

Minowa, T., Yoshikawa, M. and Honshima, M. (1989) Improvement of the corrosion resistance on Nd–Fe–B magnet with nickel plating, *IEEE Trans. Magn.*, 25: 3776–3778.

Mio, H., Lee, J., Nakagawa, T., Kano, J. and Saito, F. (2001) Estimation of Extraction Rate of Yttrium from Fluorescent Powder by Ball Milling. *Materials Transactions*, 42(11): 2460–2464.

Mishima, C., Noguchi, K., Yamazaki, M., Matsuoka, H., Mitarai, H. and Honkura, Y. (2012) Development of Dy-Free Nd-Fe-B anisotropic bonded magnet and application to the small motors. *J. Japan Inst. Metals*, 76(1): 89–95.

Miura, K. (2011) Demagnetization of neodymium magnets at room temperature. In Lecture in Tokyo on November 11, 2011, Japan Society of Material Cycles and Waste Management. Abstract available at http://jsmcwm.or.jp/jimu/event/20111111-youshi.pdf (accessed December 15, 2011).

Miura, K., Masuda, M., Itoh, M., Horikawa, T. and Machida, K. (2006) Microwave absorption properties of the nano-composite powders recovered from Nd–Fe–B bonded magnet scraps, *J. Alloys Compd.*, 408–412: 1391–1395.

Miura, K., Roh, M. and Machida, K.I. (2008) Extraction and recovery characteristics of Fe element from NdFeB sintered magnet powder scrap by carbonylation, *J. Alloys Compd.*, 466: 228–232.

Moeller, T. (1961) Chemistry of rare earths. In Spedding, F.H. and Daane, A.H. (eds.), *The Rare Earths*, John Wiley, New York.
Moeller, T. (1963) *The Chemistry of Lanthanons*, Reinhold, New York.
Moeller, T. (1967) Lanthanide elements. In Hampel, C.A. (ed.), *Encyclopedia of Chemical Elements*, pp. 338–349, Reinhold, New York.
Moeller, T. (1971) The lanthanides. In Bailer, K., Emeleus, H.J., Nyholm, R. and Trotman Dickenson, A. (eds.), *Comprehensive Inorganic Chemistry*, Vol. 4, Pergamon, Oxford.
Moeller, T. and Brantley, J.C. (1950) The rare earths. Spectrophotometric estimation of certain rare earth elements, *Anal. Chem.*, 22: 433–441.
Moeller, T. and Kremers, H.E. (1945) The basicity characteristics of scandium, yttrium and the rare earth elements, *Chem. Rev.*, 37: 97–159.
Moeller, T. and Zimmerman, P.A. (1954) Electrolysis of rare earth metal salts in basic solvents, *Science*, 120: 539–540.
Moldenhauer, M. (1914) *Chem. Z.*, 38: 147.
Moldoveanu, G.A. and Papangelakis, V.G. (2012) Recovery of rare earth elements adsorbed on clay minerals: I. Desorption mechanism, *Hydrometallurgy*, 117–118: 71–78.
Moldoveanu, G.A. and Papangelakis, V.G. (2013) Recovery of rare earth elements adsorbed on clay minerals: II. Leaching with ammonium sulfate, *Hydrometallurgy*, 131–132: 158–166.
Molycorp (2010a) Molycorp Minerals. Revised mine and reclamation plan for the mountain pass mine. Draft: Subsequent mitigated negative declaration. Submitted to County of San Bernardino, prepared by Environmental Audit, Inc., September. Available at http://www.sbcounty.gov/landuseservices/Public%20Notices/Projects/Projects.htm.
Molycorp (2010b) Molycorp minerals: Security-registration statement from 7/13/2010. Available at http://sec.edgar-online.com/molycorp-inc/s-1asecurities-registration-statement/2010/07/13/section19.aspx.
Molycorp (2010c) Molycorp minerals: Global outlook. Available at http://www.molycorp.com/globaloutlook.asp (accessed November 10, 2010).
Molycorp Application Report (1964–1970) A bibliography. Six years of research in catalysis with rare earth elements, Vol. 1, No. 7101.
Molycorp Application Report (1971–1976) A bibliography of the research in catalysis with rare earth elements, Vol. 2, No. 7907.
Molycorp, Inc. (1993) *A Lanthanide Lanthology*, Molycorp, Inc., Mountain Pass, CA.
Morais, C.A. and Ciminelli, V.S.T. (1998) Recovery of europium from a rare earth chloride solution, *Hydrometallurgy*, 49: 167–177.
Morais, C.A. and Ciminelli, V.S.T. (2001) Recovery of europium by chemical reduction of a commercial solution of europium and Gadolinium chlorides, *Hydrometallurgy*, 60(3): 247–253.
Morais, C.A. and Ciminelli, V.S.T. (2002) A study on recovery of europium by photochemical reduction, *Sep. Sci. Technol.*, 37(14): 3305–3321.
Morais, C.A. and Ciminelli, V.S.T. (2007) Selection of solvent extraction reagent for the separation of europium(III) and gadolinium(III), *Miner. Eng.*, 20(8): 747–752.
Morey, G.W. (1938) *The Properties of Glass*, pp. 435–436, Reinhold Publishing Corporation, New York.
Moriarty, Jr., J.C. (1968) The industrial preparation of the rare earth metals by metallothermic reduction, *J. Metals*, 20(11): 41–45.
Morimoto, K., Katayama, N., Akamine, H. and Itakura, M. (2012) Coercivity enhancement of anisotropic Dy-free Nd–Fe–B powders by conventional HDDR process, *J. Magn. Magn. Mater.*, 324(22): 3723–3726.
Morrice, E. (1985) Molten salt electrowinning of rare earth and yttrium metals and alloys. In Xu, G. and Xiao, J. (eds.), *New Frontiers in Rare Earth Science and Application*, Vol. II, pp. 1099–1106, Science Press, Beijing.

Morrice, E. and Henrie, T.A. (1967) Electrowinning of high purity neodymium, praseodymium and didymium metals from their oxides, Bureau of Mines Report of Investigations 6957, U.S. Department of the Interior, Washington, DC.

Morrice, E. and Knickerbocker, R.G. (1961) Rare earth electrolytic metals. In Spedding, F.H. and Daane, A.H. (eds.), *The Rare Earths*, pp. 126–144, John Wiley, New York.

Morrice, E. and Wong, M.M. (1978) Effect of temperature on the electrolytic preparation and recovery of samarium–cobalt alloy, Bureau of Mines Report of Investigations 7556, U.S. Department of the Interior, Washington, DC.

Morrice, E. and Wong, M.M. (1979) Fused salt electrowinning and electrorefining of rare earth and yttrium metals, *Miner. Sci. Eng.*, 11(3): 125–136.

Morrice, E. and Wong, M.M. (1982) Flotation of rare earths from bastnasite ore, Bureau of Mines Report of Investigations 8689, U.S. Department of the Interior, Washington, DC.

Morrice, E., Darrah, J., Brown, E., Wyche, C., Headrick, W., Williams, R. and Knickerbocker, R.G. (1960) Metallurgical laboratory data on reduction and refining of ceric oxide and cerous fluoride to cerium ingot, RI 5549, U.S. Department of the Interior, Washington, DC.

Morrice, E., Porter, B., Brown, E.A., Wyche, C. and Knickerbocker, R.G. (1961) Electrowinning of cerium group and yttrium group metals, Bureau of Mines Report of Investigations 5868, U.S. Department of the Interior, Washington, DC.

Morrice, E., Wyche, C. and Henrie, T.A. (1962) Electrowinning of molten lanthanum from lanthanum oxides, Bureau of Mines Report of Investigations 6075, U.S. Department of the Interior, Washington, DC.

Morrice, E., Shedd, E.S. and Henrie, T.A. (1968) Direct electrolysis of rare earth oxides to metals and alloys in fluoride melts, Bureau of Mines Report of Investigations 7146, U.S. Department of the Interior, Washington, DC.

Morrice, E., Shedd, E.S., Wong, M.M. and Henrie, T.A. (1969) Preparation of cobalt rare earth alloys by electrolysis, *J. Metals*, 21(1): 34–37.

Morrice, E., Whisler, N. and Wong, M.M. (1973) Electrowinning of yttrium–aluminium alloy from yttria alumina mixtures. In Kevane, C.J. and Moeller, T. (eds.), *Proc. 10th Rare Earth Research Conf., Carefree, AZ*, May, Conf-730402, P1 and P2, pp. 682–691, National Technical Information Service, Springfield, VA.

Morton, J.R. and James, D.B. (1967) Effect of temperature on the HEDTA and EDTA elution position of yttrium in the rare earth sequence. In *Proc. 6th Rare Earth Research Conference*, Report No. AFOSR-67-1214, pp. 667–677, National Technical Information Service, Springfield, VA.

Mosander, C.G. (1827) The preparation of cerium by reduction of $CeCl_3$ with potassium, *Pogg. Ann.*, 11: 406–416.

Mosen, A.W., Schmitt, R.A. and Vasilevskis, J. (1961). A procedure for the determination of the rare earth elements, lanthanum through lutetium, in chondritic, achondritic and iron meteorites by neutron-activation analysis. *Analytica Chimica Acta*, 25(1): 10–24.

Mossart, D.L. and Hoste, J. (1968) Activation analysis of rare earths, *Anal. Chim. Acta*, 42: 7–28.

Moustafa, M.I. and Abdelfattah, N.A. (2010) Physical and chemical beneficiation of the Egyptian beach monazite, *Resour. Geol.*, 60(3): 288–299.

Mueller, R.M., Buchal, Chr., Folle, H.R., Kubota, M. and Pobell, F. (1980) A double stage nuclear demagnetization refrigerator, *Cryogenics*, 20(7): 395–407.

Muller, T. and Friedrich, B. (2006) Development of a recycling process for nickel–metal hydride batteries, *J. Power Sources*, 158: 1498–1509.

Murase, K., Machida, K. and Adachi, G. (1995) Recovery of rare metals from scrap of rare earth intermetallic material by chemical-vapor transport, *J. Alloys Compd.*, 217: 218–225.

Murase, K., Ozaki, T., Machida, K. and Adachi, G. (1996) Extraction and mutual separation of rare earths from concentrates and crude oxides using chemical vapor transport, *J. Alloys Compd.*, 233: 96–106.

Murphy, A.J. and Payne, R.J.M. (1947) Magnesium–cerium–zirconium alloys: Properties at elevated temperatures, *J. Inst. Met.*, 73: 105–127.

Murphy, J.E., Adams, G.H. and Cathey, W.N. (1975) Electrotransport and diffusion of iron in a yttrium, *Metall. Trans.*, 6A: 343–348.

Murthy, D.S.R. (1995) Determination of rare earth elements and yttrium in apatites using inductively coupled plasma emission spectrometry. In *Proc. Seminar on Recent Developments in the Science and Technology of Rare Earths*, December 14–16, p. 167, Cochin.

Murthy, T.K.S. and Mukherjee, T.K. (2002) *Rare Earths Occurrence, Production and Applications*, TIFAC(DST) and Indian Institute of Metals, Calcutta.

Muthmann, W. and Weiss, L. (1904) Investigations on metals of the cerium group, *Liebigs Ann.*, 331: 1–46.

Muthmann, W. and Scheidemandel, J. (1907) On the extraction of the rare earth metals by electrolysis of the fluorides, *Ann*, 355: 116–136.

Muthmann, W., Hofer, H. and Weiss, L. (1902) On the preparation of metals of the cerium group by molten electrolysis, *Ann. Chem.*, 320: 231–269.

Naastepad, P.A., den Broeder, F.J.A. and Wassink, R.J.K. (1973) Technology of $SmCo_5$ magnets, *Powder Metall. Int.*, 5: 61–65.

Nadkarni, R.A. (1975) *Multielement analysis of coal and coal fly ash standards by instrumental neutron activation analysis*. Cornell Univ., Ithaca, NY.

Nadkarni, R.A. (1976) Feasibility study rare earths determination in rocks by instrumental neutron activation analysis. inis.iaea.org.

Nagai, H., Beaudry, B.J. and Gschneidner, Jr., K.A. (1978) Purification of gadolinium by electrorefining, *Metall. Trans.*, 9B: 25–28.

Naganawa, H., Shimojo, K. and Mitamura, H. (2007) A new "green" extractant of the diglycol amic acid type for lanthanides, *Solv. Extr. Res. Dev. Japan*, 14: 151–159.

Nair, S.G.K. and Smutz, M. (1967) Recovery of lanthanum from didymium chloride with Di (2-ethylhexyl)-phosphoric acid as solvent. *Journal of Inorganic and Nuclear Chemistry*, 29(7): 1787–1797.

Nakayama, R. and Takeshita, T. (1993) Nd–Fe–B anisotropic magnet powders produced by the HDDR process, *J. Alloys Compd.*, 193: 259–261.

Nakazato, K., Hashimoto, H., Uchida, H. and Matsumura, Y. (2000) Preparation of giant magnetostrictive thin film by magnetron and ion beam sputtering processes, *Rev. Sci. Instr.*, 71(2): 996–998.

Nan, J., Han, D., Yang, M. and Cui, M. (2006a) Dismantling, recovery and reuse of spent nickel-metal hydride batteries, *J. Electrochem. Soc.*, 153(1): 101–105.

Nan, J., Han, D., Yang, M., Cui, M. and Hou, X. (2006b) Recovery of metal values from a mixture of spent lithium-ion batteries and nickel-metal hydride batteries, *Hydrometallurgy*, 84(1): 75–80.

Narayanan, N.S., Thulasidoss, S., Ramachandran, T.V., Swaminathan, T.V. and Prasad, K.R. (1988) Processing of monazite at the rare earths division, Udyogamandal. In Gupta, C.K. and Krishnan, T.S. (eds.), *Rare Earths—Applications and Technology*, pp. 45–56, Trans Tech Publications, Switzerland.

Nash, K.L. (1994) Separation chemistry for lanthanides and trivalent actinides. In Gschneidner, Jr., K.A., Eyring, L., Choppin, G.R., Lander, G.H. (eds.), *Handbook on the Physics and Chemistry of Rare Earths*, Vol. 18, pp. 197–238, Elsevier Science B.V., Amsterdam.

Nayeb-Hashemi, A.A., Clark, J.B. and Swartzendruber, L.J. (1985) The Fe–Mg (Iron–Magnesium) system, *J. Phase Equilib.*, 6: 235–238.

Nazarov, M. and Noh, D.Y. (2010) Rare earth double activated phosphors for different applications, *J. Rare Earths*, 28(12 Suppl. 1): 1–11.

Necker, W.C. (1961) The zone purification of yttrium. In Bunshah, R.F. (ed.), *Trans. Vac. Metallurgy Conf.*, pp. 289–298, Interscience, New York.

Nemoto, T., Tanaka, Y., Tsujioka, S., Eryu, Y. and Takada, T. (2011) Resource recycling for sustainable industrial development, *Hitachi Rev*., 60(6): 335–341.

Nesbitt, E.A. and Wernick, J.H. (1973) *Rare Earth Permanent Magnets*, Academic Press, New York.

Nielsen, J.W. (1981) Bubble domain memory materials. In Gschneidner, Jr., K.A. (ed.), *Industrial Applications of Rare Earth Elements*, pp. 219–222, ACS Symposium Series 164, American Chemical Society, Washington, DC.

Niinae, M., Yamaguchi, K., Ishida, N., Djohari, A., Nakahiro, Y. and Wakamatsu, T. (1994) Study on recycling of rare earth magnet scrap, *J. MMIJ*, 110: 981–986.

Nininger, R.D. (1956) *Exploration for Nuclear Raw Materials*, D. Van Nostrand, Princeton, NJ.

Noblitt, H.C. (1965) Development of a process for the concentration of Oka pyrochlore. In Roberts, A. (ed.), *Minerals Processing*, pp. 669–678, Pergamon, Oxford.

Nolting, H.J., Simmons, C.R. and Klingenberg, J.J. (1960) Preparation and properties of high purity yttrium metal, *J. Inorg. Nucl. Chem.*, 14: 208–216.

Nourry, C., Massot, L., Chamelot, P. and Taxil, P. (2009) Electrochemical reduction of Gd(III) and Nd(III) on reactive cathode material in molten fluoride media, *J. Appl. Electrochem.*, 39(6): 927–933.

Noyes, A. and Bray, B. (1927) *A System of Qualitative Analysis for the Rare Earth Elements*, Macmillan, London.

Nozawa, Y., Iwasaki, K., Tanigawa, S., Tokunaga, M. and Harada, H. (1988) Nd–Fe–B die upset and anisotropic bonded magnets, *J. Appl. Phys.*, 64: 5285–5289.

Nozawa, N., Sepehri-Amin, H., Ohkubo, T., Hono, K., Nishiuchi, T. and Hirosawa, S. (2011) Coercivity enhancement of HDDR-processed Nd–Fe–B permanent magnet with the rapid hot-press consolidation process, *J. Magn. Magn. Mater.*, 323(1): 115–121.

Oakdene Hollins Research & Consulting (2010) Lanthanide Resources and Alternatives, A report for Department for Transport and Department for Business, Innovation and Skills, March.

Oberteuffer, J. (1974) Magnetic separation: A review of principles, devices, and applications, *IEEE Trans. Magn.*, 10(2): 223–238.

Ochsenkühn-Petropoulou, M.T., Hatzilyberis, K.S., Mendrinos, L. and Salmas, C.E. (2002) Pilot-plant investigation of the leaching process for the recovery of scandium from red mud, *Ind. Eng. Chem. Res.*, 41: 5794–5801.

Odysseos, M., De Rango, P., Christodoulou, C.N., Hlil, E.K., Steriotis, T., Karagiorgis, G. and Stubos, A. (2013) The effect of compositional changes on the structural and hydrogen storage properties of (La–Ce) Ni 5 type intermetallics towards compounds suitable for metal hydride hydrogen compression. *J. Alloys Compd.*, 580: S268–S270.

O'Driscoll, M. (1991) An overview of rare earth minerals supply and applications. In Siribumrungsukha, B., Arrykul, S., Sanguan Sai, P., Pungrassami, T., Sikong, L. and Kooptarnon, K. (eds.), *Proc. Int. Conf. Rare Earth Minerals and Minerals for Electronic Uses, Hat Yai, Thailand*, January, pp. 409–420, Prince of Songkla University, Thailand.

Ohmori, K. (1998) The use of reduction diffusion process (R/D) in magnet industry. In Preprints of the Conference, China Magnets, held on October 18–21, 1998, Beijing.

Okabayashi, Y. and Otsuka S. (1970) Method for reclaiming rare earth fluorescent substances. U.S. Patent 3,506,585.

Okabe, T.H., Deura, T.N., Oishi, T., Ono, K. and Sadoway, D.R. (1996) Electrochemical deoxidation of yttrium–oxygen solid solutions, *J. Alloys Compd.*, 237: 150–154.

Okabe, T.H., Hirota, K., Kasai, E., Saito, F., Waseda, Y. and Jacob, K.T. (1998) Thermodynamic properties of oxygen in RE–O (RE = Gd, Tb, Dy, Er) solid solutions, *J. Alloys Compd.*, 279: 184–191.

Okabe, T.H., Takeda, O., Fukuda, K. and Umetsu, Y. (2003a) Direct extraction and recovery of neodymium metal from magnet scrap, *Mater. Trans.*, 44: 798–801.

Okabe, T.H., Takeda, O., Fukuda, K. and Umetsu, Y. (2003b) Scrap combination for recycling of valuable metals: Direct extraction and recovery of neodymium metal from magnet scraps. In Kongoli, F., Itagaki, K., Yamauchi, C. and Sohn, H.Y. (eds.), *Yazawa International Symposium on Metallurgical and Materials Processing: Principles and Technologies*, 1: 1079–1091, Wiley, New York.

Okajima, Y. (1987) Rare earth metal powder, Japanese Patent 62 13 506 91987 (CA 106, 217418).

Okamoto, H. (1991) Mg–Nd (Magnesium–Neodymium), *J. Phase Equilib.*, 12: 249–250.

Oki, T. (2007) Advanced particle separation technology for rare metals recycling. In *Exhibitor Brochure at Hannover Messe 2007*, April 16–20, Hannover.

Oki, T. (2010) Recovery of rare earth magnet from waste HDD, *Rare Earths*, 56: 198–199.

Oki, T. (2011) Physical sorting technology development for the rare metal recycling, *Rare Earths*, 58: 34–45.

Oki, T., Wada, N. and Matsumoto, M. (2011) In *Proceedings of MMIJ Annual Meeting*, No. 2025, The Mining and Materials Processing Institute of Japan, Tokyo.

O'Laughlin, J.W. (1979) Chemical spectrometric and polorographic methods. In Gschneidner, Jr., K.A. and Eyring, L. (eds.), *Handbook on the Physics and Chemistry of Rare Earths*, Vol. 4, pp. 341–358, North Holland, Amsterdam.

Olson, J.C., Shaw, D.R., Pray, L.C. and Sharp, W.N. (1954) Rare earth mineral deposits of the Mountain Pass district, San Bernandino Country CA, U.S. Geol. Survey Prof. Paper 261, U.S. Govt. Printing Office, Washington, DC.

Omachi, R. (1988) Hi-tech applications of rare earths. In Gupta, C.K. and Krishnan, T.S. (eds.), *Rare Earths—Applications and Technology*, pp. 147–154, Trans Tech Publications, Switzerland.

Omori, M. (2000) Sintering, consolidation, reaction and crystal growth by the spark plasma system(SPS), *Mater. Sci. Eng.*, A287: 183–188.

Ondov, J.M., Ragaini, R.C., Heft, R.E., Fisher, G.L., Silberman, D. and Prentice, B.A. (1977) Interlaboratory comparison of neutron activation and atomic absorption analyses of size-classified stack fly ash (No. UCRL-78194; CONF-760985-2), California University, Lawrence Livermore Lab., Livermore, CA.

Ono, K. and Suzuki, R.O. (2002) The member, *J. Minerals Metals Mater. Soc.*, 54: 59–61.

Onstatt, E.I. (1953) Preparation of massive samarium metal, U.S. Atomic Energy Commission Report LA-1622, National Technical Information Service, Springfield, VA.

Onstatt, E.I. (1959) Separation of lanthanons by amalgam cathodes. III Electrochemical fractionation of the lanthanons at a lithium amalgam cathode, *J. Am. Chem. Soc.*, 81: 4451–4458.

Ooghe, W. and Verbeek, F. (1974) Atomic absorption spectrometry of the lanthanides in minerals and ores, *Anal. Chem. Acta*, 73(1): 87–95.

Orimo, S. Fujii, H. and Ikeda, K. (1997) Notable hydriding properties of a nanostructured composite material of the Mg2Ni-H system synthesized by reactive mechanical grinding, *Acta Mater.*, 45(1): 331–341.

Ormerod, J. (1985) The physical metallurgy and processing of sintered rare earth permanent magnets, *J. Less Common Metals*, 111: 49–69.

Orris, G.J. and Grauch, R.I. (2002) Rare earth element mines, deposits, and occurrences, U.S. Geological Survey Open-File Report 2002–0189, Arlington, VA.

Osborne, M.G., Anderson, I.E. and Gschneidner, Jr., K.A. (1993) Centrifugal atomization of rare earth metal and intermetallic compounds. In Lawley, A. and Swanson, A. (eds.), *Advances in Powder Metallurgy and Particulate Materials—1993 Powder Characterization, Testing and Quality Control*, Vol. 1, pp. 65–73, Metal Powder Industries Federation—American Powder Metallurgy Institute, Princeton, NJ.

OSRAM (2009) Method for recovery of rare earths from fluorescent lamps, United States Patent Application Publication. Inventors: Otto, R.; Wojtalewicz-Kasprzak, A. Assignee: OSRAM GmbH, Pub. No. US 2009/0162267 A1.

Otto, R. and Agnieszka Wojtalewicz-Kasprzak, A.W. (2011) Method for recovery of rare earths from fluorescent lamps. U.S. Patent 7,976,798.

Otto, R. and Kasprzac, A.W. (2012) Method for Recovery of Rare Earths from Fluorescent Lamps. US Patent 2012/0027651 A1.

Otsuki, A., Dodbiba, G., Shibayama, A., Sadaki, J., Mei, G.J. and Fujita, T. (2008) Separation of rare earth fluorescent powders by two-liquid flotation using organic solvents, *Jpn. J. Appl. Phys.*, 47: 5093–5099.

Otsuki, E., Otsuka, T. and Imai, T. (1990) Processing and magnetic properties of sintered Nd–Fe–B magnets. In *Proceedings of the 11th International Workshop on Rare Earth Magnets and Their Applications*, Vol. 1, pp. 328–340, Pittsburg, PA.

Overstead, W.C., Theobold, P.K. and Whitlow, J.W. (1959) Thorium and uranium resources in monazite placers of the western Piedmont, North and South Carolina, *Trans. AIME*, 214: 709–714.

Ozaki, T., Machida, K. and Adachi, G. (1999a) Extraction and mutual separation of rare earths from used polishes by chemical vapor transport, *Metall. Mater. Trans. B*, 30: 45–51.

Ozaki, T., Machida, K. and Adachi, G. (1999b) Recovery of rare earths from used polishes by chemical vapor transport process, *Mater. Sci. Forum*, 313–315: 297–305.

Ozbayoglu, G. and Umit Atalay, M. (2000) Beneficiation of bastnaesite by a multi-gravity separator, *J. Alloys Compd.*, 303–304: 520–523.

Ozumi, Y., Kato, A. and Miyake, Y. (1971) Emission-spectrometric determination of trace non-rare earth elements in yttrium oxide using AgF-Ga_2O_3 mixed carrier. *Fresenius' J. Analyt. Chem.*, 255(2): 103–109.

Palmer, P.E., Burkholder, H.R., Beaudry, B.J. and Gschneidner, Jr., K.A. (1982) Preparation and some properties of misch metal, *J. Less Common Metals*, 87: 135–148.

Pan, P.H., Fennemore, D.K., Berolo, A.J., Shanks, H.R., Beaudry, B.J., Schmidt, F.A. and Danielson, G.C. (1980) Heat capacity of high purity lanthanum, *Phys. Rev. B*, 21: 2809–2814.

Pan, M., Zhang, P., Li, X., Ge, H., Wu, Q., Jiao, Z. and Liu, T. (2010) Effect of Terbium addition on the coercivity of the sintered NdFeB magnets, *J. Rare Earths*, 28(Spec. Issue): 399–402.

Panditharatna, L. (1991) The Ceylon mineral sands industry: Profile and prospects. In Siribumrungsukha, B., Arrykul, S., Sanguan Sai, P., Pungrassami, T., Sikong, L. and Kooptarnon, K. (eds.), *Proc. Int. Conf. Rare Earth Minerals and Minerals for Electronic Uses, Hat Yai, Thailand*, January, pp. 481–500, Prince of Songkla University, Thailand.

Pankratz, L.B., Stuve, J.M. and Gokcen, N.A. (1984) Thermodynamic data for mineral technology, Bureau of Mines Bulletin 677, U.S. Department of the Interior, Washington, DC.

Park, J.K., Choi, K.J., Yeon, J.H., Yeon, J.H., Lee, S.J. and Kim, C.H. (2006) Embodiment of the warm white-light–emitting diodes by using a Ba^{2+} codoped Sr_3SiO_5:Eu phosphor, *Appl. Phys. Lett.*, 88: 043511.

Park, B., Honan, S., Billingsley, G., Chalmers, I. and London, I. (2012) Handling and management of thorium and uranium in mining and processing of rare earth minerals, White Paper Vol. 1, No. 1, Rare Earth Industry and Technology Association (REITA), Toronto, Ontario.

Parker, J.G. and Baroch, C.T. (eds.) (1971) The rare earth elements, yttrium and thorium—A materials survey, Bureau of Mines Information Circular 8476, U.S. Department of the Interior, Washington, DC.

Parthasarathy, R., Desai, H.B. and Kayasth, S.R. (1986) Radiochemical neutron activation analysis of individual rare earth elements in monazite from different geological environments, *J. Radioanal. Nucl. Chem. Lett.*, 105: 277–279.

Pasto, A.E. and Tennery, V.J. (1977) Synthesis and fabrication of EuB_6, *Trans. Am. Nucl. Soc.*, 26(1): 176.

Paul, J. and Campbell, G. (2011) Investigating rare earth element mine development in EPA region 8 and potential environmental impacts, Report on rare earth elements August 15, 2011 EPA Document-908R11003, US Environmental Protection Agency.

Pavez, O. and Peres, A.E.C. (1993) Effect of sodium metasilicate and sodium sulphide on the floatability of monazite–zircon–rutile with oleate and hydroxamates. *Miner. Eng.*, 6(3): 69–78.

Pavez, O. and Peres, A.E.C. (1994) Technical note—Bench scale flotation of a Brazilian monazite ore, *Miner. Eng.*, 7(12): 1561–1564.

Pavez, O., Brandao, P.R.G. and Peres, A.E.S. (1996) Technical note—Adsorption of oleate and octyl-hydroxamate on to rare-earths minerals, *Miner. Eng.*, 9(3): 357–366.

Payne, R.J.M. and Bailey, N. (1959–1960) Improvement of the age hardening properties of magnesium–rare earth alloys by addition of silver, *J. Inst. Met.*, 88: 417–427.

Pecharsky, V.K. and Gschneidner, Jr., K.A. (1997a) Effect of alloying on the giant magnetocaloric effect of $Gd_5(Si_2Ge_2)$, *J. Magn. Magn. Mater.*, 3(3): L179–L184.

Pecharsky, V.K. and Gschneidner, Jr., K.A. (1997b) Giant magnetocaloric effect in $Gd_5(Si_2Ge_2)$. *Phys. Rev. Lett.*, 78: 4494–4497.

Pecharsky, V.K. and Gschneidner, Jr., K.A. (1997c) Tunable magnetic regenerator alloys with a giant magnetocaloric effect for magnetic refrigeration from ~20 to ~290 K, *Appl. Phys. Lett.*, 70: 3299–3301.

Pedreira, W.R., Sarkis, J.E.S., Rodrigues, C., Tomiyoshi, I.A. and da Silva Queiroz, C.A. (2001) Determination of trace amounts of rare earth elements in highly pure praseodymium oxide by double focusing inductively coupled plasma mass spectrometry and high-performance liquid chromatography, *J. Alloys Compd.*, 323–324: 49–52.

Pei, L., Han, S., Hu, L., Zhao, X. and Liu, Y. (2012) Phase structure and hydrogen storage properties of $LaMg_{3.93}Ni_{0.21}$ alloy, *J. Rare Earths*, 30(6): 534–539.

Pengo, R., Favoron, P., Manente, G., Cecchi, A. and Pieraccini, L. (1991) The reduction of rare earth oxides to metal and their subsequent rolling, *Nucl. Instrum. Methods Phys. Res. A*, 303: 146–151.

Peppard, D.E. (1964) Fractionation of rare earths by liquid extraction using phosphorus based extractants. In Eyring, L. (ed.), *Progress in the Science and Technology of Rare Earths*, Vol. 1, pp. 89–108, Pergamon, Oxford.

Peppard, D.F. and Mason, G.W. (1961) Liquid-liquid extraction of trivalent rare earths using acidic phosphonates as extractants. In *Rare Earth Research*, pp. 37–50, The Macmillan Company, New York.

Peppard, D.E., Faris, F.J., Gray, P.R. and Mason, G.W. (1953) Studies of the solvent extraction behavior of transition elements. I. Order and degree of fractionation of the trivalent rare earths, *J. Phys. Chem.*, 57: 294–301.

Peppard, D.F., Driscoll, W.J., Siromen, S.J. and Mason, G.W. (1957a) Fractional extraction of the lanthanides as their di-alkyl orthophosphates, *J. Inorg. Nucl. Chem.*, 4: 334–343.

Peppard, D.F., Driscoll, W.J., Sironen, R.J. and McCarty, S. (1957b) Nonmonotonic ordering of lanthanides in tributyl phosphate–nitric acid extraction system, *J. Inorg. Nucl. Chem.*, 4: 326–333.

Peppard, D.E., Driscoll, W.J., Siromen, R.J. and Mason, G.W. (1958) Acidic esters of organophosphoric acids as selective extractants for metallic cations—Tracer studies, *J. Inorg. Nucl. Chem.*, 7: 276–285.

Peters, A.W. and Kim, G. (1981) Rare earths in noncracking catalysts. In Gschneidner, Jr., K.A. (ed.), *Industrial Applications of Rare Earth Elements*, pp. 117–131, ACS Symposium Series 164, American Chemical Society, Washington, DC.

Peterson, D.T. and Beernsten, D.J. (1957) Vacuum fusion determination of oxygen and nitrogen in lanthanum, *Anal. Chem.*, 29(2): 254–257.

Peterson, D.T. and Schmidt, F.A. (1969) Electrotransport of carbon, nitrogen and oxygen in lutetium, *J. Less Common Metals*, 18: 111–116.
Peterson, D.T. and Schmidt, F.A. (1972) Electrotransport of carbon, nitrogen and oxygen in gadolinium, *J. Less Common Metals*, 29: 321–327.
Pfann, W.F. (1966) *Zone Melting*, 2nd edn, Wiley, New York.
Pickarts, J. (2011) Bear Lodge Project Overview, June 22.
Pidgeon, L.M. and King, J.A. (1948) Vapour pressure of magnesium in the thermal reduction of magnesium oxide by ferrosilicon, *Discuss. Faraday Soc.*, 4: 197–206.
Pierce, T.B. and Peck, J.F. (1963) The extraction of the lanthanide elements from perchloric acid by di-(2-ethyl hexyl) hydrogen phosphate, *Analyst*, 88: 217–221.
Pietrelli, L., Bellomo, B., Fontana, D. and Montereali, M.R. (2002) Rare earths recovery from NiMH batteries, *Hydrometallurgy*, 66: 135–139.
Pilegaard, K. (1990) *Preliminary Environmental Impact Statement for the Kvanefjeld Uranium Mine*, Risø National Laboratory, Roskilde, Denmark.
Pilkington, E.S. and Wylie, A.W. (1952) Production of lanthanum and thorium compounds from monazite II, *J. Appl. Chem. (London)*, 2: 265–273.
Pin, C. and Joannon, S. (1997) Low-level analysis of lanthanides in eleven silicate rock reference materials by ICP-MS after group separation using cation-exchange chromatography, *Geostand. Geoanal. Res.*, 21(1): 43–50.
Plusa, D., Slusarek, B., Dospial, M., Kotlarczyk, U. and Mydlarz, T. (2006) Magnetic properties ofanisotropic Nd–Fe–B resin bonded magnets, *J. Alloys Compd.*, 423(1–2): 81–83.
Poirer, R.H., Calkins, G.D., Lutz, G.A. and Bearse, A.E. (1958) Ion exchange separation of uranium from thorium, *Ind. Eng. Chem.*, 50: 613–616.
Porob, D.G., Srivastava, A.K., Nammalwar, P.K., Ramachandran, G. and Ann, H. (2012) Rare earth recovery from fluorescent material and associated method. U.S. Patent 8,137,645.
Pöttgen, R., Lang, A., Hoffmann, R.-D., Künnen, B., Kotzyba, G., Müllmann, R., Mosel, B.D. and Rosenhahn, C. (1999) The Stannides YbPtSn and Yb2Pt3Sn5, *Z. Kristallogr.*, 214: 143–150.
Potts, P.J. (1997) Geoanalysis: past, present and future, *R. Soc. Chem.*, 122(11): 1179–1186.
Pourmand, A. and Dauphas, N. (2010) Distribution coefficients of 60 elements on TODGA resin: Application to Ca, Lu, Hf, U and Th isotope geochemistry, *Talanta*, 81(3): 741–753.
Pourmand, A., Dauphas, N. and Ireland, T.J. (2012) A novel extraction chromatography and MC-ICP-MS technique for rapid analysis of REE, Sc and Y: Revising CI-chondrite and Post-Archean Australian Shale, (PAAS) abundances, *Chem. Geol.*, 291: 38–54.
Powell, A.R. (1939) Treatment of rare earth minerals, British Patent 510,198.
Powell, A.R. (1957) Discussion on the paper: The extraction of thorium from monazite. In *Extraction and Refining of the Rarer Metals*, pp. 376–379, The Institution of Mining and Metallurgy, London.
Powell, J.E. (1961) Separation of rare earths by ion exchange. In Spedding, F.H. and Daane, A.H. (eds.), *The Rare Earths*, John Wiley, New York.
Powell, J.E. (1964) The separation of rare earths by ion exchange. In Eyring, L. (ed.), *Progress in the Science and Technology of Rare Earths*, Vol. 1, pp. 62–84, Pergamon, Oxford.
Powell, J.E. (1979) Separation chemistry. In Gschneidner, Jr., K.A. and Eyring, L. (eds.), *Handbook on the Physics and Chemistry of Rare Earths*, Vol. 3, pp. 81–110, North Holland, Amsterdam.
Powell, J.E. and Spedding, F.H. (1956) Basic principles involved in the macro separation of adjacent rare earths from each other by means of ion exchange, U.S. Atomic Energy Commission Report ISC-857, National Technical Information Service, Springfield, VA.
Powell, J.E. and Spedding, F.H. (1959a) Basic principles involved in the macroseparation of adjacent rare earths from each other by means of ion exchange, *Chem. Eng. Prog. Symp. Ser.*, 55(24): 101–113.

Powell, J.E. and Spedding, F.H. (1959b) The separation of rare earths by ion exchange, *Trans. AIME*, 215: 457–463.

Pradip (1981) The surface properties and flotation of rare-earth minerals, pp. 1–225, Department of Materials Science and Mineral Engineering. University of California, Berkeley, Berkeley.

Pradip, K. and Fuerstenau, D.W. (1988) Alkyl hydroxamates as collectors for the flotation of bastnasite rare earth ores. In Bautista, R.G. and Wong, M.M. (eds.), *Rare Earths*, pp. 57–70, The Minerals, Metals and Materials Society, Warrendale, PA.

Preston, J.S. (1994) Solvent extraction of the trivalent lanthanides and yttrium by some 2-bromoalkanoic acids. *Solvent Extraction and Ion Exchange*, 12(1): 29–54.

Preston, J.S. (1996) The recovery of rare earth oxides from a phosphoric acid byproduct. Part 4: The preparation of magnet-grade neodymium oxide from the light rare earth fraction, *Hydrometallurgy*, 42: 151–167.

Preston, J.S. and Du Preez, A.C. (1988) The solvent extraction of cobalt, nickel, zinc, copper, calcium, magnesium and the rare earth metals by organophosphorus acids, Mintek Report M 378, 30 pp., Mintek, Randburg, South Africa.

Preston, J.S. and Du Preez, A.C. (1990) Solvent extraction processes for the separation of rare earth metals. In Sekine, T. (ed.), *Solvent Extraction*, pp. 883–894, Elsevier, Amsterdam.

Preston, J.S. and du Preez, A.C. (1994) Solvent extraction of the trivalent lanthanides and yttrium bv mixtures of 3,5-diisopropylsalicylic acid and neutral organo phosphorous compounds. *Journal of Chemical Technology and Biotechnology* 60: 317–325.

Preston, J.S. and Du Preez, A.C. (1996) The separation of europium from a middle rare earth concentrate by combined chemical reduction, precipitation and solvent-extraction methods, *J. Chem. Technol. Biotechnol.*, 65: 93–101.

Preston, J.S., Du Preez, A.U., Cole, P.M. and Fox, M.H. (1996a) The recovery of rare earth oxides from a phosphoric acid byproduct. Part 2: The preparation of high purity cerium dioxide and recovery of a heavy rare earth oxide concentrate, *Hydrometallurgy*, 42: 21–44.

Preston, J.S., Du Preez, A.C., Cole, P.M. and Fox, M.H. (1996b) The recovery of rare earth oxides from a phosphoric acid by-product. Part 3. The separation of the middle and light rare earth fractions and the preparation of pure europium oxide, *Hydrometallurgy*, 42: 131–149.

Preston, J.S., Cole, P.M., Craig, W.M. and Feather, A.M. (1996c) The recovery of rare earth oxides from a phosphoric acid byproduct. Part 1: Leaching of rare earth values and recovery of a mixed rare earth oxide by solvent extraction, *Hydrometallurgy*, 41: 1–19.

Provazi, K., Campos, B.A., Espinosa, D.C.R. and Tenorio, J.A.S. (2011) Metal separation from mixed types of batteries using selective precipitation and liquid–liquid extraction techniques, *Waste Manage.*, 31: 59–64.

Pungrassami, T. and Sanguansai, P. (1991) An overview on rare earth mineral resources/reserves of active tin mines in Thailand. In Siribumrungsukha, B., Arrykul, S., Sanguan Sai, P., Pungrassami, T., Sikong, L. and Kooptarnon, K. (eds.), *Proc. Int. Conf. Rare Earth Minerals and Minerals for Electronic Uses, Hat Yai, Thailand*, January, pp. 557–575, Prince of Songkla University, Thailand.

Qiu, L.F., Kang, X.H. and Wang, T.S. (1991) A study on photochemical separation of rare earths: The separation of europium from an industrial concentrate material of samarium, europium, and gadolinium, *Sep. Sci. Technol.*, 26: 199–221.

Qiu, T., Fang, X., Cui, L. and Fang, Y. (2008) Behavior of leaching and precipitation of weathering crust ion-absorbed type by magnetic field, *J. Rare Earths*, 26: 274–278.

Rabah, M.A. (2008) Recyclables recovery of europium and yttrium metals and some salts from spent fluorescent lamps, *Waste Manage.*, 28: 318–325.

Rabatin, J.G. (1981) Rare earth x-ray phosphors for medical radiography. In Gschneidner, Jr., K.A. (ed.), *Industrial Applications of Rare Earth Elements*, pp. 203–218, ACS Symposium Series 164, American Chemical Society, Washington, DC.

Rabie, K.A. (2007) A group separation and purification of Sm, Eu and Gd from Egyptian beach monazite mineral using solvent extraction, *Hydrometallurgy*, 85: 81–86.
Radeke, K.H., Riedel, V., Weiss, E., Kussin, P., Gosse, I. and Reimer, B. (1998) Studies on the fluorescent recycling, *Chem. Technik*, 50(3): 126–129.
Radtke, S.F. and Herrschaft, D.C. (1983) Role of misch metal in galvanizing with a Zn–5%Al alloy, *J. Less Common Metals*, 93: 253–259.
Raslan, M.F. (2009) Mineralogical and minerallurgical characteristics of samarskite-Y, columbite and zircon from stream sediments of the Ras Baroud Area, Central Eastern Desert, Egypt, *Studia i Materialy*, 128(36): 179–194.
Reddy, M.L.P., Rao, P. and Damodarm, A.D. (1995) Liquid–liquid extraction processes for the separation and purification of rare earths, *Miner. Process. Extr. Metall. Rev.*, 12: 91–113.
Reed, T.B. (1961) Induction-coupled plasma torch, *J. Appl. Phys.*, 32: 821–824.
Reed, S.J.B. (1984) Secondary ion mass spectrometry/ion probe microanalysis for rare earths, *Scanning Electron. Microsc.*, 2: 529–535.
Reed, R. (2007) *Thorium & Rare Earth Reserves of Thorium Energy, Inc., Lemhi Pass Idaho and Montana*, 12 pp, Idaho Engineering & Geology, Inc., Boise, ID.
Reed, R. and Gillerman, V. (2008) Thorium and rare earths in the Lemhi Pass region, Idaho: Society for Mining, Metallurgy, and Exploration Inc. 60.10 U.S. Geological Survey Minerals Yearbook—2007 Meeting and Exhibit, Salt Lake City, UT, February 26, 2008, Presentation.
Reed, J.B., Hopkins, B.S. and Audrieth, L.F. (1935) Observations on the rare earths XLIV. Preparation of anhydrous rare earth compounds by the action of fused and solid "orium" salts on the oxides, *J. Am. Chem. Soc.*, 57: 1159–1160.
Reed, J.B., Hopkins, B.S. and Audrieth, L.F. (1939) Anhydrous rare earth chlorides. In Booth, H.S. (ed.), *Inorganic Syntheses*, Vol. 1, McGraw Hill, New York.
Resende, L.V. and Morais, C.A. (2010) Study of the recovery of rare earth elements from computer monitor scraps—Leaching experiments, *Miner. Eng.*, 23: 277–280.
Revel, G., Rouchand, J.C. and Pastol, J.L. (1974) Preparation and neutron activation analysis of high purity cerium. In Haschke, J. and Eick, H.E. (eds.), *Proc. 11th Rare Earth Research Conf., Traverse City, MI*, Conf.-741002, Part 2, pp. 602–612, National Technical Information Service, Springfield, VA.
RIC Insight (1990) 3 (1, 6, 12), Rare Earth Information Center, Ames Lab., Ames, IA.
RIC News (1993) XXVII (2), Rare Earth Information Center, Ames Lab., Ames, IA.
RIC News (1995) XXX (3), Rare Earth Information Center, Ames Lab., Ames, IA.
RIC News (1997) XXXII (1), Rare Earth Information Center, Ames Lab., Ames, IA.
Rice, A.C. (1959) Preparation of rare earth chloride solutions, Bureau of Mines Report of Investigations 5540, U.S. Department of the Interior, Washington, DC.
Rice, A.C. and Stone, C.A. (1962) Amines in liquid–liquid extraction of rare earth elements, Bureau of Mines Report of Investigations 5923, U.S. Department of the Interior, Washington, DC.
Richardson, F.D. and Jeffes, J.H.E. (1948) The thermodynamic of substances of interest in iron and steel making from 0 to 2400°C. I. Oxides, *J. Inn Steel Inst. (London)*, 160: 261–270.
Riker, L.W. (1981) The use of rare earths in glass compositions. In Gschneidner, Jr., K.A. (ed.), *Industrial Applications of Rare Earth Elements*, pp. 81–94, ACS Symposium Series 164, American Chemical Society, Washington, DC.
Ritcey, G.M. (2006) Solvent extraction in hydrometallurgy: Present and future, *Tsinghua Sci. Technol.*, 11(2): 137–152.
Ritcey, G.M. and Ashbrook, A.W. (1979) *Solvent Extraction: Principles and Applications to Process Metallurgy, Part 2*, Elsevier, Amsterdam.
Ritcey, G.M. and Ashbrook, A.W. (1984) *Solvent Extraction: Principles and Applications to Process Metallurgy, Part I*, Elsevier, Amsterdam.

Ritcey, G.M. and Pouskouleli, G. (1987) Non nuclear hydrometallurgical applications of TBP. In Schulz, W.W., Navratil, J.D. and Ben, T. (eds.), *Science and Technology of Tributyl Phosphate*, Vol. 2, Part A, pp. 65–121, CRC Press, Boca Raton, FL.

Robertson, D.S. and Steenland, N.C. (1960) On the Blind River uranium ores and their origin. *Economic Geology*, 55(4): 659–694.

Robinson, P., Townsend, A.T., Yu, Z. and Münker, C. (1999) Determination of scandium, yttrium and rare earth elements in rocks by high resolution inductively coupled plasma–mass spectrometry, *Geostand. Geoanal. Res.*, 23(1): 31–46.

Robjohns, N. (1989) Rare earths, *Min. Ann. Rev.*, C83–C84.

Rodewald, U.Ch., Chevalier, B. and Pöttgen, P. (2007) Rare earth–transition metal–magnesium compounds—An overview, *J. Solid State Chem.*, 180: 1720–1736.

Rodrigue, S L.E.O.C. and Mansur, M.B. (2010) Hydrometallurgical separation of rare earth elements cobalt and nickel from spent nickel–metal-hydride batteries, *J. Power Sources*, 195: 3735–3741.

Ronda, C.R. (1995) Phosphors for lamps and displays—An applicational view, *J. Alloys Compd.*, 225: 534–538.

Ronda, C.R., Kynast, U.H., Dingen, W.P.M. and Van Hal, H.A.M. (1993) Optimizing bY_2SiO_5:Tb for projection television applications, *J. Alloys Compd.*, 192: 55–56.

Rosenblum, S. and Brownfield, I.K. (1999) Magnetic susceptibilities of minerals—Report for U.S. Geological Survey, pp. 1–33.

Rosynek, M.P. (1977) Catalytic properties of rare earth oxides, *Catal. Rev. Sci. Eng.*, 16: 111–154.

Roy Choudhuri, P. (1995) Determination of rare earth elements and yttrium in silicate rocks by inductively coupled plasma–atomic emission spectrometry after cation exchange column separation. In *Proc. Seminar on Recent Developments in the Science and Technology of Rare Earths*, December 14–16, p. 143, Cochin.

Ru'an, C. (1988) Extraction of rare earths from a low-grade, kaolinitic ore by percolation leaching. In Bautista, R.G. and Wong, M.M. (eds.), *Rare Earths: Extraction, Preparation and Applications*, pp. 227–234, The Minerals, Metals and Materials Society, Warrendale, PA.

Ryason, P.R. (1977) Solar photolysis of water, U.S. Patent 4,105,517.

Rydberg, J., Cox, M., Musikas, C. and Choppin, G.R. (2004) *Solvent Extraction Principles and Practice*, Marcel Dekker, New York.

Sabot, J.L. and Maestro, P. (1995) Lanthanides. In Kroschwitz, J.I. and Grant, M.H. (eds.), *Kirk-Othmer Encyclopedia of Chemical Technology*, 4th edn, Vol. 14, pp. 1091–1115, John Wiley, New York.

Sabot, J.L. and Rollat, A. (1985) Process for separating rare earths by liquid–liquid extraction, EU Patent EP0156735.

Sagawa, M. and Hirosawa, S. (1988) Magnetic hardening mechanism in sintered R–Fe–B permanent magnets, *J. Mater. Res.*, 3(1): 45–54.

Sagawa, M. and Nagata, H. (1993) Novel processing technology for permanent magnets, *IEEE Trans. Mag.*, 29(6): 2747–2751.

Sagawa, M., Fujimura, S., Yamamoto, H. and Matsuura, Y. (1984a) New material for permanent magnets on a base of Nd and Fe, *J. Appl. Phys.*, 55: 2083–2087.

Sagawa, M., Fujimura, S., Yamamoto, H. and Matsuura, Y. (1984b) Permanent magnet materials based on the rare earth–iron–boron tetragonal compounds, *IEEE Trans. Magn.*, MAG-20: 1584–1589.

Sagawa, M., Fujimura, S., Yamamoto, H., Matsuura, Y. and Hirosawa, S. (1985) Magnetic properties of rare earth iron boron permanent magnets, *J. Appl. Phys.*, 57: 4094–4096.

Sagawa, M., Hirosawa, S., Tokuhaara, K., Yamamoto, H., Fujimura, S., Tsubokawa, Y. and Shimitzu, R. (1987a) Dependence of coercivity on the anisotropy field in the $Nd_2Fe_{14}B$ type sintered magnets, *J. Appl. Phys.*, 61: 3559–3561.

Sagawa, M., Hirosawa, S., Yamamoto, H., Fujimura, S. and Matsuura, Y. (1987b) Nd–Fe–B permanent magnet materials, *Jap. J. Appl. Phys.*, 26: 785–800.

Saguchi, A., Asabe, K., Fukuda, T., Takahashi, W. and Suzuki, R.O. (2006) Recycling of rare earth magnet scraps: Carbon and oxygen removal from Nd magnet scraps, *J. Alloys Compd.*, 408–412: 1377–1381.

Saito, T. and Motegi, T. (2004) Extraction of Tb from Tb–Fe alloys by the glass slag method, *Scripta Mater.*, 51: 1069–1073.

Saito, T., Sato, H. and Motegi, T. (2003a) Extraction of rare earth from La–Ni alloys by the glass slag method, *J. Mater. Res.*, 18: 2814–2819.

Saito, T., Sato, H., Ozawa, S. and Motegi, T. (2003b) The extraction of Sm from Sm–Co alloys by the glass slag method, *Mater. Trans.*, 44: 637–640.

Saito, T., Sato, H., Ozawa, S., Yu, J. and Motegi, T. (2003c) The extraction of Nd from waste Nd–Fe–B alloys by the glass slag method, *J. Alloys Compd.*, 353: 189–193.

Saito, T., Sato, H. and Motegi, T. (2005a) Extraction of Sm from Sm–Fe alloys by the glass slag method, *J. Alloys Compd.*, 387: 274–278.

Saito, T., Sato, H., Motegi, T. and Kobayashi, K. (2005b) Extraction of Sm from Sm–Fe–N magnets by the glass slag method, *J. Alloys Compd.*, 403: 341–344.

Saito, T., Sato, H. and Motegi, T. (2006) Recovery of rare earths from sludges containing rare earth elements, *J. Alloys Compd.*, 425: 145–147.

Saleh, M.I., Bari, M.F. and Saad, B. (2002) Solvent extraction of lanthanum(III) from acidic nitrate–acetato medium by Cyanex 272 in toluene, *Hydrometallurgy*, 63: 75–84.

Samcode (2009) Available at http://www.samcode.co.za/downloads/SAMREC2009.pdf.

Sandhage, K., Masur, L.J., Smith, G.D., Poole, J.M. and McKimpson, M.G. (1991) The metallic precursor approach to long lengths of YBa_2Cu3O_{7-x} superconducting wire. In Whang, S., Dasgupta, A. and Collings, E. (eds.), *High Temperature Superconducting Compounds III*, pp. 347–362, TMS, Warrendale, PA.

Santhi, P.B., Reddy, M.L.P., Ramamohan, T.R. and Damodaran, A.D. (1991) Liquid–liquid extraction of yttrium(III) with mixtures of organophosphorous extractants: Theoretical analysis of extraction behavior, *Hydrometallurgy*, 27: 169–177.

Santos, R., Yan, W., Huang, W. and Thaumaturgo, C. (1999) Extraction behavior and simulation of rare earths in phosphonic acid systems, *Sep. Sci. Technol.*, 34(15): 3077–3097.

Sanuki, S., Sugiyama, A., Kadomachi, K., Miyata, K. and Arai, K. (1995) Recovery of metal values from Sm-Co magnets scrap, *J. Japan Inst. Metals*, 59: 169–176.

Sasaki, Y., Zhu, Z.X., Sugo, Y. and Kimura, T. (2007) Extraction of various metal ions from nitric acid to n-dodecane by diglycolamide (DGA) compounds, *J. Nucl. Sci. Technol.*, 44(3): 405–409.

Sato, T. (1989) Liquid–liquid extraction of rare-earth elements from aqueous acid solutions by acid organophosphorous compounds, *Hydrometallurgy*, 22: 121–140.

Sato, M., and Kato, K. (2010) *Chem. Eng.*, 2010(5): 334.

Sato, N., Wei, Y., Nanjo, M. and Tokuda, M. (1997) Recovery of samarium and neodymium from rare earth magnet scraps by fractional crystallization. Fundamental study on the recycling of rare earth magnet (2nd report), *J. MMIJ*, 113(12): 1082–1086.

Sauerwald, F. (1947) The magnesium–zirconium composition diagram, *Z. Anorg. Allgem. Chem.*, 255: 212–220.

Scaife, D.E. and Wylie, A.W. (1958) A carbide–iodide process for high purity thorium. In Preprint of Paper A/CONF 15/P/1098 presented at the Second United Nations International Conference on Peaceful Uses of Atomic Energy, United Nations, Geneva.

Schiffmacher, G. and Trombe, F. (1969) Preparation du dysprosium metallique par reduction de son oxyde alaide du thorium, *C. R. Acad. Sci.*, 268: Ser. C, (2): 159–162.

Schmidt, F.A. and Carlson, O.N. (1974) Method for preparing scandium metal, U.S. Patent 3,846,121.

Schmidt, F.A., Peterson, D.T. and Wheelock, J.T. (1986) Preparations of rare earth-iron alloys by thermite reduction, U.S. Patent 4,612,047.

Schnitzke, K., Schultz, L. and Wecker, J. (1990) High coercivity in Sm, Fe, N, magnets, *Appl. Phys. Lett.*, 57(26): 2853–2855.

Schuler, D., Buchert, M., Liu, R., Dittrich, S. and Merz, C. (2011) *Study on Rare Earths and Their Recycling*, Oeko-Institut e.V, Darmstadt, Germany.

Schultz, L., Schnitzke, K. and Wecker, J. (1989) Preparation and properties of mechanically alloyed rare earth permanent magnets, *J. Magn. Magn. Mater.*, 80: 115–118.

Schulze, K.K. (1981) Preparation and characterisation of ultrahigh purity niobium, *J. Metals*, 33(5): 33–42.

Schumacher, E. and Harris, J. (1926) Investigations of the thermoionic properties of rare earth elements, *J. Am. Chem. Soc.*, 48: 3108–3114.

Schumacher, E. and Lucas, F. (1924) Photomicrographic evidence of the crystal structure of pure cerium, *J. Am. Chem. Soc.*, 46: 1167–1169.

Seeger, C. (2008) REE potential of the Pea Ridge Fe–REE–Au deposit: Society for Mining, Metallurgy, and Exploration Inc. Meeting and Exhibit, February 26, Presentation, Salt Lake City, UT.

Seith, W. and Wever, H. (1953) A new effect in the electrolytic transfer in solid alloys, *Z. Elektrochem.*, 57: 891–900.

Sen Gupta, J.G. (1976) Determination of lanthanides and yttrium in rocks and minerals by atomic absorption and flame emission spectrometry, *Talanta*, 23: 343–348.

Sen Gupta, J.G. (1984) Determination of scandium, yttrium and lanthanides in silicate rocks and four new Canadian iron formation reference materials by flame atomic absorption spectrometry with microsample injection, *Talanta*, 31: 1045–1051.

Sen Gupta, J.G. (1985) Determination of scandium, yttrium and lanthanides in silicate rocks and four new geological reference materials by electrothermal atomization from graphite and tantalum surfaces, *Talanta*, 32: 1–6.

Seon, F. and Barthole, G. (1986) Process for the Electrolytic Preparation of Rare-Earth Elements or Their Alloys, and Apparatus for Carrying Out the Process. *Ausz. Eur. Patentanmeld. I*, 2(24): 1166.

Sepehri-Amin, H., Ohkubo, T., Nishiuchi, T., Hirosawa, S. and Hono, K. (2010) Coercivity enhancement of hydrogenation–disproportionation–desorption–recombination processed Nd–Fe–B powders by the diffusion of Nd–Cu eutectic alloys, *Scripta Mater.*, 63(11): 1124–1127.

Setlur, A.A. (2009) *Phosphors for LED-Based Solid-State Lighting*, The Electrochemical Society Interface, Winter, pp. 32–36.

Sharma, R.A. (1987) Neodymium production processes, *J. Metals*, 39(2): 33–37.

Sharma, R.A. and Seefurth, R.N. (1988a) A molten salt process for producing neodymium iron alloys by reduction of Nd_2O_3 with sodium. In Bautista, R.G. and Wong, M.M. (eds.), *Rare Earths*, pp. 355–368, The Minerals, Metals and Materials Society, Warrendale, PA.

Sharma, R.A. and Seefurth, R.N. (1988b) Metallothermic reduction of Nd_2O_3 with Ca in $CaCl_2$–NaCl melts, *J. Electrochem. Soc.*, 135: 66–71.

Shastri, L.V., Mittal, J.P., Krishnan, N.P.K. and Murthy, T.K.S. (1988) Development of a photochemical route for upgrading europium from aqueous lanthanide mixtures. In Gupta, C.K. and Krishnan, T.S. (eds.), *Rare Earths—Applications and Technology*, pp. 57–60, Trans Tech Publications, Switzerland.

Shaw, V.E. (1959) Extraction of yttrium and rare earth elements from Arizona euxenite concentrate, Bureau of Mines Report of Investigations 5544, U.S. Department of the Interior, Washington, DC.

Shaw, V.E. and Bauer, D.J. (1959) Extraction and separation of rare earth elements Idaho euxenite concentrate, Bureau of Mines Report of Investigations 6577, U.S. Department of the Interior, Washington, DC.

Shaw, S. and Constantinides, S. (2012) Permanent magnets: The demand for rare earths. In *8th International Rare Earths Conference*, November 13–15, Toronto.

Shaw, K.G., Smutz, M. and Bridger, G.L. (1954) A process for separating thorium compounds from monazite sands, U.S. Atomic Energy Commission Report ISC-407, National Technical Information Service, Springfield, VA.

Shedd, E.S., Marchant, J.D. and Henrie, T.A. (1964) Continuous electrowinning of cerium metal from cerium oxides, Bureau of Mines Report of Investigations 6362, U.S. Department of the Interior, Washington, DC.

Shedd, E.S., Marchant, J.D. and Henrie, T.A. (1966) Electrowinning and tapping of lanthanum metal, Bureau of Mines Report of Investigations 6882, U.S. Department of the Interior, Washington, DC.

Shedd, E.S., Marchant, J.D. and Wong, M.M. (1970) Electrowinning misch metal from a treated bastnasite concentrate, Bureau of Mines Report of Investigations 7398, U.S. Department of the Interior, Washington, DC.

Sherer, R.L. (1990). Pajarito yttrium-zirconium deposit, Otero County, New Mexico. *New Mexico Geology*, 12: 21.

Sheridan, R.S., Sillitoe, R., Zakotnik, M., Harris, I.R. and William, A.J. (2012) Anisotropic powder from sintered Nd–Fe–B magnets by the HDDR processing route, *J. Magn. Magn. Mater*, 324: 63–67.

Sherrington, L. (1983) Commercial processes for rare earths and thorium. In Lo, T.C., Baird, M.H. and Hanson, C. (eds.), *Handbook of Solvent Extraction*, pp. 712–723, Wiley, New York.

Shi, H., Han, S., Jia, Y., Liu, Y., Zhao, X. and Liu, B. (2013) Investigations on hydrogen storage properties of $LaMg_{8.52}Ni_{2.23}M_{0.15}$ (M = Ni, Cu, Cr) alloys, *J. Rare Earths*, 31(1): 79–84.

Shibata, J. (1991) Solution chemistry and separation of metal ions in leached solution. In Siribumrungsukha, B., Arrykul, S., Sanguan Sai, P., Pungrassami, T., Sikong, L. and Kooptarnon, K. (eds.), *Proc. Int. Conf. Rare Earth Minerals and Minerals for Electronic Uses, Hat Yai, Thailand*, January, pp. 365–377, Prince of Songkla University, Thailand.

Shigeta, K., Kikuchi, T. and Furuya, K. (1986) Vacuum fusion determination of oxygen in gadolinium, terbium metal and iron-terbium alloy. *Microchimica Acta*, 90(3–4): 215–224.

Shimizu, R., Sawada, K., Enokida, Y. and Yamamoto, I. (2005) Supercritical fluid extraction of rare earth elements from luminescent material in waste fluorescent lamps. *The Journal of supercritical fluids*, 33(3): 235–241.

Shimoda, T., Akioka, K., Kobayashi, O. and Yamagami, T. (1988) High energy cast Pr–Fe–B magnets, *J. Appl. Phys.*, 64: 5290–5292.

Shimojo, K., Naganawa, H., Noro, J., Kubota, F. and Goto, M. (2007) Extraction behavior and separation of lanthanides with a diglycol amic acid derivative and a nitrogen-donor ligand, *Anal. Sci.*, 23(12): 1427–1430.

Shirayama, S. and Okabe, T.H. (2008) In *Proceeding of Annual Meeting of MMIJ*, March 27–29, Vol. II, pp. 69–70, The Mining and Materials Processing Institute of Japan, Tokyo.

Shirayama, S. and Okabe, T. (2009) Selective extraction of Nd and Dy from rare earth magnet scrap into molten salt. In Mishra, B., Fuma, A. and Bhandhubanyong, P. (eds.), *The Minerals, Metals and Materials Society—3rd International Conference on Processing Materials for Properties 2008*, Vol. 1, pp. 469–474, Curran Associates, Inc., New York.

Simandl, G.J. (2012) Geology and economic significance of current and future rare earth element sources. In Goode, J.R., Moldoveanu, G. and Rayat, M.S. (eds.), *Conference of Metallurgists 2012—Rare Earths*, pp. 15–30, Met Soc, Niagara Falls, ON, Canada.

Singer, R., Airey, H., Grimmett, L., Leech, H. and Bennett, R. (1945) The cerium industry in German territory including reports on radium and mesothorium, British Intelligence Subcommittee, Final Report 400, Item 21, pp. 1–118.

Singh, S.S. (1988) Rare earths in laser technology. In Gupta, C.K. and Krishnan, T.S. (eds.), *Rare Earths—Applications and Technology*, pp. 155–172, Trans Tech Publications, Switzerland.

Singh, D.K., Singh, H. and Mathur, J.N. (2006) Extraction of rare earths and yttrium with high molecular weight carboxylic acids, *Hydrometallurgy*, 81: 174–181.

Sklyarenko, S.I. and Sakharov, B.A. (1940) The electrochemical preparation of cerium amalgam, *J. Appl. Chem. USSR*, 13: 841–845.

Skorovarov, J.I., Kosynkin, V.D., Moiseev, S.D. and Rura, N.N. (1992) Recovery of rare earth elements from phosphorites in the USSR, *J. Alloys Compd.*, 180(1–2): 71–76.

Slusarek, B., Dlugiewicz, L., Gawrys, P. and Przybylski, M. (2005) Layered Nd–Fe–B dielectromagnets. In *Proceedings of EURO PM2005 Powder Metallurgy International Conference & Exhibition, Prague*, October 2–5, pp. 481–486, Czech Republic.

Slusarek, B., Gawrys, P. and Przybylski, M. (2007) The influence of temperature on mechanical properties of Nd–Fe–B dielectromagnets. In *Proceedings of the EURO PM2007, Powder Metallurgy International Conference & Exhibition*, October 15–17, pp. 365–370, Toulouse, France.

Smiley, W. (1958) Oxygen Determinations Using a Platinum Bath and Capillary Trap. In *Symposium on Determination of Gases in Metals*., January, ASTM International.

Smith, H.R. (1958) Electron bombardment melting techniques. In Bunshah, R.F. (ed.), *Vacuum Metallurgy*, pp. 221–235, Reinhold, New York.

Smith, M.P. and Henderson, P. (2000) Preliminary fluid inclusion constraints on fluid evolution in the Bayan Obo Fe–REE–Nb deposit, Inner Mongolia, China, *Econ. Geol.*, 95: 1371–1388.

Smith, H.R., Hunt, C. d'A. and Hanks, C.W. (1959) Electron bombardment melting, *J. Metals*, 11(2): 112.

Smutz, M. (1956) In F.R. Bruce et al. (eds.), *Progress in Nucl. Energy*, Ser. 3, Vol. 1, Process Chemistry, pp. 36–39, McGraw Hill, New York.

Smutz, M., Bridger, G.L., Shaw, K.G. and Whatley, M.E. (1954) The Ames process for separation of monazite, *Chem. Eng. Prog. Symp. Ser., No. 13*, 50: 167–170.

Sokolnicki, J. (2013) Rare earths (Ce, Eu, Tb) doped $Y_2Si_2O_7$ phosphors for white LED, *J. Lumin.*, 134: 600–606.

Song, L., Wang, Y., Lin, W. and Liu, Q. (2008) Primary investigation of corrosion resistance of Ni–P/TiO_2 composite film on sintered NdFeB permanent magnet, *Surf. Coat. Technol.*, 202(21): 5146–5150.

Song, J., Yue, M., Zuo, J., Zhang, Z., Liu, W., Zhang, D., Zhang, J., Guo, Z. and Li, W. (2013) Structure and magnetic properties of bulk nanocrystalline Nd–Fe–B permanent magnets prepared by hot pressing and hot deformation, *J. Rare Earths*, 31(7): 674–678.

Sorensen, E. and Lundgaard, T. (1966) Selective flotation of steenstrupine and monazite from Kvanefjeld Lujavrite—Report for the Danish Atomic Energy Commission, Roskilde.

Soule, J.H. (1946) Exploration of Gallinas fluorspar deposits, Lincoln County, New Mexico, U.S. Bureau of Mines Report of Investigations 3854, Department of the Interior, Washington, DC.

Sousa-Aguiar, E.F., Trigueiro, F.E. and Zotin, F.M.Z. (2013) The role of rare earth elements in zeolites and cracking catalysts, *Catal. Today*, 218–219: 115–122.

Spassov, T., Rangelova, V. and Neykov, N. (2002) Nanocrystallization and hydrogen storage in rapidly solidified Mg–Ni–RE alloys, *J. Alloys Compd.*, 334(1–2): 219–223.

Spedding, F.H. (1978) Prologue. In Gschneidner, Jr., K.A. and Eyring, L. (eds.), *Handbook on the Physics and Chemistry of Rare Earths*, Vol. 1, pp. xv–xxv, North Holland, Amsterdam.

Spedding, F.H. (1982) Rare earth elements. In Grayson, M. and Eckroth, D. (eds.), *Kirk-Othmer Encyclopedia of Chemical Technology*, Vol. 19, pp. 833–854, Wiley, New York.

Spedding, F.H. and Daane, A.H. (1952) The preparation of rare earth metals, *J. Am. Chem. Soc.*, 74: 2783–2785.
Spedding, F.H. and Daane, A.H. (1954) Production of rare earth metals in quantity allows testing of physical properties, *J. Metals*, 6: 504–510.
Spedding, F.H. and Daane, A.H. (1956) The preparation and properties of rare earth metals. In Finniston, H.M. and Howe, J.P. (eds.), *Prog. Nucl. Energy Ser., 5*, Vol. 1, pp. 413–432, Pergamon, New York.
Spedding, F.H. and Daane, A.H. (eds.) (1961) *The Rare Earths*, John Wiley, New York.
Spedding, F.H. and Daane, A.H. (1968) Metallurgy Division Research and Development Report IS-1900, Ames Laboratory, USAEC, Iowa State University, Ames, Iowa, National Technical Information Service, Springfield, VA.
Spedding, F.H. and Henderson, D.C. (1971) High temperature heat contents and related thermodynamic functions of some trifluorides of the rare earths: Y, La, Pr, Nd, Gd, Ho, and Lu, *J. Chem. Phys.*, 54: 2476–2483.
Spedding, F.H. and Powell, J.E. (1954) A practical separation of yttrium group rare earths from gadolinium by ion exchange, *Chem. Eng. Prog. Symp. Ser.*, 50(14): 7–15.
Spedding, F.H., Fulmer, E.I., Butler, T.A., Gladrow, E.M., Gobush, M., Porter, P.E., Powell, J.E. and Wright, J.M. (1947) Separation of rare earths by ion exchange. III. Pilot plant separations, *J. Am. Chem. Soc.*, 69: 2812–2818.
Spedding, F.H., Wilhelm, H.A., Keller, W.H., Ahmann, D.H., Daane, A.H., Hach, C.C. and Ericson, R.P. (1952) Production of pure rare earth metals, *Ind. Eng. Chem.*, 44: 553–556.
Spedding, F.H., Powell, J.E. and Wheelwright, E.J. (1954) The use of copper as the retaining ion in the elution of rare earths with ammonium ethylene diamine tetraacetate solutions, *J. Am. Chem. Soc.*, 76: 2557–2560.
Spedding, F.H., Hanak, J.J. and Daane, A.H. (1958) The preparation and properties of europium, *Trans. AIME*, 212: 379–383.
Spedding, F.H., Gschneidner, Jr., K.A. and Daane, A.H. (1959) The lanthanum–carbon system, *Trans. Met. Soc. AIME*, 215: 192–197.
Spedding, F.H., Daane, A.H., Wakefield, G. and Dennison, D.H. (1960) Preparation and properties of high purity scandium metal, *Trans. Met. Soc. AIME*, 218: 608–611.
Spedding, F.H., Beaudry, B.J., Croat, J.J. and Palmer, P.E. (1968) The properties, preparation and handling of pure rare earth metals. In *Materials Technology—An Interamerican Approach*, p. 151, Am. Soc. Mech. Eng., New York.
Spedding, F.H., Beaudry, B.J., Croat, J.J. and Palmer, P.E. (1970) The preparation and properties of ultrapure metals. In Les Elements Des Terres Rares 1, p. 25, Centre National de la Recherche Scientifique, Paris. Also R&D Report IS-2283, Ames Laboratory, USAEC, May.
Staatz, M.H. (1972) Thorium-rich veins of Hall Mountain in northernmost Idaho. *Econ. Geol.*, 67(2): 240–248.
Staatz, M.H., Armbrustmacher, T.J., Olson, J.C., Brownfield, I.K., Brock, M.R., Lemons, Jr., J.F., Coppa, L.V. and Clingan, B.V. (1979) Principal thorium resources in the United States, U.S. Geological Survey Circular 805, 42 pp., USGS, Reston, VA.
Staatz, M.H., Hall, R.B., Macke, D.L., Armbrustmacher, T.J. and Brownfield, I.K. (1980) Thorium resources of selected regions in the United States, U.S. Geological Survey Circular 824, 32 pp., U.S.G.S., Reston, VA.
Stablein, H. (1982) Hard ferrites and plastiferries. In Wohlfarth, E.P. (ed.), *Ferromagnetic Materials*, Vol. 3, pp. 141–601, North Holland, Amsterdam.
Staggers, J.O. (1977) Rare earth metal silicide alloys, U.S. Patent 4,018,597.
Steinnes, E. (1973) Rare earth determination by neutron activation analysis. In Michelsen, O.B. (ed.), *Analysis and Application of Rare Earth Materials*, pp. 165–181, Universitetsforlaget, Oslo.

Stewart, D.C. and Kato, D. (1958) Analysis of rare earth mixture by recording spectrophotometer, *Anal. Chem.*, 30(2): 164–172.

Strnat, K.J. (1970) The recent development of permanent magnet materials containing rare earth metals, *IEEE Trans. Magn.*, 6(2): 182–190.

Strnat, K.J. (1978) Rare earth magnets in present production and development, *J. Magn. Magn. Mater.*, 7: 351–360.

Strnat, K.J. (1985) A review of rare earth permanent magnets, applications and prospects. In Xu, G. and Xiao, J. (eds.), *New Frontiers in Rare Earth Science and Application*, Vol. II, pp. 872–878, Science Press, Beijing.

Strnat, K.J. (1988) R–Co permanent magnets. In Buschow, K.H.J. (ed.), *Ferromagnetic Materials*, Vol. 4, pp. 131–209, North Holland, Amsterdam.

Strnat, K.J. (1990) Modern permanent magnets for applications in electrotechnology, *Proceedings of the IEEE*, 78(6): 1–35.

Strnat, K.J. and Strnat, R.M.W. (1991) Rare earth–cobalt magnets, *J. Magn. Magn. Mater.*, 100: 38–56.

Strnat, K.J., Olson, J.C. and Hoofer, G. (1968) Coercivity of misch metal–cobalt alloy powders, *J. Appl. Phys.*, 39: 1263–1265.

Strnat, K.J., Wong, K.M.D. and Blaettner, H. (1976) Bonded rare earth–cobalt permanent magnets. In Lundin, C.E. (ed.), *Proc. 12th Rare Earth Research Conference, Vail, CO*, July 18–22, pp. 31–40, University of Denver, Denver Research Institute, Denver, CO.

Strnat, R.M.W., Clarke, J.P., Leupold, H.A. and Tauber, A. (1987) Metal matrix magnets for new TWT applications, *J. Appl. Phys.*, 61: 3463–3465.

Sulaiman, M.F. (1991) An overview of the rare earth mineral processing industry in Malaysia. In Siribumrungsukha, B., Arrykul, S., Sanguan Sai, P., Pungrassami, T., Sikong, L. and Kooptarnon, K. (eds.), *Proc. Int. Conf. Rare Earth Minerals and Minerals for Electronic Uses, Hat Yai, Thailand*, January, pp. 389–395, Prince of Songkla University, Thailand.

Sun, Y.H., Wang, Z.C. and Guo, L. (1998) Mutual separation characteristics of neighbouring rare earth elements Nd, Sm, Eu and Gd using stepwise chlorination–chemical vapour transport. *Journal of Alloys and Compounds*, 269(1): 88–91.

Sun, J., Zeng, F.M., Li, J.L., Cao, Y.I., Wan, Y.C. and Liu, J.H. (2005) Synthesis of Nd:GGG ultrafine polycrystalline powders by sol–gel method, *J. Rare Earths*, 23(Suppl.): 188–190.

Sun, X., Wang, J., Li, D. and Li, H. (2006) Synergistic extraction of rare earths by mixture of bis(2,4,4 trimethylpentyl)phosphinic acid and sec-nonylphenoxy acetic acid, *Sep. Purif. Technol.*, 50: 30–34.

Suzuki, R.O., Saguchi, A., Takahashi, W., Yagura, T. and Ono, K. (2001) Recycling of rare earth magnet scraps: Part II Oxygen removal by calcium, *Mater. Trans.*, 42: 2492–2498.

Szabadvary, F. (1988) The history of the discovery and separation of the rare earths. In Gschneidner, Jr., K.A. and Eyring, L. (eds.), *Handbook on the Physics and Chemistry of Rare Earths*, Vol. 11, pp. 33–80, North Holland, Amsterdam.

Takahashi, T., Takano, A., Saitoh, T. and Nagano, N. (1999) Separation and recovery of rare earth elements from phosphors in waste fluorescent lamp (part III)—Separation and recovery of rare earth elements by multistage countercurrent extraction. In Reports of the Hokkaido Industrial Research Institute, No. 298, pp. 37–47.

Takahashi, T., Takano, A., Saitoh, T., Nagano, N., Hirai, S. and Shimakage, K. (2001a) Separation and recovery of rare earth elements from phosphor sludge in processing plant of waste fluorescent lamp by pneumatic classification and sulfuric acidic leaching, *J. MMIJ*, 117(7): 37–43.

Takahashi, T., Takano, A., Saitoh, T., Nagano, N., Hirai, S. and Shimakage, K. (2001b) In *Proceedings of the 6th International Symposium on East Asian Resources Recycling Technology (EARTH 2001)*, October 23–25, pp. 421–426, The Korean Institute of Resources Recycling, Seoul.

Takahashi, T., Takano, A., Saitoh, T. and Nagano, N. (2001c) Synthesis of rare earth phosphor from phosphor sludge in processing plant of waste fluorescent lamp. In Reports of the Hokkaido Industrial Research Institute, No. 300, pp. 1–8.

Takahashi, T., Takano, A., Saitoh, T. and Nagano, N. (2003) Separation and recovery of rare earth phosphor from phosphor sludge in waste fluorescent lamp by multistage countercurrent solvent extraction. In Reports of the Hokkaido Industrial Research Institute, No. 302, pp. 41–48.

Takahashi, T., Tomita, K., Sakuta, Y., Takano, A. and Nagano, N. (1996) Separation and recovery of rare earth elements from phosphors in waste fluorescent lamp (part II)—Separation and recovery of rare earth elements by chelate resin. In Reports of the Hokkaido Industrial Research Institute, No. 295, pp. 37–44.

Takaku, Y., Masuda, K., Takahashi, T. and Shimamura, T.J. (1993) Determination of trace impurity rare earth elements in high-purity rare earth element samples using high-resolution inductively coupled plasma mass spectrometry, *Anal. Atomic Spectrom.* 9: 687–690.

Takasaki, T., Nishimura, K., Saito, M., Fukunaga, H., Iwaki, T. and Sakai, T. (2013) Cobalt-free nickel–metal hydride battery for industrial applications, *J. Alloys Compd.*, 580 (Suppl. 1): S378–S381.

Takeda, O. and Okabe, T.H. (2011) Smelting and Recycling Technologies for Rare Earth Metals. *Journal of Japanese Society of Tribologists*, 56(8): 466–471.

Takeda, O., Okabe, T.H. and Umetsu, Y. (2004) Phase equilibrium of the system Ag–Fe–Nd, and Nd extraction from magnet scraps using molten silver, *J. Alloys Compd.*, 379: 305–313.

Takeda, O., Okabe, T.H. and Umetsu, Y. (2005) Phase equilibria of the system Fe–Mg–Nd at 1076 K, *J. Alloys Compd.*, 392: 206–213.

Takeda, O., Okabe, T.H. and Umetsu, Y. (2006) Recovery of neodymium from a mixture of magnet scrap and other scrap, *J. Alloys Compd.*, 408: 387–390.

Takeda, O., Nakano, K. and Sato, Y. (2009) Resource recovery from waste of rare earth magnet by utilizing fluoride molten salts, *Yooyuen oyobi Koon Kagaku*, 52: 63–70.

Takeshita, T. and Nakayama, R. (1989) Magnetic properties and microstructures of the NdFeB magnet powder produced by hydrogen treatment. In *Proceedings of the 10th International Workshop on Rare-Earth Magnets and Their Applications*, pp. 551–557, Kyoto, Japan.

Takeshita, T. and Nakayama, R. (1990) Nd-Fe-B anisotropic magnet powders produced by the HDDR process. In *Proceedings of the 11th Workshop on Rare Earth Magnets and Their Applications*, pp. 49–52, Pittsburg, CA.

Takeshita, T. and Morimoto, K. (1996) Anisotropic Nd–Fe–B bonded magnets made from HDDR powders, *J. Appl. Phys.*, 79(8): 5040–5044.

Tanaka, Y., Zhang, Q.W. and Saito, F. (2002) Sonochemical recovery of metals from recording media, *J. Chem. Eng. Jpn.*, 35: 173–177.

Tanaka, M., Sato, Y., Huang, Y., Narita, H. and Koyama, K. (2009) Separation of dysprosium and neodymium by solvent extraction–recycling of rare earth metals from neodymium magnet. In *Proceedings of the 10th International Symposium on East Asian Resources Recycling Technology (EARTH 2009)*, November 2–6, pp. 200–203, The Korean Institute of Resources Recycling, Seoul.

Tanaka, M., Oki, T., Koyama, K., Narita, H. and Oishi, T. (2013) Recycling of rare earths from scrap. In Bunzli, J.C.G. and Pecharsky, V.K. (eds.), *Handbook on the Physics and Chemistry of Rare Earths*, Vol. 43, pp. 159–212, Elsevier, Amsterdam.

Taniguchi, J.R., Doty, A.W. and Byers, C.H. (1988) Large scale chromatographic separation using continuous displacement chromatography. In Bautista, R.G. and Wong, M.M. (eds.), *Rare Earths*, pp. 147–161, The Minerals, Metals and Materials Society, Warrendale, PA.

Tao, S., Tian, J., Lu, X., Qu, X., Honkura, Y., Mitarai, H. and Noguchi, K. (2009) Anisotropic bonded NdFeB magnets with radial oriented magnetization by 2-step warm compaction process, *J. Alloys Compd.*, 477(1–2): 510–514.

Taylor, S.R. (1979) Trace element analysis of rare earth elements by spark source mass spectrometry. In Gschneidner, Jr., K.A. and Eyring, L. (eds.), *Handbook on the Physics and Chemistry of Rare Earths*, Vol. 4, pp. 359–376, North-Holland, Amsterdam.

Taylor, R.K.A. (1991) Australian rare earth resources for the electronics industry. In Siribumrungsukha, B., Arrykul, S., Sanguan Sai, P., Pungrassami, T., Sikong, L. and Kooptarnon, K. (eds.), *Proc. Int. Conf. Rare Earth Minerals and Minerals for Electronic Uses, Hat Yai, Thailand*, January, pp. 125–136, Prince of Songkla University, Thailand.

Technology Metals Research (TMR) (2014) Available at http://www.techmetalsresearch.com/metrics-indices/tmr-advanced-rare-earth-projects-index/ (accessed November 24, 2014).

Templeton, C.C. (1949) The distribution of rare earth nitrates between water and n-hexyl alcohol at 25°C, *J. Am. Chem. Soc.*, 71: 2187–2190.

Templeton, C.C. and Peterson, J.A. (1948) Fractionation of lanthanum and neodymium nitrates by solvent extraction, *J. Am. Chem. Soc.*, 70: 3967–3968.

Terziev, A.L. and Minkova, N.L. (1997) Regeneration of waste rare earth oxides, *Bulg. Chem. Commun.*, 29: 274–284.

Thakur, N.N. (2000) Separation of rare earths by solvent extraction. *Mineral Processing and Extractive Metallurgy Review*, 21(1–5): 277–306.

Thakur, N.V., Jayawant, D. V. and Koppiker, K. S. (1990) Separation of neodymium from its concentrate using 20% saponified di-(2-ethylhexyl) phosphoric acid in kerosene as an extactant. *Solvent Extraction 1990. A. (ISEC'90)*, 1003–1008.

The Explanation of Compiling Emission Standards of Pollutants from Rare Earths Industry 2009, Ministry of Environmental Protection, The People's Republic of China. Available at http:// www.mep.gov.cn.

Thomas, R. (1977) Rare earths: New production processes based on oxides. In Thomas, R. (ed.), *Operating Handbook of Mineral Processing*, McGraw Hill, New York.

Thompson, A. (1917) *Met. Chem. Eng.*, 17: 213.

Thompson, A. and Kremers, H.E. (1925) The preparation and properties of cerium free misch metal, *Trans. Am. Electrochem. Soc.*, 47: 345–352.

Thompson, A.P., Holte, W.B. and Kremers, H.E. (1926) The electrolytic preparation and some properties of metallic yttrium, *Trans. Am. Electrochem. Soc.*, 49: 277–289.

Thornton, W.A. (1981) Lamp phosphor. In Gschneidner, Jr., K.A. (ed.), *Industrial Applications of Rare Earth Elements*, pp. 195–201, ACS Symposium Series 164, American Chemical Society, Washington, DC.

Tian, J., Chi, R. and Yin, J. (2010) Leaching process of rare earths from weathered crust elution–deposited rare earth ore, *Trans. Nonferrous Metal Soc. China*, 20(5): 892–896.

Tian, M., Song, N., Wang, D., Quan, X., Jia, Q., Liao, W. and Lin, L. (2012) Applications of the binary mixture of sec-octylphenoxyacetic acid and 8-hydroxyquinoline to the extraction of rare earth elements, *Hydrometallurgy*, 111–112: 109–113.

Tian, M., Jia, Q. and Liao, W. (2013) Studies on synergistic solvent extraction of rare earth elements from nitrate medium by mixtures of 8-hydroxyquinoline with Cyanex 301 or Cyanex 302, *J. Rare Earths*, 31(6): 604–608.

Tirnh, X.B. (1991) Mineralogical characteristics of Nam Nam Xe rare earth deposit in Vietnam. In Siribumrungsukha, B., Arrykul, S., Sanguan Sai, P., Pungrassami, T., Sikong, L. and Kooptarnon, K. (eds.), *Proc. Int. Conf. Rare Earth Minerals and Minerals for Electronic Uses, Hat Yai, Thailand*, January, pp. 636–643, Prince of Songkla University, Thailand.

Tokunaga, M., Nozawa, Y., Iwasaki, K., Tanigawa, S. and Harada, H. (1989) Magnetic properties of isotropic and anisotropic Nd–Fe–B bonded magnets, *J. Magn. Magn. Mater.*, 80: 80–87.

Tong, S., Zhao, X., Song, N., Jia, Q., Zhou, W. and Liao, W. (2009) Solvent extraction study of rare earth elements from chloride medium by mixtures of sec-nonylphenoxy acetic acid with Cyanex301 or Cyanex302, *Hydrometallurgy*, 100: 15–19.

Tong, H., Wang, Y., Liao, W. and Li, D. (2013) Synergistic extraction of Ce(IV) and Th(IV) with mixtures of Cyanex 923 and organophosphorus acids in sulfuric acid media, *Sep. Purif. Technol.*, 118(30): 487–491.

Topp, N.E. (1965) *The Chemistry of Rare Earth Elements*, Elsevier, Amsterdam.

Tourre, J.M. (1998) Rare earths 1998 market update. In Preprints of the Conference, China Magnets, held on October 18–21, 1998 at Beijing, PR China.

Tran, T. (1991) New Developments in the Processing of Rare Earths. In Siribumrungsukha, B., Arrykul, S., Sanguan Sai, P., Pungrassami, T., Sikong, L. and Kooptarnon, K. (eds.), *Proc. Int. Conf. Rare Earth Minerals and Minerals for Electronic Uses, Hat Yai*, Thailand, January, pp. 337–353, Prince of Songkla University, Thailand.

Trombe, F. (1932) Preparation of metallic lanthanum free from iron and silicon, *Compt. Rend.*, 94: 1653–1655.

Trombe, F. (1933) Preparation du néodyme métallique exempt de fer et de silicium, *C. R. Acad. Sci.*, 196: 704–706.

Trombe, F. (1935) The isolation of gadolinium, *C. R. Acad. Sci.*, 200: 459–461.

Trombe, F. (1938) On the isolation of metallic europium, *C. R. Acad. Sci.*, 206: 1380–1383.

Trombe, F. (1945) On the isolation of metallic dysprosium, *C. R. Acad. Sci.*, 220: 603–604.

Trombe, F. (1953) The vapor pressures of the rare earth metals, their separation and purification, *Bull. Soc. Chim. Fr.*, 20: 1010–1012.

Trombe, F. (1957) Preparation of rare earth metals. In *Proc. Symp. Rare Metals, Bombay*, December, pp. 402–444, The Indian Institute of Metals and Bhabha Atomic Research Center.

Trombe, F. and Mahn, F. (1943) Preparation du cerium, du neodyme et du gadolinium metalliques a partir de leurs alliages avec le magnesium, *C. R. Acad. Sci.*, 217: 603–605.

Trombe, F. and Mahn, F. (1944) The preparation and thermal dissociation of alloys of magnesium with cerium, neodymium and gadolinium, *Ann. Chim.*, 19: 345–361.

Turner, H. (1998) Radiolanthanides in nuclear oncology. In *Rare Earths' 98*, Abstracts p. 27, Free Mantle, Western Australia.

Tzanetakis, N. and Scott, K. (2004a) Recycling of nickel–metal hydride batteries. I: Dissolution and solvent extraction of metals, *J. Chem. Technol. Biotechnol.*, 79: 919–926.

Tzanetakis, N. and Scott, K. (2004b) Recycling of nickel–metal hydride batteries. II: Electrochemical deposition of cobalt and nickel, *J. Chem. Technol. Biotechnol.*, 79(9): 927–934.

Uchida, H., Okuyama, I., Wada, M., Uchida, H.H., Matsumura, Y., Koeninger, V., Koike, U., Kamada, K., Kurino, T. and Kaneko, H. (1992) In *Proceedings of the International Symposium on Giant Magnetostrictive Materials and Their Applications*, November, p. 137, Adv. Machining Technology and Development Association, Tokyo.

Uchida, H., Wada, M., Ichikawa, A., Matsumura, Y. and Uchida, H.H. (1996) Effects of the preparation method and condition on the magnetic and giant magnetostrictive properties of the (Tb, Dy) Fe_2 thin films. In *Proceedings of ACTUATOR'96*, p. 275, Bremen, Germany.

Uchida, H., Wada, M., Uchida, H.H. and Kaneko, H. (1998) Microstructure and magnetostrictive property of Tb(0.3)Dy(0.7)Fe(2) thin film. In *Proceedings of the ACTUATORS'98*, pp. 367–371, Messe Bremen GmbH, Bremen, Germany.

Uchida, H., Matsumuraa, Y., Uchida, H. and Kaneko, H. (2002) Progress in thin films of giant magnetostrictive alloys, *J. Magn. Magn. Mater.*, 239: 540–545.

Uda, T. (2002) Recovery of rare earths from magnet sludge by $FeCl_2$, *Mater. Trans.*, 43: 55–62.

Uda, T. and Hirasawa, M. (2003) Rare earth separation and recycling process using rare earth chloride. In Kongoli, F., Itagaki, K.,Yamauchi, C. and Sohn, H.Y. (eds.), *Proc. Yazawa International Symposium on Materials Processing Fundamentals and New Technologies*, March 3–6, San Diego, pp. 373–385, John Wiley, New York.

Uda, T., Jacob, K.T. and Hirasawa, H. (2000) Technique for enhanced rare earth separation, *Science*, 289: 2326–2329.

UNEP (2011) Recycling rates of metals: A status report. ISBN No: 978-992-807-3161-3. United Nations Environment Programme.

USGS (1980) Principles of a resource/reserve classification for minerals, U.S. Geological Survey Circular 831, U.S. Geological Survey, Arlington, VA.

Van Arkel, A.E. and de Boer, J.H. (1925) Preparation of pure titanium, zirconium, hafnium and thorium metals, *Z. Anorg. Allgem. Chem.*, 148: 345.

Van den Bergh, F., Adams, F. and Hoste, J. (1970) Determination of rare earths in rare-earth concentrates by neutron activation analysis. *Journal of Radioanalytical and Nuclear Chemistry*, 4(2): 347–353.

van Gosen, B.S., Gillerman, V.S. and Armbrustmacher, T.J. (2009) Thorium deposits of the United States—Energy resources for the future?: U.S. Geological Survey Circular 1336, Arlington, VA. Available at http://pubs.usgs.gov/circ/1336/.

Van Loon, J.C., Galbrairh, J.H. and Aarden, H.M. (1971) The determination of yttrium, europium, terbium, dysprosium, holmium, erbium, thulium, ytterbium and lutetium in minerals by atomic absorption spectrometry, *Analyst*, 96: 47–50.

Van Vucht, T.H.N., Kuijpers, F.A. and Brunning, H.C.A.M. (1970) Reversible room temperature absorption of large quantities of hydrogen by intermetallic compounds, *Philips Res. Rep.*, 25: 133–140.

Vargaa, Z., Katonab, R., Stefánkab, Z., Walleniusa, M., Mayera, K. and Nicholla, A. (2010) Determination of rare-earth elements in uranium-bearing materials by inductively coupled plasma mass spectrometry, *Talanta*, 80: 1744–1749.

Velge, W.A.J.J. and Buschow, K.H.J. (1968) Magnetic and crystallographic properties of some rare earth cobalt compounds with $CaZn_5$ structure, *J. Appl. Phys.*, 39: 1717–1720.

Venugopalan, M. and George, K.J. (1956) Determination of cerium by potassium periodate, *Naturwissenschaften*, 43(15): 348–349.

Venuto, P.B. and Habib, E.T. (1979) *Fluid Catalytic Cracking with Zeolite Catalysts*, Marcel Dekker, New York.

Verhaeghe, F., Goubin, F., Yazicioglu, B., Schurmans, M., Thijs, B., Haesebroek, G., Tytgat, J. and Van Camp, M. (2011) Valorisation of battery recycling slags. In Jones, P.T., Pontike, S.Y., Elsen, J., Cizer, O., Boehme, L., Van Gerven, T., Geysen, D., Guo, M.X. and Blanpain, B. (eds.), *Proceedings of the Second International Slag Valorisation Symposium: The Transition to Sustainable Materials Management*, Katholieke Universiteit Leuven, Leuven, pp. 365–373.

Verhoeven, J.D. (1966) Electrotransport arc means of purifying metals, *J. Metals*, 18(1): 26–31.

Verhoeven, J.D., Gibson, E.D., McMasters, O.D. and Baker, H.H. (1987) The growth of single crystal terfenol-D crystals, *Metall. Trans.*, 18A: 223–231.

Vickery, R.C. (1955) The extraction and purification of scandium, *J. Chem. Soc.*, 245–251.

Vierheilig, A.A. (2012) Methods of recovering rare earth elements, US Patent 8,263,028.

Vilímec, J. and Jakubec, K. (1987) Direct spectrophotometric determination of rare earths in organic extracts with chlorophosphonazo III, *Microchem. J.*, 35(3): 325–327.

Villani, F. (1980) Recovery of rare earth and thorium oxides from pyrochlore. In *Rare Earth Technology and Applications*, Chemical Technology Review No. 154, pp. 6–7, Noyes Data Corporation, Park Ridge, NJ.

Viswanathan, P. (1957) Studies on Travancore beach sands, *Indian Mining J.*, (Spec. Issue) (109): 122–139.

Vogt, T. (1998) Neutron and x-ray diffraction studies on AB5 rare earth metal hydrides. In *Rare Earths' 98*, Abstracts p. 37, Freemantle, Western Australia.

Volborth, A., Miller, G.E., Garner, C.K., Duggan, J.L. and Morgan, I.L. (1974) Accurate determination of major oxygen in inorganic and organic reagents and industrial materials as a check of purity and stoichiometry (No. CONF-741040-P2), University of California, Irvine, CA; North Texas State University, Denton, TX.

Volkov, V.T., Nikiforova, T.V., Ionov, A.M., Pustovit, A.N. and Sikharulidse, G.G. (1981) Preparation of high purity yttrium single crystals by electrotransport, *J. Less-Common Metals* 79: 199–205.

Wada, M., Uchida, H.H., Matsumura, Y., Uchida, H. and Kaneko, H. (1996) Preparation of films of (Tb, Dy) Fe_2 giant magnetostrictive alloy by ion beam sputtering process and their characterization, *Thin Solid Films*, 281: 503–506.

Walkiewicz, J.W., Winston, J.S. and Wong, M.M. (1973) Preparation of samarium cobalt permanent magnets, Bureau of Mines Report of Investigations 7784, U.S. Dept. of the Interior, Washington, DC.

Wallace, D.N. (1981) The use of rare earth elements in zeolite cracking catalysts. In Gschneidner, Jr., K.A. (ed.), *Industrial Applications of Rare Earth Elements*, pp. 101–116, ACS Symposium Series 164, American Chemical Society, Washington, DC.

Wallace, W.E. and Huang, M.Q. (1992) Magnetism of intermetallic nitrides: A review. *Magnetics, IEEE Transactions on*, 28(5): 2312–2315.

Wallace, W.E., Craig, R.S., Gupta, H.O., Pedziwiatr, A., Oswald, E. and Schwab, E. (1988) High energy $PrCo_5$ permanent magnets, *Mater. Sci. Forum*, 30: 177–186.

Walters, A., Lusty, P., Chetwyn, C. and Hill, A. (2010) Rare Earth Elements Mineral Profile, British Geological Survey, Keyworth, Nottingham. Available at http://www.bgs.ac.uk/downloads/start.cfm?id=1638.

Walton, A. and Williams, A. (2011) Rare earth recovery, *Mater. World*, 19: 24–26.

Walton, A., Han, Y., Mann, V.S.J., Bevan, A.I., Speight, J.D., Harris, I.R. and Williams, A.J. (2012) The use of hydrogen to separate and recycle NdeFeeB magnets from electronic waste. In *22nd International Workshop on Rare Earth Magnets and their Applications*, September, Nagasaki, Japan.

Wan, Y. and Liu, C. (2005) Study on adsorption of rare earth elements by kaolinite, *J. Rare Earths*, 23(3): 377–381.

Wang, Y.C., Yue, S.T., Li, D.Q., Jin, M.J. and Li, C.Z. (2002) Solvent extraction of scandium (III), yttrium (III), lanthanides (III) and divalent metal ion with sec-nonylphenoxy acetic acid, *Solvent Extr. Ion Exc.*, 20(6): 701–706.

Wang, H., Liang, Y. and Jiang, P. (2005) Recovering the rare earth from red mud generation, *Rare Earth Letter*, 1008-5939, 10-005-04.

Wang, H., Li, A. and Li, W. (2006a) Effect of Pr and Dy substitution on the impact resistance of sintered Nd–Fe–B magnets, *Intermetallics*, 15: 985–988.

Wang, X., Li, W., Meng, S. and Li, D. (2006b) The extraction of rare earths using mixtures of acidic phosphorus based reagents or their thio-analogues, *J. Chem. Technol. Biotechnol.*, 81: 761–766.

Wang, Y., Yuan, P., Xu, H. and Wang, J. (2006c) Synthesis of Ce:YAG phosphor via homogeneous precipitation under microwave irradiation, *J. Rare Earths*, 24(Spec. Issue): 183–186.

Wang, Y., Sun, X. and Qiu, G. (2007) Synthesis of scandium oxide nano power and fabrication of transparent scandium oxide ceramics, *J. Rare Earths*, 25(Suppl.): 68–71.

Wang, L., Long, Z., Huang, X., Yu, Y., Cui, D. and Zhang, G. (2010) Recovery of rare earths from wet-process phosphoric acid, *Hydrometallurgy*, 101(1–2): 41–47.

Wang, X.H., Mei, G.J., Zhao, C.L. and Lei, Y.G. (2011) Recovery of rare earths from spent fluorescent lamps. In *5th International Conference on Bioinformatics and Biomedical Engineering, (iCBBE)*, May 10–12, pp. 1–4, Wuhan, China.

Wang, L., Wanag, C., Yu, Y., Huang, X., Long, Z., Hou, Y. and Cui, D. (2012) Recovery of fluorine from bastnasite as synthetic cryolite by-product, *J. Hazard. Mater.*, 209–210: 77–83.

Wang, L., Yu, Y., Huang, X., Long, Z. and Cui, D. (2013) Toward greener comprehensive utilization of bastnaesite: Simultaneous recovery of cerium, fluorine, and thorium from bastnaesite leach liquor using HEH(EHP), *Chem. Eng. J.*, 215–216: 162–167.

Warburg, E. (1881) Magnetische Untersuchungen. I. Magnetic Investigation: I About effect of coercitive force. *Ann. Phys.*, 13: 141.

Warf, J.C. (1949) Extraction of cerium (IV) nitrate by tributyl phosphate, *J. Am. Chem. Soc.*, 64: 3257–3258.

Warf, J.C. and Kerst, W.K. (1953) Studies of the rare earth hydrides, Technical Rept. II on Project NR 356-290 Contract No. 228 (03), National Technical Information Service, Alexandria, VA.

Warf, J.C., Donahue, J. and Hardcastle, K. (1957) Technical Rept. II on Office of Naval Research Project NR 052-390 Contract Nonr. 228 (15), National Technical Information Service, Alexandria, VA.

Warner, J.D. and Barker, J.C. (1989) Columbium- and rare-earth element-bearing deposits at Bokan Mountain, southeast Alaska, U.S. Bureau of Mines Open File Report 33–89.

Wauby, P.E. (1978) Rare earth additions to steel, *Int. Met. Rev.*, 23(2): 74–98.

Weaver, B. (1974) Solvent extraction in the separation of rare earths and trivalent actinides. In Marinsky, A. and Marcus, Y. (eds.), *Ion Exchange and Solvent Extraction*, pp. 196–210, Marcel Dekker, New York.

Weaver, B., Kappelmann, F.A. and Topp, A.C. (1953) Quantitative separation of rare earths by liquid–liquid extraction. I. The first kilogram of gadolinium oxide, *J. Am. Chem. Soc.*, 75: 3943–3945.

Weber, M.J. (1979) Rare earth lenses. In Gschneidner, Jr., K.A. and Eyring, L. (eds.), *Handbook on the Chemistry and Physics of Rare Earths*, Vol. 4, pp. 275–316, North Holland, Amsterdam.

Wecker, J. and Schultz, L. (1990) Effect of Zr and Nb additions on the microstructure and the magnetic properties of melt spun Nd–Fe–B and Nd–Fe–Co–B, *J. Magn. Magn. Mater.*, 83: 189–191.

Wedepohl, K.H. (1995) The composition of the continental crust, *Geochem. Cosmochem. Acta*, 59: 1217–1232.

Weeks, M.E. (1956) *Discovery of the Elements*, 6th edn, American Chemical Society, Easton, PA.

Wei, Y., Sato, N. and Nanjo, M. (1989) Solubility of samarium sulfate and neodymium sulfate in sulfate solutions. Fundamental study on the recycling of rare earth magnet materiasls, *J. MMIJ*, 105: 965–970.

Weibke, F. (1939) Preparation of lanthanum by electrolysis of its fused chloride, *Z. Elektrochem.*, 45: 518–520.

Welcher, F.J. (1958) *Analytical Uses of Ethylene Diamine Tetra Acetic Acid*, D. Van Nostrand, Princeton, NJ.

Welker, T. (1991) Recent developments on phosphors for fluorescent lamps and cathode ray tubes, *J. Lumin.*, 48–49: 49–56.

Wellens, S., Thijs, B. and Binnemans, K. (2012) An environmentally friendlier approach to hydrometallurgy: Highly selective separation of cobalt from nickel by solvent extraction with undiluted phosphonium ionic liquids, *Green Chem.*, 14: 1657–1665.

Wernick, J. (1995) Magnetic materials. In Kroschwitz, J.I. and Grant, M.H. (eds.), *Kirk-Othmer Encyclopedia of Chemical Technology*, 4th edn., Vol. 15, pp. 723–788, John Wiley & Sons, New York.

Westendorp, F.F. and Buschow, K.H.J. (1969) Permanent magnets with energy products of 20 million gauss oersteds, *Solid State Commun.*, 7: 639–640.

Westgaard, L. and Bjornholm, S. (1966) Self-supporting metal foils prepared from the oxides of the separated isotopes of rare earth elements, *Nucl. Instrum. Methods*, 42: 77–80.
Weterings, K. and Janssen, J. (1985) Recovery of uranium, vanadium, yttrium and rare earths from phosphoric acid by a precipitation method, *Hydrometallurgy*, 15: 173–190.
Wheelwright, E.J. (1973) *Promethium Technology*, American Nuclear Society, Hinsdale, IL.
Whitten, C.W. and Yancey, R.J. (1990) Characterization of the rare-earth mineralogy at the Pea Ridge deposit, Missouri, U.S. Bureau of Mines Report of Investigations 9331.
Willard, H.H. and Young, P. (1928) Ceric sulfate as a volumetric oxidizing agent, *J. Am. Chem. Soc.*, 50: 1322–1334; also subsequent papers of the authors in JACS through 1934.
Williams, J.M. and Huffine, C.L. (1959) Solid state electrolysis of yttrium metal, *Trans. Am. Nucl. Soc.*, 2(1): 29.
Williams, J.M. and Huffine, C.L. (1961) Solid state electrolysis in yttrium metal, *Nucl. Sci. Eng.*, 9: 500–506.
Wilson, T.A. (1991) Mining, refining and marketing of bastnasite and its separated products. In Siribumrungsukha, B., Arrykul, S., Sanguan Sai, P., Pungrassami, T., Sikong, L. and Kooptarnon, K. (eds.), *Proc. Int. Conf. Rare Earth Minerals and Minerals for Electronic Uses, Hat Yai, Thailand*, January, pp. 271–277, Prince of Songkla University, Thailand.
Winckler, C. (1890) *Ber. Deutsch. Chem. Gesell.*, 23: 772.
Winckler, C. (1891) *Ber. Deutsch. Chem. Gesell.*, 24: 873.
Winge, R.K. and Fassel, V.A. (1965) Simultaneous Determination of Oxygen and Nitrogen in Refractory Metals by the Direct Current Carbon-Arc, Gas Chromatographic Technique. *Analytical Chemistry*, 37(1): 67–70.
WISE-Uranium (2010) WISE-Uranium Project. Available at http://www.wiseuranium.org/mdafko.html (accessed February 12, 2010).
World Mining (1966) Molycorp uses solvent extraction to separate europium oxide from rare earths, *World Mining*, 2(3): 16–19.
Woyski, M. and Harris, R.R. (1963) The rare earths and rare earth compounds. In Kolthoff, I.M. and Elving, P.J. (eds.), *Treatise on Analytical Chemistry*, Vol. 8, Part II, pp. 1–146, Interscience, New York.
Wu, P.C.S. (1978) Europia as nuclear control material, *Nucl. Tech.*, 39: 84.
Wu, C.S. and Segre, E. (1942) Artificial radioactivity of some rare earths, *Phys. Rev.*, 61: 203.
Wu, M.K., Ashburn, J.R., Tong, C.T., Hor, P.H., Meng, R.L., Goa, L., Huang, Z.L., Wang, Q. and Chu, C.W. (1987) Superconductivity at 93 K in a new mixed phase Y–Ba–Cu–O compound system at ambient pressure, *Phys. Rev. Lett.*, 58: 908–910.
Wu, X., Liang, Y., Liu, M., Chen, R. and Li, Y. (2010a) Synthesis and fluorescence properties of Y_2O_3:Eu by molten salt synthesis method, *J. Rare Earths*, 28(5): 688–692.
Wu, W., Xu, T., Hao, Q., Wang, Q., Zhang, S. and Zhao, C. (2010b) Applications of x-ray fluorescence analysis of rare earths in China, *J. Rare Earths*, 28(Spec. Issue): 30–36.
Wubbeke, J. (2013) Rare earth elements in China: Policies and narratives of reinventing an industry, *Resour. Policy*, 38: 384–394.
Wyoming State Geological Survey (2008) WWDC Green River Basin Water Plan II, October 22, Wyoming State Water Plan. Available at http://waterplan.state.wy.us/plan/green/2010/finalrept/gw_toc.html (accessed July 19, 2011).
Xiao, J., Otaigbe, J.U. and Jiles, D.C. (2000) Modeling of magnetic properties of polymer bonded Nd–Fe–B magnets with surface modifications, *J. Magn. Magn. Mater.*, 218: 60–66.
Xie, H., Zhao, J., and Yu, Y. (2006) New achievements in NdFeB mass production. In Wei, L., Yang, L. and Xuehui, Z.J. (eds.), *Proceedings of 19th International Workshop on Rare Earth Permanent Magnets & Their Applications (Workshop on REPM'06)*, August 30–September 2, Vol. 33, pp. 324–330, Chinese Society for Metals, Friendship Hotel 2006, Beijing, China.
Xie, F., Zhang, T.A., Dreisinger, D. and Doyle, F. (2014) A critical review on solvent extraction of rare earths from aqueous solutions, *Miner. Eng.*, 56: 10–28.

Xu, X. (1985) A new collector for bastnaesite—and a preliminary analysis of its flotation capabilities. In Xu, G. and Xiao, J. (eds.), *New Frontiers in Rare Earth Science and Applications*, Vol. 1, pp. 75–78, Science Press, Beijing.

Xu, Y. (1999) Liquid metal extraction of Nd from Nd–Fe–B magnet scrap, MSc Thesis, Iowa State University, Ames, IA.

Xu, T. and Peng, H.Q. (2009) Formation cause, composition analysis and comprehensive utilization of rare earth solid wastes, *J. Rare Earths*, 27: 1096–1102.

Xu, S., Wang, M., Niu, S. and He, M. (1985) Preparation of RE–Mg–Si alloys by silicothermic reduction of dolomite. In Xu, G. and Xiao, J. (eds.), *New Frontiers in Rare Earth Science and Applicatio*n, Vol. II, pp. 1185–1189, Science Press, Beijing.

Xu, Y., Chumbley, L.S. and Laab, S.F.C. (2000) Liquid metal extraction of Nd from Nd–Fe–B magnet scrap, *J. Mater. Res.*, 15: 2296–2304.

Xu, T., Chen, R.J., Yin, W.Z., Lin, M., Lee, D. and Yan, A.R. (2012) High performance anisotropic NdFeB magnets prepared by dual-alloy die-upsetting. *J. Appl. Phys.*, 111(7): 07B540.

Xujun, W., Xiuzhi, X., Falun, F. and Yongcheng, C. (1985) A study on the Zn–Al–Re alloy preparation by using molten salt electrolysis. In Xu, G. and Xiao, J. (eds.), *New Frontiers in Rare Earth Science and Application*, Vol. I, pp. 476–479, Science Press, Beijing, China.

Xuefang, X. (1985) A new collector for bastnasite-804# and a preliminary analysis of its flotation capabilities. In Xu, G. and Xiao, J. (eds.), *New Frontiers in Rare Earth Science and Applications*, Vol. 1, pp. 75–78, Science Press, Beijing, China.

Yagi, H., Yanagitani, T., Takaichi, K., Ueda, K. and Kaminskii, A.A. (2007) Characterizations and laser performances of highly transparent Nd^{3+}:$Y_3Al_5O1_2$ laser ceramics. *Opt. Mater.*, 29(10): 1258–1262.

Yajima, S. and Toma, H.K. (1977) Hydrogen sorption in La_2Mg_{17}, *J. Less Common Met.*, 55: 139–141.

Yamada, T., Liang, R., Kikuchi, E. and Kawashima, H. (2010) In *Proceedings of the MMIJ Annual Meeting 2010*, March 30–April 1, No. 1524, The Mining and Materials Processing Institute of Japan, Tokyo, Japan.

Yamada, T., Liang, R., Kikuchi, E. and Kawashima, H. (2011) In *Proceedings of the MMIJ Annual Meeting 2011*, No. 1114, The Mining and Materials Processing Institute of Japan, Tokyo, Japan.

Yan, J. and Xiong, J. (1998) Correlation between global NdFeB industry and Chinese rare earth industries. In Preprints of the Conference, China Magnets, October 18–21, Beijing, PR China.

Yan, C., Jia, J., Liao, C., Wu, S. and Xu, G. (2006a) Rare earth separation in China, *Tsinghua Sci. Technol.*, 11(2): 241–247.

Yan, M., Yu, L.Q., Luo, W., Wang, W. and Wen, Y.H. (2006b) Change in the microstructure and magnetic properties of sintered Nd-Fe-B induced by annealing, *J. Magn. Magn. Mater.*, 301(1): 1–5.

Yang, H.L., Wang, W., Cui, H.M., Zhang, D.L., Liu, Y. and Chen, J. (2012) Recovery of rare earth elements from simulated fluorescent powder using bifunctional ionic liquid extractants (Bif-ILEs), *J. Chem. Technol. Biot.*, 87: 198–205.

Yang, X.J., Lin, A., Li, X.-L., Wu, Y., Zhou, W. and Chen, Z. (2013) China's ion-adsorption rare earth resources mining consequences and preservation, *Environ. Dev.*, 8: 131–136.

Yao, Y.P. and Lin, J.H. (2006) Preparation of Nd-doped gadolinium–gallium garnet laser ceramic powder by sol–gel method, *Optoelectron. Lett.*, 2(4): 288–291.

Ye, J., Liu, Y., Zhu, G., Chen, M., Gao, S. and Tu, M. (2007) Microstructure and magnetic properties of $Sm_2Fe_{17}N_x$ compound and their magnets prepared by field-activated combustion, *J. Alloys Compd.*, 428(1–2): 350–354.

Yerpude, A.N. and Dhoble, S.J. (2013) Luminescence in trivalent rare earth activated $Sr_4Al_2O_7$ phosphor, *Optik*, 124: 3567–3570.

Yi, P., Lin, M., Chen, R., Lee, D. and Yan, A. (2010) Enhanced magnetic properties and bending strength of hot deformed Nd–Fe–B magnets with Cu additions, *J. Alloys Compd.*, 491(1–2): 605–609.

Ying, X., Wang, X. and Li, D. (2005) Synergistic extraction and separation of heavy lanthanide by mixtures of bis(2,4,4-trimethylpentyl)phosphinic acid and 2-ethylhexyl phosphinic acid mono-2-ethylhexyl ester, *Sep. Sci. Technol.*, 40(11): 2325–2336.

Yntema, L.F. (1930) The separation of europium by electrolytic reduction (Observations of the rare earths XXXV), *J. Am. Chem. Soc.*, 52: 2782–2785.

Yongxiu, L., Min, L., Xiaobing, H. and Pinggui, H. (1999) Gu Ziying Rare Earth Technology Research Centre, Nanchang University, Nanchang, PR China; Precipitation and crystallization process of rare earth carbonate [J]. *The Chinese Journal of Nonferrous Metals*, 1.

Yoon, H.S., Kim, C.J., Lee, J.Y., Kim, S.D., Kim, J.S. and Lee, J.C. (2003) Separation of Neodymium from NdEeB Permanent Magnetic Scrap. *Journal of the Korean Institute of Resources Recycling*, 12(6): 57–63.

Yoshida, K. and Haraguchi, H. (1984) Determination of rare earth elements by chromatography/inductively coupled plasma atomic emission, *Anal. Chem.*, 56: 2580–2585.

Yoshida, T., Ono, H. and Shirai, R. (1995) *Recycling of Used Ni–MH Rechargeable Batteries*, pp. 145–152, Minerals Metals & Materials Society, Warrendale, PA.

Yost, R.M., Russel, H. and Garner, C.S. (1947) *The Rare Earth Elements and Their Compounds*, Wiley, New York.

Yu, Z.S. and Chen, M.B. (1995) *Rare Earth Elements and Their Applications*, Metallurgical Industry Press, Beijing.

Yu, S. and Chen, L. (2006) Preparation technology and performances of Zn–Cr coating on sintered NdFeB permanent magnet, *J. Rare Earths*, 24: 223–226.

Yu, Z., Robinson, P. and McGoldrick, P. (2001) An evaluation of methods for the chemical decomposition of geological materials for trace element determination using ICPMS, *Geostand. Geoanal. Res.*, 25(2–3): 199–217.

Yu, L.Q., Zhang, J., Hu, S.Q., Han, Z.D. and Yan, M. (2008) Production for high thermal stability NdFeB magnets, *J. Magn. Magn. Mater.*, 320(8): 1427–1430.

Yuan, H., Zhang, J., Yu, R. and Su, Q. (2009) Synthesis of rare earth sulfides and their UV-vis absorption spectra, *J. Rare Earths*, 27(2): 308–311.

Yusoff, M. and Latifah, A. (2002) Rare earth processing in Malaysia: Case study of ARE and MA-REC plants. In *Proceedings of Regional Symposium on Environment and Natural Resources*, April 10–11, Vol. 1, p. 287–295, Kuala Lumpur, Malaysia.

Yüzüak, E., Dincer, I. and Elerman, Y. (2010) Giant magnetocaloric effect in the $Gd_5Ge_{2.025}Si_{1.925}In_{0.05}$ compound, *Chinese Phys. B*, 19(3): 037502.

Zadorozhnyi, V.G. (1965) Industrial flotation of sands from titanium–zirconium deposits, *Tsvetnye Metally*, 6: 7–12.

Zadorozhnyi, V.G. (1967) Industrial tests of acid still residues for flotation of titano zirconium sands, *Tsvetnye Metally*, 8: 25–27.

Zajec, O. (2010) China—Herr über die seltenen Erden. *Le Monde Diplomatique*, international edition, November.

Zakharov, A.E., Ilie, P., Pol'kin, S.I. and Solnyshkin, V.I. (1967) Reaction of sodium sulfide with pyrochlore, zircon and monazite in flotation with sodium oleate. In Plaksin, I.N. (ed.), *Flotation Properties of Rare Metal Minerals*, pp. 71–82. Primary Sources, New York.

Zakotnik, M., Devlin, E., Harris, I.R. and Williams, A.J. (2006) Hydrogen decrepitation and recycling of NdFeB-type sintered magnets, *J. Iron Steel Res. Int.*, 13: 289–295.

Zakotnik, M., Harris, I.R. and Williams, A.J. (2008a) Possible methods of recycling Nd–Fe–B–type sintered magnets using the HD/degassing process, *J. Alloys Compd.*, 450: 525–531.

Zakotnik, M., Williams, A.J., Martinek, G. and Harris, I.R. (2008b) Hydrogen decrepitation of a 2/17 sintered magnet at room temperature, *J. Alloys Compd.*, 450(1–2): L1–L3.

Zakotnik, M., Harris, I.R. and Williams, A.J. (2009) Multiple recycling of NdFeB-type sintered magnets, *J. Alloys Compd.*, 469: 314–321.

Zaluski, L., Zaluska, A. and Ström-Olsen, J.O. (1997) Nanocrystalline metal hydrides, *J. Alloys Compd.*, 253–254: 70–79.

Zang, J., Tion, S. and Guo, X. (1985) Determination of trace amounts of rare earth elements in geological samples by Direct Current Plasma Source Spectrometry. In Xu, G. and Xiao, J. (eds.), *New Frontiers in Rare Earth Science and Application*, pp. 589–594, Science Press, Beijing, China.

Zeng, Y., Guo, N., Luo, Q. and Chen, Z. (1983) The application of multiwavelength spectrophotometry to the analysis of rare earths, *J. Less Common Met.*, 94(2): 271–276.

Zhang, J. and Edwards, C. (2012) A review of rare earth mineral processing technology. In *44th Annual Meeting of the Canadian Mineral Processors*, pp. 79–102, CIM, Ottawa.

Zhang, Q. and Saito, F. (1998) Non thermal extraction of rare earth elements from fluorescent powder by means of its mechanochemical treatment, *J. MMIJ*, 114: 253–257.

Zhang, B.Z., Lu, K.Y., King, K.C., Wei, W.C. and Wang, W.C. (1982) Rare earth industry in China, *Hydrometallurgy*, 9: 205–210.

Zhang, S.X., Murachi, S., Imasaka, T. and Watanabe, M. (1995) Determination of rare earth impurities in ultrapure europium oxide by inductively-coupled plasma mass spectrometry, *Anal. Chim. Acta*, 314(3): 193–201.

Zhang, P., Tao, K. and Yang, Z. (1995) Study on material composition and REE-host forms of ion-type RE deposits in South China, *J. Rare Earths*, 13(1): 37–41.

Zhang, P.W., Yokoyama, T., Itabashi, O., Wakui, Y., Suzuki, T.M. and Inoue, K. (1998) Hydrometallurgical process for recovery of metal values from spent nickel metal hydride secondary batteries, *Hydrometallurgy*, 50: 61–75.

Zhang, Q., Lu, J. and Saito, F. (2000) Selection extraction of Y and Eu by non-thermal acid leaching of fluorescent powder activated by mechanochemical treatment using a planetary mill, *J. MMIJ*, 116(2): 137–140.

Zhang, X.Q., Liu, J.L., Yi, Y., Jiang, Y.M., Lin, P. and Tong, Y.D. (2004) *Fenxi Ceshi Xuebao*, 23: 73.

Zhang, X., Zhu, M., Li, Y., Yang, Q., Jin, H., Jiang, J., Tian, Y. And Luo, Y. (2006a) Study on fabrication process of anisotropic injection bonded Nd–Fe–B magnets, *J. Iron Steel Res., Int.*, 13(Suppl. 1): 286–288.

Zhang, X., Zoo, M., Li, Y., Yang, Q., Jin, H., Jiang, J., Tian, Y. and Luo, Y. (2006b) Study on fabrication process of anisotropic injection bonded Nd–Fe–B magnets. In Wei, L., Yang, L. and Xuehui, Z.J (eds.), *Proceedings of 19th International Workshop on Rare Earth Permanent Magnets & Their Applications (Workshop on REPM'06)*, August 30–September 2, pp. 286–288, Chinese Society for Metals, Friendship Hotel Beijing, China.

Zhang, X., Liu, J., Yi, Y., Liu, Y., Li, X., Su, Y. and Lin, P. (2007) Determination of rare earth impurities in high purity samarium oxide using inductively coupled plasma mass spectrometry after extraction chromatographic separation, *Int. J. Mass Spectrom.*, 260: 57–66.

Zhang, Z.F., Li, H.F., Guo, F.Q., Meng, S.L. and Li, D.Q. (2008) Synergistic extraction and recovery of cerium(IV) and fluorine from sulfuric solutions with Cyanex 923 and di-2-ethylhexyl phosphoric acid, *Sep. Purif. Technol.*, 63: 348–352.

Zhang, X.H., Xiong, W.H., Li, Y.F. and Song, N. (2009) Effect of process on the magnetic and mechanical properties of Nd–Fe–B bonded magnets, *Mater. Des.*, 30: 1386–1390.

Zhang, L., Xu, B., Gong. J. and Bu, T. (2010a) Membrane combination technic on treatment and reuse of high ammonia and salts wastewater in rare earth manufacture process, *J. Rare Earths*, 28(Spec. Issue): 501.

Zhang, Z.F., Guo, F.Q., Meng, S.L., Jia, Q., Li, H.F. and Li, D.Q. (2010b) Simultaneous recovery of cerium and fluorine from bastnaesite leach liquor by mixtures of Cyanex 923 and HEH(EHP), *Ind. Eng. Chem. Res.*, 49(13): 6184–6188.

Zhang, J., Yin, J., Liu, P., Gao, B. and Bie, L. (2012) Preparation and luminescent properties of $MgTiO_3:Eu^{3+}$ phosphor for white LEDs, *J. Rare Earths*, 30(10): 1009–1012.

Zhang, Y., Yang, X.U., Huang, X., Zhiqi, L.O.N.G., Dali, C.U.I. and Feng, H.U. (2012) Study on thorium recovery from bastnasite treatment process. *J. Rare Earths*, 30(4): 374–377.

Zhao, T., Li, B.W., Gao, Z.Y. and Chang, D.Q. (2010) The utilization of rare earth tailing for the production of glass–ceramics. *Mater. Sci. Eng.: B*, 170(1): 22–25.

Zheng, D., Gray, N.B. and Stevens, D.W. (1991) Comparison of naphthenic acid, Versatic acid, and D2EHPA for the separation of rare earths, *Solvent Extr. Ion Exc.*, 9(1): 85–102.

Zhong, X., Song, N. and Gong, B. (2010) Preparation of Mn–Zn ferrites powder by waste from recycling the NdFeB magnet scrap, *J. Mianyang Normal Univ.*, 5: 2010. Available at http://www.cnki.com.cn/Article/CJFDTOTAL-MYSF201005013.htm (accessed October 15, 2010).

Zhou, Z., Song, Y., Cui, S., Huang, C., Qian, W., Lin, C., Zhang, Y. and Lin, Y. (2010) Effect of annealing treatment on structure and electrochemical performance of quenched $MmNi_{4.2}Co_{0.3}Mn_{0.4}Al_{0.3}Mg_{0.03}$ hydrogen storage alloy. *J. Alloys Compd.*, 501(1): 47–53.

Zhu, T. (1991) Solvent extraction in China, *Hydrometallurgy*, 27(2): 231–245.

Zhu, M., Peng, C.H., Ouyang, L.Z. and Tong, Y.Q. (2006) The effect of nanocrystalline formation on the hydrogen storage properties of AB3-base Ml–Mg–Ni multi-phase alloys, *J. Alloys Compd.*, 426(1): 316–321.

Zijlstra, H. and Westendorp, F.F. (1969) Influence of hydrogen on the magnetic properties of $SmCo_5$, *Solid State Commun.*, 7: 857–859.

Zinner, E. and Crozaz, G. (1986) A method for the quantitative measurement of rare earth elements in the ion microprobe, *Int. J. Mass Spectrom. Ion Processes*, 69(1): 17–38.

Zintl, E. and Neumayr, S. (1933) Metals and alloys. VIII. Crystal structure of β lanthanum, *Z. Elektrochem.*, 39: 84–86.

Zoller, W.H. and Gordon, G.E. (1970) Instrumental neutron activation analysis of atomospheric pollutants utilizing Ge (Li). gamma.-ray detectors. *Analytical Chemistry*, 42(2): 257–265.

Zuttel, A., Chartouni, D., Nutzenadel, Ch., Schlapbach, L., Guether, V., Otto, A., Bartsch, M. and Kotz, L. (1999) Comparison of the electrochemical and gas phase hydrogen sorption processes, *Mater. Sci. Forum*, 315–317: 84–93.

Zwilling, G. and Gschneidner, Jr., K.A. (1978) Fused salt electrorefining of gadolinium, an evaluation of three electrolytes, *J. Less Common Metals*, 60: 221–230.

Index

Page numbers followed by f and t indicate figures and tables, respectively.

A

AAS, *see* Atomic absorption spectrometry (AAS)
Absorption bands, rare-earth ions, 690
Acetic acid, 556
Acheson graphite anode, 409
Acids, 29; *see also* Reactivity
  leaching, 269, 683
  treatment, 254, 255f; *see also* Monazite
Activators in laser glasses, 60
Active magnetic regenerative magnetic refrigerator (AMR-MR), 53
Active magnetic regenerator (AMR) cycle, 603
Adiabatic demagnetization refrigerator, 604
Advanced Material Resources Ltd. (AMR), Canada-based, 208
Air, 25–26; *see also* Reactivity
Alaska oil pipeline, 40
Alcoa and Molycorp, 528
Aliquat 336 (trioctyl methyl ammonium nitrate), 304, 305t
Alkaline fusion, 678
Alkaline igneous rocks, 102
Alkaline intrusives, 169
Alkali treatment, 255, 256f; *see also* Monazite
Alkane Resources Ltd, 740
Allanite, 94, 96t, 97
All electric vehicle (AEV), 50, 70
Allotropes, 23
Alloys; *see also* Electrolysis
  distillation of, operational data for, 440t
  electrodeposition of, operational data for, 438t
  for hydride compressor, 609
  powder, 43
Alluvial tin deposits in Malaysia, 181
AlNiCo magnet, 548, 567
  discovery of, 44
  magnet characteristics, 46t
  permanent magnet development timeline, 45t
Alumina, 546
  crucibles, 604–605
  nitric acid dissolution of, 678
Aluminum
  alloys, 41–42; *see also* Metallurgy
  non-rare-earth impurities, 692
  production, 685
  as reductants, 538
Aluminum chloride, 646
Aluminum phosphate, 100
Aluminum plating, 596
Amang, 181
American Superconductor Corporation, 620
Ames group, 475, 591
Ames lanthanum metal, 505
Ames metals, radio-frequency float-zone melting (RFFZ), 506
Ames practice, 463
Ames process, *see* Calcium reduction (Ames process)
Amines, 303–306, 304f, 305t; *see also* Solvent extraction
Amino polyacetic acids, 289
Ammonia gas, 310
Ammonia–nitrogen wastewater, 731
Ammonium bifluoride, rare-earth oxides with, 366–367, 366f
Ammonium chloride, 265, 341, 645
Ammonium double sulfates, 656
Ammonium lignin sulfonate, 248
Ammonium thiocyanate, 320
Amorphous alloys, 606
Anderson, Iver, 591
Anhydrous calcium chloride, 652
Anhydrous compounds, 30
Anhydrous HF, reaction of rare-earth oxides with; *see also* Dry methods
  fluidized bed method, 365–366
  rotary batch method, 364–365, 365f
  vibrating tray method, 366
Anion exchanger, 294t
Apatite; *see also* Minerals; Resource processing
  about, 97, 99
  calcium fluorophosphate, 97
  chemical treatment of, 277–279
  nitric acid processing of, 275f
  rare-earth distribution, 96t
  source of REE, 247
  in Western China, 177
Aqueous-based technology, 659
Aqueous hydrofluorination, 363
Aqueous systems; *see also* Rare earths
  complexes, 31
  divalent state, 32–33
  tetravalent state, 31–32
  trivalent state, 30–31
Arc-melted yttrium buttons, analysis of, 356t
Arc melting, 601

Argentina
occurrence of deposits in, 163
summary of rare-earth deposits, 108t
Argon, purified, 371
Arrhenius, Carl Axel, 2, 2t
Arsenazo III spectrophosphorimetry, 692
As-cast alloys, 593
As-mined ore, 235, 236
As-reduced rare-earth metals, 448
As-reduced yttrium, 337
Atomic absorption spectrometry (AAS), 696
Auer gas mantles, 523
Australasian Code for Reporting of Exploration Results, 154
Australia; *see also* Resources; World rare-earth production
advanced rare earth projects, 217t
Brockman (Hastings) deposit, 166
Brown's range project, 163–164
Cooljarloo/Jurien Bay, 164
Cummins Range, 165
Dubbo Zirconia Project (DZP), Toongi, 164
Eneabba mineral sand deposit, 164
Gilgai Intrusion, 165
Jangardup mineral sand deposit, 165
John Galt, 168
Mary Kathleen, 166–167
mine production of rare earths, 199t–200t
Mount Weld deposit, 167
Murray Basin deposits, 165
Nolans Bore deposit, 165–166
Norraburra RE deposit, 166
Radium Hill, 168
rare-earth production in, 205–207
summary of rare-earth deposits, 108t–116t
Syerston nickel-cobalt laterite, 168
Wimmera Industrial Minerals (WIM)-150, 165
Yangibana, 168
Australian monazite, 95t
Automotive exhaust catalysts, 58, 684
Avalon Rare Metals' Nechalacho rare-earth deposit, 742

B

Ball-milling process, 43
Band displacement technique, 290
Bangladesh
occurrence of deposits in, 168–169
summary of rare-earth deposits, 116t
Baotou concentrate, 264, 264f
Baotou Iron and Steel Company (BISC), 208
Baotou process, 541; *see also* Rare earth-silicon-iron alloys
Baotou Radiation and Environmental Management Institute, 726
Baotou rare-earth concentrates, treatment for, 264f
BARC process, 541; *see also* Rare earth-silicon-iron alloys
Barren acid solutions, 273
Barren organic (BO) solution, 272
Bases, 29; *see also* Reactivity
Basicity of rare-earth elements, 20–21
Bastnasite, 719, 732
about, 88, 93; *see also* Minerals
chemical treatment of; *see also* Resource processing
about, 261–265, 261f
Bear Lodge ore processing, 266
concentrate/chlorides of bastnasite, 263t
Goldschmidt process, 266–268, 266f, 267f, 268t
production of rare-earth chlorides from bastnasite, 262f
for treating Baotou rare-earth concentrates, 264f
for treating Beylikahir bastnasite preconcentrate, 265f
chlorination, 525
flotation, 244–246; *see also* Physical beneficiation
high-temperature chlorination of, 268t
ores from Belgian Congo, 534
physical beneficiation of, 247–249, 249f
preparation, 529–530
primary source of light REO, 93
REE distribution in, 93t
wet chemical treatment of, 524
Bayan Obo deposit, 207–208, 543
iron ore deposit, 245
physical beneficiation of, 249–251, 250f, 251f
Bayan Obo facilities, 726
Bayan Obo iron-rare earth-niobium ore body, 172, 174–175; *see also* China
Bcc phase, *see* Body centered cubic (bcc) phase
Beach sand minerals, physical beneficiation of, 240f
Bear Lodge Mountains, Wyoming, 189; *see also* United States
Bear Lodge ore processing, 266; *see also* Bastnasite
Beijing University of Iron and Steel Technology, 569
Belgian Congo, bastnasite ores from, 534
α-Benzoin oxime, 688
Beryllium iron silicate mineral, 100
Beylikahir bastnasite preconcentrate, 265f
Bismuth-214, 718
Blue-emitting LED, phosphors in, 66
Body centered cubic (bcc) phase, 503
B_2O_3-encapsulated alloy, 651
Boiling point of rare-earth metals, 22–23

Boiling water reactors (BWR), 66
Bokan Mountain, Alaska, 190; *see also* United States
Bonded magnets, 566–567, 580–584
Boric oxide, 651
Brannerite, 96t, 99; *see also* Minerals
Brazil; *see also* World rare-earth production
  advanced rare earth projects, 218t
  mine production of rare earths, 199t–200t
  occurrence of deposits in, 169–170
  rare-earth production in, 202–203
  summary of rare-earth deposits, 117t–121t
British Geological Survey, 177
Brockman deposit, 166, 206; *see also* Australia
Bromides, 30
Brown's range project, 163–164; *see also* Australia
Bubble domain memory materials, 606
Buffalo fluorspar mine, 183; *see also* South Africa
Bulb, powder-blue-colored, 60
Burundi, summary of rare-earth deposits, 121t–122t
By-products/coproducts, of rare earths, 195–197, 196t; *see also* Resources

C

$CaCl_2$ electrolyte, 517
Calcia, 54
Calcination, 570
Calciothermic reduction
  advantages, 569
  of rare-earth chloride, 350f
  of rare-earth trifluorides, 372, 373f
Calcium
  rare-earth fluorides with, reduction of, 374f
  rare-earth trifluoride reduction using, 536–537
  as reductant in preparation of samarium–cobalt alloy, 555–556
  vacuum distilled, 371
  volatile, 396
Calcium carbide, 538
Calcium chloride, 352
Calcium concentration, 477
Calcium fluoride, vapor pressures of, 456
Calcium fluorophosphate, 97
Calcium–lithium alloys, 378
Calcium reduction (Ames process), 372, 451, 648; *see also* Fluoride reduction process
  Goldschmidt process, 374–375
  overview, 371–372, 372f–374f
  semicontinuous reduction, 372–373, 375f
Calcium silicide, as reductants, 538, 539
Calcium sulfate hemihydrate, 277, 278
c-aminopropyltriethoxysilane, 581
Canada; *see also* Resources; World rare-earth production
  advanced rare earth projects, 218t–220t
  Denison mine, 170
  Hoidas Lake, 171
  Kipawa Alkaline Complex, 171–172
  Nechalacho/Thor Lake Mine Site, Northwest Territories, 170–171
  rare-earth production in, 211–212
  summary of rare-earth deposits, 122t–125t
  Yukon, 171
Canadian National Instrument 43-101, 154
Carbon, 28; *see also* Reactivity
Carbonate mineral dissolution, 719
Carbonate pressure leach (CPL) technology, 741
Carbonatites
  in Brazil, 169
  classification, 104t
Carbon-containing alloys, 651
Carbon crucible, 406
Carbon impurity, 452
Carbonyl, formation of, 646
Carbon zone refined, 514
Carbothermic reduction, 28, 401–402, 538; *see also* Reduction
Carboxylic acids, 294t, 300–301, 300t; *see also* Solvent extraction
Carrier electrolyte, 402
Cassiterite, 239
Catalysts, rare-earth application areas, 35t
Catalytic converters, 58, 75
Cathode current efficiency, varying, 558–559
Cathode ray-excited emission spectroscopy (CREE), 710
Cathode ray tubes (CRTs), 60, 673
  CRT phosphor, 682
  monitors, 79
Cation exchangers, 294t
Caustic soda digestion, 259
Cells for electrowinning
  lanthanum, 419–426, 421t, 425t
  neodymium/praseodymium/didymium, 426–428, 426f, 427f, 429t
Central Lanthanide Deposit (CLD), 167
Centrifugal atomization technique, 605
Centrifugal gravity concentrator, 237
Ceramic insulator mounting, 393f
Ceramics, 53–56; *see also* Rare-earth ceramics; Rare earths
  rare-earth application areas, 35t
Ceramic superconducting compounds, 617
Ceric fluoride, 31, 32
Ceric oxide, 31, 32
Cerite sequence, 4f
Cerium, 280
  applications, 37t
  atomic properties, 9t–10t

browning/fogging of glass, preventing, 60
chlorinating method for, 345
corrosion resistance, 41
electrolytic preparation of, 451
electrowinning of, 415t, 416
in FCC additives, 58
in high-strength nickel alloys, 40
mechanical properties, 13t
most abundant rare earth, 59
purity of, 349
separation and purification of, 292f
thermal/electrical/magnetic properties, 11t–12t
vapor pressure, 495
Cerium carboxylates, 72
Cerium chloride, 489
Cerium dioxide, 292
with boron nitride, 72
Cerium ingot, 408
Cerium oxidation, 689
Cerium oxide (CeO_2), 55, 682, 683, 688
Gray's cell for electrolysis of, 413
to metal, electrochemical reduction of, 441
Cerium production, 405
Cerium salts, as combustion additions, 72
Cerium stearate, 72
Cerium subgroup of REE, 88
Cerium sulfide, 55
Cerium trichloride, electrolysis of, 407f
CFLs, *see* Compact fluorescent lamps (CFLs)
Chelating exchangers, 294t
Chelating resins, 678
Chemical analysis of yttrium, 378t
Chemical binders, 561
Chemical methods, rare earths analysis, 687
gravimetry, 687–688
volumetry, 688
cerium, determination of, 688–689
europium, determination of, 689
Chemical process industry
rare-earth elements in, use of, 57–59
Chemical reduction, 32; *see also* Calcium reduction
Chemical treatment; *see also* Resource processing
of apatite, 277–279
of bastnasite
about, 261–265, 261f
Bear Lodge ore processing, 266
concentrate/chlorides of bastnasite, 263t
Goldschmidt process, 266–268, 266f, 267f, 268t
production of rare-earth chlorides from bastnasite, 262f
for treating Baotou rare-earth concentrates, 264f
for treating Beylikahir bastnasite preconcentrate, 265f
Elliot Lake uranium ore, Canada, 273
of euxenite, 274
of fergusonite, 276
of gadolinite, 273–274, 274f–276f
of ion-adsorption ore, 270–273, 270t, 273f
of loparite, 276
of monazite
acid treatment, 254, 255f
alkali treatment, 255, 256f
chlorination, 260–261
high-temperature process, 260
Indian Rare Earths Ltd. (IRE) plant, 255–258, 257f
monazite breakdown practices, 258–260, 259f
of pyrochlore, 277
of samarskite, 276
of xenotime, 269, 269f, 270f
Chilwa Island, 182; *see also* Malawi
China; *see also* Resources; World rare-earth production
Bayan Obo, 172, 174–175
ion-adsorption ore, 175–176, 175t
largest rare-earth deposit, 172, 173t
Mianning county, 176–177
mine production of rare earths, 199t–200t
placer deposits, 176
rare-earth production in, 207–209, 209f
summary of rare-earth deposits, 125t–127t
Chloride electrolysis, 403–408, 403t
Chloride preparation; *see also* Reduction
dehydration of hydrated rare-earth chloride, 339–344, 340f–344f
dry methods, 345–346, 346f
preparation of hydrated rare-earth chloride, 339
purification of rare-earth chlorides, 346–348, 347f
Chloride reduction processes, 22; *see also* Reduction
early attempts, 348–350, 349t
intermediate alloy processes, 353
Kroll-type processes
lithium reduction of dysprosium/holmium/erbium chlorides, 358–363, 362t
lithium reduction of rare-earth chlorides, 357–358, 357f
lithium reduction of yttrium chloride, 355–357
lithium/sodium reduction of yttrium chloride, 353–355, 354f, 355f, 356t
in refractory bomb (reactor), 350–352, 350f
in tantalum crucible, 352–353
Chlorination, 260–261; *see also* Monazite
furnace, 267, 267f
Chlorine gas, 345, 409
Chloroapatite blue phosphor, 673

Chromium, non-rare-earth impurities, 692
Chromogenic reagents
spectrophotometric determination, 692
Chuktukon deposit, 193–194; *see also* Soviet Union (USSR), former
Citric acid, complexes with, 31
Classical separation procedures, 21
C15 Laves phase compounds, 602
Clay, 546
Clean energy technology, 55
Clean slag–metal separation, 353
Climax Molybdenum Company's by-product plant, Colorado, 248
Coarse minerals, 724
Cobalt, recovery of, 660
Coercivity enhancement, 585
Coherence length, 617–618
Cold boat
solid-state electrorefining, 503
zone-refining, schematic diagram, 495
Cold isostatic press (CIP), 590–591
Cold water as leachant, 269
Collophane, 97
Coloration in glass, 59–60
Commercial mine production of rare earths, 195
Commercial phosphors, 63
Compact fluorescent lamps (CFLs), 65, 673
CREE spectrometer, 710
Complexes, 31; *see also* Rare earths
Compression molding, 580
Computerized axial tomography (CAT) scans, 37t
Comurhex, 570, 572–573
Consolidated alloys, production of, 569–570, 572–575
Comurhex, 572–573
General Motors, 573–574
Molycorp, 570
Research Chemicals, 570, 572
Ronson, 574
Santoku, 575
Th. Goldschmidt, 573
Continuous annular chromatograph (CAC), 290
Continuous displacement chromatography (CDC), 290
Continuous electrowinning, 418, 419f, 422f, 426
Continuous variable-discharge (CVD), 237
Controlled atmosphere temperature pressure (CATP), 414
Cooljarloo's deposits, 164; *see also* Australia
Copper, 591
alloys, 42; *see also* Metallurgy
condenser, air-cooled, 385
Coproducts, of rare earths, 195–197, 196t; *see also* Resources
Corrosion control by coatings on magnets, 595–598
CPL technology, *see* Carbonate pressure leach (CPL) technology
CREE, *see* Cathode ray-excited emission spectroscopy (CREE)
Cronstedt, A. F., 5
Crown Polymetallic Project, 167
CRTs, *see* Cathode ray tubes (CRTs)
Crucible, construction of, 451
Crude rare-earth chloride, 357
Crustal abundance of rare earths, 86–87, 86t, 87f; *see also* Resources
Cryogenic coolers, 604
Cryolite, 732
Crystallization, fractional, 282–283, 284f; *see also* Separation process
Crystals of monazite, 93
Crystal structures of rare earths, 23
Cummins Range, 165; *see also* Australia
Cyanex 272, 667
Cyanex 923, 324
Cyclic voltammetry, 434, 441
Czochralski method, 610
Czochralski or pulling technique, 606

D

DC-magnetron sputter (MS), 602
DCP-source spectrometry, 699
Decolorization, 59
Deep chemical weathering, 103
Dehydration of hydrated rare-earth chloride, 339–344, 340f–344f
Delafontaine, Marc, 5
Delanium carbon, 412
Demagnetization fields, 50
Demonstrated, definition, 157t
Denison Mines, 170, 309–310, 311f; *see also* Canada; Solvent extraction
Deoxidation
by oxyhalide formation, 516
refining by oxyhalide formation, 516
Department of Defense (DoD), US, 70
Department of Energy (DOE), US, 65
Deposit, defined, 154
Di-alkyl phosphinic acids, 301
1,2-diamine cyclohexane tetraacetic acid (DCTA), 289
Diamond Creek Area, Idaho, 187; *see also* United States
Dibutyl-butyl phosphonate (DBBP), 318
Dicarbides, 28
Dicyclohexyl phosphinic acid (DCHPA), 301
Didymium chloride, 298
Dielectric material, 57
Diethylene triamine pentaacetic acid (DTPA), 289
Di-2-ethyl-hexyl phosphoric acid (D2EHPA), 259, 296, 298
resin, 699

Die upsetting, 584
Diffusion-pumped vacuum system, 495
3,5-diisopropylsalicylic acid (DIPSA), 306
Dilute acids, 678
Direct melting, 568
Direct reduction technique, 396
Discovery of rare earths, 1–8, 2t–3t, 4f
Displacement chromatography, 286, 287f, 288f
Distillation apparatus
  diagram of, 360f
  rare earth-ferroalloy, 439f
Distilling, rare-earth metal, 455
Distribution coefficient, 286, 306
Divalent state, of rare earths, 32–33; *see also* Aqueous systems
DMF, *see* N,N-dimethyl formamide (DMF)
Dodecyl-amine (DDA), 293
Dodecyl ammonium acetate, 676
Dolomitic oxide, 350
Dolomitic-type ores, 174
Dong Pao deposit, 195; *see also* Vietnam
Double-chromate precipitation, 283
Double salts of rare earths, 31
Dredging operations, 241, 241f
Drum-type fluorinating reactor, 570–571
Dry ice–acetone cold trap, 341
Dry methods; *see also* Chloride preparation; Fluoride preparation
  for preparation of rare-earth chlorides, 345–346, 346f
  rare-earth oxides
    with ammonium bifluoride, reaction of, 366–367, 366f
    with anhydrous HF, reaction of, 364–366
Dry nitrogen, 563
Dry process, 328–329, 329f; *see also* Solvent extraction
Dubbo Zirconia Project (DZP), Toongi, 164; *see also* Australia
Ductile iron, 34, 36; *see also* Metallurgy
Dust emissions, 724
Dy–Nd separation factor, 666
Dysporium–terbium–iron magnetostrictive alloys, 53
Dysprosium, 455, 595
  applications, 38t
  atomic properties, 13t–15t
  and green technology initiatives, 214
  to lamp phosphor, 64
  mechanical properties, 16t–17t
  in neutron radiography, 67
  SSE processing of, 507
  substitution of, 49
  thermal/electrical/magnetic properties, 15t–16t
Dysprosium chloride, distillation of, 360
Dysprosium-doped crystals, 67
Dysprosium/holmium/erbium chlorides, lithium reduction of, 358–363, 362t

E

East ore body, 174
EBFZ, *see* Electron beam float zoning (EBFZ)
Economically exploitable deposits, definition, 154
Economic resources, 158t
Egypt
  occurrence of deposits in, 177
  summary of rare-earth deposits, 128t
Egyptian beach sands with heavy minerals, 245f
EHEHP, *see* 2-Ethylhexyl hydrogen ethylhexyl phosphonate (EHEHP)
Ekeberg, Anders Gustaf, 2
Elastic property, 25
Electrical conductivity, 55
Electric drive systems, 50
Electric energy generation, via wind power, 50
Electric motors, recycling loop, 633
Electric vehicles (EV), 50
Electrochemical extractions, 441
Electrodeposition
  of alloys, operational data for, 438t
  cell, rare earth-ferroalloy, 437f
  of europium from molten fluoride, 441
Electrodeposition-vacuum distillation process, 436
Electroless plating method, 595
Electrolysis
  of cerium trichloride, Gray's cell for, 407
  of chlorides, 432–435, 433f, 434f
  of oxide-fluoride melts
    distillation of alloys, operational data for, 440t
    electrochemical reduction of cerium oxide to metal, 441
    electrodeposition of alloys, operational data for, 438t
    electrodeposition of europium from molten fluoride, 441
    investigations, 412t
    overview, 435–441, 435f, 437f, 439f
Electrolytic cell
  current efficiency in, 442; *see also* Reduction
  with electrolyte skull hearth, 417f
  for neodymium reduction, 433f
  in protective atmosphere chamber, 416f
Electrolytic iron, 568
Electrolytic nickel coating, 596
Electrolytic preparation of rare-earth alloys, 431t
Electrolytic production of rare-earth metals; *see also* Reduction
  about, 402–403
  chloride electrolysis, 403–408, 403t

commercial electrowinning from rare-earth chlorides, 410–411, 411t
electrowinning at room temperature, 408–409
electrowinning solid metal deposits, 409
in situ preparation of electrolyte, 409–410
oxide-fluoride electrolysis
cell for electrowinning neodymium/praseodymium/didymium, 426–428, 426f, 427f, 429t
cells for electrowinning lanthanum, 419–426, 421t, 425t
Gray's cell, 412–413, 413f
high-temperature electrowinning cell, 428, 430–431, 430f
overview, 411–412, 412t
Reno cell type 6, 413–414, 415t
Reno cell type 12, 415–417, 416f, 417f, 418t
Reno continuous cell type 12, 418–419, 419f
Electromagnetic interference (EMI) problems, 652
Electron beam float zoning (EBFZ), 503, 506
Electron beam melting, 469
removed both fluorine and hydrogen, 486
Electron Energy Corporation (EEC), 48
Electronic configuration, 8, 9t–18t; *see also* Rare earths
Electronics
rare-earth application areas, 35t
use of rare-earth materials in, 56
Electronic scrap, 637, 685
Electron probe micro analysis (EPMA)
detection limits, 711
Electroreduction process
current efficiency of, 441
feasibility of, 434
Electrorefined gadolinium, 469
Electrorefining process, 478
cerium metal, 489–490
gadolinium, 482–489
yttrium, 478–482
Electrorefining process, refining, 478
cerium metal, 489–490
gadolinium, 482–489
yttrium, 478–482
Electroslag refining (ESR), 649
for RE alloy scrap recycling, 649
Electrostatic separation techniques, 238
Electrotransport, 510
mobility, 23
Electrotransport-purified rod, 502
Electrowinning; *see also* Electrolytic production of rare-earth metals
of neodymium/praseodymium/didymium, 429t
from rare-earth chlorides, commercial, 410–411, 411t
at room temperature, 408–409
solid metal deposits, 409
Electrowinning cell
with AC, 427f
high-temperature, 428, 430–431, 430f; *see also* Oxide-fluoride electrolysis
Element alloying, 591
Elevated water extraction, 739
Elk Creek Carbonatite, Nebraska, 186; *see also* United States
Ellingham diagram, 26, 27f
of compounds, 334
Elliot Lake uranium ore, Canada; *see also* Resource processing
chemical treatment of, 273
Elution chromatography, 286
EMI problems, *see* Electromagnetic interference (EMI) problems
Emission-control system in automobiles, 54
Emission spectroscopy, 693
End-of-life (EOL)
exhaust gas catalytic converters, 684
fluorescent lamps, 673, 675
recycling rates (EOL-RRs), 638
scrap, 669
vehicles, 637
Eneabba mineral sand deposit, 164; *see also* Australia
Energy-critical elements, 80t, 81
Energy-intensive process, refining of rare-earth concentrate, 725
Environmental aspects, 717
bastnasite treatment by oxidization roasting, 733
bear lodge, 738
air contamination, 739
water contamination, 738–739
cleaner production in China
research and development, 731
contaminant release points, 721
air emissions, 724
head-end processing, 725
mill, 724
mine pit, 723
mine site, 724
rare-earth mining
processing, head-end operations of, 722
risks of, 722
tailing impoundment, 723
waste rock stockpiles, 724
Dubbo Zirconia Project, 740–741
entry criteria for rare-earth industry, China, 730–731
environmental problems, technology solutions
eco-friendly RE/Th separation, 732
fluorine emission and mitigation, 731–732
wastewater treatment, 732–734

environment-friendly processing outside China
mine planning/management, 735
monazite and xenotime, 734
recovery rates, 734–735
formation of synthetic cryolite, 733
head-end operations of rare-earth mining and processing, 722
Kvanefjeld region, 741–742
mining, extraction, and separation methods, 728–729
mining/processing, main process steps, 720
REE mining and processing, 721
mining/processing in China
Bayan Obo facilities, 726
ion-adsorption deposits, 727
overview, 725
processing, 727
REE separation/refining, wastewater, 727–730
Sichuan mine, 726–727
Mountain Pass mine and refinery, 735–738
Mt. Weld deposit, 739–740
Nechalacho Project, 742–743
paste technology, 737
rare-earth element (REE), 717
rare-earth mining without/with insufficient environmental protection systems, 722
rare-earth ores, contaminant elements, 718
hard-rock mining, contaminants, 719–720
radioactive contaminants, 718–719
rare-earth elements, 720
REE mining and processing, 721
separation and recovery of RE(III), Ce(IV), Th(IV), and F(I), 733
Steenkampskrall mine, 742
technology solutions to environmental problems, 731
Environmental problems, technology solutions
eco-friendly RE/Th separation, 732
fluorine emission and mitigation, 731–732
wastewater treatment, 732–734
Environment-friendly processing outside China
mine planning/management, 735
monazite and xenotime, 734
recovery rates, 734–735
EOL, *see* End-of-life (EOL)
EPMA, *see* Electron probe micro analysis (EPMA)
Equilibrium oxygen pressures, 458
Erbia, 67
Erbium, 455
applications, 39t
atomic properties, 13t–15t
mechanical properties, 16t–17t
SSE of, 508
thermal/electrical/magnetic properties, 15t–16t
Erbium chloride, distillation of, 360
Erbium-doped fiber amplifiers (EDFA), 61
Erbium oxide
color to glass, 59
Erosion-resistant coating, 604–605
ESR, *see* Electroslag refining (ESR)
Ethylenediaminetetraacetic acid (EDTA), 31, 283, 289, 688
2-ethyl-hexyl-2-ethyl-hexyl phosphonic acid (EHEHPA), 293, 305t
2-Ethyl hexyl hydrogen ethylhexyl phosphonate (EHEHP), 702
2-ethyl-hexyl phosphonic acid mono-2-ethyl-hexyl ester (HEHEHP), 298, 307, 317f, 732
Eudialyte, 99; *see also* Minerals
European glass industry, 61
Europium, 281, 689, 694
applications, 38t
atomic properties, 9t–10t
mechanical properties, 13t
from molten fluoride, electrodeposition of, 441
preparation of, 383–384, 384f; *see also* Reduction distillation process
purification of, 316f
reduction apparatus, 384
reduction of, 379–380; *see also* Fluoride reduction process
separation by selective reduction, 282f
thermal/electrical/magnetic properties, 11t–12t
Europium-based phosphors, 677
Europium hexaboride, neutron absorber, 66
Euxenite, 99, 688; *see also* Minerals; Resource processing
chemical treatment of, 274
Excessive carbonate mineral dissolution, 719
Extractable reserves, definition, 158t
Extractant, 291

F

Falcon concentrator, 252, 253
Fanshan phosphorite ore, 278
Farafangana heavy mineral prospect region, 180
Fatty acid collector systems, 247
Fatty acids, 244
FCC, *see* Fluid cracking catalyst (FCC)
Fecralloy, 40
Fergusonite, 99, 688; *see also* Minerals; Resource processing
chemical treatment of, 276
Ferrites
lanthanum substitution in, 599–600
magnet, 44

Ferroboron, 568–569, 570
Ferromagnetism, 24
Ferrosilicon, as reductants, 538
FES, *see* Flame emission spectroscopy (FES)
FeSi intermetallic compounds, 644
Fe_2Ti intermetallic compounds, 644
Filtration, 346, 348
Fisher subsieve sizer, 593
Flame emission spectra, 694
Flame emission spectroscopy (FES), 694
Flintstone, 33
Florencite, 100; *see also* Minerals
Florida-Georgia beach placers, 191–192; *see also* Placer deposits
Flotation
  bastnasite, 244–246
  froth, 244
  monazite, 246–247
  rougher, 249
Fluid catalytic cracking (FCC)
  catalysts, 37t
  process, 57–58
Fluid cracking catalyst (FCC), 545–546, 683
  rare-earth content, 684
Fluidized bed method, 365–366; *see also* Dry methods
Fluorapatite in Egypt, 177
Fluorescent lamps, 637, 673
Fluorescent lightbulbs, 65
Fluorescent lighting, energy-efficient, 38t
Fluoride glasses, 61
Fluoride ion, 732
Fluoride preparation
  dry method
    rare-earth oxides with ammonium bifluoride, reaction of, 366–367, 366f
    rare-earth oxides with anhydrous HF, reaction of, 364–366, 364f
  purification of rare-earth fluorides, 367–368
  wet method, 363–364
Fluoride reduction process; *see also* Reduction
  about, 368–369, 368t
  calcium reduction (Ames process)
    Goldschmidt process, 374–375
    overview, 371–372, 372f–374f
    semicontinuous reduction, 372–373, 375f
  intermediate alloy process, 376–379, 377f, 378t
  lithium reduction, 369–371, 369f, 370f
  samarium/europium/ytterbium, reduction of, 379–380
  scandium preparation, 379
Fluorides, 30
Fluoridizing reactor, 572
Fluorine, 719
  impurity in, 455, 473, 508
  occurrence, 175
Fluorocarbonate mineral, magma-derived, 88
Fluorspar crucible, 406–407
Fluvial or stream placers, 169
Flux method, 617
Forecasts for rare-earth production, 232
Fractional crystallization, 282–283, 284f; *see also* Separation process
  methods, 21
Fractional precipitation, 283–285; *see also* Separation process
  methods, 21
Francolite, 278
Fray Farthing and Chen (FFC), 441
Froth flotation, 244; *see also* Physical beneficiation
Fuel cells, 55
Full width at half maximum (FWHM), 66
Fused-salt electrolysis, 22, 33
  production of alloy by, 549
Fused-salt electrorefining, 447

G

Gabon, summary of rare-earth deposits, 128t
Gadolinite, 100, 688; *see also* Minerals; Resource processing
  chemical treatment of, 273–274, 274f–276f
  sequence, 4f
Gadolinium, 308, 432, 478
  applications, 38t
  atomic properties, 13t–15t
  cold-boat zone refined, 496
  electrorefined, 486, 487, 488
  impurity profile in, 497
  in magnetic refrigeration cycles, 53
  mechanical properties, 16t–17t
  and optical glasses, 60
  refining of, 493
  and samarium, 47
  in scintillator materials, 63
  thermal/electrical/magnetic properties, 15t–16t
  volatile metal, 512
  zone refining of, 498
Gadolinium–aluminum garnet (GAG) single crystal, 53
Gadolinium–aluminum–scandium garnet (GASG), 57
Gadolinium electrolyzed, nitrogen content of, 488
Gadolinium gallium garnet, 611
Gadolinium gallium garnet (GGG), 606
Gadolinium oxide, 430, 710
  neutron absorber, 66
  for optical fibers, 57
Gallinas Mountains, New Mexico, 190; *see also* United States

Gangue minerals, 246, 247, 248
Gas cycle refrigeration, 603
Gas turbines, 56
GdPd, 603–604
Geiger-Muller (GM) counter, 710
General Electric Company's Aircraft Nuclear Propulsion Department (GE-ANPD), 491
General Motors, 569, 570, 573–574
German Federal Institute for Geosciences and Natural Resources, 177
Germany
  advanced rare earth projects, 220t
  occurrence of deposits in, 177
Giant magnetostriction (GM), 601
Giant magnetostrictive actuator (GMA), 602
Gilgai Intrusion, 165; *see also* Australia
Ginzburg and Landau (GL) theory, 617–618
Glass
  polishing, 61
  rare-earth application areas, 35t
Glass-slag method, 651
  recycling, Sm–Fe alloy, 650
Global rare-earth demand, 73–81; *see also* Rare earths
Global RE reserve estimates (2009–2010), 161t–162t; *see also* Resources
Glove box furnace, 359f
GMEL Kvanefjeld project, 741
Goldschmidt, 570
Goldschmidt process, 266–268, 266f, 267f, 268t, 374–375; *see also* Bastnasite; Calcium reduction (Ames process)
Grain orientation, 590–591
Granular alumina, 430
Graphite crucible, 428
Graphite electrodes, 22
Gravimetric methods, 687
Gravimetry
  cerium(IV), 687
  chemical methods, rare earths analysis, 687–688
Gravity preconcentration, 252
Gravity separation, 239, 250
Gravity separator, 237
Gray's cell, 407, 412–413, 413f; *see also* Oxide-fluoride electrolysis
Great Western Minerals Group (GWMG), 171, 211
Greenland
  advanced rare earth projects, 220t–221t
  occurrence of deposits in, 177–178
  summary of rare-earth deposits, 128t
Greenland and the European Environment Agency on environmental issues, 742
Green technologies, recycling, 633
Grirem Advanced Materials Co., Ltd. (GRINM), 325
Groundwater, soil contamination, 736

H

Halides, 30
Hall Mountain, Idaho, 187; *see also* United States
Halogen bulbs, incandescent, 65
Halophosphate-type phosphors
  gravities of, 675
Hard disk drives (HDDs), 665
Hard-rock deposits; *see also* Mining
  in India, 178–179; *see also* India
  mining and, 236
  in Thailand, 185
Hard-rock mining, 719
HDDs, *see* Hard disk drives (HDDs)
HDEHP, 293, 295, 296f, 305t
Heat-resistant alloys, 40
Heavy minerals (HM), 103, 237
Heavy rare-earth (HRE), 254
Heavy rare-earth element (HREE), 88, 171
  mining, 721, 741
HEHEHP, *see* 2-Ethyl-hexyl phosphonic mono-2-ethyl-hexyl ester (HEHEHP)
Height equivalent of theoretical plate (HETP), 289
HEVs, *see* Hybrid electric vehicles (HEVs)
Hexaborides of rare earths, 56
Hexagonal close packed (hcp)-hcp-to-bcc transformation temperature, 506
HF, *see* Hydrogen fluoride (HF)
Hicks Dome, Illinois, 188; *see also* United States
High-critical-temperature superconductivity, 70
High-gradient (2T) magnetic separator (HGMS), 677
High-performance liquid chromatography (HPLC), 689
High-purity calcium, 452
High-strength low-alloy (HSLA) steels, 36
High-temperature electrowinning cell, 428, 430–431, 430f; *see also* Oxide-fluoride electrolysis
High-temperature reaction of monazite, 260; *see also* Monazite
High-temperature vacuum melting, 463
High vacuum reduction distillation assembly, 354
HILOP technology, 590
HITACHI, 590
HNO_3–H_2O_2 mixture, 682
Hoidas Lake vein deposit, 171; *see also* Canada
Holmium, 455
  applications, 39t
  atomic properties, 13t–15t

mechanical properties, 16t–17t
thermal/electrical/magnetic properties, 15t–16t
Holmium chloride, distillation of, 360
Hot dip aluminizing method, 596
Hot-pressed magnets, 584–585
Hot pressing, 563
HPLC, *see* High-performance liquid chromatography (HPLC)
HREE mining, *see* Heavy rare-earth element (HREE) mining
Hubei-Sichuan belt, China, 172
Hybrid electric vehicles (HEVs), 50, 70
NiMH batteries, 638
Hydrated rare-earth chlorides; *see also* Chloride preparation
dehydration of, 339–344, 340f–344f
preparation of, 339
Hydride compressor, alloys for, 609
Hydride heat pumps, 69
Hydride refrigerator, 69
Hydrochloric acid, 257, 280, 677
Hydrofluoric acid, 29, 363
Hydrofluorination
rotary batch method, 364
of yttrium oxide, 365f
Hydrogen, 28; *see also* Reactivity
absorption, 67–68, 67–70; *see also* Rare earths
elimination, 457
vacuum/inert gas fusion, 711
Hydrogenation-disproportionation-desorption-recombination (HDDR), 577–579
Hydrogen decrepitating (HD) treatment, 577
Hydrogen fluoride (HF), 450
Hydrogen-reduced scrap powder, 652
Hydrogen storage materials, 607–610
Hydrometallurgical process, recycling, 663, 684
to treat spent borosilicate optical glass, 685
Hydrometallurgical separation process
environmentally friendly, 731
Hydrometallurgy, recycling, 652, 653
hydrothermal process, 658
leaching, 658–664
leaching and precipitation, 653–656
precipitation, 658–664
Rhône Poulenc process, 656–657
solvent extraction, 658–664
Hydrometallurgy techniques, 235
Hydrous ceric oxide, 31
Hydroxamic acids, 245, 246
Hydroxide–trisodium phosphate mixture, 256
2-hydroxy-ethylenediamine-triacetic acid (HEDTA), 31, 289, 290
Hygroscopicity, of chlorides, 450
Hypothetical resources, 158t

I

ICCD, *see* Intensified charge coupled device (ICCD)
ICP-AES, *see* Induction-coupled plasma atomic-emission spectrometry (ICP-AES)
ICP-MS, *see* Induction-coupled plasma mass spectrometry (ICP-MS)
ICP spectrometry techniques, 704
Idaho placer deposits, 190–191; *see also* Placer deposits
Identified resources, definition, 157t
IDMS, *see* Isotope dilution mass spectrometry (IDMS)
Impurities, origin of, 448–453
crucible and reactor, 451–452
environment, 452–453
starting materials, 449–451
Impurities refining, origin of, 448–453
crucible and reactor, 451–452
environment, 452–453
starting materials, 449–451
Impurity removal methods, 453
Incandescent halogen bulbs, 65
India; *see also* Resources; World rare-earth production
hard rock deposits, 178–179
mine production of rare earths, 199t–200t
placers, 179
rare-earth production in, 203
summary of rare-earth deposits, 129t–130t
Indian monazite, 95t
lanthanum to lutetium, 708
Indian rare earths, 310–318, 312f–317f; *see also* Solvent extraction
Indian Rare Earths Ltd. (IRE) plant, 255–258, 257f; *see also* Monazite
Indicated, definition, 157t
Indonesia, occurrence of deposits in, 179
Induction-coupled plasma atomic-emission spectrometry (ICP-AES), 698
Induction-coupled plasma mass spectrometry (ICP-MS), 698
acid digestion of oil samples, 700
determination of REEs, 700
double-focusing sector-field, 702
isobaric interference, 700
multicollector ICP-MS (MC-ICP-MS), 702
RE impurity determination, 700
single-collector, 702
XRF spectrometry, 704
Industrial reserves of China, 172
Industrial solvent extraction, 307–308; *see also* Solvent extraction
Inferred, definition, 157t
Inferred reserve base, definition, 157t
Infrared (IR) radiation absorption, 713

Injection-molded magnets, 566
Injection molding, 582
Inner Mongolia belt, 172
Inner transition elements, 8
In situ preparation of electrolyte, 409–410
In situ weathering, 105, 175
Instrumental neutron activation analysis (INAA), 708
Instrumental techniques, rare earths analysis, 710
  cathode ray-excited emission spectroscopy (CREE), 710
  secondary ion mass spectrometry, 711
  spark source mass spectrometry (SSMS), 711
  x-ray–excited optical luminescence (XEOL) spectroscopy, 710–711
Intensified charge coupled device (ICCD), 699
Intergranular corrosion, 595
Intermediate alloy process, 353, 376–379, 377f, 378t; *see also* Chloride reduction processes; Fluoride reduction process
Internal baffling, 392
International Commission on Illumination (CIE), 614
International Lead–Zinc Research Organization, 42
Interstitial impurities, 370
Interstitial modification, 48
Iodides, 30
  refining process, 515
Iodine, 351, 537
Ion-adsorption ore; *see also* China; Resource processing
  chemical treatment of, 270–273, 270t, 273f
  cost of mining, 176
  discovery of, 175
  distribution of, in South China, 175t
  grades of, 176
  in South China, 101
Ion exchange, 285–290, 287f, 288f
  chromatography, 286
  technology, 658, 699
Ionic liquids, 667
Ionization potentials of rare-earth elements, 8, 10t
Ionizing radiation, from radioactive decay, 719
Iron
  alloys of rare earths, 51
  chemical decolorization of, 59
  deposits of Mineville–Port Henry area, 188
  ductile, 34, 36; *see also* Metallurgy
Iron fluoride, 572
Iron Hill, Colorado, 190; *see also* United States
Iron oxide, impurity in glass, 59
Iron oxide copper–gold, 104t
Iron (Fe)–REE–thorium–apatite (FRETA) deposit, 187
Iron sulfides, 36
Isostatic press, 593
Isotope dilution mass spectrometry (IDMS), 702

J

Jangardup mineral sand deposit, 165; *see also* Australia
Japan, occurrence of deposits in, 180
Jet-milling process, 577
John Galt, 168; *see also* Australia
Joule–Brayton cycle, 603–604
Junior miner, 228
Jurien Bay sand deposits, 164; *see also* Australia

K

Kangankunde Hill rare-earth deposit, 181; *see also* Malawi
Karst bauxites, 105
Kazakhstan, advanced rare earth projects, 221t
Kenya
  advanced rare earth projects, 221t
  occurrence of deposits in, 180
  summary of rare-earth deposits, 130t
Kipawa Alkaline Complex, 171–172; *see also* Canada
Knelson concentrator, 237
Knudsen effusion technique, 22
Kramer, Matthew, 591
Kroll-type processes; *see also* Chloride reduction processes
  lithium reduction
    of dysprosium/holmium/erbium chlorides, 358–363, 362t
    of rare-earth chlorides, 357–358, 357f
    of yttrium chloride, 355–357
  lithium/sodium reduction of yttrium chloride, 353–355, 354f, 355f, 356t
Kwale Project, 180
Kyrgyzstan, 194; *see also* Soviet Union (USSR), former

L

Lamp phosphors, 63, 64, 674
  mixtures, 677
  recycling of, 675
$LaNi_5$-hydrogen system, 607
Lanthanides, 694
  carboxylates, 72
  contraction, 19–20, 19f; *see also* Rare earths
  trivalent, 303f, 304f
Lanthanothermic reduction, *see* Lanthanothermy
Lanthanothermy; *see also* Oxide reduction processes
  europium, preparation of, 383–384, 384f

samarium/europium/ytterbium/terbium, preparation of, 384–386, 385f
samarium/ytterbium, preparation of, 383
Lanthanum, 283, 523
applications, 37t
atomic properties, 9t–10t
boiling point, highest, 22
electrolysis cell in protective atmosphere chamber, 423f
electrowinning of, 420f, 421t, 422f
in high-temperature iron-based alloys, 40
largest radius, 19
mechanical properties, 13t
molten, 423
in optical glass industry, 60
oxidation of, 25
separation by fractional crystallization, 284f
thermal/electrical/magnetic properties, 11t–12t
Lanthanum chloride, 63
Lanthanum deposition
to glass imparts, 684
Van Arkel–de Boer process, 515
zone refining of, 496
Lanthanum nickel hydride, 607–610
Lanthanum oxide, 383
Lanthanum substitution in ferrites, 599–600
Lanthanum turnings, commercial, 384
Laser-induced breakdown spectroscopy (LIBS), 699
Laterite clays, 101
Laterite zone, 165
Lateritic ores, in Brazil, 169
Laves-phase alloy, 51
LCD, 637
Lead–zinc system, 647
Lead zirconate titanate (PLZT), 56
LED, 637
Lemhi Pass District, Idaho, 187; *see also* United States
Leucoxene, 240
LIBS, *see* Laser-induced breakdown spectroscopy (LIBS)
LiCl
electrolyte consisted, 480
fluoride–chloride electrolyte composed of, 482
LiCl-LiF-YF_3 system, 481
LiCl-YCl_3
electrolyte, 478
melt, 481
Light-emitting diodes (LED), 65
Light rare-earth elements (LREEs), 88, 171, 726
Light rare-earth oxide, 93
Light rare earths (LRE), 259, 288
Lignin sulfonate, 245
Limits of quantitations (LOQs), 702
Linear fluorescent lamp (LFL), 65
Liquid crystal display (LCD) screens, 38t
Liquid-liquid extraction technology, 647
Liquid rare-earth metals, tantalum solubility, 452
Lithium amalgam electrodes, 281
Lithium battery, 75
Lithium reduction; *see also* Kroll-type processes
of dysprosium/holmium/erbium chlorides, 358–363, 362t
of rare-earth chlorides, 357–358, 357f
in reduction of rare-earth fluorides, 369–371, 369f, 370f; *see also* Fluoride reduction process
of yttrium chloride, 355–357
Lithium/sodium reduction of yttrium chloride, 353–355, 354f, 355f, 356t
Lithium vapor, 356, 358
Loaded bomb for calciothermic reduction, 350f
Loaded organic (LO) phase, 272
Locations of rare-earth deposits, 154f, 155t–156t; *see also* Resources
Lodestone, 43, 44f
Long-chain quaternary ammonium salts, 303
Longnan rare-earth ore
composition of, 101t
features of, 270t
Long-range-ordered alloys, 43; *see also* Metallurgy
Loparite, 100; *see also* Minerals; Resource processing
chemical treatment of, 276
occurrence in Kola Peninsula, Russia, 253
LOQs, *see* Limits of quantitations (LOQs)
Lorentz force, 618
Lovozero Mining Company (LMC), 210
Low-pressure reverse osmosis (LPRO), 734
ammonia, removal ratio of, 734
LREEs, *see* Light rare-earth elements (LREEs)
Lutetium
applications, 39t
atomic properties, 13t–15t
mechanical properties, 16t–17t
purified by distillation, 475
with smallest radius, 19
thermal/electrical/magnetic properties, 15t–16t
Lynas Corporation Ltd, in Malaysia, 212
Lynas Malaysia, 740

M

Madagascar; *see also* World rare-earth production
advanced rare earth projects, 222t
occurrence of deposits in, 180
rare-earth production in, 213
summary of rare-earth deposits, 131t

Maghemite, 43
Magmas, 103
Magnequench powder, melt-spun, 49
Magnesia, 54
Magnesium
  alloys, 41; *see also* Metallurgy
  as reducing agent, 379
  removal, 376
Magnesium oxide, stability of, 382
Magnetic properties of rare-earth metals, 24
Magnetic refrigerants (magnetocaloric materials), 602–605
  magnetic refrigeration, 603–605
Magnetic refrigeration, 53, 603–605; *see also* Rare earths
Magnetic separation of minerals, 238–239
Magnetite, mineral, 43
Magnetizability, 240
Magnetocaloric materials, 602–605
Magnetocalorific effect (MCE), 53
Magneto-optic recording films, 38t
Magneto-optic storage media, 606–607
Magnetostriction, 51
Magnetostrictive material (TERFENOL-D), 601–602
Magnets; *see also* Rare earths
  characteristics, 46t
  naturally occurring, 43
  operating temperature range for, 48f
  permanent magnet (PM), 43
  permanent magnet development timeline, 45t
  permanent magnet generators (PMG), 50
  permanent magnet sales, 47t
  progress (of 270 years) in magnet technology, 43, 44f
  rare-earth application areas, 35t
  temperature performance, 49f
  windmill story, 51, 52t
Magnets, recycling, 668
  end-of-life scrap, 669
    collection, 669–670
    dismantling, 670–671
    mixed Sm–Co/Nd–Fe–B scrap, 671
    NdFeB, 671
    samarium–cobalt, 671
  in-plant/preconsumer scrap, 669
Magnet scrap, rare-earth magnets, 669
Main ore body, 174
Malawi; *see also* Resources
  advanced rare earth projects, 222t
  Chilwa Island, 182
  Kangankunde Hill rare-earth deposit, 181
  Nanthace Hill, 181
  occurrence of deposits in, 181–182
  Songwe, 182
  summary of rare-earth deposits, 131t
Malaysia; *see also* World rare-earth production
  mine production of rare earths, 199t–200t
  occurrence of deposits in, 180–181
  rare-earth production in, 212
Malaysian Rare Earth Corporation (MAREC), 269
Marginally economic deposits, definition, 154
Marginal reserves, definition, 158t
Marine phosphorite deposits, 191
Marine placers, 169
Mary Kathleen, 166–167; *see also* Australia
Matrix bonding, 566–567
Mauritania, summary of rare-earth deposits, 131t
MBAC Fertilizer, 169
McCallum, Bill, 591
McFarland, 553–554
Measured, definition, 157t
Mechanical alloying, 43
  for producing RE–TM–Mg alloys, 545
Mechanical milling, reduction of samarium chloride by, 380
Mechanical properties of rare-earth metals, 25
Medium rare earths, 88
Megon Company, Norway, 319–321, 320f; *see also* Solvent extraction
Melting point of rare-earth metals, 21–22
Melt spinning, 576–577
Melt synthesis, 616–617
  flux method, 617
  molten salt synthesis, 616–617
Melt texturing, 620
Mercury, fluorescent lamps and CFLs, 674
Mercury-binding functional groups, 675
Mesoproterozoic granite, 187
Metal alloys, 35t
Metal hydride process, 68
Metal ingot, 338
Metal injection molding (MIM), 591
Metallic coatings, 588
Metallic precursor (MP) approach, 620–621
Metallic reduction assembly, 355f
Metallothermic reduction
  about system, 395f
  in molten salt, 398–401, 399f, 400f, 401t; *see also* Reduction
Metallothermy, 337–338; *see also* Reduction
Metallurgy; *see also* Rare earths
  aluminum alloys, 41–42
  copper alloys, 42
  ductile iron, 34, 36
  long-range-ordered alloys, 43
  magnesium alloys, 41
  oxide dispersion–strengthened (ODS) alloys, 43
  steels, 36, 40
  superalloys, 40
  titanium alloys, 42
  zinc alloys, 42–43

Metal matrix magnets, 566
Metal-oxygen-silicon systems, 461
Metal-oxygen solid solutions, 26
Metal powder, 338
Metal refining, for research purposes, 447
Methanation catalysts, 58
Methyl-dioctyl-amine (MDOA), 293
Mianning county, 176–177; *see also* China
Microalloying, 42
Microwave plasma, 700
Middle rare earths (MRE), 283
Mine production of rare earths, 199t–200t; *see also* World rare-earth production
Mineral flotation, 244
Mineralization, rare-earth (in China), 172
Minerals; *see also* Resources
  about, 87–88
  allanite, 94, 96t, 97
  apatite, 96t, 97, 98t, 99
  bastnasite, 88, 93, 93t
  brannerite, 96t, 99
  eudialyte, 99
  euxenite, 99
  fergusonite, 99
  florencite, 100
  gadolinite, 100
  important rare-earth minerals, 92t
  ion-adsorption ore, 101
  loparite, 100
  monazite, 93–94, 95t
  perovskite, 100
  promethium, 102
  pyrochlore, 100
  scandium, 102
  in world rare-earth deposits, 89t–91t
  xenotime, 94, 96t
  zircon, 100
Mineville Iron District, New York, 188; *see also* United States
Mining; *see also* Resource processing
  activities, ventilation for exposures to radiation, 743
  hard-rock deposits, 236
  placer deposits, 236
Mining/processing in China
  Bayan Obo facilities, 726
  ion-adsorption deposits, 727
  overview, 725
  processing, 727
  REE separation/refining, wastewater, 727–730
  Sichuan mine, 726–727
Mintek, 318–319, 318f; *see also* Solvent extraction
Misch metals, 33–34, 523–538
  additions to copper, 42
  in alloy Galfan, 42
  ames process, 532–534
  commercial production, 524, 528, 531
  composition change of, 534
  contamination of, 527
  to electrical-resistance alloys, 40
  electrolysis of chlorides, 526–528
  electrolysis of oxide–fluoride melts, 528–532
  preparation of mixed rare-earth chlorides, 524–525
    dehydration techniques, 524–525
    melting and heating, 524
  pyrophoric properties of, 524
  source for, 524
Mixer–settler assemblies, 307
MMM Conference in Pittsburgh, 568
Modifier, 291
Molten fluorides, 650
  systems, 442
Molten metal, 338, 409
Molten salt, 402, 403, 407
Molten salt oxide reduction process, 401, 401t
Molten silver, 648
Molybdenum, 406, 419
Molycorp Minerals, 204, 528, 570, 572, 736, 737
Molycorp process; *see also* Solvent extraction
  chemical treatment of bastnasite, 262
  for europium oxide, 309f
  processing of Mountain Pass bastnasite, 308–309
  for pure yttrium oxide, 310f
Monazite, 93–94, 95t, 523, 688; *see also* Minerals; Resource processing
  activated by sodium oxalate, 246
  by-product in Sri Lanka, 213
  characteristics of, 201–202
  chemical treatment of
    acid treatment, 254, 255f
    alkali treatment, 255, 256f
    chlorination, 260–261, 525
    high-temperature process, 260
    Indian Rare Earths Ltd. (IRE) plant, 255–258, 257f
    monazite breakdown practices, 258–260, 259f
  composition, 523
  constituent of all of placer deposits, 206
  crystals of, 93
  first production in Brazil, 202
  Indian, 95t
  major rare-earth resource, 198
  ores from Belgian Congo, 534
  physical beneficiation of
    about, 239–243, 240f–246f
    bastnasite flotation, 244–246
    froth flotation, 244
    monazite flotation, 246–247
  processing, 523–524
  wet chemical treatment of, 524

Mongolia, summary of rare-earth deposits, 132t
Monobasic organophosphorus acids, 293
Monocarbides, 28
Mononitrides of rare earths, 26
Monovalent cations, 271
Mosander, Carl Gustaf, 5
Moseley check, 7
Mountain Pass, California, 189; *see also* United States
Mountain Pass ore, 248
Mount Weld deposit, 167, 207; *see also* Australia
Mozambique
  advanced rare earth projects, 221t
  occurrence of deposits in, 182
  summary of rare-earth deposits, 132t–133t
MRI machines, 637
Mullite bricks, 544
Multicomponent RE-Ni-Mg intermetallics, preparation of, 609–610
Murray Basin deposits, 165; *see also* Australia
Music Valley, California, 186; *see also* United States
Muthmann-type electrolysis cell, 404–405, 404f, 411
Myanmar, occurrence of deposits in, 182

N

Namibia
  advanced rare earth projects, 222t
  summary of rare-earth deposits, 133t
Nam Xe rare-earth deposit, 194–195; *see also* Vietnam
Nanthace Hill, 181; *see also* Malawi
Naphthenic acid, 300, 324, 326
National Energy Technology Laboratory (NETL), 55
Naval Ordnance Laboratory (NOL), 51
Nd alloy, Sm-Co recovery, 654
Nd-Dy separation, 667
$Nd_2Fe_{14}B$, Ames Laboratory process for, 647
Nd-Fe-O ternary, 656
Nd-H_2O systems, 656
Nd-YAG ceramics, 610–611
Nechalacho deposit, mineralogical composition of, 170–171, 251, 252t; *see also* Canada; Physical beneficiation
Neodymium, 305, 523, 647, 653
  as activators in laser glasses, 60–61
  applications, 37t
  atomic properties, 9t–10t
  electrolysis cell for reduction of, 433f
  and glass colors, 59
  light absorption, 57
  magnets, 668; *see also* Neodymium-iron-boron magnets
  mechanical properties, 13t
  metal production, 398–399
  recovery of, 314f
  supply of, 48
  thermal/electrical/magnetic properties, 11t–12t
  vapor pressure of, 506
Neodymium chloride, apparatus for dehydrating, 344f
Neodymium-containing boron trioxide, 653
Neodymium-containing oxides, recycling
  chemical treatment process, 653
Neodymium-iron-boron magnets, 44, 567–598, 637, 670
  bonded magnet scrap powder, 652
  corrosion control by coatings on magnets, 595–598
  hydrometallurgical treatments for, 671
  master alloy, calciothermic reduction, 658
  material, 652, 669
  preservation and enhancement of magnetic properties, 589–595
    super high-energy magnets, 592–594
    two-alloy process, 594–595
  production of Nd-Fe-B alloys, 568–575
    consolidation, 580–582, 584–585
    coreduction, 568–569
    direct melting, 568
    production of consolidated alloys, 569–570, 572–575
    sintered magnets, 586–589
  production of Nd-Fe-B magnets, 575–589
    consolidation, 580–582, 584–585
    hydrogenation-disproportionation-desorption-recombination (HDDR), 577–579
    melt spinning, 576–577
    sintered magnets, 586–589
    strip casting, 577
  recycling, 666
  ribbons, 643
  scrap, recycling, 655
    by liquid metal (Ag) extraction, 648
  scraps, 646
  swarf, 671
Neodymium nitrate, 570
Neodymium oxide, 60
Neodymium–praseodymium, 645
NEOMAX Co. Ltd., 591
Neutralization, 263
Neutron-absorbing isotope, 67
Neutron activation analysis (NAA), 690
  post-irradiation steps, 705, 708
Neutron radiography, 67
New Zealand
  occurrence of deposits in, 182
  summary of rare-earth deposits, 134t

Next-generation space telescope (NGST), 53
Ni, recovery of, 660
Nichia Chemical Company, 612–613
Nickel coating, 596–597
Nickel-metal hydride (NiMH) battery, 37t, 69, 608, 638
Nilson, Lars Frederick, 6
NiMH batteries, recycling, 640, 672
  direct-current (DC) electric arc furnace, 640
  Honda hybrid vehicles., 661
  by hydrochloric acid leaching and solvent extraction, 665
  industrial-scale flow sheet, 642
  pyrometallurgical treatment, 643
  recovery of, 660
  by sulfuric acid leaching, 664
NiMH battery and hydrogen storage materials, 607–610
  alloys for hydride compressor, 609
  $LaNi_5$-hydrogen system, 607
  preparation of alloys, 607–608
  preparation of multicomponent RE-Ni-Mg intermetallics, 609–610
Ni–MH type, rechargeable batteries of, 672
Nitrate system, 303
Nitric acid, 29, 30, 310
Nitrilotriacetic acid (NTA), 289
Nitrilotriacetic acid-type resin, 682
Nitrogen, 26–28, 27f; *see also* Reactivity
  vacuum/inert gas fusion
N,N-dimethyl formamide (DMF), 676
N,N-dioctyldiglycolamic acid (DODGAA), 667
N,N,NN′tetraoctyl-1,5-diglycolamide ligand (TODGA), 703
Nodular iron, 34
Nolans Bore deposit, 165–166; *see also* Australia
Nonprecipitation process, 272
Nonuniform anode burning, 417
Nonyl phenyl phosphoric acid (NPPA), 278
Norraburra RE deposit, 166; *see also* Australia
North and South Carolina placers, 191; *see also* Placer deposits
North Atlantic Mineral Resource Zone (NAMRZ), 225, 227
Northeastern Wyoming receives, 738
N-phenyl anthranilic acid, 689
Nuclear energy, rare earth applications in, 66–67

O

Ochroite earth, 5
Off-spec, 570
Olympic Dam deposit, South Australia, 105, 206
Ono and Suzuki (OS) processes, 441
Open-circuit chronopotentiometry, 434
O-phenanthroline, 689
Optical decolorization, 59
Optical emission spectroscopy, 693
Optics industry, use of rare earths in, 59–61; *see also* Rare earths
Organic coatings, 596
Organic solvents, 295
Organolanthanide phosphor (OLP), 63
Organophosphorus acids, 293, 295–300, 297t, 299t; *see also* Solvent extraction
Ormerod, 568
Oxalate precipitations, 31, 688
  during ames process, 532–533
Oxalic acid, 269
  to strip solution, 319
Oxidation
  of light rare earths, 25–26
  selective, 279–280, 280f; *see also* Separation process
Oxidation–precipitation process, 280
Oxide-deficient melt, electrolysis of, 488
Oxide dispersion-strengthened (ODS) alloys, 39t, 43; *see also* Metallurgy
Oxide-fluoride electrolysis; *see also* Electrolytic production of rare-earth metals
  cell for electrowinning neodymium/praseodymium/didymium, 426–428, 426f, 427f, 429t
  cells for electrowinning lanthanum, 419–426, 421t, 425t
  Gray's cell, 412–413, 413f
  high-temperature electrowinning cell, 428, 430–431, 430f
  overview, 411–412, 412t
  Reno cell type 6, 413–414, 415t
  Reno cell type 12, 415–417, 416f, 417f, 418t
  Reno continuous cell type 12, 418–419, 419f
Oxide-fluoride electrolysis, 451
Oxide-fluoride melt
  cerium metal electrowon from, 418t
  electrolysis of, *see* Electrolysis
Oxide reduction-distillation process, 396
Oxide reduction processes; *see also* Reduction
  about, 380–382, 381t–382t
  reduction-distillation, lanthanothermy
    europium, preparation of, 383–384, 384f
    samarium/europium/ytterbium/terbium, preparation of, 384–386, 385f
    samarium/ytterbium, preparation of, 383
  reduction-distillation, reductants, 386–397
Oxide refractories, 26, 27f
Oxidizing agents, 32
Oxychlorides, 340, 442, 450
Oxyfluorides, 450
Oxygen, 25–26; *see also* Reactivity
  diffusion, 54
  sensors, 54
  vacuum/inert gas fusion, 713

Oxygen-contaminated magnet swarf, 645
Oxygen-enriched air, 642
Oxygen-enriched residue, 461
Oxygen-free high-conductivity (OFHC), 42
Oxysulfides, at steel-making, 36

P

P204 (di-2-ethyl-hexyl phosphoric acid), 731
P507 (2-ethyl-hexyl-2-ethyl-hexyl phosphate), 731
Paint and pigment industry, rare earths in, 72
Pajarito yttrium-zirconium deposit in New Mexico, 190; *see also* United States
Paleoplacer, 104t
PC88A/tri-*n*-octylphosphine oxide (TOPO) solvent combinations, 671
Pea Ridge Iron Deposit and Mine, Missouri, 188; *see also* United States
Pegmatites, 104t, 105
Peralkaline igneous rocks, 104t
Perchloric acid, 296f
Peritectic temperature, 564
Permanent magnet (PM); *see also* Magnets
  about, 43
  development timeline, 45t
  materials, 546, 598
Permanent magnet generators (PMG), 50
Permian Phosphoria Formation, 191
Perovskite, 55, 100; *see also* Minerals
Perovskite-like structure, 617
Peru, occurrence of deposits in, 182
Petroleum ether, 563
Phalaborwa apatite source, 318f
Phalaborwa Complex, 183; *see also* South Africa
Philips Electronic Components and Materials Division, 568
Philips Research Laboratories, 607
Phosphate mine, at Tapira, 169
Phosphate rocks of magmatic origin, 192
Phosphogypsum, 278
Phosphorite deposits, 97–99
Phosphorites, rare-earth recovery from, 276f
Phosphorous acids, 294t
Phosphors; *see also* Rare-earth phosphors; Rare earths
  composition, 62
  hosts, 64
  organolanthanide phosphor (OLP), 63
  scintillation, 63
  technology transition in high-efficiency lighting, 64–66
  uses of, 61–62
Phosphors, recycling, 672
  individual phosphors, separation of, 676–682
  physical separation, 675–676
  recycled lamp phosphor, composition of, 673–674
Phosphorus, 28–29; *see also* Reactivity
Phosphor waste, recycling, pretreatment process, 681
Photochemical reduction, 281
Physical beneficiation; *see also* Resource processing
  about, 236–239
  bastnasite, 247–249, 249f
  Bayan Obo iron ore, 249–251, 250f, 251f
  of Bayan Obo ore, 251f
  of beach sand minerals, 240f
  of beach sand minerals in India, 244f
  of cassiterite-bearing mineral sands, Southeast Asia, 242f
  of coarse heavy mineral sand, 242f
  flow sheet at Cable Sands Pty Ltd. plants, Australia, 243f
  flow sheet at Zircon Rutile Ltd., Australia, 243f
  mineralogical composition of Nechalacho deposit, 251, 252t
  monazite
    about, 239–243, 240f–246f
    bastnasite flotation, 244–246
    froth flotation, 244
    monazite flotation, 246–247
  of rare earth oxide minerals, 250f
  wet high intensity magnetic separator (WHIMS) experiments, 252, 253f
Pidgeon process, 22
  for magnesium, 382
Pink coloration by erbium, 59
Placer deposits; *see also* Mining; Resources
  in China, 176
  classification, 104t
  in India, 179
  mining and, 236
  in United States
    Florida-Georgia beach placers, 191–192
    Idaho placer deposits, 190–191
    North and South Carolina placers, 191
Plasma displays, 637
Plastic bonded magnets, 561
Plug-in hybrid electric vehicles (PHEV), 50, 70
Polishing agent, 37t, 61
Polishing powder, recycling, 683
Polymeric binders, 565
Polytetrafluoroethylene (PTFE) beaker, 698–699
Potassium chlorate, 351
Pourbaix–Ellingham diagrams, 401
Praseodymium, 523
  abundance of, 47
  applications, 37t
  atomic properties, 9t–10t
  mechanical properties, 13t
  stability of, 55
  thermal/electrical/magnetic properties, 11t–12t
  for vacuum-deposited antireflection coating, 60

Precipitation, 32
fractional, 283–285; *see also* Separation process
Precipitation-hardened magnets, 564–565
machining, handling, and magnetizing, 565
Pregnant leach solution (PLS), 272
Pressure measurement, 64
Pressurized heavy-water reactors (PHWR), 66
Primordial thorium-232, 718
$PrNi_5$, 604
Promethium, 102; *see also* Minerals
applications, 37t
atomic properties, 9t–10t
mechanical properties, 13t
thermal/electrical/magnetic properties, 11t–12t
Protective atmosphere chamber, 426f
Proterozoic quartzite, 187
PtCo magnet, 548
permanent magnets, 567
PTFE beaker, *see* Polytetrafluoroethylene (PTFE) beaker
Pulsed layer deposition, 619–620
Pulverization, 608
Pure rare-earth metal production, 362
Purification, 263, 264
by distillation, 346
of rare-earth chlorides, 346–348, 347f; *see also* Chloride preparation
of rare-earth fluorides, 367–368; *see also* Fluoride preparation
Pyrochlore, 100, 103; *see also* Minerals; Resource processing
chemical treatment of, 277
Pyrometallurgical processes, recycling, 640
chemical vapor transport, 646
chlorination, 645
flux-based processes, 649
electroslag refining (ESR), 649
glass-slag method, 650–651
molten flux process, 650
oxidation–reduction, 651–652
liquid metal extraction, 646–647
Ames process, 647–648
melt spinning, 643–645
smelting, 640–643
Pyrovacuum deoxidants, 469
Pyrovacuum refining treatments, 453
Pyrovacuum techniques, refining, 462
europium purification, by UHV distillation, 475–478
lanthanum/cerium/praseodymium/neodymium, 463
samarium/europium/thulium/ytterbium, 475–478
scandium/dysprosium/holmium/erbium/lutetium, 473–475
yttrium/gadolinium/terbium/lutetium, 463–472
Pyrovacuum treatment, refining, 453–462, 470, 473
carbon deoxidation, 460–461
carbon/silicon, removal of, 462
degassing, 457
dehydrogenation, 457
denitrogenation, 457–458
deoxidation, 458
distillation, 454–455
halogens/halides, removal of, 455–457
sacrificial deoxidation, 458–460
silicon deoxidation, 461–462
vacuum distillation, 453
Pyrovacuum treatments, 453
Pyrrhotite, mineral, 43

Q

Quadrivalent titanium, non-rare-earth impurities, 691
Quantitative ion microprobe analysis, 711
Quantum efficiency (QE), 66
Quaternary ammonium nitrate, 320

R

Radiation-shielding windows, 60
Radioactivity-free rare-earth sources, 734
Radiochemical neutron activation analysis (RNAA), 705, 708
Radio-frequency float zoning (RFFZ), 503, 506
Radio-frequency heating, 493
water-cooled boats, 493
Radiometric surveys, 107
Radionuclides, 72, 719
Radiopharmaceutical therapy, 72
Radium-226, radioactive decay of, 718
Radium Hill, 168; *see also* Australia
Radon-222, half-lives of, 718
Rapid solidification (RS) technique, 42
Rare Earth Acquisitions LLC, 736
Rare earth–aluminum–zinc alloys, 543
Rare earth-bearing materials, 634–635, 634–637
Rare-earth ceramics, special, 610–612
gadolinium gallium garnet, 611
rare-earth sulphides, 612
scandia ceramics, 611–612
yttrium aluminum garnet, Nd-YAG ceramics, 610–611
Rare-earth chlorides, lithium reduction of, 357–358, 357f
Rare-earth-chloride solution, 742
Rare earth–Co permanent magnets, 546–567
preparation of magnet materials, 549–561
coreduction, 555–556
direct melting, 550

electrolysis, 556–561
reduction–diffusion, 550–555
preparation of magnets, 561–567
bonded magnets, 565–567
precipitation-hardened magnets, 564–565
sintered magnets, 561–564
Rare-earth deposits, occurrence of
in Argentina, 163
Australia
Brockman (Hastings) deposit, 166
Brown's range project, 163–164
Cooljarloo/Jurien Bay, 164
Cummins Range, 165
Dubbo Zirconia Project (DZP), Toongi, 164
Eneabba mineral sand deposit, 164
Gilgai Intrusion, 165
Jangardup, 165
John Galt, 168
Mary Kathleen, 166–167
Mount Weld deposit, 167
Murray Basin, 165
Nolans Bore, 165–166
Norraburra RE deposit, 166
Radium Hill, 168
Syerston nickel–cobalt laterite, 168
Wimmera Industrial Minerals (WIM)-150, 165
Yangibana, 168
Bangladesh, 168–169
Brazil, 169–170
Canada
Denison mine, 170
Hoidas Lake, 171
Kipawa Alkaline Complex, 171–172
Nechalacho/Thor Lake Mine Site, Northwest Territories, 170–171
Yukon, 171
China
Bayan Obo, 172, 174–175
ion-adsorption ore, 175–176, 175t
largest rare-earth deposit, 172, 173t
Mianning county, 176–177
placer deposits, 176
Egypt, 177
former USSR
Chuktukon deposit, 193–194
deposits of, 192, 193t
Kyrgyzstan, 194
Tomtor deposit, 193
Germany, 177
Greenland, 177–178
India
hard rock deposits, 178–179
placers, 179
Indonesia, 179
Japan, 180
Kenya, 180
Madagascar, 180
Malawi, 181–182
Chilwa Island, 182
Kangankunde Hill rare-earth deposit, 181
Nanthace Hill, 181
Songwe, 182
Malaysia, 180–181
Mozambique, 182
Myanmar, 182
New Zealand, 182
Peru, 182
South Africa
Buffalo fluorspar mine, 183
Phalaborwa Complex, 183
Steenkampskrall deposit, 183
Zandkopsdrift deposit, 183–184
Sri Lanka, 184
Sweden, 184
Taiwan, 184–185
Thailand, 185
Turkey, 185
United States
Bear Lodge Mountains, Wyoming, 189
Bokan Mountain, Alaska, 190
Diamond Creek Area, Idaho, 187
Elk Creek Carbonatite, Nebraska, 186
Gallinas Mountains, New Mexico, 190
Hall Mountain, Idaho, 187
Hicks Dome, Illinois, 188
Iron Hill, Colorado, 190
Lemhi Pass District, Idaho, 187
Mineville Iron District, New York, 188
Mountain Pass, California, 189
Music Valley, California, 186
Pajarito yttrium–zirconium deposit in New Mexico, 190
Pea Ridge Iron Deposit and Mine, Missouri, 188
placer deposits, 190–192
Wet Mountains Area, Colorado, 186
Venezuela, 194
Vietnam
Dong Pao deposit, 195
Nam Xe rare-earth deposit, 194–195
Zaire, 195
Rare-earth distribution
in bastnasite, 93t
in monazite, 95t, 96t
Rare-earth elements (REEs), 70, 73, 77f, 688, 717
acid drainage, 739
cation-exchange column, 702
cerium subgroup of, 88
Chinese Society of Rare Earths, 725
development of deposits, 225f
distribution of reserves, in China, 173t

environmental aspects, 717
extensive chemical characterization, 720
geology of, 102–105, 104t
hard-rock mining, 718
in situ leaching (ISL) technology, 721
drilling holes, 727
light, 88
mining and processing, 718
Mountain Pass, 738
in phosphate rocks, 98t
production of mines in 2009, 196t
radioactivity, 719
radionuclides, threats to human health, 720
recycling, 658
potential ranges, 640
scraps, recycling of, 647
supply shortages, 668
terbium group of, 88
in United States, 717
yttrium group of, 88
Rare earth-ferroalloy
distillation apparatus, 439f
electrodeposition cell, 437f
Rare-earth fluoride, from bastnasite, 530
Rare-earth hydroxides, 30
Rare-earth ions, molar absorptivity of, 690
Rare earth–magnesium–silicon alloys, 541, 543
Rare Earth Metal Corp., 528
Rare-earth-metal reduction apparatus, 370f
Rare-earth-metals, refining, 447
activated phosphor, 675
amalgamation of, 515–516
analysis of, 687
calcium concentration of, 517
C-O system, 460
solid solutions, 462
electrochemical deoxidation of, 517–520
hydrogen phase diagrams, 457
metallothermic reduction of, 462
oxygen systems, 460
purification processes, 447, 448
removal of oxygen, 517
Rare-earth-metal suboxide (REO), formation of, 459
Rare-earth nitrides, free energy of formation, 458
Rare-earth oxalates, 688
Rare-earth oxides (REOs)
about, 88
with ammonium bifluoride, reaction of, 366–367, 366f
with anhydrous HF, reaction of
fluidized bed method, 365–366
rotary batch method, 364–365, 365f
vibrating tray method, 366
electrolysis of a mixed, 528–532
electrowinning misch metal from, 528
light, 93
Rare-earth permanent magnets (REPMs), 565
Rare-earth phosphors, 673
Rare-earth phosphors, preparation of, 612–617
flux method, 617
homogeneous precipitation, 612–614
melt synthesis, 616–617
molten salt synthesis, 616–617
sol-gel synthesis, 615–616
solid-state reaction, 614–615
Rare earth projects, advanced, 217t–224t
Rare-earth recycling
aqueous-based technology for, 658
industry-level practice of, 627
Rare earths
applications
ceramics, 53–56
chemical, 57–59
electronics, 56–57
element-wise listing of uses, 37t–39t
hydrogen absorption, 67–70
magnetic refrigeration, 53
magnets, 43–51, 45t, 46t, 52t
metallurgy, 34, 36, 40–43
miscellaneous, 70–73, 71t
nuclear, 66–67
optical, 59–61
phosphors, 61–66
summary of, 35t–36t
superconductor, 70
terfenol, 51, 53
in APR resources, 232f
aqueous systems
complexes, 31
divalent state, 32–33
tetravalent state, 31–32
trivalent state, 30–31
characteristics
basicity, 20–21
electronic configuration, 8, 9t–18t
lanthanide contraction, 19–20, 19f
demand forecast, 79t
discovery of, 1–8, 2t–3t, 4f
end-use breakup (in 2010), 78t
estimated long-term availability of, 233f
global rare-earth demand, 73–81
military applications of, 71t
properties
allotropes, 23
boiling point, 22–23
magnetic, 24
mechanical, 25
melting point, 21–22
resistivity, 23–24
spectral, 24–25
reactivity
acids/bases, 29
air/oxygen, 25–26

carbon, 28
hydrogen, 28
nitrogen, 26–28, 27f
phosphorus, 28–29
refractories, 26, 27f
refractory metals, 29
selenium, 28
silicon, 28
sulfur, 28
water, 30
world consumption, growth components, 76t
Rare earths analysis
analytical separation of, 689–690
instrumental methods, 689–690
chemical methods, 687
gravimetry, 687–688
volumetry, 688
cerium, determination of, 688–689
europium, determination of, 689
detection limit/nuclear properties/interferences
NAA determination, 706t–707t
detection limits, 694t–695t
emission and absorption spectroscopy, 693–696
experimentally measured dissolved sample detection limits, 697t
ICP-AES, 698–700
ICP-MS, 700–703
interferences, 701t
induction-coupled plasma excitation, 698
instrumental techniques, 710
cathode ray-excited emission spectroscopy (CREE), 710
secondary ion mass spectrometry, 711
spark source mass spectrometry (SSMS), 711
x-ray–excited optical luminescence (XEOL) spectroscopy, 710–711
interstitials, determination of, 711–713
ions, molar absorptivity of
at analytical wavelengths, 691t
neutron activation analysis (NAA), 705–710, 706t–707t, 709t
oxygen determination, 712t
REE/thorium, important chromogenic reagents, 692t
spectroscopy
emission and absorption, 693–696
ICP-AES, 698–700
ICP-MS, 700–703
induction-coupled plasma excitation, 698
spectrophotometry, 690–692
thorium, chromogenic reagents, 692t
XRF, 703–704
Rare earth-silicon-iron alloys, 538–541
Baotou process, 541
BARC process, 541
reno (USBM) process, 538–540
Rare-earth sulphides, 612
Rare-earth transition metal alloys, 607
Rare earth–Transition Metal™ permanent magnets, 50
Rare Element Resources Ltd., 266
Reactivity; *see also* Rare earths
acids/bases, 29
air/oxygen, 25–26
carbon, 28
hydrogen, 28
nitrogen, 26–28, 27f
phosphorus, 28–29
refractories, 26, 27f
refractory metals, 29
selenium, 28
silicon, 28
sulfur, 28
water, 30
Reactor loaded for fluoride reduction, 369f
Rechargeable battery, hydrogen-based, 69
RE^{3+} contents, 688
Recoverable reserves, definition, 158t
Recovery of rare-earth metals as alloys; *see also* Reduction
about, 431–432
electrolysis of chlorides, 432–435, 433f, 434f
electrolysis of oxide-fluoride melts
distillation of alloys, operational data for, 440t
electrochemical reduction of cerium oxide to metal, 441
electrodeposition of alloys, operational data for, 438t
electrodeposition of europium from molten fluoride, 441
overview, 435–441, 435f, 437f, 439f
electrolytic preparation of rare-earth alloys, 431t
Recrystallization, 564
Recycling, 627
anode leach liquors, 662
catalysts, 683
automotive exhaust catalysts, 684
fluid cracking catalysts, 683–684
cathode leach liquors, 661
DC electric arc furnace
NiMH battery scrap by smelting, 643
end-of-life (EOL) scrap, 627
europium and yttrium oxides from fluorescent lamp wastes, 681
fluorescent lamp phosphors, 674
fluorescent lamp waste, extraction processes for, 676

glass-polishing powder, 682–683
glass-slag method, Sm–Fe alloy, 650
green technologies, 633
hydrometallurgical process, to treat spent borosilicate optical glass, 685
hydrometallurgy, 652
  hydrothermal process, 658
  leaching, 658–664
  leaching and precipitation, 653–656
  precipitation, 658–664
  Rhône Poulenc process, 656–657
  solvent extraction, 658–664
individual rare earths, separation of, 664–667
industrial RE recycling activities, 636
leaching of lamp phosphors, 679–680
magnet grinding sludge, to magnet alloy, 652
magnets, 668
  end-of-life scrap, 669
    collection, 669–670
    dismantling, 670–671
    mixed Sm–Co/Nd–Fe–B scrap, 671
    NdFeB, 671
    samarium–cobalt, 671
  in-plant/preconsumer scrap, 669
miscellaneous materials, 685
NdFeB magnets, 666
NdFeB scrap by liquid metal (Ag) extraction, 648
neodymium-containing oxides, chemical treatment process, 653
Ni, Co, and RE recovery, 660
nickel-coated sintered NdFeB magnets, to isotropic bonded magnets, 644
nickel–metal hydride batteries, 672
NiMH batteries
  by hydrochloric acid leaching and solvent extraction, 665
  by sulfuric acid leaching, 664
NiO, CeO_2, and $LaCoO_3$ from Ni–MH battery waste, 657
optical glass, 684–685
phosphors, 672
  individual phosphors, separation of, 676–682
  physical separation, 675–676
  recycled lamp phosphor, composition of, 673–674
phosphor waste, pretreatment process, 681
polishing powder, 683
potential for, 637–640
processes for, 640
pyrometallurgical processes, 640
  chemical vapor transport, 646
  chlorination, 645
  flux-based processes, 649
    electroslag refining (ESR), 649
    glass-slag method, 650–651
    molten flux process, 650
    oxidation–reduction, 651–652
  liquid metal extraction, 646–647
    Ames process, 647–648
  melt spinning, 643–645
  smelting, 640–643
rare earth-bearing materials, 634–635, 634–637
rare-earth elements (REEs), 627–632
  magnets, NiMH batteries, and phosphors, 639, 641–642
rare-earth magnets, types of, 668
rare-earth scrap
  aqueous processing for recycling, 659
  ESR process for, 649
samarium and cobalt from magnet swarf recovery, 654
solution based on mixed material, 663
USBM process
  NdFeB scrap by acid dissolution and precipitation, 655
Recycling grinding sludge, 651
Recycling NdFeB swarf, 656
Red phosphor, 38t
Reduction
  apparatus, 361f, 400f
  carbothermic, 401–402
  current efficiency in electrolytic cells, 442
  defined, 333
  electrolytic production of rare-earth metals
    about, 402–403
    chloride electrolysis, 403–408, 403t
    commercial electrowinning from rare-earth chlorides, 410–411, 411t
    electrowinning at room temperature, 408–409
    electrowinning solid metal deposits, 409
    in situ preparation of electrolyte, 409–410
    oxide-fluoride electrolysis, 411–431
  fundamentals, 333–337, 334f–336f
  metallothermic reduction in molten salt, 398–401
  metallothermy, 337–338
  oxide reduction processes
    about, 380–382, 381t–382t
    reduction-distillation, lanthanothermy, 382–386
    reduction-distillation, reductants, 386–397
  of rare-earth chlorides
    early attempts, 348–350, 349t
    intermediate alloy processes, 353
    Kroll-type processes, 353–363, 354f–361f, 356t, 362t
    in refractory bomb (reactor), 350–352, 350f
    in tantalum crucible, 352–353

rare-earth chlorides, preparation of
dehydration of hydrated rare-earth chlorides, 339–344, 340f–344f
dry methods, 345–346, 346f
preparation of hydrated rare-earth chloride, 339
purification of rare-earth chlorides, 346–348, 347f
of rare-earth fluorides
about, 368–369, 368t
calcium reduction (Ames process), 371–375, 372f–375f
intermediate alloy process, 376–379, 377f, 378t
lithium reduction, 369–371, 369f, 370f
samarium/europium/ytterbium, reduction of, 379–380
scandium preparation, 379
rare-earth fluorides, preparation of
dry methods, 364–367, 365f, 366f
purification of rare-earth fluorides, 367–368
wet method, 363–364
recovery of rare-earth metals as alloys
about, 431–432, 431t
electrolysis of chlorides, 432–435
electrolysis of oxide-fluoride melts, 435–441
retort, 377f
selective, 281–282, 282f; *see also* Separation process
Reduction bomb assembly, 356f
Reduction crucible for lithium reduction, 357f
Reduction distillation process, 22; *see also* Oxide reduction processes
europium, preparation of, 383–384, 384f
reductants, 386–397
samarium/europium/ytterbium/terbium, preparation of, 384–386, 385f
samarium/ytterbium, preparation of, 383
REE, *see* Rare-earth element (REE)
Refining
amalgamation of rare-earth metals, 515–516
in China's rare earth industry, 727
deoxidation by oxyhalide formation, 516
electrorefining process, 478
cerium metal, 489–490
gadolinium, 482–489
yttrium, 478–482
impurities, origin of, 448–453
crucible and reactor, 451–452
environment, 452–453
starting materials, 449–451
impurity removal methods, 453
iodide refining process, 515
pyrovacuum techniques, 462
europium purification, by UHV distillation, 475–478
lanthanum/cerium/praseodymium/neodymium, 463
samarium/europium/thulium/ytterbium, 475–478
scandium/dysprosium/holmium/erbium/lutetium, 473–475
yttrium/gadolinium/terbium/lutetium, 463–472
pyrovacuum treatment, 453–462
carbon deoxidation, 460–461
carbon/silicon, removal of, 462
degassing, 457
dehydrogenation, 457
denitrogenation, 457–458
deoxidation, 458
distillation, 454–455
halogens/halides, removal of, 455–457
sacrificial deoxidation, 458–460
silicon deoxidation, 461–462
vacuum distillation, 453
rare-earth-metals, 447
electrochemical deoxidation of, 517–520
purification processes, 448
solid-state electrotransport, 500–510
dysprosium/holmium, 507
erbium, 508
gadolinium, 506
lanthanum, 505
lutetium, 509
neodymium, 506
praseodymium, 505–506
residual resistivity ratio, 505
samarium, 510
solid-state electrolysis (SSE), 501, 503–504
terbium, 506
yttrium, 502, 507
ultrapurification methods, 490
zone refining, 490
interstitial impurities, redistribution of, 496–497
lanthanum/cerium/gadolinium, 493–496
lanthanum/gadolinium/terbium, 493
metallic impurities, redistribution of, 497–500
preliminary studies, 491–492
zone refining/electrotransport, 510
gadolinium, 512–515
neodymium, 510–512
Reflective coatings, 65
Refractories, 26, 27f; *see also* Reactivity
metals, 29; *see also* Reactivity
Refractory bomb (reactor), reduction in, 350–352, 350f; *see also* Chloride reduction processes
Refrigeration systems, 53
Renison Goldfields Consolidated Ltd. (RGC), US, 204

Reno cell type 6, 413–414, 415t
Reno cell type 12, 415–417, 416f, 417f, 418t
Reno continuous cell type 12, 418–419, 419f
Reno electrowinning cell, 427
Reno Metallurgy Research Center, 528
Reno (USBM) process, 538–540; *see also* Rare earth-silicon-iron alloys
REO, *see* Rare-earth-metal suboxide (REO); Rare-earth oxide
Research Chemicals, 570
Reserve base, definition, 157t
Reserves, definition, 154, 158t
Reserves, resources and
  about, 107, 154
  classification, 157t–158t
  global RE reserve estimates (2009–2010), 161t–162t
  United Nations resource categories, 160f
  USGS classification of mineral resources, 159f
Residual impurity, 452
Residual resistivity ratio (RRR), 505
Resin-bonded magnets, 582
Resistivity, 23–24; *see also* Rare earths
Resources
  by-products and coproducts, 195–197, 196t
  crustal abundance, 86–87, 86t, 87f
  definition, 157t
  immediate future, 213–229, 217t–224t–227t
  minerals
    about, 87–88, 89t–91t, 92t
    allanite, 94, 96t, 97
    apatite, 96t, 97, 98t, 99
    bastnasite, 88, 93, 93t
    brannerite, 96t, 99
    eudialyte, 99
    euxenite, 99
    fergusonite, 99
    florencite, 100
    gadolinite, 100
    ion-adsorption ore, 101
    loparite, 100
    monazite, 93–94, 95t
    perovskite, 100
    promethium, 102
    pyrochlore, 100
    scandium, 102
    xenotime, 94, 96t
    zircon, 100
  occurrence
    Argentina, 163
    Australia, 163–168
    Bangladesh, 168–169
    Brazil, 169–170
    Canada, 170–172
    China, 172–177, 173t, 175t
    Egypt, 177
    former USSR, 192–194, 193t
    Germany, 177
    Greenland, 177–178
    India, 178–179
    Indonesia, 179
    Japan, 180
    Kenya, 180
    Madagascar, 180
    Malawi, 181–182
    Malaysia, 180–181
    Mozambique, 182
    Myanmar, 182
    New Zealand, 182
    Peru, 182
    South Africa, 182–184
    Sri Lanka, 184
    Sweden, 184
    Taiwan, 184–185
    Thailand, 185
    Turkey, 185
    United States, 185–192
    Venezuela, 194
    Vietnam, 194–195
    Zaire, 195
  overview, 85–86
  rare-earth deposits
    distribution, 105–107, 106t, 108t–153t, 154f, 155t–156t
    REE, geology of, 102–105, 104t
  and reserves
    about, 107, 154
    classification, 157t–158t
    global RE reserve estimates (2009-2010), 161t–162t
    United Nations resource categories, 160f
    USGS classification of mineral resources, 159f
  world rare-earth production
    Australia, 205–207
    Brazil, 202–203
    Canada, 211–212
    China, 207–209, 209f
    former Soviet Union, 210–211
    India, 203
    Malaysia, 212
    overview, 197–202, 197f, 198f, 199t–200t
    South Africa, 211
    Sri Lanka, 212–213
    Thailand, 212
    United States, 203–205
    Zaire and Madagascar, 213
Resource processing
  chemical treatment
    apatite, 277–279
    bastnasite, 261–268, 261f–267f, 263t, 268t
    Elliot Lake uranium ore, Canada, 273
    euxenite, 274

fergusonite, 276
gadolinite, 273–274, 274f–276f
ion-adsorption ore, 270–273, 270t, 273f
loparite, 276
monazite, 254–261, 255f–257f, 259f
pyrochlore, 277
samarskite, 276
xenotime, 269, 269f, 270f
mining
hard-rock deposits, 236
placer deposits, 236
overview, 235–236
physical beneficiation
about, 236–239
bastnasite, 247–249, 249f
Bayan Obo iron ore, 249–251, 250f, 251f
mineralogical composition of Nechalacho deposit, 251, 252t
monazite, 239–247, 240f–246f
wet high intensity magnetic separator (WHIMS) experiments, flow sheet of, 252, 253f
scandium, 329
separation process
fractional crystallization, 282–283, 284f
fractional precipitation, 283–285
ion exchange, 285–290, 287f, 288f
selective oxidation, 279–280, 280f
selective reduction, 281–282, 282f
solvent extraction, 290–329
RE-TM-Mg alloys, 545
RFFZ, *see* Radio-frequency float zoning (RFFZ)
Rhône-Poulenc solvent extraction process, 321–322, 321f; *see also* Solvent extraction
RNAA, *see* Radiochemical neutron activation analysis (RNAA)
Rock-forming minerals, 87
Rock phosphate, 99
Ronson, 570, 574
Rotary batch method, 364–365, 365f; *see also* Dry methods
Rubber isostatic press (RIP), 591
Ruprecht, Antal, 2
Russia, summary of rare-earth deposits, 134t–136t

S

Samarium, 282, 510, 534
and anisotropic structure, 45
applications, 38t
atomic properties, 9t–10t
cost of, 47
mechanical properties, 13t
preparation, 383, 384–386; *see also* Reduction distillation process
recovery of, 315f
recycling
and cobalt from magnet swarf recovery, 654
thermal/electrical/magnetic properties, 11t–12t
Samarium chloride, reduction by mechanical milling, 380
Samarium–cobalt magnets, 48, 567
Samarium–neodymium, 645
Samarskite, 688; *see also* Resource processing
chemical treatment of, 276
sequence, 4f
Santoku, 570, 575
Saudi Arabia, summary of rare-earth deposits, 136t
Scandia ceramics, 611–612
Scandium, 102; *see also* Minerals; Resource processing
applications, 39t
atomic properties, 9t–10t
mechanical properties, 13t
for metal halide lamps, 63
preparation, 379; *see also* Fluoride reduction process
solvent extraction for, 329
thermal/electrical/magnetic properties, 11t–12t
Scandium–aluminum alloy, 41
Scandium iodide, hygroscopicity of, 64
Scandium oxide (Sc_2O_3), 612
Scandium trichloride, 353
Scandium–zinc alloy, 432
Scintillation, 63; *see also* Phosphors
detectors, 63
Scrap lamp phosphors, 673
ultraviolet (UV) radiation, 674
Secondary ion mass spectrometry (SIMS), 711
Selective oxidation, 279–280, 280f; *see also* Separation process
Selective reduction, 281–282, 282f; *see also* Separation process
Selenium, 28; *see also* Reactivity
Self-propagating high-temperature synthesis (SHS), 29
Semicontinuous reduction, 372–373, 375f; *see also* Calcium reduction (Ames process)
Separation of rare earths, 20–21
Separation process; *see also* Resource processing
fractional crystallization, 282–283, 284f
fractional precipitation, 283–285
ion exchange, 285–290, 287f, 288f
selective oxidation, 279–280, 280f
selective reduction, 281–282, 282f
solvent extraction
amines, 303–306, 304f, 305t
carboxylic acids, 300–301, 300t
Denison Mines, 309–310, 311f

dry process, 328–329, 329f
extractants, solvating, 301–302, 302t, 303f
Indian rare earths, 310–318, 312f–317f
industrial processes, 307–308
Megon Company, Norway, 319–321, 320f
method, 290–293, 291f, 292f, 294t
Mintek, 318–319, 318f
Molycorp approach, 308–309, 309f, 310f
organophosphorus acids, 293, 295–300, 297t, 299t
Rhône-Poulenc, 321–322, 321f
spin-off process, 327–328, 328f
synergistic effects, 306–307
Thorium Ltd., 322
Yao Lung chemical plant, Shanghai, 322–326, 323f–326f
Sesquicarbides, 28
Shallower sands, 236
Sichuan mine, 726
Silane-coupling agent, 581
Silica sol or gel, 546
Silicate-based phosphors, 616
Silicates, 614
Silicides, 28
Silicon, 28; *see also* Reactivity
as reductants, 538
Silicon deoxidation processes, for oxygen removal, 461
Silicon-enriched residue, 462
Single-crystal scintillators, 39t
Single-lens reflex (SLR) cameras, 60
Sintered lime, 350
Sintered magnets, 45, 561–564, 586–589
aligning and pressing, 563
blending, 562–563
heat treatment, 563–564
milling, 563
sintering, 563
Sintered permanent magnets, 591
SiO vaporization, 462
Slaked lime, 310
$SmCo_5$ magnet, 548–549
Sm-Co magnets
acid dissolution–precipitation/solvent extraction, 666
scrap, 659, 665
Sm–Fe alloy, 651
Sm_2Fe_{17} alloys, 598–599
$Sm_2Fe_{17}N_x$, 598
Sm-Fe-N magnets, 598–599
alloy, 650
Smith, J. Lawrence, 5
Soda ash, 266
Sodium carbonate, 260, 269
Sodium double sulfate, precipitation of, 656
Sodium fluoride, 246
Sodium hexafluorosilicate, 246
Sodium oleate, 246
Sodium oxalate, 246
Sodium silicate, 246, 247
Soil formation, 105
Solid oxide fuel cells (SOFC), 55
Solid-state electrolysis (SSE), 501
Solid-state electrotransport, refining, 500–510
dysprosium/holmium, 507
erbium, 508
gadolinium, 506
lanthanum, 505
lutetium, 509
neodymium, 506
praseodymium, 505–506
residual resistivity ratio, 505
samarium, 510
solid-state electrolysis (SSE), 501, 503–504
terbium, 506
yttrium, electrotransport purification of, 502
Solid-state laser, 57
Solid-state reaction (SSR) sintering method, 610–611, 613–616
Solvating extractants, 294t
Solvent extraction (SX), 683, 699; *see also* Separation process
amines, 303–306, 304f, 305t
carboxylic acids, 300–301, 300t
Denison Mines, 309–310, 311f
dry process, 328–329, 329f
extractants, solvating, 301–302, 302t, 303f
Indian rare earths, 310–318, 312f–317f
industrial processes, 307–308
Megon Company, Norway, 319–321, 320f
method, 290–293, 291f, 292f, 294t
Mintek, 318–319, 318f
Molycorp approach, 308–309, 309f, 310f
organophosphorus acids, 293, 295–300, 297t, 299t
Rhône-Poulenc, 321–322, 321f
spin-off process, 327–328, 328f
synergistic effects, 306–307
Thorium Ltd., 322
with tributyl phosphate (TBP), 254
Yao Lung chemical plant, Shanghai, 322–326, 323f–326f
Songwe carbonatite, 182; *see also* Malawi
South Africa; *see also* Resources; World rare-earth production
advanced rare earth projects, 224t
Buffalo fluorspar mine, 183
Phalaborwa Complex, 183
rare-earth production in, 211
Steenkampskrall deposit, 183
summary of rare-earth deposits, 137t–138t
Zandkopsdrift deposit, 183–184
South African Mineral Resource Committee (SAMREC), 154

South Korea, summary of rare-earth deposits, 138t–139
Soviet Union (USSR), former; *see also* Resources; World rare-earth production
  Chuktukon deposit, 193–194
  deposits of, 192, 193t
  Kyrgyzstan, 194
  mine production of rare earths, 199t–200t
  rare-earth production in, 210–211
  summary of rare-earth deposits, 134t–136t
  Tomtor deposit, 193
Spark plasma sintering (SPS), 584
Spark source mass spectrometry (SSMS), 711
Spectral properties of rare-earth metals, 24–25
Spectrophotometric analyses, 690
Spectrophotometric determination, 692
Spectrophotometric methods, of rare-earth determination, 690
Spheroidal graphite, 34
Spin-off process, 327–328, 328f; *see also* Solvent extraction
Split graphite resistor furnace assembly, 388f
Sputtering method, 606–607
Square wave voltammetry, 441
Sri Lanka; *see also* World rare-earth production
  occurrence of deposits in, 184
  rare-earth production in, 212–213
  summary of rare-earth deposits, 139t
SRMs, *see* Standard reference materials (SRMs)
SSE-refined gadolinium rod
  RRR profile of, 512
SSMS, *see* Spark source mass spectrometry (SSMS)
Stabilizer, 54
Stainless-steel vacuum retort, 353
Standard free energy
  change of reactions, 399f
  formation of rare-earth chlorides, 335f, 336f
  formation of selected fluorides, 336f
  formation of selected oxides, 335f
  rare-earth oxides as function of temperature, 334f
Standard reference materials (SRMs), 704
Steels, 36, 40; *see also* Metallurgy
Steenkampskrall deposit, 183; *see also* South Africa
Steenkampskrall mine, 742
Stratiform phosphate residual, 104t
Strip casting, 577
Suballoy, 594
Subcarbides, 28
Subeconomic resources, definition, 158t
Sulfates, 30
Sulfide mineral dissolution, 719
Sulfur, 28; *see also* Reactivity
Sulfuric acid, 29, 263, 308
  glass slag, 651
  method, 254
Sulfur oxide emissions, 58
Super alloys, 40; *see also* Metallurgy
Superconductivity Technology Center, 619–620
Superconductors, 70, 617–621; *see also* Rare earths
Super high-energy magnets, 592–594
Supported liquid membranes (SLMs), 667
Sweden
  advanced rare earth projects, 222t
  occurrence of deposits in, 184
  summary of rare-earth deposits, 140t
SX, *see* Solvent extraction (SX)
Syerston nickel-cobalt laterite, 168; *see also* Australia
Synergistic solvent extraction systems, 306–307; *see also* Solvent extraction

T

Taiwan
  black monazite, 95t
  occurrence of deposits in, 184–185
  summary of rare-earth deposits, 140t–141t
Tantalum, 503
  crucible, reduction in, 352–353; *see also* Chloride reduction processes
  reduction, 393f
  retort, 358
  solubility of, 29
Tanzania
  advanced rare earth projects, 223t
  summary of rare-earth deposits, 141t
Tapira phosphate mine, 169
(Tb, Dy)Fe_2 Laves compound, 601
TBP, *see* Tributyl phosphate (TBP)
Temperature in ion-exchange separations, 289
Terbium
  applications, 38t
  atomic properties, 13t–15t
  group of REE, 88
  mechanical properties, 16t–17t
  preparation of, 384–386; *see also* Reduction distillation process
  refining of, 493
  thermal/electrical/magnetic properties, 15t–16t
Terfenol, 51, 53, 605–607; *see also* Rare earths
TERFENOL-D, 601–602
Tetraethoxysilane (TEOS), 616
Tetraethyl orthosilicate (TEOS), 611
Tetravalent state, of rare earths, 31–32; *see also* Aqueous systems
Texturing, 618, 620
Th. Goldschmidt AG, 555, 568, 569, 573
Thailand; *see also* World rare-earth production

occurrence of deposits in, 185
rare-earth production in, 212
Thermal conductivity measurement, 711
Thermal gradient cells, 556–561
Thermal reduction, 32
Thermit reduction process, 601
Thermocouple, 385
Thermomechanical treatments (TMTs), 621
Thin film deposition processes, 605–607
bubble domain memory materials, 606
magneto-optic storage media, 606–607
Thiocyanate system, 303
Thorium, 391, 737, 741
in rare-earth ores, 734
Thorium-containing dust, 726
Thorium-free rare-earth solution, 687
Thorium hydroxide, 257–258
Thorium Ltd., 322; *see also* Solvent extraction
Thorium nitrate, 523
Thorium sulfate, 258
Thor Lake deposit, 170–171
Thulium, 389
applications, 39t
atomic properties, 13t–15t
mechanical properties, 16t–17t
thermal/electrical/magnetic properties, 15t–16t
Ti_2N, 598
Titanium alloys, 42; *see also* Metallurgy
Titanium dioxide, in electrorheological (ER) fluid, 72
Titanium mineral sphene, japan, 180
TMR Advanced Rare-Earth Projects Index, 216
TOA, *see* Trioctylamine (TOA)
Toluene, 563
Tomtor deposit, 193; *see also* Soviet Union (USSR), former
Topping, 367, 450
Transition elements, 8
Treibacher Chemical Works, 523–524
Tributyl phosphate (TBP), 254, 292, 293
solvent extraction, 659
Tri-isobutylphosphine oxide (TIBPO), 306
Tri-isooctylamine (TIOA), 293
Trioctylamine (TOA), 663
cobalt, 664
Tripositive rare-earth ions, 31
Trivalent iron, non-rare-earth impurities, 692
Trivalent lanthanides, 303f, 304f
Trivalent state, of rare earths, 30–31; *see also* Aqueous systems
Trombe-type electrolysis cell, 406f, 407
Tungsten, solubility of, 29
Tungsten carbide lined (WC) mortar, 645
Tungsten cathode, 409
Tungsten crucible, 475
Tungsten-lined condenser, 470
Turkey
advanced rare earth projects, 222t
occurrence of deposits in, 185
summary of rare-earth deposits, 141t
Two-alloy process, 594–595

U

Ultrahigh vacuum (UHV), 453
distillation, 475
equipment, 492
rated equipment, 503
Ultrapurification methods, 23, 490
Undiscovered resources, 158t
United Nations resource categories, 160f; *see also* Resources
United States; *see also* Resources; World rare-earth production
advanced rare earth projects, 223t
Bear Lodge Mountains, Wyoming, 189
Bokan Mountain, Alaska, 190
Diamond Creek Area, Idaho, 187
Elk Creek Carbonatite, Nebraska, 186
Gallinas Mountains, New Mexico, 190
Hall Mountain, Idaho, 187
Hicks Dome, Illinois, 188
Iron Hill, Colorado, 190
Lemhi Pass District, Idaho, 187
mine production of rare earths, 199t–200t
Mineville Iron District, New York, 188
Mountain Pass, California, 189
Music Valley, California, 186
Pajarito yttrium-zirconium deposit in New Mexico, 190
Pea Ridge Iron Deposit and Mine, Missouri, 188
placer deposits
Florida-Georgia beach placers, 191–192
Idaho placer deposits, 190–191
North and South Carolina placers, 191
rare-earth production in, 203–205
summary of rare-earth deposits, 142t–151t
Wet Mountains Area, Colorado, 186
United States Automotive Battery Consortium, 69
United States Bureau of Mines (USBM), 158
United States Geological Survey, 88
Uraniferous phosphates, 210
Uranium, 719, 741
in rare-earth ores, 734
Uranium-235, 718
Uruguay, summary of rare-earth deposits, 153t
USBM process, recycling, 656
NdFeB scrap by acid dissolution and precipitation, 655
US Bureau of Mines (USBM), 528, 556
US Department of Energy (DOE), 717
USGS classification of mineral resources, 159f; *see also* Resources

V

Vacuum calcination, 620
Vacuum-casting apparatus, 343f
Vacuum distillation, 346, 348, 355, 397f, 453
  apparatus, 434f, 437
Vacuum distillation/sublimation
  pyrovacuum treatments of, 478
Vacuum drying process, 344
Vacuum flash evaporation (FE), 602
Vacuum induction melting, 550, 568
Vacuum/inert gas fusion, 713
Vacuum melting
  during composition change of misch metals, 534
  pyrovacuum treatments of, 478
Vanadium trioxide, 60
Van Arkel–de Boer process, 448, 515
Vanquelin, Nicolas Louis, 2
Vapor pressure
  measurements, 382
  of rare earths, 22
VCM, *see* Voice coil motor (VCM)
Venezuela, occurrence of deposits in, 194
Versatic acid, 300
Vibrating tray method, 366; *see also* Dry methods
Vietnam; *see also* Resources
  Dong Pao deposit, 195
  Nam Xe rare-earth deposit, 194–195
  summary of rare-earth deposits, 152t–153t
Voice coil motor (VCM), 670
Von Welsbach, Auer, 3t, 4f, 7, 33, 523–524

W

Waste electronics and electrical equipment (WEEE), 669
Waste streams, 637
Wastewater treatment
  installations, 741
  NH_3/NH_4 content, 727
Water, 30; *see also* Reactivity
Water-cooled container, 491
Water-cooled electrodes, 500
Water treatment, traditional processes, 732
WC mortar, *see* Tungsten carbide lined (WC) mortar
WEEE, *see* Waste electronics and electrical equipment (WEEE)
West ore body, 174
Wet chemical treatment
  of bastnasite, 524
  of monazite & bastnasite, 524
Wet gravity concentration, 241
Wet high intensity magnetic separator (WHIMS)
  experiments, 252, 253f; *see also* Physical beneficiation
Wet method, 363–364; *see also* Fluoride preparation
Wet Mountains Area, Colorado, 186; *see also* United States
Wet processing, 277
Wimmera Industrial Minerals (WIM)-150, 165; *see also* Australia
Wind power, 50–51, 52t
Wind turbines, recycling loop, 633
Wolframite, 102
World Mineral Resources, Brazilian mining company, 170
World rare-earth consumption, growth components, 76t
World rare-earth deposits, summary of, 108t–153t
World rare-earth production; *see also* Resources
  Australia, 205–207
  Brazil, 202–203
  breakdown of, 1983–2013, 198f
  Canada, 211–212
  China, 207–209, 209f
  former Soviet Union, 210–211
  India, 203
  Malaysia, 212
  mine production, 199t–200t
  over past 112 years, 197f
  overview, 197–202
  South Africa, 211
  Sri Lanka, 212–213
  Thailand, 212
  United States, 203–205
  Zaire and Madagascar, 213

X

Xenotime, 94, 96t; *see also* Minerals; Resource processing
  chemical treatment of, 269, 269f, 270f
X-ray dosage, 63
X-ray–excited optical luminescence (XEOL) spectroscopy, 710–711
X-ray fluorescence (XRF), 690

Y

Yangibana, 168; *see also* Australia
Yao Lung chemical plant, Shanghai, 322–326, 323f–326f; *see also* Solvent extraction
Y–Ba–Cu–O compound (YBCO), 617–621
YCl_3 component
  in electrolyte, 480
  electrolyte consisted, 480
Y–Eu fraction, 682
YF_3, calciothermic reduction of, 463
Y–Mg alloy, 464
Ytterbium

applications, 39t
atomic properties, 13t–15t
mechanical properties, 16t–17t
preparation of, 383; *see also* Reduction distillation process
reduction of, 379; *see also* Fluoride reduction process
thermal/electrical/magnetic properties, 15t–16t
Yttria-stabilized zirconia (YSZ), 54
Yttrium, 694, 710
applications, 39t
atomic properties, 9t–10t
carbon content, 466
chemical analysis of, 378
deposition of, 515
electron beam melting, 469
electrorefining of, 478
extraction and separation of, 322
extraction with versatic acid, 308
and lanthanide contraction, 20
from laser crystals and synthetic garnets, 637
mechanical properties, 13t
as neutron moderators, 67
nitrogen content, 469
purification, 466
solubility of oxygen, 501
thermal/electrical/magnetic properties, 11t–12t
Yttrium–aluminum alloys, 544–545
Yttrium-aluminum-garnet (YAG), 57
Nd-YAG ceramics, 610–611
solid-state lasers, 37t
Yttrium chloride
dehydration assembly, 342f
lithium reduction of, 355–357
lithium/sodium reduction of, 353–355, 354f, 355f, 356t
and molybdenum crucible, 354
preparation of, 339
purification assembly, 347f
purified, 356
setup for dehydrating, 340f
Yttrium chlorination apparatus, 346f
Yttrium earths, 20
Yttrium fluoride, 378
Yttrium group of REE, 88
Yttrium hydroxide coating, 72
Yttrium–iron garnets, 57
Yttrium–lanthanum–fluoride (YLF) solid state lasers, 39t
Yttrium-magnesium alloy, 367, 376, 452
Yttrium mixed metal, 405
Yttrium orthosilicates, 64
Yttrium oxalate, 345
Yttrium oxide, 320f
in concentrated hydrochloric acid, 341
hydrofluorination of, 365f
method for chlorinating, 345
Yttrium–oxygen solid solution, 517
Yttrium phosphate, 269
Yttrium sulfate, 269
Yttrium trifluoride, 376
Yttrosynchisite ore, 210
Yukon, 171; *see also* Canada

Z

Zaire; *see also* World rare-earth production
occurrence of deposits in, 195
rare-earth production in, 213
Zandkopsdrift deposit, 183–184; *see also* South Africa
Zeolite, 545–546
cracking catalysts, 58
Zhenghai Oxygen-Free Process, 590
Zinc alloys, 42–43; *see also* Metallurgy
Zinc plating, 596
Zircon, 100; *see also* Minerals
importance of, 251, 252
Zirconia, stabilized, 54
Zirconium
mobility of oxygen, 500
non-rare-earth impurities, 692
SPADNS complex, 692
zone refining and electrotransport, 515
Zone melting, 564
Zone refining, 490
electrotransport, 510
gadolinium, 512–515
neodymium, 510–512
interstitial impurities, redistribution of, 496–497
lanthanum/cerium/gadolinium, 493–496
lanthanum/gadolinium/terbium, 493
metallic impurities, redistribution of, 497–500
preliminary studies, 491–492